



Proceedings

PRO 128

**Proceedings of the
International Conference
on Sustainable Materials,
Systems and Structures
(SMSS2019)**

**New Generation of
Construction Materials**

Edited by
**Marijana Serdar
Nina Štirmer
John Provis**

RILEM Publications S.A.R.L.

**International Conference on Sustainable
Materials, Systems and Structures
(SMSS 2019)**
New Generation of Construction Materials

International Conference on Sustainable Materials, Systems and Structures (SMSS 2019)
New Generation of Construction Materials
20-22 March 2019 – Rovinj, Croatia

Published by RILEM Publications S.A.R.L.
4 avenue du Recteur Poincaré 75016 Paris - France
Tel : + 33 1 42 24 64 46 Fax : + 33 9 70 29 51 20
<http://www.rilem.net> E-mail: dg@rilem.net
© 2019 RILEM – Tous droits réservés.
ISBN: 978-2-35158-217-6, Vol 1. ISBN: 978-2-35158-223-7
e-ISBN: 978-2-35158-218-3

Publisher's note: *this book has been produced from electronic files provided by the individual contributors. The publisher makes no representation, express or implied, with regard to the accuracy of the information contained in this book and cannot accept any legal responsibility or liability for any errors or omissions that may be made.*

All titles published by RILEM Publications are under copyright protection; said copyrights being the property of their respective holders. All Rights Reserved.

No part of any book may be reproduced or transmitted in any form or by any means, graphic, electronic, or mechanical, including photocopying, recording, taping, or by any information storage or retrieval system, without the permission in writing from the publisher.

RILEM, The International Union of Laboratories and Experts in Construction Materials, Systems and Structures, is a non profit-making, non-governmental technical association whose vocation is to contribute to progress in the construction sciences, techniques and industries, essentially by means of the communication it fosters between research and practice. RILEM's activity therefore aims at developing the knowledge of properties of materials and performance of structures, at defining the means for their assessment in laboratory and service conditions and at unifying measurement and testing methods used with this objective.

RILEM was founded in 1947, and has a membership of over 900 in some 70 countries. It forms an institutional framework for co-operation by experts to:

- optimise and harmonise test methods for measuring properties and performance of building and civil engineering materials and structures under laboratory and service environments,
- prepare technical recommendations for testing methods,
- prepare state-of-the-art reports to identify further research needs,
- collaborate with national or international associations in realising these objectives.

RILEM members include the leading building research and testing laboratories around the world, industrial research, manufacturing and contracting interests, as well as a significant number of individual members from industry and universities. RILEM's focus is on construction materials and their use in building and civil engineering structures, covering all phases of the building process from manufacture to use and recycling of materials.

RILEM meets these objectives through the work of its technical committees. Symposia, workshops and seminars are organised to facilitate the exchange of information and dissemination of knowledge. RILEM's primary output consists of technical recommendations. RILEM also publishes the journal *Materials and Structures* which provides a further avenue for reporting the work of its committees. Many other publications, in the form of reports, monographs, symposia and workshop proceedings are produced.

International Conference on Sustainable Materials,
Systems and Structures – SMSS 2019
New generation of construction materials

Rovinj, Croatia
20-22 March 2019

Edited by
Marijana Serdar
Nina Štirmer
John Provis

RILEM Publications

The following list is presenting the global offer of RILEM Publications, sorted by series. Each publication is available in printed version and/or in online version.

RILEM PROCEEDINGS (PRO)

- PRO 1:** Durability of High Performance Concrete (ISBN: 2-912143-03-9); *Ed. H. Sommer*
- PRO 2:** Chloride Penetration into Concrete (ISBN: 2-912143-00-04);
Eds. L.-O. Nilsson and J.-P. Ollivier
- PRO 3:** Evaluation and Strengthening of Existing Masonry Structures (ISBN: 2-912143-02-0);
Eds. L. Binda and C. Modena
- PRO 4:** Concrete: From Material to Structure (ISBN: 2-912143-04-7); *Eds. J.-P. Bournazel and Y. Malier*
- PRO 5:** The Role of Admixtures in High Performance Concrete (ISBN: 2-912143-05-5);
Eds. J. G. Cabrera and R. Rivera-Villarreal
- PRO 6:** High Performance Fiber Reinforced Cement Composites - HPFRCC 3
(ISBN: 2-912143-06-3); *Eds. H. W. Reinhardt and A. E. Naaman*
- PRO 7:** 1st International RILEM Symposium on Self-Compacting Concrete (ISBN: 2-912143-09-8); *Eds. Å. Skarendahl and Ö. Petersson*
- PRO 8:** International RILEM Symposium on Timber Engineering (ISBN: 2-912143-10-1);
Ed. L. Boström
- PRO 9:** 2nd International RILEM Symposium on Adhesion between Polymers and Concrete ISAP '99 (ISBN: 2-912143-11-X); *Eds. Y. Ohama and M. Puterman*
- PRO 10:** 3rd International RILEM Symposium on Durability of Building and Construction Sealants (ISBN: 2-912143-13-6); *Eds. A. T. Wolf*
- PRO 11:** 4th International RILEM Conference on Reflective Cracking in Pavements (ISBN: 2-912143-14-4); *Eds. A. O. Abd El Halim, D. A. Taylor and El H. H. Mohamed*
- PRO 12:** International RILEM Workshop on Historic Mortars: Characteristics and Tests (ISBN: 2-912143-15-2); *Eds. P. Bartos, C. Groot and J. J. Hughes*
- PRO 13:** 2nd International RILEM Symposium on Hydration and Setting (ISBN: 2-912143-16-0); *Ed. A. Nonat*
- PRO 14:** Integrated Life-Cycle Design of Materials and Structures - ILCDES 2000 (ISBN: 951-758-408-3); (ISSN: 0356-9403); *Ed. S. Sarja*
- PRO 15:** Fifth RILEM Symposium on Fibre-Reinforced Concretes (FRC) - BEFIB'2000 (ISBN: 2-912143-18-7); *Eds. P. Rossi and G. Chanvillard*
- PRO 16:** Life Prediction and Management of Concrete Structures (ISBN: 2-912143-19-5); *Ed. D. Naus*
- PRO 17:** Shrinkage of Concrete – Shrinkage 2000 (ISBN: 2-912143-20-9);
Eds. V. Baroghel-Bouny and P.-C. Aïtcin
- PRO 18:** Measurement and Interpretation of the On-Site Corrosion Rate (ISBN: 2-912143-21-7);
Eds. C. Andrade, C. Alonso, J. Fulla, J. Polimon and J. Rodriguez

- PRO 19:** Testing and Modelling the Chloride Ingress into Concrete (ISBN: 2-912143-22-5);
Eds. C. Andrade and J. Kropp
- PRO 20:** 1st International RILEM Workshop on Microbial Impacts on Building Materials (CD 02) (e-ISBN 978-2-35158-013-4); *Ed. M. Ribas Silva*
- PRO 21:** International RILEM Symposium on Connections between Steel and Concrete (ISBN: 2-912143-25-X); *Ed. R. Eligehausen*
- PRO 22:** International RILEM Symposium on Joints in Timber Structures (ISBN: 2-912143-28-4); *Eds. S. Aicher and H.-W. Reinhardt*
- PRO 23:** International RILEM Conference on Early Age Cracking in Cementitious Systems (ISBN: 2-912143-29-2); *Eds. K. Kovler and A. Bentur*
- PRO 24:** 2nd International RILEM Workshop on Frost Resistance of Concrete (ISBN: 2-912143-30-6); *Eds. M. J. Setzer, R. Auberg and H.-J. Keck*
- PRO 25:** International RILEM Workshop on Frost Damage in Concrete (ISBN: 2-912143-31-4); *Eds. D. J. Janssen, M. J. Setzer and M. B. Snyder*
- PRO 26:** International RILEM Workshop on On-Site Control and Evaluation of Masonry Structures (ISBN: 2-912143-34-9); *Eds. L. Binda and R. C. de Vekey*
- PRO 27:** International RILEM Symposium on Building Joint Sealants (CD03); *Ed. A. T. Wolf*
- PRO 28:** 6th International RILEM Symposium on Performance Testing and Evaluation of Bituminous Materials - PTEBM'03 (ISBN: 2-912143-35-7; e-ISBN: 978-2-912143-77-8); *Ed. M. N. Partl*
- PRO 29:** 2nd International RILEM Workshop on Life Prediction and Ageing Management of Concrete Structures (ISBN: 2-912143-36-5); *Ed. D. J. Naus*
- PRO 30:** 4th International RILEM Workshop on High Performance Fiber Reinforced Cement Composites - HPFRCC 4 (ISBN: 2-912143-37-3); *Eds. A. E. Naaman and H. W. Reinhardt*
- PRO 31:** International RILEM Workshop on Test and Design Methods for Steel Fibre Reinforced Concrete: Background and Experiences (ISBN: 2-912143-38-1); *Eds. B. Schnütgen and L. Vandewalle*
- PRO 32:** International Conference on Advances in Concrete and Structures 2 vol. (ISBN (set): 2-912143-41-1); *Eds. Ying-shu Yuan, Surendra P. Shah and Heng-lin Lü*
- PRO 33:** 3rd International Symposium on Self-Compacting Concrete (ISBN: 2-912143-42-X); *Eds. Ó. Wallevik and I. Nielsson*
- PRO 34:** International RILEM Conference on Microbial Impact on Building Materials (ISBN: 2-912143-43-8); *Ed. M. Ribas Silva*
- PRO 35:** International RILEM TC 186-ISA on Internal Sulfate Attack and Delayed Ettringite Formation (ISBN: 2-912143-44-6); *Eds. K. Scrivener and J. Skalny*
- PRO 36:** International RILEM Symposium on Concrete Science and Engineering – A Tribute to Arnon Bentur (ISBN: 2-912143-46-2); *Eds. K. Kovler, J. Marchand, S. Mindess and J. Weiss*
- PRO 37:** 5th International RILEM Conference on Cracking in Pavements – Mitigation, Risk Assessment and Prevention (ISBN: 2-912143-47-0); *Eds. C. Petit, I. Al-Qadi and A. Millien*
- PRO 38:** 3rd International RILEM Workshop on Testing and Modelling the Chloride Ingress into Concrete (ISBN: 2-912143-48-9); *Eds. C. Andrade and J. Kropp*
- PRO 39:** 6th International RILEM Symposium on Fibre-Reinforced Concretes - BEFIB 2004 (ISBN: 2-912143-51-9); *Eds. M. Di Prisco, R. Felicetti and G. A. Plizzari*
- PRO 40:** International RILEM Conference on the Use of Recycled Materials in Buildings and Structures (ISBN: 2-912143-52-7); *Eds. E. Vázquez, Ch. F. Hendriks and G. M. T. Janssen*

- PRO 41:** RILEM International Symposium on Environment-Conscious Materials and Systems for Sustainable Development (ISBN: 2-912143-55-1); *Eds. N. Kashino and Y. Ohama*
- PRO 42:** SCC'2005 - China: 1st International Symposium on Design, Performance and Use of Self-Consolidating Concrete (ISBN: 2-912143-61-6); *Eds. Zhiwu Yu, Caijun Shi, Kamal Henri Khayat and Youjun Xie*
- PRO 43:** International RILEM Workshop on Bonded Concrete Overlays (e-ISBN: 2-912143-83-7); *Eds. J. L. Granju and J. Silfwerbrand*
- PRO 44:** 2nd International RILEM Workshop on Microbial Impacts on Building Materials (CD11) (e-ISBN: 2-912143-84-5); *Ed. M. Ribas Silva*
- PRO 45:** 2nd International Symposium on Nanotechnology in Construction, Bilbao (ISBN: 2-912143-87-X); *Eds. Peter J. M. Bartos, Yolanda de Miguel and Antonio Porro*
- PRO 46:** ConcreteLife'06 - International RILEM-JCI Seminar on Concrete Durability and Service Life Planning: Curing, Crack Control, Performance in Harsh Environments (ISBN: 2-912143-89-6); *Ed. K. Kovler*
- PRO 47:** International RILEM Workshop on Performance Based Evaluation and Indicators for Concrete Durability (ISBN: 978-2-912143-95-2); *Eds. V. Baroghel-Bouny, C. Andrade, R. Torrent and K. Scrivener*
- PRO 48:** 1st International RILEM Symposium on Advances in Concrete through Science and Engineering (e-ISBN: 2-912143-92-6); *Eds. J. Weiss, K. Kovler, J. Marchand, and S. Mindess*
- PRO 49:** International RILEM Workshop on High Performance Fiber Reinforced Cementitious Composites in Structural Applications (ISBN: 2-912143-93-4); *Eds. G. Fischer and V.C. Li*
- PRO 50:** 1st International RILEM Symposium on Textile Reinforced Concrete (ISBN: 2-912143-97-7); *Eds. Josef Hegger, Wolfgang Brameshuber and Norbert Will*
- PRO 51:** 2nd International Symposium on Advances in Concrete through Science and Engineering (ISBN: 2-35158-003-6; e-ISBN: 2-35158-002-8); *Eds. J. Marchand, B. Bissonnette, R. Gagné, M. Jolin and F. Paradis*
- PRO 52:** Volume Changes of Hardening Concrete: Testing and Mitigation (ISBN: 2-35158-004-4; e-ISBN: 2-35158-005-2); *Eds. O. M. Jensen, P. Lura and K. Kovler*
- PRO 53:** High Performance Fiber Reinforced Cement Composites - HPRFRC5 (ISBN: 978-2-35158-046-2); *Eds. H. W. Reinhardt and A. E. Naaman*
- PRO 54:** 5th International RILEM Symposium on Self-Compacting Concrete (ISBN: 978-2-35158-047-9); *Eds. G. De Schutter and V. Boel*
- PRO 55:** International RILEM Symposium Photocatalysis, Environment and Construction Materials (ISBN: 978-2-35158-056-1); *Eds. P. Baglioni and L. Cassar*
- PRO56:** International RILEM Workshop on Integral Service Life Modelling of Concrete Structures (ISBN 978-2-35158-058-5); *Eds. R. M. Ferreira, J. Gulikers and C. Andrade*
- PRO57:** RILEM Workshop on Performance of cement-based materials in aggressive aqueous environments (e-ISBN: 978-2-35158-059-2); *Ed. N. De Belie*
- PRO58:** International RILEM Symposium on Concrete Modelling - CONMOD'08 (ISBN: 978-2-35158-060-8); *Eds. E. Schlangen and G. De Schutter*
- PRO 59:** International RILEM Conference on On Site Assessment of Concrete, Masonry and Timber Structures - SACoMaTiS 2008 (ISBN set: 978-2-35158-061-5); *Eds. L. Binda, M. di Prisco and R. Felicetti*
- PRO 60:** Seventh RILEM International Symposium on Fibre Reinforced Concrete: Design and Applications - BEFIB 2008 (ISBN: 978-2-35158-064-6); *Ed. R. Gettu*

- PRO 61:** 1st International Conference on Microstructure Related Durability of Cementitious Composites 2 vol., (ISBN: 978-2-35158-065-3); *Eds. W. Sun, K. van Breugel, C. Miao, G. Ye and H. Chen*
- PRO 62:** NSF/ RILEM Workshop: In-situ Evaluation of Historic Wood and Masonry Structures (e-ISBN: 978-2-35158-068-4); *Eds. B. Kasal, R. Anthony and M. Drdácý*
- PRO 63:** Concrete in Aggressive Aqueous Environments: Performance, Testing and Modelling, 2 vol., (ISBN: 978-2-35158-071-4); *Eds. M. G. Alexander and A. Bertron*
- PRO 64:** Long Term Performance of Cementitious Barriers and Reinforced Concrete in Nuclear Power Plants and Waste Management - NUCPERF 2009 (ISBN: 978-2-35158-072-1); *Eds. V. L'Hostis, R. Gens, C. Gallé*
- PRO 65:** Design Performance and Use of Self-consolidating Concrete - SCC'2009 (ISBN: 978-2-35158-073-8); *Eds. C. Shi, Z. Yu, K. H. Khayat and P. Yan*
- PRO 66:** 2nd International RILEM Workshop on Concrete Durability and Service Life Planning - ConcreteLife'09 (ISBN: 978-2-35158-074-5); *Ed. K. Kovler*
- PRO 67:** Repairs Mortars for Historic Masonry (e-ISBN: 978-2-35158-083-7); *Ed. C. Groot*
- PRO 68:** Proceedings of the 3rd International RILEM Symposium on 'Rheology of Cement Suspensions such as Fresh Concrete (ISBN 978-2-35158-091-2); *Eds. O. H. Wallevik, S. Kubens and S. Oesterheld*
- PRO 69:** 3rd International PhD Student Workshop on 'Modelling the Durability of Reinforced Concrete (ISBN: 978-2-35158-095-0); *Eds. R. M. Ferreira, J. Gulikers and C. Andrade*
- PRO 70:** 2nd International Conference on 'Service Life Design for Infrastructure' (ISBN set: 978-2-35158-096-7, e-ISBN: 978-2-35158-097-4); *Ed. K. van Breugel, G. Ye and Y. Yuan*
- PRO 71:** Advances in Civil Engineering Materials - The 50-year Teaching Anniversary of Prof. Sun Wei' (ISBN: 978-2-35158-098-1; e-ISBN: 978-2-35158-099-8); *Eds. C. Miao, G. Ye, and H. Chen*
- PRO 72:** First International Conference on 'Advances in Chemically-Activated Materials – CAM'2010' (2010), 264 pp, ISBN: 978-2-35158-101-8; e-ISBN: 978-2-35158-115-5, *Eds. Caijun Shi and Xiaodong Shen*
- PRO 73:** 2nd International Conference on 'Waste Engineering and Management - ICWEM 2010' (2010), 894 pp, ISBN: 978-2-35158-102-5; e-ISBN: 978-2-35158-103-2, *Eds. J. Zh. Xiao, Y. Zhang, M. S. Cheung and R. Chu*
- PRO 74:** International RILEM Conference on 'Use of Superabsorbent Polymers and Other New Additives in Concrete' (2010) 374 pp., ISBN: 978-2-35158-104-9; e-ISBN: 978-2-35158-105-6; *Eds. O.M. Jensen, M.T. Hasholt, and S. Laustsen*
- PRO 75:** International Conference on 'Material Science - 2nd ICTRC - Textile Reinforced Concrete - Theme 1' (2010) 436 pp., ISBN: 978-2-35158-106-3; e-ISBN: 978-2-35158-107-0; *Ed. W. Brameshuber*
- PRO 76:** International Conference on 'Material Science - HetMat - Modelling of Heterogeneous Materials - Theme 2' (2010) 255 pp., ISBN: 978-2-35158-108-7; e-ISBN: 978-2-35158-109-4; *Ed. W. Brameshuber*
- PRO 77:** International Conference on 'Material Science - AdIPoC - Additions Improving Properties of Concrete - Theme 3' (2010) 459 pp., ISBN: 978-2-35158-110-0; e-ISBN: 978-2-35158-111-7; *Ed. W. Brameshuber*

PRO 78: 2nd Historic Mortars Conference and RILEM TC 203-RHM Final Workshop – HMC2010 (2010) 1416 pp., e-ISBN: 978-2-35158-112-4; *Eds J. Válek, C. Groot, and J. J. Hughes*

PRO 79: International RILEM Conference on Advances in Construction Materials Through Science and Engineering (2011) 213 pp., e-ISBN: 978-2-35158-117-9; *Eds Christopher Leung and K.T. Wan*

PRO 80: 2nd International RILEM Conference on Concrete Spalling due to Fire Exposure (2011) 453 pp., ISBN: 978-2-35158-118-6, e-ISBN: 978-2-35158-119-3; *Eds E.A.B. Koenders and F. Dehn*

PRO 81: 2nd International RILEM Conference on Strain Hardening Cementitious Composites (SHCC2-Rio) (2011) 451 pp., ISBN: 978-2-35158-120-9, e-ISBN: 978-2-35158-121-6; *Eds R.D. Toledo Filho, F.A. Silva, E.A.B. Koenders and E.M.R. Fairbairn*

PRO 82: 2nd International RILEM Conference on Progress of Recycling in the Built Environment (2011) 507 pp., e-ISBN: 978-2-35158-122-3; *Eds V.M. John, E. Vazquez, S.C. Angulo and C. Ulsen*

PRO 83: 2nd International Conference on Microstructural-related Durability of Cementitious Composites (2012) 250 pp., ISBN: 978-2-35158-129-2; e-ISBN: 978-2-35158-123-0; *Eds G. Ye, K. van Breugel, W. Sun and C. Miao*

PRO 85: RILEM-JCI International Workshop on Crack Control of Mass Concrete and Related issues concerning Early-Age of Concrete Structures – ConCrack 3 – Control of Cracking in Concrete Structures 3 (2012) 237 pp., ISBN: 978-2-35158-125-4; e-ISBN: 978-2-35158-126-1; *Eds F. Toutlemonde and J.-M. Torrenti*

PRO 86: International Symposium on Life Cycle Assessment and Construction (2012) 414 pp., ISBN: 978-2-35158-127-8, e-ISBN: 978-2-35158-128-5; *Eds A. Ventura and C. de la Roche*

PRO 87: UHPFRC 2013 – RILEM-fib-AFGC International Symposium on Ultra-High Performance Fibre-Reinforced Concrete (2013), ISBN: 978-2-35158-130-8, e-ISBN: 978-2-35158-131-5; *Eds F. Toutlemonde*

PRO 88: 8th RILEM International Symposium on Fibre Reinforced Concrete (2012) 344 pp., ISBN: 978-2-35158-132-2, e-ISBN: 978-2-35158-133-9; *Eds Joaquim A.O. Barros*

PRO 89: RILEM International workshop on performance-based specification and control of concrete durability (2014) 678 pp, ISBN: 978-2-35158-135-3, e-ISBN: 978-2-35158-136-0; *Eds. D. Bjegović, H. Beushausen and M. Serdar*

PRO 90: 7th RILEM International Conference on Self-Compacting Concrete and of the 1st RILEM International Conference on Rheology and Processing of Construction Materials (2013) 396 pp, ISBN: 978-2-35158-137-7, e-ISBN: 978-2-35158-138-4; *Eds. Nicolas Roussel and Hela Bessaies-Bey*

PRO 91: CONMOD 2014 - RILEM International Symposium on Concrete Modelling (2014), ISBN: 978-2-35158-139-1; e-ISBN: 978-2-35158-140-7; *Eds. Kefei Li, Peiyu Yan and Rongwei Yang*

PRO 92: CAM 2014 - 2nd International Conference on advances in chemically-activated materials (2014) 392 pp., ISBN: 978-2-35158-141-4; e-ISBN: 978-2-35158-142-1; *Eds. Caijun Shi and Xiadong Shen*

PRO 93: SCC 2014 - 3rd International Symposium on Design, Performance and Use of Self-Consolidating Concrete (2014) 438 pp., ISBN: 978-2-35158-143-8; e-ISBN: 978-2-35158-144-5; *Eds. Caijun Shi, Zhihua Ou, Kamal H. Khayat*

- PRO 94 (online version):** HPRCC-7 - 7th RILEM conference on High performance fiber reinforced cement composites (2015), e-ISBN: 978-2-35158-146-9; *Eds. H.W. Reinhardt, G.J. Parra-Montesinos, H. Garrecht*
- PRO 95:** International RILEM Conference on Application of superabsorbent polymers and other new admixtures in concrete construction (2014), ISBN: 978-2-35158-147-6; e-ISBN: 978-2-35158-148-3; *Eds. Viktor Mechtcherine, Christof Schroefl*
- PRO 96 (online version):** XIII DBMC: XIII International Conference on Durability of Building Materials and Components (2015), e-ISBN: 978-2-35158-149-0; *Eds. M. Quattrone, V.M. John*
- PRO 97:** SHCC3 – 3rd International RILEM Conference on Strain Hardening Cementitious Composites (2014), ISBN: 978-2-35158-150-6; e-ISBN: 978-2-35158-151-3; *Eds. E. Schlangen, M.G. Sierra Beltran, M. Lukovic, G. Ye*
- PRO 98:** FERRO-11 – 11th International Symposium on Ferrocement and 3rd ICTRC - International Conference on Textile Reinforced Concrete (2015), ISBN: 978-2-35158-152-0; e-ISBN: 978-2-35158-153-7; *Ed. W. Brameshuber*
- PRO 99 (online version):** ICBBM 2015 - 1st International Conference on Bio-Based Building Materials (2015), e-ISBN: 978-2-35158-154-4; *Eds. S. Amziane, M. Sonebi*
- PRO 100:** SCC16 - RILEM Self-Consolidating Concrete Conference (2016), ISBN: 978-2-35158-156-8; e-ISBN: 978-2-35158-157-5
- PRO 101 (online version):** III Progress of Recycling in the Built Environment (2015), e-ISBN: 978-2-35158-158-2; *Eds I. Martins, C. Ulsen and S. C. Angulo*
- PRO 102 (online version):** RILEM Conference on Microorganisms-Cementitious Materials Interactions (2016), e-ISBN: 978-2-35158-160-5; *Eds. Alexandra Bertron, Henk Jonkers, Virginie Wiktor*
- PRO 103 (online version):** ACESC'16 - Advances in Civil Engineering and Sustainable Construction (2016), e-ISBN: 978-2-35158-161-2
- PRO 104 (online version):** SSCS'2015 - Numerical Modeling - Strategies for Sustainable Concrete Structures (2015), e-ISBN: 978-2-35158-162-9
- PRO 105:** 1st International Conference on UHPC Materials and Structures (2016), ISBN: 978-2-35158-164-3, e-ISBN: 978-2-35158-165-0
- PRO 106:** AFGC-ACI-fib-RILEM International Conference on Ultra-High-Performance Fibre-Reinforced Concrete – UHPFRC 2017 (2017), ISBN: 978-2-35158-166-7, e-ISBN: 978-2-35158-167-4; *Eds. François Toutlemonde & Jacques Resplendino*
- PRO 107 (online version):** XIV DBMC – 14th International Conference on Durability of Building Materials and Components (2017), e-ISBN: 978-2-35158-159-9; *Eds. Geert De Schutter, Nele De Belie, Arnold Janssens, Nathan Van Den Bossche*
- PRO 108:** MSSCE 2016 - Innovation of Teaching in Materials and Structures (2016), ISBN: 978-2-35158-178-0, e-ISBN: 978-2-35158-179-7; *Ed. Per Goltermann*
- PRO 109 (2 volumes):** MSSCE 2016 - Service Life of Cement-Based Materials and Structures (2016), ISBN Vol. 1: 978-2-35158-170-4, Vol. 2: 978-2-35158-171-4, Set Vol. 1&2: 978-2-35158-172-8, e-ISBN : 978-2-35158-173-5; *Eds. Miguel Azenha, Ivan Gabrijel, Dirk Schlicke, Terje Kanstad and Ole Mejlhede Jensen*
- PRO 110:** MSSCE 2016 - Historical Masonry (2016), ISBN: 978-2-35158-178-0, e-ISBN: 978-2-35158-179-7; *Eds. Inge Rørig-Dalgaard and Ioannis Ioannou*
- PRO 111:** MSSCE 2016 - Electrochemistry in Civil Engineering (2016), ISBN: 978-2-35158-176-6, e-ISBN: 978-2-35158-177-3; *Ed. Lisbeth M. Ottosen*

PRO 112: MSSCE 2016 - Moisture in Materials and Structures (2016), ISBN: 978-2-35158-178-0, e-ISBN: 978-2-35158-179-7; *Eds. Kurt Kielsgaard Hansen, Carsten Rode and Lars-Olof Nilsson*

PRO 113: MSSCE 2016 - Concrete with Supplementary Cementitious Materials (2016), ISBN: 978-2-35158-178-0, e-ISBN: 978-2-35158-179-7; *Eds. Ole Mejlhede Jensen, Konstantin Kovler and Nele De Belie*

PRO 114: MSSCE 2016 - Frost Action in Concrete (2016), ISBN: 978-2-35158-182-7, e-ISBN: 978-2-35158-183-4; *Eds. Marianne Tange Hasholt, Katja Fridh and R. Doug Hooton*

PRO 115: MSSCE 2016 - Fresh Concrete (2016), ISBN: 978-2-35158-184-1, e-ISBN: 978-2-35158-185-8; *Eds. Lars N. Thrane, Claus Pade, Oldrich Svec and Nicolas Roussel*

PRO 116: BEFIB 2016 – 9th RILEM International Symposium on Fiber Reinforced Concrete (2016), ISBN: 978-2-35158-187-2, e-ISBN: 978-2-35158-186-5;

PRO 117: 3rd International RILEM Conference on Microstructure Related Durability of Cementitious Composites (2016), ISBN: 978-2-35158-188-9, e-ISBN: 978-2-35158-189-6; *Eds. Changwen Miao, Wei Sun, Jiaping Liu, Huisu Chen, Guang Ye and Klaas van Breugel*

PRO 118 (4 volumes): International Conference on Advances in Construction Materials and Systems (2017), ISBN Set: 978-2-35158-190-2, Vol. 1: 978-2-35158-193-3, Vol. 2: 978-2-35158-194-0, Vol. 3: ISBN:978-2-35158-195-7, Vol. 4: ISBN:978-2-35158-196-4, e-ISBN: 978-2-35158-191-9; *Ed. Manu Santhanam*

PRO 119 (online version): ICBBM 2017 - Second International RILEM Conference on Bio-based Building Materials, (2017), e-ISBN: 978-2-35158-192-6; *Ed. Sofiane Amziane*

PRO 120 (2 volumes): EAC-02 - 2nd International RILEM/COST Conference on Early Age Cracking and Serviceability in Cement-based Materials and Structures, (2017), Vol. 1: 978-2-35158-199-5, Vol. 2: 978-2-35158-200-8, Set: 978-2-35158-197-1, e-ISBN: 978-2-35158-198-8; *Eds. Stéphanie Staquet and Dimitrios Aggelis*

PRO 121 (2 volumes): SynerCrete18: Interdisciplinary Approaches for Cement-based Materials and Structural Concrete: Synergizing Expertise and Bridging Scales of Space and Time, (2018), Set: 978-2-35158-202-2, Vol.1: 978-2-35158-211-4, Vol.2: 978-2-35158-212-1, e-ISBN: 978-2-35158-203-9; *Ed. Miguel Azenha, Dirk Schlicke, Farid Benboudjema, Agnieszka Knoppik*

PRO 122: SCC'2018 China - Fourth International Symposium on Design, Performance and Use of Self-Consolidating Concrete, (2018), ISBN: 978-2-35158-204-6, e-ISBN: 978-2-35158-205-3

PRO 123: Final Conference of RILEM TC 253-MCI: Microorganisms-Cementitious Materials Interactions (2018), Set: 978-2-35158-207-7, Vol.1: 978-2-35158-209-1, Vol.2: 978-2-35158-210-7, e-ISBN: 978-2-35158-206-0; *Ed. Alexandra Bertron*

PRO 124 (online version): Fourth International Conference Progress of Recycling in the Built Environment (2018), e-ISBN: 978-2-35158-208-4; *Eds. Isabel M. Martins, Carina Ulsen, Yury Villagran*

PRO 125 (online version): SLD4 - 4th International Conference on Service Life Design for Infrastructures (2018), e-ISBN: 978-2-35158-213-8; *Eds. Guang Ye, Yong Yuan, Claudia Romero Rodriguez, Hongzhi Zhang, Branko Savija*

PRO 126: Workshop on Concrete Modelling and Material Behaviour in honor of Professor Klaas van Breugel (2018), ISBN: 978-2-35158-214-5, e-ISBN: 978-2-35158-215-2; *Ed. Guang Ye*

PRO 127 (online version): CONMOD2018 - Symposium on Concrete Modelling (2018), e-ISBN: 978-2-35158-216-9; *Eds. Erik Schlangen, Geert de Schutter, Branko Savija, Hongzhi Zhang, Claudia Romero Rodriguez*

RILEM REPORTS (REP)

- Report 19:** Considerations for Use in Managing the Aging of Nuclear Power Plant Concrete Structures (ISBN: 2-912143-07-1); *Ed. D. J. Naus*
- Report 20:** Engineering and Transport Properties of the Interfacial Transition Zone in Cementitious Composites (ISBN: 2-912143-08-X); *Eds. M. G. Alexander, G. Arliguie, G. Ballivy, A. Bentur and J. Marchand*
- Report 21:** Durability of Building Sealants (ISBN: 2-912143-12-8); *Ed. A. T. Wolf*
- Report 22:** Sustainable Raw Materials - Construction and Demolition Waste (ISBN: 2-912143-17-9); *Eds. C. F. Hendriks and H. S. Pietersen*
- Report 23:** Self-Compacting Concrete state-of-the-art report (ISBN: 2-912143-23-3); *Eds. Å. Skarendahl and Ö. Petersson*
- Report 24:** Workability and Rheology of Fresh Concrete: Compendium of Tests (ISBN: 2-912143-32-2); *Eds. P. J. M. Bartos, M. Sonebi and A. K. Tamimi*
- Report 25:** Early Age Cracking in Cementitious Systems (ISBN: 2-912143-33-0); *Ed. A. Bentur*
- Report 26:** Towards Sustainable Roofing (Joint Committee CIB/RILEM) (CD 07) (e-ISBN 978-2-912143-65-5); *Eds. Thomas W. Hutchinson and Keith Roberts*
- Report 27:** Condition Assessment of Roofs (Joint Committee CIB/RILEM) (CD 08) (e-ISBN 978-2-912143-66-2); *Ed. CIB W 83/RILEM TC166-RMS*
- Report 28:** Final report of RILEM TC 167-COM ‘Characterisation of Old Mortars with Respect to Their Repair (ISBN: 978-2-912143-56-3); *Eds. C. Groot, G. Ashall and J. Hughes*
- Report 29:** Pavement Performance Prediction and Evaluation (PPPE): Interlaboratory Tests (e-ISBN: 2-912143-68-3); *Eds. M. Partl and H. Piber*
- Report 30:** Final Report of RILEM TC 198-URM ‘Use of Recycled Materials’ (ISBN: 2-912143-82-9; e-ISBN: 2-912143-69-1); *Eds. Ch. F. Hendriks, G. M. T. Janssen and E. Vázquez*
- Report 31:** Final Report of RILEM TC 185-ATC ‘Advanced testing of cement-based materials during setting and hardening’ (ISBN: 2-912143-81-0; e-ISBN: 2-912143-70-5); *Eds. H. W. Reinhardt and C. U. Grosse*
- Report 32:** Probabilistic Assessment of Existing Structures. A JCSS publication (ISBN 2-912143-24-1); *Ed. D. Diamantidis*
- Report 33:** State-of-the-Art Report of RILEM Technical Committee TC 184-IFE ‘Industrial Floors’ (ISBN 2-35158-006-0); *Ed. P. Seidler*
- Report 34:** Report of RILEM Technical Committee TC 147-FMB ‘Fracture mechanics applications to anchorage and bond’ Tension of Reinforced Concrete Prisms – Round Robin Analysis and Tests on Bond (e-ISBN 2-912143-91-8); *Eds. L. Elfgren and K. Noghabai*
- Report 35:** Final Report of RILEM Technical Committee TC 188-CSC ‘Casting of Self Compacting Concrete’ (ISBN 2-35158-001-X; e-ISBN: 2-912143-98-5); *Eds. Å. Skarendahl and P. Billberg*
- Report 36:** State-of-the-Art Report of RILEM Technical Committee TC 201-TRC ‘Textile Reinforced Concrete’ (ISBN 2-912143-99-3); *Ed. W. Brameshuber*
- Report 37:** State-of-the-Art Report of RILEM Technical Committee TC 192-ECM ‘Environment-conscious construction materials and systems’ (ISBN: 978-2-35158-053-0); *Eds. N. Kashino, D. Van Gemert and K. Imamoto*
- Report 38:** State-of-the-Art Report of RILEM Technical Committee TC 205-DSC ‘Durability of Self-Compacting Concrete’ (ISBN: 978-2-35158-048-6); *Eds. G. De Schutter and K. Audenaert*

Report 39: Final Report of RILEM Technical Committee TC 187-SOC ‘Experimental determination of the stress-crack opening curve for concrete in tension’ (ISBN 978-2-35158-049-3); *Ed. J. Planas*

Report 40: State-of-the-Art Report of RILEM Technical Committee TC 189-NEC ‘Non-Destructive Evaluation of the Penetrability and Thickness of the Concrete Cover’ (ISBN 978-2-35158-054-7);
Eds. R. Torrent and L. Fernández Luco

Report 41: State-of-the-Art Report of RILEM Technical Committee TC 196-ICC ‘Internal Curing of Concrete’ (ISBN 978-2-35158-009-7); *Eds. K. Kovler and O. M. Jensen*

Report 42: ‘Acoustic Emission and Related Non-destructive Evaluation Techniques for Crack Detection and Damage Evaluation in Concrete’ - Final Report of RILEM Technical Committee 212-ACD (e-ISBN: 978-2-35158-100-1); *Ed. M. Ohtsu*

Report 45: Repair Mortars for Historic Masonry - State-of-the-Art Report of RILEM Technical Committee TC 203-RHM (e-ISBN: 978-2-35158-163-6); *Eds. Paul Maurenbrecher and Caspar Groot*

Report 46: Surface delamination of concrete industrial floors and other durability related aspects guide - Report of RILEM Technical Committee TC 268-SIF (e-ISBN: 978-2-35158-201-5); *Ed. Valérie Pollet*

Conference Chair

Marijana Serdar, Faculty of Civil Engineering, University of Zagreb, Croatia

Ivana Banjad Pečur, Faculty of Civil Engineering, University of Zagreb, Croatia

Honorary president of scientific committee

Dubravka Bjegović, Faculty of Civil Engineering, University of Zagreb, Croatia

International Scientific Committee of segment *New generation of construction materials*

Susan Bernal

Alexandra Bertron

Dubravka Bjegović

Alan Carter

Valter Carvelli

Christopher Cheeseman

Ozlem Cizer

Luc Courard

Martin Cyr

Nele De Belie

Jean-Baptiste d'Espinose de Lacaillerie

Josipa Domitrović

Vilma Ducman

Guillaume Habert

Ksenija Jankovic

Dragica Lj. Jevtić

Maria Juenger

Said Kenai

Sylvie Kessler

Jamal Khatib

Miroslav Komljenović

Barbara Lothenbach

Pietro Lura

Viktor Mechtcherine

Ildiko Merta

Sree Nanukuttan

Moray Newlands

Benoit Parmentier

Gai-fei Peng

Stephane Poyet

John Provis

Tatjana Rukavina

Manu Santhanam

Marijana Serdar

Vit Smilauer

Ruben Snellings

Maria Sophia Sousa Ribeiro

Tayfun Altuğ Söylev

Nina Štirmer

Souzana Tastani

Gabriele Tebaldi

Antonio Telesca

Frank Winnefeld

Guang Ye

Organizing Committee of segment *New generation of construction materials*

Marijana Serdar, Faculty of Civil Engineering, University of Zagreb, Croatia

Nina Štirmer, Faculty of Civil Engineering, University of Zagreb, Croatia

John Provis, University of Sheffield, UK

Contents

	<i>Page</i>
Preface	XXIII
<i>Marijana Serdar, Nina Štirmer, John Provis</i>	
KEYNOTE LECTURES	1
Nanotechnology and sustainability in concrete construction	2
<i>Surendra P. Shah</i>	
Roadmap of development and application of sustainable materials	3
<i>Karen Scrivener</i>	
SESSION 1: SCM Reactivity	4
Particle size optimization in multi-component cement	5
<i>S. Adu-Amankwah, S. A. Bernal and L. Black</i>	
The limiting factors of SCMs reaction at later age	6
<i>Yosra Briki, Karen Scrivener and Mohsen Ben Haha</i>	
Comparative evaluation of use silica fume, blast furnace slag, limestone, metakaolin and red mud as supplementary cementitious materials for concrete	11
<i>Roberto Cesar de Oliveira Romano, José Augusto Ferreira Sales de Mesquita, Gabriel Carpinelli Perozzi Brasileiro, Maria Alba Cincotto and Rafael Giuliano Pileggi</i>	
Characterization and pozzolanic activity of UK alum water treatment sludge	19
<i>M. Shamaki, L. Black</i>	
Investigating the origins of metakaolin surface reactivity in the context of alkali-activated binders	27
<i>V. Benavent, Q. H. Nguyen, J.-B. d'Espinose de Lacaillerie, M. Marinova-Atanassova, A.-M. Blanchenet and C. A. Davy</i>	
SESSION 2: Special session of TC 280-CBE Cold bitumen emulsion	35
Evaluation of local aggregate with chemical additives for microsurfacing mix	36
<i>Teiborlang Lyngdoh Ryntathiang, Alan Carter, Anjan kumar Siddagangiah</i>	
Thermal impact of adding recycled glass in microsurfacing	44
<i>Apparao Gandi, Abdelghafour Zabayou, Saeed Badeli, Alan Carter and Michel Vaillancourt</i>	
Characterisation and treatment of tunnel boring muds for their valorisation in road construction	52
<i>A. Cabrerizo, D. Bulteel, J. Waligora, D. Bonneau and F. Olard</i>	

Influence of coarse recycled concrete aggregate on the durability of asphalt mixtures	60
<i>A. Radević, G. Mladenović, D. Jevtić, D. Zakić, M. Aškračić</i>	
Stone mastic asphalt reinforced by vegetable yarns	68
<i>Peter Gallo, Jan Valentin</i>	
Strength mechanism and improvement methods of cement bitumen emulsion mixture	76
<i>Jian Ouyang, Wen Xu, and Lijun Hu</i>	
Evaluation of the stiffness modulus and phase angle of cold in-place recycled mixtures for long curing periods	84
<i>Bohdan Dolzycki, Mariusz Jaczewski and Cezary Szydłowski</i>	
Evaluating the cracking resistance of cement-bitumen treated materials using the semi-circular bending test	92
<i>Chiara Mignini, Fabrizio Cardone, Alessandro Morbi, Luca Setti and Andrea Graziani</i>	
Field behaviour of cold-recycled asphalt mixtures for binder courses	100
<i>Andrea Grilli, Chiara Mignini and Andrea Graziani</i>	
Experimental application of synthetic lightweight aggregates for the production of special asphalt concretes	108
<i>P. Tataranni and C. Sangiorgi</i>	
SESSION 3: Durability of AAMs	116
Testing the durability of alkali-activated concretes	117
<i>John Provis</i>	
Behaviour of reinforced alkali-activated fly ash mortars under leaching conditions	118
<i>Petr Hlaváček, Steffi Reinemann, Gregor J.G. Gluth, Gino Ebell and Jürgen Mietz</i>	
Thermal properties and steel corrosion in lightweight alkali activated mortars	125
<i>L. Carabba, G. Masi, S. Pirskawetz, S. Krüger, G. J. G. Gluth, M. C. Bignozzi</i>	
Durability of fly ash-based alkali-activated mortars reinforced with short hemp fibres	133
<i>Bojan Poletanović, Ivan Janotka, Michal Bačuvčík, Ildiko Merta</i>	
Durability of alkali-activated concrete mixtures – a requirement for success in the market	141
<i>Katja Dombrowski-Daube, Jan Sachl</i>	
Non-classical reaction pathways in alkali-activated systems	150
<i>Luca Valentini</i>	

SESSION 4: Waste ashes as SCMs	155
Properties of cementitious materials with sewage sludge ashes	156
<i>M. Saillio, L. Andrade M. Mehdi, T. Chaussadent and Arezki Tagnit-Hamou</i>	
Early-age structural development of cement blended with flash calcined dredging sediments	164
<i>Céline Van Bunderen, Ruben Snellings, Lucie Vandewalle and Özlem Cizer</i>	
Durability of high carbon biomass ash-based binder	172
<i>Piyush Chaunsali, Hugo Uvegi, Brian Traynor and Elsa Olivetti</i>	
The effect of MSWI fly ash on mortar workability	180
<i>Benjamin A. R. Ebert, Britt-Marie Steenari, Mette R. Geiker and Gunvor M. Kirkelund</i>	
Pre-treatments of MSWI bottom ash for the application as supplementary cementitious material in blended cement paste	187
<i>Boyu Chen, Yubo Sun, Loic Jacquemin, Shizhe Zhang, Kees Blom, Mladena Luković and Guang Ye</i>	
SESSION 5: UHPC	194
Effects of different chemical pretreatments of natural fibers on the mechanical properties of cement mortar	195
<i>S. Juradin, I. Boko, I. Netinger Grubeša and S. Mrakovčić</i>	
The influence of nano SiO₂ and curing regimes on mechanical properties of UHPFRC	202
<i>Ksenija Janković, Marko Stojanović, Dragan Bojović</i>	
Strain-hardening ettringite-based composite with polypropylene fiber reinforced ladle slag: durability under combined chloride and sulfate attack	210
<i>Hoang Nguyen, Paivo Kinnunen, Valter Carvelli, and Mirja Illikainen</i>	
Mechanical and insulation properties of ultra-high performance concrete with expanded polystyrene	217
<i>Anjaneya Dixit, Sze Dai Pang and Juhyuk Moon</i>	
Effect of pre-impregnation process on the tensile behavior of glass yarn/ettringitic matrix composite	223
<i>Omayma Homoro, Marie Michel and Thouraya. N. Baranger</i>	
Rubberised concrete refinement by cement substitution and rubber particle pre-treatment	231
<i>Thomaida Polydorou, Kyriacos Neocleous, Loukas Koutsokeras, Georgios Constantinides, Nicholas Kyriakides, Kypros Pilakoutas and Diofantos Hadjimitsis</i>	
Experimental investigation of corroded steel anchorages in strain resilient cementitious composites	239
<i>Souzana P. Tastani, Christos Dakidis</i>	

SESSION 6: Trends in aggregate	247
Early-age evolution of recycled concrete strength: insights from micromechanics modeling and experimental testing	248
<i>Markus Königsberger, Brice Delsaute and Stéphanie Staquet</i>	
The study on fundamental properties and self-healing performance of concrete using belite-gehlenite clinker as fine aggregate	255
<i>Fumihiko Watanabe, Hiromi Fujiwara, Masatoshi Maruoka, Shunnosuke Ito and Kensuke Hayashi</i>	
The producing technology and improved methods of the recycled concrete aggregate	263
<i>Ting Du</i>	
Experimental study on properties of concrete containing molten slag from integrated coal gasification combined cycle as fine aggregate	264
<i>Ryotaro Kobayashi, Hiromi Fujiwara, Masanori Maruoka, Yuto Yamanaka</i>	
Recycled aggregates produced from two different feedstock materials – Applied in ready-mixed concrete	272
<i>Hernan Mujica, Egil Velde, Christian J. Engelsen, Monica S. Nodland</i>	
Variation in physical and environmental properties of recycled concrete aggregates from C&D waste in Delhi	280
<i>Christian J. Engelsen, Harsha Meenawat, Arun Kumar Sharma, Gaurav Bhatiani, Kshemendra Nath P, Monica S. Nodland</i>	
Optimizing performances of recycled aggregates for improving concrete properties	287
<i>L. Courard, E. Tabarelli, F. Michel, S. Delvoie, M. ElKarim Bouarroudj, Ch. Colman, Z. Zhao</i>	
Concrete with waste glass as a sustainable building material for precast kerbs	295
<i>Goce K. Prangovski, Georgi D. Goshev</i>	
SESSION 7: Innovation in chemistry and nanotechnology	303
Effects and potentials of plant-based chemical admixtures on the performance of cementitious construction materials	304
<i>Wolfram Schmidt, Ines L. Tchegnina Ngassam, Kolawole A. Olonade, Rose Mbugua and Hans-Carsten Kühne</i>	
Mechanical behavior and neutron shielding performances of TiO₂-incorporated cement composites	305
<i>Jaeyeon Park, Sungwun Her, Heongwon Suh, Seung Min Woo, Keunhong Jeong and Sungchul Bae</i>	
Effect of titanate nanotubes on the properties of cement-based composites	312
<i>Hyeonseok Jee, Jaeyeon Park, Sungwun Her, Erfan Zalnezhad, Keunhong Jeong and Sungchul Bae</i>	

Influence of PRAH crystalline admixtures on the durability of concretes	320
<i>Kosmas K. Sideris, Christos Tassos, Alexandros Chatzopoulos, Panagiota Manita</i>	
A comparison of graphene oxide, reduced graphene oxide and pure graphene: early age properties of cement composites	326
<i>Tanvir S. Qureshi and Daman K. Panesar</i>	
A new admixture for concrete with clay contaminated sand	334
<i>O. Mazanec, F. Morati, A. Große-Sommer</i>	
SESSION 8: Candidates for AAMs	335
Instantaneous activation energy of alkali activated materials	336
<i>Shiju Joseph, Siva Uppalapati and Özlem Cizer</i>	
Mechanical parameters of metakaolin-based geopolymer with CRT glass waste fine aggregate	337
<i>Natalia Paszek, Marcin Górski</i>	
Development of alkali-activated magnesium aluminosilicate binders from soapstone	345
<i>Z. Abdollahnejad, T. Luukkonen, M. Mastali, J. Yliniemi J, P. Kinnunen, M. Illikainen</i>	
Production of alkali-activated binders from iron silicate fines	353
<i>John L. Provis, Angel L. Muñoz Gomez, Oday H. Hussein, Gaone Koma, Emanuela Manolova, Vladislav Petrov</i>	
Mixture proportioning for alkali-activated slag-based concrete	361
<i>Ning Li, Caijun Shi, Zuhua Zhang, Deju Zhu</i>	
Alkali activation of high MgO BFS with sodium carbonate added dry vs. wet	362
<i>Abeer M. Humad, John L. Provis, Andrzej Cwirzen</i>	
SESSION 9: Alternative binders	370
Hydration of MgO in the presence of hydromagnesite	371
<i>Frank Winnefeld, Eugenia Epifania, Fabio Montagnaro and Ellis M. Gartner</i>	
Radioactive waste conditioning using alumina-silicate binary blends	379
<i>Bastien Planel, David Lambertin and Catherine A. Davy</i>	
Chemical and microstructural characterisation of lime and lime-metakaolin pastes with linseed oil	386
<i>C. Nunes, P. Mácová, D. Frankeová, R. Ševčík and A. Viani</i>	
Use of biomass fly ash for the production of low energy blended calcium sulfoaluminate cements	394
<i>M. Marroccoli, M. De Biasi and A. Telesca</i>	

A preliminary study of thermodynamic modelling of calcium sulfoaluminate cement-based material	402
<i>Yoon, H.N., Park, S.M., Kil, T.G. and Lee, H.K.</i>	
Properties of Ordinary Portland Cement Clinker with municipal solid waste incineration bottom ash as raw meal additive	408
<i>Aneeta M. Joseph, Stijn Matthys and Nele De Belie</i>	
SESSION 10: Novelties in SCMs	414
Ternary binder made from coal combustion products: mechanical properties and microstructure evolution	415
<i>Vít Šmilauer, Rostislav Šulc, Pavel Reiterman, Petr Hlaváček, Martina Šidlová, František Škvára, Adéla Peterová, Roman Snop</i>	
Use of Carbonated Waste Hardened Cement Powder as a Supplementary Cementitious Material	423
<i>Bao Lu, Caijun Shi</i>	
Early strength improvement of sustainable shotcrete	424
<i>Lukas G. Briendl, Joachim Juhart, Markus Krüger, Florian Mittermayr, Isabel Galan</i>	
Utilization of rice husk ash as reactive filler for enhancing material properties of ultra-high performance concrete	432
<i>Sung-Hoon Kang, Yang-Hee Kwon and Juhyuk Moon</i>	
Potential USE of ash from the paper industry as SCM	440
<i>Sabina Kramar, Vilma Ducman</i>	
A study on feasibility of cement clinker manufacture using oyster shell as limestone substitute	447
<i>Sungwun Her, Hyeonseok Jee, Taehoon Park, Dongcheon Park and Sungchul Bae</i>	
SESSION 11: Calcined clay	455
Comparing the reactivity of different natural calcined clays under alkali activation	456
<i>Ahmed Zohair Khalifa, Yiannis Pontikes, Jan Elsen, Özlem Cizer</i>	
Summary of 4-years of research at IIT Madras on concrete with limestone calcined clay cement (LC3)	457
<i>Ravindra Gettu, Manu Santhanam, Radhakrishna G. Pillai, Yuvaraj Dhandapani, T. Sakthivel, Sripriya Rengaraju, Sundar Rathnarajan, Fathima Suma M., Anusha S. Basavaraja, Sanoop Prakasan and Nithya Nair V.G.</i>	
Limestone calcined clay cements (LC3): effect of raw material properties on hydration and strength	465
<i>Franco Zunino, Karen Scrivener</i>	

Investigation of calcined brick clays from central Germany for use as a sustainable pozzolan	470
<i>Nsesheye S. Msinjili, Gregor J. G. Gluth, Nico Vogler, Sebastian Simon and Hans-Carsten Kühne</i>	
Pozzolanic potential of calcined clay in high-performance concrete	478
<i>Nancy Beuntner, Andrea Kustermann and Karl-Christian Thienel</i>	
Influence of temperature on the hydration of limestone calcined clay cements (LC3)	486
<i>François Avet and Karen Scrivener</i>	
SESSION 12 : Bio-based materials	492
Influence of hydric solicitations on the morphological properties of hemp concrete	493
<i>F. Bennai, C. El Hachem, K. Abahri and R. Belarbi</i>	
Sustainable Hemp-Clay-Lime Concrete	494
<i>Rotem Haik, Isaac A. Meir and Alva Peled</i>	
Self – compacting concrete with tailings and fly ash as ecological material	502
<i>Iva M. Despotović, Ksenija S. Janković, Dragan M. Bojović, Marko S. Stojanović</i>	
Influence of aggregate type on basic properties of cement mortars blended with mixture of wheat and soya straw ash	508
<i>Mirjana Malešev, Slobodan Šupić, Miroslava Radeka, Vlastimir Radonjanin, Tiana Milović, Olivera Bukvić</i>	
Improving resilience of earth construction – current perspectives and future outlook	516
<i>S. S. Lucas, F. Ahmed, H. Varum</i>	
Effect of tire powder and wood biomass ash on properties of self compacting concrete	523
<i>Robert Bušić, Nina Štirmer and Ivana Miličević</i>	
SESSION 13 : 3D printing	531
Surface modification as a technique to improve inter-layer bonding strength in 3D printed cementitious materials	532
<i>J. Van Der Putten, G. De Schutter and K. Van Tittelboom</i>	
Powder bed 3D printing with geopolymers	533
<i>Vera Voney, Pietro Odaglia, Gnanli Landrou, Coralie Brumaud, Andrei Jipa, Isolda Agustí-Juan, Benjamin Dillenburger, Guillaume Habert</i>	
High-performance 3d printable concrete enhanced with nanomaterials	541
<i>Jacques Kruger, Marchant van den Heever, Seung Cho, Stephan Zeranka and Gideon van Zijl</i>	

SESSION 14: AAMs for specific applications	549
LowCopReCon – Low Carbon Precast Concrete ProdUcts for an energy efficient built Environment	550
<i>T.E. McGrath, J. Kwansy, T. Aiken, S. Cox, M. Soutsos, J.F. Chen, J. Mariotti, R. Correia and S. Toal</i>	
Improving mechanical characteristics of lightweight geopolymers through mechanical activation of fly ash	558
<i>Tijana G. Ivanović, Miroslav M. Komljenović, Nataša M. Džunuzović, Violeta M. Nikolić and Gordana G. Tanasijević</i>	
Preliminary studies on brown coal fly ash as a cement replacement for geopolymer brick applications	566
<i>Muhamed Khodr, David Law, Chamila Gunasekara and Sujeeva Setunge</i>	
Reactivity of alkali-activated binders for stabilization/solidification of tunnel boring muds	574
<i>Thomas Watzet, Martin Cyr, Cédric Patapy, Julien Waligora, François Olard, Laurent Frouin and Nicolas Musikas</i>	
Irradiation resistance of MK-based geopolymers encapsulating oily wastes	582
<i>Daniel A. Geddes, Susan A. Bernal, Martin Hayes and John L. Provis</i>	
SESSION 15: Self-Healing	589
Chloride Migration Coefficient of Cracked Mortar Incorporating Self-Healing Materials	590
<i>Fahad R. Abro, Abdul S. Buller, Kwang Myong Lee and Seung Yup Jang</i>	
Investigation on self-healing characteristic of cementitious materials incorporating supplementary cementitious material and crystalline admixture according to exposed environment	595
<i>B. Park, S. W. Oh, Y. C. Choi, S. W. Yoo and S. W. Jung</i>	
Self-sealing of cracks in cementitious materials incorporating superabsorbent polymers under wet/dry cyclic conditions	601
<i>S. Choi, G. Hong and C. Song</i>	
Self-healing performance of engineered cementitious composites through the use of nano-silica	606
<i>Oğuzhan Öztürk, Gürkan Yıldırım, Ülkü S. Keskin and Mustafa Şahmaran</i>	
Effect of superabsorbent polymers on plastic shrinkage cracking and properties of fresh state mortars reinforced by polymeric fibres	614
<i>Rohollah Rostami, Agnieszka J. Klemm</i>	
Design and testing of anionic superabsorbent polymers for use in durable concrete structures	622
<i>Laurence De Meyst, Els Mannekens, Maria Araújo, Didier Snoeck, Kim Van Tittelboom, Sandra Van Vlierberghe, Geert Deroover, Nele De Belie</i>	

Preface

RILEM International Conference on Sustainable Materials, Systems and Structures (SMSS 2019) is a conference organised by Faculty of Civil Engineering University of Zagreb as a supporting event of RILEM Spring Convention from in Rovinj, Croatia. Both are organised in the year Faculty of Civil Engineering in Zagreb is celebrating 100 years from its establishment, making 2019 a perfect year for hosting such an important international event. The scope of the conference was to gather scientists, practitioners, members of technical committees and users of technical recommendations, to jointly at the same place discuss and envision the future sustainable development of materials, systems and structures in a holistic, global way.

SMSS 2019 conference has gathered participants from 50 countries, from Argentina to United States of America, who will exhibit a total of 290 papers. The conference was sponsored by 10 international industrial partners, supported by 6 international organisations of scientists and practitioners and organised under the patronage of 4 governmental bodies. A total of 450 contributions which arrived was reviewed by more than 150 prominent reviewers from different fields. Event was organised by 16 members of the local organising committee and 6 invited international members of organising committee.

As part of the RILEM International Conference on Sustainable Materials, Systems and Structures (SMSS 2019) the segment *New Generation of Construction Materials* covers innovation, advances and improvement of construction materials, towards sustainable, intelligent and tailor-made solutions. This volume brings a selection of 100 peer-reviewed papers that were presented within the segment on construction materials. Topics include novel advances in raw materials for classical and alternative concretes, innovations in chemistry, application of nanotechnology in construction materials, and requirements for materials to suit the needs of construction automation.

Editors wish to thank the authors for their efforts at producing and delivering papers of high standard. We are sure that this Proceedings will be a valued reference of research topics in this important field and that it will together with the other volumes from SMSS conference form a suitable base for discussion and suggestions for future development and research.

Marijana Serdar (University of Zagreb, Croatia)

Nina Štirmer (University of Zagreb, Croatia)

John Provis (University of Sheffield, UK)

International Conference on Sustainable Materials, Systems and Structures (SMSS 2019)

New Generation of Construction Materials

20-22 March 2019 – Rovinj, Croatia

NEW GENERATION OF CONSTRUCTION MATERIALS

PLENARY SESSION: Keynote lectures

NANOTECHNOLOGY AND SUSTAINABILITY IN CONCRETE CONSTRUCTION

Surendra P. Shah

Walter P. Murphy Professor of Civil Engineering (emeritus), Center for Advanced Cement Based Materials, Northwestern University

Abstract

Super tall buildings such as one kilometer high Kingdom Tower are constructed with concrete as a structural material. Such tall buildings are made with so called high performance concrete, which can have strength 5 times that of conventional concrete. The development of high strength concrete is a result of our understanding of particle packing, rheology and microstructure engineering. Concrete is a critical material for infrastructure; the world wide consumption of concrete is about 2 tons for every living human being. However, its continuing use will require improving its sustainability. Nanotechnology is playing an increasing role in making concrete more sustainable. Some examples are given.

One approach to making concrete more sustainable is to replace Portland cement (and its significant carbon foot print) with fly ash, a waste material from burning coal. When fly ash is replaced with Portland cement, the rate of strength development slows down which is not desirable. Addition of nano particle such as nano silica accelerates the chemical reaction by providing nucleation sites. In addition, characterization of nano structure of calcium silicate hydrate by nano indentation, AFM, FTIR and NMR shows beneficial nano scale modification.

Manipulation of concrete rheology has been a key to make concrete more constructible. The viscosity should be sufficiently small so that concrete can be pumped a great distance, but the material should be thixotropic to reduce the pressure on form work. Addition of a small amount of nano clay has been shown to accelerate the rate of thixotropy. Rheology of aging colloidal suspension is being studied by computation modeling as well as by measuring the dimensions of flocculated particles by using laser spectrometer.

Concrete is a brittle material, prone to cracking. Concrete structures are reinforced by steel bars at a millimeter scale. However, flaws in cement paste are in nano scale. To reinforce concrete at nano scale addition of carbon nano tube is studied. The key challenges include dispersion and rheology. Recent studies have demonstrated that adding a very small amount (0.05%) of well dispersed CNT has a profound effect on performance: mechanical properties, piezo-resistivity, transport properties as well as corrosion reinforcing steel. Such multi functionality is probably related to altered nano structure of concrete.

ROADMAP OF DEVELOPMENT AND APPLICATION OF SUSTAINABLE MATERIALS

Karen Scrivener

Construction Materials Laboratory LMC, Ecole polytechnique fédérale de Lausanne EPFL, Switzerland

Abstract

From a sustainability perspective, cement based materials are by far the best option to meet the demand for construction materials from a growing world population. Nevertheless, it is crucial to lower their environmental impact. In the presentation first, an outline will be given of the realistic options for reducing environmental impact, which should involve all steps in the construction chain, from cement, through concrete to structures. In our recent report for the European Climate foundation we illustrated that such measures could reduce the CO₂ emission from cementitious materials by 80% compared to 1990 level.

Second research questions will be identified which should be answered to achieve further gains in the sustainability of construction materials. The needs for research concern requirements for increasing the use of supplementary materials and revolve around three main areas: Placement; Hydration; Durability. For example, as concerns hydration, early properties are dominated by the clinker component and increasing the reactivity of clinker would allow higher replacement levels. In the area of durability, we need to better understand how microstructure governs transport properties. Our recent work with LC3 materials show that reductions in chloride ingress are far more than expected from the modification of pore structure and chloride binding.

International Conference on Sustainable Materials, Systems and Structures (SMSS 2019)

New Generation of Construction Materials

20-22 March 2019 – Rovinj, Croatia

NEW GENERATION OF CONSTRUCTION MATERIALS

SESSION 1: SCM reactivity

PARTICLE SIZE OPTIMIZATION IN MULTI-COMPONENT CEMENT

S. Adu-Amankwah, S. A. Bernal and L. Black

School of Civil Engineering, University of Leeds, UK

Abstract

The quest for sustainable alternatives to Portland cement has led to the exploration of a range of materials or their combinations, often with the aim of exploiting synergies in reaction or particle packing to maximize performance. Simultaneous optimization of both presents a viable option to increase the efficiency of cementitious materials. This study evaluated the effect of varying the fineness of the constituents in ternary CEM I – granulated blast furnace slag (GGBS) - limestone cement on hydration kinetics and strength development.

Eight (8) ternary cement mixes were tested at constant w/c ratio. Hydration was followed by isothermal conduction calorimetry and X-ray powder diffraction. In addition setting time and compressive strength development up to 180 days of curing were determined. The efficiency associated with changing the fineness of each component was evaluated in terms of the net heat of reaction and compressive strength after keeping all other factors constant. The results demonstrate that, finer CEM I in the ternary cement promotes hydration prominently at early age and reflected in the compressive strength accordingly. The benefits associated with a finer GGBS and similarly limestone depends on the fineness of the other constituents in the blend. Optimization of these ternary systems can be achieved by considering the inter-dependencies in terms of kinetics and microstructure development.

Keywords: Composite cement, limestone, fineness, optimization, hydration.

This work was invited for publication in the open access journal RILEM Technical Letters. You can visit the journal and benefit from the full open access to the published articles at: letters.rilem.net.

THE LIMITING FACTORS OF SCMS REACTION AT LATER AGE

Yosra Briki (1), Karen Scrivener (1) and Mohsen Ben Haha (2)

(1) Laboratory of Construction Materials, EPFL, 1015 Lausanne, Switzerland

(2) Heidelberg Technology Center GmbH, Rohrbacher Str.95, 69181 Leimen, Germany

Abstract

The objective of this study is to understand the factors inhibiting the reaction of SCMs at later ages. Different hypothesis are investigated in this paper. The availability of portlandite at later age is one possible hypothesis for preventing the reaction of calcined clay. Coarse particles in slag cement could inhibit slag reaction. Finally, the lack of large pores could be another factor, which restrains the possible growth of hydration and thus limit the reaction of SCMs.

Keywords: SCMs reaction, limitations, portlandite, large pores

1. INTRODUCTION

Replacement with different SCMs in cements is one of the potential alternatives to reduce CO₂ emissions related to cement production. However, blended cements present some limitations. First, and depending on clinker replacement levels, blended cement show lower early age strength development compared to OPC resulting from the lower reactivity of SCMs, in particular slag and fly ash. Secondly, at later age, SCMs slow down their own reaction [1], [2] and [3]. Since there is a lack of data to explain the factors that could limit or inhibit SCMs reaction, this study investigates several hypothesis that could explain this phenomenon. Not all results are presented in this paper, since some are still under investigation.

2. MATERIALS AND MIX DESIGNS

Besides OPC, clinker was blended with slag for a replacement level of 50%. Calcined clay cement (LC3) is another system of this study, which contains 30% of calcined clay and 20% of limestone. Calcined clay contains 46.5% of metakaolin in the composition and the rest are impurities. Quartz was blended with cement and in some cases with slag to check some hypothesis that will be explained in detail in later sections. The water to cement ratio was kept constant for all experiments which is 0.4. Table 1 summarize all the different systems that are studied in this paper.

Table 1. Mix design for all systems investigated (w/c=0.4).

System	Clinker	Slag	Calcined clay	Limestone	Quartz	Quartz10	Slag10
OPC	100	-	-		-	-	-
50%C 50%Slag	50	50	-	-	-	-	-
LC3	50	-	30	20	-	-	-
50%C 50%Quartz	50	-	-	-	50	-	-
50%C 25%S10 25%Q10	50	-	-			25	25

3. RESULTS

3.1 The degree of reaction of SCMs

The degree of reaction of SCMs is presented in **Error! Reference source not found..** Calcined clay shows higher reaction than slag for all ages. Slag seems to be slow in reaction and reaches only 40% at 28d. Calcined clay, differently, slows down after 28d to be constant until 90d. In the next paragraphs, several hypothesis are investigated to understand what is preventing the reaction of calcined clay and slag.

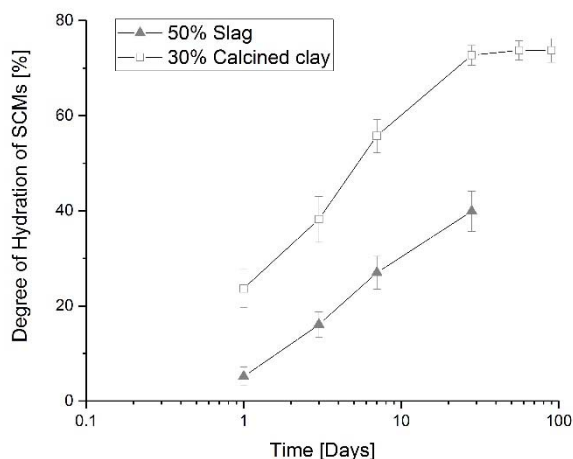


Figure 1. The degree of reaction of slag and LC3 cements.

3.2 Portlandite availability for LC3 system

Since calcined clay is pozzolanic and depends on portlandite presence, the hypothesis was that at later age, CH is not accessible anymore for calcined clay reaction. For this reason, 5% more of portlandite was added to LC3. It is clear that at early age, higher reaction of calcined clay with more portlandite. At later age, the addition of portlandite did not improve the reaction of calcined clay although the presence of portlandite. One should note that the addition of portlandite changes some parameters, for instance the addition of water coming from CH. Thus, the comparison between both systems could be not fair.

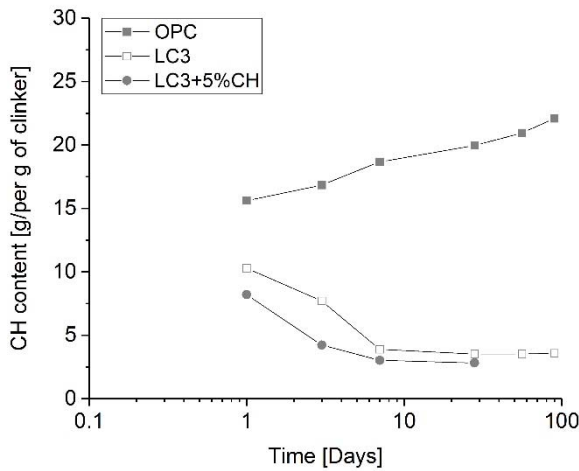


Figure 2. Portlandite content in LC3 and LC3+5%CH. #

3.3 Coarse particles inhibit slag reaction

One of the hypothesis that could explain the low reaction of slag was that the coarse particles could restrict slag reaction. To check this hypothesis, slag cement was compared with another system containing 25% of slag with particles with the size lower than 10 μm and quartz with particles with the size higher than 10 μm . The idea was to check if the coarse particles in slag behave similarly as quartz. Figure 3 shows the particle size distribution of the system used.

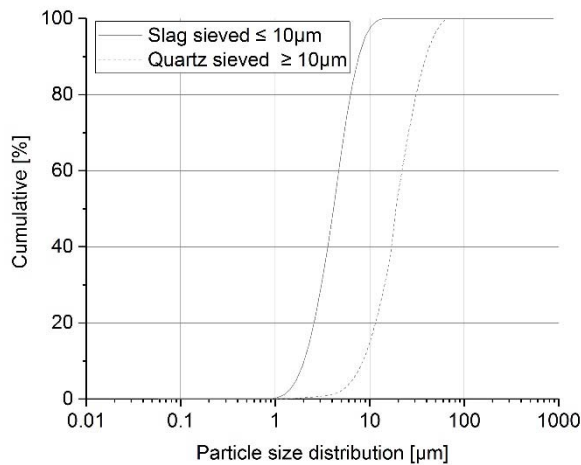


Figure 3. Particle size distribution of slag and quartz of slag cement 25S10_25Q10 #

At early age, slag cement diluted with quartz presents higher amount of reaction compared to the neat cement. This is due the available water and space for reaction when adding quartz. After 7days, the neat cement starts to develop more reaction. It seems that the coarse particles participate to the reaction of slag. The results for 90 days will be checked to confirm these results.

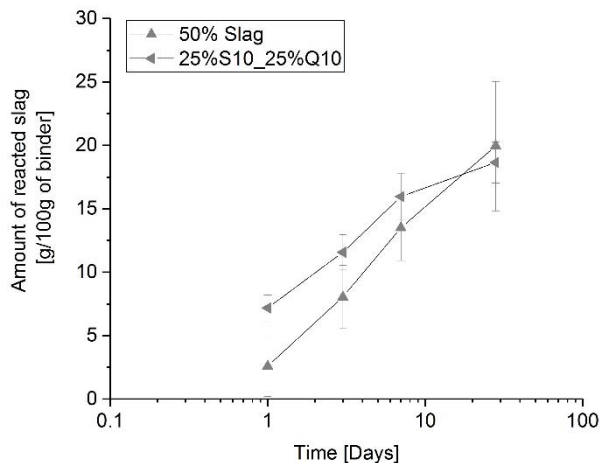


Figure 4. Amount of reacted slag in slag cement with and without dilution with quartz [g/100g of binder].

3.4 Lack of large pores

The lack of large pores could be limiting the possible growth of hydration. The critical pore entry radius is defined as the inflexion point of the cumulative curve (or the maximum of the capillary peak of the derivative curve) which can be investigated by MIP measurements.

The critical entry radius for all systems is checked and, presented in figure 5. The filling ability changes from SCM to another one. The refinement in quartz cement occurs progressively with time. On the other hand, slag and calcined clay present higher refinement of porosity and similar to the one of OPC. It seems that at later age, all blended cement except quartz; present the same “maximum” of refinement, which in this case, equal to 4nm.

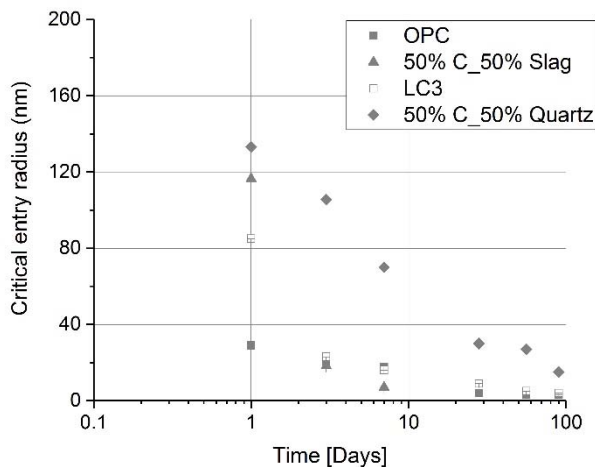


Figure 5. The critical entry radius for all blended cements

#

4. CONCLUSIONS

This paper investigated different hypothesis that could be responsible for limiting the reaction of SCMs at later ages. The availability of portlandite was one of the possible hypothesis to explain the slowing down of the reaction of calcined clay. This was checked by adding more portlandite to LC3. The results did not show any evidence for the hypothesis. Indeed, after 7days, calcined clay does not react more despite the presence of portlandite.

For slag reaction, coarse particles were suspected to be the responsible for inhibiting the reaction. This was investigated by removing all particles with size higher than 10 μ m to be replaced with quartz with the same size of particles. The results showed that coarse particles contribute to slag reaction at later age.

Finally yet importantly, the lack of large pores was investigated to check if this is restraining the possible growth of hydrates. All the blended cements tend to have similar “maximum” refinement of porosity from 28 to 90d. However, this maximum seems to be the limitation of MIP technique.

This paper confirms the need of the deep investigation for the limitation of the reaction at later age. Other hypothesis are investigated and still in progress.

ACKNOWLEDGEMENT

HeidelbergCement is greatly acknowledged for funding this project.

REFERENCES

- [1] E. M. J. BERODIER. 'Impact of the Supplementary Cementitious Materials on the kinetic microstructural development of cement hydration'. Lausanne, EPFL, 2015.
- [2] F.H. AVET. 'Investigation of the grade of calcined clays used as clinker substitute in Limestone Calcined Clay Cement (LC3)'. Lausanne, EPFL, 2017.
- [3] P. T. Durdziński. 'Hydration of multi-component cements containing cement clinker, slag, calcareous fly ash and limestone'. Lausanne, EPFL, 2016.

COMPARATIVE EVALUATION OF USE SILICA FUME, BLAST FURNACE SLAG, LIMESTONE, METAKAOLIN AND RED MUD AS SUPPLEMENTARY CEMENTITIOUS MATERIALS FOR CONCRETE

Roberto Cesar de Oliveira Romano, José Augusto Ferreira Sales de Mesquita, Gabriel Carpinelli Perozzi Brasileiro, Maria Alba Cincotto and Rafael Giuliano Pileggi

Department of Civil Construction Engineering / University of São Paulo, São Paulo, Brazil

Abstract

A comparative study of different kinds of supplementary cementitious materials (SCM) in microconcrete was done monitoring the fresh and hardened state properties. Compositions were formulated with silica fume, blast furnace slag, limestone, metakaolin or red mud (in natura or calcined at 800°C). Portland cement was partially replaced by 5 or 10%, in volume, of each SCM and the microconcretes mixed maintaining the water-to-solid ratio constant. The impact of each mineral addition during the mixing stage and in the rheological properties was evaluated using a planetary rheometer, while the changes in the hardened state properties were discussed in function of results of compressive strength, modulus of elasticity, air-permeability and dimensional variation. The aspects related to the ecoefficiency index, i.e., binder consumption by unity of strength, was used to evaluate the sustainability of each microconcrete and it was concluded that the compositions developed in this work associate high performance with very low binder consumption, representing that the concepts applied in this work to formulate the microconcretes allowed the production of cementitious components with an excellent ecoefficiency index.

Keywords: Microconcrete, supplementary cementitious materials, ecoefficiency, low binder intensity.

1. INTRODUCTION

In the modern society Portland concrete is the most produced and consumed material in the world, whose production is estimated at more than 10 km³/year. Basically, these cementitious products consist of a mixture of aggregates, binder and water and, although it is not possible to obtain an exact value for the volume produced, the volume quoted above is estimated having the production of Portland cement as a basis. In that case, the hydraulic binder reached the significant mark of 4 billion tons/year between 2013 and 2014, with a forecasted growth of 2.5 times by 2050 [1].

It is a fact that in the modern world, the environmental impact cannot be tolerated in the same rate as the production increase of cement materials, and that the technologies for producing such materials will be forced to achieve efficiency levels that guarantee high productivity levels with reduced efforts to workers.

Notwithstanding, the aforementioned obstacle, the main challenge for the future will be: how to increase the production of the most important building materials to meet the demands of a growing and aging population and the urbanization increase, without magnifying the impact of the enormous volumes produced?

Considering only the material related aspect, different routes have been developed to replace clinker with alternative materials, which are generally obtained as: i. a by-product of an industrial process (as ground blast furnace slag, fly ash, silica fume, etc.), ii. an inert material (as filler), iii. a new kind of cement of lower environmental impact, and other materials.

For that reason, the level of efficiency currently achieved in cement technology has been investigated in order to identify new opportunities to increase production without increasing cement production.

Without giving up any of the initiatives presented to reduce the environmental impact resulting from cement production, the strategies aimed at reducing the use of binders in formulations may potentially increase the production of cement materials without the need to increase cement production at the same rate.

So, it is possible to infer that to obtain a more eco-efficient scenario it is essential to look for new supplementary cementitious materials (SCMs), to improve the understanding of the characteristics of currently known SCMs and to evaluate in greater depth the physicochemical interactions with different types of binders [1].

2. MATERIALS AND METHODS

Microconcretes [1] were formulated using Portland cement (named as CPV according to the Brazilian standard), natural sand of quartz, ground sand of limestone, and the supplementary cementitious materials: silica fume, metakaolin, ground blast furnace slag, limestone and red mud (in natura or calcined at 800°C). This last one is not considered an ordinary SCM [2-4], but we have a global project to find a large-scale application for this residue and one of the stages of this project is to compare the results with different kinds of mineral addition.

2.1 Raw material characterization

Particle size distribution: coarse aggregates were evaluated in Qicpic, Sympatec equipment using Dynamic Image Analysis, while the finer particles were quantified in a Sympatec laser particle size analyzer, model Helos KR with a range between 0.1 and 350 micrometers [5].

Specific surface area: obtained by nitrogen adsorption (N₂) on a solid sample surface according to the BET method in Belsorp Max, Bel, Japan, after pretreating the samples in a Belprep-vacII, Bel Japan equipment, at 40°C for 16 hours under vacuum at a pressure of 10⁻² μmHg.

Real density: assessed using gas He pycnometry in a Multipycnometer - Quantachrome Instruments equipment.

Chemical composition: evaluated pursuant to the general guidelines from ISSO/FDIS 29581-2:2009 (E) "*Cement – Test Methods – Part 2: Chemical analysis by X-ray fluorescence*" in a Minipal Cement, PANalytical equipment with melt pastilles in a Claisse M4 model melting

machine, using lithium tetraborate/lithium metaborate blend fluxes, with a ratio of 1.0g of sample to 6.75g of melting.

Figure 1 shows the particle size distribution of the raw materials while in Table 1 are presented the specific surface area, real density and volumetric surface area of each sand and SCM.

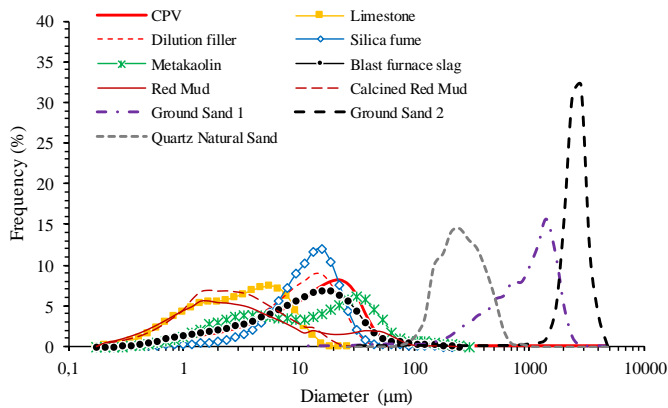


Figure 1. Particle size distribution of the raw materials used in the compositions of microconcretes.

Table 1. Specific surface area, real density and volumetric surface area of the raw materials used in the compositions of microconcretes.

Raw material	Real density (g/cm ³)	Specific surface area (m ² /g)	Volumetric surface area (m ² /cm ³)
Portland cement	3.29	1.31	4.31
Dilution filler	2.77	1.16	3.21
Limestone filler	2.78	3.73	10.4
Silica fume	2.20	22.0	48.4
Metakaolin	2.54	17.2	43.7
Ground blast furnace slag	2.91	0.60	1.75
Red mud	3.02	10.6	32.0
Calcined Red mud	3.05	20.1	61.3
Natural Quartz sand	2.64	0.65	1.72
Ground sand 1	2.76	0.30	0.83
Ground sand 2	2.76	0.20	0.55

The red mud (in natura or calcined), metakaolin and limestone filler presents a higher amount of finer particle than Portland cement. This is an important information because they can create a filler effect in the microconcrete. While silica fume (SF) presents particle size distribution higher than expected for this kind of material, the specific surface area was larger than the other materials: a large amount of agglomerates was observed, and were not broken even with the shear performed during the evaluation [5]. It is important to say that the specific surface area of raw materials with different mineralogical compositions are not to be related to its finer particle content as a comparative criterion, because they have different chemical compositions, with a distinct agglomeration potential and morphology. This comparison may only be drawn when the materials come from the same ore [6].

The chemical composition of each SCM is presented in Table 2. Portland cement presents a high amount of calcium and silicon oxides, and a smaller amount of aluminum oxide, indicating a predominance of the silicate phases in the clinker (alite and belite) and small amounts of the aluminate phases (tri-calcium aluminate and brownmillerite). The amount of SO₃ indicates a

high content of the calcium sulfates which were added to regulate the setting. The most impacting observation is the high loss on ignition (4.18%), revealing a high volatile material content, mainly CO₂ as a calcium carbonate. The standardization for this type of cement requires the addition of up to 5% of carbonate but based on this result it is estimated that a little more than 9% was added in the clinker.

Table 2. Chemical composition of raw materials

Raw material	CPV	LF	SF	MK	BFS	RM	RMc
CaO	65.4	47.8	0.51	0.06	43.4	1.05	1.20
SiO ₂	16.5	1.66	94.4	50.8	34.5	15	16.4
Al ₂ O ₃	3.71	0.07	0.12	39.1	10.5	20.6	22.8
Fe ₂ O ₃	3.02	0.03	0.13	6.07	0.30	34.4	41.5
SO ₃	3.85	0.01	0.07	0.04	2.49	0.22	0.17
Na ₂ O	0.22	<0.001	0.17	<0.001	0.21	11.0	12.7
K ₂ O	1.12	0.01	0.82	0.40	0.54	<0.001	<0.001
MgO	1.06	7.86	0.27	0.14	6.46	<0.001	<0.001
TiO ₂	0.22	<0.001	<0.001	1.26	0.63	4.64	5.50
MnO	0.09	<0.001	0.04	<0.001	0.67	<0.001	<0.001
Loss on ignition	4.18	42.6	2.99	1.98	-	12.3	0.90

CPV – Portland cement, LF – limestone filler, SF – silica fume, MK – metakaolin, BFS – ground blast furnace slag, RM – red mud and RMc – Calcined Red mud.

Silica fume and limestone filler present high purity, with more than 95% SiO₂ or CaCO₃ respectively in these SCMs. Red mud presents high amounts of iron, aluminum, and silicon oxides, with little calcium oxide and a reduced loss on ignition. As there is no technical standardization that discusses the chemical characteristics of that waste, the results obtained do not have a baseline. An information that deserves mention is that, according the Brazilian standard (NBR 12653), the red mud evaluated does not present pozzolanic activity, therefore it cannot be described as this kind of material.

For the metakaolin, as expected, the presence of high amounts of silicon and aluminum oxides was observed, but the contamination with iron was quantified, and with respect to the ground blast furnace slag, calcium was the main chemical element, while significant amounts of silicon, aluminum and magnesium were observed.

2.2 Compositions evaluated

Compositions with 5 and 10% of each raw material as partial substitution of Portland cement (in volume) were formulated, according presented, in kg/m³, in Table 3.

Table 3. Concrete compositions. Consumption of each raw material per cubic meter.

Raw material	CPV	5LF	10LF	5SF	10SF	5MK	10MK	5BFS	10BFS	5RM	10RM	5RMc	10RMc
Portland cement	263												
Dilution filler	408	397	386	398	389	398	389	396	384	396	384	396	384
Limestone filler	-	11	22	-	-	-	-	-	-	-	-	-	-
Silica fume	-	-	-	9	18	-	-	-	-	-	-	-	-
Metakaolin	-	-	-	-	-	9	18	-	-	-	-	-	-
Blast furnace slag	-	-	-	-	-	-	-	12	24	-	-	-	-
Red mud	-	-	-	-	-	-	-	-	-	12	24	-	-
Calcined Red mud	-	-	-	-	-	-	-	-	-	-	-	12	24
Natural Quartz sand	335												
Ground sand 1	380												
Ground sand 2	850												
Water	201												

The consumption of Portland cement, water and the mix of sands were kept constant for all concretes. It should be mentioned that to complete the desired amount of finer particle, a dilution filler (calcium carbonate with similar particle size distribution of Portland cement) was used.

2.3 Monitoring the mixing stage using rotational rheometry

All dry powders were homogenized and inserted into a cup in a planetary rheometer Pheso, Calmetrix. The mixing stage was carried out maintaining the rotational speed at 150 rpm by 180 seconds. The water was mixed with superplasticizer (based on polycarboxylate molecules) and added in a controlled flow of 45g/sec. After that, the microconcretes were moulded and cured at $23 \pm 2^\circ\text{C}$ for 28 days, at 98% of relative humidity.

2.4 Hardened state properties evaluations

Compressive strength: carried out according to the Brazilian test, pursuant to the ABNT NBR 7215 standard, using a Universal Test Machine, EMIC - DL 10.000, and controlling the load at 490 N/s, up to total rupture.

Modulus of elasticity: measured according to Brazilian NBR 15630/08 standard in an equipment with frequency transducers of 200 kHz, and a circular transversal section of 50 mm diameter.

Air-permeability: measured according to the vacuum-decay method [7]. The air-permeability (expressed in k_1 values, in m^2) was calculated by the *Forchheimer* equation.

Dimensional variation: the evolution of the dimensional variation was measured over time under controlled temperature (23°C) and humidity conditions (50%), but the comparison presented follow represents the measurement did with 28 days of cure [8].

3. RESULTS

3.1 Evolution of Torque during the mixing of microconcretes

Figure 2 shows the changes on the torque during the mixing of each microconcrete. Highlighted are presented the energy required for mixing each composition.

In the first stage of mixing the water is adsorbed on the surface of the particles and, consequently, the formation of the agglomerates occurs due to the van de Waals and electrostatic forces. So, part of the water required to mix is retained into these agglomerates, which, if the shear energy applied during the mix stage is not enough to broke down the agglomerates, is unavailable to hydrate the surface of the cement particles and to fluidize the mixture. In consequence, the torque is increased. At the end of this first stage the torque becomes gradually lower, indicating that the composition is flowing better.

However, the time to reach the end of this stage was different for each kind and content of SCM, but without any clear tendency.

After cure for 28 days, the hardened state properties were evaluated, and the results compiled in Figure 3 follow.

To evaluate the significance of the variation for the kind and content of SCMs, analysis of variance (one-way Anova) was used to reject or accept the hypothesis of average equality, within and among the groups, and the Tukey's test was used for a comparative evaluation of the pairs with different SCM, in order to pinpoint those which are different from the others.

The composition formulated with silica fume was the only that presented a compressive strength statistically higher from the others (independently of content). This is an expected result, due to its high pozzolanic activity, quickly reacting with the calcium hydroxide formed in the hydration of the cement, and filler effect.

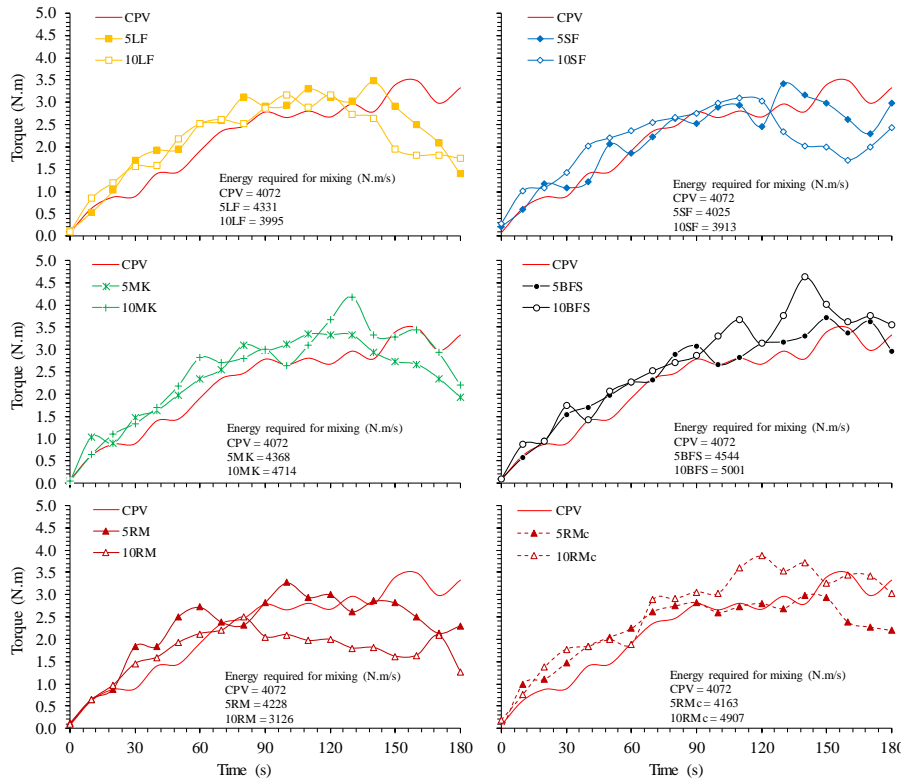


Figure 2. Changes on the torque during the mixing. Highlighted are presented the energy required for mixing each composition.

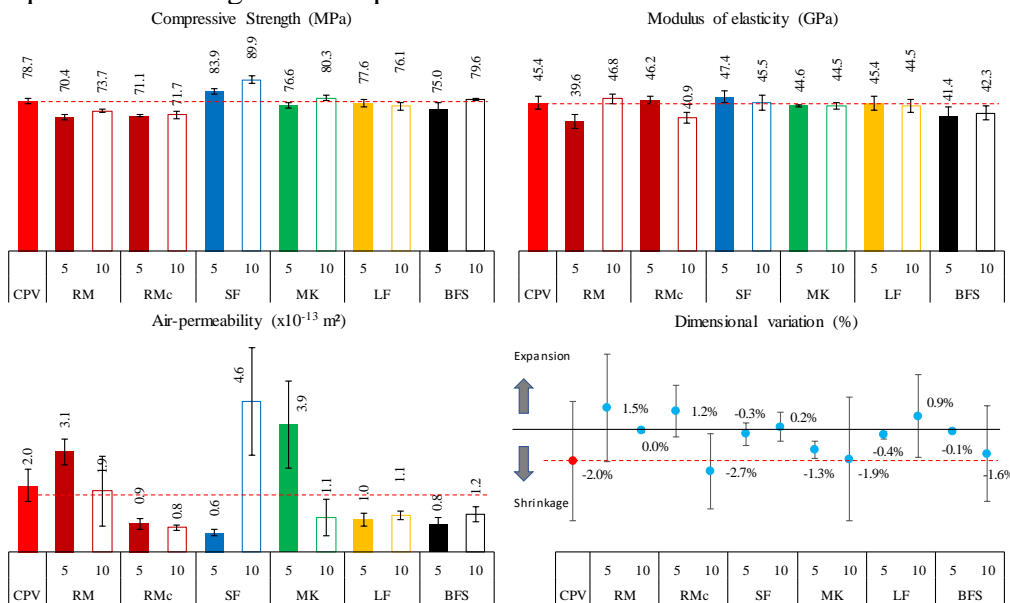


Figure 3. Results of hardened state properties of microconcretes

The lowest compressive strength was observed in the compositions with red mud, in natura or calcined at 800°C, which produced a reduction of around 10%, as compared to the Reference, but that is not a significant problem because, as represented in the binder intensity graph follow, all compositions evaluated in this work indicated eco-efficient concretes, in comparison with the cement compositions developed worldwide.

Statistically, it was proved that just the modulus of elasticity on the compositions containing red mud and ground blast furnace slag were different from the others, but similar to each other, presenting lower microstructural stiffness. Compressive strength and deformability capacity are very important properties to evaluate the mechanical performance of this kind of material. However, the air-permeability and shrinkage are important in evaluating the durability criteria of concrete types. The most common durability problems are directly associated to the diffusion of aggressive agents present in the concrete and, in general, the easier the diffusion of such agents, the faster the degradation of the cementitious product. So, air-permeability is closely related to durability and the results indicate that the air-permeability of microconcrete with calcined red mud was lower than the reference and statistically similar to silica fume, limestone filler and ground blast furnace slag. On the other hand, the composition with metakaolin was the most permeable of all, followed by the composition with red mud and Reference microconcrete. Different from the other kind of supplementary cementitious materials, the microconcrete containing red mud, in natura or calcined, presented a little expansion, indicating that it is a shrinkage compensator, and no difference in carbonation was observed as a function of the kind of SCM.

The cement consumption remained the same for all compositions, while the binder consumption did not, because SF, MK and BFS are considered binders. Figure 4 shows the relation between the binder intensity (BI) and compressive strength for the microconcrete evaluated in this study.

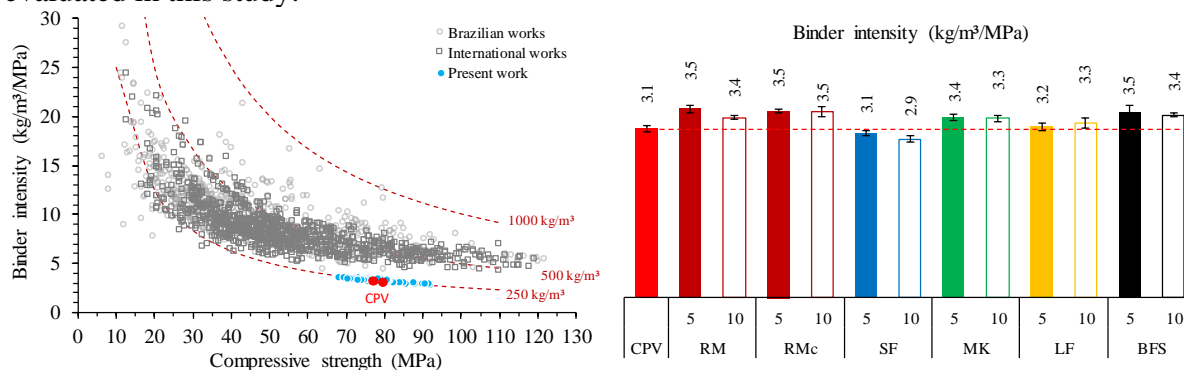


Figure 4. Binder intensity of microconcretes formulated with different kind and content of SCM. The results for the Brazilian and the International works are a compilation did by [1]

To compare the sustainability of those compositions, as the higher the BI, the higher the amount of binder to achieve the same performance and consequently, lower the concrete eco-efficiency. The minimum binder intensity, according to the literature survey by [1], indicates 5kg/m³/MPa for concretes with mechanical strength higher than 50MPa, and for compressive strength of a lower value, the minimum BI follow the corresponding values for 250kg/m³ of binder consumption.

This minimum value of binder consumption is probably due to the specifications in the standards supposed to obtain adequate durability conditions: the Brazilian standard (NBR

12655) recommends 260kg/m³ while the European recommends 240kg/m³ for concretes exposed in places subject to corrosion. However, *Wassermann, Katz and Bentur* [9] proved that a few durability referential are not affected by a reduction in the total binder amount: in some cases, they are improved. *Dhir et al* [10] concluded that it is not adequate to specify the minimum cement content in compositions, and *Popovics* [11] showed that for the same water-to-cement ratio, the higher the binder content, the lower is the compressive strength.

11. CONCLUSIONS

The use of these different kinds of SCMs affected the mixing stage of microconcretes, but without any clear tendency in function of physical properties of each mineral addition. All the microconcretes developed in this work are considered eco-efficient (low binder intensity associated to high performance) regardless of the kind and content of SCM, but the compositions with silica fume presented the best behaviour, mainly replacing 10% of Portland cement.

ACKNOWLEDGEMENTS

The authors wish to thank FAPESP – Fundação de Amparo à Pesquisa do Estado de São Paulo (Project 2014/50948-3 – INCT CEMtec – Advanced Eco-efficient Cement Technologies) and CNPq – Conselho Nacional de Desenvolvimento Científico e Tecnológico (Research Grant - 155357/2016-6) for the support during the development of this research.

REFERENCES

- [1] Daminieli, B.L. Concepts by formulation of concretes with low binder consumption. Thesis (PhD). Escola Politécnica da Universidade de São Paulo. 2013. 237p. (*in Portuguese*).
- [2] Liberato, C.C., Romano, R.C.O., Montini, M., Gallo, J.B., Gouvea, D., Pileggi, R.G. 'Effect of calcination of bauxite residue on the rheological properties and hardened state of Portland cement pastes'. *Ambiente Construído* **12** (2013) 15-25 (*in Portuguese*).
- [3] Klauber, C., Gräfe, M., Power, G. 'Bauxite residue issues: II. options for residue utilization'. *Hydrometallurgy* **108** (2011) 11–32.
- [4] Singh, M., Upadhayay, S.N., Prasad, P.M. 'Preparation of iron rich cements using red mud'. *Cement and Concrete Research* **27** (1997) 1037–1046.
- [5] Romano, R.C.O., Schreurs, H., John, V.M., Pileggi, R.G. 'Influence of dispersion technique in the properties of silica fume'. *Cerâmica*, **54**. 332 (2008), 456–461. (*in Portuguese*).
- [6] Romano, R.C.O., Maciel, M.H., Cincotto, M.A., Pileggi, R.G. 'Monitoring of Hardening of Portland Cement Suspensions by Vicat Test, Oscillatory Rheometry, and Isothermal Calorimetry'. *Applied Rheology* **27** (2017) 36006.
- [7] Innocentini, M.D.M., Rodrigues, V.P., Romano, R.C.O., Pileggi, R.G., Silva, G.M.C., Coury, J.R. 'Permeability optimization and performance evaluation of hot aerosol filters made using foam incorporated alumina suspension'. *Journal of Hazardous Materials* **162**. (2009) 212 - 221.
- [8] Varhen, C., Dilonardo, I., Romano, R.C.O., Pileggi, R.G., Figueiredo, A.D. 'Effect of the substitution of cement by limestone filler on the rheological behaviour and shrinkage of microconcretes'. *Construction and Building Materials* **125** (2016). 375–386.
- [9] Wassermann, R., Katz, A., Bentur, A. 'Minimum cement content requirements: a must or a myth?'. *Materials and Structures* **42**, 7 (2009) 973–982.
- [10] Dhir, R.H., McCarthy, M.J., Zhou, S., Tittle, P.A.J. 'Role of cement content in specification for concrete durability: cement type influences'. *Proceedings of the ICE-Structures and Buildings* **157**, 2. (2004) 113–127.
- [11] Popovics, S. 'Analysis of the concrete strength versus water-cement ratio relationship'. *ACI Materials Journal*. **87**, 5 (1990) 517–529.

CHARACTERIZATION AND POZZOLANIC ACTIVITY OF UK ALUM WATER TREATMENT SLUDGE

M. Shamaki, L. Black

School of Civil Engineering, University of Leeds, Leeds, LS2 9JT, UK.

Corresponding author: Shamaki, M, email address: cnmys@leeds.ac.uk

Abstract

Alum salts are commonly used as coagulants in the purification of surface water for potable supplies. The large volumes of waste alumina-rich sludge generated are a waste management problem and are currently disposed of at landfill sites.

As-received alum sludge was calcined at various temperatures and then blended variously with Portland cement, ground granulated blast-furnace slag (GGBS) and limestone. The raw and calcined alum sludge was characterized to probe its physical and chemical properties. The raw alum sludge is an amorphous aluminium hydroxide precipitate. Upon thermal treatment, the sludge undergoes an η -alumina transition and finally crystallizes to thermodynamically stable corundum at 1100°C.

The pozzolanic activity of calcined alum sludge was assessed by determining Strength Activity Indices (ASTM C618). In cement-sludge blends the reactivity increased with increasing calcination temperature, but remained poor. Ternary cement-GGBS-sludge blends showed improved performance when the sludge was calcined at 825°C, with slightly decreased performance following calcination at higher temperatures. However, addition of limestone to the blend led to further improved performance, out-performing a CEM I-GGBS-limestone reference. This is due to synergy between aluminates in the calcined sludge and limestone powder.

Keywords: Pozzolanic activity, Water Treatment Sludge, Ternary cement

1. INTRODUCTION

Surface waters usually contains contaminants such as sandy and clayey soils, organic matter and other impurities. These impurities are agglomerated during the coagulation-flocculation process using chemical coagulants to aid the sedimentation and filtration of the contaminants from the liquid phase to give water treatment sludge (WTS). In the UK, WTS is commonly disposed to landfill, but this is being discouraged and suitable reuse applications are being sought. The characteristics of WTS depend on the source water

quality and dosage of coagulants added during the treatment process [1]. Aluminium sulfate is commonly used as a coagulant. The solid salt is added to water forming an amorphous gelatinous precipitate of aluminium hydroxide which flocculating colloidal and suspended impurities. Meanwhile, aluminium hydroxides and their calcined forms are used in a range of applications, such as absorbents, catalyst supports and soft abrasives due to their fine particle size, high surface area and catalytically active surfaces [2]. The dehydration of gelatinous aluminum hydroxides occurs through metastable phases such as η , θ , γ , δ and ultimately thermodynamically stable α -alumina. However, the degree of structural ordering, thermal conditions, starting materials and method of synthesis have significant effects on the formation of metastable phases and the ultimate α -alumina [3,4].

Supplementary cementitious materials (SCM) offer the potential to reduce the carbon footprint of cement, while also improving technical performance. A key aspect of SCM performance is the availability of reactive silica and alumina. A number of studies have reported that alum sludge becomes reactive at (600- 800°C) due to the decomposition processes that yield reactive alumina [5–7]. Limestone powder has been shown to react with cement and SCMs to improve binder performance [8] with reactivity related to reactive alumina availability [9]. Thus, the use of calcined alum sludge offers potential for use in blended cements. Sludges have been characterized, calcined and then blended with various binders before being assessed based on strength activity indices.

2. EXPERIMENTAL

Alum sludge, CEM I 52.5R, GGBS and limestone powder, plus natural sand sieved to a maximum size of 2.0mm were used to prepare mortars. The WTS had a high water demand, so a polycarboxylate based superplasticizer (Sika Viscocrete 25MP) was used constant dosages to maintain mortar consistency within $\pm 10\%$ of the flow table spread (BS 4551) of a CEM I standard mortar mix (125mm). Potable water was used as mixing water. Physical and chemical properties of finely ground alum sludge and cementitious materials are shown in Table 1.

The alum sludge was first dried at 110°C to constant mass and then (based on thermal analysis data) calcined for 2 hours at 475, 625, 825, 1000 and 1100°C. The resultant ashes were finely ground to meet fineness specifications set by ASTM C618 [10], before further analysis and characterization by BET and particle size analysis (Table 2).

Dried raw alum sludge was studied by TGA and DTA at a heating rate of 5°C/min to 1000°C. XRD analyses were conducted using Bruker D2 phaser diffractometer with a Cu K α source operating at 30 kV and 10mA. Attenuated Total Reflectance (ATR) FTIR analysis was conducted obtaining using 128 scans over a 500- 4000 cm⁻¹ spectral range and 4 cm⁻¹ resolution. Particle size analysis was conducted laser diffraction using Malvern Mastersizer 2000. Specific surface areas were determined by nitrogen absorption (BET) technique. Specific density of samples were determined by helium pycnometry. Oxide composition and total carbon (TC) content of raw and calcined sample were determined by X-ray fluorescence spectrometer and LECO analysis respectively.

The pozzolanic reactivity of calcined alum sludge was assessed using strength activity indices (SAI) in accordance with ASTM C618. Additionally, blends were prepared using GGBS and limestone to exploit synergies between aluminates and limestone. Table 3 shows the mix proportions of mortars used. Mortar samples (1:3:0.55) were prepared in

50 x 50mm moulds and the compressive strength was determined in triplicate at 7 and 28 days. 1% superplasticizer by mass of total binder was used to maintain workability.

Table 1: Physical and chemical characteristics of cement, raw alum sludge and pozzolanic materials

Characteristic	Cement (C)	Raw alum sludge (A)	GGBS (S)	Limestone (L)
<i>Elemental Composition %:</i>				
SiO ₂	20.5	10.28	34.51	2.00
Al ₂ O ₃	4.60	44.23	11.20	0.80
Fe ₂ O ₃	2.40	2.51	0.35	0.32
CaO	63.4	2.50	43.07	53.13
MgO	2.00	0.34	7.64	0.64
SO ₃	3.60	1.24	1.76	0.07
Na ₂ O	0.13	0.15	0.14	-
K ₂ O	0.74	0.42	0.48	0.10
Organic Carbon	-	9.72	-	-
Inorganic Carbon	-	0.60	-	-
<i>Physical Properties:</i>				
Specific Gravity (g/cm ³)	3.17	2.20	2.94	2.72
Blaine fineness m ² /kg	349.0	1810.5	537.3	328
D ₁₀ (µm)	2.51	1.25	2.27	2
D ₅₀ (µm)	11.66	7.73	11.42	20
D ₉₀ (µm)	31.14	36.76	31.17	150

Table 2: Physical properties of raw and calcined alum sludge

	Raw	475 °C	625 °C	825 °C	1000 °C	1100 °C
Density g/cm ³	2.20	2.58	2.85	3.09	3.12	3.31
D ₅₀ (µm)	7.73	17.94	18.97	24.76	20.34	7.13
BET (m ² /g)	53.77	99.41	81.68	110.18	59.34	15.14

Table 3: Composition of investigated cement blends (reference blends in bold0

Mix description (%)	W/B	SP (%)	Water (g)	C (g)	A (g)	S (g)	L (g)	Sand (g)
C	0.55	1%	247.5	450				1350
C80A20	0.55	1%	247.5	360	90			1350
C50S50	0.55	1%	247.5	225		225		1350
C40S40A20	0.55	1%	247.5	180	90	180		1350
C50S40L10	0.55	1%	247.5	225	90	180	45	1350
C40S32L8A20	0.55	1%	247.5	180	90	144	36	1350

3. RESULTS AND DISCUSSION

3.1 Thermal characterization of raw alum sludge

The thermogravimetric and differential thermal analysis results are shown in Figure 1. Mass loss to 1000°C was 26.1%, with 3 significant mass losses, at 70 to 120°C and two

overlapping mass losses from 275 to 600°C. The first mass loss was due to loss of physically absorbed water. The second mass loss was due to dehydroxylation of $\text{Al}(\text{OH})_3$ to alumina and loss of organic carbon [11–13], denoted by the strong endothermic and exothermic peaks at 275°C and 400°C respectively. At 579°C there was evidence of the α - to β -quartz transition [14]. There was no significant mass loss beyond 700°C. However, the inflection at 789°C on the DTA curve may be formation of an alumina phase.

3.2 XRD analysis

The XRD pattern of raw sludge shows an amorphous structure (Figure 2) with quartz the only crystalline phase detected. This remained so after calcining at 475°C and 625°C. At 825°C characteristic peaks η -alumina (eta) phase were observed. At 1000°C there was partial crystallization of η -alumina, with conversion to α -alumina at 1100°C. η -alumina is the only transition phase derived at 825°C, consistent with studies of aluminium hydroxide gels synthesized from aluminium sulfate [15] and aluminium formate [16]. Gehlenite was observed at 1000°C, arising from CaO plus reactive Al_2O_3 and SiO_2 . Mullite had formed by 1100°C from the reaction of silica- and alumina-rich phases in the sludge,

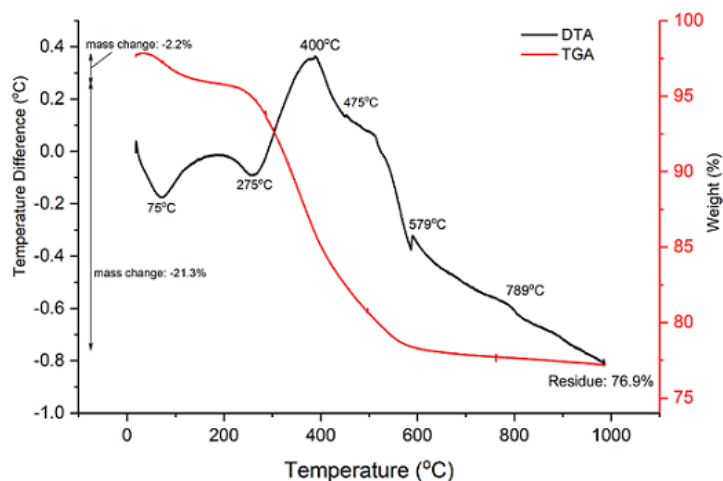


Figure 1: Thermal Analysis of raw alum sludge

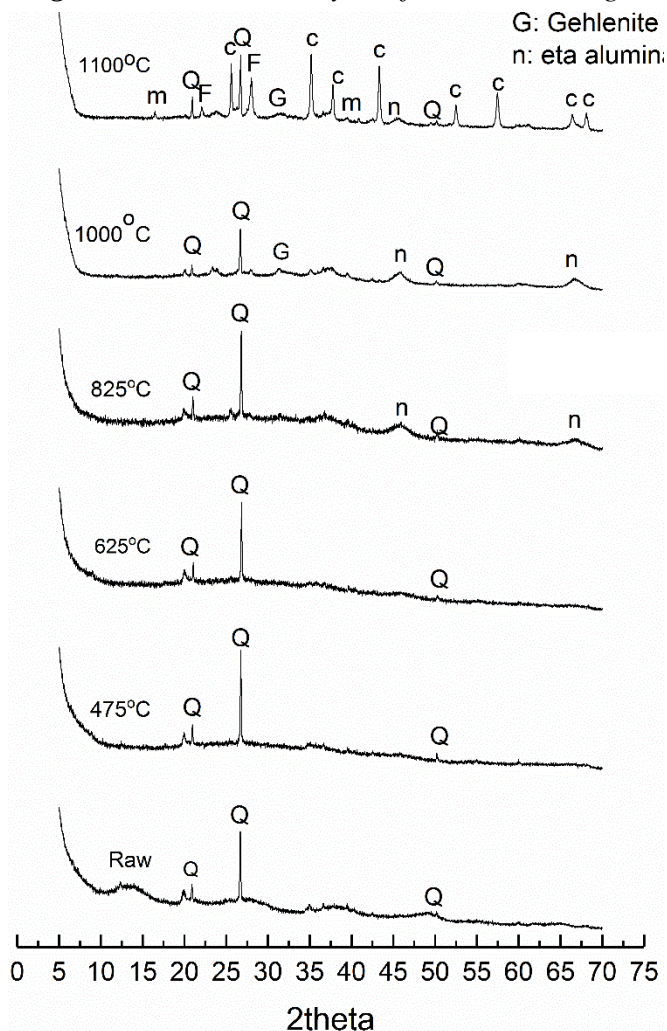


Figure 2: XRD analysis of raw and calcined alum sludge. m: mullite, Q: quartz, c: calcite, G: gehlenite, n: eta-alumina

suggesting that mullite formation and α -alumina reaction occurred concurrently. This implies that by 1100°C, η -alumina from the sludge may have reacted with silica-rich phases.

3.3 FTIR analysis

FTIR Spectroscopy (Fig. 3) was used to follow phase changes as a function of calcination temperature. Raw alum sludge is a hydrated material with bands at 1630 cm^{-1} and 3340 cm^{-1} indicating the presence of molecular and free water [17,18]. This spectra from calcined samples indicate that the decomposition of $\text{Al}(\text{OH})_3$ with release of OH species is achieved at 1100°C. The raw sludge shows bands due to carbonate species at 1435 cm^{-1} [19]. These bands diminished with temperature and completely disappeared by 825°C. This was confirmed by TOC analysis which showed a continuous decline in inorganic content with temperature.

Bands due to the silica network were in the range 800-1150 cm^{-1} [20,21]. In the raw sludge, the intense bands at 1035 and 532 cm^{-1} are Si-O stretching and Si-O-Al bending modes respectively. Heat treated samples showed bands around 790 cm^{-1} - 800 cm^{-1} assigned to ν AlO_4 [22]. Thus, η -alumina found at these temperatures has a tetrahedral structure. The transformation of $\text{Al}(\text{OH})_3$ to an oxide is related to the stepwise strengthening of the Al-O-Al band at 790 cm^{-1} [18].

At 1100°C, sharp and distinct peaks were observed ascribed to corundum. The corundum structure comprises octahedral AlO_6 only, giving rise to two strong characteristic bands near 635 cm^{-1} and 567 cm^{-1} [16]. The formation of mullite at 1100°C is indicated by the emergence of the band at 834 cm^{-1} [23], which is attributed to Si-O-Al linkages, indicating the presence of $\text{Al}_2\text{O}_3 \cdot \text{SiO}_2$ structure.

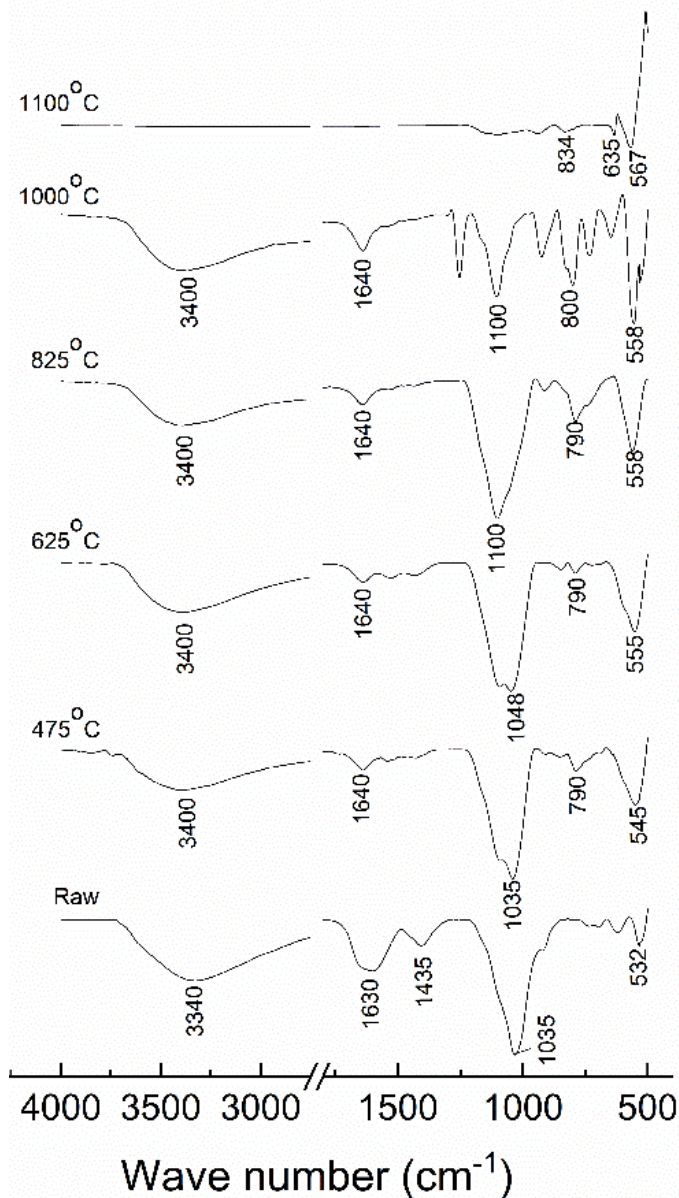


Figure 3: FTIR analysis of raw and calcined sludge.

3.4 Evaluation of cementitious activity by compressive strength

The pozzolanic reactivity of calcined sludge was assessed by two methods: the ASTM C618 strength activity index (Figure 4) and using the strengths of mortars as defined in Table 2 (Figures 5 and 6). The SAI of the sludge increases with increasing calcination temperature due to the significant removal of organic carbon. The highest SAI, 82%, was observed at 1100°C. While XRD showed the formation of highly crystalline phases. At this temperature, particle size analysis (Table 3) showed finer particles, so the superior strength may be due to a filler effect.

Moving from blending calcined sludge with CEM I to a cement-slag blend showed improved performance (Figure 5a), albeit referenced against a cement-slag blend. Performance was improved further upon the addition of limestone (Figure 5b). Additional reactive alumina from SCMs can react with limestone powder to form carboaluminate phases that lead to higher mechanical strength. However, optimum performance was observed with sludge calcined at 825°C. Higher calcination temperatures led to lower mechanical strength, likely due to the crystallization of alumina thereby preventing the reaction with limestone.

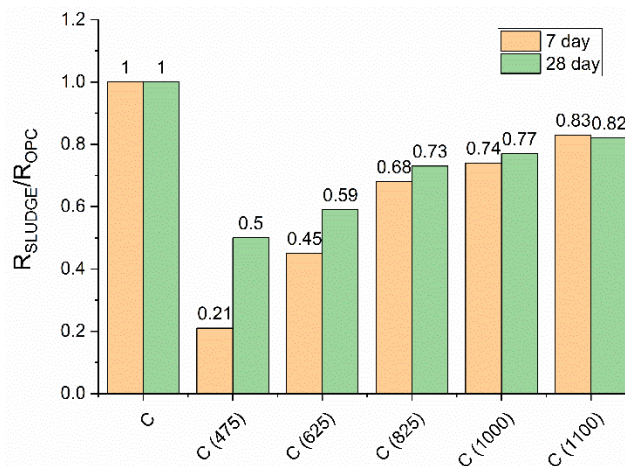


Figure 4: Strength Activity Indices of calcined alum sludge.

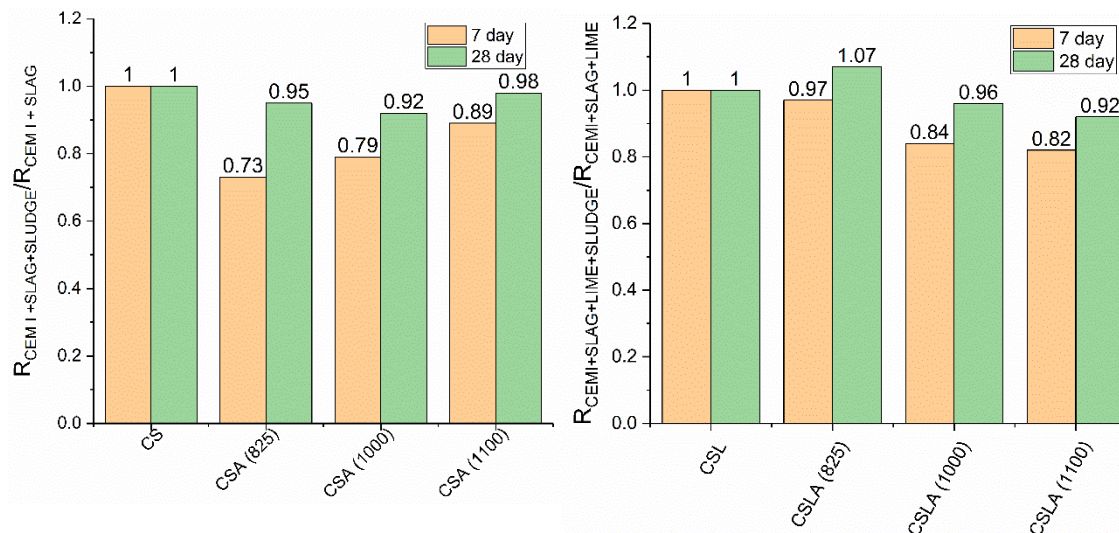


Figure 5: Relative mortar strengths of blends prepared with a) CEM I-Slag or b) CEM I-Slag-Limestone compared to equivalent blends also containing sludge.

4. CONCLUSIONS

Alum sludge is an amorphous aluminium hydroxide precipitate that undergoes thermal transformation to η -alumina, and then thermodynamically stable α -alumina at 1100°C. Detailed analysis has revealed possible solid state reactions in the 200 to 1100°C interval including $\text{Al}(\text{OH})_3$ dehydroxylation and combustion of organic matter. At 825°C, poorly crystalline η -alumina appears with a more crystalline form observed at 1000°C. At 1000°C, the formation of gehlenite occurs from CaO, reactive Al_2O_3 and reactive SiO_2 . At 1100°C, mullite and α -alumina are formed.

The calcined alum sludge showed poor pozzolanic activity with maximum SAI at 1100°C. However, sludge calcined at 825°C can exploit synergies between reactive alumina and carbonates to give improved performance over cement-slag blends.

5. REFERENCES

- [1] U.S. EPA 2011 Drinking Water Treatment Plant Residuals. Management Technical Report. Summary of residuals generation, treatment and disposal at large community water systems. 378
- [2] Malki A, Mekhalif Z, Detriche S, Fonder G, Boumaza A and Djelloul A 2014 Calcination products of gibbsite studied by X-ray diffraction, XPS and solid-state NMR *J. Solid State Chem.* **215** 8–15
- [3] Bradley S M, Kydd R A and Howe R F 1993 The Structure of Al Gels Formed through the Base Hydrolysis of Al^{3+} Aqueous Solutions *J. Colloid Interface Sci.* **159** 405–12
- [4] Wefers K and Misra C, 1987, Oxides and Hydroxides of Aluminum, *ALCOA Technical Paper No. 19*
- [5] Frias M, Vigil de la Villa R, de Soto I, García R and Baloa T A 2014 Influence of activated drinking-water treatment waste on binary cement-based composite behavior: Characterization and properties *Compos. Part B Eng.* **60** 14–20
- [6] Owaid H M, Hamid R and Taha M R 2014 Influence of thermally activated alum sludge ash on the engineering properties of multiple-blended binders concretes *Constr. Build. Mater.* **61** 216–29
- [7] Gastaldini A L G, Hengen M F, Gastaldini M C C, do Amaral F D, Antolini M B and Coletto T 2015 The use of water treatment plant sludge ash as a mineral addition *Constr. Build. Mater.* **94** 513–20
- [8] Lothenbach B, Le Saout G, Gallucci E and Scrivener K 2008 Influence of limestone on the hydration of Portland cements, *Cem. Conc. Res.*, **38(6)**, 848-860
- [9] Damidot D, Lothenbach B, Herfort D and Glasser F P 2011 Thermodynamics and cement science, *Cem. Conc. Res.*, **40(7)**, 679-695.
- [10] Pourkhorshidi A R, Najimi M, Parhizkar T, Jafarpour F and Hillemeier B 2010 Applicability of the standard specifications of ASTM C618 for evaluation of natural pozzolans, *Cem. Conc. Comp.*, **32(10)**, 794-800.
- [11] Teixeira S R, Santos G T A, Souza A E, Alessio P, Souza S A and Souza N R 2011 The effect of incorporation of a Brazilian water treatment plant sludge on the properties of ceramic materials *Appl. Clay Sci.* **53** 561–5
- [12] Ramachandran V S (Vangipuram S 2002 *Handbook of thermal analysis of construction materials* (Noyes Publications)
- [13] Rodríguez N H, Ramírez S M, Varela M T B, Guillem M, Puig J, Larrotcha E and Flores J 2010 Re-use of drinking water treatment plant (DWTP) sludge: Characterization and technological behaviour of cement mortars with atomized sludge additions *Cem. Conc. Res.* **40** 778–86

- [14] Chikouche M A, Ghorbel E and Bibi M 2016 The possibility of using dredging sludge in manufacturing cements: Optimization of heat treatment cycle and ratio replacement *Constr. Build. Mater.* **106** 330–41
- [15] Bhattacharya I N, Gochhayat P K, Mukherjee P S, Paul S and Mitra P K 2004 Thermal decomposition of precipitated low bulk density basic aluminium sulfate *Mater. Chem. Phys.* **88** 32–40
- [16] Roque-Ruiz J H, Cabrera-Ontiveros E A, González-García G and Reyes-López S Y 2016 Thermal degradation of aluminum formate sol-gel; synthesis of α -alumina and characterization by ^1H , ^{13}C and ^{27}Al MAS NMR and XRD spectroscopy *Results Phys.* **6** 1096–102
- [17] Zhang N, Liu X, Sun H and Li L 2011 Evaluation of blends bauxite-calcination-method red mud with other industrial wastes as a cementitious material: Properties and hydration characteristics *J. Hazard. Mater.* **185** 329–35
- [18] Sembiring S, Simanjuntak W, Manurung P, Asmi D and Low I M 2014 Synthesis and characterisation of gel-derived mullite precursors from rice husk silica *Ceram. Int.* **40** 7067–72
- [19] Liu X, Zhang N, Sun H, Zhang J and Li L 2011 Structural investigation relating to the cementitious activity of bauxite residue — Red mud *Cem. Concr. Res.* **41** 847–53
- [20] Fauzi A, Nuruddin M F, Malkawi A B, Al M M and Abdullah B 2016 Fly Ash Characterization as a Cementitious Material *Procedia Eng.* **148** 487–93
- [21] Madejová J 2003 FTIR techniques in clay mineral studies *Vib. Spectrosc.* **31** 1–10
- [22] Krishn G, Priya A, Pa P, Ja D, Wa Rrier K G K, Da A D, Ran M and Aruldas G, 1997, Dehydroxylation and high temperature phase formation in sol-gel boehmite characterized by Fourier transform infrared spectroscopy, *J. Mat. Sci. Lett.* **16(19)**, 1584-1587
- [23] Oréface R L and Vasconcelos W L 1997 Sol-Gel transition and structural evolution on multicomponent gels derived from the alumina-silica system *J. Sol-Gel Sci. Technol.* **9** 239–49

INVESTIGATING THE ORIGINS OF METAKAOLIN SURFACE REACTIVITY IN THE CONTEXT OF ALKALI-ACTIVATED BINDERS

V. Benavent (1), Q. H. Nguyen (1), J.-B. d’Espinoze de Lacaille (1), M. Marinova-Atanassova (2), A.-M. Blanchenet (3) and C. A. Davy (4)

(1) Soft Matter Science and Engineering laboratory, UMR CNRS 7615, ESPCI Paris, PSL Research University, Paris, France

(2) Fédération Chevreul, FR CNRS/Lille1/ENSCL ECL/Lille2/Artois n. 2638, France

(3) UMET, UMR CNRS 8207, Université de Lille, 59655 Villeneuve d’Ascq, France

(4) Centrale Lille and UCCS UMR CNRS 8181, Villeneuve d’Ascq, France

Abstract

This contribution represents our current attempt to understand the origin of metakaolin reactivity in the context of alkali-activated binders (geopolymers). To this purpose, a pure non-calcined kaolinite and two commercial metakaolinites (MK1 and MK2), are compared by using a combination of techniques. First, we investigate the potential of solid state Dynamic Nuclear Polarization (DNP) enhanced Magic Angle Spinning Nuclear Magnetic Resonance (MAS NMR) in order to reveal the specific sites of MK surface. This technique yields drastic improvements in NMR signal intensity from oxide surfaces, allowing to determine the surface coordination of aluminum and silicon on the MK surfaces under consideration. For Si, no significant difference between the bulk and surface responses is found for both MK. For Al, differences were found. Secondly, nitrogen sorption isotherms and Transmission Electron Microscopy (TEM) were coupled to investigate the pore structure, the texture and morphology of kaolinite and MK, in relation to their reactivity. Total adsorbed nitrogen volume is significantly greater for MK1 than MK2 (and than kaolinite). With careful 2D Scanning TEM (STEM) imaging, it is shown that depending on calcination, the typical platelet morphology of kaolinite can be retained, but this is not directly related to reactivity.

Keywords: geopolymer; surface reactivity; metakaolin; DNP enhanced MAS NMR; STEM; nitrogen adsorption

1. INTRODUCTION

Geopolymers (GP) are cements generally made by the alkali-activation of an aluminosilicate source, e.g. calcined kaolinite, also called metakaolin (MK) [1-4].

In this context, variable reactivity of MK is observed when manufacturing GP cement [5,6], depending on the geographical origin of kaolinite, on the exact process used to manufacture MK, on the parameters of GP formulation, etc. Controlling these parameters is of major importance for MK suppliers as well as GP end-users.

In this contribution, the focus is on the MK powders, and aims to understand the origin of their reactivity. One pure kaolinite and two commercial MK (MK1 and MK2) are compared by a combination of techniques. First, we used Dynamic Nuclear Polarization (DNP) enhanced Magic Angle Spinning Nuclear Magnetic Resonance (MAS NMR). The idea is to determine whether the reactivity difference between different MKs is related to structural differences located at the surface. DNP enhanced MAS NMR was coupled to nitrogen adsorption and Scanning Transmission Electron Microscopy (STEM). Nitrogen adsorption provided insights into the pore structure of MK, starting from the micropores, whereas STEM presented the texture and average chemical composition of kaolinite and MK. STEM was preferred to bright field TEM [3,7], in order to limit sample damage. Deeper depth of field was also achieved with STEM compared to TEM.

2. MATERIALS AND METHODS

2.1 Materials

Table 1: X-ray fluorescence results for Fluka kaolinite and MK1 commercial metakaolin

Oxide name	Kaolinite (%mass)	MK1 (%mass)	Kaolinite (%mol)	MK1 (%mol)
SiO ₂	53.2	58.4	67.3	71.2
Al ₂ O ₃	40.2	33.6	30.0	24.1
Fe ₂ O ₃	0.6	2.2	0.3	1.0
K ₂ O	2.4	1.3	1.9	1.0
TiO ₂	0.5	2.89	0.5	2.7

A pure kaolinite (Fluka Analytical brand, by Fisher Scientific, NH, USA, CAS n. 1318-74-7) is chosen as the reference clay mineral, before any calcination. Two commercial MK are used for comparison purposes, and named MK1 and MK2. Both result from calcination in a kiln (by opposition to a flash process). According to their manufacturers, the average grain diameter of MK2 is 1.3 microns, whereas it is 10-15 microns for MK1.

Despite their differences in composition and mode of preparation, MK1 and MK2 exhibit very similar reactivity towards alkali-activation. This reactivity has been assessed by Vicat setting experiment on a typical geopolymer paste (SiO₂/Na₂O =1.2 and H₂O/Na₂O =12) at 25°C. Average Vicat setting time was about 7-8 h for both MKs.

For kaolinite and MK1, average oxide chemical composition is given in Table 1 (ongoing experiment to this date for MK2). It is observed that the silicon oxide content of MK1 is greater than in pure kaolinite, possibly due to the presence of silica impurities (e.g. quartz) [9]. MK1

also contains other impurities (Fe_2O_3 and TiO_2), not present in pure kaolinite. All of these impurities modify the actual content in SiO_2 and Al_2O_3 available for geopolymerization.

2.2 DNP enhanced MAS NMR

Magic Angle Spinning Nuclear Magnetic Resonance (MAS NMR) ^{27}Al ($\pi/10$) and ^{29}Si ($\pi/2$) one-pulse as well as ^1H cross-polarization experiments were performed on a 800 MHz Bruker Avance III HD spectrometer at temperatures between 93 K and 109 K. Dynamic Nuclear Polarization (DNP) enhancement was obtained using a commercial Bruker gyrotron (9.7 T) and preliminary incipient wetness impregnation of the samples with a 15 mM AMUPOL in d8-glycerol: D_2O : H_2O 60:30:10 solution. Spinning rate was 10 kHz in all cases.

2.3 Nitrogen sorption isotherms

Nitrogen sorption-desorption experiments were conducted on an ASAP 2020 apparatus by Micromeritics (Brussels, Belgium) on kaolinite, MK1 or MK2 powders, with a mass of about 0.6-1.1g. Each powder was tested twice, by sampling twice the batch provided by the manufacturer. Prior to conducting the sorption experiments, the powders were degassed at 60°C . First, the temperature was ramped from the ambient up to 60°C at a rate of $1^\circ\text{C} / \text{h}$, and then let for 4 h at 60°C . The equilibration interval between two relative pressure (P/P_0) steps of 0.05 was of 10s. As defined by IUPAC [8], the micropore adsorbed volume was taken as the quantity adsorbed for (P/P_0) between 0 and 0.1.

2.4 2D Transmission Electron Microscopy (TEM) and Scanning TEM (STEM)

STEM (Scanning Transmission Electron Microscopy) was compared to full frame bright field TEM in order to investigate (and limit) sample damage. Both techniques were operated on a Tecnai G2 20 apparatus (FEI, now Thermo Fisher Scientific, NH, USA), at 200kV acceleration voltage. Imaging was performed individually on kaolinite, MK1 and MK2 powders, simply deposited on the sample holder surface in an ethanol suspension for kaolinite, and obtained by cryo-slicing for MK1 and MK2. Energy Dispersive X-Ray spectroscopy (EDX) analysis was coupled to STEM imaging, on square areas of more than 100 nm size, to limit sample damage due to the electron beam (during EDX data acquisition). The EDX Quantax detector and the Esprit software are both provided by Bruker. Kaolinite was used as a reference calibration material to characterize both MK.

3. RESULTS AND DISCUSSION

3.1- DNP enhanced MAS NMR

The one-pulse ^{29}Si and ^{27}Al MAS NMR spectra of the two metakaolin samples were similar to spectra already reported in the literature for metakaolinite [9]. For the ^{27}Al spectra in particular, resonances of octahedral, pentahedral and tetrahedral aluminium occurred with about equal intensities in both samples. The only difference was an additional small narrow octahedral contribution in the ^{27}Al spectrum of the MK1 sample indicating incomplete amorphization of the clay precursor. However, one-pulse MAS NMR spectra reflect the coordination in the bulk of the samples. To reveal active surface sites, DNP enhanced MAS NMR experiments were performed. Microwave excitation of the AMUPOL precursor followed

by DNP of the protons frozen at the surface of the metakaolin and subsequent polarization transfer to the metakaolin surface nuclei by cross-polarization insures that the DNP enhanced MAS NMR spectra reflects solely the coordination of the ^{29}Si and the ^{27}Al nuclei at the surface of the samples. For ^{29}Si , the DNP, surface selective, spectra of the two samples were similar to each other and to the bulk ones obtained in more usual one-pulse experiments (Figure 1).

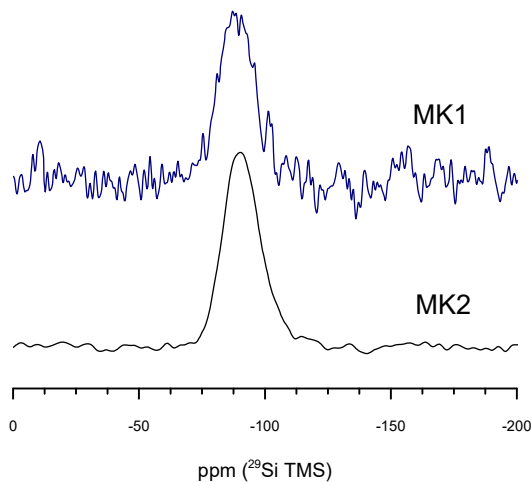


Figure 1: ^{29}Si DNP enhanced CPMAS NMR spectra of the two metakaolin samples. These spectra show the contribution of the surface nuclei only. Both samples appeared similar in that respect and the surface composition reflected roughly the one of the bulk for both samples. No specific silicon surface site was revealed.

On the contrary, the ^{27}Al DNP CPMAS spectra revealed specific features of the surfaces (Figure 2). First, no resonances attributed to tetrahedral aluminum was detected. Second, in the MK1 sample, only octahedral aluminum was detected by DNP experiments.

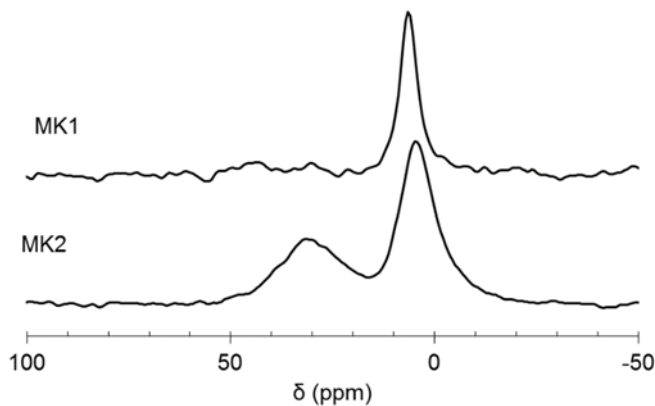


Figure 2: ^{27}Al DNP-enhanced CPMAS NMR spectra of the two metakaolin samples. These spectra show the contribution of the surface nuclei only. No tetrahedral aluminum (around 60 ppm) was present at the surface for both samples. For metakaolin MK1, pentahedral aluminum (around 30 ppm) was also absent.

The absence of tetrahedral coordination at the surfaces of the MKs was a clear indication that the reactive sites were pentacoordinated, hence explaining how calcination activates kaolinite. However, the absence of a resonance attributed to Al^V on the surface of MK1 raises questions. Most likely, it is an artefact due to the presence of iron oxide particles at the surface of this MK.

3.2- Nitrogen sorption isotherms

Table 2: Results of nitrogen sorption isotherms

	Kaolinite	MK1	MK2
BET specific surface (m^2/g)	8.4 +/- 0.2	18.5 +/- 0.3	11.9 +/- 0.2
Micropore adsorbed volume (cm^3/g STP) from $(P/P_0)=0$ to 0.1	1.83 +/-0.1	4.4 +/- 0.1	2.7 +/- 0.1
Total adsorbed volume (cm^3/g STP) from $(P/P_0)=0$ to 0.99	29.0 +/-2.0	92.3 +/- 2.0	39.9 +/- 2.0

Raw kaolinite displayed a smaller BET specific surface area, a smaller micropore volume and a smaller total adsorbed volume than both MKs (Table 2 and Fig. 3). Between the two MKs, MK1 had a significantly greater specific surface area, micropore amount and total pore amount (measured as the total adsorbed volume). These results were tested for reproducibility, and identical trends were observed for two different samples of each powder. In first instance, these elements may seem to indicate that bulk surface area might not be the determining factor for reactivity to alkali-activation. However, whenever impurities are present in a MK [9], a non negligible contribution to specific surface area may be expected from unreactive phases. Consequently, any conclusion on the impact of surface area on reactivity must be complemented by XRD to determine the nature of the impurities present in all powders.

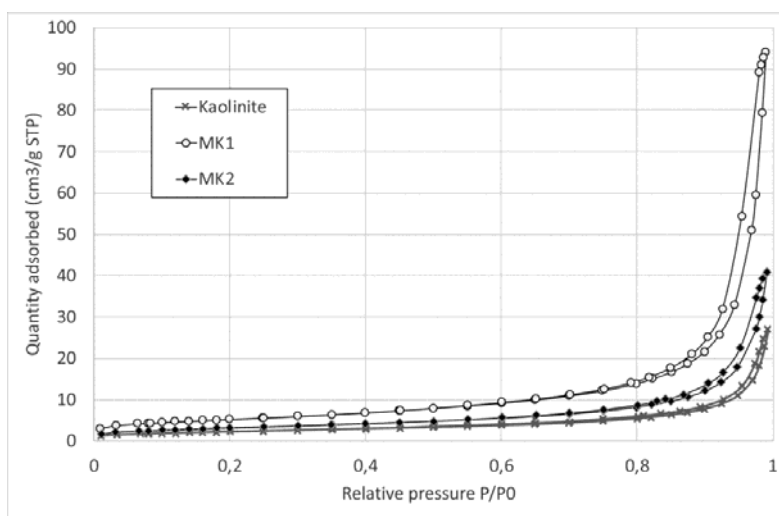


Figure 3: Sorption-desorption isotherms of pure kaolinite, compared to MK1 and MK2

3.3- Powder morphology investigated by 2D TEM and STEM

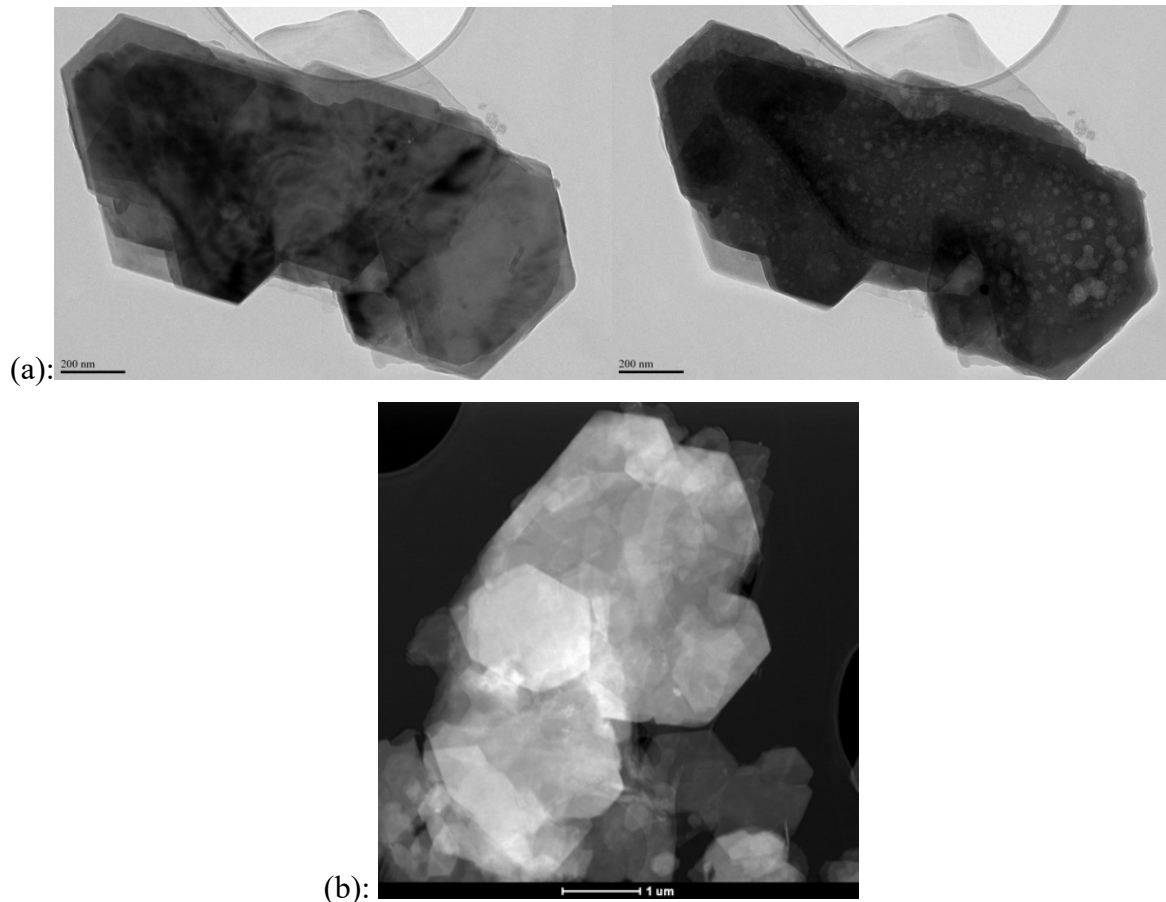


Figure 4: Observation of pure kaolinite (Fluka brand, provided by Sigma Aldrich, USA) (a): by full frame bright field TEM, on the same powder cluster (left): for the first 30 seconds, and (right) after several minutes. Sample damage is observed on the right image, as globular voids filling the clay particle space. (b): by dark field STEM at a magnification x20k. The image shows the presence of undamaged stacked hexagonal kaolinite particles.

2D TEM is performed on pure kaolinite (Fig. 4a). Hexagonal-shaped crystals are observed (Fig. 4a left), which degrade over time when subjecting kaolinite to more than 30s electron beam time. Degraded kaolinite forms “bubbles” or round lighter shades (Fig. 4a right), which may be thought to be actual pores if the photograph is not taken sufficiently rapidly. This testifies of the fragility of kaolinite under the electron beam. Such damage is much slower in STEM mode, where the beam scans the sample surface. In 2D STEM mode, imaging is possible for several minutes without powder damage (Fig. 4b). Repeated EDX analysis on several areas of 600 nm to 5 microns side provide average proportions of 17.9 +/- 0.7 at% Al and 18.3 +/- 0.4 at% Si.

The STEM mode was also chosen to characterize the MK texture and morphology (Fig. 6). When compared to reference kaolinite, MK1 and MK2 still display significant amounts of stacked platelets. More specifically, MK1 is a mix of amorphous matter, without particular shape, and of stacked platelets by about 30% of the image surface (Fig. 6 left). These stacked platelets are very similar to kaolinite platelets. On the opposite, MK2 does not display shapeless

particles (Fig. 5b right). MK2 is mainly made of stacks of roughly hexagonal platelets, organized as piles of up to more than 200 nm thickness. This is very similar to, and hardly distinguishable from actual raw kaolinite clay. When compared to MK reactivity towards alkali-activation, these texture observations imply that a visible significant amorphous content, like in MK1, is not a sufficient indicator to prove MK reactivity. Rather, the texture of both MK, observed by TEM, is not a sufficient indicator for their reactivity towards alkali-activation.

To complete the analysis, EDX provides (20.0 +/- 5.0 at% Al and 19.9 +/- 3.3 at% Si) for MK1, and (19.8 +/- 1.0 at% Al, 20.3 +/- 1.0 at% Si) for MK2. These results do not present a statistically significant difference when compared with raw kaolinite.

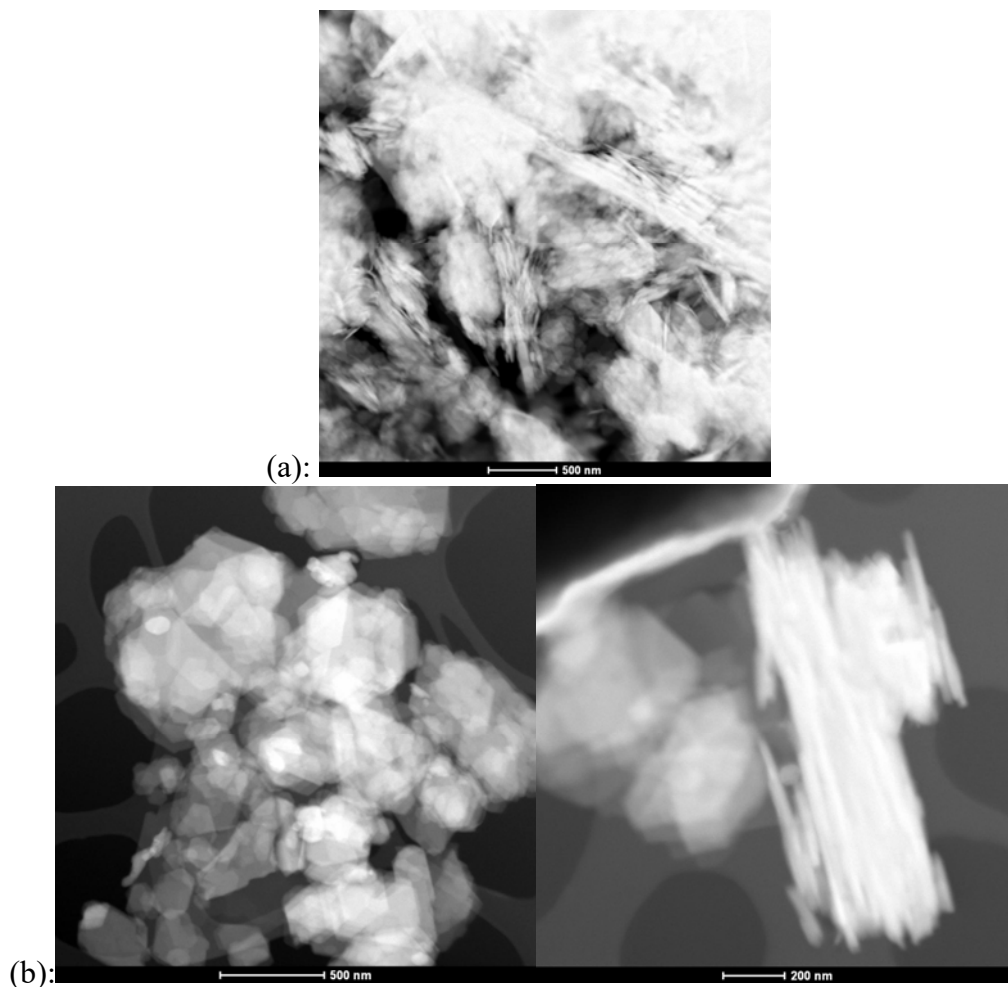


Figure 5: Observation of cryo-sliced (a): MK1 and (b): MK2 by STEM.

4. CONCLUSIONS

The comparison of two metakaolin of similar reactivity but different morphology, surface area and aluminium surface coordination, showed that a single factor was not enough to predict reactivity. In the opinion of the authors, it is not possible to define a single marker for reactivity. A full multiscale characterization of the metakaolin is required to understand reactivity. Further work is in progress in that direction.

ACKNOWLEDGEMENTS

The authors are thankful to M.-C. Willemetz (Centrale Lille, France) for performing the nitrogen sorption isotherm experiments. The SEM and TEM national facilities available at the Centre Commun de Microscopie de Lille (France) are supported by the Conseil Régional du Nord-Pas de Calais, and by the European Regional Development Fund (ERDF). DNP MAS NMR was made possible by access provided at the Biomolécules Laboratory of the ENS Paris through the TGIR-RMN. Special thanks to Dr. N. Birlirakis for assistance during these experiments.

REFERENCES

- [1] Provis J.L., and Van Deventer J.S.J., eds, 'Introduction to geopolymers. Structure, processing, properties and industrial applications', ed. J.L. Provis and J.S.J. Van Deventer. Woodhead Publishing in Materials: Cambridge, UK, 2009.
- [2] Davidovits J., 'Geopolymers', *J Therm Anal.* **37**(8) (1991) 1633-1656.
- [3] Duxson P., Fernandez-Jimenez A., Provis J. L., Lukey G. C., Palomo A., van Deventer J. S. J., 'Geopolymer technology: the current state of the art', *J. Mater. Sci.* **42**(9) (2007) 2917-2933.
- [4] Provis J. L., Palomo A., Shi C., 'Advances in understanding alkali-activated materials', *Cem. Concr. Res.* **78** (2015) 110–125.
- [5] Autef A., Joussein E., Gasgnier G., Pronier S., Sobrados I., Sanz J., Rossignol S., Role of metakaolin dehydroxylation in geopolymer synthesis, *Powder Technology* **250** (2013) 33–39.
- [6] Duxson P., Mallicoat S. W., Lukey G. C., Kriven W. M., van Deventer J. S. J., The effect of alkali and Si/Al ratio on the development of mechanical properties of metakaolin-based geopolymers, *Colloids and Surfaces A: Physicochem. Eng. Aspects* **292** (2007) 8–20.
- [7] Benavent V., Frizon F., Poulesquen A., Effect of composition and aging on the porous structure of metakaolin-based geopolymers, *Journal of Applied Crystallography* **49** (2016) 2116-2128.
- [8] Thommes M., Kaneko K., Neimark A. V., Olivier J.P., Rodriguez-Reinoso F., Rouquerol J., Sing K.S.W., Physisorption of gases, with special reference to the evaluation of surface area and pore size distribution, IUPAC Technical report, *Pure Appl. Chem.*, 19p., 2015.
- [9] Kuenzel C., Neville T. P., Donatello S., Vandeperre L., Boccaccini A. R., Cheeseman C. R., Influence of metakaolin characteristics on the mechanical properties of geopolymers, *Applied Clay Science* **83–84** (2013) 308–314.

NEW GENERATION OF CONSTRUCTION MATERIALS
SESSION 2: TC 280-CBE Cold bitumen emulsion

EVALUATION OF LOCAL AGGREGATE WITH CHEMICAL ADDITIVES FOR MICROSURFACING MIX

Teiborlang Lyngdoh Rynthiang (1), Alan Carter (2), Anjan kumar Siddagangiah (1)

(1) Indian Institute of Technology Guwahati, India

(2) École de technologie supérieure, Montréal (Qc) Canada

Abstract

Microsurfacing has been known to retard deterioration and increase the service life of the pavement by 3 to 8 years for relatively heavy traffic and could be considerably longer for low to medium traffic. In the state of Assam, the Assam PWD took up some stretches in Guwahati and Tezpur to resurface the road with microsurfacing. In order to understand the laboratory performance of such mixes with commercially available emulsion, a study is carried out on aggregate collected from three districts of Assam - Kamrup, Baksa and Udalguri respectively. Property of aggregate required for microsurfacing is carried out, and its rock classification is made. It was observed that aggregate from Kamrup and Baksa districts could pass the specifications and is of one rock type. However, the aggregate from Udalguri district over shoot the Los Angeles Abrasion Test by 4 points and composed of five rock types. Laboratory studies on microsurfacing mix at different pure asphalt requirements(PAR) was carried out on consistency test, Wet Track Abrasion Test (WTA), Loaded Wheel Test (LWT), cohesion test and compatibility test with the additives, C500, E11 and C540 respectively that are either individually or combinedly added to the emulsion. Based on the studies, it was observed that water required for consistency is the lowest with Udalguri aggregate ranging from 3% to 5.5% with the additives. Mix with Udalguri aggregate was found to pass the specification of WTA at the highest PAR with the different additives. With LWT and cohesion test, again Udalguri aggregate has been found to pass the required cycles and the required 30-minute and 60-minute torque whereas, Baksa aggregate was found to pass only the 30-minute torque. With respect to compatibility of aggregate with emulsion, Baksa and Udalguri aggregates was found to score 12 points with all additives. However, Kamrup aggregate could score 11 points with only the combined additives.

Keywords: Aggregate, additive, WTA, LWT, Cohesion test and Compatibility

1. INTRODUCTION

The state of Assam belongs to the North Eastern (NE) part of India. Assam has a total road length of 329520 km, which includes of National highways, State Highway and other roads and out of which, 64572 km are surfaced roads as of 2016 (MORTH, 2018). The public works department with the collaborative effort of emulsion producing companies majorly utilises microsurfacing to treat the distressed roads as shown in Figures 1a and 1b. Further, microsurfacing work was carried out manually in Tezpur of about 200m length as shown in Figure 1c. Likewise, Figure 1d shows the spalled blocks of plastic filled concrete block pavement where microsurfacing was laid on it with compaction to it before opening to traffic. Though microsurfacing was laid in pavements shown in Figure 1; yet, there was no scientific laboratory support for knowing the suitable usage of aggregates in such pavement. This paper presents an initial work of a sponsored project report on microsurfacing studies, with local aggregate from the different districts of Assam with the commercially available emulsion for microsurfacing that has 3.5 % natural latex in it. The objective of the present study was to evaluate the aggregates that were suitably used for cold mix in premixed carpet – a wearing course for rural roads as material for microsurfacing with the commercially available emulsion that has been modified with additive (E 11) and 3.5 % natural latex to suit the quality of emulsion required for microsurfacing.



Figure 1: (a) Road in Choygaon; (b) Road towards Airport; (c) Road at Tezpur
(d) Microsurfacing over deteriorated plastic cell filled concrete block pavement

2. MATERIALS

2.1 Aggregate

The aggregate required for the studies were collected from three districts: Kamrup, Baksa and Udalguri. Aggregate properties required for microsurfacing and specified in ISSA guidelines (ISSA, 2010) were carried out as per ASTM codes (D 2419, C 88 & C 131) and the results are presented in Table 1. Identification of rock type had been carried out visually using a magnifier and comparing the aggregate with hand-held rock specimens and by visualizing and comparing the aggregates with images of rock types from standard references (Pellant, 2002; Mottana et al., 1978, *Geology and Mineral Resources of Assam*, Geological Survey of India (2009). Based on the identification, the aggregate from the three districts was classified and shown in Table 2. It may be noted that aggregate from Udalguri district composed of two types of rocks and of five kinds.

Table 1: Properties of the collected aggregate from different districts of Assam

Properties	Aggregate from District			Specification
	Kamrup	Baksa	Udalguri	
Sand Equivalent	78	78	91	65 min
Los Angeles Abrasion Loss	20.64	21	34	30 max
Soundness of aggregates (Either by Na ₂ SO ₄ or MgSO ₄)	4.74 (by Na ₂ SO ₄)	4 (by Na ₂ SO ₄)	17.43 (by MgSO ₄)	15% max (Na ₂ SO ₄) 25% (MgSO ₄)

Table 2: Classification of aggregate according to type of Rock

Properties	Aggregate from District		
	Kamrup	Baksa	Udalguri
Classification (Rock Type)	Gneiss (Metamorphic)	Gneiss (Metamorphic)	1-Quartzite (Metamorphic-31.3%) 2-Quartz Sandstone (Sedimentary-18.1%) 3-Siliceous Sandstone (Sedimentary-3.2%) 4-Fine Greywacke Sandstone (Sedi'tary-14.6%) 5-Coarse Greywacke S'stone (Sedi'tary-32.8%)

2.2 Emulsion

The emulsion that is used in this study is collected from an emulsion manufacturer, Om Infracon Pvt. Ltd. The emulsion is a commercially available one where it is modified to suit CSS1h by adding with additives and 3.5 % natural latex, which is post added to emulsion and being sold for microsurfacing works.

2.3 Additives

Additives used for the present study are C540, C500 and E11 from a leading manufacturer of emulsifiers, AkzoNobel. The additives are mixed to the required emulsion either in combination or individual before the emulsion is mixed with known aggregate weight to carry out different tests requires for microsurfacing. The dosage of additive (C500 and C540) used was initially provided by manufacture which was subsequently fine-tuned in the lab. These additives are added to the emulsion (MS) to suit to CSS 1h and to slow down the breaking time of the microsurfacing mix. For performance evaluation of microsurfacing, the dosage for E11 was kept constant as the dosage of C500 only for comparative study.

3 EXPERIMENTAL INVESTIGATION AND RESULTS

To achieve the objectives of the paper, the experimental investigations are carried out on the collected aggregate with the above-mentioned emulsion. Studies that were carried are consistency tests, wet track abrasion tests (WTA), loaded wheel tests (LWT), cohesion tests and Schulz Breuer tests. These tests were carried out as per the specification laid in ISSA guidelines (ISSA, 2010).

3.1 Trial Mix Design Procedures

The mix design method as per ISSA TB-118 (ISSA, 2005a) describes the mix design based on pure asphalt requirements (PAR) by surface area method for an 8 μ thick coating of residual bitumen on the aggregate surface. By using this method and the absorption of

aggregate by Centrifuge Kerosene Equivalent (ISSA, 2005a), the required PARs for the three aggregate sources are calculated and the same is presented below in Table 3.

Table 3: The PAR requirement of aggregate from the three districts

	Aggregate form the District of		
	Kamrup	Baksa	Udalguri
PAR Requirement (%)	9.54	9.39	10.02

3.2 Consistency Test

Consistency is the measurement of flow of the mix. In this study, the Kansas Cone Consistency Test is followed as it is widely used and being recognized as a standard test (ISSA, 2012a). By this test, several trial mixes are made as per technical bulletin -111 of ISSA (ISSA, 2005b). The bulletin suggests determining optimum water content at three levels of residual asphalt content: 100%, 85%, and 70% PARs respectively and trial consistencies are to be made by only varying the water contents. For the comparative study, three types of the additives: combination of 1.6% C500 and 0.4% C540, 1.2% C500 and 1.2% E11 are used to prepare microsurfacing samples for the collected aggregate of the three districts. These dosages were tried from prior experience so that the microsurfacing mix does not break before the specified limit of ISSA (2010). Table 4 shows the chosen PAR after carrying out consistency tests on the aggregate. The chosen PAR is selected based on the flow of the mix and no separation of water from the mix.

Table 4: Determining required water content by consistency tests with the three types of additives at trials PAR

Consistency Test at different	Water requirement of aggregate form the District of								
	Kamrup			Baksa			Udalguri		
PAR (%)	70	85	100	90	100	110	80	90	100
1.6% C500 and 0.4% C540	7.06	8.44	12.42	10.8	11.1	12.9	4.0	4.0	4.7
1.2 % C500	2.50	4.02	7.47	16.3	21.3	23.6	3.0	4.0	5.5
1.2% E11	4.10	5.27	9.04	19.7	20.7	21.5	3.0	4.1	4.1

3.3 Compatibility test of aggregate filler-bitumen by Schulz Breuer and Ruck Method

The Schulz Breuer and Ruck Method (ISSA, 2005c) determine the relative compatibility between aggregate filler of specific gradation and the residual bitumen. The method provides a rating system or grading values for abrasion characteristics of specified filler-bitumen combination for comparison with the test values of reference combination. Samples were prepared with the three additives namely, i) additive prepared with 1.6% C500 and 0.4% C540; ii) additive of 1.2% C500; and iii) additive 1.2% E11. The ISSA A143 (ISSA, 2010) suggests that for the compatibility of the mix, the mix should have at least rating or grading of "BAA" or "AAA." Table 5 shows the results of the experiments carried out on filler-bitumen compatibility with the additives. It can be seen from table 5, the rating of the filler-bitumen compatibility; mix with all additives (individual or combined) for both aggregates from Baksa and Udalguri Districts scored 12 points, which show that the compatibility is excellent.

However, mix made with the aggregate from Kamrup could pass only with the combination of additives.

Table 5: Compatibility ranking of filler-bitumen with different additives

Additives	Abrasion loss (g)			Integrity mass (%)			Adhesion (%)			Rating		
	Districts											
	Kamrup	Baksa	Udalguri	Kamrup	Baksa	Udalguri	Kamrup	Baksa	Udalguri	Kamrup	Baksa	Udalguri
1.6% C500 and 0.4% C540	0.29	0.475	0.405	81.37	99.06	99.42	100	92	95	ABA (11)	AAA (12)	AAA (12)
1.2 % C500	1.18	0.33	0.54	62.5	99.47	98.57	100	92	95	CCA (8)	AAA (12)	AAA (12)
1.2% E11	0.81	0.055	0.185	53.43	99.15	99.66	100	92	95	BCA (9)	AAA (12)	AAA (12)

3.4 Wet Track Abrasion Test:

The Wet Track Abrasion Test (WTA) is a simulated performance test which has been correlated to wearing qualities of the field applied microsurfacing under wet abrasion conditions. Methods of conditioning samples, procedures before subjecting the samples to abrasion and testing are followed as per the guidelines of the bulletin (ISSA, 2012b). For WTA, the results of 6 days abrasion loss for the three additives that were studied namely, 1.6% C500 with 0.4% C540, 1.2% C500 and 1.2% E11 with the aggregate from the three districts of Assam were plotted and shown in Figure 3.

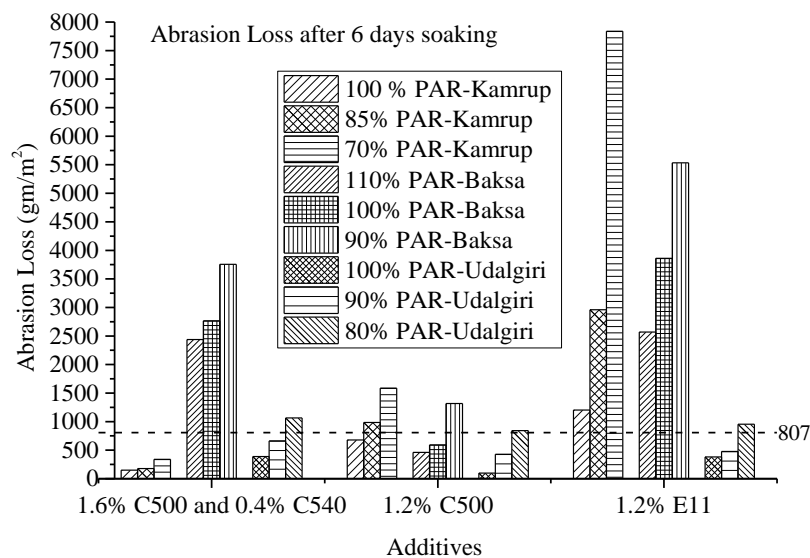


Figure 3: Six days abrasion loss of material in microsurfacing mix with different additives for the three sources of aggregate

Figure 3 illustrates that the abrasion loss of material for Kamrup aggregate is well within the limits for the mix prepared by the combination of additives and with C500 at the highest PAR. However, with the mix that has E11 as additive, the sample suffers heavy loss. With the

aggregate from Baksa, it could be seen that mix that has a combination of additives and E11 as additive could not pass the abrasion loss limit as specified in ISSA guideline. But only for additive of C500 and at highest PAR and lower to it, the mix could pass the specification. From figure 3, it could be seen that microsurfacing mix prepared with the aggregate from Udalguri fair well with all the additives - either combined or individually, except at least studied PAR.

3.5 Measurement of Stability and Resistance to Compaction by LWT

The method measures the amount of compaction or displacement characteristics of multilayered, dense graded, fine aggregate cold mixes such as slurry seal or microsurfacing under simulated rolling traffic compaction by LWT. The LWT tests on the combination (1.6% C500 and 0.4% C540) or individual (1.2% of C500 or 1.2% E11) additives with the aggregates collected from the three districts of Assam are carried out as per ISSA TB-147 (ISSA, 2005d) and ASTM D 3910. From the tests carried out, it was found that microsurfacing mix with aggregates from Kamrup and Baksa districts could not pass the specified limits (ISSA, 2005g). Since microsurfacing samples with Udalguri aggregate could pass the 1000 cycles, they are further prepared for sand adhesion test (ISSA, 2005e). Results of the sand adhesion test are shown in Figure 4. Figure 4 shows that the mix prepared at lowest PAR is suitable for all types of traffic with the studied additives. However, at 10 % more than the least PAR, the mix is suitable only for all traffics when the additives, C500 and E11 acted individually.

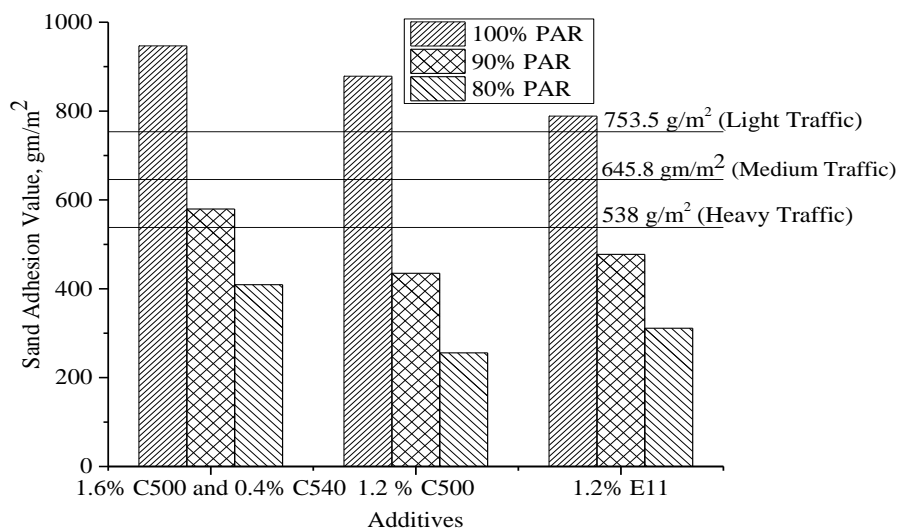


Figure 4: Sand adhesion values with different additives for Udalguri aggregate

3.6 Cohesion Test

This test method is used to determine initial set and cure development of microsurfacing systems as a function of torque over time (ISSA, 2012c). This test quantifies the time required before a microsurfacing system may be subjected to straight rolling traffic. Results of the test are shown in Table 6. Results show that microsurfacing with Kamrup aggregate fail to reach the minimum specified cohesion value for 30 and 60 minutes. But the cohesion requirement of microsurfacing mix with the aggregate from Baksa, satisfies only at 30 minutes. However,

microsurfacing mix with Udalguri aggregate; the cohesion requirements at 30 and 60 minutes respectively are satisfied.

Table 6: Results of the cohesion test at different PAR percentages

Additives	Aggregate from District																	
	Kamrup						Baksa						Udalguri					
	Residual bitumen content at different PAR																	
	9.54% (100% PAR)	8.11% (85% PAR)	6.68% (70% PAR)	10.33% (110% PAR)	9.39% (100% PAR)	8.45% (90% PAR)	10.02% (100% PAR)	9.02% (90% PAR)	8.02% (80% PAR)									
	Times (mins)																	
30	60	30	60	30	60	30	60	30	60	30	60	30	60	30	60	30	60	
1.6% C500 and 0.4% C540	*	*	*	*	*	*	14	17	14	15	14	14	17	26	16	21	14.5	20
1.2% C500	*	*	*	*	*	*	14	15	13	15	13	14	16	23	16	21.5	14	21
1.2% E11	*	*	*	*	*	*	13	15	13	13	12	13	17	23.5	14	22	14	20.5
	ISSA TB139: Minimum Torque of 12 kg-cm at 30 mins and 20 kg-cm at 60 mins * Did not pass the required minimum torque																	

CONCLUSIONS

Based on the study that was carried out on aggregates collected from different districts of Assam as an ingredient for microsurfacing with the commercially available emulsion of CSS1h having 3.5 % natural latex with the additives; the conclusions of the study are as below:

- ✓ The abrasion of microsurfacing mix with Kamrup aggregates will all combinations of additives found to be lowest compared to other aggregate sources.
- ✓ Only at lower residual asphalt content the microsurfacing was found to meet the sand adhesion requirements as per loaded wheel tracker irrespective of additive combinations used.
- ✓ Aggregates from Udalguri district found to meet the cohesion requirement at all pure asphalt requirement contents will all combinations of additives.
- ✓ In general, the aggregates showed mixed compatibility results with combinations of additives used in the study. From the results, the aggregates from Udalguri district were found to be suitable as an ingredient for microsurfacing with the commercial available emulsion of CSS 1h with added latex with all three additives – 1.6% C500 & 0.4% C500, 12% C500 and 1.2% E11. However, microsurfacing mix produced from Kamrup and Baksa sources could not fulfill the requirement with the selected combinations of additives.

ACKNOWLEDGEMENT

The authors acknowledge the Department of Science and Technology, Govt. of India for sponsoring the Microsurfacing equipments; Om Infracon Pvt. Ltd for supplying emulsion, latex and additives and also AkzoNobel India for supplying the additives.

REFERENCES:

- [1] MORTH, (2018), 'Basics Road Statistics of India 2015 - 2016', <http://morth.nic.in/showfile.asp?lid=3100&key=road%20statistics&n=1>, access September 2018.
- [2] ISSA, (2010), 'Recommended Performance Guidelines for Micro Surfacing', International Slurry Sealing Association, ISSA A143, Revised in February 2010, Annapolis, Maryland, USA.
- [3] ASTM Standard D2419, 2009, 'Standard Test Method for Sand Equivalent Value of Soils and Fine Aggregate', ASTM International, West Conshohocken, PA, 2009, DOI: 10.1520/D2419-09, www.astm.org.
- [4] ASTM Standard C88, 2013, 'Standard Test Method for Soundness of Aggregates by Use of Sodium Sulfate or Magnesium Sulfate', ASTM International, West Conshohocken, PA, 2013, DOI: 10.1520/C0088-13, www.astm.org.
- [5] ASTM Standard C131/131M, 2014, 'Standard Test Method for Resistance to Degradation of Small-Size Coarse Aggregate by Abrasion and Impact in the Los Angeles Machine', ASTM International, West Conshohocken, PA, 2014, DOI: 10.1520/C0131_C0131M-14, www.astm.org.
- [6] Pellant Chris, 'Smithsonian Handbooks - Rocks and Minerals', 2nd American Edition, (Dorling Kindersley, Inc., New York, 2002).
- [7] Mottana, A., Crespi, R. and Liborio, G., 'Guide to Rocks and Minerals', (Imon and Schuster Inc., Rockefeller Center, New York, 1978).
- [8] GSI (2009), 'Geology and Mineral Resource of Assam', Geological Survey of India, Miscellaneous Publication, No. 30, Part IV, Vol: 2(i) Assam, Govt. of India.
- [9] ISSA, (2005a), 'Surface Area Method of Slurry Seal Design', International Slurry Sealing Association, Technical Bulletin No. 118, 5th Edition, Annapolis, Maryland, USA.
- [10] ISSA, (2012a), 'Test Method for Measurement of Slurry Seal Consistency', International Slurry Sealing Association, Technical Bulletin No. 106, 5th Edition, Annapolis, Maryland, USA.
- [11] ISSA, (2005b), 'Outline Guide Design Procedure for Slurry Seal', International Slurry Sealing Association, Technical Bulletin No. 111, 5th Edition, Annapolis, Maryland, USA.
- [12] ISSA, (2005c), 'Test Method for Classification of Aggregate Filler-Bitumen Compatibility by Schulze-Breuer and Ruck Procedures', Technical Bulletin No. 144, 5th Edition, Annapolis, Maryland, USA.
- [13] ISSA, (2012b), 'Test Method for Wet Track Abrasion of Slurry Surfacing Systems', International Slurry Sealing Association, Technical Bulletin No. 100, 5th Edition, Annapolis, Maryland, USA.
- [14] ISSA, (2005d), 'Test Method for Measurement of Stability and Resistance to Compaction, Vertical and Lateral Displacement of Multilayered Fine Aggregate Cold Mix', International Slurry Sealing Association, Technical Bulletin No. 100, 5th Edition, Annapolis, Maryland, USA.
- [15] ASTM Standard D3910, 2011, 'Standard Practices for Design, Testing, and Construction of Slurry Seal', ASTM-D 3910, ASTM International, West Conshohocken, PA, 2011, DOI: 10.1520/D3910-11, www.astm.org.
- [16] ISSA, (2005e), 'Test Method Measurement of Excess Asphalt in Bituminous Mixtures by Use of a Loaded Wheel Tester and Sand Adhesion', International Slurry Sealing Association, Technical Bulletin No. 109, Annapolis, Maryland, USA.
- [17] ISSA, (2012c), 'Test Method to Determine Set and Cure Development of Slurry Surfacing Systems by Cohesion Tester', International Slurry Sealing Association, Technical Bulletin No. 139, Annapolis, Maryland, USA.

THERMAL IMPACT OF ADDING RECYCLED GLASS IN MICROSURFACING

**Apparao Gandi (1), Abdelghafour Zabayou (2), Saeed Badeli (3), Alan Carter (4), and,
Michel Vaillancourt (5)**

(1, 2, 3, 4, 5) Department of Construction Engineering, Ecole de technologie superieure,
Canada.

Abstract

Pavement albedo is an important factor when evaluating thermal performance of pavement. Information regarding albedo value for different materials is currently limited. The use of fresh coatings could help cool cities and reduce heat islands. The important thermal characteristics of the pavement, which are albedo, diffusivity, conductivity and thermal capacity, can be modified and improved by integrating new materials into its structure. Glass is one of these new materials, and it is the subject of various studies and research on its mechanical performance, but little in depth on its thermal performance.

The main objective of this study is to evaluate the impact of the addition of post-consumer glass particles on the thermal characteristics of microsurfacing. Mix design of microsurfacing with glass was first done, then we have compared the insulating capacity of a micro surfacing with and without glass, and measured the value of albedo and the thermal diffusivity of the micro surfacing with glass on an outside test section. The results have shown very little effect on the albedo, but a significant impact in the temperature in the pavement under the microsurfacing.

Keywords: Micro surfacing, Recycled glass, Albedo, Thermal performance.

1. INTRODUCTION

Increasing attention is being paid to reducing the environmental impacts associated with each phase of the life cycle of various civil infrastructures. Roadways and pavements, as one important sector of the transportation infrastructure system and the built environment, play a vital role in economic and social development of any society. While promoting economic and social growth, researchers, agencies, industries and other stakeholders in the field of the roadways and pavements are working together to reduce their environmental impacts. One environmental impact that pavements can help reduce, where local climate and urban density make it important, is the heat island effect associated with pavements [1].

Heat islands are attracting more attention from various organizations. For instance, LEED® 2009 (Leadership in Energy & Environmental Design, a green building certification program from the U.S. Green Building Council [USGBC]) awards points to new construction and major renovations for using various technologies and strategies for roofs and non-roofs (including roads, sidewalks, courtyards and parking lots, etc.) to reduce heat islands to minimize impacts on microclimates and human and wildlife habitats [2]. Some researchers from Lawrence Berkeley National Laboratory (LBNL) and some other institutes in the US and other countries also have been focusing on cool pavement technologies to help address the problem of urban heat islands, mainly through increasing pavement surface reflectivity (or albedo) [1 and 3].

Albedo (or solar reflectance) is a measure of the ability of a surface to reflect solar radiation. Solar reflectance values range from 0 (no sunlight reflected) to 1 (all sunlight reflected). Light-colored materials generally have higher solar reflectance values than dark-colored materials, although color alone is not the only indicator of solar reflectance [4]. Figure 1 illustrates how pavement surface temperatures are greatly affected by pavement albedo in Phoenix, USA [5].

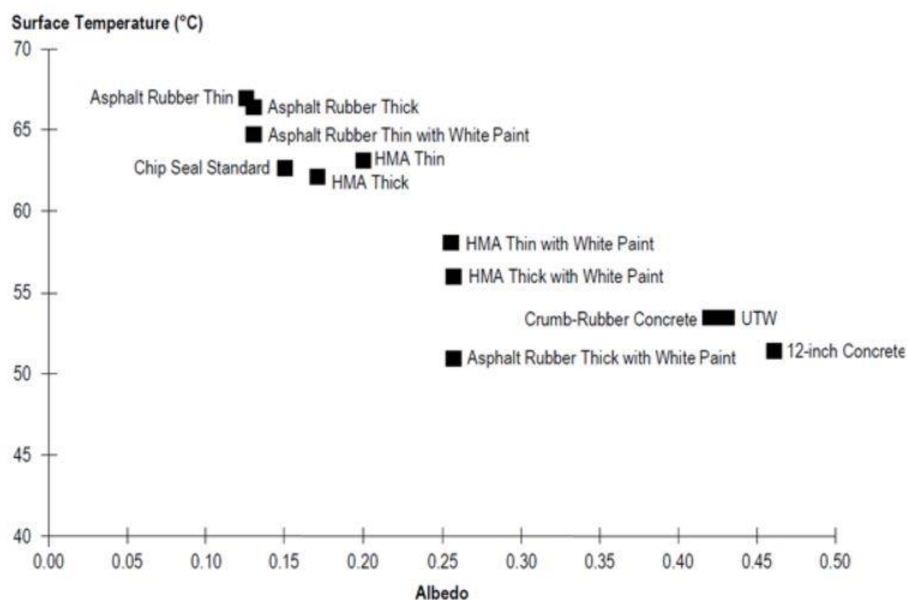


Figure 1: Albedo effect for selected types of pavements in Phoenix, Arizona (note: UTW = ultra-thin whitetopping) [5]

1.1 Recycled glass on Asphalt Pavements in Quebec

In 2012, 159,000 tons of glass was produced in the province of Quebec. Of that number, 68,000 tons were collected and sent to a recycling sorting facility [6]. Glass can be recycled over and over, and can be melted and reused to manufacture new glass products. The problem with glass recycling is the breakage of glass containers during transportation from the consumer's home to the recycling sorting facility. In the province of Quebec, all materials that are collected from the consumer's home are mixed together, which further complicates sorting in the recycling facility. Different glass types and colors are mixed with other recycled

materials, such as paper or plastic, which constitute a source of contamination. In order to reuse recycled glass to manufacture new glass products, glass collected must be separated and classified according to type and color. This part of the recycling process is really important because all glass types have specific chemical compositions. If different types of glass are mixed together to manufacture new products, the resulting quality cannot be guaranteed [7].

The integration of glass particles in asphalt is an innovative solution to ensure the proper use of post-consumer glass, to give it a new life, to generate economic benefits and to provide good thermal performance due to its insulating capacity, low conductivity and low heat capacity. A research project on the use of recycled glass in different layers of bituminous pavement is in progress in Quebec. The results have so far shown that glass can have structural capacities similar to natural aggregate when used in asphalt mixes or in granular course, that it can be used in hot asphalt mixes or in cold recycled materials with good thermomechanical properties and that it has superior insulation capacities than natural aggregate [8-11].

Microsurfacing are thin, usually under 15mm, bituminous mixes made with bituminous emulsion. Mostly used for pavement rehabilitation, microsurfacing can repair minor damage on the pavement surface, increase the texture of the pavement for safety, and limit the presence of water in the pavement [12].

2. OBJECTIVE

The main objective of this research project is to evaluate the impact of the addition of post-consumer glass particles on the thermal characteristics of the pavement and on heat islands by carrying out an experimental program.

3. METHODOLOGY AND MATERIALS

This research project is separated into two different part. The first part, in laboratory, covers the microsurfacing mix design, and the evaluation of the thermal characteristics of the microsurfacing mix with glass. In the paper, only the thermal characteristics are developed. The second part of this study is on the albedo evaluation of a trial section built outside.

3.1 Microsurfacing mix, surface and base course mix

Three different bituminous materials were designed for this project. First, a 20mm base course mix with a PG58-28 bitumen was designed. This mix was used in the laboratory tests. A 10mm HMA surface mix with a PG70-28 bitumen was also designed to serve as reference. Both those mixes were made with natural aggregate. Finally, a microsurfacing (0-5mm) mix was designed with 46% of its aggregate replaced by recycled glass. The recycled glass particles used only replaced the 0-2.5mm part of the gradation. The rest of the aggregate are the same natural aggregate used in the other two mixes. All three mixes respected the Quebec's standards.

3.2 Laboratory tests

The insulation capacity and the thermal diffusivity were measured in the laboratory. To do so, two different setups were used. In both cases, the bituminous mixes were compacted using a Shear Gyrotory Compactor (GSC) and placed in an insulated cabinet under a heat lamp (90W) placed 20cm above the mix surface (Figure 2). Expanded polystyrene was used for

insulate the mixes on the side and at the bottom.

The base course (GB-20) was first compacted with the SGC at 120mm in height. Once cooled down at room temperature, a tack coat was added on the surface (bituminous

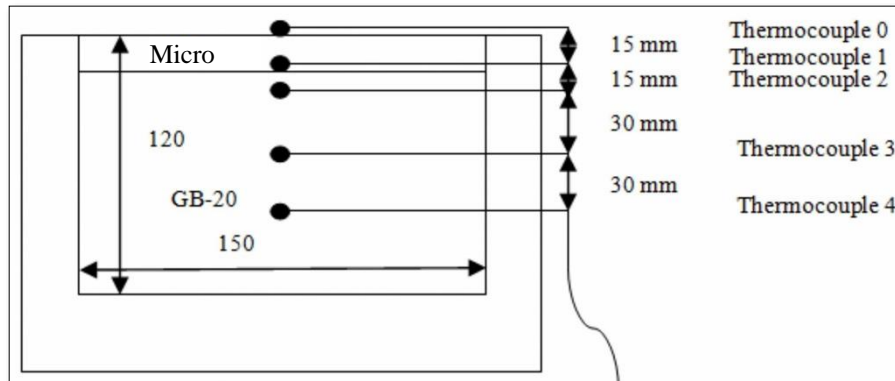


Figure 2: Setup for the insulation property measurement for the system with microsurfacing

emulsion) before adding the 20mm of the 0-10mm HMA surface course which was compacted also with the SGC. Both mixes had air voids of 5%. For the specimen with microsurfacing, the same procedure was used, but without a tack coat and without any heating. The measured air voids of the microsurfacing were 2%. Holes were drilled on the side of the specimens and thermocouples ($\pm 1^\circ\text{C}$ of precision) were inserted and maintained in place with bituminous emulsion. The microsurfacing was laid down at 20mm thick, same as the HMA surface mix in order to have the same total thickness.

The setup shown in Figure 2 is for the insulation capacity of the pavement structure. For the thermal diffusivity, only microsurfacing was placed in the insulated cabinet. The thermal diffusivity is the capacity of a material to transmit a temperature signal from one point to another. Basically, it measures the heat transfer rate from the hot to the cold side of a specimen. It is obtained by dividing the thermal conductivity by specific gravity times the thermal capacity. It is possible however to calculate the diffusivity without using the thermal conductivity of the material. The diffusivity in a semi-infinite body can be calculated with equation 1 [13].

$$\frac{\partial T}{\partial t} = \alpha \frac{\partial^2 T}{\partial x^2} \quad (1)$$

where: α is the thermal diffusivity (m^2/s)
 $T=T(x,t)$ is the temperature at a time t and a position x .

For both tests, the specimens were let under the heat lamp for 5 hours while recording the temperature every 30 seconds.

3.3 Test section – Outside

In order to measure the albedo value and to measure the temperature under a microsurfacing containing glass, a trial section was built outside in an empty parking lot on old HMA. A flat surface located in an area without shadow was selected for the test section. A

5.0 m in diameter circular section of microsurfacing was laid by hand to a thickness of 15mm \pm 2mm. It took three hours to mix and installed the microsurfacing. Thermocouples were placed below the microsurfacing, but the surface temperature was measured with a laser thermometer.

One day after the installation, it was decided to try to simulate traffic on the trial section in order to remove the thin film of asphalt on the particles to make the glass visible, as it would happen on a trafficked pavement. pedestrian traffic, mechanical brooming and even sanding barely damaged the surface; very limited glass was visible for the Albedo test.

The albedo was measured with a pyranometer centered, 50cm above the microsurfacing trial section as proposed in the ASTM 1918-16 standard. The pyranometer first measure the luminosity direct from the sun before being flipped, to face the microsurfacing, and measure the reflected luminosity. The albedo value is the ratio between the reflected and the direct luminosity value.

4. RESULTS AND ANALYSIS

The results are separated in two sections. First the laboratory results are covered, followed by the trial section results.

4.1 Laboratory results

The thermal characteristic of microsurfacing that contains recycled glass is not something found in the literature. Some generic values of diffusivity are available for bituminous materials and other pavement materials. In this study the diffusivity value obtained for microsurfacing containing 46% recycled glass is $5.04 \times 10^{-7} \text{ m}^2/\text{s}$. This is much lower than what is considered normal for bituminous materials which range from 0.37×10^{-6} to $1.44 \times 10^{-6} \text{ m}^2/\text{s}$ [14]. This result means that the heating of the microsurfacing is slower than for other bituminous material. However, since it's relatively thin, maybe this lower diffusivity is not enough to have a significant effect on the temperature in the pavement below it. This is what the second part of the lab work is all about.

As explained previously, several thermocouples were placed in the pavement structure. Figure 3a shows the temperature evolution on the surface of the specimen, and Figure 3b shows the temperature 9cm under the surface (in the base course). As it can be noted, the temperature on the surface is very similar for both specimen (microsurfacing with glass on HMA base course, or HMA surface mix over HMA base course). However, at 9 cm under the surface, the difference between the two pavement structures is quite different.

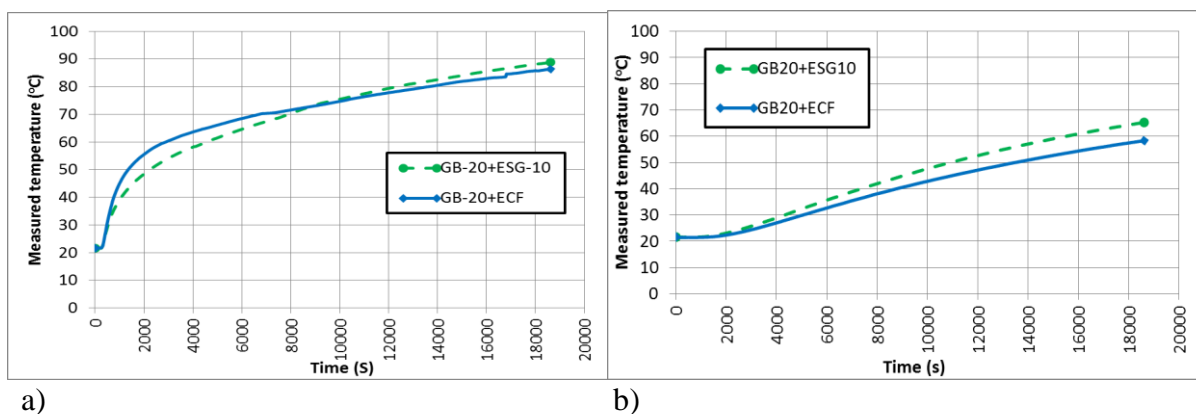


Figure 3: Temperature evolution at the surface (a) and 9cm under the surface (b) for the pavement structures with and without microsurfacing with recycled glass

The temperature differences between the two pavement structure increases with time. On Figure 4, it can be observed that, after 5 hours, for the pavement structure with microsurfacing with recycled glass, the temperature is 6.9°C lower at 9cm below the surface. This difference is rather constant throughout the thickness of the HMA base course.

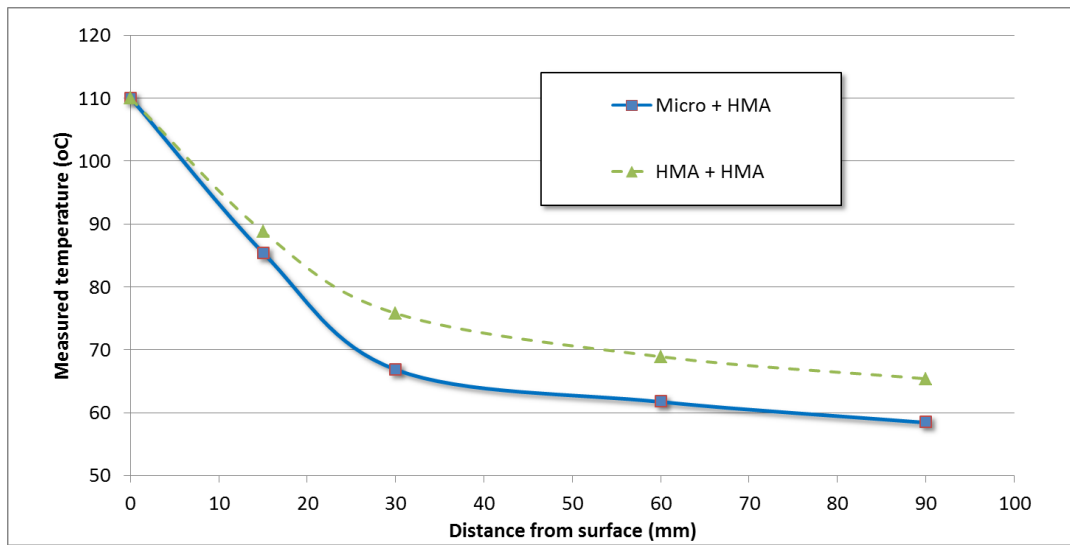


Figure 4: Temperature evolution vs the distance from the surface after 5 hours

This difference confirms the thermal properties of the microsurfacing with recycled glass. Even with its limited thickness, the impact on the pavement structure temperature is important. In North America, the bitumen is classified with the performance grade, and the grades are separated by 6°C. Since there's more than 6°C of difference between the two pavement structures, the use of microsurfacing with recycled glass could enable the usage of a bitumen with a low PG grade, which would significantly reduce the cost of the pavement.

4.2 Trial section results

The test section was monitored during two weeks in July. As mentioned earlier, it was not possible to change the level of bitumen coverage on the surface during that period, so stable results were expected.

On Figure 5, the Albedo values measured for 1 hour starting at noon can be seen. The first thing to note is the variation in the results. This is due to the sun angle of incidence that changes during that period. Also, the measured values oscillate between 6.0% and 10.6%. Those values are very low compared to what can be found in the literature (see Figure 1). Unfortunately, it was not possible to build a new trial section without glass to compare. New tests are needed to explain this, but we think that the non-modified bitumen contained in the emulsion ended up making a very mat surface, which reflected very little light. This was observed visually, and maybe even if the surface was not abraded enough to show glass particles, it did make it less shiny. The first test to measure albedo was done right after the

curing of the emulsion, and the maximum measured value was 5.5%. So even if 10.6% is low, it's still almost double from the initial reading.

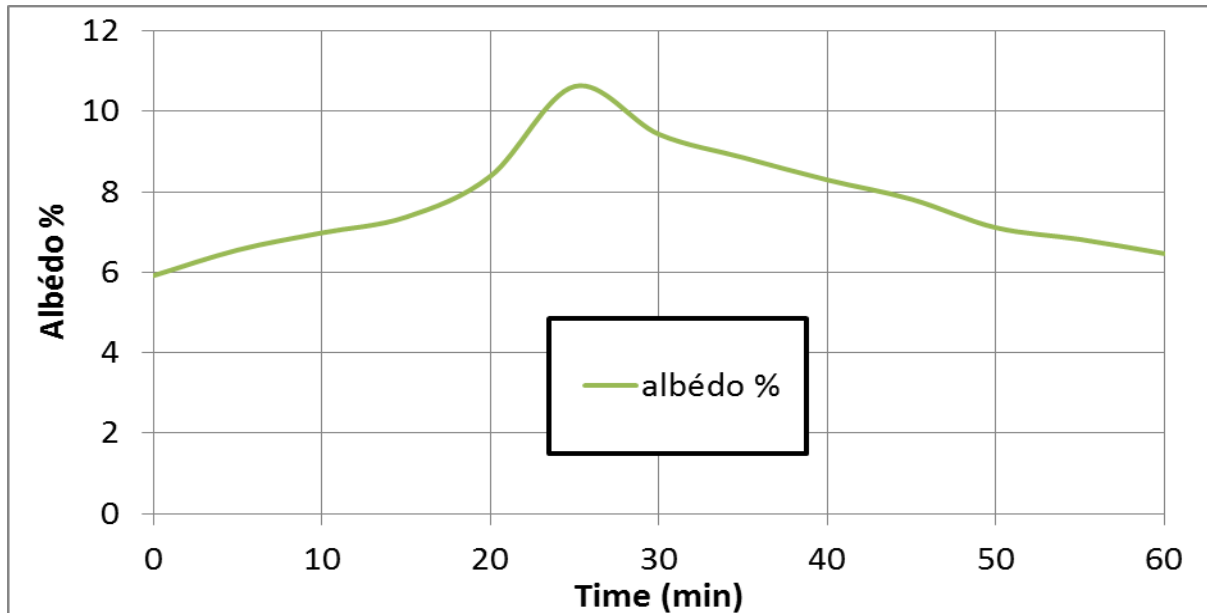


Figure 5: Albedo results measured on the microsurfacing with recycled glass test section after two weeks

The temperature at the surface of the test section was measured and compared with the temperature on an asphalt pavement beside the test section. Both section receives direct sunlight, but the pavement does have traffic on it. The maximum temperature measured on the test section is 45.9°C, it was 46.4°C at the same time on the pavement. This difference is not significant, and we believe that if the test section would have undergone traffic, the temperature difference would have been bigger. We believe that this indicates that the use of microsurfacing with recycled may be a good option to reduce the heat island effect.

5. CONCLUSIONS

In this research project, a microsurfacing mix was made with recycled glass used to replace 46% of the natural aggregate. Thermal properties tests were performed in laboratory, and albedo measurements were done outside on a test section.

The laboratory results have shown that microsurfacing with recycled glass diffuse the temperature at a lower rate than standard HMA. The results have also shown that the use of this material at the surface of a bituminous pavement structure can significantly reduce the temperature and could allow the use of a lower PG grade bitumen in the base course. The albedo measurement on the test section showed very low albedo value. However, the temperature on the test section was slightly lower than on a HMA section beside it. More work is needed to properly understand the impact of the addition of recycled glass in microsurfacing, but the results are promising.

REFERENCES

- [1] Gartland L.M., 2008, *Heat islands: understanding and mitigating heat in urban areas*. Earthscan Press in UK and USA
- [2] U. S. G. B. Council, 2009, LEED 2009 for new construction and major renovations rating system, *Washington, DC: US Green Building Council*
- [3] Akbari H., Pomerantz M., and Taha H., 2001, Cool surfaces and shade trees to reduce energy use and improve air quality in urban areas, *Solar energy*, vol. 70, no. 3, pp. 295–310
- [4] National Concrete Pavement Technology Center (NCPTC) and National Center for Asphalt Technology (NCAT), 2013, Quantifying Pavement Albedo - Phase I Final Report: Literature Review and Detailed Work Plan. Project No. DTFH61-12-C-00016. Federal Highway Administration, Washington, DC.
- [5] C. Systematics, 2008, Cool pavement report: EPA Cool pavements study–Task 5 (draft report), *Prepared for Heat Island Reduction Initiative, US EPA*, 2008.
- [6] Recyc-Québec, 2014, Bilan 2012 de la gestion des matières résiduelles au Québec, 2014. [Online]. Available: <http://www.recyc-quebec.gouv.qc.ca/client/fr/rubriques/Nouvelles.asp?id=778>.
- [7] Gagné L., 2010, Le Verre: Fiches informatives, [Online]. Available: http://icionrecycle.recyc-quebec.gouv.qc.ca/Documentation/Sections/TelechargerPieceJointe/Fiche_Verre.
- [8] Lachance-Tremblay E., Vaillancourt M., Perraton D., 2016, Evaluation of the impact of recycled glass on asphalt mixture performances, *Road Materials and Pavement Design*, Vol 17, Issue 3, pp. 600-618
- [9] Berraha Y., Vaillancourt M., Perraton D., 2017, Thermal properties of base-course material containing recycled glass under dry and wet condition, *Proceeding of the 1st GeoMEast International Congress and Exhibition, Egypt, July 2017*
- [10] Mohsenian S., Vaillancourt M., Carter A., Bilodeau J.P., 2018, Resilient modulus of pavement unbound granular materials containing recycled glass aggregate, *Current state of the art practice of use of glass in pavement structures, Materials and Structure*, 51:89
- [11] Raschia S., Badeli S., Carter A., Graziani A., Perraton D., 2018, Recycled glass filler in cold recycled materials treated with bituminous emulsion, *Transportation Research Board 97th Annual Meeting Compendium Washington DC, January 2018*
- [12] Garfa A., Carter A., Dony A., 2018, Rutting resistance of HMA rehabilitated with Micro-Surfacing, *Open Journal of Civil Engineering*, Vol 8, pp.235-255
- [13] Brunet, L, J Caillard and F Mercier. 2015. Mesure de température pariétale en temps réel, *Journal International de Technologie, de l’Innovation, de la Physique, de l’Energie et de l’Environnement*, Université Clermont Auvergne, 2015, 1 (1)
- [14] Chadbourn B.A., DeSombre R.A., Newcomb D.E., Luomo J.A., Voller V.R., Timm D.H., 1998, An asphalt paving tool for adverse conditions, Report No. MN/RC 1998-18, Minnesota Department of Transportation

CHARACTERISATION AND TREATMENT OF TUNNEL BORING MUDS FOR THEIR VALORISATION IN ROAD CONSTRUCTION

A. Cabrerizo (1), D. Bulteel (1), J. Waligora (2), D. Bonneau (3) and F. Olard (2)

(1) IMT Lille Douai, Université Lille, EA 4515 LGCgE – Laboratoire de Génie Civil et Géo Environnement, département Génie Civil & Environnemental, F-59000 Lille, France.

(2) EIFFAGE Infrastructures, Direction Recherche et Innovation, 8 rue du Dauphiné, CS 74005, 69964 CORBAS Cedex France.

(3) EIFFAGE Infrastructures, Laboratoire Central Ciry, 9 route de Condé, 02220 CIRY-SALSOGNE Cedex France.

Abstract

Projects involving tunnel boring machines (TBM) are becoming more significant, both for the creation of tunnels through mountains (Saint Gothard tunnel in Switzerland, Brenner tunnel between Austria and Italy or the Lyon-Turin line) and for the creation/optimization of metro lines (Cross rail in London, Grand Paris Express project, Hyderabad in India or Riyadh in Saudi Arabia).

Such projects lead to large amounts of excavated materials (soils or muds), characterized by variable intrinsic properties and pollutants. From both economical and environmental points of view, it is necessary to valorise them, in civil engineering and in road construction for example. However, this valuation is more or less complicated due to geographical and geological factors and it is often necessary to treat these materials with cements or hydraulic binders for improving their mechanical properties.

This research focuses on an excavated mud with high water content and weak mechanical properties. A full characterisation was undertaken using several analytical techniques. Some treatments were also performed with specific cements and hydraulic binders. Results showed that it is possible, under certain conditions, to increase mechanical properties of the studied mud, allowing its valorisation.

Keywords: excavated mud, treatments, valorisation, binders

1. INTRODUCTION

Tunnel boring machine (TMB) activity generally leads to large quantities of excavated materials (several thousand tonnes) which require special management, whether for storage or recovery. These materials could be valued in civil engineering and more particularly in road construction which needs large amounts of materials [1]–[5] : sub-base, road base and base course layers, but they have to respect several geotechnical, mechanical and environmental specifications.

- The first standard is the evaluation of the material valorisation potential, in particular its classification according to the French road grading guide (GTR) [6] based on granularity and argilosity index.
- A binder treatment is often necessary to improve mechanical properties, which is the second specification. Indeed, the treated TBM mud must respect a minimal level of mechanical properties to be used in road construction. These mechanical properties are determined by compressive (R_c) and indirect tensile strength with modulus determination (R_{it}/E) [7].
- The third criterion concerns environmental properties. Leaching tests have to be first performed on the raw material to determine if it is in accordance with the regulation. If it doesn't, a cement or hydraulic binder treatment can be carried out under two conditions: first, it has to improve the mechanical properties allowing its valorisation and secondly, it has to chemically stabilise heavy metals in time [8].

This study focuses on an excavated mud coming from the construction of a tramway line in 2014 in the Paris region. This material is called Btram in this paper. The aim is to present the obtained results of characterisation and hydraulic binder treatments associated with mechanical properties. Environmental properties are not exposed in this paper, analyses are still in progress.

2. Geotechnical properties

After its excavation, raw material has to be characterised in order to determine its valorisation potential and also if any cement or hydraulic binder treatment is necessary. Thus, tests following the GTR guidebook were first carried out. Figure 1 and Figure 2 show the dry granularity (NF P94-056) for the fraction upper than $80\ \mu\text{m}$ and the laser granularity for the fraction lower than $80\ \mu\text{m}$ (NF ISO 13320-1).

Results show that Btram granularity is relatively large with a particle size up to 20 mm and with a proportion of fine particles ($\emptyset < 80\ \mu\text{m}$) of about 40% (which is also distributed with spikes measured at 1, 5, 30 and $50\ \mu\text{m}$). It appears that the studied material should not require granular correction as it has to be generally done for the valorisation of finer materials such as sediments[9]–[11].

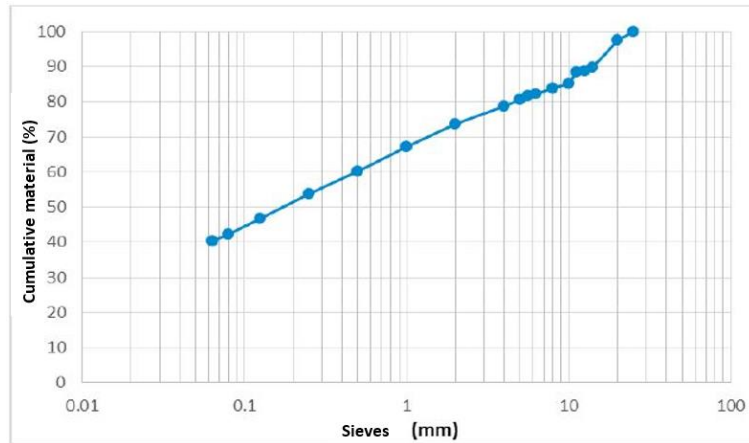


Figure 1: Btram dry particle size (fraction > 80 μm)

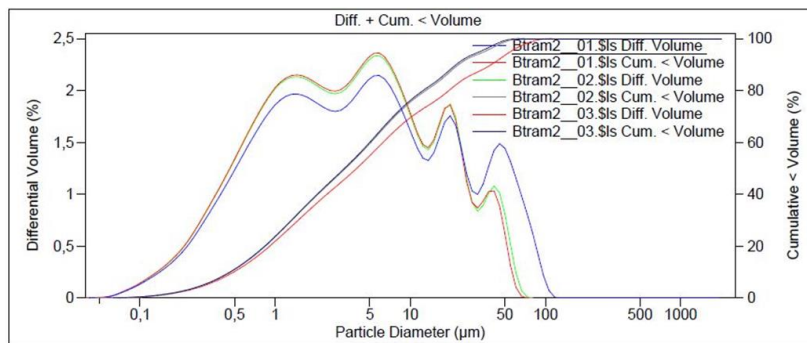


Figure 2: Btram laser particle size distribution and cumulative fraction < 80 μm

Other tests were performed to complete the characterisation: clay content, according to standard NF P 94-068 (VBs). This test quantifies the argillosity which in the case of this study is: 0.5 g/100g of analysed material. This value, associated with the granularity, allows to class the studied material as A1 according to the GTR guidebook [6] as shown in Figure 3.

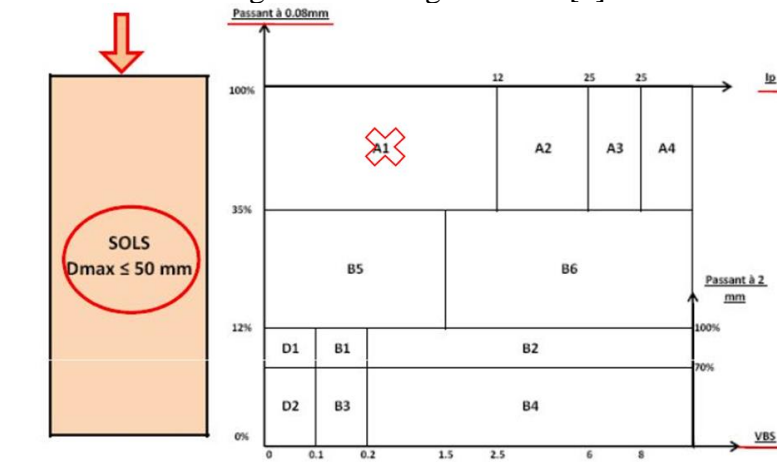


Figure 3: Btram classification according to the French GTR guidebook

The A1 classification corresponds to a fine soil, as silts or clays. Due to some difficulties to determine the plasticity index on this type of soil, the GTR classification was determined using the granularity and the VBs as allowed by the GTR guidebook.

Studied Btram is a fine material whose consistency can suddenly change with small variations in water content. This leads to modifications in its properties, showing that cement or hydraulic binder treatment can be required to stabilise and valorise it.

3. HYDRAULIC BINDER TREATMENTS AND EVALUATION OF MECHANICAL PROPERTIES

The first treatments were performed using ground granulated blast furnace (GGBF) slag-based binders rather than cement binders for interalia ecological reasons by replacing natural resources with a by-product of steel production [12] :

- A CEM III/A cement (46% of clinker, 51% of GGBF, 3% of filler + setting regulator).
- A binder containing 95 % of industrial slags ($50 \pm 4\%$ of GGBF, $40 \pm 4\%$ of blast oxygen furnace slag from Linz-Donawitz process and 5% of gypsum). This binder is named: “S binder”.

The GGBF slag is a milled material coming from the manufacturing of cast iron [13] and is composed of different oxides essentially of calcium, silicon, aluminium and magnesium [14], conferring latent hydraulic properties which can be interesting for improving mechanical properties of our material.

The CEM III/A is a cement, containing high amount of clinker whose quick hydration leads to C-S-H. These hydrates allow to rapidly obtain mechanical properties.

The S binder is a hydraulic road binder containing, in addition to GGBF slag, blast oxygen furnace (BOF) slag composed of several oxides: calcium, silicon, aluminium and magnesium. It also contains iron oxides that are not contained into GGBF slag. It is completely crystallised (the GGBF slag is amorphous) and it contains significant amount of free lime [15] which contributes to the activation of GGBF slag and the obtaining of mechanical properties.

3.1. Determination of optimum dry density and water content of treated material (Standard Proctor Optimum)

In order to determine the required parameters for making the test specimens in the laboratory (optimum dry density depending on the water content), a Standard Proctor test was performed according to NF P 94-093. It was carried out on Btram with a binder content (S binder) of 8 wt.-%. It was not necessary to perform the Proctor test with both studied binders, because their density are similar (3 Mg/m^3 for S binder and 3.1 Mg/m^3 for CEM III/A). As shown in Figure 4, the optimal obtained values under these conditions are 19.2 wt.-% for water content and 1.73 Mg/m^3 for dry density.

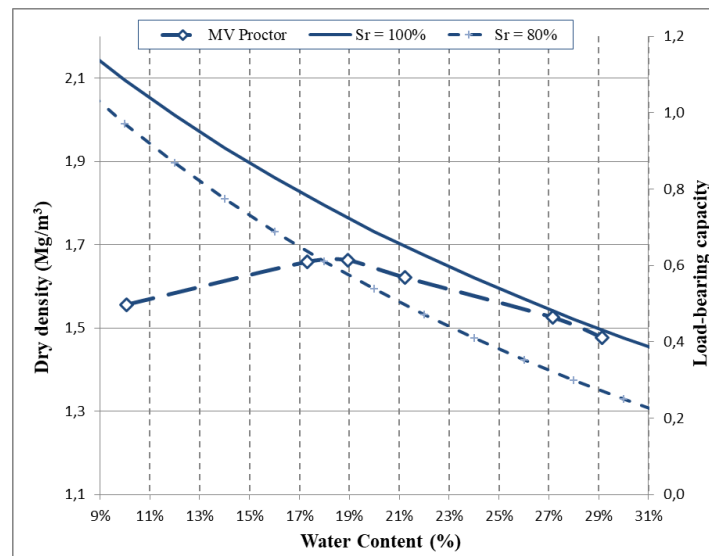


Figure 4: Standard Proctor curve for Btram treated with 8 wt.-% of S binder

The laboratory specimens were compacted to the obtained Proctor references. Both binders were used for treatment with the following contents: 6, 8 and 10 wt.-% (according to dry material). Mechanical properties were determined following two tests:

- Compressive strength tests (R_c) on $\varnothing 5 \times 10$ cm specimens with 98.5 % compactness according to standard NF EN 13286-41.
- Indirect tensile strength and elasticity modulus tests (R_{it}/E) on $\varnothing 5 \times 5$ cm specimens with 96% compactness according to standard NF EN 13286-42 and -43 (§5).

These mechanical tests are performed after several curing times (7, 14, 28 and 60 days for R_c and 7, 28, 90, 180 and 360 days for R_{it}/E) in order to determine the evolution of mechanical properties. The curing conditions are as following: specimens are stored in an air-conditioned chamber at 20°C and 90% of moisture.

3.2. Obtained results

Results obtained on Btram material treated with CEM III/A and S binder are exposed in Figure 5 and Figure 6 below.

Treatment with both binders is effective, because a good evolution is observed with curing time. 1 MPa is obtained before 7 days (depending on the binder nature and its content), allowing the treated material circulation by construction machines, except in the case of the 6% S binder treatment (7 days are required in this case). Results with CEM III/A cement are logically better in the short term. This binder contains 46% of clinker, which is quickly hydrated. However, obtained results are similar at 60 days of curing time, with an increase of 64% for the S binder and approximately 41% for the CEM III/A cement.

Mechanical properties obtained at 60 days are sufficient to allow a valorisation with compressive strengths comprised between 5 and 6.5 MPa for CEM III/A and between 3 and 5 MPa for S binder. Under these test conditions, it is possible to obtain sufficient mechanical properties at short curing time with a lower CEM III/A content. Indeed, results obtained with 6% of CEM III/A at 7 days are better to those obtained with 10% of S binder at 7 days. However, at longer curing time (90, 180 or 360 days), results obtained with CEM III/A should be weaker than those obtained with S binder because the clinker hydration will be certainly over. It will

probably not be the case with S binder mainly composed of GGBF slag, whose hydration is more progressive in time.

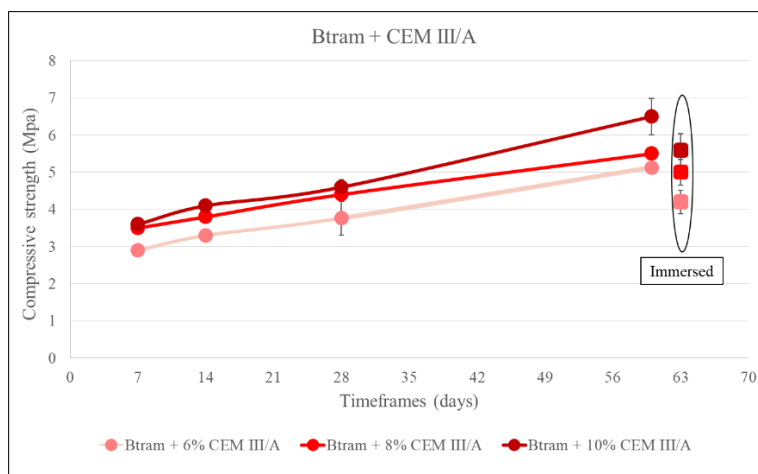


Figure 5: Compressive strength of Btram treated with CEM III/A according to curing time and content

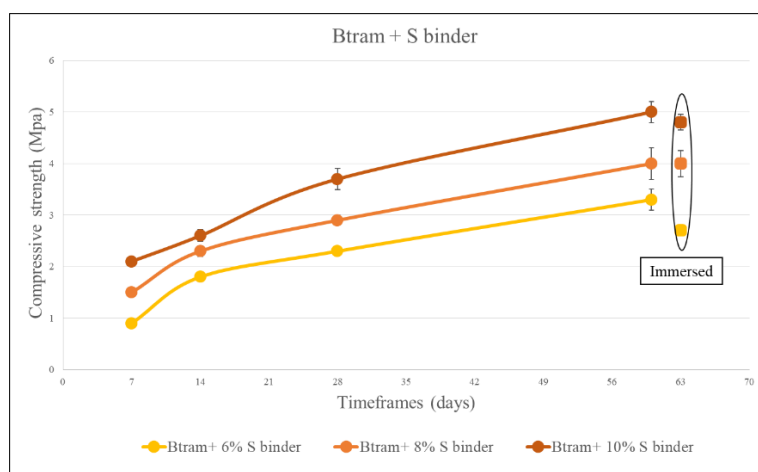


Figure 6: Compressive strength of Btram treated with S binder according to curing time and content

Another interesting result is that S binder treatment appears to give better behaviour when specimens are immersed 32 days into water. This test consists of submerging the samples in water at 20°C after 28 days of "standard" cure and then testing them at 60 days (i.e. after 32 days of immersion and noted R_{ci}). Indeed, results at 60 days with immersion show a strength loss of only 7% in the case of the S binder compared to 13% for the CEM III/A. More precisely the R_{ci60}/R_{c60} ratio for S binder formulations at 6, 8 and 10% is respectively 0.82, 1 and 0.96 against 0.84, 0.91 and 0.85 for the treatment at 6, 8 and 10% of CEM III/A. This R_{ci60}/R_{c60} ratio allows to determine the water resistance of a treated material using a classification given in the NF P 94-102-1 standard. In our case, treatments with 8 and 10% of S binder mixtures obtain the first class ($R_{ci60}/R_{c60} > 0.9$), (class 2 ($0.9 \geq R_{ci60}/R_{c60} \geq 0.8$) for the 6% assay) while CEM III/A obtains it for an 8% content (class 2 for 6 and 10%).

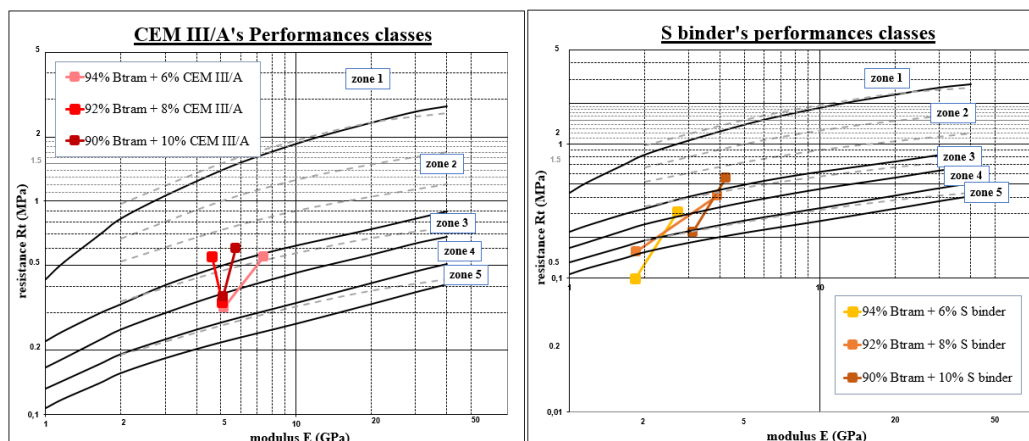


Figure 7: Tensile strength and modulus results for Btram with CEM III/A and S binder after 7 and 28 days of curing time (6, 8 and 10%)

Results of tensile strength and elasticity modulus tests are given in Figure 7. They are also interesting because they allow, according to the NF P 94-102-1 standard, to classify the treated material and to determine if its mechanical properties are sufficient to be valuable in road construction. The R_{it} obtained value is converted in tensile strength (R_t) value using the following correlation: $R_t = 0.8 \times R_{it}$. To be valorised in road construction, a treated material has to be located in zone 3 or 2. It is also better to obtain an elasticity modulus of about 10 GPa, to avoid damages with time (cracking).

After 7 days of curing time, results show insufficient mechanical properties for a valorisation in road construction: zone 4 for the CEM III/A treatment and zone 5 or less for the S binder treatment. These results can be explained by the fact that this classification is generally used at longer curing time (90 or 180 days). 7 days of curing time is not sufficient to determine if the treated material can be or not valuable in road construction.

After 28 days of curing time, mechanical properties are very interesting for both binders: mechanical zone 3 to 2 according to the content with an elasticity modulus lower than 10 GPa. These results show that our treated material can be valorised in road construction and that very good results are obtained since 28 days. It is now necessary to wait for further results at 90, 180 and 360 days of curing time.

4. CONCLUSION

Tunnel boring machines generate large amount of excavated materials that need to be finely characterised and sometime treated with cement or hydraulic binder for their valorisation. This study focused on an excavated material (mud) coming from the construction of a tramway line in 2014 in the Paris region. The first approach consisted in characterising this material at different levels, to determine if it can be valorised in road construction: geotechnical identification of the raw material, treatment with two different binders (CEM III/A and S binder) at several contents and determination of mechanical properties at different curing time.

Btram material is classified A1 according to the French GTR guidebook as a fine silty soil with low clay content, whose behaviour can be particularly sensitive to water variations. As a consequence, it requires cement or hydraulic binder treatment to be stabilised and valorised.

Obtained mechanical results on treated material are promising for both S binder and CEM III/A with classifications in zone 2 and 3 at 28 days depending on binder content. A weak

elasticity modulus (lower than 10 GPa) was obtained, that is suitable for a use in sub-base layer according to the NF EN 94-102-1 standard. It is necessary to wait for further results and the final classification of the treated material after 90 days of curing time. Mechanical tests will be also performed at 180 and 360 days of curing time. The most interesting result is that the possibility of valorisation is demonstrated since 28 days.

The main overview of this work is to study the environmental properties of the raw and treated material with the aim to chemically stabilise potential heavy metals contained into the mud using specific binders.

ACKNOWLEDGMENTS

Authors would like to thank all the staff of the EIFFAGE Infrastructures laboratory in Ciry-Salsogne - France (02220) for their valuable contribution to this work.

REFERENCES

- [1] R. Bellopede and P. Marini, "Aggregates from tunnel muck treatments. Properties and uses," *Physicochem. Probl. Miner. Process.*, **47**, (2016) 259-266.
- [2] CETU (Centre d'étude des tunnels), "Matériaux géologiques naturels excavés en travaux souterrains," (Doc. D'information, 2016).
- [3] J. Colas, "Etude de la valorisation des déblais de chantiers de tunnels riches en sulfates en granulats à béton," (Thèse Dr. Univ. Paris-Est, 2012).
- [4] C. Thalmann, C. Carron, L. Brino, and J. Burdin, "Gestion et Valorisation des Matériaux d'Excavation de Tunnels. Analyse comparative de 3 grands projets," (Communication Chambéry, 2005) 1–12.
- [5] F. Descoeurdes, A.-G. Dumont, A. Parriaux, L. Vulliet, M. Dysli, P. Robyr, M. Fontana, and G. Franciosi, "Utilisation des matériaux d'excavation de tunnels dans le domaine routier," (Etat des connaissances actuelles. Inst. des sols, roches Fond. l'Ecole Polytechnique Fédérale L, 2006).
- [6] MELT, Réalisation des remblais et des couches de forme - Guide Technique - Fascicule I Principes généraux. (2000).
- [7] D. Wang, N. E. Abriak, and R. Zentar, "Co-valorisation of Dunkirk dredged sediments and siliceous-aluminous fly ash using lime," *Road Mater. Pavement Des.*, **14** (2) (2013) 415-431.
- [8] T. Gutsalenko, A. Kiiashko, A. Darquennes, P. Seymour, L. Frouin, M. Cyr, and M. Chaouche, "Stabilization of harbor sediments contaminated with heavy metals in GGBS- based binders," (International Symposium on Sediment Management, Montreal, 2016).
- [9] M. Boutouil and L. Saussaye, "Influence de l'ajout d'un correcteur granulométrique sur les propriétés des sédiments traités aux liants hydrauliques," *Eur. J. Environ. Civ. Eng.*, **15** (2) (2011) 229-238.
- [10] Y. Liang, "Co-valorisation de sédiments et de sols fins par apport de liants et de fibres," (Thèse Dr. Univ. Caen/Basse Normandie, 2012).
- [11] F. Agostini, "Inertage et valorisation des sédiments de dragage marins," (Thèse Dr. Ec. Centrale Lille, 2006).
- [12] L. Ge, C. C. Wang, C. W. Hung, W. C. Liao, and H. Zhao, "Assessment of strength development of slag cement stabilized kaolinite," *Constr. Build. Mater.*, **184** (2018) 492–501.
- [13] Taylor H.F.W., *Cement Chemistry*, Edition 2, Thomas Telford (1997).
- [14] Glasser F.P., Chemical, mineralogical and microstructural changes occurring in hydrated slag-cement blends, *Materials Science of Concrete II*, (1991) 41-81.
- [15] J. Waligora, D. Bulteel, P. Degrugilliers, D. Damidot, J. L. Potdevin, and M. Measson, "Chemical and mineralogical characterizations of LD converter steel slags: A multi-analytical techniques approach," *Mater. Charact.*, **61** (1) (2010) 39-48.

INFLUENCE OF COARSE RECYCLED CONCRETE AGGREGATE ON THE DURABILITY OF ASPHALT MIXTURES

A. Radević (1), G. Mladenović (1), D. Jevtić (1), D. Zakić (1), M. Aškračić (1)

(1) Faculty of Civil Engineering, University of Belgrade, Serbia

Abstract

Until recently, coarse recycled concrete aggregate (RCA) has been used for the production of new concrete and soil stabilization, as well as for materials applied in road pavement construction, primarily for unbound base and sub-base layers. This paper presents the results of a study which objective was to assess the possibility of using coarse RCA in asphalt mixtures.

The experimental research, shown in this paper, included testing of four asphalt mixtures made with coarse RCA (4/22.4 mm) as a partial substitution of natural aggregate, in the amount of 0% (control mixture), 15%, 30% and 45%, by mass. All asphalt mixtures were designed for the base course.

The optimum bitumen content increased from 3.4%, for control and mixture with 15% RCA, to 3.5% for the mixtures with 30% RCA and 45% RCA. The rutting and fatigue resistance of asphalt mixtures with RCA were higher compared with the control mixture. Proportional rutting depth ranged between 3.9% and 4.8% for mixtures with RCA, while 5% was measured for the referent mixture. Estimated strain values for a lifetime of 106 load cycles increased from 124 $\mu\epsilon$, for control mixture, to 129 $\mu\epsilon$, 145.8 $\mu\epsilon$ and 137.4 $\mu\epsilon$ measured for mixtures with 15, 30 and 45% of RCA, respectively. Two out of three RCA mixtures had higher indirect tensile strength ratio, varying from +3% and +13.7% relative to the referent mixture. The results obtained by water resistance testing of mixture with 30% RCA were 4.7% lower than for the control mixture.

Keywords: asphalt, recycled concrete aggregate, rutting, fatigue, water resistance

1. INTRODUCTION

Implementation of sustainable development philosophy in civil engineering has been one of the most important topics in this area during the last decades. A huge impact that building industry has on the quality of life, as well as on the environment, challenges the scientists to discover different ways of using recycled and artificial building materials that could be implemented in common practise. Hot and cold recycling processes have already been widely acknowledged and used when asphalt rehabilitation is necessary. Another possible solution for the production of new asphalt mixtures would be the application of recycled concrete

aggregate (RCA). Most properties of RCA are the consequence of its complex structure, composed of natural aggregate grains coated with hardened cement paste [1].

RCA has been thoroughly investigated as a partial or complete replacement of natural aggregates in cementitious concrete mixtures [2, 3]. Due to the diverse nature and applications of ordinary and asphalt concrete, properties of RCA could be viewed in different light, when its usage in asphalt mixtures is concerned. For example, sharp edges of the coarse RCA grains, that can cause problems in the fresh concrete, are similar to natural crushed aggregates that are most commonly used in asphalt mixtures. On the other hand, higher porosity of these grains, due to the presence of the porous adhered mortar, may cause the increase in the optimal bitumen content (OBC) and consequently higher price of asphalt mixtures. Several authors have investigated the possibilities of application of fine, coarse or both fine and coarse RCA in asphalt mixtures, through different durability tests.

Pasandin and Perez [4] have proved that apart from increase in OBC, the use of RCA causes the decrease in effective bitumen content that can have a negative impact on the asphalt mixture properties. Absorption of bitumen in RCA grains is usually 50% lower than the water absorption of this aggregate [5]. Rafe et al. [6] have shown that the addition of fine RCA fraction results in higher values of the OBC than the addition of coarse RCA fractions.

Water resistance of asphalt mixtures with RCA aggregates has proved to be one of the weakest points of this material, since the absorption of bitumen in aggregate grains decreases the thickness of the bitumen film on the surface, which leaves more space for water passage [7-10].

Although, some of the authors conclude that the asphalt mixtures with RCA are more sensitive to permanent deformation because of the weak cement matrix [11,12], other results show that the rutting resistance increased with the higher content of coarse RCA in the mixtures [10,13,14]. When RCA originated from relatively low strength concrete, rutting deformation increased with the level of RCA replacement [15].

Only few authors investigated influence of RCA on the fatigue resistance of asphalt mixtures. Pasandin and Perez [4] showed that application of coarse RCA did not affect the fatigue resistance of asphalt mixtures. Arbani et al. [12] concluded that mixtures with coarse RCA designed for wearing course had lower fatigue resistance than the referent mixture. Wu et al. [16] tested hot asphalt mixtures with different partial replacement (20-100%) of both fine and coarse aggregate with RCA. It was concluded that the amount of RCA should be controlled, since 40% and higher quantities of RCA decreased the fatigue life of asphalt mixtures by more than 80%.

Although partial replacement of coarse natural aggregate with RCA leads to decrease in certain properties of asphalt mixtures, still most of the results comply with the conditions defined in the relevant standards and technical requirements.

2. MATERIALS AND METHODS

The tests were performed on asphalt mixtures for base course AC 22 BASE. This solution was chosen because of the potentially higher consumption of RCA compared with wearing courses, and lower bitumen content. In addition, since RCA generally possesses lower mechanical properties than the natural crushed aggregate, it is more appropriate to use it in the base courses, where they are not directly exposed to traffic loading and environmental conditions, and therefore the less strict technical requirements can be applied.

Due to the concern that RCA's lower mechanical properties would undesirably influence the performance of the asphalt mix, but also in order to avoid an excessive increase in the bitumen content, the maximum RCA amount was limited to 45%. The total of four asphalt mixtures was made: one control and three mixtures with partial replacement of coarse natural aggregate (4/22.4 mm) with RCA in amount of 15%, 30% and 45% by mass. These asphalt mixtures were labelled as E, C-15, C-30 and C-45, indicating the replacement percentage of the coarse natural aggregate by RCA. In all mixtures, the aggregate gradation was kept constant. The targeted volume of air voids was set to 5.2%. The Marshal method was adopted for the mixture design.

2.1 Materials

The RCA used in this study originated from the sub-structure of the tramway tracks consisting of cementitious concrete slabs. Although more than 30 years old, this concrete was never exposed to open ambient conditions, since it was protected by an asphalt layer. During the tramway reconstruction, the concrete core samples were taken from the structure and concrete class C35/45 was established, according to EN 206. After the crushing, the obtained RCA consisted of 98% of old concrete, 1.2% of asphalt, and 0.8% of brick material. The maximum aggregate size of 22.4 mm was adopted for all asphalt mixtures. Crushed limestone was used as the natural aggregate. Grading curves of natural and recycled aggregates are presented in Figure 1. The mineral mixture contained 5% of filler, 41% of 0/4 mm particles, 15% of 4/8 mm particles, 24% of 8/16 mm particles, and 15% of 16/22.4 mm particles. The main aggregate properties are shown in Table 1. In all mixtures, limestone filler and bitumen B 50/70 were used. The lower density of RCA is a consequence of the presence of adhered cementitious mortar. Also, RCA is characterized by increased water absorption as a result of the higher porosity of this mortar. Decreased resistance to crushing, expressed by a lower value of the Los Angeles (LA) coefficient, points to weaker mechanical properties of RCA. However, the equivalent value of LA for the mineral mixture, even with a high RCA content, is still lower than 30, which satisfies the technical requirements for bituminous base layers for medium traffic load [17].

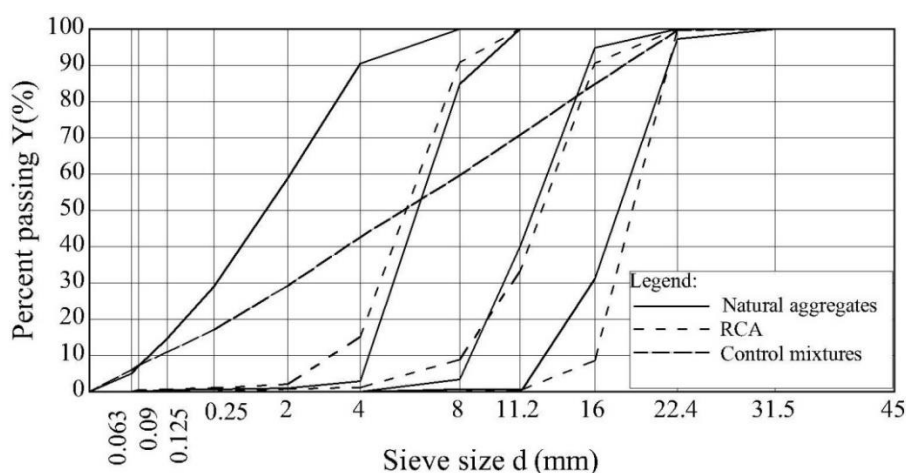


Figure 1: Sieve analysis of aggregates

Table 1: Physical-mechanical properties of aggregates

Test	Standard	RCA	Natural
Apparent specific gravity (kg/m ³)	EN 1097-6	2667	2743
Bulk specific gravity SSD (kg/m ³)		2532	2731
Bulk specific gravity (kg/m ³)		2450	2724
Water absorption (%)		3.2	0.2
Los Angeles abrasion (%)	EN 1097-2	31.5	26.1

2.2 Methods

The optimum bitumen content (OBC) for each mixture was obtained using the Marshall procedure at a temperature of 150°C and with compaction energy of two times 50 blows. The volumetric properties of mixtures are presented in Table 2.

Table 2: Properties of asphalt mixtures

Mixture type	OBC	Air voids	Voids in the mineral aggregate	Voids filled with bitumen	Density	Max density
	(%)	(%)	(%)	(%)	(kg/m ³)	(kg/m ³)
E	3.4	5.2	13.5	61.0	2419	2553
C-15	3.4	5.0	13.2	61.9	2412	2540
C-30	3.5	5.6	14.0	59.6	2388	2531
C-45	3.5	5.4	13.8	60.6	2388	2525

Water resistance of asphalt mixtures was tested by measuring indirect tensile strength (ITS) of dry and wet samples, in accordance to EN 12697-12, method A. Six Marshall cylindrical samples were prepared for each mixture and separated into two groups. Each group contained three samples with similar densities. The first group was kept in dry conditions, at the room temperature of 20°C. The second group was placed into water at the pressure of 6.7 kPa for 30 min, and afterwards conditioned in water at a temperature of 40°C during next 72 hours. Before testing, the samples were kept at 25°C for 2 h. ITS testing was conducted on the universal compression machine UTM-25, according to EN 12697-23.

Testing of resistance to rutting was performed using the small wheel tracking device in air (Figure 2), at a temperature of 60°C, after 10,000 cycles (20,000 passes), all in accordance with EN 12697-22, Annex B. In order to simulate the conditions on the asphalt plant and in situ, the mixture was conditioned before compaction at a temperature of 135°C for 4 h. For each asphalt mixture, two slabs 320×260×70 mm were compacted using a segment compactor, according to EN 12697-33.

The testing of the fatigue was performed using a four point bending beam test, in accordance with EN 12697-24, Annex D.

Fatigue testing was performed on 50×60×400 mm beams under controlled strain with a frequency of 10 Hz, with no relaxation period. Before loading, the specimens were cured at a temperature of 20°C for 2 h.

Prismatic specimens from each mixture were divided into three series. Load amplitudes were defined for each mixture and group of specimens separately, so that fatigue failure occurs in the range of 10⁴ to 2×10⁶ load cycles.

Under these conditions, the failure criterion was taken to be the number of load cycles after which the specimen's initial stiffness decreased by 50%. The initial stiffness was taken to be the specimen's stiffness after 100 load cycles.

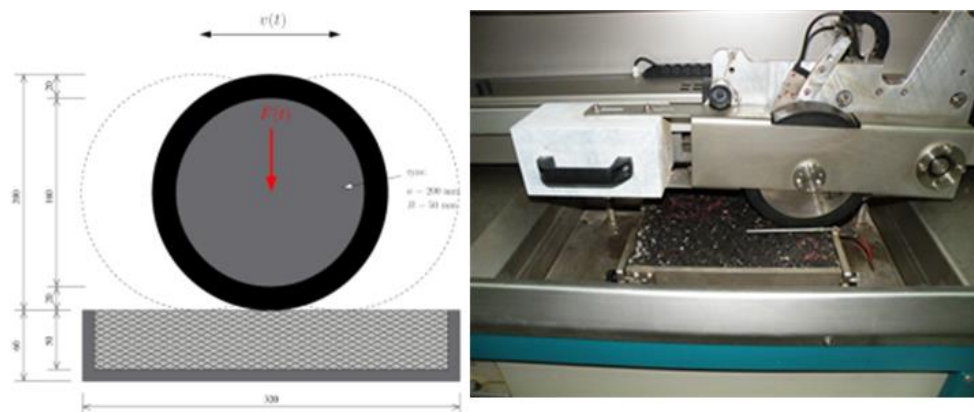


Figure 2: Rutting resistance testing

3. RESULTS AND DISCUSSION

3.1 Water resistance test

The indirect tensile strength (ITS) was calculated using the following expression:

$$ITS = \frac{2 \cdot P}{\pi \cdot h \cdot d_s} \quad (1)$$

where: P is the maximum force (kN), h - sample height (mm), d_s - sample diameter (mm).

Indirect tensile strength ratio (ITSR) that represents the measure of water resistance of asphalt mixtures is defined as a ratio between the measured indirect tensile strengths of samples conditioned in wet and dry environment. The average values of all indirect tensile strengths of dry (ITS_{dry}) and wet (ITS_{wet}) samples for each of the tested mixtures, together with their ratio (ITSR), are presented in Table 3.

Table 3: Average values of ITS and ITSR

Mix	ITS _{dry} (kPa)	ITS _{wet} (kPa)	ITSR (%)
E	937.2	692.9	73.9
C-15	771.5	676.0	87.6
C-30	981.1	679.1	69.2
C-45	879.9	676.3	76.9

As it can be seen, ITSR was higher for two out of three mixtures with RCA when compared to the control mixture. These results are the consequence of the better interaction and higher friction between the RCA particles, due to their rough surface and sharper edges.

3.3 Rutting resistance determination

The proportional rut depth, as a function of the number of loading cycles, is shown in Figure 3. The results obtained on all RCA mixtures satisfy the technical requirements [17], as the measured rut depth amounted to 5% (E), 4.8% (C-15), 3.9% (C-30) and 4.6% (C-45), which are significantly lower values than the maximum allowed 7%. It can be concluded that the structure and texture of RCA, i.e. its rough surfaces and sharp edges, which are the result of being crushed multiple times, increased the specific surface area and friction between aggregate grains and helped to improve resistance to permanent deformation.

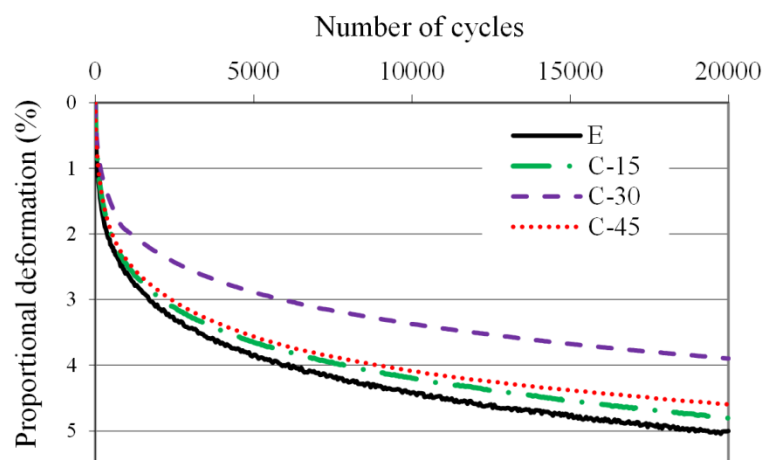


Figure 3: Proportional rut depth vs number of loading cycles [18]

3.4 Fatigue test

In order to evaluate the fatigue resistance of asphalt mixtures, the following model was adopted:

$$N_f = K_1 \cdot \left(\frac{1}{\varepsilon_0}\right)^{K_2} \quad (2)$$

$$\ln(N_f) = \ln(K_1) - K_2 \cdot \ln(\varepsilon_0) \quad (3)$$

where: ε_0 is the tensile strain at the bottom surface of the asphalt layer ($\mu\text{m}/\text{m}$); N_f is the number of load cycles; K_1 and K_2 are experimentally obtained coefficients.

By analysing the experimental results, the fatigue functions for all asphalt mixtures were defined, according to formula (3). These functions, together with the linear regression coefficients, correlation coefficients and predicted strain values for a 10^6 load cycle service life, are given on Figure 4.

If we apply the obtained functions, the calculated failure strain of the control mixture after a million cycles ($\varepsilon = 124 \mu\text{m}/\text{m}$), will be reached by mixture C-15, C-30 and C-45 after 1.2, 2.8 and 2.0 times larger number of axial loads, respectively.

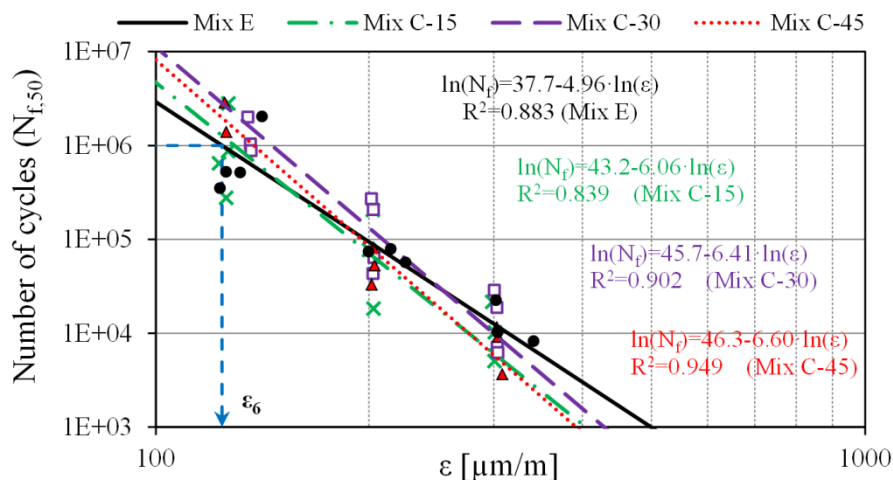


Figure 4: Fatigue performance of asphalt mixtures

Better fatigue performance of RCA mixtures could be partly explained by the higher OBC value compared to the control mixture. However, the increase in bitumen content was not substantial, since the OBC value in RCA mixtures varied between 3.4% and 3.5%, which is similar to 3.4% in the control mixture. Thus, it can be assumed that the more favourable structure and texture of RCA had again the key role in superior performance of RCA mixtures in comparison to the control mixture.

CONCLUSIONS

The main objective of the research was to evaluate the possible application of coarse RCA in asphalt mixtures for base course, to test the performance and durability of these mixtures, as well as to assess their conformity with the relevant technical requirements. Based on the presented results, the following conclusions can be drawn:

- When compared to the natural crushed aggregate, RCA has lower density and higher water absorption, due to the presence of porous adhered cementitious mortar.
- Differences between water resistance of RCA mixtures and the control mixture ranged between -2.4% and +1.7% which is negligible, regarding the potential application in asphalt mixtures; as the Technical requirements [17] do not prescribe minimal conditions for water resistance of asphalt mixtures, it can be concluded that coarse natural aggregate can be replaced with RCA in quantities up to 45%.
- Considering the fact that all asphalt mixtures containing coarse RCA showed increased resistance to permanent deformation, it can be concluded that, from this aspect, the quantity of RCA could be even higher than 45%.
- The results of fatigue test showed superior performance of RCA mixtures compared to the control mixture. These results are very encouraging, although additional research has to be made in order to establish more reliable correlation between the amount of used RCA and the fatigue performance of asphalt mixtures.

ACKNOWLEDGEMENTS

The presented study is a part of the research financially supported by the Ministry of Education, Science, and Technological Development of the Republic of Serbia under the research project TR 36048: "Research on condition assessment and improvement methods of civil engineering structures in view of their serviceability, load-bearing capacity, cost effectiveness and maintenance" and TR 36017: "Utilization of by-products and recycled waste materials in concrete composites in the scope of sustainable construction development in Serbia: investigation and environmental assessment of possible applications".

REFERENCES

- [1] Tam, V. W., Tam, C. M., Le, K. N., 'Removal of cement mortar remains from recycled aggregate using pre-soaking approaches', *Resoru. Conserv. Recy.* **50** (1), (2007) 82–101.
- [2] Oikonomou, N.D., 'Recycled concrete aggregates', *Cem. Concr. Comp.*, **27** (2005) 315-318.
- [3] Pacheco-Torgal, F., Tam, V.W., Labrincha, J., De Brito, J., 'Handbook of recycled concrete and demolition waste', *Elsevier* (2013).
- [4] Pasandín, A.R., Pérez, I., 'Laboratory evaluation of hot-mix asphalt containing construction and demolition waste', *Constr. Build. Mater.* **43** (2013) 497–505.
- [5] Atkins H.N., 'Highway materials, soils, and concretes', 3rd editions, (1997) ISBN 0-13-212862-4.
- [6] Rafi, M. M., Qadir, A. & Siddiqui, S. H., 'Experimental testing of hot mix asphalt mixture made of recycled aggregates', *Waste Manage. Res. : the journal of the International Solid Wastes and Public Cleansing Association, ISWA* **29** (12), (2011) 1316–26.
- [7] Paravithana, S. , Mohajerani, A., 'Effects of recycled concrete aggregates on properties of asphalt concrete', *Resoru. Conserv. Recy.*, **48** (1) (2006) 1–12.
- [8] Perez, I., Toledano, M., Gallego, J., Taibo, J., 'Mechanical properties of hot mix asphalt made with recycled aggregates from reclaimed construction and demolition debris' *Materiales de Construcción* **57** (285) (2007) 17-29.
- [9] Mills-Beale, J., & You, Z., 'The mechanical properties of asphalt mixtures with Recycled Concrete Aggregates', *Constr. Build. Mater.*, **24** (3) (2010) 230–235.
- [10] Wu, S., Yhong, J., Zhu, J. & Wang, D., 'Influence of demolition waste used as recycled aggregate on performance of asphalt mixture', *Road Mater. Pavement*, **14** (3) (2013) 679–688.
- [11] Pérez, I., Pasandín, A. R., Medina, L., 'Hot mix asphalt using C&D waste as coarse aggregates' *Mater. Des.* **36** (2012) 840–846.
- [12] Arabani, M., Moghadas Nejad, F., Azarhoosh, A. R., 'Laboratory evaluation of recycled waste concrete into asphalt mixtures', *Int. J. Pavement Eng*, **14** (6) (2013) 531–539.
- [13] Shen, D., Du, J., 'Application of Gray Relational Analysis to Evaluate HMA with Reclaimed Building Materials' *J. Mater. Civ. Eng.* (2005) 400–406.
- [14] Zhu, J., Wu, S., Zhong, J., Wang, D., Investigation of asphalt mixture containing demolition waste obtained from earthquake-damaged buildings. *Constr. Build. Mater.* **29** (2012) 466–475.
- [15] Zhang Z., Wang K., Liu H., Deng Z., 'Key performance properties of asphalt mixtures with recycled concrete aggregate from low strength concrete', *Constr Build Mater* **126** (2016) 711-719.
- [16] Wu S., Muhunthan B., Wen H., 'Investigation of effectiveness of prediction of fatigue life for hot mix asphalt blended with recycled concrete aggregate using monotonic fracture testing', *Constr Build Mater* **131** (2017) 50–56.
- [17] Technical requirements for road construction in the Republic of Serbia, JP 'Putevi Srbije' (2012).
- [18] Radević A., Đureković A., Zakić D., Mladenović G., 'Effects of recycled concrete aggregate on stiffness and rutting resistance of asphalt concrete', *Constr. Build. Mater.* **136** (2017) 386–393.

STONE MASTIC ASPHALT REINFORCED BY VEGETABLE YARNS

Peter Gallo (1), Jan Valentin (1)

(1) Czech Technical University in Prague, Faculty of Civil Engineering, Czech Republic

Abstract

Using materials from renewable sources in everyday life is a good way to ensure sustainable development. However, such approach is not common in road construction industry, maybe due to the underestimation of potential renewable materials can have. This paper aims to explore the possibility of using more of these materials. The objective of research done so far was to examine the effect of using vegetable fibres/yarns as reinforcement in asphalt mixtures. Two types of flax yarns and one hemp yarn were chosen for testing in the stone mastic asphalt (SMA) mixture. Referential (control) asphalt mixture was designed and prepared with standard cellulose fibres to provide a better comparison. As binder a regular polymer modified binder 45/80-65 was used. Fibre content was 0.1 %, 0.3 % and 0.6 % by mass of mixture and length of fibre element was 10-20 mm. The chosen characteristics were stiffness modulus, moisture susceptibility (by indirect tensile strength according to EN 12697-12), crack propagation resistance, resistance to permanent deformation and flexural strength test at 0 °C. Experimental results showed improvement in stiffness, indirect tensile strength and good resistance to permanent deformation of mixture variants containing vegetable fibres. Results prove that vegetable fibres can be a perspective and simple way, within the policy of sustainable development, to improve the properties of the bitumen mixtures.

Keywords: reinforcement; stone mastic asphalt; fibres; yarns; permanent deformation

1. INTRODUCTION

In asphalt mixture of stone mastic asphalt (SMA) type, cellulose fibres are used for a few decades, usually in the form of pellets. Nowadays, cellulose pellets are made almost exclusively from recycled paper. However, their function in the asphalt mixture has limits caused by the structure of cellulose fibres. Therefore, they have only a stabilizing (avoidance of bitumen drainage) function in the mixture. This paper focuses on verification whether it is possible to replace cellulose fibres by other fibres from renewable sources, which would provide additional function, not only the bitumen drainage prevention. After previous research, hemp and flax fibres in yarn form were selected.

Fibres have been used in asphalt mixtures for several decades, so their use is generally not a new technical topic.

The use of fibres in asphalt mixtures dates back many decades to the past, perhaps even further. Button and Epps (1981) claim that the first use of fibres in asphalt was the use of rocks in building plans from ancient Egypt [1]. In the modern pavement design the re-introduction of fibres might be related to asphalt concrete reinforcement done in the 60s and 70s of last century e.g. in France using asbestos fibres. Later the use of fibres was closely linked with the development of SMA mixtures.

Nowadays, the fibres in asphalt mixtures can essentially have two basic effects:

- stabilization - in mixtures with higher binder contents and gap-graded curve,
- reinforcement - in mixtures that require increased resistance to crack propagation and permanent deformation.

1.1 Reinforcing fibres

Fibres providing a reinforcing function in the asphalt mixture must provide high tensile strength to transfer tensile forces generated in pavement layers. Thus, this group includes fibres with high tensile strength and high modulus of elasticity. Theoretically, they can be used in any type of asphalt mix and pavement structural layer. However, the greatest practical application can be found in the binder and base courses.

In the past, variety of fibre materials were used as reinforcing fibres in asphalt mixtures, such as steel, basalt, fiberglass, synthetic polymers (PE, PP, aramid) or carbon [1] [2].

1.2 Stabilizing fibres

The stabilizing effect on the mixture means, that a fibre can perfectly bond bituminous binder on its surface or in inner structure and it is able to maintain the binder even at a lower viscosity, i.e. at a higher operation temperature of 50 °C and more. Fibres with stabilizing effect are used in asphalt mixtures with a higher bitumen content, where as a representative might be named SMA foremost.

For this purpose, cellulose fibres with a diameter of about 0.5 mm are usually dosed in form of pellets. Uneven surface and internal cavities of the fibre are predisposed to the purpose of stabilizing the asphalt mixture. The advantage is also their low price and production by recycling of old paper or other cellulose products. The disadvantage is their practically nil tensile strength.

2. FIBRES WITH COMBINED EFFECT

Some fibres used in asphalt mixtures may also have a combined effect due to their structure or used material. They must be able to secure a well bond between the bitumen and fine particles within the aggregate skeleton and at the same time they should have good tensile strength or tensile modulus. Such fibres include usually a special type of polyamide and polyester hollow fibres with an irregular cross-section [3].

Natural materials from renewable sources offer the possibility to use different vegetable fibres, whose tensile strength is further increased by threading individual filaments into yarns. Yarns are not only stronger in tensile strength than the fibres themselves (with the same cross-sectional area), they also provide a considerably better workability as they can be precisely cut to the desired length.

For their properties, sisal, flax and hemp fibres are the most suitable for use in asphalt mixtures. The results of tests in [4] [5] suggest that they could be applied in asphalt pavements in the future.

3. RESEARCH RESULTS

To determine the effect of vegetable yarns on selected functional and empirical properties in an asphalt mixture, a typical SMA 11 S mix for superior surface pavement layers was selected in accordance with the Czech technical standard ČSN EN 13108-5:2016, in which following vegetable yarns were used. The length of yarn elements was 10-20 mm:

- Hemp yarn with fineness of 100x3 g/km (identified as K100x3 whereas the fineness is also known as “tex”),
- Flax yarn 500 g/km (identified as L500),
- Flax yarn 105x4 g/km (identified as L105x4).

Yarn cutting was done under improvised laboratory conditions using a regular paper cutter, so the scatter of length of the elements is quite large. The yarn content was 0.1%, 0.3% and 0.6% by weight of the blend. To compare the results, identical reference mixtures were designed and mixed containing standard cellulose pellets (known by their commercial trade S-CEL 7G®). The binder used was a polymer modified bitumen 45/80-65. The compaction temperature was 160 °C, which causes a high thermal load on vegetable fibres. All mixtures have been manufactured and tested in accordance with the Czech national specifications given in the standard ČSN EN 13108-5:2016.

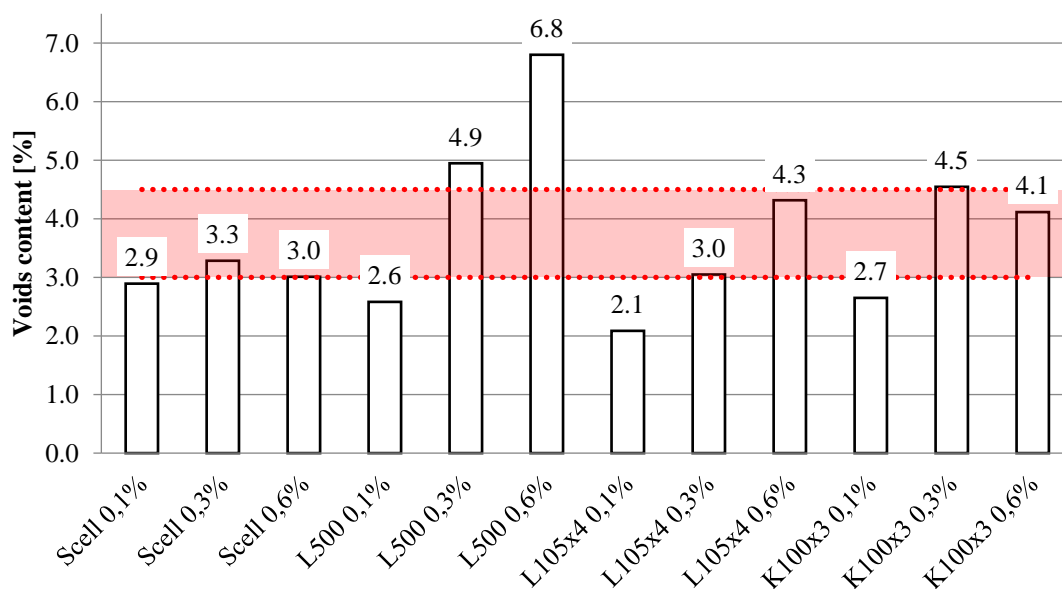


Figure 1: Voids content of tested mixtures

The red area defines minimum and maximum values for voids content according to ČSN EN 13108-5:2008. *Figure 1* shows that the defined interval of 3.0-4.5% has not been fulfilled by 6 mixtures. Four of them are mixtures with a fibre content of 0.1%. The compaction of the mixtures containing L500 fibre was particularly challenging as this yarn absorbed the bitumen

very well. Rather rigid 3D structure of coated fibres was formed as result, which caused compaction problems. The results indicate that without further treatment of the yarns, their higher proportion in the mixture will always mean the need for slightly increased binder dosage.

3.1 Water susceptibility

This test was performed in accordance with the standard ČSN EN 12697-12, the tensile strength was determined according to ČSN EN 12697-23. The effect of water has been shown in mixtures with higher yarn content. In contrast, indirect tensile strength ratio (ITSR) values reached more than 90 % in case of designed reference mixtures.

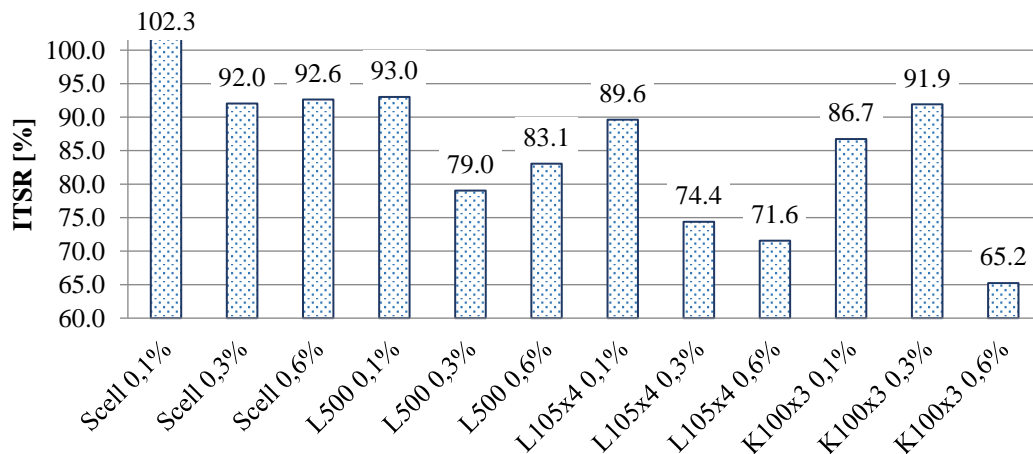


Figure 1: ITSR results of tested mixtures

The results of water susceptibility clearly show the differences in the behaviour of cellulose fibres and vegetable yarns in asphalt mixtures. Fine and short cellulose fibres are relatively well mixed in the mixture to form a mastic. Yarn elements in the contrary are 10 to 20 times longer, therefore there is an increased risk of water penetrating the asphalt mixture. However, absolute values of indirect tensile strength show a slightly different perspective and the vegetable yarns have shown the potential of their reinforcing function.

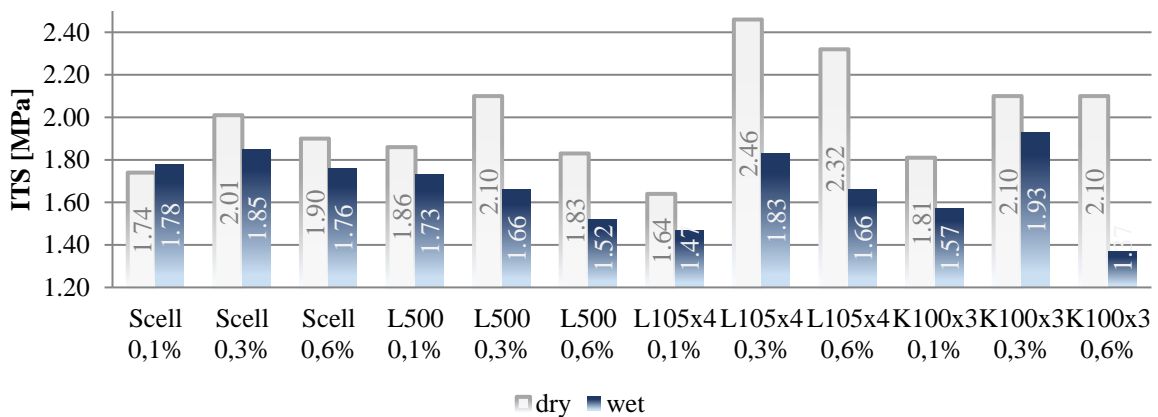


Figure 2: ITS results of tested mixtures

3.2 Stiffness modulus

The stiffness modulus was tested by a non-destructive IT-CY method (repetitive indirect tensile stress test on cylindrical test specimens) according to the standard ČSN EN 12697-26.

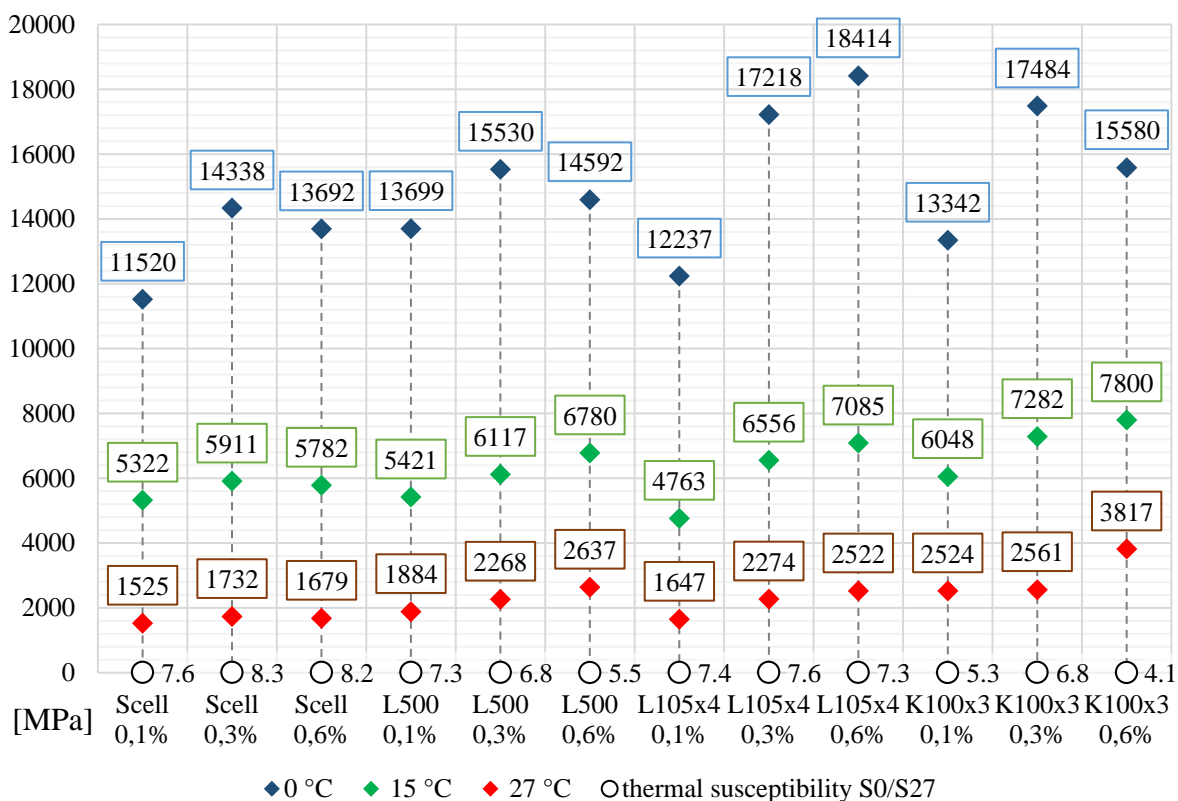


Figure 3: Stiffness modulus determined at 0 °C, 15 °C and 27 °C

On average, the stiffness modulus values of the mix variants containing yarns were greater than those of the reference mixtures. A significant increase was recorded mainly at 0 °C. Interesting are the values of mixtures with a fibre content of 0.6%. At elevated temperatures they have reached generally the highest values, but at 0 °C the stiffness modulus is smaller than in case of mixtures with lower fibre content mixtures. At 27 °C, mix variants containing yarns have usually better results than comparable control mixtures.

3.3 Crack propagation resistance

This test was carried out according to ČSN EN 12697-44, with a continuous recording of force and deformation, which also allowed fracture energy to be calculated. The standard procedure was modified based on the long-term experience at the Czech Technical University in Prague. The test specimens are compacted by Marshall compactor and not using gyratory compactor. Their diameter is 101±1 mm and not 150±1 mm as defined in the standard. Because of calculating not only fracture toughness but also fracture energy the loading rate was reduced from 5.0 mm/min (as defined in the standard) to 2.5 mm/min. The lower loading rate allows to capture more single point data from which the load-displacement curve can be more precisely depicted. A total fracture energy during the test was calculated until the loading force value

dropped to 0.30 kN on decreasing branch of the curve. For providing better understanding of cracking potential of asphalt mixtures containing fibers or yarns the test temperatures were 0 °C and -10 °C.

Achieved fracture toughness values are surprising in some mixtures. The L500 mixture with 0.1% yarn reached the best results from the L500 series and vice versa, the K100x3 mixture with 0.3% yarn reached the worst results in the K100x3 series, which do not completely match the results of the stiffness modulus. Of course, doing such comparison is difficult and in terms of mechanics not fully correct since stiffness test is run in linear viscoelastic region whereas the crack propagation test not. From fracture energy point of view, it has been confirmed that at -10 °C there is often a brittle fracture failure, as can be observed with all the mixtures. It can also be argued that asphalt mixtures containing hemp yarn were more brittle at both temperatures than other tested mixtures.

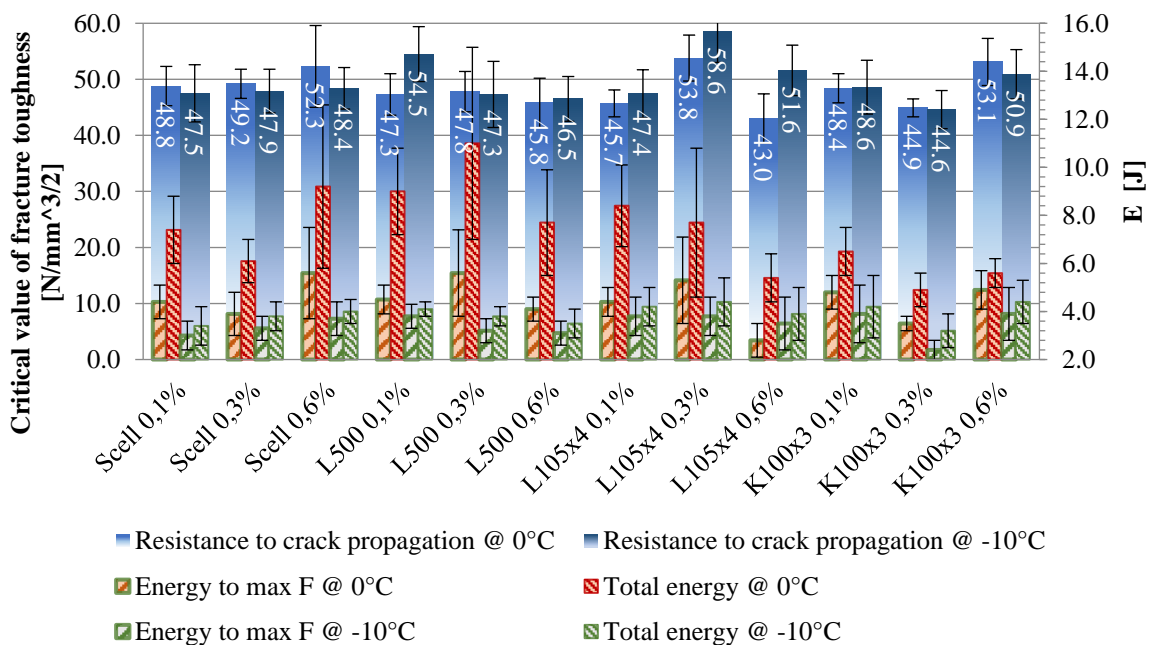


Figure 4: Critical value of fracture toughness and fracture energy at 0 °C and -10 °C

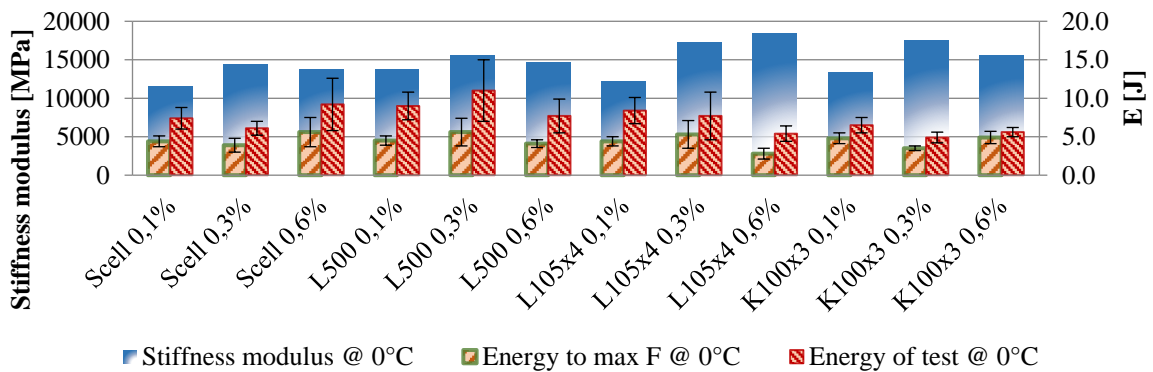


Figure 5: Comparison of stiffness and fracture energy at 0 °C

3.4 Resistance to permanent deformation

Only mix variants containing 0.3% fibres or yarns were tested by this test. Asphalt mix testing slabs with 40 mm thickness and 320x260 mm base dimensions were used for resistance to permanent deformation (rutting) test. Test was conducted in air-bath at 50 °C in a small testing device according to ČSN EN 12697-22. Key characteristics which are followed based on the test data were the proportional rut depth (PRD_{AIR}) and wheel tracking slope (WTS_{AIR}).

Table 1: Densities of slabs and resistance to permanent deformation characteristics

Mixture	Thickness [mm]	Bulk density [g.cm ⁻³]	Degree of compaction [%]	Rut after 10 000 cycles [mm]	WTS_{AIR} [mm/10 ³ cycles]	PRD_{AIR} [%]
SMA 11S PMB, Scell 0,3%	40,51	2,377	100,9	1,12	0,018	2,5
SMA 11S PMB, L500 0,3%	41,20	2,336	100,5	1,08	0,021	2,4
SMA 11S PMB, L105x4 0,3%	40,49	2,374	100,8	1,06	0,018	2,4
SMA 11S PMB, K100x3 0,3%	40,93	2,358	100,8	1,08	0,016	2,4

Results showed only small differences in the performance parameters when comparing control mix and mixtures with yarns. All mixtures met the requirements for maximum proportional rut depth (max. 0,07 mm/10³cycles) and for wheel tracking slope requirements (max. 5 %) as set by the product standard ČSN EN 13108-5:2008 and showed very good resistance to permanent deformation.

3.5 Flexural strength (3-point bending beam test)

Flexural strength was tested on beams at 0 °C and in accordance with the technical specifications of the Ministry of Transportation, TP 151. This test and resulting characteristic of flexural strength and/or relaxation ability of the mixture is mandatory only for high modulus asphalt concrete. Because of its simplicity and data collection done for several years by the Czech Technical University in Prague the test is applied on other asphalt mixtures as well. Force and deformation were continuously recorded similarly to crack propagation test, so that energy to maximum force could be calculated. The loading rate in case of this test is defined by the specifications with a value of 1,25 mm/min.

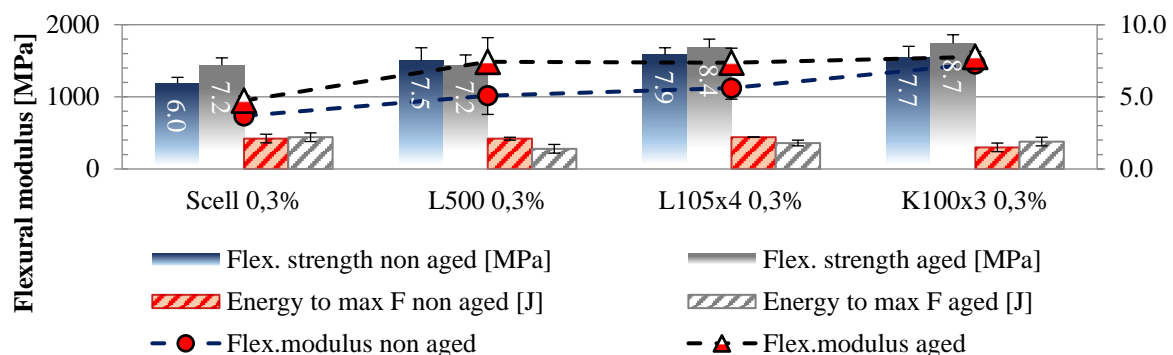


Figure 6: Flexural strength at 0 °C

Mixtures with yarns reached higher values of flexural strength and modulus than control mix values. Difference in energy was negligible, although referential mixture achieved highest values.

4. CONCLUSION

The world trend in the use of renewable materials is relentless and it also begins to be pursued in such a conservative sector as road construction is. Until now, many materials from natural renewable resources have not been used in this sector. However, with respect to the future and the necessity to keep sustainability as an important factor, it is necessary to think critically and try other, unconventional approaches as well. This was proven by this paper and many research reports published before.

Vegetable yarn mixtures gave good results following the results of selected functional (performance-based) characteristics and have demonstrated their potential for application in asphalt mixtures. Results showed their capabilities as a fiber additive with a combined effect, both with a reinforcing and stabilizing function.

In the future, research needs to be focused on this topic and other so far not analyzed effects or aspects, such as the influence of fiber length on the resulting properties, or the maximum reduction in thermal degradation, which makes vegetable fibers weaker in tensile strength. It should also be noted that reinforcing fibers find greater application in the binder and base asphalt courses. Further research will be undertaken in this direction and in terms of testing will be necessarily supplemented by fatigue assessments.

ACKNOWLEDGEMENTS

This paper was supported by the project No. TE01020168 (competence centre CESTI) within the funding scheme of the Technology Agency of Czech Republic

REFERENCES

- [1] MCDANIEL, Rebecca S. *Fiber additives in asphalt mixtures*. 1. Washington, DC: Transportation Research Board of the National Academies, 2015, pages cm. ISBN 9780309271776.
- [2] MOROVA, Nihat. Investigation of usability of basalt fibers in hot mix asphalt concrete. *Construction and Building Materials*. **2013**(47), 175-180. DOI: <https://doi.org/10.1016/j.conbuildmat.2013.04.048>. ISSN 0950-0618.
- [3] *Asphalt mixture modified with polyester and polyamide fiber possessing irregular cross section and its prepn.* b.r. CN1526767 Patent.
- [4] SHANBARA, Hayder Kamil, Felicite RUDDOCK a William ATHERTON. A laboratory study of high-performance cold mix asphalt mixtures reinforced with natural and synthetic fibres. *Construction and Building Materials*. **2018**(172), 166-175. DOI: <https://doi.org/10.1016/j.conbuildmat.2018.03.252>. ISSN 0950-0618.
- [5] RAMALINGAM, S., R. MURUGASAN a M.N. NAGABHUSHANA. Laboratory performance evaluation of environmentally sustainable sisal fibre reinforced bituminous mixes. *Construction and Building Materials*. **2017**(148), 22-29. DOI: <https://doi.org/10.1016/j.conbuildmat.2017.05.006>. ISSN 0950-0618.

STRENGTH MECHANISM AND IMPROVEMENT METHODS OF CEMENT BITUMEN EMULSION MIXTURE

Jian Ouyang, Wen Xu, and Lijun Hu

School of Transportation and Logistics, Dalian University of Technology, Dalian, China

Abstract

To increase the strength of CBEM, the voids content, strength and microstructure of CBEM were firstly studied to find the deficiency of CBEM, and then methods were proposed to overcome the deficiency of CBEM. Results indicates that CBEM at the maximum strength has much lower water content than that at the minimum voids content. This is because the strength of CBEM is not only dependent on the voids content of CBEM, but also it is related to the microstructure of cement bitumen emulsion (CBE) paste and the interface between CBE paste and aggregate. Low water content can help to form a dense microstructure of CBE paste, which is beneficial to the strength of CBEM. However, CBE paste has a poor bonding interface with aggregate at low water content. The addition of superplasticizer and wetting agent (JFC, a fatty alcohol–polyoxyethylene ether) can efficiently improve the bonding interface between CBE paste and aggregate and greatly increase the strength of CBEM. The failure face of CBEM can be changed from “adhesive failure” to “cohesive failure” and “fine aggregate fracture” when superplasticizer and JFC are added. The maximum indirect tensile strength can increase by 21.5% and 29.1% for CBEM with superplasticizer and CBEM with superplasticizer and JFC, respectively.

Keywords: Cement bitumen emulsion mixture; Indirect tensile strength; Interface; Superplasticizer.

1. INTRODUCTION

Cement bitumen emulsion mixture has been gained increasing interest in pavement engineering in recent year due to its low energy consumption and carbon emission compared to conventional hot mix asphalt (HMA) [1]. Meanwhile, CBEM has a higher rutting resistance and lower temperature sensitivity than HMA due to the effect of cement hydration [2, 3]. It is believed that CBEM can be a promising pavement material. However, the application range of CBEM is frequently limited to base and sub-base layers in high-grade road when it is used as a structural layer material. To be a structural layer material, CBEM should firstly have suitable mechanical properties. Modulus and indirect tensile strength (ITS) are two parameters of the mechanical properties of bitumen mixture in pavement design. Compared to HMA, CBEM can have higher modulus when cement content is more than 1.5% because of cement hydrates [2,

3]. However, the strength of CBEM is much lower than that of HMA. The indirect tensile strength of CBEM tested is below 0.6Mpa at ambient temperature in most references [4-7]. The low strength greatly limits the application areas of CBEM.

Factors influencing the strength of CBEM was extensively studied in the past. Generally, the strength of CBEM highly depends on cement hydration degree and the breaking of bitumen emulsion. Low curing humidity, high curing temperature and rapid-hardening cement can accelerate the strength development of CBEM [5, 7-9]. However, the long-term strength of CBEM is little improved by these methods. The strength of CBEM still remains unexplored.

In general, low strength is a weakness of CBEM. In order to efficiently increase the strength of CBEM, the strength mechanism of CBEM should be studied to find and overcome its deficiency. Therefore, effect of water content on the volumetric properties, strength and microstructure of CBEM were studied to find the deficiency of CBEM in strength. Then, efficient methods were proposed to increase the strength of CBEM and the corresponding mechanism was discussed.

2. EXPERIMENTAL PROGRAM

2.1 Materials and specimens preparation

Slow setting cationic bitumen emulsion, Portland ordinary cement P.O42.5, basalt aggregate, crushed sand and limestone powder were employed to fabricate CBEM. The solid content of bitumen emulsion was 63.2%. A uniform dense aggregate gradation for AC-13 was used in the study, which is shown in Figure 1. According to the study of Xiao et al. [10], CBEM has high strength and performances in this aggregate gradation. The total amount of filler (including cement and limestone powder) in was 6.7% by mass of dry mineral mixture (aggregates and filler).

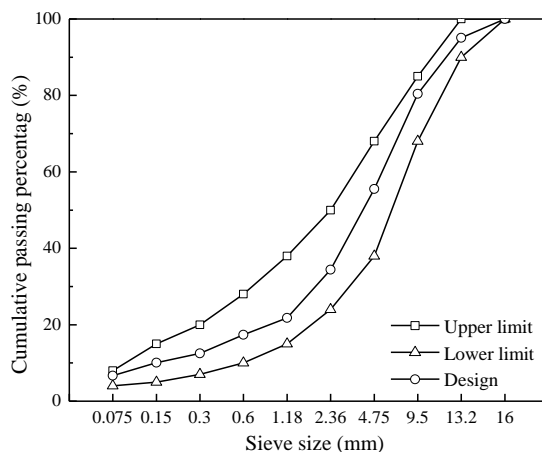


Figure 1 Gradation of CBEM

CBEM with cement content of 4.5% (cement to total dry aggregate ratio by weight) and bitumen content at 5% (bitumen to dry aggregate ratio by weight) was fabricated in this study. The high cement content was chosen in order to obtain a high strength of CBEM. The optimum bitumen content of this CBEM was 5%. Effect of different water contents were considered through adjusting additional water. Water content is the total water to dry aggregate ratio by weight, including additional water and water in emulsion.

Two kinds of surfactants were employed to improve the strength of CBEM. One is superplasticizer whose dosage is 2% of cement by weight. The other is JFC (a fatty alcohol–polyoxyethylene ether) whose function is to increase the wetting ability of bitumen emulsion. JFC is pre-added into bitumen emulsion, whose dosage is 0.5% of water in emulsion by weight. Reasons for choosing the two surfactants is discussed in the following.

Cylindrical Marshall mould with 101.6 mm diameter was used to fabricate specimens. Specimens were compacted by Marshall hammer with 50 blows per side. The specimens were cured in the mould for 3 days and then demoulded for the following 25 days curing. Specimens were kept in a chamber with controlled relative humidity of $(65 \pm 5)\%$ and temperature of 20 ± 2 °C in the whole curing period.

2.2 Indirect tensile strength test

The indirect tensile strength of pavement materials at 15 °C is a pavement design parameter in China [11]. Therefore, specimens were tested at a controlled temperature of 15 °C through a (12.7 ± 0.1) mm-wide loading strip at a constant speed of 50 mm/min. At least four specimens were tested for each mix.

2.3 Microstructure test

The microstructure of CBEM was observed by scanning electron microscopy (SEM). CBEM specimens were cut by cutting machine to ensure a relative smooth samples. Before test, specimens should be completely dried and coated by a thin film with gold-palladium to ensure a good conductivity.

3. RESULTS AND DISCUSSION

3.1 Strength mechanism and deficiency analysis of normal CBEM

3.1.1 Strength mechanism analysis

Effect of water content on the voids content and indirect tensile strength of CBEM is shown in Figure 2. It can be seen from Figure 2 that the voids content of CBEM firstly decreases and then increases with the increasing water content. The indirect tensile strength of CBEM firstly increases and then decreases with the increasing water content. CBEM has low strength at 2.9% of water content because no additional water is premixed with aggregate in this condition. As a result, bitumen emulsion is directly mixed with dry aggregate which is greatly harmful to its coating with aggregate. There are maximum strength and minimum voids content of CBEM in the test water content range. However, the water content of the maximum strength is much lower than that of the minimum voids content. The phenomenon was also observed in a previous study [2], which can be explained by the strength theory of bitumen mixture. According to the strength theory of bitumen mixture, the strength of CBEM is related to the cohesive and adhesive ability of cement bitumen emulsion (CBE) paste and the internal friction provided by aggregate skeletal structure. The internal friction of CBEM with a constant aggregate gradation is related to the voids content. Decrease in the voids content can strengthen the internal friction of bitumen mixture. However, the cohesive and adhesive ability of CBE paste are highly dependent on the microstructure of CBE paste and the interface between CBE paste and aggregate, which are affect by water content. The microstructure of the CBE pastes with different water contents is shown in Figure 3. It can be seen from Figure 3 that nearly no micro-

pores are observed in the paste of CBEM with 3.9% of water content. However, the paste of CBEM with 8.9% water content contains many micro-pores. Therefore, the increasing water content can lead to a looser microstructure of CBE paste, which can be harmful to the cohesive and adhesive ability of CBE paste. It is reasonable that the water content of CBEM at maximum strength is much lower than that at the minimum voids content.

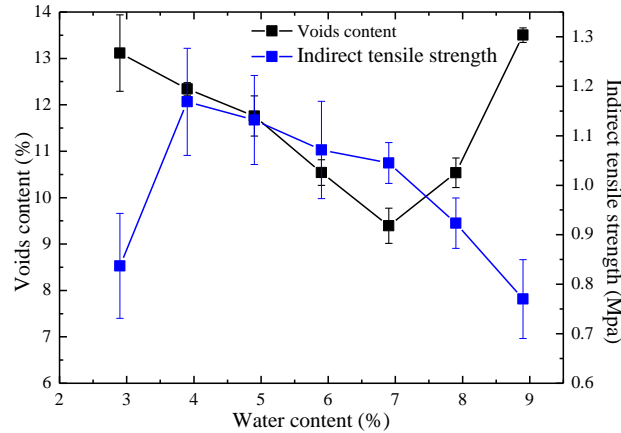
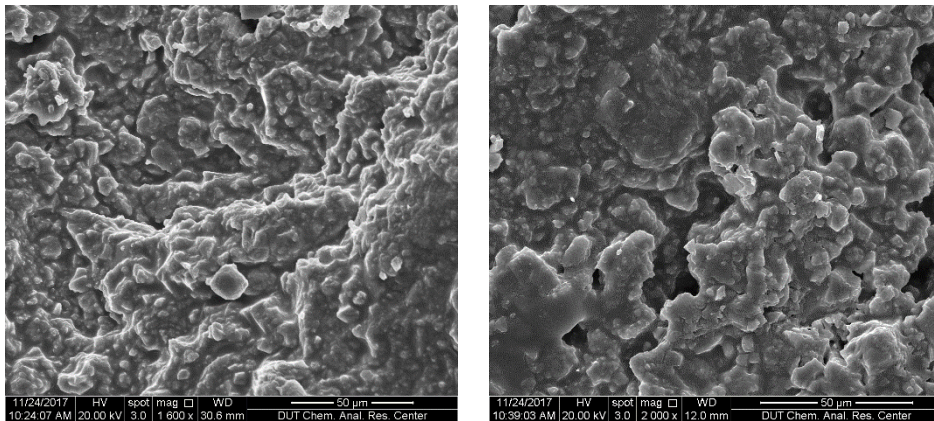


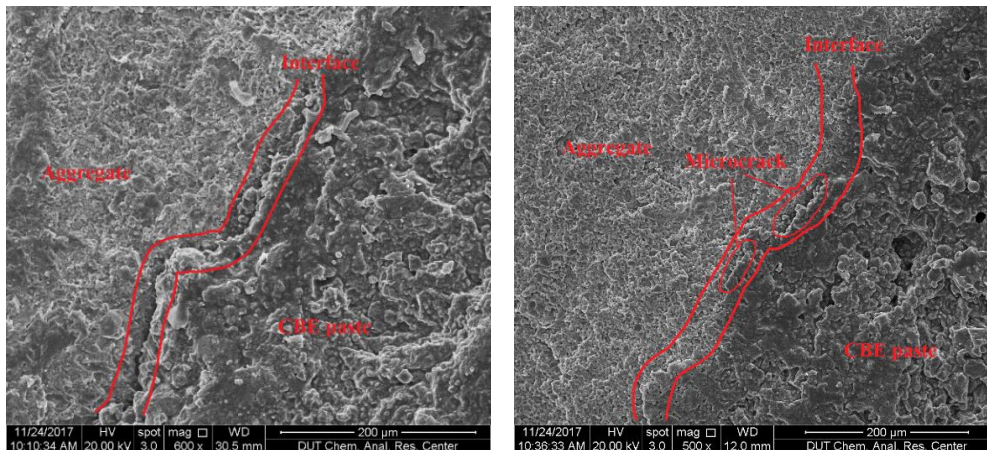
Figure 2 Voids content and strength of CBEM



(a) CBEM with 3.9% of water content (b) CBEM with 8.9% of water content
 Figure 3 Effect of water content on microstructure of CBE paste

The cohesive ability of CBE paste is also related to the interface between aggregate and CBE paste, which can affect the strength of CBEM. Effect of water content on the interface between aggregate and CBE paste in CBEM is shown in Figure 4. It can be seen from Fig.4 that a long microcrack is observed in the interface between CBE paste and aggregate at 3.9% of water content. However, microcracks are very short in the interface of CBEM with 8.9% of water content. Therefore, low water content is harmful to the interface between CBE paste and aggregate. This phenomenon is essentially related to the wetting ability of fresh CBE paste. Fresh CBE paste with low viscosity can have a good wetting ability with aggregate. The addition of water can significantly reduce the viscosity of fresh CBE paste [12]. Therefore, it is reasonable that high water content is beneficial to the bonding interface between CBE paste and aggregate.

Overall, the strength of CBEM is not only related to the voids content of CBEM, but also depends on the microstructure of CBE paste and the interface between CBE paste and aggregate. Low water content can help to form a dense microstructure of CBE paste, which is beneficial to the cohesive ability of CBE paste. Thus, the water content of CBEM at maximum strength is much lower than that at the minimum voids content. However, the wetting ability of CBE paste is related to its viscosity. It is difficult to form a good bonding interface between CBE paste and aggregate at low water content, which is harmful to the adhesive ability of CBE paste and the strength of CBEM.



(a) CBEM with 3.9% of water content (b) CBEM with 8.9% of water content
Figure 4 Interface between aggregate and CBE paste

3.1.2 Deficiency analysis

It can be seen from Figure 2 that CBEM has very high voids content compared to conventional HMA. The high voids content is harmful to the strength of CBEM. However, the total voids of CBEM are composed of voids formed during compaction and voids formed by water evaporation. The increasing water content can decrease the content of voids formed during compaction, but increase the content of voids formed by water evaporation. Therefore, it is difficult to efficiently decrease the total voids content CBEM.

It can be seen from Figure 3 that low water content is beneficial to the microstructure of CBE paste. However, it is harmful to form a good bonding interface between CBE paste and aggregate in Figure 4. Actually, it can be seen from Figure 4(b) that CBE paste does not well bond with aggregate even when water content is very high. This is because fresh CBE paste is a suspension of cement particles and bitumen droplets. It has inferior wetting and penetration ability with aggregate compared to hot bitumen. As a result, poor bonding interface between CBE paste and aggregate is a deficiency of CBEM. The interface between CBE paste and aggregate depends on the properties of fresh CBE paste. It is possible to improve this interface through adjusting the properties of fresh CBE paste.

3.2 Strength improvement methods for CBEM

The interface between CBE paste and aggregate highly depends on the wetting ability of CBE paste. Essentially, the wetting ability of a fluid is related to its viscosity and contact angle [13]. According to the authors' previous studies, superplasticizer can greatly reduce the viscosity of CBE paste [14]. Besides, JFC (a fatty alcohol–polyoxyethylene ether) is a typical

wetting agent which can greatly reduce the contact angle of aqueous emulsion. Therefore, these two surfactants are chosen to improve the strength of CBEM.

3.2.1 Strength improvement results of CBEM

Effect of superplasticizer and wetting agent on the strength of CBEM is shown in Figure 5. It can be seen from Figure 5 that the maximum indirect tensile strength of CBEM with 4.5% of cement content is only 1.17 MPa when no improvement method is employed. When superplasticizer is added, the maximum indirect tensile strength of CBEM can reach 1.42 MPa which increases by 21.5% compared to reference CBEM. When both superplasticizer and JFC are added, the maximum indirect tensile strength of CBEM can reach 1.51 MPa which increases by 29.1%. Therefore, superplasticizer and JFC do efficiently increase the strength of CBEM.

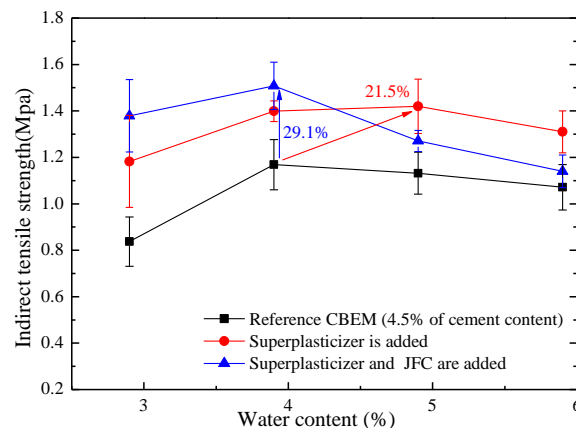


Figure 5 Effect of superplasticizer and JFC on the strength of CBEM

3.2.2 Analysis of strength improvement for CBEM

The microstructure and failure face of hardened CBEM are investigated to explain the strength improvement of CBEM. The interface microstructure of CBEM after improvement is shown in Figure 6. In comparison of Figure 6 and Figure 4, it can be seen that superplasticizer and JFC can greatly improve the interface between CBE paste and aggregate. Nearly no microcrack is observed in the interface zone of CBEM with superplasticizer and JFC. This improvement in the interface between CBE paste and aggregate can be attributed into the following reasons: (1) superplasticizer can greatly reduce the viscosity of CBE paste so that the wetting ability of CBE paste with superplasticizer is better than pure CBE paste; (2) superplasticizer can reduce the adsorption ability of cement particles with asphalt droplets [15], which is beneficial to the coating of bitumen emulsion on aggregate; (3) JFC can further increase the wetting ability of CBE paste. Because the wetting ability of fresh CBE paste is greatly improved by superplasticizer and JFC, the interface microstructure between aggregate and CBE paste is improved accordingly. Besides, the microstructure of CBE paste in Figure 6 is very dense due to the low water content.

The failure faces of CBEM before and after improvement are shown in Figure 7. It can be seen from Figure 7(a) that adhesive failures are dominant in the interface between coarse aggregate and CBE paste for reference CBEM. After improvement, not only seldom interface failures are observed in Figure 7(b) and 7(c), but also a lot of fine aggregates are fractured, which indicates a good bonding interface between CBE paste and aggregate and a high hardness of CBE paste about CBEM after improvement. The failure face of CBEM is changed from

“adhesive failure” to “cohesive failure” and “fine aggregate fracture”. It proves again that superplasticizer and JFC can both improve the interface between CBE paste and aggregate.

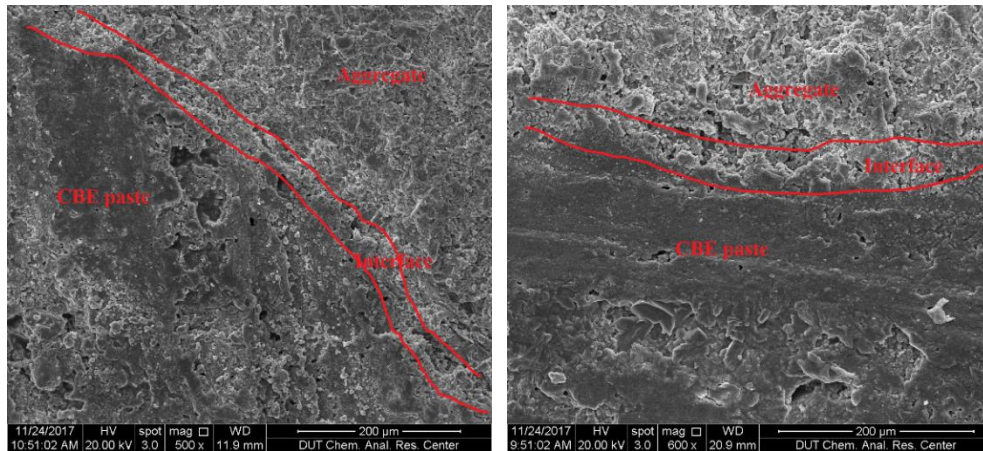


Figure 6 Interface between aggregate and CBE paste: (a) CBEM with superplasticizer (4.9% of water content) (b) CBEM with superplasticizer and JFC (4.9% of water content)



(a) Reference CBEM (b) CBEM with superplasticizer (c) CBEM with superplasticizer and JFC
Figure 8 Fracture face of hardened CBEM (3.9% of water content)

Overall, poor bonding interface between CBE paste and aggregate is a deficiency of CBEM. Superplasticizer and JFC can improve the wetting ability of fresh CBE paste, thus the coating ability of fresh CBE paste on aggregate is greatly improved. As a result, the interface between hardened CBE paste and aggregate is greatly improved so that the failure face of CBEM can be changed from “adhesive failure” to “cohesive failure” and “fine aggregate fracture”. Because of this improvement, the strength of CBEM can be improved by the superplasticizer and JFC.

4. CONCLUSIONS

(1) The water content of CBEM with the maximum strength is much lower than that with the minimum voids content. This is because the strength of CBEM is dependent on the voids content of CBEM, the microstructure of CBE paste, and the interface between CBE paste and

aggregate. Low water content can help to form a dense microstructure of CBE paste, which is beneficial to the strength of CBEM.

(2) Although CBE paste has a dense microstructure at the water content of maximum strength, a poor bonding interface between CBE paste and aggregate is observed in this condition and adhesive failure is dominant in the failure face of CBEM. Poor bonding interface between CBE paste and aggregate is a deficiency of CBEM.

(3) The addition of superplasticizer and wetting agent (JFC) can greatly increase the strength of CBEM. The maximum indirect tensile strength can increase by 21.5% and 29.1% for CBEM with superplasticizer and CBEM with superplasticizer and JFC, respectively. This is because superplasticizer and JFC can improve the bonding interface between CBE paste and aggregate. The failure face of CBEM can be changed from “adhesive failure” to “cohesive failure” and “fine aggregate fracture” when superplasticizer and JFC are added.

ACKNOWLEDGEMENTS

The authors thank National Natural Science Foundation of China (51608096) and the Fundamental Research Funds for the Central Universities (DUT17RC(4)16).

REFERENCES

- [1] Fang, X., 2016. A Fundamental research on cold mix asphalt modified with cementitious materials. Doctoral Dissertation, ETH Zurich.
- [2] Du S., 2014. Interaction mechanism of cement and asphalt emulsion in asphalt emulsion mixtures. *Mater. Struct.* 47(7), 1149-1159.
- [3] Oruc S., Celik F., Akpınar M.V., 2007. Effect of cement on emulsified asphalt mixtures. *J. Mater. Eng. Perform.* 16(5), 578-583.
- [4] Niazi Y., Jalili M., 2009. Effect of Portland cement and lime additives on properties of cold in-place recycled mixtures with asphalt emulsion. *Constr. Build. Mater.* 23(3), 1338-1343.
- [5] Bocci M., Grilli A., Cardone F., et al., 2011. A study on the mechanical behaviour of cement-bitumen treated materials. *Constr. Build. Mater.* 25(2), 773-778.
- [6] Grilli A., Graziani A., Bocci M., 2012. Compactability and thermal sensitivity of cement-bitumen-treated materials. *Road Mate. Pavement* 13(4), 599-617.
- [7] Graziani A., Godenzoni C., Cardone F., et al., 2016. Effect of curing on the physical and mechanical properties of cold-recycled bituminous mixtures. *Mater. Des.* 95, 358-369.
- [8] García A., Lura P., Partl M.N., et al., 2013. Influence of cement content and environmental humidity on asphalt emulsion and cement composites performance. *Mater. Struct.* 46(8), 1275-1289.
- [9] Fang X., Garcia A., Winnefeld F., et al., 2016. Impact of rapid-hardening cements on mechanical properties of cement bitumen emulsion asphalt. *Mater. Struct.* 49(1-2), 487-498.
- [10] Xiao J., Sha A., Jiang W., Wang Z., 2013. Gradation optimization for cement emulsified asphalt mixture. *Journal of Guangxi University: Nat. Sci. Ed.* 38(4), 936-942. [In Chinese]
- [11] Ministry of Transport of the People’s Republic of China, (2004). JTG F40–2004: Technical Specifications for construction of highway asphalt pavements. China Communications Press, Beijing, China. [in Chinese]
- [12] Ouyang J., Tan Y., Corr D.J., Shah S.P., 2017. Viscosity prediction of fresh cement asphalt emulsion pastes. *Mater. Struct.* 50(1), 59.
- [13] Rioboo, R., Marengo, M., & Tropea, C., 2002. Time evolution of liquid drop impact onto solid, dry surfaces. *Exp. Fluids* 33(1), 112-124.
- [14] Ouyang J., Corr D. J., & Shah S. P., 2016. Factors influencing the rheology of fresh cement asphalt emulsion paste. *J. Mater. Civil Eng.* 28(11), 04016140.
- [15] Ouyang J., Hu L., Li H., Han B., 2018. Effect of cement on the demulsifying behavior of over-stabilized asphalt emulsion during mixing. *Constr. Build. Mater.* 177, 252-260.

EVALUATION OF THE STIFFNESS MODULUS AND PHASE ANGLE OF COLD IN-PLACE RECYCLED MIXTURES FOR LONG CURING PERIODS

Bohdan Dolzycki (1), Mariusz Jaczewski (1) and Cezary Szydlowski (1)

(1) Faculty of Civil and Environmental Engineering, Gdansk University of Technology, Poland

Abstract

Article presents the changes in behaviour of cold-in place recycling mixtures made using cement and bituminous emulsion (CIR mixtures) after an elongated time of curing. Most of the available literature regarding change in stiffness modulus and phase angle presents results for a maximum of several dozen days, which makes it difficult to predict the behaviour over the whole life of the compacted layer. The article presents the results of stiffness modulus and phase angle for cold in-place recycled mixtures after 3 years of curing. Nine different mixtures with different combinations of cement and bituminous emulsion were tested using Simple Performance Tester. Stiffness modulus and phase angle were measured for three temperatures (4°C, 20°C and 40°C) and for 9 different frequencies (from 0.01 Hz to 25 Hz). The obtained results confirmed that despite the strong action of hydraulic bonds and their increase over three years, CIR mixtures maintained intermediate behaviour between strictly elastic and viscoelastic. While for lower test temperatures of 4°C and 20°C a steady increase in stiffness modulus and a decrease in phase angle were observed with the time of curing, there were no changes in the values of both parameters measured at the temperature of 40°C. In terms of relative values, the observed changes were not remarkably high for such a long term and ranged up to 25%. Nevertheless, in all the tested cases, with the passing of operational time materials became more elastic, which can result in improved resistance to permanent deformation, but also in higher susceptibility to reflective cracking.

Keywords: Cold recycling, Bitumen emulsion, Cement, Curing, Stiffness modulus

1. INTRODUCTION

The properties of cold recycled mixtures are dependent on the combination and properties of the binding agents used. In Poland, similarly to other countries, the most common binding agent combinations are: cement and bituminous emulsion or cement and foamed bitumen [1,

2, 3, 4, 5]. The amount of binding agents used depends on the local experience and requirements stated for the prepared and paved mixture [6, 7, 8, 9]. Bitumen (either in bituminous emulsion or foamed bitumen) is responsible for bituminous bonds, while cement is responsible for hydraulic bonds. The final properties of the mixture are the result of their proportions and the dominant type of bond. The impact of specific bonds changes with time due to ageing process of materials and hydration of cement. While for short periods of time the properties are described in numerous publications [1, 2, 10, 11, 12], the properties for longer periods are not well known. The first results of the presented research, obtained after 1.5 years of curing [13], indicated that while the stiffness of the mixtures was slowly increasing, all mixtures still presented viscoelastic behaviour due to the presence of bitumen. This paper presents the results after 3.0 years of curing. The analysis of presented results may prove helpful in proper assessment of design properties of cold recycled mixtures for the purpose of pavement design or for the assessment of risk of reflective cracking.

2. MATERIALS

CIR mixture parameters depend on gradation of mineral mixture, the amount and type of bitumen in reclaimed asphalt pavement and the combination of the binding agents used. To assess the influence of binding agents on viscoelastic parameters of CIR mixtures, one grading curve was designed according to the Polish requirements (2013) as a combination of reclaimed asphalt pavement (70%), continuously graded 0/31.5 aggregate (18%) and 0/2 fine aggregate (12%). Portland cement CEM I 32.5R and cationic asphaltic emulsion C60B5R were used as binding agents. The amount of each of the two binding agents was set to 2%, 4% or 6%, resulting in 9 different combinations of binding agent content in the tested CIR mixtures. Grading curves of the designed CIR mixtures are presented in Figure 1. For all tested mixture CxEx designation was used, where 'x' corresponds to the amount of used binding agent. For example designation C2E4 means that 2% of Portland Cement and 4% of bituminous emulsion were used.

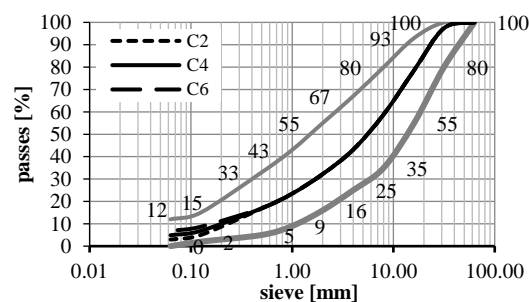


Figure 1. Grading curve of mineral mixtures.

CIR mixtures were prepared in laboratory mixer according to EN 12697-35 standard. The specimens were compacted in gyratory compactor according to EN 12697-31 standard. The limiting compaction ratio was set as 99%. The specimens were compacted to 170 mm height and 100 mm diameter. After 14 days of compaction lower and upper surfaces were cut to reach the specimen height of 150 mm. According to AASHTO TP79 (2013) procedure, the specimens should be cut out of a larger specimen (150 mm diameter), but it was impossible

due to very low initial strength of the mixtures and high amount of coarse aggregates. Detailed information regarding all mixtures are presented in [13].

3. LABORATORY TESTS

Stiffness modulus and phase angle were assessed in Simple Performance Tester according to AASHTO TP79 (2013) standard. Specimens were tested at three temperatures: 4°C, 20°C and 40°C. For every mixture and every test temperature 3 different specimens were tested in the controlled strain mode (100µstrain). Strain was measured with 3 LVDT sensors (gauge length of 70±1 mm) attached to the specimen. Stiffness modulus and phase angle were measured at 9 frequencies from 25 Hz to 0.1 Hz at temperatures of 4°C and 20°C. At the temperature of 40°C test was conducted at an additional frequency of 0.01 Hz. The view of the specimen during the test is presented in Fig. 2. In this research samples were tested three times: 28 days after compaction (first test), 1.5 year after compaction (second test) and 3 years after compaction (third test). Specimens were stored in a laboratory room, under typical temperature and moisture conditions without any special conditioning.

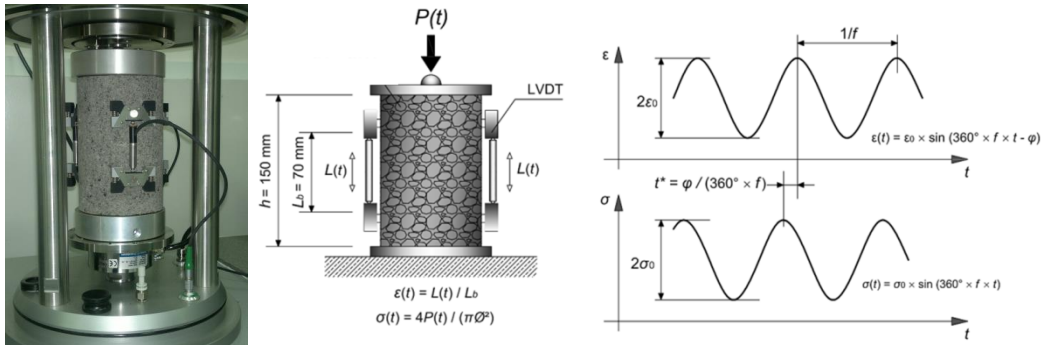


Figure 2. Specimen ready for testing (left) scheme of the test in Simple Performance Tester (centre) and plot that visualises the shift between stress and strain (right).

4. RESULTS

Values of stiffness moduli and phase angles for selected frequencies for all three curing periods (28 days, 1.5 years and 3.0 years) are presented as Black diagrams in Figures 3, 4 and 5.

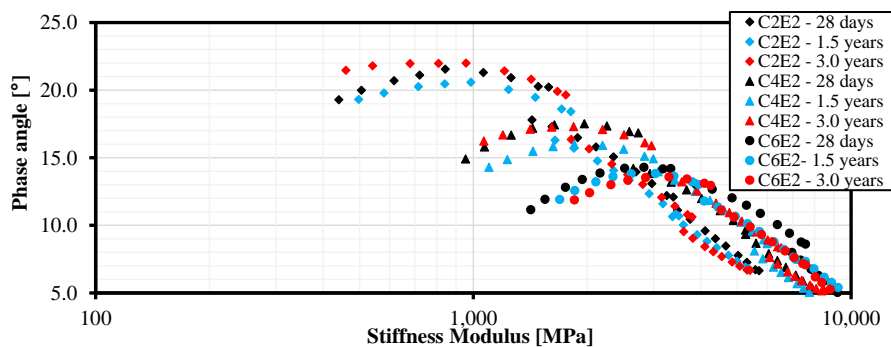


Figure 3: Black curves for mixtures: C2E2, C4E2 and C6E2 for all curing periods

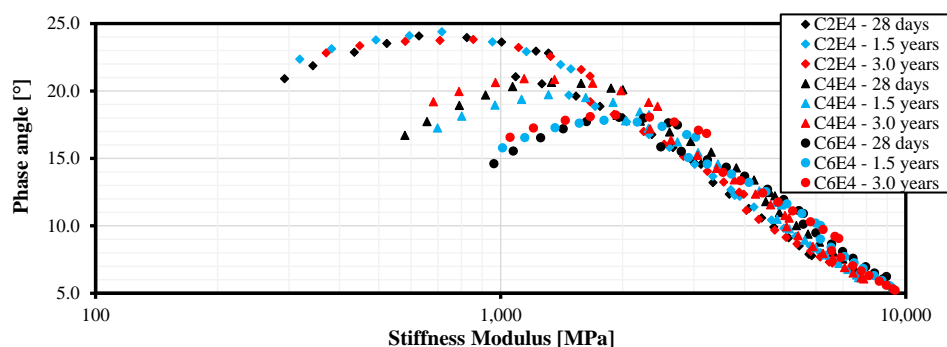


Figure 4: Black curves for mixtures: C2E4, C4E4 and C6E4 for all curing periods

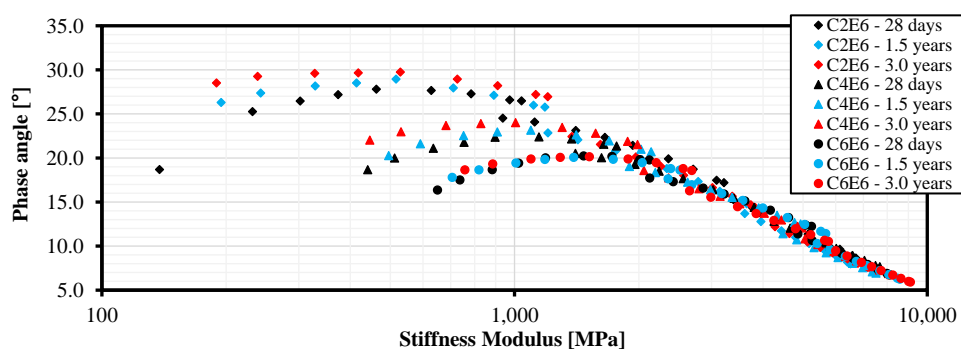


Figure 5: Black curves for mixtures: C2E4, C4E4 and C6E4 for all curing periods

5. DISCUSSION

The presented results are a continuation of the previous studies [13, 14] in which the change of two main parameters – stiffness moduli and phase angles – was analysed. The change resulted from two different aspects: material composition and the length of the curing period. While it was possible to determine the change related to the material composition, as the matrix of materials with different binding agent content was prepared, it was not possible to determine the effect of the curing periods. It was assumed that the normalized changes in strength and stiffness moduli after long curing periods will be similar to those of other cement bound materials. Due to large amount of data the analyses were presented only for mixtures with 4% of bituminous emulsion and varying amount of cement.

As expected, the curing period influenced the behaviour of tested mixtures similarly to the behaviour of cement concrete, especially in the case of stiffness modulus, as phase angle for cement bound materials is assumed as 0. The change in properties is more visible in the case of normalized values – presented as the change in comparison to the values after 28 days of curing. In the case of stiffness modulus the mean value of change is slowly decreasing – in the first test period the value of stiffness modulus increased by around 8% per year of curing and in the second test period the value of stiffness modulus increased by around 4.5% per year. In the case of the full set of mixtures with different compositions, the changes for the first and the second period are 7% per year and 3.5% per year respectively. In terms of phase angle the behaviour is more complex, especially in the case of the temperature of 40°C. While for other tested temperatures the decrease is evident and equal to around 4.5% per year (5.8% per year

in the first period and 3.5% per year in the second period for the full set of mixture compositions), for the specimens tested at the temperature of 40°C the decrease in phase angle is almost imperceptible. Moreover, some of the specimens tested at 40°C presented an increase in phase angle during the period between 1.5 and 3.0 years of curing. The cause of this phenomenon is unknown, but it is connected to the effect of the bituminous emulsion.

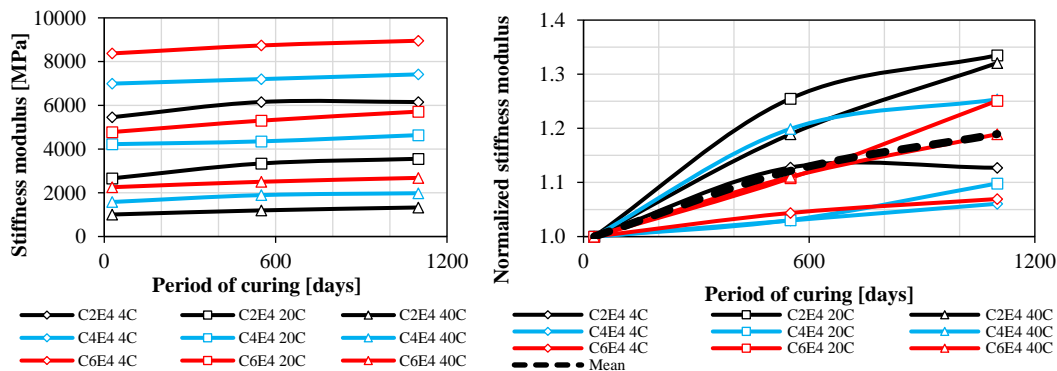


Figure 4: Change in stiffness modulus for mixtures: C2E4, C4E4 and C6E4 for all curing periods, frequency of 10 Hz

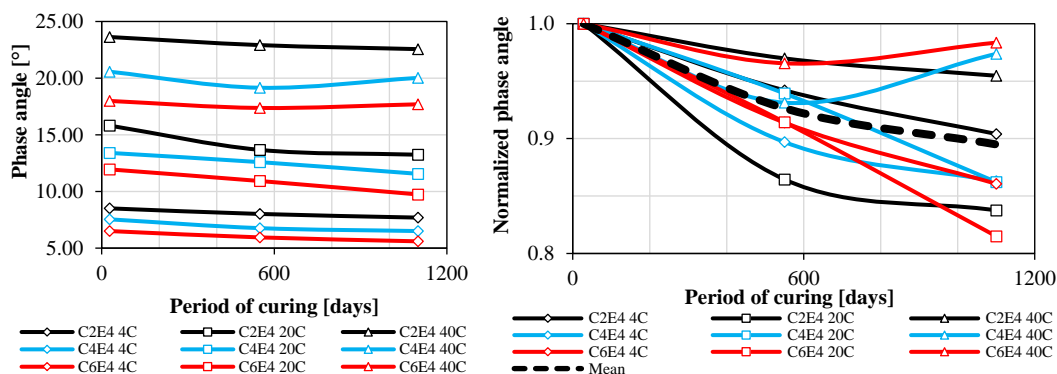


Figure 5: Change in phase angle for mixtures: C2E4, C4E4 and C6E4 for all curing periods, frequency of 10 Hz

A more detailed analysis of the change in mixture properties (stiffness modulus and phase angle) due to mixture composition and curing period was performed using multiple regression method. Literature studies [2, 3, 10, 11, 15, 9] as well as previous works [13, 14] indicate that cold recycled mixtures using cement and bituminous emulsion are a viscoelastic material and their behaviour is quite complex, as it changes with the temperature and time of loading. However, since they are a cement-bound material as well, their behaviour also changes with the time of curing. To simplify the analysis, two frequencies were selected for the analysis – 10 Hz and 0.1 Hz – to cover mixture behaviour both under fast and slow traffic. The analysis was performed on the basis of results for all compositions of mixtures. The dependent variable for each model was either the value of the stiffness modulus or phase angle. The independent variables depending on the model were: cement content [%], bituminous emulsion content [%], curing period [days] and – in a collective approach taking into account

the data across the three temperatures – test temperature [°C]. The basic equation for the multiple regression model was as follows:

$$y_i = a_i \times x_i + \dots + a_2 \times x_2 + a_1 \times x_1 + a_0 \quad (1)$$

where: y_i – dependent variable (either stiffness modulus or phase angle), x_i, \dots, x_2, x_1 – independent variables, $a_i, \dots, a_2, a_1, a_0$ – regression coefficients.

The comparison of the values predicted by multiple regression method and experimental data for a collective approach (for three temperatures) are presented in Figures 6 and 7, for stiffness modulus and phase angle respectively. The values of regression coefficients for the influence of cement and bituminous emulsion content as well as the curing period are presented in Table 1. To facilitate the data analysis, the influence of the curing period was additionally presented in the table as an increase/decrease in the value for the period of 1 month and 1 day.

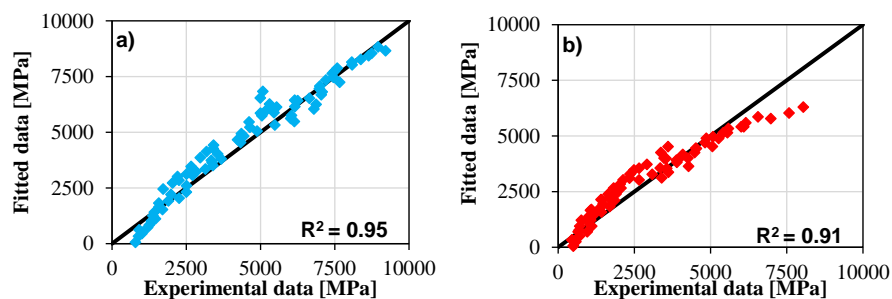


Figure 6: Validation of multiple regression for stiffness moduli: (a) full data – 10 Hz (b) full data – 0.1 Hz

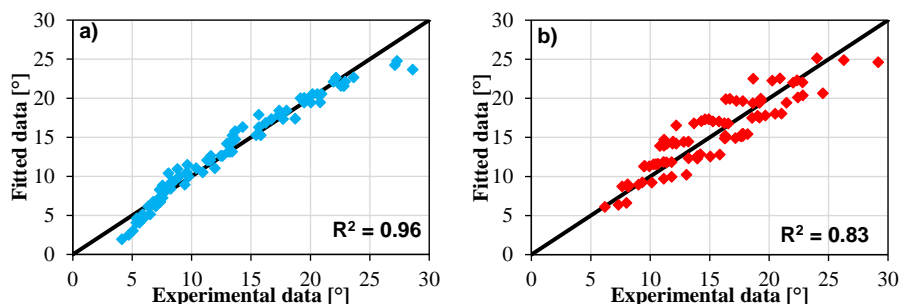


Figure 7: Validation of multiple regression for phase angles: (a) full data – 10 Hz (b) full data – 0.1 Hz

As can be seen in Figures 6 and 7, the models gave quite good accuracy of prediction – the coefficients of determination R^2 in most cases were higher than 0.9. In the case of stiffness moduli, the relationship between experimental and predicted data shows a more nonlinear behaviour. In the case of phase angle (Fig. 7(b)), the scatter of regression model results gives the lowest coefficient of determination.

Table 1: Multiple regression coefficients for cement content, bituminous emulsion content and curing period.

Property	Factor	Frequency 10 Hz				Frequency 0.1 Hz			
		4°C	20°C	40°C	4-40°C	4°C	20°C	40°C	4-40°C
Stiffness modulus [MPa]	C [1 %]	767	664	362	598	671	443	198	444
	E [1 %]	-78	-285	-225	-196	-238	-296	-150	-221
	Curing period [1 day] / [1 month]	0.556 16.67	0.688 20.63	0.332 9.95	0.525 15.75	0.736 22.08	0.580 17.39	0.097 2.91	0.485 14.45
Phase angle [°]	C [1 %]	-0.55	-0.96	-1.66	-1.06	-0.81	-1.33	-1.97	-1.31
	E [1 %]	0.50	1.09	1.57	1.06	0.82	1.43	1.46	1.29
	Curing period [1 day] / [1 month]	-0.001 -0.026	-0.002 -0.059	-0.0002 -0.007	-0.001 -0.030	-0.002 -0.056	-0.002 -0.045	+0.002 +0.066	-0.0005 -0.014

As can be seen in Table 1, the behaviour of the mixtures strongly depends on the test temperature and test frequency. As predicted, mixtures showed more elastic behaviour for higher test frequencies and lower temperatures. The influence of cement is also higher for the temperatures of 4°C and 20°C, at which:

- the increase in stiffness moduli due to additional 1% of cement is higher and ranges from 440 MPa to 770 MPa;
- the increase in stiffness moduli due to additional month of curing is higher and ranges from 16.6 MPa to 22.1 MPa;
- the changes in phase angles due to change of composition are the lowest, while the changes (decrease) in phase angles due to additional months of curing are the highest.

As previously, irregularities are visible at the temperature of 40°C. While the change (increase) in stiffness is similar in terms of relative values, the change in the phase angle is not as evident. The phase angle at the temperature of 40°C either slowly decreases or even, in some cases, increases in comparison to the values obtained for the periods of curing equal to 28 days and 1.5 years. This behaviour is more visible in the Black diagrams. While there is a small shift to the right side (higher values of stiffness moduli), the maximum values of phase angles are almost the same. Probable cause is the influence of bituminous emulsion, whose ring and ball temperature is close to the highest test temperature. On the other hand, the value of the phase angle should be affected by ageing of the bitumen, which should shift the Black curves down along the phase angle axis. The detailed mechanism behind this behaviour is not known and will be monitored in further studies.

6. CONCLUSIONS

The conducted research showed that the cold recycled mixtures are a very complicated construction material. Presented results allow to state the following conclusions:

- The curing period influences the behaviour of tested mixtures similarly to the behaviour of cement concrete, especially in the case of stiffness modulus. The mean value of change is slowly decreasing – in the first test period the value of stiffness modulus increased by around 8% per year of curing and in the second test period the same value

increased by around 4.5% per year. In the case of phase angle the decrease is evident and equal to around 4.5% per year (5.8% per year in the first period and 3.5% per year in the second period for the full set of mixture compositions).

- The behaviour of the mixtures strongly depends on the test temperature and test frequency. As predicted, mixtures showed more elastic behaviour for higher test frequencies and lower temperatures. The influence of cement was higher for the temperatures of 4°C and 20°C as well.
- At the temperature of 40°C the behaviour of cold recycled mixtures is more complex. The change of properties is not as evident and regular as it is at lower temperatures, probably due to stronger influence of bituminous emulsion. This behaviour will be monitored and analysed in further research.

REFERENCES

- [1] Buczyński P. and Iwański M., ‘Complex modulus change within the linear viscoelastic region of the mineral-cement mixture with foamed bitumen’, *Constr Build Mater.* **172** (2018) 52-62
- [2] Chomicz-Kowalska A., Gardziejczyk W. and Iwański M.M., ‘Analysis of IT-CY Stiffness Modulus of Foamed Bitumen Asphalt Concrete Compacted at 95°C’, *Procedia Eng.* **172** (2017) 550-559.
- [3] Kukielka J. and Sybilski D., ‘Durability of base courses with mineral-cement-emulsion mixes (MCEM)’, *IOP Conf Ser: Mater Sci Eng.* **356** (1) 012006.
- [4] Dolzycki B., ‘Polish experience with cold in-place recycling’, *IOP Conf Ser: Mater Sci Eng.* **236** (2017) 012089.
- [5] Miljković M., Radenberg M., Fang X., and Lura P., ‘Influence of emulsifier content on cement hydration and mechanical performance of bitumen emulsion mortar’, *Mater Struct.* **50** (2017) 185.
- [6] Graziani A., Iafelice C., Raschia S., Perraton D. and Carter A., ‘A procedure for characterizing the curing process of cold recycled bitumen emulsion mixtures’, *Constr Build Mater.* **173** (2018) 754-762.
- [7] GDDKiA, Gdansk University of Technology, ‘Instrukcja projektowania i wbudowywania mieszanek mineralno-cementowo-emulsiyjnych (MCE)’, (2013).
- [8] FGSV, ‘Merkblatt für Kaltrecycling in situ im Straßenoberbau. Vol 636’, Forschungsgesellschaft für Straßen- und Verkehrswesen Arbeitsgruppe Mineralstoffe im Straßen (2005).
- [9] Valentin J., Čížková Z., Suda J., Batista F., Mollenhauer K. and Simnofske D., ‘Stiffness characterization of cold recycled mixtures’, *Transp Res Proc.* **14** (2016) 758–767.
- [10] Godenzoni C., Graziani A., Bocci E. and Bocci M., ‘The evolution of the mechanical behaviour of cold recycled mixtures stabilised with cement and bitumen: field and laboratory study’, *Road Mater Pavement.* **19** (4) (2018) 856-877.
- [11] Graziani A., Godenzoni C., Cardone F. and Bocci M., ‘Effect of curing on the physical and mechanical properties of cold-recycled bituminous mixtures’, *Mater Des.* **95** (2016) 358-369.
- [12] Iwański M and Chomicz-Kowalska A., ‘Laboratory Study on Mechanical Parameters of Foamed Bitumen Mixtures in the Cold Recycling Technology’, *Procedia Eng.* **57** (2013) 433 – 442.
- [13] Dolzycki B., Jaczewski M. and Szydłowski C., ‘The long-term properties of mineral-cement-emulsion mixtures’, *Constr Build Mater.* **156** (2017) 799-808.
- [14] Dolzycki B., Jaczewski M and Szydłowski C., ‘The Influence of Binding Agents on Stiffness of Mineral-cement-emulsion Mixtures’, *Procedia Eng.* **172** (2017) 239-246.
- [15] Bocci M., Grilli A., Cardone F. and Graziani A., ‘A study on the mechanical behaviour of cement-bitumen treated materials’, *Constr Build Mater.* **25**(2) (2011) 773–778.

EVALUATING THE CRACKING RESISTANCE OF CEMENT-BITUMEN TREATED MATERIALS USING THE SEMI-CIRCULAR BENDING TEST

Chiara Mignini (1), Fabrizio Cardone (1), Alessandro Morbi (2), Luca Setti (2) and Andrea Graziani (1)

(1) Università Politecnica delle Marche, Department of Civil and Building Engineering and Architecture, Ancona, Italy

(2) HeidelbergCement, Global Product Innovation Department - i.lab, Bergamo, Italy

Abstract

Cement-bitumen treated materials (CBTM) are produced using cold recycling technologies for the rehabilitation of bituminous pavements. Bitumen emulsion and cement are used as binders, and thus jointly contribute to the mechanical performance of the mixtures. This paper focuses on the cracking resistance of CBTM, which is related to the presence and relative effect of bituminous and cementitious bonds within the mixtures. The objective is to evaluate the influence of different cement types, bitumen-to-cement ratios (1.3 and 0.8) and curing conditions (free and restricted evaporation). The semi-circular bending (SCB) test was used to evaluate the cracking resistance of mortar specimens whose composition was derived from the mixtures' composition removing the coarse aggregates. The SCB specimens cut from gyratory compacted specimens were tested at 10 °C after 28 days of curing at 25 °C. The results analysis indicates that in the crack initiation phase, the behaviour of CBTM mortars depends on the combined presence of cementitious and bituminous bonds, whereas, in the crack propagation phase, the effects of cement type and dosage prevail and may lead to a brittle behaviour.

Keywords: bitumen emulsion; cold recycling; cracking resistance; SCB test.

1. INTRODUCTION

Cement-bitumen treated materials (CBTM) are sustainable and low energy materials for pavement maintenance and construction. CBTM are obtained by mixing at ambient temperature aggregates, filler and bitumen emulsion [1]. Cement and other supplementary cementitious materials like fly ash, silica fume and ground granulated blast furnace slag, are added to the mixtures to improve their performance. CBTM are characterised by a dosage of fresh bitumen

(emulsion residue) generally ranging between 1% and 3%, and a dosage of cement up to 3%. Water can also be added to the mixtures to improve their workability.

CBTM require a curing period to achieve their long-term properties. During curing their physical and mechanical properties evolve because of breaking of the emulsion, moisture loss and hydration of cement [2, 3]. The development of the mechanical properties is also related to the cement type. The use of rapid-hardening cement, like calcium aluminate and sulfoaluminate cement, can accelerate the development of the mechanical properties in the early stage of curing [4].

Cracking is one of the major distress of road pavements. This means that the structural performance of pavements is strictly related to the fracture behaviour of its constituent materials. Hence, the assessment of the fracture resistance is a fundamental aspect especially for CBTM mixtures that could be prone to cracking because of the presence of cement, aged bitumen or reclaimed asphalt (RA).

Based on this background the present work investigates the cracking resistance of CBTM. In particular, CBTM mortars produced using only the fine aggregate fraction were tested with the semi-circular bending test (SCB). The effects of four types of cement, two bitumen to cement (B/C) ratios and two curing conditions were investigated.

2. MATERIALS

The CBTM mortars were characterised by an upper sieve size of 2 mm and were composed of RA aggregate, virgin aggregate, mineral filler, bitumen emulsion, cement and additional water.

The RA aggregate was obtained from an all-in RA aggregate (A1 0/16 GF₈₅ according to EN 13043) by a laboratory sieving process to obtain the fraction passing to the 2 mm sieve. Its particle density is equal to 2.424 Mg/m³ and its water absorption is 1.32% (EN 1097-6). The virgin aggregate was a crushed limestone sand with an upper sieve size of 2 mm. Its particle density is equal to 2.732 Mg/m³ and its water absorption is 1.50%. The filler was a finely ground limestone powder with particle density of 2.650 Mg/m³, Blaine surface area of 3800 cm²/g (EN 196-6) and Rigden voids of 24% (EN 1097-4).

The bituminous binder was a commercial cationic over-stabilised bitumen emulsion designated C60B10 according to EN 13808. Four different types of cement, supplied by Italcementi S.p.A., were adopted to produce the CBTM mortars (Table 1).

Table 1: Cements characteristics

		C1	C2	C3	C4
Parameter	Standard				
Particle density [Mg/m ³]	EN 1097-7	3.02±0.01	2.90±0.03	3.09±0.01	2.9±0.1
Blaine surface area [cm ² /g]	EN 196-6	3800±100	5700±200	4090±100	6100±350
Rigden voids [%]	EN 1097-4	33.23	33.53	33.38	32.34
pH value [pH]		12-13.5	11-12	12-13.5	12-13.5
Compressive strength 2dd [MPa]	EN 196-1	19±2	45±2	20±2	3±1
Compressive strength 28dd [MPa]	EN 196-1	39±3	80±3	56±3	10±2

The CBTM mortar composition was derived starting from fixed mixture compositions characterized by an emulsion dosage of 3.3% (corresponding to 2.0% of residual bitumen) and two cement dosages: 1.5% and 2.5%. Removing the coarse aggregate (retained in the 2 mm sieve) from the mixture, the resulting dosage of emulsion was 7.8% (corresponding to 4.7% of residual bitumen) and the dosages of cement were 3.5% or 5.9%. The mortars were identified using the residual bitumen to cement ratio: $B/C = 1.3$ and $B/C = 0.8$. The total water content of the mortars was 6.9%. All dosages are with respect to the dry aggregate mass. The detailed description of the adopted methodology can be found in [5]. The resulting aggregate blend was composed of 61% RA aggregate, 32% natural sand and 7% filler. The grading distributions of the aggregates and mortar are depicted in Figure 1.

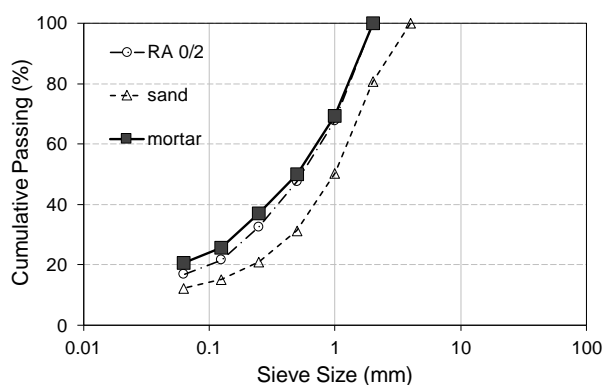


Figure 1: Grading distribution of the aggregates and the mortar.

3. LABORATORY PROCEDURES

3.1 Specimen preparation and curing

Aggregates, water, bitumen emulsion and cement were mixed at room temperature following an optimised procedure [6]. Specimens were compacted with a gyratory compactor using moulds with a diameter of 150 mm, pressure of 600 kPa, gyration speed of 30 rpm and angle of inclination of 1.25° . The compaction was stopped when the height of 50 mm was reached. Table 2 reports the average void content V_m of the mortar specimens, defined as the volume of air voids and intergranular water in the total mixture volume [7].

After the compaction, CBTM specimens were cured for 28 days in a climatic chamber at $25 \pm 2^\circ\text{C}$ and $70 \pm 5\%$ relative humidity (RH). Two curing conditions were considered: unsealed (U) and sealed inside a plastic bag (S). In unsealed condition the water evaporation was not restricted, favouring emulsion breaking. In sealed condition, the RH was close to 100%, and there was no significant amount of water evaporation. Therefore, the cement hydration was favoured. It is expected that in the unsealed specimens bituminous bonds are more developed, whereas the cementitious bonds are more developed in the sealed specimens.

At the end of the curing, specimens were conditioned at 5°C for 12 hours. Afterwards, two half-cylindrical specimens were obtained by cutting. A notch with a width of 0.35 ± 0.10 mm and a depth of 10.0 ± 1.0 mm was then cut in the middle of the base of each half-cylindrical specimen.

Table 2: Void content of the mortars investigated

B/C ratio	Vm [%]			
	C1	C2	C3	C4
1.3	14.1	14.3	15.9	15.0
0.8	14.1	14.2	15.7	15.7

3.2 Semi-circular bending test

The SCB test (EN 12697-44) was performed at 10 °C, after 4 hours of temperature conditioning. The test requires the application of a three-point bending load to a half-cylindrical specimen (Figure 2a). In this test configuration, the middle base of the specimen is subjected to an increasing tensile stress. As the test proceeds, the crack starts from the tip of the notch, where the concentration of the stress is highest, and then propagates vertically. The test was carried out at a constant vertical displacement rate of 5 mm/min. Four replicate specimens were tested for each mortar and curing condition.

The results were analysed in terms of fracture toughness K (EN 12697-44), fracture energy G_f [8] and flexibility index FI [9,10]. K describes the state of local stress around a crack and is defined as follows:

$$K = \sigma_{\max} \cdot f(a/W) \quad (1)$$

where σ_{\max} is the maximum stress at failure and $f(a/W)$ is a geometric factor. K is an intrinsic property of the material that is commonly used to define its aptitude to resist cracking initiation [11].

G_f describes the overall cracking potential of the mixture being a measurement of the work needed to increase the fractured surface until failure and is defined as follows:

$$G_f = W / A_{\text{lig}} \quad (2)$$

where W is the work of fracture (area under the load-displacement curve until failure) and A_{lig} is the crack ligament area [10].

FI is related to the fracture energy and the slope of the post-peak load-displacement curve (crack propagation phase) according to the following equation:

$$FI = A \cdot G_f / \text{abs}(m) \quad (3)$$

where G_f is the fracture energy, m is the slope of the post-peak curve at the inflection point, and A is a unit conversion factor assumed equal to 0.01. The FI was developed to better discriminate the cracking resistance of different mixtures, taking into account the crack propagation speed and the fracture process zone. Indeed, it was observed that the post-peak segment of the load-deformation curve is very sensitive to changes in the composition of the material [9].

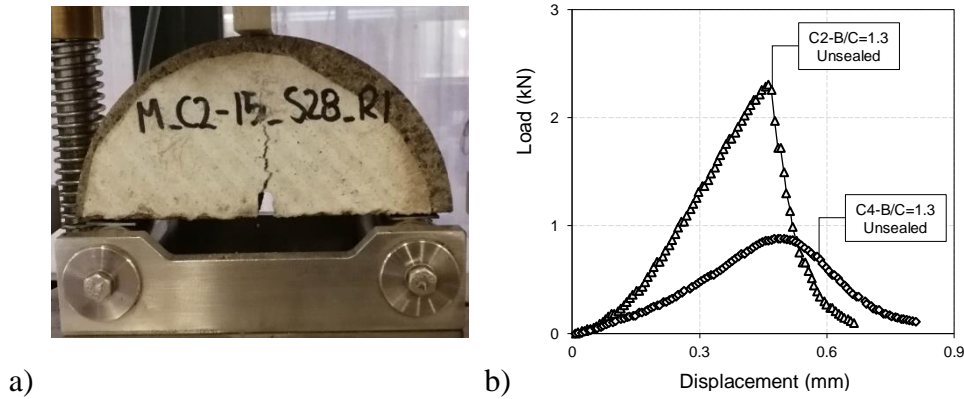


Figure 2: SCB a) test configuration, b) typical load-displacement curves

4. RESULTS

Figure 2b shows two typical load-displacement curves obtained for the studied CBTM mortars. In particular, the curves of the mortars with cements C2 and C4, with B/C ratio of 1.3 and cured in unsealed condition are depicted.

4.1 Fracture toughness

Figure 3 shows the average values of K (the standard deviations are reported as error bars). As can be observed the cement type influenced the K of the mortars. In particular, a hierarchy of the toughness can be highlighted: mortars produced with C2 always showed the highest K , followed by the mortars with C3 and C1, mortars with C4 always showed the lowest K .

Reducing the B/C ratio from 1.3 to 0.8 (thus increasing the cement dosage) improved the fracture toughness of all the mortars investigated, regardless type of cement and curing condition. In particular, the average increase of K was about 40% for mortars with C1, C2, C4 and it reached 80% for mortars with C3.

As far as curing condition is concerned, generally, sealed (S) condition of curing negatively influenced the toughness of the mortars, especially for the lowest cement dosage. In particular, for mortars with B/C=1.3, K decreased of about 25% using C1, C2 and C3 and 39% when C4 was used.

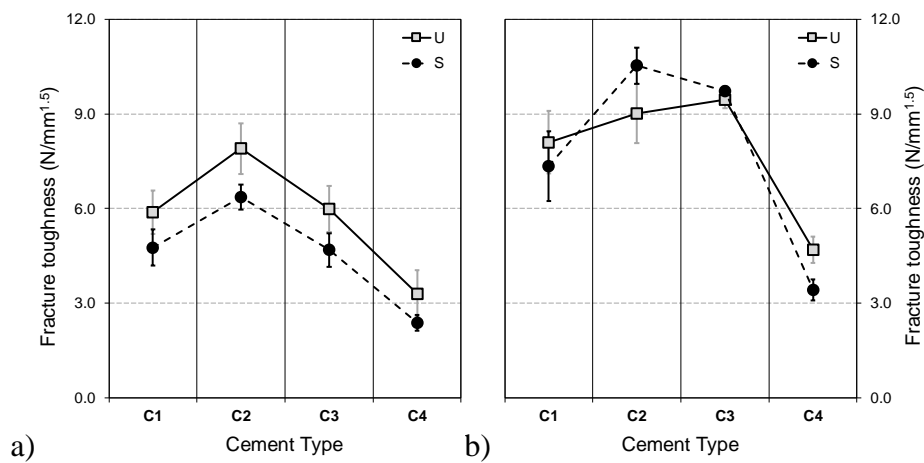


Figure 3: Fracture toughness of the mortars investigated a) B/C=1.3, b) B/C=0.8

4.2 Fracture energy

Figure 4 shows the average values of G_f (the standard deviations are reported as error bars). The influence of the type of cement on G_f was similar to that highlighted for K . Indeed, fracture energy was higher for mortars produced with C2 and C3, whereas lower values were achieved for the mortars with C4 regardless of curing conditions.

Similar to the results obtained for K , the fracture energy increased with the increase in cement dosage (lower B/C ratio). The increase in G_f was particularly high for the mortars produced with C3 (more than doubled). Whereas, the different dosage of cement had a lower influence on the mortars produced with C4 (average increase equal to 28%). Generally, the increase in cement dosage results in an increase in brittleness. However, the experimental results indicate that CBTM mortars maintain a good ability of deformation at failure due to the presence of bituminous bonds.

Allowing free water evaporation (U) resulted in an increase of G_f from 4% to 97% with respect to restricted evaporation (S). The opposite effect was observed only for the mortar produced using C1 with B/C = 0.8.

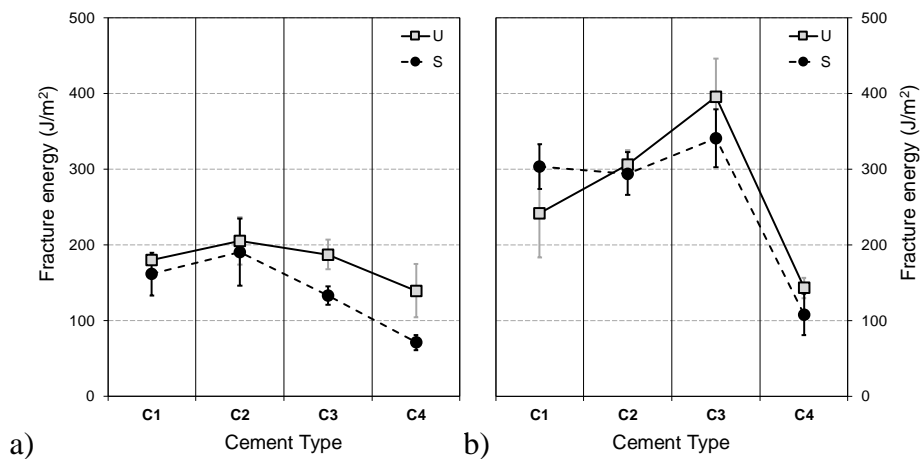


Figure 4: Fracture energy of the mortars investigated a) B/C=1.3, b) B/C=0.8

4.3 Flexibility index

Figure 5 shows the average values of FI (the standard deviations are reported as error bars). Similar to the results obtained in terms of K and G_f , the influence of the dosage of cement (and consequently of the B/C ratio) is evident. In particular, the increase in cement dosage generally causes a decrease in FI, depending on the cement type and curing condition.

FI allowed the different post-peak behaviour due to the cement type to be distinguished more clearly. Generally, mortars produced using C2 and C3 which were characterised by higher K and G_f , showed lower values of FI as compared to the mortars produced using C1 and C4. This behaviour can be explained considering the slope of the post-peak curve at the inflection point. In fact, the values of the slope obtained testing the mortars produced with C2 and C3 was, in general, 2 or 3 times higher with the respect of the slope of mortars with C1 and C4. In general, a lower slope of the post-peak peak segment is an index of a more ductile response to the crack propagation, whereas a higher slope is related to a more brittle crack propagation. Thus, the lowest FI values clearly showed the increase of brittleness of the mortars produced with C2 and C3.

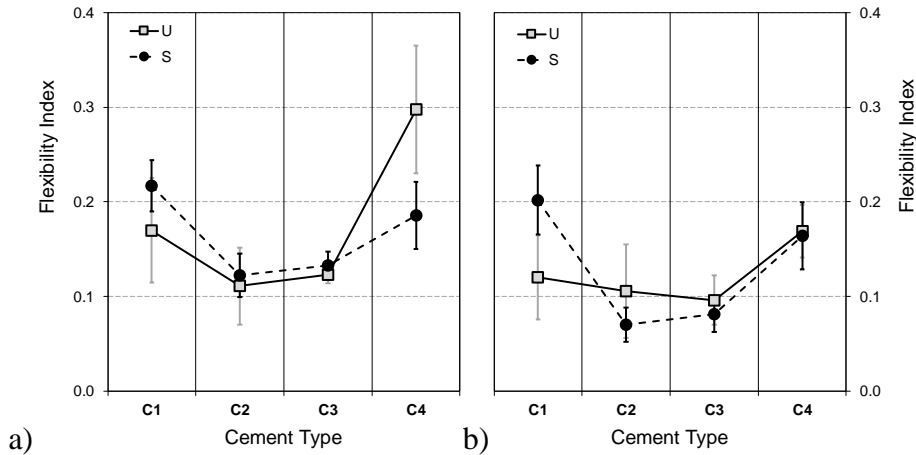


Figure 5: Flexibility index of the mortars investigated a) B/C=1.3, b) B/C=0.8

4.4 Relation among fracture parameters

Figure 6 shows the values of G_f and FI as a function of K . As can be observed, increasing the K value, G_f increases, whereas FI decreases.

In general, brittle materials show high values of K associated with low values of G_f . CBTM mortars do not follow this trend because high values of K are associated with high values of G_f . This is an effect of the simultaneous presence of cementitious and bituminous bonds. The first contribute to high values of K while the second lead to high values of G_f . The FI values reveal that the positive effect of the bituminous bonds is limited to the crack initiation phase. In fact, high values of K are associated with low values of FI which indicate a brittle behaviour during crack propagation (post-peak phase).

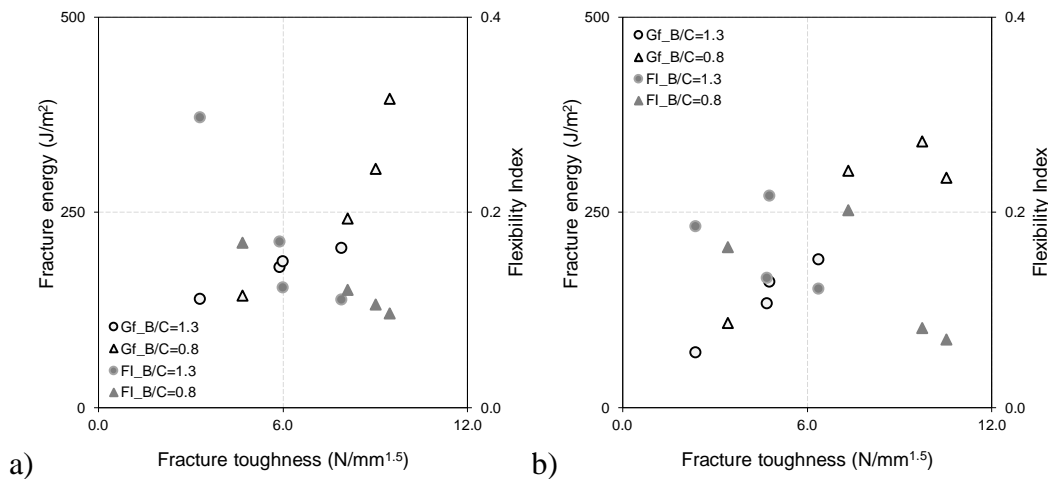


Figure 6: Fracture energy and flexibility index as a function of fracture toughness for mortars cured in a) unsealed condition, b) sealed condition

5. CONCLUSIONS

The cracking resistance of CBTM mortars was evaluated using the SCB test. CBTM mortars were produced using four cement types, two cement dosages and one bitumen emulsion dosage. Tests were carried out after 28 days of curing in two different conditions: unsealed (free water evaporation) and sealed (restricted evaporation).

The results showed that the fracture toughness K , the fracture energy G_f and the flexibility index FI allowed to discriminate among mortars produced with different type and dosage of cement. The mortars produced using cements C2, and C3 showed higher values of K and G_f , whereas the mortars produced using cements C1 and C4 showed higher values of FI.

In summary, the results analysis indicates that in the crack initiation phase, the behaviour of CBTM mortars depends on the combined presence of cementitious and bituminous bonds, whereas, in the crack propagation phase, the effects of cement type and dosage prevail and may lead to a brittle behaviour.

ACKNOWLEDGEMENTS

The Authors would like to acknowledge Italcementi – HeidelbergCement Group for funding this research and providing the cements. Furthermore, the Authors wish to express their gratitude to Valli Zabban S.p.A. and to Società Cooperativa Braccianti Riminese Companies for providing the bitumen emulsion and the reclaimed asphalt aggregate.

REFERENCES

- [1] Bocci, M., Grilli, A., Cardone, F., and Graziani, A., 'A study on the mechanical behaviour of cement-bitumen treated materials', *Constr. Build. Mater.* **25** (2) (2011) 773-778.
- [2] Cardone, F., Grilli, A., Bocci, M., & Graziani, A., 'Curing and temperature sensitivity of cement-bitumen treated materials', *Int. J. Pavement Eng.* **16** (10) (2015) 868-880
- [3] Du, S., 'Effect of curing conditions on properties of cement asphalt emulsion mixture', *Constr. Build. Mater.* **164** (2018) 84-93.
- [4] Fang, X., Garcia, A., Winnefeld, F., Partl, M. N. and Lura, P., 'Impact of rapid-hardening cements on mechanical properties of cement bitumen emulsion asphalt', *Mater. Struct.* **49** (1-2) (2016) 487-498.
- [5] Mignini, C., Cardone, F. and Graziani, A., 'Experimental study of bitumen emulsion-cement mortars: mechanical behaviour and relation to mixtures', *Mater. Struct.* **51** (6-149) (2018) 1-14.
- [6] Graziani, A., Godenzoni, C., Cardone, F., and Bocci, M., 'Effect of curing on the physical and mechanical properties of cold-recycled bituminous mixtures', *Mater. Des.* **95** (2016) 358-369.
- [7] Grilli, A., Graziani, A., Bocci, E. and Bocci, M., 'Volumetric properties and influence of water content on the compactability of cold recycled mixtures', *Mater. Struct.* **49** (10) (2016) 4349-4362.
- [8] Li, X. J. and Marasteanu, M. O., 'Using semi-circular bending test to evaluate low temperature fracture resistance for asphalt concrete', *Experimental mechanics* **50** (7) (2010) 867-876.
- [9] Ozer, H., Al-Qadi, I. L., Lambros, J., El-Khatib, A., Singhvi, P. and Doll, B., 'Development of the fracture-based flexibility index for asphalt concrete cracking potential using modified semi-circle bending test parameters', *Constr. Build. Mater.* **115** (2016) 390-401.
- [10] Ozer, H., Al-Qadi, I. L., Singhvi, P., Khan, T., Rivera-Perez, J. and El-Khatib, A., 'Fracture characterization of asphalt mixtures with high recycled content using Illinois semicircular bending test method and flexibility index', *Transportation Research Record: Journal of the Transportation Research Board* (2575) (2016) 130-137.
- [11] Saha, G. and Biligiri, K. P., 'Fracture properties of asphalt mixtures using semi-circular bending test: a state-of-the-art review and future research', *Constr. Build. Mater.* **105** (2016) 103-112.

FIELD BEHAVIOUR OF COLD-RECYCLED ASPHALT MIXTURES FOR BINDER COURSES

Andrea Grilli (1), Chiara Mignini (2) and Andrea Graziani (2)

(1) Department of Economics, Science and Law, University of the Republic of San Marino, San Marino

(2) Department of Civil and Building Engineering and Architecture, Università Politecnica delle Marche, Ancona, Italy

Abstract

A new awareness on sustainable materials and construction techniques is promoting field applications of cold bitumen emulsion mixtures. Cold in-plant recycling (CPR) techniques with bitumen emulsion ensure important benefits in terms of energy saving and amount of recycled materials while maximising the performance and production stability of mixtures.

This study describes the construction of a pavement trial section where a cold-recycled asphalt mixture (CRAM) was placed as binder course. The CRAM was manufactured in-plant, using about 90% of reclaimed asphalt, bitumen emulsion and cement. The evolution of indirect tensile stiffness modulus (ITSM) was monitored on both laboratory-compacted specimens and cores extracted from the pavement.

From the analysis of results, it can be affirmed that the increase of ITSM due to the curing process was faster for laboratory specimens with respect to field cores. However, the long-term properties of the CRAM are expected to be very similar.

Keywords: trial section, cold recycling, bitumen emulsion, curing process

1. INTRODUCTION

In pavement construction, a new awareness on sustainable construction technologies is leading researchers to move materials and techniques with low environmental impact from laboratory-scale experimental studies to real-scale field applications.

Among sustainable paving techniques, cold recycling with bitumen emulsion ensures the highest benefits in terms of energies saving and amount of recycled materials. Indeed, the extreme limitation of material heating and the use of up to 100% recycled materials are the most ambitious targets [1, 2].

Cold recycled mixtures can be used in new constructions or in maintenance projects, depending on the availability of materials to be recycled and on the performance levels to be reached. Cold in-place recycling almost eliminates the haulage phase, whereas cold in-plant recycling (CPR) maximizes the performance and the production stability of the mixtures [3].

Thanks to the recent advances in the disposal, management and selection of materials from pavement demolition and to the use of high-performance binders, such as polymer-modified bitumen emulsion, CPR allows to produce cold-recycled asphalt mixtures (CRAM) with the same level of performance as the traditional hot-mix asphalt (HMA) mixtures [4, 5].

CRAM differ from HMA mainly because of the combined use of bituminous and cementitious binders and the presence of water. Thus, a curing process is necessary to achieve the long-term mechanical properties (strength and stiffness) [6, 7].

When both bituminous and cementitious binders are employed, simulating and predicting the effects of the curing process, is still a challenge. Certainly, the curing process depends on different mechanisms: emulsion breaking, moisture loss and hydration of cementitious compounds. Moreover, the curing process in the field is also related to construction (layer thickness, drainage conditions) and environmental factors (temperature, humidity) that are extremely variable, depending on site or season [8, 9].

In the framework of the RILEM TC 280-CBE on multiphase characterization of cold bitumen emulsion materials, this paper deals with the mechanical characterization of a CRAM with bitumen emulsion, produced in a mix-plant and laid down in a trial section. The main objective is to evaluate the effect of the curing conditions on the stiffness evolution of the cores taken from the trial section (field compaction, variable curing conditions) and the laboratory-compacted specimens (fixed compaction energy and curing conditions).

2. MATERIALS AND MIXTURES

The aggregate blend consisted of reclaimed asphalt (RA), fine aggregate and mineral filler. The RA was selected by means of a screening system to produce the desired fraction passing to 20 mm sieve size. The RA was designated following the EN 13108-8 as 20 RA 0/12, where 20 is the maximum size of the RA particles in mm (smallest sieve size through which 100% of the asphalt particles pass) and 0/12 is the size designation of the extracted aggregate.

The fine aggregate (limestone sand) was designated complying with EN 13043 as 0/1 GF85. The selection of the fine aggregate was based on its high sand equivalent value (SE = 81%), low methylene blue (MB = 1.1) and water absorption values (WA₂₄ = 1%).

A filler was selected with high fineness value (Blaine surface area of 6500 cm²/g) to increase the fine content in the blend and improve the bituminous mastic consistency.

Achieving maximum density, through increased inter-particle contacts and reduced voids in the mineral aggregate, leaving enough air space in the mixture to incorporate emulsion and water, was the main object in combining of granular fractions. For this reason, the well-known Fuller's curve, which represents the densest particle packing, was selected as target gradation curve. The design gradation was obtained by combining 88% of RA, 10% of fine aggregate and 2% of filler. Figure 1 shows the particle size distribution of granular materials and the design gradation in comparison with the specification band and the Fuller's curve ($D_{max} = 20$ mm).

A Portland limestone cement was selected to accelerate the curing process of the mixture and to increase the mixture stiffness and strength. The cement was designated complying with the EN 197-1 as CEM II/B-LL 32.5R.

An over-stabilised bitumen emulsion designated according to EN 13808 as C60B10 was selected to ensure a slow setting behaviour and to act as a lubricant during the compaction phase. Its formulation was designed to mix high fine contents and cement (Table 1).

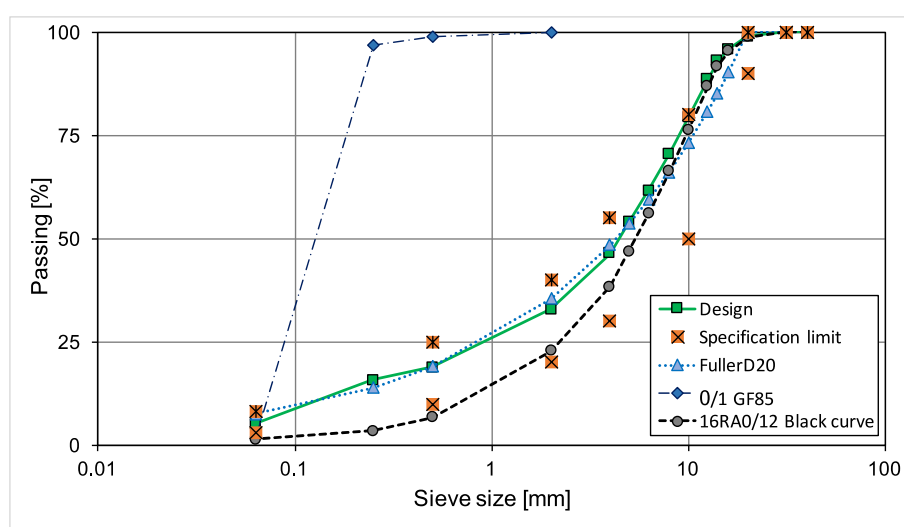


Figure 1: Particle size distribution of granular materials and design gradation

Table 1: Bitumen emulsion characteristics

Characteristic of bituminous emulsion		
Parameter	Standard	Value
pH value [pH]	EN 12850	2.45
Residual binder [%]	EN 1431	59.8
Storage stability [%]	EN 1429	0
Breaking value [-]	EN 13075-1	190
Mixing stability with cement [g]	EN 12848	< 2
Characteristic of bitumen (EN 13074)		
Penetration value [$\text{mm} \times 10^{-1}$]	EN 1426	58
Softening point [$^{\circ}\text{C}$]	EN 1427	47.8

In a previous study the mix design established the following recipe: 4.5% of bitumen emulsion (2.7% of residual bitumen), 2% of cement and 5% of water by aggregate weight (including water brought in by emulsion). According to the specification of the San Marino road agency [10], this recipe allowed obtaining an indirect tensile strength at 25 °C of 0.41 N/mm² (curing period of 72 hours at 40 °C) and a dry density of 2123 kg/m³.

3. DESCRIPTION OF THE MIXING PLANT

A mix plant for cement treated mixtures was adapted to produce CRAM by adding an inlet and a storage system for the bitumen emulsion. The mix plant (Figure 2-A) comprises four cold feed bins for aggregate and RA, a filler storage silo, a cement storage silo, an emulsion storage tank, a water pipeline, a twin-shaft counter-rotating mixer and a mixture storage silo. Working at ambient temperature (only the bitumen emulsion is kept at about 70 °C), the collection system (filter), dryer and burner are not required.

The four cold feed bins are filled by RA and fine aggregate. A vibrator keeps a constant supply of material flowing out of each cold feed bin. The variable speed feeder is located at the bottom of each cold feed bin to proportion the material fractions according to the job mix formula. An automatic weighing system monitors the mass of the aggregate flowing through a cold feed conveyor into the mixer. Emulsion, cement and filler are discharged almost simultaneously at the beginning of the mixer. The emulsion can also be supplied by connecting a tank truck to the in-let pump (delivery capacity of 15 m³/s). The mixer consists of a twin-shaft with paddles which rotate in opposite directions ensuring aggregates to be coated with emulsion in about 20 seconds (time elapsing from the constituent materials input to the fresh mixture output).

The facility continuously produces CRAM (up to 200 t/h) which is stored in a silo prior to be loaded onto a truck.

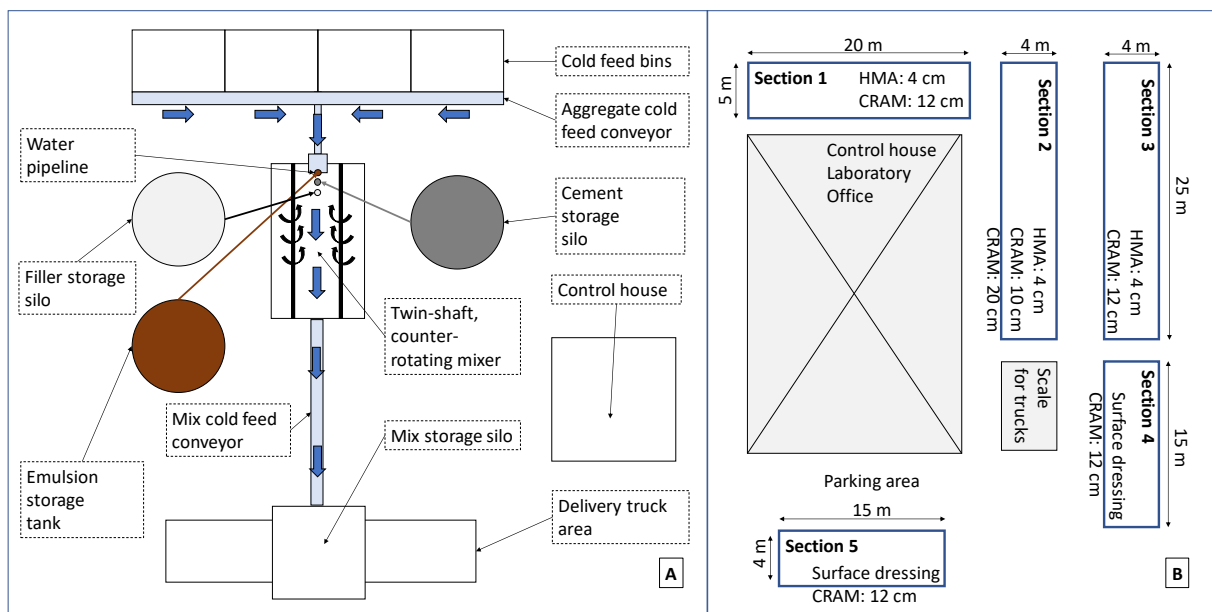


Figure 2: Scheme of the mixing plant (A) and trial section (B)

4. CONSTRUCTION OF THE TRIAL SECTIONS

Using about 150 t of CRAM, six pavement trial sections (Figure 2-B) were built using different materials, layers and compaction procedures. Before construction, a prime coat consisting of 1.65 kg/m² of slow-setting bituminous emulsion (1.00 kg/m² of residual bitumen)

saturated with filler was applied over the support layer (foundation or base course) in all sections.

Sections 1 and 3 represent a typical intermediate maintenance work for the San Marino road network. They consist of 4 cm HMA wearing course and 12 cm CRAM binder course. The binder course was immediately sealed with a tack coat consisting of 1.00 kg/m² of rapid-setting bituminous emulsion (0.60 kg/m² of residual bitumen).

Section 2 represents a typical deep maintenance work for the San Marino road network. It consists of 4 cm HMA wearing course, 10 cm of CRAM binder course and 20 cm of CRAM base course. The binder course was left unsealed for two days before applying the tack coat to verify the influence of moisture evaporation on curing process. The base and binder courses were laid down in succession without the application of a tack coat. The base course differs from the binder course only in the dosage of bitumen emulsion, 4% instead of 4.5% by aggregate weight. Section 2 was built in front of the scale to monitor the traffic (weight and number of passes).

Sections 4 and 5 represent a typical maintenance work for the San Marino rural road network. They consist of a double-layered surface dressing and 12 cm of CRAM binder course.

A paver moving at 5 m/min was employed to lay down the HMA and the CRAM layers. For all sections, the wearing course was laid down two days after the construction of the binder course. A 9-ton vibrating steel-wheeled roller, a 22-ton pneumatic roller and a 12-ton static steel-wheeled roller were used to compact the CRAM layers, following the procedures summarised in Table 2.

Table 2: Compaction procedures

Section	Layer	Material	1 st Phase		2 nd phase		3 rd phase	
			Type	passes	Type	passes	Type	passes
1	Surface	HMA	9 t SR	10	-	-	-	-
	Binder	CRAM	9 t SR	5	22 t PR	10	9 t SR	5
	Base	Existing	-	-	-	-	-	-
2	Surface	HMA	9 t SR	10	-	-	-	-
	Binder	CRAM	9 t SR	5	22 t PR	15	9 t SR	5
	Base	CRAM	9 t SR	5	22 t PR	10	9 t SR	5
3	Surface	HMA	9 t SR	10	-	-	-	-
	Binder	CRAM	22 t PR	2	9 t SR	5	22 t PR	13
	Base	Existing	-	-	-	-	-	-
4	Surface	Sur. Dressing	9 t SR	2	-	-	-	-
	Binder	CRAM	9 t SR	5	22 t PR	15	-	-
	Base	Existing	-	-	-	-	-	-
5	Surface	Sur. Dressing	9 t SR	2	-	-	-	-
	Binder	CRAM	12 t SR	20	-	-	-	-
	Base	Existing	-	-	-	-	-	-

SR = Steel roller, PR = Pneumatic roller

5. TESTING PROGRAMME

The testing programme was developed considering both laboratory-compacted specimens and cores taken from section 3.

The loose mixture produced in the mixing plant was sampled during the construction phase (before compaction) and immediately compacted using a gyratory compactor (GC). The mould

diameter was 150 mm and 2.7 kg of CRAM were compacted with 100 gyrations to obtain a suitable height (about 70 mm) for indirect tensile stiffness modulus (ITSM) testing. Other GC parameters (EN 12697-31) were: vertical pressure of 600 kPa, gyration speed of 30 rpm and external inclination angle of 1.25° [10]. After compaction, specimens were sufficiently stable to allow extrusion immediately. The specimens were cured in the laboratory, in a climatic chamber, at 40 °C and tested according to the programme shown in Table 3 (sample 1).

Cores taken from the trial section 3, at different times after construction, were also tested (samples 2, 3 and 4). After coring the specimens were cured in the same conditions as the specimens compacted in the laboratory (Table 3).

The ITSM (EN 12697-26 Annex C) was measured using a servo-pneumatic press. Load pulses with a rise time of 124 ms and a period of 3.0 s were applied. The peak load was adjusted to achieve a peak horizontal deformation of 2 microns. The measurements were carried out along two orthogonal diameters and, for each specimen, the average value was calculated.

Table 3: Experimental programme on lab-compacted specimens and cores

Sample	Specimen type	Number of specimens	Curing conditions	Testing time from construction [days]
1	Lab-compacted	4	Laboratory curing at 40 °C	3, 11, 23, 55, 73, 93, 157
2	Core	3	Field curing (23 days) followed by laboratory curing at 40 °C	23, 31, 55, 73, 93, 157
3	Core	3	Field curing (73 days) followed by laboratory curing at 40 °C	73, 74, 83, 93, 157
4	Core	4	Field curing (157 days)	157

6. RESULTS AND ANALISYS

Figure 3 shows the evolution of the average ITSM values of all the tested specimens, as a function of the curing time, starting from the construction day.

The ITSM values for lab-compacted specimens cured at 40 °C (sample 1) show a fast ITSM increase in the first 23 days. Afterwards, the increasing rate reduces and the ITSM approaches 8500 MPa after 73 days.

After 23 days of field curing the cores of sample 2 had an average ITSM value of 4128 MPa, which is about 55% of the value (7620 MPa) measured on the laboratory-compacted specimens, cured at 40 °C (Sample 1). However, after moving to laboratory curing at 40 °C, the ITSM value of sample 2 increased following the same evolution of sample 1 and reached 8028 MPa after 157 days from construction.

Similarly, after 73 days of field curing, the cores of sample 3 had an average ITSM value of 5743 MPa. At the same age, the ITSM of sample 1 and 2 were 8386 MPa and 7587 MPa, respectively. After moving to laboratory curing at 40 °C, the ITSM values of sample 2 increased with a higher rate and reached 8947 MPa after 157 days.

It can be concluded that field curing conditions slowed down the ITSM evolution with respect to laboratory curing at 40 °C. However, when the curing temperature is raised, the curing rate increases and the long-term value of ITSM does not appear penalised.

Connecting the experimental data corresponding to the ITSM values measured after only field curing for samples 2, 3 and 4, it is possible to highlight the actual evolution of stiffness in the field. Clearly, the rate of increase of ITSM is lower with respect to laboratory conditions (40 °C) because the average ambient temperature is lower. However, 157 days after construction, the ITSM still shows an increasing trend. Additional core sample will be extracted to verify the long-term stiffness of the CRAM cured in the field.

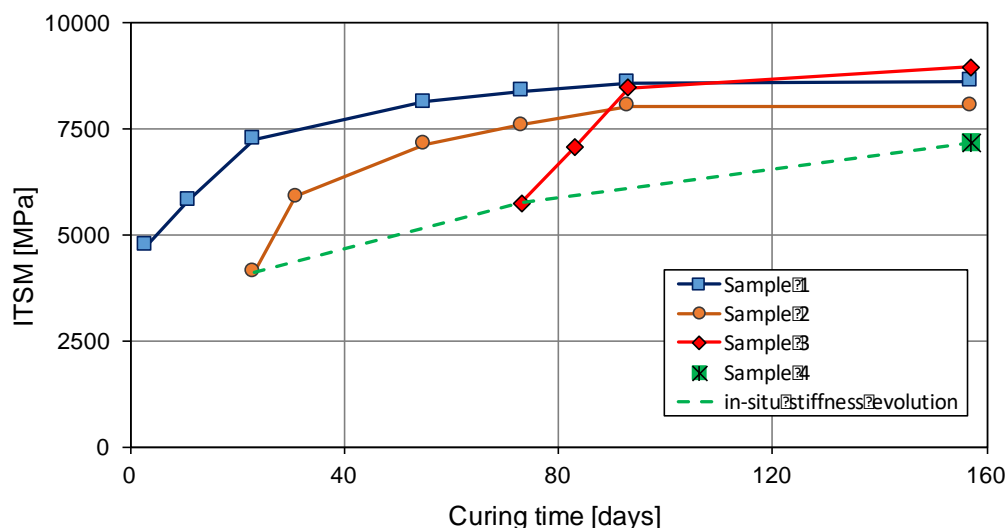


Figure 3: Evolution of ITSM over curing time

7. CONCLUSIONS

This paper describes an adapted mix plant to produce CRAM and the construction of a trial section which allowed “as produced” material sampling. Three samples were cored from the trial section at different curing age (10 cores in total). The ITSM evolution of laboratory-compacted specimens and cores as a function of curing period was monitored and the following conclusions can be drawn:

- specimens subjected to a curing temperature of 40°C show an evident increase of ITSM during the first 23 days. Afterwards, the ITSM slowly approaches to a long-term value of about 8500 MPa after 73 days at 40°C;
- in-situ curing at ambient conditions implies a slower ITSM evolution, but cores achieve similar ITSM value after 157 days;
- when the curing conditions change from ambient temperature (in-place curing) to 40°C (lab-curing), the ITSM values increase following the same evolution of lab-compacted specimens.

ACKNOWLEDGEMENTS

The Authors wish to thank the Cooperativa Braccianti Riminese (CBR) and the Valli Zabban S.p.A. that provided materials and support for the full-scale experimentation.

REFERENCES

- [1] Bocci, M., Canestrari, F., Grilli, A., Pasquini, E. and Lioi, D., 'Recycling techniques and environmental issues relating to the widening of an high traffic volume Italian motorway', *Int. J. Pavement Res. Technol.* **3** (4) (2010) 171-177.
- [2] Grilli, A., Cardone, F. and Bocci, E., 'Mechanical behaviour of cement-bitumen treated materials containing different amounts of reclaimed asphalt'. *European Journal of Environmental and Civil Engineering* **22** (7) (2018) 836-851.
- [3] Grilli, A., Graziani, A. and Bocci, M., 'Compactability and thermal sensitivity of cement-bitumen-treated materials', *Road Mater. Pavement Des.* **13** (4) (2012) 599-617.
- [4] Meocci, M., Grilli, A., La Torre, F. and Bocci, M., 'Evaluation of mechanical performance of cement-bitumen-treated materials through laboratory and in-situ testing', *Road Mater. Pavement Des.* **18** (2) (2017) 376-389.
- [5] Tebaldi, G., Dave, E. V., Marsac, P., Muraya, P., Hugener, M., Pasetto, M., Graziani, A., Grilli, A., Bocci, M., Marradi, A., Wendling, L., Gaudefroy, V., Jenkins, K., Loizos, A. and Canestrari, F., 'Synthesis of standards and procedures for specimen preparation and in-field evaluation of cold-recycled asphalt mixtures' *Road Mater. Pavement Des.* **15** (2) (2014) 272-299.
- [6] Cardone, F., Grilli, A., Bocci, M. and Graziani, A., 'Curing and temperature sensitivity of cement-bitumen treated materials', *Int. J. Pavement Eng.* **16** (10) (2015) 868-880.
- [7] García, A., Lura, P., Partl, M. N. and Jerjen, I. Influence of cement content and environmental humidity on asphalt emulsion and cement composites performance' *Mater. Struct.* **46** (8) (2013) 1275-1289.
- [8] Du, S., 'Effect of curing conditions on properties of cement asphalt emulsion mixture' *Constr. Build. Mater.* **164** 84-93.
- [9] Kim, Y., Im, S., and Lee, H. D., 'Impacts of curing time and moisture content on engineering properties of cold in-place recycling mixtures using foamed or emulsified asphalt' *J. Mat. Civil Eng.* **23** (5) (2010) 542-553.
- [10] Azienda Autonoma di Stato per i Lavori Pubblici (AASLP) 'Capitolato Speciale d'Appalto per la Manutenzione Straordinaria per Opere Stradali' (San Marino, 2017).

EXPERIMENTAL APPLICATION OF SYNTHETIC LIGHTWEIGHT AGGREGATES FOR THE PRODUCTION OF SPECIAL ASPHALT CONCRETES

P. Tataranni (1) and C. Sangiorgi (1)

(1) Department of Civil, Chemical, Environmental and Materials Engineering, University of Bologna, Italy

Abstract

This paper presents the results of a laboratory research on asphalt concretes made with synthetic expanded aggregates produced from waste materials. In the last years, the use of wastes for the production of new construction materials is constantly increasing. In the present research, through the alkali-activation process, two different wastes are used for the production of synthetic lightweight aggregates: a digested spent bentonite clay and a basalt powder. Both experimental aggregates have been fully characterized in compliance with the reference standards for lightweight aggregates. Taking as a reference some Italian specifications for special wearing course asphalt concretes, the physical and mechanical properties of two different experimental asphalt mixtures have been evaluated. For this purpose, a mixture prepared with traditional expanded clay aggregates was used as reference material.

The presented preliminary results indicate that the use of alkali-activated lightweight aggregate in total substitution of the expanded clay does not negatively affect the performances of the asphalt mixture. Moreover, the alkali-activation of these waste materials seems to be a suitable and sustainable solution for the production of lightweight aggregates for this and other purposes.

Keywords: Lightweight aggregates; alkali-activated material; special asphalt concrete; expanded clay.

1. INTRODUCTION

According to EN 13055-1 standard, a lightweight aggregate (LWA) is a granular material with a bulk density lower than 1.2 Mg/m^3 and a particle density lower than 2 Mg/m^3 . Earlier LWAs used in the engineering field as construction materials were of natural origin, generally volcanic [1]. Due to the limited availability of these natural aggregates and their changing properties, natural LWAs are not used anymore [2]. Moreover, the production of artificial lightweight materials allowed a better control of their properties and the marketing of different

products all over the world. Today their applications as construction materials is widespread due to their thermal and acoustical insulation characteristics as well as for their mechanical properties, combined with the possibility of reducing the self-weight of the final product. During years, several technologies have been developed to produce LWAs from both natural raw materials (clay, shale, slate, etc.) and industrial by-products (fly ashes, blast furnace slag, etc.). The Lightweight Expanded Clay Aggregate (LECA) is certainly the most used and widespread lightweight material that is suitable for civil engineering applications. Due to its physical and mechanical properties, LECA is used in the construction field for the production of lightweight concretes as well as for blocks and precast elements [3]. Some other applications are also known for water treatment and in the agriculture sector. In the infrastructures field, LECA is used in road and railway structures as light fill material to limit subgrade settlement and to increase the stability of structures and road embankments on weak grounds. In the last years, LECA has been also used for the production of Asphalt Concretes (ACs) with specific properties such as improved drainability or high skid resistance [4, 5]. The production of LECA takes place in rotary kilns where a special plastic clay is heated and sintered at high temperatures (1050-1250 °C). From a sustainable and eco-friendly perspective, in recent years relevant efforts have been made into finding solutions to use wastes for the production of alternative LWAs. The final aim was to limit the use of raw materials and define a functional intended use for materials otherwise disposed into landfills.

In the light of the above, in the present research two different wastes were used to produce synthetic LWAs through the so called alkali-activation process. The growing interest of researches into finding alternative and sustainable technique for the production of construction materials, lead to the development of alkali-activated materials [6, 7]. These are alternative cementitious materials, which can be synthesized by combining wastes rich in silica and alumina into a strong alkali environment. The result is the development of a strong amorphous binder, with similar or even better performances than those of traditional Portland cement, in terms of mechanical and chemical properties and fire resistance [8]. It is worth noting that from an environmental point of view, this technology involves a reduction in CO₂ emissions, if compared to the Portland cement production process, and a potential solution for wastes disposal and recycling [9]. Two different wastes were here used for the alkali-activation process: a digested spent bentonite clay (WBC) and a basalt powder (BP). Following some Italian specifications for special wearing course ACs, the produced synthetic LWAs were used in total substitution of LECA to confer a high skid resistance to the bituminous mixture.

2. MATERIALS

The alkali-activation synthesis involves two main group of materials, precursors and activators, in a chemical reaction that leads to the development of a strong amorphous binder. In the present research, the WBC and BP were used as precursors, together with a specific amount of metakaolin which confers suitable mechanical properties to the final product. A liquid mix made with sodium silicate and sodium hydroxide in specific proportions was the activator adopted for the alkali-activation synthesis.

The expansion agent used in this research was hydrogen peroxide. This foaming agent enables the expansion of the alkali-activated paste through the production of O₂. The liquid was added, in a pre-defined amount, to the mixture before curing.

A traditional LECA was used as reference material for both the LWAs characterization and for the production of special ACs.

2.1 Waste materials

WBC is a waste from the food industry process. The original material is a bleaching clay adopted for the decolouring process of vegetable oils that is subsequently processed through an anaerobic digestion for the production of biogas. At the end of this stage, the material is landfilled. After first attempts to directly use this waste into an alkali-activation process, the authors verified that a thermal treatment (calcination) improved the material reactivity [10].

The BP is a waste from the extractions and productions processes in basalt quarries. The material adopted in this research is completely passing through the 0.5 mm sieve. Due to its physical characteristics, basalt is widely used as construction material and its chemical properties make it suitable for the alkali activation process [11].

3. EXPERIMENTAL PROGRAM AND METHODS

The experimental program was divided in two consecutive steps. The first one was a preliminary characterization of the experimental LWAs. The two waste materials were used for the production of two kind of LWAs, labelled WBC_LWA and B_LWA. Taking as a reference the EN 13055-1 standard, which specifies the physical and mechanical properties of LWAs suitable for the production of construction materials, the characteristics of the synthetic aggregates were assessed and compared to the LECA ones.

The second and main step was related to the characterization of special ACs with high friction properties and produced with LWAs. Three different ACs mixtures were tested: two with the experimental LWAs (labelled WBC_AC and B_AC) and a reference one with LECA (LECA_AC) which was designed in compliance with the Italian technical specifications. The experimental program allowed the physical and mechanical analysis of the mixtures. The volumetric analysis (EN 12697-8) was carried out on three samples for each mixture that were prepared using a gyratory compactor and in accordance with the EN 12697-31 (compaction pressure of 600 kPa and 120 revolutions).

The mechanical analysis was carried out by the means of static and dynamic tests. In compliance with the EN 12697-23 standard, the Indirect Tensile Strength was evaluated at 25 °C on three SGC samples (80 gyrations) for each mixture and the reduction in ITS (EN 12697-12) after water immersion was studied on other three samples placed in water at 40 °C for 72 hours. The dynamic analysis was based on the evaluation of the Indirect Tensile Stiffness Modulus (ITSM, EN 12697-26) at three temperatures on three SGC samples (80 gyrations). The durability of the ACs was assessed by means of the Cantabro test (EN 12697-17) carried out on four Marshall samples (EN 12697-30, 50 blows) for each mixture. Finally, the surface properties of the mixture was verified measuring the skid resistance of the three ACs, in compliance with the EN 13036-4 standard.

The results obtained for the experimental LWAs and mixtures were always compared to those obtained from the traditional LECA during each step of the research.

4. LIGHTWEIGHT AGGREGATES CHARACTERIZATION

Taking as a reference the EN 13055-1 standard, which refers to LWAs that are suitable for construction materials, a full characterization of the experimental aggregates was carried out.

Data were always compared with values obtained for LECA. Table 1 summarizes the average results for each test.

Table 1: Tests and results for the experimental LWAs and LECA.

Test	Unit	WBC_LWA	B_LWA	LECA
Size distribution (EN 13043)	mm	0/14	0/16	0/12.5
Loose bulk density (EN 1097-3)	Mg/m ³	0.475	0.702	0.422
Air voids (EN 1097-3)	%	36.0	44.3	43.5
Water content (EN 1097-5)	%	4.27	1.27	0.18
Particle density (EN 1097-6)	Mg/m ³	1.18	1.69	0.87
Water absorption (EN 1097-6)	%	50	20	17
Crushing resistance (EN 13055-1)	N/mm ²	1.07	4.44	3.31

From the analysis of the results, both the experimental LWAs seem to have appropriate properties to be classified as lightweight aggregate suitable for applications as construction material. The two alkali-activated LWAs have densities lower than 2.00 Mg/m³ and a loose bulk density not exceeding 1.20 Mg/m³, in compliance with the limits imposed by the EN 13055-1 standard. In terms of mechanical properties, even if the aforementioned standard does not specify any limit, other technical specifications generally require a minimum value of crushing resistance equal to 1.00 N/mm². Both experimental LWAs exceed this threshold limit and B_LWA shows the highest crushing resistance, even if compared to the reference LECA. These results are strictly dependant on the chemical properties of the waste materials used as precursors that affect the final properties of the alkali-activated material.

5. ASPHALT CONCRETES CHARACTERIZATION

Once the physical and mechanical properties of the synthetic LWAs have been defined, two experimental ACs were prepared. Results were always compared with data obtained from a reference mixture containing LECA.

5.1 Mix Design

In compliance with relevant Italian technical specifications, a standard ACs prepared with LECA (12 % by the weight of aggregates) was taken as a reference mixture. Considering the different LWAs particles size distribution, a specific mix design was designed for each ACs, in order to have a constant amount of LWAs (12 % on the weight of aggregates) and the same grain-size distribution (Figure 1). A traditional 50/70 penetration grade bitumen was used as a binder; its rheological properties are given in Table 2.

Table 2: Rheological properties of asphalt 50/70 pen binder.

Test	Unit	Characteristic value
Penetration @ 25°C (EN 1426)	dmm	50 – 70
Soft. Point (EN 1427)	°C	50
Dynamic Visc. @ 60°C (EN 12596)	Pa·s	≥145

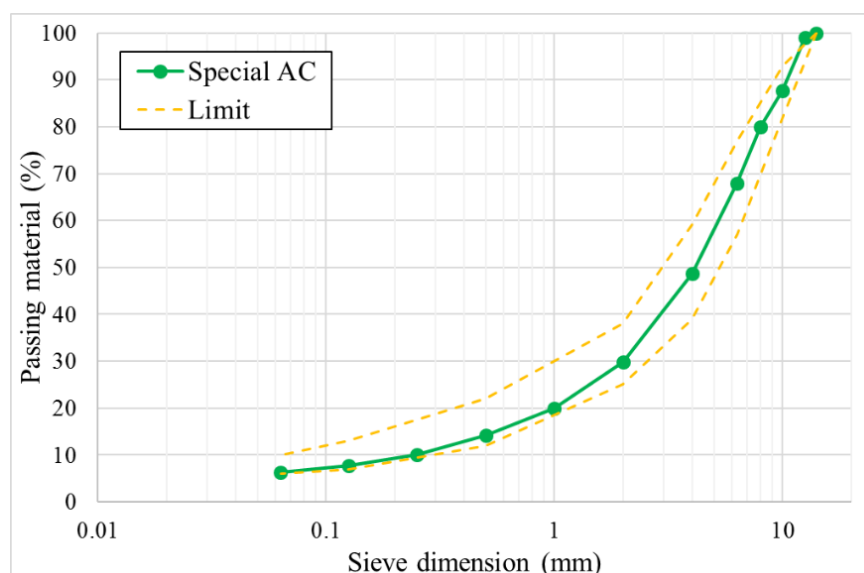


Figure 1: ACs particles size distribution.

The amount of binder was fixed according to 6 % on the weight of aggregates.

5.2 Air voids content analysis

Once the mix design of the AC was completed, three samples for each mixture were compacted by the means of gyratory compactor (EN 12697-31). To evaluate the workability properties of the mixtures and their physical properties, the air voids content (EN 12697-8) was assessed at different compaction energies corresponding to 10, 80 and 120 gyrations. Table 3 summarizes the average results.

Table 3: Average air voids content for each mixture.

Air voids content (EN 12697-8)	WBC_AC	B_AC	LECA_AC
@ 10 gyrations (%)	22.6	21.4	20.1
@ 80 gyrations (%)	17.1	14.8	13.9
@ 120 gyrations (%)	16.1	13.7	12.7

From the analysis of the results, mixtures have a high air voids content. The variation in porosity between the ACs is probably due to the different LWAs particles size distribution. The following mechanical tests will evaluate if the high air voids content has a detrimental effect on the properties of the final bituminous mixtures.

5.3 Indirect Tensile Strength and water susceptibility

The mechanical analysis was carried out by means of static and dynamic tests. The evaluation of the level of tenacity reached by the aggregates-filler-bitumen bond is generally given by the Indirect Tensile Strength (ITS) test. In compliance with the EN 12697-23 standard, three SGC samples (80 gyrations) were produced for each mixture and tested after conditioning for 4 hours at 25 °C. In order to evaluate the detrimental effect of water on the mechanical properties of the ACs, their reduction in ITS values (ITSR, EN 12697-12) was also assessed. Three additional samples for each mixture were prepared with the same compaction energy. These specimens were then kept in a water bath at 40 °C before testing at 25°C. The average results are shown in Table 4.

Table 4: Average ITS and ITSR values.

Mixture	ITS (MPa)	ITS _{wet} (MPa)	ITSR (%)
WBC_AC	0.88	0.61	69
B_AC	0.77	0.69	90
LECA_AC	0.70	0.69	98

From the analysis of results, the experimental ACs showed higher ITS values if compared to the reference mixture. This might be due to the different absorption of the synthetic LWAs, related to their porosity and to the higher specific surface. It is worth noting that the considered Italian technical specifications suggest an ITS value between 0.70 and 1.20 MPa for this kind of mixtures. Both the ACs prepared with the synthetic LWAs have suitable mechanical properties, despite the porosity of the samples. On the contrary, the high air voids content affects the performance of the mixture after the water saturation of samples. For each mixture, the reduction in ITS follows the increase in air voids content. WBC_AC, which has a significant porosity, registered the highest ITS decrease.

5.4 Indirect Tensile Stiffness Modulus evaluation

The mechanical characterization was also supported by the evaluation of the Indirect Tensile Stiffness Modulus (ITSM) according to the EN 12697-26 standard. Moreover, the thermal sensitivity of the mixtures was assessed by testing the material at three different temperatures: 10, 20 and 30 °C. For this purpose, three SGC specimens (80 gyrations) were prepared for each AC. Average results are shown in Table 5.

Table 5: Average ITSM results.

Mixture	ITSM (MPa) @ 10 °C	ITSM (MPa) @ 20 °C	ITSM (MPa) @ 30 °C
WBC_AC	7981	4952	2328
B_AC	7942	5213	2291
LECA_AC	6222	3761	1508

As overall result, all the ACs show adequate stiffness at each testing temperature. In compliance with ITS results, the experimental mixtures exhibit better mechanical properties if compared to the reference one, despite the samples high air voids content. There is not large difference in ITSM values between the experimental ACs. In terms of thermal sensitivity, the substitution of traditional LWA with synthetic materials does not affect the behaviour of the final bituminous mixtures.

5.5 Cantabro test

According to the EN 12697-17 standard, the Cantabro test was used to assess the ravelling resistance of the bituminous mixtures. The particles loss weight is traditionally one of the different method adopted to estimate the durability of ACs. For this purpose, four Marshall samples (50 blows) were prepared and kept at 20 °C for 4 hours before testing. The average results are shown in Table 6.

Table 6: Average Cantabro test results.

	WBC_AC	B_AC	LECA_AC
Particle loss (%)	5.4	6.3	8.2

The results are in line with the ITS values: the experimental mixtures show the best results if compared to LECA_AC. Once again, the high porosity of the synthetic ACs does not affect the behaviour of the bituminous mixtures. The Cantabro test results support the hypothesis of a strong aggregates-filler-bitumen bond for the experimental ACs conferred by the higher specific surface of the synthetic aggregates.

5.6 Skid resistance evaluation

The high surface friction is probably the most important functional property of the designed special AC. The EN 13036-4 standard describes a method for the laboratory evaluation of the skid resistance of bituminous surfaces. Three samples for each mixtures were tested and the average results are shown in Table 7, in terms of Pendulum Test Value (PTV).

Table 7: Average skid resistance results.

Skid resistance	WBC_AC	B_AC	LECA_AC
PTV	73	70	69

As overall results, each tested AC show a consistent skid resistance. The Italian technical specifications suggest a PTV greater than 55 after laying. The WBC_AC has the highest skid resistance, while similar values are registered for B_AC and for the reference mixture. The substitution of traditional LWAs with synthetic aggregates does not negatively affect the friction properties of the bituminous surface, which are actually improved.

6. CONCLUSIONS

On the basis of the presented results, the following conclusions can be drawn:

- The adopted waste materials seem to be suitable for the production of synthetic LWAs with adequate properties so to extend their use as construction materials.
- The substitution of traditional LECA with the experimental LWAs within a special AC needs for a specific mix design. Moreover, the dimensions of the synthetic aggregates must be taken into account since the porosity and the specific surface affect their absorption properties. This could have a negative effect on the workability and compactability characteristics of the final bituminous mixture.
- The experimental ACs show the highest mechanical performances (ITS, ITSM and Cantabro test). This is probably related to the stronger bond between aggregates and bitumen, due to the higher absorption power of the synthetic aggregate. The thermal sensitivity of the bituminous mixtures is not negatively influenced. On the other hand, as a result of the high ACs internal porosity, the mechanical properties are detrimentally affected after the saturation in water. Additional durability tests are needed.
- An increase in skid resistance is registered for the experimental ACs, more likely due to the different surface texture given by the specific LWAs dimensions.

In the light of these preliminary results, the application of synthetic LWAs within bituminous mixtures seems to be a viable solution for the production of special ACs. However, a more specific mix design needs to be optimized to decrease the air voids content.

REFERENCES

- [1] Chen, H.-J., Tsai, W.-P., Tang, C.-W. and Liu, T.-H., ‘Time-dependent properties of lightweight concrete using sedimentary lightweight aggregate and its application in prestressed concrete beams’. *Structural Engineering and Mechanics*. **39** (6) (2011).
- [2] Arioz, O., Arslan, G., Tuncan, A., Tuncan, M., Kaya, G., Karasu, B., Kilinc, K. and Kivrak, S. “Lightweight Expanded Aggregate Production from Bottom Ash”. Proceedings of the *10th international conference of the European Ceramic Society (ECerS)*, Berlin, 2007, 2051-2053.
- [3] Rashad, A.M. “Lightweight expanded clay aggregate as a building material – An overview”. *Construction and Building Materials*, **170** (2018) 757–775.
- [4] Shen, D.-H., Wu, C.-M. and Du, J.-C. “Performance evaluation of porous asphalt with granulated synthetic lightweight aggregate”. *Construction and Building Materials*, **22** (2008) 902–910.
- [5] Zhou, X., Kastiukas, G., Lantieri, C., Tataranni, P., Vaiana, R. and Sangiorgi, C. “Mechanical and Thermal Performance of Macro-Encapsulated Phase Change Materials for Pavement Application”. *Materials*. **11** (2018) 1398.
- [6] Provis, J.L. “Geopolymers and other alkali activated materials: why, how, and what?”, *Materials and Structures*. **47** (2014) 11-25.
- [7] Beghoura, I., Castro-Gomes, J., Ihsan, H. and Estrada, N. “Feasibility of alkali-activated mining waste foamed materials incorporating expanded granulated cork”. *Mining Science*. **24** (2017) 7-28.
- [8] Pacheco-Torgal, F., Castro-Gomes, J. and Jalali, S. “Alkali-activated binders: A review: Part 1. Historical background, terminology, reaction mechanisms and hydration products”. *Construction and Building Materials*, **22** (2008), 1305-1314.
- [9] Sangiorgi, C., Lantieri, C., Tataranni, P., Castro-Gomes, J. and Gabriel, M. “Reuse of mining waste into innovative alkali-activated-based materials for road pavement applications”. Proceedings of the *4th international conference of the Chinese-European Workshop (CEW) on “Functional Pavement Design”*, Delft, 2016, 1735-1744.
- [10] Tataranni, P., Besemer, M.G., Bortolotti, V. and Sangiorgi, C. “Preliminary Research on the Physical and Mechanical Properties of Alternative Lightweight Aggregates Produced by Alkali-Activation of Waste Powders”. *Materials*. **11** (2018), 1255.
- [11] Saraya, M.E.-S.I. and El-Fadaly, E. “Preliminary Study of Alkali Activation of Basalt: Effect of NaOH Concentration on Geopolymerization of Basalt “. *Journal of Material Science and Chemical Engineering*. **5** (2017) 58-76.

NEW GENERATION OF CONSTRUCTION MATERIALS
SESSION 3: Durability of AAMs

TESTING THE DURABILITY OF ALKALI-ACTIVATED CONCRETES

John Provis

Department of Materials Science and Engineering, The University of Sheffield, United Kingdom

Abstract

This presentation will summarise some of the results obtained from the round-robin testing programme of RILEM TC 247-DTA, where a set of alkali-activated concretes were designed, produced in different laboratories, and tested according to a number of standard durability test methods. The reproducibility of individual tests in each laboratory was in general very good, although with some notable exceptions including the ASTM C1202 "Rapid Chloride Permeability Test", which gave scattered results. The inter-laboratory reproducibilities of durability test results were moderate, but in several cases better than the reproducibility of compressive strength testing data for the same concretes. There was also not a clear correlation between the strength obtained in each lab for a specific mix, and the transport-related durability characteristics of the same concrete in that laboratory; durability and strength appear to be significantly decoupled in alkali-activated concretes. The results of this work provide important information highlighting areas in which further understanding of both materials and test methods is required.

Keywords: alkali activated mortar; geopolymers; fire resistance; steel corrosion; acoustic emission

BEHAVIOUR OF REINFORCED ALKALI-ACTIVATED FLY ASH MORTARS UNDER LEACHING CONDITIONS

Petr Hlaváček (1), Steffi Reinemann (2), Gregor J.G. Gluth (1), Gino Ebell (2) and Jürgen Mietz (2)

(1) Bundesanstalt für Materialforschung und -prüfung (BAM), 7.4 Technology of Construction Materials, Unter den Eichen 87, 12205 Berlin, Germany

(2) Bundesanstalt für Materialforschung und -prüfung (BAM), 7.6 Corrosion and Corrosion Protection, Unter den Eichen 87, 12205 Berlin, Germany

Abstract

Corrosion of steel reinforcement in concrete is one of the major deterioration mechanisms limiting the service life of reinforced concrete structures. While for conventional (Portland cement-based) concretes a great amount of experience exists in this regard, the factors that determine the onset of reinforcement corrosion in alkali-activated materials are incompletely understood yet.

One aspect of corrosion protection is leaching and the accompanying changes of the concrete pore solution. In the present study, alkali-activated fly ash mortars with embedded carbon steel rebars were exposed to de-ionised water for periods up to 330 days, and the electrochemical response of the steel (free corrosion potential, polarisation resistance), the alteration of the mortar (ohmic resistance, mechanical strength, pore size distribution) as well as the pore solution composition were monitored.

Although substantial alkali leaching was observed, the pH of the pore solution remained at values sufficient to protect the embedded steel from depassivation. The mortar did not exhibit indications of significant deterioration. Thus, the present results suggest that leaching is not critical for protection of steel reinforcement in alkali-activated fly ash mortars and concretes.

Keywords: alkali activation, fly ash, leaching, reinforcement corrosion

1. INTRODUCTION

One of the most important aspects of the durability of reinforced concrete structures is the protection that the concrete provides against corrosion of embedded steel reinforcement. While for conventional (Portland cement-based) concretes a great amount of experience exists in this

regard [1], knowledge about how alkali-activated concretes protect embedded steel emerged only during the last years, and many relevant aspects remain to be clarified [2].

One of the aspect that appears to be understudied is leaching of low-Ca alkali-activated materials. However, this issue seems to be particularly relevant, as these materials generally do not contain pH buffers such as $\text{Ca}(\text{OH})_2$, which could delay the onset of steel corrosion under leaching conditions [3]. Leaching of alkali ions would also affect the pH that develops on carbonation [4,5] as well as the critical chloride content (*via* the associated decrease of pH) [6].

In this contribution, we summarise free corrosion potential, polarisation resistance and ohmic resistance data for carbon steel in alkali-activated fly ash mortars, leached for 330 days in de-ionised water. In addition, we present data on the evolution of the mechanical strength, the pore structure and the pore solution composition of the mortar during that period.

2. MATERIALS AND METHODS

2.1 Starting materials and mortar preparation

Alkali-activated fly ash mortars (referred to as 'FA5' in the following) were produced from 580 kg/m³ hard coal fly ash (57.4 % SiO_2 , 17.5 % Al_2O_3 , 7.0 % Fe_2O_3 , 7.5 % CaO , 4.1 % LOI), 319 kg/m³ sodium silicate solution (18.4 % Na_2O , 20.0 % SiO_2 ; $M_s = 1.12$) and 1333 kg/m³ quartz sand (0.1–4 mm). The FA5 mortars were cured at 80 °C/80 % RH for 24 h; after this period, the specimens were removed from the moulds and further cured at 23 °C/50 % RH for one week. The chloride diffusion coefficient of these mortars, determined according to NT BUILD 443 (1995-11), was $D_e = 41.9 \times 10^{-12} \text{ m}^2/\text{s}$ [7].

As a reference for comparison, Portland cement mortars (referred to as 'CEM I' in the following) were produced from 606 kg/m³ CEM I 42.5 R, 273 kg/m³ water and 1304 kg/m³ quartz sand (0.1–4 mm). The CEM I mortars were cured at 23 °C/~99 % RH for 28 or 30 days.

2.2 Electrochemical investigations

Electrochemical measurements were done on ribbed BSt 500 carbon steel rebars with $\varnothing = 10 \text{ mm}$ and $l = 120 \text{ mm}$, embedded in FA5 or CEM I mortars. Stainless steel rods were welded to the ends of the rebars, the assemblage cleaned by grit blasting (corundum grit) and then installed in the prism moulds into pre-drilled locating holes. After curing, the mortar cover of the rebars was decreased to 5 mm by grinding off mortar from the prisms; subsequently, the prisms were cleaned in an ultrasonic bath in water.

Mortar prisms for leaching were first preconditioned at ~21 °C and ~98 % RH for 90 days, and then immersed in a container filled with de-ionised water (≤ 16 prisms in ~50 dm³ water). During the first 132 days of leaching, the water in the container was exchanged approx. weekly; subsequently, the water was exchanged continuously *via* an inlet and an outlet at a flow rate of ~15 dm³/h.

For the electrochemical measurements, specimens were removed from the container and allowed to dry in air for ~20 hours on a lab bench before being partially immersed together with a $\text{Ag}/\text{AgCl}_{(\text{sat.})}$ reference electrode in tap water in a purpose-built acrylic glass cell equipped with the counter electrode (mixed metal oxide mesh). After stabilisation and recording of the free corrosion potential (E_{corr}), the ohmic resistance (R_{el}) and polarisation resistance (R_{p}) were determined with the galvanostatic pulse technique under the following conditions: $\Delta t = 20 \text{ s}$; $I = \pm(10 \dots 50) \mu\text{A}$. Since there was always good agreement between the results obtained with

anodic and cathodic pulses, only those found with anodic pulses will be reported below. Immediately after the measurements, the samples were put back into the water-filled container for further leaching.

Further experimental details of sample production and electrochemical testing are presented in ref. [7].

2.3 Mechanical strength, mercury intrusion porosimetry and pore solution analysis

Strength testing, mercury intrusion porosimetry (MIP) and pore solution extraction was performed on samples without embedded steel, otherwise cured and treated as the samples with steel rebar.

Compressive and flexural strength were determined in accordance with the testing conditions specified in EN 196-1. The leached FA5 and CEM I mortars were dried at 23 °C/50 % RH for 5 days before strength testing.

MIP was performed on a Porotec Pascal 140/240 device using sample grit with maximum particle dimensions of ~2 mm, dried at 105 °C. Conversion from intrusion data to pore diameters (d_p) was carried out by means of the Washburn equation, assuming cylindrical pores. The surface tension was taken as 0.480 N/m, the contact angle was assumed to be 140.0°. The highest attainable mercury pressure during the measurements was 200 MPa, corresponding to a smallest accessible d_p of ~7.4 nm.

Pore solutions of the mortars were obtained by expression with the steel die method, employing a maximum pressure of 650 MPa. The mortar prisms were broken manually before being put into the die. For the non-leached FA5 mortar it was not possible to obtain pore solution by the above method, presumably because its pores were not saturated despite the storage at 98 % RH. For the leached FA5 mortars, the pressure had to be released and then increased to 650 MPa repeatedly to obtain a sufficient amount of solution. The expressed pore solutions were collected in a syringe, the solution pH analysed using a pH electrode (calibrated against standard buffer solutions) and the solutions then diluted 1:50 (v/v) with ultrapure water. Subsequently, elemental compositions were analysed by inductively coupled plasma optical emission spectrometry (ICP-OES).

3. RESULTS AND DISCUSSION

3.1 Electrochemical investigations

Figs. 1 and 2 show the results of the electrochemical investigations. These results confirm the conclusions of an earlier study, conducted for a shorter leaching duration [7]; in detail: While E_{corr} remained approx. constant with some fluctuations (in the range ~10–130 mV) for the CEM I mortar, it increased slowly from ~35 mV to ~220 mV after 330 days for the FA5 mortar (Fig. 1). The ohmic resistance of the FA5 mortar and the polarisation resistance of the steel in the FA5 mortar, too, increased steadily during leaching, though R_{el} of FA5 was always lower than R_{el} of CEM I (Fig. 2). The reason for the sharp increase of R_{el} of the CEM I mortar at the start of leaching, and its decline on changing the leaching conditions from water exchange to continuous water flow is not clear yet. Nevertheless, R_p of the steel in FA5 and in CEM I were always similar (remaining at 60–70 k Ω cm² for CEM I; evolving from ~60 to ~100 k Ω cm² for FA5), indicating a similar state of the steel in both mortars; the E_{corr} and R_p values show that this was the passive state.

These results show that in both mortars leaching did not induce a drop in pH large enough to cause depassivation. These conclusions were confirmed by visual inspection of the rebars after 316 d of leaching: the steel in both mortars showed no signs of corrosion [7]. This means that FA5 was able to protect the embedded steel under very severe leaching conditions over the observation period of 330 d, implying acceptable behaviour under real-world conditions too.

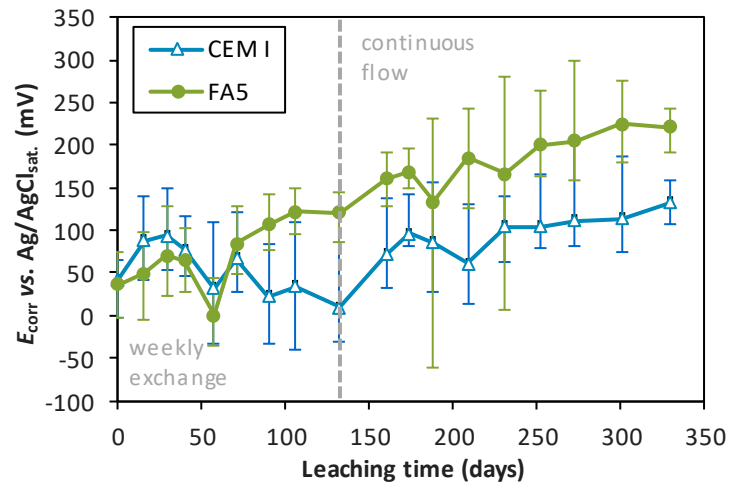


Figure 1: Free corrosion potential of steel rebars embedded in CEM I and FA5 mortars under leaching conditions (de-ionised water; 5-mm mortar cover). Error bars represent min/max values

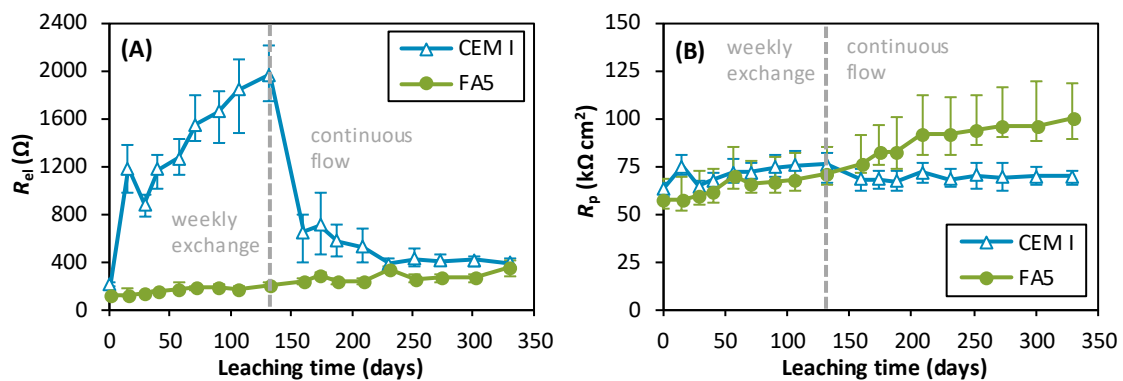


Figure 2: Ohmic resistance (A) and polarisation resistance (B) for steel rebars embedded in CEM I and FA5 mortars under leaching conditions (de-ionised water; 5-mm mortar cover). Error bars represent min/max values

3.2 Compressive strength and pore size distribution (MIP)

The compressive and flexural strengths of both mortars did not decrease during leaching; instead, a slight increase of mechanical strengths could be observed (Table 1), which can most likely be assigned to continued hydration in the case of CEM I.

Fig. 3 shows the pore size distributions (determined by MIP, *i.e.* more correctly referred to as pore entry size distributions) of the CEM I and FA5 mortars before and after leaching. Firstly, the three measurements on separate leached samples of each mortar (a, b, c in Figs. 3A and 3B)

demonstrate a good repeatability of the measurements. Second, it can be discerned that for both mortars leaching led to a slight coarsening of the pore structure, visible as a slight increase of the threshold pore diameter (from $\sim 0.10 \mu\text{m}$ to $\sim 0.15 \mu\text{m}$ for CEM I, and from $\sim 2 \mu\text{m}$ to $\sim 3 \mu\text{m}$ for FA5). In addition, some changes occurred for the mesopore region ($d_p < \sim 0.05 \mu\text{m}$) of the FA5 mortars: While the decrease of the total intruded pore volume after leaching may indicate a densification of the structure, the increasing slope at the smallest measured d_p indicates that a significant fraction of the mesopores could not be intruded at the applied maximum pressure, leaving the possibility that the porosity has remained constant or has even increased during leaching, while at the same time the mesopores have narrowed. Additional studies are required to clarify this issue.

Nevertheless, from the present data it can be concluded that leaching of FA5 for ~ 300 days did not induce severe deterioration of the mortar. However, it is noted that the FA5 mortar assumed an altered physical appearance (e.g., decreased density, different sound on tapping) after the leaching procedure.

Table 1: Compressive and flexural strengths of the CEM I and FA5 mortars before and after leaching in de-ionised water for 315 days (standard deviations after the \pm sign)

	Compressive strength after curing (MPa)	Flexural strength after curing (MPa)	Compressive strength after 315-d leaching (MPa)	Flexural strength after 315-d leaching (MPa)
CEM I	70.6 ± 1.9	7.1 ± 0.3	78.9 ± 2.6	5.5 ± 0.1
FA5	80.9 ± 2.0	7.8 ± 0.4	88.7 ± 2.6	10.4 ± 0.3

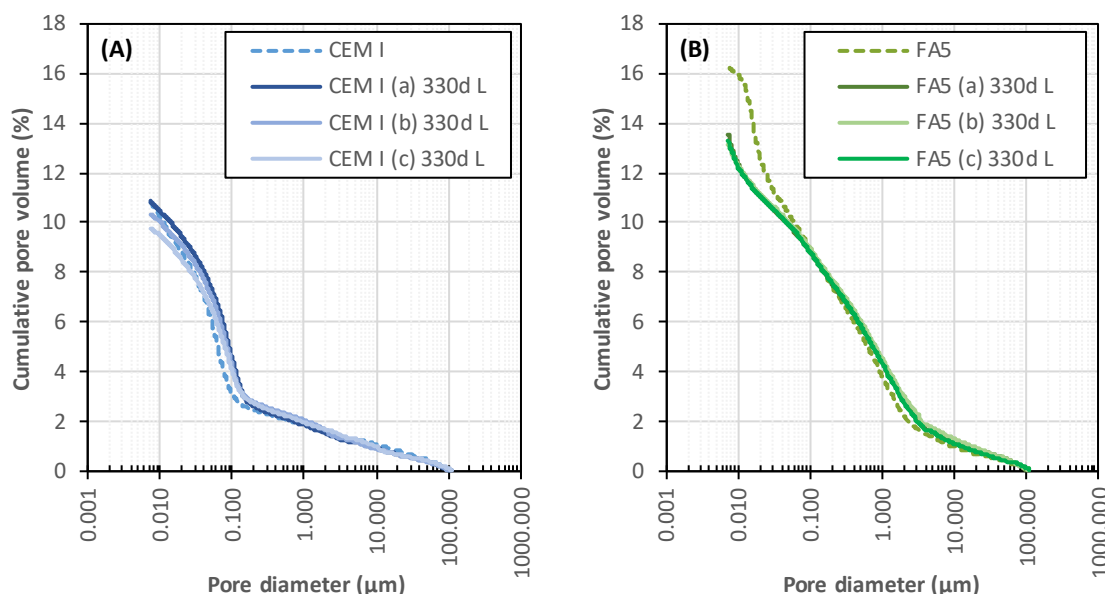


Figure 3: Pore size distributions, determined by MIP, of the CEM I (A) and FA5 (B) mortars before and after leaching in de-ionised water for 330 days

3.3 Pore solution analyses

The pore solution compositions and pH values of CEM I and FA5 after various times of leaching are shown in Table 2. The values shown represent the bulk mortars, *i.e.* not necessarily the conditions at the steel-mortar interface. Nevertheless, they serve to demonstrate general trends of the changes occurring in the pore solutions of the mortars during leaching.

In both mortars, leaching of alkalis took place, leading to Na and K concentrations on the order of few tens of mM after 330 days. This was accompanied by a significant drop of the pH in FA5, while the pH value remained above 13 in CEM I over that period. This can be assumed to be related to the buffering effect of portlandite, which is present in CEM I but not in FA5. Nevertheless, the pH value of the pore solution of FA5 was 11.4 after 330 days of leaching, evidently sufficient to protect the embedded steel from depassivation (section 3.1).

Additional notable observations include that significant sulfur leaching occurred in both mortars, while in FA5 the Al concentrations increased significantly over the leaching period. The latter observation may possibly indicate an increase of the solubility of the binding phase (*i.e.* sodium aluminosilicate gel [8]) of the FA5 mortar, but this has to be tested in future studies.

Table 2: Pore solution compositions of the CEM I and FA5 mortars after leaching in de-ionised water for various periods

	CEM I as cured	CEM I leached 90 days	CEM I leached 200 days	CEM I leached 330 days	FA5 leached 90 days	FA5 leached 200 days	FA5 leached 330 days
pH	13.9	13.2	13.7	13.0	12.3	12.2	11.4
Al (mM)	0.25	0.52	0.14	0.26	0.82	1.48	1.68
Fe (mM)	0.03	0.08	0.00	0.02	0.05	0.09	0.09
Ca (mM)	3.7	2.8	s.v.	s.v.	0.6	< 0.001	< 0.001
Mg (mM)	0.42	0.06	< 0.001	0.04	0.09	0.07	0.14
Na (mM)	299	90	34	24	113	40	24
K (mM)	327	s.v.	54	45	4	3	s.v.
Si (mM)	0.31	s.v.	< 0.001	0.12	33	30	11
S (mM)	11.0	6.0	1.6	1.2	7.4	3.7	3.0

s.v.: suspect value/outlier

4. CONCLUSIONS

Leaching of carbon steel-reinforced, alkali-activated fly ash mortar (5-mm mortar cover) in de-ionised water for 330 days did not induce depassivation of embedded steel rebars. Instead, free corrosion potential and polarisation resistance, as well as ohmic resistance, increased continuously over the leaching period. The free corrosion potential and the polarisation resistance after 330 days of leaching were ~ 220 mV vs. Ag/AgCl_(sat.) and ~ 100 k Ω cm², respectively.

The alkali-activated mortar did not deteriorate significantly during the leaching period; *viz.*, its compressive and flexural strength increased slightly, and only a slight coarsening of the pore structure was observed by mercury intrusion porosimetry. Leaching led to a substantial decrease of the Na concentration and an accompanying decrease of the pH of the pore solution of the mortar (pH = 11.4 for the bulk material). As shown by the electrochemical data, however, the pH remained high enough to protect the embedded steel from depassivation.

As the leaching procedure adopted here presents a rather severe attack, the present results imply that leaching is not a critical factor for protection of steel reinforcement in properly designed alkali-activated fly ash mortars and concretes. However, additional studies are required to investigate how leaching affects the resistance against carbonation and the protection against chloride-induced depassivation of steel in alkali-activated fly ash mortars or concretes.

ACKNOWLEDGEMENTS

Financial support by the AiF (Arbeitsgemeinschaft industrieller Forschungsvereinigungen “Otto von Guericke” e.V.) on behalf of the German Federal Ministry for Economic Affairs and Energy *via* the IGF project 18910 N of the GfKORR e.V. is gratefully acknowledged.

REFERENCES

- [1] Bertolini, L., Elsener, B., Pedferri, P., Redaelli, E. and Polder, R., 'Corrosion of Steel in Concrete', 2nd Edn (Wiley-VCH, Weinheim, 2013).
- [2] Mundra, S., Bernal, S.A., Criado, M., Hlaváček, P., Ebell, G., Reinemann, S., Gluth, G.J.G. and Provis, J.L., 'Steel corrosion in reinforced alkali-activated materials', *RILEM Tech. Lett.* **2** (2017) 33-39.
- [3] Lloyd, R.R., Provis, J.L. and van Deventer, J.S.J., 'Pore solution composition and alkali diffusion in inorganic polymer cement', *Cem. Concr. Res.* **40** (2010) 1386-1392.
- [4] Bernal, S.A., Provis, J.L., Brice, D.G., Kilkullen, A., Duxson, P. and van Deventer, J.S.J., 'Accelerated carbonation testing of alkali-activated binders significantly underestimates service life: the role of pore solution chemistry', *Cem. Concr. Res.* **42** (2012) 1317-1326.
- [5] Babae, M., Khan, M.S.H. and Castel, A., 'Passivity of embedded reinforcement in carbonated low-calcium fly ash-based geopolymer concrete', *Cem. Concr. Compos.* **85** (2018) 32-43.
- [6] Mundra, S., Criado, M., Bernal, S.A. and Provis, J.L., 'Chloride-induced corrosion of steel rebars in simulated pore solutions of alkali-activated concretes', *Cem. Concr. Res.* **100** (2017) 385-397.
- [7] Gluth, G.J.G., Hlaváček, P., Reinemann, S., Ebell, G. and Mietz, J., 'Leaching, carbonation and chloride ingress in reinforced alkali-activated fly ash mortars', *MATEC Web Conf.* **199** (2018) 02025.
- [8] Greiser, S., Gluth, G.J.G., Sturm, P. and Jäger, C., ' $^{29}\text{Si}\{^{27}\text{Al}\}$, $^{27}\text{Al}\{^{29}\text{Si}\}$ and $^{27}\text{Al}\{^1\text{H}\}$ double-resonance NMR spectroscopy study of cementitious sodium aluminosilicate gels (geopolymers) and gel-zeolite composites', *RSC Adv.* **8** (2018) 40164-40171.

THERMAL PROPERTIES AND STEEL CORROSION IN LIGHT-WEIGHT ALKALI ACTIVATED MORTARS

L. Carabba (1), G. Masi (1), S. Pirskawetz (2), S. Krüger (2), G. J. G. Gluth (2), M. C. Bignozzi (1)

(1) Department of Civil, Chemical, Environmental and Materials Engineering, University of Bologna, Italy

(2) Bundesanstalt für Materialforschung und -prüfung (BAM), Berlin, Germany

Abstract

This study aims at investigating the use of coal fly ash-based alkali activated mortars as passive fire protection system for steel structures. These systems are used to slow down the temperature rise of the steel substrate in case of fire. In addition, the protective system should guarantee the ability to prevent and/or mitigate steel corrosion phenomena. The behavior of a light-weight mortar was compared to that of a normal-weight mortar. Density and porosity were measured to better characterize the physical properties of the mortars. The degree of protection in case of fire was assessed by performing medium-scale fire tests. Acoustic emission measurements were conducted to analyze cracking phenomena during the high temperature exposure. The corrosion process was evaluated using an electrochemical approach in order to monitor the durability of the developed material. Preliminary results show that a 20 mm- thick layer of light-weight mortar is able to protect the steel substrate from reaching the critical temperature of 500 °C for 38 minutes in case of cellulosic fire. In addition, alkali activated mortars provide protection for carbon steel in presence of aggressive environment (i.e. presence of chlorides). The corrosion resistance is strictly related to the physical properties of the developed mortars.

Keywords: alkali activated mortar; geopolymer; fire resistance; steel corrosion; acoustic emission

1. INTRODUCTION

Alkali activated materials (AAMs) are increasingly investigated as an emerging technology alternative to the traditional cement-based materials and ceramics. They are obtained by the reaction between an alkaline activator and an amorphous solid aluminosilicate precursor to produce a mainly amorphous and three-dimensional matrix with binding properties [1]. The properties of the so obtained materials strictly depend by chemical and physical characteristics of the precursors as well as by the alkaline activators used [2,3].

One of the most interesting feature of AAMs is their remarkable resistance at high temperature exposure [4]. In contrast to cement-based material, the ceramic-like structure of AAMs retains its structural integrity at elevated temperatures, thus allowing to preserve the mechanical strength and the dimensional stability of the material. Therefore, AAMs are considered strong candidates for applications requiring good resistance to high temperature or fire, such as passive fire protection (PFP) [5].

PFP systems are protective layers that behave like thermal barrier to the transfer of heat to a substrate. PFP are widely used for protecting steel structures which undergo rapid mechanical degradation when heated above the critical temperature of 500 °C [6]. Besides their intrinsic thermal stability, fire resistant coatings must also exhibit good thermal insulation and low density in order to not overload the structure. Furthermore, in order to be efficient in various applications, a PFP should also prevent and/or mitigate steel corrosion phenomena. Low Ca AAMs showed promising performance in terms of corrosion resistance, as already stated in [7]. The understanding of the corrosion behavior of steel coated with alkali activated fire protective coatings is necessary for ensuring the service life of the structure.

So, this study aims at investigating the performance of light-weight fly ash-based alkali activated mortar (LWM) applied as coating onto steel, in terms of protection towards fire and corrosive agents (i.e. chlorides). In addition, normal-weight fly ash-based alkali activated mortar (M) containing quartz sand was also prepared as reference to understand advantages and drawbacks of using light-weight mortar for this specific application.

Physical and mechanical properties of the mortars were investigated. The fire resistance was assessed by performing medium-scale fire tests during which acoustic emission measurements were also conducted to analyze cracking phenomena induced by the high temperature exposure. The corrosion process was evaluated using an electrochemical approach in order to monitor the durability of the developed material. Samples were tested by accelerated ageing methods consisting of a partial immersion of the samples in an aqueous solution of sodium chloride (NaCl 3.5 wt%). The monitoring process was done measuring corrosion potentials (E_{cor}) during 30 days of exposure. In parallel, polarization curves have been also recorded at different stages of the exposure to better characterize the corrosion behavior of the steel substrates.

2. MATERIALS AND METHODS

2.1 Specimens preparation

Table 1 shows the chemical composition of the class F fly ash (FA), sourced from the Italian coal-fired power station of Torrealvaldliga Nord (RM), measured by ICP-OES after total microwave digestion.

Table 1: Chemical composition of the fly ash

Oxides (wt%)												
SiO ₂	Al ₂ O ₃	Fe ₂ O ₃	TiO ₂	CaO	MgO	Na ₂ O	K ₂ O	SO ₃	P ₂ O ₅	Mn ₂ O ₃	LOI	Residual
54.46	20.46	5.66	2.79	7.08	1.45	0.88	0.99	0.52	0.94	0.07	4.25	0.48

LOI: loss on ignition (1000°C)

Sodium silicate solution (“grade D”; composition: 29.0–30.5 wt% SiO₂, 14.5–15.5 wt% Na₂O, remainder H₂O) and 8 M sodium hydroxide (8 M NaOH) solution were used as activators. Fly

ash and alkaline solutions were mixed in order to achieve a molar ratio of Si/Al of 2.7 and an alkaline solution/fly ash ratio of 0.45 (wt/wt).

LWM was obtained using 13 wt% of expanded perlite (EP - $d_{\max} = 2$ mm) and 0.3 wt% of hydrogen peroxide solution (H_2O_2 , 30 wt% in H_2O) as light-weight aggregate and foaming agent [8], respectively. Instead, 56.2 wt% of quartz sand ($d_{\max} = 1$ mm) was used as aggregate for producing the normal-weight mortar (M). In both cases, extra-water was added for workability reasons. The extra-water amount was calculated in order to have a total content of water (extra-water + solution water) of 23 wt% for LWM and 10 wt% for M.

The mix procedure is reported elsewhere [9,10]. The slurry was poured in different size molds and cured in sealed conditions at room temperature ($T = 21 \pm 2$ °C). After 24 h, the specimens were demolded and cured in the aforementioned conditions for further 27 days. Specimens for both fire tests and corrosion measurements were obtained by pouring the fresh mortar in molds containing steel plates on the bottom. The steel plates were arranged so as to have the sandblasted surface in contact with the mortar. In the case of fire tests, stainless steel plates ($75 \times 75 \times 2$ mm) were covered by a layer of either 15 or 20 mm of thickness of mortar. For corrosion measurements, carbon steel plates ($50 \times 50 \times 2$ mm), previously connected from the backside with a braze-welded coated copper wire and sealed using an epoxy resin, were covered by a layer of 20 mm of thickness of mortar. After demolding the samples, all the mortar surfaces, except the top ones, were coated by epoxy resin, in order to have just the top surface in contact with the environment.

2.2 Physical and mechanical characterization

The bulk density (ρ_{bulk}) was obtained as dry mass divided by the volume of cylindrical samples (20 mm high, 35 mm diameter). The porosity was investigated by water absorption and capillary water absorption tests. The water absorption was obtained by immersing dried cylindrical samples (20 mm high, 35 mm diameter) in water for 24 h under vacuum ($\text{WA}_{\text{uv}}\%$). Results are expressed as percentage of the difference of saturated surface dry mass and dry mass divided by the dry mass. The capillary water absorption test, which allows to determine the capillary coefficient of water absorption, was conducted according to EN 1015-18 [11]. In addition, the height of water capillary penetration was measured after 24 h of sorptivity by longitudinally splitting the samples. At least four samples for each mortar types were tested for physical characterization. Compressive strength (R_c) of $40 \text{ mm} \times 40 \text{ mm} \times 160 \text{ mm}$ prism halves was evaluated according to the EN 196-1 [12] by an Amsler–Wolpert machine at a constant displacement rate of 50 mm/min and is expressed as average of two measurements.

2.2 Fire tests

Fire tests were conducted using a medium-scale (i.e. a furnace with an internal volume of approximately 1 m^3) fire testing set-up, as described and employed previously [9,13]. Before testing, two thermocouples (type K) were spot-welded onto the steel on the back side (side not directly exposed to the fire) of each specimen to continuously record the temperature of the samples during the fire exposure. The temperature-time curves are obtained as average of at least three measurements. In addition, a steel waveguide was also welded on the backside of the steel to couple the acoustic emission sensor type VS 150 MS to the sample. A standardized temperature-time relationship (“fire curve”), defined as cellulosic fire curve in ISO 834-1 [14], was employed to test the mortars. Heating was stopped 20 minutes after all the specimens had reached 500°C , and the specimens allowed to cool down naturally in the closed furnace.

Acoustic emissions were recorded during the complete heating-cooling circle up to 1 hour after the heating was stopped and will be expressed below as “hits” per 10 seconds.

2.4 Corrosion measurements

After 28 days of curing, the samples were partially immersed in a 3.5 wt% NaCl solution with a constant water head of 3 mm to the respect of the exposed sample surfaces. The exposure lasted for 30 days under laboratory conditions. During the exposure, the box containing testing samples was covered to avoid evaporation of the solution and the solution was weekly renewed to avoid significant variation of the chloride concentration in contact to the exposed surfaces. Electrochemical measurements were carried out using an Amel Electrochemistry Potentiostat, model 7050 and consisted in corrosion potential (E_{cor}) and in polarization curves. At least three samples for each mortar types were tested for all the corrosion measurements in order to ensure reproducibility of the results. E_{cor} was measured versus a saturated calomel electrode (SCE). Polarization curves were carried out after 1 h and 30 d of immersion in NaCl solution, using the conventional three-electrodes cell in which the mortar sample acted as the working electrode (WE), an external stainless steel net as the counter electrode (CE) and a SCE as the reference electrode (RE). The polarization curves were recorded starting 0.2 V lower than the open circuit potential (OCP) up to 1.0 V higher than the OCP, at a scan rate of 0.166 mVs^{-1} . After polarization measurements, low magnification imaging was performed on steel plates using an Olympus SZX10 optical microscope.

3. RESULTS

3.1 Physical and mechanical properties

Physical and mechanical properties of the fly ash-based alkali activated mortars are presented in Table 2.

Table 2: Physical and mechanical properties of LWM and M at 28 days

Sample	ρ_{bulk} (g/cm^3)	W_{Auv} (%)	capillary WA coefficient ($\text{kg/m}^2 \cdot \text{min}^{0.5}$)	H_{24h}	R_c (MPa)
LWM	1.26 ± 0.03	24.2 ± 1.7	0.27 ± 0.02	35 mm	8.0 ± 1.0
M	1.91 ± 0.02	8.9 ± 0.6	0.18 ± 0.01	50 mm	18.4 ± 1.3

As expected, the use of EP in combination with hydrogen peroxide solution led to 34% decrease in the bulk density and to a threefold increase of water absorption compared to the M mortar containing quartz sand. As a consequence of the increased porosity and of the presence of a light-weight aggregate, the LWM showed a reduced compressive strength.

The results of the sorptivity test are expressed in terms of capillary water absorption coefficient and height of water penetration after 24 hours of immersion (H_{24h}). This test allowed evaluate the interconnection of the pores of the hardened mortars which is an important parameter as far as durability is concerned. The capillary water absorption coefficients indicated that the water uptake was faster in LWM than M. After 24 hours of immersion, M specimens showed greater height of penetration than LWM specimens. According to these results, it can be deduced that LWM and M mortars were characterized by a different pore size distribution. In particular, M

mortar was mainly characterized by small capillary pores, which slowed down the saturation rate and increased the height of penetration. Indeed, larger pores absorb water faster than thinner pores but water can rise higher in thinner pores [15]. It is interesting to note that in both LWM and M specimens, the height of penetration after 24 hours was higher than 20 mm, which is the mortar thickness applied as coatings to the steel substrates for fire and corrosion tests in this study.

3.2 Fire resistance

The fire resistance was evaluated in terms of time necessary for the coated steel substrate to reach a temperature of 500 °C. The temperature-time curves of the specimens exposed to cellulosic fire curve are reported in Figure 1. The temperature of the back side of the bare steel plate exceeded 500 °C after only 9 minutes, thus demonstrating the urgency of using a PFP system as protective coating. Both LWM and M were effective in retarding the temperature rise of the steel plates; LWM resulted more performing than M, thus proving that expanded perlite and H₂O₂ were effective in enhancing the insulating properties of the mortar. When a 20 mm-thick layer of LWM was used, the back side of the steel plate reached the 500 °C after 38 minutes, while by using 20 mm-thick layer of M it was possible to keep the temperature of the steel plate under the critical temperature threshold for 30 minutes (Fig. 1a). The contribution of the dehydration, visible in the temperature range of 100–140 °C as temperature plateau, significantly slowed down the temperature rise of the steel. In the case of M samples, the lower overall amount of water (by weight), compared to the light-weight mortars, used to produce the mortar was responsible for a reduced duration of the dehydration plateau. This aspect highlights that, beside the porosity of the mortar and the insulating properties of the aggregate, also the amount of water contained in the mixture has critical role when fire resistance is considered.

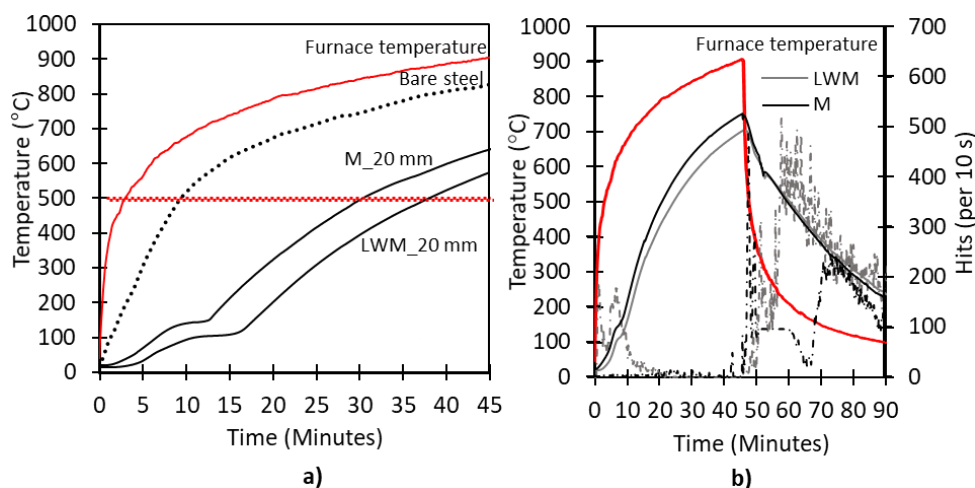


Figure 1: (a) Temperature-time curves of the specimens exposed to cellulosic fire curve (red lines) for a mortar layer thickness of 20 mm; (b) Correlation between temperature-time curves (bold lines) and acoustic emission results (dotted lines) for a mortar layer thickness of 15 mm.

The temperature-time curves of steel plates covered by 15-mm layer of mortars and exposed to cellulosic fire were correlated with the acoustic emission (AE) measurements during firing and subsequent cooling, as presented in Figure 1b. The majority of crack formation occurred on cooling, regardless of the aggregate used. These results agree with a previous study conducted

on alkali activated concrete [16]. These AE events were associated with sintering and partial melting of localized parts of the material and subsequent quenching on cooling which caused differential thermal deformations of different regions in the binder and therefore stress. From these results, it is reasonable to assume that no spalling phenomena occur during heating but adhesion problems between the coating and the steel substrate may occur during the cooling phase.

3.3 Corrosion behavior

Figure 2 reports the average E_{cor} values obtained during partial immersion of the samples in 3.5 wt% NaCl solution for 30 days. As expected, it highlights a different behavior between the corrosion potentials of steel embedded in M and LWM mortars. In particular, within 1 day of exposure, the average E_{cor} values for the sand-blasted steel in LWM mortar showed a fast drop from about $-0.18 V_{SCE}$ down to $-0.51 V_{SCE}$. Later, values around $-0.55 V_{SCE}$ were recorded for all the exposure time up to 30 days. However, more positive E_{cor} values were found for the carbon steel specimens in M mortar for longer exposure time than LWM sample. In particular, M sample exhibited E_{cor} values around $-0.1 V_{SCE}$ for the first week of partial immersion in NaCl solution. During the second week of exposure, a slight drop in E_{cor} values was detected down to $-0.25 V_{SCE}$. Finally, after 15 days up to the end of exposure, more negative potentials were obtained around $-0.50 V_{SCE}$, similarly to the E_{cor} values recorded for LWM samples. The trend described for M sample is quite in accordance with literature values reported in a previous study regarding steel rebars embedded in different alkali-activated fly ash mortars [17]. The different trend between the two mortar types is mainly related to the different porosity, as reported in Table 2. This result indicates that higher porosity in the mortar (as in the case of LWM) affected the corrosion initiation time when samples were exposed to a chloride-rich environment.

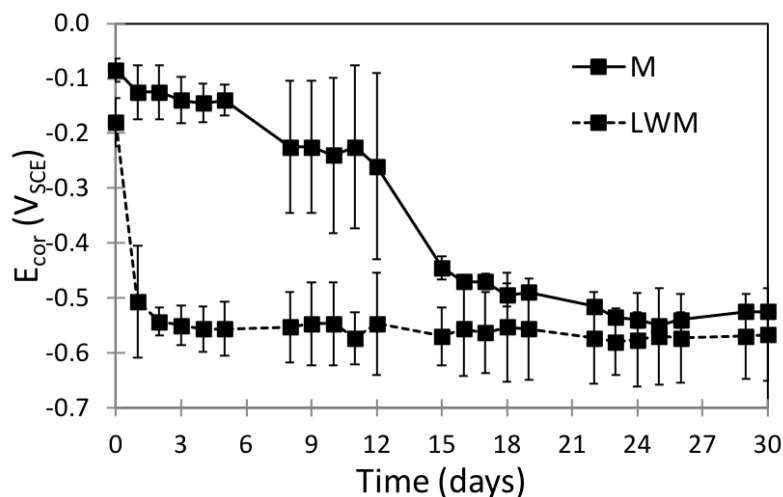


Figure 2: Average E_{cor} values recorded in M and LWM samples during the 30 days of partial immersion in 3.5 wt% NaCl solution.

In order to better highlight the different corrosion behavior obtained by M and LWM samples, polarization curves at short time of exposure (1 h) and at the end of the partial immersion (30 d) are reported in Figure 3a and b, respectively. After 1 h exposure, very low corrosion currents (i_{cor}), around $0.2 \mu A/cm^2$, were recorded for M sample. However, one order of magnitude higher

of corrosion current density ($i_{cor} \sim 1.0 \mu\text{A}/\text{cm}^2$) was measured for LWM. This different behavior is also highlighted by the images of the steel plates after the polarization measurements (Figure 3c) showing that the steel plate embedded in LWM mortar exhibited some corrosion products, contrary to what observed for carbon steel in M sample. At the end of the exposure, similar corrosion densities around $1.5 \mu\text{A}/\text{cm}^2$ were detected for all the samples, indicated similar corrosion behavior after 30 days in presence of chlorides. This result is confirmed by the optical observation of the steel plates after the measurements reported in Figure 3d and it is in good accordance with the E_{cor} trend highlighted in Figure 2.

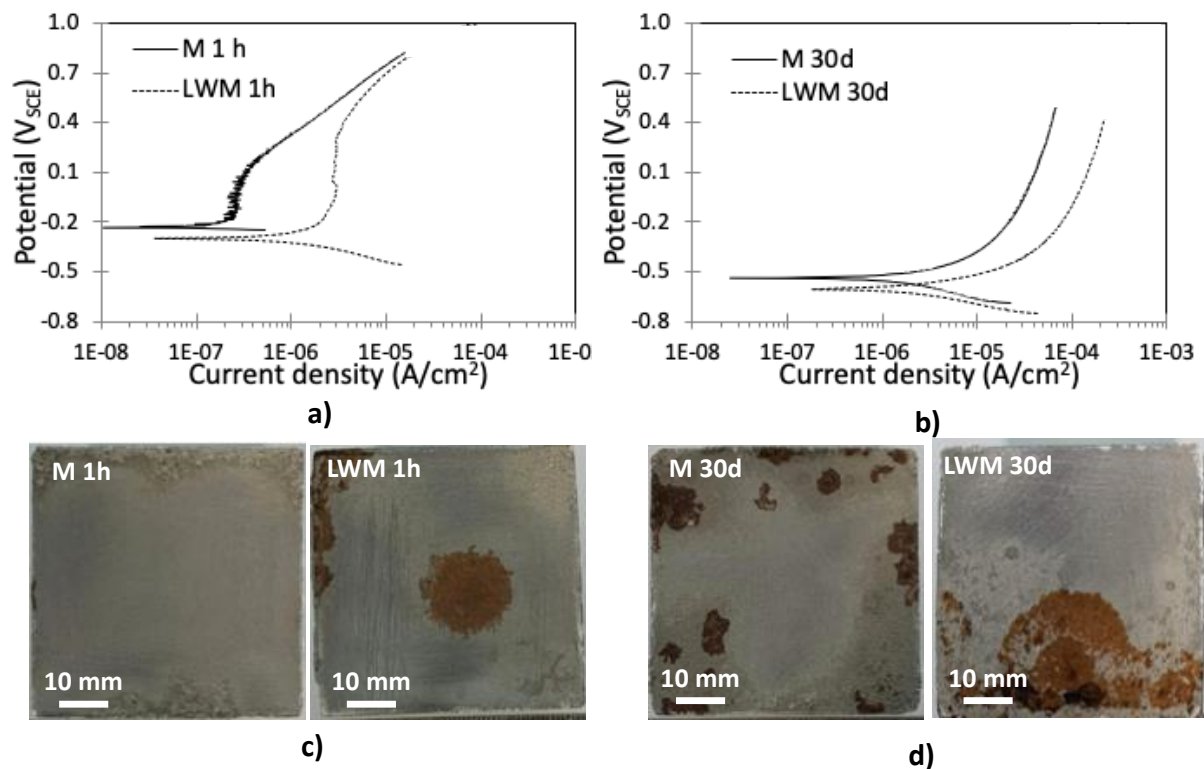


Figure 3: Polarization curves recorded in 3.5 wt% NaCl solution obtained from M and LWM samples after (a) 1 h and (b) 30 days of immersion. Low magnification images of the carbon steel plates at the end of the polarization measurements recorded after (c) 1 h and (d) 30 days of immersion.

4. CONCLUSIONS

The presented study shows that by using expanded perlite and hydrogen peroxide solution it is possible to obtain a fly ash-based alkali activated light-weight mortar with enhanced fire resistance. By medium-scale fire test it was possible to determine that 20 mm- thick layer of LWM can protect the steel substrate for 38 minutes when exposed to cellulosic fire conditions. Furthermore, AE measurements showed that cracking occurred mainly during the cooling phase and confirmed the absence of explosive spalling phenomena during heating. However, the increased and more interconnected open porosity, which characterize this type of mortar, is responsible for a reduced corrosion protection provided to the steel substrate. Indeed, corrosion

resistance is lower when carbon steel is embedded in LWM mortars and the system is exposed to an aggressive environment such as a 3.5 wt% NaCl solution compared to the use of M samples. To overcome this issue, longer exposure time is under investigation in order to understand the long-term corrosion behavior of the developed systems. In addition, studies on the control of the pore size distribution and on the development of closed porosity instead of open one are ongoing, in order to increase the protection provided by LWM. Furthermore, the passivation mechanism of carbon steel embedded in the developed low Ca AAM is currently under investigation.

REFERENCES

- [1] Provis, J.L., Bernal, S.A., 'Geopolymers and related alkali-activated materials', *Annu. Rev. Mater. Res.* **44** (2014) 299–327.
- [2] Reddy, M.S., Dinakar, P., Rao, B.H., 'A review of the influence of source material's oxide composition on the compressive strength of geopolymer concrete', *Microporous Mesoporous Mater.* **234** (2016) 12–23.
- [3] Duxson, P., Provis, J.L., Lukey, G.C., Mallicoat, S.W., Kriven, W.M., van Deventer, J.S.J., 'Understanding the relationship between geopolymer composition, microstructure and mechanical properties', *Colloids Surf. Physicochem. Eng. Asp.* **269** (2005) 47–58.
- [4] Davidovits, J., 'Geopolymers inorganic polymeric new material', *J. Therm. Anal.* **37** (1991) 1633–56.
- [5] Vickers, L., van Riessen, A., Rickard, W.D.A., 'Fire-Resistant Geopolymers - Role of Fibres and Fillers to Enhance Thermal Properties', (Springer, 2015).
- [6] American Petroleum Institute, 'Fireproofing practices in petroleum and petrochemical processing plants', 2nd Edn (API publications, 1999).
- [7] Mundra, S., Bernal, S.A., Criado, M., Hlaváček, P., Ebell, G., Reinemann, S., Gluth, G.J.G., Provis, J.L., 'Steel corrosion in reinforced alkali-activated materials', *RILEM Tech. Lett.* **2** (2017) 33–9.
- [8] Masi, G., Rickard, W.D.A., Vickers, L., Bignozzi, M.C., van Riessen, A., 'A comparison between different foaming methods for the synthesis of light weight geopolymers' *Ceram. Int.* **40** (2014) 13891–13902.
- [9] Carabba, L., Gluth, G.J.G., Pirskawetz, S.M., Krüger, S., Bignozzi, M.C., 'Fly Ash-Based Lightweight Geopolymer Mortars for Fire Protection', *ACI Spec. Publ.* **326** (2018) 26.01-26.10.
- [10] Carabba, L., Santandrea, M., Carloni, C., Manzi, S., Bignozzi, M.C., 'Steel fiber reinforced geopolymer matrix (S-FRGM) composites applied to reinforced concrete structures for strengthening applications: A preliminary study', *Compos Part B Eng.* **128** (2017) 83–90.
- [11] EN 1015-18 Methods of test for mortar for masonry - Part 18: Determination of water absorption coefficient due to capillary action of hardened mortar 2002.
- [12] EN 196-1 Methods of testing cement – part 1: Determination of strength 2005.
- [13] Watolla, M.B., Gluth, G.J.G., Sturm, P., Rickard, W.D.A., Krüger, S., Schartel, B., 'Intumescent Geopolymer-Bound Coatings for Fire Protection of Steel', *J. Ceram. Sci. Technol.* **8** (2017) 351–64.
- [14] ISO 834-1 Fire-resistance tests - Elements of building construction -Part 1: General requirements 1999.
- [15] Pia, G., Sassoni, E., Franzoni, E., Sanna, U., 'Predicting capillary absorption of porous stones by a procedure based on an intermingled fractal units model', *Int. J. Eng. Sci.* **82** (2014) 196–204.
- [16] Gluth, G.J.G., Rickard, W.D.A., Werner, S., Pirskawetz, S., 'Acoustic emission and microstructural changes in fly ash geopolymer concretes exposed to simulated fire', *Mater. Struct.* **49** (2016) 5243–54.
- [17] Monticelli, C., Natali, M.E., Balbo, A., Chiavari, C., Zanotto, F., Manzi, S., Bignozzi, M.C., 'Corrosion behavior of steel in alkali-activated fly ash mortars in the light of their microstructural, mechanical and chemical characterization', *Cem. Concr. Res.* **80** (2016) 60–8.

DURABILITY OF FLY ASH-BASED ALKALI-ACTIVATED MORTARS REINFORCED WITH SHORT HEMP FIBRES

Bojan Poletanović (1), Ivan Janotka (2), Michal Bačuvčík (2), Ildiko Merta (1)

(1) TU Wien, Vienna, Austria

(2) Building Testing and Research Institute, Bratislava, Slovakia

Abstract

The aim of this research was to investigate the durability of hemp fibre reinforced alkali-activated mortars by means of the composites mechanical properties under accelerated aging of wet/dry cycles. The mortar matrix contained fly ash as a binder, sodium water glass as an activator and sand with a particle size between 0.4 and 0.8 mm. As reinforcement hemp fibres of 10 mm in length and of volume ratio 1% in composite were used. The alkali-activated mortars underwent accelerated aging (10 wet/dry cycles) and their mechanical properties prior to and after aging compared.

It was shown that under accelerated aging conditions of wet/dry cycles hemp fibre reinforced fly-ash based alkali-activated mortars exhibit a significant decrease in their compressive- and flexural strength (36% and 34% respectively) as well as flexural toughness (34%). Thus in order to ensure the long-term durability of these composites, hemp fibres should be protected from degradation within the high alkaline matrix.

Keywords: durability, hemp fibre, fly ash, alkali-activated mortar, wet/dry cycles

1. INTRODUCTION

Due to the high utilization of Earth's minerals and significant environmental pollution caused by Portland cement production the necessity of development of alternative sustainable binders is markedly increasing. Within the last decades, it is proved that if pozzolanic materials (such as fly ash, metakaolin, blast furnace slag, volcanic ash, etc.) are mixed with high alkali solution formed materials alternative composites of comparable mechanical properties to Portland cement-based materials under significantly lower environmental pollution could be obtained [1-3]. These materials are known as alkali-activated materials.

As Portland cement-based materials, alkali-activated materials have also very limited crack resistance and energy absorption capacity under tensile load resulting in very high brittleness. Recently, natural plant fibres such as hemp, flax, coir, sisal, cotton, etc. have been considered as an environmentally friendly alternative to traditional fibre reinforcement in the improvement of the composites toughness [4,5]. Natural fibres are worldwide locally

available low-cost resources, need much less energy for production and have comparable mechanical properties to traditional microfibrils such as synthetic ones. However, the main challenges in the use of natural fibres as fibre reinforcement in an alkaline matrixes are their long-term durability [6,7]. So far there is a very limited research published dealing with the durability of natural fibres in alkali-activated materials [8].

Therefore the aim of this study was to evaluate the durability of fly ash-based alkali-activated mortars reinforced with hemp fibres under accelerated aging of wet/dry cycles by means of the composites mechanical properties.

2. MATERIALS AND EXPERIMENTAL METHODS

2.1. Mixtures and specimens preparation

The main oxides within a fly ash which is used as the source material to prepare the alkali-activated composites are SiO_2 52 wt%, Al_2O_3 25 wt%, Fe_2O_3 7 wt%, CaO 5 wt%. All particle size of the fly ash were smaller than $20\ \mu\text{m}$. For fly ash activation sodium water glass was used, with the chemical composition of 16.72 % Na_2O , 25.08% SiO_2 and 58.2% H_2O by mass. The activator to binder material ratio was defined in a way that a mass of Na_2O from the activator equals to 10% of the mass of the binder. For fibre reinforcement primary bast hemp fibres (*Cannabis sativa L*) with a diameter of 8–60 μm were used (Fig.1). The tensile strength of fibres was between 300-1100 N/mm^2 according to the literature [9] and their density was $1.5\ \text{g}/\text{cm}^3$. In all fibre reinforced geopolymer mortar mixtures the length of the fibres was 10 mm and the dosage 1% by volume. Fibres were added to the mixture in water saturated dry surface condition.

Two different groups of alkali-activated mortars (AAM) were examined, i.e. the first mixture referred to as “plain mortar” contained no fibres and the second mixture referred to as “fibre reinforced mortar” contained short hemp fibres as reinforcement.

The mortars were mixed in a laboratory Hobart mixer. Six identical specimens with dimensions of $40\times 40\times 160\ \text{mm}^3$ were cast, then covered with plastic film and cured at 80°C in an oven for 6 hours. Afterward, the samples were de-moulded and kept in laboratory condition (20°C and 50% relative humidity) for 28 days after which one group of specimens was tested, whereas the other group underwent accelerated aging.

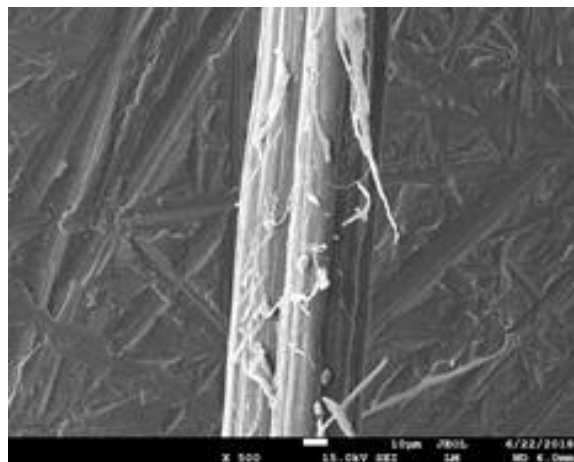


Figure1. Morphology of hemp fibres under Scanning Electron Microscope

2.2 Accelerated aging

The durability of the mortars was examined by imposing the specimens to accelerated aging of 10 wet/dry cycles. One wet cycle consisted 2 days of completely water immersion at the ambient temperature of 20°C, whereas one dry cycle consisted 2 days drying in an oven under a temperature of 65°C.

2.3. Physical tests

2.3.2. Bulk density

The measurement of the bulk density was conducted on six mortar prisms (40×40×160 mm³).

The bulk density was calculated as follows:

$$D = M/V \quad (1)$$

where M is the mass and V the volume of the test specimen.

2.3.1. Water absorption

For the water absorption test, six halves of the mortar prism specimens with a dimension of 40×40×80 mm³ were used. They were immersed in a water bath at the room temperature (20°C) for 2 days to reach water equilibrium. The percentage of the water content was determined using the following equation:

$$M_t (\%) = (W_t - W_o) / W_o \times 100 \quad (2)$$

where W_t is the weight of a water-saturated specimen and W_o the weight of a dry specimen.

2.4. Mechanical tests

Three-point bending test (3PBT) was conducted according to the norm ÖNORM EN 1015-11 on 6 identical prisms specimens of dimensions 40×40×160 mm³ [10]. The compressive test was conducted on one split half of the specimens by applying the compressive force on 40×40mm³ area on 3 identical prisms for each mortar mixture. The flexural toughness (absorbed energy) of the material was calculated from the force-mid span deflection curve of the 3PBT as the area under the curve till the deflection of 4 mm.

3. RESULTS AND DISCUSSION

3.1. Initial physical properties of the composites

Within the Fig. 2 the results of bulk density and water absorption measurements are shown. The bulk density of the plain alkali-activated mortar is 1881.70 kg/m³. Mortar containing fibres results in 4% lower density than plain mortar, which is a result of the introduced air pores by mixing of fibres into the matrix [11].

Regarding water absorption, it can be seen that alkali-activated mortars containing fibres have 23% higher water absorption than plain mortars. The reason for that is that the addition of fibres to the matrix increases the porosity of the composite resulting consequently in higher water absorption [12].

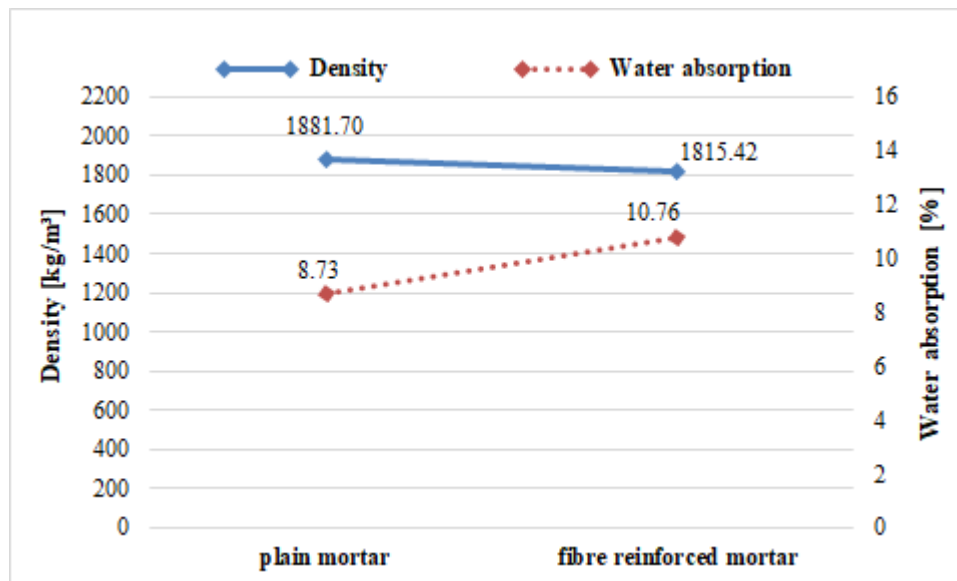


Figure 2. Initial bulk density and water absorption of the mortars

3.2. Mechanical properties of the composites

Fig. 3 shows the compressive strength of the mortar specimens tested at the age of 28 days and after exposure to wet/dry cycles. The mean compressive strength of unaged plain alkali-activated mortar is 16.54 MPa. With the addition of fibres the mortars strength reduces for 31%. The reason for the decrease is the increase in the porosity of the composites with addition of fibres, resulting consequently in lower compressive strength. The similar trend is observed in cement-based mortars and concretes reinforced with hemp fibres [4,13].

In alkali-activated (geopolymer) matrixes, however, it was reported that the compressive strength increases even up to 40% if short natural fibres (cotton fibres of 10mm length and 1% wt.) are added as reinforcement [14]. In the case of longer cotton fibres (30mm), an 18% increase in compression strength has been reported [15].

After accelerated aging, both plain and fibre reinforced mortars exhibit a strength decrease. In the case of plain mortar, the decrease is solely 4% however in case of hemp fibre reinforced mortar it is up to 20%. During exposure of the composite to wet/dry cycles the natural fibre reinforcement within it undergoes cyclic changes of i) soaking with water resulting in swelling of the cross-section of the fibers and of ii) drying out resulting in shrinkage of the cross-section of the fibres. This can lead to debonding of the fibres leaving voids (channels) within the matrix resulting in increased porosity and consequently lower compression strength.

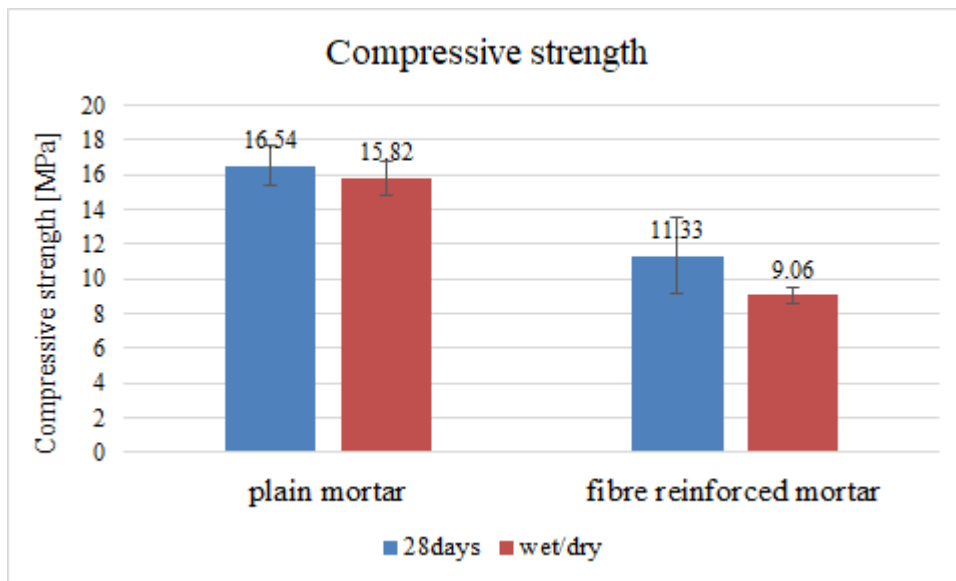


Figure 3. Compressive strengths of mortars at 28 days and after wet/dry cycles

The flexural strength of unaged and aged mortars is shown in Fig. 4. The mean value of the initial flexural strength of plain alkali-activated mortars was 4.10 MPa. When hemp fibre reinforcement is added to the mortars their flexural strength decrease for up to 25%. The similar behavior is observed in cementitious matrixes [5,13]. However, by geopolymer matrixes, it has been reported that with the addition of short fibres (cotton fibres of 10mm length and 1% wt.) the flexural strength remains the same [1] or even slightly increase if the length of the fibre is 30mm [15].

After accelerated aging, all mortars exhibit a significant loss of their initial flexural strength. In the case of plain mortars, the decrease is about 30% whereas in case of hemp fibre reinforced mortars even 36%.

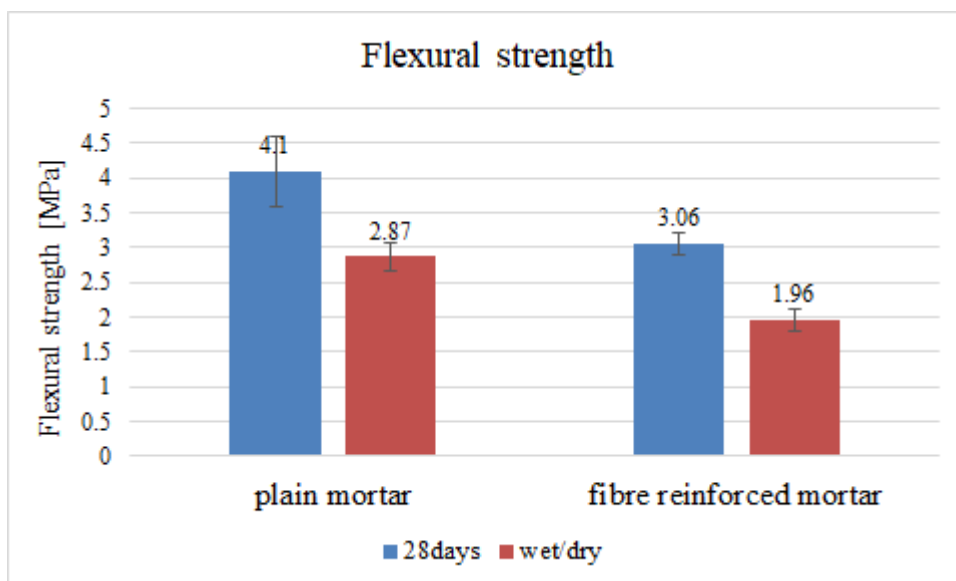


Figure 4. Flexural strengths of mortars at 28 days and after wet/dry cycles

The flexural toughness of the mortars is shown in Fig. 5. The initial toughness of plain mortar is 168.57 N/m. With the addition of hemp fibres, the toughness of mortars significantly increases, i.e. by 163%. In cement-based mortars (and concretes) reinforced with hemp fibres the similar trend is reported [4, 13].

After exposure to wet/dry cycles however the flexural toughness of all mortars decreases compared to their initial toughness. Plain mortars lose 61% of their initial toughness whereas hemp reinforced mortars only 34%. The similar severe flexural toughness degradation is observed in cement-based matrixes as well [16]. In fibre reinforced composites generally, the most crucial material property is the significant flexural (or fracture) toughness of the material. Thus, natural fibres could only be viable candidates for the eventual replacement of synthetic fibres in an alkaline environment if they do not lose their toughening effect in the matrix. This could be so far ensured only by protecting the fibres (physically or chemically) from long-term degradation within the matrix [17].

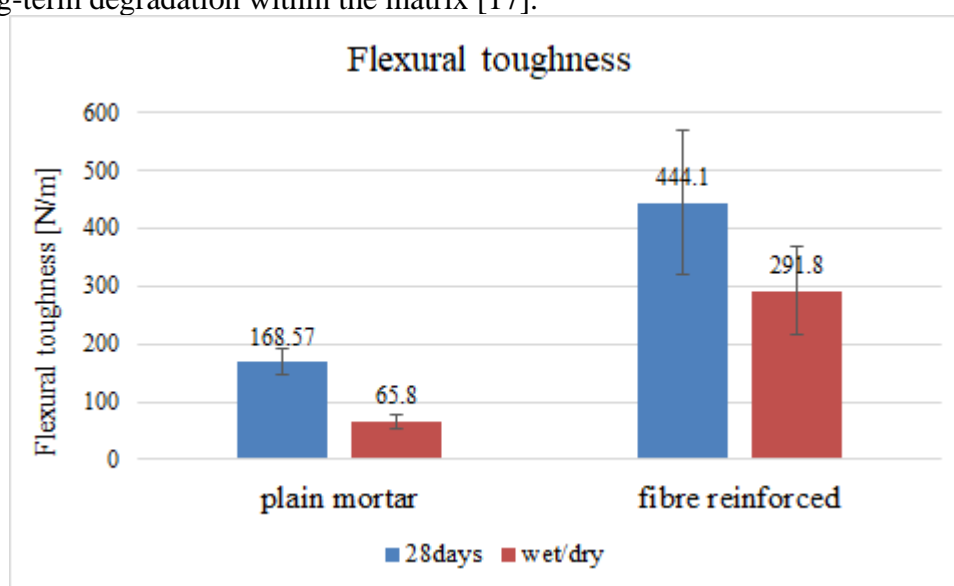


Figure 5. The flexural toughness of mortars at 28 days and after wet/dry cycles

4. CONCLUSION

In this research, the durability of fly ash-based alkali-activated mortars reinforced with short hemp fibres under accelerated aging of wet/dry cycles was determined by means of the composites mechanical properties. The specimens underwent 10 wet/dry cycles and their initial mechanical properties were compared with the properties of aged specimens.

It was shown that under accelerated aging conditions of wet/dry cycles hemp fibre alkali-activated mortars exhibit a significant decrease in their compressive- and flexural strength (36% and 34% respectively) as well as flexural toughness (34%). This indicates that hemp fibres could eventually replace synthetic fibres only if they are protected from degradation within the highly alkaline environment of the matrix.

ACKNOWLEDGEMENTS

The research is supported by the Stiftung Aktion Österreich-Slowakei in the framework of a visiting student fellowship of the first author at the Slovak University of Technology in

Bratislava. Additionally, the authors greatly acknowledge the support of NewChem from Austria for providing fly ash for the research.

REFERENCES

- [1] Fernández-Jiménez, A. and Palomo, A., 'Characterisation of fly ashes. Potential reactivity as alkaline cements', *Fuel* Volume 82 (18) (2003) 2259-2265
- [2] Weng, L., Sagoe-Crentsil, K., Brown, T. and Song, S., 'Effects of aluminates on the formation of geopolymers', *Materials Science and Engineering: B* 117 (2) (2005) 163-168
- [3] Komljenovic, M., Bascarevic, Z. and Bradic, V., 'Mechanical and microstructural properties of alkali-activated fly ash geopolymers', *J Hazard Mater*, 181(1-3) (2010) 35-42
- [4] Merta, I., Tschegg, E.K., Stanzl-Tschegg, S.E., Kolbitsch, A., *Fracture mechanics of concrete reinforced with hemp, straw and elephant grass fibres*, 2011, ICCM 18. International Conferences on Composite Materials, Jeju; South Korea
- [5] Merta, I., "Hemp Fibres-A Promising Reinforcement for Cementitious Materials", *Natural Fibres: Advances in Science and Technology Towards Industrial Applications. From Science to Market*", Springer Verlag, (2016), ISBN: 978-94-017-7513-7
- [6] Merta, I., Poletanovic, B. and Kopecko, K., 'Durability of natural fibres within cement-based materials - Review', *Concrete Structures, Journal of the Hungarian Group of fib* 18 (2017), 10-15
- [7] Merta, I., Kopecko, K., Tschegg EK, *Durability of hemp fibers in the alkaline environment of cement matrix*, 8th RILEM international symposium on fibre reinforced concrete. Guimarães, Portugal, (2012)
- [8] Alomayri T., Assaedia H., Shaikh F.U.A., Low I.M., 'Effect of water absorption on the mechanical properties of cotton fabric-reinforced geopolymer composites', *Journal of Asian Ceramic Societies*, 2 (2014) 223–230
- [9] Yan L., Kasal B. and Huang L., 'A review of recent research on the use of cellulosic fibres, their fibre fabric reinforced cementitious, geo-polymer and polymer composites in civil engineering', *Composites Part B* 92 (2016) 94-132
- [10] ÖNORM EN 1015-11: 2018 01 01, *Methods of test for mortar for masonry - Part 11: Determination of flexural and compressive strength of hardened mortar*
- [11] Alomayri T., Shaikh F.U.A., Low I.M., 'Characterisation of cotton fibre-reinforced geopolymer composites', *Composites: Part B* 50 (2013) 1–6
- [12] Assaedi H., Shaikh F.U.A., Low I.M., 'Characterizations of flax fabric reinforced nanoclay-geopolymer composites', *Composites Part B* 95 (2016) 412-422
- [13] Merta I., "Mechanical Performance of Hemp Fibre Modified Mortar"; 2nd International Conference on Bio-based Building Materials and the 1st Conference on ECOlogical valorisation of GRANular and FIBrous materials, Clearmont-Ferrand, France, (2017)
- [14] Alomayri T., Low I.M., 'Synthesis and characterization of mechanical properties in cotton fiber-reinforced geopolymer composites', *Journal of Asian Ceramic Societies* 1, Issue 1, (2013), 30-34
- [15] Korniejenko K., Fraczek E., Pytlak E., Adamski M., *Mechanical properties of geopolymer composites reinforced with natural fibres*, *Procedia Engineering* 151 (2016) 388 – 393

- [16] Mohr B.J., Nanko H., Kurtis K.E., 'Durability of kraft pulp fiber–cement composites to wet/dry cycling', *Cement and Concrete Composites* 27 (4) (2005) 435-448
- [17] Poletanovic B., Kopecsko K., Merta I., 'Durability of Hemp Fibre Reinforced Cementitious Mortars by Means of Fibre Protection and Cement Substitution with Metakaolin'; International Conference on Interdisciplinary Approaches for Cement-based Materials and Structural Concrete, Madeira Island, Funchal, Portugal; "Cement-based Materials and Structural Concrete", (2018) 957 - 962.

DURABILITY OF ALKALI-ACTIVATED CONCRETE MIXTURES - A REQUIREMENT FOR SUCCESS IN THE MARKET

Katja Dombrowski-Daube, Jan Sachl

Institute of Mining and Special Civil Engineering, TU Bergakademie Freiberg, Germany

Abstract

Alkali activated concrete (AAC) is considered to be an all-around material, meaning it has the theoretical potential to develop a wide variety of different advantages, e.g. low global warming potential (GWP) and low abiotic resource consumption (ARC) due to waste based ingredients, high strength and high resistance to environmental attacks. Durability is often the technical criteria by which customers can be convinced to choose a new type of material. Although AAC can achieve specific properties, these properties are not necessarily obtained by just mixing binder materials (containing reactive aluminates and silicates) with alkaline solutions. In order to meet the requirements for a practical application, the AAC mixtures have to be optimized.

For successful optimization procedures, large-scale investigations have been carried out to understand the correlation of composition, technical parameters, properties, durability, sustainability, and costs. Resistance to freezing and thawing as well as deicing salt is often the most important durability criteria.

It is to stated, that high strength does not necessarily mean high durability. Over-optimizing parameters towards strength might work against high durability and may also drive the costs up. All parameters, including cost, must be kept in mind when developing a product to be successful in the marketplace.

Keywords: Alkali Activated concrete, freeze-thaw/deicing-salt resistance, durability optimization parameters

1. INTRODUCTION

Portland cement based concrete is the most used building material worldwide. Its ratio of price to performance leads on the market. As a result of cement hydration, the concrete structure contains mainly strength forming solid calcium silicate hydrate (C-S-H) as well as portlandite ($\text{Ca}(\text{OH})_2$). The soluble portlandite is mostly responsible for reactions of the concrete with the environment and thus for shortcomings in terms of durability.

Among the alternatives, alkali-activated concrete as an inorganic, non-metallic material has the potential to withstand a higher variety of environmental impacts due to its inner structure based on a three-dimensional aluminosilicate network. This has already been explained and demonstrated many times [1, 2, 3, 4, 5].

Even though alkali-activated concrete is able to achieve special properties, this does not necessarily occur just by mixing reactive aluminates and silicates containing binding materials with alkaline solutions. Due to the use of wastes (such as slags and fly ashes) as binding materials for cost reasons and the need to recycle instead of landfilling, the alkaline activated binder system contains a high variety of chemical components and mineral compositions. Furthermore, the proportion of these components also differ between batches. Because of this, and similar to portland cement-based concrete, there is the need to understand the correlation of composition, technical parameters, properties, durability, sustainability, and costs, in order to produce a durable and marketable concrete free of cement.

In order to gain success on the market, the durability of the alkali-activated concrete is the benchmark. It also has to be recognized that the concrete strength might not directly correlate with concrete durability. Therefore, only systematic research can lead to marketable AAC.

On the basis of an industrial research project, extensive studies were carried out in order to investigate the correlation of composition, technical parameters, and properties for the successful development and optimization of alkali-activated concrete with a high freeze-thaw/deicing chemical resistance. Various types and qualities of waste-based binding materials, the influence of portland cement clinker contents, a range of alkaline activator solutions and chemical additives, different mixing compositions as well as technological variations contributed to mixture optimization.

2. MATERIALS AND MIXTURES

During the testing period, which lasted over at least three years, binding materials from different sources and different production dates (batches) were included in the investigations. For the investigation of the influence of different binding material qualities, ground granulated blast furnace slags (GGBFS) from two different sources were used. From source 1 (GGBFS B) only one batch and from source 2 four batches were used over time.

It is known that a combination of different binding materials helps to compensate for the shortcomings of each. Therefore, in addition to GGBFS, fly ashes (FA) from hard coal (two sources with four batches from the first and two from the second) were included into the research. In addition, a waste material (WM) from ore processing (refining bauxite to produce alumina by means of the Bayer process) was included. The binding materials were used in different compositions. The discussed results were gained from the following compositions: FA=100 %, GGBFS:FA=50:50, GGBFS:FA:WM=72:18:10, and GGBFS:FA:WM=60:20:20.

Since the reactive blast furnace slags are not freely available in Germany (as a result of the complete blast-furnace slag purchase by the cement industry), these slags can only be obtained from the cement industry or bought as a slag-containing cement (e. g. cement CEM III according to DIN EN 197-1). Since GGBFS act as AAC-improving binding materials, the influence of portland cement clinker on the structure and properties of alkali-activated concrete had to be investigated. Therefore, defined amounts of GGBFS were substituted by cement CEM I in order to simulate the application of a cement CEM III/B (20 to 34 % portland cement clinker) and CEM III/C (5 to 19 % portland cement clinker) in the laboratory tests. The

substitution of GGBFS by portland cement was marked as follows: C0: 0 % cement, C5: 5 % cement, C20: 20 % cement.

For the reaction of the reactive aluminates and silicates to form the aluminosilicate network alkaline activators were used. Here, NaOH pellets were dissolved in deionized water to set a 10 %-solution, which was then cooled to room temperature before being added to the mixture. Furthermore, alkaline silicate solutions of different quality (different alkali-types, different alkali-contents, and different silicate-contents) were used.

Besides the application of different binding materials and different activator solutions in different amounts, further optimizing parameters were investigated: water-binder-ratios, chemical admixtures (ca), chemical components (cc), aggregate grain size distributions and curing conditions.

The chosen binding materials were mixed with the alkaline solution. The fine and coarse aggregates were added and mixed to a homogeneous concrete. In optimization cases chemical admixtures were added while mixing. The fresh concrete was placed into moulds, consolidated and covered with plastic to prevent drying. After at least 24 h storage (sealed in plastic) at room temperature the de-moulded concrete samples were stored above water at room temperature until testing to avoid leaching, which occurs during storage under water.

3. LABORATORY TESTS

Within this research task concrete compressive strength and concrete durability were tested in the laboratory. The compressive strength was tested on concrete cubes according to DIN EN 206 for cement concrete at the 28th day after casting.

For the evaluation of the durability the freeze-thaw and deicing salt resistance of the concrete was investigated by means of the CDF-procedure according to CEN/TS12390-9. This procedure was originally developed to evaluate the freeze-thaw and deicing salt resistance of cement based concrete. The stated criterion of the test for cement concrete was also adopted for the AAC. The test is passed if the mass loss due to scaling does not exceed the threshold of 1500 g/m² after 28 freeze-thaw cycles (FTC). Before the start of the freeze-thaw-cycles, the samples were exposed to a 3 % sodium-chloride solution on the bottom while the sides were sealed with butyl-tape to allow penetration of the solution into the concrete only on the bottom test surface. During the freeze-thaw cycles further suction of sodium-chloride solution is possible. Investigations with deionized water as a test solution were omitted since most AAC showed high resistance to the pure freezing and thawing in previous tests.

4. DURABILITY INFLUENCING AND IMPROVING PARAMETERS

4.1 Fly ash and GGBFS qualities; binder chemistry

Initially, concrete mixtures were investigated, which were cast with the same composition concerning type, combination and amount of binding materials (GGBFS, FA, WM) and activator solution (NaOH, sodium-silicate solution), the same water-binder ratio as well as fine and coarse aggregates. The only variation was made concerning the fly ash, by casting each concrete mixture with FA from a different batch (Table 1). As a result, the samples of the different concrete mixtures showed different results for strength and durability (Figure 1a and Figure 1b). While the compressive strength (Figure 1a) increased from FA1 over Fa2 to FA3,

the resistance to freezing and thawing as well as deicing salt also increased (see less mass loss due to scaling, Figure 1b).

Secondly, concrete mixtures were investigated, which were cast with the same composition as described above, but this time with GGBFS from different batches (Table 1). Again, the samples of the different concrete mixtures showed different results for strength and durability (Figure 1c and d). While GGBFS from batch A showed highest strength (Figure 1c) and best resistance to freeze/thaw and deicing salt (Figure 1d), the strength and the durability decreases over the mixtures containing GGBFS from batch N to the mixtures with GGBFS from batch B.

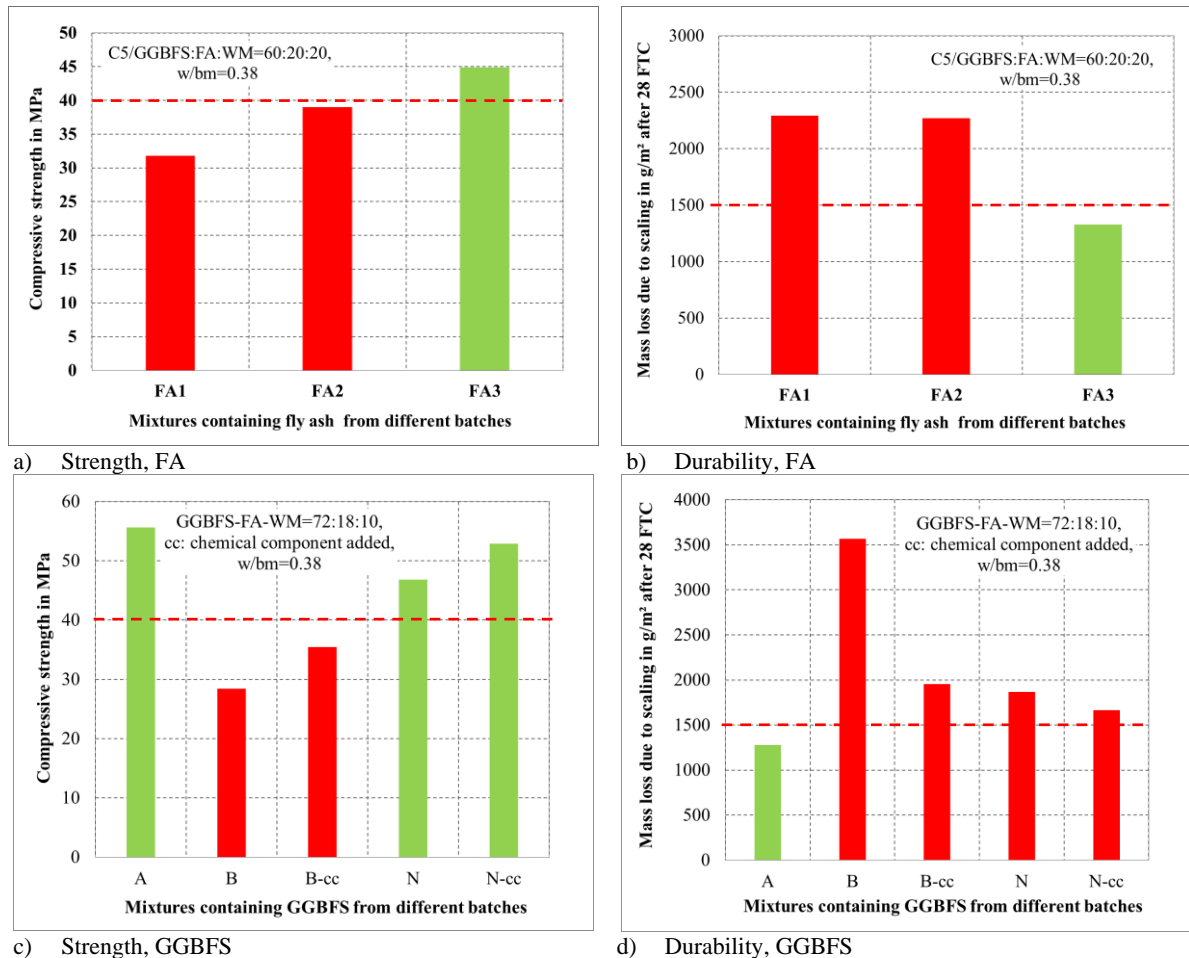


Figure 1 : Comparison of concrete cast with FA or GGBFS different from batches

In order to find the cause of the differences, the chemical composition of the binder mixtures of the concretes containing different FA and different GGBFS were compared (Table 1). It is said that in order to gain an alkali-activated concrete of good quality, binding materials containing high amounts of reactive silicates and reactive aluminates are necessary. Furthermore, the ratio of silicates to aluminates should be in the range between 1.5 and 6.

No correlations between chemical composition and strength as well as durability became evident for the mixtures containing different fly ashes (Table 1). Also, the differences between the contents of Si and Al, as well as the ratios of Si and Al are negligible.

For the GGBFS mixtures, there is no obvious correlation for either high strength or high durability with either Si or Al contents or ratios (Table 1). Although mixture A showed the best performance regarding strength and durability, the total contents of Si and Al were not the highest, only the ratio of Si and Al was lowest. A low Si/Al between 1 and 2 is the base of sufficient chemical resistance. Nevertheless, one significant difference was detected: mixture B contained approximately 6 % of sulfur containing components, which is about 2 % more than typical. All concrete mixtures, which contained GGBFS from batch B did not perform well with respect to strength and durability.

In these tests no correlation became evident between Mg content and concrete performance, neither for concrete containing FA nor for concrete containing GGBFS.

Table 1: Chemical parameters of concrete containing FA and GGBFS from different batches

Mixture/ Binder	Source of binder	Si mol	Al mol	Mg mol	Si+Al mol	Si/Al	Na/Si	Na/Al	K/Si	K/Al
FA										
FA1	S1	2,22	1,08	0,38	3,30	2,06	0,28	0,58	0,03	0,07
FA2	S1	2,22	1,05	0,4	3,27	2,12	0,29	0,60	0,03	0,07
FA3	S2	2,21	1,03	0,38	3,24	2,15	0,28	0,61	0,03	0,06
GGBFS										
A	S3	2,09	1,14	0,54	3,23	1,84	0,25	0,47	0,03	0,06
B	S4	2,08	0,87	0,57	2,95	2,37	0,26	0,61	0,03	0,08
B-cc	S4	2,08	0,87	0,57	2,95	2,37	0,26	0,61	0,03	0,08
N	S3	2,30	0,97	0,46	3,27	2,38	0,23	0,55	0,03	0,07
N-cc	S3	2,30	0,97	0,46	3,27	2,38	0,23	0,55	0,03	0,07

Parameters such as the content of the reactive (soluble) aluminates and silicates and/or physical properties such as fineness, resulting water requirement and thus workability, can also be responsible for the differences. It should be noted that the results are valid for the given mixtures. General statements about possible strength and durability of AAC based on these FA qualities can not be made on that basis. Various optimizations could be applied to improve the concrete towards the target variables. For example, the addition of an inorganic chemical component (cc: dissolved alkali salt, maximum of 1 % of the binding material content) improved strength as well as durability (see mixture B and B-cc in Figure 1a as well as mixture N and N-cc in Figure 1b).

4.2 Portland cement clinker

The reason for using portland cement clinker has been described above. In the tests carried out, concrete with the binding material composition GGBFS:FA:WM=60:20:20 and C5 (substitution of 5 % GGBFS by cement) performed best in comparison to mixtures with C0 and C20 (Figure 2a and b). Concrete with the binder-composition GGBFS:FA=50:50 showed decreased strength and decreased durability from C0 over C5 to C20.

4.3 Water to binding material ratio (w/bm)

From portland cement based concrete it is known that the freeze/thaw and deicing salt resistance increases with decreasing w/bm due to the denser pore structure. In order to investigate the influence of w/bm on the performance of AAC, identical basic mixtures of GGBFS, FA and WM were cast, but just using different dosages of water and thus showing

different w/bm. In Figure 2 results of mixtures are presented, in which the GGBFS was substituted by cement (C0: 0 %, C5: 5 %, C20: 20 %).

For the tested AAC it was noticed that the decrease of w/bm led to higher compressive strength (Figure 2c) and to improved durability (Figure 2d). The improvement of durability by reduction of the w/bm was only possibly until the optimum w/bm was reached. The optimal w/bm depends on the specific mixture. In case of the C5-mixture (optimized mixture, Figure 2b) a w/bm of 0.38 resulted in best CDF-test performance.

The results shown in Figure 2 demonstrate clearly, that concrete mixtures with the highest strength do not necessarily meet the durability requirements (mixture C0 in Figure 2a and Figure 2b; mixture 0.36 in Figure 2c and Figure 2d). Furthermore, the w/bm is not the only optimization parameter. The improvement of the grain-size distributions towards coarser aggregates was another successful optimization step. A combination of parameters such as w/bm and grain-size distribution can improve workability, compaction behaviour and finally durability (mixture 0.36* in Figure 2c and d). If in addition to w/bm, the activator content was changed, the performance got worse (mixture C20-0.36*, Figure 2b). The concrete mixtures in Figure 2a and b differ from the mixtures in Figure 2c and d by different activator contents.

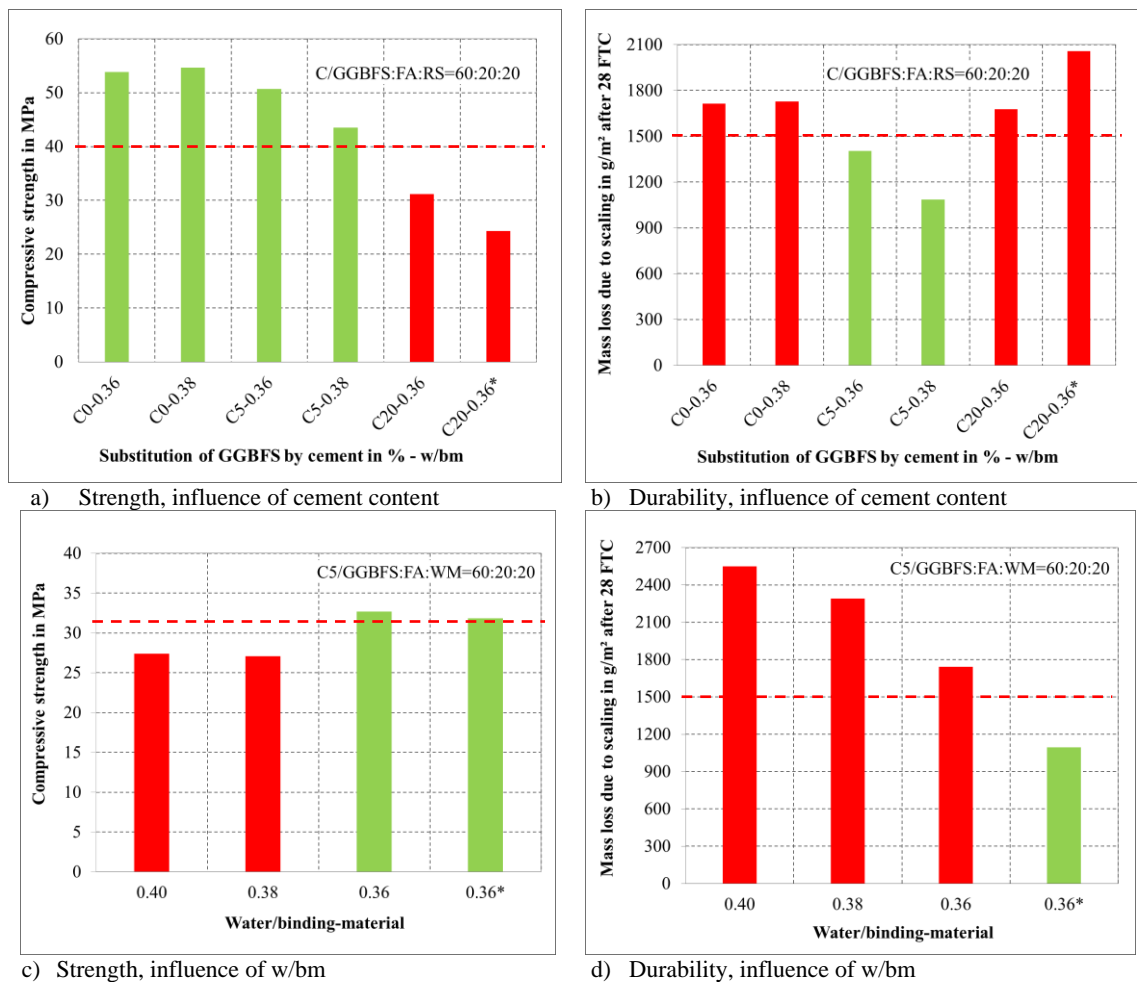


Figure 2 : Influence of cement clinker content and w/bm

4.4 Type, quality and content of activator solution

The activator influences the properties of fresh and hardened AAC as well as its durability, sustainability and costs. In previous research [6] it has been found that AAC containing potassium-based activator solutions showed better performance at elevated temperatures compared to AAC containing sodium-based activator solutions.

Figure 3 shows clearly that in these test not the type of activator but the content of silicates in the alkali silicate solutions is responsible for success. The difference in Si-contents is marked with different numbers. The activator solutions K2 and K5 contain less Si compared to K4, whereby K2 also contains less alkalis. The correlations are substantiated by results of measurements carried out on concrete mixtures C5/GGBFS:FA=50:50 (Figure 3a) as well as on concrete mixtures cast with C5/GGBFS:FA:WM=60:20:20 (Figure 3b).

In order to cast AAC, very high amounts of activator solution were often used. Figure 3c and Figure 3d show the results gained on concrete mixtures cast with different contents of activator solution. Figure 3c demonstrates that the use of low activator content can produce concrete with compressive strengths above 50 MPa. Also, it is shown in Figure 3d that reducing the activator content leads in tendency to an improved resistance to freeze/thaw and deicing salts.

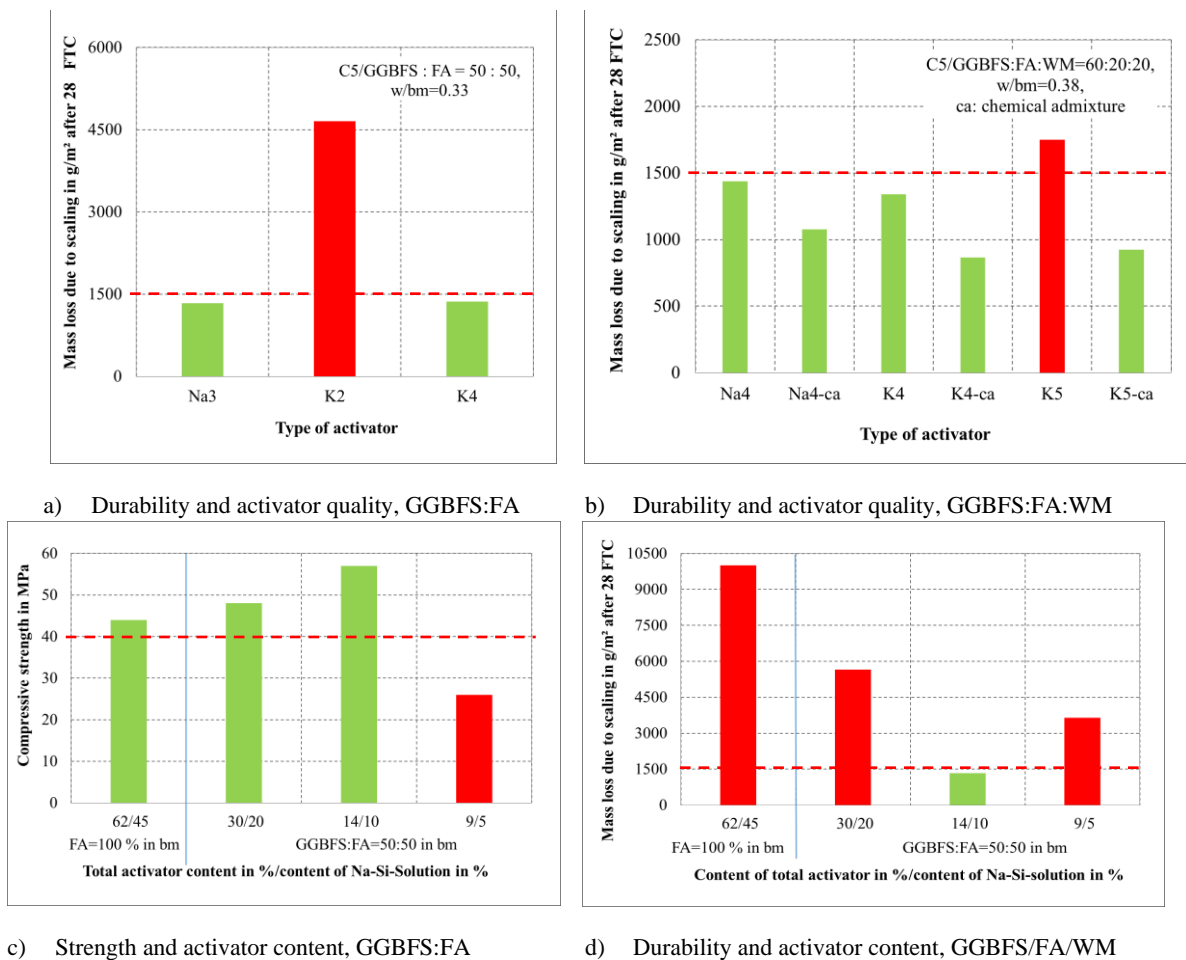


Figure 3 : Influence of activator quality and activator content on strength and durability

4.5 Chemical admixtures and consistency

It has been discussed that in addition to chemical parameters the workability plays an important role in AAC performance. By the application of chemical admixtures, the strength and the resistance to freezing and thawing and deicing salts of AAC can be improved. In this project only one superplasticizer type, normally applied for cement based concrete, was suitable for AAC mixtures. It was successfully used for mixtures containing cement clinker (C5 and C20). The improvement for mixtures C0 was rather small. Figure 3b shows test results of superplasticizer application on C5-mixtures activated with different activator solutions. Here the strength as well as the resistance to freeze/thaw and deicing salts (Figure 3b) were improved in each application case. By the use of the chemical admixture, the concrete activated with K5 achieved the freeze/thaw- and deicing-salt requirements (Figure 3b).

5. COSTS DRIVERS

The tests carried out with different amounts of activator solution showed that high dosages do not necessarily improve strength (Figure 3c) and/or the performance in freeze/thaw and deicing salt attack (Figure 3d). The activator solutions are the cost drivers in AAC. By reducing the content of sodium silicate solution from 45% to 10% (example Figure 3), the costs of the concrete mixtures can be reduced by at least 55% up to 60% [7].

In order to improve technical properties such as strength, often AAC concrete is cured at higher temperatures. Investigations showed that neither the strength nor the durability was improved if the AAC was cured at higher temperature (e.g.: 25 °C, 1 day 40 °C and 2 days 40 °C) after casting, though the energy demand and thus the costs were increased.

6. CONCLUSIONS

- No correlation became obvious between the absolute contents of Si and Al or their ratios in the binder mixture and strength as well as durability of the resulting concrete.
- Increased sulfate contents in GGBFS reduce strength and durability of AAC.
- High concrete compressive strength does not necessarily correlate with high resistance to freeze/thaw and deicing chemicals.
- AAC mixtures can be optimized to meet the technical requirements by the following parameters: binding materials (quality, content) and activator solutions (quality, content) as well as their combinations, w/bm and aggregate grain size distributions.
- The use of slag blended cement (CEMIII/C) as slag supply was acceptable for AAC, if cement content did not exceed 5%.
- Chemical additives can improve the reactivity, structure stability and/or workability, and thus the strength and durability of AAC.
- High activator contents and thermal curing (cost drivers) can reduce strength and durability.

ACKNOWLEDGEMENTS

The authors are thankful for scientific support: Prof. Dr. Donald J. Janssen, Seattle, USA, and for financial support:



Gefördert durch:



aufgrund eines Beschlusses
des Deutschen Bundestages

REFERENCES

- [1] Fernandes-Jimenez, A.; Palomo, A. 'Chemical durability of geopolymers', in: Provis, J. and Deventer J. (Eds.) 'Geopolymers: structure, processing, properties and industrial applications', Woodhead Publishing Ltd, Cambridge (2009) ISBN: 978-1-84569-449-4, 194-210
- [2] Škvára, F.; Duong, N. A., Zlámalová Cílová, Z. 'Geopolymer materials on the fly ash basis - long-term properties' *Ceramics – Silikáty* **58** (1) (2014) 12-20
- [3] Dombrowski, K.; Buchwald, A.; Weil, M. 'The influence of the calcium content on the structure formation and thermal performance of fly ash based geopolymers', in: 'Advances in Geopolymer Science and Technology', *J. Mater. Sci. – Special Section*, **42** (9), (2007), ISSN 0022-2461 (Journal), 3033-3043.
- [4] Buchwald, A; Dombrowski, K.; Weil, M. 'The influence of the calcium content on the performance of geopolymeric binder - especially the resistance against acids' in: 'Geopolymer, Green Chemistry and Sustainable Development Solutions', St. Quentin, France (2005) ISBN 2-9514820-0-0, 185-188.
- [5] Cyr, M.; Pouhet, R. 'The frost resistance of alkali-activated cement-based binders', in: Handbook of Alkali-Activated Cements, Mortars and Concretes, Woodhead Publishing (2015) 293-318
- [6] Dombrowski, K.; Buchwald, A.; Weil, M., 'Influence of alkali ions on the temperature behavior of geopolymers', in: 'Geopolymer Binders - Interdependence of composition, structure and properties', Proceedings of an International Workshop, Weimar, September 2006 (Shaker Verlag, Aachen, 2007) ISBN 976-3-8322-6179-5, 119-129.
- [7] Weil, M. personal information, cost calculation for given concrete mixtures, (KIT-ITS, Karlsruhe, Germany, 2018).

NON-CLASSICAL REACTION PATHWAYS IN ALKALI-ACTIVATED SYSTEMS

L. Valentini

Department of Geosciences, University of Padua, Italy

Abstract

With the beginning of the new millennium, society has (with some exception, sadly, especially in the last few years) embraced the idea of “sustainable development” as a key goal for the future generations to inherit a clean world. In the field of cement chemistry, this concept has boosted research oriented at designing a new generation of construction materials. Among low-CO₂ alternatives to Portland cement, alkali-activated materials gained broad consensus in the scientific community and scientific literature on this topic is now consolidated.

Nonetheless, current research is still broadly oriented towards an approach dealing with the macroscopic properties of different mix designs, and the details of alkali activation, especially for what concerns the nano-structure of the reaction products, as well as the nature of the reaction pathways leading to the formation of such products is still puzzling. This fuzzy picture is accompanied by the broad use of descriptive terms inherited from the realm of organic polymer chemistry, which may not be appropriate for a rigorous description of the alkali activation of inorganic materials such as aluminium silicates.

In this contribution, I attempt to reconcile the processes associated with alkali activation with the current views on phase separation in saturated solutions. Recent research into non-classical pathways to nucleation and growth and formation of intermediate entities, namely prenucleation clusters, is reviewed, with focus on the implementation of these theories to those materials, such as zeolitic imidazolate frameworks, which share some common structural features with the products of alkali activation. The role of computer simulations in describing the details of the dissolution-precipitation processes in alkali-activated systems is addressed.

Keywords: Alkali-activation; Modelling; Nucleation

1. INTRODUCTION

Alkali-activated materials constitute an important potential replacement for Portland cement-based concrete. Although a consolidated scientific literature is available on this subject, a knowledge gap still exists between macroscopic properties and basic physical and chemical

processes associated with the hydration of these materials. Many studies still rely on models developed during the 50s and tend to neglect the recent advances in the field of phase separation.

In this contribution, I review some current models of phase separation in saturated solution in an attempt to provide an accurate quantitative description of the dissolution-precipitation processes inherent in alkali-activated systems.

2. GLUKHOVSKY'S MODEL

The original model proposed by Glukhovsky [1] and its successive modifications [2] imply a reaction pathway consisting of three main stages.

The first stage accounts for dissolution in alkaline environment and formation of Si and Al aqueous species and is commonly named, in the referencing literature, “destruction-coagulation”. This is a fairly generic definition that, however, fails to represent the complexity of dissolution processes, resulting from a combination of etch pit nucleation and step retreat processes [3]. These latter concepts have been successfully applied to the detailed description of Portland cement dissolution [4]. Although such a formal description of dissolution is strictly applicable to crystalline phases only, it was envisaged that a similar mechanism occurs during the dissolution of amorphous silicates [5].

During the second stage (coagulation-condensation) aggregation of aqueous species occurs. The term “polycondensation” is often used in the literature to describe this process. This term is more commonly used in the field of organic macromolecules and the definition provided by the IUPAC Gold Book [6] for this term is, again, quite generic: “A polymerization in which the growth of polymer chains proceeds by condensation reactions between molecules of all degrees of polymerization”.

The third stage (condensation-crystallization) refers to the formation of larger clusters and structural reorganization, which may eventually lead to the formation of crystalline structures, although this last step is normally observed at high temperatures only [2].

3. PRENUCLEATION CLUSTERS

The Glukhovsky's model had no doubt the merit of providing a picture of the small-scale processes associated with the reaction occurring in alkali-activated systems. However, some of the terminology used may be misleading. In order to advance the knowledge into such basic processes, an implementation of the current theories on phase separation in aqueous solution, possibly framed in a rigorous mathematical formalism, is strongly needed.

In the last few years, the classical theories of nucleation and growth of new phases in aqueous solution have been revised and current theories envisage the formation of intermediate entities, named pre-nucleation clusters, which constitute stable aggregates of solute particles acting as precursors to the formation of thermodynamically stable solid phases (Figure 1). According to the entry present in the Encyclopaedia of Nanotechnology “Pre-nucleation clusters are thermodynamically stable and small (~0.5–2 nm) aggregates of ions in aqueous solution, which are solutes and form prior to the nucleation of a solid phase, in undersaturated as well as supersaturated (metastable) solution states” [7].

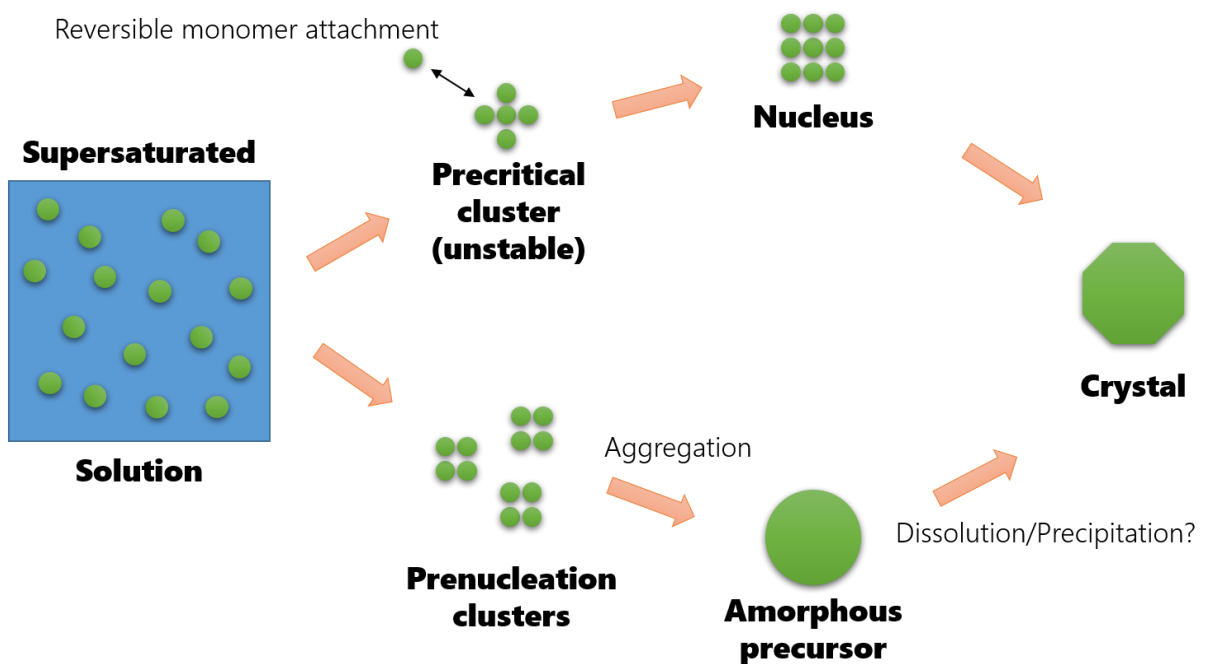


Figure 1: Idealized view of classical (top) and non-classical (bottom) pathways to phase-separation. Classical nucleation theory envisages the formation of critical nuclei by monomer-to-monomer attachment. The non-classical pathway envisages the formation of amorphous precursors by aggregation of thermodynamically stable prenucleation clusters.

Non-classical nucleation pathways, with formation of prenucleation clusters, are especially observed when poorly ordered or nano-crystalline phases (e.g. amorphous calcium carbonate) form [8]. Such “amorphous” precursors may convert or not into well-defined crystals.

This theory has been recently implemented to the formation of C-S-H in Portland cement. Small-angle X-ray scattering (SAXS) measurements suggested the occurrence of a two-step nucleation process in which amorphous spheroids of 50 nm initially form and of a second step during which nano-crystalline domains develop subsequent to aggregation of the amorphous precursors [9].

A similar two-step process was observed by means of SAXS measurements during the formation of zeolitic imidazolate frameworks (ZIF), a class of metal organic frameworks that share topological properties with zeolites, which are in turn structurally and chemical affine to N-A-S-H, the reaction product of alkali-activated cements. In this case, the development of ZIF crystalline particles is mediated by the formation and aggregation of 1-2 nm prenucleation clusters [10]. Interestingly, SAXS measurements performed on alkali-activated metakaolin indicated the occurrence of a similar process, with formation of reaction product by aggregation of previously formed 2-nm entities [11].

4. NUMERICAL MODELLING

Numerical modelling can play a decisive role in helping to define a quantitative description of the basic mechanisms pertaining to alkali-activated systems, in the context of non-classical

nucleation. Progress in this direction is being made, for example, by the use of atomistic models that could assess the nano-structural nature of N-A-S-H products [12].

Small-scale details of the basic chemical and physical processes associated with alkali-activated system may be explored by reaction-diffusion models, in which the full chemistry of the system is implemented. One such model was recently used to quantitatively assess the time-dependent dissolution, nucleation and growth rates (Figure 2) of alkali-activated metakaolin, in the presence of different alkaline activators [13].

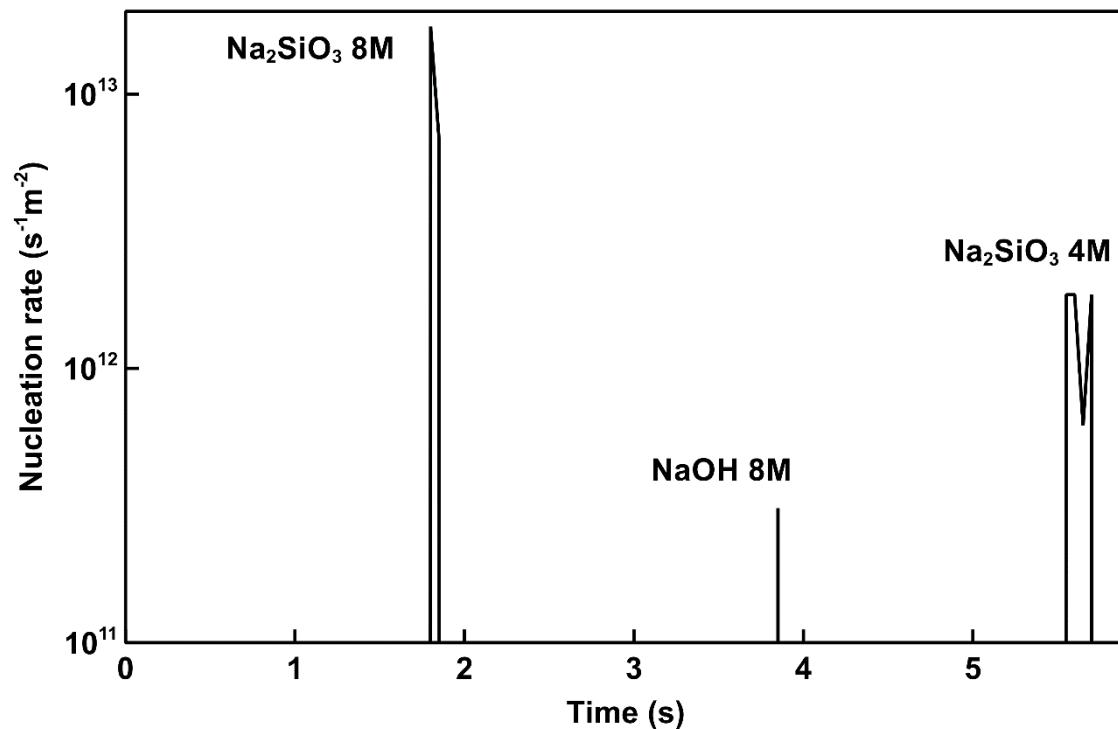


Figure 2: Simulated rates of N-A-S-H nucleation in the presence of different alkali-activated solutions.

One potential numerical approach for the implementation of non-classical nucleation pathways in alkali-activated system is “population balance modelling”. This numerical scheme can track the time variation in the size distribution of particles present in a given system, similarly to what can be experimentally achieved by SAXS methods. This approach was recently implemented to the description of C-S-H precipitation by aggregation of defective crystallites [14].

A correct implementation of population balance algorithms may likely contribute to elucidating the potential role of prenucleation clusters in the formation of N-A-S-H in alkali-activated systems.

5. CONCLUSIONS

The purpose of this contribution was that of stressing the importance of reconciling the mechanisms associated with alkali-activated systems with the most recent advances in the description of phase separation, by dissolution, nucleation and growth. Coupling beamline techniques based on SAXS with advanced numerical methods will represent a decisive strategy to understand these processes and their relationship with observed macroscopic properties of alkali-activated materials.

REFERENCES

- [1] Glukhovskiy, V.D., 'Soil Silicates' (State publishing house of literature on building and architecture of Ukrainian SSR, 1959).
- [2] Duxson, P., Fernandez-Jimenez, A., Provis, J.L., Lukey, G.C., Palomo, A., van Deventer, J.S.J., 'Geopolymer technology: the current state of the art', *J. Mater. Sci.* **42** (2007) 2917-2933.
- [3] Brantley, S.L., Kubicki, J.D., White, A.F. 'Kinetics of Water-Rock Interaction' (Springer, New York, 2008).
- [4] Juilland, P., Nicoleau, L., Arvidson, R.S., Gallucci, E., 'Advances in dissolution understanding and their implications for cement hydration', *RILEM Tech. Lett.* **2** (2017) 90-98.
- [5] Dove, P., Han, N., Wallace, A.F., De Yoreo, J.J., 'Kinetics of amorphous silica dissolution and the paradox of the silica polymorphs', *PNAS* **105** (2008) 9903-9908.
- [6] IUPAC, 'Compendium of Chemical Terminology' (2014) doi.org/10.1351/goldbook.P04722.
- [7] Bhushan, B., 'Encyclopedia of Nanotechnology' (Springer, New York, 2012).
- [8] Raiteri, P., Gale, J., 'Water is the key to nonclassical nucleation of amorphous calcium carbonate', *J. Am. Chem. Soc.* **132** (2010) 17623-17634.
- [9] Krautwurst, N., Nicoleau, L., Dietzsch, M., Lieberwith, I., Labbez, C., Fernandez-Martinez, A., van Driessche, A., Barton, B., Leukel, S., Tremel, W., 'Two-step nucleation process of calcium silicate hydrate, the nano-brick of cement', *Chem. Mater.* **30** (2018) 2895-2904.
- [10] Cravillon, J., Schroder, C.A., Nayuk, R., Gummel, J., Huber, K., Wiebcke, M., 'Fast nucleation and growth of ZIF-8 nanocrystals monitored by time-resolved in situ small-angle and wide-angle X-ray scattering', *Angew. Chem. Int. Ed.* **50** (2011) 8067-8071.
- [11] Steins, P., Poulesquen, A., Diat, O., Frizon, F., 'Structural evolution during geopolymerization from an early age to consolidated material', *Langmuir* **28** (2012) 8502 – 8510.
- [12] Lolli, F., Manzano, H., Provis, J.L., Bignozzi, M.C., Masoero, E., 'Atomistic simulations of geopolymer models: the impact of disorder on structure and mechanics', *ACS Appl. Mater. Interfaces* **10** (2018) 22809-22820.
- [13] Valentini, L., 'Modeling dissolution-precipitation kinetics of alkali-activated metakaolin', submitted to *ACS Omega*.
- [14] Andalibi, M.R., Kumar, A., Srinivasan, B., Bowen, P., Scrivener, K., Ludwig, C., Testino, A., 'On the mesoscale mechanism of synthetic calcium-silicate-hydrate precipitation: a population balance modelling approach', *J. Mater. Chem. A* **6** (2018) 363-373.

International Conference on Sustainable Materials, Systems and Structures (SMSS 2019)

New Generation of Construction Materials

20-22 March 2019 – Rovinj, Croatia

NEW GENERATION OF CONSTRUCTION MATERIALS

SESSION 4: Waste ashes as SCMs

PROPERTIES OF CEMENTITIOUS MATERIALS WITH SEWAGE SLUDGE ASHES

M. Saillio (1), L. Andrade (1) M. Mehdi (1)(2) T. Chaussadent (1) and Arezki Tagnit-Hamou (2)

(1) Université Paris-Est, MAST, CPDM, IFSTTAR, France

(2) Université de Sherbrooke, Faculté de Génie civil, Canada

Abstract

Numerous industrial by-products have potential for use as alternative supplementary cementitious materials (ASCMs) in concrete. The objective of the present study is to better understand the reactivity and the impact on durability and on hydration of one ASCMs: calcined sewage sludge ashes (SSA).

Some tests are directly performed on SSA such as the Pozzolanic test. In addition, cement pastes and mortars with SSA are mixed with the same W/B ratio. Seven binders are studied: a reference OPC and 6 mixes with OPC substituted by SSA from 5 to 30%. In order to study the hydration, setting time test, XRD, TGA/DTA are performed on cement paste and the durability tests are also performed on mortars such as water porosity, rapid chloride test and resistivity test. Various water curing time (from 7 to 365 days) are chosen in order to take into account the evolution of the materials.

The first results, based on chemical tests have highlighted the behaviour of this ASCMs and led to the design of materials which exhibit good durability properties at long age. In particular, chloride diffusion apparent coefficient is significantly reduced for material with SSA. Some properties (such as a potential pozzolanic activity) appear to be quite similar to standard fly ash or metakaolin.

Keywords: ASCMs, Sewage Sludge Ashes, Hydration, Durability

1. INTRODUCTION

The construction industry uses large quantities of cement, a material which is involved in 5 to 8% of global CO₂ emissions. To reduce these emissions, the substitution of cement with supplementary cementitious materials (SCMs), usually industrial by-products, is of particular interest [1]. The proximity between the production of these SCMs and their use is however necessary to maintain a good environmentally friendly balance. Some regions have no or few

standardized SCMs resources such as fly ash (FA), silica fume (SF), blast furnace slag (BFS) or limestone filler (LF) [2,3] and therefore other by-products should be considered for use in concrete [4-12]. Chemical reactivity synergy between these alternative SCMs (ASCMs) and cement is of primary interest considering the concrete durability, especially as regards to the corrosion of steel in reinforced concrete. This is particularly crucial in chloride or CO₂ environment.

The cement matrix not only provides a usually stable environment for steel, but it also acts as a barrier toward aggressive elements such as chlorides or carbon dioxide. The corrosion deterioration of reinforced concrete is closely related to the ability of aggressive elements to penetrate into concrete and then, reach the reinforcement. Standard SCMs are thus often used in order to optimize the performance of concrete against CO₂ or chloride ingress. SSA presents a slight pozzolanic reactivity as reported in studies [9,11] and could be used into concrete.

The objective of this study is to characterize the transport properties of mortars incorporating calcined sewage sludge ashes (SSA) in substitution of CEM I. In this paper, the characteristics of this ASCM are first presented and discussed. In a second step, durability and microstructural properties of mortars and cement pastes incorporating ASCMs are investigated and discussed.

2. EXPERIMENTAL

The Portland cement used in this study was a commercial type cement (OPC), which chemical composition is shown in Table 1. SSA is provided by industrial partners (VEOLIA). SSA had been obtained by combustion of sewage sludge at 850°C. The physical properties and chemical analysis of SSA used for this study are presented in Table 1. Chemical composition shows SSA contains high amount of SiO₂, Al₂O₃ and CaO and also high amount of P₂O₅ comparable to study [10]. In terms of mineral phases, determined by X-ray diffraction (not figured here), SSA are composed of quartz, aluminosilicates, and probably amorphous phosphorous compounds [15]. Another study [10] reports that the composition of SSA can vary between providers, which can be a drag on their use.

Standard sand are used for mortars (according CEN EN 196-1). Mortars have been cast in cylinders of diameter 100 mm and of length 200 mm for the durability investigations. Seven mixes with different SSA substitution rates of cement (0-30%) were made with the same water/binder (W/B) ratio which is equal to 0.485 (denoted M0 to M30). The influence of SSA on mortar properties was analyzed as compared to a reference mortar with only OPC. In addition, cement pastes with the same mixes and the same W/B ratio were made for studying fresh properties and for microstructural investigations (denoted P0 to P30).

Many water-curing times are chosen (7,14, 28, 91 and 365 days) in order to take into account the evolution of the materials as a function of the age.

In addition to Setting time test, various durability tests are performed on these mortars and cement pastes: porosity assessed by water (according NF P18-459, 2010), chloride migration [13], electrical resistivity [14]. Finally, microstructure is characterized by XRD, TGA-DTA.

Table 1: Chemical and physical analysis of materials (weight %)

Oxide	OPC	SSA
SiO ₂	19.1	28.6
Al ₂ O ₃	3.6	17.6
Fe ₂ O ₃	4.2	4.3
CaO	61.9	20.2
MgO	0.7	2.3
P ₂ O ₅	0.1	19.5
K ₂ O	2.7	1.9
Na ₂ O	0.3	0.6
SO ₃	2.4	1.9
Cl	0.1	0.0
LOI	2.3	3.0
D ₅₀ , μm	15.0	28.8
Blaine (m ² /kg)	394	670
Pozzolanic test NF P18-513		
Lime fixed by sample (mg per g)	-	362
Lime fixed by insoluble residues (mg per g)	-	382
% of insoluble residues	-	39

3. RESULTS AND DISCUSSION

3.1 Preliminary tests and setting time

The first step was to characterize SSA. Hydraulic test shows no reaction between SSA with regular water or in contact with KOH solution. Consequently, SSA has no self-cementitious properties. On the contrary, pozzolanic tests show reactivity between SSA and lime solution.

Results of Vicat Setting time test are presented on figure 1 for mortars with various SSA content (0 to 30% substituted to cement). The setting time is delayed with substitution. It concerns the beginning and the end of the set up and the gap between these two increases. These SSA contains high amount of P₂O₅. These can form Apatite or hydroxoapatite compounds, which are known to delay the setting time. Despite this delay, in the first days, there is no significant consequence on compressive strength as reported in another study on concrete with the same SSA in comparison to CEM I concrete [15].

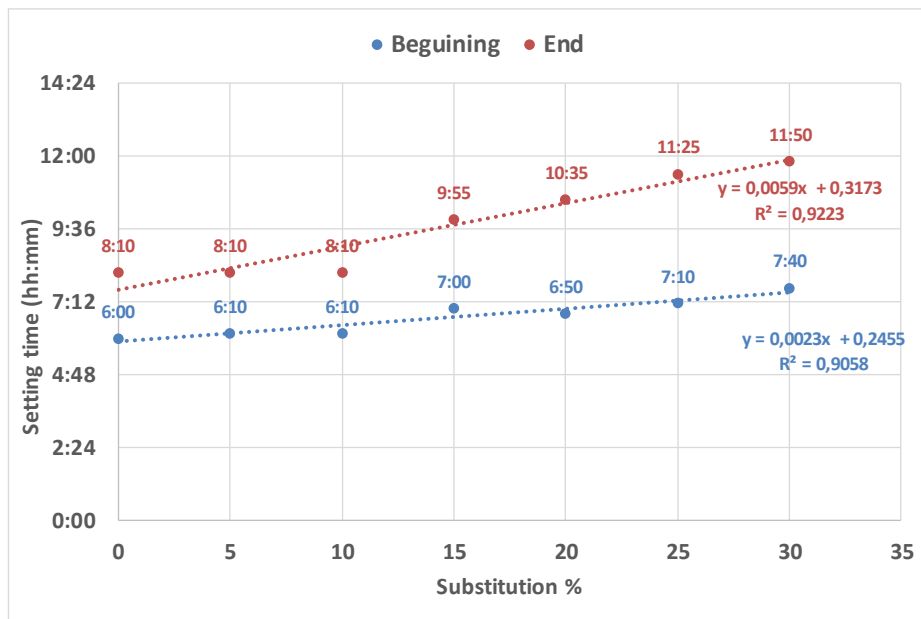


Figure 1: Vicat setting time test as a function of cement substitution by SSA performed on cement pastes.

3.2 Durability tests

Results of porosity assessed by water are presented in figure 2. This is a comparison between mortars. Porosity increases with substitution and it seems according a linear trend. This result is in opposite with some results on other SCM such as MK [16]. However, there is just one test per material for each water curing time consequently results need to be confirmed. In addition, there is no evolution with water curing time (for mortars with substitution superior to 10%). The beneficial effect of eventual pozzolanic reaction is not visible here.

Results on chloride diffusion apparent coefficient ($D_{app,Cl}$) are presented in figure 3. $D_{app,Cl}$ increases with substitution until 28 days at least in accordance to porosity results. At young age, the substitution of cement by SSA has a negative effect on chloride diffusion. However, the water curing time (between 14 and 91 days) decreases strongly $D_{app,Cl}$ for substitution superior to 15%. This is probably due to pozzolanic reactivity and the formation of C-S,(A)-H as already explain by other studies on standard SCM [5,6,16]. However, complementary tests such as SEM or maybe NMR are needed for confirmation of the formation of C-S,(A)-H.

In addition, electrical resistivity tests (ρ) are performed (see figure 4). These results are in accordance with coefficient D and show the same trends. The well known relation is found between these two values as already observed on standard SCM (see figure 3 in right).

Both D and ρ of mortars evolve with water curing time but their porosity stays constant. Consequently, it will be interesting to assess to porous network by Mercury Intrusion Porosimetry, for example, in order to better understand these results.

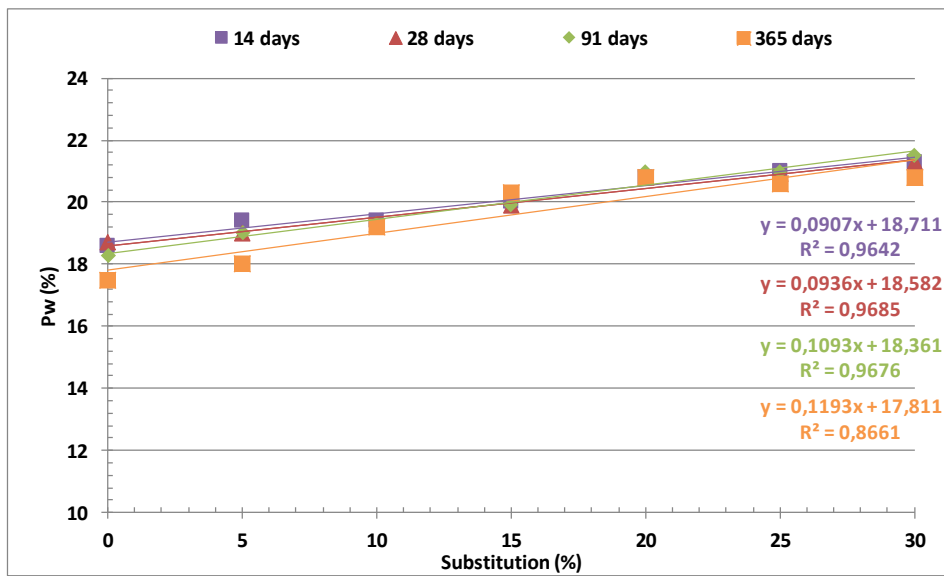


Figure 2: Porosity assessed by water as a function of cement substitution by SSA performed on mortars.

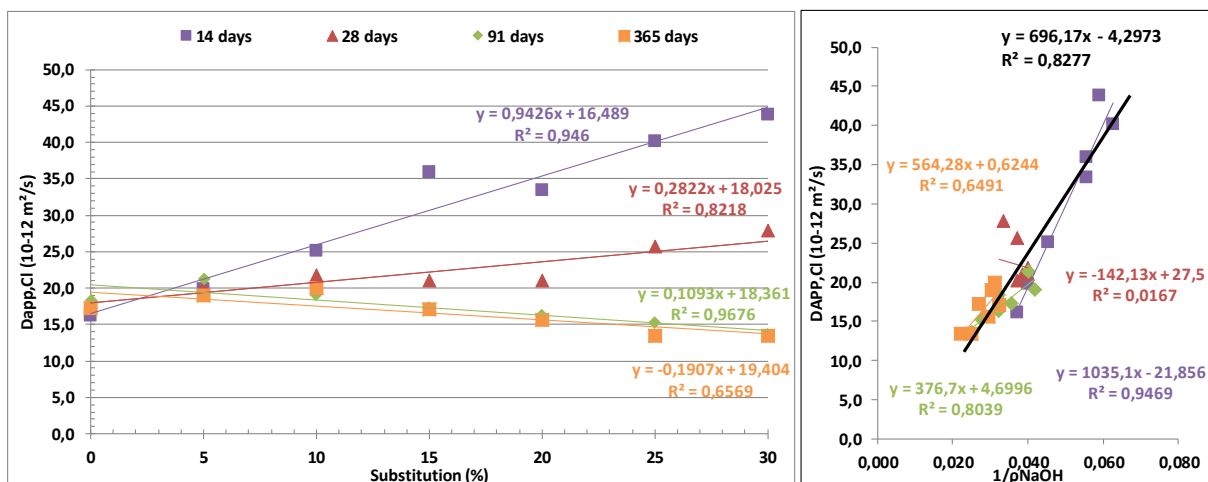


Figure 3: $D_{app,Cl}$ obtained by migration test as a function of cement substitution by SSA and water curing time (in left) or as a function of resistivity (in right) performed on mortars.

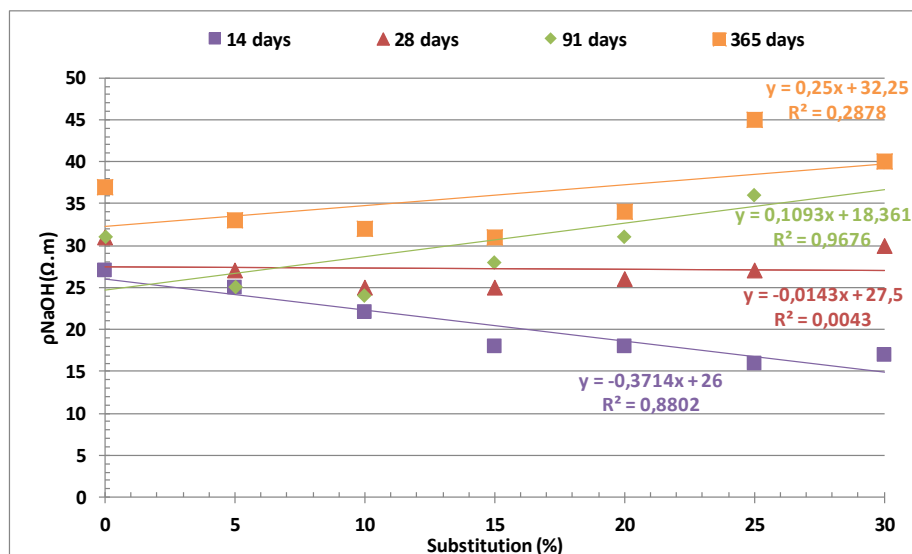


Figure 4: Resistivity as a function of cement substitution by SSA and water curing time performed on mortars.

3.3 Microstructural characterization

Portlandite amount is obtained by TGA results and presented in figure 5. Portlandite amount decreases with substitution. As already explain for other standard SCM [6], this decrease is due to the dilution effect and probably the pozzolanic reaction. In fact, less clinker means less produced portlandite and, in addition, portlandite can be consumed during pozzolanic reaction or maybe during reaction with phosphorous compounds. In order to separate the dilution effect and the portlandite consumption, the mass proportion of portlandite compared to the clinker is calculated and presented in figure 5 right. It seems there is a linear relation between this portlandite amount and the substitution but it appears between 7 and 28 days of water curing.

The water curing time increases portlandite amount for OPC. For a low substitution (inferior to 15%), it decreases between 7 and 28 days which means the supposed pozzolanic reaction or/and the reactions with phosphorous compound consume more portlandite than it is produced by clinker. Finally, this amount increases between 28 and 365 days which means production is dominant. For a higher substitution (superior to 20%), the tendency is not clear but it seems constantly decreases and consequently the consumption is dominant.

The comparison of three cement pastes after 365 days of water curing by XRD are presented in figure 9. These materials have almost the same phases but intensities are quite different. It seems there is more ettringite and portlandite in OPC as expected and more AFm phases in cement pastes with SSA. In fact, there is more SO₃ in CEM I cement paste than in SSA. Consequently, for CEM I cement paste, more AFt phases are formed in comparison to AFm phases. Quartz obviously increases with substitution since it is a part of SSA. Apatites or hydroxo-apatites are not clearly visible after 7 days but maybe they form in early hours of hydration and they change after that, explaining why they can not be observed. Another explanation is that they are amorphous.

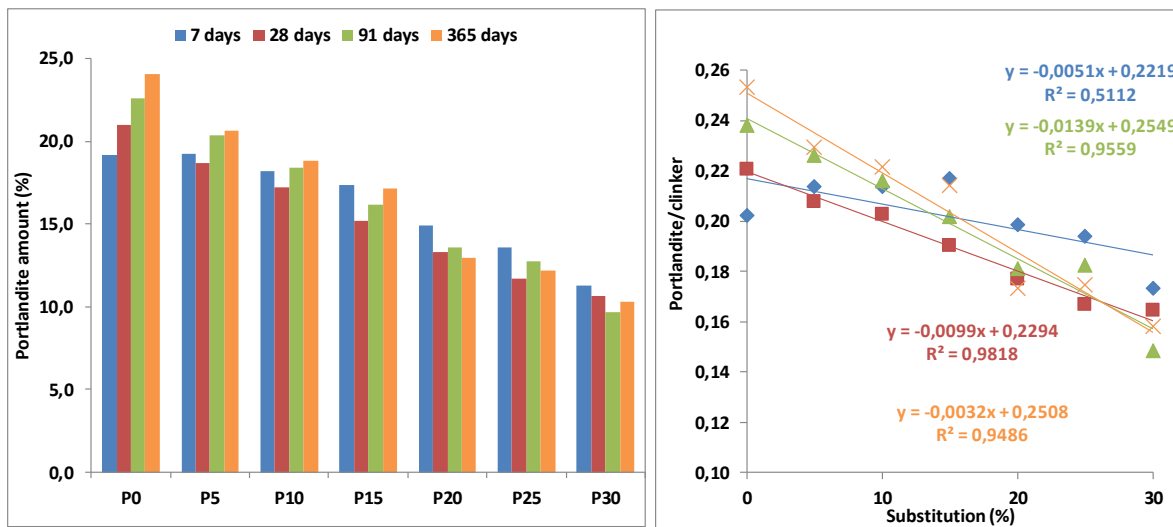


Figure 5: Portlandite amount obtained by TGA as a function of cement substitution by SSA and water curing time performed on cement paste.

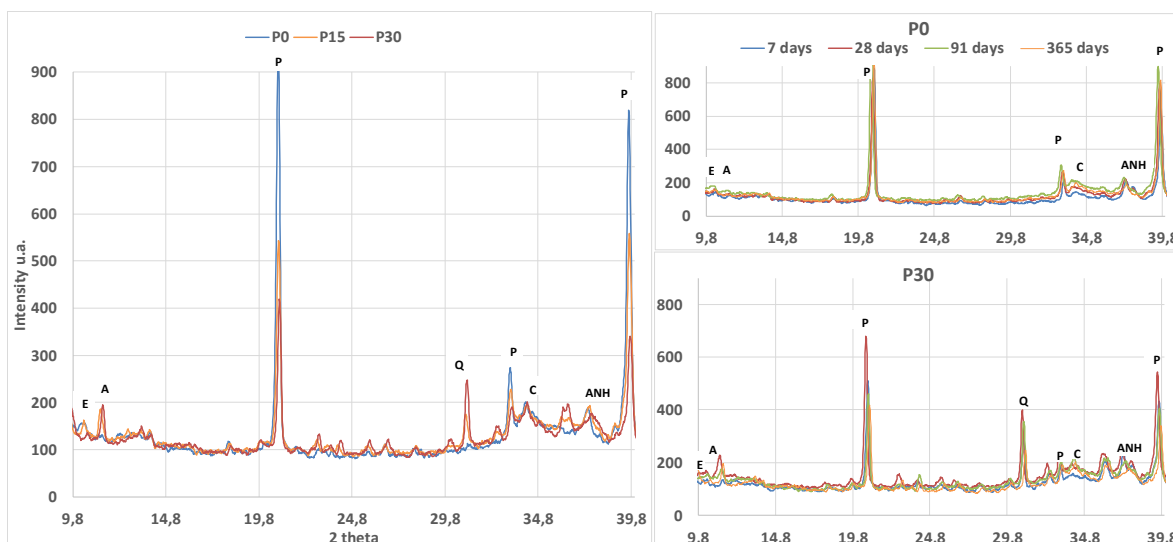


Figure 6: Diffractogram obtained by XRD as a function of cement substitution by SSA (in left) and as a function of water curing time performed on cements pastes (in right). E: ettringite, A: AFm, P: portlandite, Q: quartz, C: Calcite, ANH: anhydrous phases.

4. CONCLUSIONS

SSA seem to show pozzolanic activity. Consequently, SSA produce probably C-S,(A)-H but portlandite amount decreases with substitution (due to the dilution effect but also due to this supposed pozzolanic activity and/or maybe reaction with phosphorous compound). The equilibrium of aluminates phases is also modified. AFt phases decreases with a higher substitution. On the contrary, AFm phases seem to increase. This result is explained by SO₃ amount in cement in comparison to those of SSA. Setting time is delayed (probably due to the presence of apatites), but there is no significant consequences on compressive strength at young age. Chloride diffusion coefficient increases at young age with SSA substitution but evolve to

lower $D_{app,CI}$ with water curing time due to the supposed pozzolanic activity. Porosity assessed by water doesn't explain these results. Consequently, SSA can be used in cementitious materials and the curing time of these materials seem to be important for the hydration and therefore for the durability properties as for the other standard SCMs (fly ash for example). In perspective, technics such as Mercury Intrusion Porosimetry tests should be performed to asses to porous network but also SEM to identify actually the compound produced by lime consumption.

ACKNOWLEDGEMENTS

The presented study was funded by University of Sherbrook (Canada) and Ifsttar (France). The authors are grateful to J. Vincent, F. Ladouceur and B. Zitoun for TGA, XRD and elementary analysis.

REFERENCES

- [1] Damtoft, J. S., Lukasik J., Herfort D., Sorrentino D., Gartner E. M., 'Sustainable development and climate change initiatives', *Cement and Concrete Research*, **38** (2) (2008) 115-127.
- [2] CSA A3000-08, Cementitious materials compendium, *Canadian Standard*, 2008.
- [3] EN 197-1, Cement - Part 1: composition, specifications and conformity criteria for common cements, *European Standard*, 2000.
- [4] Zidol, A., Pavoine, A., Tagnit-Hamou, A., 'Effect of glass powder on concrete permeability', International Congress on Durability of Concrete, Trondheim, June 2012 18-21.
- [5] Schwarz, N., Cam, H., Neithalath, N., 'Influence of a fine glass powder on the durability characteristics of concrete and its comparison to fly ash', *Cement and Concrete Composites* **30** (6), (2008) 486-496.
- [6] Idir, R., Cyr, M., Tagnit-Hamou, A., 'Pozzolanic properties of fine and coarse color-mixed glass cullet', *Cement and Concrete Composites* **33** (1) (2011) 19-29.
- [7] Pera, J., Amrouz, A., 'Development of Highly Reactive Metakaolin from Paper Sludge', *Advanced Cement Based Materials* **7** (2) (1998) 49-56.
- [8] García, R., Vigil de la Villa R., Vegas I., Frías M., Sánchez de Rojas M. I., 'The pozzolanic properties of paper sludge waste' *Construction and Building Materials* **22** (7) (2008) 1484-1490.
- [9] Monzo, J., Paya, J., Borrachero, M.V., 'Use of sewage sludge ash (SSA)-cement admixtures in mortars' *Cement and Concrete Research* **26** (9) (1996) 1389-1398.
- [10] Cyr, M., Coutand, M., Clastres, P., 'Technological and environmental behavior of sewage sludge ash (SSA) in cement-based materials' *Cement and Concrete Research* **37** (8) (2007) 1278-1289.
- [11] Coutand, M., Cyr, M., Clastres, P., 'Use of sewage sludge ash as mineral admixture in mortars' *Construction Materials* **159** (4) (2006) 153-162.
- [12] Dyer, T., Halliday, J., Dhir, R., 'Hydration chemistry of sewage sludge ash used as a cement component' *Journal of Materials in Civil Engineering* **23** (5) (2011) 648-655.
- [13] Baroghel-Bouny, V., Kinomura, K., Thiery, M., Moscardelli, S., 'Easy assessment of durability indicators for service life prediction or quality control of concretes with high volumes of supplementary cementitious materials', *Cement and concrete Composites* **33** (8) (2011) 832-847.
- [14] Andrade, C., Prieto, M., Tanner, P., Tavares, F., D'Andrea, R., 'Testing and modelling chloride penetration into concrete', *Construction and Building Materials* **39** (2013) 9-18.
- [15] Frohard F., 'Durability of eco-concrete: influence of alternative supplementary cementitious material on steel corrosion in reinforced concrete', *PhD Thesis*, Paris Est University, France (in French), 2014.
- [16] Saillio, M., Baroghel-Bouny, V., Pradelle, S., 'Various durability aspects of calcined kaolin-blended Portland cement pastes and concretes', *Calcined Clays for Sustainable Concrete*, Dordrecht *RILEM Bookseries*, vol 10. Springer.

EARLY-AGE STRUCTURAL DEVELOPMENT OF CEMENT BLENDED WITH FLASH CALCINED DREDGING SEDIMENTS

Céline Van Bunderen (1), Ruben Snellings (2), Lucie Vandewalle (1) and Özlem Cizer (1)

(1) Department of Civil Engineering, KU Leuven, Belgium

(2) Sustainable Materials Management, VITO, Belgium

Abstract

Supplementary cementitious materials (SCMs) have been used in Portland cement concrete for decades and many of their effects are already well understood. Recent research on SCMs has focused on exploring new materials, since the existing SCMs will not be able to cover the growing cement demand in future, and understanding the early-age properties of concrete containing alternative SCMs.

The use of dredging sediments as a novel SCM has received considerable interest in recent years. Dredging activities play an important role in maintaining and improving navigation of ships in ports and waterways, and in Antwerp port, each year about 450.000 tons dry matter dredging material is generated. At the moment, no suitable or feasible applications exist, and the material is simply deposited. After mechanical dewatering and flash calcination, however, the dredging sediments show pozzolanic properties and have a great potential to be used as a novel SCM.

This paper presents the influence of the addition of calcined dredging sediments on the early-age properties of cement paste. Heat development (by means of calorimetry) and ultrasonic pulse velocity (UPV) are determined. It was concluded that the calcined dredging sediments had minor influence on the early age development.

Keywords: SCM, dredging sediments, calorimetry, structural development, UPV

1. INTRODUCTION

The use of supplementary cementitious materials (SCMs) is one of the most effective and feasible ways to contribute to the high CO₂-emissions associated with the cement manufacturing. After all, the cement industry is responsible for 8-10% of all man-made CO₂-emissions [1]. The use of dredging sediments as SCM for blended cements and concretes has received considerable interest in recent years [2, 3]. The clinker content of cement can be significantly reduced, producing a more sustainable concrete; as well as the waste dredging sediments become a renewable resource for construction materials.

Dredging activities play a major role in maintaining and improving navigation of ships in ports and rivers. In Antwerp port, Belgium, each year about 450.000 tons dry matter dredging material is generated, for which suitable disposal solutions are required [4]. Since the dredging sediments are rich in clay minerals, they show pozzolanic properties after a mechanical dewatering and flash calcination, and therefore have great potential to be used as a novel SCM.

This paper will focus on the early-age hydration and structural development of cement pastes containing the calcined dredging sediments from the port of Antwerp, which are proven to be pozzolanic reactive [4, 5, 6].

2. EXPERIMENTAL PROGRAM

2.1 Materials

The dredging sediments were first dewatered by membrane filter presses, and then flash calcined in a gas suspension calciner at 865 °C. This treatment ensured activation of the clay minerals, and generated an X-ray amorphous phase that constituted about half of the bulk material [5, 6]. The resulting material is further called CFC (calcined filter cakes).

Ordinary Portland cement (OPC), CEM I 52.5 N, and Portland fly ash cement, CEM II/B-V 42.5 N, were used as two reference cements. The chemical compositions of the materials are given in Table 1 and the BET specific surface areas of the CEM I, CEM II and CFC, were respectively equal to 0.93 m²/g, 2.20 m²/g and 4.94 m²/g.

Table 1: Chemical compositions of the cementitious materials [wt.%].

	Al ₂ O ₃	SiO ₂	Fe ₂ O ₃	CaO	MgO	Na ₂ O	K ₂ O	P ₂ O ₅	SO ₃	LOI
CEM I	4.90	14.04	2.79	57.42	1.63	0.50	0.88	0.29	3.06	2.69
CEM II	11.29	22.02	4.03	45.17	1.82	0.92	1.53	0.56	2.50	2.21
CFC	12.97	41.98	9.65	12.45	2.16	1.37	3.40	0.79	1.50	1.65

A PCE superplasticizer (with a dry matter content of 35 ± 1.0 % and density of 1.08 ± 0.01 kg/l) was also used, in order to contribute to the higher water demand of the CFC particles, due to their higher specific surface area than OPC.

2.2 Methods

2.2.1 Calorimetry

Heat development of the cement paste samples was measured using an isothermal heat conduction calorimeter (TAM AIR) at 20 °C. Samples of 8.4 g ± 0.2 g were taken at the end of mixing and the first measurements were acquired within less than 5 min. after the first contact between the cementitious material and the water. The reported results are the average values of two measurements, normalised to the OPC content, in order to cancel out dilution effects.

2.2.2 Ultrasonic Pulse Velocity (UPV)

An ultrasonic P-wave analysis device (multichannel IP-8, from UltraTest), equipped with a 30 kHz transducer, was used for monitoring the early age hydration of the cement paste. Each measuring cell is composed of a cylindrical silicone mould, with an ultrasonic sender and receiver and a temperature sensor. The volume of the cement paste samples was equal to 95 mL and all tests were performed with a sender-receiver distance of 40 mm ± 0.5 mm.

2.3 Mix design

The compositions of the different cement paste mixes are summarized in Table 2. Two reference mixes, respectively made with CEM I 52.5 N and CEM II/B-V 42.5 N, and three blended cement mixes, where OPC is replaced by 20, 30 and 40 wt.% of CFC, are prepared. The water-binder ratio equalled 0.42 and a PCE superplasticizer was used in order to obtain the same workability for all mixes. The amount of superplasticizer was determined on concrete samples, as described in [7, 8], and a slump class S2 and flow class F2 were achieved. The compositions of the cement paste mixes used in this study are derived from the concrete compositions used in [7, 8].

Table 2: Mix proportions of the cement paste mixes.

		RC I	RC II	CFC 20	CFC 30	CFC 40
CEM I 52.5 N	[g]	300	-	240	210	180
CEM II/B-V 42.5 N	[g]	-	300	-	-	-
CFC	[g]	-	-	60	90	120
Water	[g]	126	126	126	126	126
Superplasticizer	[wt.%/B]	0.35	0.20	0.55	0.70	0.75
W/B	[-]	0.42	0.42	0.42	0.42	0.42

3. RESULTS AND DISCUSSION

3.1 Heat development

The heat flow and cumulative heat of the cement paste samples, are shown in Figure 1. An increased heat flow and higher cumulative heat values are observed for the CFC blended cement mixes, with a higher hydration peak and cumulative heat value for higher replacement levels of OPC by CFC. This can mainly be explained by the filler effect, but also partly by the early age pozzolanic reaction of CFC [5]. Also, a small delay of the hydration peak is visible for the CFC blended cement mixtures, and this is caused by the superplasticizer retarding the cement hydration.

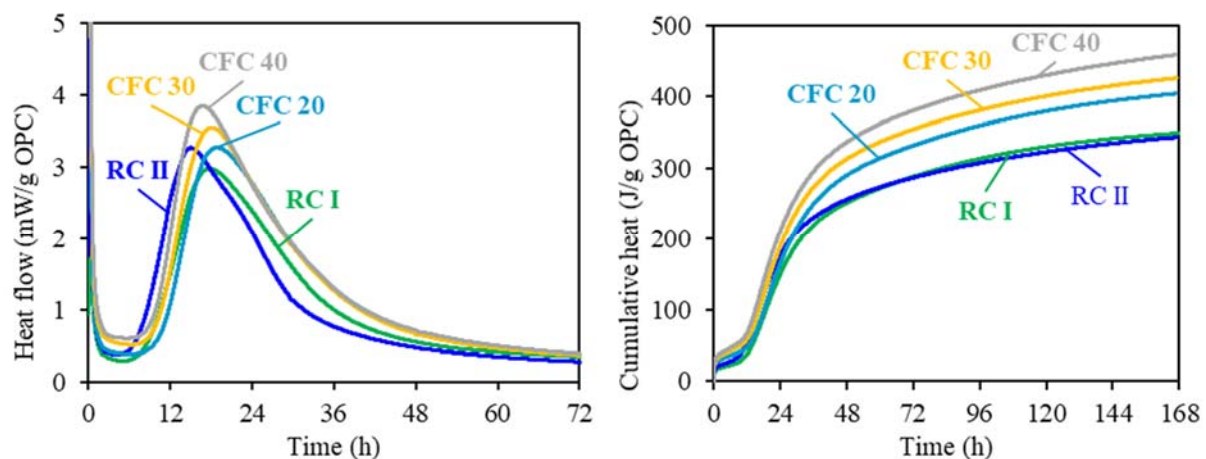


Figure 1: Heat flow and cumulative heat of the cement paste mixes, normalised to the OPC content.

3.2 Ultrasonic Pulse Velocity (UPV)

3.2.1 Ultrasonic curves

The development of the P-wave velocity for an OPC reference mix ($w/b = 0.42$) without superplasticizer, is shown in Figure 2. It can be seen that the P-wave velocity curve is composed of two S-shaped functions, resulting in two peaks in the derivative of the velocity curve. In order to explain the development of this curve, the temperature development inside the specimen is also plotted in Figure 3 and five different stages can be distinguished: a short pre-induction period (0), an induction period (I), an acceleration period (II), a deceleration period (III) and a plateau phase (IV).

0. Pre-induction period. The initial value of the P-wave velocity equals approximately 300 m/s. This value is close to the values found in [9, 10, 11]. However, for completely de-aerated fresh cement paste, values around 1500 m/s (i.e. P-wave velocity in water) are reported [12, 13, 14]. This suggests that the observed low initial value of the P-wave velocity is caused by air entrapped in the paste. However, the value of the initial P-wave velocity is even lower than the P-wave velocity in air (± 342 m/s). Chen et al. [11] reported two causes for this lower velocity: (a) the highly elongated length of the wave-path because of the suspended cement grains in fresh cement paste and (b) air entrapped in the paste because of a certain amount of air bubbles in the mixing water or a lot of tiny air bubbles entrapped during mixing [15, 16].
- I. Induction period. After the pre-induction period, there is a steep increase in the P-wave velocity (from ± 300 m/s to ± 1500 m/s), while there is not yet an increase in temperature. The velocity increase is caused by internal settling and formation of hydration products with no or little influence on the penetration resistance (e.g. ettringite) [11, 17]. At the end of the induction period, the P-wave velocity reaches approximately 1500 m/s (i.e. the initial P-wave velocity for de-aerated fresh cement paste). It is thus concluded that the influence of the entrapped air in the fresh cement paste mix is only limited to the induction period. The first S-shape of the velocity curve and the first peak in the derivative can thus be completely attributed to the removal of air in the specimen.
- II. Acceleration period. During the acceleration period, both the P-wave velocity and temperature significantly increase (the temperature increase corresponds very well with the second peak of the derivative of the P-wave velocity). This stage is a period of intense hydration and is characterized by the rapid formation of C-S-H, CH and ettringite. The connected solid phase starts to develop and the initial setting takes place [11, 14, 17].
- III. Deceleration period. During the deceleration period, the fast increase in P-wave velocity slows down and the temperature starts to decrease. In this period, hydration products with different physical properties are formed and the threshold status of the solid structure is achieved [11, 14, 17].
- IV. Plateau. Finally, a plateau is reached. Both the P-wave velocity and temperature reach to an asymptotic value. In this stage, most of the hydration has been completed, the pores are filled with hydration products and a fully connected solid frame is formed [18, 19].

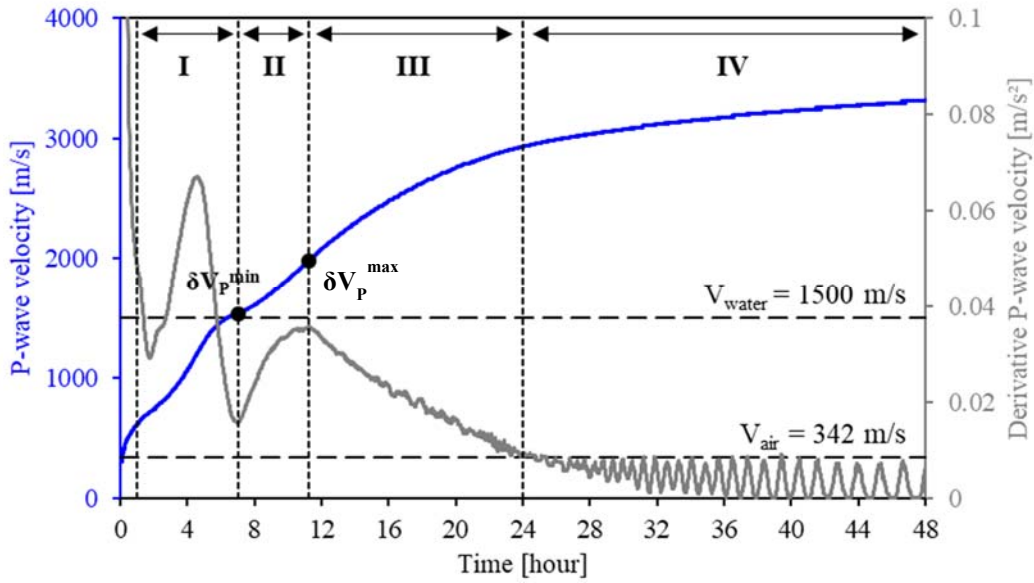


Figure 2: P-wave velocity and derivative of the P-wave velocity for an OPC cement paste ($w/b = 0.42$) without superplasticizer.

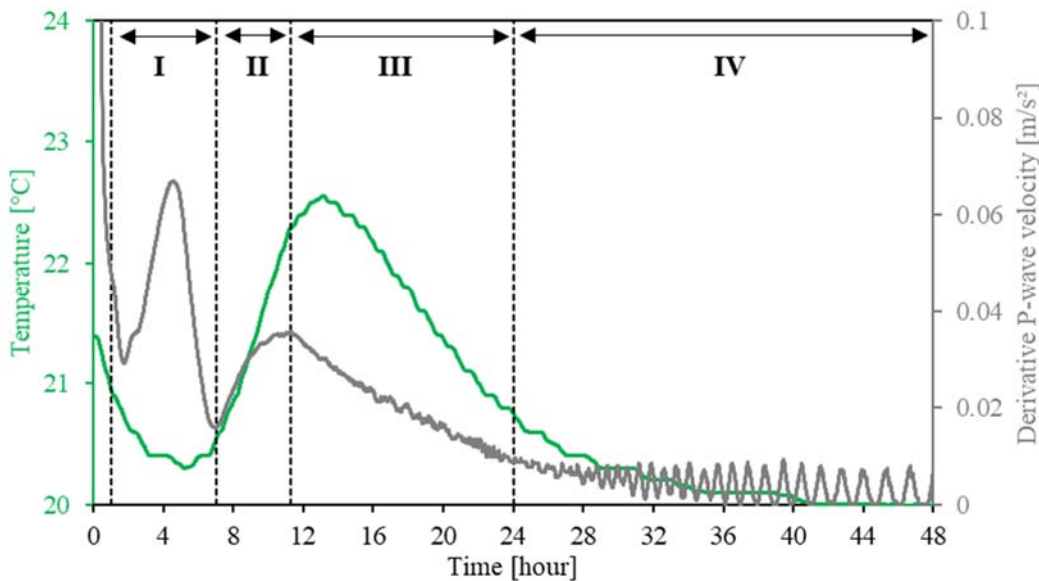


Figure 3: Temperature development versus the derivative of the P-wave velocity for an OPC cement paste ($w/b = 0.42$) without superplasticizer.

3.2.2 Effect of CFC

The effect of CFC on the P-wave velocity is shown in Figure 4 (left). The curves all develop in the same way; two S-shaped functions are observed for all mixes. During the early ages (induction and acceleration period) the difference in P-wave velocity between the different compositions is minimal. However, from the start of the deceleration period, the reference mix with OPC reaches higher P-wave velocity values, while the blended cement mixes show lower values. After 7 days, the mixes with CFC also show little lower P-wave velocities, with decreasing velocity for increasing replacement level of CFC.

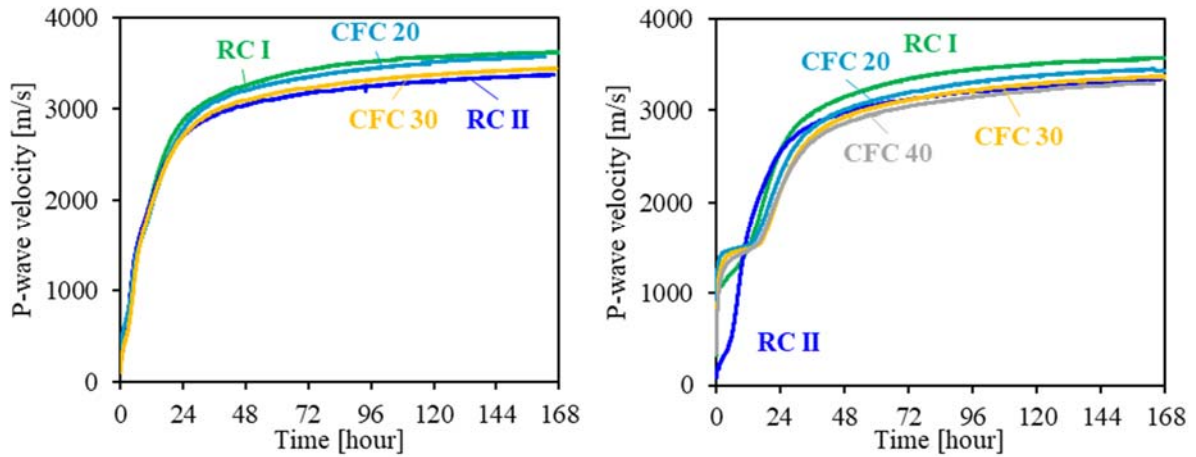


Figure 4: Effect of the addition of CFC on the P-wave velocity (left) and combined effect of the addition of CFC and PCE superplasticizer on the P-wave velocity (right).

However, when considering the cement paste mixes with the addition of superplasticizer (see Figure 4 (right)), the early age P-wave velocity development is strongly affected. This effect will be discussed in the next section.

3.2.3 Effect of superplasticizer

The addition of a PCE superplasticizer strongly affects the development of the P-wave velocity at early ages. Figure 5 shows the P-wave velocity and the derivative of the P-wave velocity for three reference mixes with different amounts of superplasticizer (0 wt.%, 0.35 wt.% and 0.7 wt.% per binder content).

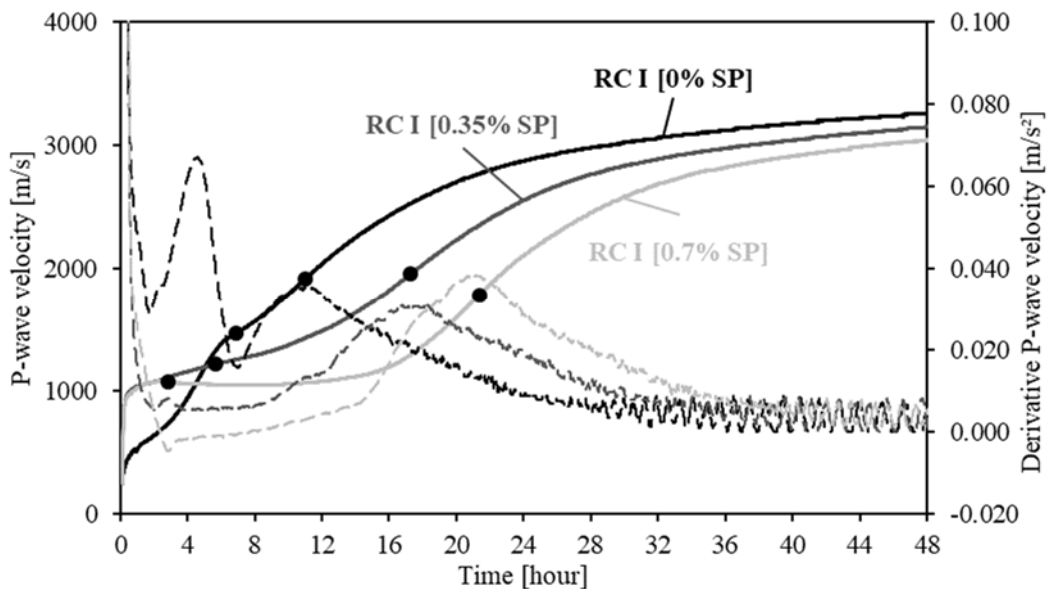


Figure 5: Effect of the addition of a PCE superplasticizer on the P-wave velocity.

During the very early ages, the P-wave velocity of the mixes with addition of superplasticizer immediately increases to a value of about 1000 m/s. This initial increase can possibly be

explained by the fact that less air is entrained in the cement paste, because of the more workable mixture. After this steep velocity increase, a long plateau is observed for the mix with the highest amount of superplasticizer. An elongation of both the induction and acceleration is visible as a result of the cement hydration retardation effect of the PCE superplasticizer [20]. From 48 hours on, the influence of the superplasticizer is less visible, and almost the same P-wave velocity values are attained for the three mixes with different amounts of superplasticizer. The influence of the superplasticizer thus only disappears when the plateau is reached.

5. CONCLUSION

It is concluded that the addition of the calcined dredging sediments influences the early-age development of blended cements in a minor way. CFC contributes to the heat development, resulting in an increased heat flow and higher cumulative heat values (per gram OPC). Considering the structural development, only slightly lower P-wave velocity values are observed for the mixes with CFC, compared to the OPC reference mix. However, the effect of the addition of a PCE superplasticizer, which is necessary in the CFC mixes, due to the lower specific surface area of CFC, strongly influences the early-age behaviour. A delay of the cement hydration is clearly visible in both the calorimetry and UPV results. Improved workability also influences early-age P-wave velocity development where a significant initial increase of the P-wave velocity is observed.

ACKNOWLEDGEMENTS

This study was carried out under the authority of the Flemish Government (Department Maritime Access, MOW); Jos Vandekeybus and Joris Dockx are gratefully acknowledged for their support.

REFERENCES

- [1] K. Scrivener, J. Vanderley and E. Gartner, *Eco-efficient cements: potential, economically viable solutions for a low-CO₂, cement-based materials industry*, UNEP, 2016.
- [2] A. Faure, A. Smith, C. Coudray, B. Anger, H. Colina, I. Moulin and F. They, “Ability of Two Dam Fine-Grained Sediments to be Used in Cement Industry as Raw Material for Clinker Production and as Pozzolanic Additional Constituent of Portland-Composite Cement,” *Waste and Biomass Valorization*, vol. 8, no. 6, pp. 2141-2163, 2017.
- [3] M. A. Chikouche, E. Ghorbel and M. Bibi, “The possibility of using dredging sludge in manufacturing cements: Optimization for heat treatment cycle and ratio replacement,” *Construction and Building Materials*, vol. 106, pp. 330-341, 2016.
- [4] R. Snellings, L. Horckmans, P. Durdzinski, C. Van Bunderen, L. Vandewalle, K. Van Balen, J. Dockx, J. Vandekeybus and Ö. Cizer, “Calcined dredged sediments as supplementary cementitious materials: properties and pozzolanic reactivity,” in *International RILEM Conference on Materials, Systems and Structures in Civil Engineering*, Lyngby, Denmark, 2016.
- [5] R. Snellings, L. Horckmans, C. Van Bunderen, L. Vandewalle and Ö. Cizer, “Flash-calcined dredging sediment blended cements: effect on cement hydration and properties,” *Materials and Structures*, vol. 50:214, 2017.

- [6] R. Snellings, Ö. Cizer, L. Horckmans, P. T. Durdzinski, P. Dierckx, P. Nielsen, K. Van Balen and L. Vandewalle, "Properties and pozzolanic reactivity of flash calcined dredging sediments," *Applied Clay Science*, vol. 129, pp. 35-39, 2016.
- [7] C. Van Bunderen, R. Snellings, L. Horckmans, L. Vandewalle and Ö. Cizer, "Mixture proportions of concrete with dredging sediments as novel SCM," in *Proceedings of the 10th ACI/RILEM International Conference on Cementitious Materials and Alternative Binders for Sustainable Concrete*, Montréal, Canada, 2017.
- [8] C. Van Bunderen, R. Snellings, L. Horckmans, J. Dockx, J. Vandekeybus, K. Van Balen, L. Vandewalle and Ö. Cizer, "Properties of concrete recycling clay-rich dredging sediments as a novel supplementary cementitious material," in *Proceedings of the International RILEM Conference on Materials, Systems and Structures in Civil Engineering - Segment on Service Life of Cement-based Materials and Structures*, pages 317-324, Lyngby, Denmark, 2016.
- [9] G. Trtnik, M. I. Valic, F. Kavcic and G. Turk, "Comparison between two ultrasonic methods in their ability to monitor the setting process of cement pastes," *Cement and Concrete Research*, vol. 39, pp. 876-882, 2009.
- [10] W. Zhang, Y. Zhang, L. Liu, G. Zhang and Z. Liu, "Investigation of the influence of curing temperature and silica fume content on setting and hardening process of the blended cement paste by an improved ultrasonic apparatus," *Construction and Building Materials*, vol. 33, pp. 32-40, 2012.
- [11] W. Chen, Y. Li, P. Shen and Z. Shui, "Microstructural development of hydrating Portland cement paste at early ages investigated with non-destructive methods and numerical simulation," *Journal of Nondestructive Evaluation*, vol. 32, pp. 228-237, 2013.
- [12] J. Zhu, S.-H. Kee, D. Han and Y.-T. Tsai, "Effect of air voids on ultrasonic wave propagation in early age cement pastes," *Cement and Concrete Research*, vol. 41, pp. 872-881, 2011.
- [13] R. M. Kmack, K. E. Kurtis, L. J. Jacobs and Y.-Y. Kim, "Assessment of air entrainment in fresh cement paste using ultrasonic nondestructive testing," *Journal of ASTM International*, vol. 7.1, pp. 1-18, 2009.
- [14] J. Zhang, L. Qin and Z. Li, "Hydration monitoring of cement-based materials with resistivity and ultrasonic methods," *Materials and Structures*, vol. 42, pp. 15-24, 2009.
- [15] J. Keating, D. Hannant and A. Hibbert, "Comparison of shear modulus and pulse velocity techniques to measure the build-up of structure in fresh cement pastes used in oil well cementing," *Cement and Concrete Research*, vol. 19, no. 4, pp. 554-566, 1989.
- [16] C. M. Sayers and R. Grenfell, "Ultrasonic propagation through hydrating cements," *Ultrasonics*, vol. 31, no. 3, pp. 147-153, 1993.
- [17] G. Trtnik, G. Turk, F. Kavcic and V. B. Bosiljkov, "Possibilities of using the ultrasonic wave transmission method to estimate initial setting time of cement paste," *Cement and Concrete Research*, vol. 38, pp. 1336-1342, 2008.
- [18] Y. Zhang, W. Zhang, W. She, L. Ma and W. Zhu, "Ultrasound monitoring of setting and hardening process of ultra-high performance cementitious materials," *NDT&E International*, vol. 47, pp. 177-184, 2012.
- [19] G. Ye, P. Lura, K. van Breugel and A. Fraaij, "Study on the development of the microstructure in cement-based materials by means of numerical simulation and ultrasonic pulse velocity measurement," *Cement & Concrete Composites*, vol. 26, pp. 491-497, 2004.
- [20] G. Trtnik and G. Turk, "Influence of superplasticizers on the evolution of ultrasonic P-wave velocity through cement pastes at early age," *Cement and Concrete Research*, vol. 51, pp. 22-31, 2013.

DURABILITY OF HIGH CARBON BIOMASS ASH-BASED BINDER

Piyush Chaunsali (1), Hugo Uvegi (2), Brian Traynor (2) and Elsa Olivetti (2)

(1) Department of Civil Engineering, IIT Madras, Chennai, India

(2) Department of Materials Science and Engineering, MIT, Cambridge, USA

Abstract

Biomass residues, such as rice husk and sugar cane bagasse, are primary source of power generation for micro, small, and medium enterprises in India. Based on feedstock type and boiler temperature, composition of biomass ash varies significantly. The residual carbon content of biomass ash can be quite high, i.e., up to 25–35%, preventing its use with Portland cement. This research aims to develop a non-Portland cement binder from an Indian biomass ash having high residual carbon (loss-on-ignition of ~26%). Biomass ash binders were formulated using biomass ash, Indo-Gangetic clay, hydrated lime and sodium hydroxide solution. The binders cured at near-ambient temperature exhibited 10–20 MPa strength after 7 days. Durability of the biomass ash binder was assessed by monitoring its water absorption, one of the key performance parameters for the masonry application. The biomass ash binder showed good water resistance as the strength was not impacted after repeated wetting and drying cycles. Moreover, 24 hours water absorption ranged from 25–37% depending on biomass ash content and bulk dry density of the binder. Chemical stability of the reaction product present in biomass ash binder was also evaluated in neutral and acidic media. In summary, this study demonstrated a value-added application of an underutilized high carbon biomass ash in masonry application.

Keywords: Biomass ash; Clay; Residual carbon; Water absorption

1. INTRODUCTION

The share of biomass-derived energy is expected to increase in the near future given its renewable nature. Globally, bioenergy is responsible for ~10% of energy production [1]. India produces about 450–500 million tons of biomass per year, and biomass provides 32% of all primary energy used in the country at present [2]. Micro, small, and medium enterprises (MSMEs) rely on the availability of agricultural residues such as rice husk, sugar cane bagasse, etc. for electricity generation. However, operational inefficiency of boilers often leads to significant residual carbon in biomass ash. Moreover, higher amounts of residual carbon in biomass ash prevents its use as a replacement of Portland cement.

Silica-rich material, such as rice husk ash, has been used as a precursor for both calcium silicate hydrate-based and sodium aluminosilicate-based binders [3-5]. In previous studies, the authors have developed a Portland cement-free biomass ash-based binder for masonry application [6, 7]. The biomass ash binder was formulated using hydrated lime and sodium hydroxide solution as reactive media to initiate the formation of the C-S-H phase, and it exhibited compressive strengths of 10–20 MPa after 7 days of curing at near-ambient temperature ($30^{\circ}\text{C} \pm 2^{\circ}\text{C}$). However, the durability of this binder has yet to be assessed. This study reports the performance of the biomass ash-based binder after long-term exposure in neutral and acidic media including the effect of wetting and drying cycles on its strength.

2. MATERIALS AND METHODS

An Indian biomass ash (source: Silverton Pulp & Papers Pvt. Ltd., Muzaffarnagar, India), derived from the burning of a mix of rice husk and sugarcane bagasse, was used in this study. Table 1 shows the oxide composition of the Silverton ash as determined by X-ray fluorescence (XRF) using ASTM C311. High loss on ignition of the ash is evident from Table 1. X-ray diffraction (XRD) analysis of Silverton ash revealed phases such as quartz, albite, cristobalite, sylvite, and arcanite [6,7]. The amorphous content of the ash was ~90% including the contribution of residual carbon. Clay from the Indo-Gangetic Plain was also used in this study and was largely crystalline [7]. Table 2 shows the mixture proportions used in this study. 1M or 2M aqueous sodium hydroxide solutions were used as activating solutions. The liquid-to-solid ratio (L/S) ranged from 0.25 to 0.4, as shown in Table 2. The mixing was performed in a Kitchen Aid mixture at the maximum speed (~220 rpm) for 15 minutes. Samples were then hydraulically pressed into 200 g cubes, compacted using a Baldwin Tate Emery Universal Testing Machine to final pressures of 10 MPa and 20 MPa with a fixed loading rate of 15000 N/min. The compaction mold had inner cross-sectional dimensions of 50 mm × 50 mm. Subsequently, samples were wrapped in plastic sheet and stored in an oven operating at $30^{\circ}\text{C} \pm 2^{\circ}\text{C}$ for at least the initial 7 days of curing.

Table 1: Chemical composition (oxide %) of biomass ash and clay using XRF

Oxide (%)	SiO ₂	Al ₂ O ₃	Fe ₂ O ₃	SO ₃	CaO	Na ₂ O	MgO	K ₂ O	P ₂ O ₅	Trace*	LOI [#]
Biomass Ash	61.73	1.12	0.63	1.96	1.6	0.17	0.81	2.22	0.86	0.15	26%
Clay	71.7	13.3	5.03	0.02	0.77	0.96	1.51	2.53	0.07	0.76	0.5%

* Includes TiO₂, MnO₂, BaO, and SrO; #loss-on-ignition (LOI) at 750°C

Table 2: Mixture proportions and associated tests

Mixtures	Ash (wt. %)	Clay (wt. %)	Lime (wt. %)	#L/S (*M) (molarity*)	Comp. Pressure (MPa)	Tests (no. of samples)
Mix 1	70	20	10	0.4 (2M)	10	Strength (3), water absorption (3)
Mix 2	70	20	10	0.4 (1M)	10	Strength (3), wetting/drying (3), leaching (1)
Mix 3	70	20	10	0.4 (1M)	20	Strength (3), water absorption (3)
Mix 4	50	40	10	0.25 (1M)	20	Water absorption (3)
Mix 5	50	40	10	0.28 (1M)	20	Water absorption (3)

#Liquid-to-solid ratio (by wt.); *Molarity of NaOH solution

Compressive strength of cube-shaped (50 mm × 50 mm × 50 mm) samples was determined at a loading rate of 15000N/min, the same as that used to compact samples. For water absorption tests, saturated samples were dried at 100°C for 24 hours. Leaching tests were performed on three different sample sizes: 1) cube (50 mm × 50 mm × 50 mm), 2) slice (1–2 mm thickness), and 3) powdered (< 45µm). Leaching tests were carried out in two solutions: neutral (pH ~ 7.5) and acidic (pH ~ 1.2). Deionized (DI) water and 0.1M HNO₃ solution were used as neutral and acidic media, respectively. The samples were weighed after 24 hours in a desiccator and immersed in one of the two solutions (neutral or acidic). The sample-to-solution ratio was 1:10 (by weight) for sliced and powdered samples. For cube-shape sample, the sample-to-solution ratio was 1:1.25 (by weight). After 28 days of soaking, leachate solutions were analyzed using inductively coupled plasma atomic emission spectrometry (ICP-AES) for the concentrations of sodium (Na) and calcium (Ca).

3. RESULTS AND DISCUSSIONS

The biomass ash binder developed in this study used NaOH solution as a chemical activator for facilitating the dissolution of ash. In an earlier study by the authors [7], it was demonstrated that calcium silicate hydrate (C-S-H) is the main reaction product in the binder. The dissolved silica from the ash reacts with hydrated lime to form C-S-H phase. In order to examine the effect of alkalinity on strength development, biomass ash binders were formulated using 1M and 2M NaOH solutions. As shown in Fig. 1, the strength of biomass ash binder increased for the activator prepared using higher alkalinity of activating solution. Both binders were able to achieve at least 10 MPa strength after 7 days of near-ambient curing (i.e., 30°C ± 2°C).

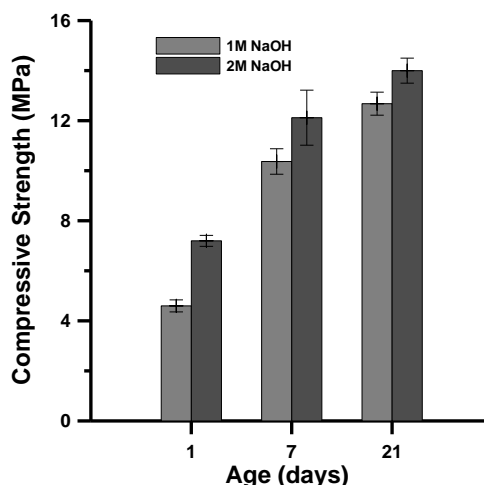


Figure 1: Strength comparison between 1M and 2M NaOH activated biomass ash binders (Note: Binder – 70% ash:20% clay:10% lime; compaction pressure – 10 MPa; L/S – 0.4)

A structure exposed to outside environment may undergo many wetting and drying cycles due to variable environmental conditions. Considering the presence of alkalis in the binder, it becomes important to investigate if alkali leaching negatively affects strength and durability. To test such an effect on durability, samples produced using 1M NaOH solution were immersed in water, and elemental leaching and compressive strength values were measured, comparing the latter with pre-wetting strength. Therefore, to simulate environmental wetting and drying cycles, a set of cube size samples (age: 7 days) were soaked in deionized water for 1 day, dried subsequently at 30°C for 2 days, and soaked again in deionized water for 1 day. It is evident from Fig. 2 that saturated samples exhibited ~10–12% strength loss.

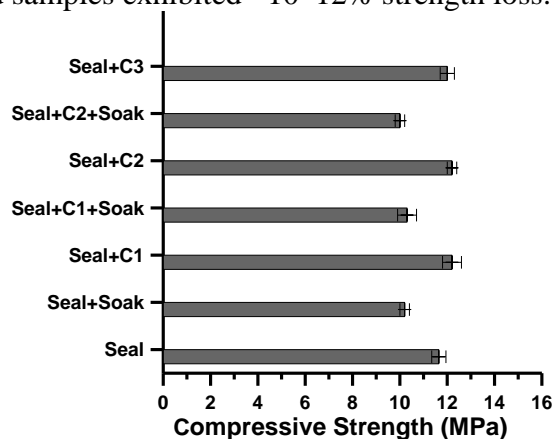


Figure 2. Influence of wetting and drying cycles on strength of 1M NaOH-activated biomass ash binder (Note: Binder – 70% ash:20% clay:10% lime; Seal – sealed for 7 days at 30°C; Soak – soaked in deionized water for 1 day at 22°C; C – cycle of soaking in deionized water for 1 day at 22°C and drying for 2 days at 30°C; C1, C2, and C3 – cycle 1, 2, and 3; Error bars represent one standard deviation of uncertainty.)

Upon subsequent drying at 30°C, the samples regained the lost strength. This observation indicates that the strength loss observed in samples after extended soaking was primarily due

to the saturation phenomenon (i.e. hydraulic stresses) [8]. After 3 wetting and drying cycles, there was no significant change in the strength of binder, as evident in Fig. 2.

Aside from its effect on strength, water absorption (i.e., % absorption after 24 hours soaking in water) is an important qualifying criterion for field application of brick masonry. Figure 3 (a) shows the water absorption values of four different mixtures. A good correlation was observed between water absorption and dry bulk density. Increase in compaction pressure from 10 MPa to 20 MPa led to a denser microstructure reducing the water absorption from ~37% to ~31%. Without changing the compaction pressure, further reduction in water absorption could be achieved by reducing the ash content to 50% (by wt.). The formulation comprising of 50% (by wt.) ash, 40% (by wt.) clay and 10% (by wt.) lime resulted in ~29% and ~25% absorption values for L/S ratios of 0.25 and 0.28, respectively. The L/S ratio of biomass ash binder had to be reduced from 0.4 to 0.25 and 0.28 to prevent the loss of liquid during sample compaction. Figure 3 (a) also suggests a way to limit the water absorption of biomass ash binder by controlling the dry bulk density. High water absorption of biomass ash binder developed in this study was a result of high fraction of ash present in binder. Therefore, limiting ash content is expected to reduce the water absorption of binder. Figure 3 (b) clearly shows that all binders exhibited strength in the range of 12–20 MPa. An increase in strength with compaction pressure is also evident due to a more compact microstructure at higher pressure.

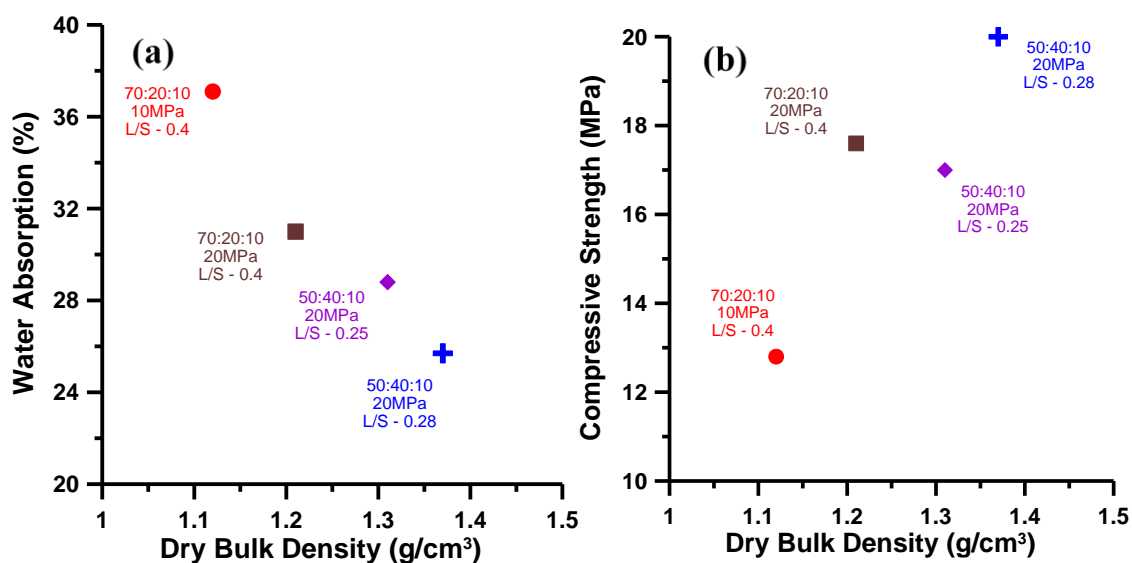


Figure 3. Water absorption (%) and 7-day strength of biomass ash binder as a function of dry bulk density (Note: Data label includes weight proportion (ash: clay: lime), compaction pressure, and liquid-to-solid ratio, L/S.)

Finally, to study alkali leaching, three different types of binder samples with varying surface area exposure were tested. This was done to examine a relationship between sample size/surface area and leaching extent in deionized water. Fine powdered samples ($< 45 \mu\text{m}$) were prepared via grinding. Due to the high specific surface area of such powders ($< 45 \mu\text{m}$), this sample type was chosen to obtain an upper bound of the extent of desorption/leaching. In addition to powdered samples, small slices (thickness of $\sim 1.5\text{--}2 \text{ mm}$) and large cubes (size $50 \times 50 \times 50 \text{ mm}$) were studied to capture the influence of sample size on the extent of alkali leaching. As

expected, sodium desorption was found to be higher from the small slice than from the large cube, also shown in Fig. 4. The extent of alkali desorption increased from 12% to 40% as the specific surface area and surface area-to-volume ratio of small size samples increased. For comparison, desorption value was normalized per unit weight of the binder, representing the total millimoles of [Na] released per gram of binder. It is evident that the alkali desorption from the large cube was small due to slower diffusion through the dense microstructure. The powdered sample exhibited the maximum extent (i.e. 60%) of sodium desorption among three sample types. Hong and Glasser [9] found that alkali (Na and K) desorption from synthesized C-S-H with 0.85 Ca/Si ranged from 55% to 70%. Therefore, the results obtained in our study are in general agreement with their study as the C-S-H phase present in biomass ash binder also had a low Ca/Si ratio [7]. In this study, powdered and sliced samples were soaked in solution at a solution-to-solid ratio (by weight) of 10, and for a period of 28 days. Any change in solution-to-solid ratio will further affect the alkali desorption, and therefore, needs to be considered.

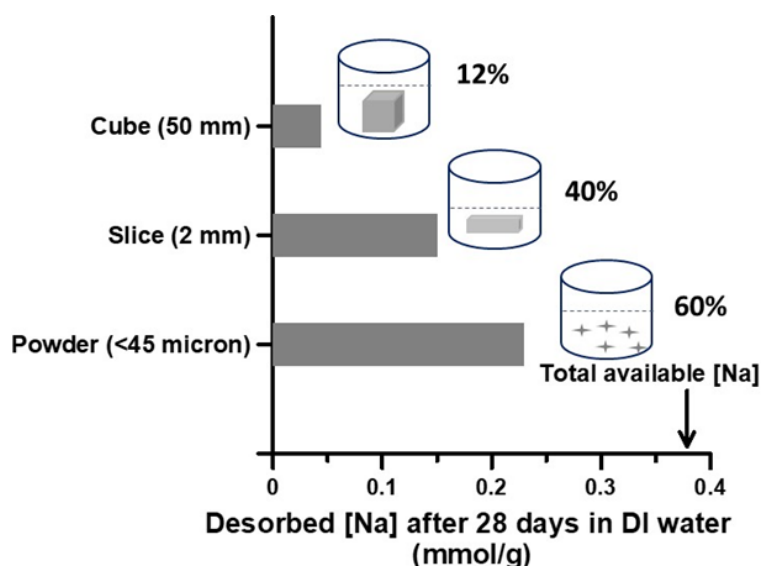


Figure 4. Influence of sample size on sodium leaching from biomass ash binder (Note: solution-to-sample ratio (by weight) was 10 for sliced and powdered samples, and 1.25 for cubes)

The extent of leaching is dependent on the pH of soaking medium. Larger pH gradient between the sample pore solution and soaking medium will result in a higher degree of leaching. Figure 5 shows that the extent of calcium and sodium leaching was higher in 0.1M HNO₃ solution than in deionized water. The difference in calcium leaching is quite evident as it was two orders of magnitude higher in 0.1M HNO₃ due to higher pH gradient and lower chemical stability of the C-S-H phase in acidic environments. However, the extent of sodium leaching was similar and high in both leaching solutions, suggesting loosely bound nature of alkalis in reaction product.

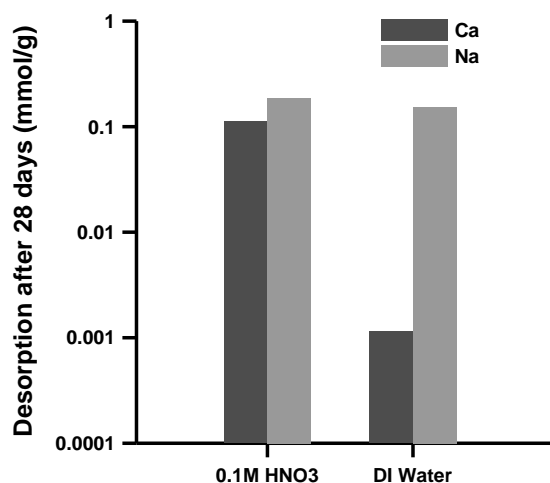


Figure 5. Influence of soaking medium on leaching of sodium and calcium from biomass ash binder (Note: Sample: 1.5–2 mm thick slice; solution-to-sample ratio: 10)

The effect of field exposure condition on durability of biomass ash binder was assessed by monitoring a brick wall (location: Muzaffarnagar, India) made of the biomass ash binder. Figure 6 compares the bricks prepared using 1M and 2M NaOH solution after long (> 1 year) exposure in outside environment. It was evident that the brick made with 2M NaOH solution had efflorescence and surface cracking, possibly due to excessing alkali leaching and associated carbonation. On the contrary, the brick made with 1M NaOH solution did not show any damage or efflorescence. Hence, it's very important to pay attention to the alkalis as they are not structurally bound in C-S-H phase present in the biomass ash binder.

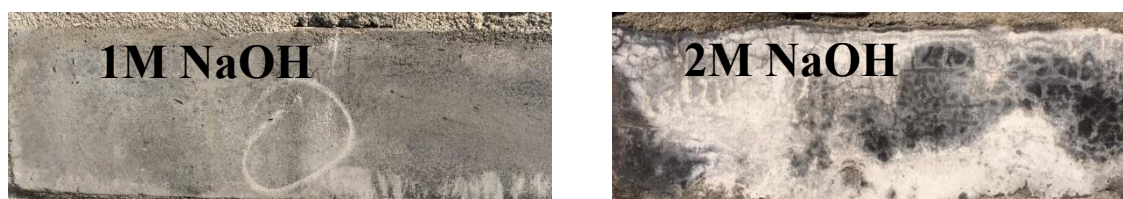


Figure 6. Comparison between bricks prepared using 1M and 2M NaOH solutions and exposed to the outside environment for extended duration (> 1 year)

4. CONCLUSIONS

The biomass ash binders formulated using 1M and 2M NaOH solution achieved at least 10 MPa strength after 7 days, exhibiting potential for structural application. Durability study revealed that the biomass ash binder retained strength after undergoing a number of wetting (in DI water) and drying (at 30°C) cycles. The water absorption of the biomass ash binder was strongly correlated with the bulk dry density. Such relationships can be utilized to formulate the biomass ash binder having target (maximum) water absorption. Exposure to 0.1M HNO₃ led to excessive leaching of calcium from the binder compared to the deionized water-treated binder. However, sodium leaching was comparable in both deionized- and 0.1M HNO₃-treated binders, suggesting loosely bound nature of alkalis. Field exposure of biomass ash binder demonstrated the benefit of having lower alkalinity of activating solution.

ACKNOWLEDGEMENTS

We would like to acknowledge the financial support for this research through the Tata Center for Technology and Design at Massachusetts Institute of Technology (MIT), Cambridge. The authors thank Mr. Pankaj Agrawal of Bindlas Duplux Ltd. (Muzaffarnagar, India) for providing the materials, and Mr. Ankur Garg of Deepak Ceramics Ltd. (Muzaffarnagar, India) for help in constructing the field prototype. This work made use of the MRSEC Shared Experimental Facilities at MIT, supported by the National Science Foundation under award number DMR-1419807.

REFERENCES

- [1] https://www.worldenergy.org/wp-content/uploads/2017/03/WEResources_Bioenergy_2016.pdf. (accessed on Sept 27, 2018)
- [2] <http://www.eai.in/ref/ae/bio/bio.html> (accessed on Sept 27, 2018)
- [3] Hernández, J.M., Middendorf, B., Gehrke, M. and Budelmann, H., 1998. Use of wastes of the sugar industry as pozzolana in lime-pozzolana binders: study of the reaction. *Cement and Concrete Research*, 28(11), pp.1525-1536.
- [4] Duxson, P., Fernández-Jiménez, A., Provis, J.L., Lukey, G.C., Palomo, A. and van Deventer, J.S., 2007. Geopolymer technology: the current state of the art. *Journal of materials science*, 42(9), pp.2917-2933.
- [5] Bernal, S.A., Rodríguez, E.D., de Gutiérrez, R.M., Provis, J.L. and Delvasto, S., 2012. Activation of metakaolin/slag blends using alkaline solutions based on chemically modified silica fume and rice husk ash. *Waste and Biomass Valorization*, 3(1), pp.99-108.
- [6] Poinot, T., Laracy, M.E., Aponte, C., Jennings, H.M., Ochsendorf, J.A. and Olivetti, E.A., 2018. Beneficial use of boiler ash in alkali-activated bricks. *Resources, Conservation and Recycling*, 128, pp.1-10.
- [7] Chaunsali, P., Uvegi, H., Osmundsen, R., Laracy, M., Poinot, T., Ochsendorf, J., & Olivetti, E. (2018). Mineralogical and microstructural characterization of biomass ash binder. *Cement and Concrete Composites*, 89, 41-51.
- [8] Bartlett, F.M. and MacGregor, J.G., 1994. Effect of moisture condition on concrete core strengths. *ACI Materials Journal*, 91(3), pp.227-236.
- [9] Hong, S.Y. and Glasser, F.P., 1999. Alkali binding in cement pastes: Part I. The CSH phase. *Cement and Concrete Research*, 29(12), pp.1893-1903.

THE EFFECT OF MSWI FLY ASH ON MORTAR WORKABILITY

Benjamin A. R. Ebert (1), Britt-Marie Steenari (2), Mette R. Geiker (3) and Gunvor M. Kirkelund (1)

- (1) Department of Civil Engineering, Technical University of Denmark, Denmark
- (2) Chemistry and Chemical Engineering, Chalmers University of Technology, Sweden.
- (3) Department of Structural Engineering, Norwegian University of Science and Technology, Norway.

Abstract

Management of fly ash from municipal solid waste incineration (MSWI) is problematic, due to the fly ash toxicity and leaching. The ash could potentially serve as a partial cement substitute, similarly to fly ash from coal incineration. In this work, the potential of two different MSWI fly ashes as partial cement substitutes were analysed by testing the ashes effect on the workability. This was achieved by investigating the variations in consistency (ease of flow), caused by increasing fly ash substitution, immediately after mixing and after 30 minutes, on mortar mixes containing 5, 10 and 20% cement replacement. The first fly ash had little impact on the consistency, except at 10% substitution where the flow was reduced by 30% compared to a reference. The second reduced the flow by 16, 29 and 70% with increasing substitution. With the addition of superplasticizer, a consistency similar to the reference was achieved. Samples with high amounts of cement replaced by ash had a higher reduction in flow after 30 minutes compared to a reference. The addition of superplasticizer reduced the flow loss after 30 minutes except for a 20% substitution.

Keywords: Mortar, MSWI Fly Ash, Consistency, Superplasticizer

1. INTRODUCTION

In recent years, countries have undergone changes to their management of municipal solid waste. Instead of landfilling, waste is recycled or incinerated at combined heat and power plants. Municipal solid waste incineration (MSWI) is a frequently used procedure, utilizing the waste for energy gain, reducing the amount landfilled. However, it results in environmentally strenuous by-products in the form of fly ash that remains underused. The high content of heavy metals in fly ash indicate that fly ash pose a potential threat to the environment, due to leaching and toxicity [1]. The fly ash could potentially serve as a partial cement substitute, similarly to

coal fly ash, when producing concrete [2,3], immobilizing the heavy metals and decreasing the environmental load [4]. In addition, cement production accounts for around 8% of the global CO₂ emission each year [5]. Substitution of cement with MSWI fly ash, could make concrete more sustainable and remove the otherwise unused fly ash from circulation.

Previous research by Aubert et al. [2] and Bertolini et al. [3] determined that the replacement of cement with MSWI fly ash led to a reduction in workability of fresh mortar, requiring alteration to the mixture design. The alterations could be changes to the water/cement ratio or the inclusion of superplasticizers in the mixing process [2]. Aubert et al. and Bertolini et al. both washed their ashes to reduce chloride and heavy metal content. Aubert et al. also stabilized the heavy metals through phosphation and calcined the ash. Additionally, they washed an ash sample with Na₂CO₃ to reduce the metallic aluminium amount and remove CaSO₄. The previously mentioned two studies focused on the mechanical strength and overall concrete properties, instead of the workability. The aim of this study is to investigate the potential of using untreated MSWI fly ash as a partial cement substitute, based on the workability properties. Accomplished by determining the changes in consistency (ease of flow) with increasing fly ash substitution, as well as studying the loss of consistency over time, and the effect of including superplasticizer.

2. EXPERIMENTAL

2.1 Materials

Two MSWI ashes were collected. The first from Nuuk incineration, a small-scale grate-fired plant in Greenland, designated Nuuk-FA, and ash from Borås Energi och Miljö, a large-scale fluidized bed plant in Sweden designated Borås-FA. The two ashes were dried for 24 hours at 50°C prior to mixing.

The experiments were done using a CEM I 52.5 N (MS) (LA) cement. The chemical composition of the cement and the two MSWI fly ashes are given in Table 1, determined by X-ray fluorescence.

Table 1: Chemical composition of cement and ashes.

	CEM I	Nuuk-FA	Borås-FA
Al ₂ O ₃	5.41	3.97	4.53
CaO	64.1	33.6	40.58
Cl	0.04	20.0	12.0
Cr ₂ O ₃	0.01	0.04	0.06
Fe ₂ O ₃	3.80	0.66	1.72
K ₂ O	0.44	10.72	2.41
MgO	1.03	0.91	1.66
Na ₂ O	0.30	21.57	6.20
P ₂ O ₅	0.30	1.26	1.67
SiO ₂	19.7	4.71	5.99
SO ₃	3.23	7.74	8.74
TiO ₂	0.22	1.13	2.34
LOI	1.56	31.16	21.36

The particle size distribution of the ashes and cement was measured by laser diffractometry using a Mastersizer 2000. Standard sand as specified in DS/EN 196-1 was used for the mortar. A modified acrylic polymer based superplasticizer was used as an additive. The plasticizer used was based on designed performance polymers and have a low viscosity of < 30 mPa·s, a pH of 6.5 ± 1 and a density of $1.06 \pm 0.02 \frac{\text{g}}{\text{cm}^3}$.

3.2 Sample Preparation

Mortar samples were prepared, based on the method described in DS/EN 196-1. 450g of cement was used, with a water-cement ratio of 0.5. For this series of testing 5, 10 and 20% of the cement was substituted with ash. Table 2 shows the series of mixes done. Superplasticizer was only used together with Borås-FA. Each mix was repeated 3 times.

Cement and fly ash blends were pre-mixed dry for 2 minutes at the mixers lowest setting, to achieve complete homogenisation. The mixer used has two settings, corresponding to the speeds described in DS/EN 196-1. At the onset of mixing, demineralised water was added to the blend and subsequently stirred as specified in DS/EN 196-1. For the samples including superplasticizer, the plasticizer was added to the mixing water before mixing.

Table 2: Series of samples prepared.

	CEM I [g]	Nuuk-FA [g]	Borås-FA [g]	Plasticizer
Ref	450.0			-
Nuuk5	427.5	22.5		-
Nuuk10	405.0	45.0		-
Nuuk20	360.0	90.0		-
Borås5	427.5		22.5	-
Borås10	405.0		45.0	-
Borås20	360.0		90.0	-
Borås5SP	427.5		22.5	+
Borås10SP	405.0		45.0	+
Borås20SP	360.0		90.0	+

3.3 Consistency Measurement

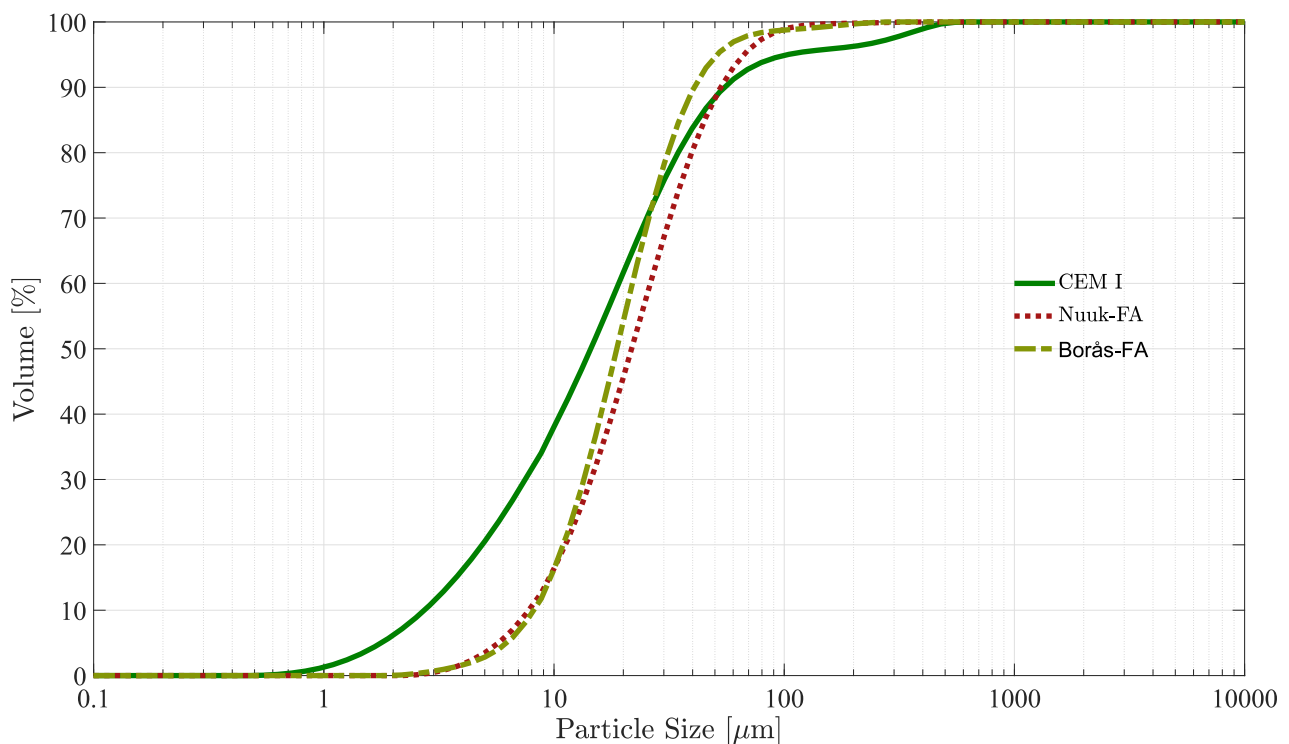
The consistency of the samples was measured with a flow table, using the technique specified in DS/EN 1015-3. The mould used had the dimensions specified in DS/EN 1015-3, except for the height, that was 50 mm instead of 60 mm. The mould was filled halfway with mortar and smoothed with at least 10 strokes of a tamper. The mould was then topped and smoothed again with at least 10 strokes of the tamper. The mould was then removed and the flow table was jolted with 1 jolt each second for 15 seconds. Finally, the diameter of the resulting circle was measured twice at 90-degree angles to each other. The mean of the two measurements was reported as the flow value. The 100 mm internal bottom diameter of the mould was subtracted from the final results. The initial consistency was measured 6 minutes after the water was added. To test the loss of consistency over time, the mortar was left to hydrate in the bowl with a plastic sheet cover. After 30 minutes of hydration, the consistency was measured again using the described procedure.

3. RESULTS & DISCUSSION

3.1 Particle Size Distribution

The particle size distribution of the ashes and cement are shown in Figure 1. The particle size distributions of the two ashes both have similar fractions between 1 and 10 μm , and curvature. However, Nuuk-FA contains a higher volume of larger particles compared to Borås-FA. The two ashes, however, deviate from CEM I. They are not as fine-grained, with the majority of their particles being larger than CEM I, and do not contain a small fraction of large particles around 100 μm .

Figure 1: Particle Size Distribution.



3.2 Initial consistency

The differences in initial consistency, and over time, with increasing cement substitution is displayed in Table 2, together with the mortar samples made with superplasticizer. The addition of MSWI fly ash is shown to have a detrimental effect on consistency. Although, the impact of the two ashes differs.

Replacement with 5% Nuuk-FA exhibited no significant changes in consistency, deviating approximately 3% from the reference. Replacement with 10% Nuuk-FA leads to a 30% reduction in flow. This indicates a loss in consistency with increasing substitution. Surprisingly, 20% substitution with Nuuk-FA resulted in a consistency similar to the 5% replacement. The decrease and increase in consistency suggest that substitution with Nuuk-FA has an initial adverse effect on the consistency; however, at higher substitution rates the ash does not affect

the consistency. With no marked effect on the consistency at 5 and 20% replacement, experiments with superplasticizer were deemed irrelevant.

Contrary to the results with Nuuk-FA, substitution with Borås-FA had a noticeable effect on the mortar consistency. Replacement with 5% Borås-FA resulted in a flow reduction of 16%, while a replacement with 10 and 20% reduced the flow by 29 and 70% respectively. Increasing substitution, therefore, results in decreased consistency. This decrease trends toward a linear interaction between the loss of consistency and replacement amount. This poses a significant challenge for concrete production, since a high replacement with Borås-FA, would be unsuited for jobs requiring a high fluidity.

The addition of superplasticizer in the mixing water negates this loss in consistency. By adding an increasing amount of plasticizer for each substitution percentile, similar flow values as the reference were achieved. An average of 0.92, 2.18 and 6.35 g superplasticizer was added to the 5, 10 and 20% mixes respectively, in order to compensate for the loss in consistency. The superplasticizer required, to achieve the desired consistency, greatly increases for higher substitutions.

It was expected, based on the results of Aubert et al. [2] and Bertolini et al. [3], that substitution with increasing amounts of MSWI fly ash would lower the consistency of the mortar, despite their ashes being treated. The results with Borås-FA corresponds to the results determined by Aubert et al. [2] and Bertolini et al. [3] using flow time testing from the French standard NF P 15-437 and Vebe respectively. Aubert et al. [2] found that the flow time was more than doubled when replacing 25% cement with fly ash, while Bertolini et al. [3] found that a 30% substitution resulted in no slump after 13 s Vebe time. Aubert et al. [2] concluded that substitution of cement with MSWI fly ash leads to a strong reduction in workability, requiring changes to the water-cement ratio or the addition of superplasticizer.

Aubert et al. [2] attribute the loss of workability to the porosity of the ashes or increase in water demand, due to the high surface area of ultrafine neoformed calcite in the ash. Although untreated, the two ashes tested in this article contain large amounts of calcium and therefore may contain calcite. The calcite is unlikely to be neoformed as in [2]. The particle size distribution showed relatively large particles, suggesting that the loss of consistency is not caused by ultrafine calcite. Although not measured during the tests in this article, differences in porosity between the Nuuk-FA and Borås-FA could be a likely cause for their different effect on the consistency as Aubert et al. [2] suggests.

Table 2: Measured flow value (mm) after 6 and 30 minutes.

	Nuuk-FA		Borås-FA		Borås-FA + Plasticizer	
	6 min	30 min	6 min	30 min	6 min	30 min
Ref	70.38±7.13	61.28±7.13	70.38±7.13	61.28±7.13	70.38±7.13	61.28±7.13
5%	68.39±4.86	59.94±5.11	58.85±6.26	53.15±0.61	67.45±1.41	59.03±2.29
10%	49.02±7.05	42.82±7.58	49.99±9.00	31.79±5.84	67.86±11.1	55.13±14.9
20%	67.43±3.70	38.99±1.29	20.87±10.4	1.79±1.43	66.81±9.11	12.92±7.70

3.3 Loss of consistency after 30 minutes

In addition to decreasing the initial consistency, substitution with MSWI fly ash is shown to further reduce the consistency after 30 minutes. For both Nuuk-FA and Borås-FA, a 5% substitution does not intensify the loss of consistency after 30 minutes, compared to the reference. In contrast, a 10 and 20% replacement with Borås-FA resulted in a loss of flow approximately twice as big as the reference loss. Although a 10% substitution with Nuuk-FA reduced the initial consistency, the loss over time remained similar to the reference. Oppositely, a 20% replacement with Nuuk-FA showed no effect on the initial consistency but greatly affected the consistency after 30 minutes, resulting in a flow loss 3 times greater than the reference.

The addition of superplasticiser had varying effects on the consistency loss over time. In the case of 5% substitution with Borås-FA, the loss of flow over time were similar to the reference, while for a 10% substitution, the superplasticizer improved the loss over time. However, it had no effect on the 20% substitution. Although the initial consistency was improved, the flow after 30 minutes was reduced by approximately 54 mm, 6 times greater than the flow loss of the reference.

The changes in consistency after 30 minutes could be caused by the chemical composition of the ashes. The two ashes both contain different elements in varying amounts that can affect the cement hydration differently. Chen et al. [6] determined that NaCl, KCl and $\text{CaCl}_2 \cdot 2\text{H}_2\text{O}$ were present in a tested MSWI fly ash, suggesting their presence in Nuuk-FA and Borås-FA. Different compounds have varying effects on hydration, such as NaCl and CaCl_2 accelerating the hydration [7] and [8], while sulphate is reported to both accelerate and retard the hydration [9] and [10]. However, further studies are required to better understand the effect of MSWI fly-ash on cement hydration.

The results show that depending on the ash, large cement replacements hampers the consistency. Superplasticizer improves the initial consistency. However, the increased loss of workability both initially and after 30 minutes would make early age concrete work increasingly difficult, when utilizing a high substitution rate.

4. CONCLUSIONS

- Depending on the type of MSWI fly ash used, the initial consistency of the mortar is either unaffected or greatly decreased with increasing ash substitution. Borås-FA reduced the consistency by 16, 29 and 70% for a 5, 10 and 20% substitution. A 5 and 20% substitution with Nuuk-FA did not affect the initial consistency, yet a 10% substitution reduced the consistency by 30%.
- High MSWI fly ash substitution results in an increased loss in consistency after 30 minutes. The two ashes showed no increase in flow loss after 30 minutes with a 5% substitution. Substitution with 10 and 20% Borås-FA increased the flow loss by a factor of two, while replacement with 20% Nuuk-FA increased the flow loss by a factor of three.
- Superplasticizer improves the initial loss in consistency. With superplasticizer, a consistency similar to the reference was achieved regardless of the substitution amount. Although increasing amounts of superplasticizer were needed for higher substitutions. The addition of superplasticizer decreased the flow loss after 30 minutes, except for a 20% substitution where the flow was reduced by a factor of 6 compared to the reference.

- To better understand the loss in initial consistency and over time, future studies will include investigations of the effect of the fly ash porosity, as well as the potential effect the chemical composition has on the consistency. Furthermore, supplementary flow and fluidity experiments with additional MSWI ashes could be made to get an overall better understanding of MSWI ashes influence on the consistency.

ACKNOWLEDGEMENTS

Nuuk Incineration and Borås Energi och Miljö are recognized for contributing the fly ash for this series of experiments.

REFERENCES

- [1] H. Zhang, Y. Zhao, Toxicity Analysis of Municipal Solid Waste Incineration (MSWI) Fly Ash, 2009 3rd Int. Conf. Bioinforma. Biomed. Eng. (2009) 1–4. doi:10.1109/ICBBE.2009.5163694.
- [2] J.E. Aubert, B. Husson, N. Sarramone, Utilization of municipal solid waste incineration (MSWI) fly ash in blended cement. Part 2. Mechanical strength of mortars and environmental impact, *J. Hazard. Mater.* 146 (2007) 12–19. doi:10.1016/j.jhazmat.2006.11.044.
- [3] L. Bertolini, M. Carsana, D. Cassago, A.Q. Curzio, M. Collepardi, MSWI ashes as mineral additions in concrete, *Cem. Concr. Res.* 34 (2004) 1899–1906. doi:10.1016/j.cemconres.2004.02.001.
- [4] L. Kozakova, T. Bakalar, M. Zelenak, M. Prascakova, Solidification of MSWI fly-ash with regard to hazardous metals leaching, *Acta Montan. Slovaca.* 18 (2013) 129–139.
- [5] Jos G.J. Olivier; Greet Janssens-Maenhout; Marilena Muntean; Jeroen A.H.W. Peters, Trends in global co 2 emissions 2016, (2016) 86.
- [6] W.S. Chen, F.C. Chang, Y.H. Shen, M.S. Tsai, C.H. Ko, Removal of chloride from MSWI fly ash, *J. Hazard. Mater.* 237–238 (2012) 116–120. doi:10.1016/j.jhazmat.2012.08.010.
- [7] F.R. Lago, J. Dweck, T. Analysis, Evaluation of Influence of Salt in the Cement Hydration to Oil Wells, 20 (2017) 743–747.
- [8] V.S. Ramachandran, Calcium chloride in concrete- applications and ambiguities., *Can. J. Civ. Eng.* 5(2) (1978) 213–221.
- [9] P.K. Metha, P.J.M. Monteiro, Concrete microstructure, properties and materials, Fourth Edi, Mc Graw Hill Education, n.d.
- [10] S. Kumar, C.V.S.K. Rao, Effect of sulphates on the setting time of cement and strength of concrete, *Cem. Concr. Res.* 26 (1996) 643. doi:Doi 10.1016/S0008-8846(96)90013-7.

PRE-TREATMENTS OF MSWI BOTTOM ASH FOR THE APPLICATION AS SUPPLEMENTARY CEMENTITIOUS MATERIAL IN BLENDED CEMENT PASTE

Boyu Chen (1), Yubo Sun (1), Loic Jacquemin (1), Shizhe Zhang (1), Kees Blom (2) Mladena Luković (3) Guang Ye (1)

- (1) Microlab, Section Materials and Environment, Faculty of Civil Engineering and Geosciences, Delft University of Technology, Stevinweg 1, 2628 CN Delft, The Netherlands
- (2) Gemeente Rotterdam, Ingenieursbureau, the Netherlands
- (3) Concrete Structures, Faculty of Civil Engineering and Geosciences, Delft University of Technology, Stevinweg 1, 2628 CN Delft, The Netherlands

Abstract

At present, most municipal solid waste incineration (MSWI) bottom ash, as being disposed of as waste, is directly landfilled, raising concern about the environmental issue and potential loss of resources. Given that the natural raw materials used for cement production are being depleted, the recycling of MSWI bottom ash for the application as building materials is meaningful and promising. The feasibility of using MSWI bottom ash as mineral additives in concrete has been demonstrated in the literature. In this research, as-received MSWI bottom ash has high mineral content and shows stable leaching behaviour. But, when used as cement substitute, the residual metallic Al in bottom ash always causes matrix swelling and strength loss by reacting with $\text{Ca}(\text{OH})_2$ and releasing H_2 gas. In this research, dry and wet pre-treatment methods were performed to remove the metallic Al in as-received bottom ash (0-2mm). The results show that both of these two methods are effective. When comparing these two methods, wet method is time-consuming but can remove the metallic Al completely; dry method is fast but always has limitation that it can only reduce the metallic Al content by 80%. Regarding compressive strength, the decrease introduced by 10% dry-treated bottom replacement in cement paste is less than that of wet-treated bottom ash. The lower strength development observed in wet-treated bottom ash blended cement may be due to the removal of soluble reactive phases during the treatment.

Keywords: MSWI bottom ash, cement substitute, metallic Al, pre-treatment, compressive strength

1. INTRODUCTION

According to the research conducted by the Worldwatch Institute for its Vital Signs Online service, the growing prosperity and urbanization could double the volume of municipal solid waste (MSW) from today's 1.3 billion tons per year by 2025, challenging environmental and public health management worldwide [1]. Currently, the waste-to-energy technology [2] is considered as an efficient method to deal with the increasing amount of MSW. The incineration process reduces the mass and volume of solid waste [3] dramatically (by 70% and 90%, respectively [4, 5]), as well as the demand of landfilling [6]. But this waste treatment method is always accompanied by the production of new types of solid wastes that include fly ash (FA) and bottom ash (BA). Compared with fly ash, the utilization of bottom ash is more important and shows greater potential, due to its large available quantities and stable leaching behavior. However, several significant drawbacks have been found limiting the utilization of MSWI BA in concrete structures. For example, the reactivity of BA is much lower than Portland cement [7]. For this reason it is commonly used as aggregates alternatives for primary sand and gravel. However, the addition of BA aggregates always causes severe volume expansion and cracking due to the release of hydrogen gas from the redox reaction of the metallic Al that BA contained in the alkaline environment [8]. The goal of this research is to eliminate the metallic Al contained in as-received bottom ash via two different pre-treatment methods and assess the possibility of using pre-treated bottom ash as supplementary cementitious material in blended cement paste.

2. MATERIALS AND METHODS

The MSWI bottom ash used in this research, having particle size of 0-2mm, was collected from one of the Dutch waste-to-energy plants. Two pre-treatment methods were selected to remove the residual metallic Al that is hard to extract in the process of metal recovery. Method one is called "dry method", in which metallic Al was sieved out by allowing milled bottom ash to pass through the sieve of 63 μ m, after enlarging its surface through low-speed ball milling. Method two is to dissolve metallic Al by immersing bottom ash in 0.1 molar NaOH solution for more than one week, and is called "wet method".

In this study, both dry- and wet-treated bottom ash were used as Portland cement substitute. For this purpose, dry-treated bottom ash (<63 μ m) was used without further treatment and is called "DBA". On the other hand, after wet treatment, the immersed bottom ash was filtered, washed, dried and further milled into fine powder. The bottom ash obtained here is called "WBA".

Cement paste samples were prepared according to EN 196-1. Each specimen has the dimension of 20mm \times 20mm \times 20mm. After casting, cement paste specimens were firstly cured at room temperature for 24 hours, then de-moulded and wet cured (room temperature, 95% RH) until 28 days. Details of mix design are listed in **Error! Reference source not found.**, where 10 wt.% Portland cement was replaced by treated bottom ash. The water to solid ratio of all the paste was 0.5. Pure Portland cement (CEM I 42.5N) samples were prepared as the reference.

Table 1 Mix design for blended cement paste

Materials			Water to solid ratio (w/s)
CEM I 42.5N	DBA	WBA	
100%			0.5
90%	10%		
90%		10%	

The chemical compositions of as-received and treated bottom ash were determined by X-ray fluorescence (XRF). The mineralogical compositions of treated bottom ash were measured by X-ray diffraction (XRD). The Al content in the bottom ash was calculated by measuring the gas volume generated upon its chemical reaction with NaOH solution.

3. RESULTS AND DISCUSSION

3.1 Metallic Al content

Table 2 shows that both dry- and wet-methods are highly effective in removing residual metallic Al. After dry-treatment, the average metallic Al content was reduced by around 80%. Comparatively, the metallic Al was removed almost completely after wet treatment. This can be attributed to the pores and cracks exist in bottom ash particles (as shown in Figure 3), which make metallic Al easily exposed to the NaOH solution even if it is incorporated inside the bottom ash particles.

Table 2 Metallic Al content in as-received and treated bottom ash

Materials	As-received BA	DBA	WBA
Metallic Al content (wt.%)	0.80 ± 0.03	0.13 ± 0.05	0.03 ± 0.03

3.2 Chemical and mineralogical compositions

The XRF results (in Table 3) indicate that in as-received and treated bottom ash the main components are SiO₂, CaO, Fe₂O₃, and Al₂O₃. When compared with Portland cement, the SiO₂ content in as-received MSWI bottom ash is 37.28%, almost two times of that in cement, but the CaO content (23.86%) is much less, only one-third of that in cement. Besides, much more Al₂O₃ and Fe₂O₃ were found in as-received MSWI bottom ash. After pre-treatment, more SiO₂, but less CaO, Fe₂O₃, and Al₂O₃ were detected in both dry- and wet-treated bottom ash. The Na₂O content in wet-treated bottom ash is slightly higher than as-received bottom ash. This is mainly introduced by the NaOH solution used in wet treatment. The content of heavy metals such as Pb and Cr are very small, less than 1% in both untreated and treated bottom ash.

Table 3 Chemical composition of CEM I 42.5N and MSWI bottom ash

Elements (wt.%)	CEM I 42.5N	MSWI bottom ash		
		As-received	DBA	WBA
SiO ₂	18.34	37.28	50.40	49.82
CaO	66.15	23.86	18.34	17.4
Fe ₂ O ₃	3.46	15.27	12.94	10.58
Al ₂ O ₃	4.41	10.48	9.84	10.2
Na ₂ O	-	0.83	0.56	2.96
K ₂ O	0.46	1.02	0.82	0.79
MgO	2.16	2.68	2.21	2.52
ZnO	-	0.9	0.75	1.4
PbO	-	0.17	0.67	0.1
Cr ₂ O ₃	-	0.16	0.12	0.09
Cl	-	1.33	0.12	0.13
SO ₃	2.63	2.32	0.86	0.36
Others	0	3.71	2.36	3.63

The XRD results (in Figure 1) show that both as-received and treated bottom ash are highly crystalline, with quartz and calcite being the two main crystalline phases along with other phases including akermanite and the main Fe-containing phase magnetite. Compared with as-received bottom ash, the mineralogical composition remains unchanged after both dry and wet treatment.

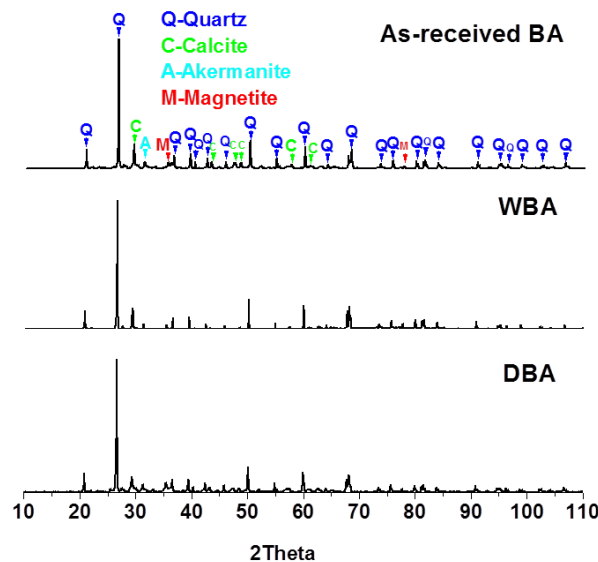


Figure 1: XRD pattern of as-received and treated MSWI bottom ash

3.3 Particle size distribution

In terms of particle size, both dry and wet treatment would lead to material loss and particle size reduction. As illustrated in Figure 2, as-received bottom ash is mainly concentrated in the range of 2-4 and 0.5-1.6mm, while the size of most wet-treated bottom ash is between 0.125-1.6mm. This is because as-received bottom ash particles have an irregular shape and are full of cracks and voids (as shown in Figure 3). When immersed in NaOH solution, the metallic Al embedded inside the particles could be dissolved easily, resulting in particles splitting. In addition, wet-treatment always leads to material loss, especially for the particles as small as dust, which easily adhere to filter paper, and are difficult to remove.

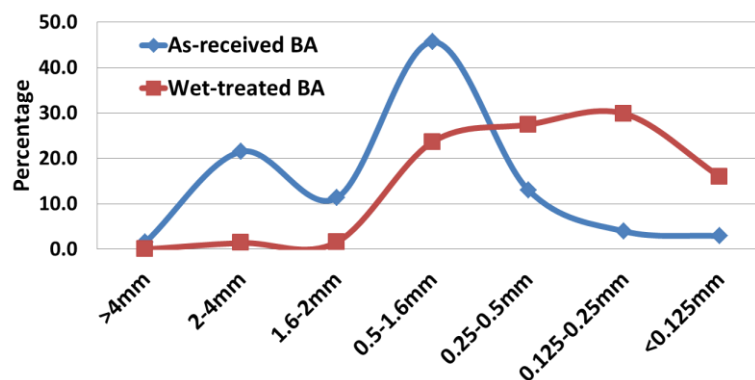


Figure 2: Particle size distribution of as-received and wet-treated bottom ash after sieve analysis

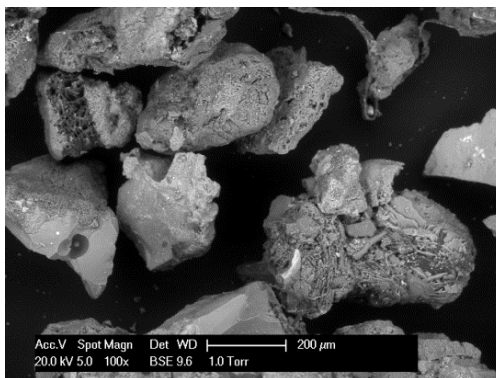


Figure 3: Morphology of as-received MSWI bottom ash (100×)

Figure 4 depicts the particle size distribution of 42.5R cement ($D_{50}=35.7\mu\text{m}$) and the bottom ash used for sample preparation including DBA and WBA. It is evident that cement has the largest particle size among these three. Besides, it is worth mentioning that considering bottom ash particles become smaller after wet treatment (as shown in Figure 2), less milling time but the same speed was applied in ball mill grinding process, to obtain similar particle distribution as DBA. However, with quartz as its main component, the abrasion resistance of wet-treated bottom ash particles remains the same. The WBA obtained having D_{50} of $27.4\mu\text{m}$ is coarser than WBA ($D_{50}=14.5\mu\text{m}$).

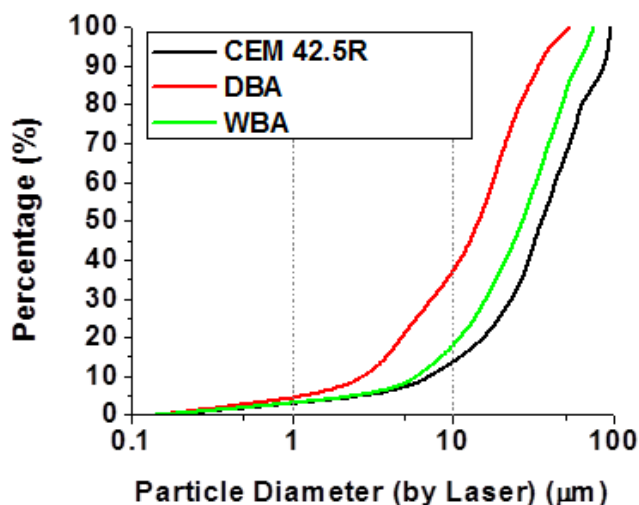


Figure 4: Particle size distribution of materials used for sample preparation

3.4 Compressive strength

As can be seen in Table 4, the replacement of cement with only 10% of WBA or DBA could already lead to dramatic decrease in compressive strength after 28 days of curing: around 62% for CEM-WBA and 40% for CEM-DBA. This can be explained by the fact that the reactive phases in treated bottom ash are deficient. Some of the WBA and DBA components may have adverse effect on the cement hydration. When comparing WBA and DBA, WBA has larger particle size, and its negative impact, due to low reactivity, on strength development seems to be higher than DBA. This can be attributed to the possible removal of soluble reactive amorphous phases in wet treatment and the high alkalinity of WBA derived from NaOH immersion. More investigation is needed in these aspects.

Table 4 Average 7- and 28-day compressive strength of pure cement and 10% WBA and DBA substituted cement specimens.

Compressive strength (MPa)	7-day	28-day
CEM	18.7 ± 1.1	41.8 ± 1.9
CEM-WBA	12.3 ± 5.3	16.0 ± 6.0
CEM-DBA	14.7 ± 1.8	25.3 ± 3.4

4. CONCLUSIONS

- Both dry- and wet-treatment are effective in removing the metallic Al presented in as-received bottom ash. Dry treatment is fast but has limitation that the maximum metallic Al it can reduce is 80%. Wet treatment is time-consuming, but it can remove the metallic Al completely.
- The mineralogical composition of bottom ash remains unchanged after dry- and wet-treatment, while the chemical composition shows small changes in the main components.

- The use of only 10% of treated bottom ash as cement substitute would decrease more than 40% of the 28-day compressive strength of pure cement. This can be attributed to the deficiency of reactive phase in treated bottom ash and the adverse impact induced by some of the components that are present in treated bottom ash on cement hydration.
- Before the application of bottom ash as supplementary cementitious material, it is necessary to improve its reactivity and remove the harmful components; further research is required in this area.

ACKNOWLEDGEMENTS

Boyu Chen would like to thank Chinese Scholarship Council for their support for her PhD study. Financial support by AVR-Afvalverwerking B.V. and Gemeente Rotterdam are acknowledged. Ruud Hendrix at the Department of Materials Science and Engineering of the Delft University of Technology is acknowledged for the X-ray analysis. Ron Penners, Maiko van Leeuwen, Ton Blom, Arjan Thijssen, and John van de Berg, from the Stevin lab and Microlab at the Faculty of Civil Engineering and Geosciences, Delft University of Technology, are acknowledged for their support for all the experiments.

REFERENCES

- [1] <http://www.worldwatch.org/bookstore/vital-signs>
- [2] Leckner, B., Process aspects in combustion and gasification Waste-to-Energy (WtE) units. *Waste management*, 2015. 37: p. 13-25.
- [3] Wiles, C.C., Municipal solid waste combustion ash: State-of-the-knowledge. *Journal of hazardous materials*, 1996. 47(1-3): p. 325-344.
- [4] Li, M., et al., Characterization of solid residues from municipal solid waste incinerator. *Fuel*, 2004. 83(10): p. 1397-1405.
- [5] Sabbas, T., et al., Management of municipal solid waste incineration residues. *Waste management*, 2003. 23(1): p. 61-88.
- [6] Bosmans, A., et al., The crucial role of Waste-to-Energy technologies in enhanced landfill mining: a technology review. *Journal of Cleaner Production*, 2013. 55: p. 10-23.
- [7] Gunning, P.J., C.D. Hills, and P.J. Carey, Production of lightweight aggregate from industrial waste and carbon dioxide. *Waste management*, 2009. 29(10): p. 2722-2728.
- [8] U. Müller, K. Rübner, The microstructure of concrete made with municipal waste incinerator bottom ash as an aggregate component, *Cement & Concrete Research* 36 (2006) 1434-1443.

International Conference on Sustainable Materials, Systems and Structures (SMSS 2019)

New Generation of Construction Materials

20-22 March 2019 – Rovinj, Croatia

NEW GENERATION OF CONSTRUCTION MATERIALS

SESSION 5: Novelties in UHPC

EFFECTS OF DIFFERENT CHEMICAL PRETREATMENTS OF NATURAL FIBERS ON THE MECHANICAL PROPERTIES OF CEMENT MORTAR

S. Juradin (1), I. Boko (1), I. Netinger Grubeša (2) and S. Mrakovčić (3)

(1) Faculty of Civil Engineering, Architecture and Geodesy, University of Split, Croatia

(2) Faculty of Civil Engineering, University Josip Juraj Strossmayer of Osijek, Croatia

(3) Faculty of Civil Engineering, University of Rijeka, Croatia

Abstract

The implementation of natural fibers in cement mortar composites can contribute to the reduction of environmental pollution with respect to the principles of global sustainability. Natural fibers are biodegradable and cheap materials, especially if they are locally available. The quality and mechanical properties of cellulosic fibers depend on the fiber type, geographic and climatic conditions where the plant is cultivated, and on the fiber extraction procedures. Owing to the presence of alkali in the cement matrix, alkaline hydrolysis of the cellulose part of fiber causes fiber degradation. Therefore, the fibers are often chemically treated prior to their addition as reinforcements to composites. Fiber modifications improve the durabilities of the fibers themselves and the fiber–cement matrix adhesion.

The aim of this study was to evaluate the influences of different chemical pretreatments of fibers on the mechanical properties of cement mortars. The cement mortar was reinforced with hemp and Spanish broom fibers. Spanish broom (*Spartium junceum* L.) is a perennial shrub that originates in the Mediterranean. Spanish broom fibers were extracted after resting for 28 days in seawater. Hemp fibers underwent alkali pretreatments with NaOH, NaOH, and Na₂SO₃. Some of these hemp fibers rested in seawater for 28 days. Twelve cement mortar mixtures with two different quantities of fibers were tested to determine the effects of seawater and alkali treatment of fibers on the mechanical properties of cement mortars.

Keywords: natural fibers, chemical pretreatments of fibers, hemp, Spanish broom, mechanical properties of cement mortars

1. INTRODUCTION

Reinforcing brittle cementitious matrices with fibers can improve the tensile strength and toughness of concrete and mortar [1]. It has been reported [2–5] that with the incorporation of fiber reinforcement in cementitious materials, the cracking due to plastic and drying shrinkages in the material as well as its permeability could be significantly reduced, the impact and abrasion resistance increased, and the tensile strain capacity of the material substantially improved.

Steel, glass, and polymer fibers, are the most frequently used fibers in fiber reinforced concrete or mortar. However, these materials are nonbiodegradable, and ecological concerns have resulted in increased interests in natural biodegradable fibers. Natural fibers are relatively cheap, low density, environmentally friendly, less abrasive, have a low cost, and are easily available [6–9]. They have a high-tensile strength but low modulus of elasticity [10]. There are three types of natural fibers: animal-based, mineral-derived, and cellulose/lignocellulose fibers [9]. Suitable animal fibers include silk, wool, and hair fibers. Mineral-derived fibers include wollastonite and palygorskite [11]. Commercially, major cellulose fiber sources include bamboo, jute, kenaf, flax, hemp, sisal, coir, ramie, abaca, sugar cane bagasse, and grass [12].

Hemp is one of the few most extensively used natural fibers for reinforcement [7]. Industrial hemp has potential for use in textiles, building materials, composite materials for automobile applications, food, and other industries.

Spanish broom (*Spartium junceum* L) is a perennial shrub and a native plant in the Mediterranean area [12–16]. It is used as a textile raw material and for paper and composite productions.

The alkaline cement matrix attacks the lignin in the natural fibers and causes degradation in the mortar/concrete strength [17]. In order to remove the parts of fibers that are sensitive to alkali action, fibers can be chemically treated before being added to concrete. The most common chemical treatment is the alkali treatment with NaOH and Na₂SO₃. For fiber alkalization, many researchers varied the concentration of NaOH from 1 to 15% [16, 18–22]. Treated fibers have darker colors, exhibit density changes, diameter texture, and improved tensile properties, compared to untreated fibers [18]. Ishak et al. [22] used a seawater treatment instead of a chemical treatment to enhance properties of sugar palm fibers. This treatment was friendlier to the environment and yielded good results.

The objective of this research is to determine the influence of different chemical pretreatments of hemp and Spanish broom fibers on the mechanical properties (tensile and flexural strength) of cement mortars.

2. MATERIALS AND METHODS

2.1 Pretreatment of fibers

Hemp: The hemp fibers were bought from a market and were divided in five groups. The first group of fibers was mixed with 2.5% NaOH for 1 h at 95 °C, and the second group was submerged in 5% NaOH for the same period and at the same temperature as that used for the first group. The fibers were then washed with distilled water (DW) and oven dried at 70 °C for

24 h. The third and the fourth groups were treated in a solution of 2.5% NaOH and 2% Na₂SO₃, and in a solution of 5% NaOH and 2% Na₂SO₃. The fifth group of 1 m long hemp fibers was soaked in seawater for 28 days, washed in water, and dried. All fibers were manually cut to have lengths equal to 10 ± 2 mm, as shown in Figure 1.

Spanish broom: Spanish broom fibers were obtained from the plant harvested in the area of Split. Freshly picked Spanish Broom shoots were soaked in seawater for 28 days. After that period, the shoots were washed in water (Figure 2a) and the fibers were manually separated from the woody parts. The fibers were dried at room temperature, and were then soaked in a solution of 5 g/l sodium alkali (NaOH). After 7 days, the fibers were rinsed with fresh water, dried (Figure 2 b) and manually cut to the length of 10 ± 2 mm.



Figure 1: Spanish broom (left) and hemp (right) fibers

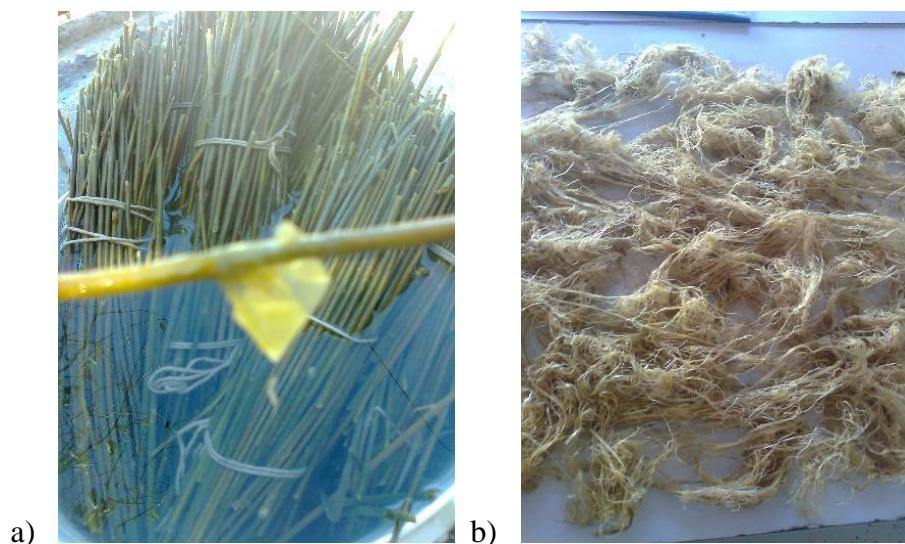


Figure 2: a) Bundle of Spanish broom in the water, and b) wet Spanish broom fibers

2.2 Mortar mixtures

For this study, twelve mortar mixtures were prepared with differently treated fibers and one reference mortar mixture (M1). The cement CEM I 42.5 R (450 g), CEN standard sand prepared according to EN 196-1 (1350 g), and water (225 g), were used in all the mixtures. Reference mortar mixture had no fibers and other mixtures contained different amounts of fibers (4.8 g and 9.6 g). To avoid the balling effect on mortar during mixing, the volume fraction of fibers was restricted to 1% according to [23]. A fiber proportion of 0.5% in the cement composite volume was selected based on other similar research findings [24]. The amounts of 4.8 g and 9.6 g of Spanish broom correspond to 0.5% and 1% of the total composite volume. The hemp fibers were added in equal quantities by mass. The same mass of hemp fibers resulted in lower percentages of the total composite volume. Table 1 lists the types and amounts of the fibers in the mixtures. The mortars were mixed in an automatic mortar mixer. After the standard mixing program for cement mortar was stopped, fibers were added and manually mixed. Mortar mixtures were compacted on a vibrating table in the standard three-gang molds. All the specimens were demolded 24 h after casting, and were placed in a water tank at 20 ± 2 °C.

Table 1: Types and amounts of the fibers in the mortar mixtures

Mixtures	Fibers	Fiber mass (g)	% of total volume
M1	-	-	-
M2	Hemp fibers treated with 2.5% NaOH	4.8	0.34
M3	Hemp fibers treated with 2.5% NaOH	9.6	0.68
M4	Hemp fibers treated with 5% NaOH	4.8	0.34
M5	Hemp fibers treated with 5% NaOH	9.6	0.68
M6	Hemp fibers treated with 2.5% NaOH and 2.0% Na ₂ SO ₃	4.8	0.34
M7	Hemp fibers treated with 2.5% NaOH and 2.0% Na ₂ SO ₃	9.6	0.68
M8	Hemp fibers treated with 5% NaOH and 2.0% Na ₂ SO ₃	4.8	0.34
M9	Hemp fibers treated with 5% NaOH and 2.0% Na ₂ SO ₃	9.6	0.68
M10	Hemp fibers treated with seawater	4.8	0.34
M11	Hemp fibers treated with seawater	9.6	0.68
M12	Spanish broom fibers treated with seawater and 5% NaOH	4.8	0.5
M13	Spanish broom fibers treated with seawater and 5% NaOH	9.6	1.0

3. RESULTS AND DISCUSSION

The properties of each mortar mixture were tested on three $40 \times 40 \times 160$ mm prisms after a curing time of 56 days. The tests were carried out on the mechanical testing machine Controls C92Z20 with a load capacity of 15 kN for the flexural strength test, and at 300 kN for the compressive strength test. The results for the relative flexural and compressive strengths, expressed as percentages of the reference mortar strength, are shown in Figures 3 and 4. The values of the flexural and compressive strengths in the mixtures with lower fiber content are mainly higher than those for the reference mortar. The authors assumed that the fibers were incorporated in the mixtures at a higher fiber percentage composition, which will likely have an impact on the reduction of the mechanical properties. The highest mechanical properties were achieved with mixtures M4 and M6, mixtures with hemp fibers treated with the 5% NaOH solution, and the mixture solution composed of 2.5% NaOH and 2.0% Na₂SO₃.

The strengths of the mortar reinforced with Spanish broom fibers were in accordance with the results obtained for mortars reinforced with hemp (M2–M7). The same weight of Spanish broom fibers takes up a larger volume than hemp fibers, as indicated in Figure 1. As stated before, higher fiber content reduces the mechanical properties of the mortar. Therefore, the properties of mortars with a lower fiber content of Spanish broom should be examined.

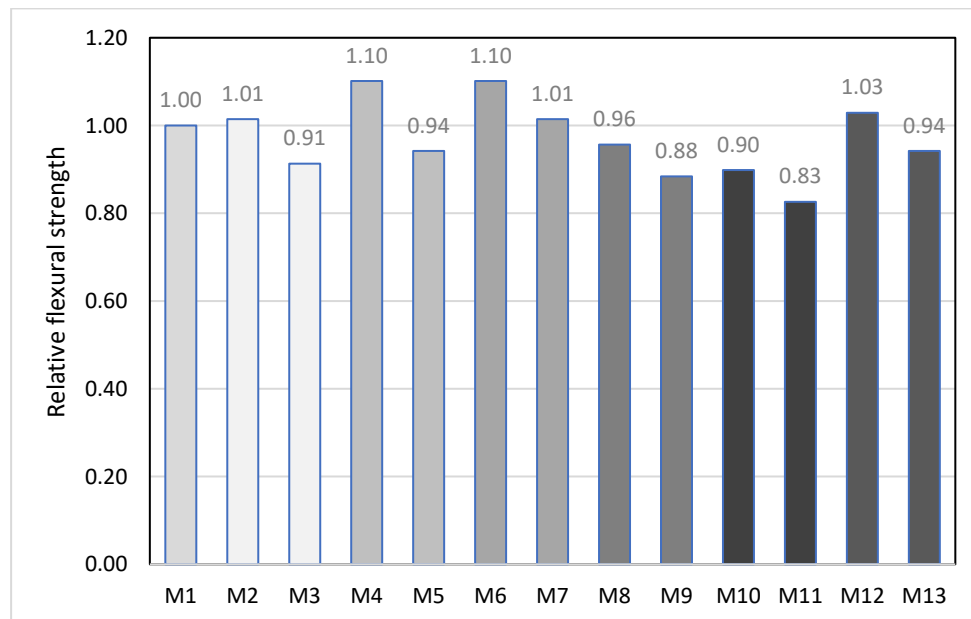


Figure 3: Relative flexural strength

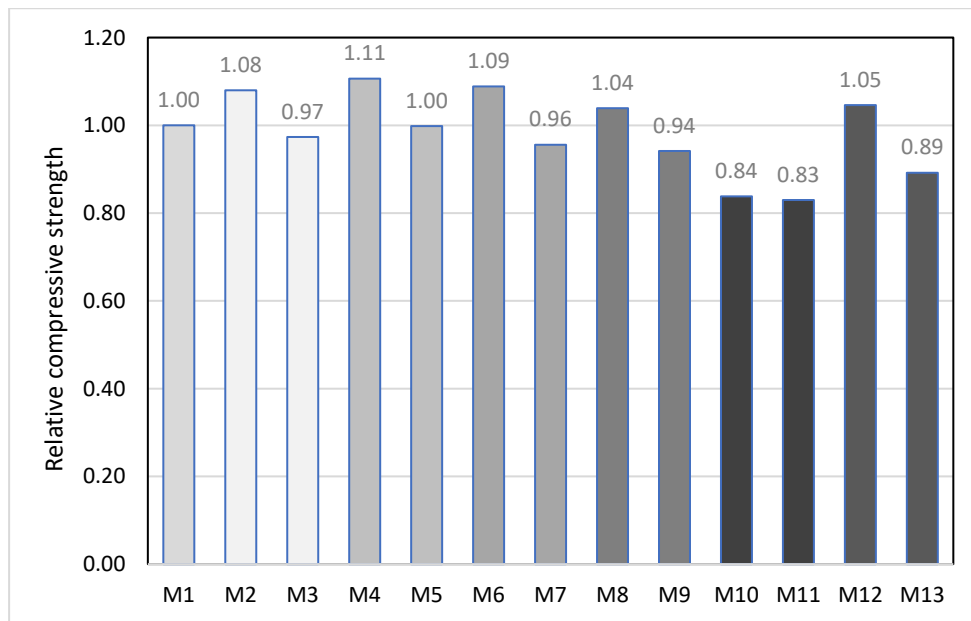


Figure 4: Relative compressive strength

4. CONCLUSIONS

Different treatments of the natural fibers of hemp and Spanish broom were used for the reinforcement of the standard mortar matrix. Based on the obtained results, the following conclusions can be drawn:

- mixtures with lower fiber content had higher flexural and compressive strengths than reference mortar
- maximum strength values were achieved with hemp fibers treated with 5% NaOH and solution which contained 2.5% NaOH and 2.0% Na₂SO₃
- hemp fiber treatment with seawater had no influences on elicited results
- Spanish broom fibers exhibited tremendous potential for reinforcing cement composites
- treating Spanish broom fibers with seawater and then with a 5% NaOH solution at room temperature was easily reproduced in areas where this plant grew
- mortars reinforced with lower quantities of Spanish broom fibers should be further examined

REFERENCES

- [1] Pereira M. V., Fujiyama R., Darwish F. and Alves G.T., 'On the Strengthening of Cement Mortar by Natural Fibers', *Mater Res*, 18 (1), (2015) 177-183.
- [2] Bentur, A. and Mindess, S., 'Fiber reinforced cementitious composites', Modern Concrete Technology Series, CRC Press, Taylor & Francis Group, (2007).
- [3] Mobasher, B., 'Mechanics of fiber and textile reinforced cement composites', CRC Press, Taylor & Francis Group, (2011).
- [4] Johnston, C.D., 'Fiber-reinforced cements and concretes', Taylor and Francis, (2010).

- [5] Alhozaimy, A.M., Soroushian, P. and Mirza, F., 'Mechanical properties of polypropylene fiber reinforced concrete and the effects of pozzolanic materials', *Cement Concrete Comp.*, vol.8, 2, (1996) 85–92.
- [6] Shahzad, A., 'Hemp fiber and its composites – a review', *J Compos Mater*, vol. 46, 8 (2011). 973-986
- [7] Madsen B., 'Properties and processing', In: Proceedings of Seminar on Bio-composites: 'The Next Generation of Composites', September 25, Shawbury, UK (2008) 1–18.
- [8] Yan, L., Kasal, B. and Huang, L., 'A review of recent research on the use of cellulosic fibres, their fibre fabric reinforced cementitious, geo-polymer and polymer composites in civil engineering', *Composites Part B, Engineering* 92 (2016) 94-132.
- [9] Pacheco-Torgal F. and Jalali S., 'Cementitious building materials reinforced with vegetable fibres: A review', *Constr. Build Mater* 25 (2) (2011) 575-581.
- [10] Faruk, O., Bledzki, A.K., Fink, H.P. and Sain, M., 'Biocomposites reinforced with natural fibers: 2000-2010' *Progress in Polymer Science* 37 (2012) 1552-1596.
- [11] Onuaguluchi, O. and Banthia, N., 'Plant-based natural fiber reinforced cement composites: A review', *Cem Concr Compos* (2016) 96-108.
- [12] Angelini, L.G., Lazzeri, A., Levita, G., Fontanelli, D. and Bozzi, C.: 'Ramie (*Boehmeria nivea* (L.) Gaud.) and Spanish Broom (*Spartium junceum* L.) fibres for composite materials: agronomical aspects, morphology and mechanical properties', *IndCrop Prod* 11 (2-3) (2000) 145 – 161.
- [13] Angelini, L.G., Tavarini, S. and Foschi, L.: 'Spanish Broom (*Spartium junceum* L.) as New Fiber for Biocomposites: The Effect of Crop Age and Microbial Retting on Fiber Quality', *Conference Papers in Materials Science*, (2013) Article ID 274359, 5 pages.
- [14] Kovačević Z., Krnčević M., Katović A. and Katović D., 'Brnista – zaboravljena tekstilna sirovina', *Tekstil* 59 (9) (2010) 410 – 421.
- [15] Katović D., Katović A. and Antonović A.: 'Extraction Methods of Spanish Broom (*Spartium Junceum* L.)', *Drvna industrija* 62 (4) (2011) 255 – 261.
- [16] Aly M., Hashmi, M.S.J., Olabi, A.G. and Messeiry, M., 'Durability of waste glass flax fiber reinforced mortar', *AIP Conference Proceedings* 1315, (2011) 241.
- [17] *Natural Fiber Composites*, Taylor & Francis Group, LLC, Boca Raton, FL, USA, 2016.
- [18] Suardana, N.P.G., Piao, Y., and Lim, J.K., 'Mechanical properties of hemp fibers and hemp/PP composites: Effects of chemical surface treatment', *Mater. Phys. Mech.* 11 (2011) 1-8.
- [19] Islam, M.S., Pickering, K.L. and Foreman, N.J., 'Influence of alkali fiber treatment and fiber processing on the mechanical properties of hemp/epoxy composites', *J AppPolymSci*, 119 (2011) 3696-3707.
- [20] Stevulova, N., Cigasova, J., Estokova, A., Terpakova, E., Geffert, A., Kacik, F., Singovszka, E. and Holub, M., 'Properties Characterization of Chemically Modified Hemp Hurds', *Materials*, 7 (2014) 8131-8150.
- [21] Netinger Grubeša, I., Marković, B., Gojević, A. and Brdarić J., 'Effect of hemp fibers on fire resistance of concrete', *ConstrBuildMater*, 184 (2018) 473–484.
- [22] Ishak, M.R. and Leman, Z.; 'The effect of sea water treatment on the impact and flexural strength of sugar palm fibre reinforced epoxy composites', *Int J Mech Mat Eng*, 4 (3) (2009) 316-320.
- [23] Sivaraja, M., Kandasamy, Velmani, N. and Pillai, M.S., 'Study on durability of natural fibre concrete composites using mechanical strength and microstructural properties', *B Mater Sci*, Vol. 33, No. 6, (2010) 719–729.
- [24] Islam, S.M., Hussain, R.R. and Morshed, M.A.Z.: 'Fiber-reinforced concrete incorporating locally available natural fibers in normal- and high-strength concrete and a performance analysis with steel fiber-reinforced composite concrete', *J Compos Mater*, Vol. 46, No. 1, (2012). 111-122.

THE INFLUENCE OF NANO SiO₂ AND CURING REGIMES ON MECHANICAL PROPERTIES OF UHPFRC

Ksenija Janković (1), Marko Stojanović (1), Dragan Bojović (1)

(1) Institute for testing of materials - IMS Institute, SERBIA

Abstract

One of the latest advances in concrete technology is Ultra High Performance Fibre Reinforced Concrete (UHPFRC). It is a fiber-reinforced, densely-packed concrete material that exhibits increased mechanical performance and superior durability to normal and high strength concretes. Nano SiO₂ can also accelerate cement hydration through a nucleation and growth mechanism, stimulate the formation of additional calcium silicate hydrates (C-S-H) through possible pozzolanic reactions, and reduce calcium leaching and weak zones of calcium hydroxide. Furthermore, curing on high temperature has a positive effect on the pozzolanic reactions between CH from the hydration of cement and Nano silica. The aim of this study was to examine the effects of curing regimes on the mechanical properties of UHPFRC with different content of nano silica (1 and 2%). Standard curing regime in water, steam curing and autoclaving were applied. Comparative test results of concrete in fresh and hardened state are shown.

Keywords: UHPFRC, Nano SiO₂, compressive strength, flexural strength, curing regime

1. INTRODUCTION

One of the most promising types of concrete, ultra-high performance concrete (UHPC) was developed in the last decade [1–3]. This innovative high-tech material's dense microstructure presents both ultra-high compressive strength and ultra-high durability [4–5]. The main composition of UHPC contains a large amount of cement, usually between 800 and 1100 kg/m³, which is around three to four times more than the quantity of cement in normal concrete [5]. Therefore, a suitable option to reduce the high volume of cement in the UHPC proportioning can be the blending of cement with high pozzolanic fine materials, such as nanosilica (nS).

Recently, nanotechnology is considered for use or already being used in many applications. It has also received a lot of attention in building materials, with potential advantages and drawbacks being underlined [6,7]. In this field, a new pozzolanic material, “nanosilica“ (NS), which is produced synthetically in the form of slurry of ultra-fine particles of amorphous silica, was introduced.

Nanosilicas can contribute to denser packing of the matrix, because, due to their small size, they can fill the voids between cement and silica fume (SF) particles. A denser matrix has a higher content of C-S-H, which improves both the mechanical properties and concrete durability [8]. Qing et al [9] performed tests to compare properties of nano-SiO₂ addition on hardened cement paste with those of SF. Their investigation showed that the pozzolanic activity of nanosilica is much greater than that of SF. It makes the cement paste thicker and speeds up the hydration process of the cement. The bond strength between cement paste and aggregates was higher for mixes with nanosilicas than to mixes with SF or the control mix with cement as the only binder.

The effect of steam-curing regime of UHPC is seen in the formation of an improved microstructure with crystalline calcium silicate phases (C-S-H phases). Results of the influence of autoclave curing at 180 °C on the physical and mechanical properties of reactive-powder concrete reinforced with brass-coated steel fibers autoclave curing at 180 °C has shown that that type of curing is beneficial both in terms of flexural and compressive strength. Specimens reached the flexural and compressive strengths of 30 and 200 MPa, respectively [10].

2. EXPERIMENTAL WORK

This study was conducted in order to examine the effects of curing regimes on the mechanical properties of UHPFRC with different nano silica content (1 and 2%). Three types of curing were applied: standard curing regime in water, steam curing and autoclaving.

2.1 Component materials and their properties

The component materials used were tested for chemical and physical-mechanical properties. The component materials used in this study are as follows:

- Cement CEM I 52.5 R, CRH – Popovac,
- Silica fume, Sika–Switzerland,
- Nano silica, Evonik – Germany,
- Quartz aggregate 0-0.5 mm – Kaolin, Valjevo,
- Quartz powder $d_{50\%} = 45\mu m$, Srbokvarc – Rgotica,
- Steel fibers (length / diameter = 8/0.17 mm), Spajić – Negotin,
- Superplasticizer "Sika Viscocrete 20HE" – Sika, Switzerland.

Cement without additives, CEM I, class 52.5 R, is obtained by grinding process of high quality portland-cement clinker with the addition of an optimal amount of plaster, and the producer CRH – Popovac was used. The chemical, physical and mechanical properties of the cement are shown in Table 1.

Silica fume - it is a secondary binder, silica fume Sika Fume HR, Sika, Switzerland, was used. According to manufacturer's technical specification bulk density is 700 kg/m³, and size of more than 95% particles is smaller than 0.1µm.

Nano silica – it is also a secondary binder, Aerosil 200 - Evonik, Germany, was used. The SiO₂ content is greater than 99.8%. Specific weight is 2.2g/cm³. Specific surface area for nano-silica is 269.31 m²/g (BET method). Mean primary particle diameter (DA) derived from the specific surface area is 14nm.

Table 1. Properties of cement CEM I 52.5R

Chemical, %		Physical		Mechanical	
SiO ₂	18.89	Specific gravity, kg/m ³	3150	Compressive strength, N/mm ²	
Al ₂ O ₃	5.60	Specific surface, cm ² /g	4220	2 days	37.2
Fe ₂ O ₃	2.61	Standard consistency, %	29.4	7 days	-
CaO	63.69	Initial setting time, min	190	28 days	65.9
MgO	2.03	Final setting time, min	250		
Na ₂ O	0.30	Specific surface area-Blaine, m ² /g	3500	Flexural strength, N/mm ²	
K ₂ O	0.73			2 days	7.1
SO ₃	2.70			7 days	-
Cl-	0.005			28 days	10.0

Quartz aggregate was used in the granulation of 0-0.5 mm Kaolin, Valjevo. The SiO₂ content was 97.54%. Specific density values were 2695 kg/m³ for quartz sand.

Steel fibers are manufactured and marketed by the company „Spaic“, Serbia. Steel fibers (length/diameter = 8/0.17 mm) are coated with brass in order to increase durability and resistance to concrete corrosion process. The tensile strength for steel fiber was ≈ 3000 MPa. Specific density values were 7850 kg/m³.

High performance superplasticiser based on modified polycarboxylate was used is "Sika Viscocrete 20HE" – Sika, Switzerland. Specific density values were 1080 kg/m³. Possibility to reduce water was up to 30%.

2.2 Concrete Composition

Mechanical properties of hardened UHPFRC concrete are shown in terms of compressive strength and flexural strength. Three types of curing were applied: standard curing regime in water, steam curing and autoclaving.

It is essential to know the properties of the component materials during the design of UHPFRC mixtures.

Considering the characteristics of UHPFRC concrete as well as its properties in the hardened state, these basic conditions for designing the composition of concrete mixture of very high strengths have been adopted:

- keep the water binding ratio under the limit value of 0.25,
- apply very high cement content > 800 kg/m³,
- the value of the air content must be reduced to the lowest possible value,
- maximum grain size of the aggregate in the range of 0.5-1mm,
- use appropriate mineral additives,
- the application of silica fume and nano silica, mandatory application of Superplasticizer with high water reduction – HRWR,

Three types of concrete were made with varying percent of nS. Mixtures with 270 kg/m³ of silica fume, 2% of steel fibers and cement suspension of 0, 1 and 2% with nano silica were designed. Mix proportions for all kinds of concrete are shown in Table 2.

Table 2. Concrete mixtures

Material	UnS0f2	UnS1f2	UnS2f2
Cement (kg/m ³)	950	940,5	931
Silica fume (kg/m ³)	270	270	270
Nano silica (kg/m ³)	0	9,5	19
Quartz powder (kg/m ³)	350	350	350
0-0.5mm Quartz sand (kg/m ³)	530	503	495
Water (kg/m ³)	235	235	235
HWR20HE (kg/m ³)	57	57	57
Steel fibers (kg/m ³)	157	157	157
HWR (kg/m ³)	31.9	31.9	31.9
w/b	0.192	0,192	0,192

Nano-silica was first mixed with water to which superplasticizer was previously added, and then added to the dry mixture of aggregate, cement and silica fume.

Finally, after 5 min when the mixture became fluid, brass coated steel fibers were added and mixing was continued for another 5 min.

UHPFRC was put into metallic prism shaped molds 40x40x160 mm.

Various types of curing of UHPFRC were applied:

First series - The samples were air cured for the first 24h, and then the water cured under ambient conditions until the moment of testing,

Second series - Samples were air cured for the first 24 hours after which they were steam-cured at a temperature of 95 ° C for a further 48 h,

Third Series - The samples were air cured for the first 24 hours after which they were autoclaved for 4 h under a pressure of 20 bar.

The mechanical properties of UHPFRC, compressive strength and flexural strength were examined on a prism after curing process. First, a flexural strength test was performed and subsequently compressive strength test on parts of the prism by a modified method. Flexural strength testing was performed according to SRPS EN 196-1. The test was carried out on a digital hydraulic press of 300 kN. During the test, a load speed rate of 0.06 MPa s was used. The beam after testing as well as the cross-section is shown in Figure 1.



Figure 1. Testing tensile strength beams and its cross-section

Testing of the compressive strength was carried out on the parts of the prisms using a modified method. Load speed rate is 0.6 MPa/s. The testing is shown in Figure 2.

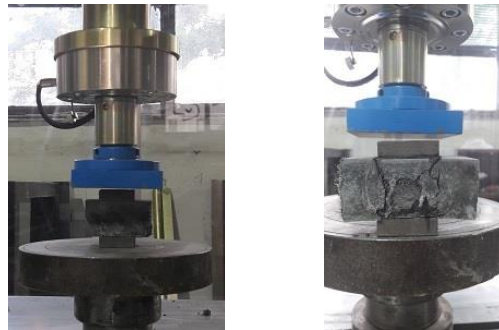


Figure 2. Testing of compressive strength UHPFRC

3. RESULTS AND DISCUSSION

To make concrete mixtures, commercial materials available in the domestic market were used. The fresh UHPFRC properties were tested in terms of workability. Concrete consistency was tested on all concrete mixes using the method of slump-flow by using a small cone. Test results for slump flow of UHPFRC are given in Figure 3.

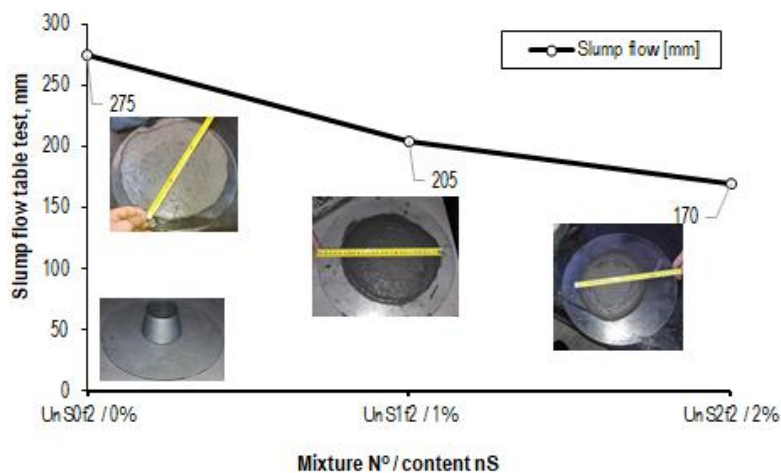


Figure 3. Consistency by slump flow test

The results of compressive and flexural strengths under 3 point flexure and uniaxial compression, in accordance with the SRPS EN 196-1 standard are presented in Figure 4 and Figure 5, respectively. For curing in water the results of compressive strengths are given in Table 3.

The obtained results are in line according to [10], the pozzolanic activity was weak when the curing temperature was 20°C in the early ages but compressive strength has grown when the curing age prolonged.

Table 3. Results of compressive strength in [N/mm²] for normal curing in water at the age of 2, 7 and 28 days

Age (days)	UnS0f2	UnS1f2	UnS2f2
2	81	75	72
7	97	99	101
28	141	142	144

The obtained values of compressive strength tests range from 141 to 144 N/mm² for normal cured samples, 155 to 165 N/mm² for steam cured samples and 174 to 179 N/mm² for autoclave cured samples.

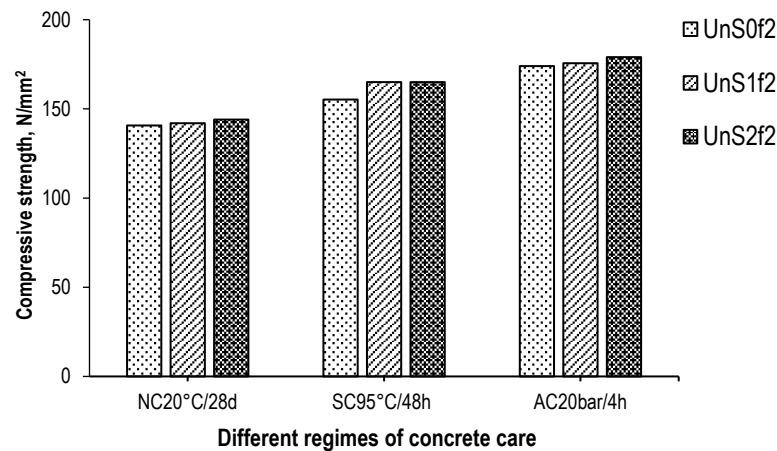


Figure 4. Results of testing compressive strength of UHPFRC in relation to the different regime of concrete care

Flexural strength testing results without nano silica and with a cement replacement of 1 and 2% nano silica range from 21.6 to 22.0 N/mm² for normal cured samples, 23.0 to 24.3 N/mm² for steam cured samples and 24.6 to 28.0 N/mm² for autoclave cured samples.

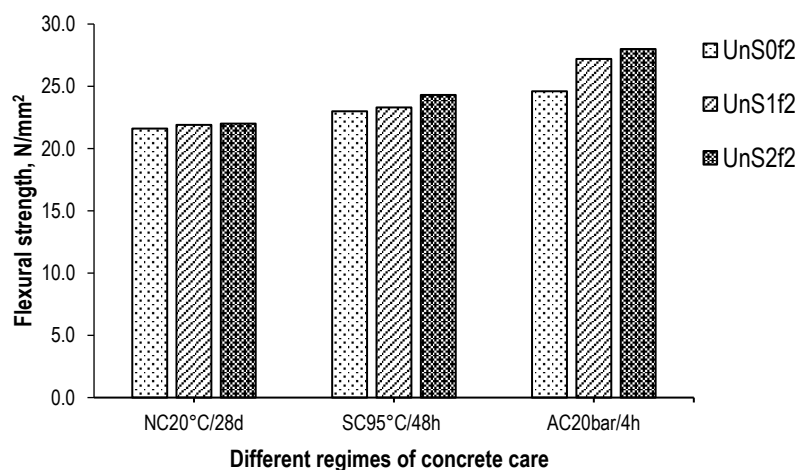


Figure 5. Results of testing flexural strength of UHPFRC in relation to the different regime of concrete care

4. CONCLUSIONS

The obtained results indicate that the addition of nano silica has an impact on the properties of fresh and hardened UHPFRC.

The mechanical properties of hardened concrete grow with the addition of nano silica in the steam curing and autoclaving regime. The obtained compressive strength values of concrete with the addition of 1 and 2% nano silica are higher in relation to concrete without the addition of nano silica in different regimes of concrete care. For steam curing regime concrete with 1% and 2% nano silica has a 6.3% higher compressive strength compared to concrete without nano silica.

Cementitious composite with nano silica did not have significant increases in compressive and flexural strength, for all curing regime which is in accordance with results [11] that a minimum quantity of nano silica with significant effect on strength of cementitious composites is 3.74%.

Steam curing regime improved compressive and flexural strength, but the influence on flexural strength was greater, and the same was found in [12].

If we compare the effects of the curing regime for concrete made with the same quantity of nano silica it can be seen that for steam curing strength was 10-15%, and for autoclaving about 24% greater in comparison with the samples cured at 20°C. The same trend was observed for tensile strength.

ACKNOWLEDGEMENTS

The work reported in this paper is a part of the investigation within the research project TR 36017 "Utilization of by-products and recycled waste materials in concrete composites in the scope of sustainable construction development in Serbia: investigation and environmental assessment of possible applications", supported by the Ministry of Education, Science and Technological Development, Republic of Serbia. This support is gratefully acknowledged.

REFERENCES

- [1] Acker P, Behloul, M. DUCTAL Technology: A large spectrum of properties, a wide range of applications. First International Symposium on Ultra High Performance Concrete. Kassel, Germany 2004.
- [2] M. Rebstroff, G.W. Experience and applications of Ultra-high Performance concrete in asia. Second International Symposium on Ultra High Performance Concrete. Kassel, Germany 2008.
- [3] E. Fehling MS, S. Stürwald, editor. The Third International Symposium on Ultra High Performance Concrete and Nanotechnology for High Performance Construction Materials. Kassel, Germany: Kassel University Press March 2012.
- [4] Graybeal BA. Material property characterization of ultra-high performance concrete. Federal Highway Administration Report No FHWA-HRT-06-103. August 2006. McLean, Virginia, USA.
- [5] Richard P, Cheyrezy M. Composition of reactive powder concrete. *Cem Concr Res* 1995;25: 1501–11.
- [6] Sanchez F, Sobolev K. Nanotechnology in concrete - a review. *Constr Build Mater* 2010; 24:2060-71.
- [7] Pacheco-Torgal, Jalali S. Nanotechnology: advantages and drawbacks in the field of building material. *Constr Build Mater* 2011; 25: 582-90.
- [8] Ghafari, E., et al., Optimization of UHPC by Adding Nanomaterials, in Proceedings of Hipermat 2012 - 3rd International Symposium on UHPC and Nanotechnology for Construction Materials. 2012, Kassel University Press: Kassel, Germany.
- [9] Qing, Y., et al., Influence of nano-SiO₂ addition on properties of hardened cement paste as compared with silica fume. *Construction and Building Materials*, 2007. 21(3): p. 539-545.
- [10] Zhang Y.S, Sun W, Liu S.F, Jiao C.J, Lai J.Z (2008), "Preparation of C200 green reactive powder concrete and its static–dynamic behaviors" *Cem. Concr. Compos.*, 30, (9) 831–838.
- [11] Rong Z, Sun W, Xiao H, Jiang G (2015), "Effects of nano-SiO₂ particles on the mechanical and microstructural properties of ultra-high performance cementitious composites", *Cem Concr Comp*, 56, 25–31.
- [12] Yazici H (2007), "The effect of curing conditions on compressive strength of ultra-high strength concrete with high volume mineral admixtures" *Build. Environ.*, 42, (5) 2083–2089.

STRAIN-HARDENING ETTRINGITE-BASED COMPOSITE WITH POLYPROPYLENE FIBER REINFORCED LADLE SLAG: DURABILITY UNDER COMBINED CHLORIDE AND SULFATE ATTACK

Hoang Nguyen (1), Paivo Kinnunen (1), Valter Carvelli (2), and Mirja Illikainen (1)

(1) Fibre and Particle Engineering Research Unit, University of Oulu, Pentti Kaiteran katu 1, 90014 Oulu, Finland

(2) Department A.B.C., Politecnico di Milano, Piazza Leonardo Da Vinci 32, 20133 Milan, Italy

Abstract

Ladle slag, an industrial waste from steel manufacturing processes, is an interesting raw material for sustainable inorganic binders. In earlier work, we have developed an ettringite-based binder (LSG) from the hydration between ladle slag and gypsum. In addition, polypropylene (PP) fiber was employed to attain a strain-hardening cementitious composite from LSG. To investigate the durability of PP fiber reinforced LSG, the composite was exposed to a combined chloride and sulfate environment under freeze-thaw cycling. The compressive and flexural behavior of PP fiber reinforced LSG after up to 180 freeze-thaw cycles was experimentally characterized. The experimental results confirm the durability of LSG under Na₂SO₄-NaCl environment. Furthermore, the PP fibers generally enhance the mechanical properties and durability of the reinforced composite. Since there is a lack of study on the durability of ettringite-based binders from industrial wastes under harsh environments, this experimental study reveals the feasibility of using fiber reinforced ettringite-based composite as an alternative construction material.

Keywords: Ladle slag cement; Durability; Recycling; Mechanical properties; Sulfate attack

1. INTRODUCTION

Ettringite-based binder is a promising alternative cementitious material. The binder can attain considerable mechanical properties [1,2], good chemical resistance [3], and has the potential to immobilize heavy metals [4]. In previous work, ladle slag (LS) and gypsum were combined together to give an ettringite-based binder (LSG) via hydration by water [2]. In addition, a fiber reinforced cementitious composite from this binder (PP-LSG) was produced.

The developed composite exhibited strain-hardening behavior when subjected to bending and uniaxial tensile load with 2% v/v polypropylene (PP) fiber as reinforcement [2]. Therefore, LSG and its composite PP-LSG are of particular interest being the hydration between water and non-hazardous industrial by-products at low pH, while still obtaining high mechanical performance.

The knowledge of the durability of ettringite-based binder is limited, as reported in the literature. In many cases, the durability of the binder is studied assuming one single factor, e.g., carbonation or chemical attacks (e.g., chloride or sulfate) [5–7]. However, the real-life conditions present a combination of different factors. The material can be subjected to the synergetic effect of multiple factors in aggressive environment. Furthermore, studies are not available in the literature considering the durability of ettringite-based composite material under harsh environments that mimic the combination of chemical and environmental stresses. As for engineered cementitious composite (ECC), the effects of freeze-thaw process and Na_2SO_4 solution on the mechanical properties of Portland cement-based ECC are of particular interest [8], as well as the chloride attack [9]. However, the mentioned work did not consider the combined effects of multiple factor (e.g., combined sulfate and chloride attack).

This experimental research is an attempt to investigate the mechanical properties of deflection-hardening ettringite-based composite under freeze-thaw and combined chloride and sulfate environment. The aim of the work is to present understanding on the durability of the developed ettringite-based composite under such aggressive conditions.

2. MATERIALS AND METHODS

2.1. Materials

LS was provided by SSAB Europe Oy (Finland). The as-received slag was removed all the leftover steel flakes and then milled by a ball mill (TPR-D-950-V-FU-EH by Germatec, Germany) to attain a d_{50} of roughly 10 μm . Additionally, fine sand (FS) ($d_{50} < 100 \mu\text{m}$) was used as fine aggregate as suggested in Ref. [10].

Pure gypsum ($\text{CaSO}_4 \cdot 2\text{H}_2\text{O}$ supplied by VWR Finland, product code 22451.360) was employed in this study. The chemical composition of the LS and gypsum was analyzed by X-ray fluorescence (XRF) (PANalytical Omnia Axiosmax) and detailed in Table 1. The hydration mechanism to form ettringite was reported in Ref. [2].

Table 1: Chemical composition (wt %) of LS and gypsum measured by XRF

Oxide	CaO	SiO ₂	Al ₂ O ₃	Fe ₂ O ₃	MgO	SO ₃	Others	Loss on ignition
LS	51.0	8.3	27.9	1.1	6.3	0.8	3.6	1
Gypsum	41.4	1.0	0.1	0.1	0.5	53.8	3.1	-

Citric acid (product code C1949 by Tokyo Chemical Industry Co., Ltd., Japan) was employed as a retarder for the reaction between LS and gypsum. As reported in Ref. [11], citric acid prevents nucleation and the subsequent crystal formation process of ettringite. Based on previous work [2], 1.8 wt.% citric acid solution was prepared to attain an initial setting time of 1.2 hours for LSG mortar. A melamine-based chemical specified for calcium sulfate cements (commercial name: Melment F10 provided by BASF, Germany) was used as superplasticizer.

As fiber dispersing agent, a sodium polymethacrylate agent named Darvan 7-N (supplied by Vanderbilt, USA) was employed. The dose of Melment F10 and Darvan 7-N were 0.5% and 1%, respectively, by weight of total binder mass.

PP fibers were employed as fibrous reinforcement to produce a deflection-hardening ettringite-based composite. The mechanical and physical properties of fibers was reported in Ref. [2,12]. The minimum fiber volume fraction of 2% was chosen to yield pseudo strain hardening (PSH) behavior with adequate workability as reported in Ref. [2,12]. Table 2 shows the recipe of the mixtures for LSG and PP-LSG

Table 2. Mix proportions of the LSG and PP-LSG

Sample ID	Slag	Gypsum	Sand	Citric acid	W/B*	Fiber volume fraction
LSG	0.7	0.3	0.5	1.8 wt.%	0.45	-
PP-LSG						2% v/v

*W/B (water-to-binder ratio) with total binder mass by the sum of the mass of slag and gypsum

2.2. Methods

The preparation of mortar specimens was detailed in [2]. It is worth noting that it usually took 20–25 minutes to complete the mixing process for one batch of mortar.

Artificial aging was conducted in a climatic chamber Weiss WK3-180/40 (Germany). The duration of aging process was approximately 2 months with approximately 180 cycles. The cycles were divided into 90 ‘cold’ and 90 ‘warm’ cycles, and changed every 45 cycles (almost 2 weeks). The adopted artificial cycles were designed based on the weather record in Oulu (Finland) during 2010–2018. The aim was to simulate the extreme weather conditions of Northern area. In the ‘cold’ cycle, the temperature ranged from 5° to -20°C, while in the ‘warm’ cycle, the temperature varied from 10° to 30°C. One single cycle lasted for 8 h. Specimens were fully covered by curing solution, hence the climatic chamber did not control the humidity during the aging scheme.

The LSG and PP-LSG were aged by combined sodium chloride and sulfate solution (SL). The SL was prepared based on Ref. [13]: 5% wt. Na₂SO₄ (product code 1.06649.0500 by Merck KGaA, Germany) and 3% wt. NaCl (product code 7647-14-5 by J. T. Baker, the Netherlands) to represent harsh marine conditions. After 28 days curing in water, specimens of LSG and PP-LSG fully immersed in SL, were submitted to freeze-thaw cycles in the climatic chamber. The mechanical performance of LSG and PP-LSG samples were assessed after 0, 90, and 180 aging cycles by 4-point bending and uniaxial compressive loading, conducted by a Zwick device (load cell of maximum 100 kN). The dimensions of 4-point bending sample were: length 280 mm, width 40 mm, height 30 mm, span 240 mm, and the distance between loading points 80 mm. The flexural tests were displacement controlled (0.4 mm/min) according to ASTM C1609 [14]. The compressive strength was measured by loading halves of the prismatic bending specimens (loading speed 1 mm/min) according to EN 196-1 [15].

3. RESULTS AND DISCUSSIONS

3.1 Flexural strength

PP-LSG attained deflection-hardening behavior regardless the aging periods. Figure 1a illustrates the stress vs. crack opening displacement (COD) curves of PP-LSG in different aging periods and in comparison with the reference LSG. LSG showed typical brittle behavior with sudden failure at very small COD. On the other hand, PP-LSG showed deflection-hardening behavior with very high ductility (large COD at the peak load). The COD at peak load of PP-LSG after 180 cycles was roughly 2.7 mm. As discussed in Ref. [12], PP fiber offered a better load transferring capacity than PVA fiber reinforced composites cured in the same conditions.

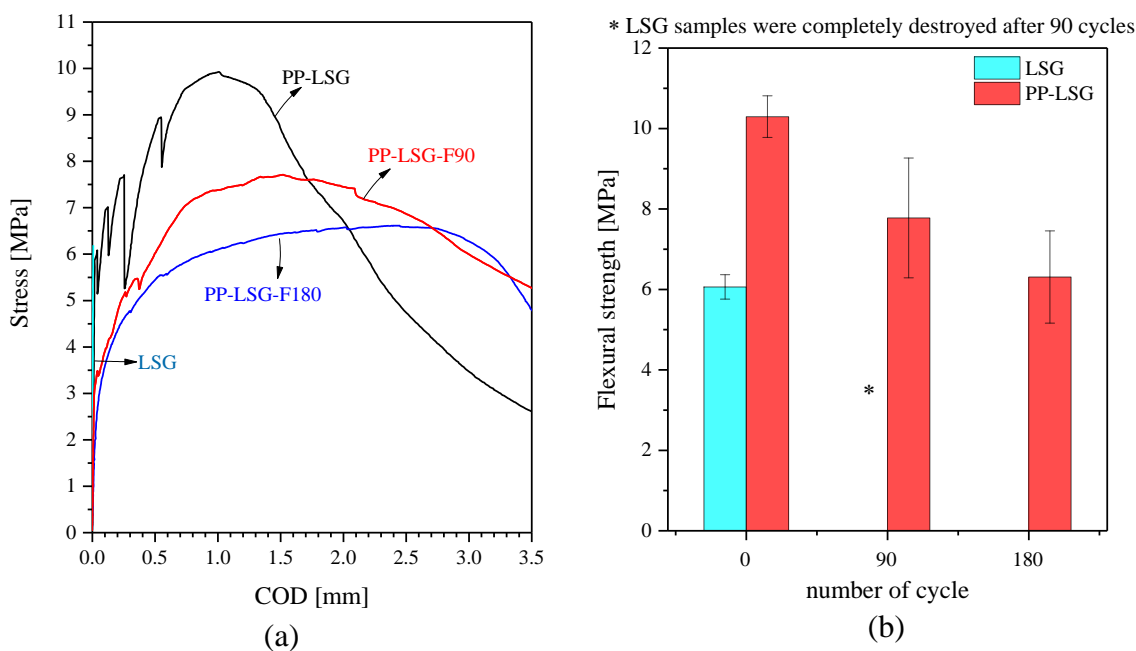


Figure 1: Flexural tests: (a) flexural strength from 4-point bending test and (b) average flexural strength of LSG and PP-LSG after different number of freeze-thaw cycles

PP-LSG had good flexural strength under the combined SO_4^{2-} and Cl^- attack. Figure 1b shows the flexural strength of the developed composite SL after different aging periods in comparison to the plain LSG. After 180 cycles, PP-LSG still retained roughly 6.2 MPa in flexural strength (almost 60% of the unaged material).

Sulfate and chloride ions were the main factors influencing the mechanical properties degradation. A reaction between these ions with cementitious materials generates a chemical volume change [16]. On the other hand, the freeze-thaw cycles contributed to the physical modification due to the expansion of water in structure pores. Therefore, the fibrous reinforcement played a vital role in controlling the cracks development and eventually preventing degradation of the mechanical properties. On the contrary, unreinforced LSG was completely destroyed after 90 freeze-thaw cycles.

3.2 Compressive strength

PP-LSG in SL gradually decreased the compressive strength, while the reference LSG was completely spoiled after the aging. Figure 2 shows the compressive strength of LSG and PP-LSG after different aging periods in SL. The composite slightly reduced the compressive strength by roughly 11% after 180 freeze-thaw cycles. PP fibers seemed delayed the crack propagation under the attacks and led a slow diffusion of sulfate and chloride ions [13,16]. As consequence, only a slight decrease in the compressive strength of PP-LSG in SL was recorded. In contrast, the unreinforced LSG suffered the combined physical and chemical attacks getting a negligible strength after only 90 freeze-thaw cycles. This result highlighted the important role of PP fibers in retaining the mechanical properties and leading to a good durability under such harsh conditions.

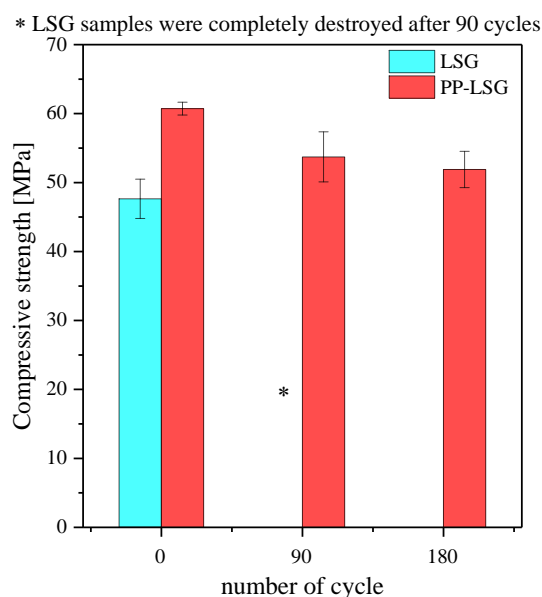


Figure 2: Compressive strength of LSG and PP-LSG after different number of freeze-thaw cycles

3.3 Phase characterization

SEM observations confirm the role played by PP fibers in slowing down the chemical attack in SL. Figure 3 shows SEM images of LSG and PP-LSG aged in SL after 180 freeze-thaw cycles. LSG reacted with SO_4^{2-} and formed visible crystal called secondary ettringite, as shown in Figure 3a. In contrast, the matrix of PP-LSG remained unreacted and structurally stable under the combined chemical attack of SO_4^{2-} and Cl^- (Figure 3b). The PP fibers showed good bonding with LSG matrix after the aging period. In addition, some micro cracks were observed on the fracture surface, which could be attributed to both the freeze-thaw and combined chemical attack. The morphology from SEM images reflects the good mechanical properties of PP-LSG, as detailed in Section 3.1 and 3.2, compared to the plain LSG.

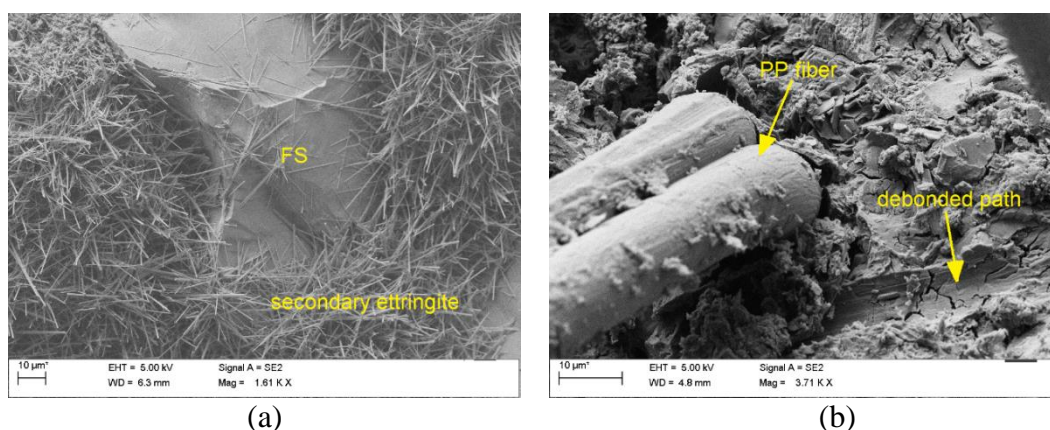


Figure 3: SEM images of (a) LSG and (b) PP-LSG after 180 freeze-thaw cycles in SL

4. CONCLUSIONS

- PP-LSG exhibited deflection-hardening behavior under flexural load after 180 freeze-thaw cycles in the combined sulfate-chloride solution.
- The mechanical properties of PP-LSG slightly decreased after the aging scheme, while the reference LSG was destructed just after 90 freeze-thaw cycles.
- The main damage mechanism in SL with freeze-thaw aging was the combined of physical attack from water uptake in structural pores and chemical attack led to volume expansion from the reaction between LSG matrix with the environment.

ACKNOWLEDGEMENTS

This work was done under MINSI project (grant number: A70189). The authors appreciate support from SSAB Europe Oy (Finland), Brasilit Saint-Gobain (Brazil), BASF (Germany), and Vanderbilt (USA) for providing the ladle slag, PP fiber, superplasticizer, and dispersing agent, respectively. Hoang Nguyen gratefully acknowledges the financial support from Tauno Tönning Foundation.

REFERENCES

- [1] J.-M. Kim, S.-M. Choi, D. Han, Improving the mechanical properties of rapid air cooled ladle furnace slag powder by gypsum, *Constr. Build. Mater.* 127 (2016) 93–101. doi:10.1016/j.conbuildmat.2016.09.102.
- [2] H. Nguyen, P. Kinnunen, V. Carvelli, M. Mastali, M. Illikainen, Strain hardening polypropylene fiber reinforced composite from hydrated ladle slag and gypsum, *Compos. Part B Eng.* (2018). doi:10.1016/j.compositesb.2018.09.056.
- [3] K. Quillin, Performance of belite–sulfoaluminate cements, *Cem. Concr. Res.* 31 (2001) 1341–1349. doi:10.1016/S0008-8846(01)00543-9.
- [4] S. Peysson, J. Péra, M. Chabannet, Immobilization of heavy metals by calcium sulfoaluminate cement, *Cem. Concr. Res.* 35 (2005) 2261–2270. doi:10.1016/j.cemconres.2005.03.015.
- [5] Edward G. Moffatt and Michael D. A. Thomas, Durability of Rapid-Strength Concrete Produced with Ettringite-Based Binders, *Mater. J.* 115 (2018). doi:10.14359/51701006.
- [6] X. Guo, H. Shi, W. Hu, K. Wu, Durability and microstructure of CSA cement-based materials from MSWI fly ash, *Cem. Concr. Compos.* 46 (2014) 26–31. doi:10.1016/j.cemconcomp.2013.10.015.

- [7] C.W. Hargis, B. Lothenbach, C.J. Müller, F. Winnefeld, Carbonation of calcium sulfoaluminate mortars, *Cem. Concr. Compos.* 80 (2017) 123–134. doi:10.1016/j.cemconcomp.2017.03.003.
- [8] E. Özbay, O. Karahan, M. Lachemi, K.M.A. Hossain, C.D. Atis, Dual effectiveness of freezing–thawing and sulfate attack on high-volume slag-incorporated ECC, *Compos. Part B Eng.* 45 (2013) 1384–1390. doi:10.1016/j.compositesb.2012.07.038.
- [9] M. Sahmaran, M. Li, V.C. Li, Transport properties of engineered cementitious composites under chloride exposure, *ACI Mater. J.* 104 (2007) 604–611.
- [10] M.L. Mustafa Sahmaran Khandaker M.A. Hossain, Ravi Ranade, and Victor C. Li, M. Lachemi, H. Khandaker M. A., R. Ranade, L. Victor C, Influence of Aggregate Type and Size on Ductility and Mechanical Properties of Engineered Cementitious Composites, *Mater. J.* 106 (2009). doi:10.14359/56556.
- [11] A.M. Cody, H. Lee, R.D. Cody, P.G. Spry, The effects of chemical environment on the nucleation, growth, and stability of ettringite $[\text{Ca}_3\text{Al}(\text{OH})_6]_2(\text{SO}_4)_3 \cdot 26\text{H}_2\text{O}$, *Cem. Concr. Res.* 34 (2004) 869–881. doi:10.1016/j.cemconres.2003.10.023.
- [12] B. Felekoglu, K. Tosun-Felekoglu, R. Ranade, Q. Zhang, V.C. Li, Influence of matrix flowability, fiber mixing procedure, and curing conditions on the mechanical performance of HTPP-ECC, *Compos. Part B Eng.* 60 (2014) 359–370. doi:10.1016/j.compositesb.2013.12.076.
- [13] H. Liu, Q. Zhang, V. Li, H. Su, C. Gu, Durability study on engineered cementitious composites (ECC) under sulfate and chloride environment, *Constr. Build. Mater.* 133 (2017) 171–181. doi:10.1016/j.conbuildmat.2016.12.074.
- [14] ASTM International, ASTM C1609 / C1609M, Standard Test Method for Flexural Performance of Fiber-Reinforced Concrete (Using Beam With Third-Point Loading), ASTM International, West Conshohocken, PA, 2015. www.astm.org.
- [15] European Standard, EN 196-1, Methods of testing cement - Part 1: Determination of strength, DIN Standards Committee Building and Civil Engineering, 2016. https://www.din.de/en.
- [16] S.-J. Lee, J.-P. Won, Resistibility of structural nano-synthetic fibre-reinforced cementitious composites in various chemical and physical environments, *Compos. Struct.* 179 (2017) 495–501. doi:10.1016/j.compstruct.2017.07.088.

MECHANICAL AND INSULATION PROPERTIES OF ULTRA-HIGH PERFORMANCE CONCRETE WITH EXPANDED POLYSTYRENE

Anjaneya Dixit (1), Sze Dai Pang (1) and Juhyuk Moon (2)

(1) National University of Singapore, Singapore

(2) Seoul National University, Seoul, Republic of Korea

Abstract

Recent advances in the field of sustainable development have witnessed an increasing effort in improving the energy-efficiency of buildings. The fundamental idea in this field of research is the inclusion of materials with high insulating characteristics in concrete. The resulting concrete-composite with low thermal conductivity (TC) helps curtail the energy required to maintain thermal comfort in buildings. However, such techniques are usually accompanied by drastic reduction in concrete strength since, the inclusion materials have low strength themselves, resulting in the composite being unsuitable for structural applications. A balance between the enhancement in thermal insulation and loss of strength in concrete is, therefore, needed. The study presented herein is an attempt of producing concrete with improved insulating behaviour with acceptable loss in mechanical properties. The insulation is achieved by mixing expanded polystyrene (EPS) beads in ultra-high performance concrete (UHPC). 5 mixtures with varying proportion of EPS by volume (0-45%) were studied. The resulting mixes show reduction in TC values (2.14 W/m-K to 0.49 W/m-K), and densities (2300 kg/m³ to 1463 kg/m³) with addition of EPS. As envisaged, the increase in EPS volume is accompanied by a decrease in compressive strength (149 MPa to 27 MPa) and elastic modulus of concrete (45 GPa to 14 GPa).

Keywords: Ultra-high performance concrete (UHPC), Expanded polystyrene (EPS), Thermal conductivity (TC)

1. INTRODUCTION

The phenomenal growth in the amount of construction projects to cater the ever increasing population has led to a proportionate escalation of humanity's impact on the environment. Consequently, the energy requirements to operate the various facilities in office and residential buildings have also seen a drastic rise. The building sector forms the largest consumer base for energy consumption with more than one-third of the total energy consumed globally. Residential and office buildings are consumers of about 40% of the global electricity produced, most of which is used to operate their heating, ventilation and air-conditioning (HVAC) systems

[1]. The largest portion of this energy owing to the HVAC systems, alone are responsible for 60% of the global energy consumption in buildings [1]. It is expected that without intervention of energy-efficient technologies, there would be a 50% increase in the energy demands of building sector, with the energy demand for cooling expected to rise by 300% by 2050 [1]. Since, fossil fuels are the major source of energy generation and will likely remain to be in the coming future, the aforementioned predictions can be directly associated to exacerbation of carbon emissions. This indirectly adds to the CO₂ emissions, since a major portion of the electricity is produced from fossil fuels.

With the increased awareness regarding global warming and the role of construction industry in exacerbating the situation, numerous researches have now been focused on making buildings energy-efficient to curtail the electricity requirements during their service life. In terms of thermally-efficient concrete, the fundamental idea is to reduce the thermal conductivity (TC) of the concrete by inducing artificial voids. Since, air has negligible TC, increase in porosity leads to an insulating concrete. This would curtail the energy requirements to operate the HVAC systems in maintaining indoor thermal comfort. A major downside to this technique is the obvious loss in mechanical properties as well as durability. Various additives like aerogel, cenospheres, glass microspheres, light-weight aggregates such as pumice, expanded clay, expanded perlite etc. have been studied in this endeavour. The study presented herein focuses on using EPS to achieve this.

The incorporation of EPS with concrete commenced in the 1970s. Due to its light weight but poor mechanical performance, initial investigations on EPS-concrete were primarily on developing non-structural elements such as partitions and wall claddings [2]. With time however, researchers have also studied the mechanical and thermal properties of EPS concrete. The combined effect of silica fume and EPS on the strength and durability of concrete was investigated by Babu and Babu [2]. Bouvard et. al. [3] conducted a comparative study between autoclaved concrete and EPS-concrete using microstructure characterization and simulation studies. The stress-strain relationship in EPS concrete under compression and its fire performance have also been studied [4]. Besides light-weight, another benefit of EPS concrete is low thermal conductivity (TC). [4], [5], [6] conducted investigations on the TC of EPS concrete. However, as mentioned earlier, a major shortcoming of EPS concrete is the considerable loss of strength and associated mechanical properties. Due to its high compressibility, EPS has negligible resistance to external loadings. This makes it inappropriate to be used in concrete beyond a certain amount. However, some progress has been made to achieve EPS concrete for structural application recently [7]– [10]. In this study, the degrading effect of EPS on strength has been countered by using ultra-high performance concrete (UHPC), which are characterized by low porosity, use of fine ingredients, low water-cement ratio and remarkably high strength (~150 MPa).

2. MATERIALS AND METHODS

The materials used in the preparation of the UHPC-EPS concrete included ordinary Portland cement (C) as per EN:197 CEM-1, quartz powder (QP) and silica sand (SS) as fillers and silica fume (SF) as supplementary cementitious material. The water-to-cement ratio was kept at 0.22 while the superplasticizer-to-cement (SP/C) ratio was 3%. The particle size distribution of the various ingredients is shown in Figure 1. The EPS used for this project were 3-5 mm in size with a density of 25 kg/m³. A total of five mixes were prepared as shown in Table 1. The volume

content of EPS was increased from 0 % in mix E0 to 45% in mix E4. The proportion of the UHPC ingredients was kept fixed at OPC: SF: SS: QP = 1: 0.25: 1.10: 0.35. The SP/C ratio plays a major role in the proportioning since, a very flowable mix would result in segregation of EPS beads on top, while a stiff mix would make the concrete difficult to work with.

The mixing was done in a Hobart mixer. The dry ingredients were mixed thoroughly, followed by addition of water and SP to prepare the UHPC mix. The EPS beads were then added gradually for uniform mixing. 50 mm cube samples were cast for compressive strength tests and 100×200 mm cylinders for modulus of elasticity (MoE) tests. For thermal conductivity tests, additional cubes were cast for E0, E1 and E2 which were then cut in half to obtain blocks of size 50×50×20 mm. For mix E3 and E4, slabs of size 300×300×30 mm were prepared. All specimens were cured in ambient conditions: relative humidity of 64% at 30°C till the time of testing. Compression and MoE tests were performed using a Denison testing machine, while the TC tests were done using HOTDISK Thermal Constants Analyzer (TPS 2500S) for the cuboids and NETZSCH Heat Flow Meter (HFM 436/3/1) for slab specimens. All tests were conducted on three specimens for each mix, except the TC tests for mix E1 where two specimens were tested. The mean values of these tests are reported in the next section.

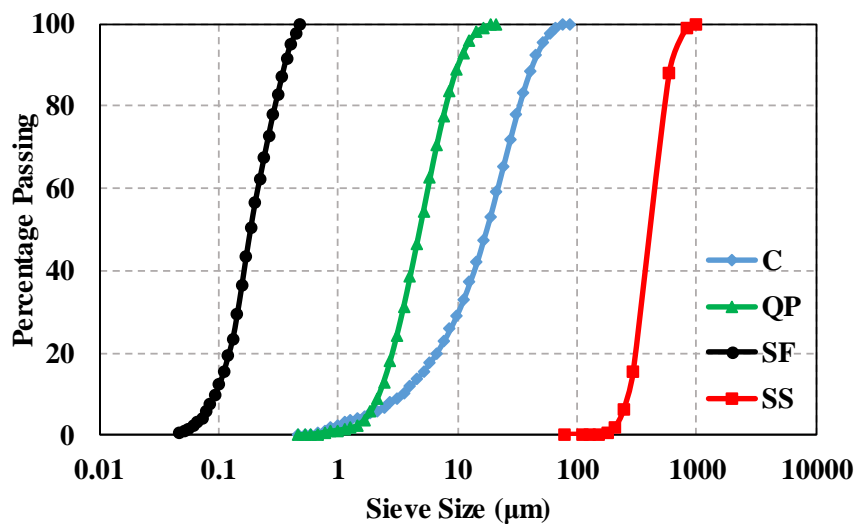


Figure 1: Particle size distribution for UHPC ingredients

Table 1: Mix proportion for UHPC-EPS concrete

Mix	C	SF	QP	SS	EPS (% volume)
E0	900	225	315	990	0
E1	720	180	252	792	16
E2	693	173	243	762	25
E3	648	162	227	713	36
E4	585	146	205	674	45

3. RESULTS AND DISCUSSIONS

The mean compressive strengths of cube specimens were determined at 7 and 28 days and are shown in Figure 2. In general, a reduction in strength was observed with increasing EPS content which is an obvious consequence of the weak EPS beads. The mean strength reduced from 149 MPa for mix E0 (0% EPS) to 27 MPa for mix E4 (45% by volume EPS). The 1-day densities measured using cube specimens by water displacement method also showed a decrease: from 2300 kg/m³ for mix E0 to 1463 kg/m³ for mix E4 as shown in Figure 3. The MoE values (Figure 4) at 28-days also showed a consistent drop with increasing EPS volume content. The mean modulus of elasticity obtained from three specimens for mix E0 was approx. 45 GPa, while for mix E4 was 14 GPa. The thermal conductivity values showed promising results (Figure 5). There was a 77% drop in the mean thermal conductivity of the composite, from 2.14 W/m-K for mix E0 to 0.49 W/m-K for mix E4.

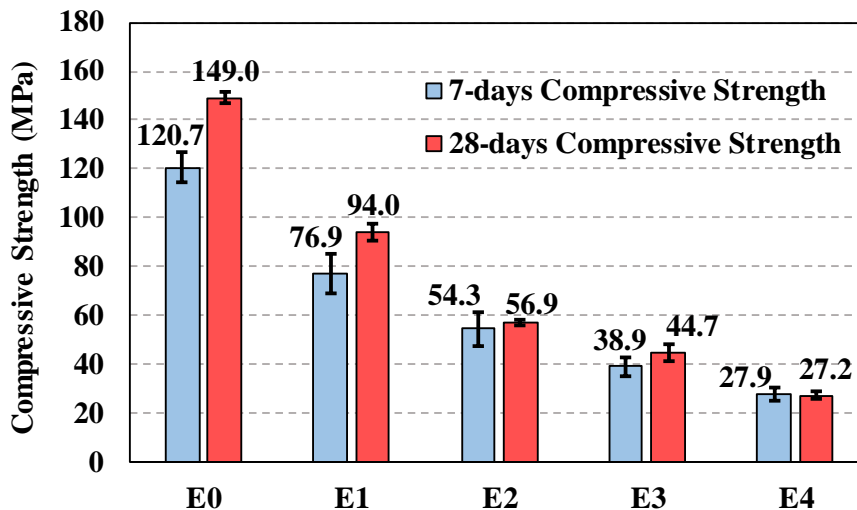


Figure 2: 7-days and 28-days compressive strength for mixtures E0-E4

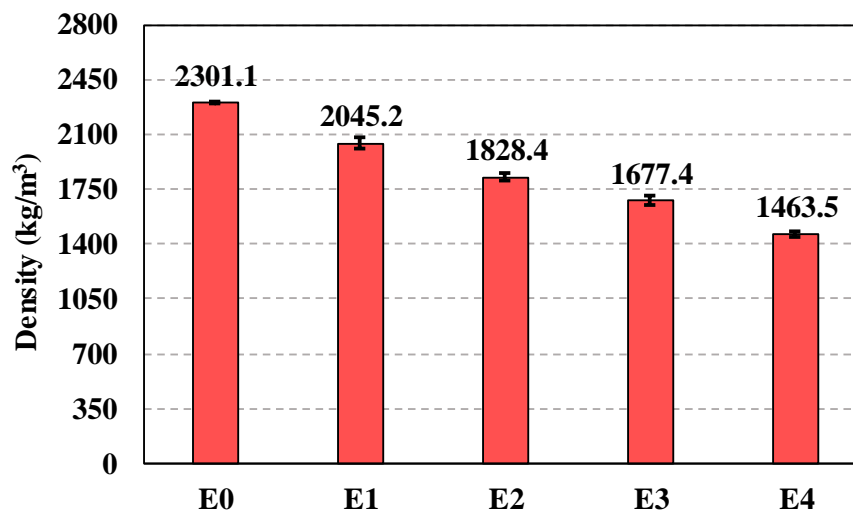


Figure 3: 1-day density for mixtures E0-E4

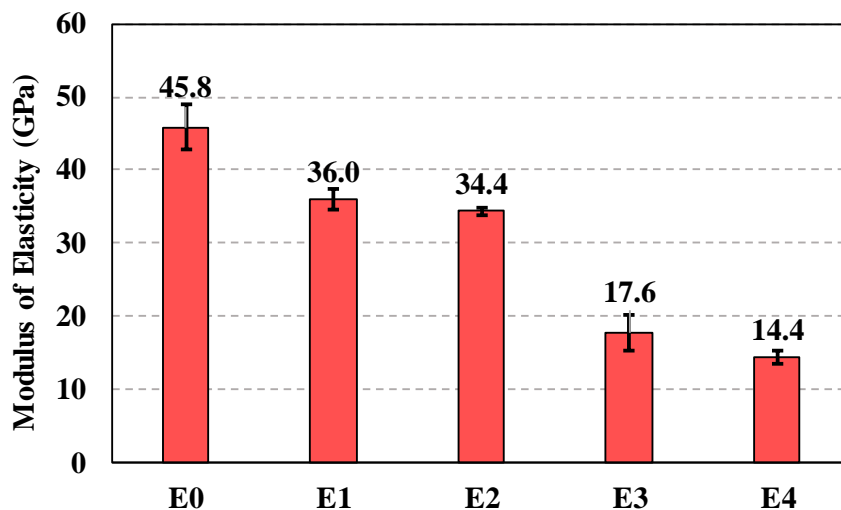


Figure 4: Modulus of elasticity for mixtures E0-E4

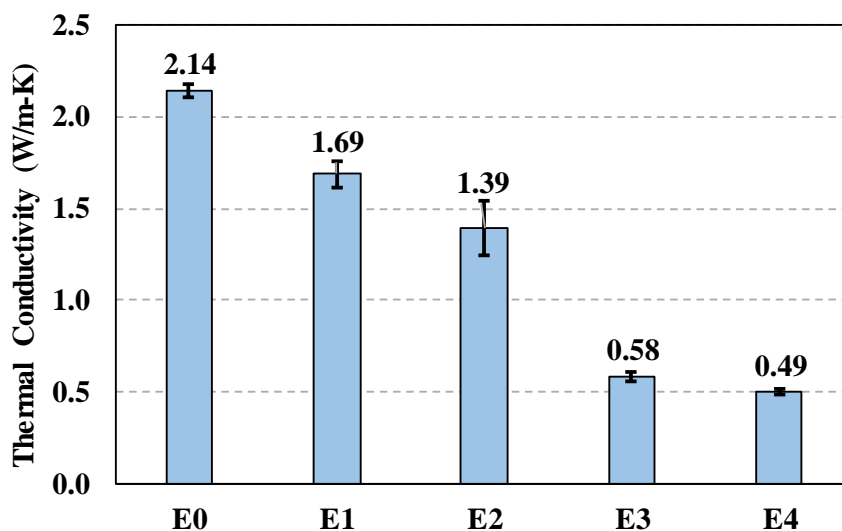


Figure 5: Thermal conductivity values for mixtures E0-E4

4. CONCLUSION

From the tests conducted and analysed, it is evident that EPS inclusion has a decreasing trend on the mechanical performance of UHPC. However, the merit lies in the decrease in density and remarkable increase in the insulating capacity of the resultant concrete. For a 45% increase in the EPS content, there was an 82% reduction in the compressive strength of the UHPC-EPS composite (from 149 MPa to 27 MPa) and a 69% loss in modulus of elasticity (from 45 GPa to 14 GPa). However, this was also accompanied by a 77% reduction in the thermal conductivity of the composite (from 2.14 W/m-K to 0.49 W/m-K) and 37% drop in density (from 2300 kg/m³ to 1463 kg/m³.) This indicates that the ultra-high strength of UHPC was, to some extent, able to mitigate the degrading effect of EPS. Based on the strength-to-thermal conductivity ratios, mix E3 was the optimal combination of insulation and strength, showing a strength of 44.7 MPa and TC value of 0.58 W/m-K.

ACKNOWLEDGEMENTS

This research was supported in the National University of Singapore by Singapore Ministry of Education Academic Research Fund Tier 1 Grant.

REFERENCES

- [1] International Energy Agency, 'Transition to Sustainable Buildings' (2013).
- [2] Babu, K. G. & Babu, D. S., 'Behaviour of lightweight expanded polystyrene concrete containing silica fume' *Cem. Concr. Res.* **33** (2003) 755–762.
- [3] Bouvard, D. et al., 'Characterization and simulation of microstructure and properties of EPS lightweight concrete', *Cem. Concr. Res.* **37** (2007) 1666–1673.
- [4] Sayadi, A. A., Tapia, J. V., Neitzert, T. R. & Clifton, G. C., 'Effects of expanded polystyrene (EPS) particles on fire resistance, thermal conductivity and compressive strength of foamed concrete', *Constr. Build. Mater.* **112** (2016) 716–724.
- [5] Brooks, A. L., Zhou, H. & Hanna, D., 'Comparative study of the mechanical and thermal properties of lightweight cementitious composites', *Constr. Build. Mater.* **159** (2017).
- [6] Remesar, J. C., Vera, S. & Lopez, M. Assessing and understanding the interaction between mechanical and thermal properties in concrete for developing a structural and insulating material. *Constr. Build. Mater.* **132**, 353–364 (2017).
- [7] Fernando, P. L. N., Jayasinghe, M. T. R. & Jayasinghe, C., 'Structural feasibility of Expanded Polystyrene (EPS) based lightweight concrete sandwich wall panels', *Constr. Build. Mater.* **139** (2017) 45–51.
- [8] Marrana, T. C., Silvestre, J. D., Brito, J. De & Gomes, R. Lifecycle Cost Analysis of Flat Roofs of Buildings. *J. Constr. Engineering Manag.* **143** (2017).
- [9] Ronald, J. D., Prabakar, J. & Alagusundaramoorthy, P. Precast concrete sandwich one-way slabs under flexural loading. *Eng. Struct.* **138** (2017) 447–457.
- [10] Wang, R. & Meyer, C. Cement & Concrete Composites Performance of cement mortar made with recycled high impact polystyrene. *Cem. Concr. Compos.* **34**, (2012) 975–981.

EFFECT OF PRE-IMPREGNATION PROCESS ON THE TENSILE BEHAVIOR OF GLASS YARN/ETTRINGITIC MATRIX COMPOSITE

Omayma HOMORO, Marie MICHEL and Thouraya. N. BARANGER

Université de Lyon, Université Lyon 1, Laboratory of Composite Materials for Construction (LMC2), 82 bd Niels Bohr, F-69622 Villeurbanne, France. Mail: omayma.homoro@univ-lyon1.fr, marie.michel@univ-lyon1.fr, thouraya.baranger@univ-lyon1.fr

Abstract

Textile Reinforced Concrete (TRC) is a composite cement-based material reinforced with alkali-resistant (AR) glass, carbon, basalt or aramid fabrics. During the last decades, these composites are being increasingly used to build thin and lightweight structures and to strengthen or repair damaged structures. However, the use of multifilament reinforcements for cements is challenging because the cement particles cannot fully penetrate the space between the inner filaments. This decreases the yarn/matrix bond and consequently the mechanical performance of the composite. To improve this bond, the glass yarns are typically pre-impregnated in a wet manner using mineral or organic matrices. The objective of this work is to compare this conventional method with an alternative method called pre-impregnation in a dry manner. It is based on using an alternating electrostatic field that allows powder to be impregnated into yarns. Classical tensile tests have been used for the mechanical characterization of glass yarn/ettringitic matrix composites. Three types of specimens have been tested: a dry yarn (D), a yarn pre-impregnated in a wet manner (PIW) with matrix particles, and a yarn pre-impregnated in a dry manner (PID) with three different types of powders. These tests allowed to identify the tensile mechanical properties of composites and to highlight the efficient pre-impregnation process.

Keywords: tensile properties, glass yarns, ettringitic matrix, pre-impregnation.

1. INTRODUCTION

Textile Reinforced Concrete (TRC) is a composite cement-based material reinforced with Alkali Resistant (AR) glass, carbon or aramid fabrics [1]. In the last decades there is a strong growing interest in this material that has been successfully used for the production of lightweight structures such as thin shells, cladding panels, ventilade façade systems and other manufactured products [2, 3] and for repairing and/or strengthening of reinforced concrete and masonry structures [4]. The great advantages offered by these composites are in their lightness, strength performance, low invasiveness, ease of installation and cost effectiveness [1, 5].

Most fabrics used for cement application are typically made of multifilament yarns composed of hundreds or thousands of filaments, each several micrometers in diameter, with very small spaces between the filaments [6]. However, this geometry does not allow penetration of cement grains (with size larger than the interfilament space) in the space between the filaments. This creates two zones: the sleeve zone in which the external filaments are in intimate contact with the hydration products of the cement matrix, and the core zone, in which the internal filaments are relatively free [7]. This special microstructure of the reinforcing bundle induces a unique failure known as ‘telescopic pullout’, whereby the external filaments, which are strongly bonded to the matrix, fracture during loading, while the internal ones remain continuous and slip against the external filaments [7,8]. This sliding mode of the inner filaments provide high ductility to the composite.

Increasing the sleeve/core ratio improves the stress transfer between the cement matrix and the inner filaments within the bundle, which is essential for increasing the efficient reinforcement of the composites. This can be achieved by filling the space between the bundles filaments. Coating bundles with polymers is an effective method that improves the mechanical performance of composites [7, 9], but it exhibits low bonding with the cement matrix leading to delamination [9]. Another solution to improve the bundle/matrix bond is to pre-impregnate bundles in a wet manner with mineral matrices. This method has already been applied and has given good results [9, 10], but it is long, difficult and suited only for the manufacturing of simple prefabricated elements. There is an alternative solution, developed by a French manufacture called Fibroline [11], which consists of pre-impregnating bundles in a dry manner using an alternating electrostatic field that allows to impregnate powder into yarns. The main advantage of this innovative process is the possibility of production of large-size building elements in site by ensuring a homogenous and controlled distribution of powder into textiles.

The goal of the present work is to compare the tensile behaviour of three types of cement based composites reinforced with AR glass yarns: (i) a dry yarn (D), (ii) a yarn pre-impregnated in a wet manner (PIW) with matrix particles, and (iii) a yarn pre-impregnated in a dry manner (PID) with three different types of powders. The effect of the reinforcement rates is also evaluated in this study.

2. EXPERIMENTAL WORK

The effect of pre-impregnation using wet and dry methods on the tensile response of cement-based composites reinforced with glass yarns is investigated. In this study, one type of AR glass yarn and specific cement matrix have been used. This section describes properties of materials, specimens manufacturing methodology, experimental configurations and tensile tests.

2.1 Materials

The yarn used in this study is a direct roving consisting of continuous AR glass filaments bonded into a single strand and wound onto a bobbin shape. The main characteristics of the yarn are given in **Error! Reference source not found.**

All specimens used in this study have a cementitious matrix named “K3 matrix”, made with a granular skeleton with a particle size of less than 300 μm , an ettringitic binder and an additive system, that consists of setting modifying agents used to adjust pot life and cure time of the grout and an association of rheology agents to ensure fluidity and stability of the

matrix. The particularity of this matrix is its rapid hardening and rise in strength. The average compression and tensile strength of this matrix after seven days of aging is 8.5 ± 0.7 MPa and 1.7 ± 0.2 MPa, respectively.

Table 1: Characteristics of the AR glass yarn (supplier's data) and composition of K3 matrix.

AR glass multi-filaments yarn		K3 matrix	
Filament diameter	19 μm	Constituents	Mass [g]
Specific Gravity	2.68 g/cm^3	Ettringitic binder	268
Linear weight	1200 Tex	Granular skeleton	624
Tensile Strength	1700 MPa	Additive system	108
Modulus of elasticity	72 GPa	Total solid	1000
Softening point	860 $^{\circ}\text{C}$	Water	240

2.2 Composite preparation

Two kinds of specimens were tested: 1Y, which was composed of the ettringitic matrix and one AR glass yarn, and 3Y, which was also composed of the same matrix, but with three AR glass yarns. The shape of all specimens is that of a rectangular parallelepiped with dimensions of 140 x 20 x 5 mm (figure 1.a). This shape is chosen to ensure homogeneous distribution of tensile stress over the whole width of the specimen. The 1Y and 3Y composites were manually prepared using silicone mold. A fresh matrix layer of 2.5 mm thickness was implemented in the mold using a spatula, then a glass yarn was positioned along the central axis of the matrix layer in the case of 1Y specimen, and three glass yarns were placed in the case of 3Y: a yarn in the center and two others located to the left and right of the central yarn making with the edges of the mold a distance of 2 mm approximately (figure 1.b). A second matrix layer of the same thickness was then applied. Specimens' upper surfaces were protected by plastic layers in order to limit drying and premature shrinkage of the upper surface. After 24 hours, specimens were removed from mold. To provide better stress transfer during testing, two aluminum plates of 50 x 20 x 4 mm, previously drilled ($\varnothing 8$ mm), were used. Each undrilled plate surface halves was glued to the edges of both faces of the specimen (figure 1.a) using an epoxy adhesive (EPONAL 380). Specimens were kept at ambient atmosphere and temperature for six days, before to be tested. Figure 1.c shows specimens ready for the tensile test.

2.3 Yarn pre-impregnation method

Before being placed into the mould, the yarn was pre-impregnated according to two different processes:

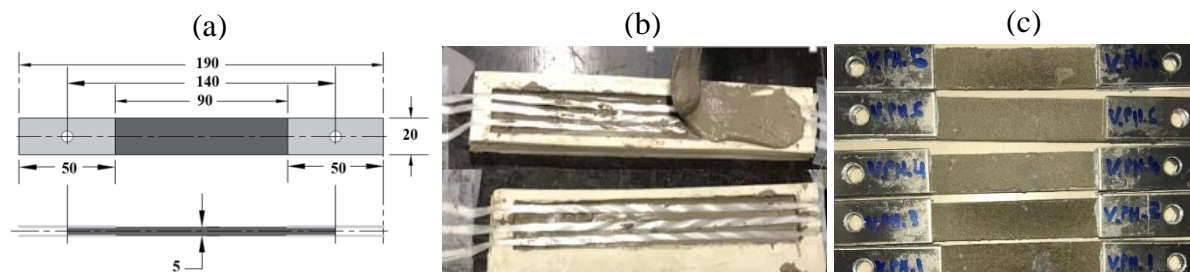


Figure 1: (a) specimen geometry (measurements in mm); (b) specimen preparation; (c) specimens ready to be tested

Wet pre-impregnation: the yarn was saturated with K3 matrix slurry by manual action (figure 2.a).

Dry pre-impregnation: the principle of this process is presented in figure 3. Three types of powder were scattered onto the glass yarn segments. The yarn/powder system was then placed between two dielectrics. A strong alternative electrostatic field is created by the high tension applied to the electrodes. At the end of the treatment, the powder scattered on top of the yarns is transferred inside (figure 2.b). A few seconds of residence time is sufficient, and leads to a homogeneous distribution of the powder inside the yarn segments. Finally, the pre-impregnated yarns were water sprayed before casting the matrix.

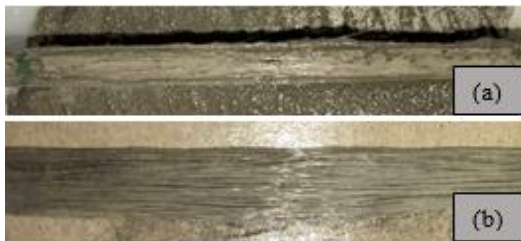


Figure 2: yarn pre-impregnated in (a) wet and (b) dry manner

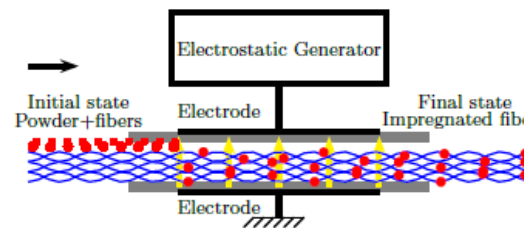


Figure 3: Principle of dry impregnation process

2.4 Experimental configurations

For both 1Y and 3Y composites, five experimental configurations were considered to study the effect of pre-impregnation of the yarn on the tensile behavior of the composite:

- D: the yarn was air dried at room temperature before casting, the penetration of cement particles into the filaments was restricted;
- PIW.K3, the yarn was wet pre-impregnated with the K3 ettringitic matrix;
- PID.B: the yarn was dry pre-impregnated with only the binder of the K3 matrix. The additive system and the fillers of K3 matrix were removed because they had a negative effect on the yarn-matrix interface [12];
- PID.SAC: the yarn was dry pre-impregnated with a SAC mono-component binder (sulfo-aluminous cement). This powder was chosen because it corresponds to a mono-component binder that is chemically similar to the K3 matrix binder consisting of three components, and ensures the homogeneity of the powder within the yarns;
- PID.P: the yarn was dry pre-impregnated with polymer powder (polyvinyl acetate) in order to compare with literature.

Specimens without yarns made with only matrix were tested for reference, designated R. At least, six specimens were tested for 1Y and 3Y composites and for each configuration. Tests were carried out 7 days after casting.

2.5 Tensile tests

All tensile tests were conducted using a zwick/Roell universal machine with a speed of 1 mm/min. The tests were performed either until a 6 mm extension was obtained (by the cross head of the machine) or, if less, until the complete failure of the specimen. The tensile effort was applied through ball joints that allow for good characterisation of the tensile behaviour (they reduce the parasitic bending). Representative specimens (with mechanical response close to the average) were graphically compared. The following average properties were

evaluated: the ultimate tensile force F_{max} , and the energy consumption W (toughness) calculated as the area under the effort–displacement curves up to F_{max} .

3. RESULTS AND DISCUSSION

3.1 Tensile test results

Figure 4.a presents the tensile behavior of the representative 1Y specimens, in terms of the axial force as a function of displacement, for the different configurations: D, PIW.K3, PID.B, PID.SAC and PID.P. In the case of D composite, the first zone of the curve corresponds to a linear evolution until reaching the maximum force. Only one crack was produced at the fracture location, leading to a force drop of around 60%. The stress is then transferred to the external filaments only (Because of the limited penetration of cement particles into the multifilament yarn) through this crack allowing a slight increase of the effort. Subsequently, the behavior is similar to that of pullout, which is characterized by a successive rupture of the external filaments followed by a slip of the internal filaments. For a wet or dry pre-impregnated yarn, the behavior is similar to that of a D yarn, characterized by the appearance of a single crack. However, the effort in this case is transferred to the external filaments and a large number of internal filaments (depending on degree of impregnation), which allowed an increase of the effort after its fall related to the crack.

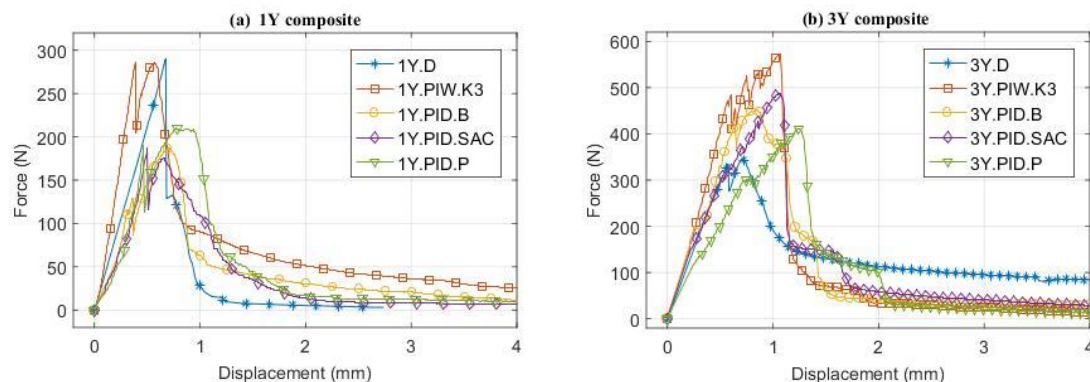


Figure 4: tensile behavior of (a) 1Y and (b) 3Y composites for different configurations

Figure 4.b presents the evolution of the axial force in the 3Y composite as a function of displacement tensile behavior for the different configurations: D, PIW.K3, PID.B, PID.SAC and PID.P. One representative curve is shown for each configuration. A common trend can be observed in the case of PIW.K3, PID.B, PID.SAC and PID.P configurations: the curves consist of a linear zone which is characterized by an uncracked matrix, followed by a non-linear zone where the matrix began to crack during the increase in the tensile axial loading until reaching the ultimate value. This behavior, which is not observed in the case of D composite (where only one or two cracks were occurred), is due to the improvement of the yarn-matrix adhesion by the pre-impregnation of the yarn. In fact, once the tensile strength of the matrix is reached, the whole force is transferred through the crack to the multifilament yarn. Owing to the bond between cement and yarn, the latter redistributes the load until the tensile strength of the matrix is reached in another section of the specimen, thus creating a new crack. Repetition of this process leads to the formation of a multicrack pattern along the composite. The width of the cracks is important in the case of the PIW.K3 composites,

represented on the curve by successive drops of the force in the second zone, unlike the composites PID.B, PID.SAC and PID.P, which are characterized by microcracks.

3.2 Failure and cracking modes

The rupture of the majority of the 1Y and 3Y specimens occurred in the section at the end of the specimen, adjacent to the aluminum heels. Three modes of rupture were observed in this study: (i) telescopic rupture of the yarns in the vicinity of the heels, corresponding to the successive rupture of the external filaments and the slip of the internal filaments (Figure 5.a). This mode of rupture was observed in the case of all 1Y specimens and 3Y.D composites in which the reinforcement was not pre-impregnated. (ii) Total rupture of the yarns (Figure 5.b). This appeared in the case of the wet pre-impregnation of 3Y composites which allowed to distribute the stress in the majority of the filaments thanks to the good adherence yarn-matrix. (iii) Intermediate failure mode in the case of 3Y composites pre-impregnated in a dry manner, characterized by the rupture, in addition to the external filaments, of a significant number of the internal filaments, followed by the slip of the unbroken filaments (Figure 5.c).

Good adhesion promotes the transfer of the reinforcement load to the matrix once the first crack occurs, leading the creation of multiple cracks on different sections of the specimen. In contrast, this cannot happen if a low reinforcement rate is used as in the case of the 1Y material, where only one crack was observed even in the case of pre-impregnated yarns. However, for the 3Y composite, wet pre-impregnation caused the production of approximately 11 cracks, while dry pre-impregnation resulted in microcracks that were only observed after the application of layer of the methylene blue solution.



Figure 5: 3Y composites failure modes (a) D, (b) PIW.K3 and (c) PID.SAC

3.3 Mechanical properties

Figure 6.a shows the maximum force F_{max} of the reference material and all glass-fiber composites (with or without pre-impregnation). The first observation that can be made from this figure is the great effect of the reinforcement rate on the ultimate load. In the case of using one glass yarn as reinforcement, whether dry (1Y.D) or pre-impregnated according to the wet and dry process (1Y.PIW.K3, 1Y.PID.B, 1Y.PID.SAC and 1Y.PID.P), the F_{max} values remain lower than that of the R material (drop of between 10 and 35%). This means that the insertion of a single yarn does not allow to reinforce the cement but rather to generate defects into the matrix, which can be related to the reduction of its compactness resulting in a weakening of its resistance. However, the insertion of three glass yarns into the cement matrix contributed to its reinforcement. Indeed, the 3Y composites showed tensile load superior to that of the reference with a gain ranging from 26 to 65% (depending on the degree of pre-impregnation of the yarn). The increase of the reinforcement rate led to a significant

improvement of F_{max} either for a dry yarn (+29%) or pre-impregnated yarn (+84% for PIW.K3, +110% for PID.B, +120% for PID.SAC and +91% for PID.P).

For the 1Y composites, the wet pre-impregnation of yarn didn't have a significant effect on the tensile force, if we take into account the fluctuation of the F_{max} values of 1Y.D and 1Y.PIW.K3 composites. This was expected since it is the matrix that governs the behavior of the material because of the low reinforcement rate. However, the ultimate strength was lower in the PID composites (by 21 %) using different types of powder, compared to D composites. This can be explained by the increase of porosity in the matrix caused by the calendaring of the yarns (This allowed penetration of powder into the yarn by dry pre-impregnation method) which is supposed to increase the inter-filament spaces. As for the 3Y composites, the results reveal that the maximum tensile effort is strongly influenced by the pre-impregnation process and the type of powder used. The wet pre-impregnation showed the greatest improvement of F_{max} with a gain of 52% compared to the D specimens, owing to the good penetrability of the cement particles between the bundle filaments, which improved the filament-matrix adhesion, and consequently the effort was transferred from the matrix to most of the filaments. The dry pre-impregnation with K3 binder, SAC binder and polymers also showed tensile strength superior to that of the D composite (by 25%, 37% and 16%, respectively), but its improvement was less marked than that of the PIW composites.

The results of the energy consumption W for the different configurations investigated are shown in figure 6.b. The results follow the same general trends as the maximum effort F_{max} . The greatest value of W for 3Y specimens was obtained in the case of a wet pre-impregnated reinforcement with a gain of 151% compared to the dry reinforcement. This is mainly due to the good yarn-matrix bond which led to the increase in strength and contributed to the multiple formation of cracks, which provide the composite a high ductility. The same effect was observed in the case of a dry pre-impregnation with K3 binder, SAC binder and polymers, but with a less significant improvement compared to the wet pre-impregnation, by 61%, 96% and 60%, respectively.

Taken together, the results of the mechanical testing of the glass yarn-matrix composites indicate that the yarn pre-impregnation have beneficial effects on the mechanical properties of these composites.

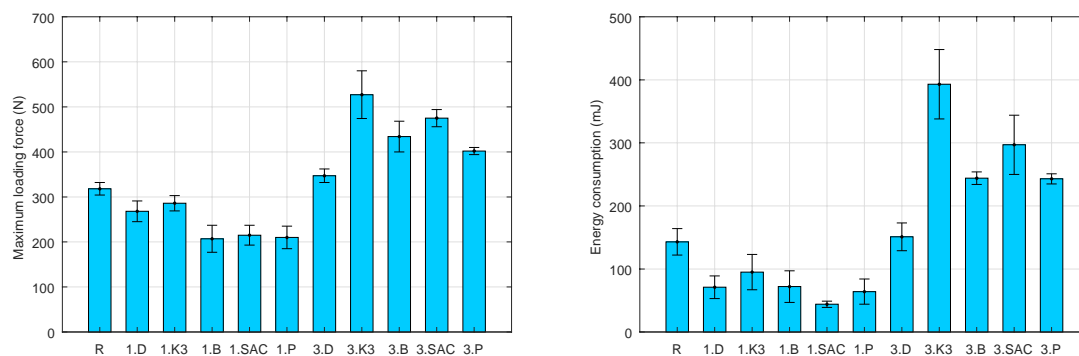


Figure 6: Evolution of the maximum force F_{max} (a); and the energy consumption W (b) according to the configurations investigated

4. CONCLUSION

From the experimental results obtained on R, 1Y and 3Y materials using two pre-impregnation methods applied to the AR glass yarn, the following conclusions can be drawn:

- The maximum tensile load is widely influenced by the reinforcement rate; the insertion of a single yarn into cement matrix reduced the mechanical properties by creating defects in matrix, while the use of three yarns as reinforcement is beneficial.
- Both wet and dry methods contributed to the improvement on the mechanical behavior of 3Y materials. The wet method showed the best improvement but with variability greater than that of dry method because it is a non-controlled process.
- The tensile failure mode of D composites was found to be slippage of the internal filaments inside the matrix. However, by using a wet pre-impregnation, the adhesion developed at the interface matrix-yarn resulted in filaments rupture. The PID composites exhibited an intermediate failure, characterized by the rupture of significant number of the internal filaments, followed by the slip of the unbroken filaments.
- Although the wet pre-impregnation method exhibited the best improvement in mechanical properties, it is suited only for the manufacturing of simple prefabricated elements, unlike the dry pre-impregnation method that allows for the production of large-size building elements on site by ensuring a homogeneous and controlled distribution of powder into the textile.

REFERENCES

- [1] Colombo, I.G., Magri, A., Zani, G., et al., 'Erratum to: Textile Reinforced Concrete: experimental investigation on design parameters'. *Materials and structures*, 2013, vol. 46, p. 1953-1971.
- [2] Naaman, N., 'Textile reinforced cement composites: competitive status and research directions'. In: *International RILEM Conference on Materials Science (MatSci) I*. 2010. p. 3-22.
- [3] Hegger, J., Zell, M. and Horstmann, M. 'Textile reinforced concrete—realization in applications'. In: *Proceedings: international fib symposium tailor made concrete structures: new solutions for our society*. 2008. p. 357-362.
- [4] Mechtcherine, V., 'Novel cement-based composites for the strengthening and repair of concrete structures'. *Construction and Building Materials*, 2013, vol. 41, p. 365-373.
- [5] Donnini, J., Corinaldesi, V. and Nanni, A., 'Mechanical properties of FRCM using carbon fabrics with different coating treatments'. *Composites Part B: Engineering*, 2016, vol. 88, p. 220-228.
- [6] Dvorkin, D. and Peled, A., 'Effect of reinforcement with carbon fabrics impregnated with nanoparticles on the tensile behavior of cement-based composites'. *Cement and Concrete Research*, 2016, vol. 85, p. 28-38.
- [7] Banholzer, B., 'Bond behaviour of a multi-filament yarn embedded in a cementitious matrix'. 2004. Thèse de doctorat. Bibliothek der RWTH Aachen.
- [8] Bentur, A. and Mindess, S., 'Fibre reinforced cementitious composites'. CRC Press, 2014.
- [9] Dvorkin, D. and Peled, A., 'Effect of reinforcement with carbon fabrics impregnated with nanoparticles on the tensile behavior of cement-based composites'. *Cement and Concrete Research*, 2016, vol. 85, p. 28-38.
- [10] Cohen, Z. and Peled, A., 'Controlled telescopic reinforcement system of fabric cement composites durability concerns'. *Cement and Concrete Research*, 2010, vol. 40, no 10, p. 1495-1506.
- [11] Caramaro, L., and Joric, M., "Imprégnation voie sèche-Procédé d'imprégnation électrostatique de la société Fibroline." (2016).
- [12] Homoro, O., Michel, M. and Baranger, N.T., 'Influence of pre-impregnation process on mechanical performance of glass/ettringitic matrix composite'. the 9th International Conference on Fiber-Reinforced Polymer Composite in Civil Engineering (CICE 2018).

RUBBERISED CONCRETE REFINEMENT BY CEMENT SUBSTITUTION AND RUBBER PARTICLE PRETREATMENT

**Dr. Thomaida Polydorou (1), Dr. Kyriacos Neocleous (1), Dr. Loukas Koutsokeras (2),
Dr. Georgios Constantinides (2), Dr. Nicholas Kyriakides (1), Prof. Kypros Pilakoutas
(3) and Prof. Diofantos Hadjimitsis (1)**

(1) Department of Civil Engineering and Geomatics, Cyprus University of Technology,
Cyprus

(2) Department of Mechanical Engineering and Materials Science and Engineering, Cyprus
University of Technology, Cyprus

(3) Department of Civil and Structural Engineering, The University of Sheffield &
Department of Civil Engineering and Geomatics, Cyprus University of Technology (Visiting
Professor)

Abstract

Re-use of End-of-life tyre components into concrete is a viable solution to the environmental issue of tyre waste that can result in promising, high added value concrete applications. End-of-life tyre particles are added to conventional concrete by replacement of a percentage of its aggregate content, improving concrete deformability. The material is currently in the initial stages of research for structural applications, with weakness observed over the interfacial transition zone between the rubber and cement paste.

This paper examines the potential of cement substitution by a combination of micro and nanoscale silica particles as well as the effect of rubber pre-treatment by coating with a Diabase quarry dust slurry for surface modification; aiming to refine the rubber/cement paste interface in rubberised concrete, thus improving its compressive strength and consequently structural performance.

The effectiveness of cement substitution and rubber treatment methods is measured by comparison of the samples compressive strength at 7 and 28 days and detected in microscopic observations of hardened rubberised concrete samples. It is indicated the rubber pre coating method investigated is a promising procedure, proven to be effective in reducing the porosity at the rubber-cement paste interface and increasing the 28-day concrete compressive strength more than twice.

Keywords: rubberised concrete, fibre reinforcement, end-of-life tyres, circular economy, cement substitution.

1. INTRODUCTION

While the world is turning to a more circular economy [1], researchers are investigating the re-use of End-of-life tyre components in high added value applications. A circular economy promotes reusing products, rather than scrapping what was formerly considered waste and then obtaining new resources. In such an economy, clothes, scrap metal and obsolete electronics, are not considered waste, but are instead returned to the economy or used more efficiently [1], [2].

Management of End-of-Life tyres is a major environmental concern in many countries; stockpiling of End-of-Life tyres is not only aesthetically unpleasing but also dangerous and in Europe has been outlawed through the implementation of EU Waste Legislation [2], [3]. Recycling of tyre rubber in construction materials and road furniture is an ideal solution to a significant environmental, health, and aesthetic problem [4], [5], [6].



Figure 1-1: Recycled Tyre Rubber Particles

Reuse of End-of-life tyre components (e.g. rubber) into concrete, the second most consumed material in the world after water [7], is considered one of the most viable solutions for this dangerous waste issue; not only eliminating large amounts of the waste rubber, but also providing a unique property to an otherwise non-deformable material. Conventional concrete lacks elasticity or flexibility unless reinforced with steel [8].

While Rubberised Concrete is a promising material, challenges regarding its performance have not been addressed sufficiently [9], [10]. High rubber content can decrease concrete compressive strength significantly thus thoughtful mix design based on the application is crucial for an effective material. The decrease in compressive strength with increasing rubber content is attributed to the higher Poisson's ratio of the rubber, compared to the replaced mineral aggregates, as well as to the poor bonding observed between the rubber particles and the cement paste, also referred to as weak Interfacial Transition Zone (ITZ). The bonding between rubber particles and cement paste at their ITZ was studied through Scanning Electron Microscopy (SEM) images, where gaps due to lack of bonding were visible and limited hydration products were observed around the rubber particles [11]. The higher porosity observed at the rubber-cement paste interface is also attributed to the hydrophobic nature of the rubber particles. In the similar case of recycled aggregates (RA), a method that was effective in improving the interfacial transition zone leading to higher compressive strengths was aggregate coating with very fine materials [12].

There are no methods established yet for the characterisation of recycled rubber properties; thus making it difficult to optimise the behaviour of rubberised concrete. Providing an optimum

gradation of rubber particles is shown to improve rubberised concrete compressive strength due to better packing of the mixture contents. In addition, admixtures such as plasticizers and super-plasticisers are used to achieve better consolidation of the mixture at predetermined water to binder ratios to control compressive strength. Even though previous research agrees that increasing rubber content results to a significant decrease in compressive strength, some argue that the rubber bonds well to the cement matrix [13], [14], [15].

Research on rubberised concrete is currently contradictory since rubber particles obtained from different recycling plants or even the same plant, vary when it comes to contamination levels (e.g. rubber dust, textile/polymeric fibre) and surface roughness. Rubber extraction and size-reduction methods are not consistent between tyre recycling plants. In addition to the traditional ambient-temperature mechanical treatment methods, water-jet cutting methods and de-vulcanization of rubber particles are also used in some tyre recycling plants worldwide, stating that de-vulcanized rubber surface is highly advantageous compared to vulcanised rubber, and can enhance the mechanical properties of rubberised concrete [16].

Mixture workability is also a primary issue in rubberised concrete, with difficulties observed due to the relatively low density of the rubber particles compared to the included natural aggregates and cement [11]. By sufficient consolidation and release of the mixture's entrapped air, rubberised concrete is able to attain satisfactory homogeneity.

In addition to rubber, tyre recycling also yields recycled tyre steel wires (Figure 1-2), which have limited alternative applications for their use; the most common one being scrap feed in steel making. It is rather preferred that recycled tyre steel wires are reused in high-value applications that can benefit from the materials' exceptional physical properties [17], [6].



Figure 1-2 : Recycled Tyre Steel Fibres

Extensive work has been undertaken on the use of recycled tyre steel fibres in concrete, where studies have compared sustainable hybrid fibre-reinforced concrete (SHFRC) to ordinary fibre-reinforced concrete with only manufactured fibres and demonstrated that SHFRC can have equal or better properties than ordinary fibre reinforced concrete [18], [19].

Methods for extracting, cleaning and sorting the recycled tyre steel tyre fibre (RTSF) were developed and optimised [20], resulting to the assembly of a RTSF product of known properties [3], [21], [19]. Unlike rebar and other types of reinforcement, RTSF allows for efficient microcrack control well before large cracks form. The unique characteristics of RTSF and the massive fibre count increase the local toughness of concrete and set new standards for sustainability [22], [23].

This research paper examines the possibilities of improving the mechanical properties of steel fibre reinforced rubberised concrete by rubber treatment with waste quarry dust paste and cement replacement by both micro and nano scale silica particles.

2. MATERIALS AND METHODS

A steel fibre reinforced concrete mix with 60% aggregate replacement by rubber particles was optimised for the development of a Steel Fibre Reinforced Rubberised Concrete Barrier, during the experimental testing rounds of the research project SAFER, funded under the Horizon 2020 Marie Skłodowska-Curie Actions, Grant Agreement No 748600. The SAFER Mix development has taken into consideration the findings of the collaborative project ‘Anagennisi’, funded under FP7 Grant Agreement No 603722.

To build on the investigation by the ‘Anagennisi’ team on enhancing the compressive strength of rubberised concrete, this research examines possible methods that could aid in improving the material compressive strength of the SAFER Steel Fibre Reinforced Rubberised Concrete Mix (S-SFRRC), by experimental examination of 3 mixture modifications.

The mixture modifications investigated by this study are summarised in Table 2.1. Mix A is a modified version of the optimised SAFER project mixture, adapted for the needs of this specific study. Mix B varies compared to Mix A only by the fact that a simple pre-treatment technique was applied to all rubber particles of the mixture, 1 day before casting and after the total amount of rubber for the Mix was weighed out and rubber particles were all blended together. The pre-treatment applied to the rubber particles of Mix B involved immersing them into a slurry made of waste diabase quarry dust from a local source and water for 1 hour. After mixing to ensure that all rubber particles’ surfaces were covered by the slurry, the particles were scooped out and let dry on a flat surface for 24 hours, resulting to a thin coating on the rubber particles’ surfaces.

Mix C and Mix D of this study examine the effect of replacing 3% of the microsilica content of Mix A with 15-20mm diameter SiO₂ particles, or nanosilica. The particles used in Mix C were nearly nonporous amorphous and spherical (S-type) but the particles used in Mix D were porous and amorphous (P-type).

As mentioned in the preceding paragraphs, the original SAFER project optimised mixture was not suitable for this study, due to the fact that when 3% of its microsilica content was replaced by nanosilica, the mixture became unworkable therefore additional water and superplasticiser were used to accommodate this issue. Accordingly, all 4 mixtures in this study included the additional amount of water and superplasticiser required to make Mix C and D workable, to ensure a fair comparison between the compressive strengths of the 4 mixture samples. It should be noted that the original SAFER mixture water to binder (w/b) ratio is 0.45 but the mixtures in this study all have a w/b ratio of 0.56. Table 2.1 shows the constituents and quantities used per cubic meter of material, for each of the 4 investigated mixtures.

The SAFER Steel Fibre Reinforced Rubberised Concrete Mix has 60% (by volume) of its natural aggregates replaced by rubber particles of equal size, keeping a fine aggregate to coarse aggregate ratio of 1.22.

The mix included rubber particles from 3 different sources coming from 3 different countries in Europe (i.e. Croatia, Cyprus and the UK) with no material properties specified. A representative sample of all types of rubber particles from the sources used in this study was tested for its apparent particle density, following EN 1097-6 (CEN 2013). The average Specific

Gravity of the representative rubber particle sample used in this mix was determined to be 0.8. For this research, liquid polycarboxilic polymer based superplasticiser conforming to EN934-2:2009 was EN 197-1 portland cement CEM I 52,5N was used.

The Recycled Tyre Steel Fibres (RTSF) used in this study are commercially cleaned, sorted and evaluated. The product properties are as follows; Tensile strength: 2,560 ±550 MPa Young's Modulus: 200,000±XXX MPa (Twincon Ltd, 2018).

Microsilica conforming to ASTM C1240 requirements and also fulfilling the requirement of Table ZA.1 in EN13263-1:2005+A1:2009 for Silica Fume-Class 1 was used in this study. In modified mixtures C and D, 3% of the Microsilica content was replaced by Nanosilica. The S-type nanosilica used in Mix C is Silicon Oxide Nanopowder / SiO₂ Nanoparticles (SiO_x, 99.5+%, 15-20nm, S-type, Spherical, Nonporous and amorphous). The P-type nanosilica used in Mix D is Silicon Oxide Nanopowder / SiO₂ Nanoparticles (SiO_x, 99.5+%, 15-20nm, Porous and amorphous).

A 60-Litre capacity drum mixer was used to make the specimens. First, all aggregates were added into the mixer and blended for 2-3 minutes before adding half of the mixing water; mixing was carried out for 2 minutes. The binders were added subsequently, followed by the rest of the water and admixture liquid. The steel fibres were added last, during the final 3 minutes of mixing. The Steel Fibre Reinforced Rubberised Concrete samples were cast and consolidated using a vibrating table. After 48 hours in their moulds, the samples were de-moulded and placed in a water tank to cure until tested. Compressive strength was tested at 7 and 28 days for all specimens and at 90 days for modified mixtures C and D only. Compressive strength testing was performed after allowing the wet specimens to dry for 24 hours.

Table 2.1 : Mixture Constituents

Mixture Constituent	Mix ID-A	Mix ID-B	Mix ID-C	Mix ID-D
Cement CEM I 52,5N	400.0 kg/m ³	400.0 kg/m ³	400.0 kg/m ³	400.0 kg/m ³
Silica Fume (Micro-silica)	100.0 kg/m ³	100.0 kg/m ³	97.0 kg/m ³	97.0 kg/m ³
P-type Nanosilica particles (15-20nm)	-	-	-	3.0 kg/m ³
S-type Nanosilica particles (15-20nm)	-	-	3.0 kg/m ³	-
Fine Crushed Aggregate (0-4mm)	310.5 kg/m ³	310.5 kg/m ³	310.5 kg/m ³	310.5 kg/m ³
Coarse Crushed Aggregate (4-20mm)	378.0 kg/m ³	378.0 kg/m ³	378.0 kg/m ³	378.0 kg/m ³
Fine Rubber Particles	169.7 kg/m ³	169.7 kg/m ³	169.7 kg/m ³	169.7 kg/m ³
Coarse Rubber Particles	207.0 kg/m ³	207.0 kg/m ³	207.0 kg/m ³	207.0 kg/m ³
Rubber Particle Treatment	-	√	-	-
Recycled Steel Fibres	25.0 kg/m ³	25.0 kg/m ³	25.0 kg/m ³	25.0 kg/m ³
Water	280.0 kg/m ³	280.0 kg/m ³	280.0 kg/m ³	280.0 kg/m ³
Super-plasticiser	4.875 (L/m ³)	4.875 (L/m ³)	4.875 (L/m ³)	4.875 (L/m ³)

3. RESULTS AND DISCUSSION

The average compressive strength and standard deviation values for each of the 4 Mixtures investigated by this study at 7, 28 and 90 days as applies, are listed in Table 3.1.

Table 3.1 : Compressive Strength Average and Standard Deviation Values

	7-day Strength (MPa)		28-day Strength (MPa)		90-day Strength (MPa)	
	Average	Standard Deviation	Average	Standard Deviation	Average	Standard Deviation
Mix A	1.63	0.06	2.17	0.06	-	-
Mix B	2.48	0.09	6.97	1.99	-	-
Mix C	4.47	0.01	4.74	0.12	4.80	0.08
Mix D	2.88	0.04	3.23	0.12	3.25	0.01

The compressive strength results indicate that both cement substitution by both silica fume (microsilica) and S or P type nanosilica, as well as the rubber pre-treatment method investigated in this research were all effective in increasing the mixture compressive strength. As expected, a significant increase of the early compressive strength is achieved by including a small amount of spherical SiO₂ nano particles in the mixture, specifically a 174% increase of the average 7-day compressive strength with the substitution of 3% of the SiO₂ micro size particles (silica fume or microsilica) by non-porous spherical SiO₂ nano size particles. Where substituted by porous SiO₂ nano size particles (Mix D), the 7-day compressive strength increase was limited to 77%. A 52% increase of the 7-day compressive strength is observed with the pre-treatment method investigated (Mix B), where unlike the cases of Mix C and D, there was no cement replacement by an expensive nanomaterial but instead, a simple pre-treatment using waste dust was applied on the rubber particles of the mixture.

At 28 days, the steel fibre reinforced rubberised concrete compressive strengths of all trial mixtures increased further, with no significant strength gains in the cases of cement replacement by combined micro and nano SiO₂ (Mix C, Mix D). Inversely, the average compressive strength of the samples where the rubber particles went through the pre-treatment increased by 181% during the additional 21 days of curing (Mix B) and having a 221% higher 28-day compressive strength compared to Mix A, between which no variant exists other than the rubber pre-treatment. It is speculated that the rubber coating achieved by pre-treatment with the waste diabase quarry dust was able to reduce the hydrophobicity of the rubber particles, thus eliminating the resulting porosity in the mixture. In contrast with the values obtained for the rest of the mixtures, a high variability was observed in the case where pre treated rubber particles were used. The variability in compressive strength in this case is attributed to the fact that the slurry coating saturation state was inconsistent within the sample range.

When comparing Mix C and Mix D, where the only difference between the two is the type of SiO₂ particles used; non-porous in Mix C and porous in Mix D, the higher compressive strength attained by Mix C samples can be explained by the contribution of density from the non-porous SiO₂ nanoparticles to the total mix density.

The apparent densities of the hardened concrete samples, listed in Table 3.2, relate to the respective compressive strengths reported in Table 3.1, suggesting that the main factor of strength improvement is the densification of the cement paste matrix.

Table 3.2 : Apparent Density of Hardened Concrete Samples

Apparent Density (kg/m ³)	Mix A	Mix B	Mix C	Mix D
7-day cured samples	1164	1335	1386	1272
28-day cured samples	1328	1618	1411	1290

This is further enforced through Scanning Electron Microscopy (SEM) images of fractured surfaces. Figure 3.1 shows images of the non-treated (Mix A) vs. the treated (Mix B) rubber surfaces suggesting that the treatment process results in a significant reduction in the volume of pores present in the microstructure. While this is in agreement with the observed density increase, it is not yet clear whether the porosity reduction relates to an enhanced hydrophilicity of the rubber particles induced by the treatment process. Furthermore, other mechanisms including the formation of cement hydration products as well as chemical interactions of the mix constituents with the waste dust used for the slurry coating need to be investigated.

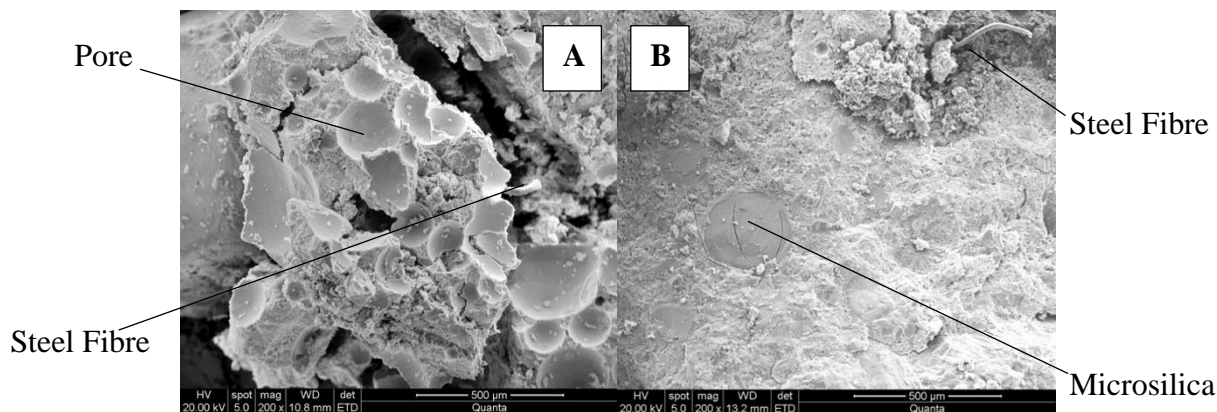


Figure 3-1 : Scanning Electron Microscopy images of fractured surfaces of hardened SFRRRC; Mix A sample (A) and Mix B sample (B)

4. CONCLUSIONS

The rubber particle treatment method investigated by this study appears to be very promising. A significant increase in the compressive strength was achieved by a simple rubber pre-treatment method using diabase quarry dust which is considered waste. Substitution of the mixture's microsilica content with non-porous nanosilica increased the material compressive strength but not to the extent where the cost of the nanomaterial is justified. Further investigation should be undertaken, to determine the chemical characteristics of the quarry dust and the effects it has on the rubber particles surface properties as well as the chemical interaction of the dust particles during the cement hydration process. In addition, the treatment process should be optimized and standardized to reduce the variability observed in the compressive strengths of samples which included the slurry treated rubber particles.

ACKNOWLEDGEMENTS

This research has received funding from the European Union's Horizon 2020 research and innovation programme under the Marie Skłodowska-Curie grant agreement No 748600.

REFERENCES

- [1] United Nations (2018), United Nations Conference on Trade and Development No.61.
- [2] Directive 2008/98/EC (2008), Official Journal of the European Union, Directive 2008/98/EC of the European Parliament and Council on Waste and Repealing Certain Directives, Brussels, Belgium.
- [3] Pilakoutas, K., Neocleous, K. & Tlemat, H. (2004), "Reuse of tyre steel fibres as concrete reinforcement", *Engineering Sustainability* 157 (ES3), 131-138.
- [4] Khaloo A. R., Dehestani, M. & Rahmatabadi, P. (2008), "Mechanical properties of concrete containing a high volume of tire-rubber particles", *Waste Management* 28 (2008) 2472– 2482.
- [5] Khatib Z. K., & Bayomy, F. M. (1999), "Rubberized Portland cement concrete", *Journal of Materials in Civil Engineering*, 1999, 11(3): 206-213.
- [6] European Tyre Recycling Association (ETRA), <http://www.etra-eu.org/joomla/projects>, 2016.
- [7] Gagg, Colin (2014), "Cement and concrete as an engineering material: An historic appraisal and case study analysis", *Engineering Failure Analysis* 40, 114-140.
- [8] Sealy, Cordelia (2018), "Nanoscale order brings flexibility to concrete", *Nano Today* 18(2018)1–7.
- [9] Elchalakani, M. (2015), "High strength rubberized concrete containing silica fume for the construction of sustainable road side barriers", *Structures* 1 (2015) 20–38.
- [10] Khalil, E., Abd-Elmohsen, M. & Anwar, A. M., (2015), "Impact Resistance of Rubberized Self-Compacting Concrete", *Water Science* 29 (2015) 45-53.
- [11] Raffoul, S., Garcia, R., Pilakoutas, K., Guadagnini, M. & Medina, N. F. (2016), "Optimisation of rubberised concrete with high rubber content: An experimental investigation", *Construction and Building Materials* 124 (2016) 391-404.
- [12] Younis, K. H. & Pilakoutas, K. (2013), "Strength prediction model and methods for improving recycled aggregate concrete", *Construction and Building Materials* 49 (2013) 688-701.
- [13] Bignozzi, M. C. & Sandrolini, F. (2006), "Tyre rubber waste recycling in self-compacting concrete", *Cem. Concr. Res.* 36 (4) (2006) 735–739.
- [14] Benazzouk A., Douzane, O., Langlet T., Mezreb K., Roucoult J. M. & Quéneudec M. (2007), "Physico-mechanical properties and water absorption of cement composite containing shredded rubber wastes", *Cem. Concr. Compos.* 29 (10) (2007) 732– 740.
- [15] Alsaif, A., Koutas, L., Bernal, S. A., Guadagnini, M. & Pilakoutas, K. (2018), "Mechanical performance of steel fibre reinforced rubberised concrete for flexible concrete pavements", *Construction and Building Materials* 172 (2018) 533-543.
- [16] Rubber Products Ltd (2016), "NRG Presentation 2016", <https://www.rubber-products.net>
- [17] Tlemat, H., Pilakoutas, K. & Neocleous, K. (2006), "Stress-strain characteristics of SFRC using recycled fibres", *Materials and Structures* 39 (3):365-377, 2006.
- [18] Baricevic, Ana & Bjegović, Dubravka & Skazlic, Marijan. (2017). Hybrid Fiber-Reinforced Concrete with Unsorted Recycled-Tire Steel Fibers. *Journal of Materials in Civil Engineering*. 29. 06017005. 10.1061/(ASCE)MT.1943-5533.0001906.
- [19] Hu H, Papastergiou P, Angelakopoulos H, Guadagnini M & Pilakoutas K (2018), "Mechanical properties of SFRC using blended Recycled Tyre Steel Cords (RTSC) and Recycled Tyre Steel Fibres (RTSF)", *Construction and Building Materials*, 187, 553-564.
- [20] Angelakopoulos H. & Waldron P., "TWINCLETOES-Tyre Wire in Concrete Leading to Environmental Sustainability", Layman's report, Twincon Ltd, Sheffield, UK (2015).
- [21] Graeff AG, Pilakoutas K, Neocleous K & Peres MVNN (2012), "Fatigue resistance and cracking mechanism of concrete pavements reinforced with recycled steel fibres recovered from post-consumer tyres", *Engineering Structures*, 45, 385-395.
- [22] Twincon Ltd., (2018), "Technical Data Sheet - Product: RTSF", www.twincon.co.uk.
- [23] Pilakoutas, K. (2016), "Mechanical behaviour of steel fibre-reinforced rubberized concrete: preliminary results of the FP7 Anagennisi project, Personal Communication, June 2016, Limassol, Cyprus".

EXPERIMENTAL INVESTIGATION OF CORRODED STEEL ANCHORAGES IN STRAIN RESILIENT CEMENTITIOUS COMPOSITES

Souzana P. Tastani (1), Christos Dakidis (1)

(1) Department of Civil Engineering, Democritus University of Thrace, Greece

Abstract

In reinforced concrete, corrosion of steel results in rust of higher volume as per the consumed metal. When exceeding a certain amount of concentration, rust generates bursting pressure to concrete cover in a similar manner to the radial bond component. In the case of a corroded anchorage, both rust and bond radial pressures are balanced by concrete cover hoop tension. Given the brittleness of concrete in tension, the exhaustion of its tensile strength results in abrupt cover spitting associated with bond strength deterioration. Strain resilient cementitious composites (SRCC) would be a promising alternative in delaying corrosion due to the control against crack initiation and widening provided by the dense fiber network. In this paper bond of corroded reinforcement in SRCC is experimentally investigated by considering short anchorages ($5D_b$, bar diameter $D_b=10\text{mm}$), developed in the shear span and in the tension zone of a four-point bending beam. Of the nine specimens, five were made from SRCC and four were casted as reference (same particle composition but without fibers). From both batches some specimens were subjected to accelerated corrosion and the rest were left uncorroded (control). The experimental results are assessed in terms of corrosion (rate and induced damage) and mechanical response.

Keywords: bond – slip, steel corrosion, strain resilient cementitious composites

1. INTRODUCTION

Steel corrosion of a reinforced concrete (r.c.) member may be critical for its structural integrity and mechanical response (i.e. under lateral sway) when exceeds certain limits of steel mass loss; by causing bar area loss, attenuation of bar rib profile, reduction of steel strain development capacity (embrittlement due to pitting) and concrete cover cracking, corrosion may alter the design hierarchy of failure modes. This is because the losses in strength and deformation are different among the response mechanisms (flexure, shear, anchorage, [1]).

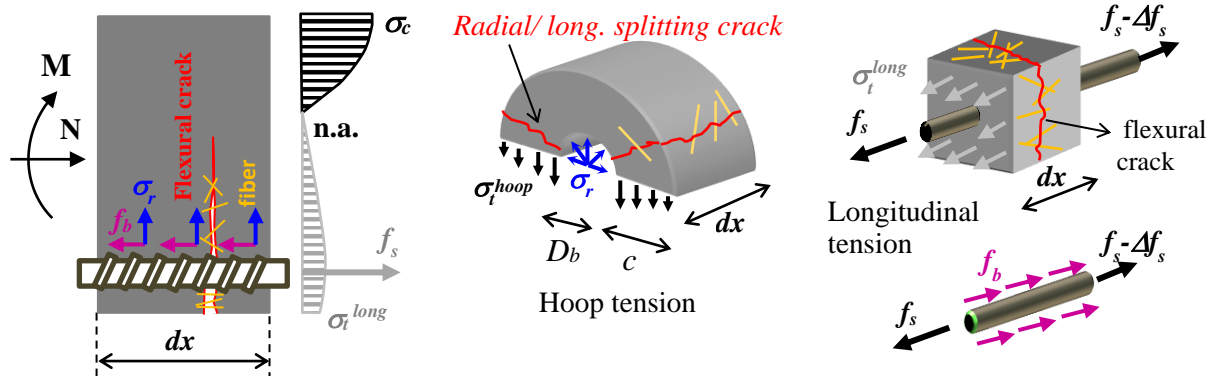


Figure 1. Tensile stresses in concrete generated by bond and flexure

In the case of corroded anchorages / splices developed in the tension zone of flexural members, bond is severely affected resulting in a less stiff response of the member, followed by premature failure [2,3]. This is because both corrosion and bond rely on the concrete cover tensile strength. Steel depletion due to corrosion results in formation of rust products which have multiple volumes as per the parent metal. When rust concentration can't any longer be accommodated in the available concrete porous space around the bar, it generates radial pressure to concrete cover. In a similar manner, stress transfer between reinforcing bar and concrete is engaged through rib translation and comprises longitudinal bond stresses f_b and radial pressure σ_r (Fig. 1). Both corrosion and bond radial pressures are balanced by hoop tension σ_i^{hoop} undertaken by concrete cover (i.e., transverse equilibrium results to $\sigma_r D_b = 2c \sigma_i^{hoop}$ where D_b = bar diameter and c = cover thickness). Given the brittle nature of concrete in tension along with its negligible deformation capacity, the quick exhaustion of the tensile strength will result in abrupt cover spitting associated with commensurate reduction of bond strength; the latter would be further degraded by the unhindered ingress of corrosive agents resulting in ribs elimination. This dual effect is well described by the frictional concept for estimating bond strength, $f_b = \mu_{fr} \sigma_r$: both deteriorations of σ_r and frictional coefficient μ_{fr} (which accounts on the fib profile), results in poor bond resistance.

Given that pressure σ_r is balanced by σ_i^{hoop} , a surrounding media of improved tensile behavior (strength sustained in a wide range of resilient deformation) should be considered as a measure to protect bond mechanism attached by steel corrosion in delaying crack initiation and widening. Such media may be engineered-designed cementitious composites of high volume, randomly distributed short plastic fibers (widely known as ECCs by V. Li) with stable cracking behavior. Maalej et al. [4] tested corroded r.c. beams made by ordinary concrete except of the region around the tensile reinforcement where a hybrid ECC (steel and PVA) was used (as a reference, they also tested specimens made exclusively by ordinary concrete). They noticed that for a predefined corrosion lever the hybrid specimens needed more time (thus they developed a slower corrosion rate) than those made by o.c. The mechanical testing revealed that, given the same corrosion level, losses of strength and deformation capacity were smaller in the case of the hybrid beams. Smaller loss of deformation capacity indicates a better bond performance of the corroded reinforcement if it is embedded in ECC. Nguyen et al. [5] reported that propagation of corrosion-induced

splitting cracking is slower in ECC resulting in less steel mass loss as compared to ordinary concrete, whereas flexural stiffness of ECC specimens is not affected.

Deformation capacity and stiffness of corroded structural members are both controlled by local bond – slip relation between bar and surrounding media [1]. While there is abundance of data for local bond of corroded bars in concrete, the relevant studies where the media is an ECC are still limited. Hou et al. [6] conducted standard pullout of corroded bars embedded in ECC. Three short embedded lengths and three predefined corrosion levels were chosen as main variables of the experimental program. Even corroded, the ECC to bar local bond – slip law a) sustained a wide plateau at strength attributed to the confinement provided by the fibers, b) sustained or even increase its toughness (energy stored). Noticeable was that for steel mass loss lower than 10% some of the above indices were unaltered or even improved. However, by adopting the standard pullout test in investigating bond, both bond strength and the shape of the bond – slip curve are enhanced by the confinement introduced by the support. To this end the extracted bond – slip law from standard pullout is not representative to the adverse conditions that occur in anchorages developed in the shear span and in tension zone of flexural members [7]. This paper aims to experimentally contribute in understanding local bond of corroded steel bars developed in ECC media under adverse tensile stress conditions.

2. EXPERIMENTAL PROGRAM

2.1 Materials: composition and properties

The strain resilient cementitious composite (SRCC) used in the present study is a class of ECCs, by following the design philosophy in terms of grain fineness of mixing materials and the high dosage of plastic fibers. However, its flexural response, after first cracking, follows a wide parabolic shape sustaining adequate tensile strength up to high levels of deformation, in where material's deformation is concentrated near a limited number of cracks emanating from the low stiffness and the bond conditions of the polypropylene fibers. Its composition (per weight) contains: one part of Cement CEM I 52.5N, three parts of Greek calcareous fly ash (with sum of SiO_2 , Al_2O_3 and Fe_2O_3 around 44%, CaO 40% and CaO_f 14%, a by-product of a lignite-combustion power plant), 1.1 parts of dried silica sand (100% passage from sieve of size 0.4mm), 1.47 parts water [the effective water to binder ratio is $1.47/(1+3)=0.37$], superplasticizer as 7% of binder weight (by SIKA, Viscocrete Ultra 200) and 2% per volume PP fibers (by ThracePlastics, TMIX-12: $d_f=25\mu\text{m}$, $\ell_f=12\text{mm}$, $f_{fu}=400\text{MPa}$, $E_f\approx 2\text{GPa}$, $\varepsilon_{fu}=0.25$,

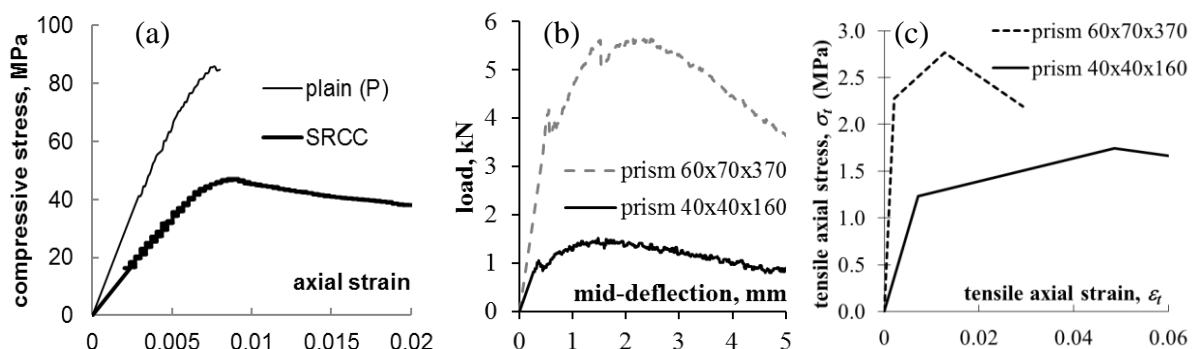


Figure 2. SRCC properties: a) compression, b) flexural tension (prisms 40x40x160 in 3-point bending with clear span 140mm and prisms 60x70x370 in 4-point bending with clear span 340mm, shear span 120mm) and c) axial tension from inverse analysis of data from (b).

$\rho_f=0.91\text{gr/cm}^3$). A plain matrix without fibers was also used as reference (superplasticizer used: 2% of binder weight). The SRCC mechanical properties are shown in Fig. 2 and were measured at the age of testing of the structural specimens (curing period in chamber: 28 days). The fracture energy of the SRCC (the area under the load-deflection curve divided by the cross section area of prism $40\times 40\times 160$) is extremely high as compared to the value of the reference matrix ($G_f^{SRCC}=2000\text{Nt}\cdot\text{m}^{-1}$ and $G_f^{ref}=70\text{Nt}\cdot\text{m}^{-1}$). The reinforcing bars used had diameter $D_b=10\text{mm}$ and nominal yielding stress $f_{sy}=500\text{MPa}$.

2.2 Structural specimens and corrosion results

The experimental program comprised nine small beams (width \times height \times length, $100\times 80\times 480$ in mm) in four-point bending, where short anchorages of length $L_b=5D_b$ were developed in the end region of one of the shear spans and in the tension zone of the cross section (Fig. 3). In the remaining segment L_s-L_b of that shear span (of length L_s) the reinforcement was covered by sleeve for bond elimination; bond elimination was also assured in the constant moment region. As a result of this configuration the internal tensile bar force at the position $x=L_s$ (and thus at maximum moment $M=QL_s/2$) is fully transmitted to the starting point of the anchorage ($x=L_b$). In the opposite shear span the reinforcement was fully bonded.

Table 1: Specimens configuration and experimental results.

Sp. ID	$\Delta D_b/D_b$ %	Bond strength (MPa)	Failure mode	Sp. ID	$\Delta D_b/D_b$ %	Bond strength (MPa)	Failure mode
cP5D-1*	8.7	10.8	Bond	cF5D-2*	12.5	12.3	Bond
cP5D-2	10.5	11.2	Bond	cF5D-3	17.9	14.3	Bond
P5D-3	0	10.4	Bond	cF5D-4	12.5	---	Shear
P5D-4	0	9.2	Bond	F5D-1	0	10.1	Bond
* P for plain and F for SRCC matrix, iD: 5 or 10 times the D_b as L_b , c for corroded specimens.				F5D-5	0	8.7	Bond

Five specimens were casted with SRCC and four with the reference mix (plain, without fibers). Configuration details and explanation of specimens code name are given in Table 1. All specimens were cured in chamber for 28 days and then left in room conditions during summer (4 months). After 5 months from casting and before any preparation most of the specimens had developed a transverse crack in the constant moment region and one near the

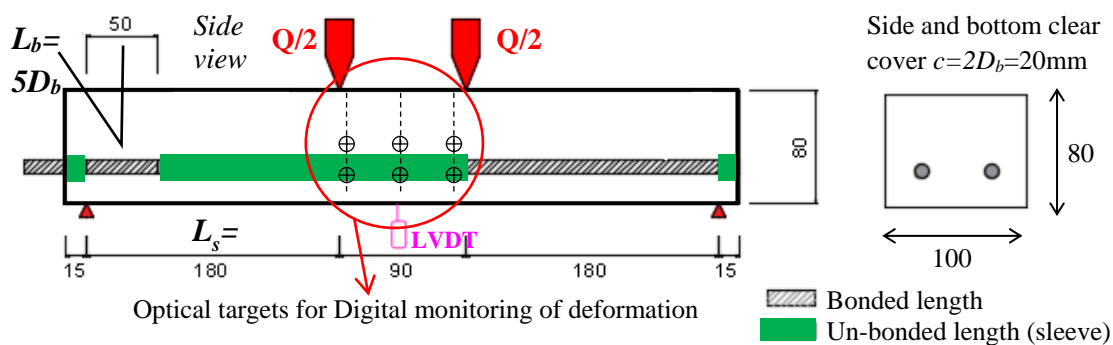


Figure 3. Beam geometry (in mm), detailing and test setup

starting point of the studied anchorage, both extended up to the position of reinforcement, as a result of restrained drying shrinkage. For those specimens that were to be connected to the accelerated electrochemical corrosion cell (denoted by letter c, Table 1), a special preparation measure was preceded; the bottom and the two sides were covered by an impenetrable resin (SIKADUR 330) leaving only the study region free to corrode (Fig. 4a, [3]). To this end, the shrinkage-induced cracks were sealed whereas only the study region was accessible to corrosion agents (O_2 , Cl^- and H_2O). A schematic depiction of the corrosion cell is shown in Fig. 4b. The corrosion process comprised four-day cycles of exposure (one day of wetting where the NaCl solution was in contact with the bottom surface of the specimen, followed by three days of drying). Records of current were taken every 24 hours.

The rate of steel mass loss $\Delta m/\Delta t$ due to oxidation was calculated following the Faraday's Law (Eq. 1), where A_m is the atomic mass of iron = 55.87grs, I is the current density (Amp), z is the valence of the reaction which is usually taken equal to 2 and F is the Faraday constant = 96486.7Coulombs/mole.

$$\frac{\Delta m}{\Delta t} = \frac{A_m \cdot I}{z \cdot F} = 2.89 \cdot 10^{-4} \cdot I \text{ (in grams/sec)} \quad (1)$$

The total mass loss ΔM_s (in grams) was estimated by integration of the current I passed through both bars of each specimen, where the time interval is 24hours. Assuming that mass loss occurred uniformly along the exposed length L_{exp} of both bars in each specimen [$L_{exp}=2 \cdot (a+L_b)$, see Fig. 3] and using the definition of iron density ($\rho_s = \Delta M_s / \Delta V_s$) it follows:

$$\frac{\Delta M_s}{M_s} = \frac{\Delta A_s}{A_s} \Rightarrow \frac{\Delta A_s}{A_s} = \frac{D_b^2 - D_{b,c}^2}{D_b^2} \approx \frac{2 \cdot (D_b - D_{b,c})}{D_b} \Rightarrow \frac{\Delta D_b}{D_b} = 0.5 \frac{\Delta M_s}{M_s} \quad (2)$$

Equation (2) denotes that the mass loss ratio $\Delta M_s/M_s$ is equal to the cross section area loss ratio $\Delta A_s/A_s$ and double of the bar diameter loss ratio $\Delta D_b/D_b$ ($D_{b,c}$ is the reduced bar diameter due to corrosion). Figure 4c shows the $\Delta D_b/D_b$ evolution during the corrosion process: a) any plateau denotes stop of the process (the current records were negligible), b) the final values of $\Delta D_b/D_b$ are given in Table 1 where for cF5D is near 14.3% (average value) and for cP5D is 9.6%. The difference, given the same duration of corrosion process, could be attributed either

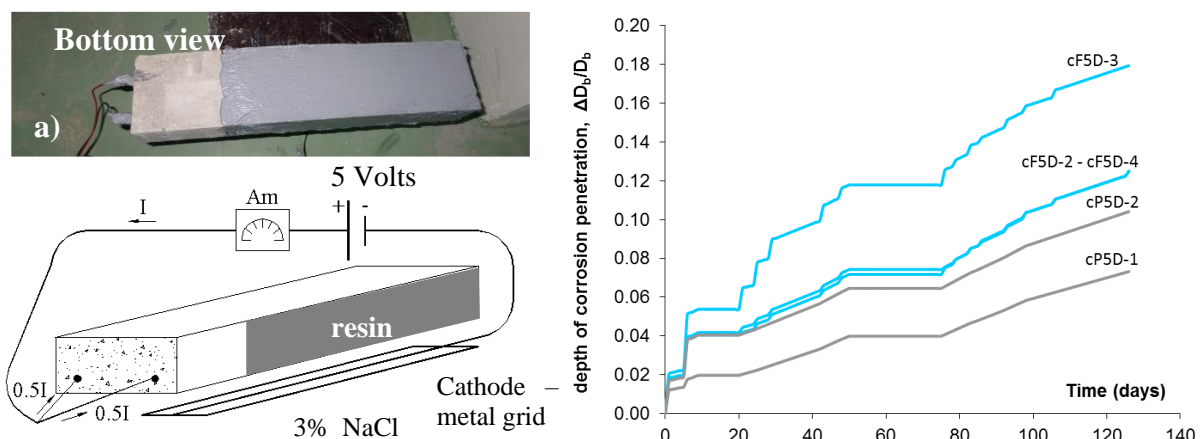


Figure 4. a) Specimen preparation before its connection to the corrosion cell. b) Accelerated electrochemical corrosion cell and c) evolution of corrosion penetration depth with time.

to the position of these specimens in respect to their proximity to the metal grid, or to the different porosity (such measurements are going to be available in near future). Specimens' damage due to corrosion is illustrated in Fig. 5: all specimens developed cracks along the exposed bonded length, more intense were found in the case of cF5D.

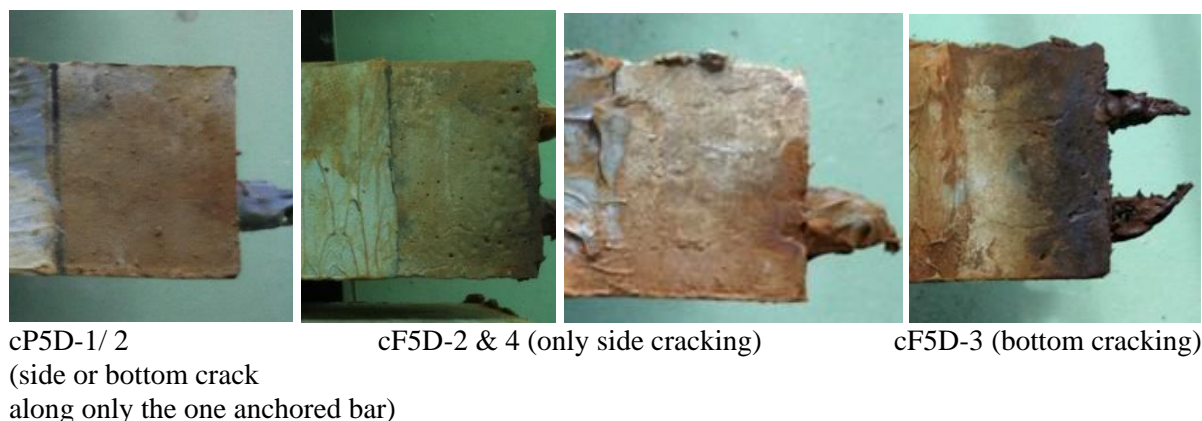


Figure 5. Cracking along the anchorage length due to corrosion of steel reinforcement.

2.3 Loading results – discussion

Figure 6 demonstrates the experimental results from mechanical testing in terms of applied load versus middle deflection curves. All tests were conducted after the end of corrosion process. The green curves correspond to the uncorroded specimens and the black curves to the corroded one; in the latter case the thicker curve corresponds to higher corrosion level. The mode of failure of each specimen is included in Table 1; term “bond” means that the specimen failed in the studied region due to bond by either developing splitting crack (the P-type specimens) or excessive slippage (the F-type specimens), whereas term “shear” corresponds to shear failure in the opposite shear span (where full bond conditions were ensured for the bar). After implementing cross section flexural analysis at bar yielding ($\varepsilon_{sy}=0.0025$) for P-type (plain matrix) and F-type (SRCC matrix) specimens, by also assuming the materials properties of Fig. 2 (i.e., for compression $f_{co/F}=45\text{MPa}$, $\varepsilon_{co/F}=0.008$, $\varepsilon_{cu/F}=0.012$ at $50\%f_{co/F}$, $f_{co/P}=80\text{MPa}$, $\varepsilon_{co/P}=0.008$, for tension $f_{ct,cr/F}=2\text{MPa}$, $\varepsilon_{ct,cr/F}=0.00015$, $f_{ct,u/F}=2.5\text{MPa}$, $\varepsilon_{ct,u/F}=0.02$, $f_{ct,cr/P}=4.5\text{MPa}$, $\varepsilon_{ct,cr/P}=0.00015$), the theoretically applied loads are calculated as $Q_{P,y} \approx 38\text{kN}$ and $Q_{F,y} \approx 41\text{kN}$. None of the specimens (corroded or control) reached such load level. Some interesting findings from the mechanical testing are:

- the corroded specimens of both matrices developed higher strength than the control; a possible explanation is that in the presence of moisture during corrosion the matrices were further hydrated (pozzolanic action); the F-type matrix was most influenced suggesting that the interfacial fiber-to-matrix bond was improved during corrosion (time-dependent effect).
- by comparing the F and P-type control specimens (green curves) that developed bond failure (pullout and splitting respectively), apparently the addition of PP fibers resulted in an impressive increase of displacement ductility and energy stored in the system (the area under the curves). The ductile response of all the F-type bond tests under sustained load (i.e. with no loss of load carrying capacity), is not a result of bar yielding but it is owing to controlled sliding of the bar from its surroundings due to the confinement provided by PP fibers.

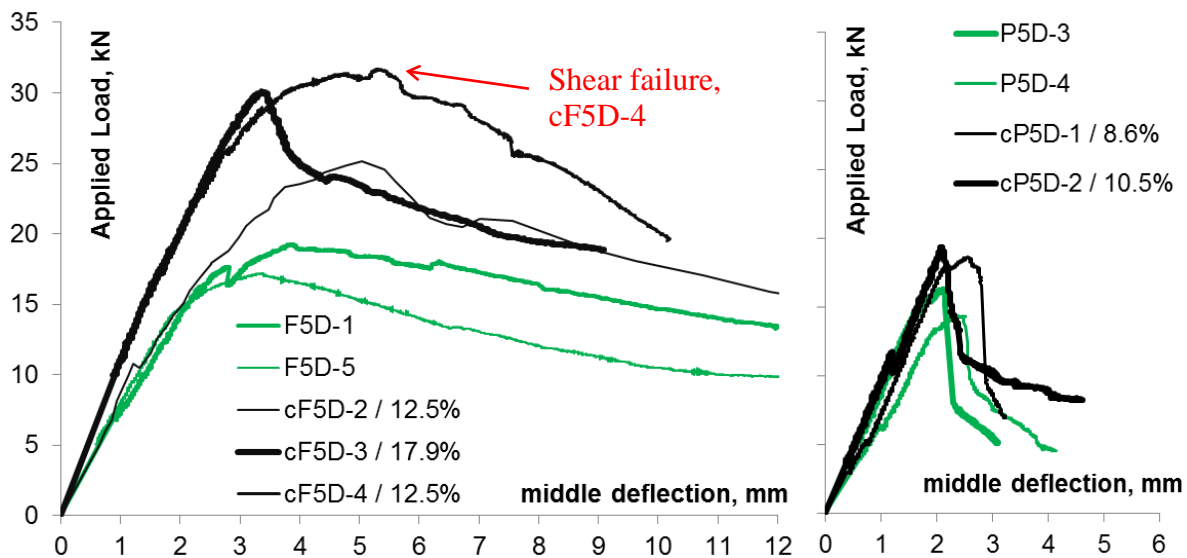


Figure 6. Load – middle deflection responses of corroded (black) and control (green) specimens (for comparison the axes scaling is identical).

c) by comparing the F-type control and corroded specimens (excluding the cF5D-4 test that failed due to shear), it seems that corrosion impaired bar-to-matrix bond resulting in a post-strength steeper response; the accommodated around the bar loose rust products, even if they are confined, after a certain magnitude of bar slip deteriorate the frictional coefficient μ_{fr} resulting in almost instant drop of load.

d) by implementing inverse cross section analysis at the attained applied peak load Q_{max} of F-type and P-type specimens, the associated bar strain ε_s at critical cross section (region of constant moment) may be approximated; given that the bar tensile force F_s is fully transmitted to the initiation point of anchorage (presence of the sleeve) and that the peak load Q_{max} is always lower than the yielding value Q_y (thus $\varepsilon_s < \varepsilon_{sy} = 0.0025$), then the bond strength may be approximated assuming uniform distribution along L_b at this ultimate stage: $f_b^{max} = (D_b E_s) / (4 L_b) \cdot \varepsilon_s$, where $E_s = 200 \text{ GPa}$. In the case of corroded specimens, where D_b is replaced by $D_{b,c}$. In Table 1 are given the f_b^{max} values for all specimens that failed due to bond. Even if f_b^{max} for all the control specimens are of similar magnitude, however the bond toughness of the F-type specimens as compared with the P-type is apparently much higher (the slip values will be extracted from the load-deflection curves in a future work). In the case of the corroded specimens, even if the F-type suffered higher degree of bar loss, they developed higher bond strength in comparison with the P-type specimens.

CONCLUSIONS

In this paper bond of corroded reinforcement in SRCC and reference matrix (without fibers) is experimentally investigated. Short anchorages developed in the shear span and in the tension zone of a four-point bending prism, were subjected to accelerated electrochemical corrosion until cover cracking. Some specimens were left in pristine conditions for comparison. From the mechanical testing and for the achieved corrosion levels, bond wasn't deteriorated, probably due to continuous hydration of the matrices. In the case of F-type specimens, the loose nature of rust induced a more abrupt strength deterioration. Further analysis of the

experimental data is required aiming to assess the full bond – slip responses of the P and F type specimens (in both conditions, corroded and control).

REFERENCES

- [1] Tastani, S., Pantazopoulou, S., ‘Recovery of seismic resistance in corrosion-damaged reinforced concrete through FRP Jacketing’, *Int. J. of Materials and Product Technology*, **23** (3/4) (2005) 389 - 415.
- [2] Goksu, C., Ilki, A., ‘Seismic Behavior of Reinforced Concrete Columns with Corroded Deformed Reinforcing Bars’, *ACI Structural Journal*, **113** (5) (2016) 1053-1064
- [3] Pantazopoulou, S., Petrou, M., Spatri, V., Archontas, N., Christofides, C., ‘The performance of corroded lap splices in reinforced concrete beams’, *Corrosion Reviews*, (2018), doi:10.1515/corrrev-2017-0086
- [4] Maalej, M., Ahmed S.F.U, Paramasivam P., ‘Corrosion Durability and Structural Response of Functional Graded Concrete Beams’, *J. Advanced Concrete Technology*, **1** (3) (2003) 307-316
- [5] Nguyen, W., Duncan, J., Jen, G., Ostertag, C., ‘Influence of matrix cracking and hybrid fiber reinforcement on the corrosion initiation and propagation behaviors of reinforced concrete’, *Elsevier Corrosion Science*, **140**, (2018) 168-181.
- [6] Hou, L., Liu, H., Xu, S., Zhuang, N., Chen, D. ‘Effect of corrosion on bond behaviors of rebar embedded in ultra-high toughness cementitious composite’, *Elsevier, Construction and Building Materials*, 138 (2017) 141-150.
- [7] Tastani, S., and Pantazopoulou, S., ‘Experimental evaluation of the direct tension-pullout bond test’, in ‘*3rd Symposium on Bond in Concrete – From research to Standards*’, Proceedings of an int. Conference, Budapest, November, 2002, 268-276.

NEW GENERATION OF CONSTRUCTION MATERIALS
SESSION 6: Trends in aggregate

EARLY-AGE EVOLUTION OF RECYCLED CONCRETE STRENGTH: INSIGHTS FROM MICROMECHANICS MODELING AND EXPERIMENTAL TESTING

Markus Königsberger, Brice Delsaute and Stéphanie Staquet

BATir Department, ULB – Université libre de Bruxelles, Belgium

Abstract

Recycled concrete, i.e. concrete which contains aggregates that are obtained from crushing waste concrete, exhibits reduced stiffness and strength as compared to virgin concrete. Micromechanics-based multiscale modeling techniques are used to study the origin and quantify the extent of the reduction of mechanical properties. Therefore, recycled aggregates are divided into three morphology classes: plain aggregates (without old cement paste), mortar aggregates (mixture of old sand and old cement paste), and aggregates entirely covered by old cement paste. Stress concentrations in interfacial transition zones (ITZs), which occur mutually between aggregates, old paste, and new paste, are quantified and allow for bottom-up strength predictions. Modeled strength evolutions are compared to novel data from an ongoing testing campaign performed at ULB as well as to experimental data available in the literature. The study shows that critical ITZs in recycled concrete are much weaker than their counterparts in ordinary concrete and that the ratio of ITZ porosity to bulk porosity of the new cement paste decreases with increasing water-to-cement ratio. This suggests that the amount of water transferred through the ITZ is responsible for the ITZ weakening.

Keywords: recycled concrete; micromechanics; multiscale modeling; interfacial transition zone; early age

1. INTRODUCTION

Recycled concrete, i.e. concrete which aggregates are produced by crushing waste concrete, is still mostly “downcycled” to be used in road sub-base. The use of recycled aggregates instead of virgin aggregates for structural concrete is far less common. The reduction of the mechanical properties of recycled concrete compared to ordinary concrete [1,2] is one of the key aspects which restricts its applicability, and which restrains recycled concrete to become widely accepted as a sustainable alternative for structural purposes. Indeed, the interplay between old paste, new paste, and (old and new) aggregates potentially results in additional stiffness

gradients in the microstructure of recycled concretes. This might lead to unfavorable stress concentration which ultimately lead to smaller compressive strengths.

The origin of the strength reduction has been recently studied by means of a micromechanical multiscale model [3,4], which is here revisited, see Section 2. Therein, the microstructure of recycled concrete is resolved all the way down to micrometer-large scales where capillary pores and hydration products are distinguished. The volumes of these material phases, as function of the hydration degree and water-to-cement ratio, are predicted by means of Powers' hydration model [10]. The model is then evaluated for recycled concrete mixes recently tested at the Civil Engineering Laboratory at ULB and for data from the literature, which allows us to compare modeled and experimentally determined strength evolutions (see Section 3). The paper is closed with conclusions and perspectives (Section 4).

2. MICROMECHANICAL MULTISCALE MODEL

Herein, we shortly summarize the model developed in Reference [3]. To represent the rather complex aggregate morphology in recycled concrete within a continuum micromechanical framework, three different recycled aggregates families are considered: (I) plain aggregates free of attached (new or old) paste or mortar, (II) old mortar aggregates which consist – at a smaller observation scale – of aggregates embedded in an old cement paste matrix, and (III) old aggregates covered by a layer of old cement paste, see Fig. 1. All aggregates are considered as spherical phases and we consider that all three classes are represented equally in terms of their volume fractions. Moreover, we consider that recycled aggregates consist of 35% of old cement paste volume and 65% of aggregates. At the millimeter scale, the old and new cement paste are built up by spherical unhydrated clinker grains, by spherical filler particles (such as limestone filler), and by a “hydrate foam” matrix. At the micrometer scale, the hydrate foam, in turn, is built up by elongated hydration products and capillary pores. This representation follows the extensively validated micromechanical model of Pichler and Hellmich [5]. Interfacial transition zones (ITZs) occur mutually between old/new aggregates and old/new cement paste. The ITZs are represented as two-dimensional, perfectly bonded interfaces at the scale of concrete and mortar, their three-dimensional nature is resolved only at the cement paste and hydrate foam scales, respectively, as it was done in [6,7].

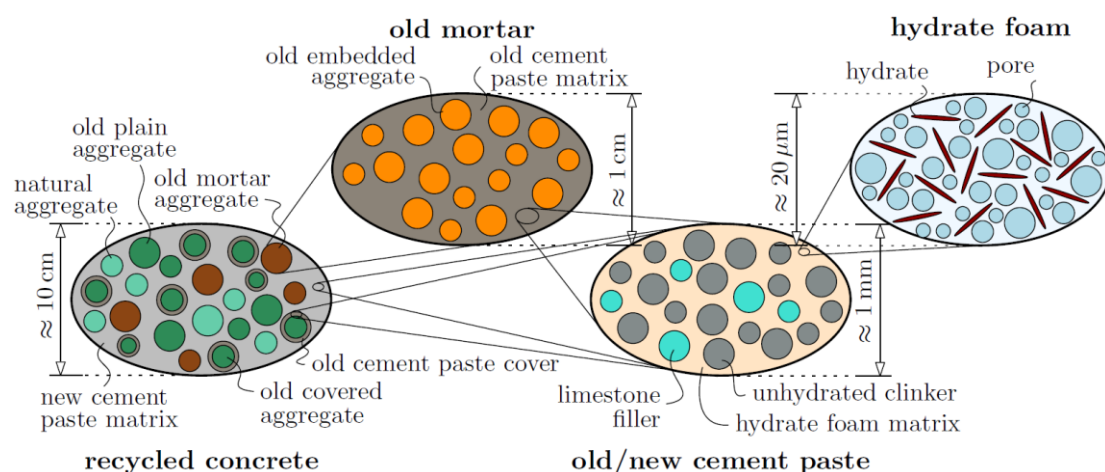


Figure 1: Hierarchical micromechanical representation of recycled concrete across four observation scales from [3].

The macroscopic elastic stiffness is obtained by mean-field homogenization techniques to upscale the phase stiffness of all constituents to the macroscopic (“homogenized”) stiffness of concrete. Thereby, we consider the self-consistent scheme for homogenization of the polycrystalline hydrate foam, and the Mori-Tanaka scheme for homogenization of the other three matrix-inclusion-type volume elements. Elastic phase properties of hydrates, pores, limestone filler, unhydrated cement clinker and (old and new) aggregates are given in Table 1.

Table 1: Isotropic elasticity constants of material phases according to [8]

	Bulk modulus [GPa]	Shear modulus [GPa]
Hydrates	18.69	11.76
Pores	0	0
Cement clinker	116.6	53.81
Filler	67.19	29.24
Aggregates (old and new)	35.35	29.91

Strength upscaling is based on a brittle failure upscaling approach, which has been successfully validated for cement paste [5] as well as for mortar/concrete [8]. Thereby, failure of the most unfavorably loaded hydration product, located in the most unfavorable ITZs, is considered to trigger concrete failure at the macroscale [8]. The hydrate failure itself is quantified by means of a Drucker-Prager failure criterion involving universal (age- and composition- independent) Drucker-Prager constants which were identified from nanoindentation tests combined with limit state analysis [9].

We aim for predicting the *evolution* of macroscopic mechanical properties of recycled concrete based on *universal* microscopic mechanical phase properties, by changing the phases’ volume fractions. Quantitative access to the phase volumes of the new cement paste is provided by Powers’ hydration model [10]. Phase volumes of the new cement paste are given as function of the water-to-cement ratio w/c_{ncp} and of the hydration degree ξ_{ncp} , i.e. the ratio of already reacted to initially available cement clinker mass. The Powers’ model is also used for predicting the (hydration degree-independent) old cement paste volume fractions, whereby we estimate $w/c_{ocp} = 0.5$ and $\xi_{ocp} = 1$. The ITZs between aggregates (whether new or old) and the new cement paste matrix are considered to be identical to the bulk of the new cement paste. By analogy, the ITZs between aggregates and the old cement paste matrix are considered to be identical to the old cement paste matrix. The ITZs between old and new cement paste, however, are potentially influenced by water migration processes [11]. Initially, mixing water might be absorbed by the old cement paste. During the (water-consuming) hydration process of the new cement paste, the absorbed water in the old cement paste, in turn, might be soaked back to the new cement paste matrix, commonly referred to as internal curing. It has been shown by several experimenters that the associated segregation effects due to the water transfer mechanisms might result in relatively porous, and therefore mechanically weak ITZs [12,13,14]. As for modeling, we phenomenologically increase the ITZ porosity between old and new cement paste by means of the factor $F_{por} > 1$, defined as the ratio between the porosity of the weak ITZs and the porosity of the new cement paste [3].

3. COMPARISON TO EXPERIMENTAL DATA

Herein, modeled strength evolutions are compared to experimental strength results from two testing campaigns. First, we report here on novel strength test and calorimetry results of a comprehensive early-age testing campaign on recycled concrete, carried out at ULB. Ordinary and recycled concrete (by replacing 100% of natural coarse aggregates with recycled coarse aggregates) were tested, denoted OC and RC in the following. The aggregates were pre-saturated. Cement CEM II/A-L 42.5N was used together with different fillers, water at w/c ratios of 0.76 (not including the water inside the saturated aggregates) and superplasticizer for the new cement paste. As for more details on the composition see Reference [15]. Strength tests were performed at approximately 24h, 30h, 2d, 4d and 7d (RC only) on cube of 10 cm side and combined with continuous quasi-adiabatic calorimetry monitoring [18] on cylinder with a diameter of 16 cm and a height of 32 cm, to deliver strength evolutions as function of the hydration degree.

Another experimental campaign combining strength and hydration degree measurement was performed from Koenders et al. [16]. Four different recycled concrete mixes were studied, whereby 30% natural aggregates were replaced by recycled aggregates, with either oven-dried or pre-saturated coarse aggregates. Cement CEM I 42.5R was used together with water at w/c ratios of 0.45 and 0.60 (not including the water inside the saturated aggregates) for the new cement paste. Compressive strength tests were carried out on concrete cubes, stored under isothermal conditions, at ages of 2, 3, 7, 14, and 28 days. The hydration process was monitored by means of thermocouple measurements inside an isolated concrete cube in semi-adiabatic conditions. By comparing the temporal evolution of measured and simulated temperature, hydration degrees of the isothermally cured samples were estimated.

Evaluating the multiscale strength model for the OC composition tested at ULB shows that model predictions agree reasonably well with experimental data, see Fig. 2(a). This corroborates the predictive nature of the strength model for ordinary concrete, which has been already extensively validated in [8].

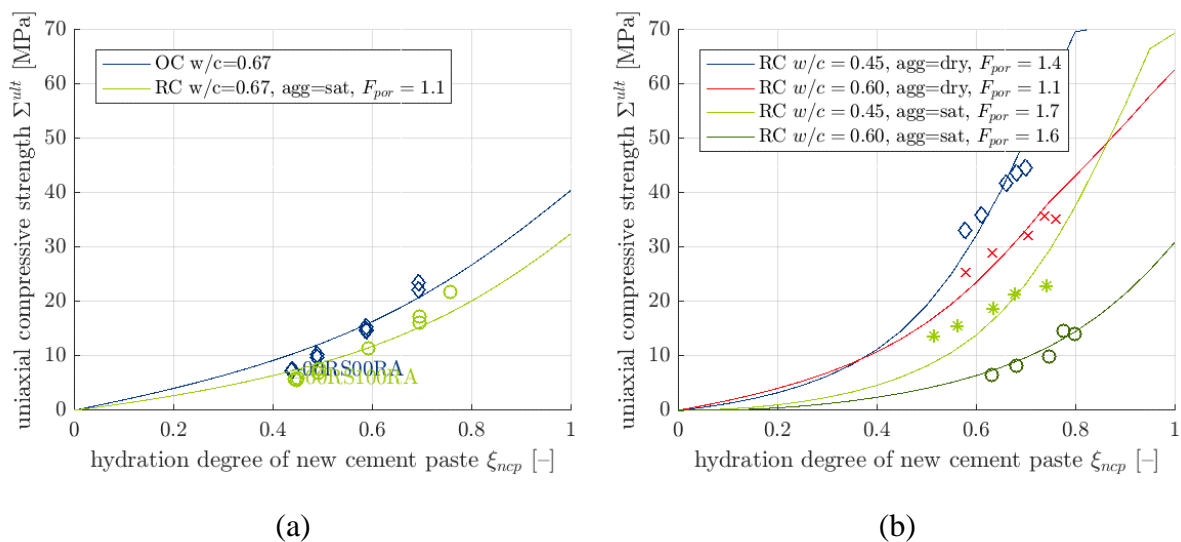


Figure 2: Modeled (lines) and experimentally determined (points) strength evolutions as function of the hydration degree of new cement paste: (a) novel tests from ULB; (b) tests from Koenders et al. [16]

As for the recycled concretes tested at ULB, see Fig. 2(a), and by Koenders et al. [16], see Fig. 2(b), we test whether the experimentally observed strength evolution can be modeled by means of a test-specific but age-independent ITZ porosity factor F_{por} . The model is therefore evaluated for the grid points $F_{por} \in \{1, 1.1, \dots, 2\}$ and the best fit is plotted in Fig. 2. For all mixes, the agreement between model results and experimental data is best when considering a weakened ITZ between old and new cement paste. This demonstrates that the ITZs around recycled aggregates are indeed considerably weaker than the adjacent new cement paste. Notably, this is in contrast to ordinary concrete (see OC results in Fig. 2(a) and the validated results of [8]), where ITZ and bulk paste were considered identical. The strength decrease observed in the ULB study of approximately 20-25% is best reproduced when considering that the old-new paste ITZ is 10% more porous than the bulk of the new paste ($F_{por} = 1.1$). Notably, the recycled concrete aggregates were pre-saturated, and the water-to-cement ratio of the new paste was very high ($w/c_{ncp} = 0.76$). As for the recycled concrete with saturated aggregates tested by Koenders et al. [16], the best fit is obtained for $F_{por} = 1.7$ for $w/c_{ncp} = 0.45$ and $F_{por} = 1.6$ for $w/c_{ncp} = 0.60$. This way, the model suggests that the old-new paste ITZ around saturated recycled aggregates is weakened more considerably, when the w/c ratio of the new cement is reduced. The latter very likely involves a more pronounced water transfer, given that low-w/c pastes develop a more pronounced capillary depression.

In case of dry recycled aggregates, the recycled concrete strength is shown to increase significantly, as compared to the saturated case [16]. The dry aggregates absorb part of the mixing water, thereby reducing the effective w/c in the cement paste. As for the modeling, we consider that the water available for hydration is equal to the added water minus the water adsorbed from the aggregates in the saturated case, and that the related effective w/c ratio is constant (no internal curing). The resulting strength evolutions exhibit kinks at high hydration degrees, due to a failure mode change, see [3] for a detailed discussion on which ITZ triggers macroscopic failure.

The best agreement of modeled and experimentally determined strength evolutions is obtained for ITZ porosity ratios of $F_{por} = 1.4$ for $w/c_{ncp} = 0.45$ and $F_{por} = 1.1$ for $w/c_{ncp} = 0.60$. Thus, the model suggests that the old-new paste ITZs around dry recycled aggregates are much less weakened than the corresponding ITZs around saturated aggregates. This could be explained, yet again, by segregation due to water transfer phenomena. It is likely that the dry recycled aggregates cannot fill up their porosity entirely with mixing water given that the new cement paste starts to stiffen already, similar observations have been made for lightweight aggregates [17]. This way, also less water would be back-transferred to the hydrating paste and thus less segregation would occur. We note that a more in-depth study of the consequences of different extents of water absorption by dry aggregates goes beyond the scope of the paper. If aggregates do not fully saturate within fresh concrete, then the modeled strength evolutions would be considerably smaller since more water (more porosity) remains in the new cement paste. This, in turn, would lead to even smaller porosity ratios, potentially even to $F_{por} < 1$, i.e. improved ITZs.

Finally, we discuss the assumption that porosity ratios F_{por} are independent of the material age. In other words, we disregard local hydration in the ITZs, since their porosity is always proportional to the porosity of the bulk paste. One might however speculate that the porosities of ITZs and bulk paste evolve in a significantly different manner during hydration, given the continuous nature of the internal curing process. We note that the model results with constant

F_{por} typically underestimate the first experimental points (obtained after 2d) while they overestimate the last experimental points (obtained after 28 days), see Fig. 2(b). The agreement would be improved if ITZ-to-bulk porosity ratios were increasing during hydration.

4. CONCLUSIONS AND PERSPECTIVES

We herein apply a recently developed micromechanics multiscale model [3] to quantify the strength evolution of recycled concrete from early up to mature ages. By comparing the model results to experimental campaigns, we obtain the following conclusions:

- The ITZs between old and new cement paste around recycled aggregates are weaker than in the adjacent new cement paste. This contrasts the results of the extensively validated strength model for ordinary concrete [3], for which ITZs and bulk paste are considered to exhibit identical porosities.
- The ratio of ITZ porosity (between old and new paste) to bulk porosity (of the new paste) decreases as the w/c ratio of the new paste increases. In other words, the ITZs around recycled aggregates are less weakened in high w/c pastes. This might be explained by segregation effects due to water transfer between recycled aggregates and hydrating new cement paste. The amount of water transferred through the ITZ decreases with increasing w/c ratio, given that the capillary depression (and thus the driving force for water transfer) considerably decreases with increasing w/c ratio.
- Considering effective w/c ratios corresponding to the absorption potential of recycled aggregates cannot explain the experimentally observed, significant strength reduction in case pre-saturated rather than dry recycled aggregates are used. This shows that the ratio between the porosity of the ITZs and the bulk cement paste is inherently different when recycled aggregates are pre-saturated.

Given the microstructural complexity of the recycled concrete, predictive micromechanical modeling is still out of reach. Water migration and therefore segregation effects between old and new cement paste (adsorption of mixing water and internal curing, respectively) are crucial for the mechanical properties of ITZs. This is important for understanding and predicting the strength behavior of recycled concrete (and its temporal evolution) since even small changes of the ITZ's porosity might lead to very significant macrostrength reductions. Future research, both modeling and experimental work, should focus on quantifying the water migration processes and the related effects for the ITZ microstructure.

REFERENCES

- [1] K. Rahal, "Mechanical properties of concrete with recycled coarse aggregate," *Building and Environment*, **42**(1):407-415, 2007.
- [2] M. C. Limbachiya, T. Leelawat and R. K. Dhir, "Use of recycled concrete aggregate in high-strength concrete," *Materials and Structures*, **33**:574, 2000.
- [3] M. Königsberger and S. Staquet, "Micromechanical Multiscale Modeling of ITZ-driven Failure of Recycled Concrete: Effects of Composition and Maturity on the Material Strength," *Applied Sciences*, **8**(6):976, 2018.
- [4] M. Königsberger and S. Staquet, "Early-age evolution of elastic stiffness and compressive strength of recycled concrete: insights from multiscale micromechanics modeling," *Proceedings of the SynerCrete'18 International Conference on Interdisciplinary Approaches for Cement-based Materials and Structural Concrete*, 2018.

- [5] B. Pichler and C. Hellmich, "Upscaling quasi-brittle strength of cement paste and mortar: A multi-scale engineering mechanics model," *Cement and Concrete Research*, vol. 41, no. 5, pp. 467-476, 2011.
- [6] M. Königsberger, B. Pichler and C. Hellmich, "Micromechanics of ITZ-aggregate interaction in concrete - Part I: stress concentration," *Journal of the American Ceramic Society*, **97**(2):535-542, 2014.
- [7] M. Königsberger, B. Pichler and C. Hellmich, "Micromechanics of ITZ-aggregate interaction in concrete - Part II: strength upscaling," *Journal of the American Ceramic Society*, **97**(2): 543-551, 2014.
- [8] M. Königsberger, M. Hlobil, B. Delsaute, S. Staquet, C. Hellmich and B. Pichler, "Hydrate failure in ITZ governs concrete strength: A micro-to-macro validated engineering mechanics model," *Cement and Concrete Research*, **103**:77-94, 2018.
- [9] E. Sarris and G. Constantinides, "Finite element modeling of nanoindentation on C--S--H: Effect of pile-up and contact friction," *Cement and Concrete Composites*, **36**:78-84, 2013.
- [10] Powers, T. C. and Brownyard, T. L. "Studies of the physical properties of hardened Portland cement paste," *ACI Journal Proceedings*, **18**(2-8):101-992, 1946-1947
- [11] C. S. Poon, Z. H. Shui and L. Lam, "Effect of microstructure of ITZ on compressive strength of concrete prepared with recycled aggregates," *Construction and Building Materials*, **18**(6):461-468, 2004.
- [12] M. B. Leite and P. J. M. Monteiro, "Microstructural analysis of recycled concrete using X-ray microtomography," *Cement and Concrete Research*, **81**:38-48, 2016.
- [13] V. W. Y. Tam, X. F. Gao and C. M. Tam, "Microstructural analysis of recycled aggregate concrete produced from two-stage mixing approach," *Cement and Concrete Research*, **35**(6):1195-1203, 2005.
- [14] S. Ismail, W. H. Kwan and M. Ramli, "Mechanical strength and durability properties of concrete containing treated recycled concrete aggregates under different curing conditions," *Construction and Building Materials*, **155**:296-306, 2017.
- [15] A. Z. Bendimerad B. Delsaute, E. Roziere, S. Staquet and A. Loukili, "Advanced techniques for the study of shrinkage-induced cracking of concrete with recycled aggregates at early age," *Construction and Building Materials*, (under Review), 2018.
- [16] E. A. B. Koenders, M. Pepe and E. Martinelli, "Compressive strength and hydration processes of concrete with recycled aggregates," *Cement and Concrete Research*, **56**:203-212, 2014.
- [17] L. Bello, E. Garcia-Diaz and P. Rougeau, "An original test method to assess water absorption/desorption of lightweight aggregates in presence of cement paste," *Construction and Building Materials*, **154**:752-762, 2017.
- [18] C. Boulay, J.M. Torrenti, J. L. Andre, R. Saintilan, "Quasi-adiabatic calorimetry for concretes: Influential factors, Bulletin des Laboratoires des Ponts et Chaussées, 19-36, 2010

THE STUDY ON FUNDAMENTAL PROPERTIES AND SELF-HEALING PERFORMANCE OF CONCRETE USING BELITE-GEHLENITE CLINKER AS FINE AGGREGATE

Fumihiko Watanabe (1), Hiromi Fujiwara (2), Masatoshi Maruoka (2), Shunnosuke Ito (1) and Kensuke Hayashi (3)

- (1) Graduate student in the department of Design and Engineering for the Global environment Utsunomiya University, Japan
- (2) Professor in the Department of Civil Engineering and Regional Design at Utsunomiya University, Japan
- (3) Research leader in the Central Research Laboratory of Taiheiyo Cement Ltd. Co.

Abstract

In Japan, the cement production has been a downward trend from a peak of 99,267 thousand tons in the 1996. Due to the effort of cement companies in Japan, the amount of wastes and by-products used for cement production has been increased. If the cement industry does not accept the wastes and by-products, which is an effective use in order to concentrate the final disposal site, the residual capacities of final disposal site is expected to be approximately 5 and a half years shorter than the estimate.

Therefore, there is a need to promote a recycling-oriented society. The cement industry has been providing basic industrial materials for a recycling-oriented society, as well as recycling the waste and by-products. In order to use wastes effectively, it's necessary to explore new utilization of a cement clinker as fine aggregate.

Belite-Gehlenite clinker is produced from large amounts of recycled industrial waste, such as construction waste soil, sewage sludge, waste clay and coal ash. Raw material used for sintering Belite-Gehlenite clinker is produced by blending and pulverizing a virgin material (limestone, quartzite, etc) with the industrial waste. And it has weak hydration performance in comparison with normal clinker, so it is expected to give self-healing performance of damaged concrete when using this clinker as aggregate.

In this study, the fundamental properties and self-healing performance of concrete using Belite-Gehlenite clinker as fine aggregate were evaluated. Compared to the properties of them using natural sand, it was found that the compressive strength increases and the drying shrinkage decreases. And then self-healing performance was also found.

Keywords: Belite-Gehlenite clinker, fine aggregate, compressive strength, drying shrinkage, self-healing

1. INTRODUCTION

In order to improve the durability of the concrete structure, technologies such as repairing cracks before it become harmful are necessary. However, concrete structures are used in various applications and places, and there are many bridges and large structures. It takes economical, temporal and human costs to repair and inspect these concrete structures.

Belite-Gehlenite clinker (GCL) is produced from large amounts of industrial waste, such as construction waste soil sewage sludge and waste clay. It contains large amounts of Belite ($2\text{CaO} \cdot \text{SiO}_2:\text{C}_2\text{S}$) and Gehlenite ($2\text{CaO} \cdot \text{Al}_2\text{O}_3 \cdot \text{SiO}_2:\text{C}_2\text{AS}$) as constituent minerals. The chemical and mineral compositions of ordinary Portland cement clinker and Gehlenite clinker are shown in Table 1 and Table 2. Raw material for sintering Belite-Gehlenite clinker is produced by blending and pulverizing virgin material (limestone, quartzite, etc) with the industrial waste to obtain the mineral composition as shown in Table 2. Then the raw material was fed into the actual rotary kiln to produce clinker 2000 tons per day. The burning temperature is around $1200\text{ }^\circ\text{C}$. 0.6 ton waste is used for producing 1 ton Belite-Gehlenite clinker. This means that the amount of waste used for Belite-Gehlenite clinker is 1.5 to 2 times as much as that used for an ordinary Portland cement clinker (NCL) commercially produced by Japanese cement plants. Therefore, this study focused on concrete aggregate as one of effective applications of clinker. In previous studies, it was found that when using Gehlenite clinker as fine aggregate in mortar, some results about fundamental properties of mortar were obtained. As the replacement rate of GCL increases, the compressive strength increases, and the drying shrinkage and the carbonation rate decrease[1]. More when cracks form in the concrete, water entering from cracks and minerals of clinker participate in the hydration reaction to produce hydration products, so it is expected that the products fill the cracks in gaps. In the field of self healing, research on self-healing by pozzolan reaction [2] is widely known by mixing fly ash, but in this research it is necessary to repair by utilizing the hydration reactivity of clinker. It aimed to develop self-healing concrete which does not do.

Table 1: Chemical compositions of clinker

Symbol	Chemical compositions (%)												
	SiO ₂	Al ₂ O ₃	Fe ₂ O ₃	CaO	MgO	SO ₃	Na ₂ O	K ₂ O	Na ₂ Oeq	TiO ₂	P ₂ P ₅	MnO	Cl
GCL	28.18	7.51	3.42	55.98	1.34	0.93	0.45	0.58	0.83	0.41	0.89	0.11	0.05
NCL	21.38	5.42	3.42	65.49	2.00	0.42	0.42	0.34	0.64	0.29	0.33	0.05	0.00

Table 2: Mineral compositions of clinker

Symbol	Mineral compositions (%)					
	C ₃ S	C ₂ S	C ₂ AS	C ₁₂ A ₇	C ₃ A	C ₄ AF
GCL	0	70	21	5	0	0
NCL	62	15	0	0	9	10

2. EXPERIMENTS ON FUNDAMENTAL PROPERTIES OF CONCRETE USING GEHLENITE CLINKER AS FINE AGGREGATE

2.1 Materials

Ordinary Portland cement was used as a binder (symbol: C, density: 3.15 g/cm^3). Crushed sand for concrete (S, density in saturated surface-dry condition: 2.63 g/cm^3) and Belite - Gehlenite clinker (GCL, absolute dry density: 3.16 g/cm^3) were used as fine aggregate. Crushed stone (G, density: 2.64 g/cm^3) was used as coarse aggregate. The particle size distributions of these fine aggregates were adjusted to same and within the range defined in JIS A 5005 [3].

Tap water (W) was used for mixing concrete. Poly-carboxylic acid-based high-performance air entraining and water reducing admixture (SP), air entraining admixture (AE) and an anti-foaming agent (DF) were also used. In this study, the researches on fundamental properties and self-healing ability of concrete when using Belite Gehlenite and Normal clinker as fine aggregate were conducted.

2.2 Mix proportions

Table 3 shows compounding conditions. The target slump (SL) was set within 10 ± 2 cm and the air volume (Air) was adjusted to within $4.5 \pm 1.5\%$ by using high performance AE water reducing agent (SP) and air entraining agent (AE).

Table 3: Mix proportions and fresh properties of concrete using Belite-Gehlenite clinker as fine aggregate

Symbol	GCL/S* vol. (%)	W/C (%)	Air (%)	Unit content (kg/m ³)					Air (%)	SL (cm)	SP (%)	DF (%)
				W	C	S	GCL	G				
GCL/S 0%	0	55	4±1.5	165	300	859	0	972	5.5	9.5	1.3	0.5
GCL/S 25%	25					644	258		5.5	11.5	1.4	0.4
GCL/S 50%	50					429	516		4.7	12.0	1.3	0.4
GCL/S 75%	75					215	774		5.3	9.5	1.0	0.4
GCL/S 100%	100					0	1032		5.5	9.5	1.3	0.4

*GCL/S: Volume ratio of Gehelenite clinker fine aggregate to total fine aggregate

2.3 Test items

For fresh properties, concrete slump, air content, concrete temperature were measured, and for hardened properties, compressive strength ($\phi 10 \times 20$ cm specimen cured in water at 20°C) was measured. For durability, drying shrinkage test (10×10×40cm specimen put at 20°C and 60% rh) was conducted. These were in accordance with Japanese Industrial Standard (JIS).

2.4 Test results

• Fresh properties

The results of the concrete slump test and the air amount are shown in Table 3. Concrete slump and air content were within the target ranges.

• Compressive strength test

Figure 1 shows the results of the compressive strength test. As the replacement rate of GCL increased, the compressive strength increased. This is due to the densification of the transition zone at the interface between the cement paste and the fine aggregate and the hardness of the GCL.

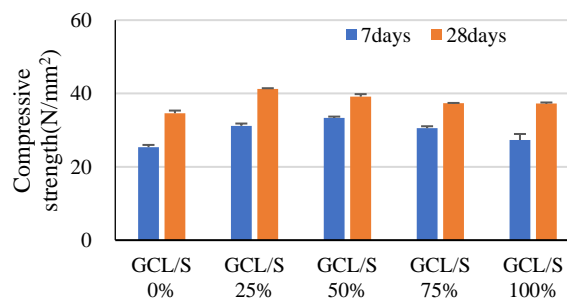


Figure 1: Compressive strength of concrete (Average of 3 specimens)

• Drying shrinkage test

The results of the drying shrinkage test are shown in Figure 2. When using GCL, the drying shrinkage decreased and showed the minimum value at GCL/S 25%.

The pore size distributions of GCL/S 0% and 100% specimens determined by MIP are shown in Figure 3. When using GCL, the compressive strength increased and the drying shrinkage decreased and showed the minimum value at GCL/S 25%. From Figure 3, it was confirmed that the pore volume between 50 nm and 2 μm in the transition zone are lower in GCL/S 100% compared with GCL/S 0%. From the Photo 1, when GCL/S was 25%, no gap was found in the part. But when GCL/S was 50%, gaps were found around coarse aggregate. It is thought that this was the trace of bleeding water stuck under the coarse aggregate. From the above results, as the GCL/S increased, the transition zone between the cement paste and the aggregate became denser and the drying shrinkage decreased. But when GCL/S is 50% or more, it is considered that the drying shrinkage increased by increasing bleeding water. However it is necessary to study more in order to confirm this.

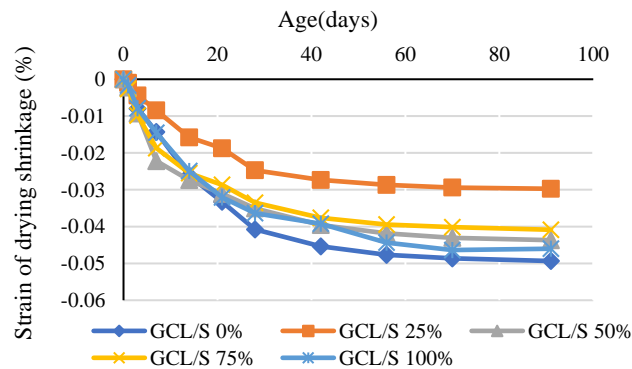


Figure 2 : Drying shrinkage tests (Average of 3 specimens)

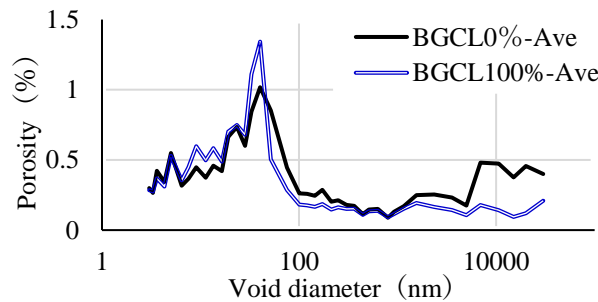


Figure 3 : Pore size distribution map

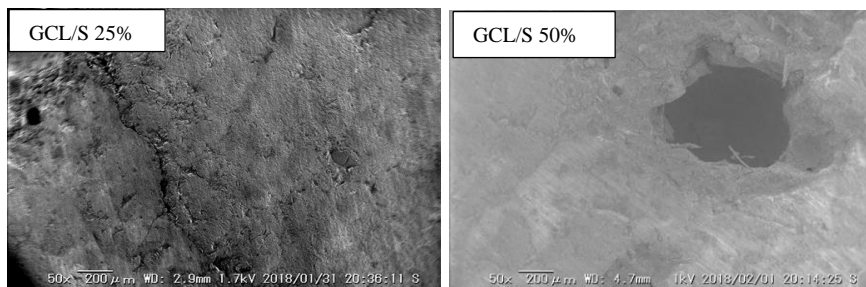


Photo 1 : Coarse aggregate interface

3. EXPERIMENTS ON SELF-HEALING PERFORMANCE OF GCL AND NCL CONCRETE

3.1 Mix proportions

The mix proportions of concrete using GCL and NCL are shown in Table 4 and 5. In this research, in order to evaluate the self-healing performance of concrete, it was necessary to damage the specimen by the freeze-thaw action. The amount of air was set to 1% or less so that the specimen could be easily damaged. No target value of slump was defined.

Table 4: Mix proportions and fresh properties of concrete using Belite-Gehlenite clinker as fine aggregate

Symbol	GCL/S vol.(%)	W/C (%)	Air (%)	Unit content (kg/m ³)					Air (%)	SL (cm)	SP (%)	DF (%)
				W	C	S	GCL	G				
GCL/S 0%	0	55	1 or less	165	300	859	0	972	0.8	8.5	1.5	3.0
GCL/S 50%	50					429	516		0.6	11.0	2.0	3.0
GCL/S 100%	100					0	1032		0.8	2.0	3.0	4.0

Table 5: Mix proportions and fresh properties of concrete using Normal clinker as fine aggregate

Symbol	NCL/S* vol. (%)	W/C (%)	Air (%)	Unit content (kg/m ³)					Air (%)	SL (cm)	SP (%)	DF (%)
				W	C	S	NCL	G				
NCL/S 0%	0	55	1 or less	165	300	859	0	972	0.9	6.5	1.5	2.0
NCL/S 50%	50					429	434		0.7	7.0	2.0	3.0
NCL/S 100%	100					0	869		0.9	5.0	3.0	4.0

*NCL/S: Volume ratio of Normal clinker fine aggregate to total fine aggregate

3.2 Test items and test methods

The self-healing performance evaluation test method is shown below. In addition, the compressive strength and the fresh properties tests described in 2.3 were carried out.

• Self-healing performance evaluation test

After producing damages in the hardened micro structure by freeze-thaw, specimen was cured in water at 20°C, and the primary resonance frequency of longitudinal vibration was measured every week, and the possibility of imparting self-healing performance was evaluated by the change in relative dynamic elastic modulus. The method of preparing the test specimen and the test method are described below.

a) Method for making specimen

The test specimen was prepared using a cylindrical mould having a diameter of 100 mm and a height of 200 mm. For the test, two cylindrical test specimens were prepared each condition. In this test, those specimens cured in water at 20°C up to 28 days of age were used.

b) Test method

The concrete specimens cured in water at 20°C up to 28 days of age were given freeze-thaw action to damage internal micro structure. In preliminary experiments, it was confirmed that the damage due to freeze-thaw effect varied in different mix proportions, so the damage level is set to the two levels. Level 1 is at the same cycle (30 cycles : the specimen were given freeze-thaw action of -18 to 5°C in each cycle) as damage level. Level 2 is at cycles that the primary resonance frequency of longitudinal vibration is 0

(the value cannot be measured). They are 60 cycles for GCL/S 0%, 50%, 100% and NCL/S 0%, and 90 cycles for NCL/S 50% and 100%.

Healing curing was carried out in water at 20°C and the day when the freeze-thaw action was over was set as the day 0 of the self-healing period. The primary resonance frequency of longitudinal vibration was measured every week. After measurement up to 8 weeks, the compressive strength test was conducted immediately and compared with the compressive strength of specimen at 28 days of the same combination without freeze-thaw action.

3.3 Test results

• Fresh properties

Tables 4 and 5 show the results of the fresh properties tests. In these tests, the target values of air content in all combinations were obtained.

• Compressive strength test

Figure 4 and 5 show the results of the compressive strength test of concrete using GCL and NCL. It was confirmed that the compressive strength increased by mixing with both GCL and NCL. This is due to the densification of the transition zone at the interface between the cement paste and the fine aggregate and the hardness of the clinker aggregate.

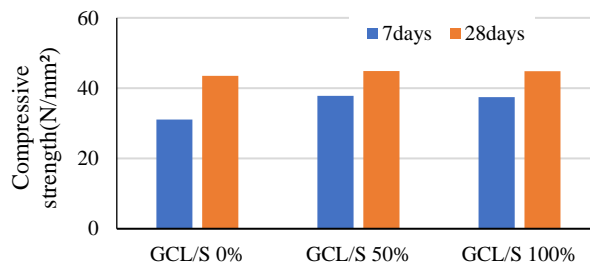


Figure 4 : Compressive strength of concrete using GCL

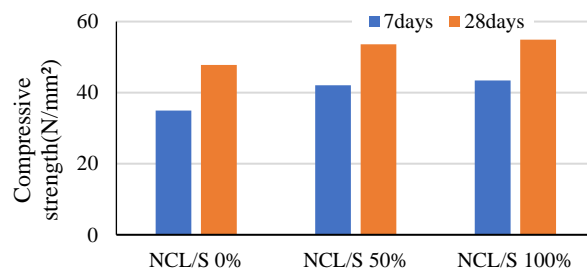


Figure 5 : Compressive strength of concrete using NCL

• Self-healing performance evaluation test

a) Relative dynamic modulus of elasticity

Self-healing performance evaluation test results are shown in Figure 6 to 9. As shown in Figure 6 and Figure 7, about the self-healing performance of concrete containing GCL, it was shown that the relative dynamic elastic modulus greatly increased at early days after healing curing was conducted and then gently stopped changing. It is presumed that this is because the hydrate from the reaction of GCL fills the part damaged by the freeze-thaw action. From Figure 6, though the specimens of GCL/S 0%, 50% and 100% were given the same cycle of freeze-thawing action, the relative dynamic elastic modulus were different. It was confirmed that the

damage was different for different mix proportions. When GCL/S was 0%, the relative dynamic elastic modulus was unable to be measured both in Level 1 and Level 2 when the specimen was damaged. But after repair curing for 8weeks, the relative dynamic modulus of specimen in Level 1 recovered to nearly 60% of that before the specimen was given the freeze thaw test. However, the relative dynamic modulus of specimen in Level 2 only recovered to about 10%. This is presumed that actually the specimen was damage heavier in Level 2 though the relative dynamic elastic modulus was unable to be measured both in Level 1 and Level 2 when the specimen was damaged.

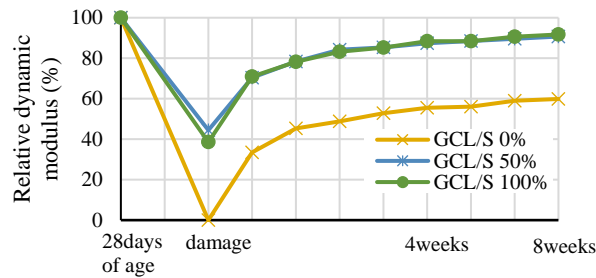


Figure 6 : Change in relative dynamic modulus of elasticity (Level 1)

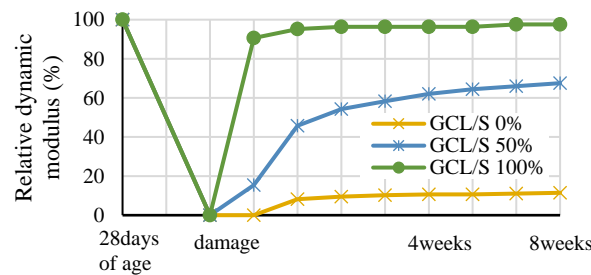


Figure 7 : Change in relative dynamic modulus of elasticity (Level 2)

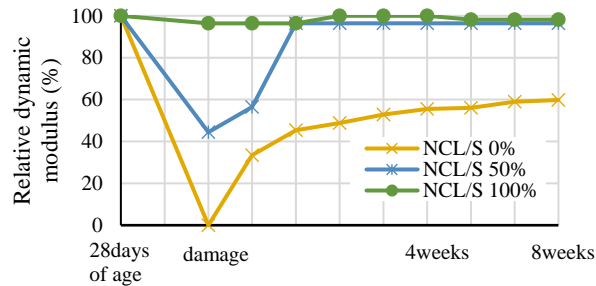


Figure 8 : Change in relative dynamic modulus of elasticity (Level 1)

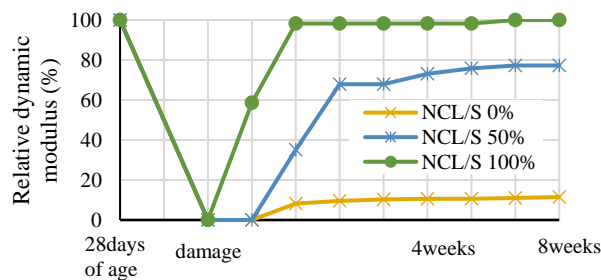


Figure 9 : Change in relative dynamic modulus of elasticity (Level 2)

b) Compressive strength after self-healing

Figure 10 and 11 show the results of the compressive strength test after self-healing of concrete using GCL and NCL. It was confirmed that compressive strength recovered by mixing with GCL and NCL. It was confirmed that the relative dynamic modulus of Level 1 and Level 2 recovered to about 90% after 8 weeks healing curing at GCL replacement rate of 100%. Moreover, the compressive strength after self-healing recovered to about 100% at NCL replacement rate of 100%. Compressive strength after self-healing of Level 2 at NCL 0% was difficult to measure because the damage given by the freeze-thaw action was too severe.

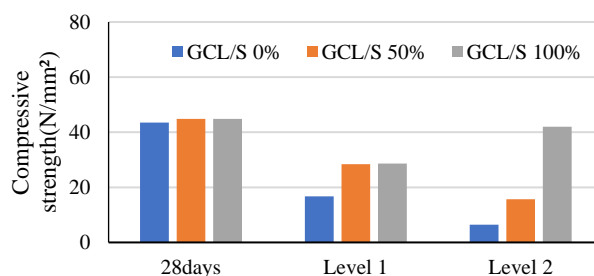


Figure 10 : Compressive strength after self-healing

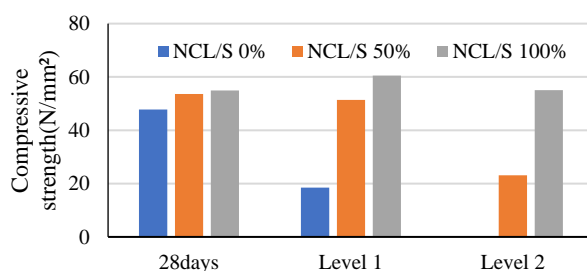


Figure 11: Compressive strength after self-healing

4. CONCLUSIONS

1. By replacing fine aggregate with GCL and NCL, increases in compressive strength were confirmed in both cases.
2. Reduction of drying shrinkage was confirmed by replacing fine aggregate with GCL. In particular, replacement with GCL of 25% resulted in the lowest drying shrinkage ratio.
3. It was also found that self-healing performance improved by replacing GCL and NCL. It was confirmed that the compressive strength after self-healing recovered.

ACKNOWLEDGEMENTS

This work was supported by JSPS KAKENHI Grant Number JP2642035.

REFERENCES

- [1] Msatoshi Nemoto, 2014. A study on hardening properties centering on self-healing performance of mortar using clinker aggregate, 31-65
- [2] Yumi Fujiwara, Investigation of frost resistance and self-restoring effect of concrete using fly ash, Concrete engineering papers annual paper, Vol.30, No. 1, pp. 873- 878, 2008
- [3] Japan Standards Association, JIS A 5005 Crushed stone and crushed sand for concrete, 2009

THE PRODUCING TECHNOLOGY AND IMPROVED METHODS OF THE RECYCLED CONCRETE AGGREGATE

Ting Du

Huazhong University of Science and Technology

Abstract

Waste concrete can be used to produce recycled aggregate instead of natural aggregate making concrete after a series of treatment, and obviously using recycled concrete aggregates will save natural resource and energy. In the paper, two technical processes of producing the recycled aggregates from the waste concrete are designed, which can obtain the primary processed recycled aggregate and the high quality recycled aggregate separately. And for the primary processed recycled aggregate, its surface are wrapped with some old cement paste, it will lead the properties of the recycled coarse aggregate is worse than the natural coarse aggregate, so four methods to improve the behaviours of the recycled coarse aggregate are put forward, such as cement-grout, Cement-grout mixed with Kim powder, Cement-grout mixed with 1-class fly ash and interfacial agent of YJ302. In the experiments, the recycled coarse aggregate was intensified by four methods independently, and the experimental results indicate that the strengths of the recycled aggregate and the recycled aggregate concrete processed with the cement-grout mixed with Kim powder and YJ302 are evidently higher than those of natural aggregate and natural aggregate concrete. It will give out some ideas for improving the recycled aggregate and making high-strength recycled aggregate concrete.

Keywords: waste concrete, recycled aggregate, produce technology, improved method

EXPERIMENTAL STUDY ON PROPERTIES OF CONCRETE CONTAINING MOLTEN SLAG FROM INTEGRATED COAL GASIFICATION COMBINED CYCLE AS FINE AGGREGATE

Ryotaro Kobayashi (1), Hiromi Fujiwara (2), Masanori Maruoka (2), Yuto Yamanaka (1)

(1) Graduate student in the department of Design and Engineering for the Global environment at Utsunomiya University

(2) Professor in the Department of Civil Engineering and Regional Design at Utsunomiya University

Abstract

Recently in Japan, the rate of coal-fired power generation among the total quantity of generated power has been increasing due to the accident of nuclear plant by the East Japan Earthquake. Among the fossil fuels, coal is economical because the price and supply are stable. However, coal-fired power generation has a large impact on the environment so the commercial application of integrated coal gasification combined cycle (IGCC) has being promoted. IGCC is a highly efficient power generating method combining a steam turbine and a gas turbine. However, it is necessary to establish effective utilization of coal gasification molten slag discharged from IGCC in order to promote the IGCC technology. In this paper, it is investigated the fresh properties and hardened properties of concrete containing the coal gasification molten slag as fine aggregate. As for the result, in comparison with the concrete using conventional fine aggregate, it is confirmed that the fluidity improves, the bleeding increases a little, the compressive strength and bending strength decrease slightly and the drying shrinkage much reduces as containing ratio of increases. As a result, it is found the possibility that the coal gasification molten slag is usable as fine aggregate for concrete.

Keywords: integrated coal gasification combined cycle (IGCC), coal gasification molten slag(CGMS), fine aggregate

1. INTRODUCTION

The depletion of aggregate used in concrete due to restrictions on the extraction of natural aggregate from the perspective of environmental preservation has become a problem for the concrete industry in Japan, and researches and developments of the substitute aggregates are underway. Moreover, as a result of the Great East Japan Earthquake and tsunami in 2011, the power supply ratio configuration that had been centered on nuclear power is shifting to thermal power generation, and currently coal-fired power generation accounts for approximately 31% of the total power generation capacity in Japan [1]. However, existing methods of coal-fired power generation emit tremendous quantities of CO₂, so technology to reduce CO₂ emissions are needed. For this reason, the use of the highly efficient Integrated Gasification Combined

Cycle (IGCC) is being promoted. In the IGCC technology, the impurities in coal that has been heated in gasification furnace is melted and discharged as coal gasification molten slag (CGMS). Establishing a method for effective use of this CGMS will be essential for the expanded use of IGCC technology. Using CGMS as concrete aggregate will make a major contribution to society. However, standards have not yet to be established for the use of aggregate derived from CGMS. In the past research, the coal gasification molten slag was used as filler component for the preparation of binder mixtures. And high strength properties were obtained even with 70% share of the milled slag [2]. According to the research using slag for mortar as fine aggregate, improvement of fluidity and suppression of drying shrinkage were confirmed [3]. This study explored the potential for the use of this aggregate, the changes in the basic properties of concrete when CGMS aggregate is used, as well as problems that must be resolved, with the aim of establishing standards for CGMS aggregate.

2. CHARACTERISTICS OF COAL GASIFICATION MOLTEN SLAG AS FINE AGGREGATE

The characteristics of the CGMS and Crushed sand used as fine aggregates in this study were compared. Figure 1 shows the CGMS (symbol: Sg) and Crushed sand (symbol: Sc) used in this study.

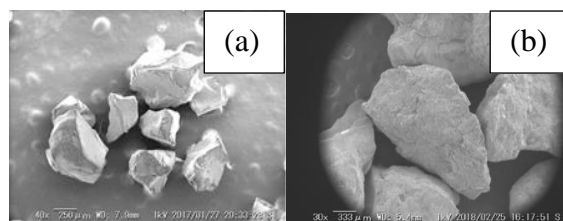


Figure 1: Coal gasification molten slag (a) and Crushed sand (b)

2.1 Test items

Density, water absorption rate, particle size distribution, bulk density, solid content, and solid volume percentage for shape determination were measured according to Japanese Industrial Standard (JIS).

And in order to grasp the strength of this aggregate and its elastic deformation capacity as aggregate, an aggregate strength indicator measurement test was performed for fine aggregate derived from CGMS and crushed sand. A steel container with an inner diameter of 33 mm and a height of 88 mm was used for the test. Figure 3 shows a schematic drawing of the aggregate strength indicator test. The test method is as follows.

From a fine aggregate test specimen in absolutely dried condition, particles within 1.2 - 2.5 mm were separated by screening. 60g of the test specimen was placed in a steel container and the upper surface was smoothed with finger. Then a round steel bar for loading was inserted and a precision universal testing machine was used to apply the compressive load P (kN), at the same time the displacement d (mm) was measured using a laser displacement gauge. The load was applied to a maximum load of 90kN. A load-displacement curve was drawn from the measurements and the gradient of the curve exhibiting proportional change was calculated out as the aggregate strength index value using Equation (1) below.

$$I(kN/mm) = P(kN) / d(mm) \quad (1)$$

Where I is the aggregate strength index value

P is the compressive load

d is the displacement

After the test, the test specimen was screened by using a 0.30 mm sieve and a 0.15 mm sieve, and the 0.30 crushing value (%) and 0.15 crushing value (%) were calculated from the quantity that passed through each sieve. These crushing values were calculated out using the following equations (2) and (3).

$$0.30 \text{ crushing value} = B(g)/A(g) \times 100\% \quad (2)$$

$$0.15 \text{ crushing value} = C(g)/A(g) \times 100\% \quad (3)$$

Where A is the crushed aggregate

B is the aggregate that 0.30 mm sieve

C is the aggregate that 0.15 mm sieve

2.2 Test results

Table 1 and Figure 2 show the results of tests of fine aggregate derived from the CGMS, as well as crushed sand aggregate. Figure 2 shows the particle size distribution of the aggregate as determined by sifting. From the test results in Table 1, CGMS used in this study had a density in saturated surface-dry condition of 2.68 g/cm³, roughly the same as ordinary natural aggregate and it is thought that it can be used in ordinary concrete as a substitute for natural aggregate. The solid volume percentage was 69.0% and the solid volume percentage determined by particle shape was 58.4%. As both of these are comparatively large values, fine aggregate derived from the CGMS can be said to have an appropriate particle shapes and sizes.

Figure 4 shows the relationship between load and displacement of the aggregate strength indicator measurement test for fine aggregate derived from CGMS. The indicators are shown in Table 1. The test results show that the aggregate strength indicator is higher for fine aggregate derived from CGMS than that for crushed sand, resulting in greater resistance to deformation due to external force. Moreover, the crushing values for each material indicate that CGMS is more likely to be brittle fractured than crushed sand.

Table 1: The results of fine aggregate tests

Test list		Test method	Test value	
			Sg	Sc
Density in saturated surface-dry condition	g/cm ³	JIS A 1109	2.68	2.64
Absolute dry density	g/cm ³		2.68	2.6
Water absorption rate	%		0.17	1.33
Bulk density	kg/L	JIS A 1104	1.85	1.75
Solid content	%		68.9	67.3
Content of materials finer than 75µm sieve	%	JIS A 1103	5.9	3
Solid volume percentage for shape determination	%	JIS A 5005	57.8	56.7
Fineness modulus		JIS A 1102	2.68	2.73
Aggregate strength index value : I	kN/mm	original	17.8	13.9
Crushing value 0.30(%)	%	original	30.3	21.7
Crushing value 0.15(%)	%	original	16.3	13.0

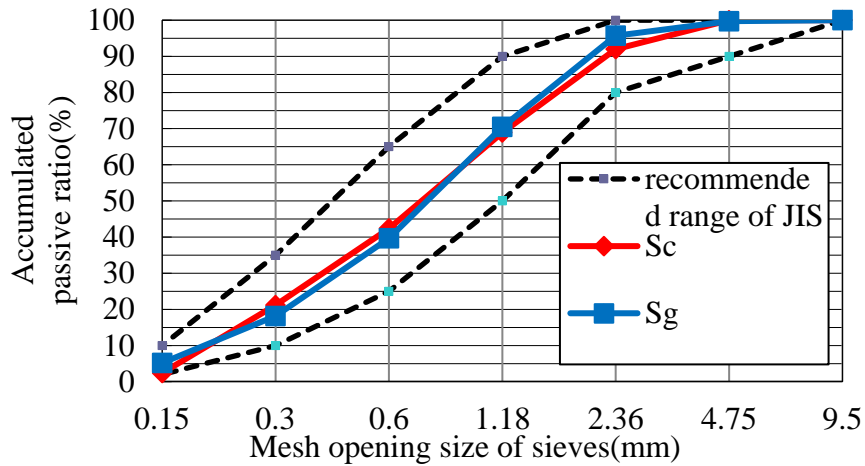


Figure 2: Particle size distribution of fine aggregate

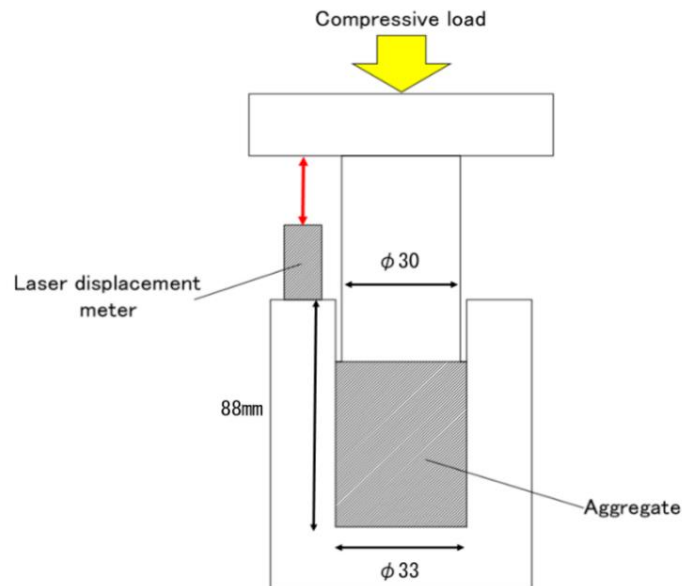


Figure 3: Outline of the Aggregate strength index value and Aggregate crushing test

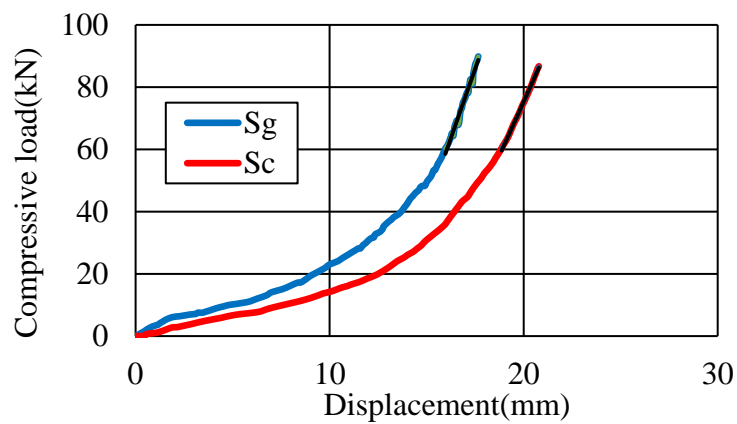


Figure 4: Displacement-Compressive load curve

3. FUNDAMENTAL PROPERTIES OF CONCRETE USING COAL GASIFICATION MOLTEN SLAG AS FINE AGGREGATE

In this section, the properties of concrete using CGMS as aggregate instead of crushed sand were investigated.

3.1 Materials

Ordinary Portland cement (symbol: C, density: 3.16g/cm^3) was used as a binder. Crushed sand (Sc) and CGMS (Sg) were used as fine aggregates. Crushed stone (symbol: G, density in saturated surface-dry condition: 2.63g/cm^3) was used as coarse aggregate. And high performance water reducing agent (SP), air entraining agent (AE) and deformer (DF) were also used as admixtures.

3.2 Mix condition

Table 2 show the mix proportions of concrete. Fine aggregate was replaced with CGMS by volume ratio (Sg/Sc) at 0%, 50% and 100%. The target values of the fresh properties were 12.0 ± 1.5 (cm) for slump, 4.5 ± 1.5 % for air content. Water-cement ratio was fixed to 50% and the addition rate of high performance water reducing agent (SP) was also fixed to 0.75% in mass. Because the target values of fresh properties were obtained when SP addition rate was 0.75% at Sg/S=100% in our study at first. And in order to obtain target values at Sg/S=0% and Sg/S=50%, the amount of unit water was adjusted.

Table 2 : Mix proportions of concrete

W/C (%)	Sg/S (%)	Unit content(kg/m ³)					Admixture addition rate(C×%)		
		W	C	Sc	Sg	G	SP	AE	DF
50	100	157	314	0	880	981	0.75	0.05	0.80
	50	169	338	421	428	954		0.05	0.50
	0	178	356	824	0	933		0.05	0.50

3.3 Test items

For fresh properties, concrete slump, air content, concrete temperature, bleeding ratio and setting time were measured and for hardened properties, compressive strength, splitting tensile strength and static elastic modulus were measured. For durability, freezing and thawing test, drying shrinkage test and accelerated carbonation test were conducted. These were in accordance with Japanese Industrial Standard (JIS).

3.4 Test results

Table 3 show the results of the fresh properties tests.

It was found that bleeding rate increased as the Sg/S value increased. And, when the Sg/S value increased, the unit water decreased but bleeding rate increased at the same time. One reason is thought to be that unit cement content decreased. However, unit cement content of all mixture is more than 300kg/m^3 . Therefore it is thought that the main reason is that Sg has smooth surface and low water absorption rate. Therefore, it is considered that the surplus water increased and the fluidity of the concrete improved.

About the setting time test, Sg mixed concrete was slower at both the start and end time. The reason for this is considered to be that the bleeding rate was large and it took time to converge.

Figure 5 shows the results of the compressive strength test. Compressive strength of Sg mixed concrete decreased 21% at 28 days and 9% at 364 days compared with Sg non-mixed

concrete. The reason for this is considered to be that the strength of Sg is smaller than that of Sc because the crushing value of Sg is larger. And, it is considered that the pore volume under the coarse aggregate increased due to the increase of bleeding so the interface bond between coarse aggregate and cement paste became weaker and the compressive strength decreased.

Figure 6 shows the results of the splitting tensile strength test. When Sg/S rate increased, the strength decreased. The reason for this is considered to be that since the surface of Sg is smooth, adhesion is not good. And it is also considered to be the same reason as that of compressive strength.

Figure 7 shows the relationship between compressive strength and static elastic modulus. When Sg replacement rate increased, the static elastic modulus at the same compressive strength also increased. It is considered that since the aggregate strength index value of Sg is larger and the elastic coefficient of Sg at low load is larger, so the deformation resistance becomes larger.

Figure 8 shows the results of the freeze - thaw test. The relative dynamic elastic modulus of Sg mixed concrete was less than 60% at 300 cycles. In general, it is known that concrete show poor frost resistance when it has high bleeding ratio. And, it is also thought that the weakness of surface adhesion between cement paste and aggregate due to bleeding caused this. Therefore, it is necessary to study more in order to improve the frost resistance.

Figure 9 shows the results of the drying shrinkage test. When Sg substitution rate increased, the drying shrinkage strain decreased. The reason for this is considered to be that since the aggregate strength index value of Sg is large, deformation resistance is large. And when the Sg/S rate increased, the unit water decreased. Therefore, it is considered that drying shrinkage was suppressed.

Figure 10 shows the results of the accelerated carbonation test. When Sg substitution rate increased, the carbonation rate increased. It is considered that when bleeding rate increased, the microstructures in the concrete became coarse, so the CO₂ entered into the concrete more easily.

Table 3: The results of the fresh properties tests

W/C (%)	Sg/S (%)	Unit water (kg)	Slump (cm)	Air volume (%)	Temperature (°C)	Bleeding rate (%)	Setting time test	
							Start time (min)	End time (min)
50	100	157	11.5	4.1	20	9.04	470	635
	50	169	11.5	4.0	21	6.89	-	-
	0	178	12.0	4.0	21	7.30	380	515

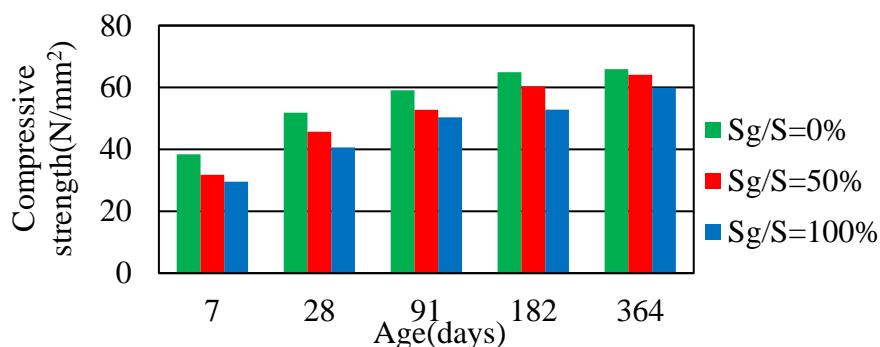


Figure 5: the results of the compressive strength test

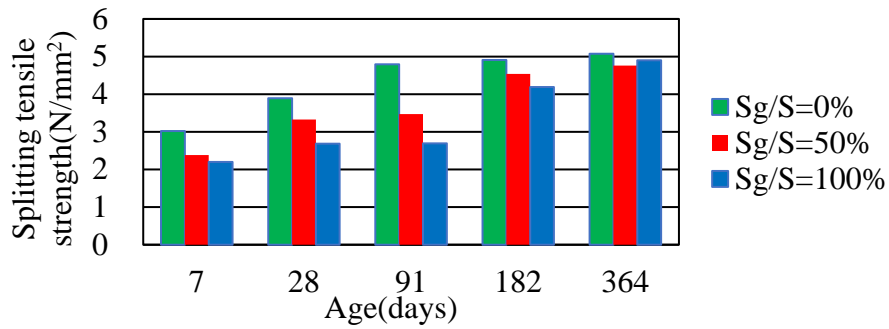


Figure 6: the results of the splitting tensile strength test

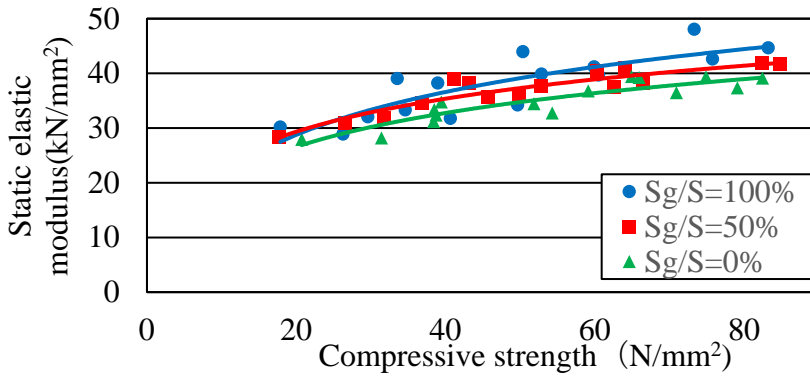


Figure 7: the relationship between compressive strength and static elastic modulus

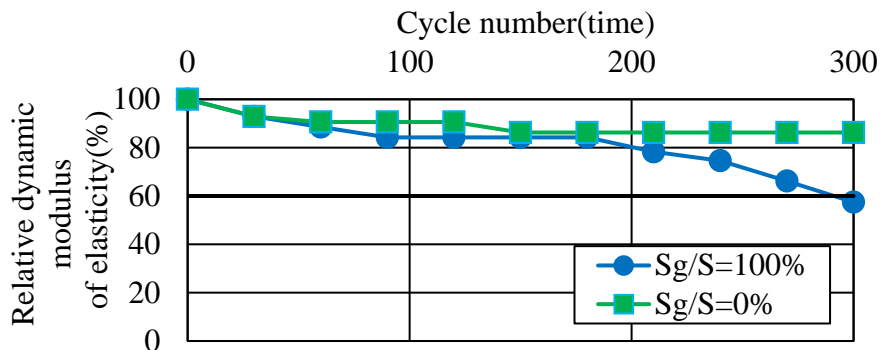


Figure 8: the results of the freeze - thaw test

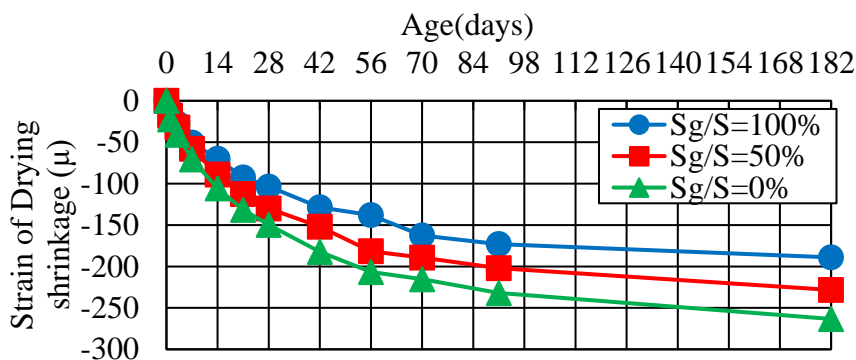


Figure 9: the results of the drying shrinkage test

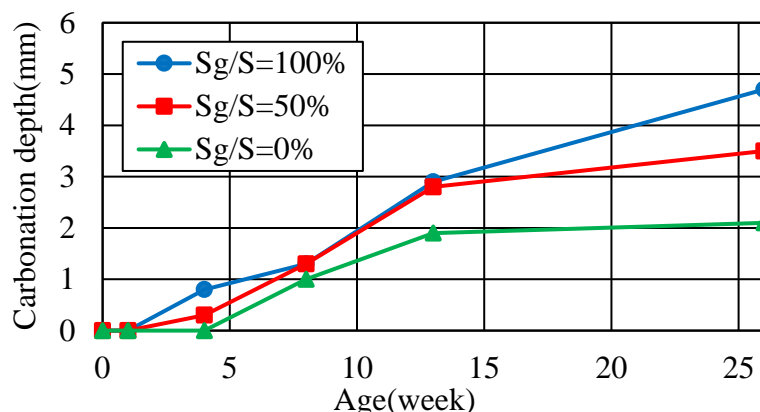


Figure 10: the results of the accelerated carbonation test

4. CONCLUSIONS

As a result of examining basic fresh properties, hardened properties and durability of Sg-mixed concrete, fluidity improved in the fresh properties. In the hardened properties, the compressive strength decreased but the static elastic modulus at the same compressive strength increased. In durability, good results were not obtained in freezing and thaw resistance. However, it seems can be improved by reducing the bleeding rate. In the drying shrinkage properties, the shrinkage strain was reduced. In carbonation resistance, the carbonation rate increased.

In this paper, only 3 mixtures were investigated. However, many other mixtures using coal gasification molten slag as fine aggregate have been being investigated. In near future, these will be presented. And in these investigations, some problems were found. Therefore, it is necessary to research more in order to solve these problems.

ACKNOWLEDGEMENTS

In this research project, Coal Energy Center of the General Foundation provided us with the slag, adjustment of granularity and opportunities for testing. And this research was entrusted by New Energy and Industrial Technology Development Organization (NEDO). Thanks for their cooperation.

REFERENCES

- [1] Sustainable Japan, Sustainability news media : 【Energy】 Amount of supply of power generation in Japan, <https://sustainablejapan.jp/2016/05/18/electricity-proportion/1396>.
- [2] Radoslaw Pomykala , The Mechanical Properties of Coal Gasification Slag as a Component of Concrete and Binding Mixtures , Pol. J. Environ. Stud. Vol. 23, No.4 (2014), 1403-1406
- [3] Yuto Yamanaka, Experimental Study on Properties of Mortar Containing Molten Slag as Fine Aggregate, American Concrete Institute 2018, 49.1-49.10

RECYCLED AGGREGATES PRODUCED FROM TWO DIFFERENT FEEDSTOCK MATERIALS – APPLIED IN READY-MIXED CONCRETE

Hernan Mujica (1), Egil Velde (1), Christian J. Engelsen (2), Monica S. Nodland (2)

(1) Velde Industri AS, Norway

(2) SINTEF Building and Infrastructure, Norway

Abstract

Construction and demolition waste (CDW) and waste excavation materials (WEM) from construction activities are important raw materials for new construction materials and products. Recycled concrete aggregates (RCA) from both waste streams are today not used in bound applications (e.g. ready-mixed concrete).

In this study, RCA was produced from a feedstock with 50% of each waste stream (WEM and CDW) and used in concrete pilot. The RCA replaced fully the natural aggregates in the concrete mix. It was found that the compressive strength complied to the requirements for C35/45 in NS-EN 206. Furthermore, the use of this type of RCA had no negative impact on the physical characteristics of the RCA and the concrete. Low content of cement paste was found in the RCA and resulted in low water absorption. This demonstrated the ability of the wet recycling process to remove significant quantities of the mortar in the CDW.

The total concentrations of inorganic and organic substances were found to be low and complied to the strict Norwegian soil quality criteria. Cr(total) exceeded the criteria. However, most of the chromium was present on the trivalent form, Cr(III), which has low solubility in the neutral to mildly basic pH region.

Keywords: Recycled aggregates, concrete, pilot demonstration

1. INTRODUCTION

The revised framework for waste management in the EU [1] which was adopted in 2008 includes a target for recovery of construction and demolition waste (CDW). Within 2020, the preparing for re-use, recycling and other material recovery of non-hazardous construction and demolition waste (excluding naturally occurring material) shall be increased to a minimum of 70 % by weight. The target was added during the final negotiations of the Directive text and instructions for verifying compliance was established in 2011 [2]. Norway has implemented the

WFD and must comply to this target through the partnership of the European Economic Area. The directive is intended to be an overall key driver for circular driven economy for C&D waste.

Furthermore, waste excavation materials (WEM) from various construction projects in urban areas represent a resource that is often not utilized [3]. In several European countries (e.g. Sweden) this mass flow is often used for landfills where it is used as a cover material. Since the recycled aggregates from WEM will largely be recycled from naturally occurring materials, it will be possible to develop products that comply to same quality criteria as natural aggregates.

Hence, CDW and WEM from construction and demolition activities are important raw materials for new construction materials and products. It is emphasised that the heavy mineral fractions in CDW have been used to some extent as recycled concrete aggregates (RCA) in unbound civil engineering applications (road construction, landscaping, etc.) for more than 20 years in Norway. Moreover, recycling of WEM into recycled natural aggregate (RNA) are to some extent also commercialised. However, recycled aggregates from both waste streams are today not commercially used in bound applications (e.g. ready-mixed concrete), although full-scale demonstrations have shown that it is technical feasible for RCA.

In the present study recycled aggregates have been produced from a feedstock with 50% of each waste stream (WEM and CDW). The production was conducted at the recycling plant at Velde Industri AS and included several separation, fractionation and washing steps. The RCA has been used in a concrete floor pilot where it fully replaced all fractions of the natural aggregates. The study is part of the Norwegian project "*Recycled aggregates from excavation materials used in road construction and concrete production*" (RESGRAM). The overall objective for the treatment and recycling plant is to convert more than 90% of the incoming excavation materials into commercial products. RESGRAM is supported by Research Council of Norway and will continue to August 2020 [4].

2. MATERIAL AND METHODS

2.1 Preparation of the RCA

In Velde's recycling plant (CDE Aggmax™ system), WEM are normally used to produce RNA in the fractions 0,063/2 mm, 2/4 mm, 4/16 mm, 16/32 mm and 32/100 mm fractions. In addition, a residual fraction (< 63 µm) is generated from the filter press which is very often landfilled. In the current study, the feedstock materials were WEM and CDW mixed in a proportion of 1:1 with a front loader.

2.2 Geometrical and physical properties determined for RCA

The cement paste content was assessed for all samples since the mortar content in RCA often represents the weaker bonding in the interfacial transition zone (ITZ) between the RCA particle and the cement paste [5]. It has been shown earlier that the acid soluble content can serve as an indicator for the cement paste content in RCA [6]. Hence, the acid soluble content was determined according to the procedure described in [6].

Furthermore, the following properties were also determined for the RCA samples:

- Particle density and water absorption
- Shape of coarse aggregates (Flakiness Index, FI)
- Resistance to fragmentation of coarse aggregates, Los Angeles coefficient (LA)
- Resistance to wear of coarse aggregates, micro-Deval coefficient (M_{DE})
- Classification of coarse RCA

2.2 Concrete mix design

The concrete mix developed is specified in Table 1.

Table 1: Concrete mix design complying to C35/45 (Norwegian class B35 M45 D32)

Parameter	Unit	Value
Cement content (CEM II/A-V) in concrete	kg/m ³	365
Water to cement ratio (w/c)	-	0.45
Admixture (Dynamon SX-N) content of cement weight	%	0.9
Steel fibre in concrete	kg/m ³	25
RCA 0/2 mm	kg/m ³	750
RCA 4/16 mm	kg/m ³	747
RCA 16/32 mm	kg/m ³	374

2.3 Chemical properties of RCA

The RCA samples were reduced in volume by splitting, quartering, crushing and pulverization. The reduction of the laboratory samples to test samples and to final test portions was conducted according to NS-EN932-2 and NS-EN 15002.

The following organic and inorganic substances were determined in the RCA samples; polychlorinated biphenyl (Σ PCB-7), polycyclic aromatic hydrocarbon (Σ PAH-16), BTEX (benzene, toluene, ethylbenzene, xylene), total hydrocarbons (THC), total organic content (TOC), As, Cd, Cr(total), Cr(VI), Cu, Pb, Hg and Ni.

GC-MS with selective ion monitoring (SIM) was used to determined Σ PCB-7, Σ PAH-16 and BTEX. THC were analyzed using GC with flame ionization detector. Heavy metals were analyzed by Inductively coupled plasma (ICP).

Humic acid was determined using the hydrochloric acid indicator test (NS-EN 1744-1).

3. RESULTS AND DISCUSSION

3.1 Geometrical and physical properties of RCA

The results from the tests are shown in Table 2. The properties of the RCA were found to be excellent and complying to the criteria specified in the table. Furthermore, the water absorption was found to be less than 1% for all grain sizes.

The classification showed that the RCA samples contained significant amount of concrete related products and also large quantity of natural unbound aggregates (Ru), see Table 3. The

latter is originating from the WEM feedstock. This indicated that the mortar content in the samples would be smaller than the corresponding content of RCA produced only with CDW.

This was also confirmed by the cement paste content determined in the samples, as shown in Table 4. The acid soluble part was found to be in region of 4-7% which is considerably lower than RCA produced from only concrete rubble [6]. In particular, the RCA 0/2 mm has a low cement paste content which is also reflected in the low water absorption obtained. Hence, the results demonstrated the mortar removing ability (washing and scrubbing) of the wet recycling technology used.

Table 2: Determination of geometrical and physical properties of the RCA samples

Parameter	RCA 0/2 mm	RCA 4/16 mm	RCA 16/32 mm	NS-EN 206 criteria
Oven dried density (kg/dm ³)	2.61	2.61	2.61	Declared value
Water absorption (%)	0.54	0.89	0.89	< 10
Flakiness index	-	15.7	9.71	≤ 35
Humic acid indicator test	No colour	-	-	No Colour
Crushed and broken surfaces (%)	-	C _{76/24}	C _{44/56}	Declared value
Los Angeles coefficient (LA)	-	30.4		≤ 35
micro-Deval coefficient (M _{DE})	-	19.8		Declared value

Table 3: Classification of coarse RCA

Material fraction	RCA 4/16 mm (%)	RCA 16/32 mm (%)
Rc (concrete products, mortar, concrete masonry units)	36.1	25.6
Ru (unbound aggregate, natural stone hydraulically bound aggregate)	34.4	61.7
Rb (clay masonry units, i.e. bricks and tiles, calcium silicate masonry units, aerated non-floating concrete)	29.3	12.7
Ra (bituminous materials)	0	0
Rg (glass)	0	0.1
Rc+Ru+Rg	70.6	87.4
X (clay and soil, metals, non-floating wood, plastic, rubber, gypsum plaster)	0	0

Table 4: Determination of the acid soluble part (n = 3)

Sample	Average (weight %)	RSD (%)
RCA 0/2 mm	4.4	0.02
RCA 4/16 mm	7.2	0.24
RCA 16/32 mm	4.0	0.20

3.2 Practical experience during casting

The pilot consumed around 100 m³ of ready-mixed concrete complying to the concrete class C35/45. The concrete mix had around 20 kg less cement than a traditional Norwegian B35. The 0/2 mm washed sand had less than 3% of the particles passing the 0.063 mm sieve. The low content of fines together with the maximum aggregate size of 32 mm (instead of the traditional 22 mm), resulted in the reduced cement content in the concrete mix even with 25 kg of steel fibres. The latter usually requires a concrete mix with more cement than a concrete without fibres.

The concrete was easy to pour out and satisfying pumpability and workability were therefore achieved (Figure 1). Furthermore, a satisfying finish with trowel machine was obtained. A curing membrane was used to prevent cracks and no presence of bleeding or cracks were observed during the pouring, finishing process and the first 24 hours. Five month after pouring, no cracks have been observed in the concrete slab that could be attributed to the aggregates.

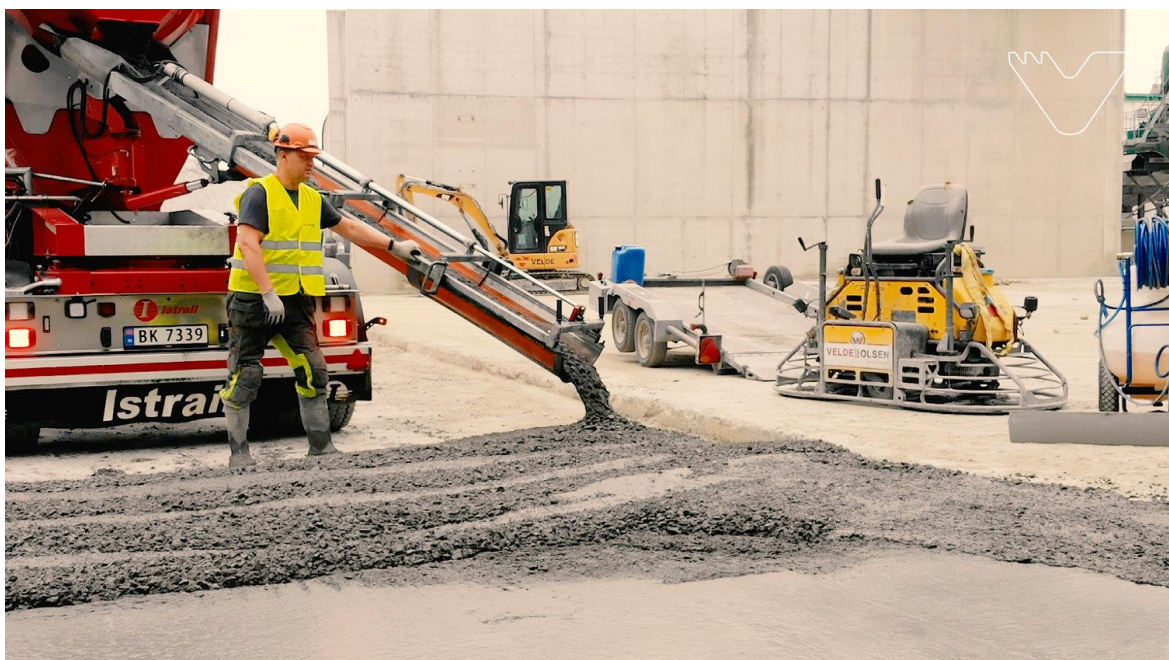


Figure 1: Concrete with 100% recycled aggregates used for casting a concrete floor

3.3 Concrete properties obtained

The fresh and hardened concrete properties obtained are shown in Table 5. It was found that the 28 days compressive strength obtained was not lower than the average compressive strength of a similar concrete with natural crushed aggregate. Compressive strength for concrete produced with natural aggregates without steel fibres from Velde's quarry is typically around 58 MPa.

Table 5: Fresh and hardened concrete properties

Parameter	Sample 1	Sample 2	Sample 3
Density (g/dm ³)	2388	2380	2367
Slump (mm)	180	200	190
Fresh concrete temperature (°C)	21.2	22.0	21.0
Compressive strength after 2 days (MPa)	22.1	26.1	25.6
Compressive strength after 28 days (MPa)	56.9	60.4	64.9
Density after 28 days (g/dm ³)	2438	2383	2403

3.4 Environmental assessment

Results from the analyses of organic substances and heavy metals in the samples are given in Table 6. The results obtained complied with the soil quality criteria (class 1) issued in the Norwegian Pollution Control Regulation. These criteria were originally developed for the handling of polluted soil. However, they are currently being used to assess the environmental ability to recycle the C&D waste. RCA complying to class 1 can normally be used without restrictions above groundwater and not directly placed into sea water or fresh water resources.

Regarding the Cr(total) and Cr(VI) concentrations, only small quantities of the latter were determined. Hence, most of the chromium content were likely on the trivalent form Cr(III). This chemical form has low solubility compared to the highly soluble hexavalent chromium, often seen as oxyanions (e.g. CrO₄²⁻) [7].

Table 6: Content of inorganic and organic substances determined in RCA samples

Substance	Total concentration (mg/kg) ^a			
	RCA 0/2 mm	RCA 4/16 mm	RCA 16/32 mm	Soil criteria ^b
As	3.1	5.5	< 3	8
Cd	0.06	0.06	0.096	1.6
Cr	103	138	126	50
Cr ⁶⁺	< 0.20	0.52	< 0.20	2
Cu	16	19	18	100
Pb	35	32	28	60
Hg	< 0.01	< 0.01	< 0.01	1
Ni	11.0	17	12.5	60
Zn	72	85	82	200
Sum PCB-7	n.d.	n.d.	n.d.	0.01
Sum PAH-16	0.16	n.d.	n.d.	2
Benzen	< 0.01	< 0.01	< 0.01	0.01
Toluene	< 0.04	< 0.04	< 0.04	0.3
Enthylbenzen	< 0.04	< 0.04	< 0.04	0.2
Xylene	< 0.04	< 0.04	< 0.04	0.2
THC > C5-C6	< 2.5	< 2.5	< 2.5	7
THC > C6-C8	8.7	< 7.0	< 7.0	7
THC > C8-C10	< 10	< 10	< 10	10
THC > C10-C12	< 10	< 10	< 10	50
THC > C12-C16	< 10	< 10	< 10	
THC > C16-C35	42	27	< 10	100
Sum > C12-C35	42	27	n.d.	100
TOC	1200	2100	1100	not issued

^a n.d. = not detected

^b Soil criteria for sensitive land use issued in Norwegian Pollution Control Regulation

4. CONCLUSION

No negative behaviour was observed during the production, pouring, finishing and curing of the concrete, compared to traditional concrete with crushed natural aggregates. The low content of fines in the sand reduced the cement content needed in the concrete, in particular for concrete mix with w/c ratio equal or below 0.45. Furthermore, low content of cement paste gave low water absorption to RCA and also demonstrated the ability of the wet recycling process to remove significant quantities of the mortar in the CDW.

The compressive strength complied to the requirements for C35/45 in NS-EN 206. From the point of view of the physical characteristics of the recycled aggregates and concrete, there was no negative impact of the use of this type of RCA.

The content of harmful chemical substances in the RCA samples was at a low level. Nearly all samples had a total concentration that complied with the strict Norwegian soil quality

criteria. Although the Cr(total) exceeded the criteria, the highly soluble hexavalent form (e.g. CrO_4^{2-}) was found to be less than 0.5% of the Cr(total). Hence, most of the chromium was present on the trivalent form, Cr(III), which has low solubility in the neutral to mildly basic pH region.

ACKNOWLEDGEMENTS

The study is part of the project RESGRAM which is supported by the Research Council of Norway.

REFERENCES

- [1] WFD (Waste Framework Directive), 'Directive 2008/98/EC of the European Parliament and of the Council of 19 November 2008 on waste and repealing certain Directives'. OJ L 312, 22.11.2008.
- [2] Arm, M., Wik, O., Engelsen, C.J., Erlandsson, M., Hjelmar, O. and Wahlström, M., 'How does the European recovery target for construction & demolition waste affect resource management?', *Waste Biomass Valor* 8 (2017) 1491–1504.
- [3] Magnusson, S., Lundberg, K., Svedberg, B. and Knutsson, S., 'Sustainable management of excavated soil and rock in urban areas - A literature review', *Journal of Cleaner Production* 93 (2015) 18-25.
- [4] RCN (Research Council of Norway), 'Recycled aggregates from excavation materials used in road construction and concrete production (RESGRAM)', RCN project number 256506/O20 (2016).
- [5] Ng, S. and Engelsen, C.J., 'Construction and Demolition wastes', in: 'Waste and Supplementary Cementitious Materials in Concrete: Characterisation, Properties and Applications', Editors: Rafat Siddique and Paulo Cachim (Elsevier, 2018).
- [6] Engelsen, C.J., van der Sloot, H.A., Wibetoe, G., Stoltenberg-Hansson, E., Petkovic, G. and Lund, W., 'Release of major elements from Recycled Concrete Aggregates and geochemical modelling', *Cement and Concrete Research*, **39** (5) (2009) 446-459.
- [7] Engelsen, C.J., van der Sloot, H.A., Wibetoe, G., Justnes, H., Stoltenberg-Hansson, E., Lund, W., 'Leaching characterisation and geochemical modelling of minor and trace elements released from recycled concrete aggregates', *Cement and Concrete Research* **40** (12): 2010: 1639-1649.

VARIATION IN PHYSICAL AND ENVIRONMENTAL PROPERTIES OF RECYCLED CONCRETE AGGREGATES FROM C&D WASTE IN DELHI

Christian J. Engelsen (1), Harsha Meenawat (3), Arun Kumar Sharma (2), Gaurav Bhatiani (3), Kshemendra Nath P (4), Monica S. Nodland (1)

- (1) SINTEF Building and Infrastructure, Norway
- (2) IL&FS Environmental Infrastructure & Services Ltd
- (3) IL&FS Academy of Applied Development
- (4) Resilient Energy Pvt. Ltd.

Abstract

Construction and demolition waste (CDW) is one of the biggest waste streams globally. The heavy inorganic part (from concrete and masonry) could be processed and refined into recycled aggregates. The Burari C&D waste recycling facility is located in the north of Delhi and is currently one of three recycling plants operating in Delhi. In relation to the Indo-Norwegian quality assessment program, the physical and environmental properties have been studied.

The physical, chemical and environmental properties determined over time were found to be relatively stable during the extensive sampling periods. Most of the parameters were complying to the requirements in IS 383. For some parameters, such as specific gravity and fines content, small modifications in the recycling process will decrease the fine particle content to the desired level. However, RCA with higher contents can be used in other applications like for example concrete block production.

The contents of inorganic and organic dangerous substances were found to comply with the strictest soil criteria (class I) in Norway. Cr(total) exceeded the criteria. However, most of the chromium was present on the trivalent form, Cr(III), which has low solubility in the neutral to mildly basic pH region.

Keywords: Recycled aggregates, mechanical and environmental properties

1. INTRODUCTION

Construction and demolition waste (CDW) is one of the biggest waste streams globally. The heavy inorganic part (from concrete and masonry) could be processed and refined into recycled aggregates. This type of aggregates could substitute natural aggregates in a range of user applications such as road construction, landscaping and concrete production. This will save natural resources, decrease transportation, reduce landfilling and bind CO₂ through increased carbonation.

The revised framework for waste management in the EU [1], which was adopted in 2008, includes a target for recovery of CDW. Within 2020, the preparing for re-use, recycling and other material recovery of non-hazardous construction and demolition waste (excluding naturally occurring material) shall be increased to a minimum of 70 % by weight. The target was added during the final negotiations of the Directive text and instructions for verifying compliance were established in 2011 [2]. Norway has implemented the WFD and must comply to this target through the partnership of the European Economic Area. The directive is intended to be an overall key driver for circular driven economy for C&D waste. In India, the estimates for the annual CDW generation vary from 50-500 million tons. However, more accurate figures could be calculated for Delhi where the generation is around 3000-4000 tons per day. Thus, it is challenging to meet the demands for treatment and recycling.

In 2016, Central Public Works Department (CPWD) under Ministry of Housing & Urban Affairs (MoH&UA), Govt. of India has signed a Memorandum of Understanding (MoU) with the Foundation for Scientific & Industrial Research (SINTEF, Norway). The institutions agree to facilitate collaboration on all aspects of waste management and building technology with special emphasis on best available technology on recycling of construction and demolition waste. The purpose of the MoU is to incept a 4-years institutional cooperation project between CPWD and SINTEF on capacity building and technical support on treatment and utilisation of construction and demolition waste in India. The Indo-Norwegian project (C&D-WIN) started in 2017 and is supported by the Royal Norwegian Embassy New Delhi. It will continue to the end of 2020.

In the present study, recycled concrete aggregates (RCA) produced in recycling facility in Delhi have been assessed for variation in essential properties (density, water absorption, etc.) over time. The aggregates produced may be suitable for bound (e.g. concrete production) and unbound use (e.g. road construction). The study was part of the C&D-WIN project.

2. MATERIAL AND METHODS

2.1 Description of the feedstock material and sampling procedure

The sampling of RCA was conducted at Burari C&D waste recycling plant in Delhi. This plant has installed the wet recycling processes (CDE Aggmax™ system). In addition, the plant has a dry processing support line for feedstock that contains mostly concrete rubble. The sampling was conducted in the period of November 2017 to February 2018. The feedstock material contained largely concrete and concrete masonry units intermixed with some soil. Small fractions of bricks and ceramics could be found occasionally. These quantities were initially evaluated to have low influence on the final RCA properties due to their relative small share.

The sampling represented a daily production shift by collecting sub-samples from the conveyer belts every 1-2 hour during the whole working shift, i.e. 5 sub-samples. These samples were mixed and homogenised to one daily bulk sample. The sampling program was developed by SINTEF who was present at site together with Bureau Veritas during the sampling period. A total of 4 daily bulk samples were prepared and analysed during the sampling period at Bureau Veritas in Delhi and at SINTEF and ALS Laboratory in Norway.

2.2 Physical properties determined in RCA

The cement paste content was assessed for all samples since the mortar content in RCA often represents the weaker bonding in the interfacial transition zone (ITZ) between the RCA particle and the cement paste [3]. It has been shown earlier that the acid soluble content can serve as an indicator for the cement paste content in RCA [4]. Hence, the acid soluble content was determined according to the procedure described in [4]

In addition, the following properties determined according to Indian standard IS 2386 [5] will be presented:

- Classification of coarse RCA
- Particle grading
- Shape of coarse aggregates (combined elongation and flakiness index)
- Specific gravity and water absorption
- Aggregate abrasion value of coarse aggregates, by Los Angeles (LA)

2.3 Chemical and environmental properties of RCA

The RCA samples were reduced in volume by splitting, quartering, crushing and pulverization. The reduction of the laboratory samples to test samples and to final test portions was conducted according to NS-EN932-2 and NS-EN 15002.

The presence of following organic and inorganic substances was determined in the RCA samples; polychlorinated biphenyl (Σ PCB-7), polycyclic aromatic hydrocarbon (Σ PAH-16), BTEX (benzene, toluene, ethylbenzene, xylene), total hydrocarbons (THC), total organic content (TOC), As, Cd, Cr(total), Cr(VI), Cu, Pb, Hg and Ni.

GC-MS with selective ion monitoring (SIM) was used to determined Σ PCB-7, Σ PAH-16 and BTEX. THC were analyzed using GC with flame ionization detector. Heavy metals were analyzed by Inductively coupled plasma (ICP). In addition, the acid soluble contents of sulphate and chloride were determined according to EN 1744-1 and IS 14959-P-2, respectively.

3. RESULTS AND DISCUSSION

3.1 Acid soluble content

The acid soluble content is shown in Table 1 and was found to be in the region of 19-33%. These contents were considered to be slightly higher than what normally can be found in only concrete rubble [4]. The presence of different types of mortar from masonry usually contribute to increase the cement paste content. Furthermore, the acid soluble contents were inorganic in

nature as the TOC levels were less than 1%, as will be shown in chapter 3.4. Hence, considerable amounts of cement paste were present in the RCA. In addition, it can be seen that the cement paste is accumulating more in the finest particle size, i.e. in RCA 0/3 mm. It is emphasised that these recycled aggregates were produced from a dry process line. In a wet recycling process, a significant amount of the cement paste can be removed by washing and scrubbing.

Table 1: Acid soluble content given weight % as the arithmetic mean of 3 replicates

Daily sampling number	RCA 0/3 mm	RCA 3/10 mm	RCA 10/20 mm
1	not determined	26	not determined
2	27	25	23
3	32	29	19
4	33	29	27

3.2 Particle grading and classification of coarse aggregates

The sieving analysis revealed that the RCA 10/20 mm was entirely according to the requirements in IS 383 [6]. Regarding the samples RCA 0/3 mm and RCA 3/10 mm, the content of particles less than 75 μm was typically higher than the criteria of 10% and 1%, respectively. Decreasing the fines content by for example a washing step will most likely result in compliance with IS 383 for RCA 0/3 mm (Zone-II) and RCA 3/10 mm.

The classification of coarse aggregates (3/10 mm and 10/20 mm) showed that only small amounts of clay masonry was found in all tested samples. The content of concrete, mortar and unbound masonry was in the region of 40-50%. Furthermore, bitumen, glass, metal, wood and gypsum were not found.

3.3 Other important physical and chemical properties

Based on previous analysis (cement paste content and classification), some variation between the sampling periods was found. The impact of this variation on the other important properties are shown in Figure 1. Water absorption and specific gravity were found to be relatively stable, except for one sample. The results also showed the expected difference between the three different particle sizes, i.e. highest density and lowest water absorption for the coarsest fraction. Furthermore, the combined elongation and flakiness, aggregate abrasion (by LA) and the acid soluble sulphate content were evaluated to be relatively stable over the sampling periods. The acid soluble chloride content varied but at a low concentration level. Some chloride results in the sampling period 2, were found to be around and insignificantly above the IS 383 criteria of 0.04 %. Except for the specific gravity of RCA 0/3 mm, the results complied to IS 383.

It is emphasised that part removal of the fines will lead to lower chloride content and increased specific gravity, in particular for the RCA 0/3 mm fraction. Decreasing the fines content without installing a washing step, may be conducted by installing a by-pass or reduce the entering of overflow materials into the recycling process.

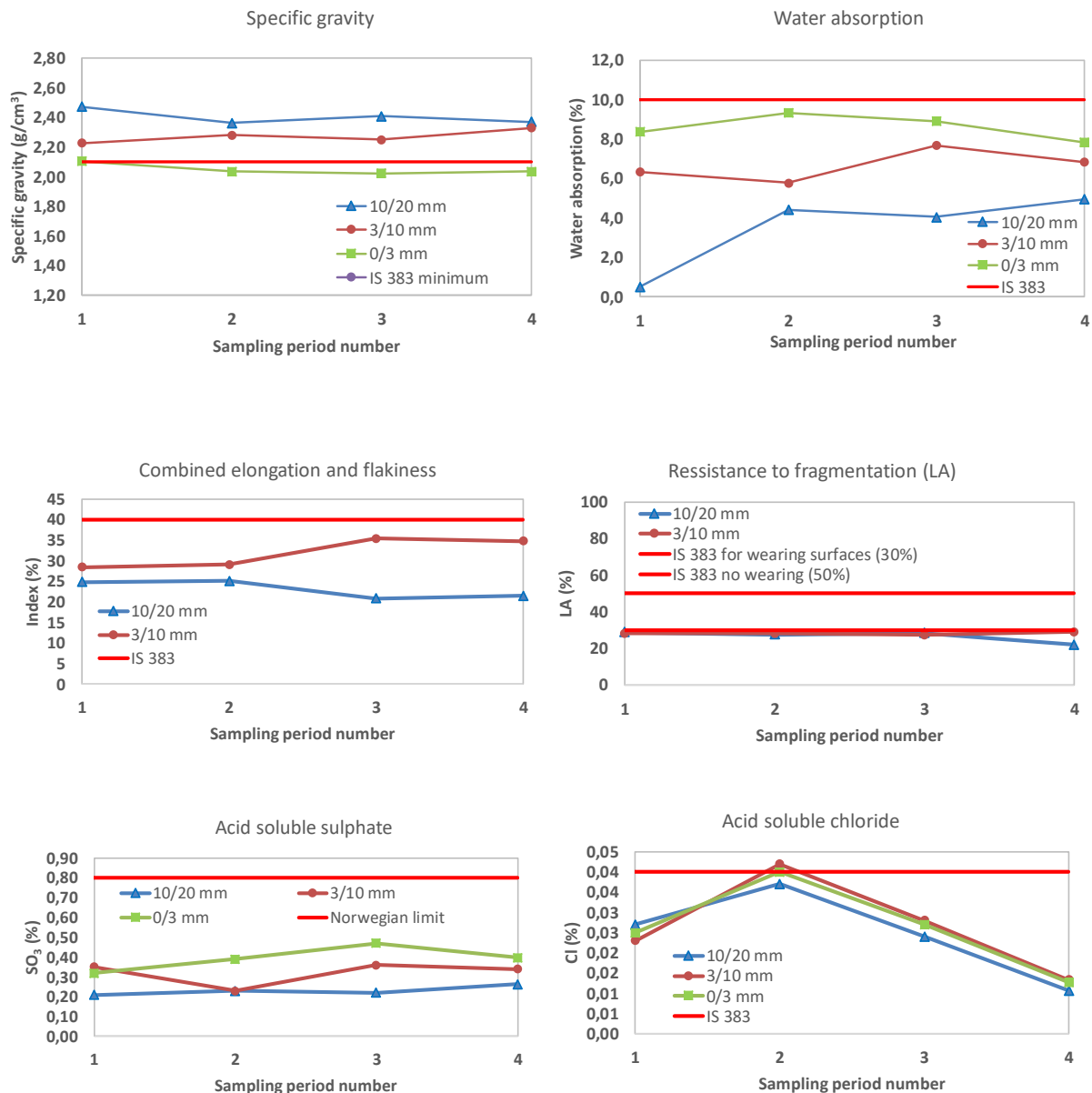


Figure 1: Variation in time of important properties of RCA

3.4 Environmental assessment

Results from the analyses of organic substances and heavy metals in the samples are given in Table 2. Except for Cr(total), the results obtained complied with the Norwegian soil quality criteria (class 1) issued in the Norwegian Pollution Control Regulation. These criteria were originally developed for handling of polluted soil. However, they are currently being used to assess the environmental ability to recycle C&D waste. RCA complying to class 1 can normally be used without restrictions above groundwater and not directly placed into sea water or fresh water resources. Regarding the Cr(total) and Cr(VI) concentrations, only small quantities of the

latter were determined. Hence, most of the chromium content were likely on the trivalent form Cr(III). This chemical form has low solubility compared to the highly soluble hexavalent chromium, often seen as oxyanions (e.g. CrO_4^{2-}) [7].

Table 2 Content of inorganic and organic substances determined in the RCA samples

Substance	Total concentration (mg/kg) ^a			
	RCA 0/3	RCA 3/10	RCA 10/20	Soil criteria ^b
As	4.8 - 4.9	3.8 - 6.1	3.4 - 5.6	8
Cd	0.10 - 0.18	< 0.05 - 0.12	0.07 - 0.12	1.6
Cr(total)	120 - 147	100 - 165	117 - 160	50
Cr(VI)	0.9 - 1.6	0.3 - 1.0	< 0.20 - 0.6	2
Cu	25 - 31	18 - 39	19 - 31	100
Pb	19 - 20	15 - 23	14 - 19	60
Hg	0.011 - 0.027	< 0.01 - 0.02	< 0.01	1
Ni	21 - 23	21 - 24	21 - 25	60
Zn	59 - 68	48 - 56	48 - 82	200
Sum PCB-7	n.d. - 0.02	n.d.	n.d.	0.01
Sum PAH-16	0.06 - 0.09	n.d. - 0.9	n.d.	2
Benzen	< 0.010	< 0.010 - 0.02	< 0.010	0.01
Toluene	< 0.040	< 0.040	< 0.040	0.3
Enthylbenzen	< 0.040	< 0.040	< 0.040	0.2
Xylene	< 0.040	< 0.040	< 0.040	0.2
THC > C5-C6	< 2.5	< 2.5	< 2.5	7
THC > C6-C8	< 7.0	< 7.0	< 7.0	7
THC > C8-C10	< 10	< 10	< 10	10
THC > C10-C12	< 10	< 10	< 10	50
THC > C12-C16	< 10	< 10	< 10	
THC > C16-C35	10 - 130	40 - 150	27 - 46	100
Sum > C12-C35	10 - 130	40 - 150	27 - 46	100
TOC	8000 - 9000	2000 - 7000	4000 - 5000	-

^a n.d. = not detected

^b Soil criteria for sensitive land use issued in Norwegian Pollution Control Regulation

4. RECOMMENDATIONS

The results suggest that the output from Burari to be broadly compliant with IS 383. Hence, efforts should be made by all stakeholders to increase the usage of recycle materials. Furthermore, two important issues need consideration. Firstly, replicating success of Burari in other cities with particular emphasis on lessons learnt, so as not to reinvent wheel after almost a decade of operational experience with CDW facilities. Secondly, ensuring financial viability of CDW facilities will require emphasis on continuous product testing, standardization and certification through independent channels to enhance confidence among the construction

contractors. This study is a step in this direction. Burari should take steps, as suggested, to further enhance quality of its output to serve more advanced needs and collaborate with large and sophisticated construction companies.

5. CONCLUSION

The results show that relatively stable physical, chemical and environmental properties were determined during the extensive sampling periods. Most of the parameters were complying to the requirements in IS 383. For some parameters like specific gravity and fines content, small modifications in the recycling process could easily decrease the fine particle content to the desired level. However, RCA with higher contents of fines have shown excellent properties, in for example, concrete block production.

The contents of inorganic and organic dangerous substances were found to comply with the strictest soil criteria (Class I) in Norway. Although the Cr(total) exceeded the criteria, most of the chromium was present on the trivalent form, Cr(III), which has low solubility in the neutral to mildly basic pH region.

ACKNOWLEDGEMENTS

The authors are grateful to Nivedita Borthakur and Aanchal Susheen for assistance in sampling and data entry. The study is part of the Indo-Norwegian project on "*Treatment and recycling of C&D waste in India*" supported by the Royal Norwegian Embassy New Delhi.

REFERENCES

- [1] WFD (Waste Framework Directive), 2008. Directive 2008/98/EC of the European Parliament and of the Council of 19 November 2008 on waste and repealing certain Directives. OJ L 312, 22.11.2008.
- [2] Arm, M., Wik, O., Engelsen, C.J., Erlandsson, M., Hjelmar, O. and Wahlström, M., How does the European recovery target for construction & demolition waste affect resource management?, *Waste Biomass Valor* **8** (2017) 1491–1504.
- [3] Ng, S. and Engelsen, C.J., 2018. *Construction and Demolition wastes*, In: *Waste and Supplementary Cementitious Materials in Concrete: Characterisation, Properties and Applications*. Editors: Rafat Siddique and Paulo Cachim, Elsevier publication.
- [4] Engelsen, C.J., van der Sloot, H.A., Wibetoe, G., Stoltenberg-Hansson, E., Petkovic, G. and Lund, W., 'Release of major elements from Recycled Concrete Aggregates and geochemical modelling', *Cement and Concrete Research*, **39** (5) (2009) 446-459.
- [5] IS 383, Indian Standard - Methods of test for aggregates for concrete, 1967 (reaffirmed 2007), Bureau of Indian Standards 2007.
- [6] IS 2386, Indian Standard – Coarse and fine aggregate for concrete - Specifications, 2016 (third revision), Bureau of Indian Standards 2016.
- [7] Engelsen, C.J., van der Sloot, H.A., Wibetoe, G., Justnes, H., Stoltenberg-Hansson, E., Lund, W., 'Leaching characterisation and geochemical modelling of minor and trace elements released from recycled concrete aggregates', *Cement and Concrete Research* **40** (12): 2010: 1639-1649.

OPTIMIZING PERFORMANCES OF RECYCLED AGGREGATES FOR IMPROVING CONCRETE PROPERTIES

L. Courard (1), E. Tabarelli (1), F. Michel (1), S. Delvoie (1), M. ElKarim Bouarroudj (1) (2), Ch. Colman (1) (2), Z. Zhao (1)

(1) Urban and Environmental Engineering, GeMME Building Materials, University of Liège, Belgium

(2) IMT Douai, Laboratoire de Génie Civil et Géo-environnement, Université de Lille, France

Abstract

Construction waste management is a quite important economic and environmental deal for our societies. More than 2 million tons demolition and construction wastes are annually produced only in Wallonia, Southern Region of Belgium: recycling has clearly to be promoted and by products to be valorised as secondary raw materials.

The influence of the fine recycled concrete aggregates (FRCA) on the mechanical and durability properties of concrete was used for producing concrete. Concretes with different substitution rates (0, 30 and 100%) of natural sand by the FRCA were manufactured. Mechanical properties (compressive strength) and durability properties (capillary absorption, carbonation depth, and freeze/thaw resistance) were investigated. The results show that the compressive strength of concrete decreased as the substitution of FRCA increased. Durability of concrete could be strongly influenced by the high porosity and water absorption of fine recycled concrete aggregates. Brick fillers (BF) have also been studied for producing Self Compacting Mortars (SCM): introduction of 50 and 100% substitution clearly show a reduction of workability properties if particles water absorption is not taken into account. However, mechanical properties at 7 and 28 days didn't show a clear impact of the substitution of limestone filler by brick filler.

Keywords: fine, recycling, concrete, bricks, self-compacting

1. INTRODUCTION

Large quantities of construction and demolition wastes (CDW) are produced each year. So far, only a small fraction of these concrete wastes is reused as aggregate for road foundations and concrete production [1]. Recycled concrete aggregates (RCA) are composed of a mix of

natural aggregates and hardened adherent cement paste. The latter is usually much more porous than natural aggregates [2] and leads to a larger water demand which makes RCA more difficult to recycle into concrete [3]. Larger porosity of aggregates could however induce lower dead load for construction and have a positive impact on structural behaviour of buildings. Finally, according to the law of mass, lower weight is correlated to lower heat transfer. Properties of RCA such as water absorption, porosity, and shape can deeply influence the properties of fresh concrete as well as mechanical properties and durability of concrete made with RCA [4].

Depending on the area and the period of construction, bricks and tiles are also present in the city. Recycled bricks usually offer less quality recycled aggregates as they are more porous which is directly correlated to lower mechanical properties. However, for specific applications like water absorption, lightweight structures or thermal insulation, such a properties may be valorised.

If coarse aggregates are commonly reused for road foundations, fine recycled concrete aggregates (RCA) and brick fillers (BF) are less commonly used. The research program which is here presented intended to evaluate the use of sand produced from crushed recycled concrete aggregates and fillers from bricks for the design mortars.

2. PROPERTIES OF CONCRETE WITH FINE RECYCLED CONCRETE AGGREGATES

The fine fraction of RCA, essentially composed of mortar and hardened cement paste, possesses a large water demand which makes it less easy to recycle into concrete compared to coarser RCA. The influence of the fine recycled concrete aggregates (FRCA) on the mechanical and durability properties of concrete is studied.

2.1 Experimental program

The cement used in concrete was an Ordinary Portland Cement (CEM I 52.5 N). Two calcareous natural aggregates (NA2/7 and NA6/14) were used for the manufacture of concretes. The water absorption of these two aggregates was 0.68 and 0.32%, respectively for NA2/7 and NA6/14 and their apparent particle density was 2.7 g/cm³ according to EN 1097-6. A natural river sand (NS0/2) was used with a water absorption of 0.70%.

Recycled concrete aggregates (RCA) (0/31.5mm) were provided by crushing concrete wastes in a recycling plant; only the fine fraction 0/2mm (noted as FRCA0/2) was used. The water absorption of FRCA0/2 was 8.8% and its apparent particle density was 2.47 g/cm³. Sieve analysis showed that the grain size distributions of NS and FRCA were comparable [2].

The concretes with different substitution rates (0, 30 and 100%) of natural sand by the same volume of FRCA were manufactured (Table 1). The absorbed water was adjusted according to the water content of the aggregates and their water absorption: half of the total water was added to pre-saturate the aggregate in the mixer for 5 minutes before the addition of cement. The other half of the water was added after introduction of the cement.

Slump and air content of fresh concrete were measured according to EN 12350-2 and EN 12350-7, respectively. After 24h, specimens were demoulded and stored in a climatic room (20±2°C and a relative humidity 95±5%). The compressive strength of concrete was measured according to EN 12390-3 on cubic samples (150mm x 150mm x 150mm) and performed after 7 days and 28 days of curing. The capillary water absorption of concrete was measured on cubic samples (100mm x 100mm x 100mm) according to Belgian standard NBN B 15-217.

The lower side of the specimen was placed into water and removed and weighed at various time intervals. The porosity of concrete was evaluated by the total immersion test in water.

Table 1: Composition of concrete (1 m³)

	B_FRCA0	B_FRCA30	B_FRCA100
NA 6/14 (kg)	550	550	550
NA 2/7 (kg)	775	775	775
NS 0/2 (kg)	600	420	0
FRCA 0/2 (kg)	0	168	559.2
Cement (kg)	320	320	320
Efficient water (kg)	160	160	160
Absorbed water (kg)	11.2	24.7	56.2
Superplasticizer (kg)	3.4	3.4	3.4
W_{eff}/C	0.5	0.5	0.5

Carbonation of concrete was evaluated on prismatic specimens (100mm x 100mm x 400mm). After curing for 28 days in the climatic room, the specimens were stored in a room at 20±2°C and a relative humidity of 60±5% until constant mass and then in a carbonation room with CO₂ concentration of 3% by volume for 4 weeks. After each week, specimens were taken out the carbonation chamber and split for measuring carbonation depth with phenolphthalein pH indicator.

Moreover, specimens (100mm x 100mm x 100mm) were subjected to 14 freeze-thaw cycles (24h cycle from -15°C to +10°C) according to Belgian standard NBN B 05-203. Freezing was carried out at -15°C in air and thawing was undertaken in the water at 10°C. The mass loss of all the specimens was recorded.

2.2 Fresh properties of concrete

Figure 1 shows the variation of slump for the three concretes after 0 and 30 minutes. It can be seen that the initial slump slightly decreased for concretes with recycled sand. After 30 minutes, the slump of all types of concrete decreased whatever the different substitutions. It is also shown that the rate of slump loss was larger as the substitution increased, which could be due to the higher water quantity absorbed by the higher percentage of recycled sand after the mix.

The air content of concrete increased (2.2% for concrete B_FRCA0, 3.3% for concrete B_FRCA30, and 5.5% for concrete B_FRCA100) when the substitution of recycled sand increased. Increased air content is also known to occur in lightweight aggregate concrete, which shows some similarities with concrete made with recycled aggregate [5].

2.3 Hardened properties of concrete

Figure 2 shows the compressive strength of the mixes at different ages. The compressive strengths of concretes with FRCA were lower than those of concrete with natural sand. The compressive strength of concrete made with 100% FRCA at 28 days decreased for 48.2% comparing with the reference concrete, while the concrete made with 30% FRCA at 28 days decreased for 15.9% comparing with the reference concrete.

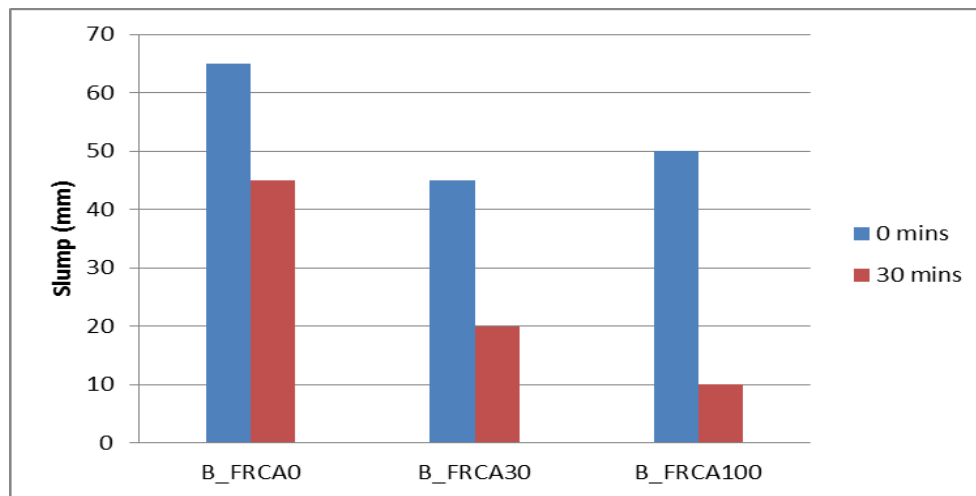


Figure 1: Change of slump as a function of three concretes

Figure 3 presents the rate of capillary absorption as a function of types of concretes. As can be seen, the rates of absorption of the recycled concrete were much larger than the reference concrete. The coefficient of capillary absorption of concrete B_FRCA100 was 0.38 kg/m²/h^{0.5}, while it was 0.11 and 0.14 g/m²/h^{0.5} for the reference concrete and B_FRCA30, respectively.

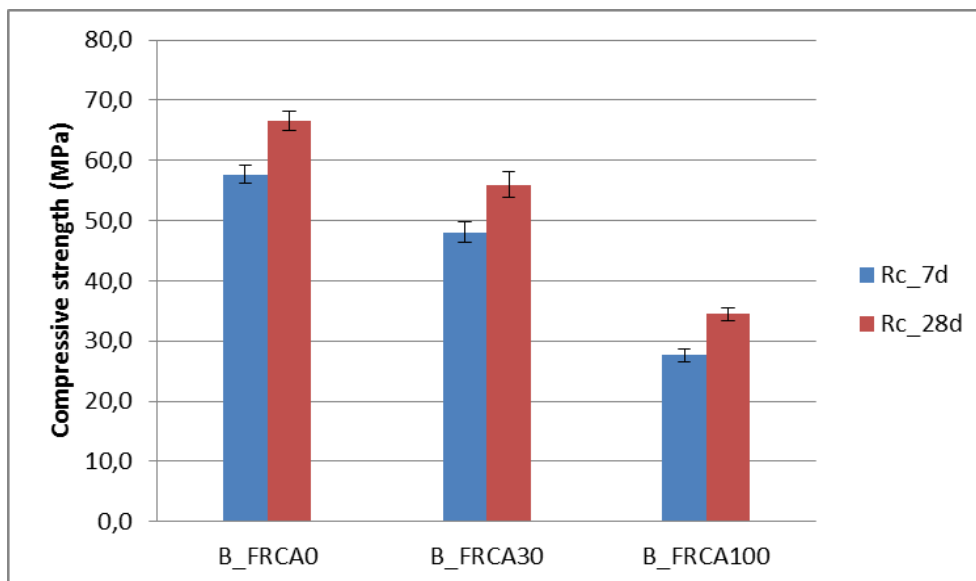


Figure 2: Compressive strength of concretes at different ages

The higher capillary absorptions of recycled concrete were certainly caused by the incorporation of FRCA, which had higher porosity comparing with the natural sand, leading to the higher porosity of concrete.

The capillary absorption of concrete was little affected by the presence of FRCA up to 30%. This was confirmed by the results of porosity of concrete measured by immersion (the total porosity estimated by water absorption for the concrete B_FRCA100 was 9.5%, while it

was estimated as 4.2% and 5.3% for the reference concrete and B_FRCA30 respectively). The rate of absorption, rather than the total absorption, is mainly affected by the structure and size distribution of the pores in the concrete.

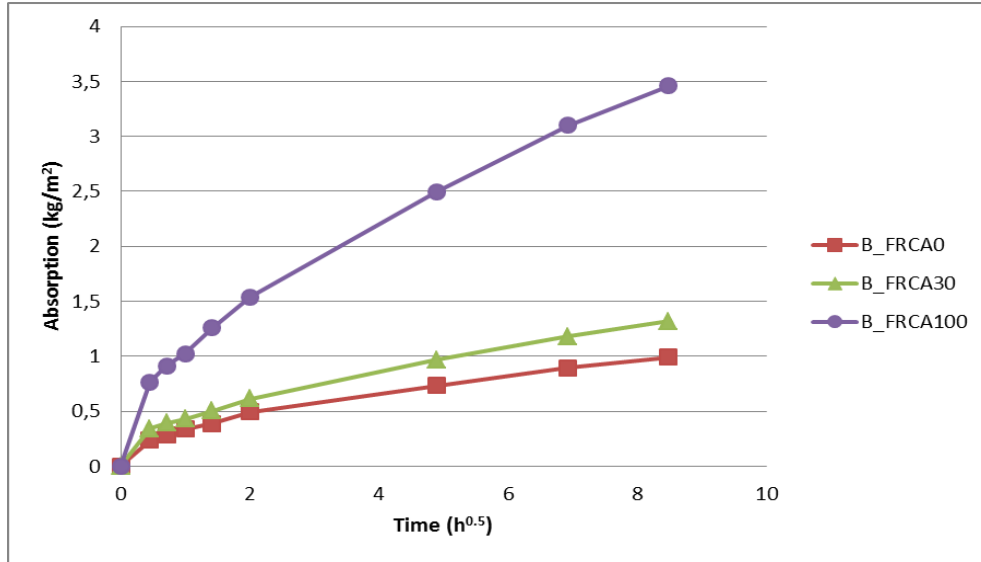


Figure 3: Capillary absorption as a function of types of concretes

These lower mechanical strengths are certainly caused by the poorer properties of FRCA in comparison to natural sand used; the presence of adherent cement paste leading to higher porosity comparing with the natural sand.

Figure 4 shows the depth of carbonation as a function of time in the carbonation room for all types of concretes. For the first 14 days, the carbonation depths of B_FRCA0 and B_FRCA30 were zero, while it was 5 mm for the concrete made with 100% recycled sand.

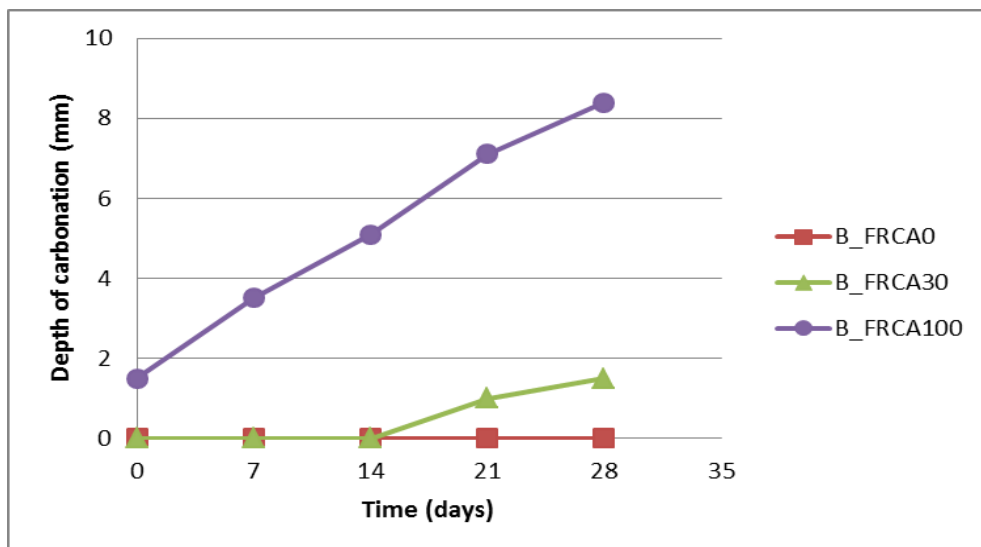


Figure 4: Depth of carbonation as a function of time in the carbonation room

After 28 days, the carbonation depth of B_FRCA100 was 9mm, while it was lower than 2mm for the B_FRCA30, and zero for the reference concrete. The higher depth of carbonation of the recycled concrete could be due to the higher porosity in concrete, inducing a faster diffusion of CO₂ into the concrete.

After 14 cycles of freeze-thaw (Fig. 5), the visual specimen's examination did not allow detecting any significant deterioration for all the concretes. The mass loss is presented in Figure 5. The recycled concretes had lower freeze-thaw resistance comparing with the reference concrete, which was due to higher porosity in the recycled concrete.

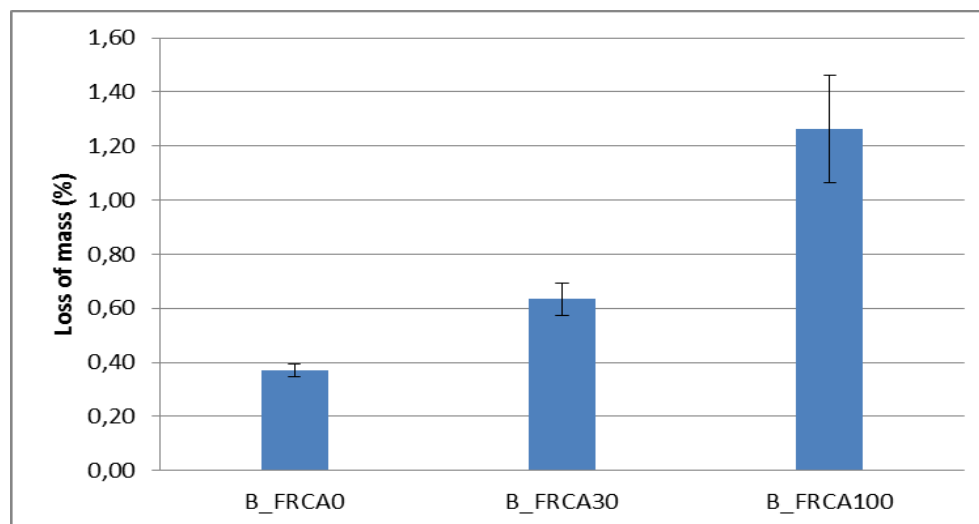


Figure 5: Mass loss due to the freeze-thaw cycles

3. SELF COMPACTING MORTARS WITH BRICK FILLER

3.1 Production and characteristics of brick filler

Brick fillers (BF) were produced from red bricks after reducing dimensions with two jaw crushers, successively, which allowed to collect particles under 4 mm. A natural limestone filler is used as a reference. Sieving curve is given on Fig. 6 in comparison with natural limestone filler. Regarding physical properties, limestone filler presents a lower β_p compared to the brick filler, which can be justified by finer particles and a more uniform sieving curve: due to the monodisperse distribution of the brick filler, the higher quantity of particles with the same dimensions induces voids in between and, consequently, a higher water demand.

3.2 Self Compacting Mortars

A reference mortar was designed with 1350g sand, 448g cement, 298g limestone filler and 358g efficient water. The gradual replacement of limestone filler is performed through a volumetric substitution of the limestone filler (eq. 1):

$$M_{Brick\ filler} = \frac{M_{Limestone\ filler}}{M_{v,limestone\ filler}} * M_{v,brick\ filler} \quad (1)$$

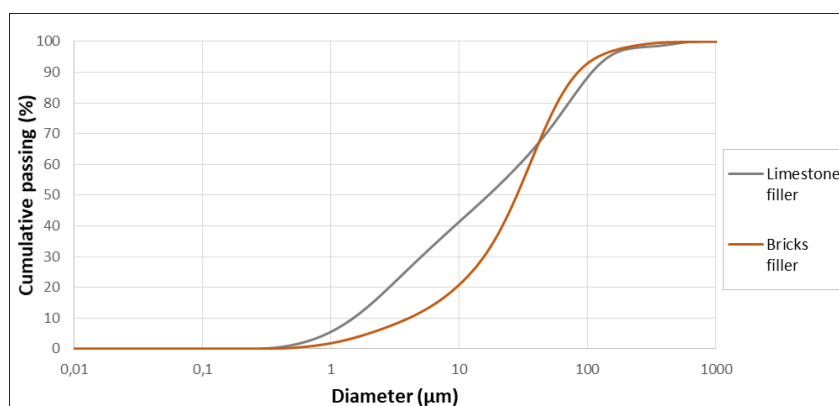


Figure 6: Comparison of the particle size distribution of natural limestone and brick fillers

Although the water absorption of a filler, due to its low particles size distribution, is not taken into consideration, the analysis was here performed to verify the presence or not of the microporosity [6]. Two kinds of samples were produced. The first, BFNWA (Brick Filler No Water Absorption), neglects the water absorption of the brick fraction. The second, BFWA (Brick Filler Water Absorption), takes into account the possible absorption of the brick particles. The limestone filler was partially replaced by the brick filler for 50% and 100% in volume, respectively.

Table 2: Mix properties of mortars with brick fillers

Sample	Substitution (%)	Cement (g)	Limestone filler (g)	Brick filler (g)	Efficient water (g)	Water absorption (%)	Sand (g)
BFWA-50	50	448	149.17	168.09	358.4	18.49	1350
BFWA-100	100		0	336.19		36.98	
BFNWA-50	50		149.17	168.09		0	
BFNWA-100	100		0	336.19		0	

At 7 days (Table 3), a slight decrease of values is recorded with the increase of the limestone filler substitution. On the other hand, after 28 days, the values offer a general decrease for the samples BFWA-50 and BFWA-100, while for the mortars BFNWA-50 and BFNWA-100 seem to be closer to the reference mix.

Table 3: Compressive strength of mortars with brick fillers brick fillers

Sample	Compressive strength at 7 days (MPa)	Compressive strength at 28 days (MPa)
BF-0	32.18	37.61
BFWA-50	31.31	36.37
BFWA-100	26.80	35.61
BFNWA-50	30.38	37.76
BFNWA-100	29.17	39.41

It means that the variations in the composition and in the quantity of the mixing water can influence the final mechanical properties of the mortar. Indeed, comparing the samples with

50% and 100% of replacement, the addition of water to face the possible absorption by the brick material leads to a decrease after 28 days. However, this is not confirmed by 7 days, where the sample BFWA-50 presents a similar compressive strength to the mortar BFNWA-50.

4. CONCLUSIONS

Concrete design with recycled materials shows that the compressive strength decreases as the substitution of FRCA increased. However, the compressive strength of concrete made with 100% FRCA could reach 35MPa after 28 days. Durability of concrete could be strongly influenced by the high porosity and water absorption of recycled concrete aggregates. The durability properties of concrete made with 30% FRCA were comparable to the reference concrete, especially for capillary absorption and carbonation. Therefore, the use of FRCA in concrete structures can be envisaged depending on their class of exposure and the concrete grade requirement (for example the concrete C25/30 with no risk of corrosion or attack). Substitution rate of natural sand up to 30% is acceptable, while for the substitution rate higher than 30%, mechanical properties of concrete should be checked while the effects on durability should be also monitored for specific applications. Brick filler could also replace natural limestone fillers when taking into account water absorption but with a very low decrease of mechanical performances.

ACKNOWLEDGEMENTS

The authors are grateful to INTERREG FWVL, which provided financial support to this study as part of VALDEM research project entitled “*Integrated solutions for the vaporization of construction and demolition wastes. Cross border approach for circular economy*”. Authors also warmly thank PREFER Company and CTP (Centre Terre et Pierre) for providing and preparing materials, respectively.

REFERENCES

- [1] Topcu I.B., Sengel S. ‘Properties of concretes produced with waste concrete aggregate’. *Cement and Concrete Research* **34** (2004) 1307-1312.
- [2] Zhao Z., Courard L., Michel F., Delvoie S., Bouarroudj MEK, Colman C., Xiao J. Properties of concrete with recycled construction and demolition wastes: a research experience in Belgium. Industry-Academia Forum on Advances in Structural Engineering IFASE (in: Sustainable structures and materials, ed. Xiao Jianzhuang, China Architecture and Building Press). Tongji University, Shanghai, 7-9 September 2018, 79-90.
- [3] Courard L., Michel F., Delhez P. ‘Use of Concrete Road Recycled Aggregates for Roller Compacted Concrete’. *Construction and Building Materials* **24** (2010) 390-395.
- [4] Poon C.S., Shui Z.H., Lam L., Fok H., Kou S.C. ‘Influence of moisture states of natural and recycled aggregates on the slump and compressive strength of concrete’. *Cement and Concrete Research* **34** 31-36.
- [5] Amnon, K. ‘Properties of concrete made with recycled aggregate from partially hydrated old concrete’, *Cem Concr Res.* **33** (2003) 703-711.
- [6] Tabarelli, E. ‘The recycling of crushed waste bricks in self-compacting mortars’. Master thesis in geological engineering, Research Unit in Urban and Environmental Engineering, University of Liège, 2018, 119p.

CONCRETE WITH WASTE GLASS AS A SUSTAINABLE BUILDING MATERIAL FOR PRECAST KERBS

Goce K. Prangovski (1), Georgi D. Goshev (2)

(1) Civil Engineering Institute Macedonia

(2) Civil Engineering Institute Macedonia

Abstract

This research shall examine the possibility for applying the concept of sustainable development during the production of concrete which is used for the manufacturing of concrete prefabricates. Waste glass is used from CRT monitors, as replacement for aggregate in the concrete, in order to achieve this aim. The exploitation of natural resources is avoided by this approach, and the same time the problem with the excessive e-waste is being solved.

Waste glass from CRT monitor is being used as partial and complete replacement for aggregate with fraction 0-4.0mm, and without addition of additives.

In order to approve the concrete properties which may be used in prefabricated concrete elements, precisely concrete kerbs, previous tests have been made of the properties of fresh and hardened concrete.

After the approval of the properties, kerbs have been manufactured in the laboratory, and all properties have been tested on them and they have been approved in accordance with the European Standard EN 1340 Concrete kerbs for sidewalks-Requirements and testing methods.

This research proves the possibility for appliance of glass from CRT monitors for manufacturing concrete which may be used for manufacturing concrete prefabricates.

Keywords: concrete, concrete mixtures, waste glass, sustainable development, kerbs

1. INTRODUCTION

Lately, one of the most popular topics is the Sustainable Development. The concept is creating the balance between the improvement of the society and the preservation of nature. The list of fields where this is applicable is endless, and one of them is the civil engineering. This filed includes multiple opportunities for application of the sustainable development concept, among which the concrete industry.

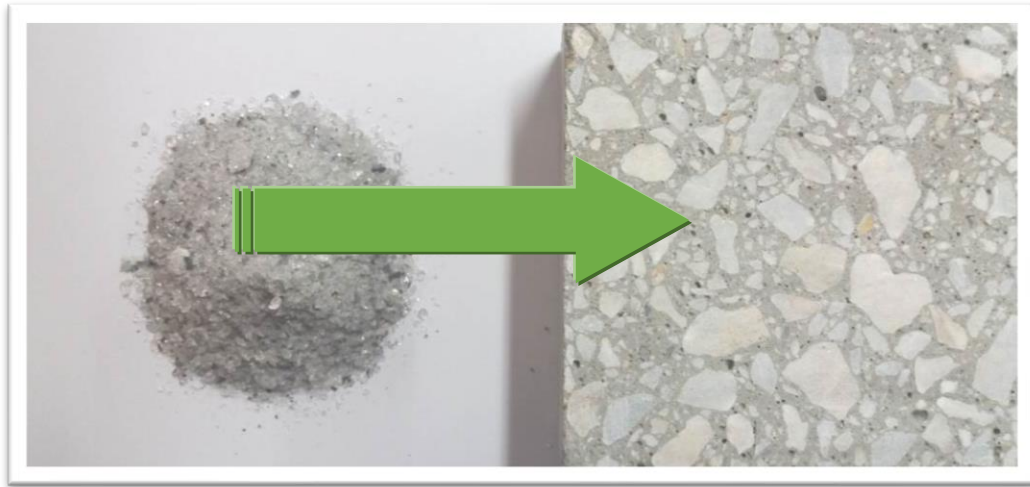


Fig. 1: Sustainable development concept during concrete production

One of the best ways to make the concrete industry sustainable is to process and apply certain waste materials as a substitute for natural materials. Such approach has multiple advantages: the excessive waste problem can be solved, the possibilities for environmental protection increased, the natural resources exploitation prevented, the energy saved, the harmful gases emission reduced, etc. This investigation should test the possibility for application of sustainable development concept during the concrete production which will be used for the precast concrete production. In order to achieve this, waste glass from CRT monitors will be used as substitute for the fine aggregate in the concrete. Such approach prevents the exploitation of the natural resources and resolves the excessive e-waste problem.

One of the most important components on each computer is the CRT monitor. The development of new technologies and the replacement of the old CRT – monitors with new, thin monitors, has shown that proper recycling is important in preserving the environment. The cathode ray tube of the CRT – monitors consists of two parts: front glass (screen) and back glass (conical). The screen is thicker and contains lead to protect the users from radiation. The back glass has a similar composition as the front one, but the difference is that it contains higher percentage of lead. The monitors with cathode ray tubes are made up of silicate glass with complex composition which is the result of the presence of different oxides. CRT monitors contain many harmful substances, which if not properly processed, have negative impact on the environment and on people's health. Therefore, the recycling of such monitors differs from the general processing of the e-waste.

2. PREPARATION AND TESTING OF THE GLASS

Glass from electronic waste – CRT monitors was used. It was obtained in cooperation with the company from Skopje which collects this type of glass and manages it. The required number of monitors was obtained from the landfill for CRT monitors.

CRT monitors were taken to the workshop where the front of the monitor was mechanically separated from the back.

Such separated front section of the CRT monitors was taken to a plant with a crushing unit and it was crushed in fraction of 0-4mm. The obtained glass aggregate of electronic waste was sent to the laboratory to be tested.

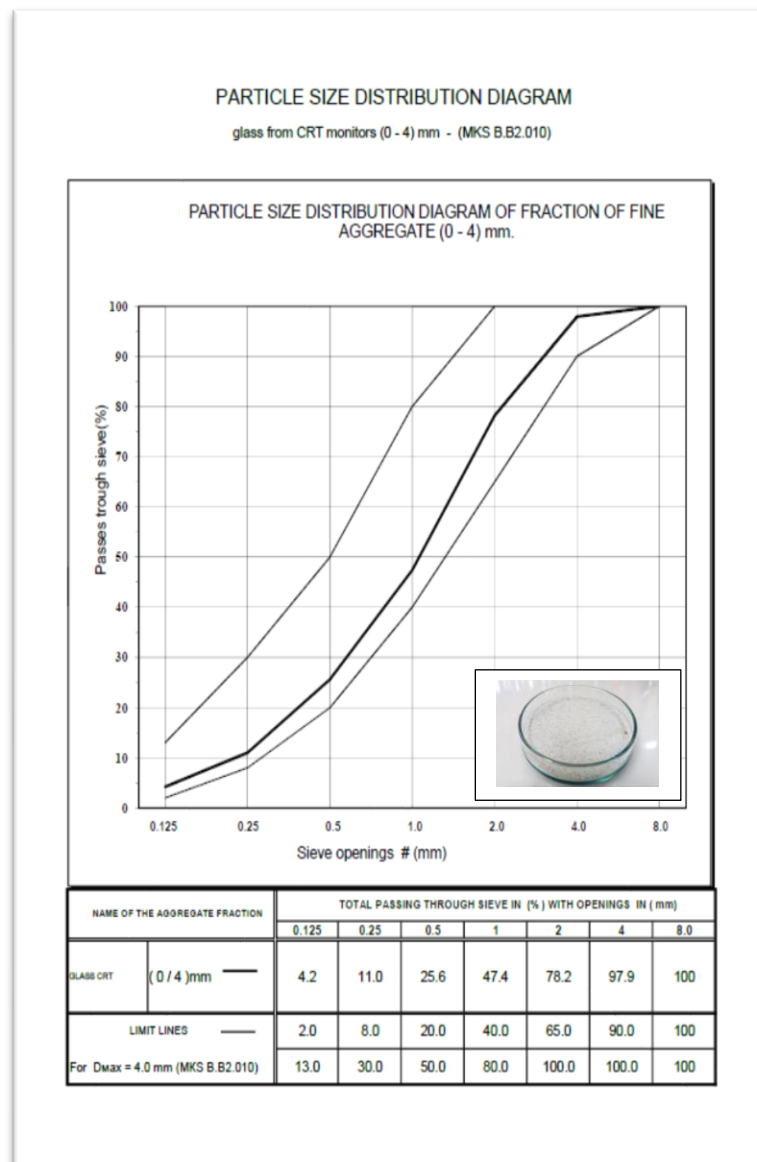


Figure 2 : CRT Glass – Appearance and particle size distribution

The diagram of the particle size distribution showed that the glass fraction between 0.0 and 4.00mm ideally fits the grain size distribution curves, thus it can be stated that based on the particle size distribution it fits as an aggregate for concrete production.

3. MIX COMPOSITION AND PREVIOUS CONCRETE TESTS

Based on the theoretical composition of the concrete mix, which is in accordance with MKC EN 206, and the conducted fresh concrete tests in accordance with MKC EN 12350, and the hardened concrete in accordance with MKC EN 12390, the optimal amount of glass which would provide the best concrete characteristics was defined.

Four mixtures were analysed, one of which was without the usage of glass and it was used as etalon for processing the other ones which had waste glass from the CRT monitors in their composition, as follows: 50% of fraction 1 from 0.0 to 4.00mm, and 100% or total substitute of fraction 1 from 0.0 to 4.0mm.

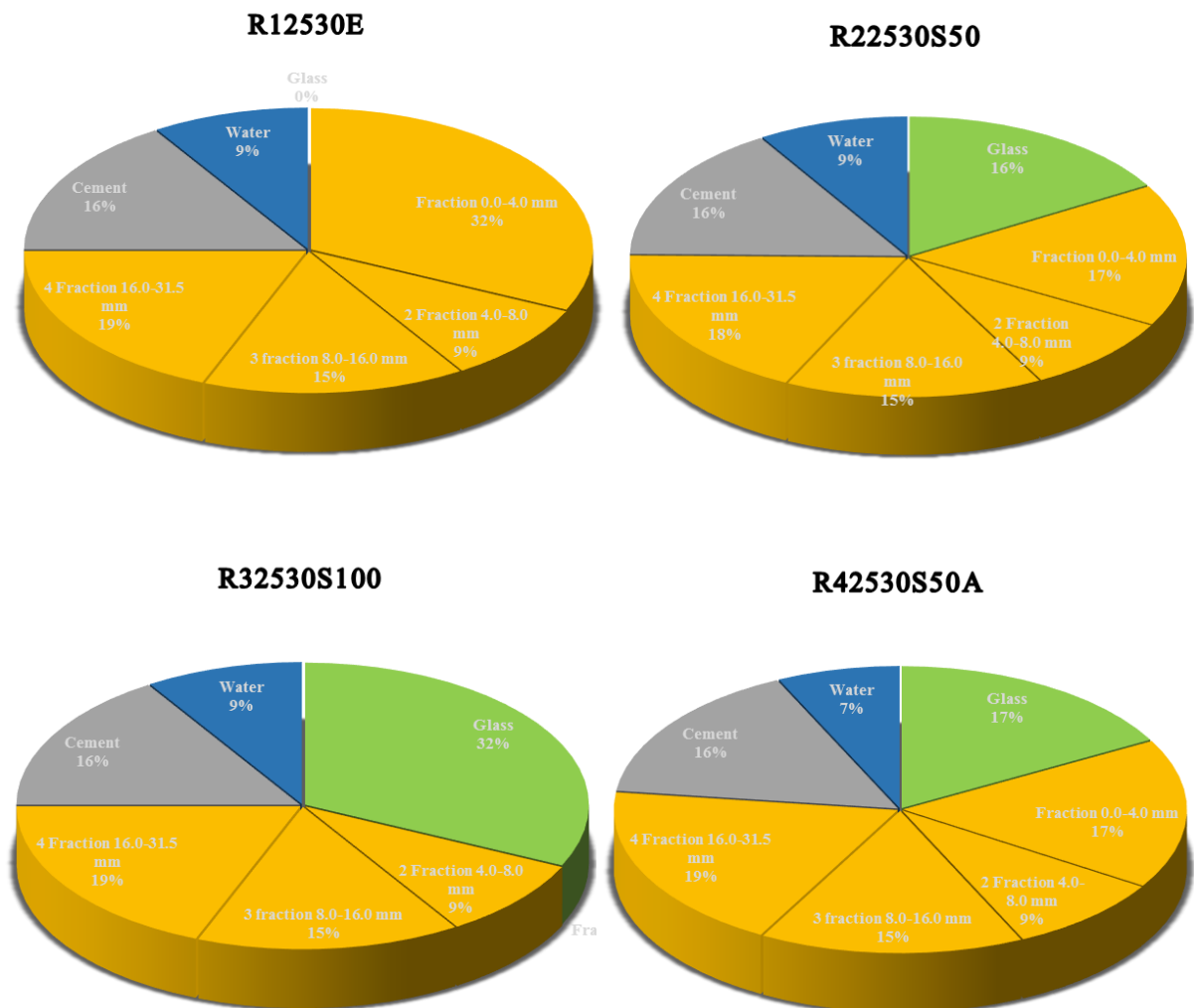


Figure 3: Percentual representation of the components in the mixtures

The performed analysis shows that the most optimal mix as basis for mix preparation for prefabricated concrete curbs is the one with partial representation i.e. 50% waste glass as substitute for fraction 1 from 0.0 to 4.0mm.

Additive, superplasticiser and aerating agent are added to the basic mix, as well as all relevant properties, in order to obtain quality composition for concrete production for prefabricated concrete curbs.

Based on the previous tests of the concrete mixtures, the following can be stated:

The mix marked R42530S50A shows that the consistency class of S3 goes into S4 regarding the mix etalon, as well as regarding the other two mixtures due to the presence of additive.

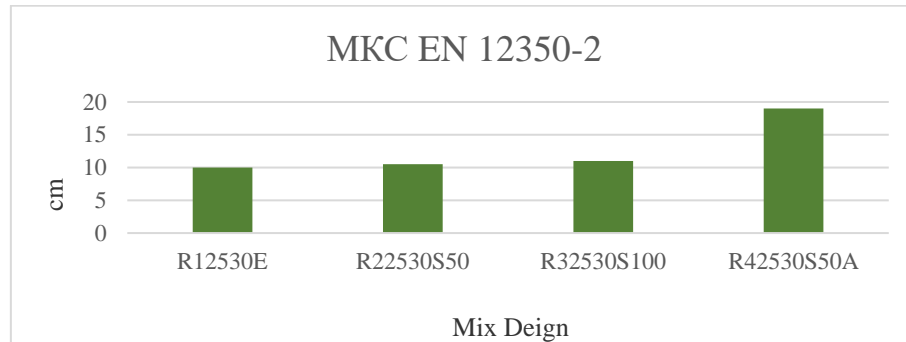


Figure 4: MKS EN 12350-2

Based on the analysis of the results of all mixtures, it can be concluded that the air content in the mixture marked R42530S50A is increasing regarding the mixture etalon with mark R12530E, and it is due to the presence of the aerating agent.

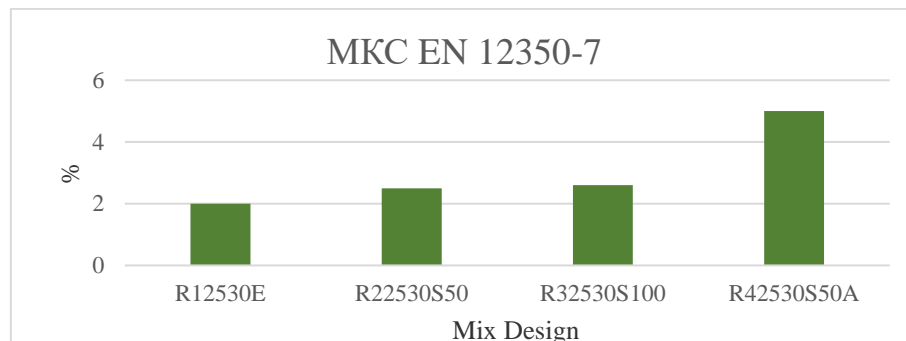


Figure 5: MKS EN 12350-7

The mix marked R42530S50A has the tendency to have constant good growth of the results regarding the other mixtures which were used as basis for its composition. The analysis of the results of 28 days shows that the compressive strength value of the mix marked R42530S50A is 12% higher in terms of the mix etalon with mark R12530E, 6.0% higher regarding the mix with 50% glass and mark R22530S50, and 4,7% higher regarding the mix with 100% glass and mark R32530S100.

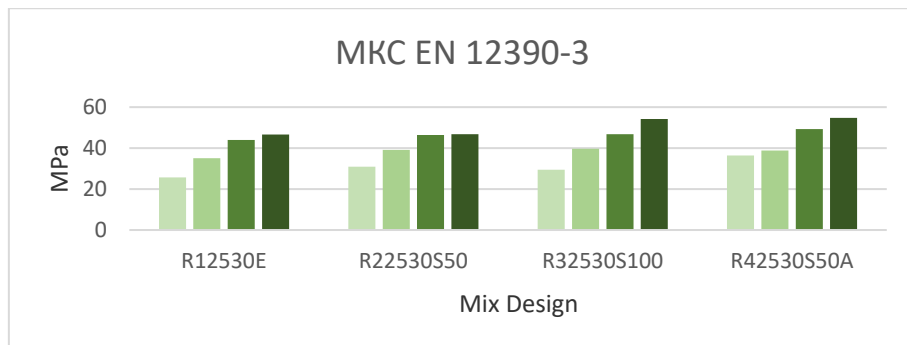


Figure 6: MKS EN 12390-3

The analysis of the results for bend strength for all mixtures of 28 days shows that the mix marked R42530S50A has higher bend strength value for 8% in terms of the mix which contains 50% glass with mark R22530S50 and 11,2% regarding the mix which contains 100% glass with mark R22530S100.

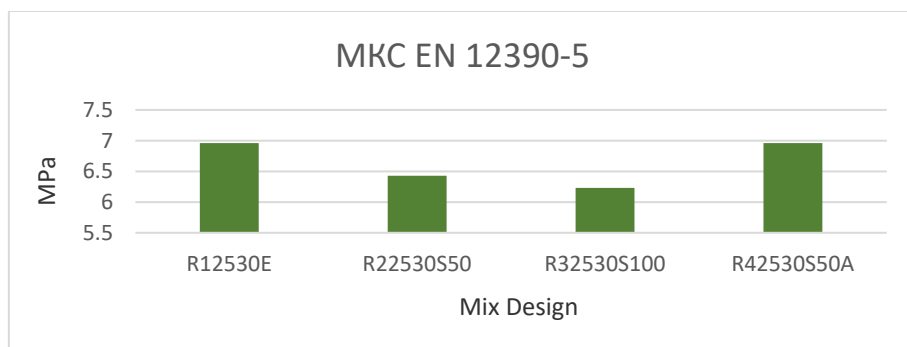


Figure 7: MKS EN 12390-5

The analysis of the results for splitting tensile strength for all mixtures of 28 days shows that the mix marked R42530S50A has higher splitting tensile strength value for 9,6% in terms of the mix which contains 50% glass with mark R22530S50 and 17,2% regarding the mix which contains 100% glass with mark R22530S100.

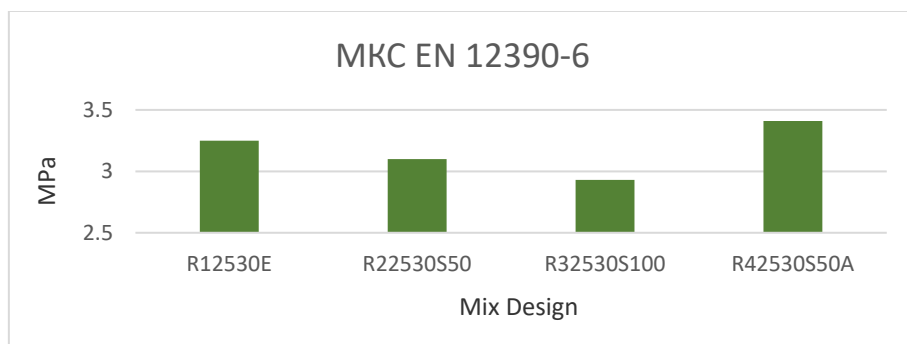


Figure 8: MKS EN 12390-6

At the mix marked R12530E the mass loss per unit area of 0,56 kg/m² is obtained, at the mix marked R22530S50 the mass loss per unit area of 0,662 kg/m² is obtained, at the mix marked R32530S100 the mass loss per unit area of 0,726 kg/m² is obtained, and at the mix marked R42530S50A the mass loss per unit area of 0,588 on 56 cycles as average value of 3 results is obtained. It is noted that the difference in the mass loss regarding the mix etalon is 0,028 kg/m².

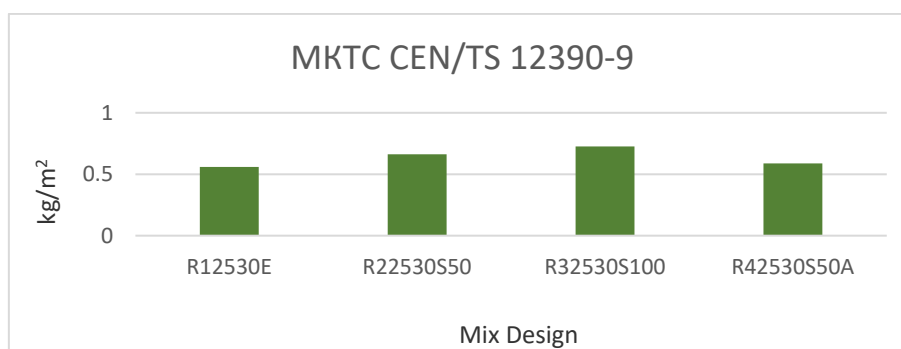


Figure 9: MKS CEN/TS EN 12390-9

All of the mixtures are prepared with the same amount of cement which was one of the aims of this investigation.

4. PREPARATION, TESTING AND ANALYSIS OF THE RESULT

Based on the previous tests of the fresh and hardened concrete for mix marked R42530S50A in the following scope:

MKC EN 12350-2 Determination of consistency - SLUMP TEST

MKC EN 12350-7 Determination of air content

MKC EN 12350-8 Determination of density

MKC EN 12390-3 Compressive strength

MKC EN 12390-5 Bend strength

MKC EN 12390-6 Splitting tensile strength

MTS CEN / TS 12390-9: 2009 Freezing and thawing resistance

and after determining the physical and mechanical properties which correspond to the preparation of the concrete mixture, the preparation of the prefabricated concrete curbs commenced.

The metal moulds for preparation of prefabricated concrete curbs with 190/240/1000mm dimensions were delivered to the laboratory.

Based on the determined mix marked R42530S50A, composition of the mixture was made, all of the components were dosed in the automatic mixer for that purpose.

After the construction of the curbs, they were under a treatment in the air conditioning chamber with a constant temperature of 20°C ± 2°C and a relative humidity of 95% ± 2%.

After 28 days of treatment of the concrete curbs in the air conditioning chamber, they were processed for the required further tests of finished product.

The tests of the prefabricated concrete curbs were conducted in accordance with the MKC EN 1340:2006 standard Concrete curbs, requirements and test methods.

All of the points from the standard were covered in the following form:

Shape and dimensions in accordance with Annex C

Ice resilience and soils in accordance with Annex D

Water absorption in accordance with Annex E

Tensile strength during bending in accordance with Annex F

Abrasion Bohme test in accordance with Annex H

Sliding resilience in accordance with Annex I

Visual appearance in accordance with Annex J

Based on the result analysis of the finished product, the prefabricated concrete curb, the following results were obtained:

The calculated values of the dimensions met the allowed deviations.

The mass loss per 56 cycles ice and soils is 0,709, so the curb based on the standard belongs to class 3 and marking D.

The water absorption was 4,84%, making this property to belong to class 2, marking B.

The bend strength was 5,52MPa which characterizes the curb with class 2, marking T.

The volume loss was 14755 mm³/5000 mm², so the curb belongs to class 4, marking I.

5. CONCLUSIONS

Taking into consideration that this concrete meets all properties, it could be used in other prefabricated elements for landscape design.

The investigation will contribute in opening new opportunities for the application of the waste materials. This would increase the interest in production of such concrete, which would provide greater environmental and economic savings.



Figure 10: Structure of concrete with glass

REFERENCES

- [1] Аранѓеловски Т. – Печатени предавања по технологија на бетон , април, 2006
- [2] <http://www.isrm.gov.mk>
- [3] <http://usje.mk/Default8c48.html>

NEW GENERATION OF CONSTRUCTION MATERIALS
SESSION 7: Innovation in chemistry and nanotechnology

EFFECTS AND POTENTIALS OF PLANT-BASED CHEMICAL ADMIXTURES ON THE PERFORMANCE OF CEMENTITIOUS CONSTRUCTION MATERIALS

Wolfram Schmidt (1), Ines L. Tchegnina Ngassam (1), Kolawole A. Olonade (2), Rose Mbugua (3) and Hans-Carsten Kühne (1)

(1) Bundesanstalt für Materialforschung und -prüfung, Germany

(2) University of Lagos, Nigeria

(3) Walter Sisulu University, South Africa

Abstract

While today, engineers can choose from a wide range of rheology modifying admixtures, in some parts of the world, these are difficult to access, due to their complex processing. However, alternatives can be bio-based polymers such as polysaccharides from various sources. These are easily accessible all over the world, do not demand for complicated processing, and typically they are more sustainable than many established materials, which are crude oil-based.

The paper presents the effects of acacia gum, cassava starch and the gum of *triumfetta pendrata* A. Rich on the rheological performance of cementitious systems. It is shown that acacia gum can be as efficient as polycarboxylate based superplasticisers, cassava starch can reduce the yield stress slightly with little effect on the plastic viscosity, and the gum of *triumfetta pendrata* A. Rich increases the thixotropy of cement pastes with plasticizing polymers significantly.

Keywords: polysaccharides, rheology, cement, chemical admixtures, bio-based concrete

This work was invited for publication in the open access journal RILEM Technical Letters. You can visit the journal and benefit from the full open access to the published articles at: letters.rilem.net.

MECHANICAL BEHAVIOR AND NEUTRON SHIELDING PERFORMANCES OF TiO₂-INCORPORATED CEMENT COMPOSITES

Jaeyeon Park (1), Sungwun Her (1), Heongwon Suh (1), Seung Min Woo (2), Keunhong Jeong (3) and Sungchul Bae (1)

(1) Department of Architectural Engineering, Hanyang University, Republic of Korea

(2) Department of Nuclear Engineering, Texas A&M University, USA

(3) Department of Chemistry, Nuclear and WMD Protection Research Center, Korea Military Academy, Republic of Korea

Abstract

Cementitious materials have been variously used in various nuclear facilities because of their cost-effective neutron shielding ability. In this study, the mechanical properties of cement paste containing nano-TiO₂, which has a wide range of neutron reactivity cross-sections and a chemically-stable character was analyzed using compressive strength, density comparison, and pore distribution. The neutron shielding performance was quantitatively analyzed by the Monte Carlo N-Particle transport code (MCNP). The mechanical properties of the cement paste incorporated with 10 wt.% nano-TiO₂ (T10) were found to be higher than that of ordinary Portland cement paste (T0) due to the filling effect of the nano-TiO₂ by the compressive strength test and porosimetry analysis. Thermal neutron (0.025 eV), epithermal neutron (1 keV), and fast neutron (10 MeV) regions were exposed to the shielding walls, which were 5, 10, 20, 30, and 50 cm thick, comprising T0 and T10, by the MCNP simulation. As a result of these simulations, the shielding performance of T10 was higher than that of T0 at the thermal and epithermal neutron energy levels. As the thickness of the shielding wall increased, the effect of the neutron shielding ability also increased.

Keywords: Cement; Nano-TiO₂; Neutron; MCNP; Simulation

1. INTRODUCTION

The handling of radioactive materials or devices by research institutes and industrial organizations is increasing worldwide [1, 2]. These facilities emit different types of radiation, including alpha-rays, beta-rays, gamma rays, X-rays, and neutrons. Exposure to such radiation

has a fatal impact on nature and the human body [3]. Therefore, it is essential to improve the shielding performance of cementitious material, which is the most economical and effective shielding material [4]. Shielding materials differ depending on the radioactivity. Alpha-rays can be shielded with thin paper, while beta-rays can be effectively shielded with plastic, gamma rays and X-rays are shielded with lead, and neutrons with concrete [4, 5]. Numerous studies have been conducted to improve the neutron shielding performance of cementitious materials. In a previous study, the neutron shielding performance was enhanced using cement mortar, increasing the hydrogen content via a thermosetting epoxy resin as an alternative for fine aggregate. However, low density thermosetting epoxy resins have been found to weaken the mechanical performance of the mortar [6]. In addition, studies have been conducted to incorporate boron oxide into cement to improve the neutron shielding performance [7]. However, it has been found that boron oxide is not suitable for cement admixture because it interferes with the formation of ettringite and calcium silicate hydrates (C-S-H) in the cement hydration reaction, significantly decreasing the mechanical performance [8].

In this study, we evaluate the effects of nano-TiO₂ powder incorporation on the mechanical properties and neutron shielding performance of cement paste. Nano-TiO₂ is known as a chemically-stable structure and has been used to enhance the mechanical properties of cement paste through the filling effect as nanoparticles [9]. Further, the titanium element possesses a greater neutron reaction cross-section in most energy ranges, except for the resonance range, compared to the main component of conventional cement, such as the calcium and silicon elements [10]. Hence, the addition of nano-TiO₂ was used to improve the neutron shielding performance of cement paste. We conducted compressive strength tests and mercury intrusion porosimetry (MIP) to evaluate the mechanical performance of nano-TiO₂-incorporated cement paste. To quantitatively evaluate the neutron shielding performance, each sample was analyzed by X-ray fluorescence (XRF) and thermogravimetry-differential thermal analysis (TG-DTA). By assessing the Monte Carlo N-Particle transport code (MCNP) simulation based on the experimentally obtained chemical composition data, the neutron shielding performance of nano-TiO₂-incorporated cement paste was quantitatively evaluated with respect to: i) the types of neutrons with different energy levels; and ii) the thickness of the wall.

2. EXPERIMENTAL PROCEDURE

2.1 Materials

Ordinary Portland cement (Sungshin Co., Korea) and nano-TiO₂ (Titanium (IV) dioxide anatase, <25 nm, Sigma Aldrich, USA) were used for the preparation of the specimen. Table 1 shows the chemical composition of the OPC used in the sample measured by XRF (ZSX Primus II, Rigaku, Japan). Polycarboxylate superplasticizer (ADVA 149, GCP Applied Technologies, USA) was used to disperse the nano-TiO₂ powder and was used to achieve proper workability of the paste.

Table 1: Chemical compositions of ordinary Portland cement (via XRF)

Chemical Compositions	MgO	Al ₂ O ₃	SiO ₂	SO ₃	K ₂ O	CaO	TiO ₂	Fe ₂ O ₃	LOI	Total
(wt.%)	8.47	2.23	17.34	2.86	1.05	64.14	0.14	2.05	1.72	100

2.2 Sample preparation

A sample of nano-TiO₂-incorporated cement paste was prepared by controlling the amount of nano-TiO₂ added. The ordinary Portland cement paste was named T0 and the cement paste with 10 wt.% of nano-TiO₂ was named T10. The water-to-cement weight ratio (W/C) of the samples was 0.3 and 0.4, a 0.8 wt.% of superplasticizer was added to the T0 and T10, respectively. The nano-TiO₂ was dispersed with the superplasticizer added to the water solution by ultrasonic dispersion treatment for 5 min [11]. Thereafter, cement powder was added to the nano-TiO₂ water solution. The prepared mixture was placed into the paste mixer (SPS-1, Malcom, Japan) and was mixed for 12 min, it was then cast into the mold of size 5 × 5 × 10 mm³. After a day of casting, the specimens were demolded and cured at 27°C and 60% RH.

2.3 Compressive strength test and bulk density measurement

The compressive strength of each specimen (T0, T10) was measured by using a compression testing machine (Deben Microtest, UK) at 1, 3, 7 and 28 days of hydration time. Simultaneously, the bulk density of the specimens (T0, T10) was also measured using an electron density meter (GP-300S, Matsuhaku, Japan).

2.4 Mercury intrusion porosimetry (MIP) analysis

Automated MIP (Autopore IV 9520, Micromeritics, USA) was used to measure the total porosity and pore size distribution of each specimen. Before the test, the specimens were prepared as 6 pieces of 5×5×5 mm³ samples, then the specimens were soaked in isopropanol for 24 h and dried by the ThermoStable™ SOF dry oven (Daihan scientific, Korea) at 60°C for 6 h to remove moisture.

2.5 X-ray fluorescence spectrometry (XRF) analysis

XRF spectrometry (ZSX Primus II, Rigaku, Japan) was used to analyze the chemical compositions of each sample hydrated for 28 days. Each specimen was crushed by a ball mill grinder (Pulverisette 23, Fritsch, Germany) for 5 min. This powder was then sieved in a 200 mesh (75 μm) filter.

2.6 Thermogravimetry-differential thermal analysis (TG-DTA)

TG-DTA was performed to quantify the hydrogen and oxygen elements of the bound water and carbonates in the sample. Each specimen was treated the same as in the XRF analysis preprocessing procedure. TG data was obtained by a DTG-60A (Shimadzu, Japan), heated at a rate of 10 °C/min.

2.7 Monte Carlo N-particle transport code (MCNP) simulation

The geometry designed for MCNP simulation, such as the neutron source, shielding wall, and detection point, is displayed in Figure 1. The energy level of the neutron source (Fig. 1 (a)) modeled by a point shape was set to 0.025 eV, 1 keV, and 10 MeV. Each energy value represents the thermal, intermediate, and fast neutrons, respectively. The element composition ratio and density information of T0 and T10 obtained by XRF and TG-DTA are shown in Fig. 1 (b). The thickness was adjusted to 0 cm, 5 cm, 10 cm, 20 cm, 30 cm, and 50 cm, respectively. The detector (Fig. 1 (c)) is modeled as a sphere with a radius of 30 cm and a distance of 300 cm from the shielding wall (Fig. 1 (b)). Each simulation was run 10⁷ times to improve reliability [12].

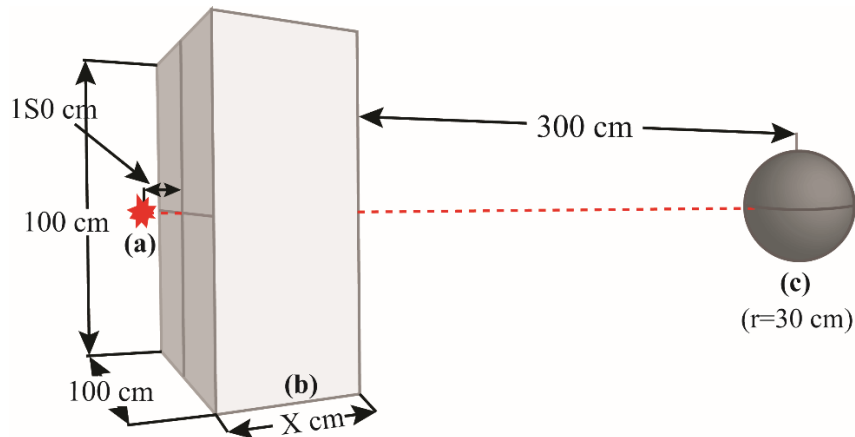


Figure 1: Geometry of the MCNP simulation. (a) Neutron source, (b) Shielding wall (X: 0, 5, 10, 20, 30, and 50 cm), and (c) Detector

3. RESULTS AND DISCUSSION

3.1 Mechanical behavior of nano-TiO₂-incorporated cement paste

Figure 2 (a) shows the compressive strength results for each hydration time of T0 and T10. The compressive strength of T10 was about 120%, 112%, 119%, and 105% in the specimens with a hydration period of 1, 3, 7 and 28 days compared to T0, respectively. The density improved to 2.326 g/cm³ and 2.341 g/cm³ in the hydrated T0 and T10 specimens for 28 days, respectively.

The distribution of the pore size and the accumulated porosity of the T0 and T10 analyzed by MIP are shown in Fig. 2 (b). As can be seen in Fig. 2 (b), the pore size of 12 nm to 36 μm (range II) significantly reduced and the pore size of 5 nm to 12 nm (range I) increased in T10 by the filling effect of nano-TiO₂. In addition, micropores ranging from 36 μm to 221 μm (range III) slightly increased due to the incomplete dispersion of nano-TiO₂. According to the above results, it can be claimed that the incorporation of nano-TiO₂ improves the mechanical properties of the cement paste, even if the micropores increase due to insufficient dispersion of the nano-TiO₂ in the cement paste.

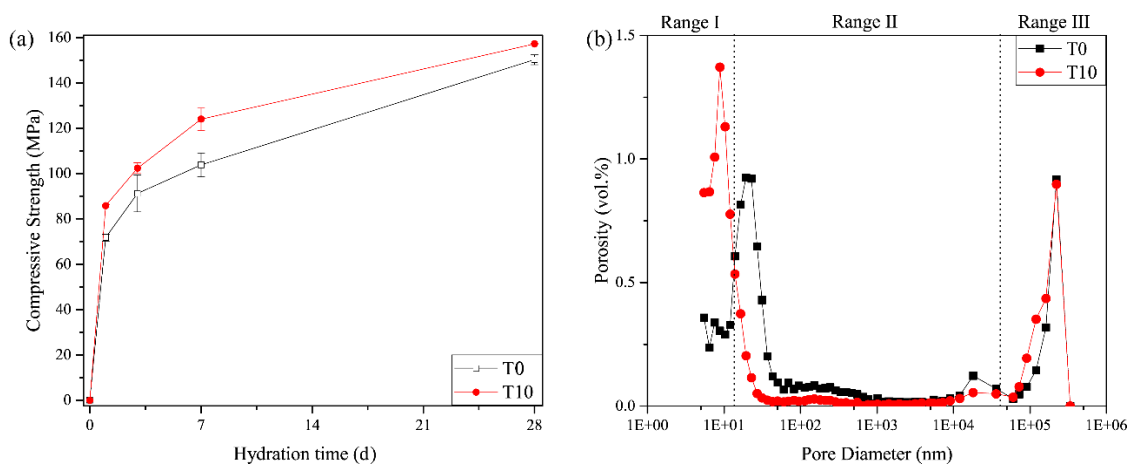


Figure 2: (a) Compressive strength with hydration time, and (b) Pore size distribution

3.2 Element composition ratio calculation result

We experimentally quantified the element composition ratio and density of T0 and T10 as input parameters of the MCNP simulation. Table 2 presents the oxide composition ratios of each sample (T0, T10) by XRF analysis. Figure 3 shows the thermal gravimetric results by TG-DTA, the solid and dotted lines indicate the TG and DTA values, respectively. The TG results were used to analyze the free and bound water and the amount of CaCO_3 . The weight of free water in T0 (6.96 wt.%) was slightly larger than T10 (5.90 wt.%). The weight percent of chemically bound water in T0 and T10 was 15.88 wt.% and 15.65 wt.%, respectively. The values of the element composition ratios of the respective samples calculated from the XRF and TG-DTA results are shown in Table 3. The final element ratio and density values were used in the MCNP simulation.

Table 2: Chemical compositions of T0 and T10 at 28 days of curing (XRF)

Chemical Compositions (unit: wt.%)	MgO	Al ₂ O ₃	SiO ₂	SO ₃	K ₂ O	CaO	TiO ₂	Fe ₂ O ₃	Total
T0	1.97	2.46	17.6	2.27	1.13	71.9	0.16	2.52	100
T10	1.80	2.27	16.0	2.03	1.17	66.6	7.89	2.27	100

Table 3: Input elemental composition parameters and density for MCNP simulation

(unit: wt.%)	H	C	O	Mg	Al	Si	S	K	Ca	Ti	Fe	Density
T0	2.51	0.51	46.2	0.92	1.01	6.36	0.71	0.73	39.6	0.08	1.37	2.326
T10	2.36	0.47	45.8	0.85	0.95	5.89	0.65	0.76	37.3	3.71	1.26	2.341

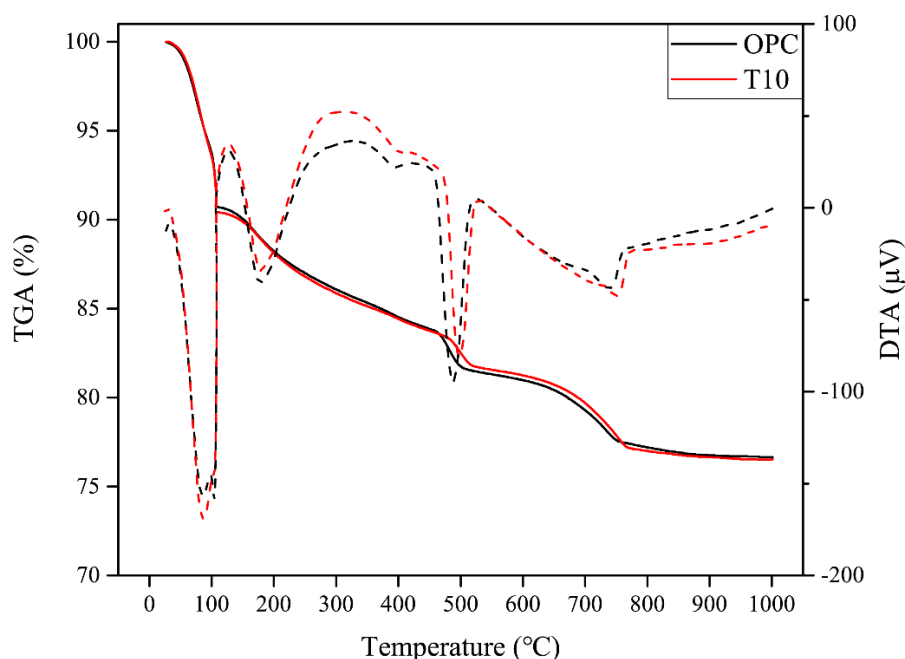


Figure 3: Results of thermogravimetric-differential thermal analysis (TG-DTA)

3.3 Neutron shielding performance of nano-TiO₂-incorporated cement paste

MCNP simulations were used to compare the neutron shielding performances of cement pastes with those containing nano-TiO₂. Figure 4 shows the normalized flux values detected after penetrating the shielding wall (Fig. 1 (b)) for each neutron energy (0.025 eV, 1 keV, and 10 MeV). Based on the comparison of flux values for each sample upon thermal neutron irradiation (0.025 eV), shown in Fig. 4 (a), when the thickness of the shielding wall was 50 cm, the flux rate decreased by approximately 21% in T10 compared with T0. Figure 4 (b) shows a comparison of the flux values of each sample during intermediate neutron irradiation (1 keV). When the shielding wall thickness was 50 cm, the flux reduced by about 21%, compared to T0, at T10. This is because the neutron reaction cross-sections of the titanium element in the thermal neutron and intermediate energy regions are larger than that of calcium and silicon, which are the main components of cement. Additionally, as the shielding wall is thicker, the absolute value of the neutron flux detected is lower, however, the influence of the addition of nano-TiO₂ to the shielding performance increases dramatically. This is because as the thickness of the shielding wall increases, the time and frequency of the neutron reaction with the titanium element increases.

However, the flux values of T0 and T10 are almost the same when the thickness of the shielding wall is 50 cm, when comparing the flux values of each sample at fast neutron irradiation (10 MeV), as shown in Fig. 4 (c). This is because there is little difference between the neutron reaction cross-section of the titanium element and that of calcium and silicon in the fast neutron energy region.

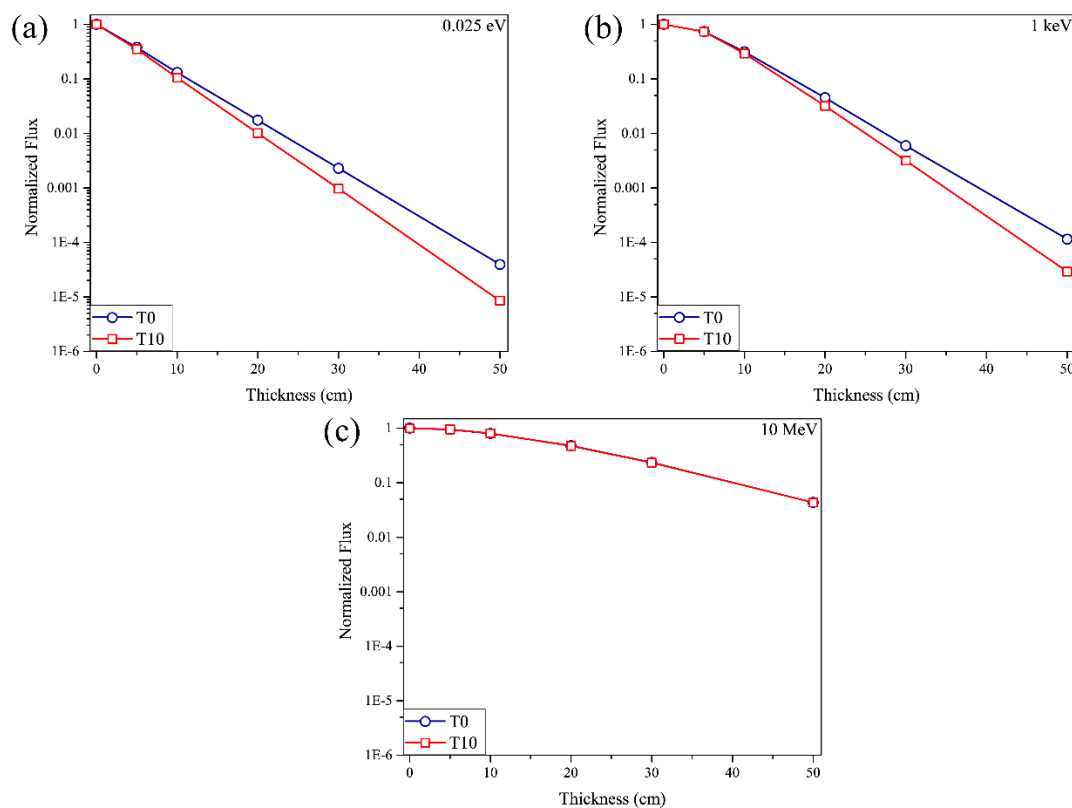


Figure 4: The normalized flux results of MCNP simulation in (a) thermal neutron, (b) intermediate neutron, and (c) fast neutron irradiation

4. CONCLUSIONS

- Due to the filling effect of nano-TiO₂ powder, the nano-TiO₂-incorporated cement paste showed a higher compressive strength and density than ordinary Portland cement paste.
- The neutron shielding performance improved in the energy range of thermal neutrons and intermediate neutrons in the nano-TiO₂-incorporated cement paste due to the relatively large neutron reaction cross-section of the titanium element.
- As the thickness of the shielding wall increases, the effect of neutron shielding increases significantly with the incorporation of nano-TiO₂ in thermal neutron and intermediate neutron irradiation. This is because as the thickness of the shielding wall increases, the number and rate of reactions of the neutron and titanium element increases.
- However, the incorporation of nano-TiO₂ showed no significant improvement on the neutron shielding performance when irradiating the fast neutron energy region because there is little difference in the neutron reaction cross-section of the titanium, calcium and silicon elements in the fast neutron energy region.

ACKNOWLEDGEMENTS

This research was supported by the Basic Science Research Program through the National Research Foundation of Korea (NRF) funded by the Ministry of Science, ICT & Future Planning (NRF-2016R1C1B1014179).

REFERENCES

- [1] Nuclear energy data 2017, OECD Publishing.
- [2] International Status and Prospects for Nuclear Power 2017, IAEA.
- [3] S. Nagataki, Radiation Effects on Humans, The Japan Radiation Research Society Annual Meeting Abstracts The 47th Annual Meeting of The Japan Radiation Research Society, Journal of Radiation Research Editorial Committee, 2004, pp. 45-45.
- [4] E. Yılmaz, H. Baltas, E. Kırıs, I. Ustabas, U. Cevik, A. El-Khayatt, Gamma ray and neutron shielding properties of some concrete materials, *Annals of Nuclear Energy* 38(10) (2011) 2204-2212.
- [5] K. Maruoka, H. Imoto, S. Saito, H. Yamamoto, Virtually Complete Blocking of. alpha., beta.-Unsaturated Aldehyde Carbonyls by Complexation with Aluminum Tris (2, 6-diphenylphenoxide), *Journal of the American Chemical Society* 116(9) (1994) 4131-4132.
- [6] L. Aggarwal, P. Thapliyal, S. Karade, Properties of polymer-modified mortars using epoxy and acrylic emulsions, *Construction and Building Materials* 21(2) (2007) 379-383.
- [7] M. Kharita, S. Yousef, M. AlNassar, Review on the addition of boron compounds to radiation shielding concrete, *Progress in Nuclear Energy* 53(2) (2011) 207-211.
- [8] I. Bell, P. Coveney, Molecular modelling of the mechanism of action of borate retarders on hydrating cements at high temperature, *Molecular simulation* 20(6) (1998) 331-356.
- [9] T. Meng, Y. Yu, X. Qian, S. Zhan, K. Qian, Effect of nano-TiO₂ on the mechanical properties of cement mortar, *Construction and Building Materials* 29 (2012) 241-245.
- [10] ENDF: Evaluated Nuclear Data File.
- [11] A. Yousefi, A. Allahverdi, P. Hejazi, Effective dispersion of nano-TiO₂ powder for enhancement of photocatalytic properties in cement mixes, *Construction and building materials* 41 (2013) 224-230.
- [12] J.T. Goorley, M. James, T. Booth, MCNP6 User's Manual, Version 1.0, LA-CP-13-00634, Los Alamos National Laboratory (2013).

EFFECT OF TITANATE NANOTUBES ON THE PROPERTIES OF CEMENT-BASED COMPOSITES

Hyeonseok Jee (1), Jaeyeon Park (1), Sungwun Her (1), Erfan Zalnezhad (2), Keunhong Jeong (3) and Sungchul Bae (1)

(1) Department of Architectural Engineering, Hanyang University, Seoul 04763, Korea

(2) Department of Metrology-Photo, TowerJazz Texas, 9651 Westover Hills Blvd, San Antonio, TX 78251, USA

(3) Department of Chemistry, Nuclear and WMD Protection Research Center, Korea Military Academy, Seoul 01805, Korea

Abstract

Recently, nano-reinforcing technology using nanotubes has attracted significant attention as a method of compensating for poor tensile strength and improving the performance of various cementitious materials. In this study, for the first time, we investigated the mechanical properties, microstructure, and early hydration kinetics of cement paste with titanate nanotubes (TNTs). The microstructures of the fracture surfaces of samples were investigated with scanning electron microscopy (SEM). TNTs were successfully synthesized using a hydrothermal method. With 0.5 wt.% addition of TNTs, both compressive and flexural tensile strength were improved for all curing days, but it was found that TNT reinforcement was more effective for flexural strength enhancement. Moreover, the analysis of the hydration kinetics by isothermal conduction calorimetry clearly showed that the TNTs improved the hydration kinetics of the pure cement clinker phase (C₃S) at the initial stage of hydration. Pore analysis showed that nano-sized TNTs filled pores between 10 to 100 nm in size, resulting in a denser microstructure of the cement paste. SEM images clearly showed that TNTs bridged cracks and voids in the cement paste, which mitigated and altered crack propagation in the cement paste. These results suggest that TNTs have great potential as a new nano-reinforcing agent for cementitious materials.

Keywords: nanotubes; cements; strength; microstructure; kinetics

1. INTRODUCTION

Cementitious materials such as concrete and mortar are currently some of the most widely used construction materials [1]. However, due to the poor tensile performance and brittle nature of cementitious materials, there is a need for reinforcement to compensate for these problems.

As one feasible solution, methods involving the incorporation of steel reinforcing bars or various fibers into cementitious materials have been used. The incorporated reinforcements resist tensile forces generated in the cementitious matrix and improve the tensile strength and strain performance of the composite while preventing cracking and constantly resisting tensile forces after crack occurrence [2].

In recent years, various nano-reinforcing techniques for cementitious materials have attracted attention. One of the most popular nano-reinforcing materials for cementitious materials is carbon nanotubes (CNTs). CNTs have many features that make them attractive reinforcements for cementitious materials, such as their high aspect ratio [3] and high Young's modulus [4]. To date, most research regarding CNT strengthening has been directed toward improving the mechanical performance of cementitious materials. Campillo et al. [5] found that the addition of single-walled CNTs (SWCNTs) or multi-walled CNTs (MWCNTs) improved the compressive strength of a cementitious material by 6 % and 30 %, respectively. Li et al. [6] also observed an improvement of about 25 % in a 28-day cement mortar composite when mixed with 0.5 % surface modified MWCNTs.

Although CNTs have great potential as a nano-reinforcing material, several disadvantages have been observed when they are applied to cementitious materials. The main problem in applying CNT to cementitious composites is poor dispersion due to inter-tube van der Waals attraction [7]. The homogeneous dispersion of CNTs is known to be one of the key factors affecting the mechanical performance of cementitious composites containing CNTs. Konsta-Gdoutos et al. [8] reported that if the dispersion of CNTs in the composite was sufficient, adding a small amount of about 0.05 wt.% MWCNTs resulted in a 30% increase in the flexural toughness of the cement composite after 28 days. However, obtaining a proper dispersion of CNTs in the cement matrix is a big challenge because of the large aspect ratio of and strong attractive forces between the CNTs [9]. Moreover, it is known that the insufficient dispersion of CNTs could cause many defects in the cement composite and lower the efficiency of the CNTs in the matrix [10].

Meanwhile, since Kasuga et al. [11] reported the synthesis of titanate nanotubes (TNTs) for the first time in 1998, TNTs have received attention in a variety of fields. Similar to CNTs, TNTs also have a large specific surface area [12] and can be used in a variety of applications. TNTs have great potential as a nano-reinforcing material and have been studied extensively in a variety of research areas, but previous research on TNTs for cement materials is extremely limited. Therefore, we investigated the effects of TNT addition on the mechanical properties and hydration kinetics of cement paste. The basic properties of hydrothermally synthesized TNTs were characterized using transmission electron microscopy (TEM). Scanning electron microscopy (SEM) and mercury porosimetry (MIP) were used to observe morphological details of fracture surfaces and the pore distributions of cement pastes incorporating TNTs. Moreover, the early hydration kinetics of cement paste with TNTs were also characterized by isothermal conduction calorimetry.

2. MATERIALS AND EXPERIMENTAL PROCEDURES

2.1 Materials and preparation of specimens

TNTs were synthesized by hydrothermal synthesis methods [13]. Ordinary Portland cement was used to produce cement paste reinforced with TNTs. The chemical composition of the cement as measured by an X-ray fluorescence spectrometer (XRF, ZSX Primus II, Japan) is shown in Table 1. Ordinary cement paste (hereafter referred to as OPC) and TNT-reinforced cement paste

(hereafter referred to as OPC-TNTs) were prepared with a water-cement ratio (w/c) of 0.3. In order to obtain proper workability and dispersibility of TNTs, polycarboxylate superplasticizer (SP) of 0.4% by weight of cement was used. The amount of TNTs added to make OPC-TNTs was 0.5 wt.% of the cement. TNTs were added to a mixture of distilled water and SP and then ultrasonicated for 5 minutes using a sonicator (SD-100H, Korea) to disperse the TNTs in the solution. Next, the TNT solution was added to the cement and mixed in a paste mixer (SPS-1, USA) for 12 minutes. After curing for 24 hours, the paste was demolded from the mold and cured at 20 °C and 60 % RH.

Table 1: Chemical Composition of Ordinary Portland Cement (%)

SiO ₂	Al ₂ O ₃	Fe ₂ O ₃	CaO	MgO	K ₂ O	SO ₃	TiO ₂	LOI	Total
18.43	2.83	2.17	68.17	2.37	1.11	3.03	0.15	1.72	100

2.2 Mechanical tests

Compression and bending tests were performed to evaluate the mechanical performance of cement paste when TNTs were added. The dimensions of the test specimens for the compression strength tests were 5×5×10 mm³. The flexural strength was measured using a 3-point bending test with a test piece of dimensions 4×8×40 mm³. The compressive strength and flexural strength of the specimens were measured after 1, 3, 7, and 28 days of curing using a 5 kN compression and tensile test apparatus (Microtest, Deben, UK).

2.3 Mercury intrusion porosimetry (MIP) analysis

The effects of TNT addition on the total porosity and pore size distribution were investigated using MIP (Autopore IV 9520, USA). Samples of 28-day hydrated cubic paste (5×5×5 mm³) were soaked in isopropanol and diethyl ether to block additional moisture. The treated samples were then dried in a 40 °C oven for 48 hours before measurement.

2.4 Electron microscopy analysis

The morphological characteristics of the synthesized TNTs were observed by transmission electron microscopy (TEM, JEM 2100F, Japan). To prepare the TEM sample, an appropriate amount of TNTs was first added to ethanol and ultrasonicated for dispersion. A few drops of the sonicated solution were then placed on a carbon film Cu grid and dried in a vacuum desiccator for 48 hours.

The fracture surface of the OPC-TNTs (4×8×40 mm³) formed after testing the flexural strength at 28 days was examined using a scanning electron microscope (SEM, Nova NanoSEM, USA). SEM samples were produced by increasing the amount of TNTs (1.5%) to clarify the bridge effect of TNTs. SEM analysis was performed at an acceleration voltage and magnification of 15.00 kV and 150,000×, respectively, and the working distance was 5.8 mm.

2.5 Isothermal conduction calorimetry analysis

Isothermal conduction calorimetry (TAM-air, TA instrument, USA) measurements were performed to monitor the effect of TNTs on the initial hydration rate of cement and pure C₃S paste. The cumulative value of the hydration heat was calculated based on heat flow data from

the isothermal calorimeter. The boundary nucleation model (BN model) was used to quantitatively explain the effect of TNT addition on C₃S hydration kinetics [14].

3. RESULTS AND DISCUSSION

3.1 Properties of synthesized TNTs

Figure 1(a) and (b) show the morphology of the hydrothermally synthesized multi walled TNTs that were examined by TEM. Based on the TEM images, the size distribution of the TNTs was calculated manually for about 200 nanotubes (Figure 1(c)) and the related physical parameters of the TNTs are shown in Table 2. Unlike CNTs, which often have an aspect ratio greater than 1000 [8], the calculated aspect ratio of TNTs was about 9. However, since TNTs have a relatively small size compared to CNTs, the effect of filling the pores of the cement paste with TNTs can be greater than that of CNTs. In addition, since the hydrophilic TNTs can improve the adhesive properties of cement hydration products, a strength improving effect is expected [15]. The BET surface area of the TNTs was calculated as ~200 m²/g, which is about 4 times that of untreated nano-TiO₂.

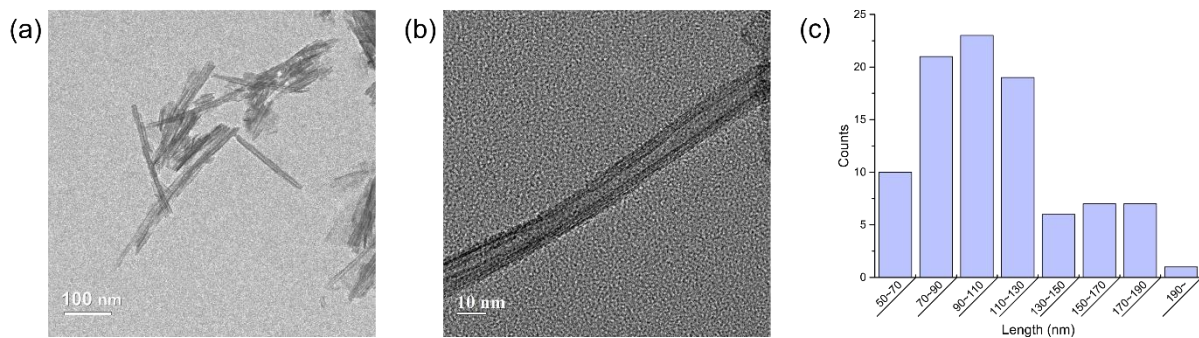


Figure 1: (a, b) Morphology of hydrothermally synthesized TNTs. (c) Size distribution of TNTs.

Table 2: Physical parameters of TNTs

Products	Outer Diameter (nm)	Inner Diameter (nm)	Length (nm)	Surface Area (m ² /g)
TNTs	11 ± 1.9	5 ± 0.8	100 ± 36	~200

3.2 Mechanical properties and microstructure of TNTs-cement composites

Compressive and flexural strength were measured to determine the reinforcing effect of TNTs on the mechanical properties of cement paste. In general, nanoparticles can fill the pores and provide a compact microstructure matrix [16]. Figure 2 shows the changes in compressive strength and flexural strength of OPC and OPC-TNTs on days 1, 3, 7, and 28 of the curing process. The compressive strength of the TNT-reinforced samples was higher than the compressive strength of ordinary Portland cement paste for all curing durations. In particular, the compressive strength of OPC-TNTs increased significantly after 28 days (11.7%). TNT reinforcement improved the flexural strength by 19.0, 21.6, 7.3, and 23.2% after 1, 3, 7, and 28

days, respectively. Like the compressive strength, the flexural strength was significantly improved after 28 days.

In previous studies, CNTs have shown a positive impact on the mechanical properties of cementitious materials. Konsta-Gdoutos et al. reported that CNT-containing cement paste increased the production rate of calcium silicate hydrate (C-S-H) gel with high stiffness [8]. In addition, CNTs having a large specific surface area per unit volume promoted the formation of hydrate by providing nucleation sites at which cement hydrate could be formed [17]. Like CNTs, TNTs have the ability to improve the mechanical properties of cement pastes, especially their long-term strength.

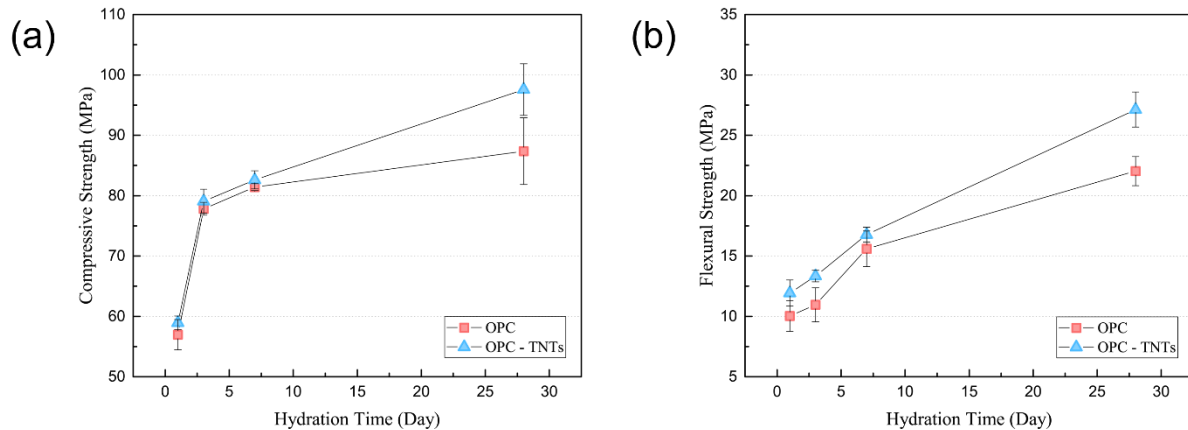


Figure 2: Compressive and flexural strength of ordinary Portland cement paste with and without TNTs.

Porosity analysis of cement pastes with and without TNTs was performed to further investigate the effect of porosity and pore size distribution on the strength of OPC and OPC-TNTs (Figure 3). The incorporation of TNTs reduced the number of voids in the cement paste in the range of 10 to 100 nm (Figure 3(a)) and reduced the total porosity (Figure 3(b)). Similar results were obtained for MWCNTs-cement composites by Nochaiya et al. [16]. As the content of CNTs was increased, the total porosity of the CNTs-cement mixture decreased and the CNTs filled the spaces between the hydration products of the cement, which supported the increased compressive strength of the cement composite [16]. Therefore, the improvement in the compressive strength of the OPC-TNTs can be explained by the relatively small size of the TNTs which can fill the pores between the cement hydration products.

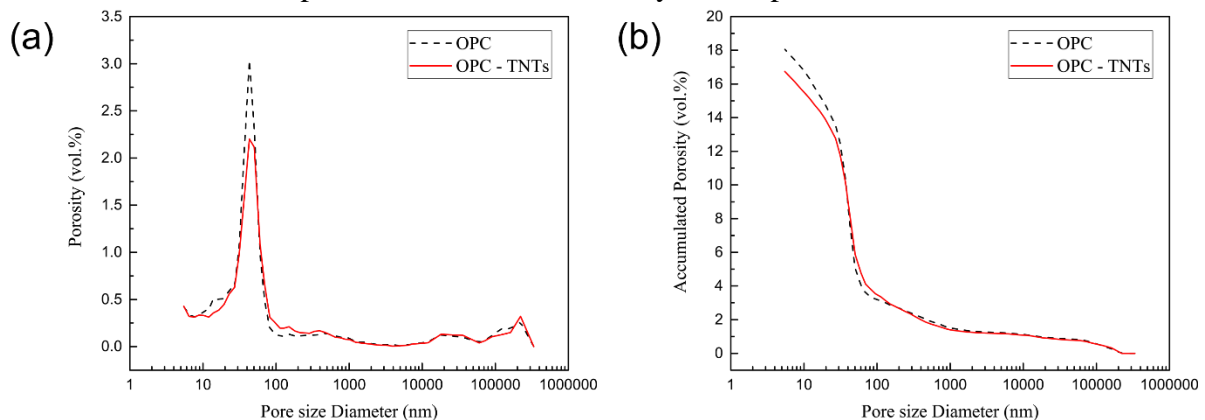


Figure 3: (a) Pore size distribution and (b) total porosity of OPC and OPC-TNTs

Figure 4 shows an SEM image of the fractured surface of the OPC-TNTs. In the SEM image, it can be clearly observed that TNTs appear bridging nano-sized cracks between the hydration products in the cement paste. This shows the crack-bridging effect of TNTs, even if their aspect ratio is relatively small compared to that of CNTs. It is also worth noting that the average thickness of TNTs in the cement paste increased to 22 nm compared to that measured before mixing into the cement paste (outer diameter = ~11 nm). The increased thickness was induced by the formation of cement hydrates, such as C-S-H, tightly wrapped around the TNTs. The surface of the hydrophilic TNTs [18] provides a better site for cement hydrate to form, thereby increasing the bond strength between the TNT and the cement paste. Thus, it is proved that the effect provided by the bridging TNTs improved the flexural strength of the cement paste prepared in this study.

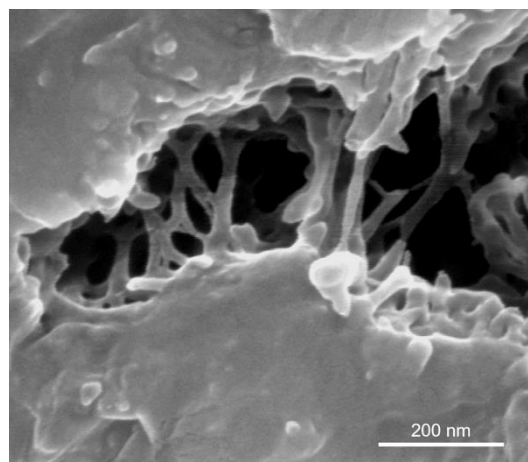


Figure 4: Crack bridging effect at the fractured surface of the OPC-TNTs (SEM image).

3.3 Effect of TNTs on hydration of cement paste and tricalcium silicate (C_3S)

Pure C_3S has been widely used as a model system to study the hydration kinetics of Portland cement [14]. Isothermal calorimetry was used to investigate the effect of TNTs on the hydration kinetics of C_3S and the results are shown in Figure 5.

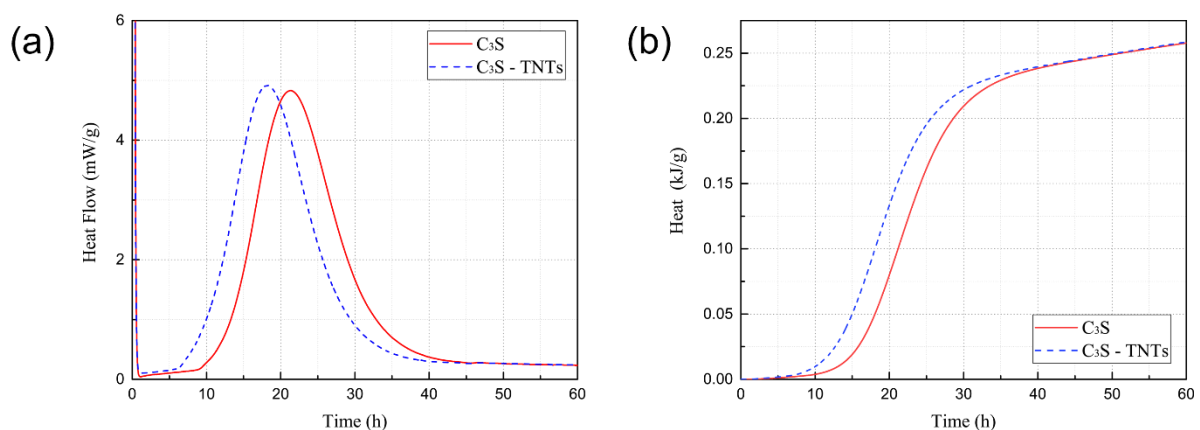


Figure 5: (a) Heat flow through C_3S with and without TNTs measured by isothermal conduction calorimetry. (b) The hydration heat calculated by integration of the data in (a).

The presence of TNTs accelerated the onset of the C₃S hydration peak by ~5 hours. However, the total hydration heat was not significantly different, as shown in Figure 5(b). The degree of hydration (α) was calculated assuming the enthalpy of hydration of C₃S to be 121 kJ/mol [19]. The hydration degree after 50 hours of hydration was calculated as 55.6% in pure C₃S and 55.7% in the TNTs-incorporated C₃S mixture. This means that TNTs accelerated the hydration of C₃S at an early stage but did not significantly affect its total degree of hydration.

The hydration kinetics were modeled using the BN model to further study the experimental results of pure C₃S and the related parameters are shown in Table 3, where k_B is the rate constant for transformation at the grain boundary (particle surface), and k_G is the rate constant for transformation at the non-nucleation particles (intergranular space). The ratio of k_B to k_G represents the type of kinetic behavior. When k_B/k_G is large, the conversion occurred early in the overall process [14]. A slight reduction in k_B/k_G could be explained by additional nucleation sites provided by TNTs delayed the diffusion-controlled hydration kinetics and increased the amount of early nucleation and growth hydration [19]. However, a very small difference in k_B/k_G confirms that TNTs do not significantly affect the overall hydration of cement paste. On the other hand, the addition of TNTs decreased t_0 by 2.93 h compared to the control. This decrease in t_0 was found to shift the fit of the BN model to the left, which implies that TNTs exert a promoting effect only at the initial reaction stage of the cement paste hydration process [20].

Table 4: Fitting parameters obtained by applying the boundary nucleation and growth model to C₃S and C₃S-TNTs hydration data.

	A (kJ/mol)	t_0 (h)	k_B (h ⁻¹)	k_G (h ⁻¹)	k_B/k_G
C ₃ S	67.47	7.12	0.06314	0.06262	1.0083
C ₃ S - TNTs	66.76	4.19	0.06419	0.06381	1.006

4. CONCLUSIONS

- The TNTs had a beneficial effect on the strength of the cement paste, especially in the long-term strength. It is also believed that the addition of TNTs is more effective in increasing flexural strength than compressive strength.
- The SEM measurements of the crack surfaces of cement paste clearly showed the effect of TNT bridges between microcracks of cement paste.
- In the case of C₃S, it was confirmed that addition of TNTs promoted hydration for several hours. However, there was no significant difference in total hatching rate between control and TNTs-incorporated samples.
- Based on these results, we conclude that TNTs have great potential as a nano-reinforcing material for cementitious materials.

ACKNOWLEDGEMENTS

This research was supported by the Basic Science Research Program through the National Research Foundation of Korea (NRF) funded by the Ministry of Science, ICT & Future Planning (NRF-2016R1C1B1014179).

REFERENCES

- [1] Balaguru, P. and Chong, K., 'Nanotechnology and concrete: research opportunities.' *Proceedings of the ACI Session on Nanotechnology of Concrete: Recent Developments and Future Perspectives* (2006).
- [2] Song, P. and Hwang, S., 'Mechanical properties of high-strength steel fiber-reinforced concrete.' *Construction and Building Materials* **18**(9) (2004) 669-673.
- [3] Yu, M.-F., Files, B. S., Arepalli, S. and Ruoff, R. S., 'Tensile loading of ropes of single wall carbon nanotubes and their mechanical properties.' *Physical review letters* **84**(24) (2000) 5552.
- [4] Salvétat, J.-P., Bonard, J.-M., Thomson, N., Kulik, A., Forro, L., Benoit, W. and Zuppiroli, L., 'Mechanical properties of carbon nanotubes.' *Applied Physics A* **69**(3) (1999) 255-260.
- [5] Campillo, I., Dolado, J. and Porro, A., 'High-performance nanostructured materials for construction.' *Special Publication-Royal Society of Chemistry* **292** (2004) 215-226.
- [6] Li, G. Y., Wang, P. M. and Zhao, X., 'Mechanical behavior and microstructure of cement composites incorporating surface-treated multi-walled carbon nanotubes.' *Carbon* **43**(6) (2005) 1239-1245.
- [7] Grobert, N., 'Carbon nanotubes—becoming clean.' *Materials today* **10**(1-2) (2007) 28-35.
- [8] Konsta-Gdoutos, M. S., Metaxa, Z. S. and Shah, S. P., 'Highly dispersed carbon nanotube reinforced cement based materials.' *Cement and Concrete Research* **40**(7) (2010) 1052-1059.
- [9] Bastos, G., Patiño-Barbeito, F., Patiño-Cambeiro, F. and Armesto, J., 'Nano-inclusions applied in cement-matrix composites: A review.' *Materials* **9**(12) (2016) 1015.
- [10] Xie, X.-L., Mai, Y.-W. and Zhou, X.-P., 'Dispersion and alignment of carbon nanotubes in polymer matrix: a review.' *Materials Science and Engineering: R: Reports* **49**(4) (2005) 89-112.
- [11] Kasuga, T., Hiramatsu, M., Hoson, A., Sekino, T. and Niihara, K., 'Formation of titanium oxide nanotube.' *Langmuir* **14**(12) (1998) 3160-3163.
- [12] An'amt, M., Huang, N., Radiman, S., Lim, H. and Muhamad, M., 'Triethanolamine solution for rapid hydrothermal synthesis of titanate nanotubes.' *Sains Malaysiana* **43**(1) (2014) 137-144.
- [13] Kim, J.-Y., Sekino, T., Park, D. J. and Tanaka, S.-I., 'Morphology modification of TiO₂ nanotubes by controlling the starting material crystallite size for chemical synthesis.' *Journal of Nanoparticle Research* **13**(6) (2011) 2319-2327.
- [14] Thomas, J. J., 'A new approach to modeling the nucleation and growth kinetics of tricalcium silicate hydration.' *Journal of the American Ceramic Society* **90**(10) (2007) 3282-3288.
- [15] Anandan, S., Narasinga Rao, T., Sathish, M., Rangappa, D., Honma, I. and Miyauchi, M., 'Superhydrophilic graphene-loaded TiO₂ thin film for self-cleaning applications.' *ACS applied materials & interfaces* **5**(1) (2012) 207-212.
- [16] Nochaiya, T. and Chaipanich, A., 'Behavior of multi-walled carbon nanotubes on the porosity and microstructure of cement-based materials.' *Applied Surface Science* **257**(6) (2011) 1941-1945.
- [17] Makar, J. M. and Chan, G. W., 'Growth of cement hydration products on single-walled carbon nanotubes.' *Journal of the American Ceramic Society* **92**(6) (2009) 1303-1310.
- [18] Miyauchi, M. and Tokudome, H., 'Low-reflective and super-hydrophilic properties of titanate or titania nanotube thin films via layer-by-layer assembly.' *Thin Solid Films* **515**(4) (2006) 2091-2096.
- [19] Thomas, J. J., Jennings, H. M. and Chen, J. J., 'Influence of nucleation seeding on the hydration mechanisms of tricalcium silicate and cement.' *The Journal of Physical Chemistry C* **113**(11) (2009) 4327-4334.
- [20] Lee, B. Y. and Kurtis, K. E., 'Influence of TiO₂ nanoparticles on early C₃S hydration.' *Journal of the American Ceramic Society* **93**(10) (2010) 3399-3405.

INFLUENCE OF PRAH CRYSTALLINE ADMIXTURES ON THE DURABILITY OF CONCRETES

Kosmas K. Sideris (1), Christos Tassos (1), Alexandros Chatzopoulos (1), Panagiota Manita (1)

(1) Laboratory of Building Materials, Democritus University of Thrace, Department of Civil Engineering, Greece

Abstract

The influence of crystalline admixtures on the durability of concretes was the objective of the present study. We produced four concrete mixtures – two reference concretes and two alternative mixtures- The properties measured were the compressive strength and different durability indicators. The results revealed that crystalline admixtures enhanced the strength and the durability of alternative mixtures.

Keywords: Crystalline admixtures, durability, carbonation, chlorides, water absorption.

1. INTRODUCTION

Permeability Reduction Admixtures under Hydrostatic Pressure (PRAH) is a class of sealing admixtures mentioned by ACI 212.3-R10. These materials use a mechanism for sealing the pores of the concrete through the crystal growth mechanism. The material is added to the concrete during the production phase and is activated in the presence of moisture, developing insoluble crystals that fill the pores and prevent further moisture penetration.

In the current paper examined the effect of PRAH crystalline admixtures on the durability of reinforced concrete structures. In particular, concrete of different strength classes were prepared with and without the addition of crystalline admixtures. The compressive strength of mixtures was measured as well as durability indices such as water absorption, chloride penetration and carbonation of mixtures.

2. EXPERIMENTAL PROGRAM

Four concrete mixtures were produced - two conventional and two alternatives with added crystalline admixtures. Concrete mixtures were C25/30 and C30/37 strength class, according to ELOT EN206-1. CEM I 42.5R and CEM II 32.5 (B-M) N cement were used to produce the mixtures. Aggregates were of limestone origin with a maximum grain diameter of 32 mm. Appropriate doses of retarder and polycarboxylate superplasticizer were used to achieve the desired workability.

The mixing ratio as well as the properties of the fresh concrete mixtures prepared, are shown in Table 1. C30/37 PRAH mixture was produced with CEM II 32.5N cement instead of CEMI 42.5R in order to reduce the cost of the alternative mixture.

Cubic edge specimens of 150mm and cylindrical dimensions of 100x200mm were prepared. All samples were maintained in a maintenance chamber ($T = 20^{\circ}\text{C}$, $\text{RH} > 98\%$) until the test age. Cylindrical specimens with dimensions of 60X100mm were also used to measure the carbonation depth.

The 150mm cubes were used to measure the compressive strength at the ages of 2 and 28 days as well as to determine the water absorption. Resistance to chloride penetration of concrete was measured in cylindrical specimens with a diameter of 100mm and a height of 50mm cut off from the 100x200mm rollers. These specimens were maintained as above until the age of 28 days. The chloride diffusion coefficient D_e was then evaluated according to the procedure described in NT Building 492.

Table 1: Mixing ratio of concrete mixtures

kg/m ³	C 25/30	C 25/30- PRAH	C 30/37	C 30/37- PRAH
CEM I 42,5R	0	0	330	0
CEM II/(B-M) 32.5N	400	320	0	350
Sand	1042	1105	1133	1133
Gravel	180	190	195	195
Coarse	575	610	625	625
Water	200	160	165	160
superplasticizer	1.40	1.12	1.16	1.16
retarder	5.60	4.80	5	3.5
PRAH	--	2.56	--	2.8
W/C	0.50	0.50	0.50	0.46
S0 (cm)	25	23	24	21
S30 (cm)	20	22	22	19

Carbonation resistance was measured in cylindrical specimens 60x100mm. These specimens were maintained in the above-mentioned wet chamber for 3 days and then remained in a laboratory environment until the age of 28 days. After this age they were imported into the accelerated carburization chamber (RH = 55-60%, T = 20°C, CO₂ = 1%) where they remained for 60 days.

3. EXPERIMENTAL RESULTS AND DISCUSSION

3.1 Resistance to compression

The compressive strength was measured for all concrete mixtures at the ages of 2 and 28 days. These values are shown in Table 2.

Table 2: Compressive strength of concrete mixtures (MPa)

(MPa)		C25/30	C25/30 -PRAH	C30/37	C30/37- PRAH
2 days	f _{c2}	26.9	21.2	31.4	31.6
	S _{dev}	0.35	0.49	0.1	0.28
28 days	f _{c28}	39.3	41.1	54.2	64.0
	S _{dev}	0.3	0.1	0.7	0.5

The values of the above table show the positive effect of crystalline admixture on the compressive strength of the mixtures. Specifically, the C30/37 strength class mixtures show the same strength at the age of 2 days. However, the mixture prepared by addition of crystalline admixtures exhibits an increased strength of 9.8 MPa (18.15%) relative to the reference mixture at the age of 28 days.

In the case of C25/30 mixtures, the 2 day strength of alternative concrete is reduced by 5.65 MPa (21.04% reduction) relative to the reference mixture, due to the 20% reduced cement content in the this mixture. However, the gradual growth of the crystals resulted in an increase in the later strength of the alternative mixture, which at 28 days was measured at 41.10 MPa, ie 1.8 MPa higher than the reference mixture (4.6 percent increase).

3.2 Water absorption

The water absorbability measurements of the concrete mixtures were taken at the age of 28 days on 150mm edge specimens. The specimens remained in the laboratory maintenance chamber until the age of 28 days. Then they were dried at 65 °C until their weight was stabilized. The specimens were then properly prepared (wrapped around the insulating tape to ensure absorption only from the bottom of the specimen) and after weighing they were placed in basins of clean water in such a way that the water covered 3-5 mm of height of the specimen.

Measurements of weight change of the specimens were performed at 10 minutes, 30 minutes, 60 minutes, 90 minutes, 120 minutes, 180 minutes, 240 minutes, 480 minutes and 24 hours. These weights were divided by the exposed surface of the specimen into the water to calculate the water absorbance in gr/m².

Table 3: Water absorption of concrete mixtures

mm/min ^{0.5}	C25/30	C25/30-PRAH	C30/37	C30/37-PRAH
S _{index}	1.21	0.76	1.09	0.81

3.3 Chloride penetration coefficient

The Dnssm chloride diffusion coefficient values were measured according to NT Building 492 Standard and are presented for all mixtures in Table 4.

Table 4: Dnssm chloride penetration coefficient (x10⁻¹²m²/s) of concrete mixtures

x10 ⁻¹² m ² /s	C25/30	C25/30-PRAH	C30/37	C30/37-PRAH
Dnssm	15.27	12.54	11.6	8.61
S _{dev}	1.08	0.32	1.90	0.49

The above coefficients were used to calculate the lifetime of reinforced concrete constructions concreted with these mixtures. For this purpose the Life 365 program was used. The following assumptions were made: Exposure class XS1, time for the propagation of corrosion 10 years, 50 mm reinforcement cover. The total service life time is shown in the following diagram:

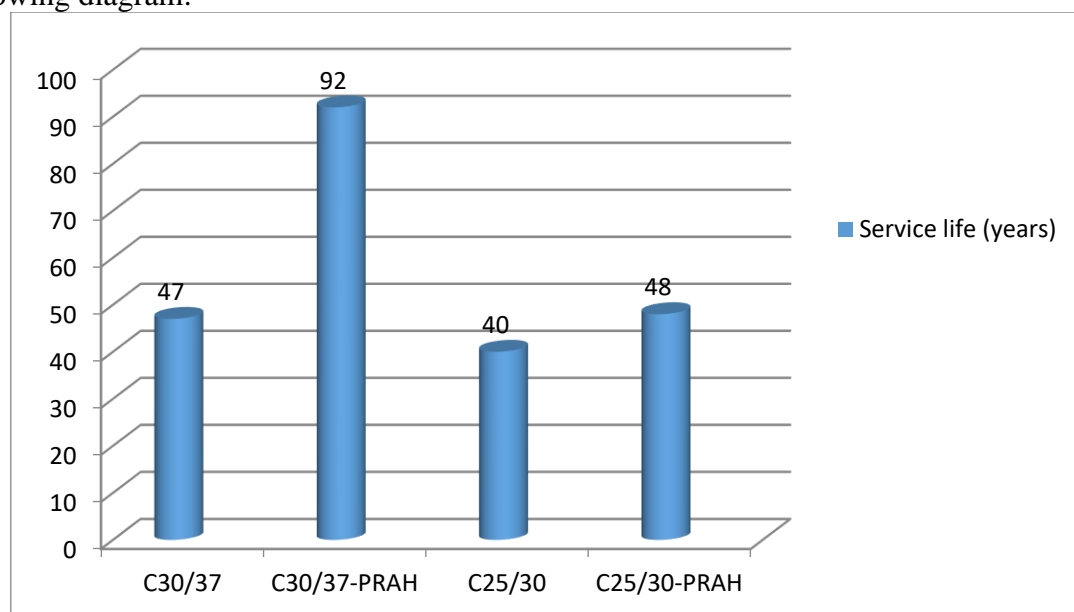


Figure 1: Estimated construction lifetimes

The figure above shows the particularly positive effect of the crystalline admixtures on the strength of the concrete. Specifically, the C30/37-PRAH mixture develops twice the lifetime of penetration of chlorides compared to the reference C30/37, while the C25/30-PRAH mixture

has an increased lifetime of 20% over the reference C25/30. Crystal activation in both cases led to a drastic reduction in porosity, thus preventing penetration of chlorides into the mixtures.

3.4 Carbonation depth

The carbonation depth was measured according to the procedure described in EN 14630 Standard. The specimens remained for 60 days in the Accelerating Carbonation Chamber of the Building Materials Laboratory. The carbonation depth of all mixtures is shown in Table 5.

Table 5: Carbonation depth of concrete mixtures

mm	C25/30	C25/30-PRAH	C30/37	C30/37-PRAH
Carbonation	8,7	9,1	2,9	4,5
S _{dev}	1.15	1.28	0.68	0.75

Based on the values of Table 5 it appears that the carbonation depth of the prepared mixtures is affected by the addition of the crystalline admixtures in a different way. In particular, the C25/30-PRAH mixture exhibits a slightly increased 5% carbonation depth relative to the reference mixture while the C30/37-PRAH mixture exhibits a carbonation depth increased by 55% relative to the C30/37 reference mixture. This may be due to the non-activation of the crystals; the specimens remained in a wet curing chamber for only three days, unlike the specimens used in the previous tests and which were maintained in the laboratory's wet curing chamber for 28 days. In addition, it should be noticed that the alternative C25/30-PRAH mixture was prepared with a 20% lower cement, while the C30/37-PRAH alternative was prepared using CEM II (B-M) 32.5N cement more prone to carbonation due to its high pozzolan content.

Long-term outdoor exposure experiments are underway in the Building Materials Laboratory in Xanthi in order to calculate the carbonation coefficient k and to assess more accurately the life span against carbonation of reinforced concrete structures exposed to XC4.

4. CONCLUSIONS

The crystalline PRAH additives used in the present study appear to be an effective way of sealing the porosity of the concrete prepared therewith. The presence of moisture is a catalytic factor for the activation of crystals which thus clog the pores of the cement and prevent the penetration of harmful fluids and gases. The alternative mixtures with crystalline PRAH additives that have been tested in the present study show increased compressive strength, lower water absorption coefficient, and significantly lower permeability to chlorides than reference mixtures, thus giving reinforced concrete constructions increased lifetime against seawater originated chlorides. These mixtures also exhibited a low carbonation depth, due to the use of a different dosage and type of cement as well as to the low maintenance time, which did not help to activate the crystals.

ACKNOWLEDGMENTS

Crystal admixtures and chemical additives used in the above experiments were provided by Penetron Hellas SA and NORDIA SA. Their support to the research work of the Building Materials Laboratory is greatly acknowledged.

REFERENCES

- [1] ELOT EN 206 Concrete - Specification, performance, production and compliance.
- [2] Concrete Technology Regulation 2016 (Government Gazette B / 02-06-2016).
- [3] ACI 212.3R-10 Report on Chemical Admixtures for Concrete.
- [4] NT Build 492 - Concrete Mortar and Cement-based Repair Materials - Chloride Migration Coefficient from Non-steady-state Migration Experiments (1999).
- [5] EN 14630 Committee of European Normalization. Products and systems for the protection and repair of concrete structures - Test methods - Determination of carbonation depth in hardened concrete by the phenolphthalein method (2006).

A COMPARISON OF GRAPHENE OXIDE, REDUCED GRAPHENE OXIDE AND PURE GRAPHENE: EARLY AGE PROPERTIES OF CEMENT COMPOSITES

Tanvir S. Qureshi (1) and Daman K. Panesar (1)*

(1) Department of Civil and Mineral Engineering, University of Toronto, Toronto, Ontario, Canada. M5S 1A4

*corresponding author: d.panesar@utoronto.ca

Abstract

This study compares the hydration, mechanical and transport properties of cement based composites containing graphene oxide (GO), reduced graphene oxide (rGO), and pure graphene (G). The only mix design variable other than the type of graphene material (GO, rGO, and G) that was considered is the concentration of graphene materials which ranged from 0.01% to 0.16% of cement weight. Outcomes from this research indicate that the physical and chemical properties of GO, rGO and G influence the early age properties of the cement based composites. A high amount of oxygen-containing functional groups of GO considerably enhances the cement hydration and forms a compacted composite bond which improved the 14-day compressive and flexural strength by 44% and 83%, respectively compared to the control mix. The reduced amount of functional groups and moderately high physical strength of rGO gradually enhances cement hydration and reinforces the composite matrix which improved the 14-day compressive and flexural strength by 42% and 52%, respectively compared to the control mix. The high physical strength of G reinforces the composite matrix which improved the 14-day compressive and flexural strength by 34% and 56%, respectively compared to the control mix. The microscopic imaging and electrical resistivity performance also confirms the influence of graphene materials in the composite.

Keywords: Graphene, graphene oxide (GO), reduced graphene oxide (rGO), dispersion, mechanical and transport properties, microstructure.

1. INTRODUCTION AND LITERATURE REVIEW

The incorporation of reinforcing materials in concrete has become common practice owing to its benefits to the mechanical properties. As such, graphene nanomaterials have the potential to improve both the mechanical and durability properties of the nano-cement composites. There are three common forms of graphene based nanomaterials herein: graphene oxide (GO),

reduced graphene oxide (rGO) and pure graphene (G). All three graphene materials exhibit different properties due to their different molecular structure arrangement. The physical properties of graphene materials are presented in Table 1. G is hexagonally connected carbon atoms with σ -bonds forming 2D planes. G exhibits an extraordinarily high elastic modulus, nearly 1 TPa, and a tensile strength of nearly 130 GPa [1], as well as high electrical conductivity (approximately 1000 S/m) [2]. G is hydrophobic which limits its dispersibility in water. GO is composed of G layers with active oxygen-containing functional groups on its surface, such as hydroxyl, epoxide, carboxyl, and carbonyl groups [3]. GO is not conductive and has reduced mechanical properties compared to G (Table 1), due to the presence of functional groups [2] which breaks the sp^2 bonding of crystal planes. However, the functional groups of GO makes it hydrophilic and highly dispersible in water. rGO is produced through removing the functional groups from GO [4], which partly restores the mechanical and electrical conductivity properties of the graphene layers (Table 1).

Table 1: Physical properties of graphene materials.

Physical properties	GO- Graphene oxide	rGO- Reduced graphene oxide	G- Pure graphene
Tensile strength	~0.13 GPa*	unknown	~130 GPa*
Elastic modulus	23-42 GPa*	250±150 GPa**	1000 GPa*
Elongation at break	0.6 %*	unknown	0.8%*
Electrical conductivity	Non conductive	~667 S/m***	~1000 S/m
Dispersibility in water	Highly dispersible	Moderately dispersible	Not dispersible

Note: * Reference [1,5], ** Reference [6], ***Measured in a 20 nm thickness film.

GO has been most commonly studied form of graphene in the cement based composites [7]. In contrast, the literature on rGO and G in cement composites is limited, possibly owing to the hydrophobicity and the challenging aspects of dispersion in the composite. In water, the agglomeration of G has been found to be a common limitation at the nanoscale [1].

The functional group's reduction level from GO to rGO was reported to considerably vary the degree of hydration of the cement composite in the range of 16.5 to 22.5% [4]. The hydration process of cement is influenced by GO [7] which regulates the formation of flower-like hydration crystals [8].

The use of 0.08 wt% GO in cement based composites increased the compressive strength by 46.8%, compared to that of 100% cement paste [9]. However, 0.04 wt% GO in the composite increased the flexural strength by 14.2%, compared to the 100% cement paste [9]. The cement composite with 0.02 wt% rGO of cement increased the flexural strength by 23% compared to the 100% cement paste at 28 days [10]. The composite of 0.03 wt% G was reported to increase the flexural strength by 40% compared to the 100% cement paste [11].

The GO-cement composites have been reported to have higher electrical resistivity and lower sorptivity compared to the 100% PC paste [7]. The presence of rGO in the cement based composite decreased water sorptivity and mass porosity in 7 days then, both properties increased by 28 days [10], compared to the control mix.

Despite advancements in the last five years, there is a lack of understanding on the characteristics, mechanisms and the relative influence of GO, rGO and G materials on the cement based composites. Hence, the objective of this research is to evaluate and compare the impact of GO, rGO and G on the properties of cement based composites up to 14 days.

2. MATERIALS AND METHODS

2.1 Materials

Three forms of graphene materials (GO, rGO, and G) were supplied by Zenyatta Venture Ltd. The major characterisation factors of graphene materials are: chemical structure, size, *d*-spacing, layer thickness, stack thickness in water dispersion, Raman I_D/I_G ratio (Table 2). For example, the functional groups are reduced in rGO compared to GO which is indicated by the lower oxygen element (%), lower *d*-spacing and higher I_D/I_G ratio. Both G and rGO were treated with surfactants to improve their dispersibility in water, which is evidenced by the markedly greater stack thickness in water dispersion values of rGO, and G compared to GO. The general use cement was supplied by CRH Mississauga plant, and its chemical composition is shown in Table 3.

Table 2: Characterization of graphene materials.

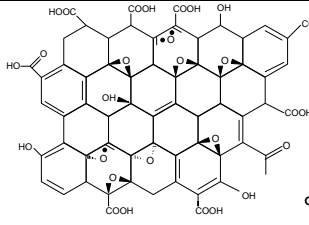
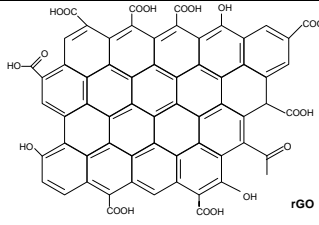
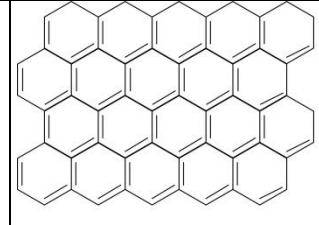
	GO	rGO	G
Chemical structure			
C, O Element (%)	C (62-65%) O (35-38%)	C (77-87%) O (13-22%)	C (99%) O (--)
Crystal size	21.14 nm	15.13-15.95 nm	175.49 nm
<i>d</i> spacing	0.93 nm	0.36	0.33 nm
Plane size	1-2 μm	1-7 μm	0.5-5 μm
Number of layers	1-3	1-3	3-5
Layer thickness	0.76-0.84 nm	0.35-0.36 nm	0.34 nm
Stack thickness in water dispersion	1.00-1.20 nm	125-175 nm	180-230 nm
Raman (I_D/I_G) ratio	0.79	1.10-1.16	0.25

Table 3: The chemical composition of general use cement in percentage.

SiO ₂	Al ₂ O ₃	Fe ₂ O ₃	CaO	MgO	SO ₃	Total Alkali	Free Lime	LOI
19.3	5.50	2.70	61.20	2.60	4.00	0.92	0.60	2.50

One 100% cement paste (control) plus fifteen (15) paste mix designs of the graphene-cement composite were prepared. GO, rGO and G were used at 0.01, 0.02, 0.04, 0.08 and 0.16 wt% of cement. For all paste composites, 3000 g of cement was used with a water to cement ratio of 0.45.

2.2 Dispersion of graphene materials in water

Graphene materials were dispersed in deionised water prior to mixing with cement. The dispersion method was as follows: (i) graphene materials were first mixed with deionized water for 3 hr at 1000 rpm, (ii) the mixture was sonicated for 3 hr and left for 18 hr, and (iii) the mixture was stirred for 1 hr and sonicated for 1 hr prior to mixing with cement.

2.3 Graphene-cement composite mixing and casting

Cubes (50x50x50 mm), and prisms (25x25x100 mm) of the graphene-cement composite were cast following ASTM C1738 [12] using a high-shear mixer. Triplicates of all of the samples were prepared for each test in order to present the corresponding statistics.

2.4 Test Methods

The workability of the composites was assessed using a mini-slump test, and the static and dynamic flow diameters were measured according to [13] and ASTM C1437-07 [14], respectively. From ~5 min to 72 hr, hydration kinetics of the composite paste was measured using a thermometric TAM air calorimeter. The compressive and flexural strengths of graphene-cement composites were measured at 3 and 14 days. The compressive strength test was conducted on 50 mm cubes according to ASTM C109 [15]. The flexural strength test was performed on prisms (25x25x100 mm) following ASTM C348 [16]. The microstructure of the composite samples was analysed by SEM imaging on 14-day samples. The electrical resistivity was measured on 50 mm cubes using the uniaxial two-electrode method [17].

3. RESULTS AND DISCUSSION

3.1 Workability

Both the static and dynamic flow diameter results are presented in Fig. 1. Increasing the proportion of GO reduces both the static and dynamic flow of the composites compared to the control paste mix. This is due to the absorption of additional water by high d -spacing and the functional groups of hydrophilic GO in the composite. Both rGO and G were treated with surfactants which result in similar or slightly higher static flow in the composite (Fig. 1a). However, increasing the percentage of rGO in the paste, reduces the dynamic flow due to the presence of some remaining functional groups (Fig. 1b). Varying the percentage of G has the least impact on the workability of the composites since G is hydrophobic.

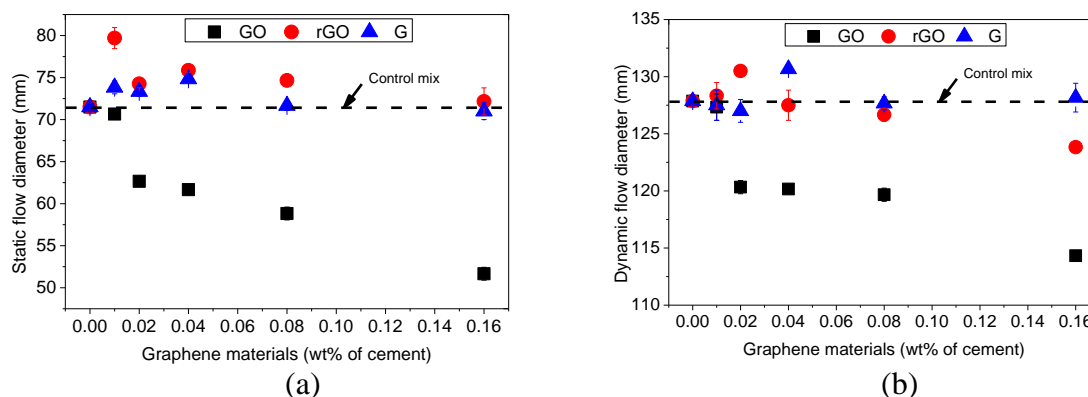


Figure 1: Flow diameter in mini-slump test, (a) Static flow, and (b) Dynamic flow.

3.2 Hydration kinetics

The heat of hydration of the graphene-cement composites in the first 48 hr is shown in Fig. 2. GO accelerates the cement hydration process by increasing the rate of heat of hydration at the C_3S and C_3A hydration phases (Fig. 2a). This is due to the contribution of oxygen-containing functional groups on the cement hydration process. On the other hand, rGO slightly delays the cement hydration and does not show much impact on heat release (Fig. 2b) within the first 48 hours, owing to its reduced amount of functional groups. However, the rate of heat

of hydration was higher for the rGO composite compared to the control specimens, particularly during 8 to 12 hours which corresponds to the C_3A hydration phase. The rate of heat of hydration is minimally impacted by the G composites, compared to the control specimens as shown in Fig. 2c. Although there are no functional groups in G, the sp^2 bonded carbon planes of G may act as nano nucleation sites during the cement hydration process.

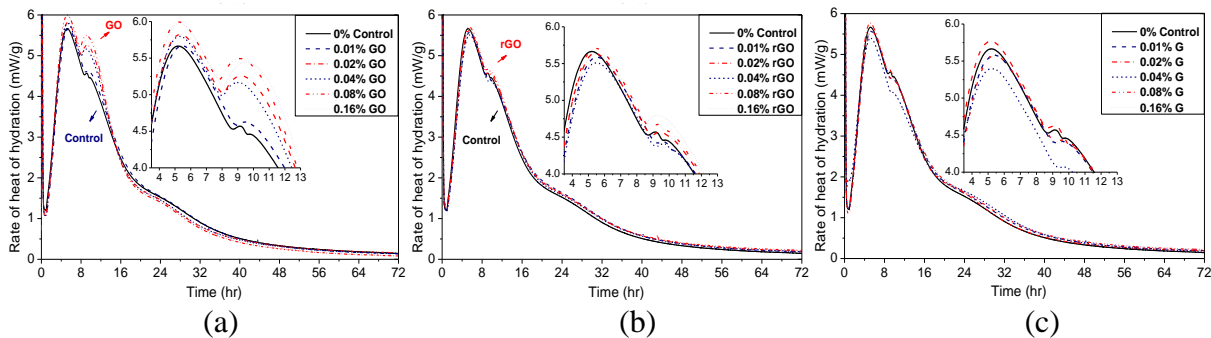


Figure 2: Effect of graphene materials on the hydration heat release of composite pastes during 48 h hydration: (a) GO composites, (b) rGO composites, and (c) G composites.

3.3 Mechanical properties

The 3 and 14 day compressive strength results are presented in Fig 3a and Fig 3b, respectively. GO increases the compressive strength of the composites at 3 and 14 days, compared to the control mix. At 14 days, increasing the percentage of GO increases the compressive strength of the composites, which results by 44% in the 0.16% GO composite, compared to the control mix. This is due to the participation of GO functional groups in the cement hydration process within the first 24 hr which enhanced hydration and reinforced the hydration compounds such as C-S-H, portlandite, and ettringite at the nano-micro scale. The compressive strength of the rGO composites at 3 days slightly increases up to 0.04% rGO then decreases with higher content of rGO, compared to the control mix. However, at 14 days, increasing the percentage of rGO increases the compressive strength of the composites (except for 0.08% rGO) resulting in a maximum increase of 43% compressive strength of the 0.16% rGO composite, compared to the control mix. This is due to rGO's moderately higher physical strength compared to GO. rGO slowly influences the cement hydration process due to the reduced amount of functional groups, which reflects on the 14-day compressive strength results. The G cement composites have a 3-day compressive strength similar to that of the control mix except for 0.02% G which have 25% increased compressive strength than the control mix. The 14-day compressive strength increased around 34% in 0.01% G, 0.02% G and 0.16% G, compared to the control mix. The high physical strength and micro size planes (1-7 μm) of G plays a vital role in compressive strength enhancement.

The 3-day and 14-day flexural strength of the graphene-cement composites increased compared to the control mix (Fig. 4). The maximum flexural strength at 14 days increased by 83%, 52% and 56%, respectively in 0.04% GO, 0.16% rGO, and 0.02% G, compared to the control mix. The reason for flexural strength increase in the graphene-cement composites is similar as explained for the compressive strength enhancement. The large error bar resulted in flexural strengths of the G cement composites (example, 0.02% G and 0.16% G) may be due to the challenge of G dispersion in water and composites regardless of surfactant treatment.

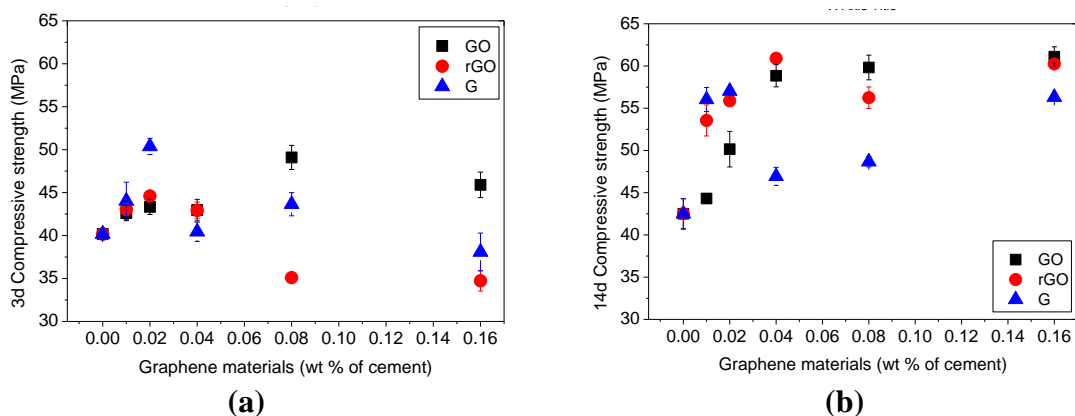


Figure 3: Compressive strength of the composites, (a) 3-day, and (b) 14-day.

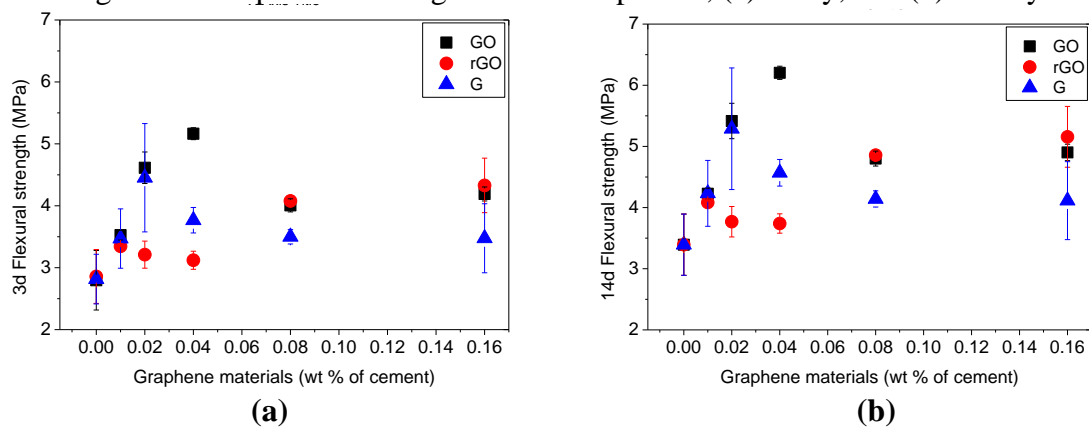


Figure 4: Flexural strength of the composites, (a) 3-day, and (b) 14-day.

3.4 Microstructure

Typical SEM backscattered images of the 14-day graphene-cement composites are presented in Fig. 5. Common cement hydration products such as C-S-H, portlandite, and ettringite are observed in all specimens. Graphene materials were observed to be well distributed as indicated by arrows which densified the composite microstructure (Fig. 5 b-d). GO is shown to be well compacted within the C-S-H gel materials. Further comprehensive analysis is required to understand the influence of nanomaterials on the microstructure of the graphene-cement composites.

3.5 Transport properties

The 3-day electrical resistivity of the graphene-cement composites decreased compared to the control mix. However, the composites with up to 0.02% GO and 0.02% G have a higher or similar electrical resistivity compared to the control mix (Fig. 6a). At 14 days, all of the GO cement composites have similar or higher electrical resistivity compared to the control mix (Fig. 6b). This is due to GO's nonconductive properties and the densification of the composite by additional hydration products by GO. The resistivity gradually decreases in the rGO composites with the increasing percentage of rGO due to rGO's higher electrical conductivity. In the G cement-composites, the 14-day resistivity was slightly increased with G up to 0.02% G. The resistivity of the G composites decreases starting from a concentration of 0.04% G due to its high electrical conductivity (Fig. 6b).

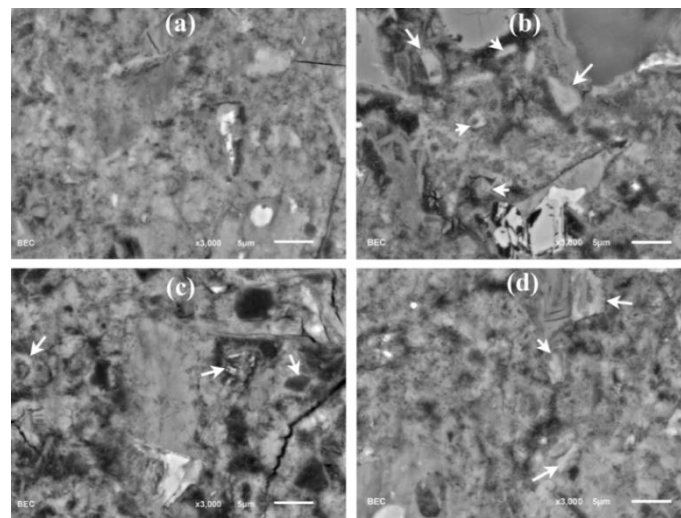


Figure 5: SEM backscattered images of control paste and composites thin section after 14 days hydration, (a) control, (b) GO, (c) rGO, and (d) G.

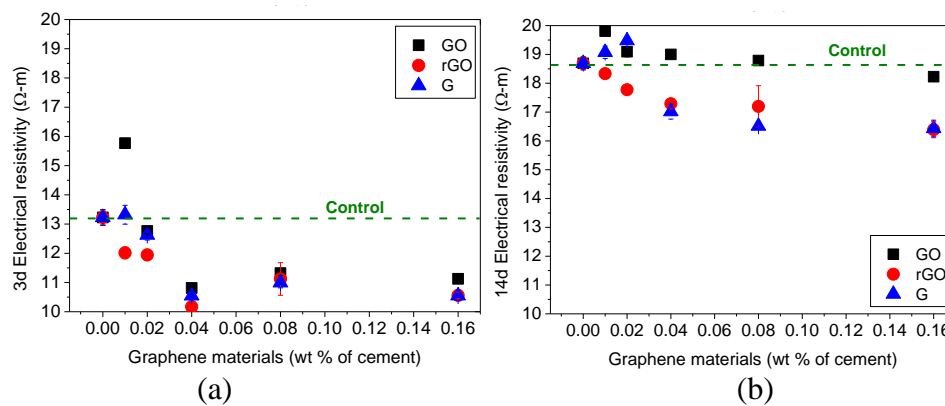


Figure 6: Electrical resistivity of the composites, (a) 3 days, and (b) 14 days.

4. CONCLUSIONS

- Characteristics such as oxygen-containing functional groups, size, *d*-spacing, layer thickness, and the physical properties of graphene materials impact the properties of the graphene-cement composites.
- The high amount of oxygen-containing functional groups of GO considerably enhances the cement hydration which improves the mechanical properties.
- The reduced amount of functional groups and moderate physical strength of rGO enhance cement hydration and improve the mechanical properties.
- The high physical strength of G improves the mechanical properties.
- The microstructural analysis of the composites shows that graphene materials influence cement hydration and reinforce the composite at a nano-micro scale. Graphene materials are well compacted within the C-S-H gel materials, where GO is the most effective followed by rGO and G.
- The electrical resistivity of the graphene-cement composites was influenced by the electrical conductivity, functional groups and dispersion properties of GO, rGO and G.

- In the future, self-sensing, long-term properties and performance graphene materials in complex cement based systems such as mortar and concrete, should be investigated.

ACKNOWLEDGEMENTS

The authors are grateful for support from an NSERC Engage grant in collaboration with Zenyatta Ventures Ltd. and Prof. Panesar's Early Career Award, Hart Professorship.

REFERENCES

- [1] S. Chuah, Z. Pan, J.G. Sanjayan, C.M. Wang, W.H. Duan, Nano reinforced cement and concrete composites and new perspective from graphene oxide, *Constr. Build. Mater.* 73 (2014) 113–124.
- [2] H. Chu, J. Jiang, W. Sun, M. Zhang, Effects of graphene sulfonate nanosheets on mechanical and thermal properties of sacrificial concrete during high temperature exposure, *Cem. Concr. Compos.* 82 (2017) 252–264.
- [3] T.N. Lambert, C.A. Chavez, B. Hernandez-Sanchez, P. Lu, N.S. Bell, A. Ambrosini, T. Friedman, T.J. Boyle, D.R. Wheeler, D.L. Huber, Synthesis and Characterization of Titania–Graphene Nanocomposites, *J. Phys. Chem. C.* 113 (2009) 19812–19823.
- [4] A. Gholampour, M. Valizadeh Kiamahalleh, D.N.H. Tran, T. Ozbakkaloglu, D. Losic, From Graphene Oxide to Reduced Graphene Oxide: Impact on the Physiochemical and Mechanical Properties of Graphene–Cement Composites, *ACS Appl. Mater. Interfaces.* (2017)
- [5] W. Lv, Z. Li, Y. Deng, Q.-H. Yang, F. Kang, Graphene-based materials for electrochemical energy storage devices: Opportunities and challenges, *Energy Storage Mater.* 2 (2016) 107–138.
- [6] Y. Zhu, S. Murali, W. Cai, X. Li, J.W. Suk, J.R. Potts, R.S. Ruoff, Graphene and Graphene Oxide: Synthesis, Properties, and Applications, *Adv. Mater.* 22 (2010) 3906–3924.
- [7] T.S. Qureshi, D.K. Panesar, B. Sidhureddy, A. Chen, P.C. Wood, Nano-cement composite with graphene oxide produced from epigenetic graphite deposit, *Compos. Part B Eng.* 159 (2019) 248–258.
- [8] S. Lv, Y. Ma, C. Qiu, T. Sun, J. Liu, Q. Zhou, Effect of graphene oxide nanosheets of microstructure and mechanical properties of cement composites, *Constr. Build. Mater.* 49 (2013) 121–127.
- [9] W. Li, X. Li, S.J. Chen, Y.M. Liu, W.H. Duan, S.P. Shah, Effects of graphene oxide on early-age hydration and electrical resistivity of Portland cement paste, *Constr. Build. Mater.* 136 (2017) 506–514.
- [10] M. Murugan, M. Santhanam, S. Sen Gupta, T. Pradeep, S.P. Shah, Influence of 2D rGO nanosheets on the properties of OPC paste, *Cem. Concr. Compos.* 70 (2016) 48–59.
- [11] G. Li, J.B. Yuan, Y.H. Zhang, N. Zhang, K.M. Liew, Microstructure and mechanical performance of graphene reinforced cementitious composites, *Compos. Part A Appl. Sci. Manuf.* 114 (2018) 188–195.
- [12] ASTM International, ASTM C1738, Standard Practice for High-Shear Mixing of Hydraulic Cement Pastes, 2011.
- [13] F. Collins, J. Lambert, W.H. Duan, The influences of admixtures on the dispersion, workability, and strength of carbon nanotube-OPC paste mixtures, *Cem. Concr. Compos.* 34 (2012) 201–207.
- [14] ASTM Standard C1437-07, Standard Test Method for Flow of Hydraulic Cement Mortar, 2007.
- [15] ASTM C109 / C109M-16a, Standard Test Method for Compressive Strength of Hydraulic Cement Mortars (Using 2-in. or [50-mm] Cube Specimens), 2016.
- [16] ASTM C348-14, Standard Test Method for Flexural Strength of Hydraulic-Cement Mortars, 2014.
- [17] H. Layssi, P. Ghods, A.R. Alizadeh, M. Salehi, Electrical resistivity of concrete, *Concr. Int.* 37 (2015) 41–46.

A NEW ADMIXTURE FOR CONCRETE WITH CLAY CONTAMINATED SAND

O. Mazanec (1), F. Morati (2), A. Große-Sommer (3)

(1) BASF Construction Solution GmbH, Trostberg, Germany

(2) BASF Construction Chemicals Italia Spa, Treviso, Italy

(3) BASF SE, Ludwigshafen, Germany

Abstract

Our daily lives are built on sand. A report by the United Nations Environment Programme (UNEP) found that no solid raw material is used more than sand and gravel. But these fine grains are in short supply. This is primarily due to the construction boom. In 2014, the UNEP estimated that between 26 and 30 billion metric tons of sand are poured into concrete mixers every year worldwide. Since then, these numbers will have only increased. The demand for this raw material in expanding metropolises, such as Singapore, Shanghai, Paris, or Dubai, is always growing. Mega construction projects in these cities are already devouring vast quantities of sand, as we see with the major public transfer projects in Paris.

This shortage has made sand a scientific priority. We are now looking for ways to make better use of the resources. One of these methods has been in use since 2016: a process developed by BASF to convert sand that was previously unsuitable for high-quality concrete into a valuable raw material. This involves using clayey sand or sand with a high proportion of ultra-fine additives, such as mica. Clay and mica absorb large amounts of water due to their large surface area and their special, partially expandable structure – they also absorb the commonly used polycarboxylate superplasticizer (PCE) needed for concrete mixing by superficial adsorption via electrostatic interactions between the anionic groups and positively charged sites by adsorbed Ca²⁺ cations or the intercalation of ether units of the PCE grafts in the interlayer space of the aluminosilicate layers. This has unwanted consequences: concrete cannot be processed.

A clay blocking superplasticizer has been synthesized to increase the performance in concrete with challenging sands. It ensures that water and PCE superplasticizer are not absorbed by the sand, and instead the concrete is generously liquefied. The use of the clay blocking superplasticizer as counter measure will be discussed, including underlying mechanistical principles and sustainable aspects. Sands that were previously unsuitable can now be used and existing deposits can be exploited more intensively.

Keywords: superplasticizer, clay contamination, sand, sustainability

NEW GENERATION OF CONSTRUCTION MATERIALS
SESSION 8: Candidates for AAMs

INSTANTANEOUS ACTIVATION ENERGY OF ALKALI ACTIVATED MATERIALS

Shiju Joseph (1), Siva Uppalapati (1) and Özlem Cizer (1)

(1) Department of Civil Engineering, KU Leuven, Belgium

Abstract

Alkali activated materials (AAM) are generally cured at high temperatures to compensate for the low reaction rate. Higher temperature accelerates the reaction of AAM as in cement-based materials and this effect is generally predicted using Arrhenius equation based on the activation energy. While apparent activation energy is calculated from parallel isothermal calorimetry measurements at different temperatures, instantaneous activation energy is typically measured using a differential scanning calorimeter. Compared to the apparent activation energy, instantaneous activation energy has minimal effects on the microstructural changes due to the variation in temperature. In this work, the evolution of activation energy was determined by traditional methods and was compared with the instantaneous activation energy. It was found that while the activation energy changed with the progress of reaction over traditional methods, the instantaneous activation energy did not show any changes / or remained the same. The instantaneous activation energy was also found to be higher compared to the apparent activation energy determined with traditional methods.

Keywords: Activation energy, Alkali activated materials, calorimetry, blast furnace slag, fly ash

This work was invited for publication in the open access journal RILEM Technical Letters. You can visit the journal and benefit from the full open access to the published articles at: letters.rilem.net.

MECHANICAL PARAMETERS OF METAKAOLIN-BASED GEOPOLYMER WITH CRT GLASS WASTE FINE AGGREGATE

Natalia Paszek (1), Marcin Górski (2)

(1) Faculty of Civil Engineering, Silesian University of Technology, Poland

(2) Faculty of Civil Engineering, Silesian University of Technology, Poland

Abstract

The paper presents tests performed on a metakaolin-based geopolymer containing crushed cathode-ray tube (CRT) glass waste in a form of an aggregate. CRT glass constitutes a problematic type of waste which is hard to recycle. The paper describes the possibility of CRT glass application in the geopolymer matrix. During the research, six mixtures containing different metakaolin to CRT glass ratio were subjected to flexural and compressive strength tests. Samples containing glass waste showed very good strength results. Samples prepared with the use of a mixture containing 50% of crushed glass exhibited the highest average flexural strength (6,6 MPa) and the highest compressive strength (51,0 MPa). One mixture was deemed the most promising, and as such was subjected to further testing which showed that the increase of NaOH concentration leads to an increase in mechanical strength.

Keywords: geopolymer, metakaolin, CRT glass, aggregate, mechanical parameters

1. INTRODUCTION

Geopolymer can be classified as an aluminosilicate cementitious binder material. Geopolymers are synthesized during the geopolymerization reaction of alumino-silicate minerals with alkaline activators [1]. The term “alumino-silicate minerals” (also known as “raw materials”) covers an endless list of different substances. Metakaolin, fly ash and blast furnace slag are raw materials most often used in the geopolymerization process [2].

Some research covers geopolymers containing only raw material and activator, which can be compared to cement paste without sand addition [1, 3]. However, geopolymer mixtures frequently contain some kind of aggregate, most often sand [4, 5]. Some scientists try to add different type of aggregate to the mixture. Pacheco-Torgal et al. [6] carried out tests of tungsten mine waste mud-based geopolymer with addition of three different types of aggregates: limestone, granite and schist. The test showed that the type of aggregate influences strength differently depending on the aggregate/binder ratio, but total differences are not significant.

Top et al. [7] describe a successful attempt at lightweight geopolymer concrete prefabrication with use of basaltic pumice aggregate. Panizza et al. [8] present metakaolin and slag-based geopolymer with environment-friendly aggregate recycled from construction and demolition waste. Authors reused grinded concrete and fired clay scraps. Complex research was concluded with promising results related to possible use of the new geopolymer as a building material.

The following paper presents tests performed on a metakaolin-based geopolymer with crushed cathode-ray tube (CRT) glass waste in form of a fine aggregate. The recycling of CRT glass waste is problematic because of its diverse character, inhomogeneous composition and presence of heavy metals [9]. CRT glass waste often finds application in the civil engineering branch for glass-ceramic composites production or as an aggregate in concrete [9]. The usage of crushed glass as an aggregate in the geopolymer binder allows to decrease the metakaolin content in the mixture and to reuse glass waste in an environment-friendly way.

2. LABORATORY TESTS

The main goal of the tests was to determine the influence of metakaolin to crushed glass ratio on the flexural and compressive strength of the geopolymer. An additional goal of the tests was to determine the influence of NaOH concentration on the flexural and compressive strength on the example of one chosen mixture. Table 1 presents the chemical composition of metakaolin. Figure 1 presents the particle size distribution of the aggregate (CRT crushed glass).

Table 1: Chemical composition of metakaolin

	SiO ₂	Al ₂ O ₃	K ₂ O	TiO ₂	Fe ₂ O ₃	CaO	MgO	H ₂ O ⁻	Na ₂ O	P ₂ O ₅	Cl	S
[%]	53,12	42,24	0,73	0,64	0,45	0,44	0,26	0,22	0,09	0,03	0,02	0,01

During the preliminary tests, the authors tried to make samples containing only the CRT glass and activators mixed in different ratios. Neither mixtures gave any sign of hardening within 7 days. The authors concluded that CRT glass cannot be treated as a precursor itself.

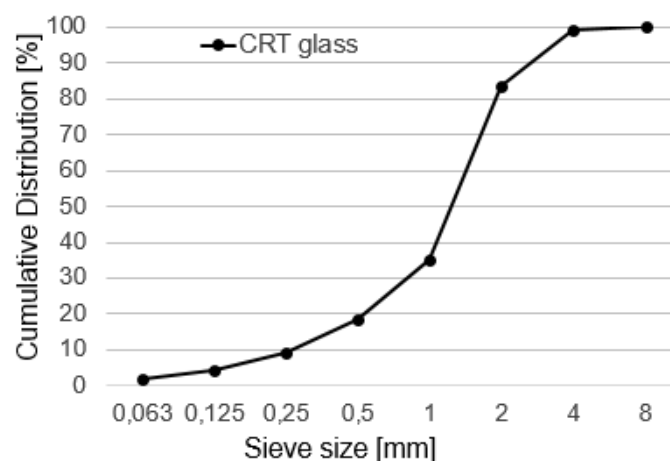


Figure 1: The particle size distribution of crushed CRT glass

Metakaolin and crushed waste CRT glass were the only dry components of the mixtures. Sodium silicate and sodium hydroxide were used as activators. The prismatic specimens of dimensions 4x4x16 cm were used during the flexural strength test. Then, the compressive strength test was carried out on the halves of prisms broken during the flexural strength test (as is required by the European standard EN 196-1:2016 [10]).

2.1 Mixtures compositions

Six geopolymer mixtures containing different metakaolin to crushed glass ratios were prepared. Table 2 presents the precise composition of all prepared mixtures including quantity of each ingredient and its percentage contribution. All mixtures listed in Table 2 were prepared with use of a sodium silicate solution and a water solution of NaOH. The sodium hydroxide solution was prepared no later than 24 hours before the tests by dissolving the NaOH pellets in demineralized water, to obtain a solution of desired concentration (8, 10 or 12 mol/L). The used sodium silicate solution (which was a commercial sodium water glass used in building chemistry) has a ratio of SiO₂ to Na₂O between 2,4 and 2,6. The minimum content of oxides (SiO₂&Na₂O) in the sodium hydroxide solution was 39%.

Samples were named with codes where the first number indicates metakaolin content and the second crushed glass content (see Table 2). Sodium silicate to sodium hydroxide ratio in each mixture was equal to 2:1. Authors tried to keep metakaolin to activators mass ratio similar (between 1,1:1 and 1,3:1). The variations come from simultaneous endeavours to keep a useful workability of mixtures.

Table 2: Mixtures compositions

Sample		Metakaolin	Crushed glass	Sodium silicate	Sodium hydroxide
M25/75:1	Quantity [kg/m ³]	449	1348	449	225
	Contribution [%]	18,2	54,5	18,2	9,1
M25/75:2	Quantity [kg/m ³]	524	1572	314	157
	Contribution [%]	20,4	61,3	12,2	6,1
M40/60	Quantity [kg/m ³]	755	1133	417	208
	Contribution [%]	30,1	45,1	16,6	8,3
M50/50	Quantity [kg/m ³]	898	898	449	225
	Contribution [%]	36,4	36,4	18,2	9,1
M60/40	Quantity [kg/m ³]	995	663	521	260
	Contribution [%]	40,8	27,2	21,4	10,7
M75/25	Quantity [kg/m ³]	1078	359	586	293
	Contribution [%]	46,5	15,5	25,3	12,6
M100/0	Quantity [kg/m ³]	1083	0	675	337
	Contribution [%]	51,7	0	32,2	16,1

The mixture M25/75 was prepared two times. The first time (M25/75:1) too much activator was added in an effort to achieve high workability: unfortunately this disturbed the proportions. The second variant of this mixture (M25/75:2) had better proportions of ingredients. The mixture M60/40 was used for reference during estimation of the NaOH concentration influence on mechanical strength (reasons for this choice are outlined in Section 3.2). Two new mixtures were prepared. Quantities of ingredients were the same as for mixture M60/40 (see Table 2). The only difference was the concentration of sodium hydroxide used for activation. The first mixture was activated with a 8 mol/L NaOH solution, the second with 12 mol/L.

2.2 Preparation of samples

All samples were prepared according to the same procedure. The process started with mixing of metakaolin and crushed glass in planned proportions. Then, the activators were weighed, poured together into a vessel and mixed for 5 minutes. At the end, metakaolin, crushed glass and activators were mixed together with a mechanical mixer. Mixtures were poured into prismatic moulds, condensed, covered and put into a climatic chamber. Samples were cured in a temperature of 60°C and humidity of 40% for 24 hours. After this time, samples were demoulded and kept in room temperature for the next 6 days. Tests were carried out after 7 days since samples preparation. Immediately after demoulding (and before tests), samples were weighed: this allowed determination of density and mass loss during the curing process.

It was decided to cure the samples in a temperature of 60°C for the first 24 hours, because previous research showed that this temperature is optimal for achieving good mechanical parameters of geopolymer [1, 3, 4]. Samples were cured in 40% humidity to enable future comparison with samples cured in the same conditions during other experiments. In all similar work carried out by the authors (e.g. [11]), geopolymer samples were cured in 40% humidity. Samples have never shown any cracks after curing.

3. RESULTS

3.1 Different metakaolin to crushed glass ratios

Figure 2 presents a few geopolymer samples made of various mixtures just before the flexural strength test. As it can be seen, the surface of samples is plain, samples did not exhibit any cracking. The only irregularity were small voids caused probably by air trapped between the mould surface and the geopolymer mixture.

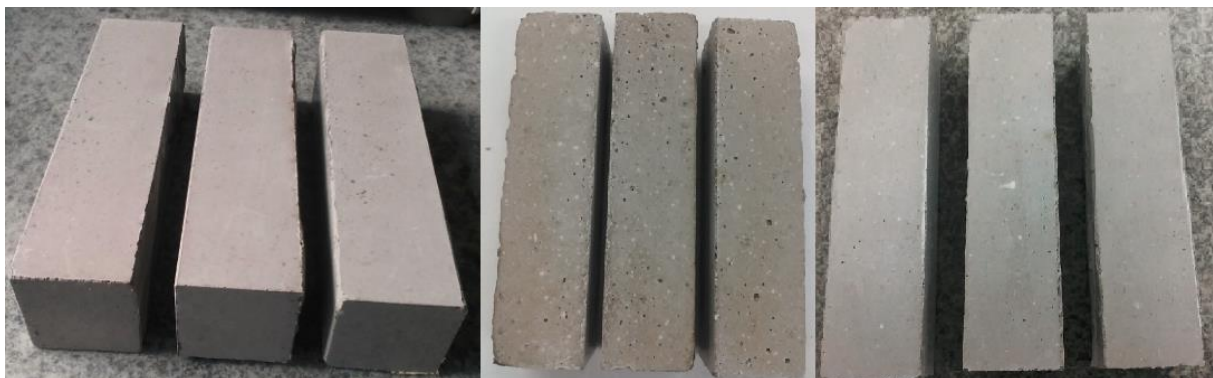


Figure 2: Geopolymer samples just before strength tests

Figure 3 and Figure 4 present respectively the flexural and compressive strength tests' results.

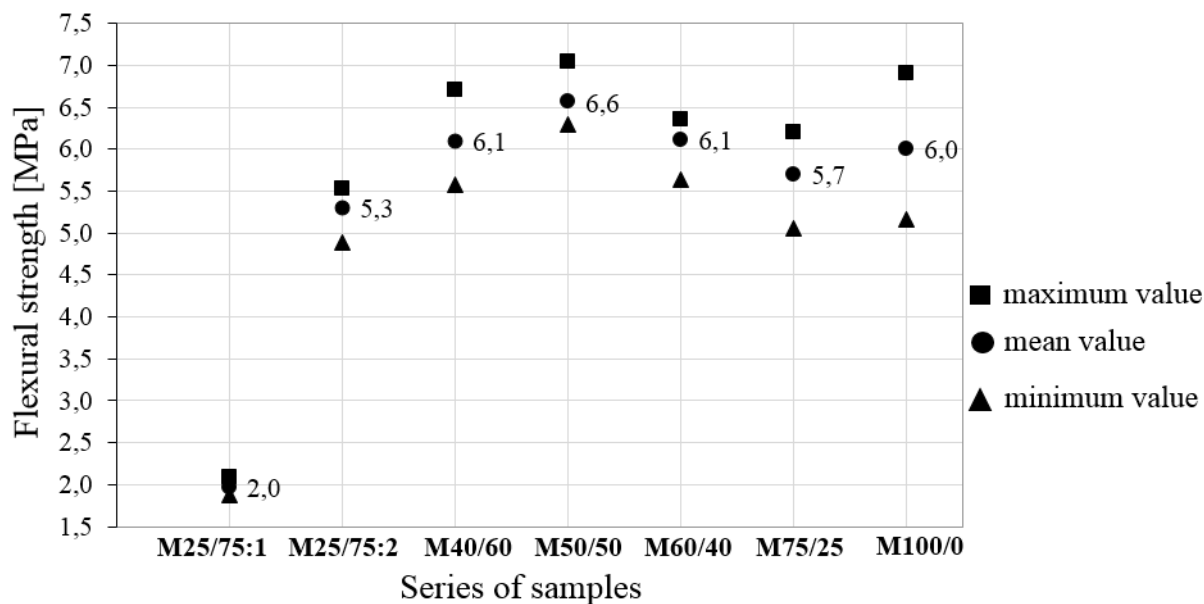


Figure 3: Flexural strength of metakaolin-based geopolymer samples after 7 days

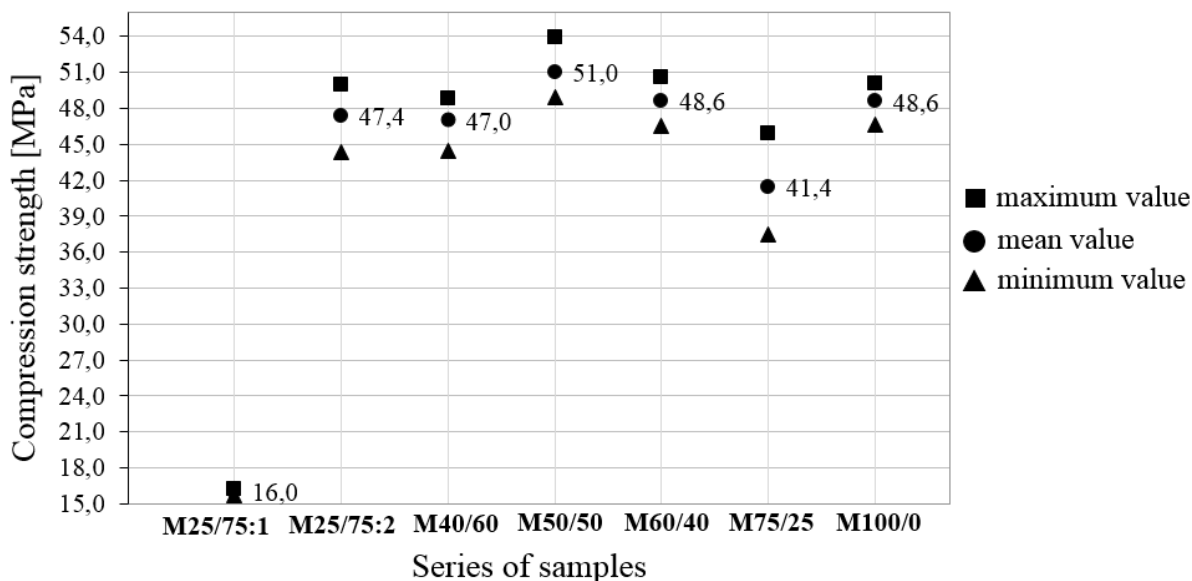


Figure 4: Compressive strength of metakaolin-based geopolymer samples after 7 days

The test did not show any evident dependency between the metakaolin to crushed glass ratio and geopolymer mechanical properties. Only specimens made of mixture M25/75:1 containing the least amount of metakaolin obtained flexural (2,0 MPa) and compressive (16,0 MPa) strength significantly lower than the rest of the samples. The already mentioned overuse of

activators in this mixture (see section 2.1) is the most probable reason of such disparity. Samples made of mixture M25/75:2 (in which metakaolin to glass ratio was the same but the amount of activators was reduced), obtained much better results. It shows that the proper amount of activators can be crucial for the mechanical strength of geopolymer. The rest of the samples obtained similar values of both flexural and compressive strengths. The highest average flexural (6,6 MPa) and compressive (51,0 MPa) strengths were obtained by samples made of mixture M50/50.

The standard deviation of flexural and compressive strength values was the highest for samples made of mixture M75/25 and smallest for ones made of mixture M25/75:1. Among the samples which contained aggregate and obtained good flexural and compressive strength, the mixture with the smallest standard deviation among its specimens was M60/40.

Table 3 presents the average density of samples made of each mixture and the average mass loss during the process of curing in room temperature. Density was established by samples' weighing before the strength tests and dividing the result by the volume of samples. The mass loss was established by comparison the samples' weight after the demoulding process and before the tests. The mass loss applies only to the period when samples were cured in room temperature.

Table 3: Average density and mass loss of geopolymer samples made of each mixture.

Mixture	M25/75:1	M25/75:2	M40/60	M50/50	M60/40	M75/25	M100/0
Density [kg/m ³]	2060	2220	2070	2040	1880	1790	1590
Mass loss [%]	5,6	5,6	4,8	5,8	6,5	7,1	12,5

According to the results, the density of the metakaolin-based geopolymer with crushed glass aggregate increases with the increase of aggregate content. The samples containing 75% had the highest density (2220 kg/m³). The lowest density (1590 kg/m³) was obtained by the samples without aggregate. It was also noticed that samples made of mixture M25/75:2 achieved higher density than samples made of mixture M25/75:1. Oppositely to the density, the mass loss during the curing process decreased with the decrease of aggregate content.

Both during the compressive and flexural strength tests it was noticed that the smaller aggregate content, the more rapid and resounding is the rupture of the sample. During the flexural strength tests, samples containing more metakaolin broke rapidly into two halves with loud reverberation. Samples containing less metakaolin at the end of the test had only a crack in the middle of the length.

3.2 Different NaOH concentrations

The relatively high content of CRT glass, the second largest flexural and compressive strength and small standard deviation of the obtained results were the reasons why mixture M60/40 was chosen for determination of NaOH concentration influence on the mechanical behaviour of metakaolin-based geopolymer. Obtained results were compared with results of M60/40 mixture activated with 10 mol/L NaOH (Figure 5). Samples are signified as M8(60/40), M10(60/40) and M12(60/40) where the first number stands for the NaOH molarity, the second for metakaolin content and the third for glass content.

The test showed that increase of NaOH concentration causes an increase of flexural and compressive strength of metakaolin-based geopolymer. The increase of compressive strength

is linear. The average compressive strength of samples containing 10 mol/L NaOH is 6,7 MPa greater than samples containing 8 mol/L NaOH while the difference between samples activated with 12 mol/L and 10 mol/L NaOH is 6,6 MPa. In case of flexural strength, the difference between samples activated with 8 mol/L NaOH and 10 mol/L NaOH is two times smaller than between samples activated with 10 mol/L and 12 mol/L NaOH. The mixture M10(60/40) has the largest standard deviation in its results in this test. No dependency between NaOH concentration increase and samples density was registered. Samples made of mixtures M8(60/40), M10(60/40) and M12(60/40) had following densities (1920 kg/m³, 1880 kg/m³ and 1950 kg/m³) and mass losses (6,2%, 6,5% and 5,8%).

Similar conclusions can be found in the literature. According to Wang et al. [12] both flexural and compressive strength of metakaolin-based geopolymer increase with the increase of activator molarity although the increase is not linear. The difference in compressive strength between samples activated with 8 mol/L NaOH and 10 mol/L NaOH is over 20 MPa but no further increase in strength for samples containing 12 mol/L NaOH was registered. Wang et al. [12] noticed the increase of samples density with the increase of NaOH molarity. The same dependency connected with density was registered by Steveson [13], who also reported the rapid increase of compressive strength with the increase of NaOH molarity.

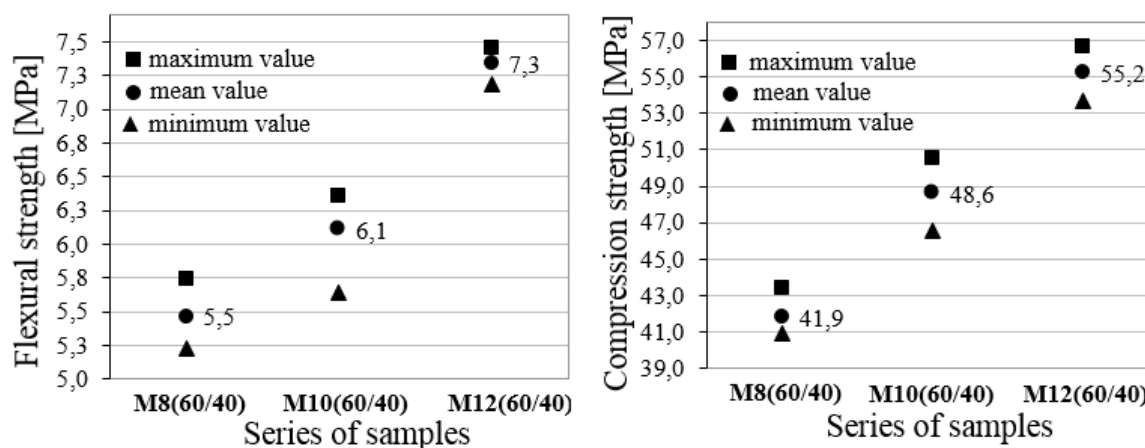


Figure 5: Flexural and compressive strength of metakaolin-based geopolymer samples after 7 days activated with NaOH of different concentrations

The results of mechanical strength obtained during the test are consistent with the results of similar tests presented in the literature. Results concerning the connection between NaOH molarity increase and samples density are divergent. The possible reason of the divergence is the relatively small NaOH to sodium silicate ratio in the mixture. Since the amount of NaOH in the mixture is smaller than in the cited research [12], the influence on samples density can be also smaller.

4. SUMMARY

Research presented in this paper shows that addition of crushed CRT glass in a role of aggregate allows obtaining geopolymer of desirable strength properties. Samples containing addition of crushed glass achieved results as good as, and even better than those made of pure

metakaolin. It means that in the mechanical strength aspect, crushed glass can be considered as a potential aggregate alternative for geopolymer elements. The use of waste in form of CRT glass in metakaolin-based geopolymer elements allows also for savings of the raw material.

No evident influence of metakaolin-crushed glass ratio on the mechanical parameters of the geopolymer was noticed. However, it was shown that the improper (too big) amount of activator can significantly decrease mechanical strength of geopolymer.

The increase of crushed glass content causes the increase of geopolymer density. Simultaneously, the increase of the aggregate content decreases the loss of mass during the curing process. The biggest repeatability of flexural and compressive strength results was achieved by samples containing 25% of metakaolin and the smallest by samples containing 75% of metakaolin.

Tests showed also that both flexural and compressive strength increase with the increase of NaOH concentration. No influence of NaOH concentration on samples density nor on the mass loss during the curing process was registered.

ACKNOWLEDGEMENTS

The paper and works are financed from BKM funds (BKM-547/RB6/2018).

REFERENCES

- [1] Bing-hui, M., Zhu, H., Cui, X. M., He, Y. and Gong, S. Y., "Effect of curing temperature on geopolymerization of metakaolin-based geopolymers", *Appl. Clay. Sci.* **99** (2014), 144-148.
- [2] Provis J. L. and van Deventer J. S. J., "Alkali Activated Materials", State-of-the-Art Report, RILEM TC 224-AAM, (Springer, London, 2014).
- [3] Pecheco-Torgal F., Castro-Gomes J.P. and Jalali S., "Investigations of tungsten mine waste geopolymeric binder: Strength and microstructure", *Constr. Build. Mater.*, **22** (2008), 2212-2219.
- [4] Ekaputri J.J., Junaedi S., Wijaya, "Effect of curing temperature and fiber on metakaolin-based geopolymer", *Procedia Eng.* **171** (2017) 572-583.
- [5] Hardjito, D. and Rangan, B. V., "Development and properties of low-calcium fly ash-based geopolymer concrete", Research Report GC 1 Faculty of Engineering Curtin University of Technology, Perth (2005).
- [6] Sathonsaowaphak A., Chindaprasirt P. and Pimraksa K., "Workability and strength of lignite bottom ash geopolymer mortar", *J. Hazard. Mater.*, **168** (2009) 44-50.
- [7] Top S., Vapur H., "Effect of basaltic pumice aggregate addition on the material properties of fly ash based lightweight geopolymer concrete", *J. Mol. Struct.*, **1163** (2018) 10-17.
- [8] Panizza M., Natali M., Garbin E., Tamburini S., Secco M., "Assessment of geopolymers with Construction and Demolition Waste (CDW) aggregates as a building material", *Constr. Build. Mater.* **181** (2018) 119-133.
- [9] Mrowiec K., Kubica S., Kuczyńska H., "Recykling odpadowego szkła kioskowego", *CHEMIK* **65** (11) (2011), 1212-1217.
- [10] EN 196-1:2016, Method of testing cement – Part 1: Determination of strength, Brussels (2016)
- [11] Paszek N., Górski M. "Influence of sodium hydroxide concentration on mechanical parameters of fly ash-based geopolymer", in the Proceedings of International Conference Synercrete18, Funchal, October, 2018 (RILEM Publications S.A.R.L., Paris, 2018), 461-466.
- [12] Wang, H., Li, H. and Yan, F., "Synthesis and mechanical properties of metakaolinite-based geopolymer", *Colloids. Surf., A Physicochem. Eng. Asp.* **268** (2005), 1-6.
- [13] Steveson, M., "Relationships between composition, structure and strength of inorganic polymers. Part I: Metakaolin-derived inorganic polymers", *J. Mater. Sci.*, **40** (2005), 2023-2036.

DEVELOPMENT OF ALKALI-ACTIVATED MAGNESIUM ALUMINOSILICATE BINDERS FROM SOAPSTONE

Z. Abdollahnejad (1), T. Luukkonen (1), M. Mastali (1), J. Yliniemi J (1), P. Kinnunen (1), M. Illikainen (1)

(1) Fibre and Particle Engineering, Faculty of Technology, Univ. of Oulu, P.O. Box 4300, 90014 Oulu, Finland

Abstract

Soapstone plays an important role in the economy of many countries and it is mainly used for architectural applications, such as counter tops and floor tiles. However, the extraction processing of soapstone stone can generate a large amount of waste powder, which represents disposal problems and environmental damages.

To minimize its negative environmental impacts, it would be useful to develop new technique to reuse these industrial wastes in construction applications and minimise their negative environmental effects.

This paper presents the experimental results regarding the use of soapstone as a precursor for alkali-activated materials. Based on earlier published results, the main component of soapstone, talc ($\text{Mg}_3\text{Si}_4\text{O}_{10}(\text{OH})_2$), is poorly reactive in alkali-activation due to its chemical structure and a lack of amorphous components. Consequently, mechanical properties of these materials are mostly too low to be used in the construction applications. Thus, these materials require co-binder, high temperature curing and high alkalinity to achieve high strength alkali-activated material.

In this study, the blended soapstone/metakaolin binders were activated by using an alkali solution, which consists of sodium hydroxide (10 M) and sodium silicate (molar ratio of $\text{SiO}_2/\text{Na}_2\text{O} = 2.5$). The specimens were cured by using the thermal curing (60°C) during the first 24 hours and then they were exposed to the controlled environmental conditions (23°C and 35% RH).

The results showed that substitution of soapstone by metakaolin up to 20 wt.% results in increased compressive strength to above 30 MPa after 28 days. This strength facilitates the application of the proposed binders for construction applications.

Keywords: Soapstone, metakaolin, alkali activation, thermal treatment, strength development.

1. INTRODUCTION

Talcoses rock is one of the massive world rock reserves containing various minerals mainly around 50% talc with a soft and soapy characteristics. Due to their soft and soapy nature, they mostly called soapstone [1]. The total world production of talc is estimated about 7.8 million tonnes in 2011 [2] and the main producing countries are listed in Table 1.

Table 1: World production of talc (tone/year), (By principal countries) [2]

Country	2009	2010	2011
World total	7500	7400	7800
Argentina	22	25	25
Australia	92	80	99
Austria	111	138	132
Brazil	578	655	650
Canada	44	100	147
China	2300	2000	2200
Egypt	72	35	13
Finland	375	419	429
France	420	420	420
India	876	896	939
Iran	66	95	95
Italy	110	110	110
Japan	24	24	24
Korea. Dem.P.R.of	50	50	50
Mexico	33	10	51
Russia	150	150	150
Spain	47	52	12
USA	511	604	615
Other countries	1618	1546	1639

During natural stone excavations, waste production is inevitable, which resulted in various negative environmental impacts. The global recovery of soapstone is only 40 wt% and approximately 60 wt% of the rock is discharged as residue [3]. One of the effective parameters to minimize this environmental impact is achieving balance between side stream production and reusing it in a same area or in the other purpose [4-8]. Due to an increasing population around the world, the demand for new construction materials has increased and this demand can be employed as one of the side stream reuse areas [9]. Increasing population around the world results in increasing demand for the construction materials, which this increment could increase the CO₂ emission through production of these materials especially ordinary Portland cement. To minimise the CO₂ emission, there is increasing need for alternatives. One of the proposed solutions is alkali-activated binders, which are mainly distinguished for lower CO₂ emissions compared to Portland cement and utilizing side streams in their production [10]. Based on the research performed on the waste rock production in Finnish natural stone queries, this area can be counted as one of the side stream production sources [11]. Recycling and employing side stream materials in the construction area can result in minimising the consumption of natural resources and producing more eco-efficient materials [12]. At the first stage of this study, four metakaolin additions were used to replace soapstone. After casting, the

specimen were cured at 60°C for 24 hours, then, the specimens were demolded and kept at the lab conditions up to the test day. In this study, the final product will be used in fireplaces and exposed to high temperature. Therefore, two different fibres were added to reinforce the mix compositions and to improve the performance of mix compositions under elevated temperature. Also, microstructural analysis was employed to justify the results obtained. Finally, the effects of using metakaolin and fibres on the efflorescence were assessed visually.

2. EXPERIMENTAL PLAN

2.1 Materials and mix design

The designed alkali-activated mortars are composed of waste soapstone powder, fine aggregate (standard sand according to EN 196-1), sodium silicate (molar ratio $\text{SiO}_2/\text{Na}_2\text{O}=2.5$), sodium hydroxide with molarity of 10M, and high purity Metakaolin (99%). The chemical compositions of the soapstone and metakaolin, which were determined by X-ray fluorescence (XRF, PANalyticalAxiosmAX), are presented in Table 2. The main components of soapstone are SiO_2 (39 wt.%) and MgO (38 wt.%). The particle size of the soapstone is smaller than 250 μm . Metakaolin was used as a co-binder with soapstone. Regarding this replacement, the designed mix compositions are listed in Table 3. In the first stage of the study, the impacts of replacing soapstone with metakaolin on compressive and flexural strength was investigated. It will be shown that using metakaolin improves mechanical characteristics. Moreover, the preliminary results depicted that the reduction of sand to binder ratio from 2 to 1 enhanced mechanical properties. Therefore, in the second phase, the mix composition comprised of 20 wt.% metakaolin and a sand to binder ratio 1 polyvinyl alcohol (PVA) and basalt fibres were added to the mix compositions and their impacts on mechanical properties were studied. The used mix compositions and fibre details are presented in Tables 4 and 5, respectively. Fibre contents were constant in this stage and it was equal to 6% of the total mass binder.

Table 2: The chemical compositions of precursors determined by XRF analysis

Element/oxide, (wt.%)	Soapstone	Metakaolin
SiO_2	38.4	53.0
Al_2O_3	1.6	44.5
Fe_2O_3	16.6	0.4
Na_2O	0.1	0.3
K_2O	0.1	0.1
P_2O_5	0.0	0.1
TiO_2	0.1	1.4
MgO	38.0	-
SO_3	0.4	-
CaO	1.7	-
CrO_3	0.60	-
MnO	0.2	-
NiO	0.3	-
LOI (950 °C)	21.3	0.6

LOI*=Loss on ignition

2.2 Specimens synthesis and aging

Dry ingredients (soapstone, metakaolin, and sand) were mixed for 3 min and alkali activator solution (sodium silicate to sodium hydroxide mass ratio of 2.5) were added and mixed with medium mixer speed (mixing paddle at a rate of 140 ± 5 rpm and planetary motion of 65 rpm). All the mix ingredients were mixed for a further 2 minutes to provide homogenous mix and ready for casting. A low mixing speed was used. For the reinforced mix compositions, in the last step, fibres were gradually added. The addition of fibres reduces the workability, therefore, 1% superplasticizer (of the total binder mass) was added to the reinforced beams, which it was added to the mix after adding the activator.

Fresh mortar was cast in prismatic beams with dimension $20 \times 20 \times 80$ mm for executing the first phase and in beams with dimension $40 \times 40 \times 160$ mm for the second phase.

Equal curing regime was considered for all mix compositions (60°C for 24 hours and then kept in the laboratory conditions (24°C and RH 35%) until the test day).

Table 3: Mix proportions of the first phase

Mixture	Soapstone	MK*	Alkali activator/binder	Sand/binder
Mk-0	100	0	0.6	2
Mk-5	95	5		
Mk-10	90	10		
Mk-15	85	15		
Mk-20	80	20		

Mk*=Metakaolin

Table 4: Mix proportions of the second phase (mass, %)

Mix notations	Soapstone	Metakaolin	Activator/binder	Sand/binder	Fibre (% mass of binder)
Mk-20-Plain	80	20	0.6	1	0
Mk-20-PVA					6
Mk-20-Basalt					6

Table 5: Fibre properties

Fibre type	Basalt	PVA
Diameter (μm)	18	14
Cut length (mm)	6	12
Tensile strength (MPa)	4100-4840	1500
Elastic modulus (GPa)	93.1-110	41.7
Density (g/cm^3)	2.63-2.80	1.19-1.31
Elongation (%)	3.100	7

3. TEST PROCEDURE AND SETUPS

3.1 Three-point bending test (TPB)

The beams were tested under three point bending test (TPB) in according to the ASTM C78 recommendation [13]. The flexural load was submitted by a 0.6 mm/min displacement rate and

using 100 kN load cell capacity. The flexural strength obtained under TPB test for each tested specimen.

All the flexural strengths were obtained from the average of two prismatic beams. The half-crushed samples obtained from the flexural test were used for the compressive test based on the ASTM C116-90 recommendation [14].

3.2 Compressive test

The portions of the prismatic beams broken in the flexural test were used to measure the compressive strength based on the ASTM C116-90 recommendation [14]. The Zwick Z100 Roell testing machine with 100 kN capacity and a constant displacement rate of 1.8 mm/min was used to measure the maximum compressive load. The result is the average of four tested specimens from each mix composition.

3.3 Microstructure analysis

To provide chemical composition and micrograph of the selected specimens, scanning electron microscope with energy dispersive spectrometer (SEM-EDS, Zeiss Ultra Plus) was used. Prior to the measurement the small samples from the selected mix compositions were submerged in acetone, to stop any further reaction and then carbon coated. The SEM images in this investigation were obtained by employing backscatter electron detector with 15 KV acceleration voltage and a working distance of 6-8 mm.

4. RESULTS AND DISCUSSION

Figure 1a indicates that replacing soapstone with metakaolin improves the flexural strength up to 4 times compared to the reference mix composition with 100% soapstone. Additionally, metakaolin as co-binder increases compressive strength more than 4 times (reached almost 18 MPa) compared to the reference sample. It can be stated that adding metakaolin can improve the binding properties of the mix composition, which result in improvement of the strengths even at early age. Replacing soapstone by metakaolin results in decreasing the amorphous content and the main strength of the mix composition with 100% soapstone came from formation of magnetite. Moreover, thermal curing also played an important role in improving the compressive strength of the soapstone mix compositions, while the preliminary results revealed that the ambient curing resulted in slow hydration reactions and the mix composition was even fresh after 24 hours. In addition, low compressive strength was obtained.

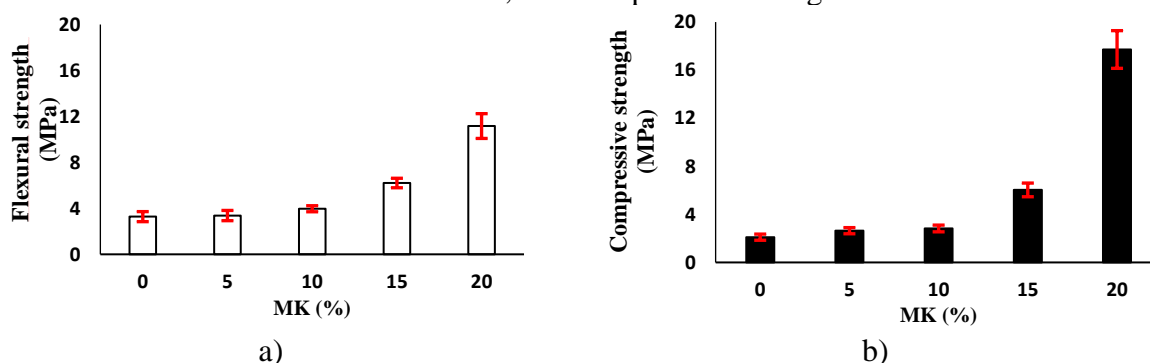


Figure 1: Results for 7 days: a) Flexural strength; b) Compressive strength

To improve the flexural strength, the best performance of the plain mix compositions in terms of mechanical properties from the previous step was selected and reinforced with basalt fibre with 6 mm length or PVA fibre with length of 12 mm.

PVA fibre showed the greatest improvement on the flexural strength compared to the plain mix composition and basalt fibre. As shown in Figure 2a the minimum and the maximum flexural strengths were recorded around 8 MPa and 10 MPa for the plain specimens and specimens reinforced with PVA fibre, respectively. This improvement was caused by forming hard bond between PVA fibres and their embedded matrix. Figure 2b represents the effects of adding two types of fibres on the compressive strength. The obtained results showed that the addition of fibres decreased the compressive strength compared to the plain mix composition, regardless of the fibre type, which can be explained due increasing porosity that can reduce the compressive strength. The minimum compressive strength was recorded around 22 MPa and the maximum around 28 MPa in the reinforced mix composition with basalt fibre and plain mix composition, respectively.

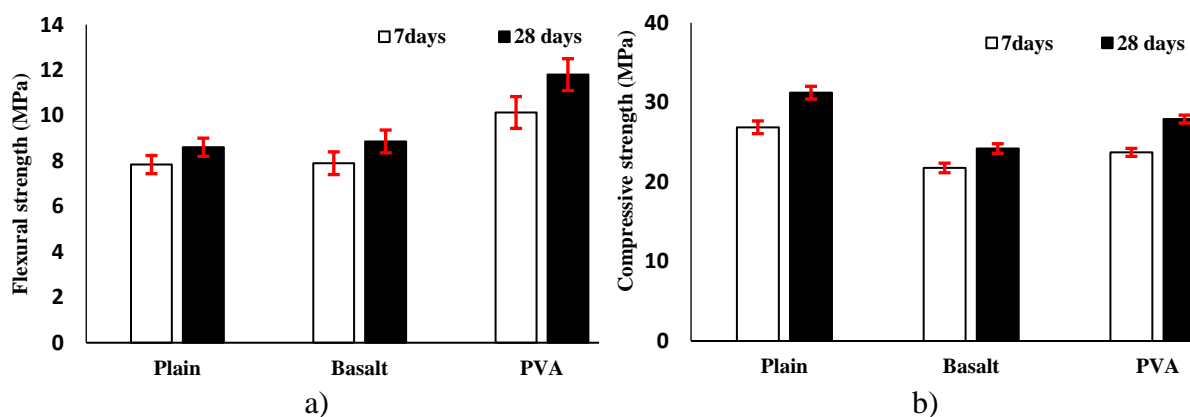


Figure 2: a) Flexural strength; b) Compressive strength

Figure 3 depicts the differences caused on the morphology of the mix compositions, through replacement of soapstone by 20 wt.% metakaolin. The SEM images show that addition of metakaolin result in formation of uniform chemical products, which justify the enhancement of the mechanical characterizations of the mix composition containing 20% metakaolin (Figure 3b).

Efflorescence is often observed in alkali activated materials originated by the fact that alkaline or soluble silicates that are added during processing cannot be totally consumed during geopolymerisation [15]. Efflorescence is caused by migration of alkali or earth alkali ions from pore solution to the sample surface and reacting with atmospheric CO₂. Therefore, this phenomenon was also evaluated for the developed material and the effects of replacing metakaolin and fibres were studied visually. This assessment in Figure 4 showed that replacement of soapstone with metakaolin and employing fibre were effective solutions in controlling the efflorescence.

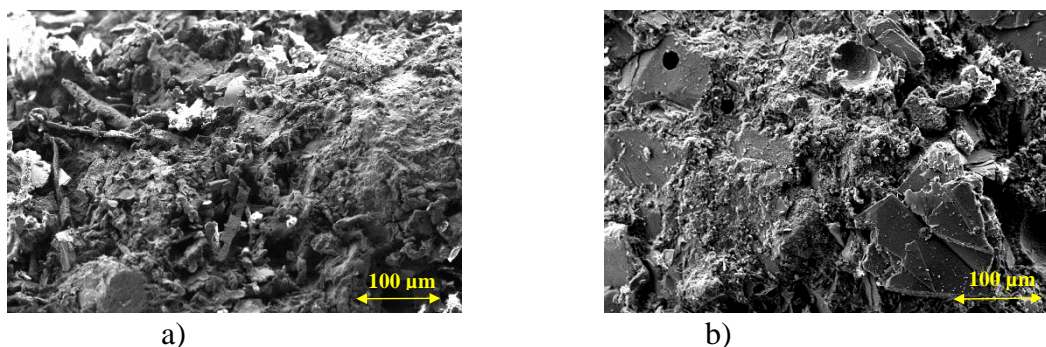


Figure 3: SEM image: a) 100% soapstone; b) 80% soapstone and 20% metakaolin



Figure 4: Visual monitoring of the designed mix compositions

5. CONCLUSIONS

This paper reports an experimental investigation on the feasibility of using soapstone in alkali activation process. To obtain this aim, metakaolin was used as replacement of soapstone. Then, two different fibres were added to reinforce. Regarding the results, following remarks could be highlighted:

- Replacing soapstone by 20% (in weight) metakaolin improved both compressive and flexural strengths up to 4 times compared to the reference mix composition (100% soapstone).
- Using thermal curing conditions (60°C) significantly enhanced hardened state properties.
- Reinforcing the mix compositions through PVA fibre improved the flexural strength around 80% at 7 days and about 70% at 28 days. On the contrary, the addition of basalt fibres reduced the compressive strength by 10% and 12% at 7 and 28 days, respectively, when compared to the plain mix composition. Moreover, no improvement in terms of flexural strength was registered for the mix compositions reinforced with basalt fibres.
- The morphology of mix compositions showed that using metakaolin resulted in forming denser matrix. This justifies the enhancement of the mechanical characterizations.
- The visual monitoring confirmed that the combination of metakaolin as a co-binder and fibre could successfully mitigate the efflorescence.

ACKNOWLEDGEMENTS

This work was supported by the Finnish Funding Agency for Technology and Innovation (Tekes) [grant number 1105/31/2016] (project GEOBIZ).

REFERENCES

- [1] Indian Minerals Yearbook, Part III :Mineral Reviews 51st Edition Talc, Soapstone and steatite, Government of India ministry of mines Indian bureau of mines, Indira Bhavan, Civil Lines, (2012) NAGPUR-440001.
- [2] World Mineral Production, (2007-2011), 'Including talc, agalmatolite and pyrophyllite'.
- [3] Rodrigues, M. L. M. and Lima, R. M. F., 'Cleaner production of soapstone in the Ouro Preto region of Brazil: a case study', *J.Clean.Prod.* **32** (2012) 149–156.
- [4] Ferreira, W.L. Reis, E.L. R.M. and Lima, F., 'Incorporation of residue from the minero- metallurgical industry in the production of clay-lime brick', *J.Clean.Prod.* **87** (2015) 505–510.
- [5] Acchar, W., Vieira, F.A., and Segadães, A.M., 'Using ornamental stone cutting rejects as raw materials for red clay ceramic products: properties and microstructure development', *Mater. Sci. Eng.* **435** (2006) 606–610.
- [6] Gencel, O., Sutcu, M., Erdogmus, E., Koc, V., Cay, V.V., and Gok, M.S., 'Properties of bricks with waste ferro chromium slag and zeolite', *J. Clean. Prod.* **59** (2013) 111–119.
- [7] Gencel, O., Ozel, C., Koksal, F., Erdogmus, E., Martínez-barrera, G., Brostow, W., 'Properties of concrete paving blocks made with waste marble ', *J. Clean. Prod.* **21** (2012) 62–70.
- [8] Silva, F.L., Araújo, F.J.S., Teixeira, M.P., Gomes, R.C., VonKrüger, F.L., 'Study of the recovery and recycling of tailings from the concentration of iron ore for the production of ceramic', *Ceram. Int.* **40** (2014) 16085–16089.
- [9] UN Energy for a sustainable future The Secretary-General's Advisory Group on energy and climate change, New York (2010).
- [10] Gartner, E., and Hirao, H., 'A review of alternative approaches to the reduction of CO₂ emissions associated with the manufacture of the binder phase in concrete', *Cem. Concr. Res.* **78** (2015) 126–142.
- [11] Website: <https://www.suomalainenkivi.fi/en/finnish-natural-stone-association/natural-stone-industry-finland/natural-stone-quarries-in-finland/>, Access date: 19.10.2018.
- [12] Abdollahnejad, Z., Hlavacek, P., Miraldo, S., Pacheco-Torgal, F., and Aguiar, J.B., 'Compressive strength, microstructure and hydration products of hybrid alkaline cements', *Mat. Res.* **16** (2014) No 4.
- [13] ASTM C78. (2016). Standard Test Method for Flexural Strength of Concrete (Using Simple Beam with Third-Point Loading), ASTM International, West Conshohocken, PA, USA.
- [14] ASTM C349-14. (2014). Standard Test Method for Compressive Strength of Hydraulic-Cement Mortars (Using Portions of Prisms Broken in Flexure), ASTM International, West Conshohocken, PA, USA.
- [15] Abdollahnejad, Z., Pacheco Torgal, F., Aguir, J.B., and Jesus, C., 'Performance of fly ash based one/part mortars in durability tests', (2014), Guimaraes, Portugal.

PRODUCTION OF ALKALI-ACTIVATED BINDERS FROM IRON SILICATE FINES

John L. Provis (1), Angel L. Muñoz Gomez (1), Oday H. Hussein (1), Gaone Koma (1), Emanuela Manolova (2), Vladislav Petrov (2)

(1) Department of Materials Science & Engineering, University of Sheffield, Sheffield S1 3JD, United Kingdom

(2) Aurubis Bulgaria AD, BG-2070 Pirdop, Bulgaria

Abstract

The refinement of copper from its ores results in the generation of a large quantity of an iron silicate by-product, which holds potential value as a precursor for the production of alkali-activated cementitious binders. This paper reports the results of the analysis and optimisation of the chemical processes by which this can be achieved, with assessment of the leaching characteristics of the particulate precursor, the design and development of cementing systems of useable strength based on this precursor, and the microstructural characteristics of the products of this reaction process. Hybrid alkali-Portland activation of the iron silicate fines is demonstrated to give cementitious binders with desirable strength development characteristics, offering the opportunity for valorisation of this by-product into a useful material.

Keywords: Iron silicate fines, alkali activation, waste valorisation, hybrid cements

1. INTRODUCTION

In the extraction of copper from its ores, the slags from the flash furnace and the converters contain residual copper which is extracted through grinding and flotation. Two products are obtained at the slag flotation plant: flotation copper concentrate and flotation product called iron-silicate fines. This is a powdery material with a high content of iron and silicon dioxide in the form of minerals, mainly fayalite, magnetite, and quartz. Some of the iron-silicate fines are used in the cement industry as a ferrous additive for clinker manufacture. They can also be used in other areas of construction and as an initial raw material in iron production.

The aim of this study is to use these iron silicate fines as a raw material for obtaining alkali-activated or related cementitious binders [1], using different alkali-activators, and other additional solid precursors as needed to obtain a commercially valuable product.

2. MATERIALS AND METHODS

The materials used in this study are the iron silicate fines (abbreviated ISF) supplied by Aurubis, which is used as the main precursor in development of cementitious binders, along with steel slag (SS), blast furnace slag (BFS), and Portland cement (PC), grade CEM I 52.5N according to EN 197-1. Chemical and mineralogical characterisation of these powders is shown in Table 1 and Figure 1.

Table 1: Chemical composition of slags and Portland cement determined by X-ray fluorescence, reported on an oxide basis. L.O.I: loss on ignition at 1000°C.

wt. %	CaO	SiO ₂	Al ₂ O ₃	MgO	SO ₃	Fe ₂ O ₃	MnO	K ₂ O	Na ₂ O	Others	LOI
BFS	41.8	36.0	11.3	6.5	0.7	0.3	0.3	0.4	0.1	0.7	2.0
SS	56.9	17.4	9.9	4.9	2.0	1.5	0.1	2.8	0.3	0.5	3.6
ISF	2.7	27.5	3.5	0.7	0.7	66.5	<0.1	0.9	0.4	2.0	-4.9 ^a
PC	64.7	19.5	4.9	1.1	3.3	3.2	<0.1	0.6	0.1	0.6	2.1

^a Mass gain probably due to oxidation of FeO [2]

From the XRF analysis, the iron silicate fines mainly consist of iron oxides, represented here as Fe₂O₃ (more than 60 wt. %) but most likely also with some Fe(II) minerals as observed by the negative LOI value which indicates gain upon a mass ignition, and SiO₂ (26 wt.%). There is a very low content of CaO and Al₂O₃. Dissolution testing in 5 mol/L NaOH at 20°C and a solid/liquid ratio of 1:20 showed the release of 592 mg/L Si, 110 mg/L Al, and 18 mg/L Fe from the iron silicate fines after 14 days.

The steel slag and blast furnace slag contain significant amounts of CaO, and this is higher in the case of steel slag, with a correspondingly lower silica content.

The X-ray diffraction (XRD, Bruker D2 Phaser) patterns of the precursors were obtained using Cu-K α radiation under conditions of 40 kV and 20 mA, in the range $2\theta = 5-60^\circ$. Figure 1 shows that BFS is fully amorphous. The iron silicate fines show a structure containing fayalite, magnetite, and augite, but also most likely with a significant X-ray amorphous (glassy) component. Steel slag contains lime olivine, lime, tricalcium silicate (which may indicate some Portland cement contamination, as this is not a usual slag constituent), mayenite, calcium ferrite, and magnesium aluminate spinel, again with a probably amorphous constituent. Portland cement is composed of alite, belite, tricalcium aluminate, tetracalcium aluminoferrite, and a minor amount of periclase. The sulfate constituents of the Portland cement were not evident in this mineralogical analysis, but likely contain gypsum and/or its partially dehydrated forms added during cement grinding, as well as some minor mixed calcium-alkali sulfate salts formed in the clinkerisation process.

Compressive strength testing was carried out using samples of various geometries and sizes, as described in the Results and Discussion section below. All samples were cured under sealed conditions, in polymeric or steel moulds, and demoulded directly before testing.

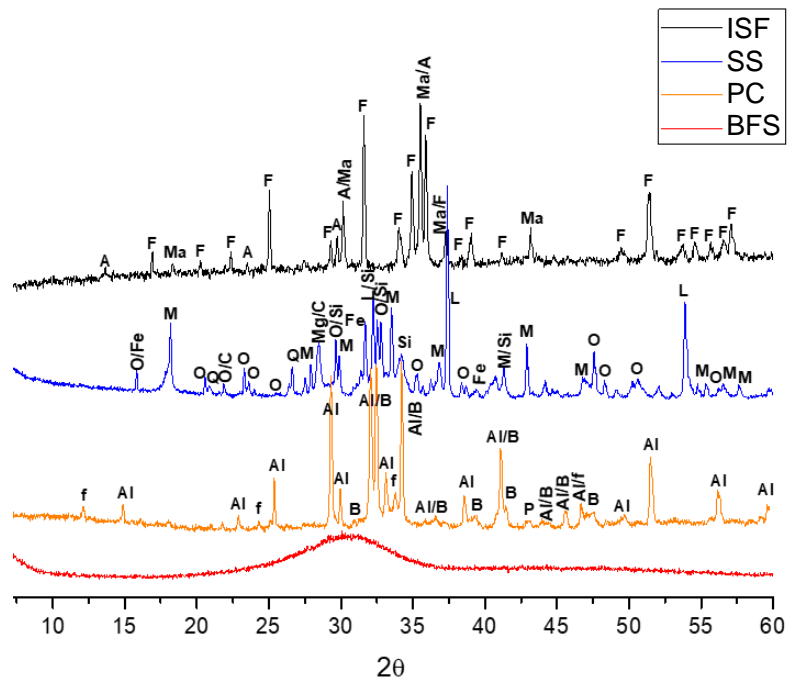


Figure 1: XRD analysis of iron silicate fines (ISF), steel slag (SS), Portland cement (PC), and blast furnace slag (BFS). Mineral phases identified are:

Iron silicate fines: **A**: Augite ($\text{Ca}(\text{Fe}, \text{Mg})\text{Si}_2\text{O}_6$; PDF #24-0201). **F**: Fayalite ($(\text{Fe}_{0.94}\text{Mg}_{0.06})_2\text{SiO}_4$; PDF #07-0164). **Ma**: Magnetite (Fe_3O_4 ; PDF #01-1111).

Steel slag: **O**: Lime olivine (γ -dicalcium silicate, Ca_2SiO_4 ; PDF #80-0941). **Q**: Quartz (SiO_2 ; PDF #33-1161). **L**: Lime (CaO ; PDF #37-1497). **Si**: Tricalcium silicate (Ca_3SiO_5 ; PDF #42-0551). **M**: Mayenite ($\text{Ca}_{12}\text{Al}_{14}\text{O}_{33}$; PDF #09-0413), **Fe**: Calcium ferrite ($\text{Ca}_4\text{Fe}_9\text{O}_{17}$; PDF #17-0105). **Mg**: Magnesium aluminate spinel (MgAl_2O_4 ; PDF #33-0853). **C**: Cristobalite (SiO_2 ; PDF #03-0272).

Portland cement: **Al**: Alite (impure tricalcium silicate, Ca_3SiO_5 ; PDF #73-0599), **B**: Belite (β -dicalcium silicate, Ca_2SiO_4 ; PDF #01-1012), **AL**: Tricalcium aluminate ($\text{Ca}_3\text{Al}_2\text{O}_6$; PDF #01-1051), **f**: Tetracalcium aluminoferrite ($4\text{CaO} \cdot \text{Fe}_2\text{O}_3 \cdot \text{Al}_2\text{O}_3$; PDF #74-0803), **P**: Periclase (MgO ; PDF #87-0653).

3. RESULTS AND DISCUSSION

Different alkaline activators were used in initial tests to activate iron silicate fines: a commercial sodium silicate solution (PQ Grade D, Na_2O : 14.7%, SiO_2 : 29.4% by mass), and a mixture of this sodium silicate solution with NaOH pellets to achieve a silicate modulus (M_s = molar ratio $\text{SiO}_2/\text{Na}_2\text{O}$) of 1.0. These were trialled at different dosages: 5, 10, 15, and 38.6 wt.% by mass of iron silicate fines, but they did not work effectively; the samples (prepared by filling centrifuge tubes and holding at room temperature) did not set after 15 hours, when the iron silicate fines were used as the sole solid precursor. Research published by Onisei et al. [3], as part of their extensive research programme on fayalitic slags (industrial and lab-synthesised) showed that fayalite slag activated with sodium silicate solution did not exhibit any peaks of heat release when monitored by isothermal calorimetry, even after 142 hours, suggesting low

reactivity. Those workers also tested the addition of BFS as a supplemental source of CaO, SiO₂, and Al₂O₃ at 5 wt.%, but the result was the same.

So, potassium silicate solution (K₂O: 21.8%, SiO₂: 47.11%) was tested as activator solution. The activation of iron slag pastes did not work; the samples did not set. When blast furnace slag was included at 5 and 10 wt.% at a dose of 50.0 wt.% activator, the samples set within 2 hours. However, this activator dose is very high, which would make the materials unreasonably expensive. So, a lower activator dose was tested, 38.6 wt.%, and both mixes with 5 and 10 wt.% blast furnace slag were able to set within 2 hours.

Compressive strength tests were carried out for these pastes at 7 days (cured at room temperature and at 35°C), and 28 days; the results are shown in Table 2. The temperature effect was also studied in several samples, to determine if thermal curing is able to improve the mechanical properties of this material.

Table 2: Compressive strength at 7 and 28 days (50 mm paste cubes) under room temperature (RT) and elevated temperature (35°C) curing conditions

Sample ID	Compressive strength (MPa) 7 days		Compressive strength (MPa) 28 days
	RT	35°C	RT
T6 (10 wt.% BFS, 38.6 wt.% activator)	14.0	21.5	41.0
T7 (5 wt.% BFS, 38.6 wt.% activator)	6.64		15.0

Steel slag was introduced, to study its use as an alternative to blast furnace slag. The following formulations were tested, preparing small cylinders (28 x 25 mm), due to limitations in materials availability for testing. In parallel testing with CEM I PC specimens using the same loading frame, cylinders of this size were found to give compressive strength readings up to 25% higher than standard 50 mm cubes at 7 days, so this should be taken as an approximate correction factor to interpret the data for these very small samples.

Samples with 10 wt.% blast furnace slag showed much higher values of compressive strength than those prepared with steel slag at the same replacement level; the samples hardened/stiffened more or less within the same time, but the appearance was notably different. With blast furnace slag, they look harder and are stronger; they had a more polished finish. Conversely, with steel slag, they hardened/stiffened, but the surface was easily scratched. When the activator solution dose was decreased to 20 wt.%, with steel slag there was no great difference between 5, 10, and 30 wt.% slag content in terms of the compressive strength values obtained, these were all low. Higher-temperature curing increased these values.

Comparing the samples with 10 wt.% blast furnace slag and 10 wt.% steel slag: compressive strength values of only about 2.0 MPa were obtained with steel slag but setting happened in an acceptable time, while the paste with blast furnace slag took long time to set, ~20hours, and an upper liquid phase (bleed liquid) was observed. However, when it was set, it was stronger than the steel slag one. Compressive strength at 7d was 12.55 MPa at room temperature, and 27.6 MPa at 35°C, for the sample with 10 wt.% BFS.

It seems that the best performance is obtained with blast furnace slag, and at the highest activator dose (38.6 wt. %).

It was also considered to study some samples adding Portland cement, because due to its high alkalinity and reactivity, it could contribute to the reaction process, and a better performance could potentially be obtained. So, Portland cement, CEM I 52.5N, was included at 5 wt.%. Samples with this Portland cement along with 10 wt.% steel slag were also prepared too.

Cubes of 20 mm in size were prepared for testing for compressive strength at 7 and 28 days (3 cubes per each age), because the cylinders were prepared cutting them from centrifuge tubes, and it was difficult to get a flat and parallel surface, whereas with cubes, no such preparation was needed, and more accurate compressive strength values would be obtained. Several other samples (from Table 3) were repeated for preparation of cubes of them, to enable direct comparison of compressive strengths for the same sample size and geometry. Iron silicate fines, with Portland cement and/or slag powders, were mixed for 3 minutes. Then, the activator solution was added and mixed by hand for 2 minutes. After that, 6 moulds were filled, and manually compacted on the preparation table (15 times, x2).

Sample hardening times were not very different between the full set containing Portland cement, falling between 2.5-4 h, and the workability was also comparable between them. They were tested for compressive strength after 7 and 28 days, at room temperature.

Taking into account the compressive strength values obtained, it could be said that the samples with Portland cement and steel slag, activated with potassium silicate (ICK) presented higher compressive strength values than that with only cement added (see Table 3). These showed higher compressive strength values than those with the 50:50 blended activator (potassium and sodium silicate), although the overall molar dose of the activator component was higher in the blended systems due to the lower molar mass of Na than K.

Table 3: Summary of the main formulations tested, with and without Portland cement

Sample ID	Iron silicate fines (g)	Blast furnace slag (g)	Steel slag (g)	CEM I 52.5N (g)	Activator (g)		Compr. strength (MPa) 7d	Compr. strength (MPa) 28d
					KSil	NaSil		
T6	90	10		0	38.6	0	19.9	39.3
ES4	90	10		0	19.3	19.3	14.5	29.2
T9	90		10	0	38.6	0	7.8	16.7
ES5	90		10	0	19.3	19.3	6.0	12.5
ICK	95	0		5	38.6	0	8.5	18.4
ICM	95	0		5	19.3	19.3	6.9	15.1
ICKSK	85	0	10	5	38.6	0	13.9	30.5
ICSM	85		10	5	19.3	19.3	9.7	18.9

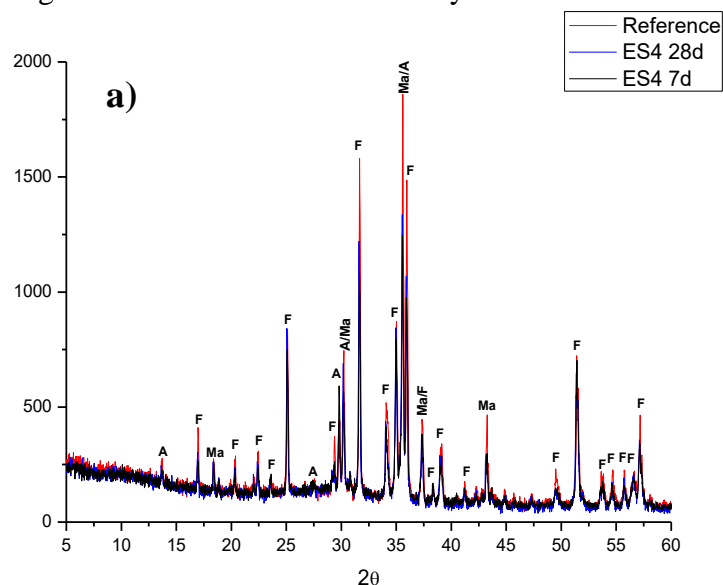
Incorporation of Portland cement in a small proportion in addition to steel slag showed a great improvement in the mechanical strength development, when potassium silicate was used as activator. In light of this result, an increase of the content of cement (from 5 to 10 wt.%) was tested. However, the sample was not workable, and extra water was needed. When the w/b ratio was increased (to 0.22, 0.26, 0.32, and 0.45), the samples showed a very slight increase in the hardening time, but in all cases they hardened very quickly, and it was not possible to produce uniform samples in moulds. This line of development was not further pursued.

5. ANALYSIS OF HARDENED PRODUCTS BY X-RAY DIFFRACTION

XRD analysis was carried out to study the mineralogy of the alkali-activated binders at 7 and 28 days. No new crystalline phases were observed in the alkali-activated pastes in comparison to the anhydrous starting materials at 7 or 28 days. All the peaks correspond with the phases presented by the anhydrous precursor powders. However, all the samples presented a small halo between 25 and 35°, at 7 and 28 days, indicating the presence of a disordered gel reaction product, and this was identified as the strength-giving phase in the solid binders.

Since the XRD patterns of all the alkaline activated pastes studied were very similar, it was decided to compare them with their respective reference precursor powder blends, mixing the raw materials in the same proportions used to formulate the pastes, but without activation. This was intended to enable identification of any reaction taking place involving crystalline phases in the precursor powders. The data are then plotted directly overlaid, with no offset, to enable visualisation of which peaks have altered in intensity due to the chemical reaction process taking place during binder formation and strength development. An example of this type of analysis is shown in Figure 2.

The samples at 7 and 28 days for T6 (Figure 2b) and ES4 (Figure 2a) mixes showed the same peaks as were observed for the original iron silicate fines (ISF), since the blast furnace slag used as a secondary blend component is fully amorphous (Figure 1). However, important peaks present in the X-ray diffractograms of the samples have lower intensity than in the original powder blends, indicating that the phases associated to these peaks (fayalite, magnetite and augite) could take part in the reaction process. In a study by Lemougna et al. [4], the formation of a geopolymer product with ferric iron in the tetrahedral network was observed via reaction of augite, consistent with the observations here. No further intensity decrease of these peaks is evident when the curing time increases from 7 to 28 days.



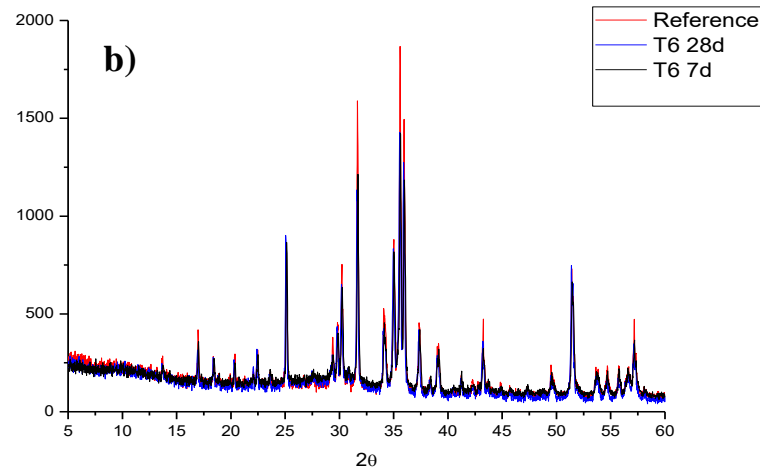


Figure 2: XRD analysis of samples ES4 (a), and T6 (b) at 7 and 28 days, compared to their respective reference powder blends.

From the XRD data in Figure 3, the peaks observed in ICK are those associated with anhydrous iron silicate fines, whose intensities are once again lower than those of the reference powder blend. The small peaks at 25.58° , 32.25° , and 32.69° associated to alite (A1) and belite (B) present in the original Portland cement are either not observed, or decrease significantly from 7 to 28 days, suggesting that these phases have reacted, taking part in the hydration and/or alkali activation reaction process.

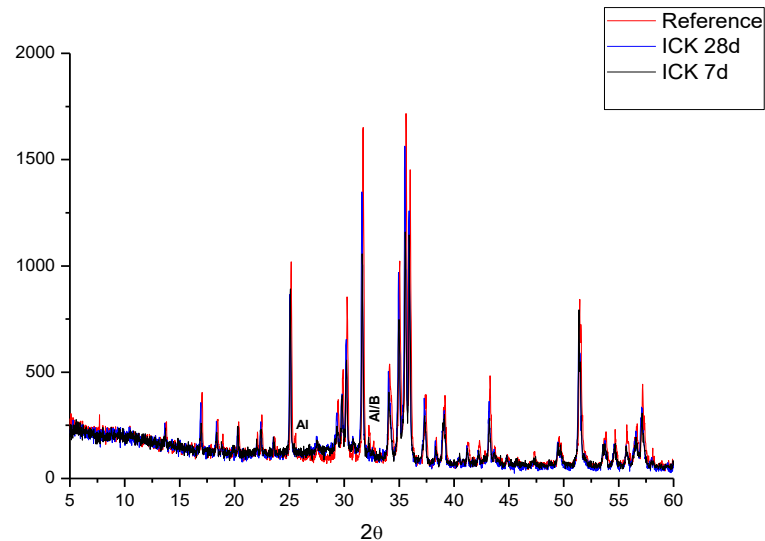


Figure 3: XRD analysis of ICK at 7 and 28 days, compared to the reference powder blend.

In Figure 4, a peak is observed at 37.37° 2θ due to lime (L), overlapping in part the magnetite (Ma) and fayalite (F) from the iron silicate fines. Peaks at 25.58° , 32.25° , and 32.69° associated to alite and belite in Portland cement are also observed. These four peaks decrease in intensity when the paste is activated, confirming their participation in the reaction process. In addition, the peaks associated with the crystalline phases in the iron silicate fines decrease in intensity.

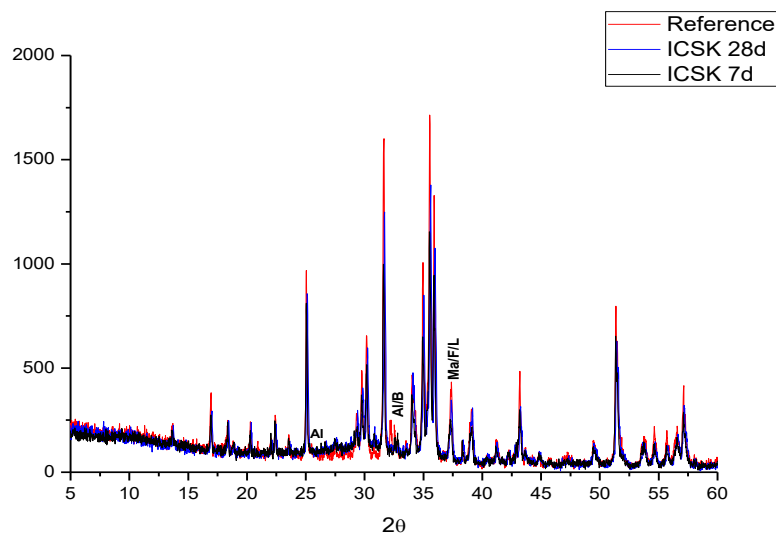


Figure 4: XRD analysis of ICSK at 7 and 28 days, compared to the reference powder blend.

4. CONCLUSIONS

Production of alkali-activated binders from iron silicate fines has been demonstrated through activation with potassium silicate. The fayalite phase within the iron silicate fines is reactive during alkali activation, and the addition of a small quantity of either Portland cement, ground granulated blast furnace slag, or steel slag, brings advantages in strength development. The alkali-activator doses used in this study were rather high and need to be reduced for a more practical and cost-effective binder system, but this work has demonstrated a proof of concept for this process.

ACKNOWLEDGEMENTS

This study has been funded by Aurubis Bulgaria AD.

REFERENCES

- [1]. Bernal, S.A., Rodríguez, E.D., Kirchheim, A.P. and Provis, J.L.: 'Management and valorisation of wastes through use in producing alkali-activated cement materials', *J. Chem. Technol. Biotechnol.* **91** (9) (2016) 2365-2388.
- [2]. Gorai, B. and Jana, R.: 'Characteristics and utilisation of copper slag—a review', *Resourc. Conserv. Recyc.* **39** (4) (2003) 299-313.
- [3]. Onisei, S., Lesage, K., Blanpain, B. and Pontikes, Y.: 'Early age microstructural transformations of an inorganic polymer made of fayalite slag', *J. Am. Ceram. Soc.* **98** (7) (2015) 2269-2277.
- [4]. Lemougna, P.N., MacKenzie, K.J.D., Jameson, G.N.L., Rahier, H. and Chinje Melo, U.F.: 'The role of iron in the formation of inorganic polymers (geopolymers) from volcanic ash: a ⁵⁷Fe Mössbauer spectroscopy study', *J. Mater. Sci.* **48** (15) (2013) 5280-5286.

MIXTURE PROPORTIONING FOR ALKALI-ACTIVATED SLAG-BASED CONCRETE

Ning Li (1), Caijun Shi (1)*, Zuhua Zhang (1, 2)*, Deju Zhu (1)

(1) Key Laboratory for Green & Advanced Civil Engineering Materials and Application Technology of Hunan Province, College of Civil Engineering, Hunan University, Changsha, 410082, China, cshi@hnu.edu.cn

(2) Centre for Future Materials, University of Southern Queensland, Toowoomba, QLD 4350, Australia

Abstract

This paper reports a general mix design procedure for alkali-activated slag concrete, which is an essential step towards industrial application of this new type of materials. The procedure includes 1) determination of coarse and fine aggregate ratio according to close packing model, as determined by measuring mixed bulk density; 2) determination of liquid phase (water content and activator) based on compressive strength; 3) determination of excess paste content by workability measurement. Effects of mix proportional factors, including activator composition, water content, fly ash content, and binder/aggregate ratio are examined on consistency, setting time and compressive strength. The relationship between performance and precursor composition is established using simplex centroid design method, by which a range of alkali-activated concretes with compressive strength grades of C40, C60, and C80 are successfully prepared with initial setting time of 1 to 3 h and slump of more than 200 mm.

Keywords: alkali-activated concrete, proportional design, simplex centroid design method, slump, setting time, compressive strength

ALKALI ACTIVATION OF HIGH MGO BFS WITH SODIUM CARBONATE ADDED DRY VS. WET

Abeer M. Humad^{1,2}, John L. Provis³, Andrzej Cwirzen¹

1Structural Engineering Division, Luleå University of Technology, Luleå, Sweden.

2Civil Engineering Department, University of Babylon, Iraq.

3Department of Materials Science and Engineering, University of Sheffield, Sheffield, UK.

Abstract

The use of sodium carbonate to alkali activate blast furnace slag has several advantages over the typically used sodium silicate, including for example easier, safer handling and less negative environmental impacts. In this study, sodium carbonate (SC)-activated blast furnace slag (BFS) pastes and concretes were produced using a high MgO content BFS activated with 3, 5, 10 and 14 wt.% (by binder) of SC. The activator was added either as a dry powder or dissolved in water one hour before mixing. The setting time, workability and compressive strength after 1,7 and 28 days were determined. Concrete cubes were cured in two setups: sealed specimens at 65 °C for 24 hours followed by storage at laboratory conditions (20±2°C), or simply sealed storage at laboratory conditions (20±2°C and 50-55% RH), until testing. The results showed that, increasing the dosage of SC decreases the initial and the final setting time regardless of whether the mixing procedure was dry or wet. However, addition of the SC dissolved in water increased the slump at higher SC dosage, while increasing addition of the dry SC resulted in a lower slump. A higher dose of SC increased the 28d compressive strength when added as a dry powder or wet, with higher values in laboratory curing compared with heat curing.

Keywords: Alkali Activated Slag, Blast Furnace Slag, Alkali activation, Sodium carbonate.

1. INTRODUCTION

The contribution of Portland cement manufacture to greenhouse gas emission is estimated to be at least 6% of total anthropogenic greenhouse gas emissions¹. Alkali activated slag is indicated as an environmentally friendly alternative to Portland cement, having lower CO₂ emissions and energy cost, particularly when near-neutral salt activator are used as these can be generated with very low carbon footprints. However, sodium carbonate (SC), which was used in the present research, is less effective as an alkali activator in comparison with, for example, sodium silicate (SS). Consequently, some SC-activated mixes have a longer initial

setting time which can span even from 2 to 5 days²⁻⁶. The rate of reaction of sodium carbonate activated slag is also influenced by factors including the fineness and the chemical composition of the slag, curing temperature, W/B ratio and SC dosage⁶⁻⁹ and might be accelerated to a certain extent by several means, for example higher alkali dosage, addition of additional activators such as sodium hydroxide or SS or the use of reactive admixtures such as lime or active MgO^{4,10-13}. It has been reported that SC-activated slag required around 100-130 h to reach the reaction peak with variable dosages of SC, when using a slag with moderate MgO content. The initial formation or precipitation of CaCO₃ was indicated as the main reason^{7,8}. Increasing the SC content and lowering the water to binder ratio shortened the time required to reach the reaction peak to 48h or less^{9,12}, but this is still unacceptably slow for partial concreting. The pH of the activator solution is playing a significant role in the initial dissolution and reaction of the precursor followed by the precipitation of the C-S-H gel. The minimum required pH value was higher than 9.5¹⁴. In spite of the lower initial pH of the SC, it exhibited better activation results than the NaOH in terms of mechanical properties and durability⁶, which is linked to the reaction kinetics of the SC-activated slag. The dissolution of slag releases Ca²⁺, which react with CO₃²⁻ from the SC activator to form calcite and gaylussite Na₂Ca(CO₃)₂·5H₂O. This occurs earlier than the precipitation of the C-(A)-S-H gel, consuming the Ca²⁺ released by the slag at an initial pH below 12. As a result, the dissolution of silicate species is slow. After consuming CO₃²⁻ ions, the pH will rise to approximately 13.5 at the later stage of the reaction^{6,8}.

Concrete produced with SC-activated slag usually showed slower strength development, and sometimes lower late strength, in comparison with mixes activated by sodium silicate¹⁵. Recent studies showed significantly higher compressive strength of SC-activated fly ash-slag materials, reaching up to 80 MPa after 90 days of curing¹⁶. The SC-activated slag showed similar or lower shrinkage in comparison with PC mortar, while mixes activated with waterglass had 3-6 times higher shrinkage values⁴. The strength development of slags activated with various activators can be listed in the following order Na₂SiO₃ > Na₂CO₃ > Na₂SO₄ > NaOH^{17,18}. In a recent study, the reaction products of SC-activated slag at early age were identified as gaylussite, calcite and C-(A)-S-H gel^{6,9}, and the formation of gaylussite tended to occur much earlier in the binder based on slag with higher fineness⁶. Hydrotalcite-group minerals (Mg-Al layered double hydroxides) are also important reaction products in these binders as they evolve^{6,8}. SC or NaOH alkali activated slag with moderate content of MgO in the slag glass showed longer setting times in comparison with SS activated mixes^{7,8}, whereas, a high MgO content slag (14.6 wt.%) activated with SC revealed a faster setting in comparison with mixes activated with SS¹⁹. Consequently, the composition of slag has a significant role in defining the kinetics of reaction SC-activated slag at very high MgO content (16.1wt.% in the slag) had a final setting time under 21h when activated with 14 wt.% SC, and a rapid loss of workability⁹. The MgO content also affect the microstructure and the strength development of alkali-activated slag, associated with the availability of Al and the formation of hydrotalcite-type phases^{20,21}.

In alkali-activation, the alkaline component can be added to slag in different ways, for example in an aqueous solution, or in the solid state by mixing the dry alkali powder with slag. The dry alkali powder can be also ground together with the slag^{9,13,22,23}. Producing a binder that can be used with only the addition of water, requiring a dry activator, will promote the use of AAS cements²³. So, the present study is focused on the effect of mixing methods (dry or wet activator addition) on selected properties of sodium carbonate-activated slag pastes and

concretes, using a slag with high MgO content due to its superior compatibility and reaction with this particular activator type.

2. EXPERIMENTAL WORK

A commercially available ground granulated blast furnace slag (BFS) in Sweden was used in this study. Table 1 shows the chemical composition, which was determined using a Pananalytical-Zetium XRF spectrometer. Powdered sodium carbonate (SC) with purity > 99% was used. The sodium carbonate dosages varied between 3 and 14wt.% Table 2. All concrete mixes contained 450 kg/m³ of BFS. The water to binder (w/b) ratio was 0.45 for concrete mixes and 0.36 for pastes. The granite aggregates having a particle size 0-8 mm, with fine aggregate content of 80 wt.% were used. The total aggregate content for concrete mixes was 1663 kg/m³.

Table 1: Chemical composition of BFS used in this work, measured by X-ray fluorescence and reported on an oxide basis.

Component	CaO	SiO ₂	Al ₂ O ₃	Fe ₂ O ₃	MgO	Na ₂ O	K ₂ O	TiO ₂	MnO	SO ₃	L.O.I
Oxide wt. %	30.4	35	14.3	0.3	16.1	0.6	0.7	2.8	0.5	0.7	0.9
Physical data	Specific surface cm ² /g			Particle density kg/m ³				Bulk density kg/m ³			
	5000			2950				1100			

Table 2: Mix proportions of concrete

Mix ID	Binder content kg/m ³	w/b ratio	Aggregate content kg/m ³	Sodium carbonate doses wt. %
3 SC	450	0.45	1663	3%
5 SC	450	0.45	1663	5%
10 SC	450	0.45	1663	10%
14 SC	450	0.45	1663	14%

Note: For all mixes above there were two mixing procedures; dry D and wet W and two curing types; laboratory curing (20±2°C and 50-55% RH) and heat curing (65°C for 24h then laboratory conditions until testing).

Different mixing procedures were used for dry and wet activators. The dry procedure included 3 min of mixing of all the dry ingredients (slag + aggregates + powder sodium carbonate), followed by addition of water and mixing for another 4 minutes. The Hobart mixer model A200N was used. In the wet procedure, the sodium carbonate was dissolved in the mixing water and left to stand for one hour before being added to the mixed dry materials (slag + aggregate). Specimens for compressive strength testing were casted in alkali-resistant polymer 100 mm cube moulds. Immediately after casting, all samples were sealed with plastic film. Curing was carried out following two procedures. In the first procedure, specimens were sealed and kept at 20±2°C and 50-55% relative humidity (RH) until testing, whereas in the second procedure, specimens were sealed and heat cured at 65°C for 24 hours, then at 20±2°C

and 50-55% RH until testing. Compressive strength values were determined at 1, 7 and 28-days after casting, following the SS-EN 12390-3 standard (SS-EN 12390-3). The compressive strength values were determined using an Ele-autotest 3000 instrument. The loading rate was set to 10 kN/sec. The concrete slump was determined following ASTM C143 (ASTM International 2015). Initial and final setting times of SC-activated slag pastes were determined following the IS 4031 process of the Vicat test (IS: 4031-PART 5-1988), measuring the penetration using a 1-mm diameter needle and a plunger mass of 300 g. The initial setting times was defined as to occur when the penetration depth was 5-7 mm from the bottom of the material in its mould, and the final setting time when there was no longer any visible penetration of the outer circle of the needle plunger.

3. TEST RESULTS AND DISCUSSION

The amount of sodium carbonate and the mixing procedure strongly affected the fresh concrete properties. Mixes produced with dry SC showed decreasing workability with an increasing amount of activator, Figure 1. This can be related to the increased water uptake of the dry activator while it is in the process of dissolving. Conversely, the mixes with SC dissolved in water prior to the mix showed increasing slump values with an increasing SC dosage. In that case, no rapid water uptake by the SC was present. The initial setting time appeared to be slightly shortened for mixes produced with the wet activator. A higher alkali concentration caused more extensive dissolution of the slag which was followed by more intense precipitation of the reaction products and thus a shorter setting time^{24,25}, Figure 2.

Concrete activated with the dry SC activator showed a longer initial setting time. This could be related to a slower formation of C-A-S-H due to the lack of the advanced dissolution as in the case of the wet SC, Figure 2a. Furthermore, a high concentration of MgO (16.1 wt.%) in the blast furnace slag used in this study gives more extensive formation of hydrotalcite-group phases at early age, which could also contribute to the observed short initial setting times²⁶. The final setting times were unaffected by the SC preparation pathway, Figure 2b.

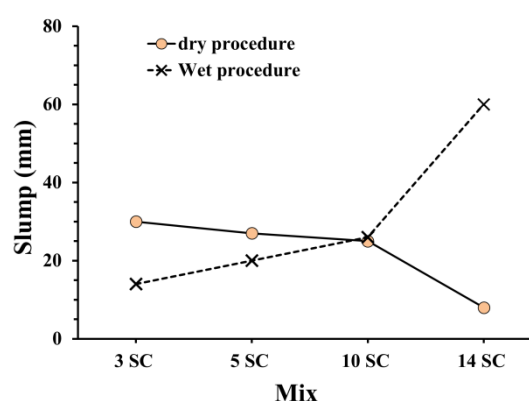


Figure 1: Slump test results

The compressive strength results are presented in Figures 3 and 4. Generally, a higher dosage of sodium carbonate led to increased 1, 7 and 28-day compressive strength values. The 1-day compressive strength was higher for the heat-cured specimens, Figure 3, due to the increased dissolution of BFS and acceleration formation of the reaction products². The laboratory cured specimens activated with less than 14 wt.% SC did not harden after one day of curing, Figure 4. After 7-days of laboratory curing, concrete cube strength values varied between 22 and 35 MPa, and between 32 and 50 MPa after 28 days. There was not a statistically significant difference between mixes produced with dry and wet alkali activators. Longer curing times are known to stimulate further strength development of concrete based on blast furnace slag, which was also observed in the present research²⁷. The 28-day old concretes cubes cured at 20°C for all mixes showed higher late (28 day) strength values than the heat-cured specimens which is similar to the know behaviour of Portland cement based concrete²⁸. Usually, lower curing temperature tends to promote development of denser and more homogenous microstructure.

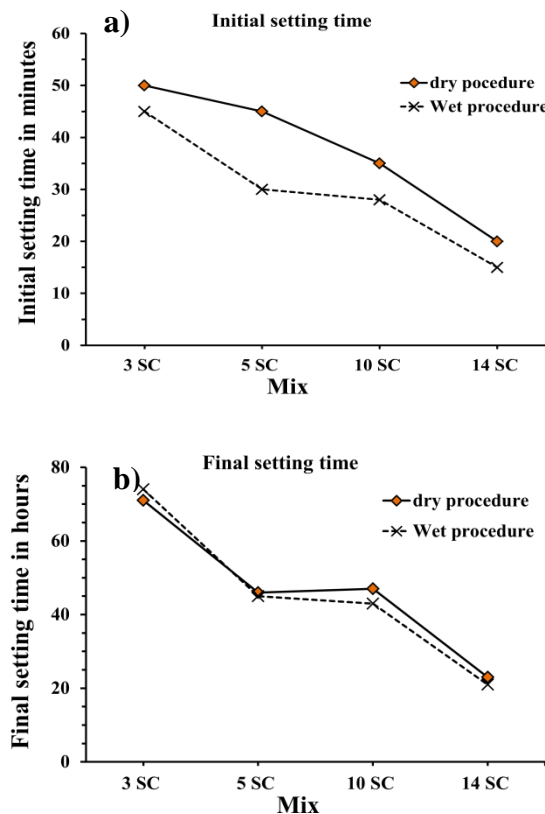


Figure 2: Initial and final setting times of SC-activated slag pastes.

The heat curing could decrease the crystallinity of the C-A-S-H²⁹. In addition, it also tends to coarsen the pore structure due to a higher reaction rate for C-A-S-H, in comparison with the rate of diffusion. As a result, the pores formed between denser precipitates create a barrier inhibiting additional dissolution and dispersion of ions¹⁵.

4. CONCLUSIONS

The effects of carbonate activator dosage, mixing procedures and curing temperatures on sodium carbonate activated high-MgO blast furnace slag pastes and concretes were studied. The key findings include:

Increasing the dosage of the sodium carbonate reduced the initial and the final setting time regardless of the mixing procedure mostly due to the slow reaction of the sodium carbonate. Addition of the sodium carbonate dissolved in water one hour before mixing, enhanced the workability at higher activator dosage. In contrast, increasing the amount of dry sodium carbonate worsened the workability. Higher amounts of sodium carbonate increased the 28d compressive strength when added either as dry or wet powder. The recorded final compressive strength values were generally higher for the laboratory cured samples, however, early age strength (1 and 7 days) were higher for the heat cured concretes.

ACKNOWLEDGEMENTS

This research was funded by the Iraqi Ministry of Higher Education and Scientific Research, Iraq. The authors would like to thank the technical staff of the laboratory at LTU, Sweden, and Dr Oday Hussein and Dr Xinyuan Ke (University of Sheffield) for conducting the XRF analysis.

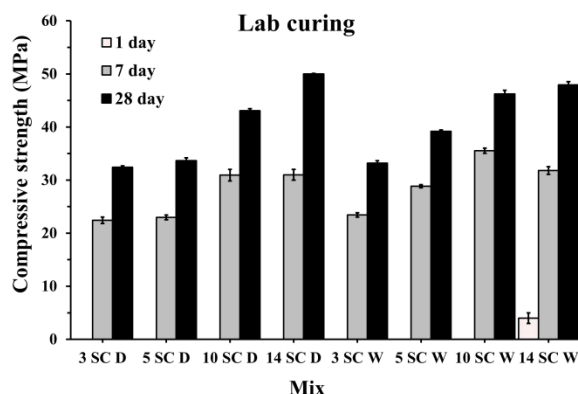


Figure 3: 1, 7 and 28 days compressive strength results of heat-cured concrete cubes using the two mixing procedures; dry (D) and wet(W).

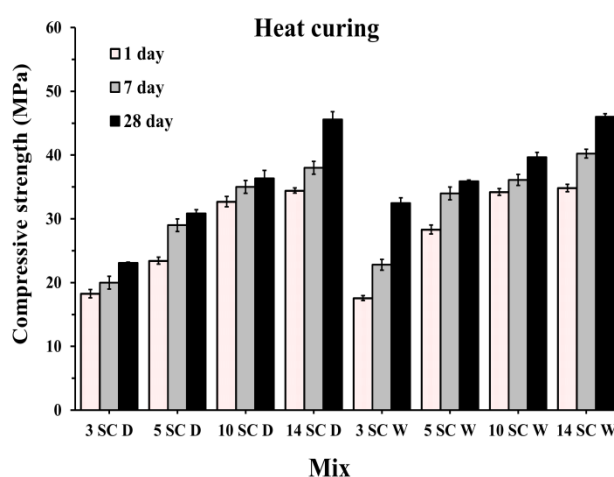


Figure 4: 1, 7 and 28 days compressive strength results of laboratory-cured concrete cubes using the two mixing procedures; dry (D) and wet(W).

REFERENCES

- [1] Islam A, Alengaram UJ, Jumaat MZ, Bashar II. The development of compressive strength of ground granulated blast furnace slag-palm oil fuel ash-fly ash based geopolymer mortar. *Mater Des.* 2014;56:833-841.
- [2] Bakharev T, Sanjayan J, Cheng Y. Effect of elevated temperature curing on properties of alkali-activated slag concrete. *Cem Concr Res.* 1999;29(10):1619-1625.
- [3] Živica V. Effects of type and dosage of alkaline activator and temperature on the properties of alkali-activated slag mixtures. *Constr Build Mater.* 2007;21(7):1463-1469.
- [4] Atiş CD, Bilim C, Çelik Ö, Karahan O. Influence of activator on the strength and drying shrinkage of alkali-activated slag mortar. *Constr Build Mater.* 2009;23(1):548-555.
- [5] Yuan B, Yu Q, Brouwers H. Investigation on the activating effect of Na_2CO_3 and NaOH on slag. In the *5th International Conference on Non-Traditional Cement and Concrete (NTCC2014)*, 16-19 June 2014, Brno, Czech Republic, 2014.
- [6] Yuan B. *Sodium carbonate activated slag: Reaction analysis, microstructural modification & engineering application*. [PhD Thesis]. Technische Universiteit Eindhoven; 2017.
- [7] Fernández-Jiménez A, Puertas F. Setting of alkali-activated slag cement. influence of activator nature. *Adv Cem Res.* 2001;13(3):115-121.
- [8] Bernal SA, Provis JL, Myers RJ, San Nicolas R, van Deventer JS. Role of carbonates in the chemical evolution of sodium carbonate-activated slag binders. *Mater Struct.* 2015;48(3):517-529.
- [9] Humad AM, Provis JL, Cwirzen A. Alkali activation of a high MgO GGBS–fresh and hardened properties. *Mag Con Res.* 2018: in press, DOI 10.1680/jmacr.17.00436.
- [10] Puertas F, Torres-Carrasco M. Use of glass waste as an activator in the preparation of alkali-activated slag. mechanical strength and paste characterisation. *Cem Concr Res.* 2014;57:95-104.
- [11] Yuan B, Yu Q, Brouwers H. Reaction kinetics, reaction products and compressive strength of ternary activators activated slag designed by taguchi method. *Mater Des.* 2015;86:878-886.
- [12] Abdalqader AF, Jin F, Al-Tabbaa A. Characterisation of reactive magnesia and sodium carbonate-activated fly ash/slag paste blends. *Constr Build Mater.* 2015;93:506-513.
- [13] Kovtun M, Kearsley EP, Shekhovtsova J. Dry powder alkali-activated slag cements. *Adv Cem Res.* 2015;27(8):447-456.
- [14] Song S, Jennings HM. Pore solution chemistry of alkali-activated ground granulated blast-furnace slag I. *Cem Concr Res.* 1999;29(2):159-170.
- [15] Bakharev T, Sanjayan JG, Cheng Y. Alkali activation of australian slag cements. *Cem Concr Res.* 1999;29(1):113-120.
- [16] Abdalqader A, Al-Tabbaa A. Factors affecting the properties of Na_2CO_3 -activated fly ash/slag paste. In the *34th Annual Cement and Concrete Science Conference*. 2014(14-16):329-332.
- [17] Wang S, Scrivener KL, Pratt P. Factors affecting the strength of alkali-activated slag. *Cem Concr Res.* 1994;24(6):1033-1043.
- [18] Fernández-Jiménez A, Palomo J, Puertas F. Alkali-activated slag mortars: Mechanical strength behaviour. *Cem Concr Res.* 1999;29(8):1313-1321.
- [19] Shi C, Day RL. A calorimetric study of early hydration of alkali-slag cements. *Cem Concr Res.* 1995;25(6):1333-1346.
- [20] Ben Haha M, Lothenbach B, Le Saout G, Winnefeld F. Influence of slag chemistry on the hydration of alkali-activated blast-furnace slag—Part I: Effect of MgO. *Cem Concr Res.* 2011;41(9):955-963.
- [21] Bernal SA, San Nicolas R, Myers RJ, et al. MgO content of slag controls phase evolution and structural changes induced by accelerated carbonation in alkali-activated binders. *Cem Concr Res.* 2014;57:33-43.

- [22] Collins F, Sanjayan J. Microcracking and strength development of alkali activated slag concrete. *Cem Con Compos.* 2001;23(4):345-352.
- [23] Luukkonen T, Abdollahnejad Z, Yliniemi J, Kinnunen P, Illikainen M. One-part alkali-activated materials: A review. *Cem Concr Res.* 2018;103:21-34
- [24] Chang J. A study on the setting characteristics of sodium silicate-activated slag pastes. *Cem Concr Res.* 2003;33(7):1005-1011.
- [25] Bernal SA, Mejía de Gutiérrez R, Pedraza AL, Provis JL, Rodriguez ED, Delvasto S. Effect of binder content on the performance of alkali-activated slag concretes. *Cem Concr Res.* 2011;41(1):1-8.
- [26] Ke X, Bernal SA, Provis JL. Controlling the reaction kinetics of sodium carbonate-activated slag cements using calcined layered double hydroxides. *Cem Concr Res.* 2016;81:24-37.
- [27] Bernal SA, San Nicolas R, van Deventer JSJ, Provis JL. Alkali-activated slag cements produced with a blended sodium carbonate/sodium silicate activator. *Advances in Cement Research.* 2016;28(4):262-273.
- [28] Verbeck GJ, Helmuth RH. Structures and physical properties of cement paste. . 1968;3:1-32.
- [29] Wang S, Scrivener KL. ²⁹Si and ²⁷Al NMR study of alkali-activated slag. *Cem Concr Res.* 2003;33(5):769-774.

International Conference on Sustainable Materials, Systems and Structures (SMSS 2019)

New Generation of Construction Materials

20-22 March 2019 – Rovinj, Croatia

NEW GENERATION OF CONSTRUCTION MATERIALS

SESSION 9: Alternative binders

HYDRATION OF MgO IN THE PRESENCE OF HYDROMAGNESITE

Frank Winnefeld (1), Eugenia Epifania (1,2), Fabio Montagnaro (2) and Ellis M. Gartner (3*)

(1) Empa, Swiss Federal Laboratories for Materials Science and Technology, Laboratory for Concrete and Construction Chemistry, Dübendorf, Switzerland

(2) Dipartimento di Scienze Chimiche, Università degli Studi di Napoli Federico II, Naples, Italy

(3) Department of Civil and Environmental Engineering, Imperial College London, London, United Kingdom

* Deceased as of February 13, 2018

Abstract

The hydration of reactive periclase (MgO) in the presence of hydromagnesite ($\text{Mg}_5(\text{CO}_3)_4(\text{OH})_2 \cdot 4\text{H}_2\text{O}$) was investigated by a variety of physical and chemical techniques. This system is of potential interest as low CO_2 binder, if the magnesium carbonate is produced by carbonation from naturally occurring magnesium silicates such as olivine or serpentine.

In contrary to thermodynamic prediction not artinite ($\text{Mg}_2(\text{CO}_3)(\text{OH})_2 \cdot 3\text{H}_2\text{O}$), but a very poorly-crystalline form of brucite ($\text{Mg}(\text{OH})_2$), and an unknown amorphous hydrate which partially loses its crystal water at about 100°C were the main hydration products.

Mortars based on such a binder show a reasonable compressive strength of 21 MPa after 28 days of hydration, which could be further optimized.

Keywords: MgO, cement, hydration, hydromagnesite, artinite, brucite

1. INTRODUCTION

Most of the alternative low CO₂-clinkers that have been proposed are based on calcium silicates and aluminates [1-3]. Their main calcium source is limestone, even though the amounts required may be somewhat lower than for Portland cement clinker.

MgO can be used to make a variety of hydraulic binders as well as binders that harden by carbonation [4]. Potential raw materials for MgO production are magnesium silicates or Mg-containing brines, which could be carbonated and partially calcined afterwards to obtain mixture of MgO and basic magnesium carbonates [5]. If the final composition of the hardened binder were sufficiently rich in carbonate, the CO₂ sequestered by it could fully compensate for the CO₂ emitted by the binder manufacturing process. Then we could talk of a truly carbon-neutral binder. We could even envisage carbon-negative binders for which there would be net consumption of CO₂ during manufacture and use. This was the original concept behind the “Novacem” start-up venture, which was built on the discovery that reactive MgO, when hydrated together with certain magnesium carbonates, gave a relatively strong hydraulic binder, compared to MgO hydrated alone, which had almost no binding capacity [6-9].

The current study aimed at a more detailed investigation of the hydrates formed in such binders. The hydration of reactive periclase (MgO) in the presence of hydromagnesite (Mg₅(CO₃)₄(OH)₂·4H₂O) was investigated by a variety of physical and chemical techniques. Isothermal calorimetry, X-ray powder diffraction, thermal analysis and vibrational spectroscopy (Raman spectroscopy) were applied to assess the hydration mechanism.

2. MATERIALS AND METHODS

3.1 Materials

Pure magnesium oxide (MgO-p) was prepared by igniting laboratory-grade brucite in a furnace at 900°C for 6 h. For compressive strength measurements on mortars a technical magnesium oxide calcined at low temperatures (MgO-t, 83 M.-% periclase) was used as well as a superplasticizer based on polycarboxylate ether and standard sand according to EN 196-1. Laboratory grade hydromagnesite (HY) was used.

The mix designs given in Table 1 were used in the experiments. Due to the high water demand, a water/binder ratio of 1.20 was used in the hydration study. For strength measurements, the water/binder ratio was decreased by means of the superplasticizer to 0.95 and 0.70, respectively.

Table 1: Mix designs referring to 100 g binder. Mixes No. 1-3 were used in the hydration experiments, whereas Mixes No. 4-6 were used to determine compressive strength.

Mix. No.	MgO-p g	MgO-t g	HY g	Water g	superplasticizer M.-% of binder
1	100			120	
2	70		30	120	
3	50		50	120	
4		70	30	120	
5		70	30	95	1.5
6		70	30	70	3.0

3.2 Methods

Isothermal conduction calorimetry was performed using a Thermometric TAM Air at 20°C for 72 h. Approximately 5-6 g of freshly mixed paste were transferred into a glass vial which was then capped and placed into the calorimeter.

For phase analyses at different hydration steps 15 g of paste was mixed by hand for 2 minutes using a spatula. The pastes were cast and stored in a sealed PE container at 20°C until testing. Hydration was stopped by solvent exchange, first with isopropanol and then with diethyl ether. Before further analysis, the samples were freshly ground by hand below a particle size of 63 µm using an agate mortar.

X-ray diffraction analyses (XRD) were performed with a Panalytical X'Pert Pro in a Θ - Θ configuration using $\text{CoK}\alpha$ -radiation and the X'Celerator detector.

Thermogravimetric analyses (TGA) were performed using a Mettler Toledo TGA/SDTA 851e under nitrogen atmosphere. Weight changes were measured while heating about 50 mg samples from 30-980° C with a heating rate of 20°C per minute in 150 µl alumina crucibles.

Mortars for compressive strength testing with a binder to sand ratio of 1:3 were produced according to EN 196-1 with the exception that smaller prisms (2.5 cm x 2.5 cm x 10 cm) were used and that the specimens were cured at 20°C / 95% rH until testing.

Thermodynamic modelling was used to calculate the thermodynamically stable phases in the system $\text{MgO-CO}_2\text{-H}_2\text{O}$ at ambient temperature and pressure. The geochemical GEMS-PSI software [10,11] was applied together with the Nagra/PSI database [12], the SLOP98 [13,14] database and additional data for lansfordite [15,16] and nesquehonite [17]. For dypingite, $\text{Mg}_5(\text{CO}_3)_4(\text{OH})_2 \cdot 5\text{H}_2\text{O}$, no thermodynamic data was found in open literature.

3. RESULTS

3.1 Thermodynamic modelling

Thermodynamic modelling reveals that artinite, $Mg_2(CO_3)(OH)_2 \cdot 3H_2O$, should be the thermodynamic stable hydrate phase in MgO-hydromagnesite blends (Figure 1), however it has to be considered that thermodynamic data for dypingite is not available. Based on artinite formation, a ratio of 80% hydromagnesite and 20% MgO would be the optimum to incorporate as much CO_2 in the mix as possible.

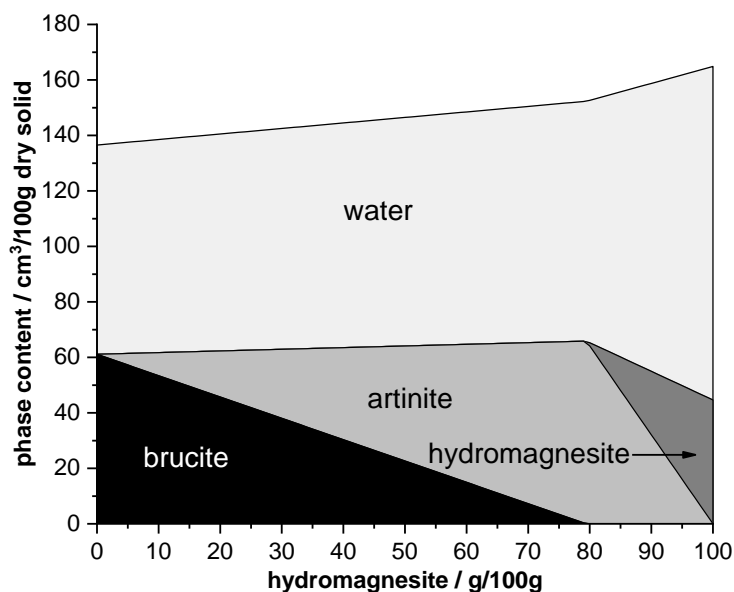


Figure 1: Thermodynamic modelling of the stable hydrate assemblage in MgO-hydromagnesite blends hydrated at 20°C using a water/binder ratio of 1.20.

3.2 Isothermal calorimetry

The replacement of MgO with hydromagnesite accelerates the early hydration of the pure MgO at early ages as shown in the heat flow calorimetry data (Figures 2).

The heat of hydration of MgO to brucite is estimated to be about 930 J/g MgO [18]. On this basis, all three samples were about 80-85% hydrated after three days (Figure 3). It seems that the acceleratory effect is not very strongly dependent on the MgO/HY ratio.

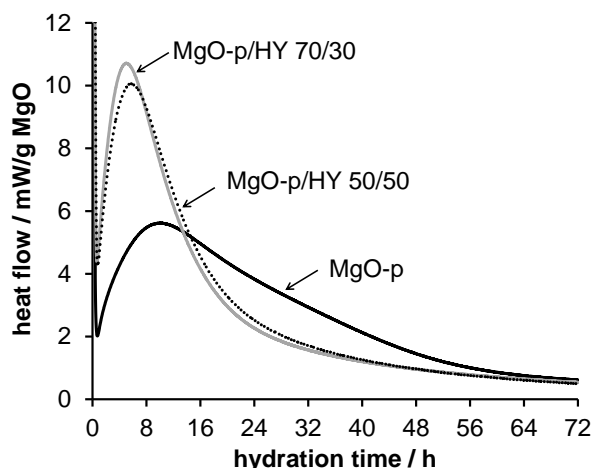


Figure 2: Hydration heat flow normalized to 1 g of MgO

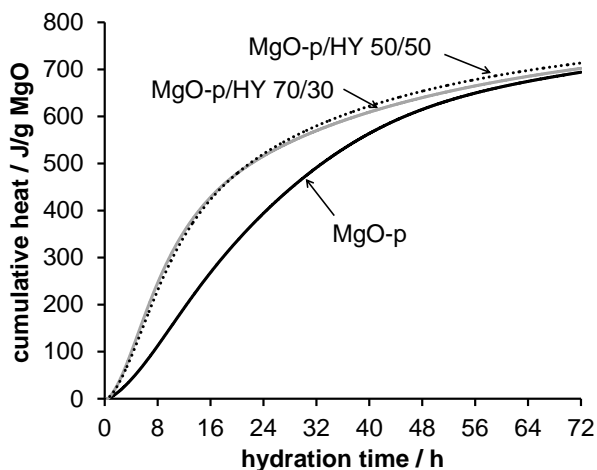


Figure 3: Development of heat of hydration normalized to 1 g of MgO

3.3 X-ray diffraction analysis and thermogravimetry

After 28 d of hydration the XRD pattern of hydrated MgO shows well crystalline brucite and traces of periclase (Figure 4). In the blend of MgO with hydromagnesite, periclase disappears as well and brucite appears instead, but the brucite peaks are extremely broad and some of them even shifted, as has been observed before whenever a reactive magnesium carbonate is present [9]. Some unreacted hydromagnesite is present as well. Two additional reflections can be observed, one at a very low angle (about 6°) which we tentatively refer to as “dypingite-like” since it is close to the literature basal peak reported for dypingite. Another broad peak at $17\text{--}19^\circ$ which is quite strong and well separated from expected brucite peaks, and which we refer to as “artinite-like”.

Thermogravimetric analysis of MgO hydrated for 28 d confirm the presence of brucite (Figure 5). TGA analysis of hydrated pastes of MgO blended with hydromagnesite the

appearance of a dehydration peak centred at about 100°C, which belongs neither to hydromagnesite, nor to brucite. This as well indicates the presence of a hydrate phase, which cannot be clearly identified neither by XRD nor by TGA. Furthermore, the CO₂-release of the hydrated MgO-p/HY 70/30 is shifted to a lower temperature (around 460°C) compared to pure hydromagnesite (around 520°C), which confirms that hydromagnesite is mainly consumed and that the CO₂ is bound into a new hydrate phase.

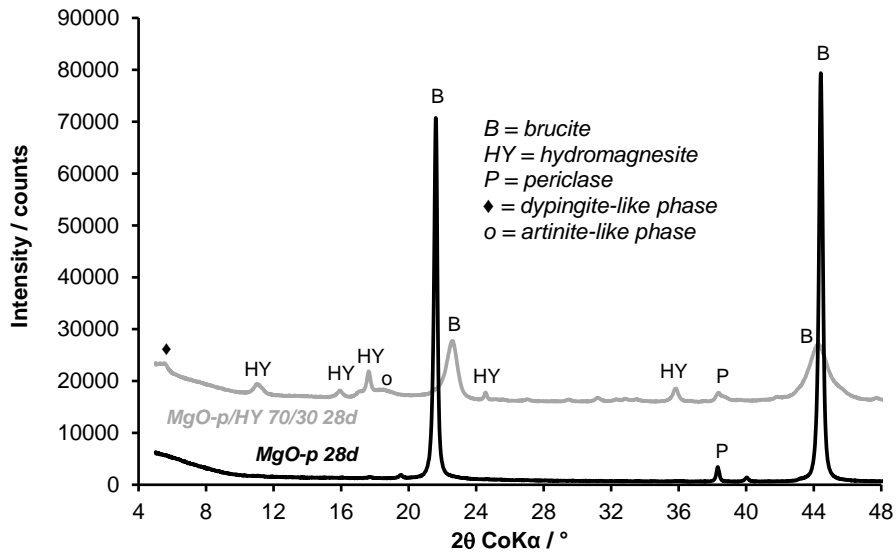


Figure 4: X-ray diffraction analyses of MgO-p and MgO-p/HY 70/30 after 28 days of hydration

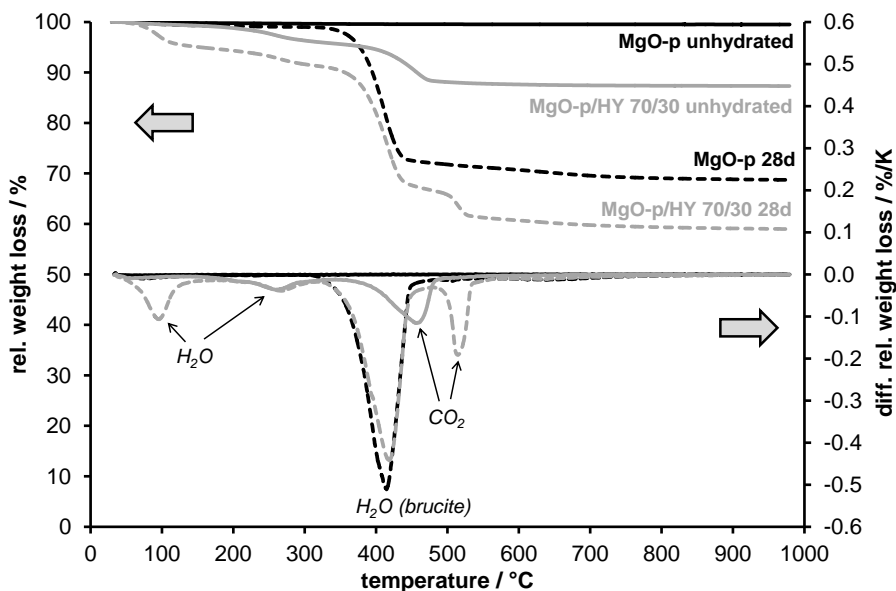


Figure 5: Thermogravimetric analyses of unhydrated MgO-p and MgO-p/HY 70/30 and after 28 days of hydration

3.4 Mortar compressive strength

Figure 6 shows the results of the mortar compressive strength. Without superplasticizer, a very high water/binder ratio of 1.20 was used, which is much higher than the water demand for full hydration. Thus, only low strength is achieved. By the addition of a superplasticizer, the water/binder ratio could be lowered. With a water/binder ratio of 0.70, a compressive strength of 21 MPa after 28 days could be achieved.

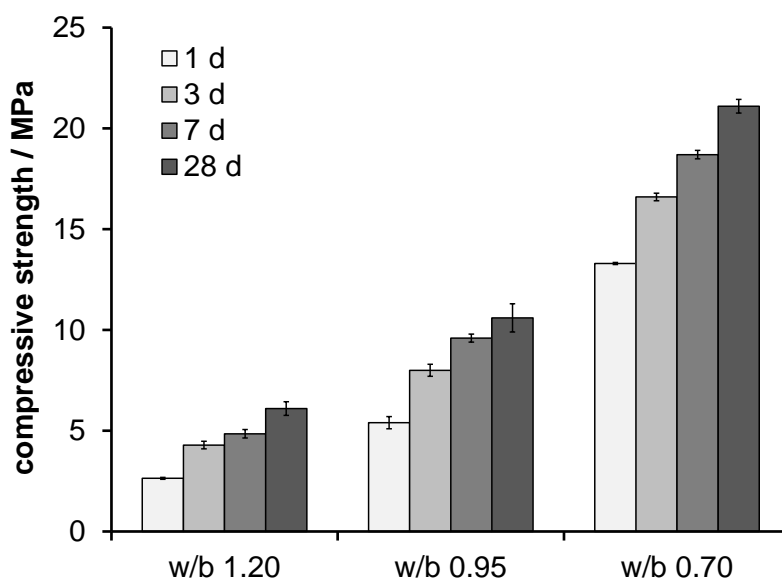


Figure 6: Mortar compressive strength of MgO-t/HY 70/30 using different water/binder ratios

4. CONCLUSIONS

Isothermal calorimetry showed that partial replacement of the MgO with hydromagnesite accelerated the hydration of the pure MgO at early ages (i.e. for about the first half day). The MgO-HY blends always produced a significant amount of an unknown hydrate with a thermal decomposition peak centred at about 100°C as determined by thermogravimetry. We hypothesise that this peak represents an amorphous or very poorly-crystalline phase that leads to cohesive binding in these blends. The other main difference between the hydrated MgO-hydromagnesite pastes and the pure MgO paste is the observation of very broad X-ray diffraction peaks for brucite whenever hydromagnesite is present. Furthermore, reflections of a dypingite-like phase ($\text{Mg}_5(\text{CO}_3)_4(\text{OH})_2 \cdot 5\text{H}_2\text{O}$) and an artinite-like phase ($\text{Mg}_2(\text{CO}_3)(\text{OH})_2 \cdot 3\text{H}_2\text{O}$) were identified by X-ray diffraction. However, the formation of artinite, which was calculated to be the thermodynamic stable phase, could not be fully confirmed. Mortars produced based on this binder system show reasonable strengths in case a superplasticizer is used to lower the water/binder ratio.

ACKNOWLEDGEMENTS

Ellina Bernard, Boris Ingold and Luigi Brunetti are acknowledged for their support in the experiments and Barbara Lothenbach for fruitful discussions.

REFERENCES

- [1] Gartner, E., 'Industrially interesting approaches to "low-CO₂" cements', *Cem. Concr. Res.* **34** (9) (2004) 1489-1498.
- [2] Juenger, M.C.G., Winnefeld, F., Provis, J.L., Ideker, J.H., 'Advances in alternative cementitious binders', *Cem. Concr. Res.* **41** (12) (2011) 1232-1243.
- [3] Gartner, E., Sui, T., 'Alternative cement clinkers', *Cem. Concr. Res.*, in press.
- [4] Walling, S.A., Provis, J.L., 'Magnesia-based cements: A journey of 150 years, and cements for the future?', *Chem. Rev.* **116** (7) (2016) 4170-4204.
- [5] Gartner, E., Gimenez, M., Meyer, V., Pisch, A., 'A novel atmospheric pressure approach to the mineral capture of CO₂ from industrial point sources', Thirteenth Annual Conference on Carbon Capture, Utilization and Storage, April 28 – May 1, 2014, Pittsburgh, Pennsylvania, USA.
- [6] Vlasopoulos, N., Cheeseman, C.R., 'Binder composition', PCT Patent Application PCT/GB2009/001610, International Publication Number WO 2009/156740 A1 (12/30/2009).
- [7] Vlasopoulos, N., 'Waste minimisation through sustainable magnesium oxide cement products', PhD Thesis, Imperial College, London, UK, 2007.
- [8] Zhang, F., 'Magnesium oxide based binders as low-carbon cements', PhD Thesis, Imperial College, London, UK, 2012.
- [9] Kuenzel, C., Zhang, F., Ferrándiz-Mas, V., Cheeseman, C.R., Gartner, E.M., 'The mechanism of hydration of MgO-hydromagnesite blends', *Cem. Concr. Res.* **103** (2018) 123-129.
- [10] Wagner, T., Kulik, D.A., Hingerl, F.F., Dmytrieva, S.V., 'GEM-Selektor geochemical modelling package: TSolMod Library and data interface for multicomponent phase models', *Can. Mineral.* **50** (5) (2012) 1173-1195.
- [11] Kulik, D.A., Wagner, T., Dmytrieva, S.V., Kosakowski, G., Hingerl, F.F., Chudnenko, K.V., Berner, U.R., 'GEM-Selektor geochemical modeling package: revised algorithm and GEMS3K numerical kernel for coupled simulation codes', *Comput. Geosci.* **17** (1) (2013) 1-24.
- [12] Hummel, W., Berner, U., Curti, E., Pearson, F.J., Thoenen, T., 'Nagra/PSI chemical thermodynamic data base 01/01', *Radiochim. Acta* **90** (9-11) (2002) 805-813.
- [13] Helgeson, H.C., Delany, J.M., Nesbitt, H.W., Bird, D.K., 'Summary and critique of the thermodynamic properties of rock-forming minerals', *Am. J. Sci.* **278A** (1978) 1-229.
- [14] Johnson, J.W., Oelkers, E.H., Helgeson, H.C., 'SUPCRT92 - A software package for calculating the standard molal thermodynamic properties of minerals, gases, aqueous species, and reactions from 1 to 5000 bar and 0 1000°C', *Comput. Geosci.* **18** (7) (1992) 899-947.
- [15] Königsberger, E., Königsberger, L.C., Gamsjäger, H., 'Low-temperature thermodynamic model for the system Na₂CO₃-MgCO₃-CaCO₃-H₂O', *Geochim. Cosmochim. Acta* **63** (19-20) (1999) 3105-3119.
- [16] Hill, R.J., Canterford, J.H., Moyle, F.J., 'New data for lansfordite', *Mineral. Mag.* **46** (341) (1982) 453-457.
- [17] Robie, R.A., Hemingway, B.S., 'Heat-capacities at low-temperatures and entropies at 298.15 K of nesquehonite, MgCO₃·3H₂O, and hydromagnesite', *Am. Mineral.* **57** (11-12) (1972) 1768-1781.
- [18] Thomas, J.J., Musso, S., Prestini, I., 'Kinetics and activation energy of magnesium oxide hydration', *J. Am. Ceram. Soc.* **97** (1) (2014) 275-282.

RADIOACTIVE WASTE CONDITIONING USING ALUMINA-SILICATE BINARY BLENDS

Bastien Planel (1), David Lambertin (2) and Catherine A. Davy (3)

(1) CEA DAM, F-21120 Is sur Tille, France

(2) CEA DEN, DE2D, SEAD, LCBC, F-30207 Bagnols sur Cèze, France

(3) Centrale Lille and UCCS UMR CNRS 8181, Villeneuve d'Ascq, France

Abstract

For radioactive waste conditioning, geopolymer (GP) cements, and their blends with ground granulated blast furnace slag (GGBFS), are considered as encapsulating media for organic radioactive waste. In practice, fresh GP pastes are mixed with organic waste (oil). They harden and form homogeneous GP-oil composites.

In situ, these composites will be placed in contact with Portland concretes, so that interactions with the highly alkaline pore water of Portland concretes is expected. This may induce chemical reactions, degrade the GP-oil composites and their durability.

In this contribution, leaching experiments are conducted on GP-oil mortars. Each sample is injected with a pressure gradient of highly alkaline water (similar in composition to Portland concrete porewater). Water carbonation is avoided by continuously flowing argon over the water container. Water permeability is deduced in the Darcy's sense over several weeks. GP mortar made with metakaolin (MK) alone has a water permeability smaller than high performance Portland concretes ($1.3 \times 10^{-18} \text{ m}^2$ instead of $3.2\text{-}4.0 \times 10^{-18} \text{ m}^2$). By replacing MK with 20% mass GGBFS, water permeability decreases down to $3.9 \times 10^{-19} \text{ m}^2$, hence increasing mortar durability. When adding 20% vol oil, the pure MK GP mortar provides a stable cement matrix (with smaller water permeability than without oil), contrarily to GGBFS-added GP.

Keywords: geopolymer, oil, composite, waste management, alkali-activation

1. INTRODUCTION

In the industrial context of radioactive waste conditioning, geopolymer (GP) cements [1-4], and their blends with ground granulated blast furnace slag (GGBFS) [5-8], are considered as encapsulating media for organic radioactive waste. In practice, fresh GP pastes are mixed with organic waste (oil) so that they harden to form homogeneous GP-oil composites [9-12].

In situ, the GP-oil composites will be placed in contact with Portland concretes, widely used as containers, overpacks and structural elements in the engineered barrier of the storage site (e.g. in France). Interactions with the highly alkaline pore water of Portland cements is expected. This may induce chemical reactions (e.g. dissolution and re-precipitation of swelling phases), degrade the GP-oil composites and limit their durability.

The aim of this contribution is precisely to investigate the durability of GP-oil composites when subjected to an accelerated flux of highly alkaline water mimicking Portland concrete porewater.

To this purpose, GP-oil mortar composites are made with various GGBFS or oil content (20% each), and compared to composed Portland High Performance Concrete (HPC). Their durability is assessed through accelerated leaching tests, using an original set-up imposing a water pressure gradient to the sample. Test duration is of one to several weeks.

2. MATERIALS AND METHODS

2.1 Materials

Reference concrete is retrieved from former research in our laboratory [13-15]. This High Performance Concrete is made of CEMV (Type V) composed Portland cement, silica-limestone aggregates and super-plasticizer, as detailed in Table 1. It is matured for six months, cored to 37 mm diameter cylinders, and cured again for several years at 20°C under lime-saturated water, and finally cut to a height of 26.5mm +/-0.1 before being tested for water permeability.

Table 1: Composition of CEMV reference HPC (water-to-cement ratio of 0.39)

Nature	Source	Amount (kg/m ³)
CEMV/A 42.5 N	Calcia, France	450
Limestone (0-4 mm)	Boulonnais quarry, France	800
Limestone (0-4 mm)	Boulonnais quarry, France	984
Glenium 27	BASF	11.5
water	tap	176.3

Table 2: Composition of GP mortars, added with GGBFS or oil or not

Nature	Source	Amount (kg/m ³)
Metakaolin	Grace Construction, France	557.4
Sodium silicate	Woellner, Germany	635.0
Sodium hydroxyde	VWR International, USA	99.9
GGBFS	Ecocem, France	0 or 111.5
Silica sand	Le Beausset, Lafarge, France	557.4
Water	demineralized	47.5
Oil	Spirax, Shell, USA	175.4

GP cement is made with a stoichiometry of 1 Al₂O₃ 1 Na₂O 3.8 SiO₂ 12 H₂O. It uses metakaolin (MK) purchased under the brand name Pieri Premix MK from Grace Construction

(France), sodium silicate solution (Betol® 39T) obtained from Woellner (Germany), sodium hydroxide NaOH (purity >99%) from VWR International (USA) and GGBFS from Ecocem (France). This research investigates mortars solely, so that GP cement is consistently combined with pure silica sand (Fulchiron LS 0/2, France) to a sand-to-MK mass ratio (S/MK) of 1. GGBFS powder is mixed in the GP cement by replacing 20% mass metakaolin in the initial dry powders. These changes lead to the combined formation of a geopolymer network and of Calcium Silicate Hydrates (C-S-H), which are the main binding elements of Portland cements. GP mortar is mixed with 20% total volume of non reactive industrial Spirax oil (Shell, USA), as expected for radioactive organic waste conditioning.

In practice, the dry powders (metakaolin and sand) are mixed until homogeneity, the sodium silicate solution is adjusted with NaOH to the adequate stoichiometry, let to cool down and mixed with the powders to make a fresh mortar paste. Mixing is continued to incorporate non reactive oil by emulsification, until homogeneity.

Each mortar paste is poured into 37mm diameter plastic moulds up to a height H ranging between 12 and 22mm, and cured in hermetic bags at 20°C for at least 7 days. After this period, it is assumed that geopolymerization is sufficiently advanced not to modify anymore the pore network useful for fluid transport.

Table 3: Summary of the samples tested in this study

Material	Sample quantity	Metakaolin proportion (%mass)	GGBFS proportion (%mass)	Oil proportion (%vol)
CEMV concrete	2	0	0	0
GP mortar	1	100	0	0
	1	100	0	20
	1	80	20	0
	1	80	20	20

A summary of all samples tested with the accelerated leaching test set-up is given in Table 3.

2.2 Description of the accelerated leaching experiment

The experiment (Fig. 1) is derived from a typical triaxial cell experiment for fluid permeability measurement [14,16]. The sample is wrapped in a Viton protective membrane and placed in the triaxial cell, which is filled with confining fluid at a given pressure of 3MPa (+/- 0.2). This avoids any fluid leakage around the sample, so that fluid passes consistently through its pores, while being a low enough value not to damage the mortar. The triaxial cell also allows to inject fluid at a given pressure $P_{upstream}$ on its upstream side, while the sample downstream side is at atmospheric pressure $P_{upstream} = P_{atmospheric}$. This provides an imposed pressure gradient $\Delta p = P_{upstream} - P_{downstream}$ of 0.5MPa. The injecting pump (Gilson, USA) provides the measurement of volumetric fluid flowrate Q_v (in m^3/s) versus time. By assuming a unidirectional flow of a Newtonian fluid through the sample, and by neglecting gravity effects [16], Darcy's law provides water permeability as:

$$K = \frac{\mu H Q_v}{A \Delta p} \quad (1)$$

where H is sample height (in m), A is its surface area (in m²), μ is fluid dynamic viscosity in Pa.s at the considered temperature (here 20°C, for water, it is taken at a value of 1 mPa.s). Each permeability experiment is performed until several days after fluid percolation on the downstream sample side.

Synthetic CEMV porewater is made according to Andra's technical note RTS.NT.ASCM.17.0002 by mixing 2.666g NaOH, 7.48g KOH and 0.074 g Ca(OH)₂ in 1l demineralized water. Andra is the French national agency in charge of radioactive waste management. The pH of the solution is checked after mixing at an average value of 13.3 +/-0.1 with a Mettler-Toledo (USA) pH-meter.

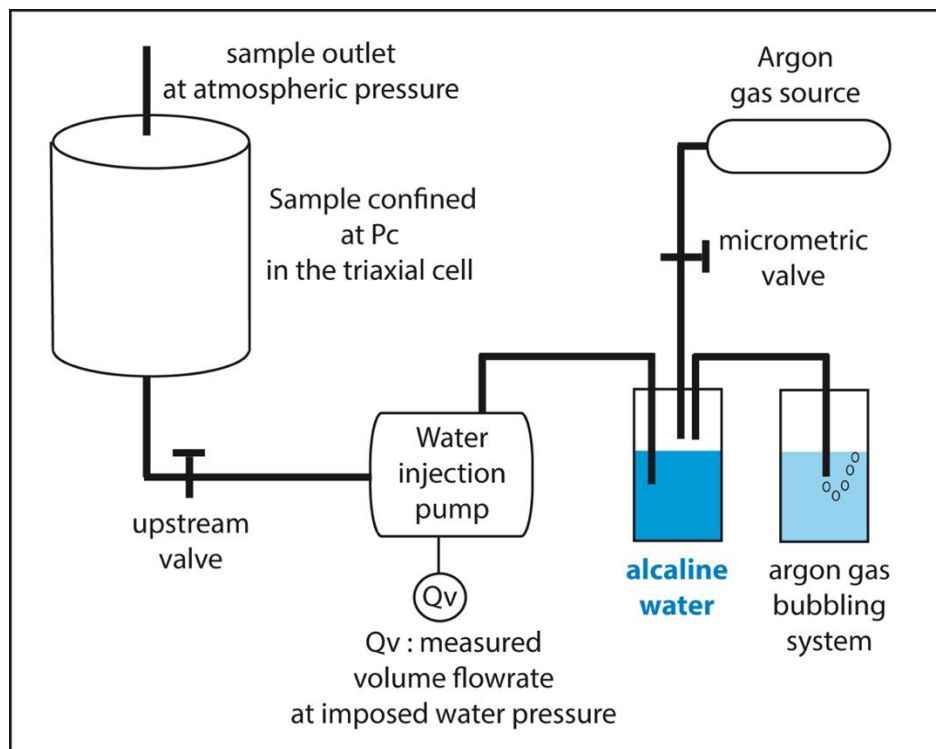


Figure 1: Principle of the accelerated leaching experiment. A pressure gradient of alkaline water is applied to a centimetric sample placed in a triaxial cell to avoid fluid leakage. Water carbonation is avoided using a small argon flux above the water reservoir.

3. RESULTS AND DISCUSSION

First results (Fig. 2) compare two reference HPC concrete samples to the reference GP mortar, made only with MK and no oil. Both materials have stable water permeability values over time, meaning that no progressive degradation is observed over the few days experiments (1 to 3 days). It is observed that on average, water permeability K of GP mortar is of $1.3 \times 10^{-18} \text{ m}^2$ instead of $3.2\text{-}4.0 \times 10^{-18} \text{ m}^2$ for the two CEMV concrete samples. This means that GP mortar is less permeable than CEMV concrete, although K is on the same order of magnitude.

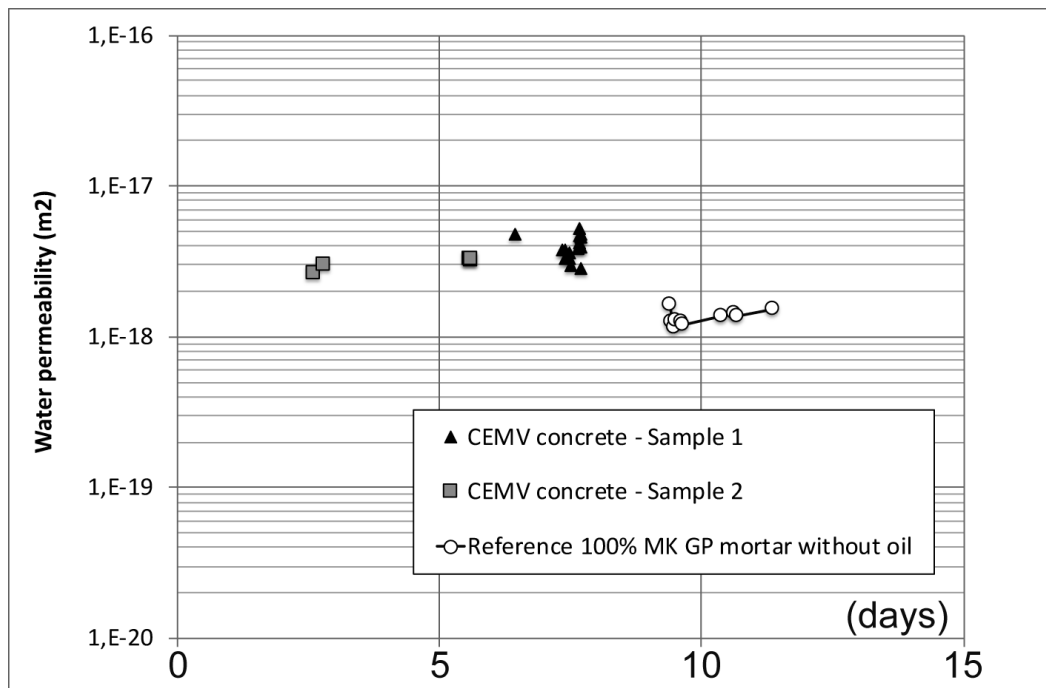


Figure 2: Water permeability results for two samples of CEMV concrete compared to a sample of reference GP mortar (made with MK only). All of these samples are mixed without oil

Fig. 3 compares reference GP mortar (neither with oil nor GGBFS) to the same mortar added with 20% vol. oil, and to GP mortar made with 20% mass GGBFS substitution (80%MK-20%GGBFS), without and with 20% vol oil.

For reference GP mortar made with pure MK, water permeability is decreased by the addition of 20% vol oil. Oil addition also increases fluctuations around the average, with $K_{\text{mean}} = 4.4 \times 10^{-19} \text{ m}^2 \pm 4.0 \times 10^{-19}$ over 40 days water injection. This means that emulsifying 20% vol oil inside a pure MK-GP mortar provides low fluid transport ability, which is considered related to good durability in the investigated experimental conditions.

Moreover, over the course of one month (27 days), water permeability of the GGBFS-substituted GP mortar decreases significantly when compared to reference GP mortar, from $2.0 \times 10^{-18} \text{ m}^2$ on the first day down to $1.9 \times 10^{-19} \text{ m}^2$ after 27 days, i.e. a decrease by one order of magnitude. It is anticipated that the alkaline water flow through the GGBFS-substituted mortar helps advance the hydration of GGBFS, by forming more calcium silicate and aluminate hydrates, owing to a better affinity with GGBFS than the MK-based GP porewater. From a durability point of view, the 80%MK-20%GGBFS mortar has better performance. This is consistent with former research on the subject [17].

However, when adding 20% vol oil to 80%MK-20%GGBFS mortar, Fig. 3 shows that after 16 days, K increases by more than two orders of magnitude, starting from $2.4 \times 10^{-19} \text{ m}^2$ on day 1, and going up to $2.6 \times 10^{-17} \text{ m}^2$ on day 16. After a decrease of more than one decade, on the course of 9 days, permeability goes from $9.2 \times 10^{-20} \text{ m}^2$ up to $2.6 \times 10^{-17} \text{ m}^2$. This means that despite displaying smaller permeability than pure MK GP mortar, the 80%MK-20%GGBFS mortar degrades significantly after about two weeks when emulsified with 20% vol oil.

Comparatively, a stable permeability over time (for more than 30 consecutive days) is obtained for pure MK GP mortar when emulsified with the same oil amount (20% vol).

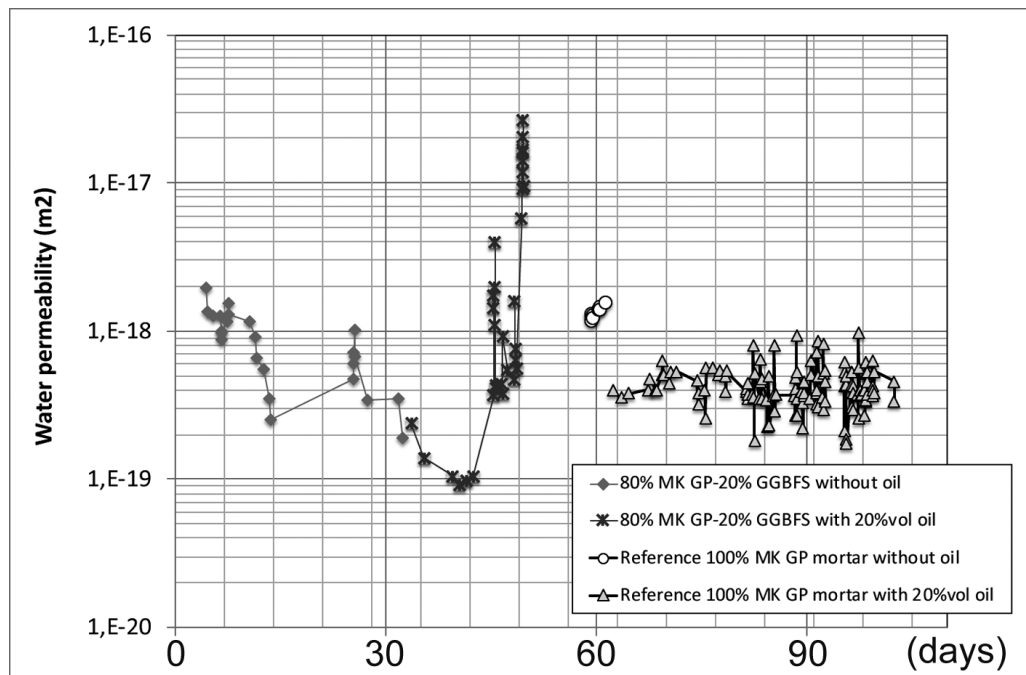


Figure 3: Water permeability results for (1) reference GP mortar (made with MK only) without oil, (2) reference GP mortar with 20% vol oil, (3) mortar made with 80%MK-20%GGBFS without oil, (4) mortar made with 80%MK-20%GGBFS and 20% oil

4. CONCLUSIONS

Our results show that GP mortars made with metakaolin (MK) alone have a water permeability similar to high performance Portland concretes (10^{-18} m^2). When GP formulation is modified by replacing part of MK with GGBFS, its permeability is lowered and its durability improved. However, mixing the GP-GGBFS paste with 20 %vol oil destabilizes the pore system, so that water permeability increases by several orders of magnitude within 9 days. This is not observed with pure MK GP mortar with 20 % oil, which retains a low permeability on the order of $4.4 \times 10^{-19} \text{ m}^2$ +/- 4.0×10^{-19} over 40 days water injection. Emulsifying 20% vol oil inside a pure MK-GP mortar provides low fluid transport ability, which is considered related to good durability in the investigated experimental conditions.

It is possible that the presence of oil (similar to an over-dosage in super-plasticizer) does not allow an adequate hydration of the GGBFS in the GP-GGBFS paste, expected to lead to C-A-S-H, so that the solid structure is not as stable and strong as in pure GP-MK paste. In further research, we will study the effect of varying the formulation parameters: oil proportion, GGBFS, etc.

REFERENCES

- [1] Provis J.L., and Van Deventer J.S.J., eds, 'Introduction to geopolymers. Structure, processing, properties and industrial applications', ed. J.L. Provis and J.S.J. Van Deventer. Woodhead Publishing in Materials: Cambridge, UK, 2009.
- [2] Bai C., Colombo P., 'Processing, properties and applications of highly porous geopolymers: A review', *Ceram Int*, in press, 2018.
- [3] Davidovits J., 'Geopolymers', *J Therm Anal.* **37**(8) (1991) 1633-1656.
- [4] Duxson P., Fernandez-Jimenez A., Provis J. L., Lukey G. C., Palomo A., van Deventer J. S. J., 'Geopolymer technology: the current state of the art', *J. Mater. Sci.* **42**(9) (2007) 2917-2933.
- [5] Provis J. L., Palomo A., Shi C., 'Advances in understanding alkali-activated materials', *Cem. Concr. Res.* **78** (2015) 110–125.
- [6] Borges P. H. R., Banthia N., Alcamand H. A., Vasconcelos W. L., Nunes E. H. M., Performance of blended metakaolin/blasfurnace slag alkali-activated mortars, *Cem Concr Res* **71** (2016) 42-52.
- [7] Wang S.D., Scrivener K. L., Pratt P. L., 'Factors affecting the strength of alkali-activated slag', *Cem. Concr. Res.*, **24**(6) (1994) 1033-1043.
- [8] Ding L., Ning W., Wang Q., Shi D., Luo L., 'Preparation and characterization of glass–ceramic foams from blast furnace slag and waste glass', *Mat Lett*, **141** (2015) 327–329.
- [9] Cantarel V., Nouaille F., Rooses A., Lambertin D., Poulesquen A., Frizon F. Solidification/stabilisation of liquid oil waste in metakaolin-based geopolymer. *J Nuc Mat* **464** (2015) 16-19.
- [10] Cantarel V., Lambertin D., Poulesquen A., Leroux F., Renaudin G., Frizon F. Geopolymer assembly by emulsion templating: Emulsion stability and hardening mechanisms. *Ceram Int* **44** (2018) 10558-10568.
- [11] Cantarel V., Etude de la synthèse de composites liquides organiques/géopolymère en vue du conditionnement de déchets nucléaires. Université Blaise Pascal, Clermont-Ferrand, France. PhD thesis, 2017.
- [12] Davy C. A., Hauss G., Planel B., Lambertin D., '3D structure of oil droplets in hardened geopolymer emulsions', *Journal of the American Ceramic Society*, doi: 10.1111/jace.16142, in press, 2018.
- [13] F. Brue, C. A. Davy, F. Skoczylas, N. Burlion, X. Bourbon, Effect of temperature on the water retention properties of two high performance concretes, *Cem Concr Res*, **42** (2012) 384-396.
- [14] Chen W., Liu J., Brue F., Skoczylas F., Davy C. A., Bourbon X., Talandier J., Water retention and gas relative permeability of two industrial concretes, *Cem Concr Res*, **42** (2012) 1001-1013.
- [15] F. Brue, C. A. Davy, N. Burlion, F. Skoczylas, X. Bourbon, Five year drying of high performance concretes: effect of temperature and cement-type on shrinkage, *Cem Concr Res*, **99** (2017) 70-85.
- [16] C. A. Davy, F. Skoczylas, J.-D. Barnichon, P. Lebon, Permeability of macro-cracked argillite under confinement: gas and water testing, *Phys Chem Earth*, **32** (2007) 667-680.
- [17] Provis J. L., Myers R. J., White C. E., Rose V., van Deventer J. S. J., X-ray microtomography shows pore structure and tortuosity in alkali-activated binders, *Cem Concr Res* **42** (2012) 855-864.

CHEMICAL AND MICROSTRUCTURAL CHARACTERISATION OF LIME AND LIME-METAKAOLIN PASTES WITH LINSEED OIL

C. Nunes (1), P. Mácová (1), D. Frankeová (1), R. Ševčík (1), and A. Viani (1)

(1) Institute of Theoretical and Applied Mechanics of the Czech Academy of Sciences, Czech Republic

Abstract

Linseed oil has been used since the Classical times as a water-repellent additive in lime mortars and other types of lime-based coatings to protect building structures exposed to severe weathering conditions, e.g., direct exposure to wind-driven rain. Recent studies have confirmed the potential of this environmentally-friendly additive in improving the durability of lime-based mortars. This study aims to investigate the effect of linseed oil on the microstructure of lime and lime-metakaolin pastes. The specimens were analyzed after a long period of curing in laboratory conditions. The results of thermal analysis, Fourier transform infrared spectroscopy, and powder X-ray powder diffraction (XRPD) demonstrated that linseed oil significantly hindered the carbonation reaction in both lime and lime-metakaolin pastes. Scanning electron microscopy analysis showed the presence of large hexagonal crystals of portlandite in the lime paste with linseed oil. The lime-metakaolin pastes exhibited common calcium silicate hydrates morphologies (fibres, flakes) and the paste with linseed oil exhibited a denser structure than the reference. This observation was in line with the results of XRPD quantitative phase analysis which indicated the double content of amorphous phases in the specimen with linseed oil in comparison with the reference. The results confirm previous indication that linseed oil can have a beneficial effect on the hardening reaction of lime-metakaolin by favoring hydration reactions to the detriment of carbonation under the curing conditions tested and/or by contributing to its stabilization.

Keywords: lime, metakaolin, linseed oil, carbonation, hydration

1. INTRODUCTION

The use of lime-based materials in the repair of historic structures is widely recommended by authorities and scientific institutions dealing with the conservation of cultural heritage, thanks to its well-established compatibility with masonry and coatings based on these materials. However, lime mortars and coatings produced nowadays do not usually achieve the higher performance of the ancient ones [1]. It is believed that the use of organic additives in the past

may have significantly improved the performance of lime-based materials [2]. However, there is little knowledge about the effect of traditional additives on the materials' microstructure, which will, in turn, influence its performance and durability. Likewise, there is a lack of knowledge about the reaction products resulting from mixing the binders with organic additives. The need for sustainable development is bringing attention to the use of materials from renewable natural resources. Linseed oil is a material with long usage tradition in buildings, either as a coating resin or as an additive in mortars and paints. Recent investigations have proved its potential to improve the durability of lime-based mortars by imparting water-repellent properties to the system [3], [4].

Vegetable oils consist predominantly of esters of glycerol and fatty acids (glycerides). Fatty acids are the part of the molecule which mainly determines the physical and chemical properties of the glycerides. The degree of saturation of the fatty acids, i.e., the number of conjugated double bonds between carbon atoms, determine its chemical reactivity. The main fatty acids present in linseed oil are rich in double bonds: linolenic acid with three double bonds (48-60%), linoleic acid with two double bonds (4-19%), and oleic acid with one double bond (14-24%) [5], which makes it highly chemically reactive. When mixed with lime and water, the fatty acids react with calcium hydroxide to form water-repellent calcium salts of fatty acids [3], [6].

The goal of this work is to study the effect of linseed oil on the microstructure and composition of lime and lime-metakaolin pastes. Metakaolin is a pozzolanic material which reacts with calcium hydroxide producing calcium silicate hydrates (CSH) and alumina-containing phases (CAH). It has been given vast importance thanks to its high pozzolanic activity but has been mainly studied in cementitious composites [7]. Combinations of lime with metakaolin have been recently studied with promising results [8]. Hence, metakaolin was selected as the pozzolanic material to use in this study.

2. EXPERIMENTAL

2.1 Materials and specimen preparation

Lime hydrate (class CL90), metakaolin produced from Czech clay shale [9], and raw linseed oil were used to prepare the pastes. The composition of the specimens is given in Table 1. The same water/binder ratio (1.06) was used to prepare the four types of pastes. Oil was added to the binder/oil ratio of 1:0.1, which corresponds to 9wt% of oil in relation to the binder. A higher amount of oil than what is usually recommended (1-3wt%) for preparing mortars with satisfactory durability against salt and frost cycles [3], [4], was used to maximize the microstructural changes and to try to identify calcium salts of fatty acids, which have not been detected in previous work. The consistency of the fresh pastes was determined according to ASTM C110 [10].

Lime and metakaolin were first hand-mixed in the dry state for 3 min. Linseed oil was mixed with the dry components in five stages, by adding increasing portions of binder to the vessel containing oil while mixing. In the first three stages mixing was performed with a mortar and pestle, whereas, in the last one, with a spoon. The dry mixes were then blended with water for 3 min.

The fresh pastes were cast into cylinders of 70 mm in diameter and 10 mm thick. The pastes were left for seven days in the moulds at 20°C and 90% relative humidity (RH) to facilitate demolding. After demolding, they were cured for 68 months over grid-lined shelves at 20°C,

60% RH, and 500 ppm of atmospheric CO₂. These conditions were selected based on the average environmental RH and temperature in the Czech Republic during the construction/repair activity period (April-September) and used to compare all paste types cured under the same conditions [15].

Table 1: Composition by weight and fresh consistency of the fresh paste.

Specimen	Materials	Ratio	Consistency (mm)
L	Lime	-	20 ±2
LO	Lime:Oil	1:0.1	16 ±3
LM	Lime:Metakaolin	0.75:0.25	21 ±3
LMO	Lime:Metakaolin:Oil	0.75:0.25:0.1	18 ±4

A film of fresh linseed oil was left exposed to air under the same conditions to study its composition with some of the analytical techniques described in the next section to help in the interpretation of the results obtained from the pastes. The curing room had no natural nor artificial light.

2.2 Methods of analysis

The wettability of the pastes was determined by measuring the contact angle of water drops with the surface of the pastes which was measured by pouring a water drop of $0.20 \pm 0.05 \mu\text{l}$ at ca. 50 mm distance from the surface. After 10s, a picture was taken and the angle determined with image analysis. The porosity and pore size distribution (PSD) of the samples was determined with mercury intrusion porosimetry (MIP) using two specimens of each type of paste. The hardening reaction was studied with thermogravimetry (TG) and the mineralogical composition with X-ray powder diffraction (XRPD) using the Rietveld method for the quantitative phase analysis (QPA). Amorphous quantification was obtained adopting the internal standard method. The molecular composition of the pastes was further studied with attenuated total reflection Fourier-transform infrared spectroscopy (ATR-FTIR). Images of the freshly broken surface of the pastes were analyzed with a scanning electron microscope (SEM).

3. RESULTS AND DISCUSSION

The measured contact angle of water drops with the surface of the pastes revealed their hydrophobicity as both measured angles were higher than 90°; LO measuring 125° and LMO measuring 123°. The reference pastes absorbed the water drop within 10s after contact.

The PSD curves determined with MIP are given in Fig. 1. Linseed oil promoted a relevant increment of the pore volume maxima of the lime paste (from ca. 0.60 to 1.10 μm) and porosity (from 49 to 58 %). The increment in the pore size and porosity is attributed to air entrapment during mixing resulting from the saponification reaction between lime and oil [4]. This phenomenon lead to the development of rounded macropores in the pastes (20-200 μm as observed under SEM and macroscopically). High-pressure injection of mercury can have caused microcracking in the matrix giving access to the macropores through the so-called 'ink bottle' effect; this would explain the significant increment in porosity.

In the case of the lime-metakaolin system, the addition of oil slightly reduced the pore volume maxima (from ca. 0.77 to 0.73 μm) and porosity (from 61 to 58 %). In this case, the microstructure was probably not damaged during high-pressure Hg injection, so the closed macropores were not accessed by mercury thanks to the higher strength of the matrix granted by metakaolin. The reduction of the PSD and porosity with oil addition to lime-metakaolin is further explained along with the SEM observations.

Linseed oil retarded the carbonation reaction in both lime and lime-metakaolin pastes as shown by the results of TG (Fig. 2), XRPD (Fig. 3), and FTIR (Fig. 4). Even after 68 months of curing, the lime paste was still not completely carbonated. This fact can be due to the formation of a dense calcium carbonate skin on the surface of the specimen in the first stage of curing hence preventing the diffusion of CO_2 through the calcium hydroxide matrix or to premature drying, as proposed by Cizer [11].

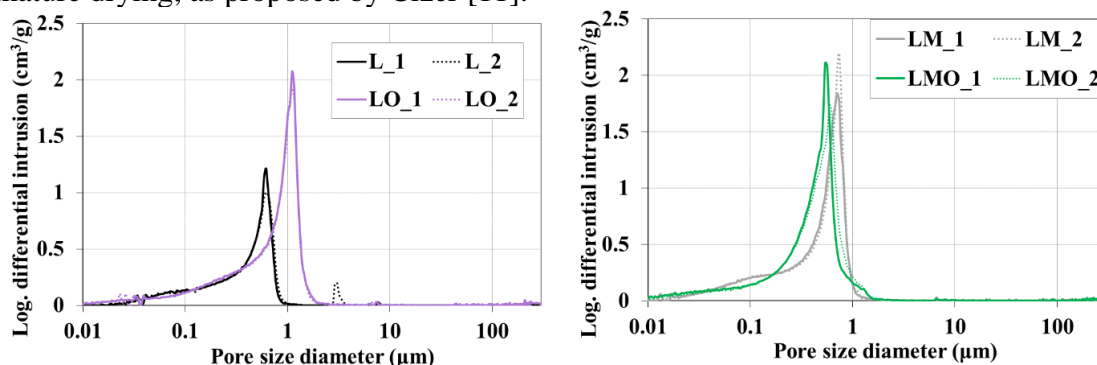


Figure 1: PSD curves of the pastes.

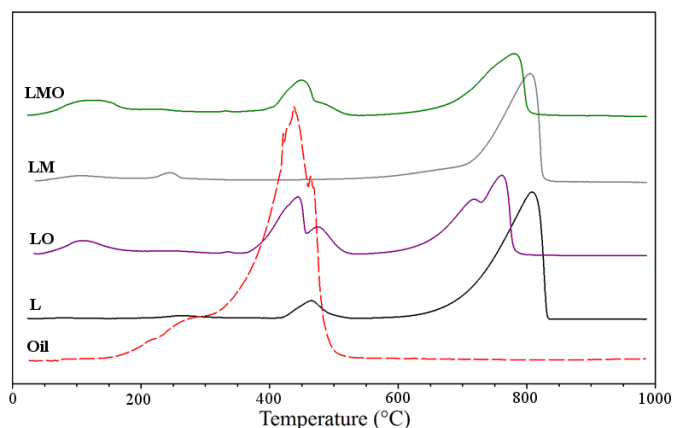


Figure 2: Derivative thermogravimetric curves of the pastes and polymerized oil

The weight loss detected by TG (Fig. 2) at ca. 450°C is attributed to $\text{Ca}(\text{OH})_2$ dehydroxylation and the weight loss at ca. 750°C is attributed to CaCO_3 decarbonation. In the pastes with oil, the decarbonation peak is slightly shifted to a lower temperature and, in LO paste, there is also a shoulder linked to the main peak. These thermogravimetric features could be attributed to the different size of the particles as seen under SEM (Fig. 5), but further analyses are needed to corroborate this hypothesis. The additional peak interlinked with the $\text{Ca}(\text{OH})_2$ dehydroxylation peak in the pastes with oil is attributed to the decomposition of the oil's fatty acids [16]. Both LO and LMO also show a broad peak around 150°C, which can be assigned to

the presence of amorphous hydrated calcium carbonate [11]; in LMO this band can also be attributed to hydration products (CSH and CAH) resulting from the pozzolanic reaction [11].

The results of XRPD showed that only two main crystalline phases are present in the pastes: calcite and portlandite. LM is the only paste which does not show the presence of portlandite, which, therefore is assumed to have been consumed in the carbonation reaction. A significant amount of amorphous phases was detected in the specimens with linseed oil, being more relevant in LMO paste.

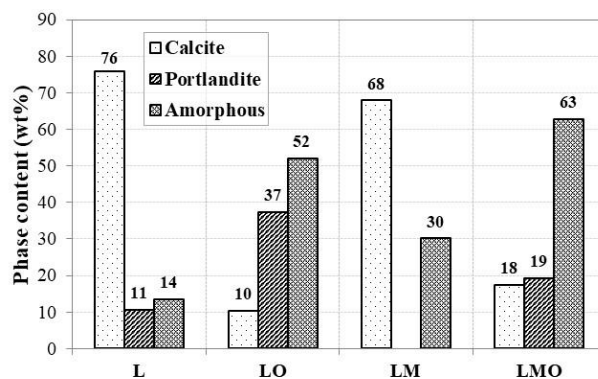


Figure 3: Results of the XRPD-QPA

The FTIR spectra (Fig. 4) confirmed the previous results regarding the progress of carbonation and pozzolanic reactions. The peak at 3641 cm^{-1} denotes the presence of portlandite (O-H) which has a higher intensity in LO compared to LMO, and significantly lower intensity compared to L, which is in line with the TG and XRPD results. The peaks at 1708 and 1732 cm^{-1} assigned to the C=O vibration in oil are absent in the pastes with oil, thus, indicating that oil reacted with the binder likely to form hydrophobic calcium salts of fatty acids, though these salts were not identified due to the low limit of detection of FTIR. To the authors' knowledge, these compounds have been only detected with XRPD and FTIR in lime and vegetable oil samples collected from ancient structures [12]. Also, for this reason, the testing pastes were cured for a long time.

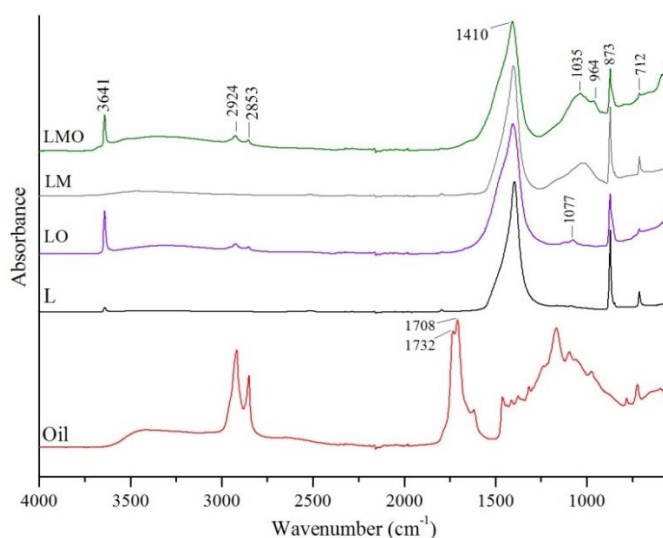


Figure 4: FTIR spectra of the pastes and polymerized oil

The results of TG, XRPD, and FTIR may help in explaining the difference in the PSD between L and LO (Fig. 1): linseed oil hinders the carbonation reaction, hence delaying the reduction of porosity and pore size [13]. The development of amorphous phases can also significantly contribute to the change in PSD. The slight reduction of the pore size distribution in LMO in relation with LM can be assigned to a higher amount of hydraulic phases, as suggested by the high amorphous content of LMO and by its morphology as observed under SEM.

Representative views of the freshly fractured surface of the pastes seen under SEM are given in Fig. 5. The lime paste is characterized by small grains of calcium carbonate and plate-like structures with irregular edges. A few portlandite hexagonal plate-like crystals were also observed sporadically. LO paste showed a less dense structure, and portlandite crystals (often showing sub-angular shape) were more abundant than in L paste and also showed larger size (up to ca. 10 μm) and thickness (ca. 1 μm). LM and LMO paste showed flakes and fibers, which are characteristic habits of hydration products (CSH and CAH) [11]. LM also showed grains and plates resembling those observed in L paste and which probably correspond to calcium carbonate. The latter was detected in a high amount with TG and XRPD. Fig. 6a shows the aspect of the rounded pores formed in the pastes with oil described previously.

LMO paste showed a denser structure than LM. A few cracks were observed in LM paste with visible aggregated rhombohedral calcite formed along the crack edges (Fig.6b) which explains its higher porosity and calcite content in comparison with LMO. This phenomenon is probably linked with the decalcification of hydration phases, further leading to shrinkage and decrease in strength [14]. The water-repellency imparted by linseed oil can contribute to moisture retention in the matrix thus hindering decalcification and shrinkage.

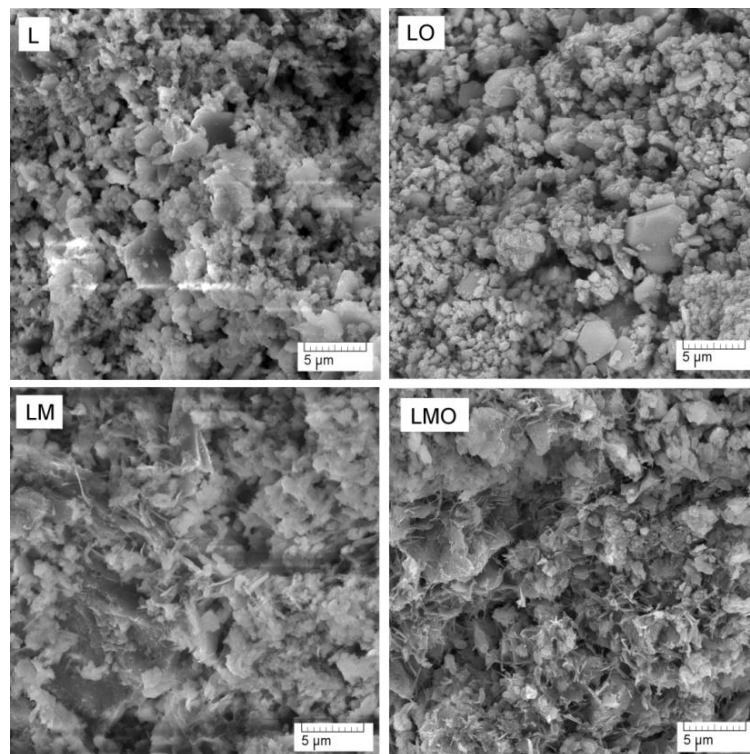


Figure 5: SEM photomicrographs of the pastes

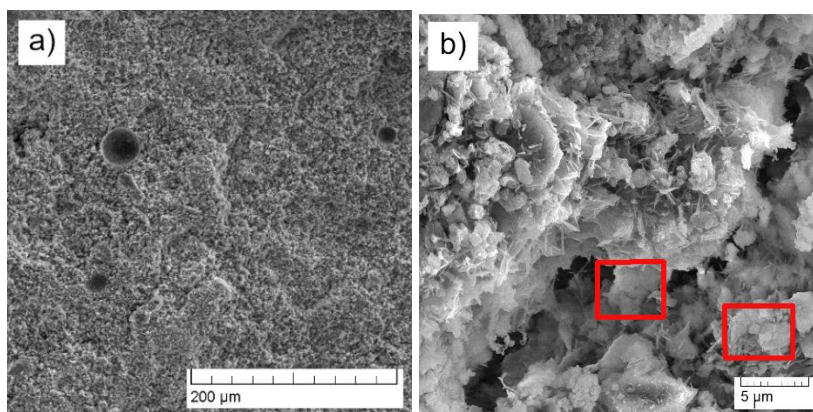


Figure 6: Aspect of the rounded pores developed in LMO (a) and aspect of a crack observed in LM paste under SEM with indication of rhombohedral calcite particles in red (b).

4. CONCLUSIONS

This work provides the microstructural characterization of lime and lime-metakaolin pastes and the influence of linseed oil addition. Paste specimens were analyzed after a long curing time under 20°C, 60% RH and studied with TG, FTIR, XRPD, and SEM. The main findings are summarized as follows:

- Linseed oil granted a similar degree of water-repellency to both lime and lime-metakaolin pastes.
- Oil promoted the development of rounded macropores as a result of air entrapment during the mixing of the fresh paste, attributed to the saponification reaction between oil and the binder.
- Linseed oil significantly hampered the carbonation reaction in both lime and lime-metakaolin pastes and promoted the formation of amorphous phases.
- The lime-metakaolin pastes exhibited common CSH morphologies, the paste with linseed oil exhibiting a denser structure than the reference. This observation was in line with the results of XRPD quantitative phase analysis which indicated the double content of amorphous phases in the specimen with linseed oil in comparison with the reference.

The results confirm previous indication that linseed oil can have a beneficial effect on the hardening reaction of lime-metakaolin by favoring hydration reactions to the detriment of carbonation under the curing conditions tested. For future work, further analysis of the specimens regarding the mechanical strength should be performed.

ACKNOWLEDGMENTS

This work has been supported by the Czech Science Foundation through the grant 18-28142S. P. Mácová, R. Ševčík, and A. Viani acknowledge support by the project No. LO1219 under the Ministry of Education, Youth and Sports, National sustainability programme I of the Czech Republic.

REFERENCES

- [1] Veiga R., 'Mortars in conservation' (in Portuguese), (LNEC, Lisbon, 2005).
- [2] Chandra S. and Ohama Y., 'Historical background of the use of natural polymers. Polymers in Concrete', Ch. 1 (CRC Press, Boca Raton, 1994).
- [3] Čechová E., 'The effect of linseed oil on the properties of lime-based restoration mortars', Ph.D. thesis (Università di Bologna, 2009).
- [4] Nunes, C. and Slížková, Z., 'Hydrophobic lime-based mortars with linseed oil: Characterization and durability assessment,' *Cem. Concr. Res.* 61–62 (2014) 28-39.
- [5] Mills J.S., and White R., 'Oils and fats.' In: 'The organic chemistry of museum objects', (Butterworth and Heinemann, Oxford, 1994).
- [6] Justnes H., Ostnor T.A., Barnils Vila N., 'Vegetable oils as water repellents for mortars', Proceedings of the First International Conference of Asian Concrete Federation, Chiang Mai, October, 2004 (Asian Concrete Federation) 689–698.
- [7] Siddique, R. and Klaus, J., 'Influence of metakaolin on the properties of mortar and concrete: A review', *Appl. Clay Sci.* 43 (3–4), (2009) 392–400.
- [8] Gameiro, A., Santos Silva, A, Veiga, R. and Velosa, A., 'Hydration products of lime–metakaolin pastes at ambient temperature with ageing', *Thermoch. Acta* 535 (2012) 36–41.
- [9] Vejmelková, E., Keppert, M., Rovnaníková, P., Keršner, Z. and Černý, R., 'Properties of lime composites containing a new type of pozzolana for the improvement of strength and durability', *Comp. Part B: Eng.* 43 (8) (2012) 3534–3540.
- [10] ASTM C110 – 16e1: Standard Test Methods for Physical Testing of Quicklime, Hydrated Lime, and Limestone, Ch. 5: Standard consistency of lime putty.
- [11] Cizer O., 'Competition Between Carbonation and Hydration on the Hardening of Calcium Hydroxide and Calcium Silicate Binders', PhD thesis (KU Leuven, 2009).
- [12] Fang S., Zhang H., Zhang B. and Li G., 'A study of Tung-oil-lime putty: a traditional lime-based mortar', *Int. J. Adhesion Adhesives* 48 (2014) 224–230.
- [13] Arandigoyen M., Bicer-Simsir B., Alvarez J.I., Lange D.A., 'Variation of microstructure with carbonation in lime and blended pastes', *Appl. Surf. Sci.* 252 (20) (2006) 7562–7571.
- [14] Chen J.J., Thomas J.J., Jennings H.M., 'Decalcification shrinkage of cement paste', *Cem. Concr. Res.* 36 (5) (2006) 801-809.
- [15] Data retrieved on 2018.9.17 from the website of the Czech Hydrometeorologic Institute: <http://portal.chmi.cz/>
- [16] Lazzari M., Chiantore O., 'Drying and oxidative degradation of linseed oil', *Polymer Degradation and Stability* 65 (1999) 303-313.

USE OF BIOMASS FLY ASH FOR THE PRODUCTION OF LOW ENERGY BLENDED CALCIUM SULFOALUMINATE CEMENTS

M. Marroccoli, M. De Biasi and A. Telesca

School of Engineering, Basilicata University, ITALY

Abstract

Ordinary Portland cement (OPC) manufacture accounts for about 7% of the global anthropogenic CO₂ emissions. This has pushed both cement producers and scientific community to develop new cementitious materials characterized by a production process with a reduced CO₂ generation.

In this regard, calcium sulfoaluminate (CSA) cements undoubtedly represent an important alternative to OPC; as matter of fact, their peculiar composition can be exploited not only for achieving considerable technical properties but also for giving a more pronounced environmentally friendly feature to their manufacturing process. However, in order to lower the high costs, mainly related to the use of bauxite in the clinker generating raw mix, and further reduce the amount of carbon dioxide associated with their production, CSA cements can be mixed with supplementary cementitious materials (SCMs) such as industrial wastes.

In this paper, biomass fly ash (BFA) was employed as SCM in CSA-blended cements; it was preliminarily washed in order to reduce its alkali content (WBFA). The effect of WBFA on both hydration properties and technical behaviour of different CSA blended cements was investigated by means of X-ray diffraction analysis, thermogravimetry and mercury intrusion porosimetry as well as shrinkage/expansion and compressive strength measurements.

Keywords: biomass fly ash, CO₂ emissions reduction, calcium sulfoaluminate-blended cements, hydration, mechanical behaviour.

1. INTRODUCTION

In 2016 the World cement production accounted for about 4.7 billion tons and the total CO₂ generation from cement plants reached almost 2.8 billion metric tons, representing more than 6% of the global anthropogenic carbon dioxide emissions [1, 2]. Over the last years many efforts have been made toward the manufacture of low-CO₂ cements [3]; they are hydraulic binders whose manufacture is associated with a reduced carbon footprint achievable through three main different approaches, namely 1) the use of a non-carbonated CaO source instead of limestone as a constituent of the Portland clinker-generating raw mix; 2) the increased

production of blended cements, obtained by mixing Portland clinker with significant amounts of supplementary cementitious materials (SCMs); 3) a larger use of special cements, namely hydraulic binders obtained from non-Portland clinkers [4]. In this regard, a considerable attention has been paid by researchers and engineers towards calcium sulfoaluminate (CSA) cements which have aroused the interest of the international cement research community for both their valuable technical properties and by virtue of the environmentally friendly features mainly related to their manufacturing process [5-9]. CSA cements contain C_4A_3S as main component and, depending on the synthesis temperature as well type and proportioning of raw materials, calcium sulfates, C_2S , C_4AF , C_5S_2 and various calcium aluminates. The most relevant technical properties of CSA cements (e.g. shrinkage compensation/self-stressing behaviour, good dimensional stability, high impermeability, rapid hardening) are mainly regulated by the formation of ettringite ($C_6A_3H_{32}$) generated by the hydration of calcium sulfate (belonging and/or added to CSA clinker) with C_4A_3S .

Moreover, compared to that of ordinary Portland cements (OPC), the manufacturing process of CSA binders is characterized by both lower synthesis temperatures ($<1350^\circ\text{C}$) and reduced limestone requirement ($<40\%$) which imply a decreased kiln fuel consumption as well as CO_2 emissions. In order to further decrease the CO_2 generation and cut the high costs (principally related to the use of bauxite in the clinker generating raw mix), CSA cements can be blended with SCMs [10-14].

The addition of biomass fly ash (BFA) to OPC is reported in several papers [15-19]). BFA commonly derives from the combustion process of wood, herbaceous biomass and agriculture wastes carried out in thermal power plants. Chemical and mineralogical composition of BFA mainly depend on the biomass characteristics and combustion technology; it is usually disposed in landfill [20] or employed in forest agricultural fields [21] thanks to its generally high alkali content.

In this paper, the possibility of using BFA, formerly submitted to an alkali reduction treatment by means of a water-washing process, as SCM for CSA blended-cements, was evaluated; these binders were subjected to physical-mechanical and hydration tests for curing times ranging from 4 hours to 56 days. X-ray diffraction (XRD) and thermogravimetric (TG) analyses as well as mercury intrusion porosimetry (MIP) were employed as main characterization techniques.

2. EXPERIMENTAL

2.1 Materials

The industrial CSA cement used in this investigation was kindly supplied by an Italian cement manufacturer. BFA come from the woodchips combustion carried out in a thermal power plant located in Basilicata Region (ITALY); the sample was collected from the baghouse filter.

The chemical composition of both materials, evaluated by means of X-ray fluorescence apparatus (BRUKER Explorer S4), is reported in Table 1; a BRUKER D2 PHASER diffractometer ($\text{CuK}\alpha$ radiation and $0.02^\circ 2\theta$ s^{-1} scanning rate) was employed for the identification of the main BFA and CSA cement phases. The Rietveld refinement (carried out through the TOPAS software, Table 1) was employed only for the quantitative mineralogical determination of the binder.

In order to strongly decrease the high amount of both Na₂O and K₂O, BFA was submitted to a water-washing treatment by using a tap water:BFA ratio equal to 10:1. The process was carried out with a magnetic stirrer at 1500 rpm for 2 hours at 20°C. The chemical composition of washed BFA (WBFA) is reported in Table 1 which also contains the specific gravity values (evaluated by means of a pycnometer) of all the investigated materials.

Table 1: Chemical, mineralogical composition (mass %) and physical properties (kg/m³) of the used binder components.

Chemical composition				Mineralogical phase composition		
	CSA cement	BFA	WBFA	CSA cement	ICDD ref. number	
CaO	44.58	40.09	42.20	Ye'elimite	30-0256	43.0
SiO ₂	8.95	26.30	27.68	β-belite	33-0302	21.7
Al ₂ O ₃	22.42	6.82	7.18	Celite	38-1429	3.8
Fe ₂ O ₃	1.86	3.04	3.20	Anhydrite	37-1496	19.1
TiO ₂	1.10	0.34	0.36	Calcite	05-0586	1.1
K ₂ O	0.30	7.38	3.62	Brownmillerite	30-0256	4.5
MnO	0.08	0.19	0.19	Gehlenite	73-2041	1.6
Na ₂ O	0.08	2.08	1.25	Others		5.2
MgO	0.94	3.09	4.20			
Cl	0.07	1.02	0.23			
SO ₃	16.85	2.07	2.18			
P ₂ O ₅	0.05	3.38	3.40			
LOI*	2.16	4.09	4.30			
Total	99.44	99.89	99.99	Total		100.0
Specific gravity	3.11	2.57	2.51			

*LOI=loss on ignition measured at 950±10°C

Analogously, WBFA was submitted to XRD analysis; both spectra and amorphous content of BFA and WBFA were evaluated by means of the EVA software

Three mixtures were investigated, namely: (a) 100% CSA cement (used as a reference term, CSAR); (b) two CSA blended cements (CSA10 and CSA20) respectively containing WBFA in concentrations equal to 10% and 20% by mass.

2.2 Measurements on mortars

Mortar prisms were prepared according to the European Standard EN 196-1 and cured after demolding under water at 20±1°C; they were submitted to compressive strength measurements at curing periods ranging from 4 hours to 56 days.

2.3 Measurements on pastes

Cement pastes were prepared with a 0.50 water/solid mass ratio, then cast into small plastic cylindrical molds and finally placed inside a thermostatic bath at 20°C. At the end of each aging period, the cylinders were broken in half: one part was tested with MIP, the other pulverized (grain size <63µm) for TG (Netzsch Tasc TG/SDTA 414/3 apparatus operating in the temperature ranges 20°–1000°C, with a heating rate of 10°C/min) and XRD analyses.

Specimens were treated with acetone (to stop hydration) and diethyl ether (to remove water); subsequently, they were stored in a desiccator containing silica gel-soda lime (to ensure protection against H₂O and CO₂). TG and XRD tests were carried out on samples cured from 4 hours up to 56 days.

The MIP (Thermo-Finnigan Pascal 240 and 140 Series porosimeters) measurements were conducted on samples cured from 4 h up to 56 days.

For the expansion–shrinkage measurements, eight paste samples, shaped as small prisms (15X15X78 mm), were air cured at 20°C for 4 hours and then demolded. One set of samples was then aged at 20°C under tap water, the other stored in a humidity (H) chamber at 50% R.H. and 20°C. The length changes were determined as average values of four measurements with a caliper accurate to ±1 µm; the reference length for them was that evaluated just after demolding [6-7].

3. RESULTS AND DISCUSSION

CSA cement contained ye'elimitite (43.0 mass-%), belite, brownmillerite, celite and gehlenite; moreover, CaSO₄, mainly deriving from the addition of natural anhydrite, was also present.

The BFA chemical composition data revealed that CaO (40.09 mass-%) and SiO₂ (26.30 mass-%) were the main oxides (“high-calcium biomass fly-ash”); it was also rich in alkalis (Na₂O_{eq}=6.95 mass-%), especially in K₂O (7.38 mass-%), and contained quite low amounts of sulphates (2.07 mass-%) and chlorides (1.02 mass %). After the water treatment, WBFA contained a much lower alkalis content (Na₂O_{eq}=3.64 mass %). Moreover, quartz, mullite, hematite and free CaO were the main detected crystalline phases of both BFA and WBFA whose amorphous content was respectively equal to 45% and 48%.

The specific surfaces of both CSA and WBFA (measured according to EN 196-6) were comprised in the ranges 4500±50 and 4800±50 cm²/g, respectively.

Table 2 reports the compressive strength development of CSA-based mortars as a function of curing time; at all the investigated periods, the compressive strength of CSAR and CSA10 based-mortars were almost similar to each other; on the contrary, the compressive strength of CSA20 is higher after 4 hours of hydration, almost equal after 1 day and constantly lower of about 8% at longer curing periods.

Table 2: Results of compressive strength measurements of CSAR, CSA10 and CSA20 at various aging periods.

Days	CSAR	CSA10	CSA20
0.17	28.1±0.2	28.6±0.4	31.2±0.2
1	45.7±0.4	44.7±0.5	45.3±0.3
2	52.1±0.3	51.9±0.2	48.0±0.5
7	57.4±0.2	58.0±0.6	54.0±0.5
14	58.9±0.1	57.7±0.3	55.7±0.8
28	60.6±0.5	60.3±0.1	55.9±0.7
56	62.4±0.7	61.3±0.5	56.3±0.8

The compressive strength results refer to three prisms (six determinations)

The results of the expansion–shrinkage tests are illustrated in Figure 1. They indicate that CSA10 and CSA20 differed very little from CSAR, both when submerged under water and cured in air. In particular, under water the maximum expansion values, reached after about 14 days of curing, are comprised in the narrow range of 0.06-0.19%. When cured in air, the investigated pastes show a continuous shrinkage till 14 days when a minimum length change is reached (-0.17%, -0.15% and -0.13% for CSAR, CSA10 and CSA 20, respectively); since that period the values remain constant for the three investigated systems.

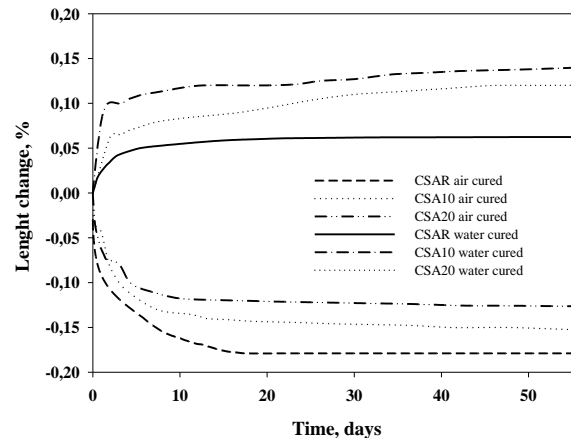


Figure 1: Dimensional stability curves for CSA-based cements (air and water cured).

Figure 2 shows the differential TG results for CSA, CSA10 and CSA20 cured at 4 hours and 1, 7, 28, 56 days. On the basis of the scientific literature data [18], the following phases (in the order of increasing temperature of the related endothermal effect) were attributed: calcium silicate hydrate (CSH), ettringite (E) and aluminium hydroxide (AH).

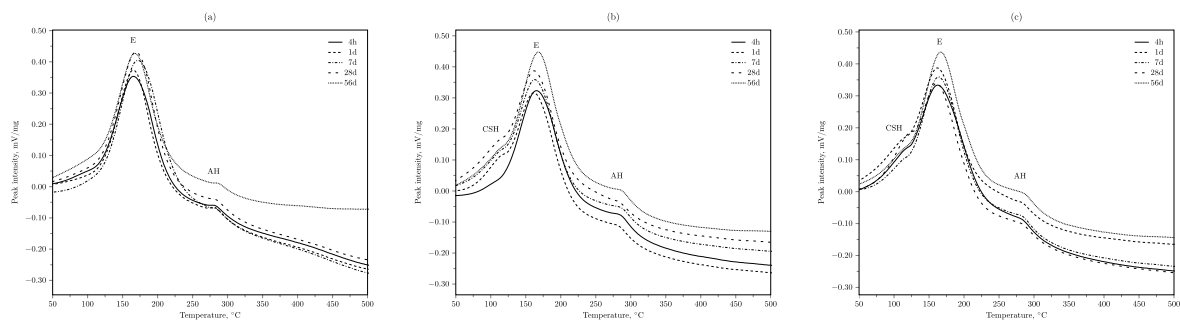


Figure 2: Differential TG results for CSAR (a), CSA10 (b) and CSA20 (c) hydrated for 4 hours, 1, 7, 28, 56 days. Legend to symbols: CSH=calcium silicate hydrate; E=ettringite; AH=aluminium hydroxide.

With the exception of the peak related to CaCO_3 present in WBFA, no significant effects were recorded by TG analysis above 500°C . From an overall examination of the obtained results it can be argued that:

- E and AH are detected in the three systems already after 4 hours of hydration;
- the presence of CSH was observed only in the systems containing WBFA due to the hydration of reactive CaO and SiO_2 belonging to the biomass ash.

On the whole, the TG results indicate that the hydration behaviour of CSAR is basically regulated by the ye’elinite reaction with calcium sulfate alone, while that of CSA10 and CSA20 is also related to the self-cementing properties exhibited by WBFA reactive components. XRD results confirm the indications obtained from TG analyses; in fact, as far as the hydration products are concerned, together with ettringite, no- and very weak-signals for CSH and AH were observed respectively due to the absence and poor crystallinity of the two phases.

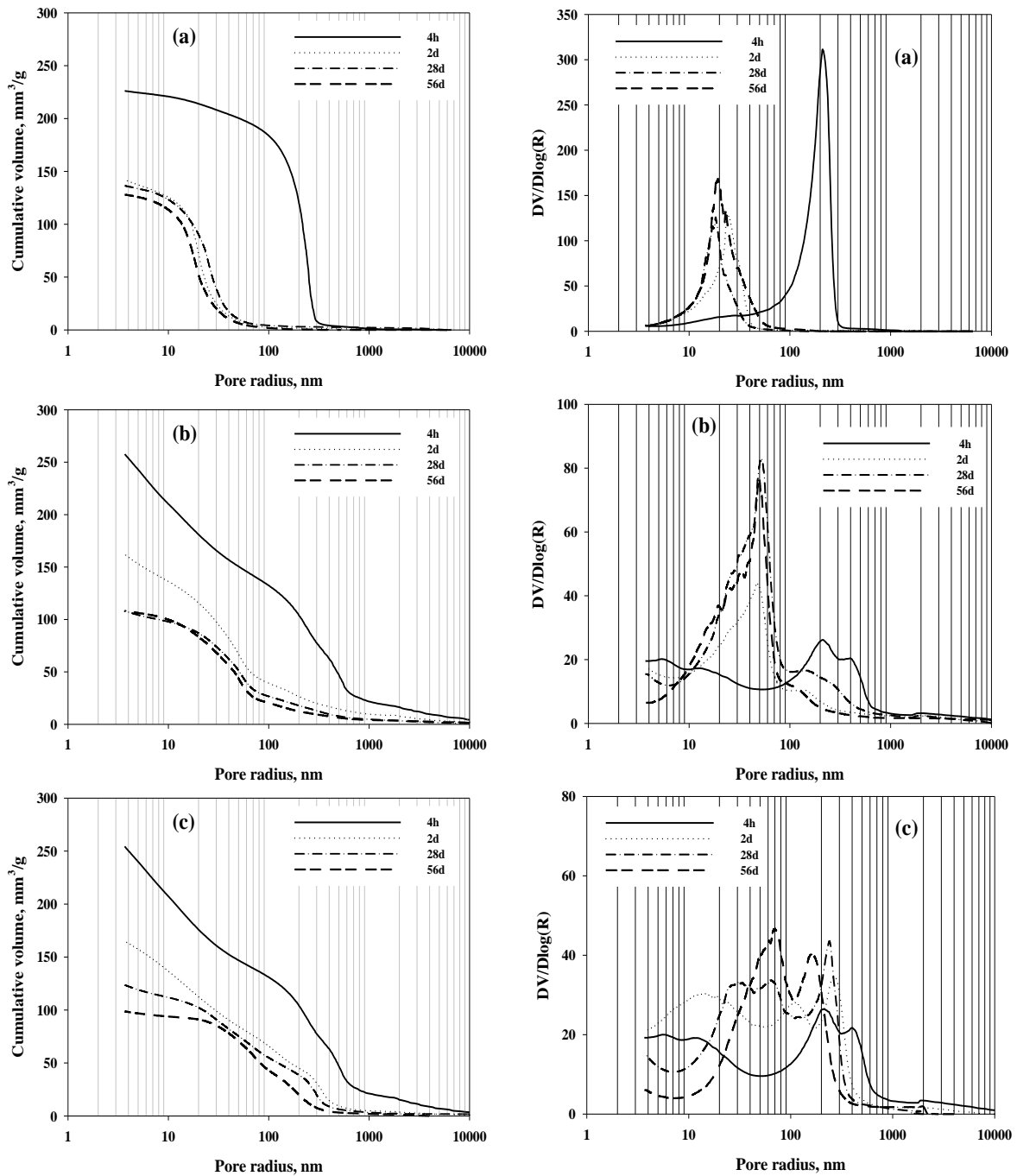


Figure 3 : Cumulative (left) and derivative (right) Hg volume vs. pore radius for CSAR (a), CSA10 (b) and CSA20 (c) cement pastes cured at 4 hours and 2–28–56 days.

The WBFA hydraulic activity does not influence the mechanical properties of CSA10, while only a low decrease (about 8%) of the compressive strength is shown when 20% of biomass ash was added to CSA cement; these results are confirmed by MIP investigations.

As already established, increased curing time give rise to both lower total porosity and threshold pore width [9]. Figure 3 reports the porosimetric curves for the pastes of the three investigated systems; in particular, the left and the right part of the Figure respectively show the cumulative and derivative plots for intruded Hg volume of CSA-based cements vs. pore radius at various curing times (4 hours and 2-28-56 days). For CSAR (Figure 3 (a)), the differential curves display a sharply peak at all the curing periods, indicating a unimodal pore size distribution centred on the lowest width of pore necks connecting a continuous system [6]. In particular, as curing time increases, both cumulative pore volume and threshold pore width decrease from 225 to 120 mm³/g and from about 210 to 20 nm. Compared to CSAR, both WBFA-based cements exhibit a different behaviour: a multimodal pore size distribution, already present after 4 hours of hydration, is shown at all the investigated curing times. For CSA10, due to high reaction rate, the cumulative pore volume reduces of about 37% (from 258 to 162 mm³/g) from 4 hours to 2 days, while at longer curing times it reaches an almost constant value (about 108 mm³/g); likewise, at the earliest and longest curing times, the first and the last thresholds pore widths respectively range from 400 to 118 nm and from 5 to less than 3.6 nm. These porosimetric features are also observed for CSA20 system.

4. CONCLUSIONS

The results reported in this paper highlight that biomass fly ash (duly water treated, WBFA, carried out for the reduction of its alkali content) represents a very interesting waste inasmuch as its utilization as secondary cementitious material (SCM) in calcium sulfoaluminate (CSA) cements, allows the saving of raw materials as well as the clinker dilution; this implies a CO₂ emissions reduction together with a noticeable energy saving per unit mass of cement.

In terms of phase composition, WBFA contains reactive components (based on calcium, silicon and aluminum) which, when mixed with water, display self-cementitious properties thanks to the development of calcium silicate hydrate. It has been found that the use of WBFA (as CSA cement substitute up to 20% by mass) does not significantly influence both mortars compressive mechanical strength and pastes dimensional stability. In addition, by following the hydration behaviour through mercury intrusion porosimetry, thermal and diffractometric analyses, similarities were shown by the two CSA-blended cements when compared to the plain CSA cement.

REFERENCES

- [1] Activity Report 2016, The European Cement Association, 2017 (<http://www.cembureau.be/>).
- [2] Habert, G., 'Environmental impact of Portland cement production', in Woodhead Publishing Series in Civil and Structural Engineering (Eco-efficiency of Portland Cement Concrete, Cambridge, UK, 2013) 3–25.
- [3] Gartner, E., Hirao, H., 'A review of alternative approaches to the reduction of CO₂ emissions associated with the manufacture of the binder phase in concrete', *Cem. Concr. Res.* **78** (2015) 126–142.
- [4] Telesca, A., Marroccoli, M., Tomasulo, M., Valenti, G.L., Dieter, H., Montagnaro, F., 'Low-CO₂ Cements from Fluidized Bed Process Wastes and Other Industrial By-Products', *Comb. Sci. Tech.* **188**(4–5) (2016) 492–503.

- [5] Telesca, A., Marroccoli, M., Tomasulo, M., Valenti, G.L., Dieter, H., Montagnaro, F., ‘Calcium looping spent sorbent as a limestone replacement in the manufacture of Portland and calcium sulfoaluminate cements’ *Env. Sci. Tech.* **49** (2015) 6865–6871.
- [6] Telesca, A., Marroccoli, M., Pace, M.L., Tomasulo, M., Valenti, G.L., Monteiro, P.J.M., ‘A hydration study of various calcium sulfoaluminate cements’, *Cem. Concr. Comp.* **53** (2014) 224–232.
- [7] Valenti, G.L., Marroccoli, M., Pace, M.L., Telesca, A., ‘Discussion of the paper “Understanding expansion in calcium sulfoaluminate–belite cements’ by I.A. Chen et al.’, *Cem. Concr. Res.*, **42** (2012) 1555-1559.
- [8] Marroccoli, M., Pace, M.L., Telesca, A., Valenti, G.L., Montagnaro, F., ‘Utilization of coal combustion ashes for the synthesis of ordinary and special cements’, *Comb. Sci. Tech.* **182** (2010) 588–599.
- [9] Bernardo, G., Telesca, A., Valenti, G.L., ‘A porosimetric study of calcium sulfoaluminate cement pastes cured at early ages’, *Cem. Concr. Res.* **36** (2006) 1042–1047.
- [10] Lukas, H.J., Winnefeld, F., Tschopp, E., Müller, C.J., Lothenbach, B., ‘Influence of fly ash on the hydration of calcium sulfoaluminate cement’, *Cem. Concr. Res.* **95** (2017) 152-163.
- [11] Hargis, C.W. Telesca, A., Monteiro, P.J.M., ‘Calcium sulfoaluminate (Ye’elimite) hydration in the presence of gypsum, calcite, and vaterite’, *Cem. Concr. Res.* **65** (2014) 15–20.
- [12] Martin, L.H.J., Winnefeld, F., Müller, C.J., Lothenbach, B., ‘Contribution of limestone to the hydration of calcium sulfoaluminate cement’, *Cem. Concr. Compos.* **62** (2015) 204–211.
- [13] Garcia-Mate, M., De la Torre, A.G., Leon-Reina, L., Aranda, M.A.G., Santacruz, I., ‘Hydration studies of calcium sulfoaluminate cements blended with fly ash’, *Cem. Concr. Res.* **54** (2013) 12–20.
- [14] Pelletier-Chaignat, L., Winnefeld, F., Lothenbach, B., Müller, C.J., ‘Beneficial use of limestone filler with calcium sulfoaluminate cement’, *Constr. Build. Mater.* **26** (2012) 619-627.
- [15] Tosti, L., van Zomeren, A., Pels, J.R., Comans, R.N.J., ‘Technical and environmental performance of lower carbon footprint cement mortars containing biomass fly ash as a secondary cementitious material’, *Res. Cons. Rec.* **134** (2018) 25–33.
- [16] Berra, M., Mangialardi, T., Paolini, A.E., ‘Reuse of woody biomass fly ash in cement-based materials’, *Constr. Build. Mater.* **76** (2015) 286–296.
- [17] Rajamma, R., Senff, L., Ribeiro, M.J., Labrincha, J.A., Ball, R.J., Allen, G.C., Ferreira, V.M., ‘Biomass fly ash effect on fresh and hardened state properties of cement-based materials’, *Comp. P. B* **77** (2015) 1–9.
- [18] Rajamma, R.J.B.R., ‘Characterisation and use of biomass fly ash in cement-based materials’, *J. Hazard. Mater.* **172** (2009), 1049–1060.
- [19] Siddique, R., ‘Utilization of wood ash in concrete manufacturing’, *Res. Cons. Rec.* **67** (2012) 27–33.
- [20] van Eijk, R.J., Obernberger, I., Supancic, K., ‘Options for increased utilization of ash from biomass combustion and co-firing (No. 30102040- PGR/R& E 11-2142)’, IEA Bioenergy Task 32. (2012).
- [21] Kwapinski W, Byrne CMP, Kryachko E, Wolfram P, Adley C, Leahy JJ, Novotny, E.H., Hayes, M.H.B., ‘Biochar from biomass and waste’, *Waste Biomass Valoriz.* **1** (2010) 77–89.
- [22] Taylor, H.F.W., ‘Cement Chemistry’, 2nd Edn. (Thomas Telford, London, 1997).

A PRELIMINARY STUDY OF THERMODYNAMIC MODELLING OF CALCIUM SULFOALUMINATE CEMENT-BASED MATERIAL

Yoon, H.N. (1), Park, S.M. (1), Kil, T.G. (1) and Lee, H.K. (1)

(1) Department of Civil and Environmental Engineering, Korea Advanced Institute of Science and Technology (KAIST), South Korea

Abstract

Ordinary Portland cement (OPC) is the most commonly used construction material, however, it produces a lot of CO₂ during its manufacturing process [1,2]. Calcium sulfoaluminate (CSA) cement has been attracted attention due to its reduced CO₂ footprint during the production, in comparison with that of OPC [2,3]. The production, hydration process, characteristics, and physicochemical properties of CSA cement have been widely investigated, while their durability aspects has still to be revealed. In this regard, this paper provides an overview on the current understanding and perspectives of the durability of CSA cement-based material. In addition, a preliminary study on thermodynamic modelling of the phase development of CSA cement blended with slag was investigated. The preliminary study indicated that the replacement of slag affected the formation of ettringite, monosulfate, aluminium hydroxide, and strätlingite of CSA cement-based materials. The volume of ettringite, monosulfate, and aluminium hydroxide decrease as the replacement of slag content increases. In the future research, the experiments on the chemical reactions of CSA cement blended with slag will be conducted and will be compared to results of the thermodynamic modelling.

Keywords: Calcium sulfoaluminate cement, Blast furnace slag, Thermodynamic modelling

1. INTRODUCTION

Ordinary Portland cement (OPC) is the most commonly used construction material in the World; however, a significant amount of CO₂ is generated during its production [1,2]. On a global scale, OPC accounts for about 29% of industrial CO₂ emissions, corresponding to 5-8% of the total anthropogenic CO₂ emissions [2,7]. For this reason, several methods for reducing CO₂ emissions were explored for the production of environmentally friendly binders, such as blended cements (by using supplementary cementitious materials) and alternative cementitious materials (e.g. alkali-activated materials) [2].

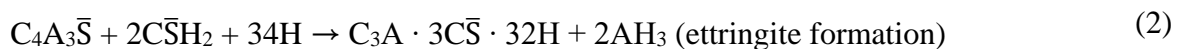
Calcium sulfoaluminate (CSA) cement has received attention due to its reduced CO₂ footprint during manufacturing process, in comparison with that of OPC [2,3]. CSA cement can be produced by sintering raw materials such as natural gypsum, limestone, and bauxite at a temperature of about 1250 °C, which is about 200 °C lower than that related to the synthesis of OPC clinker [2,8]. In addition, production of CSA cement requires less amount of limestone input (~60% less than OPC) and requires lower grinding energy [17], hence CO₂ footprint and energy associated with the production can be vastly lowered.

CSA clinkers are mainly composed by ye'elimite and generally together with belite, calcium sulfate, and calcium aluminoferrite as well as other minor components [4]. The CSA cement is manufactured by incorporating calcium sulfate (as gypsum or anhydrite) to the CSA clinker [9]. The main hydration products of CSA cement are ettringite and aluminium hydroxide while monosulfate is produced when calcium sulfate is depleted [4]. Based on these characteristics CSA cement can be an alternative to the traditional cements, and can contribute to reduce the CO₂ footprint.

Meanwhile, understanding of external factors such as chloride and carbonation, which cause deterioration of cement-based material, is important for preventing deterioration of cement-based material and maintaining its structural integrity [5]. The production, hydration process, characteristics, and physicochemical properties of CSA cement have been widely investigated, while their durability aspects has still to be revealed. In this regard, this paper provides an overview on the current understanding and perspectives of the durability of CSA cement-based material. In addition, a preliminary study on thermodynamic modelling of the phase development of CSA cement blended with slag conducted by the authors to investigate the influence of slag on the chemical reaction of CSA cement-based material is summarized.

2. LITERATURE REVIEW

Generally, CSA cement contains calcium sulfoaluminate (i.e., ye'elimite (4CaO·3Al₂O₃·SO₃)) of over 50 wt% [9]. According to Eqs. (1) and (2), the main hydration products of CSA cement are monosulfate and amorphous aluminium hydroxide; ettringite is produced depending on the presence of sulfate source [2,9].



Note that the following notations are used in Eqs. (1) and (2) to denote the chemical oxides: CaO as C; Al₂O₃ as A; SiO₂ as S; SO₃ as \bar{S} ; and H₂O as H. Other hydration products such as C-S-H phases, strätlingite, monocarboaluminate may be produced depending on the minor components in CSA cement as well as their reactivity [4,10,11]. As CSA cement reacts faster than OPC, most of the hydration heat is related during the first 12 h of curing [2]. For this reason, CSA cement has short setting time and high early-age strength and its development of strength and volume stability significantly rely on the amount of addition of the calcium sulfate [3,4].

Meanwhile, the two main factors, (1) carbonation and (2) chloride ions can be the most critical aspects for the durability of concrete, since these factors can destroy the passivation layer of steel reinforcement bars and accelerate the corrosion of the steel [12]. Therefore,

understanding of external factors such as chloride and carbonation is important for preventing deterioration of cement-based material, and several studies on the carbonation characteristics and chloride ingress of CSA cement were carried out.

A previous study on the carbonation characteristics of CSA mortars as a function of w/c ratios and anhydrite contents showed that the carbonation of CSA mortar occurred at a much faster rate than that of OPC mortar [13]. In particular, the carbonation rate of CSA mortar was affected by w/c ratio and content of anhydrite and decreased with decreasing w/c ratio and intermediate anhydrite content [13]. Moreover, these results indicated that reaction kinetics of ye'elimite is significantly affected by w/c ratio and anhydrite content of the CSA mortar [13]. The corrosion resistance of steel embedded in the CSA-based binder was also investigated; it has been observed that the corrosion rate of steel in CSA concrete was lower than that in OPC concrete [14].

A study of chloride ingress in the CSA cement matrix showed that chloride binding capacity of high sulfate CSA pastes indicated negligible binding potential at low chloride concentrations [15]. At high chloride concentration, the chloride binding capacity of CSA pastes was inversely proportional to the total content of calcium sulfate, concluding that CSA cement can be utilized for the concrete construction industry in chloride environments [15].

By-product materials (e.g., fly ash and blast furnace slag) are widely used for supplementary cementitious materials to enhance the performance of OPC-based materials, and can effectively enhance the various properties of OPC-based materials. There have been several attempts to enhance the performance of CSA cement-based materials using the supplementary cementitious materials [3,4]. These studies showed that the addition of fly ash in the CSA cement can increase the mechanical properties of CSA cement-blended with fly ash, and indicating that using the CSA cement with fly ash has economic and environmental benefits [3,4]. However, only few efforts were given to investigate the influence of blast furnace slag on the chemical reaction of CSA cement-based materials.

3. THERMODYNAMIC MODELLING: A PRELIMINARY STUDY

The thermodynamic modelling of the phase development of CSA cement blended with slag was carried out to investigate the influence of slag on the chemical reaction of CSA cement-based materials. The chemical composition of CSA clinkers and blast furnace slag are shown in Table 1. M-value denotes the molar ratio of calcium sulfate to ye'elimite, and is often used as an indicator for the degree of expansive behaviour with reference to the value [18]. CaSO₄ (anhydrous, 99% purity) was added to achieve the M-value of the binder to 0.75. Phase quantification was conducted by Rietveld refinement method, and results are shown in Table 2.

Table 1. Chemical composition by XRF of CSA clinkers and slag used in this study

(wt%)	CaO	SiO ₂	Al ₂ O ₃	MgO	Na ₂ O	K ₂ O	SO ₃	Fe ₂ O ₃	TiO ₂	Mn ₂ O ₃	SrO	LOI*
CSA clinkers	43.0	8.4	30.2	2.0	0.1	0.4	9.0	1.9	1.4	-	1.0	2.2
Slag	44.8	33.5	13.7	2.9	0.2	0.5	1.7	0.5	0.5	0.2	0.1	1.4

*Loss on ignition, determined in accordance with ASTM C114

Table 2. Phase composition of CSA clinkers obtained by Rietveld refinements method

(wt%)	$C_4A_3\bar{S}$	C_2S	C_2A	CT	M	C_2AS
CSA clinkers	63.7	19.6	5.8	3.3	1.1	1.1

Thermodynamic modelling was carried out using the GEMS-Selektor software [16]. The phase assemblage was predicted using CEMDATA 18.01 database which contains various solid solution models including hydration products of Portland, calcium aluminate, calcium sulfoaluminate and blended cements, as well as of alkali-activated materials [16]. A reaction degree of slag after 28 days of curing was determined by ^{29}Si MAS NMR deconvolutions, and was 29%, 17% and 3% when the dosage of the slag was 30%, 50% and 70%, respectively. The water-to-binder ratio was fixed at 0.50 for all modelling.

The thermodynamic modelling of the phase development of CSA cement blended with slag as a function of the content of slag is shown in Fig. 1. In the case of the CSA cement without slag, main hydration products are predicted to be ettringite, monosulfate, aluminium hydroxide, strätlingite and a small amount of layered double hydroxides (LDH) phase after hydration reaction. As the slag content increases, the volume of strätlingite is predicted to increase gradually owing to the supply of Si source, reaching the maximum at about 30 wt% slag content, and then decreasing due to decrease of reaction degree of slag. On the other hand, the volume of ettringite, monosulfate, and aluminium hydroxide decrease as the replacement of slag content increases. The formation of CASH phase due to slag incorporation was not observed. As the slag content increases, the free water in the CSA cement-based materials increases, which lead to more porosity in the paste, therefore, lower strength to be predicted in the samples with more slag. The details of the modelling methods and experiments results will be presented.

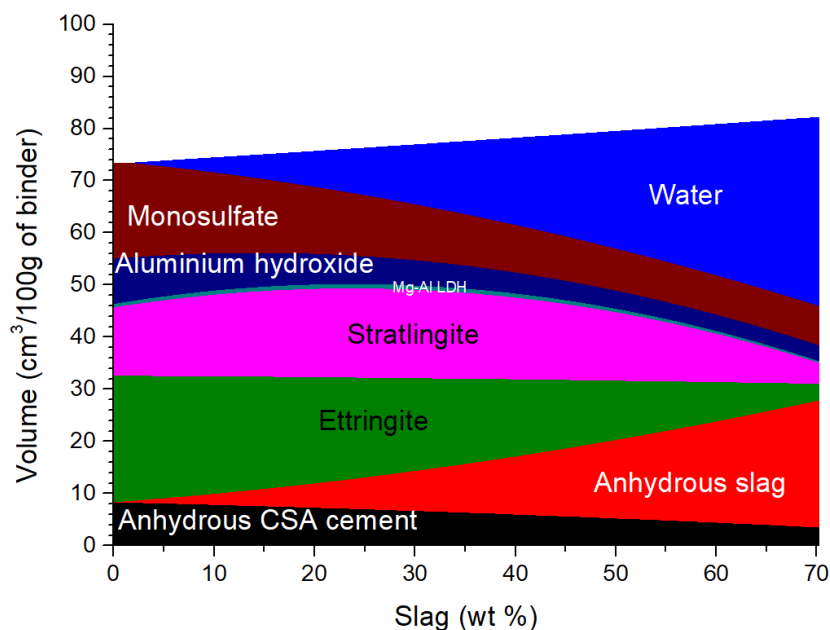


Fig. 1. Thermodynamic modelling of the phase development of CSA cement blended with slag as a function of the content of slag

4. CONCLUDING REMARKS

This paper provides an overview on the current understanding and perspectives of the durability of CSA cement-based materials. Based on these studies it can be said that CSA cement can potentially be an alternative to conventional cement, and it can contribute to reducing CO₂ footprint during the production. In addition, use of the supplementary cementitious materials such as fly ash can improve its mechanical properties, and provide both economic and environmental benefits. However, the effect of blast furnace slag, another supplementary cementitious material, on the chemical reaction of CSA cement-based materials has been rarely investigated in the relevant literature.

For this objectives, a preliminary study on thermodynamic modelling of the phase development of CSA cement blended with slag was briefly summarized. In conclusion, the preliminary study indicated that the replacement of slag affected the formation of ettringite, monosulfate, aluminium hydroxide, and strätlingite of CSA cement-based materials. In the future research, the experiments on the chemical reactions of CSA cement blended with slag will be conducted and will be compared to results of the thermodynamic modelling.

ACKNOWLEDGEMENTS

This study was supported by the National Research Foundation (NRF) of the Korean government (Ministry of Science & ICT) [Grant Number: 2017R1A5A1014883] through Smart Submerged Floating Tunnel System Research Center.

REFERENCES

- [1] Gartner, E., 'Industrially interesting approaches to "low-CO₂" cements', *Cem. Concr. Res.* **34**(9) (2004) 1489-1498.
- [2] Winnefeld, F., & Lothenbach, B., 'Hydration of calcium sulfoaluminate cements—experimental findings and thermodynamic modelling', *Cem. Concr. Res.* **40**(8) (2010) 1239-1247.
- [3] García-Maté, M., De la Torre, A. G., León-Reina, L., Aranda, M. A., & Santacruz, I., 'Hydration studies of calcium sulfoaluminate cements blended with fly ash', *Cem. Concr. Res.* **54** (2013) 12-20.
- [4] Martin, L. H., Winnefeld, F., Tschopp, E., Müller, C. J., & Lothenbach, B., 'Influence of fly ash on the hydration of calcium sulfoaluminate cement', *Cem. Concr. Res.* **95** (2017) 152-163.
- [5] Papadakis, V. G., 'Effect of supplementary cementing materials on concrete resistance against carbonation and chloride ingress', *Cem. Concr. Res.* **30**(2) (2000) 291-299.
- [6] D.A. Kulik, T. Wagner, S.V. Dmytrieva, G. Kosakowski, F.F. Hingerl, K.V. Chudnenko, U.R. Berner, 'GEM-Selektor geochemical modeling package: revised algorithm and GEMS3K numerical kernel for coupled simulation codes', *Comput. Geosci.* **17** (2013) 1-24.
- [7] Damtoft, J. S., Lukasik, J., Herfort, D., Sorrentino, D., & Gartner, E. M., 'Sustainable development and climate change initiatives', *Cem. Concr. Res.* **38**(2) (2008) 115-127.
- [8] Ali, M. M., Gopal, S., & Handoo, S. K., 'Studies on the formation kinetics of calcium sulphoaluminate', *Cem. Concr. Res.* **24**(4) (1994) 715-720.
- [9] García-Maté, M., Angeles, G., León-Reina, L., Losilla, E. R., Aranda, M. A., & Santacruz, I., 'Effect of calcium sulfate source on the hydration of calcium sulfoaluminate eco-cement', *Cem. Concr. Compos.* **55** (2015) 53-61.
- [10] Glasser, F. P., & Zhang, L., 'High-performance cement matrices based on calcium sulfoaluminate–belite compositions', *Cem. Concr. Res.* **31**(12) (2001) 1881-1886.

- [11] Zhang, L., & Glasser, F. P., 'Investigation of the microstructure and carbonation of CSA-based concretes removed from service', *Cem. Concr. Res.* **35**(12) (2005) 2252-2260.
- [12] Arbi, K., Nedeljković, M., Zuo, Y., and Ye, G., 'A review on the durability of alkali-activated fly ash/slag systems: advances, issues, and perspectives', *Ind. Engng. Chem. Res.* **55**(19) (2016) 5439-5453.
- [13] Hargis, C. W., Lothenbach, B., Müller, C. J., & Winnefeld, F., 'Carbonation of calcium sulfoaluminate mortars', *Cem. Concr. Compos.* **80** (2017) 123-134.
- [14] Carsana, M., Canonico, F., & Bertolini, L., 'Corrosion resistance of steel embedded in sulfoaluminate-based binders', *Cem. Concr. Compos.* **88** (2018) 211-219.
- [15] Jen, G., Stompinis, N., & Jones, R., 'Chloride ingress in a belite-calcium sulfoaluminate cement matrix', *Cem. Concr. Res.* **98** (2017) 130-135.
- [16] Lothenbach, B., Kulik, D., Matschei, T., Balonis, M., Baquerizo, L., Dilnesa, B.Z., Miron, D.G., Myers, R., 'Cemdata18: A chemical thermodynamic database for hydrated Portland cements and alkali-activated materials', *Cem. Concr. Res.* (2018), <https://doi.org/10.1016/j.cemconres.2018.04.018>
- [17] Telesca, A., Marroccoli, M., Tomasulo, M., Valenti, G. L., Dieter, H., & Montagnaro, F. (2015). Calcium looping spent sorbent as a limestone replacement in the manufacture of Portland and calcium sulfoaluminate cements. *Environmental science & technology*, 49(11), 6865-6871.
- [18] Winnefeld, F., Martin, L. H., Müller, C. J., & Lothenbach, B. (2017). Using gypsum to control hydration kinetics of CSA cements. *Construction and Building Materials*, 155, 154-163.

PROPERTIES OF ORDINARY PORTLAND CEMENT CLINKER WITH MUNICIPAL SOLID WASTE INCINERATION BOTTOM ASH AS RAW MEAL ADDITIVE

Aneeta M. Joseph (1,2), Stijn Matthys (1) and Nele De Belie (1)

(1) Magnel Laboratory for Concrete Research, Universiteit Gent, Belgium

(2) Strategic Initiative Materials (SIM vzw), project ASH-CEM within the program ‘MARES’, Technologiepark Zwijnaarde 935, Ghent B-9052, Belgium

Abstract

Around 1.3 billion tonnes of municipal solid wastes are generated all around the world and out of that around 10% is incinerated generating a vast amount of incineration residues [1]. In Belgium, around 400 kilo tonnes of bottom ash is generated, out of which only 102kT is utilised, mainly as aggregate and road subbase material. Environmental stipulations prevent utilisation of 0-2mm fraction due to exceedance of the leachability of Cu. Therefore this fraction cannot yet be reused. However, due to the mineral transformation in the cement kiln, by using as part of the cement raw meal, limited amounts of Cu can be incorporated into C_3S and C_4AF phases, and after cement hydration, can be bound in C-S-H phases. Also the chemical composition of bottom ash makes it suitable to be used in raw mix for clinker production. In this study, a clinker was produced with 5% bottom ash as an additive in the raw meal and was characterised for its mineralogy. The early age hydration kinetics were studied using isothermal calorimetry. These measurements show that the properties of clinker with bottom ash as part of the raw meal has comparable properties with that of conventional clinker.

Keywords: Municipal solid waste incineration bottom ash, cement clinker, Alternate fuel and raw materials (AFR), clinker mineralogy, isothermal calorimetry

1. INTRODUCTION

Cement industry, the major contributor to CO_2 emission and energy consumption, has been focusing on use of alternative fuels and raw materials since long. The main raw materials used are calcareous materials such as limestone which acts as source of calcium, argillaceous materials such as shale, sandstone etc. as source of silica and alumina, ferruginous materials such as iron ore to correct the iron content and other corrective materials to adjust the composition. Using alternative fuels contributes to energy recovery from waste materials and

reduces the need for primary (fossil) energy sources. Exploitation of by-products as alternative raw materials prevents them from going into landfills. The main types of wastes used as alternative fuels include waste oils, tyres, impregnated saw dust, plastic, industrial and household waste, meat and bone meal, agricultural waste, wood chips and other biomass, sewage sludge, refuse derived fuel etc. [3]. Alternative raw materials used include lime sludge from water treatment plants, calcium fluoride, used foundry sand, roasted pyrite, contaminated ore, dusts from steel plants, mill scale, blast furnace slag, fly ash, oil shale, trass, paper residuals, incineration ashes, oil contaminated soil, gypsum from flue gas desulphurisation, ceramic waste etc. The sustainability of production depends on a lot of factors, one of the important ones being transportation of materials. Hence, local solutions have the highest probability to be the most sustainable ones. Municipal solid waste incineration plants are widespread and the residues have a high potential to be used as corrective additions in cement raw meal. The parameters considered while formulating a raw mix and its effects on properties of cement are given below [4].

Lime Saturation Factor (LSF) – This is the ratio of lime (and MgO) present in the mix to the amount of lime required to react with silica, alumina and iron oxide. Excess lime leading to a LSF above 1 leads to undesirable free lime in the resulting clinker.

$$LSF = \frac{100 (CaO + 0.75 MgO)}{2.85SiO_2 + 1.18 Al_2O_3 + 0.65 Fe_2O_3} \quad (1)$$

Silica Ratio (SR) – The acceptable value of SR ranges from 1.9 to 3.2. A SR higher than the limit leads to very low burnability of the mix, and also very slow setting and hardening of cement.

$$SR = \frac{SiO_2}{Al_2O_3 + Fe_2O_3} \quad (2)$$

Alumina Ratio – The acceptable value of AR ranges from 1.0 to 4.0. Alumina ratio governs the ratio of aluminate to ferrite phases, and the liquid formed. The quantity of liquid formed, melt phase is maximum at AR of 1.38. [4]

$$AR = \frac{Al_2O_3}{Fe_2O_3} \quad (3)$$

Hydraulic Modulus (HM) - The prescribed value of hydraulic modulus is between 1.7 and 2.3. Mixes with higher HM show poor volume stability and those with lower HM show poor strength.

$$HM = \frac{CaO}{SiO_2 + Al_2O_3 + Fe_2O_3} \quad (4)$$

Cement is produced by sintering raw meal to approximately 1450°C. The main phases of cement formed are C₃S, C₂S, C₃A and C₄AF.

Based on the point of collection, the residues from incineration plants are classified as bottom ash, boiler ash and fly ash, out of which bottom ash constitutes about 85% of the whole residue. The composition of bottom ash is specific to the size fraction. The ash used in this study was collected from the grate furnace installation of Indaver in Doel, Belgium. The residues are sorted into different size fractions, >50mm, 6-50mm, 2-6mm and 0-2 mm. The fraction of

bottom ash between sizes 0 and 2 mm is used in this study and has the highest organic carbon content out of different bottom ash fractions from the incinerator. That makes it unsuitable to be used as supplementary cementitious material in cement. Another characteristic that makes it unsuitable is the presence of heavy metals such as Cu, Zn and Pb. Limited quantities of these heavy metals can be incorporated into cement phases. Presence of Cu above a threshold of 0.35% has the effect of decomposition of C_3S to C_2S and free lime [5]. Zn can be fixed in C_3S , C_3A and C_4AF . Its content up to 1% does not affect the stability of clinker phases. However, increased Zn content above a threshold of 0.7% causes retardation of hydration [6]. Further, Cu and Pb is fixed in C-S-H, the main phase in hydrated cement [7]. In this study, 0-2 mm fraction of bottom ash is used as a corrective agent in raw mix for clinker production, which is identified as an excellent opportunity to valorize this fraction.

2. MATERIALS AND METHODS

The raw materials used for making raw meal were limestone, shale, two types of bauxite, overburden limestone and bottom ash. For the bottom ash, the 0-2 mm fraction was used as a corrective agent and constituted 5% of the cement raw meal. The chemical composition of all the raw materials were determined by XRF. The milled raw materials were proportioned, and mixed into a slurry, which was then dried into pellets of 5 mm size. These pellets were sintered in a platinum crucible in a bottom loading furnace up to a temperature of 1500°C with a residence time of one hour, and then quenched by exposing suddenly in air to prevent C_3S decomposing back to C_2S and lime. The chemical composition of the raw materials and the percentage of each in the raw meal is shown in Table 1. The values of all the parameters for the raw mix used, raw meal-BA in present study are shown in Table 2.

Table 1 Chemical composition of raw mix, constituents and control CEM I 52.5N

Raw material	Limestone	Shale	Bauxite 1	Bauxite 2	Overburden limestone	BA 0/2	CEM I 52.5N
%	80.5	1	1	1.5	11	5	
CaO	86.42	1.87	0.96	5.32	5.56	18.90	63.00
SiO ₂	6.69	56.75	34.30	5.52	71.17	47.46	21.40
Al ₂ O ₃	1.34	22.59	33.21	60.12	11.67	10.75	5.00
Fe ₂ O ₃	1.17	9.02	26.30	25.04	4.97	11.65	2.46
MgO	2.64	2.15	1.20	0.31	2.13	1.61	2.17
Na ₂ O	0.10	0.80	0.17	0.00	1.10	3.18	nd
K ₂ O	0.21	3.74	0.06	0.18	2.35	1.84	0.41
SO ₃	0.10	1.02	0.00	0.44	0.07	2.00	4.64
TiO ₂	0.07	0.99	3.27	2.82	0.73	1.28	0.31
P ₂ O ₅	0.05	0.23	0.23	0.08	0.13	2.57	nd
MnO	0.21	0.30	0.24	0.06	0.10	0.15	0.20

Table 2 Parameters of raw mix (raw meal – BA)

LSF	1.03
SR	1.95
AR	1.62
HM	2.22

The obtained clinker was ground in isopropanol medium to preserve mineralogy of clinker and dried in air. Then, the ground clinker was mixed with zincite as internal standard and mineralogical examination was carried out with a thermo-scientific diffractometer with Cu-K α radiation, angular scan 5-70°C with a step size of 0.02, and the constituents were quantified by Rietveld analysis. The clinker was mixed with 3% gypsum and the resulting cement was mixed with water at a w/c ratio of 0.5. The heat of hydration of the cement paste was measured in a TAM Air isothermal calorimeter at 20°C.

3. RESULTS AND DISCUSSIONS

Table 3 shows the cement phase composition in commercial CEM I 52.5N and in the laboratory-made cement CEM I - BA. The laboratory preparation of clinker with BA0/2 yielded marginally higher C₃S and C₃A. It is difficult to make a real evaluation of the reasons, since the raw mix composition of the commercial cement is unknown. Figure 1 shows the hydration kinetics of cement from the laboratory mix CEM I –BA compared to commercial cement CEM I 52.5N. Presence of anhydrite content in commercial cement is due to the high temperature during grinding. In the laboratory mix, sulphate was added in form of gypsum and mixed by hand. In presence of anhydrite, early hydration of C₃A is lower. This, combined with higher aluminate content in the lab mix CEM I – BA may have resulted in the lower heat release during the induction period for commercial cement [8]. Figure 2 shows cumulative heat of hydration of both cements under study. The laboratory mix CEM I – BA shows a marginally higher cumulative heat release. It could be due to the higher C₃S and C₃A content, difference in fineness or also experimental error.

Table 3 Phase composition of commercial cement CEM I 52.5N and laboratory mix CEM I – BA

	CEM I 52.5N	CEM I - BA
C ₃ S	51.6	57.1
C ₂ S	20.8	13.8
C ₃ A	3.4	5.3
C ₄ AF	8.2	9.3
Gypsum	2.5	3
Anhydrite	2.1	-
Amorphous / Undetected	10.6	11.3

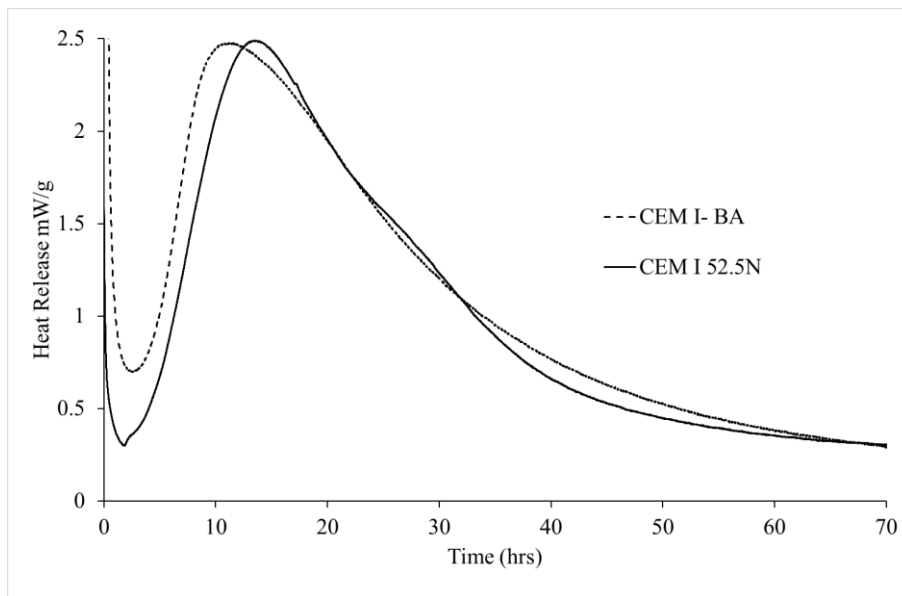


Figure 1 Heat of hydration of commercial cement CEM I 52.5N and CEM I – BA made in the laboratory

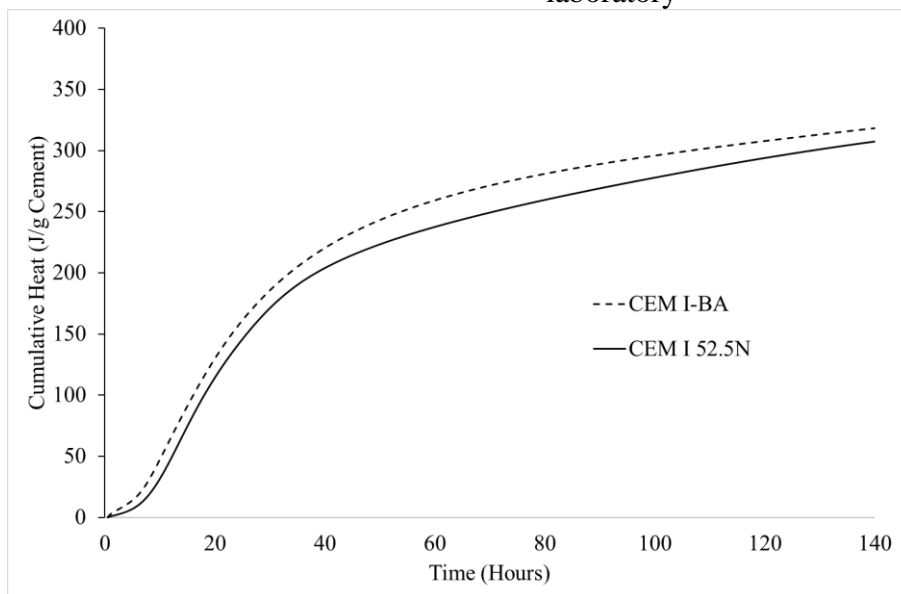


Figure 2 Cumulative heat of hydration of commercial cement CEM I 52.5N and clinker CEM I – BA made in the laboratory

4. CONCLUSIONS

- In this study, first feasibility tests validates the use of municipal solid waste incineration ash as a secondary raw material in the raw meal for clinker production.
- Clinker produced by replacement of 5% of raw meal generated clinker with comparable mineralogy and hydration kinetics as that of commercial cement.

- Higher heat release during the induction period for the lab cement CEM I – BA in comparison with the commercial cement could be attributed to the combined effect of lower C₃A content and higher anhydrite content in the commercial cement.

ACKNOWLEDGEMENTS

The authors are grateful to Indaver nv for the bottom ash and VVM for the cements required for research, and Mr. Joe Rice from Irish Cements for helping in mix formulation of raw meal. This research is a part of the ASHCEM project, which in itself is a part of the bigger program MaRes aimed at creating and demonstrating an operational, flexible toolbox to recover metals and valorize the residual matrix into building materials, funded by SIM (Strategic Initiative Materials in Flanders) and VLAIO (Flanders Innovation & Entrepreneurship). The financial support from the foundations for this study is gratefully appreciated.

REFERENCES

- [1] D. Hoornweg, P. Bhada-Tata, and A. Joshi-Ghani, “What a waste: A global review of solid waste management,” 2009.
- [2] E. C. Gentil, “Municipal waste management in Belgium,” 2013.
- [3] A. A. Uson, A. M. Lopez-Sabiron, G. Ferreira, and E. L. Sastresa, “Uses of alternative fuels and raw materials in the cement industry as sustainable waste management options,” *Renew. Sustain. Energy Rev.*, vol. 23, pp. 242–260, 2013.
- [4] H. F. W. Taylor, *Cement chemistry*. 1990.
- [5] N. Gineys, G. Aouad, F. Sorrentino, and D. Damidot, “Effect of the clinker composition on the threshold limits for Cu, Sn or Zn,” *Cem. Concr. Res.*, vol. 42, no. 8, pp. 1088–1093, 2012.
- [6] N. Gineys, G. Aouad, and D. Damidot, “Managing trace elements in Portland cement - Part II: Comparison of two methods to incorporate Zn in a cement,” *Cem. Concr. Compos.*, vol. 33, no. 6, pp. 629–636, 2011.
- [7] N. Gineys, G. Aouad, and D. Damidot, “Managing trace elements in Portland cement - Part I: Interactions between cement paste and heavy metals added during mixing as soluble salts,” *Cem. Concr. Compos.*, vol. 32, no. 8, pp. 563–570, 2010.
- [8] S. Pourchet, L. Regnaud, J. P. Perez, and A. Nonat, “Early C₃A hydration in the presence of different kinds of calcium sulfate,” *Cem. Concr. Res.*, vol. 39, no. 11, pp. 989–996, 2009.

International Conference on Sustainable Materials, Systems and Structures (SMSS 2019)

New Generation of Construction Materials

20-22 March 2019 – Rovinj, Croatia

NEW GENERATION OF CONSTRUCTION MATERIALS

SESSION 10: Novelties in SCMs

TERNARY BINDER MADE FROM COAL COMBUSTION PRODUCTS: MECHANICAL PROPERTIES AND MICROSTRUCTURE EVOLUTION

Vít Šmilauer (1), Rostislav Šulc (1), Pavel Reiterman (1), Petr Hlaváček (2), Martina Šídllová (3), František Škvára (3), Adéla Peterová (3), Roman Snop (4)

- (1) Czech Technical University in Prague, Faculty of Civil Engineering, Czech Republic
- (2) Bundesanstalt für Materialforschung und –prüfung (BAM), Berlin, Germany
- (3) Institute of Chemical Technology in Prague, Prague, Czech Republic
- (4) ČEZ Energetické produkty, s.r.o., Hostivice, Czech Republic

Abstract

Coal combustion products present industrially interesting source of aluminosilicate materials. Based on previous experience, a ternary binder is proposed, consisting of circulating fluidized bed combustion (CFBC) fly ash, conventional fly ash and $\text{Ca}(\text{OH})_2$ activator. The binder yields reasonable compressive strength of 32 MPa after 28 days of standard sealed curing and can be used for soil stabilization or concrete production.

Volumetric evolution of crystalline and amorphous phases during hydration were quantified using XRD analysis, differential thermal gravimetry, porosimetry and electron microscopy. A micromechanical model is applied to interpret the evolution of compressive strength due to the growing proportions of C-S-H and ettringite in the system. Long-term monitoring of the binder showed excellent volume stability and no detrimental expansion due to late ettringite formation.

Keywords: ternary binder, properties, microstructure, evolution, ettringite

1. INTRODUCTION

Circulating fluidized bed combustion (CFBC) is a widely used technique to reduce SO_2 and NO_x emissions in coal-burning thermal power plants. The sulphur-containing coal is burned together with limestone so that the SO_2 emissions are in-situ transformed to anhydrous CaSO_4 . Since the SO_2 is captured directly in the furnace, no wet scrubber of exhaust gases is needed to be installed separately and no waste gypsum is produced. The first CFBC boilers were installed in the 1970's able to process a wide range of fuel quality, high-moisture fuels or high-ash fuels [1].

Compared to conventional thermal power plants, where the combustion of pulverized coal runs under temperatures between 1200 and 1700°C, the CFBC boilers operate under temperatures around 850°C. The CFBC fly ash particles are therefore, on the contrary to the conventional fly ashes, unsintered and their reactivity is considerably higher. On the other hand, the CFBC fly ashes contain about 11% of free lime and about 13.5% of gypsum anhydrite causing delayed formation of Ca(OH)_2 , crystallization of ettringite and excessive expansion [2]. This prohibits addition of CFBC fly ashes to standard Portland-based cements and concretes and alternative utilizations are therefore sought.

To date, CFBC fly and bottom ashes have been used for geopolymer synthesis, production of autoclaved bricks, non-autoclaved aerated concretes, manufacturing of compressed earth bricks, and for preparation of self-cementing binders, see references in [4].

This paper aims at quantification of the phases formed during hydration of a CFBC fly ash-based ternary binder, followed with micromechanical prediction of compressive strength based on a multiscale model. A model of volumetric phase evolution during hydration is proposed, based on experimental data.

2. MATERIALS AND METHODS

CFBC fly ash from a circulating fluidized bed combustion power plant (d_{50} 36.3 μm , Blaine 603 m^2/kg) and conventional class F fly ash (FA) (d_{50} 44.9 μm , Blaine 484 m^2/kg) served as the raw materials. Commercially available calcium hydroxide is used as an alkali activator. Table 1 summarizes the chemical composition of the fly ashes.

Table 1: Chemical composition of conventional and CFBC fly ashes (wt. %).

	SiO ₂	Al ₂ O ₃	Fe ₂ O ₃	CaO	K ₂ O	TiO ₂	SO ₃
CFBC ash	31.4	26.2	4.9	21.9	0.4	5.5	8
Fly ash	52.4	35	5.1	1.8	2.1	1.5	0.2

All experiments were carried out at the level of paste. The mix composition was optimized for workability, maximal compressive strength at 28 days of curing and volumetric stability after an accelerated aging test (curing for an extra 28 days in 95°C water). The ratio between CFBC and conventional fly ash during the mixture optimization experiments varied from 0:1 to 1:0; the Ca(OH)_2 content remained constant. The 28 day compressive strength of 100% CFBC fly ash paste was found as 54 MPa, however it dropped by 30% after accelerated aging. The 100% conventional fly ash paste exhibits only 4 MPa after 28 days.

The optimal composition was found as a mixture of 50% CFBC and 50% conventional fly ash. The optimized mix composition of the ternary binder (TB) is given in Table 2. A high range water-reducing admixture (superplasticizer) was added to reach a feasible workability with an acceptable water/binder ratio.

Table 2: Mix compositions of the ternary binder (wt. %).

	CFBC fly ash	Conventional fly ash	Ca(OH) ₂	Water	Superplasticizer
Paste from TB	31.3	31.3	9.4	26.3	1.7

The mixing sequence started with 1 min of dry stirring to homogenize the source materials; addition of water; 10 min of mixing (285 rpm.); addition of the superplasticizer followed by another 5 min of mixing. The paste was subsequently cast into molds and vibrated for 2 min. Samples for determination of the phase evolution were ambient cured in sealed ampoules to prevent water evaporation and carbonation. After a given curing period (3, 7, 28 and 60 days) the hydration was stopped by water removal using acetone and a vacuum drying approach; the specimens were cut on a diamond saw to 3 mm slices, immersed in acetone for 24 h and vacuum dried for 48 h. Samples for the XRD and DTG analyses were ground in a laboratory small-scale planetary ball mill (Retsch PM 400). Beams for strength measurements were cast into $40 \times 40 \times 160$ mm molds and covered by a foil to prevent water evaporation. After 7 days of sealed curing, the samples were unmolded and again wrapped in foil. The compressive strength was measured on half beams.

Further methods and details are described in [4], particularly XRD measurements with the Rietveld method, TGA, Helium pycnometry, SEM images and EDX analyses.

3. RESULTS AND DISCUSSION

3.1 Experimental data

Table 3 presents the results of XRD-Rietveld analysis on the hydrated samples. Eight phases are distinguished using the XRD, namely quartz, ettringite, mullite, calcite, portlandite $\text{Ca}(\text{OH})_2$, anhydrite, hematite, and (indirectly using the addition of a Zincite internal standard) an amorphous content. The amorphous content is expected to consist of two general phases, i.e. the glassy phase originating from the conventional fly ash, and the C-S-H gel which is formed during the hydration. Since the two phases could not be easily distinguished using the XRD approach, a thermal gravimetric analysis is proposed to access the C-S-H gel fraction.

Table 3: Quantitative XRD phase analysis of pastes at 0, 3, 7, 28 and 60 days of curing (wt. %).

	Density (g/cm ³)	0D	3D	7D	28D	60D
Amorphous content	2.0	51	56	62	51	58
Quartz	2.7	6	5	5	5	6
Ettringite	1.8	0	2	3	16	12
Mullite	3.3	14	15	14	13	13
Calcite	2.7	4	4	4	5	5
Portlandite	2.3	15	11	7	6	3
Anhydrite	3	6	3	1	0	0
Hematite	5.3	4	4	4	4	3

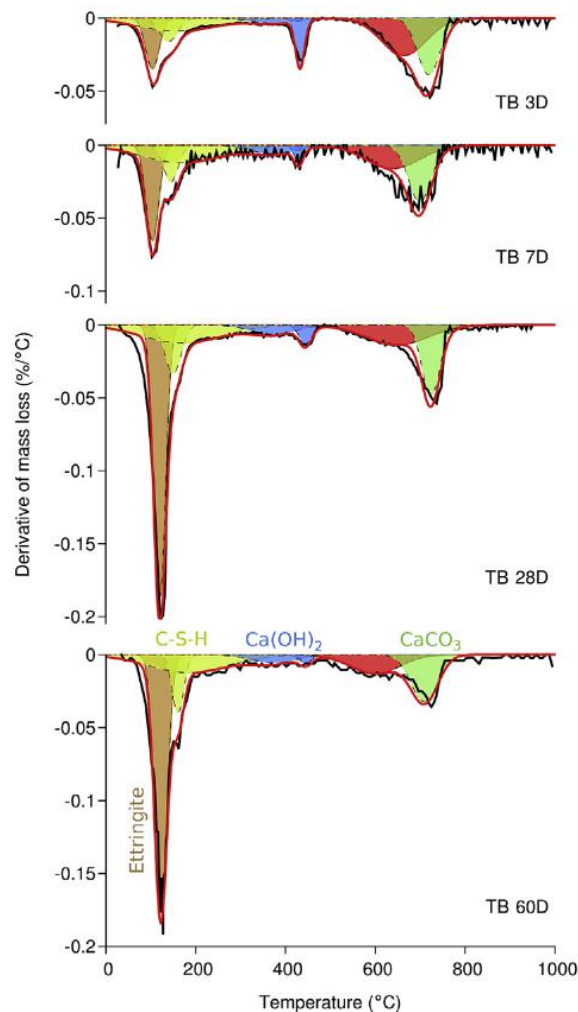


Figure 1: Differential thermal gravimetry of TB pastes at 3, 7, 28 and 60 days of curing. Derivative of mass loss. Proposed fit of particular phases using Gaussian curves.

The main goal of the DTG analysis lies in C-S-H gel quantification. This is done using deconvolution of the total mass loss during the DTG analysis to assess contributions of ettringite, C-S-H gel, Ca(OH)_2 and CaCO_3 , see Figure 1. The first question is the amount of ettringite and possible conversion to metaettringite during extensive drying procedure. Comparing virgin undried sample with dried sample led to similar DTG curves hence little or no metaettringite was formed [4]. Temperature peaks were assigned for deconvolution; ettringite 120°C [7], C-S-H 150°C [8], Ca(OH)_2 450°C, CaCO_3 750°C. Table 4 summarizes final mass fractions from DTG deconvolution. It should be emphasized that DTG deconvolution is sensitive to overlapping regions, such as ettringite and C-S-H, sensitive for the selection of peak temperatures and width (in case of ettringite was chosen to match area around peak based on [7]). At the end, the results for ettringite, portlandite and calcite are consistent with XRD analysis and support quantified phase evolution in the system.

Table 4: Mass fractions from DTG analysis. Quantitative phase analysis of pastes at 3, 7, 28 and 60 days of curing (wt. %).

	3D	7D	28D	60D
Ettringite	3	5	14	14
C-S-H	28	39	42	42
Ca(OH) ₂	5	5	5	4
CaCO ₃	5	5	5	5

Two types of porosities are here distinguished. Gel pores with a nominal diameter under 3 nm in the C-S-H, and capillary pores above [30]. The volume of entrapped air is neglected. Total porosity corresponds to the sum of gel and capillary porosities. Immediately after the mixing, the total porosity corresponds to the water volume in the fresh paste. Decrease of total porosity was determined with the combination of He pycnometry and measured bulk density on vacuum-dried cylindrical samples; it was 48% before hardening and decreased systematically to 38% at 60 days [4]. Scanning electron microscopy provided insight into microstructure formation, see Figure 2 for fractured surface.

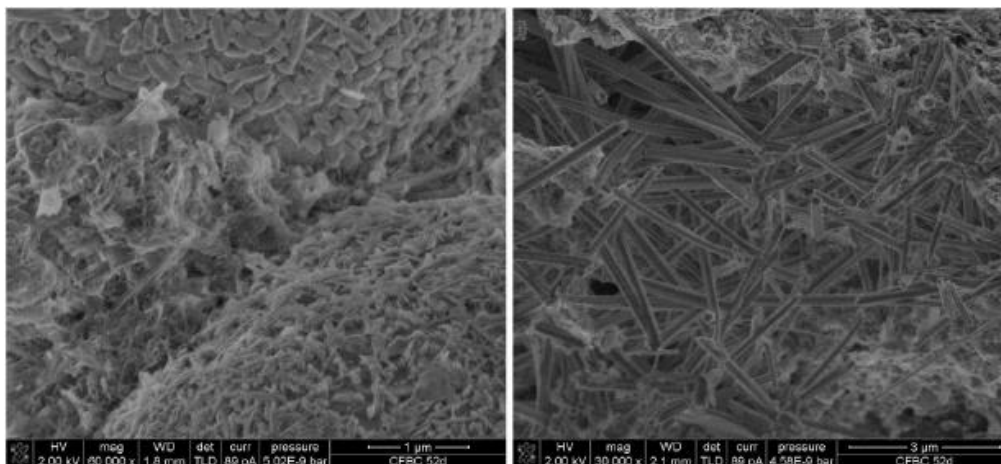


Figure 2: SEM-SE of TB paste after 52 days of sealed curing, fractured surface with visible hydration products and unreacted fly ash particle (left) and ettringite crystals (right).

3.2 Model of volumetric phase evolution

The model of volumetric phase evolution is constructed from measured total porosity, mass fractions from XRD, and mass fractions from deconvoluted DTG curves. The SEM/EDX results are only indicative. Seven phases are distinguished in the volumetric model: capillary pores, C-S-H gel consisting of C-S-H globules and gel pores, ettringite, amorphous glass, calcium hydroxide, and nonreactive crystalline phases.

The amount of non-reactive crystalline phases, calcium hydroxide and total amorphous content originates from XRD analysis; the amount of ettringite and C-S-H gel comes from DTG deconvolutions. The identified mass fractions are recalculated to volume fractions using known densities of the particular phases, and normalized to 100% volume (without total porosity). The density of C-S-H globules is assumed as 2.25 g/cm³ for a globule with 1.3 mol of H₂O, i.e. C_{1.7}SH_{1.3} [3]. The density of amorphous glass is fitted, so the theoretical

calculated bulk density from the volumetric model corresponds to the measured one. The density is identified as 2.0 g/cm³.

The total measured porosity is divided into the capillary and the gel contributions. The fraction of C-S-H-gel pores is derived from the identified volume of C-S-H gel using its characteristic porosity 0.37 (for a LD C-S-H gel with a packing density 0.63) [3]. It is unlikely that any significant portion of high-density HD C-S-H forms in such a porous system, in fact, transition from LD to HD type requires confined space under reduced capillary space, which would occur in significantly lower w/b ratios [3,5].

Figure 3 shows the proposed volumetric model of phase evolution during hydration of the ternary binder. The measured/calculated data for 0, 3, 7, 28 and 60 days of curing are shown and a smooth monotonic fit is proposed.

The coexistence between C-S-H and ettringite seems not to be detrimental in terms of volume changes since both products evolve simultaneously during 28 days. Linear length change on similar TB paste showed no expansion; up to 5 years, maximum shrinkage was 1900 µε for air storage and 1900 µε for wet storage [6]. This is in contrast with the crystallization pressure of delayed ettringite formation which causes expansion with cracking of a mature C-S-H matrix, due to limited creep capacities. This hypothesis of simultaneous growth explains why CFBC ash alone causes significant expansion due to ettringite formation but causes no problems in this TB.

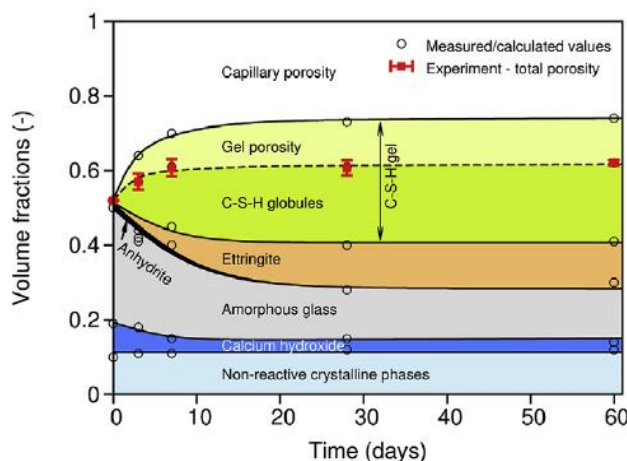


Figure 3: Volumetric model of phase evolution during hydration of ternary binder.

3.3 Compressive strength prediction

Compressive strength evolution is generally governed by the weakest solid percolating phase in a microstructure, which has been linked to a gel in Portland cement-based materials. Therefore, the gel/space ratio belongs to a traditional descriptor coined by Powers and TB can be tested for this hypothesis as well. Figure 4 shows the relationship with CemBase, a public database [5] devoted mainly to microstructure characterization of ordinary and blended Portland cement pastes, often complemented with compressive strength and elastic moduli. It contains mix designs for 83 pastes and 27 mortars, covering water/binder ratios of 0.16-0.69. The ternary binder in Figure 4 left exhibits a slight underestimation which points to an inaccurate gel descriptor, i.e. gel composed of C-S-H and ettringite.

Better results are obtained for C-S-H/space descriptor, showing that this ternary binder comes exactly on the average predicted value of the multiscale micromechanical model [5]. It becomes likely that ettringite does not contribute substantially to the compressive strength since including ettringite into the gel shows even worse results. However, ettringite likely contributes to early-strength gain and also efficiently fills capillary pores, contributing to strength indirectly, as a space-filling agent. The micromechanical models points also to little or no damage of C-S-H percolating matrix due to the growing ettringite, consistent with measurements of expansions.

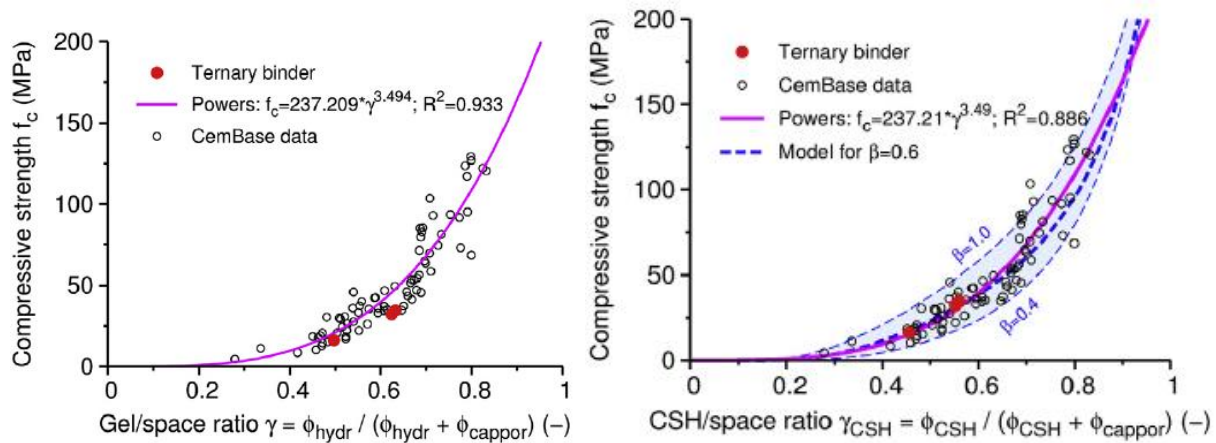


Figure 4: Compressive strength of ternary binder with regards to OPC and blended cements in the form of gel/space (left) and CSH/space (right) descriptor.

Detailed evolution of compressive strength evolution is depicted in Figure 5 using standard parameters for the micromechanical model such as tensile strength of C-S-H globule as 320 MPa [5]. It signals a formation of characteristic C-S-H gel as found within Portland cement-based pastes. The choice of different C-S-H stoichiometry would have impact on identified volume fraction of C-S-H. However, since C-S-H globule volume is identified directly from total porosity measurement, the question remain rather on porosity distribution between gel and capillary types, affecting Gel/space and CSH/space ratio in Fig. 4. Not much changes occur then for strength prediction; C-S-H with lower gel porosity would attain higher strength which is lowered by increased capillary porosity and vice versa.

4. CONCLUSIONS

A ternary binder synthesized from CFBC fly ash, conventional fly ash, and calcium hydroxide exhibits hydraulic properties resulting in 32 MPa compressive strength after 28 days of curing. The binder utilizes CFBC fly ash, which is otherwise unsuitable for OPC blending due to its high sulphate content and free CaO. The ternary binder could be used for low-demanding applications such as soil stabilizations, void fillings, temporary road constructions, etc. For a deeper understanding in the microstructure-strength links, the evolution of phase volumes is determined using a combination of XRD, TGA, SEM and porosimetry. A multiscale micromechanical model provides a good validation of the compressive strength evolution with standard model parameters derived from Portland cement-based binders.

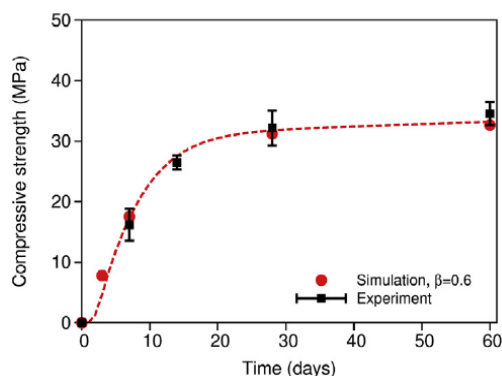


Figure 5: Evolution of compressive strength of ternary binder.

ACKNOWLEDGEMENTS

The authors gratefully acknowledge financial support from Technology Agency of the Czech Republic (TA CR) under projects TE01020168, TH03020404, TH02020163 and INTER-COST LTC18063.

REFERENCES

- [1] J. Koornneef, M. Junginger and A. Faaij, “Development of fluidized bed combustion - An overview of trends, performance and cost,” *Progress in Energy and Combustion Science*, pp. 19-55, 2007.
- [2] J. Havlica, J. Brandštetr and I. Odler, “Possibilities of utilizing solid residues from pressured fluidized bed coal combustion (PSBC) for the production of blended cements,” *Cement Concr. Res.*, vol. 28, no. 2, pp. 299-307, 1998.
- [3] H. Jennings, “Refinements to colloid model of C-S-H in cement: CM-II,” *Cement and concrete research*, vol. 3, pp. 275-289, 2008.
- [4] P. Hlaváček, R. Šulc, V. Šmilauer, C. Rössler and R. Snop, “Ternary binder made of CFBC fly ash, conventional fly ash, and calcium hydroxide: Phase and strength evolution,” *Cement and concrete composites*, vol. 90, pp. 100-107, 2018.
- [5] M. Hlobil, V. Šmilauer and G. Chanvillard, “Micromechanical multiscale fracture model for compressive strength of blended cement pastes,” *Cement and Concrete Research*, vol. 83, pp. 188-202, 2016.
- [6] F. Škvára, R. Šulc, R. Snop, A. Peterová and M. Šídlová, “Hydraulic clinkerless binder on the fluid sulfocalcic fly ash basis,” *Cement and concrete composites*, vol. 93, pp. 118-126, 2018.
- [7] L. Baquerizo, “Impact of Water Activity on the Mineralogy of Hydrated Cement,” EPFL, Lausanne, 2015.
- [8] E. Stepkowska, J. Blanes, F. Franco, C. Real and J. Perez-Rodriguez, “Phase transformation on heating of an aged cement paste,” *Thermochim. Acta*, vol. 420, no. 1, pp. 79-87, 2004.

USE OF CARBONATED WASTE HARDENED CEMENT POWDER AS A SUPPLEMENTARY CEMENTITIOUS MATERIAL

Bao Lu (1), Caijun Shi (1*)

(1) Key Laboratory for Green & Advanced Civil Engineering Materials and Application Technology of Hunan Province, College of Civil Engineering, Hunan University, Changsha 410082, China

(2) College of Transportation Engineering, Tongji University, Shanghai, 201804, China

Abstract

Recovering aggregates from recycled concrete produces a large amount of powder, which contains hardened cement paste and is classified as a corrosive hazardous material. This work used CO₂ to treat hardened cement powder and to investigate how incorporation of uncarbonated and carbonated waste hardened cement powder into cement affect the hydration and microstructure development of cement. Carbonated waste hardened cement powder consists mainly of calcite and silica gel. Replacement of cement by uncarbonated waste paste powder content from 10 to 30% by the mass of cement decrease the strength of cement, while replacement of cement with 10-20% carbonated waste paste powder, but with 30% carbonated waste paste powder decrease the early strength of the cement. The presence of calcite in carbonated waste paste powder leads to the formation of hemicarbonate and monocarbonate thus to a stabilization of ettringite compared with the pure cement paste, in which a part of ettringite converts to monosulphate. Hemicarbonate is less stable than monocarbonate. It exists only for one week, then transforms to monocarbonate. The presence of silica gel significantly reduces the calcium hydroxide and results in the formation of more C-S-H. Replacement of cement by carbonated waste paste powder also leads to a lower porosity and a higher compressive strength compared with the pure cement paste.

Keywords: waste cement paste powders; carbonation treatment; hydration; monocarbonate; pore structure

EARLY STRENGTH IMPROVEMENT OF SUSTAINABLE SHOTCRETE

Lukas G. Briendl (1), Joachim Juhart (1), Markus Krüger (1), Florian Mittermayr (1), Isabel Galan (2)

(1) Institute of Technology and Testing of Building Mat., Graz University of Techn., Graz

(2) Institute of Applied Geosciences, Graz University of Technology, Graz, Austria

Abstract

Sprayed concrete formulations commonly used in practice have a high content of ordinary Portland Cement (OPC) and consequently high global warming potential and primary energy demand. The substitution of OPC by pozzolanic and/or inert filler materials can significantly improve eco-friendliness of shotcrete; however, this should not compromise the early strength development. The outlined contribution focuses on the effects of micro- fillers (MF), with average particle sizes $\leq 1/10-1/3$ from d_{50} of OPC's ($\approx 10\mu\text{m}$) [1], on the hydration and early strength evolution of sprayed concrete mixes. OPC systems accelerated by means of alkali-free, aluminum- sulfate based setting accelerators were analysed by: Isothermal calorimetry, X-ray diffraction, determination of the specific surface area (SSA) and standard compressive strength tests according to EN-196-1. The results show a strong influence on the early strength development, hydrations characteristics and –products due to the addition of UF limestone powders.

Keywords: shotcrete, filler, early- strength, resource efficiency

1. INTRODUCTION

The hydration reactions of accelerated systems such as shotcrete differ to those of normal concrete due to the presence of the so-called ‘setting accelerators’. The most commonly used accelerators these days are those based on aluminium sulfate and alkali-free. These products react immediately after contacting the concrete mix. As a result of the first reaction high amounts of ettringite are formed. This, together with the high-speed shooting, allows for the shotcrete mix to stick to the surface where it is applied. Apart from contributing to the formation of ettringite, the low pH of the accelerator ($\text{pH} \approx 3$) helps increasing the solubility (re-activity) of alite [2-5].

The substitution of clinker by supplementary cementitious materials (SCMs) and fillers in shotcrete has become a common practice in the last years. However, only a reduced number of combinations (cement + SCMs) are currently being used, the main reason for this being the potential reduction of early strength and the current standards and guidelines for shotcrete. In the course of laboratory- tests on accelerated mortar prisms and real scale tests it could be

demonstrated that low clinker mixtures can achieve sufficient early strength, as for example the J2 class requirement of the Austrian Guidelines for Shotcrete [6,7], if the mix design is adequate. Ultrafine limestone powders proved more effective than silica- fume with similar BET- surface at improving the early strength development of laboratory-tests samples. [8].

The contribution of MF, in particular limestone, to the early- strength development systems is associated to several possible mechanisms:

a.) Filler effect: increase of nucleation sites but also affecting the interparticular distance between the solid particles due to a strong influence on the water- layer thickness by controlling the packing density and the volumetric- surface of the fines [9-11].

b.) Chemical participation in the hydration process: the presence of limestone contributes to the formation of hemi- and monocarboaluminate and inhibits the transformation of ettringite to monosulfate [12-15]. This point is also discussed in chapter 3.3.

c.) A strong (probably ionic and/or covalent) bond between Ca^{2+} ions adsorbed on calcitic surfaces (from the pore solution) and C-S-H phases can form, so that C-S-H binds strongly to limestone surfaces [16].

2. EXPERIMENTAL

2.1 Materials

For all the tests and the different mixes only CEM I 52.5 R according to EN 197-1 (2011) was used. The composition of the cement is shown in *Table 1*.

Table 1: Cement composition determined by XRD + Rietveld Analysis

Phase	%	Phase	%	Phase	%
Alite	55.0	Anhydrite	3.8	Ferrite	7.4
Belite	13.1	Arcanite	2.0	Periclase	4.2
Aluminate c	0.7	Bassanite	1.7	Portlandite	0.3
Aluminate o	10.8	Calcite	0.9	Total	99.9

In addition to the cement, various types of fillers were used for the investigations: quartz powder (97% SiO_2), four limestone powders (99.9% $CaCO_3$) with different grain sizes, and dolomite ($CaCO_3 \cdot MgCO_3$) powder. The dry particle density, average grain size (d_{50}) and BET surface of the cement and fillers are shown in *Table 2*.

Table 2: Used powders and their parameters

Material	Dry particle density ρ_s [g/cm ³]	d_{50} [μ m]	BET [m ² /g]
CEM I 52.5 R	3.16	7.1	1.32
Quartz powder	2.67	13.6	2.62
Limestone powder 1	2.72	2.6	3.9
Limestone powder 2	2.72	0.9	8.2
Limestone powder 3	2.72	0.4	18.4
Dolomite powder	2.9	1.1	8.2

For the mortar specimens, a carbonate- siliceous sand in a grain fraction 1-4mm was used in order to exclude possible influences of the finer fraction aggregates on the hydration processes. For all specimens (mortar and paste) a commercial liquid, alkali- free aluminium sulfate based setting accelerator was used. The pH value of the accelerator was 2.4 at 14.4°C. All specimens were mixed with water at a temperature of $\approx 20^\circ\text{C}$. Except from the accelerator no more concrete additives (e.g. superplasticizer, retarder) were used for the mixtures.

2.2 Mix Design

To quantify the effect of the different amounts of the various filler types and sizes keeping the water/cement ratios constant, the mixes were design based on the substitution of quartz (and not cement) from a reference-mix, containing 60 wt.% cement and 40 wt.% quartz powder (*Table 3*). The water/binder (w/b) ratio for the mortar was 0.5 and the aggregate/binder ratio 2.0. The binder includes the cement and any filler material (limestone, quartz, dolomite).

The specific surface area (SSA) per volume of solids was calculated by means of the BET Surface and the bulk density (*Equation (1)*).

$$\text{SSA} [\text{m}^2/\text{cm}^3] = \text{BET} [\text{m}^2/\text{g}] \times \rho_s [\text{g}/\text{cm}^3] \quad (1)$$

Table 3: Composition and specific surface area (SSA) of the investigated binders (QP= quartz powder, LP=limestone powder, DP=dolomite powder).

ID	QP		MF		SSA [m ² /cm ³]	ID	QP		MF		SSA [m ² /cm ³]
	wt. %	V%	wt. %	V%			wt. %	V%	wt. %	V%	
QP-40	40	44	-	-	5.42	LP2-25	15	17	25	27	9.57
LP1-2	38	42	2	2	5.48	LP3-2	38	42	2	2	6.19
LP1-7	33	37	7	7	5.68	LP3-7	33	37	7	7	8.53
LP1-15	25	28	15	16	6.0	LP3-15	25	28	15	16	12.42
LP1-25	15	17	25	27	6.39	LP3-25	15	17	25	27	17.12
LP2-2	38	42	2	2	5.69	DP-2	38	42	2	2	5.7
LP2-7	33	37	7	7	6.52	DP-7	33	37	7	7	6.55
LP2-15	25	28	15	16	7.91	DP-25	15	17	25	26	9.74

2.3 Strength development

To determine the effect of the various fillers on the strength development of accelerated systems, mortar prisms were produced and tested at different times: 6h, 24h, 28d and 56d. For the preparation of mortar prisms (40x40x160mm) the following procedure was applied: water was first given into a common 5l Hobart mixer. Then the whole amount of well mixed solids (binder and aggregates) was added and mixed for 90 seconds at ~ 150 rpm. After 60 seconds the mixer was stopped to scrape the mixer and the mixing bowl. The mix was then left for 10 minutes, after which the alkali-free accelerator (6 wt.% of binder) was added by means of a syringe (25ml), while mixing at 300 rpm for 15 seconds (zero time). The mix was then rapidly poured into the prism molds while vibrating them for 30 seconds. The prisms were then covered with a glass plate and stored at $\approx 100\%$ RH and 20°C for 6h (wet storage). The specimens were then demolded and kept under wet storage until they were tested. The compressive

strength tests were carried out within the first 24h using an electronically controlled testing machine with a testing speed of 1mm/min on 4 prism halves. After 28 and 56 days the test was carried out according to ÖN EN 196-1 (2016) on 2 prism halves also by an electronically controlled testing machine.

2.4 Isothermal calorimetry

For the continuous measurement of the heat of hydration, \approx 50-100g of mortar were given into an isothermal calorimeter (Calmetrix; I-Cal 4000 HPC) shortly (\approx 2 minutes) after the accelerator dosage and left for 24 hours at 20 °C. The amount of binder in the samples was recalculated using the initial weight. The measuring interval was 1/min. In case of multiple determinations of one mix, the average value for each measurement point was calculated from the measurements.

2.5 X- Ray Diffraction

The development of the crystalline phases during the early hydration of selected samples was followed by means of powder X- Ray diffraction (Panalytical X'Pert Pro; $\text{CoK}\alpha$ radiation) for 24h. Cement pastes were mixed with the same procedure and composition, as the mortar samples described above, but without any aggregates. The accelerated paste was quickly filled into the sample holder, the surface smoothed with a small glass plate, and finally covered with a Kapton foil (7.6 μm) to prevent water loss. About 2 minutes after accelerator addition, the sample was transferred to the X-ray diffractometer.

The sample was measured in time steps of about 20 minutes continuously during 24h from 9 to 50° 2 θ . The contribution to the background of the Kapton foil was determined using a single crystal silicon wafer and then subtracted from the measurements.

Additionally, the hydration of the mixes was stopped shortly after accelerator dosage=0h, after 3h, 6h and 24h, by solvent exchange with isopropanol and subsequently drying under 300mbar vacuum. On those samples XRD measurements were also carried out.

3. RESULTS AND DISCUSSION

3.1 Early strength

The early strength of the mortar specimen increased with the SSA of the powdery materials. For example the 6h compressive strength ($R_{c,6h}$) of the reference mix (QP-40), 1.82 MPa, was improved by a factor of 3 in the LP3-25 mix (*Figure 1*).

The results show a logarithmic function between the specific surface area of the powdery materials and the R_c after 6h. No significant difference between limestone, dolomite powders or quartz powder could be found. After 24h of hydration the strong strength increasing effect of the fine limestone- and dolomite powders is also noticeable (*Figure 2*). Mixtures with dolomite powders and the reference mix show slightly lower strength than formulations with limestone powders with similar volume-specific surface. A faster growth of C-S-H phases and/or a stronger bond between the limestone particles and C-S-H compared to dolomite or quartz is indicated by this behaviour. Neither the limestone nor the dolomite powder had an influence on the long-term strength after 28 or 56 days of hydration, reaching all mixes very similar values (around 30 MPa).

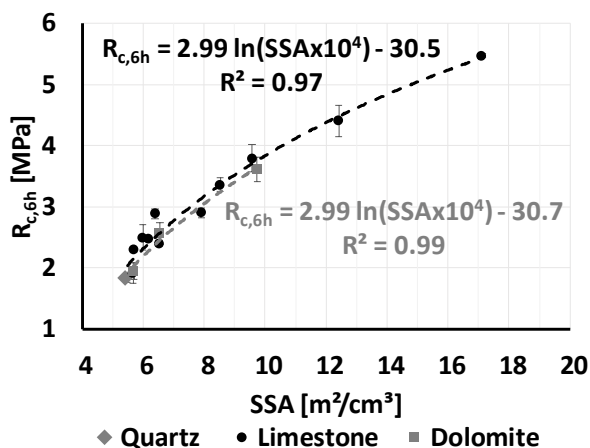


Figure 1: $R_{c,6h}$ of accelerated mortar prisms (n=4) with standard deviation

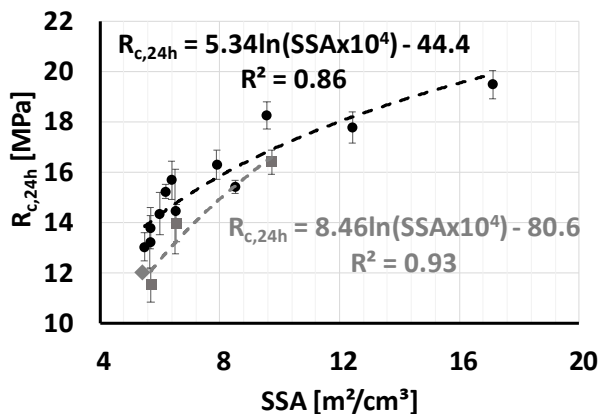


Figure 2: $R_{c,24h}$ of accelerated mortar prisms (n=4) with standard deviation

3.2 Heat of hydration

In the investigated systems with aluminium sulfate based accelerators, the heat evolution during hydration can be divided in 3 phases. Phase I shows the massive ettringite formation, due to the accelerator addition. Since the addition of water and that of the accelerator take place with a time delay (~10 minutes), in addition to the ettringite formation there may be a residual heat of the free lime, sulfate and alkali dissolution included in this first peak. Afterwards, analogous to non-accelerated systems, the dormant period in which no exothermic reaction takes place, can be observed. The end of the dormant period was characterized in the studies as the lowest point of heat flux between 2 and 4 hours after accelerator addition. Thereafter, in the phases II and III of the hydration mainly the formation of strength-giving calcium-silicate-hydrates (C-S-H), portlandite and AFm phases (monosulfate, hemi- or monocarbonate) take place. Both periods can be divided into an acceleration and decay phase.

Figure 3 shows the measured curves for samples with 25% substitution of quartz powder by limestone- and dolomite powders with different fineness. The cumulative heat is plotted here in two parts. The left curve shows the first hour contribution during hydration phase I. During this time no significant differences between limestone- and dolomite powders are visible in the heat evolution, the most noticeable effect being the slight lower values achieved in the mix with the finest limestone powder.

On the right graph the contribution of the cumulative heat from period I has been removed and only the corresponding cumulative heat after the dormant period is considered.

In the second period of hydration (Stage II) it is clearly visible that the addition of UF limestone powder enhances the silicates hydration, resulting in an earlier and higher peak as compared to the reference mix. There is no clear correlation between the SSA and the height and time of the second peak of hydration, but the increase of cum. heat from the end of the dormant period to 6h is similar in all mixes with MF ($43.5 \pm 1.12 \text{ J/g}_{\text{powder}}$). UF dolomite powder seems to not have an effect on the time when the C-S-H growth starts, but the peak is much higher and broader than in the reference mix. The heat flow during the third phase of the hydration is higher for all substituted mixes in comparison to the quartz reference.

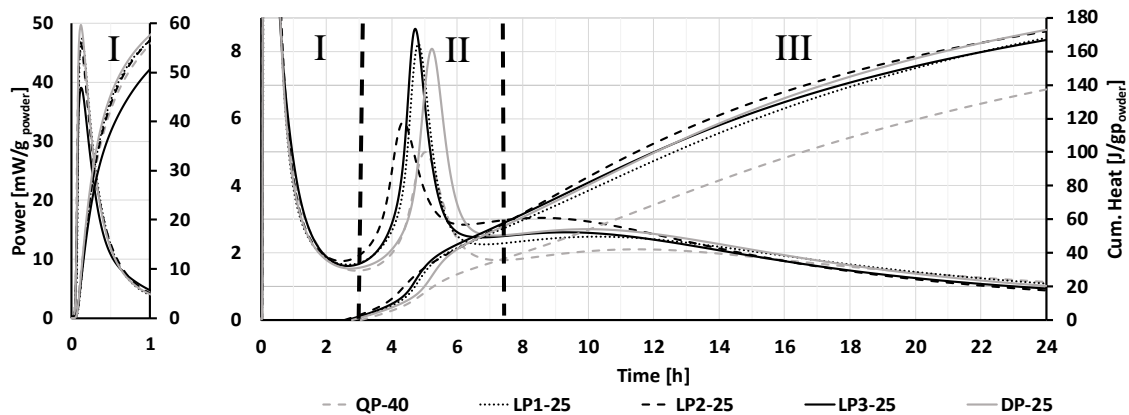


Figure 3: Heat of hydration of mortar mixes with 25% addition of limestone and dolomite powders with different fineness (n=5)

Figure 4 shows the cum. heat of all mixes from Table 3 after 6 and 24h versus the corresponding compressive strength data. Similar to non-accelerated systems [17] a linear correlation between the heat released by the hydration process and the R_c of the mortar prisms is observed. This correlation can be used to estimate the expected R_c in the time range from 6 to 24 hours using calorimetry data. It should be noted that the fitted function is valid for the cement, w/c, w/b ratio, and accelerator type and dosage used. For other conditions, other functions may be applicable.

Higher mix SSA is in most cases related to shorter dormant period (Figure 5). This trend is however not clear in the case of dolomite powders.

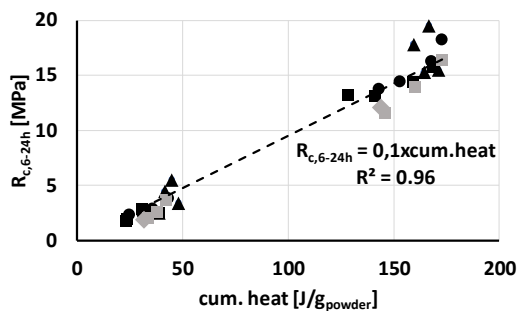


Figure 4: Correlation between cum. heat of hydration and $R_{c,6-24h}$ (QP-40, LP1-25, LP2-25, LP3-25, DP-25: n=5; rest: n=1)

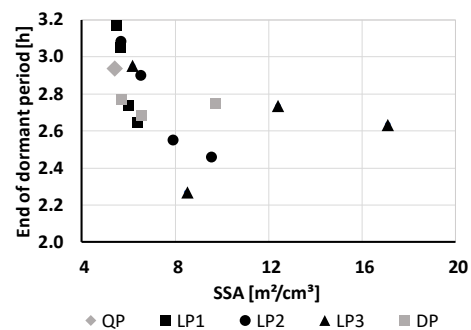


Figure 5: SSA vs. end of dormant period (QP-40, LP1-25, LP2-25, LP3-25, DP-25: n=5; rest: n=1)

3.3 Development of crystalline phases during early hydration

Figure 6 & Figure 7 show the evolution of the crystalline phases during hydration over 24h. The reference mix (QZ-40) is compared to mix LP3-25. In both mixes the main ettringite peak at $\approx 10.5^\circ$ (2θ) grows until 3 hours of hydration. This time coincides with the end of the dormant period from calorimetry measurements. Therefore, it can be assumed that the primary ettringite formation is finished at the end of dormant period. After that in the reference mix the absolute intensity of the ettringite peak decreases. (Figure 6a) This is associated with the transformation of ettringite to monosulfate (2):



In the presence of fine limestone, hemihydrate (main peak at $\approx 12,5^\circ$) and/or monohydrate are formed and the transformation of ettringite to monosulphate is suppressed [13,14].

Gypsum can be observed in the initial XRD patterns of both mixes at $\approx 13,5^\circ$ (Figure 6a). It is likely that the gypsum crystallized from a supersaturation of the pore solution with respect to sulfate, soon after the contact with water (false setting was observed).

Portlandite starts to form in both samples after $\approx 4h$ of hydration (main peak at $\approx 21^\circ$).

Alite is continuously hydrated over time. Observing for example the peak at $48,4^\circ$, the higher hydration rate of alite in case of limestone powder addition can be clearly appreciated (Figure 6b). The higher amount of nucleation sites provided by the high surface of the used limestone powder can be, at least partly, the reason for this behaviour.

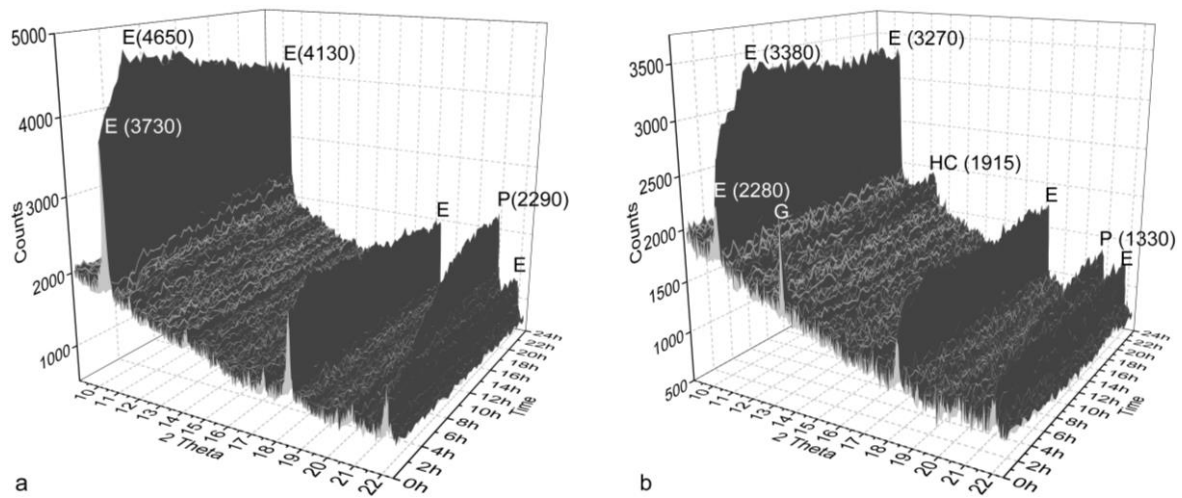


Figure 6: 24h in-situ XRD plot from $9-23^\circ$ (2θ): a=QZ-40, b=LP3-25†

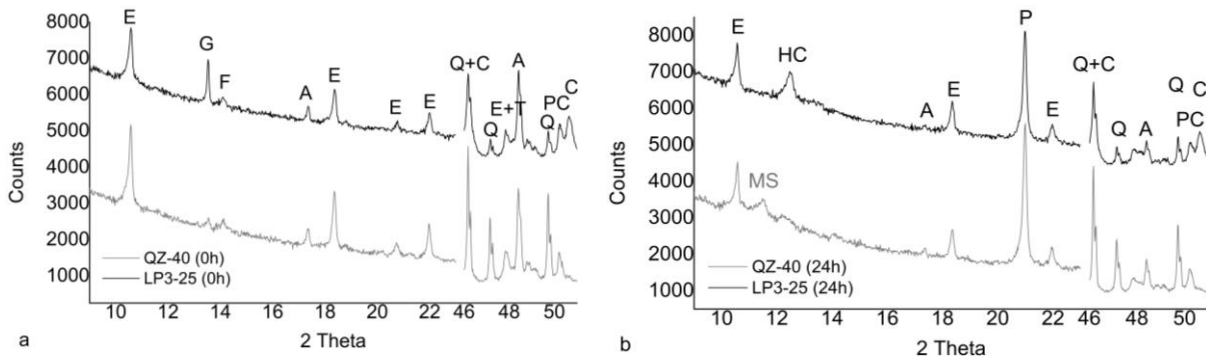


Figure 7: XRD measurements from stopped samples at 0 and 24 h.: a=0h, b=24h†

4. CONCLUSION

Ultrafine limestone and dolomite powders increase the early strength and enhance the hydration of cement systems accelerated by means of alkali-free sulfate based setting accelerators. This effect increases for larger volume-specific filler surface.

For the used cement and $w/b=0.5$ and $w/c=0.83$ ratio a correlation between the compressive strength after 6 hours ($R_{c,6h}$) and the particle surface of the fines, independently from their nature (limestone, quartz, dolomite), can be described by a logarithmic relationship. A better performance of limestone in comparison to quartz and dolomite is seen after 24 hours of hydration. Additionally, UF calcite contributes to shorten the dormant period.

The early strength of accelerated mortar can be assessed with the use of cumulative heat release data obtained from calorimetry measurements.

Ultrafine limestone powders inhibit the transformation of ettringite to monosulfate and contribute to the formation of carbonate- AFm phases.

ACKNOWLEDGEMENTS

The authors gratefully acknowledge the funding by the industry partners, the Austrian Research Promotion Agency FFG (ASSpC Project-No. 856080) and the Austrian Building Technology Association ÖBV.

REFERENCES

- [1] Juhart, J., et al., 'A practical approach to increase the functional and environmental performance of cementitious composites by mineral fillers', Paper submitted, (2018).
- [2] Juilland, P., 'Early Hydration of Cementitious Systems', Dissertation, Ecole polytechnique fédérale de Lausanne (2009).
- [3] Paglia, C., et al. 'The influence of alkali-free and alkaline shotcrete accelerators within cement systems: I. Characterization of the setting behavior', *Cem. Concr. Res.*, **31**(6) (2001), 913–918.
- [4] Salvador, R. P., et al., 'Early age hydration of cement pastes with alkaline and alkali-free accelerators for sprayed concrete', *Constr. and Building Mat.*, **111** (2016), 386–398.
- [5] Xu, Q., 'Chemische Wirkung von Erstarrungsbeschleunigern auf die frühe Hydratation des Portlandzements', Dissertation, Bauhaus-Universität Weimar (2005).
- [6] ÖVBB-Richtlinie: 'Spritzbeton', Österreichische Bautechnik Vereinigung ÖBV, Wien, (2009).
- [7] Stauffacher, A., Galan, I., et al., 'Einfluss von Hüttensand und ultrafeinem Kalksteinmehl auf die Hydratation von jungem Spritzbeton', Conference Proc., Spritzbetontagung 2018, Alpbach, (2018).
- [8] Juhart, J., Briendl, L., et al., 'Optimierte Eigenschaften von Spritzbeton durch kombinierte Zusatzstoffe', Conference Proc., Spritzbetontagung 2018, Alpbach, (2018).
- [9] Lothenbach, B., Scrivener, K., Hooton, R.D., 'Supplementary Cementitious Materials', *Cement and Concrete Research*, **41**(12) (2011), 1244–1256.
- [10] Berodier, E., Scrivener, K., 'Understanding the Filler Effect on the Nucleation and Growth of C-S-H', *J. Am. Ceram. Soc.*, **97** (12) (2014), 3764–3773
- [11] Kumar, A., Oey, T., et al., 'The filler effect: The influence of filler content and type on the hydration rate of tricalcium silicate', *J. Am. Ceram. Soc.*, (2017), 1–13
- [12] Kakali, G., Tsvivilis, S., Aggeli, E., Bati, M., 'Hydration Products of C3A, C3S, and Portland Cement in the Presence of CaCO₃', *Cement and Concrete Research*, **30** (2000), 1073–1077.
- [13] Pommersheim, J., Chang, J., 'Kinetics of hydration of tricalcium aluminate in the presence of gypsum', *Cement and Concrete Research*, **18** (1988), 911–922.
- [14] Kuzel, H.-J., 'Initial Hydration Reactions and Mechanisms of Delayed Ettringite Formation in Portland Cements' *Cement and Concrete Research*, **18** (1996), 195–203.
- [15] Kuzel, H.-J., Pöllmann, H., 'Hydration of C3A in the presence of Ca(OH)₂, CaSO₄•2H₂O and CaCO₃', *Cement and Concrete Research*, **21** (1991), 885–895.
- [16] Ouyang, X., Koleva, D.A., Ye, G., van Breugel, K., 'Understanding the adhesion mechanisms between CSH and fillers', *Cement and Concrete Research*, **100** (2017), 275–283.
- [17] De Schutter, G., Taerwe, L., 'Degree of hydration-based description of mechanical properties of early age concrete', *Materials and Structures*, **29** (1996), 335–344.

UTILIZATION OF RICE HUSK ASH AS REACTIVE FILLER FOR ENHANCING MATERIAL PROPERTIES OF ULTRA-HIGH PERFORMANCE CONCRETE

Sung-Hoon Kang (1), Yang-Hee Kwon (2), Juhyuk Moon (3)

(1) Department of Architecture and Architectural Engineering, Seoul National University, Republic of Korea

(2) Department of Traditional Architecture, Korea National University of Cultural Heritage, Republic of Korea

(3) Department of Civil and Environmental Engineering, Seoul National University, Republic of Korea

Abstract

Significant amounts of rice husk ash (RHA) are currently being generated annually as a byproduct of rice production. In this study, we used this waste product as a reactive filler to produce an eco-friendly ultra-high performance concrete (UHPC). This approach replaced inert quartz filler with the reactive RHA filler, with the intention of increasing the amorphous silica content in UHPC while maintaining the physical role of the micron-sized conventional filler. In addition, due to the porous structure of RHA, internal curing effect may be expected, which can promote the hydration reaction over a long period of time. Experimental results proves this approach as we confirmed outstanding mechanical strength of UHPC without heat treatment.

Keywords: rice husk ash; agricultural waste; ultra-high performance concrete; reactive filler

1. INTRODUCTION

Rice husk is an agricultural byproduct of the rice milling process. Enormous amount of the rice husk is produced annually [1, 2]. However, most (> 80%) of them are simply discarded as wastes, which causes water and soil pollutions [3, 4]. Therefore, the utilization of the husk as a biomass fuel to produce electricity is gaining some interests in the field of green technology [2, 5]. After the combustion process of the fuel, rice husk ash (RHA) remains as much as about 20% of the weight of the husk [5]. This is also usually discarded, which causes another environmental issue [6].

RHA can be used as a supplementary cementitious material (SCM) in cement-based composites. It can provide crystalline or amorphous silica, depending on the combustion conditions [2]. Since the RHA burnt below 700 °C is a highly reactive pozzolanic material, it has been successfully used to replace some of cement [7] or silica fume (SF) [1, 8-9] in concretes. It has been generally accepted that the optimal combustion temperature regarding the purity of amorphous silica is 500–700 °C [4, 7]. The silica contents of RHA can reach 90 wt.%, which is comparable to that of SF [7, 9]. For this reason, the RHA has been utilized to replace SF in ultra-high performance concrete (UHPC) which requires a large amount of amorphous silica for the pozzolanic reaction [8].

However, RHA is completely different material with SF in terms of physical characteristics such as particle shape and size. SF is a key material to optimize the particle packing of UHPC, and it has spherical shape which helps to improve fresh properties of the concrete [10]. However, the average particle size of RHA (generally 5–20 µm) is generally 50–100 times that of SF. Therefore, the use of RHA as a substitute of SF can change the microstructure of UHPC. The incorporation of micro-sized filler is also important for the maximum particle packing of UHPC. Conventionally, 5–25 µm of quartz powder (QP) in average particle size has been used [11]. Physically, RHA is more similar with irregular QP than spherical SF. While QP is composed of almost perfectly crystalline silica which is inert in UHPC below 150 °C of curing temperature, an appropriately produced RHA can be used as a reactive pozzolan at a room temperature, like SF [12]. Thus, there is a potential that the use of RHA as a micro-sized filler instead of QP can further improve the pozzolanic reactivity of UHPC.

Therefore, we investigated two types of RHAs burnt below 700 °C were tested as candidates of reactive fillers in UHPC instead of QP. Since the purity of amorphous silica in RHA is related to the brightness, white RHA (WRHA) and black RHA (BRHA) were prepared as a high- and low-purity siliceous materials, respectively. Therefore, various material characteristics such as mechanical properties, hydration reaction and pore structure were investigated as a function of replacement ratio of QP, and the purity of RHA.

2. MATERIALS AND METHODS

2.1 Rice husk ash

BRHA and WRHA were prepared by different combustion conditions, as shown in Figure 1. BRHA was collected in a plant which uses an uncontrolled combustion with the maximum temperature of about 400 °C. WRHA was obtained by a controlled combustion in a programmable temperature furnace: maximum temperature of 650 °C for 2 h with the heating and cooling rates of 2 °C/min. The ashes were ground in a ball mill.

The result of X-ray diffraction (XRD) analysis confirmed that the RHAs burnt below 700 °C do not contain crystalline phase (Figure 1). However, X-ray fluorescence (XRF) analysis in Table 1 revealed that chemical composition of the two ashes was significantly different. WRHA was mostly composed of silicon dioxide (SiO₂), similar to SF and QP. Based on the two results in Figure 1 and Table 1, it is concluded that WRHA and SF are mostly composed of amorphous silica, while QP is composed of crystalline silica. On the other hand, amorphous silica content in BRHA is very low because of impurities such as organic materials, as indicated in loss on ignition (LOI).

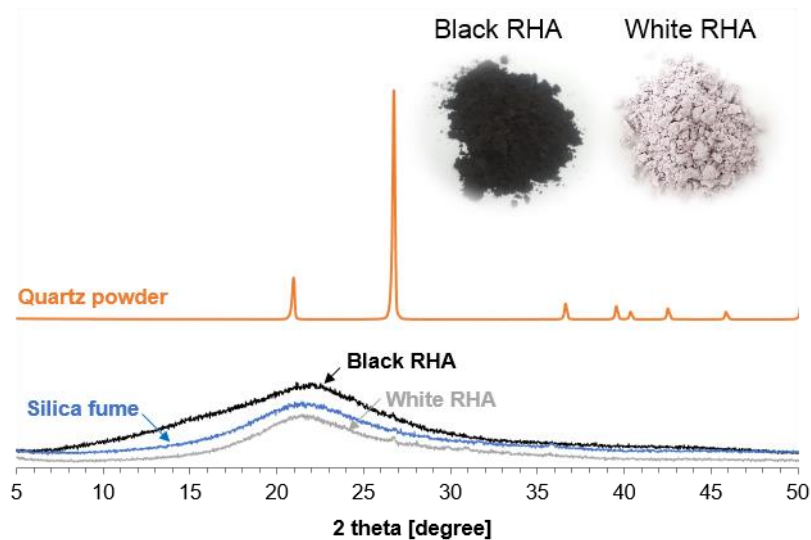


Figure 1: Two types of RHAs by different combustion programs, and XRD patterns of quartz powder, silica fume and RHA. All peaks in quartz powder are induced by crystalline quartz.

Table 1: Chemical composition of quartz powder, silica fume and RHA (wt.%)

Materials	SiO ₂	Al ₂ O ₃	TiO ₂	Fe ₂ O ₃	MgO	CaO	Na ₂ O	K ₂ O	MnO	P ₂ O ₅	LOI	Total
BRHA	23.8	0.1	-	0.1	0.1	0.3	0.1	1.0	0.1	0.2	74.3	100
WRHA	92.0	0.3	-	0.4	0.5	1.0	0.2	3.9	0.3	0.8	0.8	100
SF	96.9	0.3	0.0	0.2	0.2	1.5	0.2	0.6	0.0	0.1	0.0	100
QP	97.7	0.5	0.1	0.1	0.2	1.4	0.0	0.0	0.0	-	0.0	100

2.2 Manufacturing UHPC samples with RHA filler

The UHPC samples were prepared using ordinary Portland cement (OPC)-type I, SF, QP, silica sand, RHA (WRHA or BRHA), water and polycarboxylate-ether based superplasticizer (SPPL). The microscope images showed that the shape of RHAs is entirely different with that of SF; it is irregular like QP. Furthermore, the analysis of the particle size distribution confirmed that the size of RHA is almost 100 times that of SF. Table 2 shows the mix proportions of the samples and the main test parameter, filler composition, respectively. Sample name indicates the ratio of WRHA or BRHA in the filler. The fresh concrete samples were manufactured using a 5 L Hobart mixer. In addition, paste samples which do not include silica sand were also prepared for the tests on the hydration reaction such as heat of hydration reaction, XRD and thermogravimetric (TG) analysis. All specimens were subjected to ambient curing of 20 °C and 60% relative humidity (RH), after 1 day of sealed curing.

Table 2: Mix proportion and filler composition of UHPC samples

Materials	Mix proportion		Filler composition (wt.%)	
	Mass (kg/m ³)	Sample name	QP : RHA	
Cement	800	RHA0	100:0	
Silica fume	200	WRHA50	50:50	

Mix proportion		Filler composition (wt.%)	
Filler	200	WRHA100	0:100
Silica sand	880	BRHA50	50:50
Total water ^a	200	^a Water in SPPL is included.	
SPPL (dry content)	9.6 (or 14.4 ^b)	^b In the case that filler is composed of RHA only (i.e., the sample, WRHA).	

2.3 Experiments

The hydration heats of the paste samples were measured at 20 °C by an isothermal calorimetry (TAM Air). The released calories from 15 g of the pastes were recorded and normalized by the weight of cement in each paste.

On the planned test day (7, 28 and 91 days), the compressive strength of cubic specimens (50 mm for one side length) was measured, according to ASTM C109 [13].

The powder specimens were used in XRD and TG analysis. On the 28th days, the hardened pastes specimens were crushed and ground into powder form, and their hydration reactions were stopped by solvent removal technique [14]. After the drying process at 40 °C, the prepared powders were placed in the XRD analyzer, to investigate the mineralogical characteristics of the samples.

The portlandite contents in the pastes were determined by the TG analysis. The prepared powders were inserted in the analyzer and heated with a heating rate of 10 °C/min (from 40 °C to 1000 °C) in a nitrogen atmosphere. The weight loss between 400–500 °C was used to estimate the portlandite content by the tangential method [15]. The estimated results were again rescaled on basis of the dry sample weight at 500 °C [14, 15].

Mercury intrusion porosimetry (MIP) was used to investigate the pore structure of the UHPC samples. At 28 days, small concrete cubes (5 mm of one side length) were prepared by cutting large specimens, and their hydration reactions were stopped using isopropanol. After drying the cubes, the pore size distribution was measured using an equipment.

3. RESULTS AND DISCUSSION

3.1 Early age-hydration reaction

Figures 2a and b show heat of hydration and cumulative heat of the paste samples, respectively. When half of QP was replaced with WRHA, early age-hydration reaction was significantly accelerated; that is, the beginning of acceleration period of cement hydration was shortened and the maximum heat flow increased. The reduction of effective w/c by the absorption of porous RHA filler might cause this result, as reported in the previous studies [16, 17]. Seemingly, this is not the case when all of QP were replaced by WRHA, because the hydration was delayed. However, this is probably due to the increased SPPL-to-cement ratio, rather than the addition of RHA [18]. Therefore, the early hydration was delayed despite the addition of the porous filler. However, the use of WRHA filler slightly reduced the cumulative heat at 60 h, due to the decreased effective w/c [16]. Meanwhile, when BRHA was used, early hydration was significantly decelerated. The beginning of acceleration period was delayed, and also the heat flow and cumulative heat decreased. This indicates that the unburned organic materials in BRHA significantly disrupt the cement hydration at early ages. A significant high LOI in BRHA, as shown in Table 1, confirms that the ash contained high

amount of carbon-based materials that are decomposed between 400 °C and 650 °C. Furthermore, Figure 2 demonstrates that these unburned carbons decelerate the initial hydration reaction of cement.

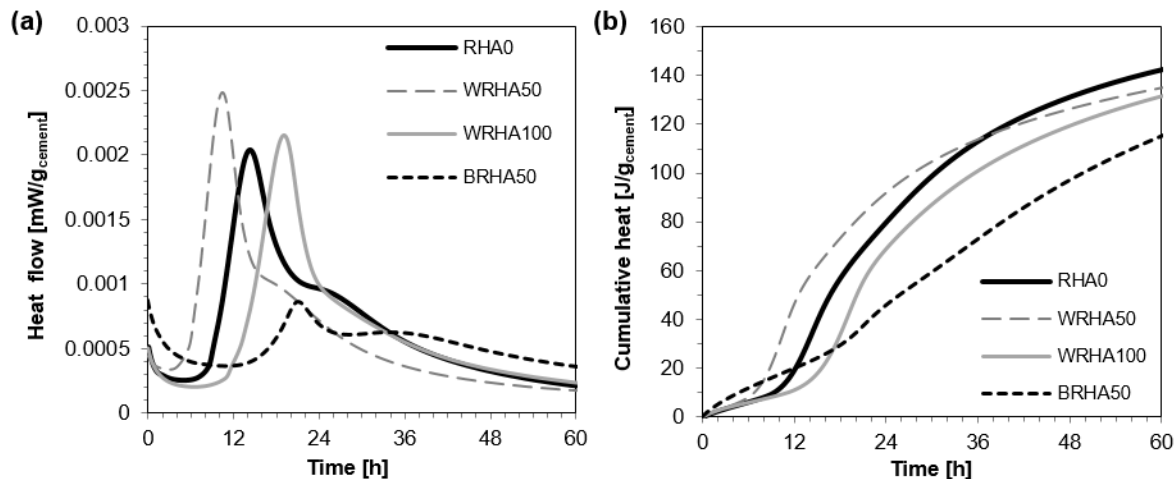


Figure 2: (a) Heat flow and (b) cumulative heat of paste samples

3.2 Microstructural investigation

The results of XRD analysis showed notable differences in the peaks of cement clinkers (alite, belite and ferrite) and ettringite among the samples. The most significant difference was found in quartz peak which depends on the filler composition. It was also found that the peak intensity of the portlandite (2θ =near 18°) is exceptionally strong in the sample containing BRHA. This indicates poor pozzolanic reaction of the sample compared with the other samples. In addition, the results of TG analysis confirmed that the portlandite content in the paste samples is decreased when WRHA is used instead of QP. The contents of RHA0, WRHA50, WRHA100 were 2.6 wt.%, 1.5 wt.% and 1.6 wt.%, respectively.

The replacement of QP with WRHA was effective to make pore structure of UHPC finer, especially in the pore size of 10–50 nm which corresponds to the capillary pores in low w/c concretes [19]. It should be noted that the pore size measured by MIP is not real but the pore entry size due to the ink-bottle effect [15]. Among the three samples (RHA0, WRHA50, WRHA100), there was no notable difference in the critical pore diameter formed around 20 nm, whereas the volume of the capillary pores (10–50 nm) decreased by 10-30% in the sample containing WRHA, compared to the sample RHA0. This might be due to additionally formed C-S-H gels which can fill up the capillary pores [20]. The promoted pozzolanic reaction, confirmed by the TG analysis also supports this. Nevertheless, as shown in Table 3, total porosity of WRHA100 was almost similar to that of RHA0. This is due to the increase in the pore volume between 50 nm–10 μ m of size range, which could be caused by the pores inside WRHA particles. Meanwhile, the pore structure of UHPC changed undesirably when BRHA was used. Especially, the volume of large pores (> 50 nm) increased significantly.

Table 3: Total porosity by MIP

Samples	RHA0	WRHA50	WRHA100	BRHA50
Porosity (%)	9.66	8.17	9.90	16.42

3.3 Strength development

Figure 3 shows the compressive strength of UHPCs as a function of time. The results reveal the significance of combustion conditions of RHA when it is used as a filler or SCM of concrete. The use of WRHA filler had a crucial impact on the strength development of UHPC, especially in long-term ages. When 50% and 100% of QP were replaced with WRHA, 91 days-strength was improved by 8% and 19%, respectively. However, surprisingly, the strength was decreased by 24%, when half of QP was replaced with BRHA. This is due to the unburned carbon contents in BRHA which negatively affects hydration reaction and pore structure.

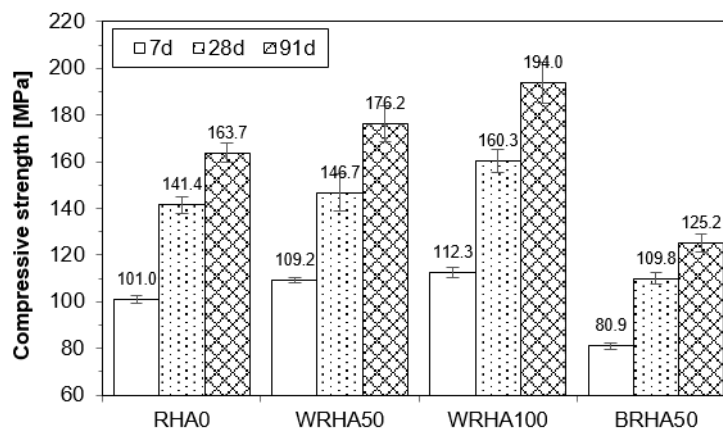


Figure 3: Compressive strength of UHPC samples

4. CONCLUSIONS

In this study, two types of RHAs, produced by different combustion processes were used in UHPC, instead of the conventional filler, QP. Due to the similarity in chemical composition, the ash has been considered as a substitute of SF. However, we considered to use this agricultural waste as reactive and functional fillers for its wide application in concrete industry. Furthermore, it was demonstrated that the RHA filler has positive effects on the mechanical properties and the pozzolanic reaction. In this regard, the compressive strength of UHPC remarkably improved and the volume of capillary pores was decreased. Further improvements in mechanical properties can contribute to mitigating heat-treatment process of UHPC, which is generally 48 hours of steam curing at 90 °C; thus, the method can reduce manufacturing cost of precast UHPC elements. However, this positive effect was only effective in the case of WRHA. When BRHA was used, hydration significantly delayed and strength loss occurred. Thus, this study also emphasized the importance of combustion process in the manufacturing of RHA filler.

ACKNOWLEDGEMENTS

This research was supported by Basic Science Research Program through the National Research Foundation of Korea (NRF) funded by the Ministry of Education (NRF-2018R1C1B6003058).

REFERENCES

- [1] Zhang, M.H., R. Lastra, and V.M. Malhotra, 'Rice-husk ash paste and concrete: Some aspects of hydration and the microstructure of the interfacial zone between the aggregate and paste', *Cem. Concr. Res.* **26** (6) (1996) 963-977.
- [2] Prasara-A, J. and Gheewala, S.H., 'Sustainable utilization of rice husk ash from power plants: A review', *J. Clean. Prod.* **167** (2017) 1020-1028.
- [3] Cheah, W.-K., Ooi, C.-H. and Yeoh, F.-Y. 'Rice husk and rice husk ash reutilization into nanoporous materials for adsorptive biomedical applications: A review', *Mesoporous Biomaterials* **3** (1) (2016).
- [4] Msinjili, N.S., Schmidt, W., Rogge, A., and Kühne, H.-C., 'Performance of rice husk ash blended cementitious systems with added superplasticizers', *Cem. Concr. Compos.* **83** (2017) 202-208.
- [5] Rodríguez de Sensale, G., 'Strength development of concrete with rice-husk ash', *Cem. Concr. Compos.* **28** (2) (2006) 158-160.
- [6] Alex, J., Dhanalakshmi, J., and Ambedkar B., 'Experimental investigation on rice husk ash as cement replacement on concrete production', *Constr. Build. Mater.* **127** (2016) 353-362.
- [7] Nair, D.G., Fraaij, A., Klaassen, and A.A.K., Kentgens, A.P.M., 'A structural investigation relating to the pozzolanic activity of rice husk ashes', *Cem. Concr. Res.* **38** (6) (2008) 861-869.
- [8] Van Tuan, N., Ye, G., van Breugel, K., and Copuroglu, O., 'Hydration and microstructure of ultra high performance concrete incorporating rice husk ash', *Cem. Concr. Res.* **41** (11) (2011) 1104-1111.
- [9] Van, V.-T.-A., Rößler, C., Bui, D.-D., and Ludwig, H.-M., 'Rice husk ash as both pozzolanic admixture and internal curing agent in ultra-high performance concrete', *Cem. Concr. Compos.* **53** (2014) 270-278.
- [10] Kang, S.-H., Lee, J.-H., Hong, S.-G., and Moon, J., 'Microstructural investigation of heat-treated ultra-high performance concrete for optimum production', *Materials* **10** (9) (2017) 1106.
- [11] Richard, P. and Cheyrezy, M., 'Composition of reactive powder concretes', *Cem. Concr. Res.* **25** (7) (1995) 1501-1511.
- [12] Schachinger, I., Hilbig, H., and Stengel, T., 'Effect of curing temperature at an early age on the long-term strength development of UHPC', Proceedings of the 2nd International Symposium on Ultra High Performance Concrete, Kassel, Germany, March, 2008 (Kassel University, Kassel, 2008) 205-212.
- [13] ASTM C109 / C109M-16a, 'Standard test method for compressive strength of hydraulic cement mortars (Using 2-in. or [50-mm] cube specimens)' (ASTM International, 2016).
- [14] Schöler, A., Lothenbach, B., and Winnefeld, F., 'Hydration of quaternary Portland cement blends containing blast-furnace slag, siliceous fly ash and limestone powder', *Cem. Concr. Compos.* **55** (2015) 374-382.
- [15] Scrivener, K., Snellings, R., and Lothenbach, B., 'A practical guide to microstructural analysis of cementitious materials', (CRC Press, 2016).
- [16] Justs, J., Wyrzykowski, M., Bajare, D., Lura, P., 'Internal curing by superabsorbent polymers in ultra-high performance concrete', *Cem. Concr. Res.* **76** (2015) 82-90.
- [17] Snoeck, D., Schaubroeck, D., Dubruel, P., and De Belie, N., 'Effect of high amounts of superabsorbent polymers and additional water on the workability, microstructure and strength of mortars with a water-to-cement ratio of 0.50', *Constr. Build. Mater.* **72** (2014) 148-157.
- [18] Kong, F.-r., Pan, L.-s., Wang, C.-m., Zhang, D.-l., and Xu, N. 'Effects of polycarboxylate superplasticizers with different molecular structure on the hydration behavior of cement paste', *Constr. Build. Mater.* **105** (2016) 545-553.
- [19] Aligizaki, K.K., 'Pore structure of cement-based materials: testing, interpretation and requirements', (Taylor & Francis, 2006).

- [20] Cheyrezy, M., Maret, V., and Frouin, L., 'Microstructural analysis of RPC (Reactive Powder Concrete)', *Cem. Concr. Res.* **25** (7) (1995) 1491-1500.

POTENTIAL USE OF ASH FROM THE PAPER INDUSTRY AS SCM

Sabina Kramar (1), Vilma Ducman (1)

(1) Slovenian National Building and Civil Engineering Institute, SI

Abstract

The study investigates the potential of use of ash from paper industry in mortars. For that purpose the influence of 5%, 10% and 20% substitution of cement with two different ashes (K4-fly ash from co-combustion of coal, bark, biomass and/or paper sludge, and K5-mixture of bottom ash and fly ash from co-combustion of paper sludge) on mortar properties was studied. Properties of fresh mixtures and hardened mortars were assessed using various methods. Among fresh properties workability and setting time were investigated. The evolution of compressive and flexural strength of hardened mortars was studied through test performed at 7, 28, 56, 180 and 365 days. Furthermore durability properties of mortars with addition of ash were determined. Results showed that by higher replacement level the workability was in general enhanced while initial and final setting times were prolonged. In a hardened state the addition of ash decreases early age and long term compressive strength of the mortars.. However, bond strength of mortars can be considerably increased, by applying K4 or K5. While frost resistance is higher in case of K5 ash, mixtures with K4 showed better sulfate resistance and resistance to carbonation.

Keywords: ash, SCM, cement replacement, mortars, durability

1. INTRODUCTION

Supplies of currently used supplementary cementitious materials (SCM), like fly ash and slags are limited, therefore most recent research has focused on the potential of alternative SCMs and their performance in building materials [1]. Among SCMs, fly ash is by far the most widely used in the manufacture of cement and concrete products. However, current standards (EN 197-1, EN 450-1) allow the use of fly ash from power stations, which originates from the combustion of coal with or without co-combustion of biomass materials or other sources. However, the amount of ash derived from co-combustion must not exceed 30% by mass of the total ash. Ashes of other origin, such as municipal and industrial waste incineration ashes, are excluded from addition to cements or concrete. In contrast to those obtained from coal combustion, biomass fly ashes are characterised by a high content of

calcium oxide and a low content of iron oxide [2]. Although biomass-combustion fly ashes are today typically disposed of in landfills or recycled on agricultural fields and forest land, they do, similarly to coal-combustion fly ashes, possess a certain capacity to react chemically with $\text{Ca}(\text{OH})_2$, producing a relatively stable C–S–H gel [3]. Properties of paper mill ash depend on the fuel and the type of incineration plant and this affects their reactivity.

Within the previous research [4] it was shown that according to the tests of pozzolanic activities (SAI index and Fratini test) these ashes cannot be classified as pozzolanic additives. In the present work two different types of ash originating from the paper industry were assessed with respect to their potential use as additive to the mortars. The properties of mortars with different amounts of cement replacement by the two ashes on properties of fresh mixtures as well as physical-mechanical and durability properties of mortars were investigated.

3. EXPERIMENTAL

3.1 Materials

Two types of ash were obtained from a paper mill, ash K4 representing fly ash from the combustion of coal, biomass and/or paper sludge, and K5 the combustion residue from a steam boiler in which de-inking fibre paper sludge, waste wood and bark are used as fuel, producing a mixture of ca. 90% bottom ash and 10% fly ash. Chemical and physical data are shown in Table 1. K4 ash consists of the following phases: quartz, periclase, hematite, gehlenite, lime and brownmillerite, while K5 ash contains calcite, larnite, lime, portlandite, mayenite and periclase.

Six different mortar mixtures were prepared by mixing cement and two different types of ash at substitution levels of 5 %, 10% and 20% by weight. Mortars were prepared at a constant flow value ($182 \pm 5 \text{ cm}^3$). The reference mixture consisted entirely of CEM I.

Table 1: Main chemical and physical parameters of ash

Parameter	K4	K5
SiO ₂	27.84	13.53
Al ₂ O ₃	9.01	9.35
Fe ₂ O ₃	13.92	0.42
CaO	25.92	53.02
P ₂ O ₅	0.72	0.23
MgO	9.79	2.14
K ₂ O	2.18	0.31
Na ₂ O	1.04	0.25
SO ₃	1.87	0.27
LOI	3.99	18.6
Reactive CaO	26.18	31.65
Reactive SiO ₂	15.12	11.80
Free CaO	7.05	17.26
Cl ⁻	0.25	0.07
BET	10.99	7.21

3.2 Methods

The workability of the fresh mortar mixtures was investigated by means of the flow test according to EN 13395-1, 10 min and 30 min after mixing, while setting time was determined according to EN 480-2.

Compressive and flexural strength of mortars were determined after 7, 28, 56, 180 and 365 days in accordance with EN 196-1. Bond strength determination by pull-off was performed according to EN 1542. Sulfate resistance of mortars was determined according to ASTM C 1012/C1012M-09.

Length change was measured at 1, 2, 3, 4, 8, 13 and 15 weeks, using the length comparator. Subsequent measurements were made at 4, 6, 9 and 12 month.

The carbonation of the mortar samples was assessed on mortar prisms having dimensions of 40 mm × 40 mm × 160 mm, according to EN 13295. The samples were cured for 24 h in a mould, wrapped in film. After de-moulding, the samples were cured for 48 h, wrapped in film, and then for 25 d at (21 ± 2) °C and at a RH of (60 ± 10) %. After this, they were placed in a chamber containing CO₂ 1 %, at a RH of (60 ± 10) %. The depth of the carbonation was determined by spraying a phenolphthalein indicator solution onto the freshly broken surface at 28 and 56 days of exposure.

For the investigation of the resistance to freezing/thawing in the absence of de-icing salt, mortar samples having dimensions of 40 mm × 40 mm × 160 mm were cured for 28 d in water at (20 ± 1) °C. After this, some of the samples were exposed to freeze/thaw cycling, whereas the remaining samples were left in the water at (20 ± 1) °C. Freeze/thaw cycling was performed according to the standard SIST 1026: 2008. All the samples were exposed to 50 cycles of freezing/thawing, where one cycle consisted of 4h at (-20 ± 2) °C and 4h at (20 ± 2) °C.

4. RESULTS AND DISCUSSION

4.1 Fresh properties of mortars

The properties of the fresh mortars are presented in Table 2. As seen from the table the flow value after 10 min increased with the replacement level of ash which is most obvious for K4 ash. After 30 min the flow value of the K4 ash increased as well, but remained quite constant for K5 ash. With respect to the reference mixture, workability is not enhanced much in case of addition of K5 ash, while in lower amount for K4 is even reduced, which is probably related to the fineness of the ash (for instance, % of particles < 0,125 mm for K4 is 90.5 wt.% and for K5 31.6 wt.%).

The values of initial and final setting times differed between the mixtures of K4 and K5. While replacement of cement with K5 ash prolonged the initial and setting time with increasing its amount, the replacement of cement by K4 ash in smaller amount slightly reduced the setting times. Ash K5 contain high fraction of inert phases (calcite, quartz). When compared to reference mixture, with exception of K4 5% the initial setting time was prolonged. On the other hand, final setting time was prolonged for all except for K4 5 % and K4 10%.

Table 2: Properties of the fresh mortars

Replacement level	Initial setting time (min)	Final setting time (min)	Workability 10 min (mm)	Workability 30 min (mm)
0 %	280	370	175.5	169.0
K4 5 %	273	358	159.0	150.5
K4 10 %	295	350	173.0	156.0
K4 20 %	340	385	181.5	171.5
K5 5 %	340	425	173.0	167.0
K5 10 %	340	420	177.5	170.5
K5 20 %	355	440	179.5	170.0

4.2 Mechanical properties of mortars

As seen from the Figure 1, compressive strength of the mixtures decreased with replacement levels for both K4 and K5 ash. The decrease is higher for K5 ash, which is due to the high amount of its inert fraction, and decreased significantly at 20 % of replacement level. On the other hand, compressive strength of the K4 ash gradually decreased with replacement level from 5 to 20 wt.%. Moreover, with the time the compressive strength of the K4 ash increased gradually over the period of 365 days. As regards K5 mixture, compressive strength increased with the time as well. However, when 20wt.% of K5 ash is added the compressive strength remained quite constant over the time period. The similar trend is observed for flexural strength. However, no deterioration of mechanical properties was noted with time of curing.

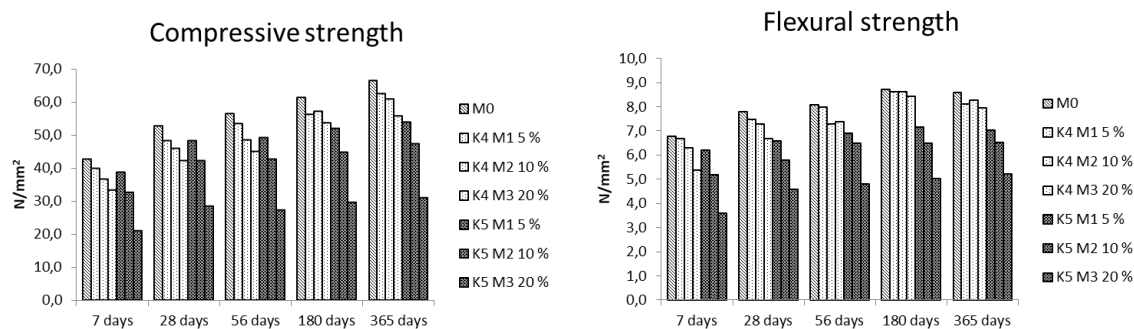


Figure 1: Compressive and flexural strengths of the investigated mortars.

Bond strength of the mortars ranged from 1.21 to 1.35 N/mm² and from 0.56 to 1.40 N/mm² for K4 and K5 ash, respectively. As observed from the results (Table 4), addition of ash improved the bond strength of mortars with respect to reference mixture. In the case of K5 ash a 100% cohesion failure was observed in mortar layer indicated that the mortar is the weakest part of the system. The type of the failure was more variable in the case of mortars with K5 ash, where the observed failure was adhesion failure and cohesion failure in mortar substrate. However, with respect to the reference mortars, the failure is in much higher respect of type B when cement is replaced by fly ash.

Table 4: Bond strength of investigated mixtures: A: cohesion failure in concrete substrate, B: cohesion failure in mortar layer, A/B: adhesion failure.

Mixture	Replacement level (%)	Bond strength (N/mm ²)	Type of failure (%)
M0	0	0.98	94% A/B, 6% B
K4	5	1.35	62% A/B, 38% B
	10	1.23	84% A/B, 16% B
	20	1.21	64% A/B, 36% B
K5	5	1.37	100% B
	10	1.40	100% B
	20	0.56	100% B

4.2 Durability properties of mortars

The depth of carbonation of the mortar samples exposed to accelerated carbonation was highest in the case of K5 ash. While there is no significant difference observed for different replacement levels for K4 ash, the carbonation depth of mortars with K5 ash increased with higher replacement level and with 20% penetrated the sample after 56 days of exposure to accelerated carbonation.



Figure 2: Carbonation depth of mortars after 28 day curing in air (up) and 56 days of exposure to accelerated carbonation (below): left : reference mixture, middle : 20% of K4 ; right : 20% of K5.

The results showed (Table 6) that, after the freeze/thaw cycling, the compressive strength of the samples decreased by 40 to 50 % for K4. However compressive strength of mortars with K5 ash did not change significantly after freeze/thaw cycling. Similar trend was observed for flexural strength.

Table 6: Compressive and flexural strengths of the investigated mortar samples after freeze/thaw cycling.

Mixture	Compressive strength (N/mm ²)		Flexural strength (N/mm ²)	
	Water cured	Freeze/thaw cycling	Water cures	Freeze-thaw cycling
Ref.	50.6	31.5	6.4	2.3
K4 5%	46.5	26.8	6.2	2.2
K4 10%	46.7	23.2	6.1	1.1
K4 20%	41.6	25.0	6.4	1.3
K5 5%	44.4	42.4	6.3	5.9
K5 10%	38.1	39.7	6.0	5.8
K5 20%	25.3	26.4	5.0	3.9

Length change of mortars exposed to sulphate solution is shown in Figure 3. While the K4 mixtures significant change in length, mixtures with higher amounts of K5 ash showed expansion in later periods. After 8 weeks, mixture with 20wt% of K5 ash showed more than 0.10 % of length change and prisms deteriorated after 13 weeks. However, all mortars with K4 ash showed the value below the limit of the standard ASTM C 1012/C1012M-09 which requires value below 0.10 %.

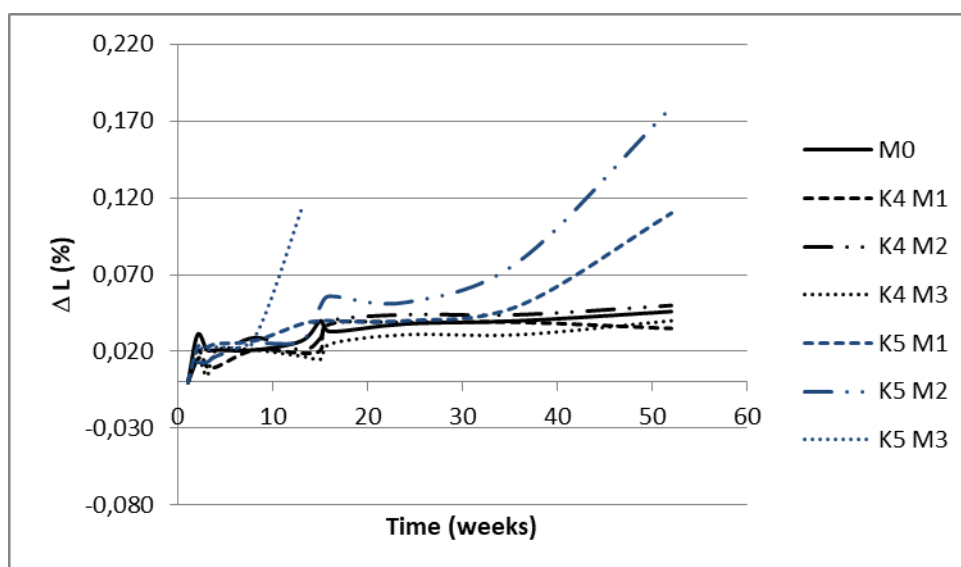


Figure 3: Length change of mortars with investigated ash after exposure to sulfate solution.

5. CONCLUSIONS

In order to determine how ash from paper industry influences the selected properties of mortars, mixtures were prepared at 5%, 10% and 20% levels of substitution of cement with ash by weight. Two types of ash were studied: K4-fly ash from co-combustion of coal, bark, biomass and/or paper sludge, and K5-mixture of bottom ash and fly ash from co-combustion of paper sludge.

Results showed that the two ashes, which differentiate in their mineralogical, chemical and physical characteristics influences differently the properties of fresh and hardened mortars as well as their durability. In general, workability of mortars is enhanced by the increasing ash replacement level, which is more significant for K4 ash. Furthermore, initial and final setting times are prolonged notably for K5 ash with respect to the reference mixture. Both ashes, when replaced cement, decrease compressive and flexural strength of the mortars, which increased with percentage of replacement level. Decrease in strength is higher for K5 ash. Addition of ash contributes to the improved bond strength with respect to reference mortar. Moreover, while frost resistance is higher in case of K5 ash, mixtures with K4 showed better sulfate resistance and resistance to carbonation.

Eventough addition replacement of cement with investigated ashes in general worsen the characteristics of mortars, certain improvement, like bond strength deserves further investigations, especially with K4 mortar which might provide at lower percentage still satisfactory mechanical strength, and improved bond strength in certain cases might justify the slight loss of mechanical strength.

ACKNOWLEDGEMENTS

The work was carried out within the RDI project Cel.Cycle: “Potential of biomass for development of advanced materials and bio-based products”, co-financed by the Republic of Slovenia, Ministry of Education, Science and Sport, and the European Union under the European Regional Development Fund, 2016-2020. The Metrology Institute of the Republic of Slovenia is acknowledged for the use of XRF.

REFERENCES

- [1] Juenger, M.C.G. and Siddique, R., 'Recent advances in understanding the role of supplementary cementitious materials in concrete', *Cement and Concrete Research*, 78 (2015)71-80.
- [2] Rajamma R., Ball, R.J., Tarelho L.A., Allen, G.C., Labrincha, J.A., Ferreira, V.M., Characterisation and use of biomass fly ash in cement-based materials. *J Hazard Mater.* 172 (2009) 1049-1060.
- [3] Esteves TC, Rajamma R, Soares D, Silva AS, Ferreira VM, Labrincha J.A. Use of biomass fly ash for mitigation of alkali-silica reaction of cement mortars. *Cons Build Mat.* 26 (2012) 687-693.
- [4] Kramar, S., Ducman, V. Evaluation of ash pozzolanic activity by means of the strength activity index test, Frattini test and DTA/TG analysis, *Technical Gazette*, (2018), in press

A STUDY ON FEASIBILITY OF CEMENT CLINKER MANUFACTURE USING OYSTER SHELL AS LIMESTONE SUBSTITUTE

Sungwun Her (1), Hyeonseok Jee (1), Taehoon Park (1), Dongcheon Park (2), and Sungchul Bae (1)

(1) Department of Architectural Engineering, Hanyang University, Seoul, 04763, Republic of Korea

(2) Department of Architecture and Ocean Space, Korea Maritime and Ocean University, Busan, 49112, Republic of Korea

Abstract

Since the development of shellfish-farming, oyster shells have caused environmental problems along the coast because they are not recycled enough. Previous papers studied recycling oyster shells in construction materials, but they only focused on replacing fine aggregate. This study focuses on the use of oyster shells to replace limestone in manufacturing Portland cement clinker, in order to use a waste material, shells, to make the manufacturing process more sustainable than current cement production methods. The performance of oyster shell cement (OSC) was compared with ordinary Portland cement (OPC) using X-ray powder diffraction, and its structures were identified by Rietveld quantitative phase analysis. The OSC was compared with specimens manufactured with limestone in same conditions (LPC). Cement paste of OPC, OSC and LPC were measured at 1,3, and 7 days to compare strength development. The compressive strength of OPC and OSC developed equivalently over the long-term. The results show that Portland cement clinker can be manufactured using oyster shells, replacing 100% of the limestone. Through this series of analyses, the overall properties of OSC were found to be similar to OPC

Keywords: Oyster Shell, Cement Clinker, Limestone, Recycle, Waste Management

1. INTRODUCTION

Oysters, which are distributed throughout the ocean, are cultivated in the southern and western coastal areas for supplying commercial markets. However, only the oyster content is consumed, and the shell remains on the island due to the difficulty of waste management. Each year, almost 300,000 tons of oyster shells are produced in Korea, but only 10% of shells are properly recycled. Many of the remainder are buried, causing environmental problems due to illegal dump.

One method for recycling oyster shells has been studied: pulverizing shells to use as a substitute for fine aggregate in mortar [1, 2]. However, that study concluded that there is no positive effect on the strength of the mortar from the oyster shell addition. Moreover, as the substitution rate of shells in mortar increased, the strength of the mortar was drastically reduced.

The components of oyster shells are more than 95% trigonal calcite (CaCO_3), which possesses a crystal structure identical to that of limestone, one of the main raw materials in ordinary Portland cement (OPC). Therefore, it may be possible to reuse shells as a substitute for limestone in OPC.

To manufacture OPC, limestone is synthesized at high temperature with the other raw materials. The manufacturing process of OPC uses high energy consumption for firing, extracting, crushing, and producing the final product. Mining of limestone causes not only high energy consumption but also environmental destruction and depletion of natural resources.

Although there are numerous studies on the reuses of waste or industrial byproducts in cement production, most of the research suggests to replacing clay, quartz, and slag as opposed to limestone [3-5].

In this study, we synthesize oyster shell cement (OSC) and limestone Portland cement (LPC) to investigate the feasibility of oyster shells as a substitute for limestone in the manufacture of OPC clinker. To determine the proper proportion of oyster shell and other raw materials in the OSC clinker production, the Bogue calculation and X-ray fluorescence spectroscopy (XRF) were used. The crystalline phases of the synthesized OSC clinker at different temperature were identified by X-ray powder diffraction (XRD). A compressive strength test was performed to determine the reactivity of OSC and LPC.

2. METHODS

2.1 Bogue Calculation

The compositions of the cement are calculated by the Bogue equation, which is widely used on the cement industry. Generally, OPC is composed mainly of alite (C_3S), belite (C_2S), aluminite (C_3A), and ferrite (C_4AF), and is synthesized at high temperatures in a kiln. The Bogue calculation gives proper ratios for the blending process of the raw material. [6]

In the Bogue calculation, the lime saturation factor (LSF), silica modulus or silica ratio (SM or SR), and iron modulus (IM) values are formulas that can control the composition of clinker, and their values should be adjusted depending on the type of cement. In this study, the composition of the cement was calculated based on type I OPC according to ASTM C150.

The Bogue formula values based on type I OPC are shown in Table 1.

Table 1: Bogue Calculations for Type I OPC

Bogue Calculation	LSF	SM	IM	C₃S (%)	C₂S (%)	C₃A (%)	C₄AF (%)
OPC	91	2.7	1.7	55	19	10	7

2.2 Mix Proportion of OSC and LPC

Oyster shell and limestone were pulverized from raw material and filtered through 200 mesh (75 μm) before dry mixing in its proper ratio from the Bogue calculation, respectively. Quartz, slag, and clay were also filtered and mixed in the same method as the oyster shell and then all those materials were mixed in a paste mixer for up to 8 minutes. The optimum mixture ratio of raw materials is shown in Table 2.

Table 2: Mix Proportion of Raw Materials in Weight Percent for OSC and LPC

Oxides	Oyster Shell/ Limestone	Quartz	Slag	Clay
OSC (wt %)	78.52	11.12	2.98	7.37
LPC (wt %)	80.41	10.42	2.58	6.59

The chemical composition of the oyster shell was measured by XRF (ZSX PrimusIV, Rigaku) and is shown in Table 3. From the XRF data, it was concluded that the major component of oyster shell, like limestone, is calcite.

Table 3: Chemical Composition of the Oyster Shell and Limestone Measured by XRF

Oxide	Chemical Unit								
	SiO ₂	Al ₂ O ₃	Fe ₂ O ₃	CaO	MgO	Na ₂ O	K ₂ O	SO ₃	LOI
Oyster Shell (%)	0.05	0.04	0.01	53.79	0.30	0.57	0.08	0.43	44.50
Limestone (%)	1.77	0.54	0.37	53.41	0.52	0.01	0.07	0.01	43.24

2.3 Synthesis Process for OSC and LPC

The OSC and LPC were synthesized at a temperature of 1470°C for about 30 min in an electric furnace (Nabertherm, 17/LB), after which they were quenched for about 8 min for rapid cooling at nature temperature (laboratory environment temperature of 20°C). The structure phases of OSC and LPC were characterized using XRD (D2 Phaser, Bruker) and the phases were quantified by Rietveld refinement (TOPAS, Bruker).

The OSC and LPC clinkers were pulverized with gypsum of 3 wt% in a ball mill (Planetary Mono Mill, Fritsch). Thereafter, OSC and LPC were filtered to collect particle under 100 μm .

OPC, OSC and LPC paste specimens were produced with distilled water (water/cement ratio=0.48) in a 5×5×10 mm³ column-shaped mold and put into a thermos-hygrostat for 24 h at 20 °C and 60% relative humidity (RH). Specimens were then cured in distilled water at a temperature of 20 °C.

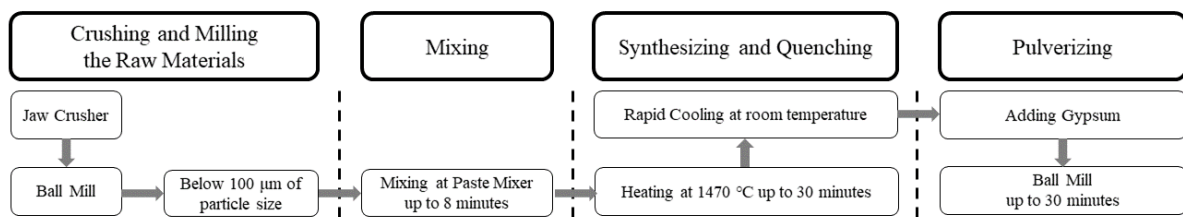


Figure 1: Flowchart of OSC synthesis method

3. RESULTS

3.1 Identifying Structure of Limestone and Oyster Shell

The oyster shell was compared with limestone using XRD analysis to identify the structure, and the result are illustrated in Figure 2.

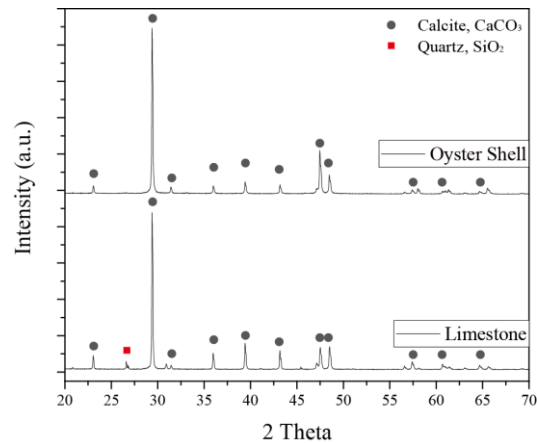


Figure 2: XRD Patterns from Limestone and Oyster Shell

The XRD data shows trigonal-calcite (COD 900965), which quantified(EVA Software, Bruker), a main phase in both limestone and oyster shell. However, quartz (COD 9009666) was measured slightly in limestone, whereas there was no quantified quartz in oyster shell. This result also followed previous data from XRF, it is the reason of differences in mix proportion between OSC and LPC. Consequently, oyster shell has the potential to replace limestone in cementitious raw material.

3.2 OSC Synthesis at Different Temperature

To study the reactions of oyster shells at different temperature, mixed raw materials for OSC were heated at 1200, 1250, 1300, 1350, 1400, and 1450 °C for up to 30 minutes.

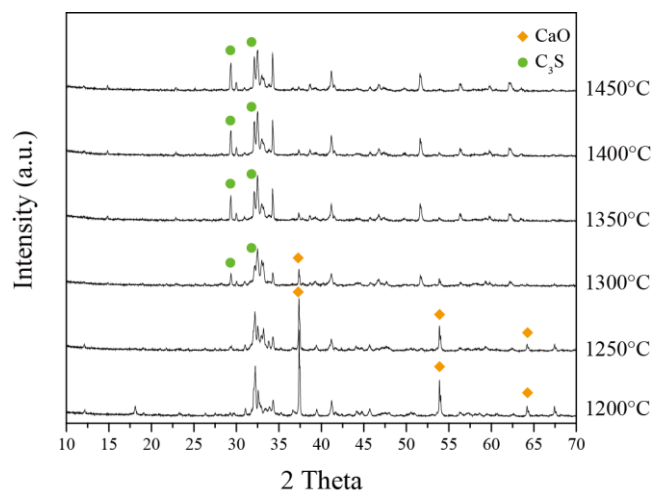


Figure 3: XRD Patterns of OSC Clinker at Different Temperatures

The figure 3 shows that free CaO is decreased gradually at up to 1200 °C. Free CaO, calcium carbonate, pyrolyze between 600 to 800 °C and is released by reacting with alumina, slag, and silica [6]. It transforms as C₃S, C₂S, C₃A, and C₄AF at temperatures more than 1400 °C. As confirmed in Figure 3, the XRD results observed the characteristic peaks of C₃S at more than 1300 °C.

3.3 Rietveld Quantitative Phase Analysis

Rietveld refinement analysis was performed in order to characterize anhydrous cementitious materials. Rietveld method is a very useful tool for identifying the crystal structures and measuring the quantification in cement [7]. Figure 4 shows a comparison of OPC, OSC, and LPC results from Rietveld quantitative refinement.

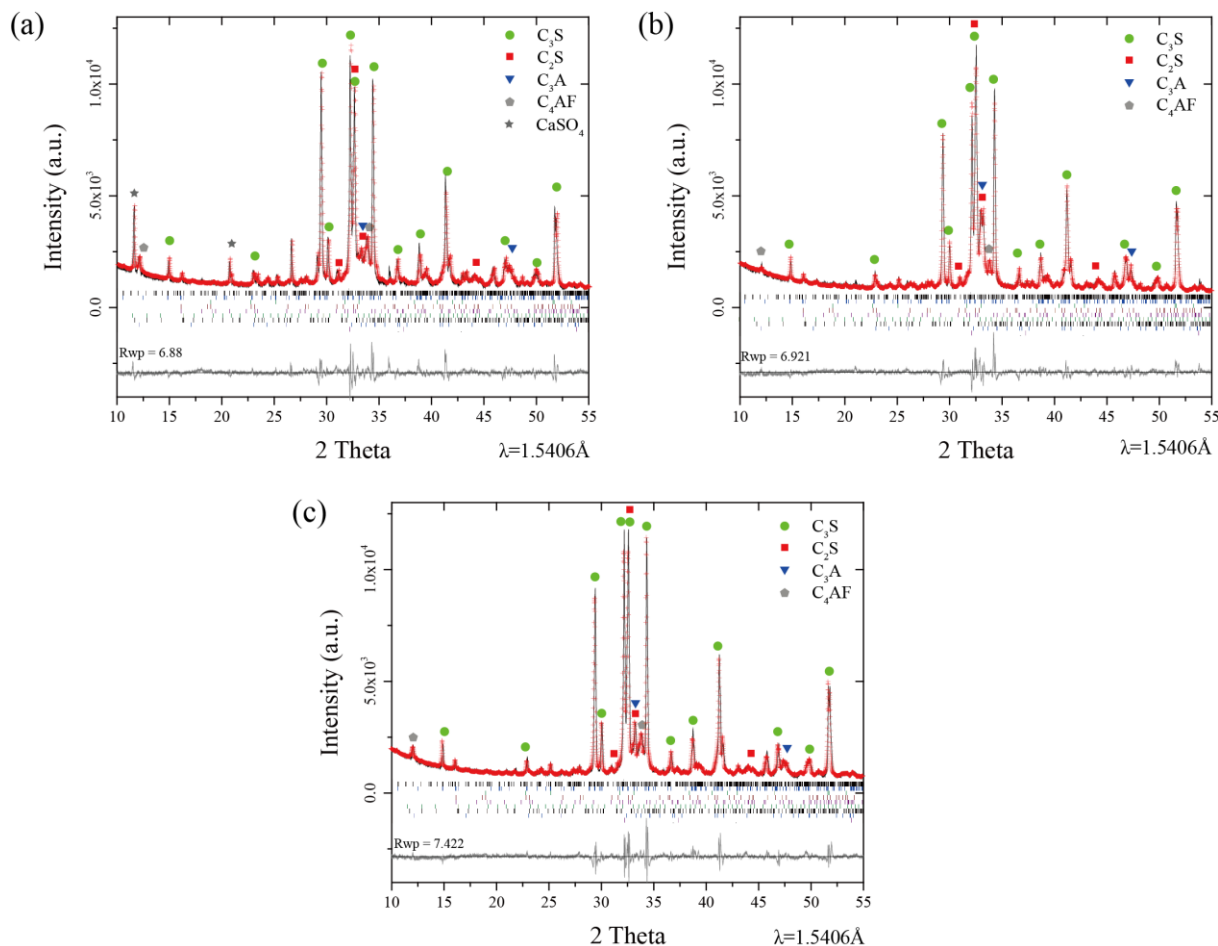


Figure 4: Rietveld Quantitative Phase Analysis of (a) OPC, (b) OSC, (c) LPC

By using Rietveld quantitative analysis, cementitious structure phases, such as C₃S, C₂S, C₃A, and C₄AF, were analyzed and labeled in Figure 4. The composition of the OPC, OSC, and LPC were compared quantitatively by TOPAS and are listed in Table 4. The main

cementitious structures were quantified similarly, concluding that clinker could be synthesized with oyster shells instead of limestone. However, because of differences in cooling the OPC and OSC clinker, the C_2S structures were differently quantified and are labeled as α' - C_2S and β - C_2S in Table 4.

Table 4: Phase Compositions of OPC and OSC

Oxide	$C_3S<M3>$	$C_3S<M1>$	α - C_2S	α' - C_2S	β - C_2S	C_3A Cubic	C_3A Ortho
OPC(%)	35.23	24.6	1.11	3.37	10.82	1.24	1.40
OSC(%)	31.61	28.92	1.86	20.42	2.07	1.93	6.06
LPC(%)	35.50	35.59	0.37	4.27	8.84	3.91	0.59
Oxide	C_4AF	Lime	Periclase	Quartz	Gypsum	Anhydrite	Calcite
OPC(%)	11.89	0.05	1.20	2.35	3.22	0.14	3.37
OSC(%)	5.91	0.35	0.04	0.46	0	0.16	0.21
LPC(%)	10.26	0.14	0.18	0.11	0	0.08	0.17

3.4 Compressive Strength

The compressive strength of OPC, OSC, and LPC paste were measured in each of three specimens after 1, 3, and 7 d of curing and the results are displayed in Figure 5.

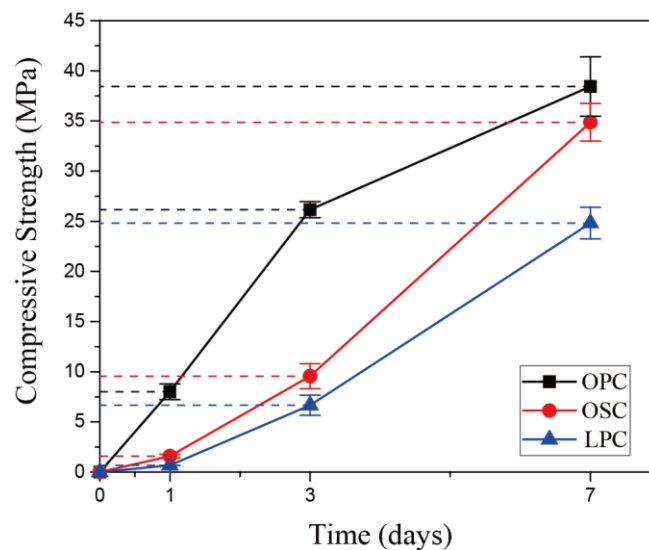


Figure 5: Compressive Strength of OPC and OSC Paste

The results show the OSC and LPC specimens exhibited a lower compressive strength compared to OPC specimens after 1 and 3 days of curing. The low compressive strength could be caused by the pulverized OSC and LPC particle size being dissimilar to OPC's particle size [8]. Figure 6 shows the calorimetry test results for OPC, OSC, and LPC.

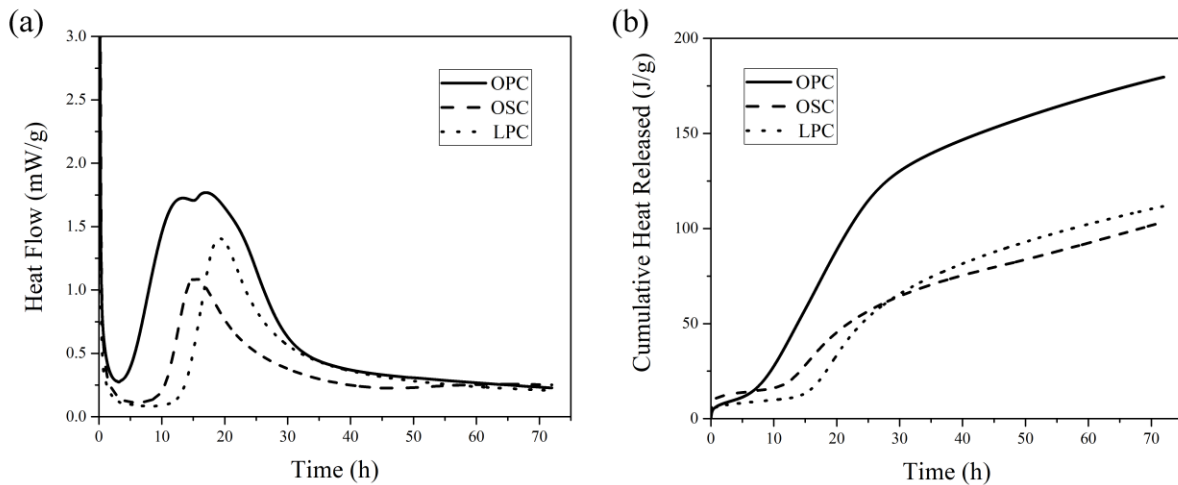


Figure 6: Calorimetry Measurements (a) Rate of Cement Hydration as a Function of Time
 (b) Cumulative Heat of Cement Hydration as a Function of Time

Consequently, properties such as strength, in Figure 5, and heat processing, in Figure 6-(b), are different because of differences in particle size distribution [9]. Cumulative heat released figure results followed as the compressive strength and heat flow. However, the results between OSC, LPC and OPC did not seem to be completely different. As shown in Figure 6-(a), although heat flow of OSC and LPC paste was slower and smaller than for OPC paste, the profile of the heat flow tended to be similar for both materials.

4. CONCLUSION

Those of results in this study can be summarized as follows.

- The main composition of oyster shell is trigonal calcite (CaCO_3), which has the same phase characteristic as limestone.
- OSC and LPC clinkers are synthesized properly at more than $1450\text{ }^\circ\text{C}$ for transforming to C_3S , C_2S , C_3A , and C_4AF from free CaO with clay, slag, and silica.
- XRD and Rietveld analyses show that clinker manufactured from pulverized oyster shells as a limestone substitute, is composed of cementitious materials as C_3S , C_2S , C_3A , and C_4AF . However, some C_2S composition is different because of differences between cooling environments in a laboratory versus and manufacturing plants.
- From the calorimetry test, heat flow of OSC and LPC pastes were delayed and less than OPC paste, although the heat flow profile of the OSC and LPC pastes are similar to that of OPC pastes.
- OSC specimens showed lower compressive strength at an early curing age than OPC specimens. The reason for lower strength is that the heat proceeding of OSC was not enough than OPC. Increasing strength of OSC will be further investigated in the near future.

ACKNOWLEDGEMENTS

This research was supported by the Basic Science Research Program through the National Research Foundation of Korea (NRF) funded by the Ministry of Science, ICT & Future Planning (NRF-2016R1C1B1014179).

REFERENCES

- [1] Yang, E.-I., Kim, M.-Y., Park, H.-G. and Yi, S.-T., 'Effect of partial replacement of sand with dry oyster shell on the long-term performance of concrete.' *Construction and Building Materials* 24(5) (2010) 758-765.
- [2] Liang, C.-F. and Wang, H.-Y., 'Feasibility of Pulverized Oyster Shell as a Cementing Material.' *Advances in Materials Science and Engineering 2013* (2013) 1-7.
- [3] Puertas, F., Garcia-Diaz, I., Barba, A., Gazulla, M. F., Palacios, M., Gomez, M. P. and Martinez-Ramirez, S., 'Ceramic wastes as alternative raw materials for Portland cement clinker production.' *Cement Concrete Comp* 30(9) (2008) 798-805.
- [4] Tsakiridis, P. E., Papadimitriou, G. D., Tsvivilis, S. and Koroneos, C., 'Utilization of steel slag for Portland cement clinker production.' *Journal of Hazardous Materials* 152(2) (2008) 805-811.
- [5] Aouad, G., Laboudigue, A., Gineys, N. and Abriak, N. E., 'Dredged sediments used as novel supply of raw material to produce Portland cement clinker.' *Cement and Concrete Composites* 34(6) (2012) 788-793.
- [6] Taylor, H. F. W. (1997). *Cement chemistry*. London, T. Telford.
- [7] Le Saout, G., Kocaba, V. and Scrivener, K., 'Application of the Rietveld method to the analysis of anhydrous cement.' *Cement and Concrete Research* 41(2) (2011) 133-148.
- [8] Sajedi, F. and Razak, H. A., 'Effects of curing regimes and cement fineness on the compressive strength of ordinary Portland cement mortars.' *Construction and Building Materials* 25(4) (2011) 2036-2045.
- [9] Bullard, J. W., Jennings, H. M., Livingston, R. A., Nonat, A., Scherer, G. W., Schweitzer, J. S., Scrivener, K. L. and Thomas, J. J., 'Mechanisms of cement hydration.' *Cement and Concrete Research* 41(12) (2011) 1208-1223.

NEW GENERATION OF CONSTRUCTION MATERIALS
SESSION 11: Calcined clay

COMPARING THE REACTIVITY OF DIFFERENT NATURAL CALCINED CLAYS UNDER ALKALI ACTIVATION

Ahmed Zohair Khalifa (1), Yiannis Pontikes (2), Jan Elsen (3), Özlem Cizer (1)

(1) KU Leuven, Department of Civil Engineering, Kasteelpark Arenberg 40, 3001 Leuven, Belgium

(2) KU Leuven, Department of Materials Engineering, Kasteelpark Arenberg 44, 3001 Leuven, Belgium

(3) KU Leuven, Department of Earth and Environmental Sciences, Celestijnenlaan 200C, B-3001 Heverlee, Belgium

Abstract

Metakaolin is one of the most popular solid aluminosilicate precursors for the synthesis of geopolymers. Despite its high reactivity and availability, there is a noticeable move towards the use of other natural clays as alternative precursors, due to their plentiful supply and widespread availability. Natural clays usually consist of a combination of 1:1 and 2:1 layer silicates. Four various natural clays with different proportions of 1:1 and 2:1 clay minerals were used in this study. The presence of different clay minerals yields a range of Si/Al ratio from 1.2 to 3.4.

This study aims firstly to determine the optimum calcination conditions to activate the clay minerals. Clays were calcined at different temperatures (700 to 900 °C) for different holding times (10 seconds to 60 minutes). The thermal transformations were studied by TGA and XRD analyses. The reactivity of the calcined clays with alkalis was assessed by the dissolution test and isothermal conduction calorimetry. The second aim of this study is to compare the reactivity of the calcined clays under alkali activation using NaOH. The chemical, mineralogical and physical properties of natural and calcined clays were characterized using XRD, calorimetry, ICP-OES, PSD, and BET analyses.

Keywords: Geopolymer; Common clays; Alkali activation; Thermal activation.

This work was invited for publication in the open access journal RILEM Technical Letters. You can visit the journal and benefit from the full open access to the published articles at: letters.rilem.net.

SUMMARY OF 4-YEARS OF RESEARCH AT IIT MADRAS ON CONCRETE WITH LIMESTONE CALCINED CLAY CEMENT (LC3)

**Ravindra Gettu, Manu Santhanam, Radhakrishna G. Pillai, Yuvaraj Dhandapani,
T. Sakthivel, Sripriya Rengaraju, Sundar Rathnarajan, Fathima Suma M.,
Anusha S. Basavaraja, Sanoop Prakasan and Nithya Nair V.G.**

Department of Civil Engineering, Indian Institute of Technology (IIT) Madras, Chennai, India

Abstract

Various properties of limestone calcined clay cement (LC3) as a binder and those of concretes made with LC3 were assessed during the last four years at IIT Madras to understand its potential as an alternative mainstream cement. LC3 from two major industry-scale productions was used in the evaluation, and the major findings from the research are summarized in this paper. LC3 concretes exhibit compressive strength development comparable to that of concrete made with ordinary portland cement (OPC). In general, they were found to have higher resistance to chloride ingress, moisture ingress, gas permeation, sulphate attack and corrosion-induced cracking, when compared to that of concretes of similar strength grade and/or mixture proportions but having other binders. From the assessment of chloride threshold and carbonation, LC3 concretes were found to have a lower chloride threshold for rebar corrosion and higher carbonation rate than similar strength concretes with OPC and fly ash. However, the service life under chloride attack is expected to be significantly longer for a reinforced concrete structure with LC3 than other commonly used concretes. The ecological impact of LC3 on the cement and concrete production was also found to be positive with a dramatic decrease in carbon footprint when LC3 replaces OPC.

1 INTRODUCTION

The global projection of cement consumption is expected to see a major rise in emerging economies [1]. In a technology roadmap by WBCSD and IEA, clinker substitution was identified as a major solution for sustainable transition to a controlled 2°C emission scenario [1, 2]. A ternary cement made of clinker, calcined clay and limestone, known as limestone calcined clay cement (LC3), has been shown to be promising as a low-clinker cement with comparable strength development characteristics to ordinary portland cement [2, 3]. In LC3, there is a two-fold reaction mechanism leading to the cementing matrix being enhanced through a combination of pozzolanic reaction and limestone-clay interaction.

In the present paper, an overview of major findings from the research projects (see Fig. 1 for project outline) at the Indian Institute of Technology (IIT) Madras, in Chennai, India, during the last four years, on the assessment of various properties of LC3 as a binder, and the potential areas of benefits and concerns is presented. To understand the suitability of the LC3 binder for the wide range of construction applications, it was necessary to study several properties relevant to different possible service/exposure conditions. To evaluate such properties, LC3 was produced on an industrial pilot scale in India [4]. Detailed investigations of the concrete properties including the workability, compressive strength, elastic modulus, shrinkage, chloride/carbonation/sulphate resistance, and corrosion characteristics were carried out. The sustainability potential of the cement and concrete was assessed by a systematic life cycle assessment (LCA) on energy and emission. The knowledge base created has the potential to help the uptake of LC3 technology for standardization and field applications for a transition to the large-scale use of this low carbon cement.

Fresh properties	<ul style="list-style-type: none"> • Setting time characteristics • Flow properties of cement paste • Compatibility with PCE and SNF based superplasticizers
Microstructural characteristics	<ul style="list-style-type: none"> • Porosity and pore size distribution • Hydrate phase assemblage and phase transformation on exposure to chlorides, sulphates and carbonation exposure
Mechanical properties	<ul style="list-style-type: none"> • Concrete mixture proportioning • Compressive strength evolution of concretes • Elastic modulus of concretes
Shrinkage characteristics	<ul style="list-style-type: none"> • Autogeneous shrinkage • Drying shrinkage • Mass loss in different binder systems –Drying potential
Durability characteristics	<ul style="list-style-type: none"> • Transport properties (permeation, diffusion, migration and sorption) • Resistance to Chloride/Sulphates/Carbonation ingress
Service life parameters	<ul style="list-style-type: none"> • Diffusion coefficient of concrete • Chloride threshold • Carbonation rate
Studies on curing conditions	<ul style="list-style-type: none"> • Steam curing • Retention for RMC applications • Curing effects -Field-crete Vs Lab-crete
Life cycle assessment for CO₂ and Energy	<ul style="list-style-type: none"> • LCA for cement production • LCA for concrete production

Figure 1. Outline of the research studies on LC3 at IIT Madras

2. HIGHLIGHTS OF THE MAJOR FINDINGS

2.1 Fresh properties

The flow behaviour of LC3 in the fresh state was studied by conducting various tests on cement paste and concrete with various water-to-binder ratios (w/b), and different types and dosages of superplasticizers (i.e., PCE - Polycarboxylic ether and SNF - Sulphonated naphthalene formaldehyde). The major conclusions from these test results are summarized in Table 1, where OPC denotes binders with only ordinary portland cement and FA30 denotes binders with 30% of the ordinary portland cement replaced with Class F fly ash.

Table 1. Summary of the fresh property tests and conclusions drawn.

Material type/ properties	Methodology	Major conclusions
Cement paste/ compatibility	Marsh cone and mini-slump test	Superplasticizer saturation dosage followed the order LC3>FA30>OPC, and the level of flow at saturation dosage was LC3≈FA30>OPC.
Cement paste/ rheology	Brookfield HA DV II + vane spindles	At higher w/b, the plastic viscosity is drastically reduced in the case of LC3 (at optimum dosages); indicating better ability to flow at higher w/b
Concrete/ workability	Slump test	Superplasticizer requirement for equivalent flow in paste/workability in concrete is higher for LC3 concretes. The retention of workability with LC3 concretes is poor.

2.2 Microstructure evolution

The influence of the highly pozzolanic nature of calcined clay and the formation of the additional hydrate phases result in the early reduction of pore sizes. The threshold diameters obtained from mercury intrusion porosimetry reflect early refinement in the pore structure of LC3 pastes with respect to the OPC and FA30 pastes. This difference in the microstructural development can be attributed to the difference in microstructural composition of LC3, in terms of CSH, with much lower Ca/Si ratio compared to OPC and FA30. It can be noted that early reactivity of calcined clay and the corresponding improvement in resistivity and pore structure are major governing factors leading to significant improvement in the properties in LC3 concrete, in contrast to those of FA30, where fly ash tends to react relatively slower and contribute to performance only after extended curing.

2.3 Mechanical properties and compressive strength evolution

Concrete mixes were prepared with two strength grades (M30 and M50, corresponding to 28-day characteristic compressive strengths of 30 and 50 MPa, respectively), along with C-mixes (i.e., ‘common mix designs’ with same binder content and water-binder ratio as the reference concretes). The mix details and other properties are provided in Table 2; further details can be found in [5-7]. The evolution of compressive strength for the same grade was

comparable for LC3 and OPC concretes. However, in the case of fly ash blended concrete (designated as FA30, for 30% replacement of cement by Class F fly ash), there was a need to reduce the w/b to produce a similar grade of concrete compared to LC3 and OPC. In the case of C-mixes, LC3 concrete systems exhibited faster compressive strength development than the other mixes. Also, the elastic moduli of all the concretes were found to be comparable (see Table 3).

2.4 Shrinkage characteristics

Nine concrete mixes were prepared, and 150 × 300 mm cylinders were cast from them and moist cured for 28 days. Later, the specimens were exposed to a controlled environment (65%±5% relative humidity and 25±3°C) and the total shrinkage was monitored as per RILEM TC 107-1998 procedure. Data from the results presented in [7] are summarised in Table 3; it was seen that in the same grade of concrete, the total shrinkage was predominantly controlled by the w/b. In the common mixes (C-mixes), the total shrinkage strains of all concretes at the end of one year were comparable/similar as given in Table 3.

2.5 Transport properties

The transport properties of concretes made with LC3 were evaluated after 28 and 90 days of curing. It was found that concretes made with LC3 attained higher resistivity, which in turn results in better resistance to the ingress of chloride as per the Rapid Chloride Penetration Test and Migration co-efficient assessment. Results of chloride resistance of LC3 concrete are presented in Table 3, with data from [7]. The chloride resistance always followed the order of LC3 > FA30 > OPC. With respect to oxygen permeability and water sorptivity, the ranking for concretes of equivalent strength grade was LC3 ≈ FA30 > OPC, and for concretes in the C-mixes (i.e., similar mixture proportions) the ranking was LC3 > FA30 > OPC.

Table 2 Mix design for the nine concretes studied

Concrete Set	Grade	Mix I.D.	w/b	Quantity (kg/m ³)				
				Binder content	Water	Fine aggregate	Coarse aggregate	
							10 mm	20 mm
1	M30	OPC M30	0.5	310	155	695	496	744
		FA30 M30	0.45	310	139.5	723	491	737
		LC3 M30	0.5	310	155	708	491	736
2	M50	OPC M50	0.4	360	144	703	477	716
		FA30 M50	0.35	380	133	699	475	713
		LC ³ M50	0.4	340	136	704	488	732
3	Common Mix (C-mix)	OPC – C Mix	0.45	360	162	721	463	694
		FA30 – C Mix	0.45	360	162	721	463	694
		LC ³ – C Mix	0.45	360	162	687	476	715

Table 3 Summary of results from nine concretes studied at IIT Madras [5-7]

Properties	Age (days)	OPC			FA30			LC3			
		M30	M50	C-Mix	M30	M50	C-Mix	M30	M50	C-Mix	
Compressive strength (MPa)	28	45.65	54.85	47.32	38.31	53.44	42.73	44.90	55.31	49.16	
	365	49.29	57.24	48.93	48.67	62.60	51.11	53.24	61.86	55.44	
Elastic modulus (GPa)	28	45.95	54.85	47.32	38.31	53.44	42.73	44.90	55.31	49.16	
Total shrinkage strain, for concrete subjected to drying after 28 days of curing (microstrain)	90	295	320	290	280	260	300	300	330	315	
	365	450	455	390	430	335	380	490	520	430	
Critical pore size (nm) from mercury porosimetry	28	41.1	32.7	74	31.6	43.8	41.3	24.4	16.4	20.4	
	90	31.9	23.0	74.5	20.8	14.9	18.3	17.3	23.4	19.8	
Charge passed in the RCPT (Coulombs)	28	2635	2040	2315	1355	1000	1665	125	100	100	
	90	2270	1760	2310	470	425	665	75	55	55	
	365	1260	2490	1590	210	210	200	60	50	20	
Chloride migration coefficient ($10^{-12} \text{ m}^2/\text{s}$)	28	18.8	10.8	11.8	12.5	6.3	13.6	1.9	1.2	1.2	
	90	18.3	8.9	15.3	3.9	2.3	5.1	1.1	0.8	0.9	
	365	10.9	3.4	10.6	1.7	1.2	1.6	0.5	0.5	0.5	
Chloride diffusion coefficient ($10^{-12} \text{ m}^2/\text{s}$)	365	18.7	15.6	12.6	2.6	1.9	3.5	3.5	1.7	1.3	
Carbonation depth (mm)	Accelerated – 1%	120	5.4	0	4.1	7.5	3.9	7.8	10.2	7.2	8.6
	Accelerated – 3%	120	11.9	0	7.2	15.0	6.4	13.6	19.9	12.9	16.8
	Natural-Sheltered	730	8.0	6.7	6.7	11.3	5.5	8.0	10.6	8.7	7.7
	Natural-Unsheltered	730	5.7	3.8	5.6	10.1	3.7	6.6	10.1	8.5	8.5
Time for corrosion-induced cracking (hours)		100-160	340-380	NA	200-280	380-480	NA	>500	>500	NA	
Energy consumed for production (MJ/m^3 of concrete)		330	370	375	260	300	290	250	270	280	
Emissions associated with the production ($\text{kg CO}_2 \text{ eq.}/\text{m}^3$ of concrete)		2750	3000	3025	2300	2600	2500	2500	2600	2700	

2.6 Sulphate resistance

Specimens were exposed to sodium and magnesium sulphate solutions to assess the damage caused. Changes in length were measured, as per ASTM C1012 procedures, over a period of 2 years. When exposed to sodium sulphate, LC3 and FA30 showed better performance (say, negligible expansion) than the OPC specimens, as shown in Table 4, see details in [8]. However, the LC3 samples exposed to magnesium sulphate solution experienced severe disintegration due to decalcification of C-(A)-S-H, and the formation of brucite and gypsum.

2.7 Chloride-induced corrosion

To study the corrosion resistance of LC3 against chlorides, short- and long-term tests were performed. The short-term tests include the determination of chloride threshold and the resistance against corrosion-induced cracking. The ASTM G109 test method was chosen for long-term monitoring against chloride induced corrosion. The chloride threshold was found to be higher for OPC than for FA30 and LC3, as given in Table 4, which is attributed to the higher consumption of $\text{Ca}(\text{OH})_2$ in the FA30 and LC3 systems [9]. When subjected to 15 volts for about 500 hours, the resistance of LC3 against corrosion-induced cracking was found to be better than the OPC and FA30; the LC3 specimens did not crack even after 500 hours. The ranking of corrosion cracking resistance is found to be as follows: LC3 >> FA30 > OPC. In the G109 tests, the specimens with LC3 exhibited lower macrocell current due to the higher resistance against ionic movement than in OPC and FA30.

Table 4 Summary of test results from mortar studies

Properties		OPC	FA30	LC3
Chloride threshold (%bwob)		0.44	0.32	0.17
Sulphate expansion (%)	336 days	0.1	Negligible	Negligible
	672 days	0.89	Negligible	Negligible

2.8 Carbonation

Concrete specimens of $100 \times 100 \times 500$ mm were cast and exposed to accelerated (i.e., concentrations of 1% & 3% CO_2) and natural carbonation (0.04% CO_2) after 28 days of curing. Accelerated carbonation (measured using phenolphthalein indicator) at both CO_2 concentrations showed the ranking for carbonation resistance as OPC > FA30 > LC3. The mean carbonation depths are given in Table 3.

2.9 Studies on the effect of curing conditions

Properties of steam cured concretes

For accelerated curing applications, the strength after steam curing and the ultimate strength at 28 days were assessed. The steam curing cycle includes curing at ambient temperature for 4 hours from the time of concrete fabrication, followed by steam curing at 60°C for 5 hours, cooling until 24 hours and curing in a mist room till the time of testing. From the results presented in Table 5, it can be seen that the strength after 1 day was relatively higher in LC3 concrete compared to OPC and FA30. In terms of 1-day and 28-day

strengths, the ranking was OPC > LC3 > FA30. In terms of the relative increase in strength and ultimate strength loss, LC3 gave the best results.

Table 5. Summary of results from normally cured (NC) and steam cured (SC) concretes (with binder content: 360 kg/m³ and w/b: 0.40)

Binder type	1-day compressive strength (MPa)		28-day compressive strength (MPa)		% increase in strength at 1 day due to steam curing	% difference in strength at 28 days due to steam curing
	NC	SC	NC	SC		
OPC	14.6	21.8	48.2	43.2	49	-10
FA30	9.5	12.6	38.2	38.0	32	0
LC3	11.1	21.1	38.2	41.0	91	+7.0

Performance of LC3: Lab-crete versus Field-crete

The durability properties of the core specimens from the field and laboratory environments, i.e., denoted as field-crete and lab-crete, respectively, were also compared [5]. Results of the total charge passed in the RCPT suggest that the charge passed in field specimens are marginally higher than the laboratory specimens for all binders; the charge passed in the LC3 lab and field specimens were 120 and 160 Coulombs, respectively. In both instances, the concrete has very low chloride ion penetrability (corresponding to the range of 100-1000). In the fly ash-based concrete, there was a large variation between the laboratory (1800 Coulombs) and field specimens (3050 Coulombs). The results from chloride migration tests indicated lower chloride migration in concretes with LC3 in both laboratory and field specimens, with negligible difference between the two cases. The migration coefficient in the PPC field specimens was 30 % higher.

2.10 Life cycle assessment (LCA)

The energy and CO₂ footprint of LC3 depend predominantly on the trade-off between the effects of clinker reduction and additional material processing energy for the calcination of clay (see Table 4). LCA was conducted for LC3 (hypothetically assumed to be produced in a plant in South India) and compared with those of conventional cements, such as OPC and portland pozzolana cement with fly ash (PPC). Further details of the LCA can be found in [10]. Energy and CO₂ footprint of LC3 were estimated considering a range of clays (47 samples) with varying kaolinite contents (40-100%), and conservatively, the highest values of calcination energy were considered for estimation. The study was also extended to concrete using the SimaPro 8.0.5.13 software for the ground-to-gate system boundary, which gives a more holistic assessment. The CO₂ equivalent emitted and energy consumption are estimated using the impact assessment methods following IPCC 2013 GWP 100a and the Cumulative Energy Demand, respectively. The results are provided in Table 3. Emissions were estimated to be lower in LC3 concretes by 250-400 kg CO₂ eq./ m³ compared OPC concretes.

3. CONCLUSIONS

Studies conducted over the last four years on LC3 for evaluating its robustness for application, have shown that the new cement is promising for countries like India with a

growing demand for cement and concrete and dwindling resources of slag and fly ash in certain geographical locations. Durability performance with respect to chloride exposure, sulphate attack, carbonation and corrosion resistance was studied. LC3 systems were found to have better resistance (than OPC and PFA systems) against chlorides, sulphates and corrosion-induced cracking. However, LC3 systems exhibited lower resistance against carbonation than OPC systems. Although the LC3 systems exhibited slightly lower chloride threshold than the OPC and FA30 systems, the significantly lower chloride diffusion coefficient results to much longer service life estimates for chloride exposure. Lower carbon footprint and better durability performance are seen as the major benefits from using LC3 in concrete applications.

4. REFERENCES

- [1] WBCSD, IEA, Technology Roadmap: Low-Carbon Transition in the Cement Industry, 2018. doi:10.1007/SpringerReference_7300.
- [2] K.L. Scrivener, Options for the future of cements, *Indian Concr. J.* 88 (2014) 11–21.
- [3] M. Antoni, J. Rossen, F. Martirena, K. Scrivener, Cement substitution by a combination of metakaolin and limestone, *Cem. Concr. Res.* 42 (2012) 1579–1589.
- [4] A.C. Emmanuel, P. Haldar, S. Bishnoi, S. Maity, Second pilot production of Limestone Calcined Clay Cement (LC 3) in India : The experience, *Indian Concr. J.* 90 (2016) 57–64.
- [5] Y. Dhandapani, M. Santhanam, Durability of Concrete Prepared with Ternary Binder Systems Involving Limestone and Calcined clay, in: XIV DBMC Durab. Build. Mater. Components, 2017.
- [6] Y. Dhandapani, M. Santhanam, Assessment of pore structure evolution in the limestone calcined clay cementitious system and its implications for performance, *Cem. Concr. Compos.* 84 (2017) 36–47.
- [7] Y. Dhandapani, T. Sakthivel, M. Santhanam, R. Gettu, R.G. Pillai, Mechanical properties and durability performance of concretes with Limestone Calcined Clay Cement (LC3), *Cem. Concr. Res.* 107 (2018) 136–151.
- [8] M. Santhanam, F. Suma, Y. Dhandapani, Sulphate Resistance of Limestone Calcined Clay Cement, in: 2nd ACF Symp. 2017 - Innov. Sustain. Concr. Infrastructures, 2017.
- [9] R.G. Pillai, R. Gettu, M. Santhanam, S. Rengaraju, Y. Dhandapani, S. Rathnarajan, A. Basavaraj S., Service life and life cycle assessment of reinforced concrete systems with limestone calcined clay cement (LC3), *Cem. Concr. Res.*, DOI: 10.1016/j.cemconres.2018.11.019, in press (2018) 9 p.
- [10] R. Gettu, A. Patel, V. Rathi, S. Prakasan, A. Basavaraj S., S. Palaniappan, Influence of incorporating supplementary Cementitious materials on the sustainability parameters of cements and concrete in the Indian context, *Materials and Structures*, under review.

LIMESTONE CALCINED CLAY CEMENTS (LC³): EFFECT OF RAW MATERIAL PROPERTIES ON HYDRATION AND STRENGTH

Franco Zunino (1), Karen Scrivener (1)

(1) Laboratory of Construction Materials, EPFL STI IMX LMC, École Polytechnique Fédérale de Lausanne (EPFL), Station 12, CH-1015 Lausanne, Switzerland

Abstract

Limestone calcined-clay cements (LC³) take advantage of the synergetic effects of calcium carbonate reaction with the additional aluminum provided by the calcined clay. Previous research showed that calcined kaolinite content is an important factor that governs the strength development of these materials. This study explores the effect of kaolinite content from 20 to 95% on mechanical properties of LC³-50 and LC³-65 (50% and 65% clinker factor respectively) systems by dilution of pure metakaolin. The effect of metakaolin dilution was coupled with other factors that were observed to have a significant impact on hydration kinetics and strength, such as limestone particle size. Compressive strength was monitored on mortar specimens in accordance with EN196 standard. Different strategies to increase the early-age strength (before 7 days) were explored. Chemical (alkali content adjustment) and physical (limestone particle size adjustment) approaches were tested and compared to control systems.

Keywords: sustainability, calcined clay, carbon footprint, blended cement, calcite

1. INTRODUCTION

The use of supplementary cementitious materials (SCMs) as a means to reduce the cement content in concrete mixes [1–4] and enhance the durability of the material to increase the service life of concrete structures [5] have become of increasing interest among researchers.

The available amounts of commonly used supplementary cementitious materials (SCMs), such as fly ash, blast furnace slags and natural pozzolan are much lower than the worldwide demand for cement (OPC). Consequently, research interest has shifted towards alternative and more abundant sources of SCM's such as calcined clays and limestone.

The combination of metakaolin and limestone in OPC-based systems produces a synergy that enables the production of high performance cement with a significantly lower clinker factor. The reactive alumina supplied by metakaolin enhances the limestone reaction and allow higher replacement levels with improved performance. For this reason, LC³ (limestone calcined clay cements) have become of great interest.

This study explores the effect of calcined metakaolin content on early-age performance of LC³ by dilution of pure metakaolin using limestone. The effect of particle size of the limestone fraction and alkali content adjustment on strength are also discussed.

2. MATERIALS AND METHODS

Portland cement classified as CEMI 42.5R was used for the preparation of blended cement pastes. The limestone powders were supplied from commercial manufacturers and were used as received. For the base mixtures of this study, a limestone with $D_{V50} = 4.1 \mu\text{m}$ was used. A pure metakaolin (95% purity) was used in this study as calcined clay. Lower grades of clay were achieved by dilution of the pure metakaolin with limestone. A base mixture design of LC³-50 with clay-to-limestone ratio of 2:1 was used (50% clinker, 30% calcined clay, 15% limestone and 5% gypsum). From there, different levels of dilution were explored by combining pure metakaolin and additional limestone in the 30% clay fraction of the binder, ranging from 95% metakaolin content (30% calcined clay and 15% limestone) down to 20% metakaolin (6.3% calcined clay and 38.7% limestone) content.

The LC³-65 systems were designed by increasing the clinker factor up to 65% and keeping the relative proportions between limestone and clay constant in the remaining fraction for comparison with LC³-50.

A constant w/b ratio of 0.4 by mass was used for all mixtures. Compressive strength was measured in mortar samples in conformity with EN 196-1 standard procedure. For the limestone particle size study, mortar samples were cast at w/b 0.4 in the same way as the base mixtures. Two additional limestone sizes were used: D15 (coarse limestone, with $D_{V50} = 17.5 \mu\text{m}$) and BUG (fine limestone, with $D_{V50} = 1.8$). The coarse and fine limestone replaced the limestone used to dilute down the 95% metakaolin down to the desired values (therefore, an increased amount of fine or coarse limestone is added as the metakaolin content goes down), while the initial 15% base limestone content of the LC³-50 with clay-to-limestone ratio of 2:1 system was always kept constant with the $D_{V50} = 4.1 \mu\text{m}$ limestone. For the mixtures where the alkali content was adjusted, KOH was used to achieve a total alkali content, expressed as percentage of $\text{Na}_2\text{O}_{\text{EQ}}$ of the total binder, of 0.8% and 1.0%.

3. RESULTS AND DISCUSSION

3.1 Effect of metakaolin content and clinker factor on compressive strength

Results for compressive strength of mortar with 50% and 65% clinker factors are presented on Figure 1. It can be observed that in general, LC³-65 exhibits a higher strength at 1 day as compared to LC³-50. This is attributed to the higher clinker content. At this age, the hydration of clinker dominates the production of hydrates. However, this difference starts to disappear already at 2 days, starting from the systems with higher metakaolin content. At 7 days, the difference is negligible across the whole range explored. LC³-65 formulations are currently allowed in the European EN 197 standard as CEMII/B-Q-L, but not the LC³-50 based formulations. From a strength point of view, it appears that the difference between both clinker factors is restricted to the very early stage of hydration. Furthermore, as it will be shown in the next section, this difference can be shortened even further by the refinement of the limestone fraction of the adjustment of the alkali content.

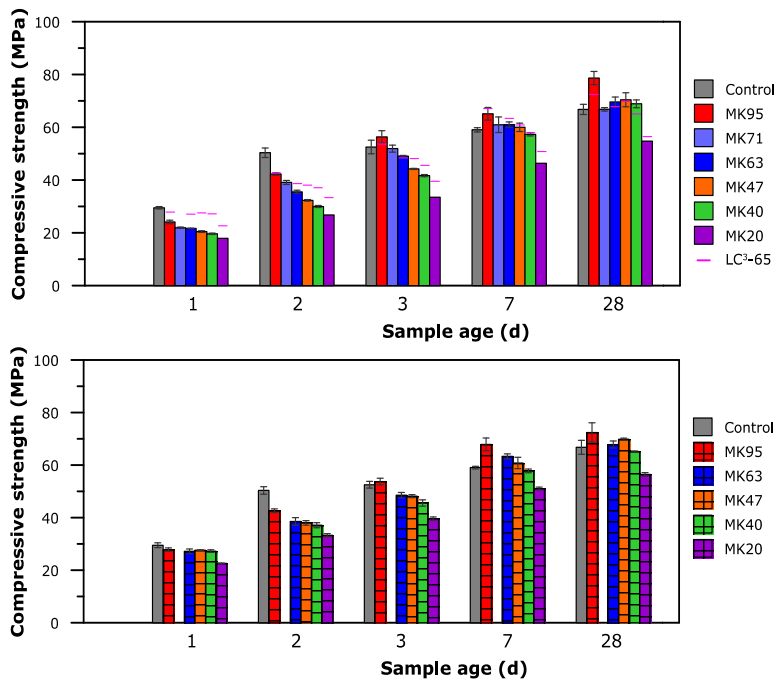


Figure 1: Compressive strength of LC³-50 (top) and LC³-65 (bottom) mortar mixtures with different amounts of metakaolin. Eye guides are included in the top figure referring to the LC³-65 strength at each metakaolin level.

3.2 Effect of limestone particle size on compressive strength of LC³-50

Figure 2 shows the compressive strength results of LC³-50 mixtures where coarse (D15) or fine (BUG) limestone is incorporated. It can be observed that for the same metakaolin content, the surface area of limestone has a strong effect on compressive strength, specially at early age. In fact, at 1, 2 and 3 days the effect of limestone refinement on strength is higher for a given mixture than the observed variation (Figure 1) for a reduction in metakaolin content. Thus, limestone particle size is a relevant factor that influence the strength of LC³ at early age, and could be used to increase the performance of binders in scenarios where only low-grade clays are available. Furthermore, the use of fine limestone allows to approach to the strength level of LC³-65 formulations at 1 day.

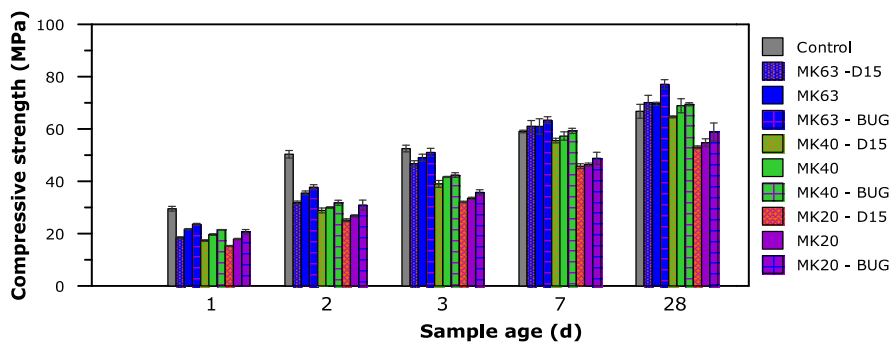


Figure 2: Compressive strength of LC³-50 mortar mixtures with coarse (D15) and fine (BUG) limestone additions.

3.2 Strategies to increase early-age strength: chemical vs physical acceleration

To further explore the possibilities to increase early age strength of LC³-50 systems, alkali adjustment was used. Figure 3 shows the studied mixtures with 63 and 40% metakaolin content, with adjusted alkali content, fine limestone (BUG) addition or a combination of both. In addition, the reference values for the MK63 and MK40 with the reference limestone are also included for comparison. As seen, for the two metakaolin contents studied, the mixtures with an increased alkali content up to 1% Na₂O_{EQ} shown higher strength at early ages. A decrease of strength is observed at 7 and 28 days as compared to the reference system, but within the error of the experiment. The combination of fine limestone and alkali adjustment exhibited an even higher increase of strength at 1, 2 and 3 days.

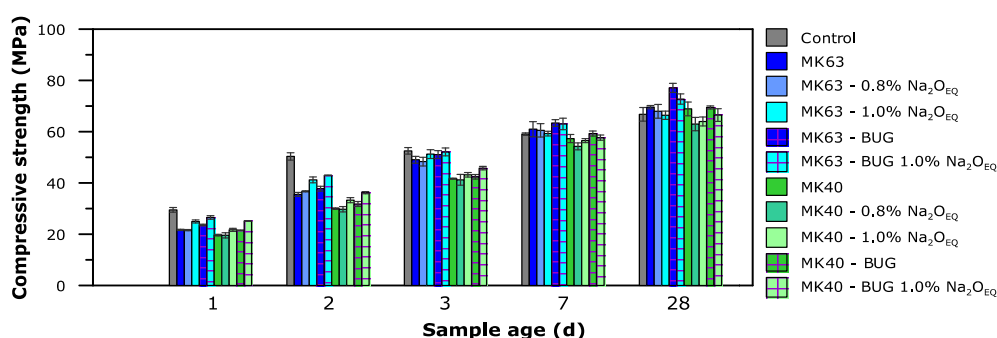


Figure 3: Compressive strength of LC³-50 mortar mixtures that incorporate different strategies to increase early age strength (alkali adjustment, limestone refinement or a combination of both).

4. CONCLUSIONS

Based on the presented results, the following conclusions can be drawn:

1. Calcined kaolinite content is linked with compressive strength of LC³ systems. However, other design parameters such as limestone fineness shown a strong influence in strength and therefore, can be managed to achieve the desired performance of the mixture.
2. The inclusion of fine limestone in LC³-50 mixtures proved to be an effective way to increase early-age strength to levels comparable to LC³-65 formulations.
3. Further increase can be achieved adjusting the alkali content of the binder, with no negative impact observed at later age strength at the amounts below 1% Na₂O_{EQ}.

ACKNOWLEDGEMENTS

The authors would like to acknowledge financial support by the Swiss Agency of Development and Cooperation (SDC) grant 81026665. The Swiss federal commission for scholarships for foreign students (FCS) is acknowledged for supporting Franco Zunino's studies through scholarship 2016.0719.

REFERENCES

- [1] R.C. Lara, M. Antoni, A.A. Díaz, K. Scrivener, J. Fernando, M. Hernández, Estudio de la adición de arcillas calcinadas en la durabilidad de hormigones, *Rev. Ing. Construcción*. 26 (2011) 25–40.
- [2] B. Lothenbach, K. Scrivener, R.D. Hooton, Supplementary cementitious materials, *Cem. Concr. Res.* 41 (2011) 1244–1256. doi:10.1016/j.cemconres.2010.12.001.
- [3] N. Jain, Effect of nonpozzolanic and pozzolanic mineral admixtures on the hydration behavior of ordinary Portland cement, *Constr. Build. Mater.* 27 (2012) 39–44. doi:10.1016/j.conbuildmat.2011.08.006.
- [4] E. Karim, K. El-Hadj, B. Abdelkader, B. Rachid, Analysis of Mortar Long-Term Strength with Supplementary Cementitious Materials Cured at Different Temperatures, *ACI Mater. J.* (2010) 323–331.
- [5] P. Mehta, Durability - Critical Issues for the Future, *Concr. Int.* 19 (1997) 69–76.

INVESTIGATION OF CALCINED BRICK CLAYS FROM CENTRAL GERMANY FOR USE AS A SUSTAINABLE POZZOLAN

Nsesheye S. Msinjili, Gregor J. G. Gluth, Nico Vogler, Sebastian Simon and Hans-Carsten Kühne

Bundesanstalt für Materialforschung und -prüfung (BAM), Germany

Abstract

The production of Portland cement causes a substantial environmental impact, since the calcination of limestone results in high emissions of carbon dioxide. The use of supplementary cementitious materials such as calcined clays as partial replacement for Portland cement offers a solution to limit this environmental impact. This paper investigates four clays from deposits in central Germany with the aim of obtaining pozzolans for the production of Portland-pozzolana cement. The results obtained show that the calcined clays possess pozzolanic properties, which differ depending on calcination temperature and the relative amounts of kaolinite and 2:1 clay minerals.

Keywords: supplementary cementitious materials; calcined clays; dehydroxylation; strength

1. INTRODUCTION

In recent years, it has become apparent that the use of supplementary cementitious materials (SCMs) such as fly ash or slag in concrete cannot be easily expanded, because of limited supply and availability [1, 2]. Calcined clays have emerged to be an alternative SCM due to their worldwide availability. The activation of clays requires a lower temperature than Portland clinker production and does not involve release of chemically bound CO₂, leading to lower greenhouse gas emissions, and can render the clays highly pozzolanic. Metakaolin, produced from high-grade kaolinite has shown excellent properties in concrete. However, kaolinite-rich clays are comparatively expensive and primarily used in the ceramic, paper and paint industries [3]. Low-grade kaolinitic clays, *i.e.* clays with lower amounts of kaolinite and often a high fraction of 2:1 clay minerals (illite/muscovite and smectite groups), are relatively cheaper and much more widely available, thus, appear to be a viable alternative as feedstocks for SCMs in large-scale manufacturing for the cement industry. Cement replacement of 15-35% with calcined clays is feasible for production of Portland-pozzolana cement. Therefore, the present work investigates the use of clays from central Germany with low to moderately high contents of kaolinite, and varying amounts of 2:1 clay minerals, in blended cement systems.

2. MATERIALS AND METHODS

2.1 Raw materials

The raw materials used in this study were Portland cement, CEM I 42.5 R (PC), and clays from four deposits in central Germany. The nomenclature used throughout this study is as follows: PL x X (x X denoting deposit and batch/location); R (raw clay, dried at 120 °C for 48 hours, ground in an impact mill and sieved through a 2-mm sieve); C yyy (calcined clay, yyy indicating calcination temperature in °C). Two of the employed clays, PL1B and PL3C, are brick clays. Quartz powder (Q) was used as an inert filler. The chemical composition and physical properties of the raw materials are shown in Table 1.

Table 1: Chemical composition and physical properties of raw materials used in this study

Constituent (wt.%)	PC	PL1B_R	PL3C_R	PL5D_R	PL7B_R	Q
SiO ₂	19.82	77.31	65.18	74.05	62.60	99.40
Al ₂ O ₃	4.56	10.55	13.81	8.97	23.53	0.10
Fe ₂ O ₃	1.97	1.78	5.87	0.87	1.07	0.03
TiO ₂	0.13	1.00	1.38	3.41	1.05	0.07
CaO	62.87	0.32	1.19	0.17	0.24	-
MgO	1.73	0.52	1.50	0.10	0.11	-
Na ₂ O	0.31	0.37	0.86	0.23	0.37	-
K ₂ O	0.86	1.87	2.93	1.19	0.33	-
SO ₃	3.26	0.13	0.08	0.11	0.23	-
P ₂ O ₅	0.20	0.22	0.47	0.26	0.20	-
Mn ₂ O ₃	0.02	0.01	0.07	0.01	0.01	-
Other	0.74	0.19	0.56	0.50	0.11	-
Loss on ignition	3.57	5.75	6.13	10.15	10.20	0.15
Density (g/cm ³)	3.15	2.58	2.66	n/a	2.53	2.65
Specific surface area, a_s (m ² /g)	1.07	16.74	15.50	35.64	17.21	0.45
Median particle size, d_{50} (μm)	4.87	13.29	20.48	10.7	8.38	12.17

2.2 X-ray diffraction

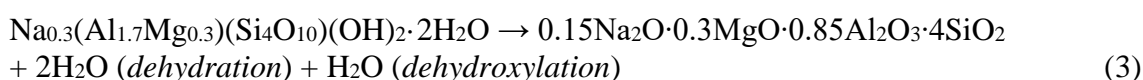
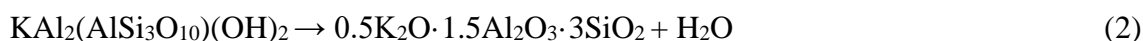
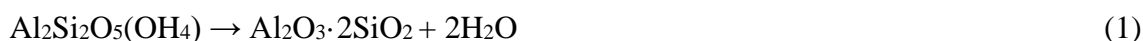
Powder (XRD) patterns were recorded in Bragg–Brentano geometry on a Rigaku Ultima IV diffractometer under the following conditions: CuK α radiation ($\lambda = 1.541874 \text{ \AA}$), 40 kV, 40 mA; sampling interval: $0.02^\circ 2\theta$; scan rate: $0.5^\circ 2\theta \text{ min}^{-1}$; scanning range: $5^\circ\text{--}65^\circ 2\theta$; divergence slit: in-plane 0.5° , axial 10 mm; strip detector D/teX Ultra with 5° Soller slits. Samples were filled into sample holders by top-loading and spun at 15 rpm during the measurements. Because of the top-loading procedure, preferred orientation effects are expected to occur, thus, the XRD measurements served for qualitative analyses (phase ID) only.

2.3 Thermogravimetric analysis

TGA/DTG was used to estimate the contents of clay mineral species in the raw and calcined (see Section 2.4) clays, using a Mettler Toledo TGA/DSC 3+ STARE device. Sample masses

of ca. 10 mg were tested in Al₂O₃ crucibles at a heating rate of 5 °C/min from ambient temperature (ca. 23°C) up to 1000°C and a nitrogen flux of 80 ml/min. At 40°C, the temperature was kept constant for one hour before gradually increasing to 1000 °C.

The tangent method was used to obtain the mass losses due to dehydroxylation from the TG curves. The mass losses in the ranges 400–600, 600–700 and 800–900°C were assigned to the dehydroxylation of kaolinite, illite/muscovite and smectite (assumed to be montmorillonite), respectively [4-7]. Typical stoichiometries of these minerals, assumed to hold for the studied clays, together with their dehydroxylation reactions are given in equations (1), (2) and (3), respectively [7-9].



The mass fractions of the clay minerals (wt.%_{clay mineral}) in each raw or calcined clay was calculated, assuming complete dehydroxylation of the clay minerals, from Equation (4), where wt.%OH_{clay mineral} is the measured mass loss due to dehydroxylation of the clay mineral; $M_{\text{clay mineral}}$ and M_{water} are the molar masses of the clay mineral and water, respectively; and n_{dehydrox} is the number of moles of water released on dehydroxylation of the clay mineral.

$$\text{wt.\% clay mineral} = (\text{wt.\% OH}_{\text{clay mineral}}) \times [M_{\text{clay mineral}} / (n_{\text{dehydrox}} \times M_{\text{water}})] \quad (4)$$

For the calcined clays, the degree of dehydroxylation (D_{TG}) was calculated from Equation (5), considering the D_{TG} of kaolinite and 2:1 clay minerals (illite/muscovite, smectite) separately. In Equation (5), wt.%_{clay mineral, calcined} is the mass fraction of clay mineral remaining after calcination, which was obtained following Equation (4).

$$D_{\text{TG}} = [(\text{wt.\% clay mineral} - \text{wt.\% clay mineral, calcined}) / \text{wt.\% clay mineral}] \times 100\% \quad (5)$$

2.4 Calcination of clays

Each raw clay was calcined in a laboratory muffle furnace at 3 temperatures: 650, 850 and 900°C. The retention time was 3 hours. After calcination, the clays were left to cool down on a lab bench for ca. 15 mins before storing in a desiccator.

2.5 Blended cement pastes and compressive strength testing

Blended cements were produced by replacing PC with 15% and 30% by volume of calcined clay or quartz powder. From these blends, pastes were prepared with a constant water to solid ratio by volume (w/s_v) of 1.26 (*i.e.* w/s by weight in the range 0.40–0.42), using de-ionised water. The dry powders were first homogenised manually for 30 seconds, subsequently the water was added, and the pastes mixed in a planetary centrifugal mixer at a rotational speed of 1250/min, for 4 minutes. The pastes were then cast into 20 mm × 20 mm × 20 mm cube moulds and cured for 1, 7 or 28 days at 20°C and ~99% RH. Compressive strength testing of the cubes after curing was done on a ToniPRAX testing machine at a loading rate of 0.6 MPa/s.

3. RESULTS AND DISCUSSION

3.1 Mineralogical characterisation of the raw clays

The diffractograms of the bulk raw clays are shown in Figure 1. In PL1B_R and PL3C_R, high intensity reflections of illite/muscovite-type minerals were detected (002 at $\sim 8.8^\circ 2\theta$), whereas PL5D_R and PL7B_R exhibited lower intensities at the corresponding angles. Also, kaolinite was detected in all clays (001 at $\sim 12.3^\circ 2\theta$), but most prominently in PL7B_R. A minor peak at $6.2^\circ 2\theta$ was present in PL3C_R, indicating the presence of a smectite-type or vermiculite-type clay mineral. All clays contained considerable amounts of quartz and minor amounts of other accessory minerals.

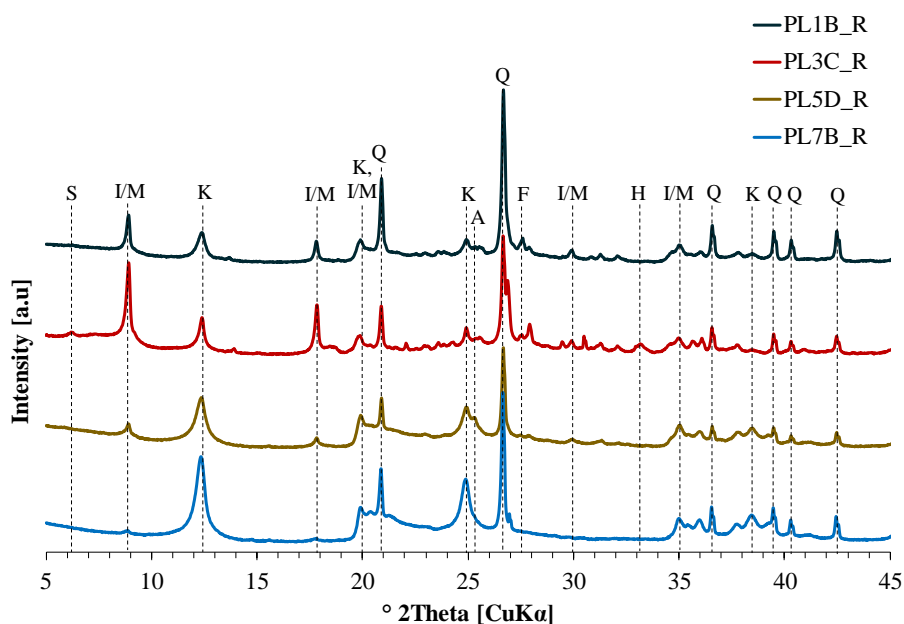


Figure 1: XRD diffractograms of raw clays
(S-smectite; I/M-illite/muscovite; K-kaolinite; Q-quartz; F-feldspar; A-anatase; H-hematite)

Figure 2 shows the DTG curves (see Figure 3 for example TGA curves) and the fractions of clay minerals (wt.%_{clay mineral}) calculated from TGA/DTG. The mass loss up to 200°C shown in Figure 2 (left) is due to the presence of surface water on the clays, whereas the existence of a shoulder as observed with PL3C_R, reflects the evaporation of interlayer water, primarily associated with smectite clay minerals [7, 10]. Dehydroxylation of clay minerals is discerned at temperatures $400\text{--}900^\circ\text{C}$, with the peaks and shoulders attributed to the different clay species (Section 2.3) sufficiently well separated.

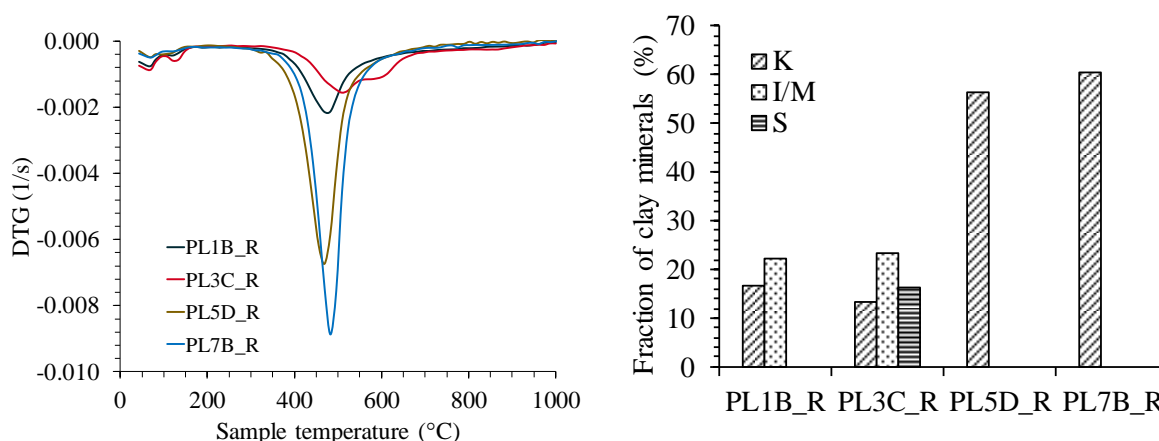


Figure 2: DTG curves of raw clays (left) and fraction of clay mineral content (right) (S-smectite; I/M-illite/muscovite; K-kaolinite)

In accord with the XRD results, the highest content of kaolinite was calculated for raw clays PL5D_R and PL7B_R, whereas PL1B_R and PL3C_R exhibited significant contents of 2:1 clay minerals. Also, PL5D_R and PL7B_R show illite/muscovite minerals in their XRD diffractograms, but due to their low amount their dehydroxylation could not be discerned from the TGA/DTG curves and hence their content could not be quantified. Smectite was only detected in PL3C_R, in line with the XRD results.

3.2 Characterisation of the calcined clays

In Figure 3, TGA example curves of raw clays and calcined clays are compared. The calcined clays exhibited substantially diminished steps in the TGA curves, proving that calcination led to dehydroxylation of the clay minerals. However, minor mass losses in the dehydroxylation ranges of the different clay minerals were still present for the calcined clays, showing that dehydroxylation was not complete, particularly for calcination at 650°C.

The degrees of dehydroxylation (D_{TG}) of the different clay mineral species in the calcined clays, calculated according to Equation (5), are shown in Table 2. For calcination at 650°C, the D_{TG} of kaolinite is ca. 99% for all clays (except PL3C), whereas for the 2:1 clay mineral it is less than 70%. The D_{TG} for the 2:1 clay minerals of PL5D and PL7B could not be quantified due to the difficulty in discerning their initial value by the tangent method.

Figure 4 shows the effect of calcination on the median particle diameter (d_{50} ; determined by laser granulometry, wet-dispersed in propan-2-ol) and the specific surface area (a_s ; determined by N_2 sorption) of the clays. The d_{50} is seen to increase with increasing calcination temperature, due to agglomeration of the clay particles during thermal treatment. PL3C shows the largest median particle diameter before calcination and at all calcination temperatures, presumably due to the presence of smectite minerals, which are reported to agglomerate more than kaolinite and illite [5, 11].

For a calcination temperature of 650°C, a_s remains almost constant, compared to the raw clays. At higher calcination temperatures, a_s decreases significantly. This decrease is least significant for PL7B and most pronounced for PL1B and PL3C. This may be attributed to partial sintering and the corresponding reduction of the pore volume caused primarily by the dehydroxylation of the 2:1 clay minerals occurring at temperatures above 800°C [11, 12].

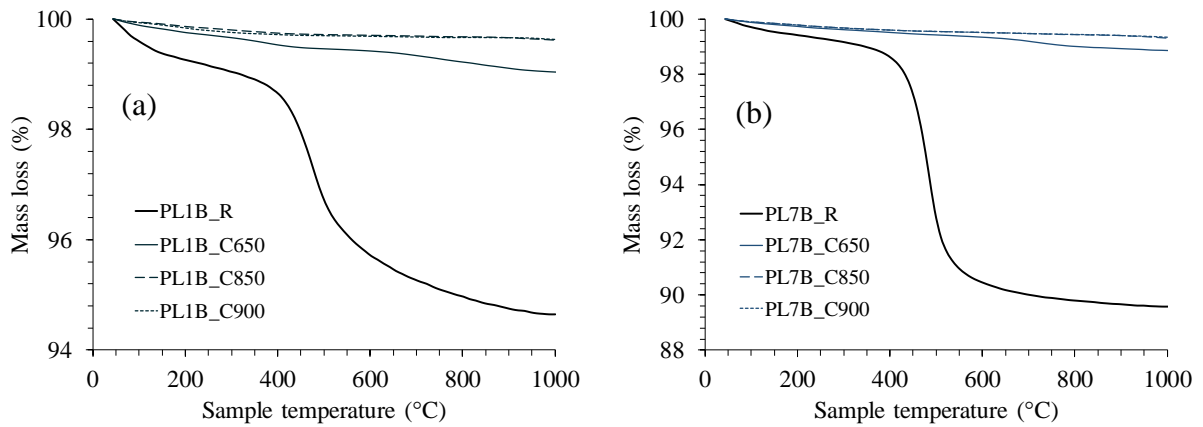


Figure 3: Comparison of thermogravimetric analysis (TGA) curves of raw and calcined clays

Table 2: Degree of dehydroxylation of the calcined clays

Clay	Degree of dehydroxylation (D_{TG}) (%)						LOI (%)		
	Calc. @ 650°C		Calc. @ 850°C		Calc. @ 900°C		Calc. @ 650°C	Calc. @ 850°C	Calc. @ 900°C
	1:1	2:1	1:1	2:1	1:1	2:1			
PL1B	98.72	59.55	100.00	95.10	100.00	96.08	0.77	0.23	0.21
PL3C	96.76	67.71	99.05	n/a	n/a	n/a	1.01	0.40	0.17
PL5D	99.11	-	100.00	-	100.00	-	1.22	0.41	0.16
PL7B	99.64	-	100.00	-	100.00	-	0.98	0.55	0.25

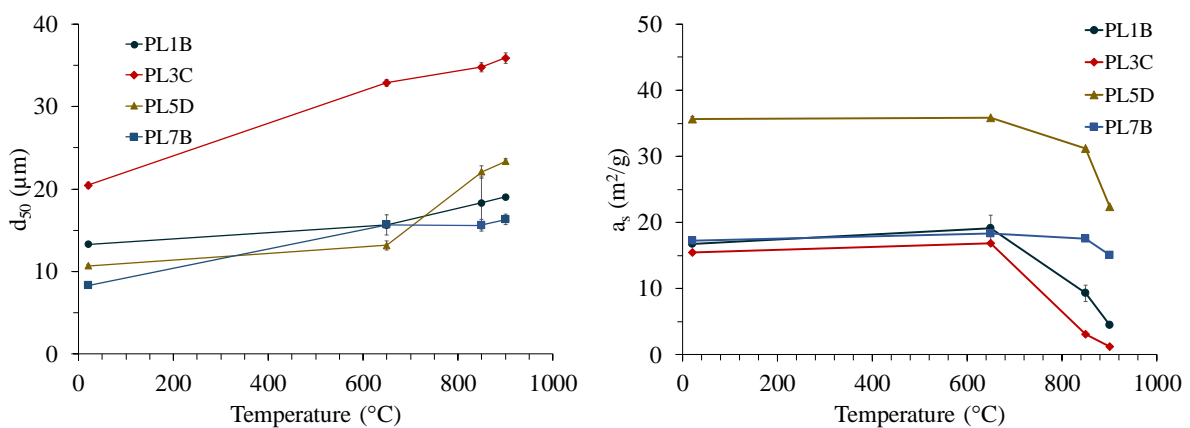


Figure 4: Median particle size (left) and specific surface area (right) of raw and calcined clays

3.3 Compressive strength of blended cements

Figure 5 shows the relative compressive strength of the blended cement pastes (all values referred to a pure PC paste with $w/s = 0.40$ by weight at the respective age, *i.e.* 1, 7 or 28 days). At early ages (*i.e.* 1 and 7 days), the relative strength of all systems with 15% replacement of clay for cement was either similar or surpassed the systems with 15% quartz powder, except PL1B (calcined at 650°C) and PL3C (calcined at 850°C). That means, assuming that quartz is inert and merely acts as a filler, the latter show low or no pozzolanic reactivity due the high median particle size (for PL3C) and the seeding effect [13]. However, at 28 days, all pastes with clays calcined at 850°C or 900°C exhibited a significant higher strength than the system with quartz. The pastes with PL5D (calcined at 900°C) and PL7B (calcined at 650°C) exhibited relative strengths of almost 100% relative to that of pure PC. This can be assumed to be due to their high kaolinite content (Figure 2) compared to the brick clays (PL1B and PL3C) having lower kaolinite content. Despite the low kaolinite content in PL1B, its relative strength at 28 days is ca. 95% compared to pure PC when calcined at 850°C (Figure 6: left). This could mean that the effect of the calcined 2:1 clay minerals present in PL1B significantly contributed to the pozzolanic reactivity, in line with their high degree of dehydroxylation (D_{TG} is only ca. 60 % at 650 °C but increases to ca. 95% at 850°C, Table 2).

Similarly, for the systems with 30 % replacement (Figure 5: right), only PL3C (calcined at 650°C) shows no pozzolanic reactivity at early ages and shows a slight increase in pozzolanicity at 28 days. Although the relative strength of the blended systems is lower than that of pure PC at 28 days, the calcined clay systems show pozzolanic reactivity, as evidenced by their higher strength, compared to the paste with 30% quartz.

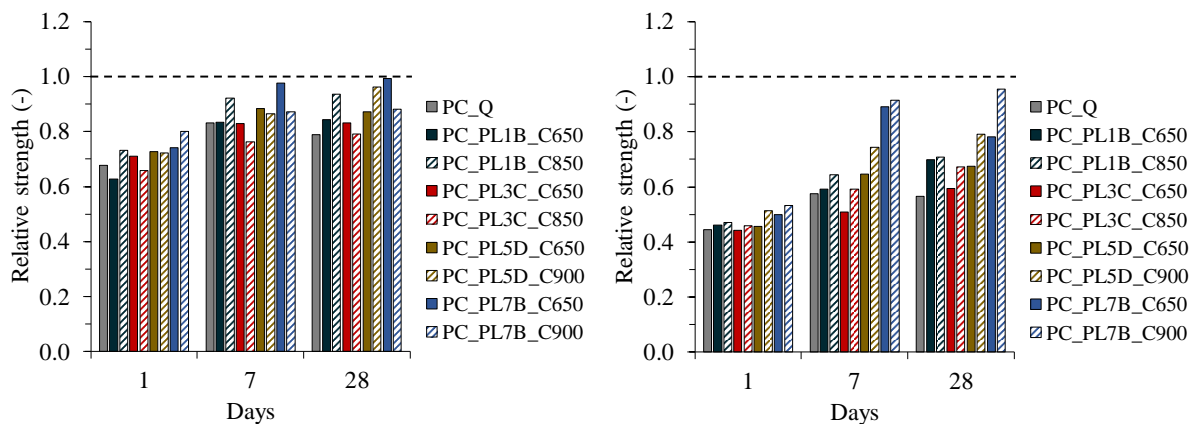


Figure 5: Relative compressive strength of blended cement pastes with a PC replacement of 15% (left) and 30% (right)

4. SUMMARY AND CONCLUSIONS

From this study, the following could be summarised:

- At calcination temperatures of $\geq 850^\circ\text{C}$, the median particle size of the clays increased, and their specific surface area decreased. This was seen to be most significant for the clay with a significant smectite content.

- At calcination temperatures of $\geq 850^{\circ}\text{C}$, the degree of hydroxylation of the 2:1 clay minerals was increased, compared to calcination at 650°C , which improved the pozzolanic reaction of the brick clays, as observed by compressive strength testing.
- For all the paste systems blended with 15% calcined clays, a minimum of 83% and a maximum of 99% relative strength was observed at 28 days for the studied clays (except PL3C calcined at 850°C – showing similar relative strength to that of quartz). At the same age and 30% replacement, a minimum of 59% and a maximum of 95% relative strength was observed. The highest relative strengths at 28 days for all replacement ratios were achieved with kaolinite-rich clays.

Thus, although clays with a high kaolinite content generally perform better than brick clays, the latter develop sufficient reactivity on calcination to yield strengths that are significantly higher than those of systems blended with quartz powder. Work is in progress to study the hydration kinetics and transport coefficients and durability at later ages of the blended cement pastes in more detail and to confirm the present results with clays calcined at pilot plant scale.

REFERENCES

- [1] Antoni, M., Rossen, J., Martirena, F., *et al.*, 'Cement substitution by a combination of metakaolin and limestone', *Cement and Concrete Research*. 42 (12), (2012) 1579-1589.
- [2] Tironi, A., Castellano, C.C., Bonavetti, V.L., *et al.*, 'Kaolinitic calcined clays – Portland cement system: Hydration and properties', *Construction and Building Materials*. 64 (2014) 215-221.
- [3] Murray, H.H., 'Overview — clay mineral applications', *Applied Clay Science*. 5 (5), (1991) 379-395.
- [4] Guggenheim, S. and Koster van Groos \ddagger , A.F., 'Baseline studies of the clay minerals society source clays: Thermal analysis', *Clays and Clay Minerals*. 49 (5), (2001) 433-443.
- [5] Fernandez, R., Martirena, F. and Scrivener, K.L., 'The origin of the pozzolanic activity of calcined clay minerals: A comparison between kaolinite, illite and montmorillonite', *Cement and Concrete Research*. 41 (1), (2011) 113-122.
- [6] Bernal, S.A., Juenger, M.C.G., Ke, X., *et al.*, 'Characterization of supplementary cementitious materials by thermal analysis', *Materials and Structures*. 50 (1), (2016) 26.
- [7] McIntosh, A., Lawther, S.E.M., Kwasny, J., *et al.*, 'Selection and characterisation of geological materials for use as geopolymer precursors', *Advances in Applied Ceramics*. 114 (7), (2015) 378-385.
- [8] Chukanov, N.V., *Infrared spectra of mineral species vol. 1*. Dordrecht (Springer, 2014).
- [9] Meunier, A., *Clays*. Berlin (Springer, 2005).
- [10] He, C., Makovicky, E. and Osbaeck, B., 'Thermal treatment and pozzolanic activity of Na- and Ca-montmorillonite', *Applied Clay Science*. 10 (5), (1996) 351-368.
- [11] Hollanders, S., Adriaens, R., Skibsted, J., *et al.*, 'Pozzolanic reactivity of pure calcined clays', *Applied Clay Science*. 132-133 (2016) 552-560.
- [12] Trümer, A., Ludwig, H.-M. and Rohloff, K., 'Investigations into the application of calcined clays as composite material in cement', *ZKG International*. 09/2014 (9), (2014) 52-57.
- [13] Thomas, J.J., Jennings, H.M. and Chen, J.J., 'Influence of Nucleation Seeding on the Hydration Mechanisms of Tricalcium Silicate and Cement', *The Journal of Physical Chemistry C*. 113 (11), (2009) 4327-4334.

POZZOLANIC POTENTIAL OF CALCINED CLAY IN HIGH-PERFORMANCE CONCRETE

Nancy Beuntner (1), Andrea Kustermann (2) and Karl-Christian Thienel (1)

(1) Institute for Construction Materials, Bundeswehr University Munich, Germany

(2) Building chemistry and construction materials, faculty of civil engineering, University of Applied Sciences Munich, Germany

Abstract

Supplementary cementitious materials (SCM) are required to improve the technical and environmental characteristics of high-performance concrete. They will substitute conventional binders to a greater extent than previously common. Calcined clays are considered to provide huge potential in this regard. Besides the well-known, highly reactive but relatively expensive metakaolin, which can be used in concrete only to a limited extent, calcined mixed layer clays are an alternative solution that appears to be very promising both in environmental and economic terms. In this study, the suitability and efficiency of a calcined mixed layer clay as SCM is compared to a metakaolin and a silica fume. The latter served as reference since it is the most common SCM used in high-performance concrete. The pozzolanic reaction kinetics and the formation of hydrate phases were specifically affected by the calcined clays' specific surface, their high water demand and did depend in addition on their aluminum content. These factors influence fresh and hardened concrete properties as well. The study investigates the impact of different calcined clays on microstructure and on strength, young's modulus of high performance concrete. The pozzolanic efficiency of calcined clay in blended pastes for high-performance concrete with low water-binder ratio was also determined by thermogravimetric analyses. Other than for metakaolin and silica fume the application of low-grade calcined mixed layer clays in concrete and mortar is especially interesting even for high substitution levels of up to 30 wt.% of cement due to their lower and retarding reactivity.

Keywords: supplementary cementitious material, bound water, hydration kinetics, microstructure, pozzolanic reaction

1. INTRODUCTION

The increasing use of binders with low clinker content requires effective and sufficient supplementary cementitious materials (SCMs) in future [1]. Calcined mixed layer clays with varying amounts of phyllosilicates, especially kaolinite, illite and mica, and a range of inert components (e.g. quartz and feldspar) are promising materials with great potential [2-5]. They are an attractive option for use in concrete at high cement substitution levels of up to 30 wt.% [6]. The low kaolinite content and physical properties like a high specific surface area and a comparatively high water demand (about 30 to 60 % higher than cement) are critically discussed aspects for use as SCM in high-performance concrete with low water-binder ratios [7, 8]. Dinakar et al. illustrate the impact of highly reactive metakaolin in high performance concrete [9]. The optimal substitution level is 10 wt.% of cement which is in the range that is common for silica fume [9, 10]. The pozzolanic reaction of calcined clays indicates C-(A)-S-H and AFm-phases including Strätlingite (C_2ASH_8). The aluminate reaction plays an decisive role for the pozzolanic efficiency of calcined mixed layer clays [11]. A low C_3A -content in cement reduced for instance the reactivity of metakaolin according to Cyr et al. [12].

This study addresses the influences of aluminate level in calcined clays and the interaction with cement composition for pozzolanic reaction is compared with the purely siliceous reactivity of silica fume. The effects on microstructure, especially porosity, and mechanical characteristics were investigated in combination with three different cements and water-binder ratios of 0.4 and 0.6 on cement/blended pastes and concrete. Results reveal possibilities to control the properties of ecological high-performance concrete made with calcined clay as SCM.

2. EXPERIMENTAL INVESTIGATION

The first part of the investigation focuses on the pozzolanic reactivity of calcined clays in blended cement pastes with different cement substitution levels. This was accomplished using thermogravimetric analysis to determine bound water (20 to 400 °C) and portlandite consumption. Furthermore, microstructural analysis was performed following [13] by means of mercury intrusion porosimetry (MIP). The variables include differing cement types (ordinary Portland cement (OPC), Portland limestone cement (PLC), calcined clay content (10, 20 and 30 wt.% for calcined mixed layer clay, 20 wt.% for metakaolin. For PLC calcined clay content of 20 and 30 wt.%, a combination of 10 wt.% metakaolin with 20 wt.% of calcined mixed layer clay and the addition of 10 wt.-% silica fume were investigated. Water-binder ratio was 0.4 for OPC mixes and 0.6 for PLC mixes. PCE-based superplasticizer was added to the PLC mixes for adjusting the workability. Compressive strength of the OPC based binder matrices was tested on micro-prisms ($10 \times 10 \times 40 \text{ mm}^3$). Pure cement pastes served as references.

In the second part of the investigation concentrated on compressive strength and Young's modulus of high strength concrete. The SCMs were calcined mixed layer clay, a combination of calcined mixed layer with metakaolin and silica fume. Again, PCE-based superplasticizer was needed for adjusting the workability.

2.1 Materials and specimens

Two ordinary Portland cements (OPC1 and OPC2) and one Portland limestone cements (PLC) were used having a strength grade 42.5R and complying with DIN EN 197-1. Two calcined clays were selected: A commercially available metakaolin (Mk) and a calcined mixed layer clay (CT). The source material of CT originates from Amaltheen (black jura) in Southern

Germany and was calcined at 750 °C in a rotary kiln on industrial scale [6]. Silica fume (Sf) served as reference SCM for high-strength concrete mixes. The physical properties and chemical analysis of the cements, both calcined clays and silica fume are listed in Table 1.

Table 1: Physical and chemical compositions of investigated binders

	OPC1	OPC2	PLC	CT	Mk	Sf
Particle density [g/cm ³]	3.14	3.14	3.08	2.63	2.42	1.40
Specific surface area (BET) [m ² /g]	1.23	1.08	1.24	5.3	14.1	-
Water demand [wt.%]	28	32	30	39	70	-
Loss of ignition [wt.%]	3.0	2.8	4.9	0.9	1.5	0.2
C ₃ S [wt.%]	54.1	59.0	56.8			
C ₂ S [wt.%]	20.1	14.0	8.5			
C ₃ A [wt.%]	6.3	8.0	8.6			
C ₄ AF [wt.%]	9.0	10.0	8.1			
SiO ₂ [wt.%]	20.4	19.6	18.2	54.0	55.0	97.0
Al ₂ O ₃ [wt.%]	5.0	5.3	5.4	21.4	42.5	-
Fe ₂ O ₃ [wt.%]	3.1	3.5	2.9	9.0	0.5	-
CaO [wt.%]	60.8	61.4	61.1	4.3	0.1	-
MgO [wt.%]	1.8	1.7	1.9	2.0	0.1	-
SO ₃ [wt.%]	3.0	3.4	3.2	2.0	0.1	-
Na ₂ O _{eq} [-]	0.6	1.2	1.1	3.0	0.5	-
TiO ₂ [wt.%]	0.2	0.3	0.2	0.0	1.0	-
Cl ⁻ [wt.%]	0.06	0.08	0.07	0.01	0.01	< 0.10

Cement pastes were mixed in a Hobart type laboratory mixer for 5 minutes and cast into molds with a size of 10x10x40 mm³ for testing compressive strength and in sealed plastic containers for analytical investigations. The latter samples were crushed after 2 and 28 days resp., and the hydration of 250 mg samples was stopped with acetone [14, 15]. The nomenclature of the specimens gives the type of cement followed by the replacement level and the type of SCM, e.g. (OPC1_30CT).

Table 2 summarizes the high strength concrete compositions. The nomenclature system is identical to the one used for the paste specimens. Aggregates were river sand and crushed granite coarse. W/b ratio was 0.4. Workability was adjusted with a PCE-based superplasticizer (ACE 430).

Table 2: Concrete compositions

Components	PLC_10Sf	PLC_20CT	PLC_30CT	PLC_10Mk/20CT
Cement [kg/m ³]	297	264	231	231
SCM [kg/m ³]	33	66	99	33/66
Aggregate [kg/m ³]	2019	2030	2040	2038
Water [kg/m ³]	132	132	132	132
PCE [wt.% of cement]	1.6	3.5	6.5	6.5

Concrete was mixed in a pan-type mixer. The specimens were compacted on a vibration table and cured following DIN EN 12390-2. Compressive strength was tested on 150-mm-cubes according to DIN EN 12390-3. Young's modulus was measured on 150/300-mm-cylinders according to DIN EN 12390-13.

2.2 Analytical investigation

Bound water and portlandite consumption were evaluated by thermogravimetric analysis (TGA) using a STA 449 F3 Jupiter (Netzsch) by measuring the weight loss in the temperature range 20-400 °C for bound water (H) and 450-550 °C for portlandite (CH) [13]. Porosity parameters are determined by mercury intrusion porosimeter Pascal 140/440 (Thermo Fisher Scientific). Results are the accessible porosity [vol.-%], the quantity of pores smaller than 30 nm [vol.-%], the median pore diameter [nm] and the threshold pore entry radius [nm] [16].

3. EXPERIMENTAL RESULTS AND DISCUSSION

3.1 Evaluation of pozzolanic reactivity by bound water and portlandite consumption

The pozzolanic reactivity was determined by bound water and portlandite consumption after two and 28 days. The results are presented in Table 3. The bound water in the temperature range of 20-140 °C (H_1) characterizes C-S-H phases and ettringite in cementitious systems [17]. The AFm phases typically show water loss over a wide temperature range of 140-400 °C (H_2) [18].

The total bound water (H_{total}) is higher after two days for the blended cement pastes containing Mk or silica fume than for those made with even higher replacement levels of CT. After two days higher values of H_1 as compared to H_2 indicate a more pronounced formation of C-S-H phases and ettringite than AFm. Nevertheless, the amount of H_2 indicates a distinctive formation of AFm phases in blended binders with the alumina-rich SCMs used here already after two days.

In the following the aluminate reactions are intensified and after 28 days significantly more water is bound in AFm phases (H_2) compared to C-S-H phases and ettringite (H_1) in the mixes containing CT. With increasing alumina content in SCMs the formation of AFm phases is typical and becomes dominant in blended cement pastes. This holds especially for mixes based on PLC [19]. Portlandite consumption increases in the course of hydration and with increasing substitution levels of CT, but it remains significantly below the one measured for Mk. The portlandite consumption for the silica rich, highly pozzolanic silica fume in PLC_10Sf is in the range of PLC_20CT after 28 days. Especially, the Mk blended cements (OPC1/OPC2_20Mk and PLC_10Mk/20CT) show a significantly lower portlandite content of less than 6 g/100 g cement after 28 days which was already indicated after two days where 12 g CH/100 g cement and less were measured for OPC1_20Mk and PLC_10Mk/20CT.

Figure 1 provides for OPC based binders the compressive strength values of the micro-prisms as a function of the amount of bound water. In all systems, there is a good correlation between the amount of bound water and compressive strength. For alumina rich binders, containing Mk or CT, this phenomenon can be attributed to the AFm phases formed during hydration [9, 11, 12]. In consequence, AFm phases seem to have a strength-enhancing effect since they densify the paste. The influence of AFm phases upon volume stability might be significant in blended systems containing alumina rich SCMs, like calcined clays and can reduce drying shrinkage [20].

Table 3: Amount of bound water (H) and portlandite (CH) content after 2 and 28 days determined by TGA

System	H _{total} [%]	H ₁ [%]	H ₂ [%]	CH [%]	CH [g/100 g cement]
	2 d / 28 d	2 d / 28 d	2 d / 28 d	2 d / 28 d	2 d / 28 d
OPC1	12.7 / 16.2	7.9 / 8.2	4.8 / 8.0	11.4 / 17.3	19.2 / 22.7
OPC1_10CT	12.0 / 17.2	7.1 / 8.8	4.9 / 8.4	11.0 / 13.3	17.2 / 19.6
OPC1_20CT	10.6 / 17.6	6.1 / 8.7	4.5 / 8.9	6.5 / 10.2	11.6 / 16.2
OPC1_30CT	11.6 / 16.0	6.7 / 7.8	4.9 / 8.2	9.1 / 7.5	18.5 / 14.3
OPC1_20Mk	12.6 / 18.2	6.2 / 6.7	6.4 / 11.5	6.9 / 1.9	12.0 / 3.1
OPC2	12.9 / 16.7	7.9 / 8.3	5.0 / 8.4	9.1 / 20.3	12.7 / 26.5
OPC2_10CT	13.2 / 17.6	9.8 / 9.1	3.4 / 8.5	8.4 / 16.9	10.1 / 24.8
OPC2_20CT	10.9 / 18.2	5.7 / 9.4	5.2 / 8.8	6.1 / 14.3	10.8 / 23.5
OPC2_30CT	12.6 / 17.9	9.6 / 9.4	3.0 / 8.5	6.9 / 12.1	10.9 / 22.6
OPC2_20Mk	14.6 / 17.5	6.8 / 6.2	7.8 / 11.3	10.0 / 1.2	17.1 / 2.0
PLC_10Sf	13.7 / 17.6	8.7 / 11.6	5.0 / 6.0	10.3 / 7.4	16.0 / 11.6
PLC_20CT	13.5 / 17.9	8.4 / 10.6	5.1 / 7.3	8.4 / 6.4	14.7 / 11.2
PLC_30CT	10.8 / 17.9	6.1 / 10.9	4.7 / 7.0	7.3 / 4.0	14.6 / 8.1
PLC_10Mk/20CT	13.7 / 17.5	8.4 / 10.8	5.3 / 6.7	6.0 / 2.9	12.0 / 5.8

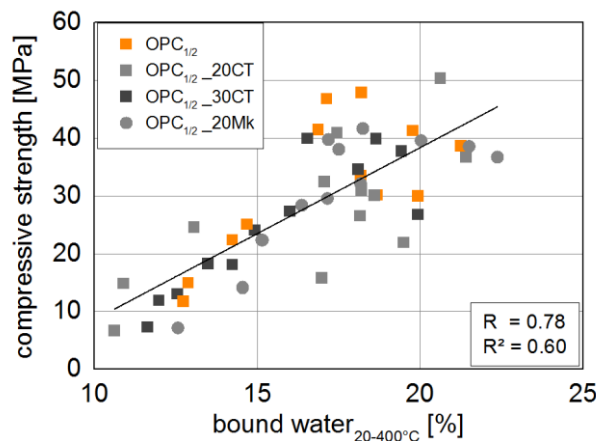


Figure 1: Compressive strength [MPa] related to the amount of bound water [wt.%]

3.2 Porosity

For blended binders, the accessible porosity decreases with increasing substitution levels of SCMs after 28 days of hydration (Table 4). The volume of pores below a pore size of 30 nm increases slightly for OPC systems blended with CT. The effect is more pronounced for binders containing Mk. The pore volumes below a pore size of 30 nm in the PLC systems exhibit a similar trend. After 28 days, the median pore diameter of systems containing Mk has decreased even to less than 20 nm, as already stated e.g. by [21, 22]. The silica fume containing binder has a median pore diameter of 4.7 nm which is hardly surprising due to the high specific surface area of Sf. A comparable low value was obtained for the Mk/CT blended PLC system. In terms of durability, the threshold pore entry radius [16] is a significant parameter to evaluate the possible threat of transportation mechanisms. It decreases with increasing substitution level of CT and provides the lowest values for OPC systems containing Mk. The threshold for the blended PLC systems was even lower. The results confirm a significant refinement of

microstructure due to the SCMs used. The modification of porosity originates from differences in hydration products and is also valid for blended binders with 20 and 30 wt.% of CT.

Table 4: Porosity parameters determined by MIP after 28 days of hydration

System	Accessible porosity	Pore size < 30 nm	Median pore diameter	Threshold pore entry radius
	vol.-%	vol.-%	nm	nm
OPC1	37.3	15.9	41.0	110
OPC1_10CT	35.6	13.9	49.5	105
OPC1_20CT	37.0	17.5	50.1	70
OPC1_30CT	36.8	18.6	29.2	75
OPC1_20Mk	34.8	22.6	20.0	30
OPC2	37.3	16.7	38.3	150
OPC2_10CT	36.5	16.8	39.2	110
OPC2_20CT	36.1	18.5	28.4	115
OPC2_30CT	36.8	17.3	34.0	116
OPC2_20Mk	34.8	22.6	20.0	80
PLC_10Sf	22.3	12.1	4.7	64
PLC_20CT	24.4	15.3	28.3	52
PLC_30CT	23.3	18.5	21.9	37
PLC_10Mk/20CT	11.4	21.3	7.2	28

3.3 Compressive strength and Young`s modulus in concrete

Error! Reference source not found. presents compressive strength and modulus of elasticity of high performance concretes with different substitutions levels of SCMs at an age of 28 days. Concretes made with calcined clays yield comparable strength results as the reference high strength concrete made with silica fume even though high amounts of superplasticizer were necessary for the calcined clay mixes. It is interesting that it is possible to obtain the same strength with 30 wt.% of pure or mixed calcined clays as with 10 wt.% of silica fume. Such a high replacement level is needed in future for a more ecological mix design.

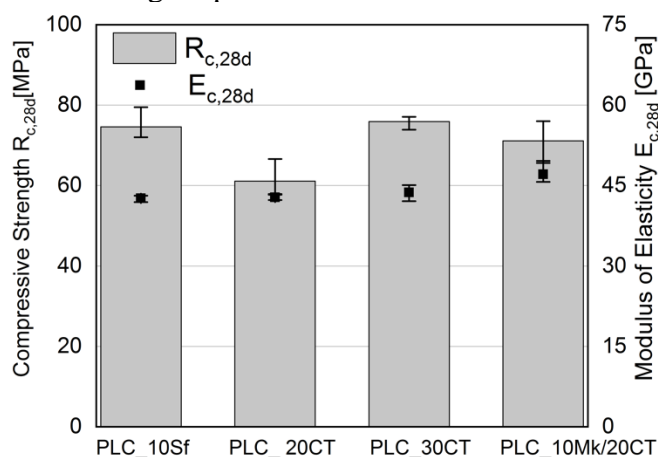


Figure 2: Compressive strength ($R_{c,28d}$) and modulus of elasticity ($E_{c,28d}$) after 28 days

The modulus of elasticity is in the same range of about 43 GPa for PLC_10Sf, PLC_20CT and PLC_30CT and is slightly higher for the combined calcined clay substitution in

PLC_10Mk/20CT. Furthermore, positive synergetic effects between the calcined clays and limestone in the PLC may have an impact which result in a preferred formation of strength-enhancing AFm phases according to Antoni et al. [23]. In addition, a higher alkali and C₃A content of the PLC both promote the pozzolanic reactivity and confirms the findings of Cyr et al. [12] for metakaolin blended cements.

4. FURTHER RESEARCH

The poor workability of high strength concretes with a high substitution level of calcined clays due to the latter's high water demand represents the biggest challenge so far. It is indispensable to test the interaction of calcined clays with superplasticizers. The investigations show that high concrete strength can be achieved with PLC blended with calcined clays. The combination of calcined mixed layer clays with other composite cements should be evaluated in further investigations.

6. SUMMARY AND CONCLUSIONS

Based on the results of this investigation the following conclusions are drawn:

1. The investigated calcined mixed layer clay exhibits a high pozzolanic reactivity comparable to other highly reactive SCMs. Its benefit consists in higher substitution rates becoming possible than recommendable with common SCMs like metakaolin and silica fume. With an increasing alumina content in blended binders, the aluminate reaction is preferred over the well-known pozzolanic reaction which is until now often primarily seen as silicate reaction only.
2. The favored AFm phase formation leads to an increasing volume of hydrate phases, resulting in higher density of the microstructure and pore structure refinement. Both effects contribute to an increased compressive strength of blended binders.

Environmentally friendly high strength concrete can be achieved with low water-binder ratio and a cement replacement of up to 30 wt.% by calcined mixed layer clays. Properties of concretes with 30 wt.% of calcined mixed layer clays or mixes of CT with metakaolin are comparable to concrete made with 10 wt.% of silica fume, even though necessary dosages of superplasticizer may exceed dosages recommended by producers.

ACKNOWLEDGEMENTS

The authors like to thank Liapor GmbH & Co. KG for supplying the calcined mixed layer clay and Schwenk Zement KG for providing the cements.

REFERENCES

- [1] Müller, N. and Harnisch, J., 'A Blueprint for a Climate Friendly Cement Industry – How to Turn Around the Trend of Cement Related Emissions in the Developing World, ed. Report prepared for the WWF-Lafarge Conservation Partnership, (Nürnberg, 2008) 94.
- [2] Beuntner, N. and Thienel, K.-C. 'Calcined clays as alternative supplementary cementitious materials (Calcinierte Tone als alternative Betonzusatzstoffe)', in '61. BetonTage', (Neu-Ulm, Germany, Bauverlag, 2017) 50.
- [3] Beuntner, N. and Thienel, K.-C. 'Performance and properties of concrete made with calcined clays', in 'ACI SP 320 - 10th ACI/RILEM International Conference on Cementitious Materials and Alternative Binders for Sustainable Concrete', (Montreal, Canada, Sheridan Books, 2017) 7.1-7.12.

- [4] Alujas, A. et al., 'Pozzolanic reactivity of low grade kaolinitic clays: Influence of calcination temperature and impact of calcination products on OPC hydration', *Applied Clay Science*, **108** (2015) 94-101.
- [5] Lemma, R., Irassar, E.F. and Rahhal, V., 'Calcined Illitic Clays as Portland Cement Replacements', in 'Calcined Clays for Sustainable Concrete', K. Scrivener and A. Favier, Editors, (Dordrecht, Springer Netherlands, 2015) 269-276.
- [6] Thienel, K.-C. and Beuntner, N. 'Effects of calcined clay as low carbon cementing materials on the properties of concrete', in 'Concrete in the Low Carbon Era', (Dundee, UK, University of Dundee – Concrete Technology Unit, 2012) 504-518.
- [7] Beuntner, N., Rapp, K. and Thienel, K.-C. 'Efficiency of Calcined Clay in Cementitious Systems', in 'ACI SP 289 - 12th International Conference on Recent Advances in Concrete Technology and Sustainability Issues', (Prag, Sheridan Books, 2012) 413-424.
- [8] Juenger, M.C.G. and Siddique, R., 'Recent advances in understanding the role of supplementary cementitious materials in concrete', *Cement and Concrete Research*, (2015).
- [9] Dinakar, P., Sahoo, P. and Sriram, G., 'Effect of Metakaolin Content on the Properties of High Strength Concrete', *International Journal of Concrete Structures and Materials*, **7** (3) (2013) 215-223.
- [10] Mehdipour, I. and Khayat, K.H., 'Effect of Supplementary Cementitious Material Content and Binder Dispersion on Packing Density and Compressive Strength of Sustainable Cement Paste', *ACI Materials Journal*, **113** (03) (2016) 361-372.
- [11] Beuntner, N. and Thienel, K.-C. 'Solubility and kinetics of calcined clay: study of interaction by pore solution', in '2nd International Conference on the Chemistry of Construction Materials (ICCCM 2016)', (Munich, Germany, Gesellschaft Deutscher Chemiker e.V., 2016) 157-160.
- [12] Cyr, M. et al., 'Effect of cement type on metakaolin efficiency', *Cement and Concrete Research*, **64** (2014) 63-72.
- [13] Bazzoni, A. et al., 'A Practical Guide to Microstructural Analysis of Cementitious Materials', 1st edn. (Boca Raton, CRC Press, 2016) 558.
- [14] Lothenbach, B. and Winnefeld, F., 'Thermodynamic modelling of the hydration of Portland cement', *Cement and Concrete Research*, **36** (2) (2006) 209-226.
- [15] Tironi, A., Scian, A.N. and Irassar, E.F. 'Hydration of ternary cements elaborated with limestone filler and calcined kaolinitic clay', in '14th International Congress on the Chemistry of Cement (ICCC 2015)', (Beijing (China), 2015) 7.
- [16] Antoni, M., 'Investigation of cement substitution by blends of calcined clays and limestone', in *Faculté des Sciences et Techniques de L'ingénieur. (École Polytechnique Fédérale de Lausanne, Lausanne, 2013)*, 254.
- [17] Taylor, H.F.W., 'Cement Chemistry', 2. edn. (London, Thomas Telford Ltd, 1997) 459.
- [18] Lothenbach, B. et al., 'Influence of limestone on the hydration of Portland cements', *Cement and Concrete Research*, **38** (6) (2008) 848-860.
- [19] Antoni, M., Baquerizo, L. and Matschei, T., 'Investigation of ternary mixes made of clinker limestone and slag or metakaolin: Importance of reactive alumina and silica content', in 'Calcined Clays for Sustainable Concrete', K. Scrivener and A. Favier, Editors, (Dordrecht, Springer Netherlands, 2015) 545-553.
- [20] Baquerizo, L.G. et al., 'Hydration states of AFm cement phases', *Cement and Concrete Research*, **73** (2015) 143-157.
- [21] Frías, M. and Cabrera, J., 'Pore size distribution and degree of hydration of metakaolin–cement pastes', *Cement and Concrete Research*, **30** (4) (2000) 561-569.
- [22] Kadri, E.H. et al., 'Combined effect of chemical nature and fineness of mineral powders on Portland cement hydration', *Materials and Structures*, **43** (5) (2010) 665-673.
- [23] Antoni, M. et al., 'Cement substitution by a combination of metakaolin and limestone', *Cement and Concrete Research*, **42** (12) (2012) 1579-1589.

INFLUENCE OF TEMPERATURE ON THE HYDRATION OF LIMESTONE CALCINED CLAY CEMENTS (LC³)

François Avet (1) and Karen Scrivener (1)

(1) Swiss Federal Institute of Technology (EPFL), Switzerland

Abstract

This paper investigates the influence of temperature on the hydration of Limestone Calcined Clay Cements (LC³). The increase from 20°C to 40°C leads to an acceleration of hydration. Both clinker hydration and metakaolin reaction are faster. However, similar amounts of reacted clinker and metakaolin are measured at late ages. The influence of temperature on C-A-S-H density was also studied. The grey level of the C-A-S-H was determined and the differences observed between plain cement and LC³ blends are related with the difference of chemical composition. There is no clear evidence that the density of C-A-S-H increases with temperature.

Keywords: calcined clay, limestone, temperature, hydration

1. INTRODUCTION

In the recent years, more and more attention has been brought on decreasing the environmental impact of cement and concrete production. The decrease of the clinker content of cement using Supplementary Cementitious Materials (SCMs) is very promising. Traditional SCMs such as fly ashes and slags are facing global shortage [1]. The combination of widely available calcined clay and limestone in Limestone Calcined Clay Cements (LC³) permits to reduce the clinker content of cement to 50% in LC³-50 blends [2].

Recent studies showed that pure calcined kaolinitic clays are not the most suitable in LC³. Clays with only 40-50% of kaolinite permit to get the best compromise in terms of rheological, mechanical and durability properties, compared with plain cement [3,4]. Most of previous studies were carried out at laboratory conditions, i.e. 20°C. However, LC³ cements have high potential in tropical countries with higher temperature. Thus, the goal of this study is to investigate the influence of the temperature increase on the hydration and the properties of LC³, from 20°C to 40°C.

2. MATERIALS AND METHODS

Five clays were used in this study from various countries. The kaolinite content was determined by thermogravimetric analysis (TGA) using tangent method. The calcined kaolinite content is used to consider the grade of calcined clay and the efficiency of calcination [5]. Table 1 details the characteristics of the clays used, their calcined kaolinite content, origin, calcination method and physical properties. The properties of the cement and limestone used to make LC³ are also shown in Table 1.

Table 1: Characteristics of the calcined clays, cement and limestone used in this study.

Calcined clay	1	2	3	4	5	Quartz	Cement	Limestone
Origin	North America	South Asia	South-east Asia	South America	South Asia	-	-	-
Calcination process	Flash	Furnace	Furnace	Furnace	Furnace	-	-	-
Calcined kaolinite content (wt.%)	95.0	62.6	50.3	35.0	17.0	0	-	-
D _{v, 50} (µm)	5.1	25.3	10.9	23.5	5.9	11.2	8.4	7.2
Specific surface (m ² /g)	9.6	15.2	45.7	18.5	18.7	1.2	0.9	1.8

For the mix design, LC³-50 was used, with a clinker content down to 50%, 30% of calcined clay, 15% of limestone and 5% of gypsum. Pastes were cast using a fixed water to binder ratio of 0.4. For the casting at 40°C, the powders and water were stored at 40°C, then cast and stored at 40°C until testing.

3. RESULTS

3.1 Clinker hydration

Figure 1 shows the degree of hydration of clinker determined by XRD combined with Rietveld method. At 20°C, the degree of hydration slows down from 3 days onwards for LC³-50 blends containing more than 60% of calcined kaolinite in the calcined clay. The reason for this slowing down is the lack of pores large enough to enable hydrate growth [5]. At 40°C, the hydration of clinker is accelerated. The slowing down of clinker hydration occurs even earlier. From 1 day onwards, the hydration of clinker does not significantly increase anymore for blends

with a calcined kaolinite content in clay higher than 60%. At 28 days of hydration, the amount of clinker reacted reaches quite similar values at 20°C and 40°C.

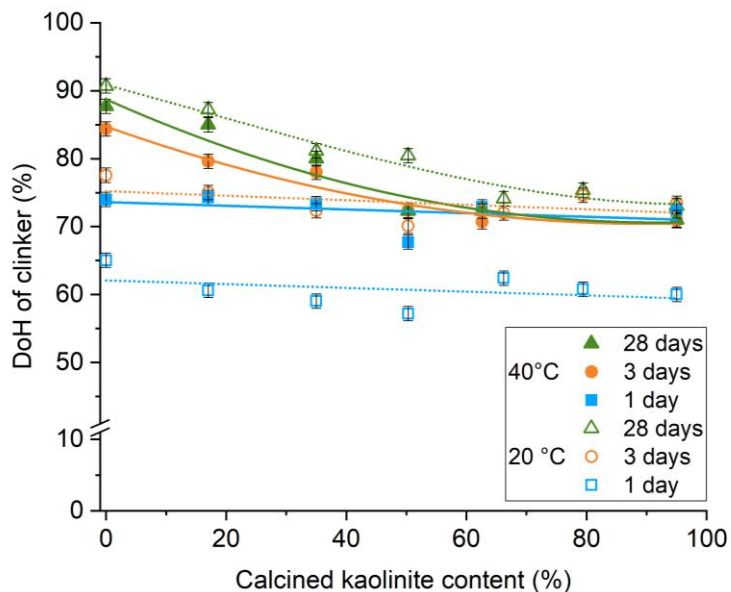


Figure 1. Degree of hydration of clinker at 20°C and 40°C for LC³-50 systems.

3.2 Pozzolanic reaction

The amount of reacted metakaolin is obtained by mass balance [6] and is shown in Figure 2. As previously observed for the hydration of clinker, the reaction of metakaolin is accelerated with the increase of temperature. This acceleration is observed especially at 1 and 3 days. At 28 days of hydration, the amount of reacted metakaolin is very similar for both temperatures. The reaction of metakaolin reaches a plateau for blends containing clays with more than 50% of calcined kaolinite. This limit of reaction is likely to be due to the lack of portlandite.

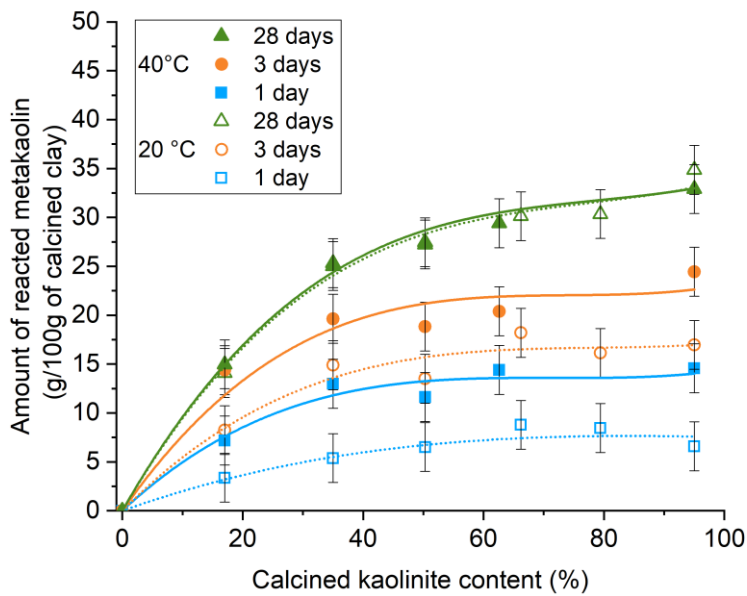


Figure 2. Amount of reacted metakaolin at 20°C and 40°C for LC³-50 blends.

3.3 C-A-S-H characterization

The grey level was determined on polished cross-sections in backscattered electron mode (BSE) [7]. Only blends with visible uniform inner C-A-S-H layers were investigated. Results are shown in Figure 3. It shows that the C-A-S-H of LC³-50 blends is darker than the C-S-H of PC. This is explained by the difference in chemical composition of the C-A-S-H between the plain cement system and the blends. There is no clear evidence of the increase of the brightness of the C-A-S-H with temperature. The differences observed are in the range of error of the measurement. Thus, the increase of C-A-S-H density with temperature cannot be verified.

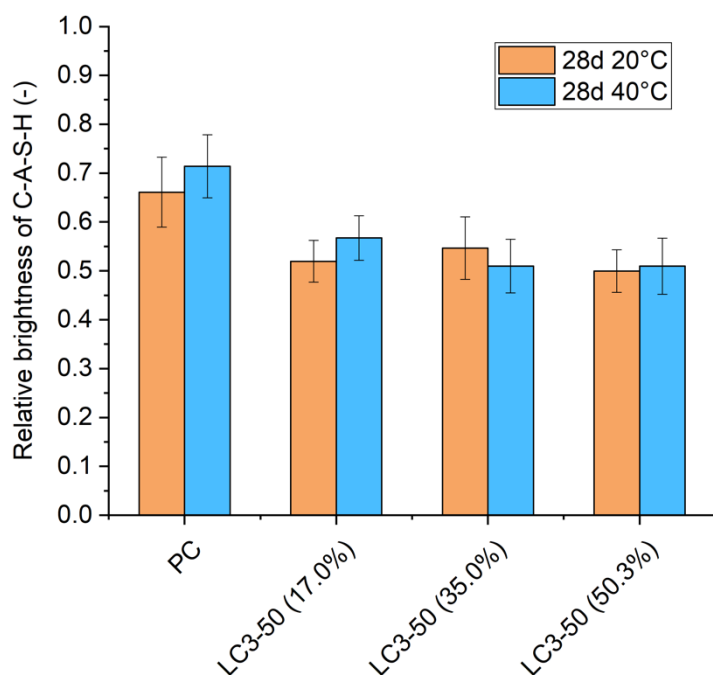


Figure 3. Relative brightness of C-A-S-H for PC and LC³-50 blends at 28 days of hydration.

11. CONCLUSIONS

- The hydration of clinker is accelerated at higher temperature. The clinker hydration significantly slows down from 1 day onwards for LC³-50 blends containing more than 60% of calcined kaolinite in clay.
- The pozzolanic reaction of calcined clay is also enhanced at 1 and 3 days of hydration. At 28 days, the amount of reacted metakaolin is similar at 20°C and 40°C.
- The increase of temperature does not impact the density of C-A-S-H, since similar grey levels are obtained.

ACKNOWLEDGEMENTS

The authors gratefully acknowledge the Swiss Agency for Development and Cooperation (SDC) grant 81026665 for their financial support.

REFERENCES

- [1] Scrivener K., Vanderley J., Gartner E., 'Eco-efficient cements: Potential, economically viable solutions for a low-CO₂ cement based materials industry', UNEP, (2016).
- [2] Bishnoi, S., Mallik, A.; Joseph, S.; Krishnan, S., 'Pilot scale manufacture of limestone calcined clay cement : The Indian experience', *The Indian Concrete Journal*, **88** (2014) 22-28.
- [3] Avet F., Snellings R., Alujas Diaz A., Ben Haha M., Scrivener K., 'Development of a new rapid, relevant and reliable (R3) test method to evaluate the pozzolanic reactivity of calcined kaolinitic clays', *Cement and Concrete Research*, **85** (2016) 1-11.
- [4] Maraghechi H., Avet F., Wong H., Kamyab H., Scrivener K. 'Performance of Limestone Calcined Clay Cement (LC³) with various kaolinite contents with respect to chloride transport'. *Materials and Structures* **51:125** (2018) 1-17.

- [5] Avet F., Scrivener K. 'Investigation of the calcined kaolinite content on the hydration of Limestone Calcined Clay Cement (LC3)'. *Cement and Concrete Research* **107** (2018) 124-135.
- [6] Avet F., Li X., Scrivener K. 'Determination of the amount of reacted metakaolin in calcined clay blends'. *Cement and Concrete Research* **106** (2018) 40-48.
- [7] Gallucci E., Zhang X., Scrivener K. 'Effect of temperature on the microstructure of calcium silicate hydrate (C-S-H)'. *Cement and Concrete Research* **53** (2013) 185-195.

NEW GENERATION OF CONSTRUCTION MATERIALS
SESSION 12: Bio-based materials

INFLUENCE OF HYDRIC SOLICITATIONS ON THE MORPHOLOGICAL BEHAVIOR OF HEMP CONCRETE

F. Bennai (1, 2, 3), C. El Hachem (3), K. Abahri (3) and R. Belarbi (1, 2),

(1) LMT, ENS Paris-Saclay, CNRS, Université Paris Saclay, 61 Avenue du Président Wilson, 94230 Cachan, France.

(2) LaSIE UMR 7356, CNRS, Université de La Rochelle, Avenue Michel Crépeau, 17042 La Rochelle Cedex 1, France.

(3) 4ev Lab, EDF R&D, CNRS, LaSIE, Université de La Rochelle, Avenue Michel Crépeau 17042 La Rochelle cedex1, France.

Abstract

The use of bio-based materials such as hemp concrete in the field of construction allows limiting environmental impacts and improving the energy performances of buildings. The aim of this paper is to understand the influence of adsorption and desorption of moisture in hemp concrete on its internal morphology and its dimensional variations. That's why, the high porosity and the adsorption capacity of hemp concrete were discussed. Then, an experimental cell was developed to follow the geometric evolution over time of hemp concrete microstructure under hydric solicitations: humidification and drying. The digital image correlation was used to determine the strains fields on the surface of the material. This technique showed the behavior of this hygroscopic material subjected to different hygrometries. Indeed, the hemp shiv undergoes larger strains than the binder, thus affecting the morphology of hemp concrete. The results obtained highlighted the influence of the hydric state of hemp concrete on its very heterogeneous microstructure. It has also been revealed that the durability of the material can be affected by the dimensional variations caused by the relative humidity variations.

Keywords: Hemp concrete, microstructure, digital image correlation, adsorption, strain.

This work was invited for publication in the open access journal RILEM Technical Letters. You can visit the journal and benefit from the full open access to the published articles at: letters.rilem.net.

SUSTAINABLE HEMP-CLAY-LIME CONCRETE

Rotem Haik (1), Isaac A. Meir (2) and Alva Peled (2)

(1) Unit of Energy Engineering, Ben Gurion University of the Negev, Israel

(2) Department of Structural Engineering, Ben Gurion University of the Negev, Israel

Abstract

Buildings are responsible for approximately 40% of the global energy consumption and CO₂ emissions. These values only include the operational energy (OE) and operational carbon (OC), but they are even greater if the embodied energy (EE) and embodied carbon (EC) are also included. In this research, sustainable building materials based on bio-aggregate made of Hemp and low energy / low carbon footprint binders were developed. The research was based on Lime-Hemp Concrete (LHC), which was already proven to be an energy efficient and environment friendly construction material and its use is rapidly increasing. However, lime, like other fired materials, has relatively high EE and EC values. This research studied the influence of replacing the lime in LHC with alternative unfired binders in several different contents. Five alternative binders were examined (based on clay, limestone and basalt), including waste by-products of aggregate quarries, these last ones presenting additional environmental benefits. The thermal properties were investigated, aiming to obtain a good balance between thermal insulation and heat capacity, which will allow reducing the OE and OC of the building while the EE and EC of these materials are reduced as well. Physical, chemical and mechanical properties were also examined.

Keywords: Hemp bio-aggregate, lime, clay, thermal insulation, energy efficiency.

1. INTRODUCTION

Buildings are responsible for approximately 40% of the global energy consumption and CO₂ emissions [1-2]. These values only include the operational energy (OE) and operational carbon (OC), which is the energy and carbon requirements for heating, cooling, ventilation, etc. These values are significantly higher if they also include the embodied energy (EE) and the embodied carbon (EC) involved with materials production [3]. Therefore, current requirements for sustainability are essential to find ways to reduce the levels of energy and carbon requirements of the building industry.

Concrete is by far the most widespread building material in the industrialized world, used for a wide range of structural and non-structural applications in the construction industry.

Worldwide, more than 10 billion tons are produced each year. Cement production requires kiln temperature of 1450°C, and as such it possesses high EE. Furthermore, the production of each ton of cement releases almost one ton of CO₂ into the atmosphere [4]. Therefore, cement is widely perceived as being incompatible with the demands of sustainable development. Moreover, in order to keep a building on a low level of OE and OC, the use of insulation materials is essential. However, in many cases such materials imply a high level of EE and EC, which very often is not compensated by their OE and OC savings over the life span of the building [5-6]. Thus, development of innovative building materials is required to meet the demand for a sustainable industry. One recent innovative development is that of Lime-Hemp Concrete (LHC), which is already gaining popularity in Europe due to its great energy efficiency, as well as its low environmental impact.

LHC is a new environment friendly construction material that is composed of hemp shives and lime binder [7]. The EE of LHC is relatively low due to the fact that hemp is a natural plant possessing low levels of EE and due to the relatively low kiln temperature of lime (~900°C) as compared to that of cement. The EC of LHC is actually negative due to the active carbon sequestration of the hemp plant during its growing phase [8-9] and the carbonation process of the lime during its hardening. Furthermore, the high porosity of the hemp shives provides low values of density and thermal conductivity, the latter defining its property as thermal insulation. However, these values depend on the hemp: lime ratio, higher hemp content leads to lower thermal conductivity, i.e., better insulation [10-11]. Research has shown that a building made of LHC has the ability to lessen the impact of external temperature oscillations. Furthermore, LHC can regulate the indoor relative humidity (RH). The ability of LHC to lessen the impact of external oscillations of temperature and RH is fundamental to the avoidance of summer overheating and winter overcooling [12]. The mechanical properties of LHC are relatively low and therefore it cannot be used as a load bearing material, but can be used for non-structural applications [11, 13-15], for example as a substitute for the current commonly used concrete blocks or as a replacement for lightweight materials such as Autoclaved Aerated Concrete (AAC). In addition, LHC can be used as an insulation layer for walls, floors and ceilings.

However, lime, like other fired materials, possesses relatively high EE and EC. Thus, alternative unfired binders should be considered for further reduction in EE and EC of LHC [16-18]. Partial replacement of the lime with an unfired material can significantly reduce the EE and EC [17-18].

The objective of this research was to develop novel environment friendly building materials based on LHC with alternative unfired binders which possess low levels of EE and EC on the one hand, and satisfactory thermal and mechanical properties on the other hand. Two alternative unfired binders having different chemical composition were studied with and without hemp. The work was divided into three stages: (i) physical and chemical characterization of the binders, (ii) selection of the binder, (iii) variable contents of the selected binder.

2. EXPERIMENTAL PROGRAM

2.1 Alternative binders' characterization tests

The first stage of the research focused on identifying optimal alternative unfired binders. Two alternative binders were examined, Mamshit which is a clay-based material, and Kalgir

which is a limestone-based material. The chemical compositions of the binders were examined by XRF (x-ray fluorescence) and EDS (energy dispersive spectroscopy). Their particles size distribution (PSD) was studied as well as their morphology by SEM (scanning electron microscope).

2.2 Compressive strength and thermal conductivity tests

2.2.1 Constant binder's content

The second stage of the research studied the behavior of samples composed of 50% alternative binder and 50% lime. Tradical PF70 lime [19] was used for that purpose. The mixtures were tested without hemp and with hemp as follows:

Without hemp - A mixtures of 50% alternative binder and 50% lime were mixed with water as the binders (lime + alternative binder): water ratio was 0.76 (by weight). Cubic specimens with side dimensions of 5 cm were prepared and the compressive strength was tested at an age of 28 days, 4 specimens were tested and the average is reported.

With hemp - A mixtures of 50% alternative binder and 50% lime were mixed with hemp as the binders (lime + alternative binder): hemp ratio was 2:1 (by weight). The water content was 2.92 times the hemp content (by weight). These proportions were chosen in order to achieve a density of approximately 330 kg/m³. Cylindrical specimens with dimensions of 10 cm diameter and 20 cm height were prepared. Each sample included 6 specimens, 4 specimens were used for testing the compressive strength and 2 specimens for testing the thermal conductivity.

For both cases, the compression tests were conducted using an INSTRON 5982 test system [20] at a rate of 0.5 mm/min. The thermal conductivity was tested by Decagon KD2-Pro Thermal Analyzer [21].

2.2.2 Variable binder contents

The third stage of the research examined the influences of replacing the lime in LHC with different contents (0%, 30%, 50%, 70%, and 100% replacement) of Kalgir, which is the alternative binder that was selected since it presented the most attractive results, this will be discussed at stage 3.2.1. The parameters that were tested at this stage are the thermal conductivity and the compressive strength. These properties were tested at the same methods as in stage 2.2.1.

3. RESULTS

3.1 Alternative binders' characterization

Fig. 1a presents the chemical composition of the two alternative unfired binders, Mamshit and Kalgir, examined by XRF. As expected, Mamshit presents a composition which is typical for clay (~22% Si, ~13% Al, ~10% Ca, and ~5% Fe) while Kalgir presents significantly higher content of Ca (~47%) and lower contents of the other elements (~11% Si, ~2% Al, and ~1% Fe) indicating a limestone-based material. These results were also confirmed by EDS. The particle size distribution of the alternative binders is presented in Fig. 1b showing approximately similar size distribution of the two binders, mainly in the range of 1µm to 100µm with 80% smaller than 20µm. Fig. 2 presents SEM images of the binders (at a magnitude of x1000) showing that their morphology is approximately similar as well.

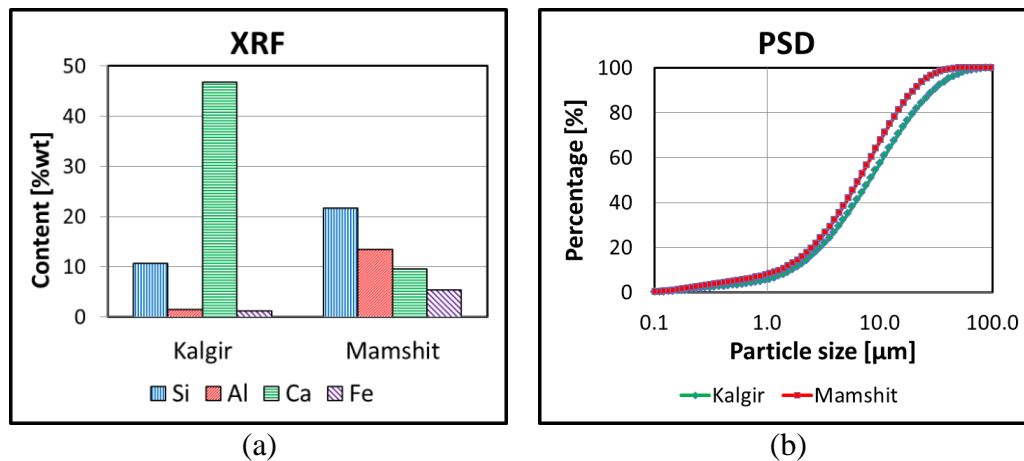


Figure 1: Analysis of the alternative binders: (a) chemical composition measured by XRF; (b) particles size distribution (PSD)

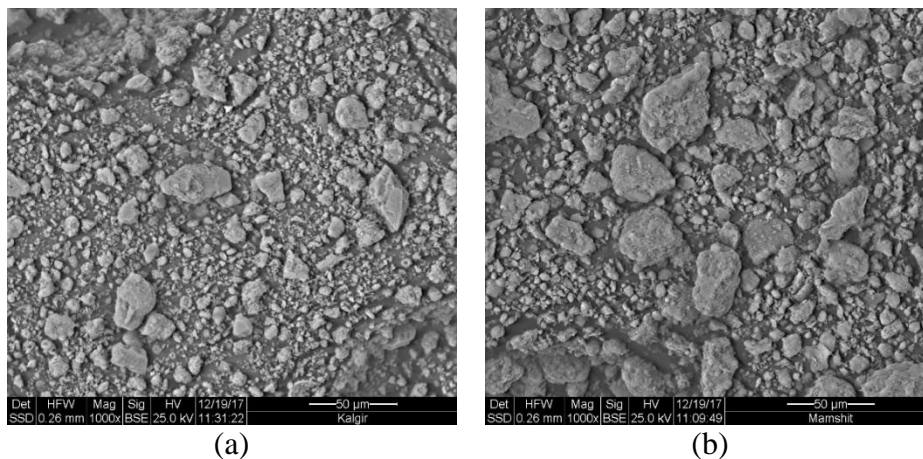


Figure 2: Morphology of the alternative binders taken by SEM of: (a) Kalgir; (b) Mamshit

3.2 Compressive strength and thermal conductivity

3.2.1 Alternative binder selection

Lime-based mixtures with and without hemp were examined, a mixture with 100% lime was compared to mixtures with 50% lime and 50% alternative binders, i.e., mixtures with 50% replacement of the lime with Kalgir or Mamshit. Fig. 3a presents the compressive strength of these mixtures without hemp. It shows that both samples containing alternative binders present significantly lower strength than the sample of 100% lime. While the mixture with Kalgir presents significantly higher strength of twice as much as that with Mamshit. When hemp is added, the strengths of all mixtures is significantly lower (Fig. 3b) as compared to the mixtures without hemp. However, the trend is completely different as both mixtures with Kalgir and Mamshit present higher compressive strengths than that with 100% lime only, in contrary to the compression results of the samples without hemp. One possible reason for this difference might be due to absorption of water by the hemp during mixing (thanks to the porous structure of the hemp), and thus not enough water is left for the reaction of the lime; as a result, the strengthening process of the lime was incomplete. Also here with

the addition of hemp, the mixture with Kalgir is the strongest, presenting improvement of 36% as compared to the reference with lime only; but the compressive strength of the mixture with Mamshit is only 8% lower than the one with Kalgir, suggesting that when hemp is involved the main influence on mixture strength is not highly related to the type of the alternative binder but rather to the lime reaction process as was suggested above.

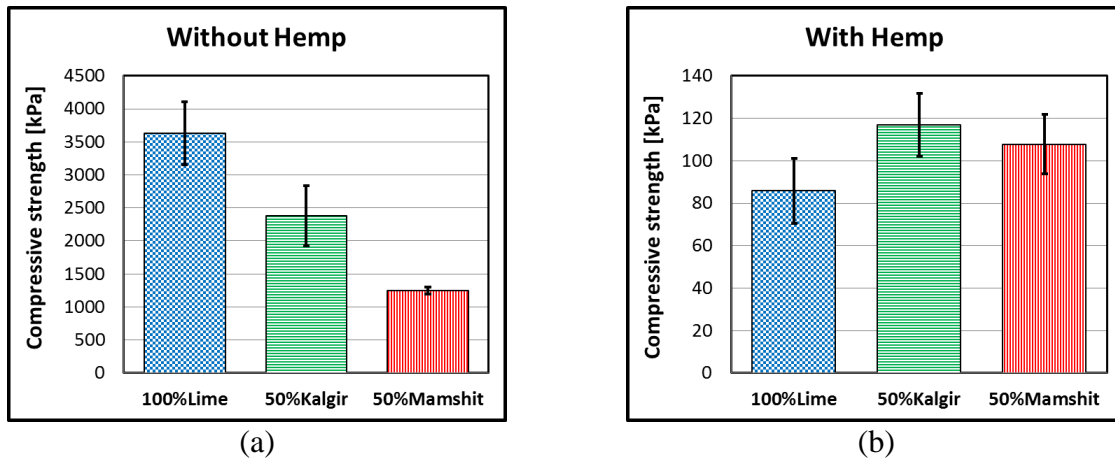


Figure 3: Compressive strengths of samples made with 50% alternative binder and 50% lime: (a) without hemp; (b) with hemp

Fig. 4 presents the thermal conductivity of samples made of 50% alternative binder and 50% lime with hemp, compared to a reference sample composed of 100% lime. It shows that both mixtures with the alternative binders present slightly higher thermal conductivity than that of the reference with lime only. The thermal conductivity of the mixture with Kalgir is 5% lower than the one with Mamshit, i.e., Kalgir functions slightly better as an insulator, as compared to Mamshit. However, the difference is not significant enough. Hence, it is difficult to draw conclusions.

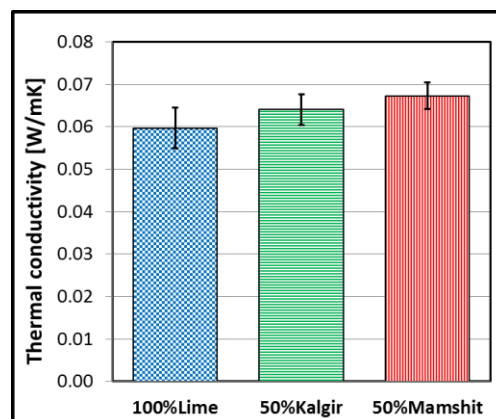


Figure 4: Thermal conductivity of samples with hemp, 50% alternative binder and 50% lime

The above results indicate that Kalgir is more attractive than Mamshit as a partial replacement of the lime when LHC mixtures are considered, as the mixture with Kalgir exhibited greater mechanical properties and higher thermal properties than the mixture with Mamshit. Therefore, it was decided to choose Kalgir as the alternative binder for the third

stage of the research, which examines the influences of different contents of the selected alternative binder as lime replacement.

3.2.2 Alternative binder contents

The influences of replacing the lime in LHC with variable contents of Kalgir, the selected alternative binder, were examined. Fig. 5a presents the compressive strengths of samples made with different contents of Kalgir: 0%, 30%, 50%, 70%, and 100%. Note that the 50% content was tested again having a complete series with the exact same conditions. In general, it shows that higher content of Kalgir leads to higher compressive strength (with an exception of 70% Kalgir), i.e., replacing the lime with Kalgir improves the compressive strength of the LHC component. Such improvement is most significant up to 50% lime replacement as the compressive strength of the mixture with 50% Kalgir is 39% higher than that of the reference with lime only (similar to the results presented previously in section 3.2 above). Above 50% replacement the improvement by the addition of Kalgir relative to the reference mixture with lime only is almost the same as the 50% one, the mixture with the 100% Kalgir is 44% higher than that of the reference with lime only.

Fig. 5b presents the thermal conductivity of samples made with variable contents of Kalgir (0%, 30%, 50%, 70%, and 100%). It shows that replacing the lime in LHC with Kalgir hardly affects the thermal conductivity, with an exception of 100% Kalgir, which its thermal conductivity is 16% higher than that of the reference with lime only. However, note the high standard deviation (STDV) of this system. The thermal conductivity values of the other mixtures (30%, 50%, and 70% Kalgir) are approximately similar; of only 5% higher than that of the reference with lime only.

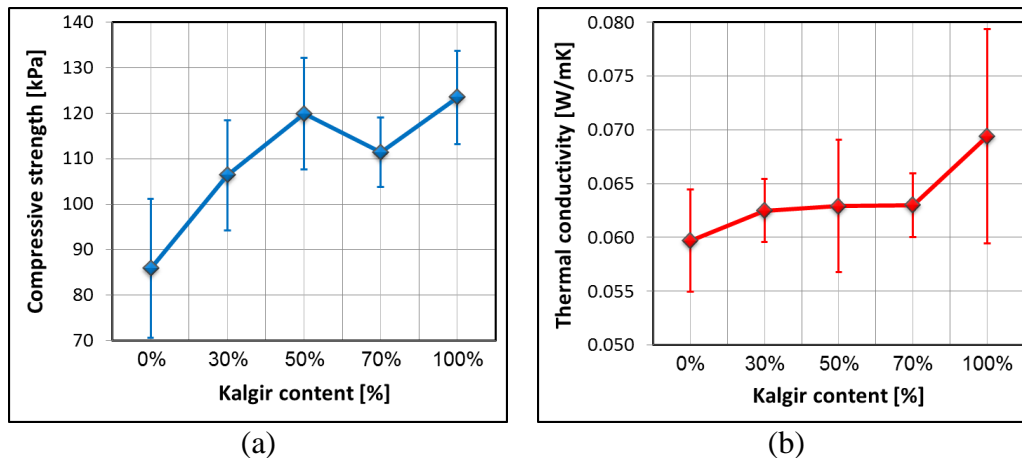


Figure 5: Properties of samples made with variable contents of Kalgir. (a) Compressive strength; (b) thermal conductivity

Fig. 6 presents the total embodied energy of samples made with different contents of Kalgir (0%, 50%, and 100%). The embodied energy included the energy required for materials production (hemp, lime and Kalgir), was calculated based on the values taken from the *Inventory of Carbon and Energy (ICE)* [16]. It clearly shows the benefit of replacing the lime with alternative binder from an energy saving point of view. When the lime is replaced by 50% alternative binder (Kalgir) 49% of the EE can be saved. Furthermore, if all the lime is

replaced by alternative binder (Kalgir), i.e. 100% lime replacement, the EE saving is higher than 98%.

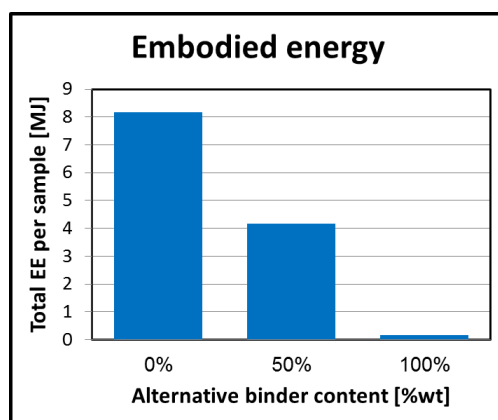


Figure 6: Embodied energy of samples made with different contents of alternative binder (Kalgir)

4. CONCLUSIONS

This research studied the influences of replacing the lime in LHC with two alternative unfired binders, Kalgir and Mamshit. Mixtures with and without hemp were explored. In general, for mixtures without hemp partly replacing the lime with the alternative binders reduced their compression strengths. However, when hemp was added the situation was different: the alternative binders improved the compressive strengths as compared with the mixture of 100% lime. A possible reason can be related to the ability of the hemp to absorb water during mixing (thanks to the porosity of the hemp), leading to incomplete chemical reaction of the lime. When hemp was added to the mixture the following trends were observed:

- The thermal conductivity of LHC was almost not affected by the replacement of the lime with the alternative binders.
- Using Kalgir as lime replacement was more attractive than Mamshit, as the mixture with Kalgir exhibited improved mechanical properties and improved thermal properties than the mixture with Mamshit.
- The content of Kalgir in the mixture highly influenced LHC compressive strength, with higher Kalgir content resulting in higher compressive strength.
- Replacing the lime with alternative binder was found to be attractive from the sustainability prospective, as it led to significantly lower embodied energy.

It can be concluded that the findings of this research clearly show the high potential of using alternative unfired binders as partial replacement for lime in LHC, in terms of mechanical properties, thermal insulation, as well as embodied energy savings.

REFERENCES

- [1] European Commission, '20% energy savings by 2020 – Memo', European Commission - Directorate General for Energy and Transport (2005).
- [2] Gabay H., Meir I.A., Schwartz M. and Werzberger E., 'Cost-benefit analysis of green buildings: An Israeli office buildings case study', *Energy and Buildings* 76 (2014) 558–564.
- [3] Huberman N. and Pearlmutter D., 'A life-cycle energy analysis of building materials in the Negev desert', *Energy and Buildings* 40(5) (2008) 837-848.
- [4] Mayer C., 'The greening of the concrete industry', *Cement & Concrete Composites* 31 (2009) 601–605.
- [5] Meir I.A. and Pearlmutter D., 'Building for climate change: planning and design considerations in time of climatic uncertainty'. *Corrosion Engineering, Science and Technology* 45 (2010) 70-75.
- [6] Meir I.A., 'Green technologies in planning and design vis-à-vis climatic uncertainty', *Encyclopedia of Energy Engineering and Technology* (2nd Edition). Taylor & Francis (2015) 796-803.
- [7] Bevan R. and Wooley T., 'Hemp Lime Construction: A Guide to Building with Hemp Lime Composites', (IHS BRE Press, 2010).
- [8] Hirst E.A.J, Walker P., Paine K.A. and Yates T., 'Characterisation of low density hemp-lime composite building materials under compression loading'. 2nd International Conference on Sustainable Construction Materials and Technologies (2010) 1395–1405.
- [9] Ip K. and Miller A., 'Life cycle greenhouse gas emissions of hemp–lime wall constructions in the UK', *Resources, Conservation and Recycling* 69 (2012) 1–9.
- [10] Evrard A. and De Herde A., 'Dynamical interactions between heat and mass flows in Lime-Hemp Concrete', *Research in Building Physics and Building Engineering*, Taylor & Francis Group (2006) pp. 69-76.
- [11] Cérézo V., 'Propriétés mécaniques, thermiques et acoustiques d'un matériau à base de particules végétales: approche expérimentale et modélisation théorique' (Thesis), Institut national des sciences appliquées de Lyon, France (2005).
- [12] Shea A., Lawrence M. and Walker P., 'Hygrothermal performance of an experimental hemp–lime building', *Construction and Building Materials* 36 (2012) 270–275.
- [13] De Bruijn P.B., Jeppsson K.H., Sandin K. and Nilsson C., 'Mechanical properties of lime–hemp concrete containing shives and fibres', *Biosystems Engineering* 103 (2009) 474–479.
- [14] Arnaud L. and Gourlay E., 'Experimental study of parameters influencing mechanical properties of hemp concretes', *Construction and Building Materials* 28 (2012) 50–56.
- [15] Florentin Y.(2015), 'A Comparative Life-Cycle Energy and Carbon Analysis of Hemp-based Building Materials in an Arid Environment' (Thesis), The Jacob Blaustein Institutes for Desert Research, Ben-Gurion University of the Negev, Israel (2015).
- [16] Hammond G. and Jones C., 'Inventory of Carbon and Energy (ICE)'. Sustainable Energy Research Team, Department of Mechanical Engineering, University Of Bath, UK (2008).
- [17] Wilkinson S., 'A Study of the Moisture Buffering Potential of Hemp in Combination with Lime and Clay-Based Binders' (Thesis). School of Computing and Technology, University of East London, UK (2009).
- [18] Busbridge R. and Rhydwen R., 'An investigation of the thermal properties of hemp and clay monolithic walls', School of Computing and Technology 5th Annual Conference, University of East London, UK (2010) 163-170.
- [19] <http://www.tradical.com/tradical-pf70.html>
- [20] <http://www.instron.us/en-us/products/testing-systems/universal-testing-systems/electromechanical/5900/5980-floor-model>
- [21] http://manuals.decagon.com/Manuals/13351_KD2%20Pro_Web.pdf

SELF – COMPACTING CONCRETE WITH TAILINGS AND FLY ASH AS ECOLOGICAL MATERIAL

Iva M. Despotović¹, Ksenija S. Janković², Dragan M. Bojović², Marko S. Stojanović²

(1) Belgrade University College of Applied Studies in Civil Engineering and Geodesy, Serbia

(2) IMS Institute, Belgrade, Serbia

Abstract

Concept of sustainable development, which beside sociological and economic aspects, includes saving of energy, environment protection and preservation of restorable natural resources, presents strategic determination of various economic sectors. During the ore flotation in the mine large amounts of flotation tailings are generated and as waste material disposed in the specially determined areas. With the increase in metal production, the amount of tailings also increases, which is a major environmental problem because it takes up large areas. Great production of fly ash, which is the main residue from combustion of coal, also "managed" by landfilling, is a huge risk and danger for environment. Unlike vibrated concrete, self-compacting concrete contains significant amounts of fine particles, i.e. a mineral additive that greatly affects its performance, where potential use of fly ash is very important ecological aim. Tailing test results showed no pozzolanic activity and so its application in concrete can be only a partial replacement of aggregate. This paper presents the possibility of using tailings and fly ash, which are waste products, in Self – Compacting Concrete. The obtained results indicate that these materials can successfully be used.

Keywords: Self – Compacting Concrete, Tailings, Fly ash, Compressive strength.

1. INTRODUCTION

During the ore flotation in the mine large amounts of flotation tailings are generated and as waste material it is disposed in the specially determined areas in the industrial site. With the increase in metal production, the amount of tailings also increases, which is a major environmental problem because it takes up large areas. Great production of fly ash, which is the main residue from combustion of coal, also "managed" by landfilling, is a huge risk and danger for environment. By its technology, Self – Compacting Concrete (SCC), requires a certain amount of powder component for the production, so the possibility of using fly ash and tailings in the area of the concrete creates space for various research.

It is possible to use copper tailing in cement concrete as a partial replacement of natural river sand (up to 60% substitution) – the copper tailing concrete exhibited good strength and durability characteristics [1]. The effect of the application of copper tailings, which substitute 0%, 5% and 10% of cement mass on the properties of fresh and hardened mortar was investigated [2]. Copper tailings blended mortars showed higher strength and abrasion resistance. The study [3] showed that increasing the tungsten mine waste content in mortar mixes decreased both flowability and compressive strength. The aim of the paper [4] was to study combined effects of pre-firing and firing dwell times on the chemical, physical and microstructural properties of artificial lightweight aggregates produced from mining and industrial waste, including polluted mine soil and coal combustion products. The same authors presents a study about the effectiveness of thermal treatment in the immobilization of different chemical elements within the structure of artificial lightweight aggregates manufactured with contaminated soil and fly ash [5].

The utilization of fly ash in the SCC resulted in a lower wet density, mechanical properties and a higher water porosity, carbonation depth and chloride ion diffusion coefficient [6]. Increasing the fly ash content has been found to decrease the compressive strength at all the curing ages tested in investigation [7]. A maximum decrease in the compressive strength of the order of 25% at 28 days of curing.

2. EXPERIMENT

2.1 Materials used in experiment

Self – Compacting Concrete was prepared with: cement CEM I 42.5R Lafarge, natural separated aggregate 0/4mm, 4/8mm and 8/16mm, mineral additive limestone (when tailing was used), superplasticizer (polycarboxylate) and potable water.

For the purpose of this study the tailings was taken from the Pb and Zn mines, from the tailings dump. Complete testing of chemical, physical and mechanical properties of the samples was performed. The chemical composition of the tailings sample was determined by chemical analysis according to SRPS EN 196-2. There active SiO₂ and CaO content was calculated on the basis of the results of chemical analysis according to SRPS EN 197-1 standard. The test results are shown in Table 1.

The physical properties of the tailings were determined in accordance with SRPS B.C1.018 standard. The samples were milled because of a high content of coarse particles so that the residue on the 0.063 mm sieve was up to 10%, and then tested for pozzolanic activity using lime. Pozzolanic activity of the tailing was determined as the strength of mortar samples prepared with 300g of milled tailing sample, 1350g of quartz sand, 150g of hydrated lime and 270g of water. The results of pozzolanic activity were extremely low (flexural strength 0 MPa, compressive strength 0.4 MPa), which confirmed the results of the reactive SiO₂ content calculation. The conclusion is that this material is not suitable for cement replacement in concrete and mortar or as a pozzolanic cement additive. So, tailings can only be used for replacement a part of the fine aggregate.

Table 1: The chemical properties of tailings

Loss on ignition on 950 °C, %	5.61
SiO ₂ , %	43.26
Al ₂ O ₃ , %	11.11
Fe ₂ O ₃ , %	15.57
CaO, %	20.01
MgO, %	4.31
SO ₃ , %	0.32
Na ₂ O, %	0.92
K ₂ O, %	1.00
CO ₂ , %	4.42

When fly ash is added to concrete, pozzollanic reaction starts between silicon dioxide (SiO₂) and calcium hydroxide (CaOH₂) or lime, which is a by-product of hydration of Portland cement. The resulting products of hydration fill pores reducing the porosity of the matrix. These products differ from the products formed in concrete containing only Portland cement. In the reactions of Portland cement and water, hydrated lime (CaOH₂) is formed first, in the space between particles, because of its limited solubility. In the presence of water, lime reacts pozzollanic with fly ash to form new hydration products with fine pore structures. So, fly ash can be used as pozzollanic cement additive. For the purpose of this study, fly ash was taken from thermal power plant “Obrenovac B” – direct from filter. It’s chemical composition is shown in Table 2.

Table 2: The chemical properties of fly ash

SiO ₂ , %	53.84
Al ₂ O ₃ , %	30.29
Fe ₂ O ₃ , %	3.6
CaO, %	5.15
MgO, %	3.0
SO ₃ , %	1.86
Na ₂ O, %	0.51
K ₂ O, %	0.83
P ₂ O ₅ , %	0.23
TiO ₂ , %	0.73

2.2 Self-Compacting Concrete

Composition of concrete mixtures is shown in Table 3. Two different types of Self – Compacting Concrete were made: A: SCC-T₁₀ – Self – Compacting Concrete made with Portland cement and a partial replacement of 10 and 20% of fine aggregate with tailings; B: SCC-L – Self Compacting Concrete made with lime as mineral addition; SCC-FA – Self Compacting Concrete made with fly ash as mineral addition. The criteria in the mixture design was achieving slump - flow class SF1 for type A (spreading from 550 to 650 mm), and SF2 for

type B, which includes the usual application of concrete and involves spreading from 660 to 750 mm, according to SRPS EN 206-1.

Table 3: Compositions of concrete mixtures

	Concrete mixture	Cement kg/m ³	0/4mm kg/m ³	4/8mm kg/m ³	8/16mm kg/m ³	Lime kg/m ³	Fly ash kg/m ³	Tailing kg/m ³	Superpl kg/m ³	Water kg/m ³
A	SCC-T_0%	350	782	434	521	100	0	0	3.6	180
	SCC-T_10%	350	703.8	434	521	100	0	78.2	3.6	180
	SCC-T_20%	350	625.6	434	521	100	0	156.4	3.6	180
B	SCC-L	400	770.86	306.28	532	120	0	0	4.94	170.8
	SCC-FA	400	770.9	306.3	532	0	120	0	4.94	193

3. RESULTS AND DISCUSSION

3.1 Properties of fresh concrete

The properties of fresh concrete are shown in Table 4. Slump flow test, testing with V-funnel and L-box and sieve segregation were done according to SRPS EN 12350-8, SRPS EN 12350-9, SRPS EN 12350-10 and SRPS EN 12350-11.

Table 4: The properties of fresh Self – Compacting Concrete

	Concrete mixture	Slump-flow mm	V funnel sec	L-box H2/H1	Sieve segregation (%)	Density in the fresh state (kg/m ³)
A	SCC-T_0%	610	6.7	0.84	6.8	2335
	SCC-T_10%	600	7.1	0.91	6.6	2371
	SCC-T_20%	600	7.6	0.96	5.5	2375
B	SCC-L	730	6.3	1.0	12.4	2418
	SCC-FA	700	5.8	0.96	11	2288

By Slump-flow test is checked first of the four key characteristics of SCC: flowability. Spreading was between 600 to 610 mm, and it ranked all the projected mixtures with tailings in class SF1. Mixture with fly ash “fitted” in class SF2 corresponding to the most common use of concrete in construction.

V –funnel test represents checking of the mixture viscosity. Time period less than 9 seconds puts them in a class of viscosity VF1. There was no segregation nor any accumulation of water at the surface that could be collected.

L-box test is used for checking of the third key property: the passing ability of SCC between reinforcing bars without blocking. All mixtures meet the criterion for the relative height of the concrete at the ends of L-box is at least 0.8; and how the testing was done with three reinforcing bars (which is a requirement for densely reinforced structures) their class is PA2. The test results are in the range from 0.84 – 1.0). Resistance to segregation as a fourth property of fresh SCC has been tested in sieve paste. The results show that all blends/mixtures are resistant to segregation and belong to the class SR2 (<15%).

It should be noted that the usage of tailings did not affect self – compacting properties of concrete a lot, while fly ash increased slump-flow.

3.2 Compressive strength

Testing compressive strength of concrete at the age of 3, 7 and 28 days was carried out according to SRPS EN 12390 -3 standard. Bulk density of hardened concrete was tested according to SRPS EN 12390-7 standard and ranged from 2262 to 2462 kg/m³. The test results are shown in Figure 1 and Figure 2.

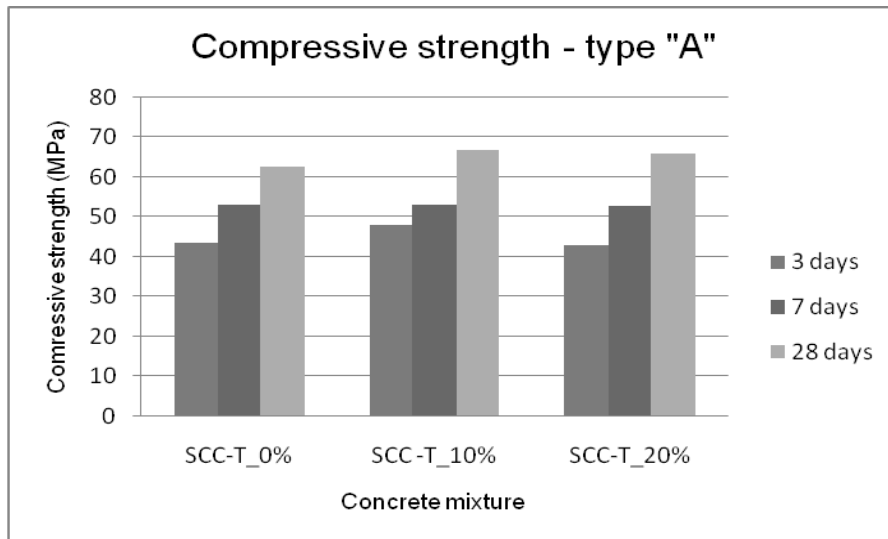


Figure 1: Compressive strength of concrete “A”

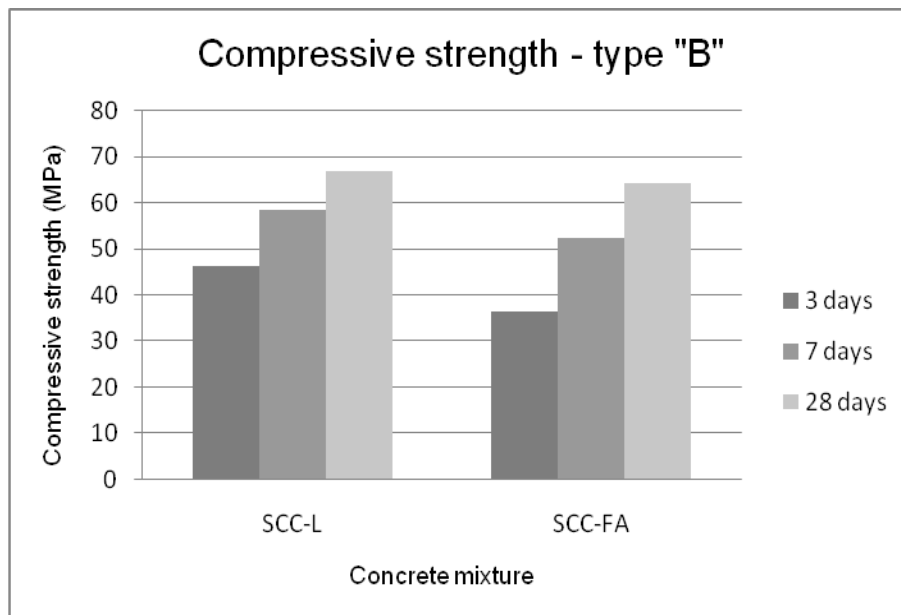


Figure 2: Compressive strength of concrete “B”

The differences between obtained results do not exceed 10%. Concrete with 10% and 20% addition of tailings achieved higher strengths when compared to the reference concrete at 28 days of age.

Slower growth of concrete strength with fly ash prevents its application, at the expected high early strength, which can be solved by applying the accelerator. At the available literature sources has been recommended process of the design and monitoring of the 90 - day long concrete strength. The obtained results are very good: Compressive strength differences between concrete with fly ash and limestone does not exceed 5% (after 28 days) at the same cement quantity. This fact should be borne in mind, especially if we include the economic factor in the equation.

4. CONCLUSIONS

The results of pozzolanic activity of tailings were extremely low, which has confirmed the results of the calculation of reactive SiO₂ content. Thus it was concluded that this material is not suitable as a material for cement replacement in concrete and mortar or as a pozzolanic cement additive. The results presented in this paper show that it is possible to use tailings from the Pb and Zn mine in Self – Compacting Concrete and that the best effect is achieved by replacing the fine fractions of aggregate with 10% of the tailings.

On the other hand, fly ash is pozzolanic cement additive and it's usage opens possibility for obtaining self-compacting concretes of high performances.

Self-Compacting Concrete, also an innovation in the field of concrete technology, contains a certain amount of powder material - filler. There are different possibilities of choosing these components. In case of use some of the industrial by – products the problem of depositing these materials would be solved, and that type of concrete could be certainly named eco-friendly.

ACKNOWLEDGEMENTS

The work reported in this paper is a part of the investigation within the research project TR 36017 "Utilization of by-products and recycled waste materials in concrete composites in the scope of sustainable construction development in Serbia: investigation and environmental assessment of possible applications", supported by the Ministry for Science and Technology, Republic of Serbia. This support is gratefully acknowledged.

REFERENCES

- [1] Thomas, B.S. et al: Strength and durability characteristics of copper tailing concrete, *Construction and Building Materials*, Vol.48 (2013), pp. 894-900.
- [2] Onuaguluchi, O.; Eren, O.: Recycling of copper tailings as an additive in cement mortars, *Construction and Building Materials*, Vol.37 (2012), pp.723-727.
- [3] Choi, Y. Et al.: Utilization of tailings from tungsten mine waste as a substitution material for cement, *Construction and Building Materials*, Vol.23 (2009), pp.2481-2486.
- [4] Gonzales-Corrochano, B. et al.: Effect of pre-firing and firing dwell times on the properties of artificial lightweight aggregates, *Construction and Building Materials*, Vol.53 (2014), pp.91-101.
- [5] Gonzales-Corrochano, B. et al.: Effect of thermal treatment on the retention of chemical elements in the structure of lightweight aggregates manufactured from contaminated mine soil and fly ash, *Construction and Building Materials*, Vol.35 (2012), pp.497-507.
- [6] Hui Z. et al.: The properties of the self – compacting concrete with fly ash and ground granulated blast furnace slag mineral admixtures, *Journal of cleaner production*, Vol.95 (2015), pp. 66 -74.
- [7] Singh N., Singh S.P.: Carbonation resistance and microstructural analysis of Low and High Volume Fly Ash Self Compacting Concrete containing Recycled Concrete Aggregates, *Construction and Building Materials*, Vol.127 (2016), pp.828-842.

INFLUENCE OF AGGREGATE TYPE ON BASIC PROPERTIES OF CEMENT MORTARS BLENDED WITH MIXTURE OF WHEAT AND SOYA STRAW ASH

Mirjana Malešev (1), Slobodan Šupić (1), Miroslava Radeka (1), Vlastimir Radonjanin (1), Tiana Milović (1), Olivera Bukvić (1)

(1) University of Novi Sad, Faculty of Technical Sciences, Department of Civil Engineering and Geodesy, Serbia

Abstract

In this paper, the effects of fine aggregate type on consistency, capillary water absorption and compressive strength were evaluated for cement mortars blended with 0%, 10%, 20%, 30%, and 50% biomass ash, by mass. Following types of fine aggregate were varied: standard quartz sand, fractionated aggregate of river origin - fraction 0-4mm and sand for plastering of river origin. The ash generated by combustion of mixture of wheat and soya straw (1:1, by mass) was used as a SCM. The results indicate that it is possible to produce mortar, with 30% of biomass ash, with physical and mechanical properties comparable with those of reference mortar.

Key words: fine aggregate, biomass ash, mortar, strength, absorption

1. INTRODUCTION

In light of concerns referring to the sustainable use of natural resources and the adverse effects of improper waste disposal, the beneficial use of municipal and industrial by-products becomes the subject of growing interest. Incorporation of otherwise discarded materials into construction products for buildings, roads, and other infrastructure is one of the more commonly proposed beneficial use applications [1]. In addition to reducing the volume of waste disposed of in landfills, this practice reduces the use of natural mineral materials, thus, reducing this negative footprint and impact of the construction industry on the natural environment. In addition, the replacement of OPC with such alternative materials has the potential to mitigate previously mentioned environmental problems (such as CO₂ emission, climate change, etc.). Alternative materials used to replace portions of OPC within PCC are referred to as supplementary cementitious materials (SCM).

A great part of the Serbian economy is based on agricultural production and agriculture related industry. The agricultural biomass wastes are coming from cereals, mostly wheat, barley and corn, and from industrial crops mostly sunflower, soya, and rapeseed. It is

estimated that every year a total amount of 12.5 million tons of biomass waste is produced in Serbia, of which 9 million tons (72%) is produced in Vojvodina [2].

In Serbia, there are many small individual landowners who deal with production of cereals or industrial plants, like sunflower or soya. A lot of crop farming production, almost 75% is achieved in small or medium size private ownership, while only about 25% of crop farming production belongs to agricultural companies of relatively larger size [3]. It is considered that about half of harvest residues at large agricultural farms can be used for energy purposes, while only about 20% harvest residues generated on relatively small private farms can be used for energy purposes.

In the process of harvest residues combustion, significant quantities of biomass ash are generated. These ashes are not further utilised, but disposed of at the landfills and companies which are involved in this process pay considerable high price for their storage, transportation and disposal. In this paper, the results of testing the influence of aggregate type on basic properties of cement mortars blended with mixture of wheat and soya straw ash are presented.

2. EXPERIMENTAL INVESTIGATION

2.1 Mortar constituents

For the experimental investigation of the influence of fine aggregate type on the basic properties of cement mortars blended with mixture of wheat and soya straw ash, the following component materials were used:

- Ordinary Portland cement CEM I 42,5R (Lafarge-BFC Serbia), OPC,
- Mixture of wheat and soya straw ash, “Soya Protein”, Bečej, Serbia,
- CEN standard sand in accordance with EN 196-1 (aggregate type 1),
- Fractionated aggregate of river origin, fraction 0-4mm (type 2),
- Sand for plastering of river origin (type 3),
- Superplasticizer (HRWRA) (Sika ViscoCrete 3070, Sika Switzerland),
- Deionized water.

2.2 Methods

Specific surface and density of biomass ash were determined according to SRPS EN 196-6 [4]. The Blaine air permeability method was used for determination of specific surface.

The chemical composition of cement and biomass ash was determined using SRPS EN 196-2 [5].

The consistency of fresh mortars was determined by flow table test - a measure of horizontal spread that a cement mortar experiences due to successive dynamic impacts, in accordance with SRPS EN 1015-3 [6].

The compressive strength of mortars was tested according to SRPS EN 196-1 [7].

The capillary water absorption of investigated mortars was measured according to ASTM C1585. The method is used to determine the rate of water absorption by measuring the increase in the mass of a specimen resulting from the absorption as a function of time when only one surface of the specimen is exposed to water [8].

X-ray diffraction (XRD) was conducted via XPert Pro diffractometer (PANalytical, Netherlands) with Cu anode as the X-ray source. X-ray diffractograms for aggregate types 2 and 3 were measured at 25 °C in the 2 Θ range from 5 to 80° with a step of 0.033° and step time of 100 s.

2.3 Composition of mortars

The experimental study was carried out on five different mortar mixtures for each type of fine aggregate. The composition of mixtures was defined in accordance with EN 196-1: the ratio (by mass) of cement and aggregate was 1:3, while two water to binder ratios (w/b) were used: w/b=0,5 (for mixtures prepared with aggregate types 1 and 2) and w/b= 0,7 (for mixtures prepared with aggregate type 3). Referent mortar (C) was prepared with ordinary portland cement. In the next four types of mortar mixtures (SP10, SP20, SP30 and SP50) the part of cement was replaced with 10%, 20%, 30% and 50% of biomass ash, respectively.

3. TESTING OF PROPERTIES OF COMPONENT MATERIALS

3.1 Biomass ash

Preparation of biomass ashes included sieving and grinding phase. The ash was roughly sieved (through a 4mm sieve) in order to separate unburnt straw and other large impurities. Then, it was ground in laboratory ball mill in order to obtain material with high specific surface. After grinding phase, specific surface (Blaine) of biomass ashes exceeded $15.500\text{cm}^2/\text{g}$.

The chemical compositions of OPC and biomass ash are given in Table 1. Obtained chemical composition of wheat straw ash points out relatively high total content of SiO_2 , (~56%) and moderate content of reactive SiO_2 (~41%). With respect to this chemical composition, the mixture of wheat and soya straw ash can be potentially used as a SCM.

Table 1: Chemical composition of OPC and biomass ash

Material (%)	SiO_2	Al_2O_3	Fe_2O_3	CaO	MgO	Na_2O	K_2O	SO_3	P_2O_5	LOI
Cement	21.25	5.55	25.3	61.6	2.37	0.25	0.72	3,75	-	1.77
Biomass ash	56.36	2.03	1.53	7.13	3.54	0.20	20.02	0.18	3.72	4.85

3.2 Fine aggregate

The particle size distribution of chosen fine aggregates was determined by a sieve analysis according to EN 933-2 [4]. The results are given in Figure 1.

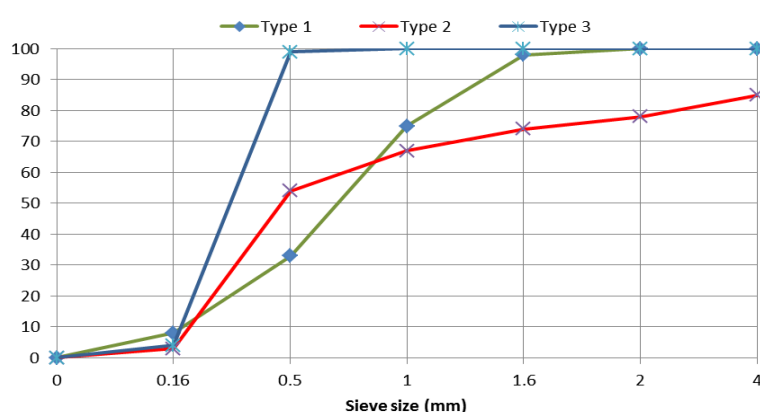


Figure 1 - Particle size distribution of different types of fine aggregate

It can be observed that sand for plastering (aggregate type 3) has finer particles, which are concentrated in one interval of sieve size (0.16-0.5mm) compared to other two types of

aggregate. According to passing results, it can be concluded that aggregate type 1 (CEN standard sand) has the smallest content of particles smaller than 0.5mm.

The results of XRD analysis of sand for plastering of river origin revealed quartz as a dominant mineral (82%). Additionally, albite, calcite and microcline were present, Fig 2. The mineralogical content of fractionated river aggregate showed quartz (76%) as a prevailing one. Besides quartz, calcite and albite, dolomite is also present, Figure 3 [9].

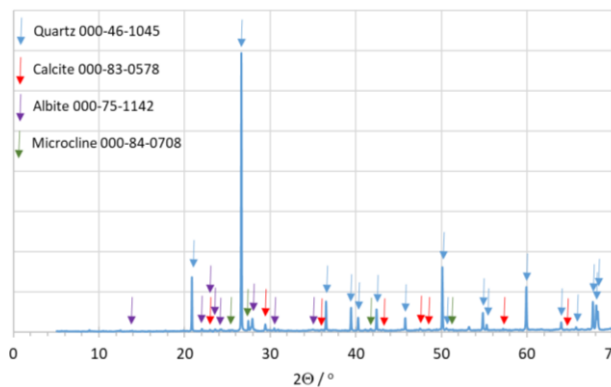


Figure 2 - X-ray mineralogical analysis for sand for plastering of river origin

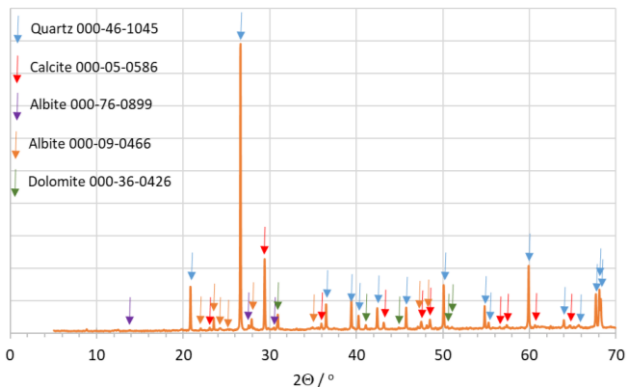


Figure 3 - X-ray mineralogical analysis for fractionated river aggregate

4. PROPERTIES OF CEMENT MORTARS BLENDED WITH WHEAT AND SOYA STRAW ASH

4.1 Consistency

Consistency of mortars, determined by flow table, is shown in Figure 4.

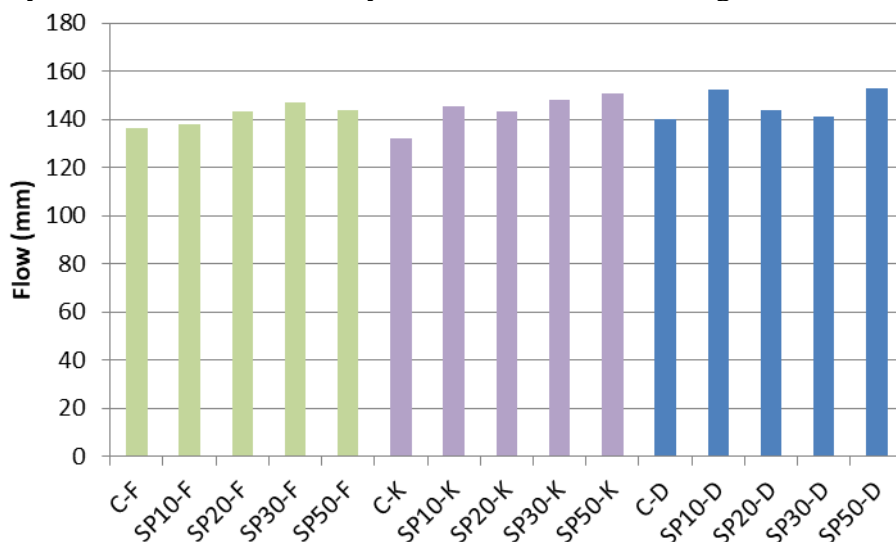


Figure 4 – Consistency of fresh mortars

Regarding the mortars with aggregate types 1 (K) and 2 (F), at the replacement level of mixture of wheat and soya straw ash in cement up to 30%, the workability of mortars was not

greatly affected. In mortars with 50% replacement level, superplasticizer has been used for flow correction, in amount of 0,2% (by mass of cement).

As previously mentioned, the sand for plastering has finer particles; because of this, it tended to adsorb water in mortar mixtures (D) leading to a decrease in mortar flow and a reduction in mortar workability. Even with the use of superplasticizer, mortar mixtures with $w/b=0.5$ could not be cohesive enough and they required a higher w/b ratio to achieve the flow properties of the reference one. Therefore, w/b ratio was increased from 0.5 to 0.7 and superplasticizer was not used in these mixtures.

The flow of all types of mortar mixtures was in the range of 130 to 160mm.

4.2 Compressive strength

The compressive strengths of tested mortars, at the age of 28 days, are presented in Fig 5.

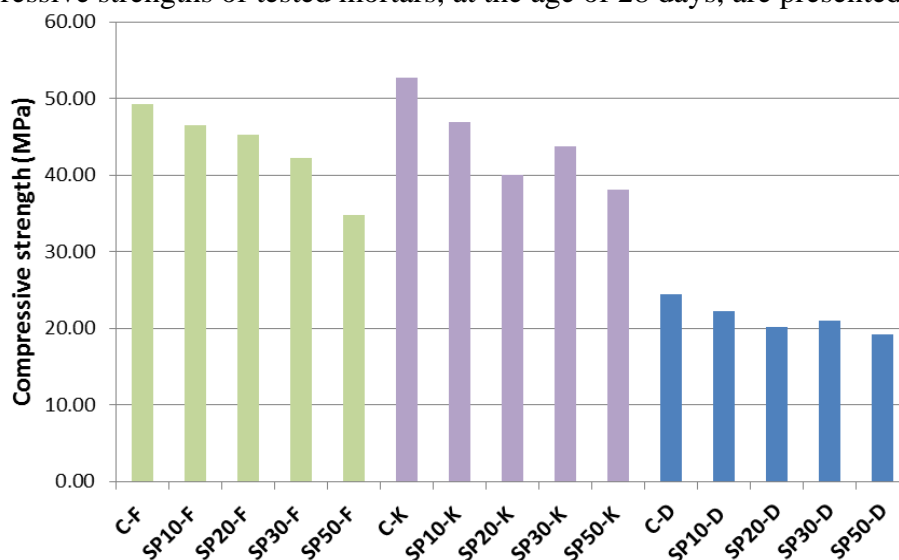


Figure 5 – Compressive strength of mortars at the age of 28 days

In the case of mortars with aggregates types 1 (K) and 2 (F), the compressive strength decreases as the replacement level of cement with biomass ash increases. The compressive strength varies from 38MPa to 52MPa and from 35MPa to 49MPa for mortars prepared with the aggregate type 1 (K) and 2 (F), respectively. All obtained compressive strengths are very high for ordinary cement mortars, even when 50% of cement was replaced with chosen biomass ash. Nevertheless, it is supposed that pozzolanic reaction of mixture of wheat and soya ash has not been intensified yet up to the age of 28 days.

Due to the increase w/b ratio, the compressive strength of mortars with sand for plastering, type 3 (D), is reduced at least 50%, in relation to mortars with aggregates type 1 and 2. The substitution of cement with biomass ash did not have a significant impact on compressive strength of these types of mortars. The difference between compressive strengths of reference mortar and mortar containing up to 30% biomass ash is negligible. The compressive strength varies from 19,2MPa (mortar containing 50% biomass ash) to 24,5MPa (reference mortar).

4.3 Capillary water absorption

The capillary water absorption of mortars was tested at the age of 28 days. Recorded changes in mass over time were used to calculate the absorption, as the change in mass divided by the cross-sectional area of the test specimen and the density of water. The results

sorted by the aggregate type, are presented in Figures 6-8. By comparison of the obtain results it can be concluded that the type of aggregate has significant influence on capillary water absorption. Mortars with CEN standard sand (type 1) have the lowest water absorption, with the exception of mortar containing 50% biomass ash, while mortars with sand for plastering (type 3) have the highest values.

Results of testing of capillary water absorption of mortar with aggregate type 1 (K) indicate that replacement of cement with biomass ash, up to 30%, did not affect capillary water absorption. The absorption of mortar with 50% of biomass ash was significantly higher.

Regarding capillary water absorption of mortar with aggregate type 2 (F), absorption rates of reference and mortar with 30% of biomass ash are in the same range, while significantly higher absorption rate was observed for mortars containing 10%, 20% and 50% of biomass ash.

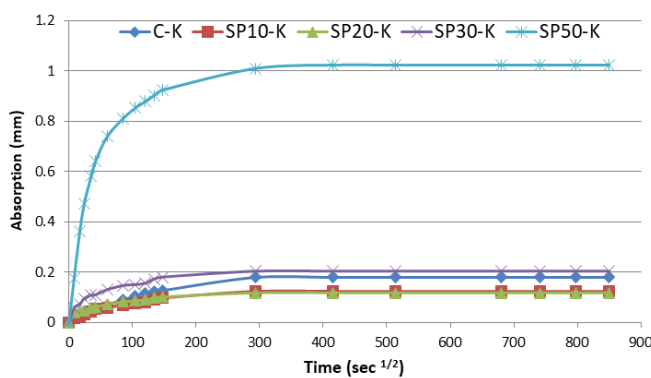


Figure 6 – Capillary water absorption of mortars with aggregate type 1

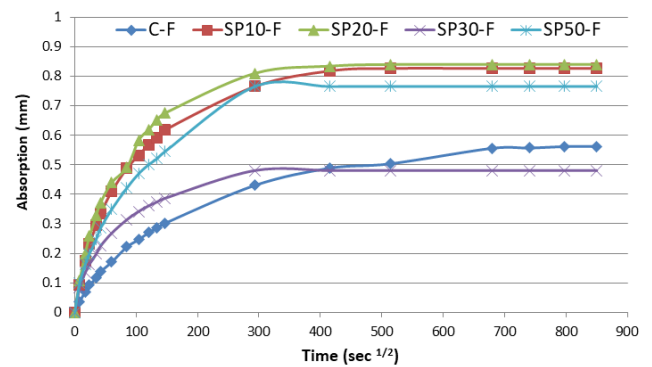


Figure 7 – Capillary water absorption of mortars with aggregate type 2

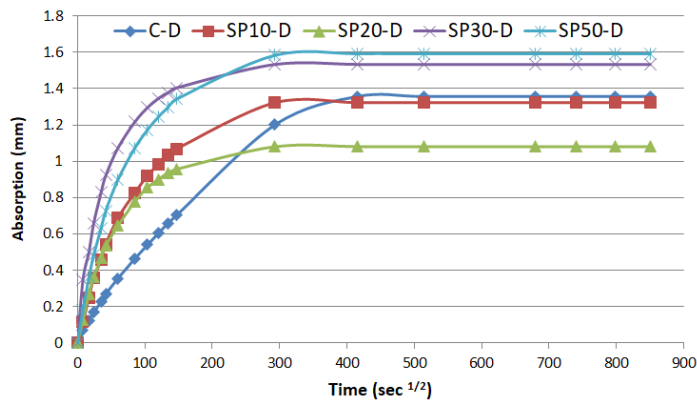


Figure 8 – Capillary water absorption of mortars with aggregate type 3

The results of testing of capillary water absorption of mortars with aggregate type 3 (D) in the initial period (up to 6h), generally indicate that, greater replacement level of cement with biomass ashes (noticeably 30% and 50%) leads to higher water absorption rate. The absorption rates of mortars with 10% and 20% of biomass ash are in the same range.

The initial rate of water absorption (S_i , mm/s^{1/2}) is calculated as the slope of the line that is the best fit to data between 1 min and 6 h. The secondary rate of water absorption (S_s ,

mm/s^{1/2}) is calculated as the slope of the line that is the best fit to data between 1 and 7 days. The results are shown in Table 2. By analysing the results for initial absorption it is concluded that initial rate of water absorption has been determined only for 4 of 15 mortars, as the other mortars show a systematic curvature. The secondary rate of water absorption has not been determined for any mortar type since any mortars did not show significant changes in water absorption in observed period (1-7 days).

Table 2: Initial and secondary rates of absorption

Mortar type	Initial absorption	Initial rate of absorption Si (mm/s ^{1/2})	Secondary absorption	Secondary rate of absorption Ss (mm/s ^{1/2})
C-F	$0.002t^{1/2} + 0.0363$	0,002	$0.0002t^{1/2} + 0.376$	*
SP10-F	$0.0038t^{1/2} + 0.1131$	*	$0.0001t^{1/2} + 0.7652$	*
SP20-F	$0.0041t^{1/2} + 0.1254$	*	$0.0001t^{1/2} + 0.809$	*
SP30-F	$0.0023t^{1/2} + 0.0888$	*	$y = 0.4807$	*
SP50-F	$0.0034t^{1/2} + 0.0987$	*	$y = 0.7651$	*
C-K	$0.0008t^{1/2} + 0.0156$	0,0008	$y = 0.1792$	*
SP10-K	$0.0006t^{1/2} + 0.1555$	*	$y = 0.1240$	*
SP20-K	$0.0005t^{1/2} + 0.0322$	*	$y = 0.1182$	*
SP30-K	$0.0009t^{1/2} + 0.0551$	*	$y = 0.2042$	*
SP50-K	$0.0053t^{1/2} + 0.2691$	*	$0.0001t^{1/2} + 1.0105$	*
C-D	$0.0046t^{1/2} + 0.0487$	0.0046	$0.0002t^{1/2} + 1.2137$	*
SP10-D	$0.007t^{1/2} + 0.1526$	0.007	$y = 1.3224$	*
SP20-D	$0.0061t^{1/2} + 0.1749$	*	$y = 1.0802$	*
SP30-D	$0.0082t^{1/2} + 0.3847$	*	$y = 1.5328$	*
SP50-D	$0.0085t^{1/2} + 0.2326$	*	$0.0001t^{1/2} + 1.584$	*

* a linear regression cannot be established, a correlation coefficient of less than 0.98.

5. CONCLUSION

The following conclusions can be drawn based on the test results of this study:

- Mixture of wheat and soya straw ash can be used as a supplementary cementitious material with an amount of up to 50% without compromising the workability. The flow of all types of mortar mixtures was in the range of 130 to 160mm.
- The type of aggregate affects the workability of mortars. To achieve the required consistency of mortars with sand for plastering, an increase of water to binder ratio is indispensable.
- The substitution of cement with the mixture of wheat and soya straw ash generally leads to the reduction of mortar's compressive strength. Based on the obtained results, it can

be concluded that this type of biomass ash can be used as a cement substitute up to the level of 30%, without compromising mortar's mechanical properties to a larger scale.

- A remarkable increase in water to binder ratio of mortars with sand for plastering caused a significant reduction of compressive strength, but the achieved values still overcame the requirements of mortars for masonry.
- The type of aggregate has significant influence on capillary water absorption. Mortars with CEN standard sand have the lowest water absorption, while mortars with sand for plastering have the highest values. In general, the results of capillary water absorption indicate that a greater replacement level of cement with biomass ash (noticeably 50%) leads to a higher water absorption rate.
- The results prove that it is possible to obtain eco-friendly mortar with comparable properties with the reference ones. The application of mixture of wheat and soya straw ash as SCM leads to substantial cost savings, as well as benefits to the environment, such as lower consumption of cement, reduction of CO₂ emissions during the production of cement and sustainable waste management.

ACKNOWLEDGMENT

The authors acknowledge that full financial support for this study was provided by Agricultural Waste – Challenges and Business Opportunities, Eco build project financed within Interreg IPA Cross-border Cooperation Programme Croatia-Serbia 2014-2020.

REFERENCE

- [1] Jerry M. P., Justin G. R., Christopher C. F., Harvey D. D., Timothy G. T.. *A review of waste products utilized as supplements to Portland cement in concrete*, Journal of Cleaner Production Vol. 121 (2016): pp. 1-18.
- [2] Šupić S., Malešev M., Radonjanin V., Radeka M, Laban M. *Application of Biomass Ashes as Supplementary Cementitious Materials in the Cement Mortar Production*. International Journal of Structural and Construction Engineering - WASET Vol. 12 (2018), Stockholm.
- [3] Ilić M., Grubor B., Tešić M. *The state of biomass energy in Serbia*. Thermal Science Vol. 8 (2004): pp. 5-19.
- [4] SRPS EN 196-6, Methods of testing cement - Determination of fineness.
- [5] EN 196-2, Methods of testing cement - Chemical analysis of cement.
- [6] SRPS EN 1015-3, Methods of test for mortar for masonry – Part 3: Determination of consistence of fresh mortar (by flow table).
- [7] SRPS EN 196-1:2008, Methods of testing cement - Part 1: Determination of strength.
- [8] ASTM C1585-13, Standard Test Method for Measurement of Rate of Absorption of Water by Hydraulic-Cement Concretes.
- [9] Malešev, Šupić, Radeka, Radonjanin, Draganić, Laban. *Influence of aggregate type on basic properties of mortars with wheat straw ash*. Indis - Eco build Vol. 14 (2018): pp. 1241-1250.

IMPROVING RESILIENCE OF EARTH CONSTRUCTION – CURRENT PERSPECTIVES AND FUTURE OUTLOOK

S. S. Lucas (1), F. Ahmed (2), H. Varum (3)

(1) Eindhoven University of Technology, Faculty of the Built Environment, The Netherlands

(2) University of Greenwich, Faculty of Engineering and Science, United Kingdom

(3) University of Porto, Faculty of Engineering, Civil Engineering Department, Portugal

ABSTRACT

Earth has been, for thousands of years, the main source of construction materials and, as of today, roughly one-third of the world's population still lives in earth buildings. With increasing concerns about our environmental footprint, this ancient technique has regained interest. Whereas before, the focus was on studying the techniques with the main goal of preserving building's heritage, more recently, the focus shifted to the development of new and innovative solutions to reintroduce this technique as a viable alternative to cement and concrete.

The use of adobe bricks as a sustainable and affordable alternative for construction has many advantages, however, poses nonetheless, some challenges. The major threats to this type of building are heavy rainfall, flooding and earthquakes. Finding a solution that can make adobe bricks more resilient to heavy rain and flooding – while keeping it low cost and based on local sources – is at the basis of this work. To reach this goal, several types of natural fibres have been used as an alternative to traditional straw. The results show that some of these fibres can improve the bricks' mechanical strength, allowing the structures to resist adverse weather conditions.

From this research, it also became apparent that the low quality of many of these adobe blocks is related with the inconsistency in the preparation methods. There is clearly a need to provide local communities with guidelines and procedures that allow for higher quality standards. In this paper, it will be presented a new strategy to improve and standardise the fabrication of these bricks, overcoming the lack of quality often associated with these traditional products.

Keywords: earth construction, adobe, natural fibres, flood-resistant buildings

1. INTRODUCTION

Earth construction is an ancient building technique that is still elected in many developing countries as the primary construction method. The possibility of using local materials and the low cost of these buildings is the main reason why it is still so popular in some of the poorer regions on Earth [1]. Earth unfired building blocks have been given different names in different regions – adobe, mud or rammed earth – generally, they are prepared as a mixture of clay, sand and sometimes fibres (straw) and gravel, moulded into bricks.

Amongst the main advantages are [2]:

- Earth materials are locally available, are affordable and renewable
- Preparing earth blocks does not require high energy demand
- Construction techniques are simple and can be performed by non-specialised labour
- Adobe buildings can balance the indoor humidity levels much more effectively than any other construction material
- It can store solar heat helping to balance room temperature
- These bricks can be recycled and reused

Though from an economic and environmental perspective it is indeed an interesting solution, the quality of some of these buildings can be a cause for concern, particularly in areas with heavy rainfall and prone to flooding. Rammed earth (adobe) blocks do not perform well when exposed to water and their durability can be severely compromised by excessive rain [3,4].

They can present some problems that often compromise the building's structural integrity:

- Earth is a non-standard material and its properties can differ from site to site [5];
- Bricks undergo substantial shrinkage during drying
- They are not water resistant and require protection from rainfall

However, if structural resilience is improved, earth-based bricks can be a good alternative to cement and concrete blocks [6]. It is only rational that, by looking at the main pros and cons of this traditional material, building with earth is regaining interest as an alternative to reach the 2020 goal of net-zero energy buildings across Europe.

The main difficulty for a widespread use of this technique is still the water resistance of these blocks and their overall structural resilience.

In this work, different alternatives to improve the bricks' durability will be presented and studied. The main objective is to establish viable solutions that can help communities in regions with heavy rainfall to build safer buildings, but also, to explore the use of this material in sustainable buildings across the globe.

2. MATERIALS

The adobe bricks were prepared using a sharp sand and clay with 38% w/w of moisture. For the bricks' reinforcement, it was selected a jute fibre with a diameter of 2 mm, 7 mm length and a specific density of 2.05 g/cm³. The fibres were added in 0.1 % and 0.2 % relative to the total amount of solid material. The sand was graded by sieve analysis; its particle distribution is represented in Figure 1. The mineralogical composition of the clay was determined by X-ray diffraction (XRD) analysis (Figure 1) – it is formed mostly by quartz and kaolinite, with a minor content of muscovite. The Atterberg limits of the sample were determined according to the standard ASTM D4318, retrieving a liquid limit $w_L = 43\%$, plastic limit $w_p = 17\%$ and plasticity

index $I_p = 26\%$. For the adobe-cement composites it was selected an ordinary Portland cement, CEM I 42.5 N.

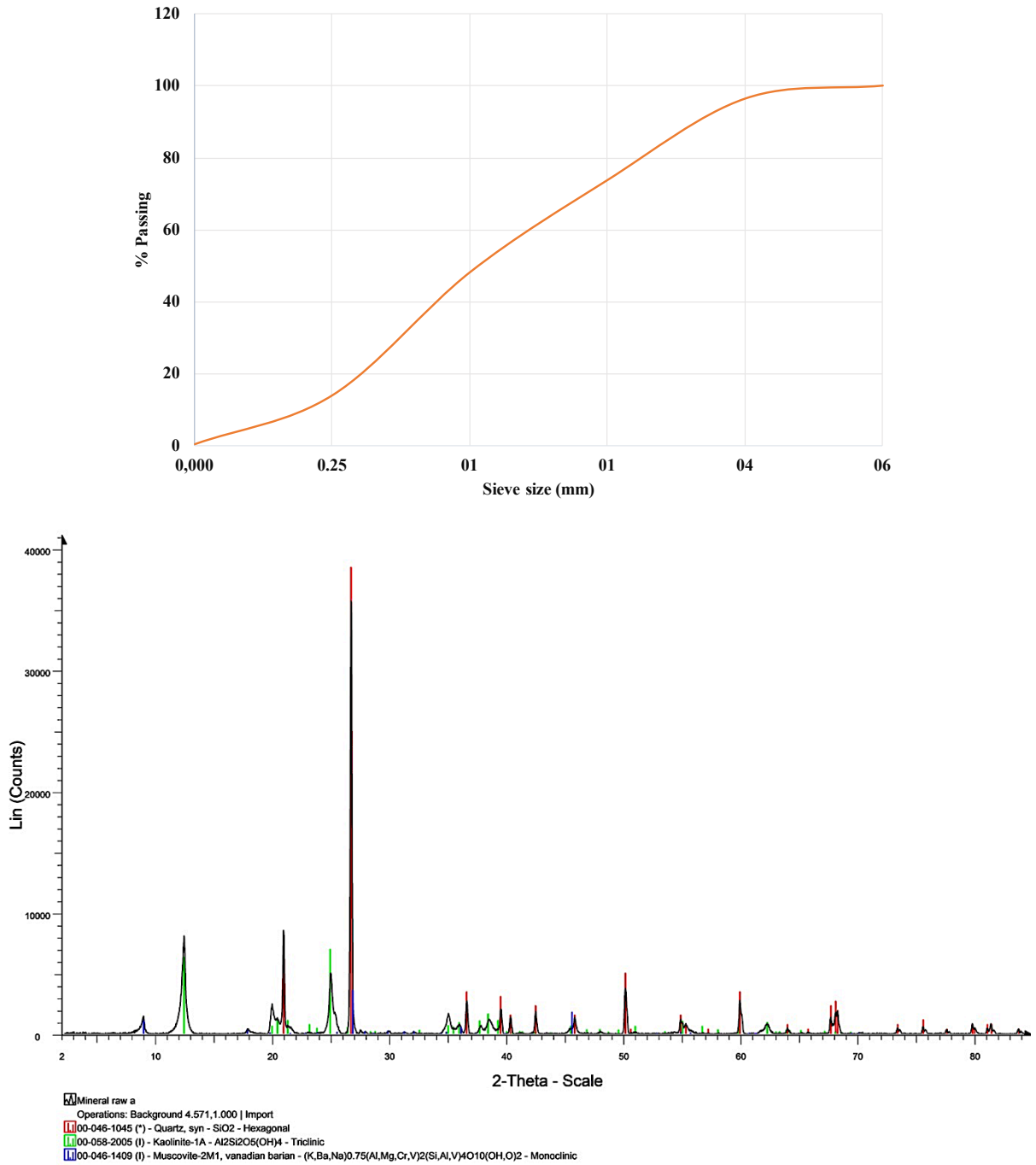


Figure 1 - Sieve analysis for the sand (left) and XRD analysis of the clay (right)

The composition of the samples to be tested is detailed in .. The sand and clay were weighted and mixed with 4% w/w of water to provide adequate plasticity to the mix. In a final step, the additive – fibres, cement or lime – was added and thoroughly mixed. The specimens were then oven dried for 24 h at 80 °C and left to cure naturally for 28 days. The samples have been moulded with 100 x 100 x 100 mm and vibrated on a shaking table to ensure proper compaction.

Table 1 - composition of the adobe bricks tested (weight %)

% Sand	% Clay	% Jute fibres	% cement	% lime
50	50	0	0	0
50	50	0.1	0	0
50	50	0.2	0	0
60	40	0	0	0
60	40	0.1	0	0
60	40	0.2	0	0
60	40	0	0	0
60	40	0	1	0
60	40	0	3	0
60	40	0	5	0
60	40	0	0	0
60	40	0	0	1
60	40	0	0	3
60	40	0	0	5

3 RESULTS AND DISCUSSION

Compression testing was carried out using an Avery Dension testing machine type 7226CB calibrated in accordance with BS 1610: Part1:1992. The load was applied at the rate of 2.5 kN/s through the steel plates on which the adobe specimen was placed. The compressive strength is given by the maximum uniaxial compressive stress of the specimen, which is the ratio of the axial force applied and the cross-sectional area of the specimen, according to equation 1.

$$\sigma = \frac{F}{A} \left(\frac{\text{kN}}{\text{mm}^2} \right) \quad (1)$$

The results of the compression tests for the fibre reinforced adobe cubes are presented in Figure 2. While the introduction of fibres has increased the overall strength, there is a limit for how much fibre can be beneficial. A total content of 0.2 % has proven to be excessive with a decrease in strength starting to show.

Although fibre reinforcement shows some promising results, strength remains below 2 MPa and it might not be sufficient to ensure adequate resistance to rainfall and flooding. Though this strategy might not be the best approach for preventing water damage it is a good option to improve structural resilience in structures that are not in regions with heavy rainfall. Several authors are currently exploring the use of natural fibres for reducing shrinkage and improve

mechanical strength in adobe bricks [2,7,8]. The use of natural fibres is also a good way of reducing agricultural waste through valorisation [6].

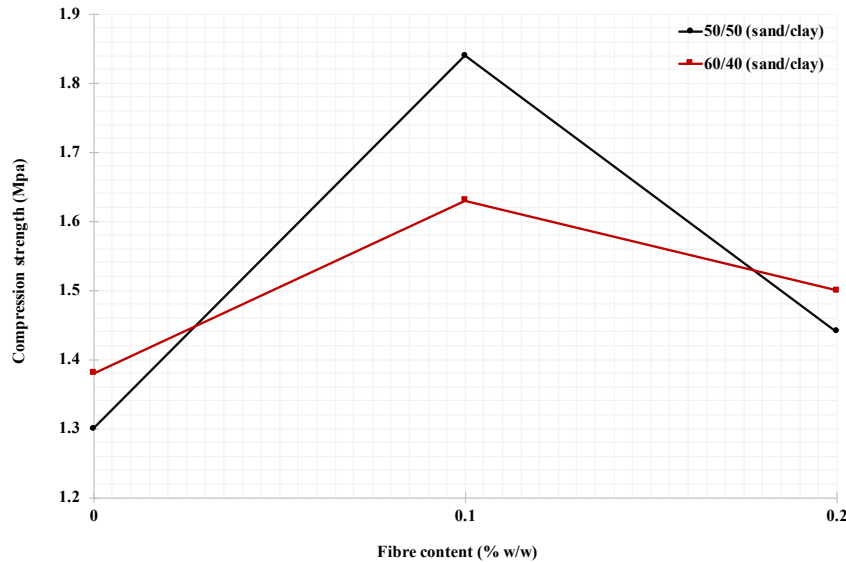


Figure 2 – Compressive strength of the adobe samples with jute fibres

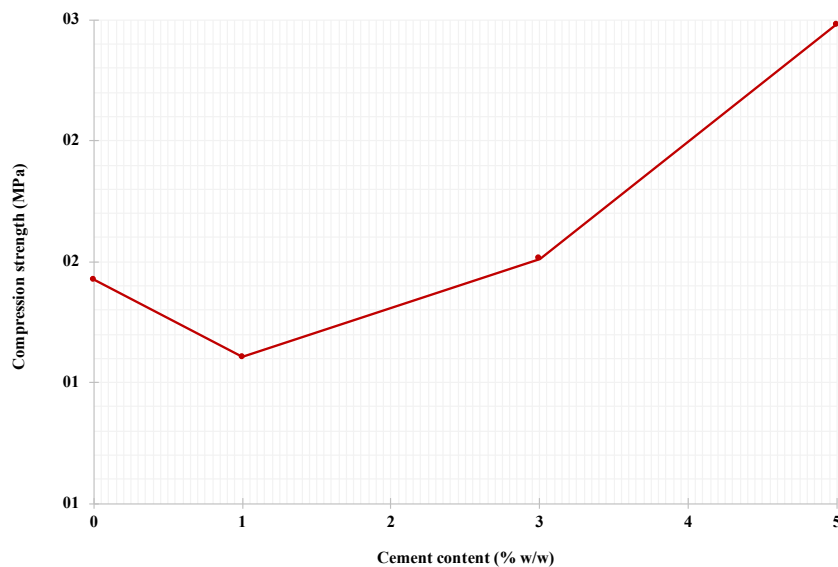


Figure 3 – Compressive strength of the adobe samples with cement

Another alternative that has been explored to increase water tightness in adobe bricks is the incorporation of small amounts of cement to the mix. While cement is more expensive and not as sustainable as adobe, small amounts up to 5 % in weight do not influence significantly the final cost and, if successful, can improve durability. In Figure 3, it is possible to see the positive

effect that introducing 3 to 5 % of cement can have in the final mechanical strength. Considering the promising results obtained with this strategy, a test of the bricks' durability to flooding has been conducted.

For the water resistance test, the samples were weighted after 28 days and placed in water at a temperature of 25 ± 2 °C for 24 hours (M_0). After soaking in water, the samples were removed and wiped with a wet cloth. The specimens were then dried again until reaching a constant mass. The final mass of the cubes was taken as M_f . The loss of weight by water immersion (L_w) is given by Equation 2.

$$L_w = \frac{M_0 - M_f}{M_0} \quad (1)$$

The difference between the control samples and the specimens with 3 and 5 % of cement to withstanding 24 h immersion in water is remarkable, as seen in Figure 4. The samples move from total loss to a decrease in weight of only 3 and 2 % respectively, proving that adding a small amount of cement to the composition can potentially increase resistance to heavy rainfall.

These results are in line with studies conducted by other groups, being demonstrated that adding more than 2% and up to 5% of cement is indeed beneficial. Higher amounts do not significantly increase water tightness and can be detrimental to the overall mechanical strength [9].

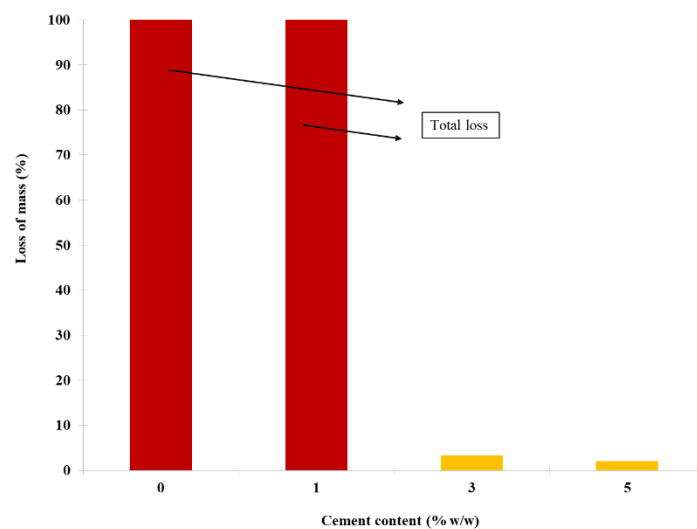


Figure 4 – Mass loss of adobe' cement composites after 24h immersed in water

4. CONCLUSION

With this preliminary study, it has been demonstrated that fibre reinforcement can successfully improve the mechanical strength of adobe bricks and the use of small amounts of cement can increase the composite's durability under heavy rain. More research is required to

establish what type of fibres show higher efficiency and to explore other alternatives to cement for water protection.

A possible alternative can be introducing additives such as metal stearates or surfactants that can provide hydrophobicity.

REFERENCES

- [1] F.W. Kanjumba, A. Njuguna, G. Achoki, Economic Factors Influence on Funding of the Supply-Side of Housing in Kenya: Case Study Nairobi, *Int. J. Bus. Manag.* 11 (2016) 194. doi:10.5539/ijbm.v11n10p194.
- [2] V. Sharma, B.M. Marwaha, H.K. Vinayak, Enhancing durability of adobe by natural reinforcement for propagating sustainable mud housing, *Int. J. Sustain. Built Environ.* 5 (2016) 141–155. doi:10.1016/j.ijbsbe.2016.03.004.
- [3] V.E. García-Vera, M. Lanzón, Physical-chemical study, characterisation and use of image analysis to assess the durability of earthen plasters exposed to rain water and acid rain, *Constr. Build. Mater.* 187 (2018) 708–717. doi:10.1016/J.CONBUILDMAT.2018.07.235.
- [4] T. Martins, J. Fernández, H. Varum, Influence of Moisture on the Mechanical Properties of Load-Bearing Adobe Masonry Walls, *Int. J. Archit. Herit.* (2018) 1–14. doi:10.1080/15583058.2018.1482384.
- [5] I. Duarte, E. Pedro, H. Varum, J. Mirão, A. Pinho, Soil mineralogical composition effects on the durability of adobe blocks from the Huambo region, Angola, *Bull. Eng. Geol. Environ.* 76 (2017) 125–132. doi:10.1007/s10064-015-0800-3.
- [6] E. Christoforou, A. Kylili, P.A. Fokaides, I. Ioannou, Cradle to site Life Cycle Assessment (LCA) of adobe bricks, *J. Clean. Prod.* 112 (2016) 443–452. doi:10.1016/J.JCLEPRO.2015.09.016.
- [7] G. Araya-Letelier, J. Concha-Riedel, F.C. Antico, C. Valdés, G. Cáceres, Influence of natural fiber dosage and length on adobe mixes damage-mechanical behavior, *Constr. Build. Mater.* 174 (2018) 645–655. doi:10.1016/J.CONBUILDMAT.2018.04.151.
- [8] V. Sharma, H.K. Vinayak, B.M. Marwaha, Enhancing sustainability of rural adobe houses of hills by addition of vernacular fiber reinforcement, *Int. J. Sustain. Built Environ.* 4 (2015) 348–358. doi:10.1016/j.ijbsbe.2015.07.002.
- [9] K. Dao, M. Ouedraogo, Y. Millogo, J.-E. Aubert, M. Gomina, Thermal, hydric and mechanical behaviours of adobes stabilized with cement, *Constr. Build. Mater.* 158 (2018) 84–96. doi:10.1016/J.CONBUILDMAT.2017.10.001.

EFFECT OF TIRE POWDER AND WOOD BIOMASS ASH ON PROPERTIES OF SELF COMPACTING CONCRETE

Robert Bušić (1), Nina Štirmer (2) and Ivana Miličević (1)

(1) Faculty of Civil Engineering Osijek, University of Osijek, Croatia

(2) Faculty of Civil Engineering, University of Zagreb, Croatia

Abstract

The paper presents possibility of usage of recycled materials, tire powder and wood biomass ash, as fillers for self-compacting concrete (SCC). Fly ash and dolomite powder are found to be the traditional materials used in controlling the segregation potential and deformability of fresh SCC. This research deals with the utilisation of an alternative materials, tire powder and wood biomass ash, instead of 5%, 10%, 15% and 20% of dolomite powder, to produce SCC. For this study, nine mixtures were prepared. Fresh SCC properties were assessed by means of slump flow, L-box and J-ring, while hardened properties were evaluated by means of compressive strength and modulus of elasticity at age of 28 days. The results are positive: recycled fillers can partially replace dolomite filler and at the same time satisfactory maintain fresh and hardened concrete properties.

Keywords: tire powder, wood biomass ash, self-compacting concrete, hardened SCC properties, fresh SCC properties.

1. INTRODUCTION

Every year quantity of wood biomass ash (WBA) and waste tires is rapidly increasing. Number of waste tires produced each year counts almost 1 billion [1] and up to 2030 this number will approach 1.2 billion [2]. In year 2013, the number of end-of-life tires in Europe has grown up to 2.88 million tons [3]. On the other side, total amount of wood biomass ash (WBA) waste will increase up to 42,000 tons per year by 2020 and 126,000 tons per year by 2030 [4]. Because of these disturbing numbers, European Union was forced to adjust legal frameworks to new challenges given by these two materials.

According to waste hierarchy given by European Parliament and the Council [5], the priority of waste management is waste prevention, re-use and recycling. Waste tires disposal has been avoided as much as possible, due to the ecological problems caused by landfilling and burning, causing air pollution and fast depletion of the site [6], [7]. Human health and environment

should not be affected by waste management. In Republic of Croatia, Directive 2008/98/EC is applied through Act on sustainable waste management [8]. Waste tires considered to be special waste category and from year 2015 separate collection of waste tires had to be ensured in Croatia. According to Croatian Regulation [9] the annual goal of waste tires recovery by the R3 recovery operation, i.e. recycling of organic substances, is at least 80% of the mass of separately collected waste tires. By implementing waste tire rubber into concrete, this problem can be mitigated or even completely solved, as concrete industry is one of the biggest industries in the world and only in European Union the average production of concrete for year 2015 was over 340 million m³ [10].

To date, waste tire rubber was incorporated into self-compacting concrete (SCC) as a partial replacement of natural fine and coarse aggregate. Depending on rubber particle size, there are three types of most frequently used waste tire rubber as a partial replacement of natural aggregate in SCC so far: (i) chipped rubber particles (size 13 and 76 mm) as coarse aggregate replacement, (ii) crumb rubber particles (size 0.075 and 4.75 mm) as a fine aggregate replacement and (iii) ground rubber particles (size 0.15 and 19 mm) as a fine and coarse aggregate replacement [2]. Because of its improved impact resistance and energy dissipation, rubberized concrete has been used in several non-structural applications, i.e. pavement, sidewalks, sport courts, traffic noise barriers [11]–[14]. However, latest experimental investigations on rubberized reinforced concrete structural members under cyclic loading could be promising, as reinforced rubberized concrete specimens show favourable ductility and energy dissipation [15] which is encouragement for further investigation of SCRC on the material and structural level. In this work waste tire powder (TP) will be used as replacement for inert filler, i.e. dolomite filler.

Regulations which concerns WBA, Directive 2009/28/EC [16] and Croatian Act on renewable energy sources and highly effective cogeneration [17] defined biomass as a biodegradable part of products, waste and residues from biological origin from agriculture, forestry and related industries. According to these two regulations and Framework for climate and energy in the period from 2020 to 2030 [18], each European Union Member State had to ensure that the share of renewable energy sources (RES) in gross final energy consumption is at least 20% until year 2020 and 27% until year 2030. Because of economically low operational cost, availability and continuously regeneration of the fuel, forestry and agricultural biomass represents satisfactory source of fuel for energy production in bio-power plants [19]–[21]. Unlike coal fly ash which is generated as a by-product in thermal power plants, wood biomass fly ash occurs as a by-product in bio power plants, which are working on solid biomass, i.e. forestry and agricultural management residues, as a fuel. Most of the produced WBA is landfilled (70%) or used in agriculture as a soil supplementary material (20%) [19], [22], [23] although using of wood ash as soil supplementary material may cause serious ground water pollution [19]. Another problem is concentration of heavy metals in wood ash [24] which is over acceptable values to use wood ash as soil mineral fertilizers [4].

Wood biomass ash can be used as supplementary cementitious material (SCM) in concrete mixtures as an active pozzolanic material [23] and incorporation of wood ash into concrete can solve the problem of harmful substances in the ash as they will be immobilized [25]. However, biomass ash chemical composition can vary and depends on geographical location, combustion technology and type and source of wood [4], [22]. In this work WBA will be used as replacement for inert filler, i.e. dolomite filler. Cuenca et al. [26] reported that agricultural olive residue biomass fly ash can be used in SCC as a replacement for filler and still maintain structural

application grade after replacement. However, Cuenca et al. [26] used agricultural biomass fly ash obtained from combustion of agricultural waste.

As it is mentioned earlier, most of the research focused their experimental work on using WBA as replacement of cement or TP as replacement for fine and coarse aggregate. The most similar experimental work was provided by Cuenca et al. [26], but in mentioned work biomass fly ash was obtained from combustion of agricultural, and not from forestry management residues. The main objective of this work is to study utilization of wood biomass ash (WBA) and tire powder (TP) partially replacing inert dolomite filler in self-compacting concrete (SCC) and to show potential of application of WBA and TP in concrete industry.

2. EXPERIMENTAL PART

2.1 Material characteristics and mixtures design

All test specimens were fabricated using locally available materials. EFNARC dosage parameters were respected in creation of SCC mixture proportions [27]. CEM I 42.5R type Portland cement was used in the study, from cement factory in Našice, Croatia, which conform to EN 197-1:2012 standard [28]. Density of cement was $3,17 \text{ g/cm}^3$. Tap water from local water supply that complies with HRN EN 1008 standard was used [29]. Chemical admixtures, superplasticizer Sika® Viscocrete® 20 Gold and viscosity modifying admixture Rheomatrix® 100, were used in order to achieve desirable SCC properties and flowability and viscosity classes. Dolomite powder, wood biomass ash and tire powder with density of 2.97, 2.49 and 1.23 g/cm^3 , respectively, were used as fillers. Dolomite powder (size $< 0.063 \text{ mm}$) from local quarry, wood biomass fly ash (size $< 0.063 \text{ mm}$) from electrostatic precipitator of biomass co-generation plant and tire powder (size $0 - 0.5 \text{ mm}$) obtained from mechanical grinding of local waste tires were used and the source of these material was also from Croatia. Density of cement, dolomite powder, wood biomass ash and tire powder was tested according to ASTM C188-17 [30]. Materials used as a filler replacement are presented in Figure 1. Natural crushed aggregate with nominal sizes of 0-4 mm, 4-8 mm and 8-16 mm and natural sand were used for the coarse and fine aggregates.

A total of 9 self-compacting mixtures were tested in fresh and hardened state, reference mixture SCC-0 with 0% of WBA and TP, 4 mixtures with 5, 10, 15 and 20% of WBA as a replacement for dolomite powder and 4 mixtures with 5, 10, 15 and 20% of TP as a replacement for dolomite powder. SCC mixtures compositions are shown in Table 1.



Figure 1. Materials used as a filler replacement in experimental work: (a) wood biomass ash (WBA); (b) tire powder (TP)

Table 1. SCC mixtures design

#	Mixture	Cement (kg)	Water (kg)	w/c	SP (%)	VMA (%)	Filler (kg)			FA and CA (kg)
							Dolomite powder	WBA	TP	
1	SCC-0	450	180	0.40	1.5	0.3	150	-	-	1600
2	SCC-5-WBA	450	189	0.42	1.5	0.3	142.5	7.5	-	1573
3	SCC-10-WBA	450	189	0.42	1.5	0.3	135	15	-	1572
4	SCC-15-WBA	450	198	0.44	1.8	0.3	127.5	22.5	-	1542
5	SCC-20-WBA	450	198	0.44	1.8	0.3	120	30	-	1541
6	SCC-5-TP	450	180	0.40	1.5	0.3	142.5	-	7.5	1597
7	SCC-10-TP	450	180	0.40	1.5	0.3	135	-	15	1595
8	SCC-15-TP	450	180	0.40	1.5	0.3	127.5	-	22.5	1593
9	SCC-20-TP	450	180	0.40	1.5	0.3	120	-	30	1591

SP - superplasticizer, VMA - viscosity modifying admixture, WBA - wood biomass ash, TP - tire powder, FA - fine aggregate, CA - coarse aggregate

Originally, identical water to cement ratio (w/c) and same amount of superplasticizer (SP) were used in design of SCC mixtures. During mixing procedure, with w/c = 0.4 and SP = 1.5%, SCC, loss in workability of mixtures with 5, 10, 15 and 20% of WBA was observed. Therefore, w/c ratio had to be increased from 0.40 to 0.42 for mixtures SCC-5-WA and SCC-10-WA and from 0.40 to 0.44 for mixtures SCC-15-WA and SCC-20-WA, and percentage of superplasticizer had to be increased from 1.5 to 1.8 for mixtures SCC-15-WA and SCC-20-WA.

2.2 Methodology

In this research, testing of fresh and hardened SCC properties were carried out. Tests on fresh and hardened SCC were performed according to relevant European Standards. Slump flow test, L-box test and J-ring test were measured according to HRN EN 12350-8 [31], HRN EN 12350-10 [32] and HRN EN 12350-12 [33], respectively. Flowability and viscosity of SCC were measured and classified through the slump flow test, while passing ability of SCC was measured and classified through L-box and J-ring tests. All specimens were demoulded 24 h after the casting and placed in a water tank for 4 weeks. The mechanical properties tests were carried out after the specimens had been moist-cured for 28 days. Two mechanical properties were tested, compressive strength test on cubes 150×150×150 mm and cylinders 150×300 mm, and modulus of elasticity test on cylinders 150×300 mm. Compressive strength was measured according to HRN EN 12390-3 [34] and modulus of elasticity was measured according to HRN EN 12390-13 [35].

3. TEST RESULTS AND DISCUSSION

3.1 Fresh SCC test results

Results of testing the fresh SCC are given in Table 2. In fresh SCC state, aggregate segregation or bleeding was not observed, therefore the concrete was embedded in moulds without compaction.

Table 2. Test results of fresh SCC

#	Mixture	J-ring		Slump flow			L - box		
		PJ (mm)	Class	d (mm)	T500 (s)	Class	H ₂ /H ₁	Class	
1	SCC-0	6.25	< 10	695	2.01	SF2/VS2	0.80	= 0.80	PA2
2	SCC-5-WBA	8.75	< 10	685	2.21	SF2/VS2	0.77	< 0.80	PA2
3	SCC-10-WBA	12.00	> 10	662	2.29	SF2/VS2	0.75	< 0.80	PA2
4	SCC-15-WBA	15.25	> 10	600	2.48	SF1/VS2	0.69	< 0.80	PA2
5	SCC-20-WBA	18.75	> 10	565	2.61	SF1/VS2	0.56	< 0.80	PA2
6	SCC-5-TP	6.75	< 10	825	1.78	SF3/VS1	0.95	> 0.80	PA2
7	SCC-10-TP	7.75	< 10	810	2.43	SF3/VS2	0.90	> 0.80	PA2
8	SCC-15-TP	16.25	> 10	693	3.40	SF2/VS2	0.81	> 0.80	PA2
9	SCC-20-TP	21.25	> 10	680	3.50	SF2/VS2	0.79	< 0.80	PA2

From Table 2. it can be seen that the implementation of WBA as filler replacement in SCC causing reduction in passing ability and flowability and increase in viscosity. By increasing WBA from 0% to 20% PJ value was increased by 3 times, therefore exceed maximum typical range value of 10 mm [36]. With reduction of WBA content in SCC from 20% to 0% slump flow diameter is reduced for 19%, meaning transition in slump flow class from SF1 to SF2. Reduction in flowability of SCC with increase of WBA replacement level from 0% to 20% is as well followed by increase in viscosity, i.e. slump flow time T500 is increased by 0.60 s. Despite presented results, slump flow values of all SCC mixtures with WBA are in accordance with EFNARC Guidelines [27]. Test results from L-box confirmed results obtained with J-ring test. By implementing WBA in SCC, passing ability is reduced. Similar trends in test results of SCC with TP as a filler replacement can be observed. Larger amount of TP in SCC caused reduction in passing ability and flowability and enhancement in viscosity, which is in accordance with several previous investigations carried out by different authors, where crumb rubber, grain size 0-4 mm, was replaced with fine aggregate in SCC [1], [7], [12], [37], [38]. With 20% of TP as filler replacement material, PJ value was increased by 3.4 times, and slump flow diameter was reduced by 2%, maintaining same slump flow class, SF2. Slump flow time T500 is increased by 1.49 s which may refer to the increase in viscosity with increasing TP replacement level. However, results of slump flow test for SCC-5-TP and SCC-10-TP gives contradictory results, as in this case slump flow diameter is increased comparing to diameter of reference mixture SCC-0, which is, on the other hand, not in accordance with investigations carried out so far.

3.2 Hardened SCC test results

Results of testing the hardened SCC are given in Table 3. And Figure 2. Compared to reference mixture SCC-0, reduction in compressive strength of SCC cubes was 24% and 16% with implementation of 20% of WBA and TP, respectively. Similar reduction in compressive strength of SCC cylinders was observed, i.e. 29% and 21% with implementation of 20% of WBA and TP, respectively. However, replacing 10% of filler with TP caused only 7% of reduction in compressive strength of cubes. For all SCC mixtures compressive strength values of cubes were over 40 MPa, while compressive strength values of cylinders were over 35 MPa.

With WBA and TP replacement level of 20%, compressive strength values of cubes were satisfying 49.67 and 55.13 MPa, respectively.

Table 3. Mechanical properties of tested SCC mixtures

Mixture #	Mixture	$f_{ck,cube}$ (N/mm ²)	$f_{ck,cyl}$ (N/mm ²)	E (GPa)
1	SCC-0	65.39	53.02	45.43
2	SCC-5-WBA	61.17	48.90	44.33
3	SCC-10-WBA	52.71	41.86	36.37
4	SCC-15-WBA	49.41	36.01	38.82
5	SCC-20-WBA	49.67	37.71	41.68
6	SCC-5-TP	64.77	52.34	50.41
7	SCC-10-TP	60.74	47.90	50.17
8	SCC-15-TP	56.82	49.17	43.78
9	SCC-20-TP	55.13	41.84	43.56

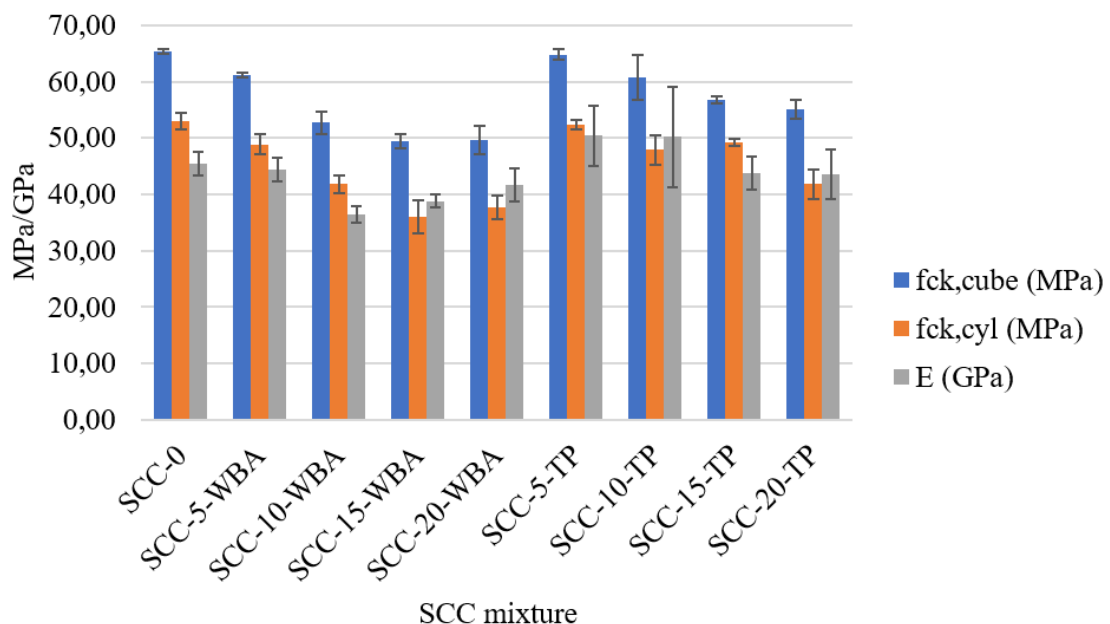


Figure 2. Compressive strength and modulus of elasticity of SCC mixtures

Regarding modulus of elasticity, reduction was occurred when filler was replaced with WBA. With WBA replacement level of 10, 15 and 20% reduction in modulus of elasticity was 20, 15 and 8%. On the other hand, with TP replacement level of 5 and 10% increase in modulus of elasticity occurs by 11 and 10%, respectively. However, TP replacement level of 15 and 20% caused reduction in modulus of elasticity by 3.6 and 4.1%.

4. CONCLUSIONS

Quantity of wood biomass ash (WBA) and tire powder (TP) as a waste material rapidly grows each year. Therefore, the European regulations are becoming more rigorous in terms of recycling and re-use of these materials. In order to give a solution to this environmental problem, utilization of these two waste materials into self-compacting concrete are presented

in this paper. WBA and TP were implemented into SCC as a filler replacement in different amounts. From obtained results, several conclusions can be made:

- Implementation of WBA as filler replacement in SCC caused reduction in passing ability and flowability and increase in viscosity.
- Implementation of TP as filler replacement in SCC caused increase in flowability and viscosity and reduction in passing ability of fresh SCC mixtures.
- Partial replacement of filler, i.e. dolomite powder with WBA and TP caused reduction of SCC compressive strength and modulus of elasticity, although slight increase in modulus of elasticity was observed when 5 and 10% of filler was replaced with TP.
- Compressive strength values of cubes and cylinders of all SCC mixtures were over 40 MPa and 35 MPa, respectively, which are promising results for further experimental work.

This research showed that WBA and TP can be used as partial replacement material of dolomite powder in SCC, and that acceptable SCC fresh and hardened properties can be obtained. However, further long-term research of SCC with WBA and TP as a filler replacement is recommended to determine a possibility for potential use of these type of SCC in structural applications.

ACKNOWLEDGEMENTS

This paper was supported by Croatian Science Foundation under the project UIP-2017-05-7113 Development of Reinforced Concrete Elements and Systems with Waste Tire Powder – ReCoTiP and under the project IP-2016-06-7701 Transformation of Wood Biomass Ash into Resilient Construction Composites – TAREC².

REFERENCES

- [1] M. M. Rahman, M. Usman, and A. A. Al-Ghalib, "Fundamental properties of rubber modified self-compacting concrete (RMSCC)," *Constr. Build. Mater.*, vol. 36, pp. 630–637, 2012.
- [2] H. Liu, X. Wang, Y. Jiao, and T. Sha, "Experimental investigation of the mechanical and durability properties of crumb rubber concrete," *Materials (Basel)*, vol. 9, no. 3, pp. 1–12, 2016.
- [3] ETRMA, "End-of-life Tyre Report 2015," 2015.
- [4] N. Ukrainczyk, "Reuse of Woody Biomass Ash Waste in Cementitious Materials," *Chem. Biochem. Eng. Q.*, vol. 30, no. 2, pp. 137–148, 2016.
- [5] Directive 2008/98/EC of the European Parliament and the Council of 19 November 2008 on waste and repealing certain Directives.
- [6] M. Emiroğlu, S. Yildiz, O. Keleştemur, and M. H. Keleştemur, "Bond performance of rubber particles in the self-compacting concrete," *Bond Concr. 2012 - Bond New Mater. under Sev. Cond.*, pp. 779–786, 2012.
- [7] M. K. Ismail and A. A. A. Hassan, "Use of metakaolin on enhancing the mechanical properties of self-consolidating concrete containing high percentages of crumb rubber," *J. Clean. Prod.*, vol. 125, pp. 282–295, 2016.
- [8] Zakon o održivom gospodarenju otpadom (NN 94/2013, 73/2017).
- [9] Pravilnik o gospodarenju otpadnim gumama (NN 113/16).
- [10] ERMCO, "Ready-mixed concrete industry statistics," 2015.
- [11] A. Moustafa and M. A. Elgawady, "Mechanical properties of high strength concrete with scrap tire rubber," *Constr. Build. Mater.*, vol. 93, pp. 249–256, 2015.
- [12] R. Si, J. Wang, S. Guo, Q. Dai, and S. Han, "Evaluation of laboratory performance of self-consolidating concrete with recycled tire rubber," *J. Clean. Prod.*, vol. 180, pp. 823–831, Apr. 2018.
- [13] M. Jedidi, A. Gargouri, and A. Daoud, "Effect of Rubber Aggregates on the Thermophysical Properties of Self-Consolidating Concrete," *Int. J. Therm. Environ. Eng.*, vol. 8, no. 1, pp. 1–7, 2014.

- [14] R. B. Murugan, E. R. Sai, C. Natarajan, and S.-E. Chen, "Flexural fatigue performance and mechanical properties of rubberized concrete," *Gradjevinar*, vol. 69, no. 11, pp. 983–990, 2017.
- [15] A. Y. Elghazouli, D. V. Bompa, B. Xu, A. M. Ruiz-Teran, and P. J. Stafford, "Performance of rubberised reinforced concrete members under cyclic loading," *Eng. Struct.*, vol. 166, no. November 2017, pp. 526–545, 2018.
- [16] Directive 2009/28/EC of the European Parliament and of the Council of 23 April 2009 on the promotion of the use of energy from renewable sources and amending and subsequently repealing Directives 2001/77/EC and 2003/30/EC.
- [17] Zakon o obnovljivim izvorima energije i visokoučinkovitoj kogeneraciji (NN 100/15, 123/16, 131/17).
- [18] Communication from the Commission to the European Parliament, the Council, the European Economic and Social Committee of the Regions, A policy framework for climate and energy in the period from 2020 to 2030, Brussels, 2014. .
- [19] C. B. Cheah and M. Ramli, "Mechanical strength, durability and drying shrinkage of structural mortar containing HCWA as partial replacement of cement," *Constr. Build. Mater.*, vol. 30, pp. 320–329, 2012.
- [20] I. Carević, I. Banjad Pečur, and N. Štirmer, "Utilization of Wood Biomass Ash (WBA) in the Cement Composites," in *Proceedings of the 2nd International Conference on Bio-based Building Materials & 1st Conference on ECological valorisation of GRAnular and FIBrous materials, Clermont-Ferrand, France, June 21th - 23th 2017*, pp. 196–201.
- [21] S. Chowdhury, M. Mishra, and O. Suganya, "The incorporation of wood waste ash as a partial cement replacement material for making structural grade concrete: An overview," *Ain Shams Eng. J.*, vol. 6, no. 2, pp. 429–437, 2015.
- [22] I. Carević, N. Štirmer, I. Banjad Pečur, B. Milovanović, and M. Rukavina Jelčić, "Potential of use wood biomass ash in the cement composites," *Proceedings 1st Int. Conf. Constr. Mater. Sustain. Futur. Zadar, Croat. 19 - 21 April 2017*, pp. 109–114.
- [23] I. Carević, I. B. Pečur, N. Štirmer, B. Milovanović, and A. Baričević, "Potencijal biopepela i stanje u Republici Hrvatskoj," in *Sabor hrvatskih graditelja 2016, Hrvatski savez građevinskih inženjera, Cavtat, 17. i 18. listopada 2016*, pp. 133–142.
- [24] I. Obernberger and K. Supancic, "Possibilities of ash utilisation from biomass combustion plants," in *Proceedings of the 17th European Biomass Conference & Exhibition, Hamburg, Germany, 29 June - 3 July 2009*.
- [25] M. Berra, T. Mangialardi, and A. E. Paolini, "Reuse of woody biomass fly ash in cement-based materials," *Constr. Build. Mater.*, vol. 76, pp. 286–296, 2015.
- [26] J. Cuenca, J. Rodríguez, M. Martín-Morales, Z. Sánchez-Roldán, and M. Zamorano, "Effects of olive residue biomass fly ash as filler in self-compacting concrete," *Constr. Build. Mater.*, vol. 40, pp. 702–709, 2013.
- [27] EFNARC, "The European Guidelines for Self-Compacting Concrete," 2005.
- [28] HRN EN 197-1:2012 Cement - Part 1: Composition, specifications and conformity criteria for common cements.
- [29] HRN EN 1008:2002 Mixing water for concrete – Specification for sampling, testing and assessing the suitability of water, including water recovered from processes in the concrete industry, as mixing water for concrete.
- [30] ASTM International, Standard Test Method for Density of Hydraulic Cement (ASTM C188-17).
- [31] HRN EN 12350-8:2010: Testing fresh concrete - Part 8: Self-compacting concrete - Slump flow test.
- [32] HRN EN 12350-10:2010: Testing fresh concrete - Part 10: Self-compacting concrete - L box test.
- [33] HRN EN 12350-12:2010: Testing fresh concrete - Part 12: Self-compacting concrete - J-ring test.
- [34] HRN EN 12390-3:2009: Testing hardened concrete - Part 3: Compressive strength of test specimens.
- [35] HRN EN 12390-13:2013: Testing hardened concrete - Part 13: Determination of secant modulus of elasticity in compression.
- [36] EFNARC, "Specification and Guidelines for Self-Compacting Concrete," 2002.
- [37] T. Uygunoğlu and I. B. Topçu, "The role of scrap rubber particles on the drying shrinkage and mechanical properties of self-consolidating mortars," *Constr. Build. Mater.*, vol. 24, no. 7, pp. 1141–1150, 2010.
- [38] E. Güneş, "Fresh properties of self-compacting rubberized concrete incorporated with fly ash," *Mater. Struct. Constr.*, vol. 43, no. 8, pp. 1037–1048, 2010.

International Conference on Sustainable Materials, Systems and Structures (SMSS 2019)

New Generation of Construction Materials

20-22 March 2019 – Rovinj, Croatia

NEW GENERATION OF CONSTRUCTION MATERIALS

SESSION 13: 3D printing

SURFACE MODIFICATION AS A TECHNIQUE TO IMPROVE INTER-LAYER BONDING STRENGTH IN 3D PRINTED CEMENTITIOUS MATERIALS

J. Van Der Putten (1), G. De Schutter (1) and K. Van Tittelboom (1)

(1) Ghent University, Ghent, Belgium

Abstract

The structural capacity of 3D printed components mainly depends on the inter-layer bonding strength between the different layers. This bond strength is affected by many parameters (e.g. moisture content of the substrate, time gap, surface roughness,..) and any mismatch in properties of the cementitious material may lead to early failure. A common technique to improve inter-layer bonding strength between a substrate and a newly added layer is modifying the substrate surface. For the purpose of this research, a custom-made 3D printing apparatus is used to simulate the printing process and layered specimens with a different delay time (0 and 30 minutes) are manufactured with different surface modification techniques (wire brushing, addition of sand or cement and moisturizing substrate layer). The surface roughness was measured and the effect of the modification technique on the inter-layer-bonding strength was investigated. Results showed that the most effective way to increase the inter-layer bonding is increasing the surface roughness by a comb. This creates a kind of interlock system that will provide a higher inter-layer strength. The compressive strength is most influenced by the addition of cement, where the changing W/C-ratio will create a higher degree of hydration and consequently a higher strength.

Keywords: 3D printing – surface modification – inter-layer bonding

This work was invited for publication in the open access journal RILEM Technical Letters. You can visit the journal and benefit from the full open access to the published articles at: letters.rilem.net.

POWDER BED 3D PRINTING WITH GEOPOLYMERS

Vera Voney (1)*, Pietro Odaglia (2), Gnanli Landrou (1), Coralie Brumaud (1), Andrei Jipa (2), Isolda Agustí-Juan (1), Benjamin Dillenburger (2), Guillaume Habert (1)

(1) Chair of Sustainable Construction, ETH Zürich, Switzerland,

(2) Digital Building Technologies, ETH Zürich, Switzerland.

Abstract

With digital fabrication, complex formworks for high performance concrete can be manufactured, which help to save material. The drawback of the current method is the organic binder, because it releases volatile organic compounds. Therefore, in this study, the organic binder is replaced with a geopolymer in a custom-built binder jet 3D printer. The geopolymer is printed in a selective binder activation approach: the sand bed of the printer contains a mix of metakaolin and silica sand, on which we print with a sodium silicate solution.

In order to find the optimal settings of the printer, the immersion of silicate droplets into powder beds with different metakaolin contents was studied, to get an insight of the spreading of the liquid in the powder bed. The analysis of the weight and the size of the different droplets shows that the printing layer height can be adjusted by changing the metakaolin content in the powder, keeping the same geopolymer.

Keywords: Geopolymers, 3D printing

1. INTRODUCTION

Digital fabrication allows the production of very complex shapes with no extra cost for complexity and customization. This mass customization revolution opens new possibilities for the construction industry [1]. For instance, structural elements can be designed with the exact amount of materials positioned in the right place. Recently, binder jet 3D printing has been used to produce a formwork for high performance fibre reinforced concrete [2, 3], which would reduce the environmental impact of the structure, by one third (Figure 1).

Binder jet 3D printing is a technique in which a liquid binding agent is deposited to join powder particles, previously placed on a movable platform. Another layer of powder is then spread and the binder is added. Over time, layers of material are bonded to form an object (Figure 2). The main advantages of this 3D printing technique compared to extrusion is that overhangs can be printed easily and the leftover powder can be reused.



Figure 1: Stay-in place formwork for a concrete slab 3D printed with organic binder. High performance fiber reinforced concrete is poured inside. (Image: Chair of digital building technologies)

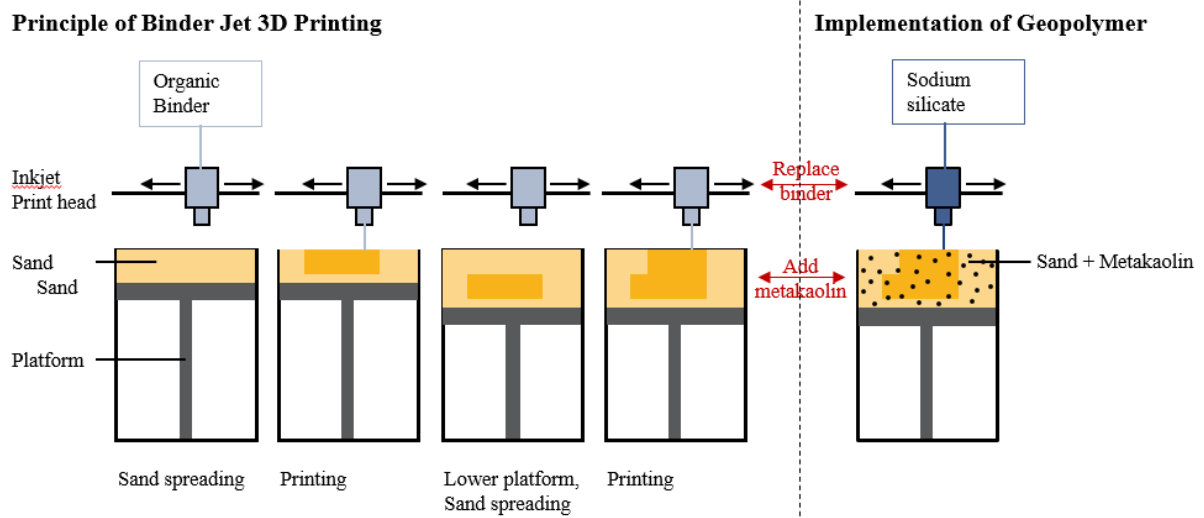


Figure 2 : Left. Working principle of binder jet 3D printing. Right. Implementation of a geopolymer binder system.

However, this large scale binder-jet technology, commonly used with organic binders as additive, causes serious problems for the indoor environmental quality of buildings through the release of volatile organic compounds when they are used as building structure [4].

Therefore in this work the usual system organic binder/non-reactive powder bed is replaced by an inorganic solution/reactive powder, resulting in a binder between grains: a geopolymer. Geopolymers are inorganic amorphous materials that consist of a covalently bond aluminosilica network with sodium or potassium (or other ions) as charge compensators. Geopolymers are used in construction as a cement replacement or fire resistant coatings [5]. The synthesis of a geopolymer requires a reactive aluminosilicate powder which is activated with an alkaline solution. The implementation of the geopolymer in the binder jet 3D printing follows the principle of selective binder activation [6] (cf. Figure 2): the reactive aluminosilicate powder (metakaolin) is added to the sand and the organic binder is replaced by an activating solution (sodium silicate). Everywhere where solution is printed on the powder bed, the two components react and build up a geopolymer which acts as a glue between the sand grains.

The aim of the project is to develop guidelines which allow the definition of all the printing parameters such as layer height, line spacing, nozzle size, printing speed, injection speed and volume from the properties of the powder bed and of the printed liquid. Reis et al. [7] identified

the main governing parameters to model the penetration depth and width of a droplet on a porous powder bed. It was shown in literature, that the shape of the dispersion of the liquid in the powder depends also on the pore size distribution and the particle shape [8, 9].

2. MATERIALS

2.1. Powder bed

All the powder bed experiments were conducted with a mixture of fine sand (Quartz sand FS003 from Strobel Quartz Sand GmbH) and metakaolin (Metastar501 from Imerys) (here referred to as MK). With laser scattering (Horiba Partica LA-950), BET analysis (Quantachrome Autosorb-1) and helium pycnometry (AccuPyc II 1340) the mean grain size, the surface area and the specific density was measured respectively. All the values as well as the SiO₂ and Al₂O₃ contents (from data sheet of corresponding material) are reported in Table 1. Different compositions of powder beds were produced by varying the MK contents (substitution of 0, 5, 10, 15, 20, 40, 60, 80, 100 wt% of sand part by MK) and the random loose packing of the grains was measured (35 % for 20 wt% of MK) according to [10].

Table 1 : Specifications of the used powders

	Mean grain size d ₅₀ [μm]	Surface area [m ² /g]	Specific density [g/cm ³]	SiO ₂ content [wt%]	Al ₂ O ₃ content [wt%]
Sand	240	0.09	2.6	>99.1	<0.2
Metakaolin	4	13.17	2.58	51.63	44.37

2.2. Activating solution

A sodium silicate solution (here referred to as NaSil) was used as activating solution and was produced with deionized water at 20°C, NaOH in pellets form (Sigma Aldrich) and silica gel in powder form (Davisil grade 635, Sigma Aldrich). The SiO₂/Na₂O ratio of 1.69 results in a fast initial strength of the geopolymer, which allows the printing of the next layer in the 3D printing [11]. Since the layers should still connect, an intermediate final setting time is needed, therefore a H₂O/Na₂O ratio of 12.93 was chosen [11]. The viscosity of the solution was measured using a stress-controlled rheometer (Kinexus, Malvern Instrument Switzerland) equipped with parallel plates (0.06 Pa.s at 20°C). The specific density of the solution (1.46 g/cm³) was measured with a Densito 30 PX (Mettler Toledo).

3. DROPLETS EXPERIMENTS

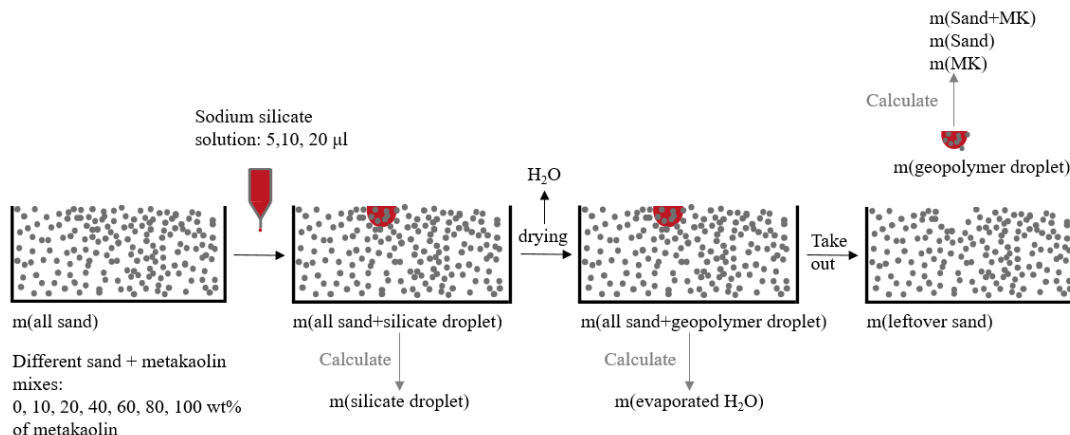


Figure 3 : Schematics of the droplet experiment.

In order to get an insight of the spreading of the liquid in the powder bed during the 3D printing depending on the powder bed composition, first experiments consisted in simulating the 3D printing process by dropping NaSil solution with a pipette on different sand/MK mixes (loose packing state) (Figure 3). With this method, droplets were produced and characterized. Through the analysis of the droplet weight after removal and knowing the powder bed composition, the Si/Al ratio can be calculated. The Si/Al ratio of around 2 is constant for MK contents higher than 20wt% (Figure 4 left). With an Al-NMR measurement (

Figure 4 right) of the solid droplet and of the sand/MK mix (20wt% of MK), the existence of a geopolymer could be validated: the characteristic AlVI peak is clearly higher in the droplet than in the sand/MK mix. The size of the obtained droplets (diameter and height) were determined by image analysis (microscopy and Matlab code), 3 mm for 20 wt% MK (Figure 5a,b). Micro tomography images were taken in order to evaluate the internal structure of the droplets (Figure 5c).

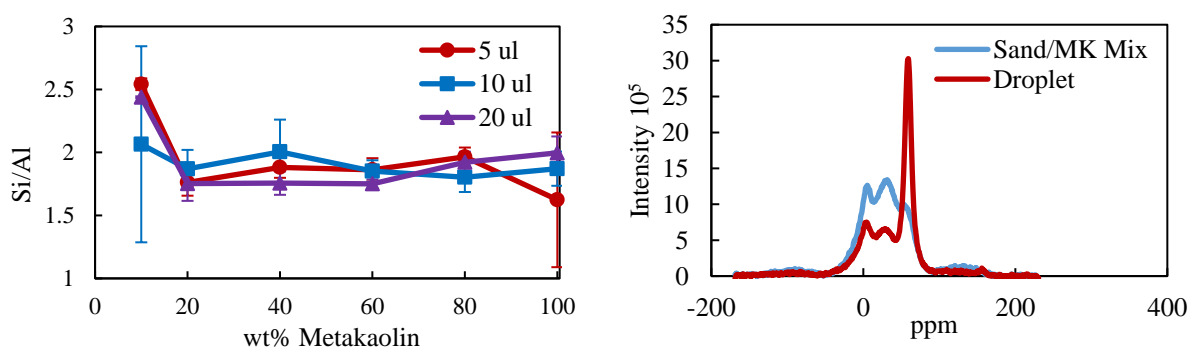


Figure 4 : Left. Si/Al ratios of geopolymer droplets built up from different powder mixes prepared with different MK contents. Right. Al-NMR of geopolymer built with a sand/MK mix containing 20wt% of MK.

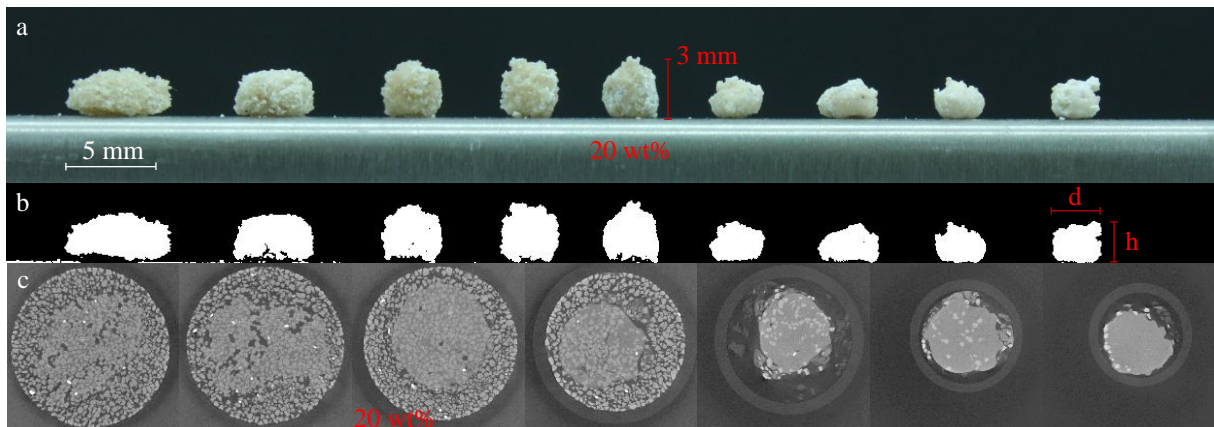


Figure 5 : a : Droplets of 10 μ l NaSil solution dropped on different sand/MK mixes, with an increasing MK content from left to right (0, 5, 10, 15, 20, 40, 60, 80, 100 wt%). b: Output from Matlab code to analyse the diameter (d) and the height (h). c: Microtomography images (0, 10, 20, 40, 60, 80, 100 wt% MK)

On the first sight, the shapes of the droplets look like spheres. Assuming that the liquid distributes as a sphere in the powder bed and occupies all the voids ($V_{liquid} = V_{voids}$), a theoretical diameter of this sphere can be calculated from the loose porosity of the powder bed ($\epsilon_{loose} = \frac{V_{pores}}{V_{theor}}$) and the volume of the liquid:

$$d_{theor} = h_{theor} = \left(\frac{6V_{liquid}}{\pi\epsilon_{loose}} \right)^{1/3} \quad (1)$$

Comparing this theoretical diameter with the measured diameter, the results separate in two regimes (Figure 6 left): for MK contents lower than 20 wt%, the ratio between the measured and the theoretical diameter (equation 1) is decreasing, whereas it is constantly close to one for MK contents higher than 20 wt%. Comparing this result with the available surface per droplet, it can be observed a regime change at the same MK content (Figure 6 right). An increasing surface area is related to smaller pore sizes [8], therefore we can assume significantly smaller pore sizes in powder mixtures with MK contents > 20 wt%. This leads to higher capillary forces, hindering the liquid from penetration into the powder, leading to more defined droplet shapes and less spreading across the surface [7, 9]. The less homogeneous spreading in powders with larger pores is also supported by the microtomography images: droplets from sand mixes with a MK content < 20 wt% show more air voids (cf. Figure 5c).

The height of the droplets (corresponding to the penetration depth) follows a similar pattern: it shows a maximum height at 20 wt% of metakaolin (cf. Figure 5a). From the calculations of the droplet weights we know that the Si/Al content in the droplet is constant for MK contents > 20 wt% (cf.

Figure 4 left), therefore it is possible to adjust the layer height in the printer by adjusting the MK content of the powder bed, keeping the same geopolymer composition.

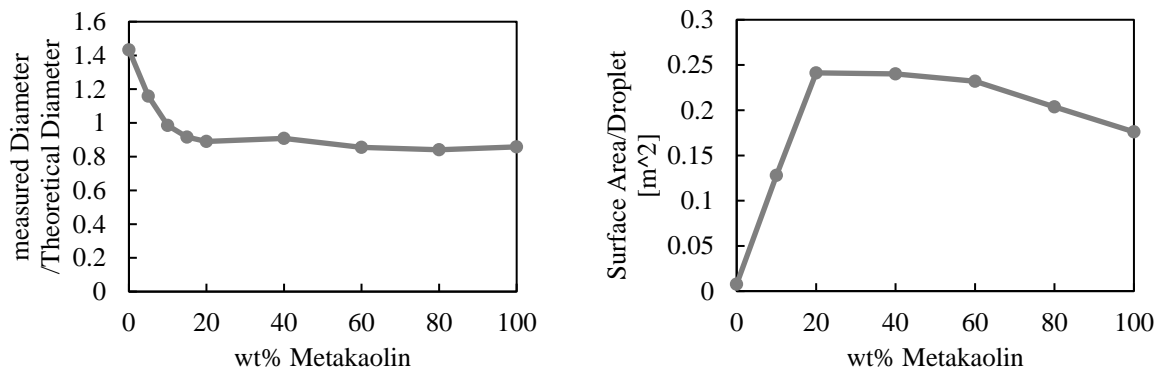


Figure 6 : Left. Ratio of measured and theoretical diameter (equation 1) of geopolymer droplets. Right. Available surface area per droplet.

4. 3D PRINTING

The printing was done on a self-built setup (Figure 7, left), designed and developed using affordable and easily accessible components and with the main aim of providing a robust testing platform for multiple material combinations. The software interface, built from scratch in the .NET framework, allows for full flexibility in settings and printing parameters.

The printer allows the control of different parameters: nozzle diameter, moving speed, injection volume per distance, layer height and the spacing between the printed lines (Figure 7 right). The range of acceptable nozzle sizes is affected by the viscosity and surface tension of the NaSi solution: a valid compromise between achievable resolution and time between subsequent cloggings was found in 0.25 mm. The layer height depends on the powder bed composition: the prints were done with a powder mix containing 20 wt% of MK, therefore a layer height of 3 mm was chosen. The moving speed of the print head was set to 30 m/min and the injection volume per distance as well as the line spacing were varied. These two values can be combined in the saturation of the printed part, which can be defined as:

$$\text{Saturation} = \frac{V_{\text{liquid}}}{V_{\text{pores}}} \quad (2)$$

To evaluate the mechanical performances of the produced material, 4x4x16 cm bars were printed and submitted to compression testing (Unitronic, Matest) after 7 days curing at room temperature and 50% relative humidity.

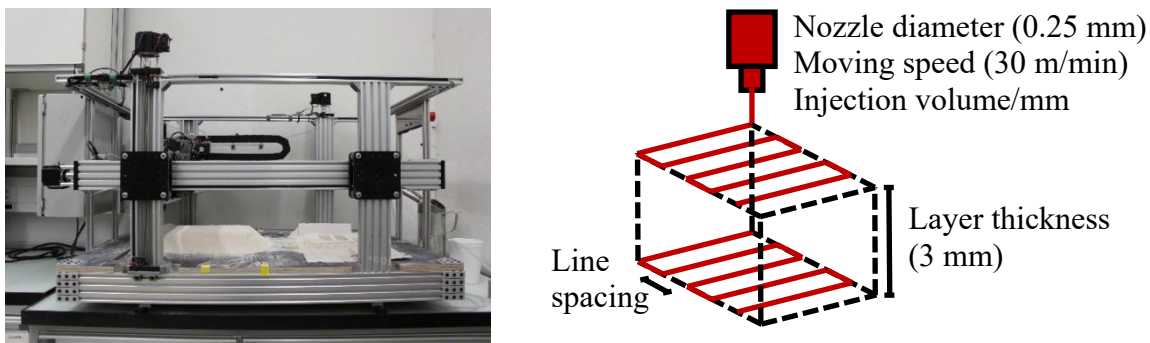


Figure 7 : Left. 3D printer. Right. Different printing parameters that can be adjusted.

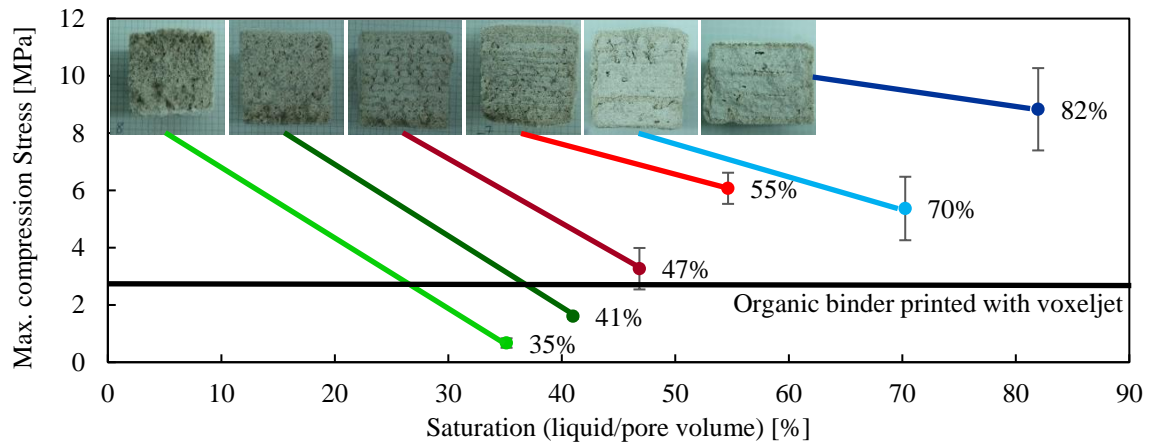


Figure 8 : Maximum compression strength of printed parts with different saturation index

Table 2 : Saturation index values for the different printing parameters

Layer thickness: 3 mm Nozzle diameter: 0.25 mm	Line spacing: 0.5 mm	Line spacing: 0.75 mm	Line spacing: 1 mm
0.6 $\mu\text{l}/\text{mm}$	70%	55%	35%
0.7 $\mu\text{l}/\text{mm}$	82%	47%	41%

Figure 8 shows the maximum compression strength of bars printed with different printing parameters resulting in different values of saturation (Table 2). With an increasing saturation value, an increasing compression strength is observed, but also an increase in the flow out in the bottom. Already at 47% saturation the bars are stronger than the reference, printed in a commercial powder bed 3D printer (Voxeljet VX 1000) with sand and organic binder.

5. DISCUSSION

The main parameters influencing the penetration radius and depth of a liquid in a porous powder, identified by Reis *et al.* [7], are either related to the fluid (viscosity, density), the powder (porosity, permeability, pore size, grain size) or to the printing conditions (impingement velocity, initial droplet radius). Assuming spherical particles in the current study, the pore and grain sizes could be calculated from the porosity and all the relevant parameters would be present. However, in the studied mixes, due to the non-spherical particle shape of MK, this assumption would not be valid. Therefore, further measurements on the relevant powder properties should be performed in order to model the penetration depth and diameter of the droplet. An additional difference to the experiments of Reis *et al.* [7] lies in the reactivity of the powder bed. In the MK/NaSi system a volume change could occur due to the geopolymer reaction and the rearrangement of the plate like MK particles in liquid.

Finally, the results of the droplet experiment gave a valid assumption for the printing layer height. Since the volume of the droplet is much larger per millimetre, it is surprising that the layer height still corresponds. It could be explained by the fact that the injection speed in the

printer is much higher than for the droplet, therefore the jet pushes away the upper layer and then starts to penetrate.

For the printing an important parameter is the saturation, because it correlates with the compression strength (*cf.* Figure 8). It was found that the saturation of a printed part can be controlled by the printing parameters $\mu\text{l}/\text{mm}$ and the line spacing.

6. CONCLUSION

In this study, the system of organic binder/non-reactive powder bed usually employed for binder jet 3D printing was replaced by a sustainable solution which consists of an inorganic solution and a reactive powder bed. As a result, the concept of printing geopolymers in a selective binder activation approach could be proofed. The penetration depth varies with varying MK content within the sand bed, whereas the Si/Al ratio stays constant at around 2 which should give a strong geopolymer. Therefore we can vary the layer thickness of the printed part by changing the amount of MK in the powder bed, without changing the final material properties. To relate the printing parameters with the material properties of the sand and the liquid, the penetration behaviour needs to be studied in more detail.

REFERENCES

- [1] I. Agustí-Juan and G. Habert, "Environmental design guidelines for digital fabrication," *Journal of cleaner production*, vol. 142, pp. 2780-2791, 2017.
- [2] T. Wangler *et al.*, "Digital concrete: opportunities and challenges," *RILEM Technical Letters*, vol. 1, pp. 67-75, 2016.
- [3] A. Jipa, M. Bernhard, B. Dillenburger, and M. Meibodi, "3D-Printed Stay-in-Place Formwork for Topologically Optimized Concrete Slabs," in *2016 TxA Emerging Design+ Technology conference*, 2016: Texas Society of Architects.
- [4] I. Agustí-Juan, A. Jipa, and G. Habert, "Environmental assessment of multi-functional building elements constructed with digital fabrication techniques," *The International Journal of Life Cycle Assessment*, pp. 1-13, 2018.
- [5] P. Duxson, A. Fernández-Jiménez, J. L. Provis, G. C. Lukey, A. Palomo, and J. S. van Deventer, "Geopolymer technology: the current state of the art," *Journal of materials science*, vol. 42, no. 9, pp. 2917-2933, 2007.
- [6] D. Lowke, E. Dini, A. Perrot, D. Weger, C. Gehlen, and B. Dillenburger, "Particle-bed 3D printing in concrete construction—possibilities and challenges," *Cement and Concrete Research*, vol. 112, pp. 50-65, 2018.
- [7] N. C. Reis Jr, R. F. Griffiths, and J. M. Santos, "Parametric study of liquid droplets impinging on porous surfaces," *Applied Mathematical Modelling*, vol. 32, no. 3, pp. 341-361, 2008.
- [8] K. P. Hapgood, J. D. Litster, S. R. Biggs, and T. Howes, "Drop penetration into porous powder beds," *Journal of Colloid and Interface Science*, vol. 253, no. 2, pp. 353-366, 2002.
- [9] H. Miyanaji, S. Zhang, and L. Yang, "A new physics-based model for equilibrium saturation determination in binder jetting additive manufacturing process," *International Journal of Machine Tools and Manufacture*, vol. 124, pp. 1-11, 2018.
- [10] V. Lédée, F. De Larrard, T. Sedran, and F. Brochu, "Essai de compacité des fractions granulaires à la table à secousses," *Laboratoire Central des Ponts et Chaussée—IST Diffusion des éditions, Juillet 2004, Paris*, 2004.
- [11] A. Favier, "Mécanisme de prise et rhéologie de liants géopolymères modèles," Université Paris-Est, 2013.

HIGH-PERFORMANCE 3D PRINTABLE CONCRETE ENHANCED WITH NANOMATERIALS

Jacques Kruger, Marchant van den Heever, Seung Cho, Stephan Zeranka and Gideon van Zijl

Division for Structural Engineering and Civil Engineering Informatics, Stellenbosch University, South Africa

Abstract

The development of high-performance concrete (HPC) suitable for 3D printing is restricted by the fresh state of concrete i.e. a narrow workability concrete range that will yield appropriate printability and buildability. Thus, the main focus is to first obtain sufficient concrete rheology, followed by enhanced mechanical characteristics in the hardened state. A HPC material that appertains to 3D printing should therefore yield superior properties in both the fresh and hardened concrete state.

In this research, silicon carbide (SiC) and silica (SiO₂) nanoparticles are added and compared to a reference HPC material suitable for 3D printing. Fresh state properties that result in improved buildability are depicted by means of novel static yield shear stress evolution curves. The effect of nanoparticle addition on the performance in the hardened state, in terms of mechanical strength and stiffness, is also characterised. Furthermore, the effect on the interlayer bond strength between successive filament layers is determined, which typically is the weakest section in 3D printed elements.

Keywords: 3D printing of concrete; rheology; nanomaterials; silicon carbide; nano-silica

1. INTRODUCTION

Prominent Industry 4.0 technologies such as 3D printing and nanotechnology are augmenting several industry sectors, resulting in increased productivity, quality and reduced costs. In contrast, the construction industry's productivity has regressed over the last 50 years, mainly due to their lack of embracing automation technologies [1]. However, 3D printing of concrete (3DPC) is enjoying significant attention in the academia [2], and together with industry partners resulted in the realisation of a bridge [3] as an example of practical application.

Nanoparticles are defined as particles with a diameter of less than 100 nm. Due to their small size, their behaviour is influenced by atomic, molecular and ionic interactions [4]. Research on nanoparticle addition to concrete concludes that increased mechanical strength is obtained [5,6] as well as improved rheological behaviour, specifically yield stress and

cohesion [7]. These effects are largely attributed to increased pozzolanic reactivity [8]. A well-dispersed nanoparticle microstructure has the further benefit of increasing re-flocculation of particles e.g. after shearing induced by pumping, hence increasing thixotropic behaviour that is ideal for 3DPC purposes [9].

HPC is defined as concrete having high strength or improved durability properties, however, a wide range of strengths (60 – 130 MPa) are defined as HPC depending on the era and institute [10]. For 3DPC purposes, a HPC must demonstrate thixotropic behaviour to yield acceptable buildability. Thus, a HPC for 3DPC consists of a hybrid model: firstly improved rheology and secondly increased mechanical or durability properties. Typical HPC employs very low w/c ratios, which results in incompatible workability in terms of printability for 3DPC. With the use of nanoparticles, higher w/c ratios can be used to obtain concrete rheology suitable for 3DPC, while also conforming to the hardened property requirements for HPC.

In this research, silicon carbide (SiC) and silica (SiO₂) nanoparticles are added to a reference HPC material that is suitable for 3DPC. Its effect on rheology is depicted by means of novel static yield shear stress evolution curves [9], which encompasses the static and dynamic yield strength, as well as re-flocculation and structuration rates that characterises the degree of thixotropy of a material. Its effect on mechanical properties, in particular compressive and flexural strength and the Young's Modulus, are examined. The interlayer bond strength between successive filament layers with and without nanoparticle addition is determined by means of 4-point bending tests. This is a crucial test for 3DPC, as the interlayer bond strength is typically weaker than the concrete itself. Adequate rheology can result in filament layers merging to form a homogenous concrete section, resulting in stronger structures without weak interlayer bonds.

2. MATERIALS AND EXPERIMENTAL METHODS

2.1 Nanomaterial properties

Two different types of nanomaterials are used for this study and the respective material properties of each are indicated in Table 1. Both materials are purchased from Nanostructured and Amorphous Materials [11].

Table 1: Nano-silica and silicon carbide material properties [11].

Property	SiO ₂	SiC
Purity	99.5 %	97.5 %
Average Particle Size (APS)	15 – 20 nm	45 – 55 nm
Specific Surface Area (SSA)	640 m ² /g	35 – 40 m ² /g
Colour	White	Dark Grey
Morphology	Spherical	Spherical
Bulk Density	0.1 g/cm ³	0.068 g/cm ³
True Density	2.2 – 2.6 g/cm ³	3.22 g/cm ³
Synthesis Method	-	Plasma CVD

The nano-silica particles have a specific surface area that is 16 times greater than that of the silicon carbide, due to the particles being more than twice as small in diameter. It is therefore theorised that the nano-silica particles will have a bigger influence on rheology. The silicon carbide particles have greater mechanical properties than the nano-silica particles, and

is theorised to increase the concrete's mechanical strength more than the silica [6]. Thus, two materials that are theorised to exhibit different effects are tested in this research.

2.2 HPC mix design

The reference HPC mix used in this research, with quantities depicted in Table 2, is developed at Stellenbosch University. The mix comprises of a w/c ratio of 0.45 and its grading follows closely with Fuller's ideal grading in order to achieve maximum particle packing density [12]. A constant polycarboxylate ether superplasticizer dosage is used to achieve dispersion of the nanoparticles, which are added to the concrete by replacement of cement content.

Table 2: Reference HPC mix constituent quantities and nanoparticle content.

Constituent	kg
Cement	579
Fly Ash	165
Silica Fume	83
Fine Aggregate	1167
Water	261
Superplasticizer	1.48 % by mass of binder
Nanoparticles	1, 2, 3 % by mass of cement

2.3 Rheology test

Thixotropic behaviour consists of two phases namely break-down and rebuilding. The rebuilding phase depicts the shear stress increase after cessation of agitation e.g. after extrusion and is characterised by re-flocculation and structuration respectively. This is important for 3DPC as it influences the buildability of a material. Figure 1 depicts a static yield shear stress evolution model applicable especially to 3DPC [9]. Re-flocculation occurs immediately after extrusion of the material and starts at the material's initial dynamic yield shear stress. The static yield shear stress then increases linearly according to the re-flocculation rate (R_{thix}) until it reaches the material's initial static yield shear stress. Thereafter, the static yield shear stress increases linearly according to the structuration rate (A_{thix}) [13]. A larger re-flocculation rate correlates with increased thixotropic behaviour. A lower initial dynamic yield shear stress increases a material's pumpability while a higher initial static yield shear stress increases a material's buildability for 3DPC.

The Germann Instruments ICAR rheometer is utilised in this research to facilitate concrete rheology testing in order to obtain the static yield shear stress evolution curve. A stress growth rheology test is performed at the following resting time intervals: 0, 10, 20, 30, 40, 50, 60, 90, 120, 1200, 2400 and 3600 seconds, at a constant shear rate of 1/s. The short term time scale (0 - 120s) depicts re-flocculation while the long term time scale (0, 1200, 2400 and 3600s) depicts structuration. The static and dynamic yield shear stress are obtained from each stress growth test that corresponds to its respective resting time interval. The static yield shear stress values are then plotted for both the short and long term time scales and the derivative of each linear regression function determined to obtain R_{thix} and A_{thix} respectively. Together with the initial static and dynamic yield shear stress values (0s time interval), the evolution curve depicted in Figure 1 can be plotted. A more detailed explanation of the rheology test method can be found in [9].

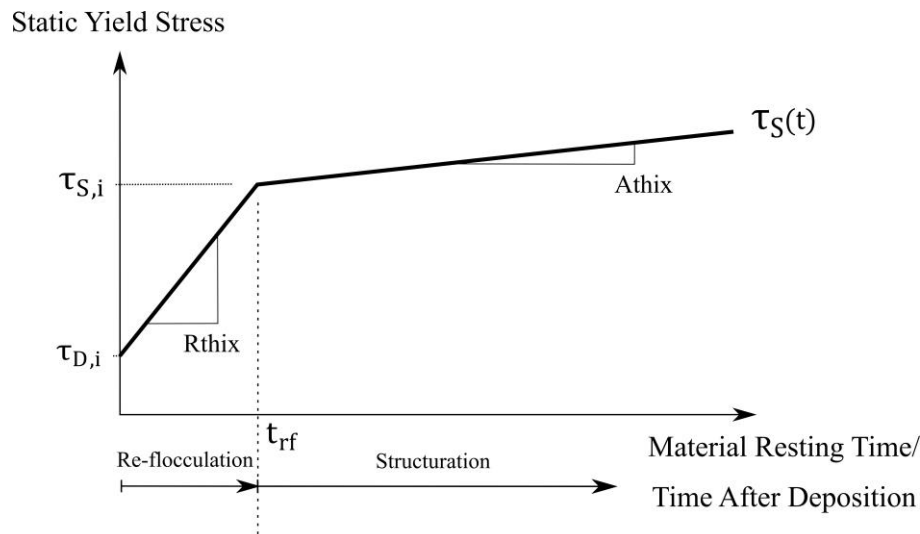


Figure 1: Static yield shear stress evolution curve as a function of time illustrated by re-flocculation and structuration mechanisms [9].

2.4 Mechanical tests

The respective mixes are cast into 40x40x160 mm moulds for four-point flexure tests (EN 196-1) and in cylinder moulds with height 200 mm and diameter 100 mm for Young's Modulus tests (ASTM C469-02). All specimens are initially cured in laboratory conditions at 23°C and 65% relative humidity. After one day, the specimens are stripped and cured in water at 23±2°C until testing age.

Flexural tests are performed in a Zwick Z250 materials testing machine with a span length of 150 mm and loading points at 50 mm spacing. After conducting the flexural tests, an undamaged 40x40 mm part of the beam specimen is tested for compression strength in the same machine by placing 40x40x10 mm plates above and below the sample (EN 196-1). The cylindrical specimens are instrumented with three LVDT's at 120° intervals around the circumference, over a 70 mm gauge length. The tests are conducted in a 2 MN Contest cube press machine, and the load on the specimen recorded with a 2 MN load cell. The displacement and load cell readings are recorded via a HBM Spider8 data acquisition system.

The interlayer bond strength is determined from 3D printed specimens. A 175x175x350 mm square hollow column with layer width 40 mm and height 10 mm is printed at 60 mm/s, yielding a time interval between layer depositions of 11.67s. The day after printing, four specimens are cut from the column with dimensions 40x40x160 mm, which is exactly the same dimensions used for the flexural tests. Four point bending tests are performed on the specimens (28 days) with layers aligned vertically and the same setup is used as for the conventional flexure tests described previously. With the layers aligned vertically, the interlayer bond strength can be classified in terms of the maximum normal stress achievable before delamination of layers occur i.e. failure of the flexural specimen.

3. RESULTS AND DISCUSSIONS

3.1 Static yield shear stress evolution curves

The static yield shear stress evolution curves are illustrated in Figure 2 and its parameters depicted in Table 3. The same reference mix (Table 2) is used for both nanomaterials,

however, different rheological parameters are obtained for the respective reference materials due to a new batch of constituents being used for the silicon carbide tests. The SiO₂ particles, which possess a significantly larger surface area to volume ratio than the SiC particles, drastically increased the static yield shear stress of the reference material for each % increment of nanomaterial. However, it was visually observed that the 2 and 3% SiO₂ mixes are not suitable for 3DPC due to the mixes being too stiff. The SiC particles have a substantial influence on the thixotropy mechanisms, yielding more than a 100% increase in R_{thix} and A_{thix} at 1% dosage. Although increased thixotropy mechanisms are important for 3DPC, the stiffness ($\tau_{s,i}$) contributes the most towards increased buildability and hence the 1% SiO₂ mix is favoured for 3DPC.

It is clear from the results that the SiC nanoparticles significantly improve thixotropic behaviour while SiO₂ particles have a considerable effect on the static yield shear stress. The clear difference in rheological effect is due to the 16:1 surface area ratio between the SiO₂ and SiC particles respectively. Consequently, more superplasticizer is required to completely adsorb onto the SiO₂ particles and disperse particles to release entrapped water. However, due to the smaller SSA of the SiC particles they require less superplasticizer to yield adequate workability and effectively decreases the distance between all particles in the concrete that increases the strength of the van der Waals forces. Subsequently, a more optimal zeta potential [14] is reached resulting in increased thixotropic behaviour while maintaining good workability.

Table 3: Static yield stress evolution curve parameters with normalised values in brackets.

	SiO ₂				SiC			
	SM	1%	2%	3%	SM	1%	2%	3%
$\tau_{s,i}$	2730	3944	5618	6483	1545	1647	2007	1636
(Pa)	(1)	(1.44)	(2.06)	(2.37)	(1)	(1.07)	(1.3)	(1.06)
$\tau_{D,i}$	1146	1532	2702	2803	560	480	738	966
(Pa)	(1)	(1.33)	(2.36)	(2.45)	(1)	(0.86)	(1.32)	(1.73)
R_{thix}	6.88	8	6.11	4.2	2.04	5.07	3.9	3.01
(Pa/s)	(1)	(1.16)	(0.89)	(0.61)	(1)	(2.49)	(1.91)	(1.48)
A_{thix}	1.08	0.91	0.61	0.61	0.32	0.77	0.63	0.66
(Pa/s)	(1)	(0.84)	(0.56)	(0.56)	(1)	(2.41)	(1.97)	(2.06)
t_{RF} (min)	3.84	5.03	7.95	14.6	8.05	3.84	5.42	3.71

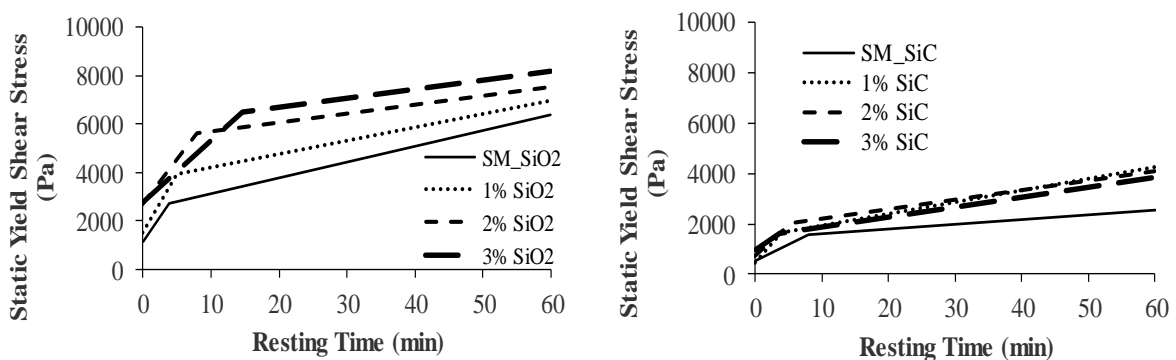


Figure 2: Static yield shear stress evolution curves for (left) silica (SiO₂) and (right) silicon carbide (SiC) nanoparticle addition to a reference concrete mix.

3.2 Mechanical properties

The mechanical properties of the reference and nano-concretes are depicted in Table 4. Three specimens were tested in flexure, four in compression and three for Young's Modulus for each percentage at every testing age. The coefficient of variation (CoV) is calculated for each entry as a means of assessing the variability of the test results, which in general is found to be acceptable. With 1% SiO₂ addition, the early age compressive strength increased by more than 100%. SiO₂ addition yielded very high 1-day compressive strengths, whereas SiC decreased the early age strength, with 3% being the exception. SiO₂ also yielded better performance than SiC at 28 days, especially with 1% addition that results in a 14% strength increase, although with a relatively high CoV. Notably, 3% SiC also yielded 80 MPa after 28 days, with a significantly lower CoV. In the long term (56 days), SiO₂ seems to reduce the compressive strengths for unknown reasons, whereas this effect is not evident for SiC.

In flexure, 1% SiO₂ yielded an 82% increase after 1 day with a very high CoV. In general, SiO₂ increased early age flexural strength whereas SiC yielded a decrease with 3% again being the exception. 2% SiO₂ yielded the highest flexural strength of 9.2 MPa after 28 days. A decrease in flexural strength of SiO₂ is observed in the long term, as was also noted for compression strength, whereas SiC yielded its best results after 56 days.

SiO₂ generally increased the Young's Modulus at 7 days (6% increase at 2% dosage), whereas a constant decrease is noted with every percentage increase in SiC. At 28 days, the effect of SiO₂ as well as SiC on the stiffness is negligible.

Table 4: Mechanical properties (MPa) with CoV values in brackets.

		% Particles\Days	1	7	28	56
Compression Strength	SiO ₂	0	7.9 (2.6)	55.6 (0.6)	70.6 (10.3)	80 (15.1)
		1	16.5 (2.1)	60.4 (7.7)	80.3 (13.4)	72.2 (10)
		2	15.2 (2.5)	59.8 (3.6)	76 (5.5)	77.2 (9.9)
		3	13.7 (4)	63 (5.9)	73.4 (6.4)	61.1 (5.2)
	SiC	0	8.1 (3.6)	58.5 (0.6)	74.3 (10.3)	78.2 (15)
		1	4 (2.8)	56.1 (6.3)	79.5 (4.8)	83.8 (5.7)
		2	7.1 (5.1)	55.3 (4.4)	77.9 (2.9)	80.2 (0.8)
		3	11.1 (2.6)	57.2 (5.4)	80 (0.4)	83.4 (3.3)
Flexural Strength	SiO ₂	0	1.7 (8.1)	7.3 (5)	8.4 (5.7)	8.7 (2)
		1	3.1 (18.3)	7.3 (6.1)	8.1 (13.9)	8.4 (22.8)
		2	2.9 (4.7)	7.3 (5.4)	9.2 (4.4)	7.9 (9)
		3	2 (10.7)	6.8 (2.5)	6.8 (6.2)	7.7 (9.5)
	SiC	0	1.7 (8.2)	7.3 (5)	8.4 (5.7)	8.9 (2)
		1	0.9 (5.3)	6.9 (4.3)	8 (3.4)	9 (2.6)
		2	1.3 (6.8)	6.9 (4.9)	7.6 (4)	9.2 (4.1)
		3	2.2 (6.9)	6 (3.5)	8.5 (4.9)	9.3 (7.5)
Young's Modulus	SiO ₂	0	-	26.6 (2.3)	30.7 (2)	-
		1	-	27.6 (1)	30.5 (2.2)	-
		2	-	28.1 (3.9)	30.3 (3.4)	-
		3	-	27.8 (0.1)	33.2 (3.3)	-
	SiC	0	-	26.6 (2.3)	30.7 (2)	-
		1	-	25.6 (2)	29.2 (5.3)	-
		2	-	23.6 (0.3)	30.6 (3.7)	-
		3	-	20.6 (8.7)	28.9 (7.4)	-

3.3 Interlayer bond strength

The results of the interlayer bond strength (IBS) tests are depicted in Table 5. It is determined that the IBS test results are all lower than the conventional flexure strength test results. Typical failure encountered for this test is depicted in Figure 3. Although the layers seem homogenous on the sawed section, it is believed that the outer lubrication layer of the extruded filament, which is mainly comprised of colloidal particles, holds them together. Hence, the layers do not become fully homogenous, creating weak planes between layers. Cold joints can also form at longer printing times. Therefore, it is theorised that enhanced thixotropy, especially R_{thix} , via nanomaterial addition could prove significant to enhance the IBS of 3D printed elements.

A 19% reduction in flexural strength is obtained with the reference concrete mix for the IBS compared to the conventional prism test. As noted in Figure 3b, failure mainly occurred at the narrowest section and between filament layers. With 2% SiC and an increased R_{thix} (refer to Table 3), only a 6.6% reduction in flexural strength is observed. Interestingly, the conventional concrete flexural strength of the reference mix is stronger than that of the 2% SiC mix. However, the 2% SiC yielded larger IBS results than that of the reference mix. This indicates that although the bulk concrete of the reference mix is stronger than the 2% SiC mix, the interlayer strength of the layers limit flexural capacity of 3D printed elements. Consequently, enhanced thixotropy increases layer strength and yields less reduction in flexural strength of printed elements compared to the less thixotropic reference mix. This observation is consistent with the SiO₂ IBS, however to a lesser degree than that of the SiC IBS.

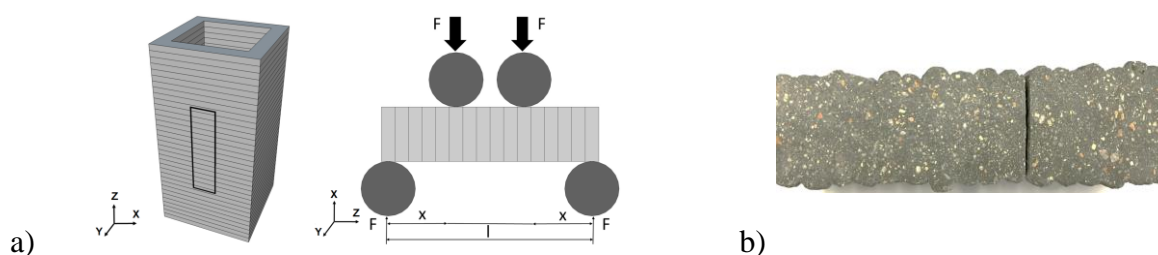


Figure 3: a) IBS specimen cut from 3DP square hollow section and loaded at third points; b) typical failure of the IBS tests.

Table 5: Interlayer bond strength of 3D printed filament layers with CoV in brackets.

Concrete Mix	IBS (MPa)	Conventional Flexure (MPa)	% Reduction
0% (ref.)	6.8 (2.1)	8.4 (5.7)	19
1% SiO ₂	7 (2.3)	8.1 (13.9)	13.6
2% SiC	7.1 (7.1)	7.6 (4)	6.6

4. CONCLUSIONS

Limited research has been performed to characterise the rheology and mechanical properties of HPC used for 3DPC. In order to enhance the printability and buildability, while retaining the properties of a HPC, silicon carbide (SiC) and silica (SiO₂) nanoparticles are added to the HPC in 1, 2 and 3% increments. Rheology is depicted by means of novel static yield shear stress evolution curves. 1% SiO₂ addition yields the most appropriate static yield

shear stress increase for 3DPC, while 1% SiC addition yields the largest increase in thixotropy, characterised by R_{thix} and A_{thix} respectively. Furthermore, 1% SiO₂ yields almost a 100% increase in compressive and flexural strength compared to the reference mix after 1 day of curing. In the long term (56 days) SiC addition increases compressive and flexural strength while SiO₂ decreases these strengths. Lastly, an increase in thixotropy (especially R_{thix}) yields stronger IBS of 3D printed elements in flexure. 2% SiC addition results in a 6.6% reduction in flexure strength of 3D printed elements compared to the conventional flexure test strength.

ACKNOWLEDGEMENTS

This research is funded by The Concrete Institute (TCI) and the Department of Trade and Industry of South Africa under THRIP Research Grant TP14062772324.

REFERENCES

- [1] A.L. Huang, R.E. Chapman, D.T. Butry, Metrics and tools for measuring construction productivity: Technical and empirical considerations, U.S. Dep. Commer. Natl. Inst. Stand. Technol. (2009). www.nist.gov/publications/metrics-and-tools-measuring-construction-productivity-technical-and-empirical.
- [2] S.C. Paul, G.P.A.G. van Zijl, M.J. Tan, I. Gibson, A Review of 3D Concrete Printing Systems and Materials Properties : Current Status and Future Research Prospects, *Rapid Prototyp. J.* (2017). doi:10.1108/RPJ-09-2016-0154.
- [3] T.A.M. Salet, Z.Y. Ahmed, F.P. Bos, H.L.M. Laagland, Design of a 3D printed concrete bridge by testing, *Virtual Phys. Prototyp.* 13 (2018) 222–236. doi:10.1080/17452759.2018.1476064.
- [4] S. Panneerselvam, S. Choi, Nanoinformatics: Emerging databases and available tools, *Int. J. Mol. Sci.* 15 (2014) 7158–7182. doi:10.3390/ijms15057158.
- [5] A. Said, A. Ayad, M. Zeidan, Beneficial Use of Nano-Silica in Concrete : A Review, *Trends Civ. Eng. Mater. Sci.* (2018) 1–3.
- [6] A. Mahawish, S.I. Ibrahim, A.H. Jawad, F.M. Othman, Effect of Adding Silicon Carbide and Titanium Carbide Nanoparticles on the Performance of the Cement Pastes, *J. Civ. Environ. Eng.* 07 (2017). doi:10.4172/2165-784X.1000277.
- [7] L. Senff, J.A. Labrincha, V.M. Ferreira, D. Hotza, W.L. Repette, Effect of nano-silica on rheology and fresh properties of cement pastes and mortars, *Constr. Build. Mater.* 23 (2009) 2487–2491. doi:10.1016/j.conbuildmat.2009.02.005.
- [8] E. Garcia-Taengua, M. Sonebi, K. Hossian, M. Lachemi, J. Khatib, Effects of the addition of nanosilica on the rheology, hydration and development of the compressive strength of cement mortars., Leeds, 2015.
- [9] P.J. Kruger, S. Zeranka, G.P.A.G. van Zijl, An ab initio approach for thixotropic characterisation of nanoparticle-infused 3D printable concrete, (2019). IN REVIEW
- [10] M.A. Rashid, M.A. Mansur, Considerations in producing high strength concrete, *J. Civ. Eng.* 37 (2009) 53–63.
- [11] Nanostructured & Amorphous Materials, About Us, (n.d.). www.nanoamor.com/about_us (accessed July 24, 2018).
- [12] W.B. Fuller, S.E. Thompsom, The laws of proportioning concrete, *Trans. Am. Soc. Civ. Eng.* 57 (1907) 67–143. archive.org/details/transactionsofam59amer.
- [13] N. Roussel, A thixotropy model for fresh fluid concretes: Theory, validation and applications, *Cem. Concr. Res.* 36 (2006) 1797–1806. doi:10.1016/j.cemconres.2006.05.025.
- [14] AZOM, The Influence of Particle Size, Zeta Potential and Rheology on Suspension Stability, (2015) 1–8. <http://www.azom.com/article.aspx?ArticleID=10221>.

NEW GENERATION OF CONSTRUCTION MATERIALS
SESSION 14: AAMs for specific applications

LOWCOPRECON – LOW CARBON PRECAST CONCRETE PRODUCTS FOR AN ENERGY EFFICIENT BUILT ENVIRONMENT

T.E. McGrath (1), J. Kwansy (1), T. Aiken (1), S. Cox(1), M. Soutsos (1), J.F. Chen (1), J. Mariotti (1), R. Correia (2) and S. Toal (2).

(1) School of Natural & Built Environment, Queen’s University Belfast, Northern Ireland

(2) Creagh Concrete Ltd., Toomebridge, Northern Ireland.

ABSTRACT

The production of Portland cement is well acknowledged as having a significant impact on the environment, accounting for 8% of global CO₂ emissions (4bn tonnes per annum). Concrete is the most widely used material in the world and therefore has vast potential to absorb high volumes of waste and by-product materials. These materials can act as partial replacements, i.e. supplementary cementitious materials, or total replacements and be the cement-like precursors for geopolymer concretes.

The LowCoPreCon project brings together academic and industrial partners from the UK and Malaysia with the aim of identifying available waste streams with which to manufacture geopolymer concretes on a commercial scale.

Initial laboratory work was conducted by academic partners to design geopolymer concretes that had both optimum strength and workability. These mixes were then used in factory trials to successfully cast structural elements, including building blocks, wall slabs and staircases. To ensure commercial viability, the geopolymer concretes developed in the project will undergo rigorous testing to establish their long term durability and product specifications will be developed. To determine the potential environmental benefits of geopolymer concrete, a detailed life cycle assessment will be conducted. Two demonstration projects using the novel material will be constructed in Malaysia; a domestic building and a FlexiArch bridge.

Keywords: Geopolymer; Malaysia, circular economy, life cycle assessment, precast dwelling.

1. INTRODUCTION

In October 2014 EU Leaders agreed a target of 40% reduction in greenhouse gas (GHG) emissions by 2030 (based on 1990 levels) [1]. The Eleventh Malaysian plan has set the goal of reducing Malaysia’s GHG emission intensity of GDP by 40% (compared to 2005 levels) by 2020 [2]. These EU and Malaysian targets reflect the global commitment to reducing GHGs

manifested at COP21 in Paris. Portland cement production produces 5-8% of global CO₂ emissions and contributes significantly to the 40% of total GHGs attributed to the built environment [3]. Annual cement production in GB is in the region of 10 million tonnes and in Malaysia is over 20 million tonnes [4]. The environmental impact of cement is well acknowledged with significant emissions from three distinct areas; emissions produced as the raw materials are calcined at high temperatures to form clinker, emissions associated with fuel combustion in the cement kiln and the emissions associated with energy used to operate the cement plant [5].

The raw materials used in cement manufacture are rich in calcium carbonate and may be quarried from limestone, chalk or shale deposits. Depending on the location, the quarrying process involves the use of drilling, blasting, excavating and crushing [6]. The calcination process, which is responsible for approximately 50% of cement CO₂ emissions, requires the burning of the calcium carbonate, forming calcium oxide and carbon dioxide. So whilst there is potential to reduce environmental emissions associated with fuel and energy use, the nature of the calcination process means that potential reduction of the environmental impact of cement is constrained.

Alkali activated concrete (AAC) or geopolymer concrete has emerged as a promising alternative to traditional Portland cement based concrete. Geopolymer is an umbrella term which refers to a wide range of synthetic aluminosilicate polymeric materials. Geopolymer materials can be produced from a range of natural and synthetic pozzolanic binder materials, activated with alkaline solutions such as sodium hydroxide and sodium silicate. Geopolymers can act as “cementless” binders to replace Portland cement pastes in concrete products. Previous studies comparing geopolymer materials to cement have reported a reduction in CO₂ emissions of between 30[7] – 80% [8], with other studies finding values within this range [9][10].

The LowCoPreCon project aims to develop geopolymer products from locally available waste streams. The project is supported by the Newton-Ungku Omar Coordination Fund which facilitates innovative research between the UK and Malaysia. The work brings together industrial and academic partners and is jointly funded by Innovate UK and MIGHT (Malaysian Industry Government Group for High Technology). The project team consists of academic and industrial partners in both the UK and Malaysia. In the UK, Queen’s University is the project co-ordinator with industrial input provided by Creagh Concrete Ltd and Macrete Ltd. In Malaysia, University of Malaya and Monash University are the academic partners with industrial input provided by Sunway and Ikhmas Jaya Group Berhad. Each project partner is responsible for leading a minimum of one work package, providing their particular expertise and facilitating advancement of the project objectives. This paper will provide an overview and summary of the work that is being undertaken, from identification of suitable waste streams, laboratory and factory scale trials, and the planned demonstration projects using these novel materials.

2. WASTE STREAMS FOR GEOPOLYMER CONCRETE IN MALAYSIA AND THE UK

LowCoPreCon offers multiple simultaneous benefits; the construction industry is uniquely placed to be able to incorporate high-volumes of waste materials or by-products whilst at the same time developing concrete alternatives that have a lower economic and environmental cost. Whilst geopolymer concretes have been used in applications world-wide, the use of expensive

chemical activators has made their use cost prohibitive. The initial focus of the project was the identification and characterisation of suitable local waste alumina-silicate rich ash and alkali activator sources. Detailed microstructural characterisation was carried out to assess the suitability of these materials as geopolymer components.

Fly ash, (FA) is produced by power generating stations during the production of electricity using coal as the fuel. Finely powdered (pulverized) coal is mixed with heated air and burned. The resultant ash is transported by the exhaust gases and recovered as 'fly ash' with fine particles. Over 22Mt of coal is consumed annually in Malaysia providing a readily exploitable source of over 3Mt of FA. While FA is an established additive to cement and concrete manufacture, typically 2Mt of FA is still landfilled annually in the UK and there is an estimated 60Mt of FA stockpiled in the UK. These stockpiles of FA are usually stored in lagoons or ash ponds. Even in circumstances where these lagoons have liners, seepage, spills and overflows may be hazardous to the groundwater and subsurface soil.

Ground granulated blast-furnace slag (GGBS) is a by-product from the manufacturing of iron and steel and it is available in both the UK and Malaysia. In iron and steel production blast-furnaces are fed with carefully controlled mixtures of iron-ore, coke and limestone, with temperatures of about 1500°C. Once the metal has been separated from the ore the material that remains is referred to as slag. The slag is rapidly quenched in large quantities of water. The process of quenching improves the cementitious properties and produces granules similar to coarse sand particles. The 'granulated slag' is dried and ground to a fine powder that is called GGBS.

Whilst a number of alkali waste activator sources were investigated the most promising material identified in the UK was powdered glass cullet particles. According to the most recent waste statistics there was more than 2 million tonnes of glass waste produced in the UK, the majority of which came from household waste. Of this glass waste, the vast majority was recycled, with the remainder deposited in landfill or used as backfill. During the recycling process of the glass, the glass is broken down by impact crushers and sieved. Ultra-fine powdered glass cullet particles are gathered during the screening phase and cannot be reintroduced to the recycling process. As a result this material is usually landfilled. This material when combined with sodium hydroxide, using a thermochemical process, forms a powdered silicate source that can be used as the alkali activator in the geopolymer system. In Malaysia the silicate sources being investigated include rice husk ash (the ash residue after rice husk is burned) and coastal sand.

2. UK LABORATORY TRIALS

As part of the LowCoPreCon project, extensive laboratory trials were conducted using fly ash obtained from Kilroot Power Station in Northern Ireland, GGBS and the glass cullet (GC) based alkali activator. The alkali dosage (M+) used in the geopolymer concretes is defined as the percentage mass ratio of the total sodium oxide (Na₂O) in the activating solution to the binder. The alkali modulus (AM) is defined as the mass ratio of sodium oxide to silica in the activating solution. Initially the materials were trialled individually at a mortar level. In the case of the GC silicates the compressive strength values compared well with commercial silicates. For example, in a 60/40 FA/GGBS mortar (AM=1.0 and M+7.5) the GC silicates achieved a 28 day compressive strength values of 45MPa compared with 40MPa using commercial silicates.

Likewise the Kilroot fly ash was compared with a laboratory control fly ash (Drax) achieving comparable compressive strength values of up to 70MPa at 28 days with curing at 70°C.

To ensure a successful outcome for the factory trials, the required strength and workability properties were specified by Creagh. A high slump value after 30 minutes was required to ensure the mix did not set before batching, casting and finishing the products had been completed. Characteristic compressive strength values of between 40 - 50MPa after 28 days were required for the manufactured precast elements. Given the high volume nature of precast manufacturing, there was also an early age strength compressive strength of 15MPa after 16 hours, which allows for the product to be demoulded and lifted. Moving on from mortar mixes to concrete mixes a range of parameters were tested; including paste volume, water/solid ratio and M+/AM varied, to develop a mix that could achieve both the required workability and compressive strength needed in the industry setting. Similar laboratory trials are being undertaken in the University of Malaya and Monash University to facilitate Malaysian factory trials, that are due to commence in December, 2018.

3. GEOPOLYMER UK FACTORY TRIALS

In May and June 2018, factory scale trials using geopolymer concretes were successfully carried out by Creagh Concrete, Toomebridge. Overall 8 batches were manufactured and used to cast specimens such as walls, slabs, stairs and building blocks. Partner visits were scheduled to coincide with factory trials to ensure effective transfer of knowledge and sharing of best practice. For the precast elements two mixes were selected to progress onwards for the factory trials 100% FA and 30/70 FA and GGBS mix. The 100% FA products were activated with commercial silicates and the 30/70 FA/GGBS mix was activated using the GC silicates. To successfully manufacture the 100% FA mix a heated chamber was manufactured to provide elevated temperatures (up to 70°C) for curing the samples, as shown in Figure 1.



Figure 1. Curing chamber in use during manufacturing and specimens being demoulded during partner visits – May 2018

Both mixes were found to be sufficiently workable for the factory setting with the 30/70 FA/GGBS mixes having slump values of between 220 – 260mm and the 100% FA mixes having table flow values of between 720 – 750 mm after approximately 30 minutes.

Of crucial importance for any precast concrete product is the early age of 15MPa compressive strength which is needed to allow for lifting and demoulding of the specimen after

approximately 16 hours. The 30/70 FA/GGBS trialled on site, achieved an impressive 22MPa after 16 hours. After 28 days the 30/70 GA/GGBS blend achieved compressive strength values up to 48 MPa. Given that the 100% FA mix required elevated temperature that could not be fully guaranteed during the trial, it was decided to leave specimens for a full 24 hours before compression tests were carried out. After 24 hours, the samples achieved 18MPa. The 28 day compressive strength result was 29MPa. However, given that the 7 day compressive strength had measured at 34MPa the low result at 28 days may be due to a faulty cube. Some cracking was visible on the 100% FA mix panels which could possibly be linked to poor heat circulation within the chamber with a 15°C temperature differential between the top and bottom of the chamber.

For the block trials a 30/70 FA/GGBS mix was activated with commercial silicates. A conventional Portland cement (PC) mix was cast at the same time to act as a control mix. The first batch manufactured was too dry and while blocks were cast, they were not successful. For the next two batches, additional water was added. Two sets of blocks were cast from each batch. One set of each batch was covered with timber boxes (as shown in 2) and the other set remained uncovered. The blocks that remained uncovered had a higher level of efflorescence than the covered blocks as can be seen in Figure 2. Despite the efflorescence there is little difference between the compressive strength values of the covered vs. uncovered mixes. In Creagh, the target compressive strength for conventional concrete blocks is 3MPa at 4 days, to allow for strapping and moving blocks, and 7MPa strength at 28 days. Both mixes achieved above the minimum 4 day strength, whilst for the 28 day strength one mix achieved just below the requirement with 6MPa whilst the other mix achieved 10MPa.



Figure 2. Covered blocks (left) and uncovered blocks with signs of efflorescence (right)

4. DEMONSTRATION PROJECTS IN MALAYSIA

As well as the traditional approaches to dissemination including publication of findings in conferences proceedings and academic journals, a significant opportunity for publicising the work will be carried out via the two proposed demonstration projects. Macrete's FlexiArch bridge system will be used to construct a pedestrian bridge on the campus of University of Malaya in Kuala Lumpur in 2019. Sunway will be producing the bridge components using the geopolymer mixes developed at the University of Malaya and Monash University. Ikhmas Jaya Group Berhad will be carrying out the necessary geotechnical surveys, groundwork and constructing the bridge on the campus.

The second demonstration project is a low cost precast residential dwelling, again manufactured from the developed geopolymer mixes. The dwelling will be cast and constructed in a Sunway factory site in Batang Kali, Selangor. The demonstration dwelling will be externally insulated with panels made of a novel lightweight geopolymer foamed concrete material and finished with a geopolymer based rainscreen façade as shown in

Figure 3. These elements will improve the thermal insulation of the building envelope, leading to a reduction in electrical energy consumed for air-conditioning and ensuring comfort for the occupants. To assess these potential energy savings and occupancy comfort levels in the demonstration dwelling, dynamic energy simulation will be carried out using IES-VE – Integrated Environmental Solution - Virtual Environment.



Figure 3. Rainscreen façade elements cast with pigmented geopolymer concretes and a lightweight geopolymer foamed concrete sample made using a pre-formed foam technique, manufactured in Queen’s University Belfast

The “flat-pack” FlexiArch bridge and the precast structure of the dwelling are both novel methods of construction with benefits including speedy construction, excellent quality control of manufactured products and potential to scale for large applications. It is expected that there will be significant interest from a range of stakeholders including government, construction and professional bodies. The proposed demonstration projects are shown in Figure 4.

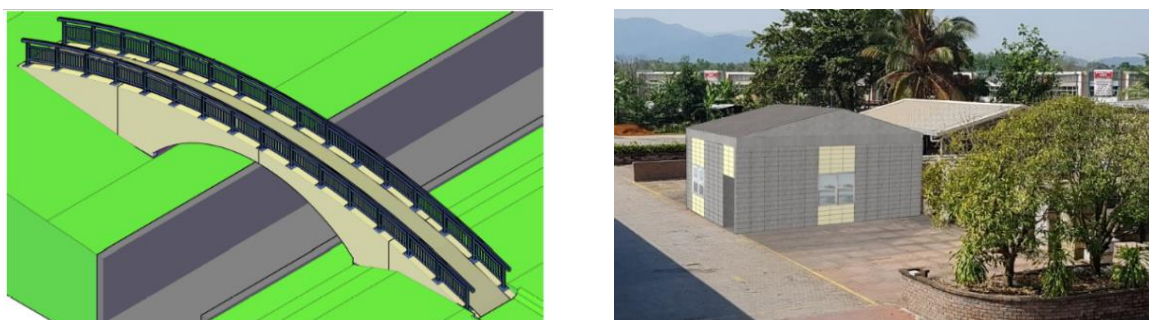


Figure 4. Demonstration projects – proposed FlexiArch design for University of Malaya Campus (left) and proposed precast demonstration dwelling in Sunway, Batang Kali, Selangor, Malaysia (right).

4. ASSESSING SUSTAINABILITY OF PRODUCTS THROUGH LIFE CYCLE ASSESMENT AND STAKEHOLDER ENGAGEMENT IN A MALAYSIAN CONTEXT

Life cycle assessment (LCA), internationally standardised through the ISO14040 [11] series, can be used to quantify and compare the environmental impacts of products or processes. All products or processes have various stages in their life cycle and during each of these stages, energy and resources are consumed and emissions to the environment and wastes are produced. In an LCA study the function of the product is taken into consideration to ensure a fair and accurate comparison between products. In the LowCoPreCon project the life cycle assessment methodology will be used to quantify and compare the environmental impact of FA precast concrete products utilised in the demonstration building and an equivalent PC residential building for a Malaysian context.

The system boundary, which outlines which stages of the product life cycle will be included in calculating the environmental impact, will be set to include a cradle to grave analysis. This will consider all impacts including those associated with extraction of raw materials, processing and manufacturing of the concrete, operating life such as maintenance/repairs, energy consumed and end-of-life scenarios, such as how the item will be disposed/reused/recycled. Primary data will be gathered during manufacturing of the geopolymer products in Malaysia and secondary data sources including SIRIM MY-LCID (Malaysia Life Cycle Inventory Database) will be used to complete the inventory analysis [12].

The socio-economic impact of the use of geopolymer materials and novel construction methods of the demonstration dwelling will be assessed through engagement with stakeholders pre- and post- construction. A variety of participatory workshops will generate outcomes that will help to facilitate adoption of these products in a wider market. The demonstration dwelling has been designed with flexibility of internal layout in mind. Focus groups will be organised with scale models of the demonstration dwelling and samples of geopolymer so that participants can interact and consult on potential design options and variations that would best suit their lifestyle and family needs.

5. CONCLUSIONS

Successful completion of large scale factory trials using a variety of waste materials to manufacture precast concrete units with geopolymer concrete have demonstrated the vast potential of this material to utilise substantial quantities of waste materials whilst potentially significantly reducing the carbon footprint of construction projects. Having successfully completed trials in the UK the next focus for the LowCoPreCon project is to investigate the long term durability of the geopolymer materials produced with tests examining the performance of the material, including sulphate resistance, freeze thaw and reinforcement corrosion. Similar laboratory trials are also being undertaken in Malaysia, with Malaysian factory trials due to commence in December 2018.

Concurrently, work is ongoing to collect inventory data to complete a detailed LCA of the demonstration dwelling to be constructed by Sunway in Malaysia and feedback is being gathered from participatory workshops in Malaysia to enhance understanding and improve prototyping of precast dwellings constructed from geopolymer concrete.

Upon completion of the project, two innovative demonstration projects will have been constructed in Malaysia with research disseminated amongst key stakeholders including academic, policy and construction audiences.

ACKNOWLEDGEMENTS

Authors gratefully acknowledge the funding provided for LowCoPreCon, Low Carbon Footprint Precast Concrete products for an energy efficient built environment, provided by the Newton-Ungku Omar Fund which is supported by Innovate UK and Malaysian Industry-Government Group for High Technology (MIGHT).

REFERENCES

- [1] European Commission, “EU leaders agree 2030 climate and energy goals,” *Climate Action News*, 2014. [Online]. Available: https://ec.europa.eu/clima/news/articles/news_2014102401_en.
- [2] P. M. D. The Economic Planning Unit, “Eleventh Malaysia Plan 2016-2020.” 2016.
- [3] J. L. Provis and J. S. J. Van Deventer, *Alkali activated materials*. Netherlands: Springer, 2014.
- [4] M. Department of Statistics, *Statistics yearbook of Malaysia*, 1st Editio., no. December. Putrajaya, Malaysia: Jabatan Perangkaan Malaysia, 2017.
- [5] P. Van Den Heede and N. De Belie, “Cement & Concrete Composites Environmental impact and life cycle assessment (LCA) of traditional and ‘ green ’ concretes : Literature review and theoretical calculations,” *Cem. Concr. Compos.*, vol. 34, no. 4, pp. 431–442, 2012.
- [6] M. Suhr *et al.*, *Best Available Techniques (BAT). Reference Document for the Production of Cement, Lime and Magnesium Oxide*. 2015.
- [7] B. Tempest, O. Sanusi, J. Gergely, V. Ogunro, and D. Weggel, “Compressive Strength and Embodied Energy Optimization of Fly Ash Based Geopolymer Concrete,” *2009 World Coal Ash Conf.*, pp. 1–17, 2009.
- [8] E. Von Weizsacker, K. Hargroves, M. Smith, C. Desha, and P. Stasinopoulos, *Factor Five: Transforming the Global Economy through 80% Improvements in Resource Productivity*. London: Earthscan/Routledge, 2009.
- [9] B. C. McLellan, R. P. Williams, J. Lay, A. Van Riessen, and G. D. Corder, “Costs and carbon emissions for geopolymer pastes in comparison to ordinary portland cement,” *J. Clean. Prod.*, vol. 19, no. 9–10, pp. 1080–1090, 2011.
- [10] D. Stengel, T., Reger, T., Heinz, “Life Cycle Assessment of Geopolymer Concrete – What is the Environmental Benefit?,” *CIA*.
- [11] BS EN ISO 14040, *Environmental Management - Life Cycle Assessment - Principles and Framework*, vol. 3. 2006.
- [12] SIRIM, “Malaysia Life Cycle Inventory Database,” 2018. [Online]. Available: <http://lcamalaysia.sirim.my/>. [Accessed: 23-Mar-2018].

IMPROVING MECHANICAL CHARACTERISTICS OF LIGHTWEIGHT GEOPOLYMERS THROUGH MECHANICAL ACTIVATION OF FLY ASH

Tijana G. Ivanović (1), Miroslav M. Komljenović (1), Nataša M. Džunuzović (1), Violeta M. Nikolić (1) and Gordana G. Tanasijević (1)

(1) Institute for Multidisciplinary Research, University of Belgrade, Serbia

Abstract

The present paper investigated the influence of mechanical activation of fly ash and various parameters, such as curing temperature and concentration of foaming agent (Al powder), on physical-mechanical characteristics of lightweight geopolymers. Prior to alkali activation, fly ash was mechanically activated in a high energy planetary ball mill. Lightweight geopolymers were obtained by mixing the mechanically activated fly ash with various amounts of Al powder and sodium silicate solution ($\text{SiO}_2/\text{Na}_2\text{O}$ mass ratio of 1.5). Geopolymer paste samples were cured covered in plastic either at room temperature for 28 days or at elevated temperature (95 °C) for 4 hours. It was observed that the mechanical activation of fly ash resulted in a drastic increase of geopolymer compressive strength regardless of curing conditions, preserving the lightweight properties at the same time. The lightweight geopolymers based on mechanically activated fly ash might be used both in constructive and insulating applications.

Key words: mechanical activation, lightweight geopolymers, compressive strength, aluminum powder

1. INTRODUCTION

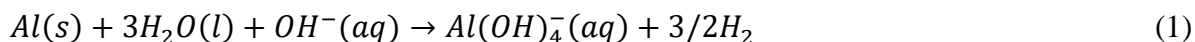
Alkali activated materials (AAMs) represent a group of inorganic binding materials, formed by chemical (alkali) activation of aluminosilicate and calcium silicate material with concentrated alkali activator solution. Research in the field of AAMs has shown that binding materials based on alkali-activated industrial waste materials and/or by products, such as fly ash (FA) from thermal power plants and blast furnace slag from pig iron production, have great potential especially in terms of valorization of different types of industrial waste materials and/or by product [1-3]. It is well known that these binding materials show properties comparable with the properties of commercial binders based on Ordinary Portland Cement (OPC) including good flexural and compressive strength, good durability in aggressive environments, high temperature resistance, etc. Therefore, the main application of

AAMs is in the industry of building materials, as an alternative for concrete and binders based on OPC. Depending on the selection of the initial materials and synthesis conditions, AAMs can show improved properties compared to binders based on OPC.

Lightweight geopolymers represent relatively new research field within research of alkali activated materials. For creating porosity during their synthesis various chemical (pore forming or foaming) agents such as aluminum (Al) powder [4-8] or hydrogen peroxide [9-14] can be used. Chemical agents react in an alkaline environment releasing the gases generating bubbles i.e. creating porous structure, whereby the materials with low density, low thermal conductivity and good high-temperature resistance are obtained. The advantage of lightweight geopolymers over conventional thermal insulating materials based on OPC primarily is in less detrimental environmental impact, i.e. industrial waste recycling and lower carbon dioxide emission. Reducing carbon dioxide emissions by using appropriately-selected materials is of critical importance. Besides that, according to some recently published research data [15, 16], lightweight geopolymers could show better properties comparing to conventional thermal insulating and high-temperature resistant materials.

Fly ash (FA) is generated as an industrial by product in the process of coal combustion in thermal power plants. The mechanical activation was proved to be quite successful method for FA reactivity improvement [17], as well as for enhancing the adsorptive properties of FA [18], the improvement of thermal stability of FA based geopolymers [19], and for the stabilization/solidification of hazardous waste [20]. The changes induced in material during the mechanical activation process include not only the obvious reduction of particle size, but also the changes in particle morphology, increase in specific surface area, structural defects, as well as the decrease in crystallinity degree, implying significant structural rearrangement [21, 22]. This paper investigated the influence of mechanical activation of fly ash and various synthesis parameters on physical-mechanical characteristics of lightweight geopolymers. The most important outcome of the use of mechanically activated fly ash for the geopolymer synthesis was the increase of FA reactivity and consequently the improvement of mechanical strength of ensuing geopolymers [17].

For lightweight geopolymers synthesis aluminum powder was used as a foaming agent. Chemical foaming agents react in an alkaline environment releasing the gases generating bubbles i.e. creating porous structure, whereby the materials with low density and low thermal conductivity were obtained. Regarding the reactive metal powders, these react with water and hydroxide in an alkaline environment, liberating bubbles of hydrogen and forming hydrolyzed metal complexes [23]. This reaction takes place according to the following equation:



The H_2 gas produced leads to expansion of the paste, provided the latter possesses a suitable consistency to entrap it.

2. MATERIALS AND METHODS

2.1 Materials

Fly ash from Serbian thermal power plant “Nikola Tesla”, Unit B, Obrenovac, was used as a solid precursor (as-received FA). FA sample used in this study belongs to the ASTM

Class F [24]. Sodium silicate solution (so-called water glass) was used as an alkaline activator (“Galenika-Magmasil”, Serbia: 26.25 % SiO₂, 13.60 % Na₂O, 60.15 % H₂O). Modulus (n) of sodium silicate solution (SiO₂/Na₂O mass ratio) was modified by adding NaOH (VWR, Germany, p.a. 99 %).

2.1.1 Mechanical activation of fly ash

Mechanical activation of fly ash was carried out in planetary ball mill (Fritch Pulverisette type 05 102, Germany). The diameter size of stainless steel balls was 13 mm, while the FA to ball mass ratio was 1:20, according to the previously optimized procedure [25]. FA samples were mechanically activated in an air atmosphere for 15 min, at maximum speed of 380 rpm.

2.1.2 Lightweight geopolymer synthesis

Lightweight geopolymer pastes were prepared by adding the activator solution to water and then mixing the solution with FA or MFA and aluminum powder for 2 minutes. Modulus of sodium silicate solution used as alkaline activator in this study was 1.5, while the concentration of the activator was 10% of Na₂O with respect to the dry FA or MFA mass. These values of modulus and concentration were selected as optimum values for alkali activation reaction, based on our previous research [26]. Various amount of Al powder was used (0.1 % or 0.5 % with respect to the FA or MFA mass). Dimensions of the paste samples were approximately 160×40×40 mm and the samples were cured covered in plastic either at room temperature for 28 days or at elevated temperature (95 °C) for 4 hours.

2.2 Methods

The compressive and flexural strength of the geopolymer pastes were tested according to the SRPS EN 196–1 standard, using “Controls-Advantest 9” (Italy).

The water absorption test was also carried out in this study. Principally, the test consists of two major steps. First, the geopolymers specimens are immersed in water until the change in mass during 24 hours is less than 0.1 %. The obtained saturated mass is called M_s . Afterwards; the specimens are dried in a ventilated oven at a temperature of 105 °C until the difference in mass during 24 hours is less than 0.1 %. The dry mass is called M_D . The water absorption by immersion (W) is expressed as the water uptake relative to the dry mass:

$$W = [(M_s - M_D)/M_D] * 100 \quad (2)$$

3. RESULTS

3.1 The influence of mechanical activation of FA and concentration of foaming agent on mechanical strength and density of geopolymers

The mechanical activation can drastically enhance the FA reactivity in the process of geopolymerization, which was previously established by the exceptional increase of compressive strength of geopolymers based on mechanically activated FA [17]. The results presented here are confirming the previous findings.

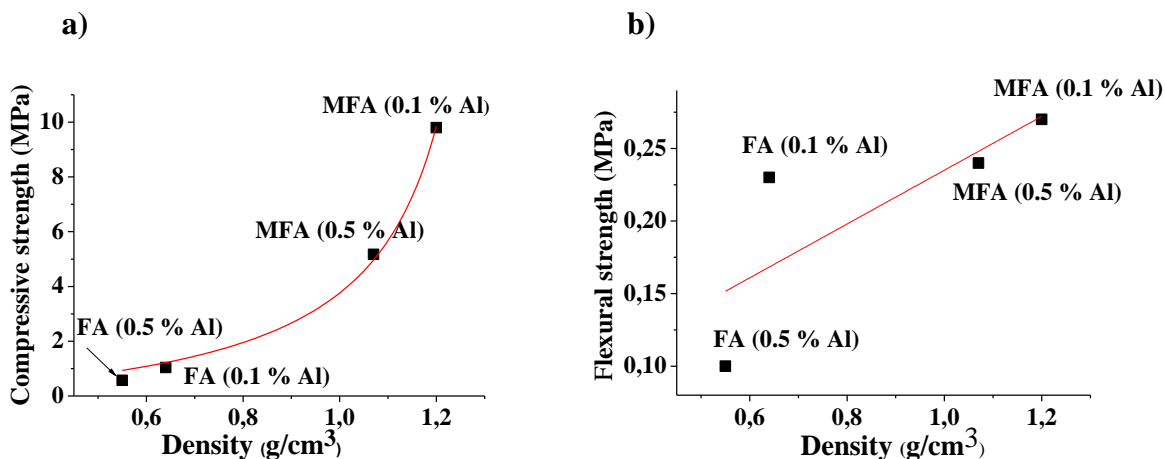


Figure 1: Correlation of FA and MFA-based lightweight geopolymers strength and density: a) compressive strength and b) flexural strength.

The mechanical strength of lightweight geopolymers based on as-received FA after curing at 95 °C for 4 h, was very low in all cases (Figures 1a and b). In sharp contrast to that, the compressive strength of geopolymers based on MFA (developed under the same curing conditions), increased 8 fold when the content of Al powder was 0.1 %. In the case of 0.5 % of Al powder added, the MFA-based geopolymer samples showed both higher density and compressive strength (increased 5 fold), compared to the lightweight geopolymers based on as-received FA.

3.2 The influence of mechanical activation of FA and concentration of foaming agent on water absorption of geopolymers

The results of water absorption by immersion of FA and MFA-based lightweight geopolymers are shown in Figure 3. The lowest water absorption by immersion (8.3 %) was noticed for the sample FA (0.1% Al), while the highest water absorption (47.7 %) was for the sample MFA (0.5% Al). As it can be seen in Figure 2, the mechanical activation had a significant influence both on density and water absorption of lightweight FA-based geopolymers. On the other hand, the concentration of Al powder added also had an effect on the water absorption of lightweight geopolymers i.e. the higher concentration of Al powder added is connected with the higher water absorption of lightweight geopolymers, which is in an agreement with the published data [4 - 8]. This effect was more pronounced in the case of MFA.

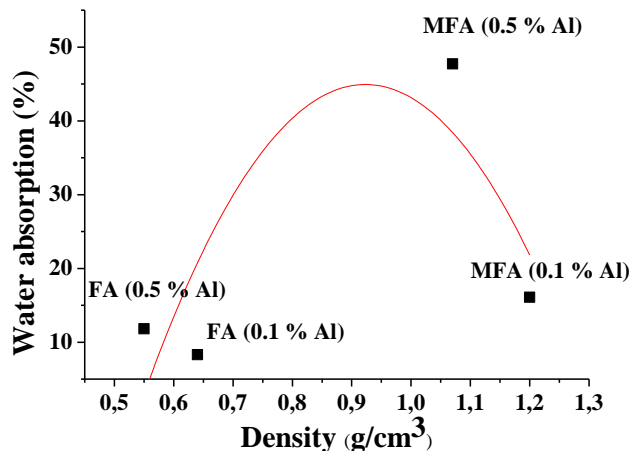


Figure 2: Water absorption of FA and MFA-based lightweight geopolymers versus density.

3.3. Prediction of thermal conductivity of mechanically activated geopolymers

As it can be seen from the literature data given in Figure 3, the thermal conductivity of AAMs can be correlated with the materials' density [12, 13, 16, 27 - 30].

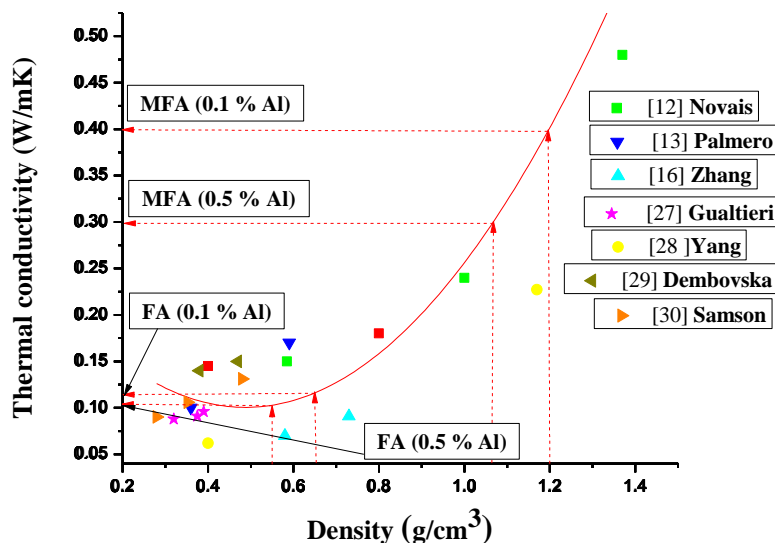


Figure 3: Thermal conductivity versus density of lightweight geopolymers (literature data).

According to the literature data given in Figure 3 and in agreement with the low densities reached, the as-received FA-based lightweight geopolymers produced most probably possess low thermal conductivity (0.10-0.12 W/mK). On the other hand, it is estimated that the values of thermal conductivity of mechanically activated FA-based lightweight geopolymers might be approximately 0.40 W/mK for MFA (0.1 % Al) and 0.30 W/mK for MFA (0.5 % Al) samples. It is also possible to further optimize the thermal conductivity of FA-based lightweight geopolymers, for example by mixing the MFA and as-received FA. This mixing

will lead to density and strength reduction of geopolymers in comparison to the MFA-based lightweight geopolymers, as well as to lower thermal conductivity.

3.4. The influence of concentration of foaming agent and curing conditions on physical-mechanical characteristics of MFA-based geopolymers

Both mechanical strength and density are crucial properties for application of lightweight building materials in constructions, either as porous building blocks or insulating materials. The mechanical strength of lightweight geopolymers was directly affected by the amount of foaming agent. The compressive strength of samples cured for 4 h at 95 °C decreased from 9.80 MPa down to 5.16 MPa when Al content increased from 0.1 to 0.5 mass %. The compressive strength of samples cured for 28 days at 20 °C decreased from 6.14 MPa down to 5.45 MPa when Al content increased from 0.1 to 0.5 mass%. This trend could be directly translated into a relation between density and compressive strength, as presented in Figure 4.

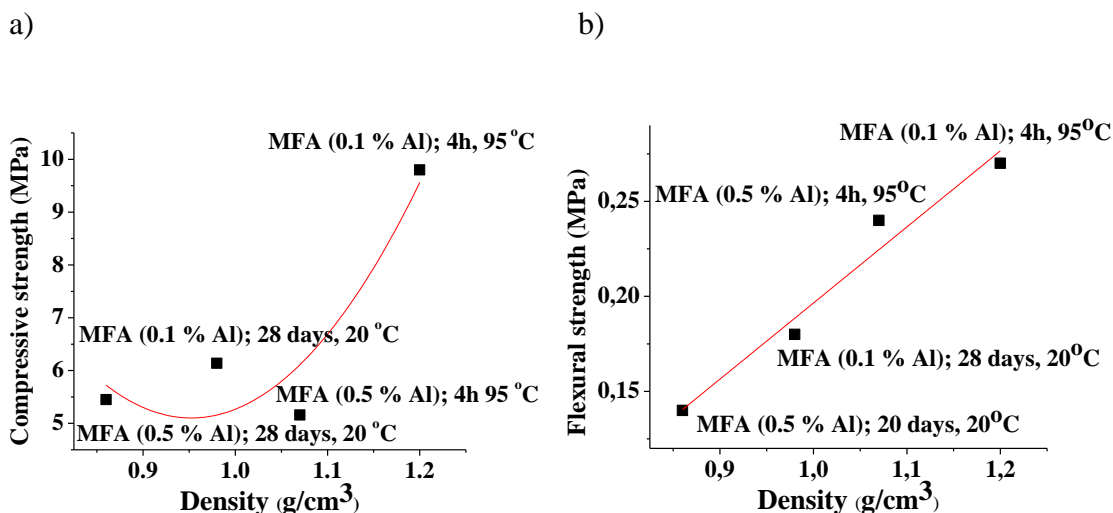


Figure 4: Strength of MFA-based lightweight geopolymers versus density for different curing conditions and Al concentrations: a) compressive strength and b) flexural strength.

As presented above, the sample MFA with 0.1 % of Al powder cured for 4 h at 95 °C showed a higher density (22.4 %), but also 60 % higher compressive strength compared to the sample MFA with 0.1 % of Al powder cured for 28 days at 20 °C. Curing conditions had a significantly lower impact for the samples with higher content of Al powder (0.5 %). In that case the sample MFA cured 4 h at 95 °C showed a higher density (24.4 %), and slightly higher compressive strength (5.62 %) compared to the sample MFA cured 28 days at 20 °C.

4. CONCLUSION

Lightweight geopolymers were synthesized by alkali activation of as-received fly ash (FA) and mechanically activated fly ash (MFA), with addition of various amounts of foaming agent (Al powder), and under different curing conditions (at room and at elevated temperature).

Mechanical activation of fly ash resulted in a significant improvement of mechanical properties of synthesized geopolymers. Presented results demonstrated that the mechanical

activation of fly ash had a major effect on the compressive strength and density of synthesized lightweight geopolymers, whereby their flexural strength was less influenced. It can be concluded that mechanical activation significantly enhanced FA reactivity in the process of geopolymerization.

On the other hand, the density of the lightweight geopolymers, and consequently the thermal conductivity, is strongly influenced by the dosage of Al powder in all cases. The effects of Al powder strongly depended on the curing conditions. The amount of Al powder had a major effect on the compressive strength of lightweight geopolymers when they were cured at elevated temperature (4h at 90 °C) and minor effect when they were cured at room temperature (28 days at 20 °C).

ACKNOWLEDGEMENT

This work was carried out within the projects TR34026, financed by the Ministry of Education, Science and Technological Development of the Republic of Serbia and SPS 985402 funded by the NATO Science for Peace and Security (SPS) Programme.

REFERENCES

- [1] Pacheco-Torgal, F., Labrincha, J.A., Leonelli, C., Palomo and A., Chindaprasirt, P., (Editors), *Handbook of Alkali-activated Cements, Mortars and Concretes*, Woodhead Publishing Series in Civil and Structural Engineering, 2014.
- [2] Duxson, P., Provis, J.L., 'Designing precursors for Geopolymer Cements', *J. American Ceram. Soc.* 91 (2008) 3864-3869.
- [3] Shi, C., Fernandez-Jimenez, A., Palomo, A., 'New cements for the 21st century: The pursuit of an alternative to Portland cement', *Cem. Concr. Res.* 41, (2011) 750-763
- [4] Ducman, V., Korat, L., 'Characterization of geopolymer fly-ash based foams obtained with the addition of Al powder or H₂O₂ as foaming agents', *Mater. Charact.* 113 (2016) 207-213.
- [5] Sanjayan, J., Nazari, A., Chen, L., Nguyen, G., 'Physical and mechanical properties of lightweight aerated geopolymer', *Constr. Build. Mater.* 79 (2015) 236-244.
- [6] Hlavaček, P., 'Inorganic foams made from alkali-activated fly ash, 'Mechanical, chemical and physical properties', *J. Europ. Ceram. Soc.* 35 (2015) 703-709.
- [7] Masi, G., Rickard, W., Vickers, L., Bignozzi, M.C., Riessen, A., 'A comparison between different foaming methods for the synthesis of light weight geopolymers', *Ceram. Int.* 40 (2014) 13891–13902.
- [8] Kamseu, E., Nait-Ali, B., Bignozzi, M.C., Leonelli, C., Rossignol, S., Smith, D.S., 'Bulk composition and microstructure dependence of effective thermal conductivity of porous inorganic polymer cements', *J. Europ. Ceram. Soc.* 32 (2012) 1593–1603.
- [9] Vaou, V., Pnias, D., 'Thermal insulating foamy geopolymers from perlite', *Min. Eng.* 23 (2010) 1146-1151.
- [10] Bay, C., Franchin, G., Elsayed, H., Conte, A., Colombo, P., 'High strength metakaolin-based geopolymer foams with variable macroporous structure', *J. Europ. Ceram. Soc.* 36 (2016) 4243–4249.
- [11] Novais, R., Ascensão, G., Seabra, M.P., Labrincha, J.A., 'Waste glass from end-of-life fluorescent lamps as raw material in geopolymers', *Waste Manage.* 52 (2016) 245–255.
- [12] Novais, R., Buruberri, L.H., Ascensão, G., Seabra, M.P., 'Labrincha, J.A., "Porous biomass fly ash-based geopolymers with tailored thermal conductivity', *J. Clean. Product.* 119 (2016) 99-107.
- [13] Palmero, P., Formia, A., Antonaci, P., Brini, S. and Tulliani, J., 'Geopolymer technology for application-oriented dense and lightened materials. Elaboration and characterization', *Ceram. Int.* 41 (2015) 12967–12979.

- [14] Cilla, M., Morelli, M., Pcolombo, 'Open cell geopolymer foams by a novel saponification/peroxide/gelcasting combined route', *J. Europ. Ceram. Soc.* 34 (2014) 3133–3137.
- [15] Zhang Z., Provis J., Reid A., Wang H., 'Geopolymer foam concrete: An emerging material for sustainable construction', *Construction and Building Materials* 56 (2014) 113–127.
- [16] Zhang, Z., Provis, J., Reid, A., Wang, H., 'Mechanical, thermal insulation, thermal resistance and acoustic absorption properties of geopolymer foam concrete', *Cem. Concr. Comp.* 62 (2015) 97–105.
- [17] Marjanović, N., Komljenović M., Baščarević Z., Nikolic, V., 'Improving reactivity of fly ash and properties of ensuing geopolymers through mechanical activation', *Constr. Build. Mater.* 57 (2014) 151–162.
- [18] Stellacci, P., Liberti, L., Hotarnicola, M., Bishop, P.L., 'Valorization of coal fly ash by mechanochemical activation. Part I: Enhancing adsorption capacity', *Chem. Eng. J.* 149 (2009) 11–18.
- [19] Babu Rao, J., Harayanaswami, P. and Prasad, S. K., 'Thermal stability of nano structured fly ash synthesized by high energy ball milling', *Int. J. Eng. Sci. Technol.* 2 (2010) 284–299.
- [20] Stellacci, P., Liberti, L., Hotarnicola, M., Bishop, P.L., 'Valorization of coal fly ash by mechanochemical activation. Part II: Enhancing pozzolanic reactivity', *Chem. Eng. J.* 149 (2009) 19–24.
- [21] Fernandez-Bertran JF., 'Mechanochemistry: an overview', *Pure Appl Chem*, 71 (1999) 581–6.
- [22] Zhang Q, Saito F., 'A review on mechanochemical synthesis of functional materials', *Adv Powder Technol* 23 (2012) 523–31.
- [23] Shi, Z., et al., Geopolymer foam concrete, 'An emerging material for sustainable construction', *Constr. Build. Mater.* 56 (2014) 113-127.
- [24] ASTM C618–12a Standard Specification for Coal Fly Ash and Raw or Calcined Natural Pozzolan for Use in Concrete.
- [25] Zdujić, M., Jovalekić, Č., Karanović, Lj., Mitrić, M., Poleti, D. and Skala, D., 'Mechanochemical treatment of α -Fe₂O₃ powder in air atmosphere'. *Mater. Sci. Eng.* 245 (1998) 109–117.
- [26] Komljenović, M., Baščarević, Z., Bradić, V., 'Mechanical and microstructural properties of alkali-activated fly ash geopolymers', *J. Hazard. Mater.* 181 (2010) 35–42.
- [27] Gualtieri, M., Romagnoli, M., Gualtieri, A.F., 'Preparation of phosphoric acid based geopolymer foams using limestone as pore forming agent – thermal properties by in situ XRPD and rietveld refinements', *J. Eur. Ceram. Soc.* 35 (2015) 3167–3178.
- [28] Yang, K.H., Lee, K.H., Song, J.K., Gong, M.H., 'Properties and sustainability of alkali-activated slag foamed concrete', *J. Clean. Product.* 68 (2014) 226-233.
- [29] Dembovska, L., Bajare, D., Ducman, V., Korat, L., Bumanis, G., 'The use of different by-products in the production of lightweight alkali activated building materials', *Constr. Build. Mater.* 135 (2017) 315–322.
- [30] Samson, G., Cyr, M., Gao, X., 'Thermomechanical performance of blended metakaolin-GGBS alkali-activated foam concrete', *Constr. Build. Mater.* 157 (2017) 982–993.

PRELIMINARY STUDIES ON BROWN COAL FLY ASH AS A CEMENT REPLACEMENT FOR GEOPOLYMER BRICK APPLICATIONS

Muhamed Khodr (1), David Law (1), Chamila Gunasekara (1) and Sujeeva Setunge (1)

(1) School of Engineering, RMIT University, Australia

Abstract

The continued use of Portland Cement (PC) as the main binder in concrete has raised economic and environmental concerns due to PC production being a pivotal contributor to the growing CO₂ emissions. Thus, research into alternatives using industrial by-products has become well established in recent years, with much attention being focussed on Ground Granulated Blast Furnace (GGBS) and Fly Ash (FA). The studies have shown that 100% Class F FA concrete can produce similar strengths to that achieved by from PC concrete, but unlike Class F FA, Brown Coal Fly Ash (BC FA) has high Sulphur and Calcium content and low aluminosilicate content which are detrimental to the strength that can be achieved. However, the opportunity may exist to use BC FA as a geopolymeric material for low strength application such as geopolymer concrete bricks. This paper reports a preliminary study conducted to investigate the feasibility of using Yallourn BC FA for geopolymer concrete brick production. The physical and chemical characteristics of the BC FA have been identified, and an optimum mix design has been generated by varying both the activator modulus (AM) and the Na₂O dosage. Compressive strength results were obtained at 7, 14 and 28 day intervals. Moreover, a standard flow table test was conducted for each mix design to understand the impact of flowability of this new material, which is essential in concrete casting.

Keywords: Brick, Brown-Coal-Fly-Ash, Compressive-strength. Flowability, Environmental-friendly-material, Geopolymer, Mix-design optimisation

1. INTRODUCTION

Cement production is linked to environmental issues such as high carbon emissions and substantial energy consumption. It had been forecast that cement production worldwide was expected to increase from 2.54 to 4.38 billion tonnes annually from 2006 to 2050, but according to Schneider et al. [1] the projected levels have already been surpassed with current production reaching 4.6 billion tonnes of cement. An alternative to cement are alkali activated materials

(AAM). As 100% FA based AAM (geopolymers) require heating, not all concrete application can be readily manufactured. Thus, concrete brick production has been identified as a suitable application. Geopolymer concrete bricks would produce less energy and carbon output than standard concrete bricks. Much research undertaken on geopolymer concrete has been centred around Class F FA, due to its high aluminosilicate content. In contrast, there has been little research on BC FA in the last decade [2-4], though past research has shown that BC FA has the ability to produce geopolymer concrete with strengths that meet the standards. However, it has also shown strengths can vary significantly, with values reported in the range from 5-40 MPa. However, concrete bricks require lower compressive strengths that range from 5-20 MPa, allowing it to be a suitable pathway into geopolymeric application.

This research addresses the physical and chemical properties of BC FA taken from a storage pond and dump at the Yallourn power plant located in the Latrobe Valley, Victoria, Australia, as well as the optimisation process for geopolymer mortar mix design. This was examined by manipulating the Activator Modulus (AM) while maintaining a fixed Na₂O dosage for the mix designs. The compressive strengths data were obtained at 7, 14 and 28 day periods. Furthermore, a standard flow table test was conducted to understand the relationship between flow and compressive strength.

2. MIX PROPORTIONS, CASTING, AND TESTING

2.1 Material selection

An initial visit to the Yallourn power plant provided BC FA from two different locations, Y1 being from a storage pond, whereas Y2 was from a storage dump. It is understood that Y2 is a material that has undergone storage in the pond and been removed to a dry location on land. To determine the chemical composition X-ray fluorescence (XRF) was carried out on the source materials, Table 1. The particle size distribution was determined with the use of a Malvern particle size analyser (Mastersizer 3000), Table 2. X-ray diffraction (XRD) analysis was undertaken on a Bruker AXS D4 endeavour wide angle X-ray diffractometer with the copper anode at 40 Kv and 35 mA to determine the amorphous and crystalline content.

The aggregate utilised for the mixtures was normal river sand with a specific gravity of 2.5 and a fineness modulus of 3.0. The makeup of the alkali activators comprised sodium silicate (Na₂SiO₃) solution and 15M sodium hydroxide (NaOH) solution. The alkali modulus of the sodium silicate solution was 2 (Na₂O of 14.7% and SiO₂ of 29.4% by weight), whereas the sodium hydroxide solution made up a total of 32.89% NaOH and 67.11% water.

Table 1– Chemical compositions of Loy Yang BC FA

FA	Weight (%)												
	SiO ₂	Al ₂ O ₂	Fe ₂ O ₃	Na ₂ O	MgO	CaO	TiO ₂	P ₂ O ₅	K ₂ O	SO ₃	BaO	MnO	LOI
Y1	4.68	5.58	45.10	0.00	13.72	7.75	0.27	0.32	0.15	1.46	1.06	0.56	19.08
Y2	4.32	2.05	45.29	0.00	12.57	8.88	0.12	0.36	0.10	3.56	0.98	0.50	20.81

Table 2– Particle size distribution of fly ash

F A	Passing Size (%)										
	10μ m	20μ m	30μ m	40μ m	45μ m	50μ m	60μ m	70μ m	80μ m	90μ m	100μ m
Y1	36.25	53.28	64.46	71.52	74.7	77.55	82.14	83.87	85.27	92.39	98.32
Y2	44.99	64.4	76.17	82.95	85.85	88.4	92.42	93.92	95.12	96.07	99.08

2.2 Mix design proportioning

The optimisation of the mix design was based on a previous study by Dirgantara et al. [3], that utilised BC FA gathered from the precipitators of the Yallourn power plant. The optimal mix suggested states that the highest strength achieved was with an activator modulus of 1.56. Further modifications were applied to the optimal mix design to understand the influence that varying AM has on the strength. The AM is the proportion of SiO₂ to Na₂O in the alkaline activator solution and the Na₂O dosage is determined as the proportion of Na₂O in the alkaline activator solution to the mass of the FA [5]. To keep consistent mixes, the Na₂O dosage has been taken as 30% as this had proved to be the optimal dosage in previous work completed on Yallourn BC FA [3]. The ratio between the sodium silicate and sodium hydroxide allow for the AM to be modified. In this study, the AM is varied from 1 to 1.9 by mixing the activator solutions in different proportions, Table 3 and Table 4.

Table 3– Mix design proportions for material Y1 BC FA geopolymer mortar

Geopolymer Mix Design	Related AM	Mass ratio of materials per m ³ (kg)					Water / Solid
		FA	Sand	Water	Activator Solution		
					Na ₂ SiO ₃	NaOH	
Y1-1	1	263	1535.7	19	268.7	120.1	0.57
Y1-2	1.25	263	1535.7	10.5	335.9	90	0.57
Y1-3	1.56	263	1535.7	0	418.9	53	0.57
Y1-4	1.75	263	1535.7	0	470.3	30.1	0.58
Y1-5	1.9	263	1535.7	0	510.6	12	0.59

Table 4– Mix design proportions for material Y2 BC FA geopolymer mortar

Geopolymer Mix Design	Related AM	Mass ratio of materials per m ³ (kg)					Water / Solid
		FA	Sand	Water	Activator Solution		
					Na ₂ SiO ₃	NaOH	
Y2-1	1	263	1535.7	19	268.7	120.1	0.57
Y2-2	1.25	263	1535.7	10.5	335.9	90	0.57
Y2-3	1.56	263	1535.7	0	418.9	53	0.57
Y2-4	1.75	263	1535.7	0	470.3	30.1	0.58
Y2-5	1.9	263	1535.7	0	510.6	12	0.59

The FA to sand ratio is kept consistent at 1:5.83. The Water to Solid ratio ranges from 0.57-0.59, the increase in the ratio is due to the increasing water mass located within the sodium

silicate solution. The water content is defined as the total amount of liquid comprised within the sodium silicate, sodium hydroxide and added water, whereas the solid content is defined as the total solids comprised within the activator solutions and mass of the FA [6].

2.3 Mixing, casting and testing of specimens

The BC FA was dried in an oven at 80° degrees C for 24 hours and removed to cool down at ambient temperature. From previous studies, it is understood that 80% of the particle size required to achieve good strength should be 45 µm or less, however, due to commercial consideration and low strength requirements for brick production 80% at 75 µm was adopted [7]. As the particle size required for this mix is needed to pass through 75 µm, a ball grinding mill was used to crush the material to the required limit. Mixing was performed using a 5 litre Hobart mixer. The dry materials, BC FA and sand were initially mixed for 5 minutes at 150 revs/min, while the activator solutions and added water were pre-mixed by hand to allow the liquids to combine systematically. The activating solution was then added to the solids and blended by hand for 2 minutes. The resultant mixture was then stirred at two speeds 150 and 300 revs/min for 4 and 2 minutes respectively. A flow table test was performed for each mix design as per the ASTM C1437, the results are reported in Table 5. The percentage of flow is defined as the displacement of the mortar material after undergoing tampering. The percentage is calculated as the change in base diameter over the initial base diameter [8]. This was followed by the mortar mix being placed in 50 mm cubic Teflon moulds and compacted with two-layer placing and tamping, then vibrated for 20 seconds for each layer on a vibrating table. The moulds were then placed to cure at ambient temperature for 24 hours followed by oven curing at 120° for 24 hours. The curing temperature adopted is based on previous research that showed 120° as being the optimal curing temperature for BC FA [9]. After the oven curing phase was completed, the moulds were taken from the oven and stored at ambient temperature to cool down for 4 hours. The mortar samples were then removed from the Teflon moulds and kept at ambient temperature until tested at 7, 14, 28 days. The compressive strength test was undertaken in accordance with the ASTM C109/C109M standards [10]. A total of 4 specimens were tested at each interval, thus comprising of 12 specimens per mix at a loading rate of 0.34 N/mm²/S on Tecnotest concrete testing machine. The specimens were tested until failure.

Table 5– Flowability of geopolymer mix - Y1 and Y2

Geopolymer Mix Design	Y1-1	Y1-2	Y1-3	Y1-4	Y1-5	Y2-1	Y2-2	Y2-3	Y2-4	Y2-5
Avg. Diam (cm)	110	120	120	147.5	148.8	125	136	140	142.5	150
Flow (%)	10	20	20	48	49	25	36	40	43	50

3. RESULTS AND DISCUSSION

The mean compressive strengths and standard deviations (SD) of the different mix designs for material BC FA Y1 and Y2 are shown in Figure 1. In relation to the results obtained with the use of material Y1, the strengths reached a maximum mean strength of 7.59 MPa, mix Y1-4 at 7 days and a minimum mean strength of 1.74 MPa, mix Y1-2 at 28 days. Whereas the strengths obtained by material Y2 ranged from 2.38 MPa, mix Y2-2 at 14 days to 12.32 MPa,

mix Y2-5 at 14 days. The strengths acquired are similar to strengths obtained from mortar specimens with Yallourn precipitator ash [11], indicating that there is no significant variation in strengths from different material gathered within the same power plant. This would indicate that material obtained from the Yallourn power plant can yield stable strengths if optimised.

The strengths themselves are significantly lower than the minimum requirement (25 MPa) for structural concrete [12], this is attributed to the low SiO_2 , Al_2O_3 and high Fe_2O_3 . A similar composition was observed for the Hazelwood power plant in the same location, but considerably different to the Loy yang power plant also in the La Trobe Valley, Victoria [11].

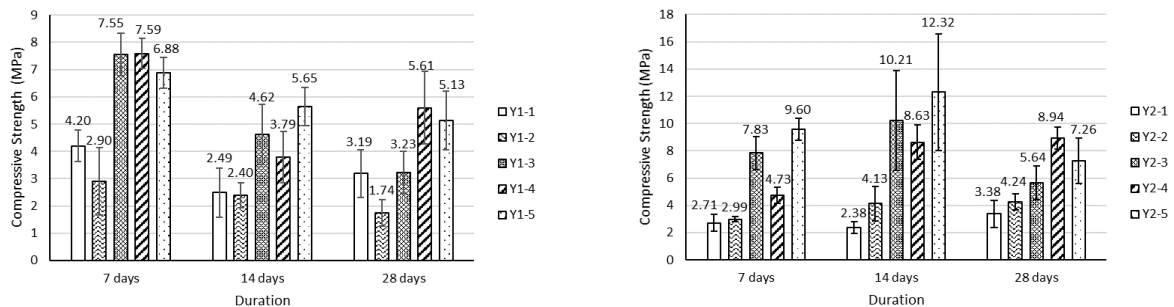


Fig. 1– Mean compressive strength and SD of BC FA geopolymer mortars Y1 (Left) & Y2 (Right)

As a construction material concrete bricks are required to have a 5 MPa characteristic strength. It can be noted that all Y1 mixes failed to achieve sufficient strengths required for low strength concrete brick. In comparison, mix Y2-4 and Y2-5 produced strengths surpassing the minimum characteristic strengths needed for brick production, with strengths of 7.88 MPa and 5.12 MPa, respectively. The results show fluctuations between all mixes, apart from mix Y2-4, which shows a steady rise in its characteristic strength over the 28 day period.

The development of strength of geopolymer mortar specimens has been identified as being affected by the SiO_2 to Al_2O_3 (Si/Al) ratio [13]. It has been reported that the Si/Al ratio impacts the pore volume and microstructure distribution of Na activated geopolymers, where an increase in the ratio produces a homogenous product with reduced dispersed pores [14]. Regarding the strength against Si/Al ratio, it can be noted that material Y2 has a much higher ratio, 2.28 compared to material Y1, 0.84; suggesting this could be a factor into the higher strengths achieved by Y2 FA. Other reports state a high Si/Al ratio can reduce the rate of early age reaction during the dissolution stage of the polymerisation process. As Y2 has a higher ratio, this suggests that the activation of the geopolymer product was slowed by the deprotonation of hydrated silica molecules and the utilisation of sodium in the arrangement of the alumina silicate reaction product, resulting in delayed reaction leading to low initial strengths across the mixes [15]. The AM is established as being a highly significant factor in the strength development of the geopolymeric material. Duxson et al. [16] suggested the ratios of the AM significantly alters the rate of polymerisation in an alkali silicate solution. The optimal strength was found to be at 1.75 AM, as the strength dropped at AM 1.9 in both Y1 and Y2 mixes [5, 17-19]. Hence, it is hypothesized that the combination of both the high Si/Al and AM ratio contribute to the improved compressive strength observed in the Y2 geopolymer specimens.

The quantity of SiO_2 and Al_2O_3 and their relative ratio is critical in the geopolymerisation reaction. The selected BC FA shows a chemical composition comprising of 5.78% (SiO_2) and 6.89% (Al_2O_3), for Y1, compared with 5.45% (SiO_2) and 2.49% (Al_2O_3) for the Y2 ash. Given the low aluminosilicate concentration, the relatively higher quantity in Y1 would have suggested it would perform better of the two. There are a number of reasons that can explain the overall low strengths achieved. Both materials have high amounts of Fe_2O_3 , 55%-57% and of CaO , 9%-11%. High Fe_2O_3 content has been reported as decreasing the strength in geopolymer, whereas the CaO improves the final strength of geopolymer specimens [20]. It is also understood that the dissolution stage is influenced by the proportion of the crystalline and amorphous content. The Y1 ash has only 7% amorphous content while the Y2 has 14 % amorphous content.

The characteristic strength is illustrated in Figures 2 for the respective materials, the characteristic strengths were calculated based on the 90th percentile with a z value of 1.29. As a construction material concrete bricks are required to have a 5 MPa characteristic strength. It can be noted that all Y1 mixes failed to achieve sufficient strengths required for the low strength concrete brick. In comparison, mix Y2-4 and Y2-5 produced strengths surpassing the minimum characteristic strengths needed for brick production, with strengths of 7.88 MPa and 5.12 MPa, respectively [21].

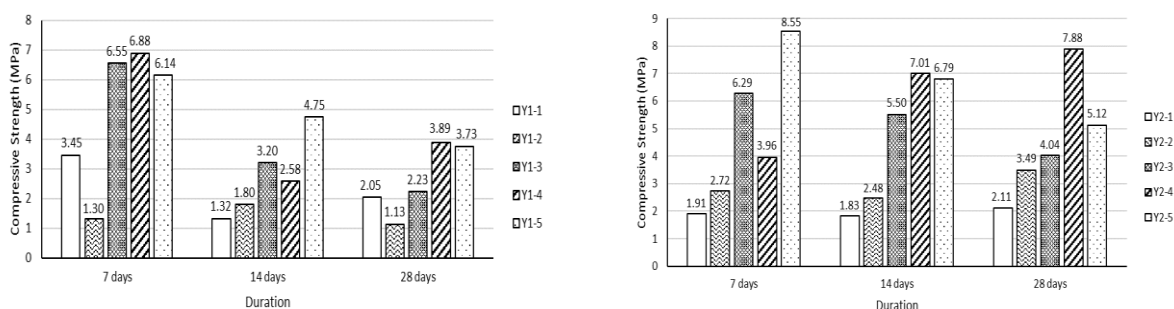


Fig. 2– Characteristic compressive strength of BC FA geopolymer mortars Y1 (Left) & Y2 (Right)

Amorphous compounds dissolve readily during the dissolution phase. Therefore, a higher percentage of amorphous content is expected to result in an improved geopolymeric reaction. Dissolution leads on to the speciation equilibrium and gelation phases, where the leached Si and Al ions come into contact with the activator solution to form the aluminosilicate gel. The formation of the gel leads to the development of the strength of the geopolymer mortar. Thus, a higher amorphous content leads to an increased concentration of ions in solution which leads to increased gel formation and higher compressive strength. The amorphous content of Y2 is double the amount of Y1, indicating that although Y1 has higher aluminosilicate content, the improved strength achieved by the Y2 mixes indicate that the amorphous content has a greater influence. The high crystalline content will also inhibit the rate of dissolution, leading to fewer SiO_2 and Al_2O_3 compounds being leached by the activating solution. This will result in fewer leached particles and a higher number of unreactive particles in the geopolymer matrix. The unreactive particles impair gel formation and increase the porosity within the matrix. This

increased porosity coupled with the evaporation of water on completion of dissolution stage contributes to the formation of microcracks [16, 17]. The widening of these microcracks with time is postulated as the reason for the reduction of overall strength from 7 days to 28 days. It also is hypothesised that the high crystalline content and also contributes to the lower strength observed in the Y1 specimens when compared to the Y2 specimens.

The results of the slump flow tests are illustrated in Figure 3. The data shows a clear relationship between the flowability and compressive strength, as the strengths generally increase with an increase in flow for both Y1 and Y2. The behaviour seen is unusual as the flow increases with increasing AM, corresponding to an increase in sodium silicate. However, according to Chindaprasirt et al. [22], high concentration levels of sodium hydroxide solution can thicken the flow. It is also known that sodium hydroxide is hygroscopic which enables it to absorb water molecules physically. Both factors could lead to a decrease in sodium hydroxide resulting in the improved flowability observed. Particle size can also significantly influence the flow of the mortar produced and the resultant performance. The Y2 ash has 93.92% passing at 75 μm , with 85.85 % passing at 45 μm , while the Y1 ash has 83.87% passing at 75 μm and 74.7 % passing at 45 μm . This would indicate that the fineness of the material also plays a critical role in the flow of the mortar mixes, as Y2 BC FA had a higher percentage of finer particles than that of the Y1 material. The data would indicate that there is an optimum flow range with regard to compressive strength as observed by Chidaprasirt [22].

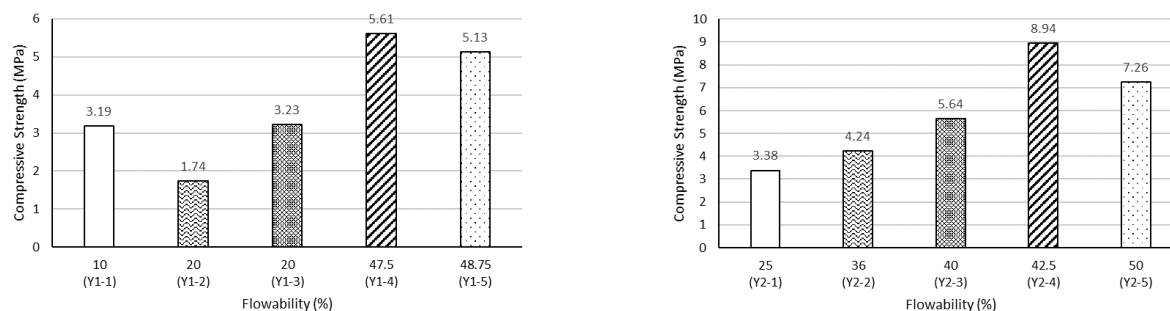


Fig. 3– Flowability Vs Compressive strength at 28 days – Y1 (Left) & Y2 (Right)

4. CONCLUSIONS

- The combination of the source material, BC FA and the optimal alkali activators provide strengths that can reach similar strengths found in low strength concrete bricks. However, the results indicate that further investigation is required to achieve the minimum strength requirement reliably.
- The optimal characteristic compressive strength obtained from all mixtures was with an AM of 1.75 that gave a compressive strength of 7.88 MPa at 28 days for material Y2.
- The properties that have been identified as influencing the strength of the material are the low aluminosilicate content, the high crystalline content and the high Si/Al and AM ratios.
- The data indicates a relationship between flowability and strength.
- The factors that influenced flowability of the mixtures were identified as the angular shape of the BC FA, the particle size and the relative combination of the alkali activators.

REFERENCES

1. Schneider, M., et al., *Sustainable cement production—present and future*. Cement and Concrete Research, 2011. **41**(7): p. 642-650.
2. Tennakoon, C., et al., *Characteristics of Australian brown coal fly ash blended geopolymers*. Construction and Building Materials, 2015. **101**: p. 396-409.
3. Dirgantara, R., et al., *Suitability of Brown Coal Fly Ash for Geopolymer Production*. Journal of Materials in Civil Engineering, 2017. **29**(12): p. 04017247.
4. MINAŔÍKOVÁ, M. and F. ŠKVÁRA, *Fixation of heavy metals in geopolymeric materials based on brown coal fly ash*. Ceramics– Silikáty, 2006. **50**(4): p. 200-207.
5. Dirgantara, R., *Development of Brown Coal Fly Ash Geopolymer Concrete in School of Engineering* 2016, RMIT University.
6. Law, D.W., et al., *Long term durability properties of class F fly ash geopolymer concrete*. Materials and Structures, 2015. **48**(3): p. 721-731.
7. Fernández-Jiménez, A. and A. Palomo, *Characterisation of fly ashes. Potential reactivity as alkaline cements* ✱. Fuel, 2003. **82**(18): p. 2259-2265.
8. Rahier, H., J.F. Denayer, and B. Van Mele, *Low-temperature synthesized aluminosilicate glasses Part IV modulated DSC study on the effect of particle size of metakaolinite on the production of inorganic polymer glasses*. Journal of MS, 2003. **38**(14): p. 3131-3136.
9. Dirgantara, R. and L.D. W.; *Effects of elevated temperature curing of brown coal fly ash geopolymer*. in *Mechanics of Structures and Materials:Advancements and Challenges*. 2016. Pert, Australia: CRC PRESS / BALKEMA.
10. Rahier, H., et al., *Low-temperature synthesized aluminosilicate glasses Part I low-temperature reaction stoichiometry and structure of a model compound*. Journal of Materials Science, 1996. **31**(1): p. 71-79.
11. Dirgantara, R., et al., *Suitability of Brown Coal Fly Ash for Geopolymer Production*. Journal of Materials in Civil Engineering, 2017. **29**(12).
12. AS3600, ed. *Concrete Structures*. 3rd edition ed.. 2018, Australian Standard: Sydney, Australia.
13. Sakulich, A.R., et al., *Influence of Si: Al ratio on the microstructural and mechanical properties of a fine-limestone aggregate alkali-activated slag concrete*. Materials and Structures, 2010. **43**(7): p. 1025-1035.
14. Duxson, P., et al., *Understanding the relationship between geopolymer composition, microstructure and mechanical properties*. Colloids and Surfaces A: Physicochemical and Engineering Aspects, 2005. **269**(1): p. 47-58.
15. Bernal, S.A., R.M. de Gutiérrez, and J.L. Provis, *Engineering and durability properties of concretes based on alkali-activated granulated blast furnace slag/metakaolin blends*. Construction and Building Materials, 2012. **33**: p. 99-108.
16. Duxson, P., et al., *Geopolymer technology: the current state of the art*. Journal of Materials Science, 2007. **42**(9): p. 2917-2933.
17. Gunasekara, C.M., *Influence of properties of fly ash from different sources on the mix design and performance of geopolymer concrete*. 2016, RMIT University Melbourne, Australia.
18. Fernández-Jiménez, A. and A. Palomo, *Composition and microstructure of alkali activated fly ash binder: Effect of the activator*. Cement and concrete research, 2005. **35**(10): p. 1984-1992.
19. Wardhono, A., *The durability of fly ash geopolymer and alkali-activated slag concretes*. 2014.
20. Fernandez-Jimenez, A. and A. Palomo, *Characterisation of fly ashes. Potential reactivity as alkaline cements*. Fuel, 2003. **82**(18): p. 2259-2265.
21. AdBriMasonry, *Characteristic Strength for Masonary Brick*, R. UNIVERSITY, Editor. 2016:
22. Chindaprasirt, P., T. Chareerat, and V. Sirivivatnanon, *Workability and strength of coarse high calcium fly ash geopolymer*. Cement and Concrete Composites, 2007. **29**(3): p. 224-229.

REACTIVITY OF ALKALI-ACTIVATED BINDERS FOR STABILIZATION/SOLIDIFICATION OF TUNNEL BORING MUDS

Thomas Wattez (1), Martin Cyr (1), Cédric Patapy (1), Julien Waligora (2), François Olard (2), Laurent Frouin (3) and Nicolas Musikas (4)

(1) LMDC, Université de Toulouse, INSA, UPS, Génie Civil, 135 Avenue de Rangueil, 31077 Toulouse Cedex 04, France

(2) EIFFAGE Infrastructures, 8 Rue du Dauphiné, 69960 Corbas, France

(3) ECOCEM Materials, 4 place Louis Armand, 75012 Paris, France

(4) ECOCEM France, 970 Rue René Descartes, 13100 Aix-en-Provence, France

Abstract

This work aims to develop innovative cementitious solutions for stabilization/solidification process of tunnel boring muds. These muds are characterized by a high CaCO_3 content, a high water content and a relatively high fineness, where the material fraction smaller than $80\ \mu\text{m}$ represents almost 50% of its mass. Our interest mainly focuses on the study of alkali-activated slag binders based on sodium hydroxide and sodium metasilicate, both used in powder forms. These two specific binders were compared with regular cements such as ordinary Portland and slag blended cements. Compressive strengths measurements up to 28 days were coupled with a one week long isothermal calorimetry test. Pore solution extraction and analysis were also performed to evaluate binders' performance at early age and up to 28 days. Soda-activated slag binder showed the highest suitability for the targeted application, both in terms of mechanical properties and chemical reactivity. On the other hand, the use of sodium metasilicate significantly delayed reactivity whereas this binder showed higher mechanical performance compared to sodium hydroxide activated system when used in normalized mortars. Hypothesis regarding the activator interactions with the mud solid matrix and the high water content of the samples are then proposed.

Keywords: alkali-activated slag, subgrade layer, stabilization/solidification, pore solution, compressive strength

1. INTRODUCTION

The *Lyon-Turin* high-speed railway aims to dig a 60 kilometres long tunnel through the Alps. The *Grand Paris* project aims to build about 200 kilometres of new metro lines. By 2030, in between these two major Civil Engineering projects, about 60 to 80 million of m³ of boring muds will be extracted. These boring muds, due to the variety of the geological depths, are expected to present a great diversity of mineralogical components, organics content and pollutants either from natural occurrences (sulfate, molybdenum) or humanly induced (heavy metals, TBT, ...) [1]. With the expected important volumes of extracted material, authorities are imposing contractors to come up with environmentally friendly and economically viable solutions for their upcycling.

One possible application that would lead to the re-use of important volumes is the development of a subbase layer for road infrastructures. The stabilization and solidification of soils being usually performed with ordinary Portland or slag blended cements. An innovative and low carbon footprint inducing solution consists in the use of alkali-activated binders [2]. In this work, the focus concerns the suitability of alkali-activated binders when used in road infrastructures applications by studying exclusively Ground Granulated Blast Furnace Slag (GGBS) mixed with either sodium hydroxide or sodium metasilicate.

Performances of such alternative binders are evaluated in terms of mechanical strength at different curing ages and compared to binders that are considered of standard use for such application: an Ordinary Portland Cement (OPC) and slag blended cement made of up to 90% of GGBS. Hydration kinetics and chemistry of the binders when mixed with one type of calcareous soil are evaluated by isothermal calorimetry during the early age and by pore solution extractions and analysis for the whole period of interest.

2. MATERIALS AND METHODS

The raw mud studied in this work comes from the south-western underground region of Paris (France). At delivery, the mud presents a total water content of 25%. Its mineralogy, obtained by XRD with a Bruker D8 advance diffractometer based on a Cu-K α radiation source, is essentially composed of calcite, aragonite and dolomite. Traces of quartz (SiO₂) are also detected. Total Organic Carbon (TOC) content measured according to French standard XP P 94-047 [3] leads to a value of 1.6%. Methylene blue absorption test, which relates to the clay content of the soil, carried according to the French standard NF P 94-068 [4], produces a relatively low value of 0.8.

Ordinary Portland Cement (OPC) used is provided by Vicat and enters the category of CEM I 52.5N according to the European standard EN 197-1 [5]. It presents a density of 3.17 g/cm³ and a Blaine fineness of 4300 cm²/g.

GGBS is provided by Ecocem France Ltd. It presents a density of 2.90 g/cm³ and a Blaine fineness of 4500 cm²/g. All raw materials compositions are determined using ICP OES (Optima 7000DV - Perkin Elmer) and summarized in Table 1.

Table 1 - Chemical compositions and Blaine fineness of the mud, the Ordinary Portland Cement and the GGBS.

	Mass (%)										
	SiO ₂	Al ₂ O ₃	CaO	Fe ₂ O ₃	MgO	TiO ₂	SO ₃	Cr ₂ O ₃	Mn ₂ O ₃	Na ₂ O _{eq}	LOI (%)
Mud	6.8	1.3	47.6	0.9	3.2	<0.1	0.4	<0.1	<0.1	0.3	40,56
CEM I	19.9	3.9	64.0	4.5	2.5	0.2	2.1	N.D.	N.D.	0.4	1,12
GGBS	37.7	10.2	43.8	0.6	6.4	0.7	0.1	N.D.	N.D.	0.4	< 1,5

For the alkali-activation of the GGBS, sodium hydroxide and sodium metasilicate (molar ratio SiO₂/Na₂O = 1) were used, both of analytical grade and in powder form.

Stabilized mud samples are prepared with four different types of binders: one exclusively based on OPC, one based on a slag rich binder that is prepared in the lab with proportions of OPC and GGBS equivalent to a CEM III/C as defined in EN 197-1 [5], one soda-activated GGBS binder and one sodium metasilicate activated GGBS binder. Masses used of mud, precursors, activators and added water to prepare three prismatic samples are given in Table 2.

Table 2 - Masses of materials used to prepare three 4cm x 4cm x 16cm prismatic samples.

	Masses (g)					
	Mud (w=25%)	OPC	GGBS	NaOH	Na ₂ SiO ₃	Added Water
CEM I	1500	120	-	-	-	120
CEM III/C		12	108	-	-	120
AAS-NaOH		-	120	9.6	-	96
AAS-Na ₂ SiO ₃		-	120	-	14.7	96

The ratio between precursors (OPC and/or GGBS) and the dry mud is kept constant at a value of 10%. Activators proportions are chosen in order to obtain a sodium oxide equivalent content of Na₂O_{eq} = 6%. For each mix presented in Table 2, the added water is selected in order to attain sufficient rheology for casting samples in prismatic molds using exclusively a vibrating table. Finally, the stabilized mud samples prepared with these proportions present a total water to binder ratio between 3.0 and 3.5. Samples are demolded 24 hours after mixing.

Unconfined compressive strengths measurements are done after 3, 7 and 28 days of endogenous curing performed in sealed bags and using a constant loading rate of 0.4 kN/s for the four different mix designs described earlier.

Hydration kinetics is assessed through isothermal calorimetry for a period of 7 days. The preparation of the samples is done by sieving the mud at 10 mm beforehand. Then, for each mix design, an initial 100 grams batch is prepared keeping constant the proportions given in Table 2. Each testing bottle is filled with 10 grams of the mixture and placed in the apparatus.

Pore solution extractions are performed on additional stabilized mud samples of the four types of binder and after the same three curing durations considered for mechanical performances evaluation. The apparatus and protocol employed to perform such extractions are described by Cyr et al. [6]. Immediately after extraction, the pH of the solution is measured with a LPH430T pH-meter. The solution is then filtered at 0.45 µm and acidified by adding 2% of nitric acid to avoid the precipitation of species. Liquid samples are stored at 5°C until chemical composition comes to be determined by ICP OES.

3. RESULTS

3.1 Compressive strengths

Figure 1 summarizes results obtained in terms of compressive strength performed on prismatic samples of stabilized mud for the four different mixes considered in Table 2 and after three distinct curing durations. For each prism, three tests are done, the value displayed in the graph being the average value plus or minus the standard deviation.

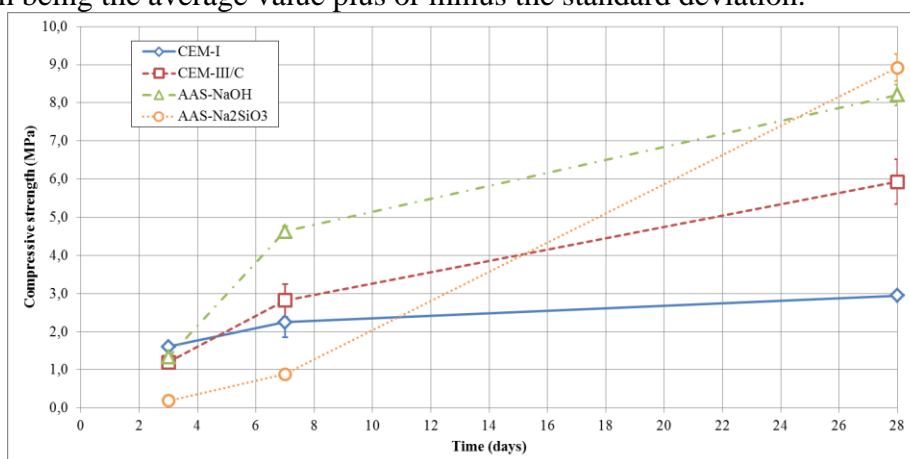


Figure 1 - Compressive strengths after 3, 7 and 28 days of curing for the four different mixes.

After three days of curing, all mix designs except the AAS-Na₂SiO₃ ($f_c = 0.2$ MPa) develop a compressive strength above 1 MPa, which satisfies requirements for traffic rehabilitation in the road construction environment. After 7 and 28 days, CEM I based stabilization shows a rather limited evolution which is typical of OPC when used in soil stabilization and with high water content [7]. Slag-rich binder and AAS-NaOH develop performances significantly higher after 7 days and especially for the soda activation that reaches a value around 8 MPa after 28 days of curing. At the same time, the sodium silicate activation still lacks mechanical strength after 7 days of curing by not meeting the requirement for traffic re-use ($f_c = 0.9$ MPa), but suddenly displays the highest value of all four mixes at 28 days curing ($f_c = 8.9$ MPa).

3.2 Isothermal calorimetry

Figure 2 displays the normalized heat flow for the whole testing period and for the four different mix designs of interest.

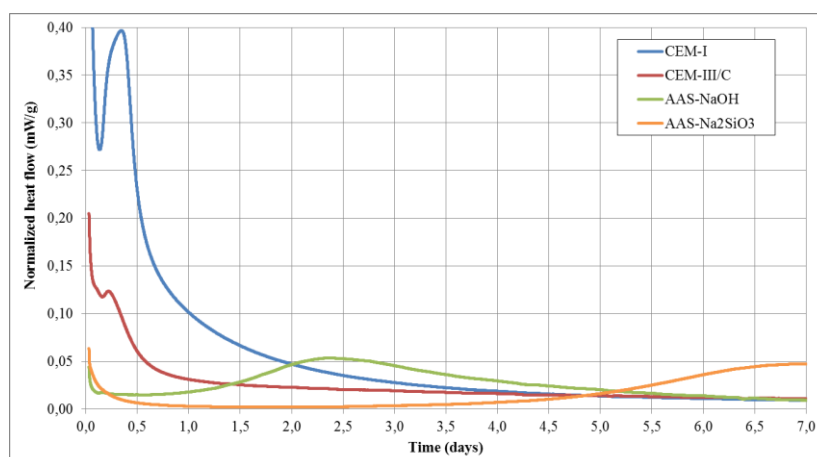


Figure 2 - 7 days long isothermal calorimetry of the four different types of stabilized mud.

Curves obtained for regular binders (CEM I and CEM III/C) are in good agreement with usual data from the literature where maximum heat is obtained early on (≤ 8 hours) and slag rich binder develop an overall heat significantly lower than OPC. In the case of soda activation, the total heat flow is within the same order of magnitude of the CEM III/C binder, but with a clear delay in the time to reach maximum value compared to behavior observed on paste samples [8], as it appears almost 2.5 days after mixing. In the case of the sodium metasilicate activation, the delay is even greater. After 7 days of measurement, the overall heat is about half the value measured for the soda-based activation and the last measurement corresponds to the maximum of the curve. This delayed reactivity correlates with the compressive strengths measured on samples of the same mix design (Fig. 1).

3.3 Pore solutions analysis

The following part assesses the properties and compositions of the pore solutions obtained at three different curing ages and for the four different mix designs of stabilized mud (Fig.3).

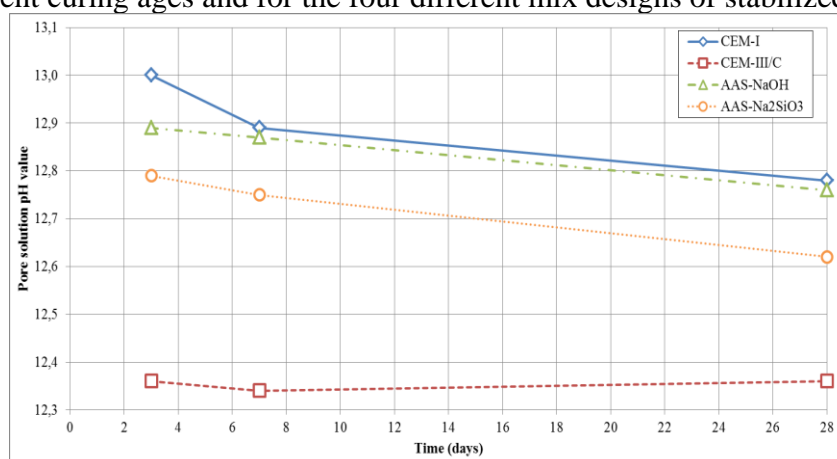


Figure 3 - pH values of the extracted pore solutions from stabilized mud samples at three different deadlines for the four different types of mixes studied.

The pH values measured directly after extraction show a steady decrease with time for all mixes except for the slag-rich binder that displays a relatively constant value around 12.35. In the case of the CEM I binder (Fig. 4a), the decrease is due to the slow and continuous

consumption of the alkalis (potassium essentially, not measured here) initially contained in the OPC from the pore solution to precipitate hydration products [9]. In the case of the CEM III/C samples (Fig. 4b), the constant concentrations in calcium and sodium go accordingly with the steady pH value of the pore solution, showing a slower rate of hydration of the GGBS in such system. As shown in Figs. 4c and 4d, the same process happens to alkali-activated binders associated with a decrease in sodium concentrations due to its uptake by C-A-S-H gels. As shown in [10], a constant pH of the pore solution through time for a binder containing 75% or more GGBS is expected because of the slower reactivity of this cementitious addition.

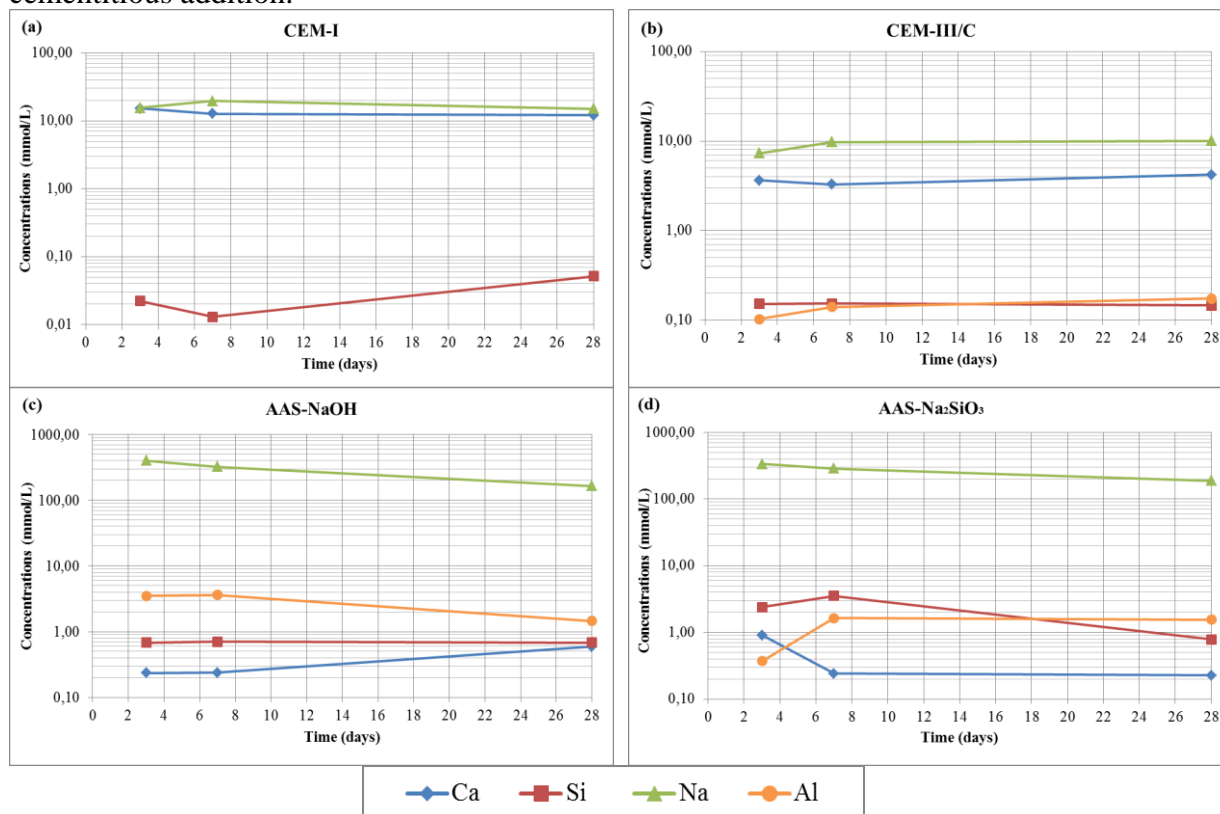


Figure 4 - Chemical composition of pore solutions. (a) From CEM I; (b) from CEM III/C; (c) from sodium-hydroxide activated slag; (d) from sodium metasilicate activated slag.

Silicon concentrations in solution for regular binders are relatively low because of its low solubility in this range of pH values. Due to the OPC chemical composition (Table 1), concentrations in aluminum are below the apparatus detection limit (not displayed in Fig. 4a). In the case of the CEM III/C, concentration in calcium remains relatively constant as for the pH measured in associated pore solutions. In the case of the AAS-Na₂SiO₃ solutions, the silicon concentrations are significantly higher than for other binders due to the activator contribution but also show a decrease in time.

4. DISCUSSIONS

The coloring of the pore solutions extracted from mud stabilized with sodium metasilicate activated GGBS (Fig. 5) comes from the organic acids initially present in the sample of soil. In the case of the sodium hydroxide activated slag stabilized mud, pore solutions extracted

after 3, 7 and 28 days of endogenous curing all display the same color, light yellow, as obtained for AAS- Na_2SiO_3 samples after 28 days of curing. Eventually, pore solutions extracted from regular cement binders, here being CEM I and CEM III/C, do not display any particular color and remain totally clear even after the addition of the acid solution and the long term conservation.



Figure 5 - Pore solutions extracted from AAS- Na_2SiO_3 samples. Left is after 3 days. Centre is after 7 days. Right is after 28 days.

In the case of the alkali-activated mixes, as shown in [11], the addition of alkali provokes the separation of the clay-humus complex and the leachate of humic acids into the pore solution. In a second time, the addition of the nitric acid (HNO_3) to the pore solution extracted leads to the precipitation of those organics. After the period of storage at 5°C , the colored pore solutions are filtered ($0.45\ \mu\text{m}$), once more to obtain a transparent solution.

In the work presented by Puertas et al. [12], the pore solutions of alkali-activated GGBS are studied for the first seven days of hydration. Those solutions are extracted from paste samples that are prepared with a water to binder ratio of 0.5 and a total equivalent sodium oxide content of $\text{Na}_2\text{O}_{\text{eq}} = 4\%$. Both activation with sodium hydroxide and sodium silicate, presenting a molar ratio of $\text{SiO}_2/\text{Na}_2\text{O} = 1.5$, are evaluated. In our study, samples of stabilized mud with a water to binder ratio between 3.0 and 3.5 are prepared, with a total equivalent oxide content of $\text{Na}_2\text{O}_{\text{eq}} = 6\%$ and sodium metasilicate (molar ratio equal to 1.0). By applying suitable factors to the calculated species concentrations to take into account those differences, it was found that the evolution of sodium and silicon concentrations of both alkali-activated slag mixes agree with the data presented in [12]. Meanwhile in the specific case of the AAS- Na_2SiO_3 , the concentration profiles through time for calcium and is significantly higher after 3 and 7 days than the ones reported in the literature.

As shown in Fig. 5, the use of sodium silicate leads to the leaching of higher amounts of humic acids from the soil than sodium hydroxide, for a fixed $\text{Na}_2\text{O}_{\text{eq}}$. Humic acids are known to be strong complexing agents of cations such as Ca^{2+} [13]. When mixing the mud, the sodium silicate and the GGBS, the pH of the system rises, as shown by in-situ measurements, therefore the humic acids are freed from the soil into the pore solution while the GGBS particles start dissolving. The cations that are released from the GGBS tend to associate with the humic acids instead of precipitating hydration products. Until all the extracted organic molecules are complexed with cations, the hydration products do not start to precipitate, therefore, the associated heat released, measured by isotherm calorimetry, is delayed. As seen in Fig. 2, the smaller amounts of HA in solution for NaOH activation lead to a shorter delay (1.5-2.0 days) compared to the sodium metasilicate activation (5.5-6.0 days). This lack of reactivity also appears to be correlated with mechanical performances, or in the case the silicate activation lack of performances, measured at different curing ages.

Eventually, when the pore solutions are extracted, cation – humic acids complexes are broken down by the acidification step, precipitating the organics. As a consequence, calcium ions are released back into the solution which comes to explain the abnormal values measured in the pore solutions of sodium silicate activated stabilized mud after the extraction and preparation protocols.

5. CONCLUSIONS

- Upcycling of tunnel boring muds for road applications involving low carbon footprint binders is technically possible.
- This work proves sodium hydroxide activated GGBS is a suitable binder for soil stabilization and solidification. The performances developed through time meet both early age requirement and long term performances development.
- Sodium silicate brings new challenges regarding interactions with organics and clay-humic acid complexes.
- Cost might be an issue and should be taken into account.
- This work is limited to the study of non-polluted, low clay and low organics contents type of soil. Suitability of alkali-activated binders should be assessed on more diverse source of materials such as sediments or heavily polluted boring muds.

REFERENCES

- [1] Trincal, Vincent, et al. "Use of hydraulic binders for reducing sulphate leaching: application to gypsiferous soil sampled in Ile-de-France region (France)." *Environmental Science and Pollution Research* (2018): 1-21
- [2] Corrêa-Silva, Manuela, et al. "Improvement of a clayey soil with alkali activated low-calcium fly ash for transport infrastructures applications." *Road Materials and Pavement Design* (2018): 1-15.
- [3] XP P 94-047. "Sols : reconnaissance et essais - Détermination de la teneur pondérale en matières organiques d'un matériau - Méthode par calcination."
- [4] NF P 94-068. "Sols: Reconnaissance et essais, mesure de la capacité d'adsorption de bleu de méthylène d'un sol ou d'un matériau rocheux, détermination de la valeur de bleu de méthylène d'un sol ou d'un matériau rocheux par l'essai à la tache."
- [5] NF EN 197-1. "Ciment - Partie 1 : composition, spécifications et critères de conformité des ciments courants."
- [6] Cyr, Martin, et al. "High-Pressure Device for Fluid Extraction from Porous Materials: Application to Cement-Based Materials." *Journal of the American Ceramic Society* 91.8 (2008): 2653-2658.
- [7] Yi, Yaolin, et al. "Comparison of reactive magnesia-and carbide slag-activated ground granulated blastfurnace slag and Portland cement for stabilisation of a natural soil." *Applied Clay Science* 111 (2015): 21-26.
- [8] Shi, Caijun, and Robert L. Day. "A calorimetric study of early hydration of alkali-slag cements." *Cement and Concrete Research* 25.6 (1995): 1333-1346
- [9] Gruskovnjak, Astrid, et al. "Hydration of alkali-activated slag: comparison with ordinary Portland cement." *Advances in cement research* 18.3 (2006): 119-128.
- [10] Vollpracht, Anya, et al. "The pore solution of blended cements: a review." *Materials and Structures* 49.8 (2016): 3341-3367.
- [11] Theng, Benny Kian Goan. Formation and properties of clay-polymer complexes. Vol. 4. Elsevier, 2012.
- [12] Puertas, F., A. Fernández-Jiménez, and María Teresa Blanco-Varela. "Pore solution in alkali-activated slag cement pastes. Relation to the composition and structure of calcium silicate hydrate." *Cement and Concrete Research* 34.1 (2004): 139-148.
- [13] Tremblay, Helene, et al. "Influence of the nature of organic compounds on fine soil stabilization with cement." *Canadian Geotechnical Journal* 39.3 (2002): 535-546.

IRRADIATION RESISTANCE OF MK-BASED GEOPOLYMERS ENCAPSULATING OILY WASTES

Daniel A. Geddes (1), Susan A. Bernal (2), Martin Hayes (3) and John L. Provis (1)

(1) Department of Materials Science and Engineering, University of Sheffield, UK

(2) School of Civil Engineering, University of Leeds, UK

(3) National Nuclear Laboratory (NNL), UK

Abstract

Geopolymerisation is proposed as a potential method for the safe disposal of intermediate-level radioactive nuclear waste, which are considered to be problematic when adopting other cementation methodologies. It is particularly difficult to encapsulate oils and/or organic materials in conventional Portland cement based systems, at a sufficient waste loading. In this study a potassium silicate/metakaolin geopolymer grout has been developed, where 20 wt.% of silicone oil can be incorporated without affecting setting characteristics. This grout withstands gamma irradiation to a total dose of 1 MGy without showing significant changes in its microstructure. Irradiation appeared to modify the structure of a secondary phase forming in the geopolymer grout loaded with oil, and increase the susceptibility to carbonation of these materials, as carbonates are the main products identified in irradiated samples. X-ray diffractograms show a slight change in the ordering of the structure of the irradiated sample, which is consistent with thermogravimetry results. The fact that crystalline polymorphs of sodium carbonates are not observed by X-ray diffraction, indicates that the amount of these phases present in irradiated samples is small. In order to better understand the effect of irradiation in these materials, additional studies applying solid-state NMR spectroscopy and scanning electron microscopy will be carried out in the future. The results of this study demonstrate that oils can be incorporated within geopolymers at higher waste loadings than conventional Portland cement, and the loaded grouts appear to withstand gamma irradiation.

Keywords: Geopolymers, Solidification/Stabilisation, Oily Wastes, Nuclear Waste Disposal, Gamma Irradiation

1. INTRODUCTION

Exposure of cementitious systems, both geopolymers and conventional Portland cements, to irradiation has potential to cause changes within the chemical and physical structure of this system [1, 2]. Therefore, when these systems are proposed as a potential disposal route for nuclear wastes, it is imperative to determine their chemical and physical stability upon radiation exposure. Cementation is the suggested route for disposal of intermediate level radioactive waste (ILW) in the UK. Nuclear wastes are classified as ILW in the UK, if they are not significantly heat generating but emit at least 4GBq per tonne of alpha particles, and/or 12 GBq per tonne of beta/gamma radiation. Hence, any grout to be used for this disposal of ILW must withstand a significant dose of radiation over their projected service lifetime.

Geopolymers, are materials produced via a chemical reaction between poorly crystalline aluminosilicate sources (e.g. calcined clays) and an alkaline activating solution. If these materials are properly formulated and cured, they can exhibit attractive properties for the treatment of radioactive waste, such as high chemical resistance and resistance to high temperatures [3]. This has aided the motivation in recent years to consider geopolymers as suitable grouts for cementation of wastes, with the potential to withstand exposure to gamma irradiation.

In cementitious systems, exposure to irradiation can lead to radiolysis of the water present in the pores and in the hydrated products, compromising the microstructure of the binder and releasing hydrogen [1, 4, 5]. It has been shown [1] that radiolysis can induce small changes in the pore size distribution when materials are exposed to moderate radiation doses (<750 kGy). The introduction of a corrosion inhibitor in the form of NaF, which are attractive additions that provide benefits when trying to incorporate metals such as Al into a high-pH cementitious grout, appears to inhibit the radiolysis process [5]; however the mechanisms leading to this hydrogen generation reduction are not well understood.

The solidification and stabilisation of oil-based wastes, in a sufficient loading volume to make disposal via cementation a viable option, is challenging. The main issue is separation of the oils and the cement over time, due in part to the cement particles being surrounded in an oily film that prevents the hydration from taking place [6]. Therefore, as geopolymers do not harden via a hydration mechanism, the chemical and physical interaction when blended with oils is expected to be completely different from that which is observed in Portland cement based system. The hardening mechanism of a geopolymer follows a dissolution, rearrangement/nucleation mechanism [7]. As a further benefit, the highly alkaline activating solution can react with the oil to provide a further immobilisation/encapsulation step through saponification. The UK nuclear stockpile contains a variety of oils/organics as problematic wastes, however the majority of these wastes are silicone oils/lubricants [8].

The immobilisation of oil within geopolymers has been investigated by Cantarel et al. [9], who reported that the assessed grouts were stable up to a waste loading of 20 vol.%, when using sodium silicate and metakaolin as the precursors. The oil droplets become entrained within the geopolymer binder, and had a maximum droplet size of 50 μm . The leachability of the oils from the binder appeared to be minimal. Studies by the authors [10-12] have demonstrated that

potassium silicate activation of calcined clays offers a potentially suitable alternative to produce geopolymer grouts for the immobilisation/encapsulation of oil based wastes. The use of potassium ions as a constituent in the aluminosilicate type gel phase, over the commonly used sodium silicate, reduces alkali leaching, and also produces a grout with a more controllable rheology [11]. Therefore, this study will present the effects of gamma irradiation on potassium aluminosilicate geopolymers, loaded with 20 wt. % of a silicone oil.

2. EXPERIMENTAL PROCEDURE

Geopolymer samples were produced using MetaMax (BASF, UK), a rotary calcined metakaolin (chemical composition shown in Table 1) that is activated using a potassium silicate stock solution (K120, PQ Silicates, UK). The molar composition of the silicate is adjusted by blending with reagent grade KOH (Fisher Sci., UK) and distilled water. The base composition of the initial geopolymer was formulated with the molar ratios K_2O/SiO_2 and $Al_2O_3/K_2O = 1.0$ and $H_2O/K_2O = 11$. Silicone Oil 47 V 350 (VWR, UK) was incorporated into a pre-mixed base formulation as waste simulant, at a 20 wt.% loading.

Table 1 – X-ray fluorescence analysis of metakaolin

	SiO ₂	Al ₂ O ₃	TiO ₂	Fe ₂ O ₃	CaO	K ₂ O	Na ₂ O	LOI	Others
MetaMax	52.54	44.54	1.31	0.36	trace	0.15	0.21	0.63	0.20

Geopolymer monoliths were cured for 48 hours at 20 °C, prior to radiation exposure, and then they were exposed to gamma irradiation for 96 hours, using the ⁶⁰Co irradiator at the Dalton Cumbrian Facility (DCF) [13]. These samples were irradiated to a total dose of 1 MGy, using a dose rate of approx. 12 kGyhr⁻¹.

The effect of irradiation was assessed using a Perkin Elmer TGA4000 coupled with a Hiden mass spectrometer, using 40 mg of sample, using a ‘wet’ sample that had not undergone solvent exchange. The potential effects of the oil incorporation and irradiation exposure on the mineralogy and phase assemblage of these grouts were evaluated using X-ray diffraction, analysing a solvent exchanged sample (using isopropanol), that has been ground to pass through a 63 µm sieve. A Panalytical X’pert³ instrument was used, with CuK α radiation. The scans were taken over a 2 θ range of 5 – 70 °, with a step size of 0.02 ° and a time per step of 2.2 s. Control samples were produced and cured at 20 °C (RT Control) and heated to 50 °C (Heated Control), to identify potential effects of heating the specimens inside the irradiator.

3. RESULTS AND DISCUSSION

3.1 Thermogravimetry

Comparison of the thermogravimetric results for non-encapsulated geopolymer grouts (previously presented in [14]), and those of heated and irradiated samples, shows that exposure of this grout to 50 °C causes a reduction in the weight loss below 150 °C, which corresponds to free water present in the sample, and loosely bound water present in the geopolymeric gel [15]. A higher reduction in the weight loss in this range of temperature is observed in irradiated

samples, demonstrating that irradiation is inducing further removal of water from the geopolymer gel. Significant differences are observed in the range 150–200 °C between the control, heated and irradiated samples. The distinctive weight loss at this temperature range cannot be associated with decomposition of the simulant waste, as this will take place at higher temperatures, Figure 1. Hence, the results suggest the formation of a secondary reaction product with water more tightly bound to the geopolymer structure than that formed in specimens without oil loading. This might suggest that the addition of oil into the geopolymer gel is leading to the formation of new reaction products in the system. Therefore, a chemical interaction taking place in these systems. The thermogravimetric information is not sufficient to identify accurately which phase is decomposing at this range of temperature, hence future analysis will be carried out using in-situ heating XRD analysis of these samples.

After the samples have been irradiated, the secondary phase decomposing around 200 °C is no longer observed. Instead, distinctive weight losses between 400 – 700 °C are identified.

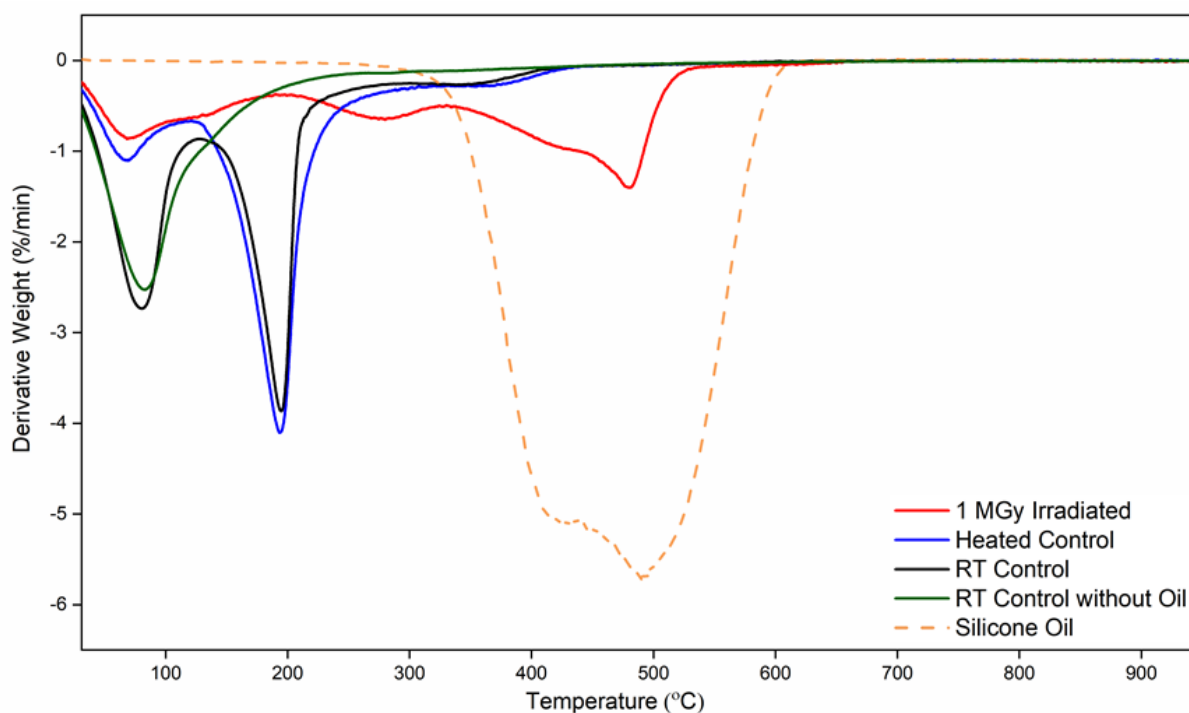


Figure 1 – Comparison of the derivative TG data for the control samples and the irradiated formulation containing the oil. The TG curve for the RT control without oil and for the silicone oil waste simulant are also presented

In order to understand the effects and changes caused by irradiation of an encapsulation matrix, thermogravimetry coupled with mass spectroscopy was used. Figure 2 shows that effectively the mass loss below 200°C corresponds to release of H₂O from the samples. The MS traces show an increase in the release of CO₂ and N₂/CO between 200 – 700 °C, which would be expected due to decomposition of carbon-based materials such as the oil simulant. However, it has been reported for conventional Portland cement systems that one of the effects of irradiation is an increase in the susceptibility to carbonation, hence the weight loss in this temperature range might be also be associated with decomposition of alkali carbonates present in the geopolymer system.

The resolution of the instrument used does not allow for discrimination between nitrogen and carbon monoxide gases, which both have a molecular weight of $24 \text{ g}\cdot\text{mol}^{-1}$. However, the N_2 is flowing at a constant flow rate from the gas supply, therefore any variations from a horizontal line can be associated with the release of CO. This appears to occur when oil is expected to be released.

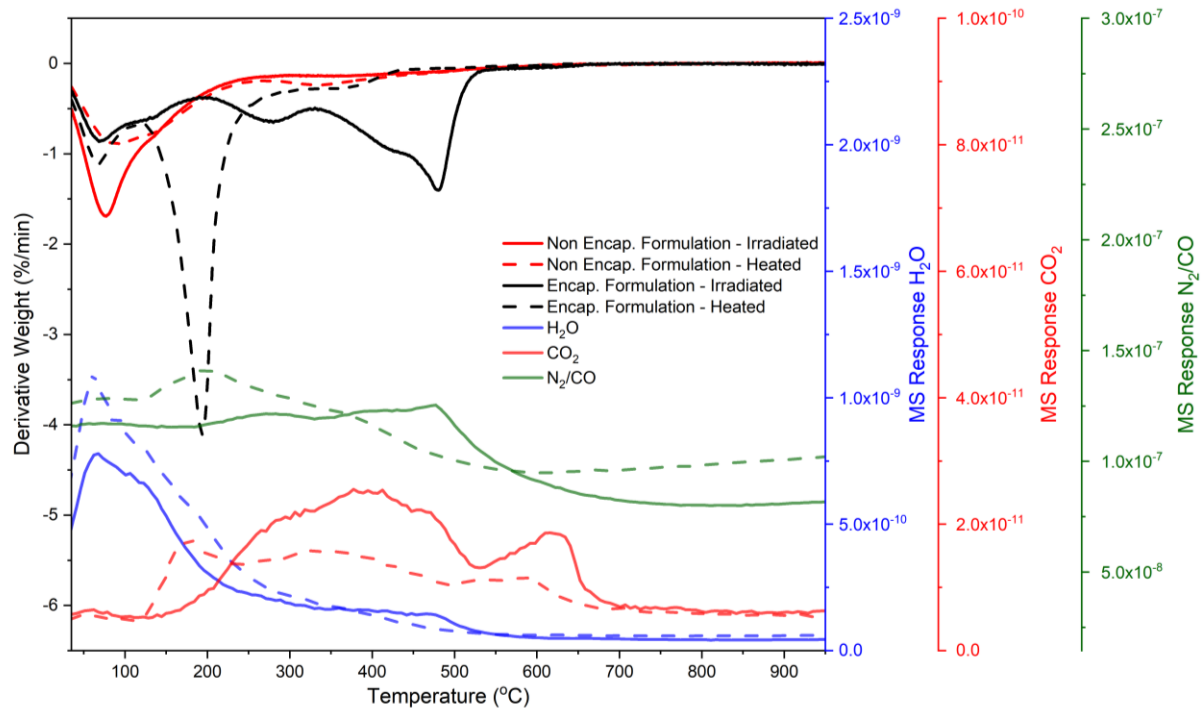


Figure 2 – TG-MS data comparing oil encapsulated (black) and non-oil containing (red) formulations. The solid lines represent the irradiated samples and the dashed lines represent heated controls.

3.2 X-ray Diffraction

In order to determine any differences in the mineralogy and phase assemblage of the irradiated sample, XRD (Figure 3) was used. Irradiation to 1 MGy induced minimal changes in the diffractograms compared with the control and heated samples. There is a slight increase in intensity of a broad reflection between 10-15 2θ degrees (noted as A_{m1} in the diffractogram), that could be related to the secondary phase identified by TG-MS (Figure 2). The inclusion of oil within this system is seen to reduce the ordering of the geopolymer gel, labelled A_{m1} , and whose reflection is centred at $\sim 12^\circ 2\theta$, when compared to the results for control and heated specimens. Anatase is the only crystalline product identified in these samples, and is an impurity present in the MK used to produce the geopolymer grouts.

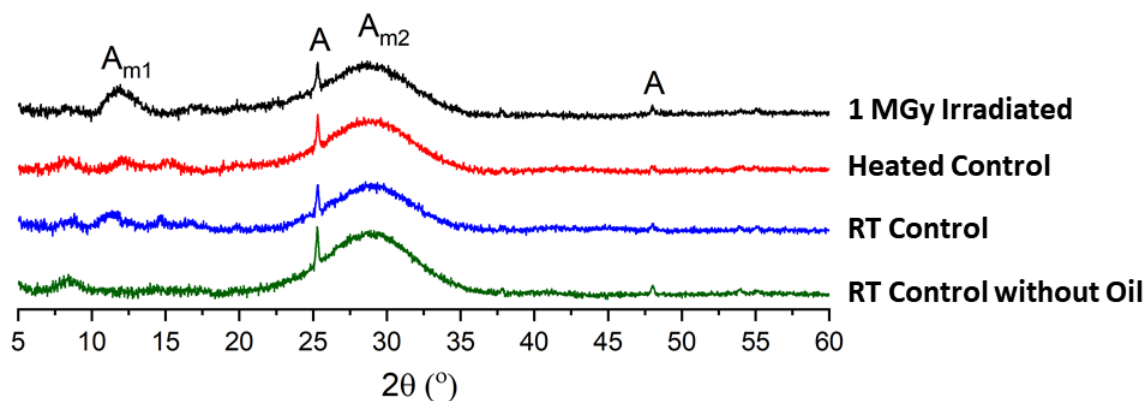


Figure 3 - XRD patterns of the encapsulated and non-encapsulated RT control geopolymer formulations. A_{m1} and A_{m2} represent different poorly crystalline phases and A represents anatase (TiO_2).

4. CONCLUSIONS AND FUTURE WORK

- Oils can be successfully incorporated within geopolymer grouts.
- These oils withstand irradiation (upto 1 MGy) and appear to induce structural changes within the geopolymer matrix.
- The system appears to become slightly less ordered with the inclusion of oils and upon gamma irradiation.
- Further work is required to understand the effect of clay type and activator composition on the waste loading and the physical and chemical properties of geopolymers.
- Future irradiation studies should include exploring different formulations and total radiation dose to fully understand the effect of irradiation in causing structural changes in these materials. The use of solid state NMR and SEM will help to develop this understanding.

ACKNOWLEDGEMENTS

The PhD of D. Geddes is funded by the UK Nuclear Decommissioning Authority (NDA) with valuable input from the National Nuclear Laboratory (NNL). This research was performed in part at the MIDAS facility, at the University of Sheffield, which was established with the support of the Department for Energy and Climate Change. The authors would gratefully like to thank PQ Silicates for the supply of the alkali silicate activating solution, and the Dalton Cumbrian Facility, via Dr Laura Leay and Dr Ruth Edge, for use of the ^{60}Co irradiator. The participation of S. Bernal in this study has been funded in part by EPSRC grant EP/P013171/1. D Geddes would also like to acknowledge the help and guidance of Dr Oday H. Hussein in this work.

REFERENCES

- [1] D. Lambertin, C. Boher, A. Dannoux-Papin, et al. 'Influence of gamma ray irradiation on metakaolin based sodium geopolymer', *J. Nucl. Mater.*, **443**, 1–3, 2013, 311-315.
- [2] F. Vodák, K. Trtík, V. Sopko, et al. 'Effect of γ -irradiation on strength of concrete for nuclear-safety structures', *Cem. Concr. Res.*, **35**, 7, 2005, 1447-1451.
- [3] J.L. Provis and J.S.J. van Deventer. 'Alkali Activated Materials - State of the Art Report, RILEM TC 224-AAM', Springer/RILEM. 2014.

- [4] L. Leay, A. Potts, and T. Donoclift. 'Geopolymers from fly ash and their gamma irradiation', *Mater. Lett.*, **227**, 2018, 240-242.
- [5] A. Rooses, P. Steins, A. Dannoux-Papin, et al. 'Encapsulation of Mg–Zr alloy in metakaolin-based geopolymer', *Appl. Clay Sci.*, **73**, 2013, 86-92.
- [6] S. Trussell and R.D. Spence. 'A review of solidification/stabilization interferences', *Waste Manage. (Oxford)*, **14**, 6,1994, 507-519.
- [7] J.L. Provis and S.A. Bernal. 'Geopolymers and related alkali-activated materials', *Annu. Rev. Mater. Res.*, **44**, 2014, 299-327.
- [8] M. French and I. Tanase, *Management of Contaminated Oils - Feasibility Study*, LLW Respository Ltd, March 2015, 2015.
- [9] V. Cantarel, F. Nouaille, A. Rooses, et al. 'Solidification/stabilisation of liquid oil waste in metakaolin-based geopolymer', *J. Nucl. Mater.*, **464**, 2015, 16-19.
- [10] D.A. Geddes, S.A. Bernal, M. Hayes, et al., 'Geopolymerization is an innovative solution for the treatment of problematic nuclear wastes', presented at the 4th International Conference on Service Life Design for Infrastructures, Delft. 2018.
- [11] D.A. Geddes, X. Ke, S.A. Bernal, et al., 'Metakaolin-Based Geopolymers for Nuclear Waste Encapsulation', Dordrecht, 2018, 183-188.
- [12] P. Duxson, G.C. Lukey, and J.S. van Deventer. 'Thermal evolution of metakaolin geopolymers: Part 1–Physical evolution', *J. Non-Cryst. Solids*, **352**, 52,2006, 5541-5555.
- [13] L. Leay, W. Bower, G. Horne, et al. 'Development of irradiation capabilities to address the challenges of the nuclear industry', *Nuclear Instruments and Methods in Physics Research Section B: Beam Interactions with Materials and Atoms*, **343**, 2015, 62-69.
- [14] D.A. Geddes, S.A. Bernal, M. Hayes, et al., 'Early age geopolymers exposed to gamma irradiation', in *NUWCEM - Cement-based materials for Nuclear Waste*, Avignon, 2018, 1-4.
- [15] S.A. Bernal, E.D. Rodríguez, R. Mejía de Gutiérrez, et al. 'Mechanical and thermal characterisation of geopolymers based on silicate-activated metakaolin/slag blends', *J. Mater. Sci.*, **46**, 16,2011, 5477.

NEW GENERATION OF CONSTRUCTION MATERIALS
SESSION 15: Self-Healing

CHLORIDE MIGRATION COEFFICIENT OF CRACKED MORTAR INCORPORATING SELF- HEALING MATERIALS

Fahad R. Abro (1), Abdul S. Buller (1), Kwang Myong Lee (1) and Seung Yup Jang (2)

(1) Department of Civil Engineering, Sungkyunkwan University, Republic of Korea

(2) Graduate School of Transportation, Korea National University of Transportation, Republic of Korea

Abstract

One of the key factors for early deterioration of most concrete structures subjected to marine and coastal environment is the corrosion of steel bar induced by chloride ions. Cracks present in concrete would significantly accelerate the penetration of chloride ions into concrete. Thus, the self-healing of cracks has a great impact on the resistance of chloride penetration and the durability of the concrete structures. In this study, for the characterization of self-healing capacity with regard to the durability of concrete structures, rapid chloride migration (RCM) tests were conducted to measure the chloride migration coefficients of mortar specimens made of OPC and special binders incorporating self-healing materials. Chloride ion concentration in the upstream cell of ASTM C1202 test set-up was measured for 36 hours, and the chloride migration coefficients were calculated based on the change rate of chloride concentrations in the steady-state condition. Test results reveal that self-healing can reduce the penetration of chloride ions and improve the resistance to chloride ingress of the cracked mortar specimens. The self-healing efficiency can be defined in terms of the decrease of chloride migration coefficients and the RCM test can be a satisfactory method to evaluate the self-healing capacity of cement-based materials.

Keywords: Crack, Self-Healing, Durability, Chloride ion, Migration

1. INTRODUCTION

Most marine structures are built with reinforced concrete which has high durability. However, concrete is vulnerable to cracking. Cracks have an adverse impact on the durability performance of the structures, especially built in marine and coastal environment because the chloride ions ingress faster through cracks which cause the corrosion of steel reinforcement [1]. Generally, in the practice, to prevent the deterioration of the structures, immediate repairs are required upon the formation of cracks to avoid the chloride ingress. This crack repairing is very costly and labor-intensive [2]. In this regard, the self-healing of cracks would be helpful to minimize the ingress of chloride ions through the cracks without manual crack repairs. Recently, there is a growing interest in the self-healing technology and various technologies including

autogenous self-healing by mineral additives, crystalline admixtures, or superabsorbent polymers and autonomous self-healing by incorporating, e.g., encapsulated polymers, minerals, or bacteria are being studied [3,4]. However, there found very limited research in the literature regarding the evaluation of self-healing capacity with regard to the chloride penetration [4-6]. This study has been undertaken to investigate the influence of self-healing against the chloride penetration and to characterize the self-healing capacity of cracked mortars using steady-state migration tests. An evaluation method of self-healing performance is also suggested in this study.

2. EXPERIMENTAL WORK

2.1 Materials

Mortar specimens made of OPC with and without self-healing (SH) materials were cast. Details of the mix proportions of mortars are given in Table 1. The SH material is the mixture of several expansive mineral admixtures and comprises 8% by the mass of binder.

Table 1: Mix proportions of mortar mixtures

Binder	Mass ratio			
	Water	Cement	SH materials	Sand
OPC	0.4	1.0	0.0	2.0
SH	0.4	0.92	0.08	2.0

2.2 Test method

After 28-day water curing, the mortar specimens having a size of $\text{Ø}100 \times 50$ mm were split into two semi-circles under the compressive load with the help of UTM. The target crack widths of 0.1 and 0.3 mm were achieved with silicon tapes of a specific size kept on the ends of semi-circle specimens and the two semi-circle specimens were tied with a steel band as shown in Figure 1.

The crack widths were measured at three points on top and bottom of the specimen by using an optical microscope immediately after the preparation of each cracked specimen. The mean value was taken as the crack width of the specimen. The test setup of ASTM C1202 was modified, the upstream cell was filled with 0.5M NaCl solution and the downstream cell with 0.3M NaOH solution. Under the potential difference of 36V, the chloride ion concentration in the upstream cell was measured for 36 hours with an ion selective electrode at an interval of 1 hour for initial 6 hours and of 2 hours for remaining 30 hours. Details of the tests can be found in references [7,8].



Figure 1: Preparation of cracked specimen

3. RESULTS AND DISCUSSION

3.1 Steady-state migration coefficient

The steady-state migration coefficients of the specimens were calculated at the healing age of 28 days using the Nernst-Planck equation as follows [7].

$$D_{ssm} = \frac{RTL}{zFU} \frac{V}{A} \frac{1}{C_1} \times |\Delta C_1 / \Delta t| \quad (1)$$

where D_{ssm} is the diffusion-migration coefficient at steady-state condition (referred as “migration” coefficient hereafter), R is the gas constant = 8.3145 J/mol/K, T is the absolute temperature (K), L is the specimen height (cm), z is the absolute value of ion valence, for Cl^- , $z = |-1| = 1$, F is the Faraday constant = 96,485 C/mol, U is the potential difference applied (V), V is the cell volume = 300 cm^3 , A = Area for ion penetration = 78.50 cm^2 and $\Delta C_1 / \Delta t$ is the rate of change of the chloride concentration in the upstream cell. Since $(1/C_1)(\Delta C_1 / \Delta t) = \Delta \ln(C_1) / \Delta t$, Eq. (1) can be rewritten as [7]

$$D_{ssm} = \frac{RTL}{zFU} \frac{V}{A} \times |\Delta \ln(C_1) / \Delta t| \quad (2)$$

Figure 2 shows the calculated migration coefficients of both mortar mixtures before and after healing for 28 days as per the crack widths. As shown in the figure, the migration coefficients of both OPC and SH specimens were decreased after the healing of 28 days, but the decrease rates of SH specimens are greater. This shows that the self-healing capacity of the SH mixture used in this study is higher than that of the OPC mixture. Also, the decrease rates of cracked specimens are greater than those of uncracked specimens. This is attributed to the higher contribution of cracks to the transport of chloride ions.

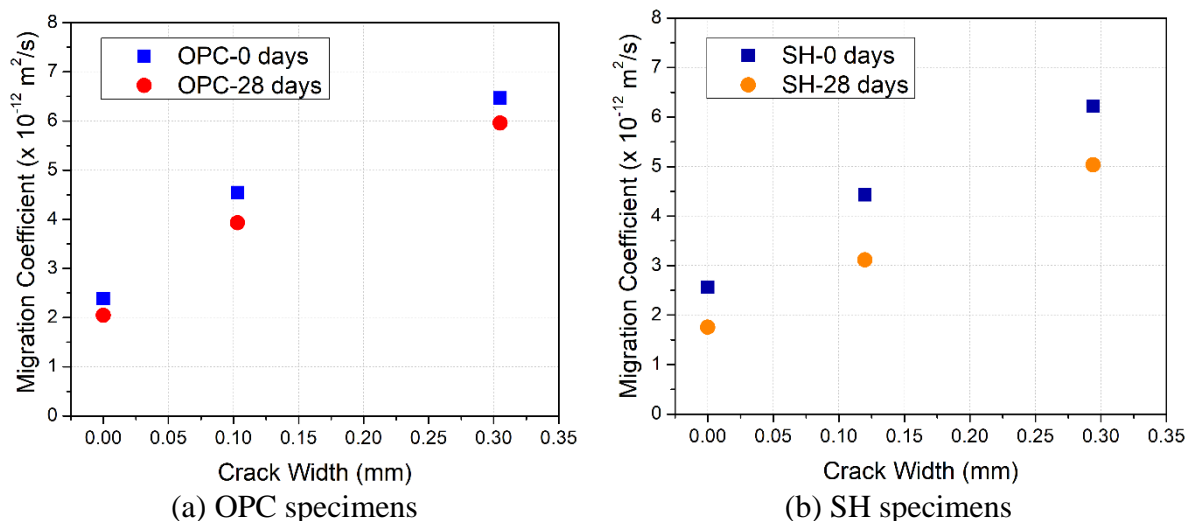


Figure 2: Migration coefficients vs crack widths

3.2 Evaluation of the self-healing performance

In this study, the self-healing efficiency is defined as an index of the self-healing capacity on the basis of the rate of chloride ion ingress through the crack as follows.

$$SH(t) = 1 - \frac{Q_{cr}(t)}{Q_{cr,i}} = 1 - \frac{D_{cr}(t)A_{cr}(t)}{D_{cr,i}A_{cr,i}} = 1 - \frac{[D_{eq}(t) - D_{ucr}(t)] A_{tot}}{[D_{eq,i} - D_{ucr,i}] A_{tot}} \quad (3)$$

$$SH(t) = 1 - \frac{D_{eq}(t) - D_{ucr}(t)}{D_{eq,i} - D_{ucr,i}}$$

where SH is the self-healing efficiency, and $Q_{cr}(t)$ and $Q_{cr,i}$ are the ionic flow rates at the healing age t and initial stage, respectively ($\text{kg}/\text{m}^3/\text{s}$). $D_{cr}(t)$ and $D_{ucr}(t)$ are the migration coefficient through crack and that of the uncracked part at the healing age t (m^2/s), respectively. $D_{eq}(t)$ is the equivalent migration coefficient of the entire mortar including crack and uncracked part. $D_{eq,i}$ and $D_{ucr,i}$ are the migration coefficients at the initial stage (m^2/s).

Table 2 summarizes the calculated self-healing efficiency at the healing age of 28 days according to the mix type and the crack width. The results show that the self-healing efficiencies of the SH specimens are greater than those of OPC specimens. Also, it is noted that at the smaller crack width, the higher self-healing efficiencies were obtained.

Table 2: Summary of chloride migration coefficients and self-healing efficiencies

Binder	Crack width (mm)	$D_{eq,i}$ at the initial stage ($\times 10^{-12} \text{ m}^2/\text{s}$)	D_{eq} after 28-day healing ($\times 10^{-12} \text{ m}^2/\text{s}$)	Self-healing efficiency (%)
OPC	0	2.389	2.047	-
	0.103	4.543	3.931	12.55
	0.305	6.468	5.957	4.14
SH	0	2.566	1.756	-
	0.120	4.430	3.116	27.04
	0.294	6.218	5.035	10.22

4. CONCLUSIONS

In this study, a method to characterize the self-healing capacity of cement-based materials with regard to the chloride penetration was proposed. The results have shown that it is possible to utilize the self-healing efficiency obtained from the steady-state migration tests using the conventional RCM test set-up as an index of the self-healing capacity of concrete.

ACKNOWLEDGEMENTS

This research was supported by a grant (18SCIP-B103706-04) from Construction Technology Research Program funded by the Ministry of Land, Infrastructure, and Transport of the Korean Government.

REFERENCES

- [1] Maes, M., Snoeck, D., and Belie, N. D., 'Chloride penetration in cracked mortar and the influence of autogenous crack healing', *Constr. Build. Mater.* **115** (2016) 114–124.
- [2] Belleghem, B.V., Kessler, S., Heede, P.V.D., and Tittelboom, K., V., 'Chloride induced reinforcement corrosion behavior in self-healing concrete with encapsulated polyurethane', *Cem. Concr. Res.* **113** (2018) 130-139.
- [3] De Nardi, C., Bullo, S., Ferrara, L., Ronchin, L. and Vavasori, A., 'Effectiveness of crystalline admixtures and lime/cement microcapsules in engineered self-healing capacity of lime mortars', *Mater. Struct.* **50** (2017) 191.
- [4] Ferrara, L., Mullem, T.V., Alonso, M.C., Antonaci, P., Borg, R.P., Cuenca, E., Jefferson, A., Ng, P.-L., Peled, A., Roig-Flores, M., Sanchez, M., Schroefl, C., Serna, P., Snoeck, D., Tulliani, J. M. and Belie, N.D., 'Experimental characterization of the self-healing capacity of cement-based materials and its effects on the material performance: A state of the art report by COST Action SARCOS WG2', *Constr. Build. Mater.* **167** (2018) 115-142.
- [5] Bjorn, V.B, Philip, V.D.H and Nele, D.B, 'Resistance to Chloride Penetration of Self-Healing Concrete with Encapsulated Polyurethane', in 'Sustainable Construction Materials and Technologies', The 4th International Conference on Sustainable Construction Materials and Technologies (SCMT4) Las Vegas, USA, August 7-11 (2016), 1386–1395.
- [6] Darquennes, A., Olivier, K., Benboudjema, F. and Gagne, R., 'Self-healing at early-age, a way to improve the chloride resistance of blast-furnace slag cementitious materials', *Constr. Build. Mater.* **113** (2016) 1017-1028.
- [7] Jang, S.Y, Kim, B.K. and Oh, B.H., 'Effect of crack width on chloride diffusion coefficients of concrete by steady-state migration tests', *Cem. Concr. Res.* **41** (2011) 9–19.
- [8] Abro, F.R., Buller, A.S., Jang, S.Y. and Lee, K.M., Chloride Ion Migration Coefficient of Cracked Mortar Specimens Using Steady-State Migration Test Method, in 'Sustainability and Innovation in Concrete Materials and Structures' 8th International Conference of Asian Concrete Federation Fuzhou, China, November 4-7 (2018).

INVESTIGATION ON SELF-HEALING CHARACTERISTIC OF CEMENTITIOUS MATERIALS INCORPORATING SUPPLEMENTARY CEMENTITIOUS MATERIAL AND CRYSTALLINE ADMIXTURE ACCORDING TO EXPOSED ENVIRONMENT

B. Park (1), S. W. Oh (1), Y. C. Choi (2), S. W. Yoo (2) and S. W. Jung (1)

(1) High-Tech Construction Materials Center, Korea Conformity Laboratories, South Korea

(2) Department of Civil and Environmental Engineering, Gachon University, South Korea

Abstract

In recent years, many research papers have been published to investigate self-healing performance incorporating supplementary cementitious materials (SCMs) and crystalline admixtures (CA). It has been confirmed that the self-healing products are changed by the incorporation of SCMs and CA. And, in some papers, it was shown crack width of 0.25 mm was self-healed incorporating CA. However, most studies using inorganic binders focus on the self-healing performance of cementitious materials depending on the type of inorganic binder, and there is a lack of research on the investigation of self-healing characteristics according to environmental conditions. Since the concrete structure is exposed to various environments, it is necessary to examine the self-healing performance depending on the exposure environment.

In this study, the crack self-healing characteristics of cementitious materials incorporating SCMs and CA were investigated according to exposure environment conditions. Experiments were conducted under three environmental conditions of exposure: $\text{Ca}(\text{OH})_2$ solution, high temperature (55°C) and room temperature environment. XRD and SEM analysis were performed to analyze the components of the self-healing materials.

Keywords: Self-healing; Cementitious materials; Exposed Environment; Mineral admixture; Healing products

1. INTRODUCTION

The cracks in the concrete act as the path of the harmful ions same like Cl^- and promote the inflow of harmful ions into the concrete, which is a main cause of reducing the durability of

the concrete structure. Self-healing concrete is a technique to improve the durability of concrete by crack healing autogenously without any repair work. Most studies on self-healing concrete have been conducted on the development of self-healing materials such as bacteria, capsules, inorganic binder. Self-healing concrete technology using inorganic has been studied to improve self-healing performance incorporating of supplementary cementitious materials (SCMs) such as fly ash (FA), ground granulated blast-furnace slag (GGBFS), silica fume (SF) and crystalline admixture (CA). The self-healing properties of the self-healing concrete are different depending on the exposure environment of the crack because the crack is healed by the further hydration of the unreacted binder located in the crack and precipitation of calcite. However, there is still a lack of research on crack self-healing characteristics according to the exposure environment.

In this study, The self - healing properties of inorganic self - healing materials were investigated according to exposure conditions. GGBS and Na₂SO₄ were used as inorganic self-healing materials. Experiments were conducted under three environmental conditions: Ca(OH)₂ solution, high temperature (55°C) and room temperature environment. XRD and SEM analysis were performed to analyze the components of the self-healing materials.

2. EXPERIMENTAL PROGRAM

2.1 Materials

In this study, research cement (RC) and ground granulated blast-furnace slag (GGBS) were used as inorganic binder. RC was prepared by inter-grinding 96% of Portland cement clinker and 4% of Gypsum to eliminate the influence of impurities contained in OPC. The density of RC is 3.19 g/cm³, and the specific surface area is 3,880 cm²/g. GGBS is a product from P Company of Korea. The specific surface area and density of GGBS are 4,280 cm²/g and 2.87 g/cm³, respectively. The mean diameters of RC and GGBS are 11.8µm and 14.02µm, respectively. Table 1 shows the chemical composition of RC and GGBS measured by XRF.

Table 1: Chemical compositions of RC and GGBS

	CaO	SiO ₂	Al ₂ O ₃	Fe ₂ O ₃	MgO	K ₂ O	Na ₂ O	SO ₃	LOI	Total
RC	63.70	21.22	4.09	3.55	2.73	0.97	-	1.40	1.28	98.94
GGBS	42.51	29.13	15.82	0.67	4.43	0.52	1.20	3.34	0.26	97.88

Table 2 shows the blend ratio of cement paste. The water-to-binder ratio was 0.35. A 100x100x10mm slice specimen was prepared for self-healing product analysis.

Table 2: Mixture proportion

	Water	RC	GGBS	Na ₂ SO ₄
MH-1	35	100		
MH-2	35	60	35	5

2.2 Test methods

Cracks occurring in cement and concrete specimens are generated in irregular type, and it is very difficult to obtain self - healing products in the crack plane. Therefore, in order to analyze chemical composition of the self-healing products in crack, it is necessary to acquire the self-healing product newly formed on the crack surface separately from the original cement matrix. In this study, self-healing products were obtained in the same way as study of Huang. 32 slices of 100×100×10 mm paste slice were prepared using the mixture proportion of Table 2 to make artificial cracks for the self-healing product. After mixing, the specimens were cured at 23°C and RH 100% chamber for 24 hours, then demolded and cured in a 20 ± 1°C water container until 7 days. At 7 days, the specimens were taken out, dried for 4 hours, and polished to make the surface of the specimen uniform. 8 slice specimens were bundled into specimens with artificial cracks.

In order to describe the crack self-healing, the specimen is placed in the container and the solution is filled with 2 cm of the bottom of the specimen. The solution used was tap water and Ca(OH)₂ solution. To analyze the effect of temperature, the specimens placed in tap water were self-healed in a chamber of 23°C and a chamber of 55°C. After curing for 7 days, all specimens were separated. Self-healing products between the artificial crack surfaces of the specimen were collected using a plastic putter. The obtained self-healing material was dried for 24 hours at a 40°C chamber for component analysis.

3. RESULTS AND DISSCUTIONS

3.1 XRD analysis

Figures 1~3 show the XRD patterns of crack self-healing products according to environmental conditions. Figure 1 shows the XRD pattern of self-healing product at tap water (23°C). In the case of MH-1, calcite, arcanite, and portlandite were the major products. In MH-2, calcite and Na compounds such as trona and thermonatrite were the main compounds. In the XRD pattern of MH-2, portlandite did not appear, probably because the portlandite was exhausted during the hydration of GGBS. Also Na compounds were included in self - healing products due to Na₂SO₄ used as a crystalline admixture.

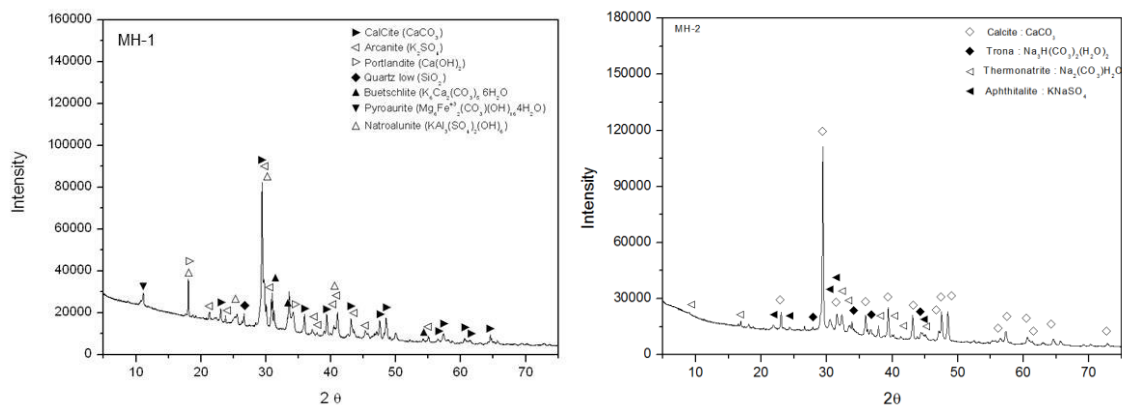


Figure 1: XRD pattern of self-healing product at tap water (23°C)

Figure 2 shows the XRD pattern of self-healing product at tap water (55°C). In MH-1 self-healing substances, portlandite was the main self-healing substance and calcite was partially present. In MH-2 self-healing substances, compounds containing Al ions appeared, unlike self-healing substances at room temperature.

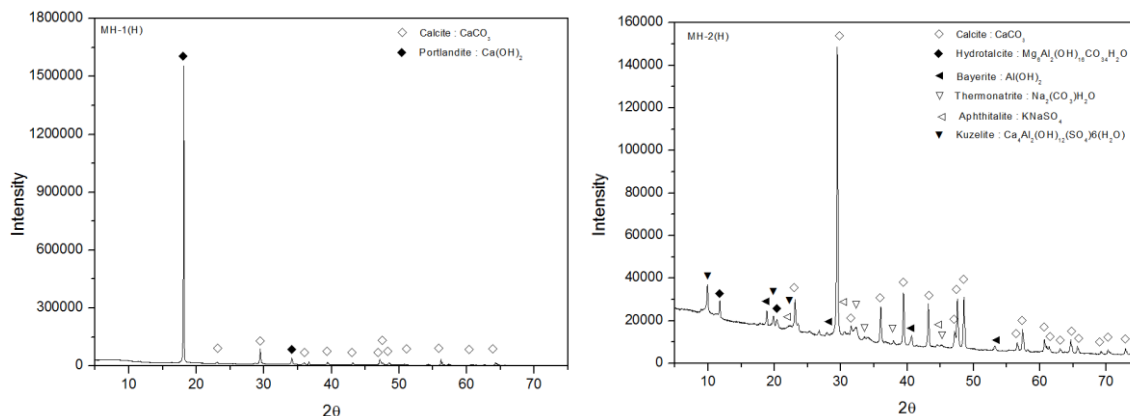


Figure 2: XRD pattern of self-healing product at tap water (55°C)

Figure 3 shows the XRD pattern of the self-healing product at Ca(OH)₂ solution. As a result of XRD pattern analysis of MH-1, there was no significant difference from tap water (23°C), and in case of MH-2, portlandite was confirmed unlike tap water (23°C).

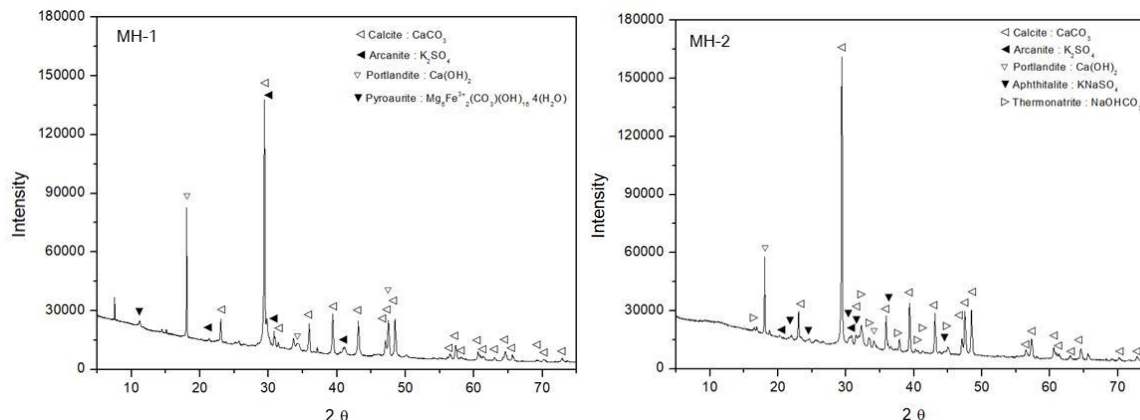


Figure 3: XRD pattern of self-healing product at Ca(OH)₂ solution

3.2 SEM analysis

Figure 4 and Figure 5 show SEM observations of self-healing products. Figure 4 shows the SEM observations of MH-1 self-healing products. portlandite was predominant in self-healing products at 55°C tap water and calcite and portlandite were found at 23°C tap water. Figure 5 shows the SEM observations of MH-2 self-healing products. Unlike the self-healing substances produced at 23°C tap water, portlandite was found in the self - healing substances

produced in $\text{Ca}(\text{OH})_2$ solution. This suggests that the formation of self-healing substances by further hydration of GGBS is advantageous in the $\text{Ca}(\text{OH})_2$ solution.

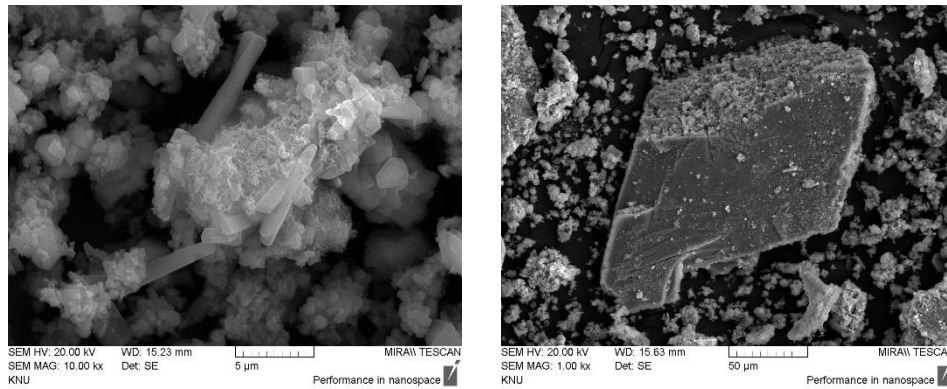


Figure 4: SEM observations of self-healing products of MH-1; (Left) 23°C Tap water, (Right) 55°C Tap water

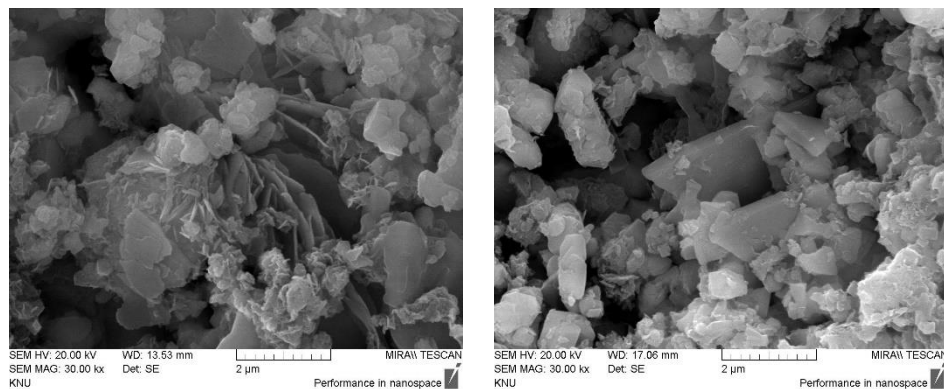


Figure 5: SEM observations of self-healing products of MH-2; (Left) 23°C Tap water, (Right) $\text{Ca}(\text{OH})_2$ solution

4. CONCLUSION

In this study, the self-healing properties of cementitious materials were investigated according to the exposure environment conditions of the cracks. As an inorganic binder, GGBS and CA were used in addition to the RC manufactured by using cement clinker and anhydrite. Experiments were conducted under three environmental conditions of exposure: $\text{Ca}(\text{OH})_2$ solution, high temperature (55°C) and room temperature environment. The self-healing materials in crack of cementitious materials were investigated by XRD and SEM analysis. In the case of MH-1, portlandite increased with increasing temperature, and no other substance was observed. In the case of MH-2, the number of compounds containing Al ions increased with increasing temperature. When exposed to $\text{Ca}(\text{OH})_2$ solution, the peak of

portlandite increased in both specimens, so it can be concluded that $\text{Ca}(\text{OH})_2$ was sufficient to further hydration of GGBS contained in MH-2. It is confirmed that results of SEM analysis showed similar conclusions of XRD analysis. Therefore, the autogenous healing properties of the inorganic binder depend on the exposure environment, and self-healing materials optimized for environmental conditions are needed to improve the crack healing performance.

ACKNOWLEDGEMENTS

This research was supported by a grant(18SCIP-B103706-04) from Construction Technology Research Program funded by Ministry of Land, Infrastructure and Transport of Korean government. And this work was also supported by the Korea Institute of Energy Technology Evaluation and Planning(KETEP) and the Ministry of Trade, Industry & Energy(MOTIE) of the Republic of Korea (No. 20181110200070).

REFERENCES

- [1] Ahn, T.H. and Kishi, T., 'Crack Self-healing Behavior of Cementitious Composites Incorporating Various Mineral Admixtures', *J. Adv. Concr. Technol.* **8** (2010) 171-186.
- [2] Qiu, J., Tan, H.S. and Yang, E.H., 'Coupled effects of crack width, slag content, and conditioning alkalinity on autogenous healing of engineered cementitious composites', *Cem. Concr. Compos.* **73** (2016) 203-212.
- [3] Termkhajornkit, P., Nawa, T., Yamashiro, Y. and Saito, T., 'Self-healing ability of fly ash–cement systems', *Cem. Concr. Compos.* **31** (2009) 195-203.
- [4] Huang, H., Ye, G., Damidot, D., 'Characterization and quantification of self-healing behaviors of microcracks due to further hydration in cement paste', *Cem. Concr. Res.* **52** (2013) 71-81.
- [5] Park, B. and Choi, Y.C., 'Quantitative evaluation of crack self-healing in cement-based materials by absorption test', *Constr. Build. Mater.* **30** (2018) 1-10.

SELF-SEALING OF CRACKS IN CEMENTITIOUS MATERIALS INCORPORATING SUPERABSORBENT POLYMERS UNDER WET/DRY CYCLIC CONDITIONS

S. Choi (1), G. Hong (1), C. Song (1)

(1) Department of Civil and Environmental Engineering, Chung-Ang University, Seoul 06974, South Korea

Abstract

This study experimentally investigated the hysteretic behavior of crack self-sealing and self-healing in superabsorbent polymer (SAP)-added cementitious materials due to the repeated swelling/deswelling of SAPs exposed to wet/dry cyclic conditions. Water flow test and image analysis were used to analyze both the short-term self-sealing by repeated swelling of SAPs and the long-term self-healing by internal curing of SAPs. The cement paste and mortar specimens including different dosages of SAPs were fabricated and the cracks were induced at the different ages of the specimens. The water flow test results showed that rapid swelling of SAPs by absorbing ingress water effectively sealed cracks in cementitious materials. From the point of view of a self-sealing, the reduction ratio of flow rate through cracks initially increased and then gradually converged as the wet/dry cycles repeated. From the point of view of a self-healing, meanwhile, the water runoff through cracks decreased as the cracks were healed by the internal curing of SAPs under wet/dry cyclic conditions. The results of this study suggest that SAPs are effective in both self-sealing and self-healing of cracks in the cementitious materials exposed to wet/dry cyclic environment.

Keywords: Self-sealing, Self-healing, Superabsorbent polymer (SAP), Wet/dry cycles

1. INTRODUCTION

Concrete is the most widely used construction material even though it has the property of easily cracking due to shrinkage, hydration heat and limited tensile strength. Cracks occurring in concrete cause durability to deteriorate by allowing harmful ions to reach the internal cementitious matrix from the outside [1]. For this reason, many researches have been conducting using superabsorbent polymers (SAPs) for the purpose of resolving the problem of durability degradation of concrete due to cracking [2,3]. Research results have shown that SAPs improve the self-sealing and self-healing performance of cracks in cementitious materials [4,5].

Generally, cracks in concrete structures are not constantly exposed to moisture, and in most cases the water is supplied by rainfall from time to time. However, studies on crack self-sealing and self-healing evaluation by SAPs in wet/dry cyclic condition are insufficient. Therefore, in this study, crack self-sealing and self-healing performance of cracked cementitious materials including SAP exposed to wet/dry cyclic condition were evaluated experimentally through water flow test.

2. EXPERIMENT

2.1 Materials

Table 1 shows the composition of the mixture of cement pasted and mortar specimens used in the experiment. In the case of a mixture of cement paste, the water-cement ratio (w/c) was 0.35. And in case of cement mortar mixture, w/c and sand-cement ratio (s/c) were 0.5 and 1.7, respectively. The SAP contents were used with 0.5% and 1.0% of the cement weight.

Because one of the purposes in this study is to evaluate hysteretic behaviour of crack self-sealing in cementitious materials including SAPs exposed to wet/dry cyclic condition, the series II mortar specimens adopted a relatively high water-to-cement ratio so that the self-healing caused by the internal curing of SAPs can be minimized. In addition, the amount of additional water absorbed in SAPs was decided to ensure that the workability of SAPs-added specimens was the same as that of the reference specimen without SAPs [5]. Two different shapes of SAPs were used in the test; the labels S_i and S_r in Table 1 denote irregular-shaped and spherical-shaped SAPs, respectively.

Table 1: Cement paste and mortar mixture proportions

Specimen	ID	Free w/c	Component (kg)			
			Cement	Sand	SAP	Water in SAP
<i>Series I</i>						
Cement paste (reference)	CP-R	0.35	1.0	-	-	-
Cement paste – 0.5% S_i	CP- S_i -0.5	0.35	1.0	-	0.005	0.05
Cement paste – 1.0% S_i	CP- S_i -1.0	0.35	1.0	-	0.01	0.1
<i>Series II</i>						
Cement mortar (reference)	CM-R	0.5	1.0	1.7	-	-
Cement mortar – 0.5% S_r	CM- S_r -0.5	0.5	1.0	1.7	0.005	0.05
Cement mortar – 1.0% S_r	CM- S_r -1.0	0.5	1.0	1.7	0.01	0.1

2.2 Specimen preparations and test methods

The specimens for water flow test were disc-shaped ones, of which the diameter and height were 70 mm and 30 mm, respectively. For the series I specimens in Table 1, after standard curing (23 ± 1 °C; 100% RH) for 7 days, the through-crack was induced at the center of the

specimens, in which the induced crack width of $300 \pm 50 \mu\text{m}$ was controlled by wrapping the specimens with the silicon sheet. For the series II specimens in Table 1, after standard curing ($23 \pm 1 \text{ }^\circ\text{C}$; 100% RH) for 28 days, the through-crack was induced in the same way as in the series I specimens and their crack width were $400 \pm 50 \mu\text{m}$. During the water flow test, the water head was maintained at 20 mm from the top surface of the specimens and the distilled water used in the test. Table 2 presents the test conditions for the water flow test and the amount of water runoff through the crack was measured at every cycle.

Table 2: Test conditions for the water flow test

Specimen	The number of cycles	Wetting condition	Drying condition
<i>Series I</i>	8 cycles	1 h ($20 \pm 1 \text{ }^\circ\text{C}$)	47 h ($25 \pm 1 \text{ }^\circ\text{C}$, $50 \pm 1\% \text{ RH}$)
<i>Series II</i>	10 cycles	20 min ($20 \pm 1 \text{ }^\circ\text{C}$)	47 h 40 min ($40 \pm 1 \text{ }^\circ\text{C}$, $2 \pm 1\% \text{ RH}$)

3. RESULTS

3.1 Water flow test

Fig. 1 shows the mean and standard deviation of the reduction ratio of flow rate for the series II specimens exposed to wet/dry cyclic condition. The reduction ratio of flow rate of the CM-R was overall smaller than those of the CM-S_r-0.5 and CM-S_r-1.0. In addition, the reduction ratio of CM-R changed little over the number of cycles whereas those of CM-S_r-0.5 and CM-S_r-1.0 increased as the wet/dry cycle was repeated and was stabilized after 6-cycle. The reduction ratio of the specimens incorporating SAPs increased with the increase of SAPs dosage.

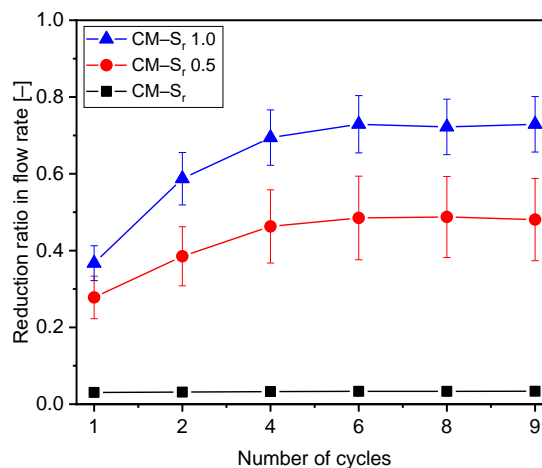


Figure 1: Reduction ratio in flow rate for mortar specimens under wet/dry cyclic conditions

Fig. 2 shows the variation in the flow rate of the series I specimens over the number of wet/dry cycle. The flow rate represents the amount of water runoff through the crack per unit time every cycle. The flow rates of the CP-R in 6-cycle was about 38–45% lower than that in 1-cycle. However, the flow rates of the CP-S_i-0.5 and CP-S_i-1.0 decreased more rapidly than the CP-R as the wet / dry cycle was repeated. The flow rates CP-S_i-0.5 and CP-S_i-1.0 in 6-cycle was about 68–86% and 94-97%, respectively, lower than that in 1-cycle. This is because the further hydration was promoted as the additional moisture absorbed in SAPs was released to the cracks of the specimens including SAPs under dry condition.

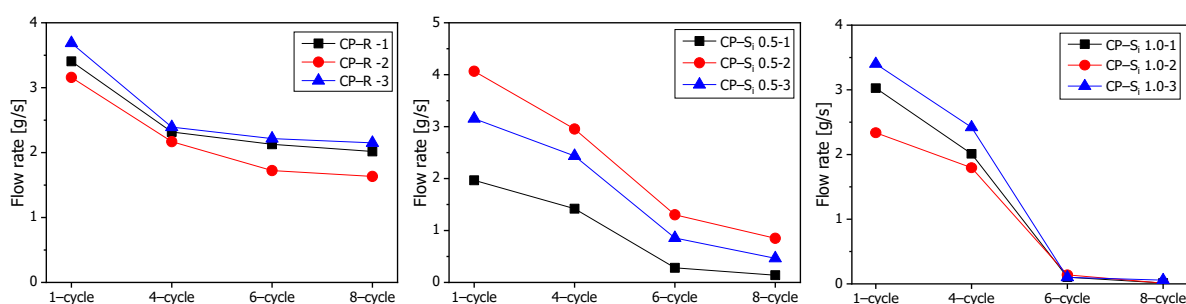


Figure 2: Flow rate development for paste specimens under wet/dry cyclic conditions

4. CONCLUSIONS

In this study, long term crack self-healing and hysteretic behavior of crack self-sealing in cementitious materials were analysed experimentally, considering SAP dosage and crack width.

- SAPs are repeatedly effective for rapid crack self-sealing in cementitious materials under wet/dry cyclic conditions. In addition, as the cycle was repeated, the self-sealing performance of SAPs improved. The reduction ratio of flow rate of the specimens including round-shaped SAPs gradually increased and then converged as wet/dry cycle was repeated. The mean reduction ratios of CM-S_r-0.5 and CM-S_r-1.0 in 6-cycle were about 1.74 time and 1.98 times those of 1-cycle.
- SAPs are highly effective for self-healing of cracks in cementitious materials by internal curing effect under wet/dry cyclic conditions. The water flow test result shows that the flow rate of CP-S_i-1.0 was almost converged to '0' in 6-cycle.

ACKNOWLEDGEMENTS

This research was supported by a grant(18SCIP-B103706-04) from Construction Technology Research Program funded by Ministry of Land, Infrastructure and Transport of Korean government.

REFERENCES

- [1] Otieno, M., Beushausen, H., Alexander, M., 'Chloride-induced corrosion of steel in cracked concrete-Part I: Experimental studies under accelerated and natural marine environments', Cem. Concr. Res. 79 (2016) 373-385.

- [2] Mechtcherine, V., Reinhardt, H.W. (Eds.), 'Application of superabsorbent polymers in concrete construction', in: State-of-the-art Report prepared by the RILEM TC 225-SAP, Springer, Heidelberg (Germany) (2012)
- [3] Mechtcherine, V., 'Use of superabsorbent polymers (SAP) as concrete additive', RILEM Techn. Lett. 1 (2016) 81–87.
- [4] Snoeck, D., Dewanckele, J., Cnudde, V., De Belie, N., 'X-ray computed microtomography to study autogenous healing of cementitious materials promoted by superabsorbent polymers', Cem. Concr. Comp. 65 (2016) 83–93.
- [5] Hong, G., Choi, S., 'Rapid self-sealing of cracks in cementitious materials incorporating superabsorbent polymers', Constr. Build. Mater. 143 (2017) 366–375.

SELF-HEALING PERFORMANCE OF ENGINEERED CEMENTITIOUS COMPOSITES THROUGH THE USE OF NANO-SILICA

Oğuzhan Öztürk (1), Gürkan Yıldırım (2), Ülkü S. Keskin (1), Mustafa Şahmaran (3)

(1) Civil Engineering Department, Konya Technical University, Turkey

(2) Civil Engineering Department, Kırıkkale University, Turkey

(3) Civil Engineering Department, Hacettepe University, Turkey

Abstract

The COST Action CA15202 – Self-healing As preventive Repair of CONcrete Structures (SARCOS), has gathered European researchers active in the field of self-healing cement-based materials and within this context has secured the financial support of the European Commission. Within the frameworks of different working groups of SARCOS, several review papers focusing on self-healing cementitious materials have already been published. Engineered Cementitious Composite (ECC) is reported to be one of such promising materials which combine superior mechanical and durability properties. These superior characteristics make the material a favorable preference for various infrastructures. ECCs exhibit strain/deflection-hardening behavior by forming multiple micro-cracks under severe loading conditions unlike normal or conventional fiber reinforced concrete. It is also known that autogenous self-healing is an inherent property of ECCs and the extent of intrinsic self-healing is substantially dependent on crack widths. This behavior can provide decrements of detrimental substance ingress in structures so that longer service life can be possible. However, studies available in the literature reported that success of self-healing becomes limited when larger cracks and repetitive mechanical loadings take place. Here, efforts were made to confront the abovementioned limitations of intrinsic self-healing of ECC compositions with nano-silica. Results of experiments revealed that nano-silica utilization triggered more robust and expedited self-healing products in the cracks of cementitious system along with unhydrated cement particles that also contributed for higher strength grades. Micro analysis indicated that wider cracks ($>250\ \mu\text{m}$) can be fully closed by nano-silica incorporation in ECCs. In addition, preloaded nano-silica incorporated ECC specimens attained permeability properties similar to uncracked specimens. It can be concluded that autogenous self-healing of ECCs can be further improved in terms of both mechanical and transport properties with the use of nano-silica which tailors the microstructure and contributes to enhanced healing mechanisms of conventional ECC mixtures.

Keywords: Engineered Cementitious Composites (ECC), self-healing, nano modification, nano-silica.

1. INTRODUCTION

Despite the efforts to cope with difficulties of short service life, concrete structures still underperform under severe environmental effects and mechanical loadings. Moreover, to externally repair the damage occurrences is costly [1]. One of the main contributors of this adverse condition is the natural tendency of plain conventional concrete to crack in a brittle manner under tensile loads. For this reason, concrete is often produced with steel reinforcement to compensate for resistance to tensile loads. However, it is almost inevitable to offset crack formation in reinforced concrete elements which leads to the ingress of deleterious materials such as chloride, sulfate, salts and other undesirable substances in water.

Penetrations of such materials can drastically reduce the long term performance of reinforced concrete structures. To overcome this shortcoming of conventional concrete, High-Performance Fiber Reinforced Cementitious Composites (HPFRCCs) have been developed in the last few decades. The most distinctive characteristic of HPFRCCs is the tensile strain-hardening response coupled with the formation of multiple microcracks. This behavior is due to micromechanical engineering of fiber, matrix and interface interaction [2,3]. Engineered Cementitious Composites (ECC) is one of the special types of HPFRCCs developed by Victor Li [4] and has been of topic to many studies so far [5,6].

To functionalize the benefits of ECC in wide range of infrastructures, many efforts have been made to investigate the self-healing capability of ECC under different conditions [7]. Although different mechanisms are reported to be influential on autogenous self-healing capability of ECCs, presence of cracks with small widths is crucial for the completeness of the mechanism [8].

Recently, the use of nano materials in cement-based materials such as paste, mortar and concrete has become popular. Given its relatively high specific surface area and reactivity, nano-silica (NS) is also used in literature to modify the early-age strength problem of cement-based mixtures with high volumes of fly ash. The literature survey reveals that studies which include cement-based systems with different nano materials focus mostly on the fresh-state, hydration, microstructural characterization, pore structure, mechanical/transport/durability properties of concrete [9]. Unlike studies in the literature, the work at hand focuses on favoring self-healing capability of ECCs with the use of NS. It is believed that the outcomes of current research will contribute to existing knowledge by proposing a novel way to use nano-materials in the systems of cementitious composites.

2. EXPERIMENTS

2.1 Materials

The experimental program was conducted on ECC specimens produced with NS. The specimens were prepared by using Class-F fly ash (FA), CEM I 42.5 Portland cement (PC) silica sand (with maximum aggregate size of 0.4 mm), polyvinyl-alcohol (PVA) fibres, water and polycarboxylic-ether based high range water reducing admixture (HRWRA). Nano-silica particles (NS, used by 3% of the total weight of cementitious materials) were used to accelerate and increase the rate of self-healing. Physical properties and chemical compositions of PC, FA, silica sand and NS are given in Table 1.

Table 1: Physical properties and chemical compositions of PC, FA, silica sand and NS

Materials	Chemical composition, %								Physical properties		
	SiO ₂	Al ₂ O ₃	Fe ₂ O ₃	MgO	CaO	Na ₂ O	K ₂ O	LOI*	Specific gravity	Blaine fineness (m ² /kg)	BET (m ² /kg)
PC	20.8	5.55	3.35	2.49	61.4	0.19	0.77	2.20	3.06	325	-
FA	60.8	21.7	5.48	1.71	3.48	0.74	1.95	1.57	2.10	290	-
Sand	99.8	0.06	0.02	0.01	0.02	0.02	0.01	0.07	2.60	-	-
NS	99.2	0.38	0.18	0.25	0.00	0.02	0.00	-	2.40	-	163.2

*LOI: Loss on ignition

2.2 Mixture Proportions

Two different ECC mixtures (ECC/Ref and ECC/NS) were produced with a water to cementitious materials (CM=FA+PC) ratio (W/CM) of 0.27 and a fly ash to Portland cement (FA/PC) ratio of 1.2. PVA fibres were used by 2% of total mixtures' volume. High range water reducing admixture (HRWRA) was adjusted (5.1 and 6.9 kg/m³ for ECC/Ref and ECC/NS, respectively) considering the similar flow consistency of different ECC mixtures. The amount of NS used in the mixtures was 3% of total weight of CM. The proportions for ECC mixtures are given in Table 2.

Table 2. Mass of ECC ingredients¹

Mix ID	Cement	Fly ash	Water	PVA	NS	SP	Sand
ECC/Ref	566	679.2	336.2	26	-	5.1	438.5
ECC/NS	566	679.2	336.2	26	30.4	6.9	405.5

¹ in kg/m³

2.3 Mixing

To prepare ECC/Ref mixture, dry raw materials were initially mixed together at 100 rpm for a minute in a mortar mixer. After dry mixing, total amounts of water and HRWRA were added into the mixture and mixing was continued at 150 rpm for a minute and later at 300 rpm for additional 2 minutes. Lastly, PVA fibres were added into fresh mixture and mixing was continued for 3 minutes at 150 rpm. ECC/NS mixture was produced with the uniformly distributed NS solution added into dry ingredients. To do this, a previously verified mixing procedure of NS was followed [10]. All mixing water and 25% of the total HRWRA were ultrasonically mixed with the NS powder for 5 minutes. At the same time, ECC ingredients were prepared in a separate mortar mixer similar to ECC/Ref mixture. At the end of the dry mixing of ECC ingredients, prepared NS solution was poured into ECC mixture and mixing was kept on for an additional minute at low speed. The rest of the HRWRA was added and mixing was continued for 3 more minutes. Finally, PVA fibers were added into fresh mixture and mixing was continued for another 3 minutes. After mixing and casting, all mixtures were kept in their molds for 24 hours at 50±5% RH, 23±2°C. Then, specimens were removed and cured in isolated plastic bags until predetermined ages at 95±5% RH, 23±2°C.

2.4 Experimental Methods

Tests were performed in terms of compressive strength, chloride ion permeability and microscopic observations. At least three separate 50-mm cubic specimens from each mixture

were tested in accordance with the ASTM C109 at 7 and 28 days for compressive strength. Self-healing performance was assessed in terms of rapid chloride permeability test (RCPT) (according to ASTM C1202) and microscopic observations on disc specimens measuring $\text{Ø}100 \times 50$ mm cut out of larger $\text{Ø}100 \times 200$ mm cylinders. Six different disc specimens were prepared for each mixture. Four of them were preloaded up to their 75% of ultimate deflection capacity at 7 days by performing splitting tensile test. Preloading level (75%) was preferred in order to simulate severe damage occurrences on ECC specimens in real conditions. Splitting tensile loading was applied by a closed-loop controlled universal testing system at a loading rate of 0.005 mm/s (Figure 1). Two of the specimens were kept uncracked for comparison. Both uncracked and preloaded specimens were cured under water after 7 days. The cracks of preloaded specimens were identified after the preloading and tracked at 7+0, 7+7 and 7+28 days by the use of video microscope with a maximum enlargement capacity of 125X.

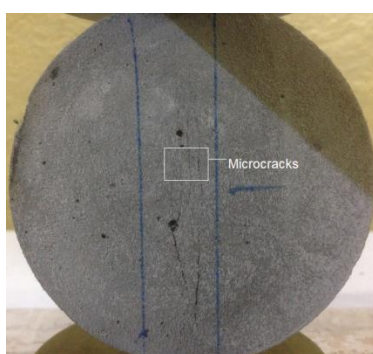


Figure 1. Preloading of cylindrical specimens under splitting tensile loading

3. RESULTS AND DISCUSSION

3.1. Compressive Strength

Compressive strength results of 7- and 28-day-old cubic specimens are given in Table 3. Incorporation of NS into ECC systems increased the compressive strength both at 7 and 28 days compared to ECC/Ref specimens.

Table 3. Results of compressive strength tests

Mix ID	7 days			28 days		
	ECC/Ref	28.9	29.9	30.7	53.8	58.1
ECC/NS	31.6	36.3	36.1	63.8	65.2	66.4

7-day-old cubic specimens modified with NS exhibited 16.4% higher compressive strength than the average compressive strength of ECC/Ref specimens (Figure 2). At 7 days, higher average compressive strength of NS-incorporated specimen can be explained by the superior pozzolanic activity of NS particles [10]. In addition, NS particles may have provided nucleation sites for additional C-S-H gel formation due to very small average particles size. Therefore, it can be stated that NS stimulates the hydration and triggered accelerated pozzolanic activity [10, 11]. The amorphous structure of NS is likely to accelerate pozzolanic reactions with CH activating high-volume-fly ash system for early age development [12].

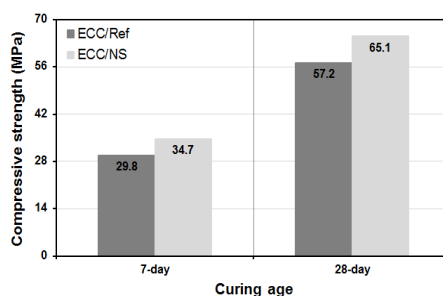


Figure 2. Average compressive strength results of ECC mixtures at 7 and 28 days

Average of compressive strength results of NS-bearing cubic specimens was 13.8% higher than ECC/Ref at 28 days as depicted in Figure 2. The improved microstructure of nano-modified ECC specimens also resulted in higher compressive strength at 28 days. The higher improvements in compressive strength are probably due to lesser porosity of ECC/NS mixtures [10]. Thanks to smaller average particle size of NS compared to FA and PC, particle size distribution of cementitious systems may have improved thus contributing to denser microstructure. Despite size factor of 50 mm-cubic specimens, two mixtures (ECC/Ref and ECC/NS) were acceptable even at 7 days in terms of minimum 28-day old compressive strength (30 MPa) with regards to latest Turkish Building Code [13].

3.2. Rapid Chloride Permeability Test (RCPT)

RCPT results are presented in Table 4 in terms of total amount of charge (Coulomb) [C] passed through the specimens. Average RCPT results of 7-day-old uncracked specimens reveal that ECC/NS (250 C) exhibited lower chloride ion permeability compared to ECC/Ref (635 C). 7-day-old ECC/NS specimens were more resistant to chloride ion penetration than ECC/Ref specimens. This result may be attributed to NS particles being much finer than cementitious materials (PC, FA) of reference mixture and having higher pozzolanic capacity that contributes to better particle distribution and denser microstructure.

Table 4. Chloride ion permeability of ECC specimens (Coulomb)

Mix ID.		7+0 days	7+7 days	7+28 days
ECC/Ref	Uncracked	630	233	152
		640	214	146
	Preloaded	2831	1270	395
		2982	1048	279
ECC/NS	Uncracked	2296	1486	436
		2450	884	297
	Preloaded	214	117	83
		286	143	100
		2234	1237	947
		1330	682	421
Preloaded	1774	1005	545	
	1624	1029	586	

RCPT results of uncracked specimens decreased with the application of further curing irrespective of mixture type. This can be explained with the gradual maturation of matrix properties for both mixtures. This behaviour is clearly seen in Figure 3 as percental decrements of results. Decrements in RCPT results were very sudden especially after 7+7

days of curing although continuing reductions were also registered for uncracked ECC specimens at 7+28 days.

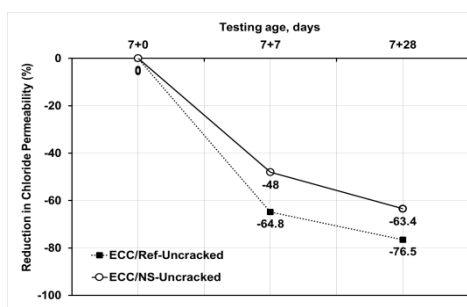


Figure 3. Reduction of chloride ion permeability for uncracked specimens

At 7+7 days, reduction of RCPT results were more pronounced for uncracked ECC/Ref specimens. These higher reductions of RCPT results of uncracked ECC/Ref specimens compared to uncracked ECC/NS specimens were due to faster exhaustion of unhydrated cementitious particles after 7 days of curing. It can be stated that faster exhaustion of nano-silica explicitly lowered the RCPT results until first 7 days of curing for uncracked ECC/NS specimens (250 C and 635 C for ECC/Ref and ECC/NS) while slow hydration of fly ash particles seems to contribute to decrease of RCPT results for uncracked ECC/Ref specimens only after 7+7 days (64.5% and 53% for uncracked ECC/Ref and ECC/S specimens, respectively). Similar behaviour can be also seen for the RCPT results of uncracked specimens at 7+28 days in Figure 3. At 7+28 days, further consumption of portlandite after pozzolanic capability of fly ash in ECC/Ref specimens [14] could be already preceded compared to ECC/NS specimens. This capability may have triggered higher decrement of RCPT results for uncracked ECC/Ref specimens at 7+28 days (76.5% and 57.5% for uncracked ECC/Ref and ECC/NS specimens). Despite the higher average RCPT results obtained for ECC/Ref specimens compared to ECC/NS specimens at 7+0, 7+7 and 7+28 days, respectively, all values were lower than 1000C which can be considered “very low” in terms of the chloride ion penetration levels according to ASTM C 1202.

Initial preloading of uncracked specimens at 7+0 days increased the RCPT results. Interconnection of pores and additional paths for ionic travelling increased after inducing of the cracks on the specimens [15]. The average rate of increment of RCPT results after preloading was 316% and 596% for ECC/Ref and ECC/NS specimens, respectively. This higher increment of ECC/NS specimens can be attributed to the stronger chemical bonding between individual PVA fibres and matrices resulting in fibre rupture instead of pull-out. This behaviour leads to a lower number of cracks with increased widths (Figure 4). Although wider crack widths of NS incorporated specimens were expected to increase RCPT values compared to reference specimens, this was not the case. Higher maturation of specimens in the presence of NS may have lowered the chloride permeability. However it is important to note that the average RCPT results of ECC/Ref (2640C) and ECC/NS (1740) specimens after preloading can be accepted as moderate ion penetrability level in accordance with the ASTM C 1202.

After curing for additional 7 days, RCPT results of preloaded specimens revealed considerable reductions taking into account of their previous values at preloading day. Preloaded ECC/Ref specimens fell from a “moderate” to “low” penetrability level (1172C) while preloaded ECC/NS specimens fell from a “moderate” to “very low” penetrability

level (988C). So it can be deduced that values of NS bearing specimens can be regarded as negligible in terms of chloride penetration only after 7 days of curing. However, it should be noted that chloride penetrability level of preloaded ECC/NS specimens (625C) fell behind the level of preloaded ECC/Ref specimens (352C) at 7+28 days of curing due to similar reason of uncracked specimens at same age as previously explained (Figure 5).

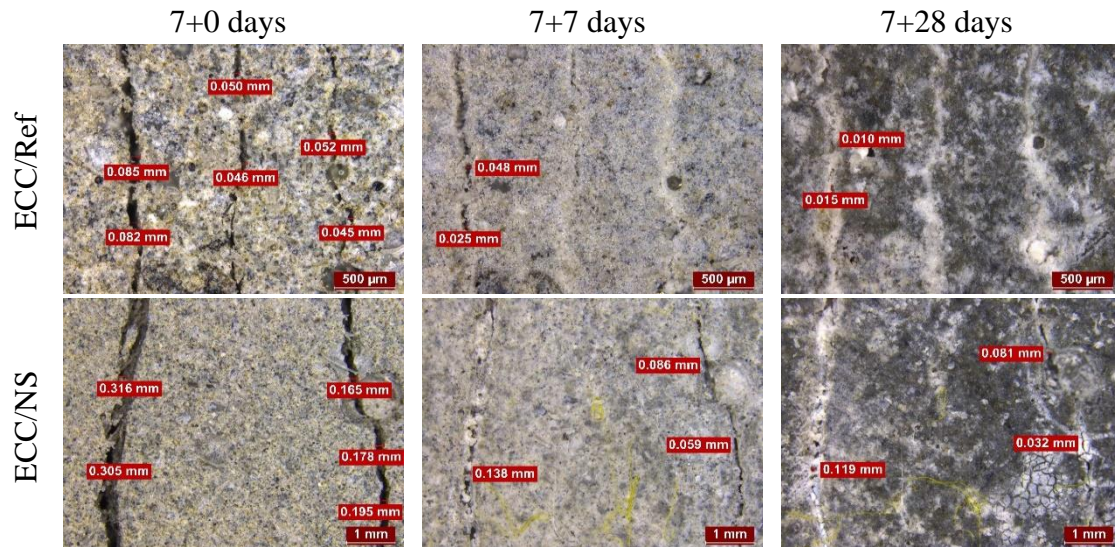


Figure 4. Self-healing of cracks in ECC specimens

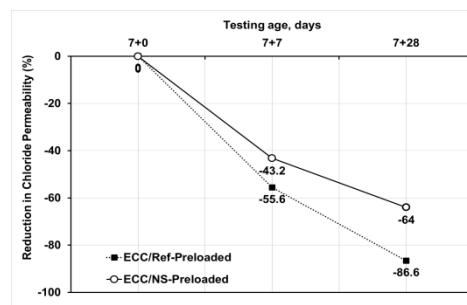


Figure 5. Percental changes in chloride ion permeability results of preloaded specimens

4. CONCLUSIONS

Following conclusions can be drawn from the current study:

- Incorporation of NS into ECC matrices increased the compressive strength both at 7 and 28 days compared to the reference mixtures.
- RCPT results of uncracked specimens were more favoring for ECC/NS specimens from 7+0 days to 7+28 days. However, RCPT values of uncracked ECC/Ref specimens were also acceptable to be considered as “very low” in all ages according to chloride penetrability level.
- Preloaded ECC/NS specimens exhibited higher percental increment in RCPT tests at 7+0 days in comparison with the reference specimens. Self-healing of ECC/NS specimens in terms of chloride permeability resistance was promising at 7+7 days although this behavior was likely to change at 7+28 days in favor of ECC/Ref specimens.

- Although accelerated higher self-healing rate is registered for ECC/NS specimens at 7+7 days, additional supportive materials for further promoting self-healing in ECC materials can be preferably used. In this sense, binary use of NS and carbon nanotubes (CNTs) in engineered cementitious composites to stimulate self-healing phenomenon is under investigation by the authors.

ACKNOWLEDGEMENT

The authors gratefully acknowledge the financial assistance of the Scientific and Technical Research Council (TUBITAK) of Turkey provided under project: 117M954 and COST Action CA15202 (SARCOS). <http://www.sarcos.enq.cam.ac.uk>.

REFERENCES

- [1] Tittelboom K.V. and Belie, N.D., ‘Self-Healing in Cementitious Materials—A Review’, *Materials*, **6** (2013) 2182-2217.
- [2] Naaman, A. E., and Homrich, J.R., ‘Tensile Stress Strain Properties of SIFCON’. *ACI Materials Journal*, **86** (1989) 244–251.
- [3] Li, V.C., and Leung C.K.Y., ‘Theory of Steady State and Multiple Cracking of Random Discontinuous Fiber-Reinforced Brittle Matrix Composites’, *Journal of Engineering Mechanics*, **118** (1992) 2246–2264.
- [4] Li, V. C., ‘On Engineered Cementitious Composites (ECC)—A Review of the Material and Its Applications’, *Advanced Concrete Technology*, **1** (2003) 215–230.
- [5] Şahmaran, M., Li, M., and Li. V. C., ‘Transport Properties of Engineered Cementitious Composites Under Chloride Exposure’, *ACI Materials Journal*, **104** (2007) 604–611.
- [6] Şahmaran, M., and Li. V. C., ‘Influence of Microcracking on Water Absorption and Sorptivity of ECC’. *RILEM Materials and Structures*, **42** (2009) 593–603.
- [7] Yıldırım, G., Keskin, Ö. K., Keskin, S. B., Şahmaran, M., and Lachemi, M. ‘A review of intrinsic self-healing capability of engineered cementitious composites: Recovery of transport and mechanical properties’, *Construction and Building Materials*, **101**, (2015) 10-21.
- [8] Neville, A., ‘Autogenous healing—A concrete miracle?’, *Concrete International*, **24** (2002) 76–82.
- [9] Safiuddin M, Gonzalez M, Cao J, Tighe SL. ‘State-of-the-art report on use of nano-materials in concrete’ *Int. J Pavement Eng* **15** (2014) 940–949.
- [10] Al-Najjar, Y., Yeşilmen, S., Al-Dahawi, A.M, Şahmaran M., Yıldırım G., Lachemi M., and Amleh L., ‘Physical and Chemical Actions of Nano-Mineral Additives on Properties of High-Volume Fly Ash Engineered Cementitious Composites’, *ACI Materials Journal*, **6** (2016) 791-801.
- [11] Li. G., ‘Properties of high volume fly ash concrete incorporating nano SiO₂’ *Cement and Concrete Research*, **34** (2004) 1043-1049.
- [12] Zhang M.H., Islam, J., ‘Use of nano-silica to reduce setting time and increase early strength of concretes with high volumes of fly ash or slag’, *Construction and Building Materials*, **29** (2012) 573-580.
- [13] Turkish Earthquake Code, 2018, Specification for Buildings to be Built in Seismic Zones, Ankara, Turkey, 2018.
- [14] C. Andrade C., ‘Calculation of chloride diffusion coefficients in concrete from ionic migration measurements’ *Cement and Concrete Research*, **23** (1993) 724-742.
Yıldırım, G., Aras, G.H., Banyhussan, Q.S., Şahmaran, M., Lachemi M., ‘Estimating the self-healing capability of cementitious composites through non-destructive electrical-based monitoring’, *Ndt&E Int.* **76** (2015) 26-37.

EFFECT OF SUPERABSORBENT POLYMERS ON PLASTIC SHRINKAGE CRACKING AND PROPERTIES OF FRESH STATE MORTARS REINFORCED BY POLYMERIC FIBRES

Rohollah Rostami (*), Agnieszka J. Klemm

School of Computing, Engineering and Built Environment, Glasgow Caledonian University, UK

(*), corresponding author

Abstract

Superabsorbent polymers (SAPs) in cementitious materials can be successfully used as internal curing agents by providing continuous supply of water for hydration processes. The kinetics of absorption and desorption of water play a critical role in formation of dense and uniform microstructure and hence significantly influence long term durability and sustainability of mortars. However, the effect of SAPs on shrinkage cracking in early age fibre reinforced mortars (FRM) still remains unclear and deficient. The current study aims to address this issue by evaluating the effect of SAPs on plastic shrinkage cracking in cementitious mortars reinforced by polymeric fibre and made with three types of cement (CEM I–PC, CEM II –FA and CEM III–GGBS). The plastic shrinkage cracking was analysed by the optical microscopy according to ASTM C1579-13 standard. Fresh state properties were characterised by flow table, air content and setting time tests. The results showed that SAPs significantly reduce development of plastic shrinkage cracking and enhance its serviceability. It was also found that the fresh state properties of fibre reinforced mortars with different type of cements are strongly affected by different SAPs as governed by their particles size and absorption/desorption kinetics.

Keywords: Superabsorbent polymers, Fibre Reinforced Mortars, Plastic Shrinkage, Fresh state Properties

1. INTRODUCTION

Supplementary cementitious materials (SCMs) are commonly used to improve sustainability of Portland cement-based materials and reduce its environmental impact. The use of SCMs, leads to a significant reduction in carbon dioxide emissions from cement industry [1]. However, early age shrinkage of cementitious systems is still a major concern due to the complex hydration reactions. This often leads to early cracking induced by self-desiccation processes [2]. Even within the first hours after casting before final set, plastic shrinkage can take place, leading to crack formation in concrete and to compromising its

serviceability. Addition of Superabsorbent Polymers (SAPs) may mitigate Autogenous [3] and plastic shrinkage [4]. SAP is a natural or synthetic water-insoluble three-dimensional network of polymeric chains, with the ability to absorb aqueous fluids from the environment dispersed throughout the structure. Although there are some studies on SAP application in terms of plastic shrinkage mitigation [4, 5], its influence on shrinkage cracking at early age in fibre reinforced mortars (FRM) still remain unclear. Therefore, the main purpose of this study is to assess the effect of different SAPs on plastic shrinkage and properties of FRM in fresh state. Three types of SAPs with SAP with different particles size and different water absorption capacities and three types of cement (CEM I– Portland cement (PC), CEM II– fly ash (FA) and CEM III– Ground Granulated Blastfurnace Slag (GGBS)) were analysed.

2. MATERIALS AND METHODS

Three types of cement have been used, including CEM I 52.5N (PC), CEM II/B-V 42.5N (FA), and CEM III/A 42.5N (GGBS). CEM I, II and III have been supplied by Hanson Cements (UK), Lafarge (UK) and Ecocem (Ireland) respectively. Chemical and physical characteristics of cements provided by manufacturers are presented in Table 1.

Table 1: Chemical and physical analysis of CEM I, II and III

Compound (%)	SiO ₂	Al ₂ O ₃	Fe ₂ O ₃	CaO	MgO	K ₂ O	Cl	MnO	TiO ₂	ZnO	Mn ₃ O ₄	Loss on ignition
CEM I	20.76	4.99	2.57	64.30	2.19	0.27	0.06	0.00	0.00	0.00	0.00	2.39
CEM II	32.69	13.13	3.29	43.48	1.33	1.26	0.00	0.07	0.56	0.02	0.00	0.00
CEM III	24.50	8.99	1.76	57.13	5.33	0.00	0.04	5.33	0.58	0.00	0.16	1.19

The micro polypropylene fibres used in this study were provided by ADFIL Construction Fibres (UK). The length of fibre is 6-mm, diameter 18 μ m and density 0.91 kg/m³.

Three different types of SAPs (BASF) have been considered: SAP A, SAP C and SAP E with water absorption capacities (WAC) in cement paste solution of 20 g/g, 25-30 g/g and 30 g/g respectively. SAPs were characterized by SEM analysis (Fig. 1). The chemistry of SAP C and E are the same, but different particle sizes (Fig. 2a). Figures 2(a) and (b) show results of particle size distribution tests of SAPs by the Laser Diffraction and the fine sand (Fife Silica Sands, UK) determined by sieving test (BS EN13139:2013[6]).

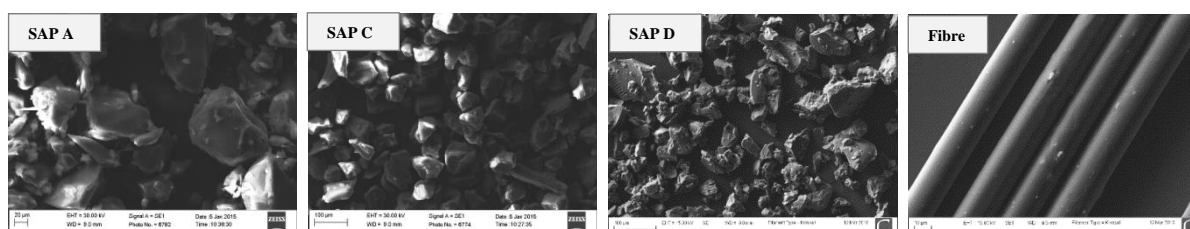


Figure 1: The SEM micrographs of SAP A, C, E and Fibre

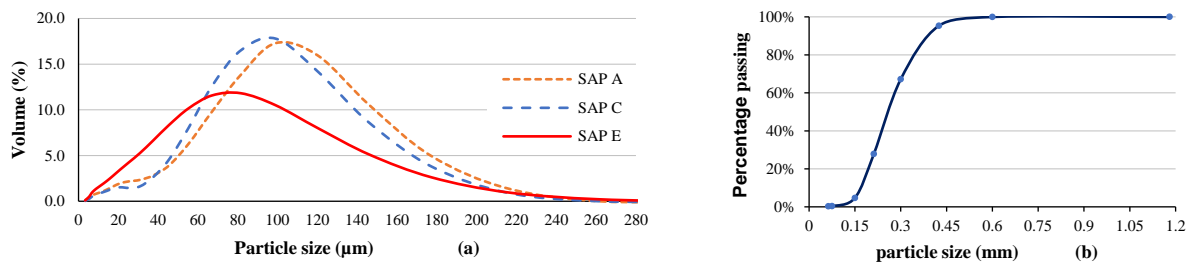


Figure 2: (a) Particle size distribution of SAPs and (b) Sand

All studied mortars had cement to fine sand ratio of 1:2 (by weight). In order to obtain similar consistencies of plastic mortars total water/binder ratios have been adjusted to achieve flow values in a range of 140 - 200 mm according to EN 1015-6:1999 [7]. The theoretical calculation of the amount of water/binder ratio (0.47) was based on the adopted concepts of water bound by cement hydration [8]. The additional water-to-binder ratio $(w/b)_{add}$ is the amount of water absorption by the SAP [9]. Three types of SAPs were added to mixtures in equal amounts of 0.25 % by mass of cement as previously adopted in studies by [3, 8]. The amount of fibre used was constant 0.50 % by mass of cement. The chosen dosage of PP fibres was based on the previously published reports [10, 11]. Table 2 shows the mix proportions of materials used in this study together with effective water/binder ratio $(w/b)_{eff}$, additional water/binder ratio $(w/b)_{add}$ and the total water/binder ratio $(w/b)_{tot}$ and flow values (EN 1015-3:1999 [12]).

Table 2: Mix proportions of materials, water/binder ratios and flow values

cement	Sample name	SAP type	SAP content	Fibre type	Fibre content	Binder : Sand	$(W/b)_{eff}$	$(W/b)_{add}$	$(W/b)_{tot}$	Flow of $(W/b)_{tot}$
CEM I	I	-	-	-	-	1 : 2	0.47	0.01	0.48	141
	II	-	-	1	0.50%	1 : 2	0.47	0.05	0.52	141
	IA1	A	0.25%	1	0.50%	1 : 2	0.47	0.11	0.58	142
	IC1	C	0.25%	1	0.50%	1 : 2	0.47	0.11	0.58	141
	IE1	E	0.25%	1	0.50%	1 : 2	0.47	0.11	0.58	140
CEM II	II	-	-	-	-	1 : 2	0.47	-0.02	0.45	140
	III	-	-	1	0.50%	1 : 2	0.47	0.03	0.5	140
	IIA1	A	0.25%	1	0.50%	1 : 2	0.47	0.09	0.56	142
	IIC1	C	0.25%	1	0.50%	1 : 2	0.47	0.09	0.56	141
	IIIE1	E	0.25%	1	0.50%	1 : 2	0.47	0.1	0.57	139
CEM III	III	-	-	-	-	1 : 2	0.47	0.01	0.48	142
	IIII	-	-	1	-	1 : 2	0.47	0.05	0.52	142
	IIIA1	A	0.25%	1	0.50%	1 : 2	0.47	0.11	0.58	142
	IIIC1	C	0.25%	1	0.50%	1 : 2	0.47	0.11	0.58	141
	IIIE1	E	0.25%	1	0.50%	1 : 2	0.47	0.11	0.58	140

Fresh state mortars were characterised with respect to their consistency (flow table method, EN 1015- 3:1999[12]), air content (pressure method, EN 1015-7:1999[13]), and initial and final setting times (Vicat apparatus, EN 460- 3:2006[14]) in laboratory environment (temperature $21 \pm 2^\circ\text{C}$ and RH $40 \pm 5\%$).

The effect of SAPs on plastic shrinkage cracking in cementitious mortars reinforced by PP fibres and made with three types of cement (CEM I-PC, CEM II –FA and CEM III- GGBS) were determined and compared. The plastic shrinkage was analysed by the optical microscope according to ASTM C1579-13 [15] standard. According to ASTM C1579-13[15], the temperature during the first 24 hours of experiment was maintained at 36 ± 3 °C, and the relative humidity at 30 ± 10 %. Free shrinkage measurements were done on mortar specimens of $160 \times 140 \times 40$ mm. For the restraint conditions, three $140 \times 20 \times 0.2$ mm aluminium plates were placed equally and symmetrically on each steel threaded bar (Φ 8 mm) (Fig. 4). The moulds were filled with mortar in two layers and compacted for 10 seconds (using vibrating table).

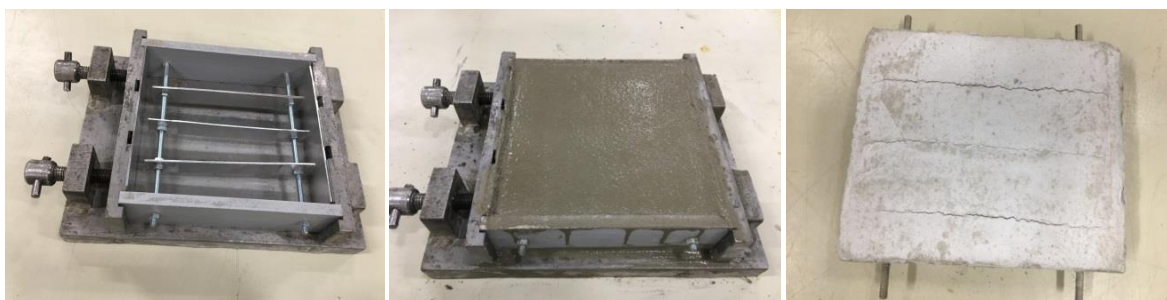


Figure 4: Moulds used for plastic shrinkage tests

The water evaporation was recorded after 30 min, 60 min and afterwards every hour after mixing. An optical microscope system was used to measure the crack widths on the free surface.

3. RESULTS AND DISCUSSION

As shown in Table 2, in order to achieve the similar flow values different amounts of water had to be added and hence different total w/b ratios have been used. It is clear that both SAPs and PP fibres decrease workability, however, the effect of SAPs is more pronounced in all three sets of samples (cement types). Mortars with CEM III (GGBS) had only slightly reduced consistencies in comparison with CEM I mortars. However, as anticipated the biggest adjustments were required for mortars containing CEM II (FA).

Physical properties of fly ash particles, their spherical shape, glassy surfaces and usually finer particles than PC and GGBS result in lower water demand [16]. As it can be seen, the addition of PP fibres required additional water to keep the same consistency of mortars. This effect is directly linked to the characteristics of fibre, including fibre type, geometry, content, distribution and its orientation as well as matrix properties [17]. The addition of SAPs to FRM leads to decreased workability of mortars due to its high water absorption capacity. By comparing the additional w/b values used for SAP mortars, it can be concluded that SAP A has the highest effect on consistency for all three types of cement. SAP E had lower consistency. This can be explained by the lowest (WAC) of SAP A and finer particles of SAP E.

The corresponding air content of mortars is shown in Figure 4. The presence of PP fibres lead to the increase of air content. Addition of SAPs only slightly decreased air content for CEM I and III. The strongest effect was recorded for CEM II, where air content dropped by

approximately 2.6%. This could be attributed to reduce total water/binder ratios in CEM II mortars and lower additional water in SAPs with CEM II mortars. Higher air content values have been recorded for FRM containing CEM I and III in comparison to their reference samples. Addition of SAPs to CEM I and III had very limited effect on air content; however, SAP E had the lowest air content. Likely reasons for this wide variety of results can be associated, on one hand, with the effect of different WAC of SAPs (SAP C has higher WAC) and on the other hand with different particles size (SAP E has smaller particles).

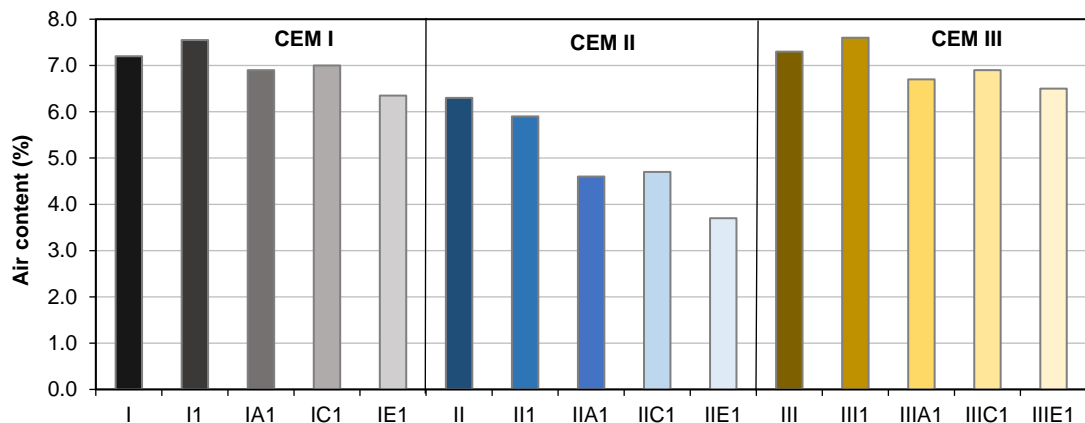


Figure 5: Air content of fresh state mortars

In addition, it can be concluded that the addition of SAP leads to slightly reduced air content for most of FRM. However, SAPs in CEM II mortars can have a noticeable effect on air content of mortars, probably due to finer cement particles [16]. The results of initial and final setting times of mortars are shown in figure 6. Initial setting times for mortars with fibres occur slightly earlier then for the reference samples. However, the time of initial setting is increased for all SAP samples regardless the type of cement.

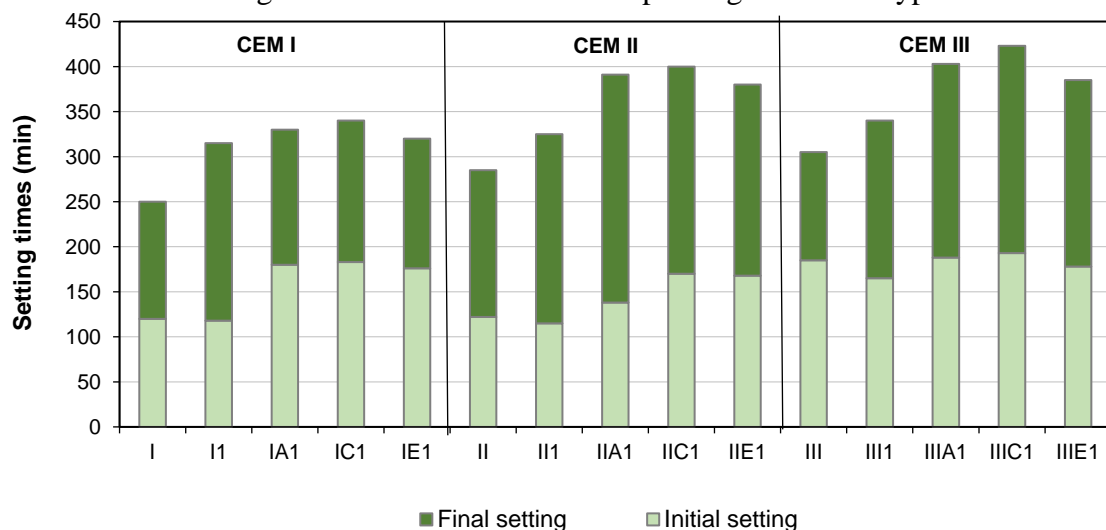


Figure 6: Setting times of mortars

The similar trends have been also observed for the final set times, although it was more pronounced for blended cements. Samples with CEM III (GGBS) had longer setting times than with CEM I and CEM II (FA). These times were further prolonged by addition of fibres and SAPs, as previously reported in [18]. When analysing samples within three different sets (cement types) the common feature was identified: all SAP C mortars had the longest final setting times, followed by SAP A and SAP E mortars. The bigger differences were observed between mortars with SAP C and SAP E (of the same chemistry) leading to the conclusion that the particle sizes are more important than the total water absorption capacities.

The shrinkage due to capillary pressure is the main reason of plastic shrinkage cracking [3]. The visible cracks displayed on all reference samples were measured according to the ASTM C1579-13 standard [15] (Fig.7). Cracks below 0.05 mm are very fine and difficult to be identified. Furthermore, the minimum visible cracks that can be identified by the naked eyes are around 0.1 mm width [19]. The optical microscope was used for measurements of cracks 0.05 mm wide. Therefore, in this study the maximum of large cracks (above 0.1 mm) and minimum of fine cracks (below 0.05 mm) were considered for determining total average for all mortars. Figure 7 shows representative micrographs of the average largest crack found on the surfaces of each mortar after 24 hours under severe environmental conditions. The crack distributions on the surfaces of mortars for different type of cement with PP fibre and different types of SAPs are presented.

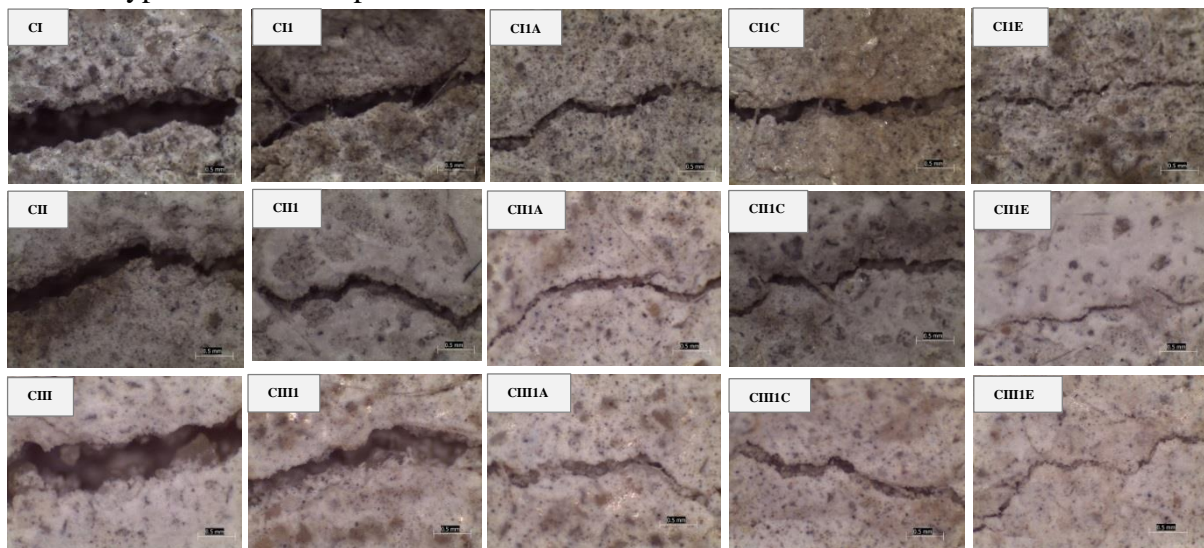


Figure 7: Comparison of the largest cracks formed in different mortars (35x magnification)

Overall, SAPs significantly reduced the development of plastic shrinkage cracking in all samples. By comparing (Figs. 7 and 8), it can be concluded that CEM II mortars had the smallest crack width and CEM III mortars had the widest cracks. Also CEM I mortars showed smaller crack width when compared to CEM III. It can be attributed to the fineness of cement [16]. As it has been reported by [4] the increased cement fineness reduces the maximum crack width. Moreover, the cements with SAP E, which had smaller particle sizes, lead to the finest crack width than those with other SAPs. On the other hand, SAP C mortars showed the largest crack formation than SAP A and E, probably due to the larger particle sizes of SAP C. It can be concluded that the smaller SAP is more suitable for reduction of plastic shrinkage.

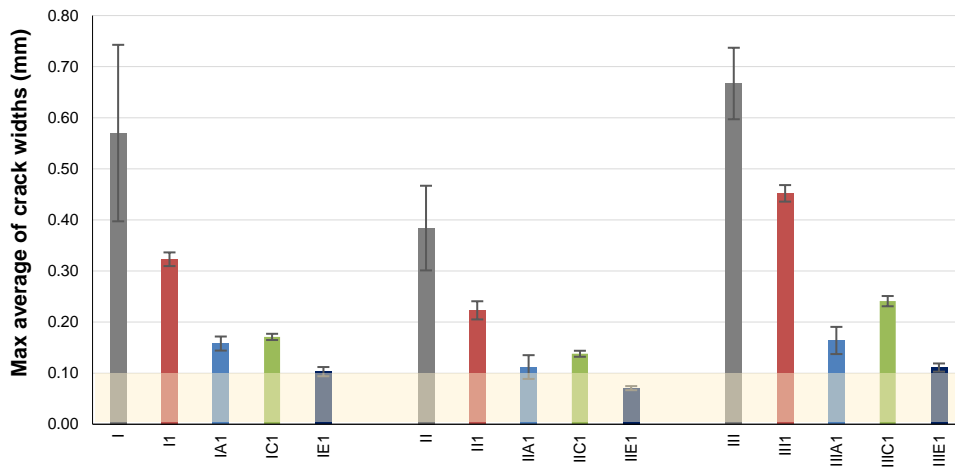


Figure 8: Maximum averages of crack widths (mm)

Figure 9 shows the evaporation rates of all mortars over time at 24h. For clarity purpose, the Figure only shows the results of references samples, SAP E and CEM III were presented. However, other samples had similar pattern. These evaporation rates are shown around 5-6%, which confirm effectiveness of designed system used in this study according to the ASTM C1579-13 standard [15].

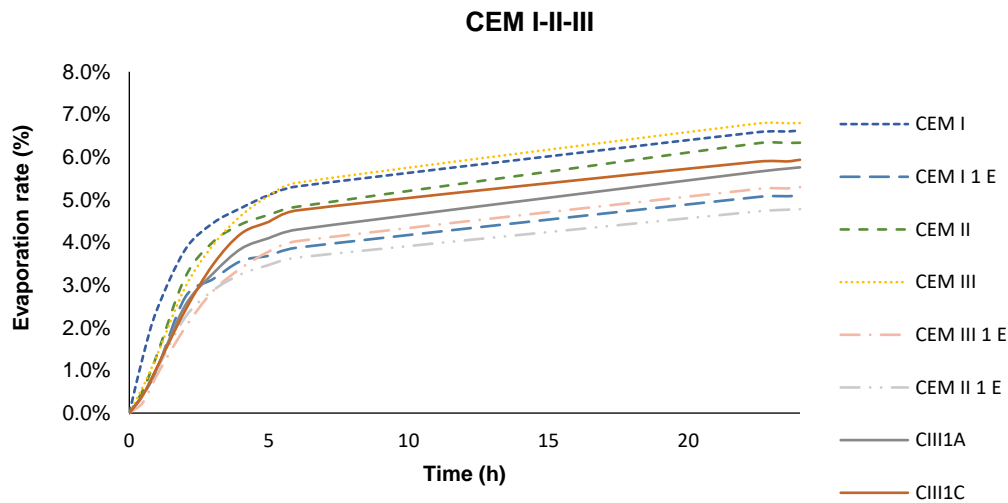


Figure 9: Water evaporation rates during plastic shrinkage tests

As shown in Figure 9, the highest water evaporation rates were recorded for the reference mortars. This in turn resulted in formation of larger cracks. The samples with SAPs had the lowest evaporation rates when compared to the reference. Furthermore, SAP E in mortars with CEM II had the lowest evaporation rate due to smaller particle sizes. Consequently, smaller SAP had significant effects on reduction of plastic shrinkage and is more suitable for mitigation of plastic shrinkage.

4. CONCLUSION

The reinforced mortars made with three types of cement (CEM I–PC, CEM II–FA and CEM III–GGBS) and three types of SAP with different particles size and different water absorption capacities have been analysed. It was found that the addition of SAPs have major influence on the fresh state properties of FRM and different SAPs (particle sizes and absorption/desorption kinetics) behave differently in blended cements with SCM. From the obtained experimental results, the following can be concluded:

- The addition of SAP to FRM leads to decreased workability of mortars due to its high WAC. The highest workability was recorded for samples with SAP A (lowest WAC) and the lowest workability was displayed by samples containing SAP E (with finest SAP particles);
- SAPs slightly reduce air content for most of FRM, but the strongest effect was recorded for CEM II with SAP E, where air content dropped by approximately 2.6%. Furthermore, SAP C had the highest air content (higher WAC) and SAP E had the lowest air content (smaller particles);
- Addition of SAP retards both initial and final set times of FRM. SAP C mortars had the longest final setting times, followed by SAP A and SAP E mortars. The bigger differences were observed between mortars with SAP C and SAP E (of the same chemistry) leading to the conclusion that the particle sizes are more important than the total water absorption capacities;

SAPs significantly reduce the development of plastic shrinkage cracking in all mortars. Evaporation rates for all SAP samples were lower than for the reference ones, hence the cracks widths were smaller. The biggest effect on crack reduction can be achieved by application of fine SAPs (SAP E). The effect of different water absorption capacities (SAP A and C) is of less importance.

REFERENCES

- [1] Miller, S. A., (2018), *Journal of Cleaner Production*. 178 (2018) 587-598.
- [2] Wyrzykowski, M. and Lura, P. 2016. *Cement and Concrete Research*. 85, pp.75–81.
- [3] Schröfl, C. Mechtcherine, V., Gorges, M. (2012). *Cem Concr Res* 42(6):865–873.
- [4] Ghourchian, S., et al., (2018). *Cement and Concrete Composites* 91 (2018) 148–155.
- [5] Snoeck, D. Pel, L. and De Belie, N. (2018). *Cement and Concrete Composites*. 93 (2018) 54–62.
- [6] BSI 2013. BS EN 13139. *Aggregates for Mortar*. British Standards Institution.
- [7] BSI 1999. BS EN 1015-3. British Standards Institution.
- [8] Lura, P., Winnefeld, F., Fang, X., (2017). *J Therm Anal Calorim* (2017) 130:653–660.
- [9] Snoeck, D., Jensen, O. M., & De Belie, N. (2015). *Cement and Concrete Research*, 74, 59–67.
- [10] Richardson, A. E. (2006). *Structural Survey* 24(2): 138–153.
- [11] Yazici S, et al. (2015). *Concrete Research* 67(16): 867–875.
- [12] BSI 1999. BS EN 1015-3. British Standards Institution.
- [13] BSI 1999. BS EN 1015-7. British Standards Institution.
- [14] BSI 2006. BS EN 480-2. Part 2: Determination of Setting Time. British Standards Institution.
- [15] ASTM, “C1579-13. Standard Test Method for Evaluating Plastic Shrinkage Cracking, 2013.
- [16] De Belie, N. Soutsos, M. Gruyaert, E. (2018). *RILEM*. 238-SCM.
- [17] Sadrinejad I, et al., (2018). *Construction and Building Materials* 178 (2018) 72–82.
- [18] D. Suresh and K. Nagaraju, *IOSR J. Mech. Civ. Eng.*, vol. 12, no. 4, pp. 2278–1684, 2015.
- [19] Serpukhov, I., and Mechtcherine, V., (2015). *ASCE, Rest*, 2015, pp. 1504–1513.

DESIGN AND TESTING OF ANIONIC SUPERABSORBENT POLYMERS FOR USE IN DURABLE CONCRETE STRUCTURES

Laurence De Meyst (1), Els Mannekens (2), Maria Araújo (1, 3), Didier Snoeck (1), Kim Van Tittelboom (1), Sandra Van Vlierberghe (3), Geert Deroover (2), Nele De Belie (1)

- (1) Magnel Laboratory for Concrete Research, Department of Structural Engineering, Ghent University, Tech Lane Ghent Science Park, Campus A, Technologiepark Zwijnaarde 904, B-9052 Ghent, Belgium
- (2) ChemStream bvba, Drie Eikenstraat 661, B-2650 Edegem, Belgium
- (3) Polymer Chemistry and Biomaterials Group, Centre of Macromolecular Chemistry, Department of Organic and Macromolecular Chemistry, Ghent University, Krijgslaan 281, Building S4-bis, 9000 Ghent, Belgium

Abstract

Superabsorbent polymers (SAPs) can be added to a concrete mixture to provide internal curing and reduce the risk for early-age shrinkage cracking. Hence, they help to increase the overall durability of concrete structures. The type, swelling characteristics, kinetics of water release, amount and particle size of the SAPs will dictate their effectiveness for this purpose. An anionic SAP was synthesized with varying amounts of cross-linker and ground to particle sizes with d_{50} varying between 10 and 100 μm . The swelling capacity in demineralised water of 40 μm particles increased with a decreasing degree of cross-linker from 87 g/g SAP to 270 g/g SAP, and was about 3 to 4 times larger than the swelling capacity in cement filtrate. The SAPs were tested for their effect on mortar workability, cement hydration kinetics and mechanical properties of the hardened mortar. With proper compensation for the absorbed water by the SAPs, the mortar workability was not negatively affected and a reduction in flow over the first two hours remained limited. The SAPs with the lowest swelling capacity, resulting in the least macro pore formation, showed the smallest negative effect on mortar compressive strength and a negligible effect on cement hydration. The difference in strength with the reference decreased as a function of mortar age. Different SAP particle sizes in the range of 10 – 100 μm had no significant effect on mortar properties.

Keywords: Superabsorbent polymers (SAPs), mortar properties, particle size, cross-linker

1. INTRODUCTION

Superabsorbent polymers (SAPs) are 3D polymer networks that can retain large amounts of liquids, up to thousand times their own dry weight without dissolving¹. This special feature makes SAPs very interesting to use in concrete applications for different reasons¹: mitigating autogenous shrinkage^{2,3,4}, self-healing of cracked concrete^{5,6}, self-sealing of concrete^{7,8}, increasing the freeze-thaw resistance of concrete^{9,10}, modifying the rheology of fresh concrete^{2,3} etc. Hence, they can help to increase the durability of concrete structures in different ways.

Various types of SAPs are already available. On a chemical base, two extreme types can be distinguished: ionic (charged) and anionic (neutral) polymers¹¹. Commercially available SAPs are mostly ionic polymers and show higher absorption capacity. Another distinction can be made based on the type of cross-links occurring between the polymers: covalent, ionic or hydrogen bonding. These cross-links are the most essential part of the SAPs, as these bonds prevent the SAPs from dissolving.

Besides the aforementioned different properties of SAPs, also other parameters can be used to distinguish SAPs: type (synthetic, semi-synthetic, natural) and cross-linking degree, particle size, etc.. By varying these parameters, insight can be gained in the influence of each of these parameters on SAP properties such as the swelling capacity. In a next step, the SAPs can be implemented in mortar to assess their influence on mortar properties like workability, compressive strength, hydration kinetics. Based on these results, the 'ideal' SAP with tuneable properties for a specific concrete application can be synthesized.

2. MATERIALS & METHODS

2.1. Materials

A reference mortar mixture with a water-to-cement ratio of 0.43 was composed of ordinary Portland cement (CEM I 52.5 N, 510 kg/m³, HOLCIM), silica sand 0/2 (1530 kg/m³) and tap water (219.3 kg/m³). A constant dosage of 0.25 m% (of cement weight) polycarboxylate superplasticizer (Glenium 51, conc. 35%, BASF) was added to obtain an initial flow of 20 cm directly after mixing. In case of SAP-containing mixtures, a constant amount of 0.5 m% SAPs by cement weight was added, as well as additional water to compensate for the water uptake by the SAPs. The amount of additional water was 1.5 times the swelling capacity in cement filtrate obtained from a filtration test. This amount was based on previous tests performed by the author and was found to be the average amount needed to keep the consistency.

The studied SAPs were developed and produced by the Belgian chemical R&D company ChemStream bvba. The SAPs are formed through a copolymerization of sodium vinyl sulfonate (SVS) with 2-acryloylamino-2-methyl-propane-1-sulfonate (NaAMPS) using potassium persulfate (KPS) as thermal initiator and were obtained by a radical bulk polymerization reaction carried out at 70°C. Three different amounts of the cross-linker N,N'-methylenebisacrylamide (MBA) (i.e. 0.15, 0.38 and 0.775 mol% with respect to the used monomer) were used in order to obtain SAPs with different swelling capacities, see Table 1. The obtained SAPs were ground to particle sizes with d_{50} of 10, 40 and 100 μm using a RETSCH ZM200 centrifugal mill.

To prepare the SAP-containing mortar mixtures, first the dry components (cement and SAPs) were mixed for 30 s at low speed (140 rpm) to ensure a homogeneous distribution of the SAPs in the cement. The rest of the mixing procedure was according to the standard NBN EN 196-1.

In this paper, two different test series were made to study two different influences: series 1: the influence of the degree of cross-linking and series 2: the influence of the particle size. For the reference mixture, the code (see Table 1) is REF. For the mixes with SAPs, the

code starts with CS (CS for ChemStream), followed by the degree of cross-linker used in mol% and ending with the particle size in μm (i.e. 10, 40 or 100).

Table 1: Studied mortar mixtures with their code, amount of cross-linker, extra water and corresponding water-to-cement ratios (additional and total), series 1 and 2.

Code	cross-linker amount (mol%)	Extra water (kg/m ³)	(w/c) _{add} (-)	(w/c) _{tot} (-)
REF	/	0	0	0.43
CS_0.15_40	0.15	238	0.47	0.90
CS_0.38_40	0.38	126	0.25	0.68
CS_0.775_10	0.775	106	0.21	0.64
CS_0.775_40	0.775	90	0.18	0.61
CS_0.775_100	0.775	97	0.19	0.62

At the age of two days, all specimens (nine prisms of 40x40x160 mm³ for every mixture) were demoulded, wrapped in plastic foil and subsequently stored in an air-conditioned room with a relative humidity of $60 \pm 5\%$ and a temperature of $20 \pm 2^\circ\text{C}$ until the age of testing.

2.2. Characterisation of SAPs

The synthesized SAPs were characterised by the amount of solubles (i.e. the percentage of the non-cross-linked polymer fraction after synthesis), the swelling capacity in both demineralized water and cement filtrate solution and the mean particle size (d_{50}) of the ground SAPs.

To determine the fraction of the non-cross-linked polymer or the amount of solubles, the following procedure was followed. An excess of water was added to the SAP particles dried in an oven at 80°C . After the SAPs had reached their maximum swollen state, the swollen hydrogel was filtered from the excess of water. Next, the hydrogel was dried in an oven at 80°C to constant mass. The weight loss between the dried SAP after swelling (M_1) and the initial dry SAP before starting the swelling procedure (M_0) was measured. The % solubles was then calculated according to formula (1):

$$\% \text{ solubles} = \frac{(M_0 - M_1)}{M_0} \times 100 \quad (1)$$

The swelling capacity of the SAPs in demineralized water and cement filtrate was determined by the filtration method described in the RILEM TC-RSC WG1 recommendation¹². Therefore, approximately 100 g of fluid was added to around 0.15 g dry SAP particles (exact mass of fluid and SAPs to be recorded). After 24 hours, the SAP particles definitely reached their equilibrium swelling and everything was filtered using filter paper with particle retention 12-15 μm . In order to exclude possible absorption of the fluid by the filter paper, the latter was first saturated with the testing fluid. To minimize evaporation during the test, the test setup was covered with a lid. After filtration, the amount of fluid that was not absorbed by the SAPs, was recorded. The test was performed in triplicate. The swelling ratio, i.e. the amount of fluid that can be absorbed by 1 g of SAPs can be calculated by formula (2):

$$\text{Swelling ratio [g fluid/g SAP]} = \frac{W_{\text{fluid added}} - W_{\text{fluid not absorbed}}}{W_{\text{dry SAP}}} \quad (2)$$

With

- $W_{\text{fluid added}}$ [g]: the amount of fluid before filtration;

- $W_{\text{fluid not absorbed}}$ [g]: the amount of fluid that was not absorbed by the SAPs;
- $W_{\text{dry SAP}}$ [g]: the amount of dry SAPs.

The cement filtrate was obtained by mixing 100 g Portland cement in one litre of demineralized water for at least 24 h, followed by filtration with filter paper with particle retention 12-15 μm .

The particle size distribution of the ground SAP powders was determined using a Malvern Mastersizer 2000 instrument that measures the size distribution of particles in the wet state by laser diffraction. Measurements were obtained by adding some ethyl acetate to the dry SAP powders in a vial, stirring with caution in a sonicating bath and then transfer those with a pipet into the measuring system that was already filled with ethyl acetate as the solvent medium. Ethyl acetate was chosen as this type of SAP does not swell in this fluid. The mean value (d_{50}) of the particle size distribution is represented in μm .

2.3. Initial flow and flow over time

The workability of the fresh mortar mixture was measured by a flow test according to the standard NBN EN 1015-3. The test was executed directly after mixing, 30 min, 60 min, 90 min and 120 min after mixing. Before testing, the mixture was first mixed for 30 sec at low speed.

2.4. Hydration kinetics

The hydration kinetics of the mixtures were measured with a TAM AIR isothermal heat conduction calorimeter (TA instruments). For this test, ampoules with 14 g of mortar were filled. As the components were mixed manually outside the calorimeter, the first hydration peak was not fully registered and will not be further analysed. The isothermal calorimetric tests were performed at 20°C for 7 days. The data from the calorimetric tests were processed and converted to obtain the heat production rate q (J/g/h).

2.5. Flexural and compressive strength

The flexural strength was determined by means of a three-point-bending test on three mortar prisms with dimensions 40 x 40 x 160 mm^3 . The compressive strength was measured on the halves resulting from the bending test. Both tests were performed according the standard NBN EN 196-1 with the testing machine Walter + Bai DB 250/15. The mechanical properties were tested at 3, 7 and 28 days after casting.

3. RESULTS & DISCUSSION

3.1. Influence of cross-linking

SAPs with three different amounts of cross-linker (mol%) were produced, namely 0.15 mol%, 0.38 mol% and 0.775 mol%, as indicated in Table 2. The higher the degree of cross-linker, the lower the swelling capacity. The SAP with the highest amount of cross-linker (CS_0.775_40 with 0.775 mol% cross-linker) has a swelling capacity in demineralised water of 87 ± 2 g/g SAP. The SAP with the lowest degree of cross-linker (CS_0.15_40 with 0.15 mol% cross-linker) has a three times higher swelling capacity in demineralised water of 270 ± 17 g/g SAP. This result is logical as the crosslinks will impede the SAPs from swelling. The same trend is seen for the swelling in cement filtrate solution. However, the results of all SAPs show that their swelling capacities in cement filtrate solution are much lower compared to their swelling capacity in demineralized water. Cations like K^+ , Na^+ , Mg^{2+} or Ca^{2+} present in cement filtrate solution give rise to a so-called charge screening effect of the negatively charged polymer chains, resulting in a lower repulsion of chains and a lowered fluid absorption and less

swelling of the SAP particles. Furthermore, the presence of divalent cations like Ca^{2+} gives rise to an additional reduction of the swelling properties as these cations form strong complexes with the sulfonate groups and can therefore act as cross-linkers^{13, 14}.

Table 2: Characterization of SAPs: amount of cross-linker, solubles, swelling capacity in demineralised water and in cement filtrate (n=3), series 1

Code	Amount of cross-linker (mol%)	Solubles (%)	Swelling capacity in	
			demineralised water (g/g SAP)	cement filtrate (g/g SAP)
CS_0.15_40	0.15	28	270 ± 17	62 ± 3
CS_0.38_40	0.38	44	133 ± 14	33 ± 2
CS_0.775_40	0.775	36	87 ± 2	23 ± 3

In case no additional water is added to the mixture, the workability would be negatively affected as the SAPs will absorb part of the mixing water. Therefore, it was decided to add an amount of additional water of 1.5 times the swelling capacity in cement filtrate obtained from the filtration test. With this amount of extra water, the mortar workability was not negatively affected as the targeted initial flow of 20 ± 2 cm was reached, as shown in Figure 1. The reduction in flow over the first two hours was limited and comparable with the reference mixture without SAPs. In fact, the reference mixture shows one of the largest losses in flow as it goes from an initial value of 20.5 cm to a value of 16.8 cm after 120 min.

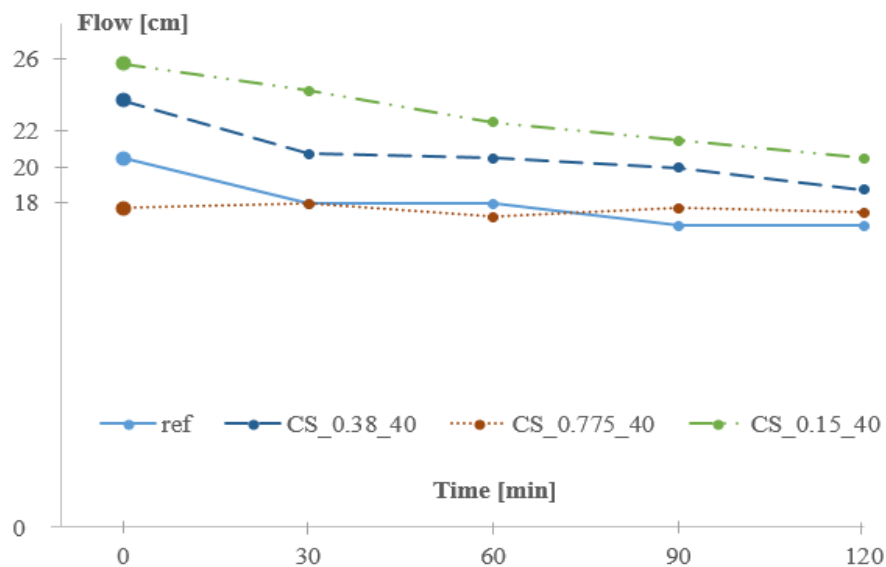


Figure 1: Initial flow and flow over time of the reference mixture and the mixtures containing SAPs with different amounts of cross-linker, series 1

Figure 2 shows the heat production rate as a function of time. It can be seen that the hydration of the mixtures containing SAPs is slightly retarded compared to the reference mixture as indicated by the small shift to the right and by the reduction in maximum heat flow values. A retardation in setting time caused by the addition of SAPs was already reported by several authors^{15,16,17}. However, the SAPs with the lowest swelling capacity, i.e. CS_0.775_40 with 0.775 mol% cross-linker, show a negligible effect on cement hydration.

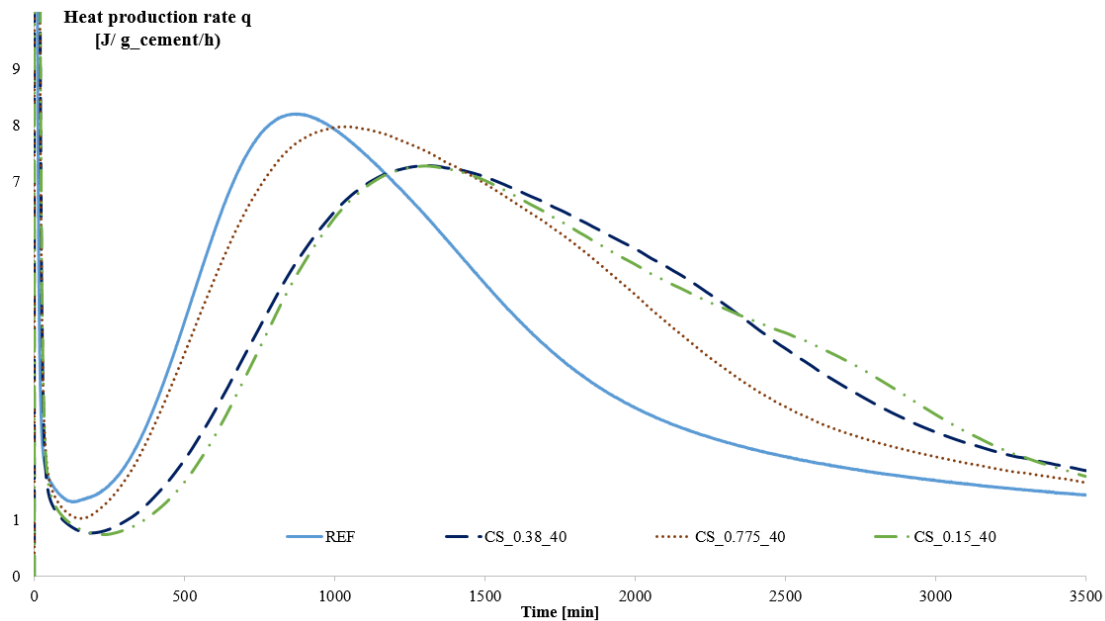


Figure 2: Hydration kinetics of the reference mixture and the mixtures containing SAPs with different amounts of cross-linker, series 1

The compressive strength of the different mixtures after 3, 7 and 28 days is shown in Table 3, together with the swelling capacity in cement filtrate of the SAPs. Different conclusions can be made based on these results:

1) the higher the swelling capacity (i.e. the lower the amount of cross-linker), the lower the compressive strength. This result is logical as the swollen SAPs will create macro pores in the matrix, negatively affecting the compressive strength compared to the reference^{1, 18, 2, 3}. After 28 days, the compressive strength of SAP CS_0.15_40 (i.e. with the lowest amount of cross-linker) is 67% lower than the reference. SAP CS_0.775_40 (i.e. with the highest amount of cross-linker) has a compressive strength at that age which is 27% lower than the reference.

2) The difference in strength with the reference decreases as a function of the mortar age. For example for SAP CS_0.775_40 this difference decreases from -37% after 3 days to -34% after 7 days and to -27% after 28 days compared to the reference. This trend is observed for all the SAPs with different cross-linking degrees.

Table 3: SAP swelling capacity in cement filtrate (n=3) and mortar compressive strength (n=6) after 3, 7 and 28 days for SAPs with different amounts of cross-linker, compared to the reference

Code	Swelling capacity in cement filtrate [g/g SAP]	Compressive strength [MPa]		
		After 3 days	After 7 days	After 28 days
REF	/	53.0 ± 2.4	63.9 ± 0.7	68.4 ± 6.7
CS_0.15_40	62 ± 3	9.7 ± 0.3	14.9 ± 1.1	22.4 ± 0.4
CS_0.38_40	33 ± 2	24.9 ± 0.7	34.4 ± 1.3	41.6 ± 1.0
CS_0.775_40	23 ± 3	33.3 ± 0.8	42.2 ± 2.6	50.0 ± 0.9

3.2. Influence of particle size

In a second test series, the influence of different particle sizes was investigated. For this purpose, the SAPs from series 1 resulting in the lowest strength reduction and with the smallest effect on the hydration rate were selected, namely CS_0.775 (0.775 mol% cross-linker). These SAPs were ground to particle sizes with d_{50} of 10, 40 and 100 μm . Similar tests as for test series 1 were performed. The results are summarized in Table 4 and

Table 5. The results between the SAPs with particle sizes of 10, 40 and 100 μm were not significantly different ($\alpha = 0.05$) concerning the swelling capacity in both demineralised water and cement filtrate solution, flow after 120 min and compressive strength of mortar after 28 days.

Table 4: Characterization of SAPs: amount of cross-linker, solubles, swelling capacity in demineralised water and cement filtrate (n=3), series 2

Code	Amount of cross-linker (mol%)	Solubles (%)	Swelling capacity in	
			demineralised water (g/g SAP)	cement filtrate (g/g SAP)
CS_0.775_10	0.775	30	75 \pm 6	28 \pm 1
CS_0.775_40	0.775	36	87 \pm 2	23 \pm 3
CS_0.775_100	0.775	30	79 \pm 3	25 \pm 2

Table 5: Characterization of mortar: flow after 120 min, mortar compressive strength after 3, 7 and 28 days (n=6), series 2

Code	Flow after 120 min [cm]	Compressive strength [MPa]		
		3 days	7 days	28 days
REF	16.75	53.0 \pm 2.4	63.9 \pm 0.7	68.4 \pm 6.7
CS_0.775_10	19.75	23.8 \pm 0.3	36.2 \pm 1.1	48.4 \pm 0.6
CS_0.775_40	17.5	33.3 \pm 0.8	42.2 \pm 2.6	50.0 \pm 0.9
CS_0.775_100	18.75	24.2 \pm 1.7	36.7 \pm 0.6	49.1 \pm 1.2

4. CONCLUSIONS

The following conclusions can be drawn based on the results of this study:

- The swelling capacity of the SAPs can be fine-tuned by varying the cross-linking degree of the SAPs.
- With an additional amount of water of 1.5 times the swelling capacity in cement filtrate obtained from the filtration test, the mortar workability was not negatively affected.
- The hydration of mixtures containing SAPs is slightly retarded compared to the reference mixture as indicated by the small shift to the right and the reduction in maximum heat flow values resulting from the TAM AIR tests.
- The higher the swelling capacity (i.e. the lower the degree of cross-linker), the lower the compressive strength. This result is logical as the swollen SAPs will create macro pores in the matrix, negatively affecting the compressive strength compared to the reference.
- The difference in strength with the reference decreases as a function of the mortar age.

- The SAP particle size (10, 40 and 100 μm) has no significant effect on the studied mortar properties (swelling capacity in both demineralised water and cement filtrate, flow after 120 min and compressive strength after 28 days).

ACKNOWLEDGEMENTS

These results are part of a project that has received partial funding from the European Union's Horizon 2020 research and innovation programme under grant agreement N°685445 – LORCENIS and partial funding from the Research Foundation Flanders (FWO Vlaanderen) under project No G.0A28.16.

REFERENCES

1. Mechtcherine, V. & Reinhardt, H.-W. *STAR 225-SAP Application of Superabsorbent Polymers (SAP) in Concrete Construction*. (2012).
2. Jensen, O. M. & Hansen, P. F. Water-entrained cement-based materials I. Principles and theoretical background. *Cem. Concr. Res.* **31**, 647–654 (2001).
3. Jensen, O. M. & Hansen, P. F. Water-entrained cement-based materials II. Experimental observations. *Cem. Concr. Res.* **32**, 973–978 (2002).
4. Dudziak, L., Mechtcherine, V. & Hempel, S. Mitigating early age shrinkage of Ultra-High Performance Concrete by using Super Absorbent Polymers (SAP). *Creep Shrinkage Durab. Mech. Concr. Concr. Struct.* 847–853 (2009). doi:10.1201/9780203882955.ch115
5. Kim, J. S. & Schlangen, E. Super Absorbent Polymers To Stimulate Self Healing in Ecc. in *2nd International Symposium on Service Life Design for Infrastructure* 849–858 (2010).
6. Van Tittelboom, K., Snoeck, D., Wang, J. & Belie, N. De. Most recent advances in the field of self-healing cementitious materials. in *ICSHM 2013: 4th international conference on self-healing materials* 406–413 (2013).
7. Lee, H., Wong, H. S. & Buenfeld, N. Potential of superabsorbent polymer for self-sealing cracks in concrete. *Adv. Appl. Ceram.* **109**, 296–302 (2010).
8. Tsuji, M., Shitama, K. & Isobe, D. Basic Studies on Simplified Curing Technique, and Prevention of Initial Cracking and Leakage of Water through Cracks of Concrete by Applying Superabsorbent Polymers as New Concrete Admixture. *J. Soc. Mater. Sci. Japan* **48**, 1308–1315 (1999).
9. Mönnig, S. & Lura, P. Superabsorbent Polymers – An Additive to Increase the Freeze-Thaw Resistance of High Strength Concrete. *Adv. Constr. Mater.* 351–358 (2007).
10. Mechtcherine, V. *et al.* Effect of superabsorbent polymers (SAP) on the freeze–thaw resistance of concrete: results of a RILEM interlaboratory study. *Mater. Struct.* **50**, 14 (2017).
11. Jensen, O. M. Water absorption of superabsorbent polymers in a cementitious environment. *Int. RILEM Conf. Adv. Constr. Mater. Through Sci. Eng.* 22–35 (2011).
12. Snoeck, D., Schröfl, C. & Mechtcherine, V. Recommendation of RILEM TC 260-RSC: testing sorption by superabsorbent polymers (SAP) prior to implementation in cement-based materials. *Mater. Struct.* **51**, 116 (2018).
13. Schröfl, C., Snoeck, D. & Mechtcherine, V. A review of characterisation methods for superabsorbent polymer (SAP) samples to be used in cement-based construction materials: report of the RILEM TC 260-RSC. *Mater. Struct. Constr.* **50**, (2017).
14. Zhu, Q., Barney, C. W. & Erk, K. a. Effect of ionic crosslinking on the swelling and mechanical response of model superabsorbent polymer hydrogels for internally cured concrete. *Mater. Struct.* **48**, 2261–2276 (2014).
15. Rizwan, S. A., Mustafa, S. & Ahmed, W. MITIGATION OF EARLY AGE SHRINKAGE IN SELF- CONSOLIDATING PASTE SYSTEMS USING SUPERABSORBENT. 443–453 (2016).
16. Dudziak, L. & Mechtcherine, V. Deliberations on kinetics of internal curing water migration and consumption based on experimental studies on SAP-enriched UHPC. (2010).
17. Piérard, J., Pollet, V. & Cauberg, N. Mitigating autogenous shrinkage in HPC by internal curing using superabsorbent polymers. *Int. RILEM Conf. Vol. Chang. Hardening Concr. Test. Mitigation,*

20-23 August C, 97–106 (2006).

18. Esteves, L. P., Cachim, P. & Ferreira, V. M. Mechanical properties of cement mortars with superabsorbent polymers. in *Advances in Construction Materials 2007* (ed. Grosse, C. U.) 451–462 (Springer Berlin Heidelberg, 2007).

UNIVERSITY OF ZAGREB FACULTY OF CIVIL ENGINEERING



100
Years

1919-2019

www.grad.unizg.hr



Mision, Vision and Strategy

Mission

The Faculty of Civil Engineering of the University of Zagreb is the oldest civil engineering faculty in Croatia conducting university education at an undergraduate, graduate and postgraduate level in all branches of civil engineering. It is continually developing and advancing higher education, scientific research activities and overall education, and actively participates in the development of the profession and implementation of new technologies.

Vision

- to retain and strengthen the leading position as a university and scientific-research centre in the country, which covers all branches of civil engineering
- to achieve international recognisability by developing a culture of quality higher education and research work by implementing the best European and world practices, promoting the mobility of students and researchers, and by becoming one of the regional centres of excellence in individual disciplines, as well as a "cooperation bridge" for countries of the European Union and the region
- to retain and strengthen cooperation with the business sector in high-expertise tasks and developmental projects, specialised life-long higher education, and the development of an alumni network for mutual support and progress

Objectives

- further harmonisation of the outcome of learning with the demands of the profession and market, with continual modernisation of the teaching process and content
- connecting and expanding cooperation with related university institutions and scientific institutions, primarily in the European Union, along with promoting the international mobility of students and researchers
- participation in joint research projects and joint studies with partners from EU countries and the region
- founding individual study programmes in the English language, and organising life-long learning and non-formal education in the English language
- development and modernisation, and certification of laboratories
- increasing spatial and personnel capacities for teaching and research needs
- further ties with the business sector and searching for adequate organisational forms

ENABLING BETTER CONSTRUCTION AND REPAIR

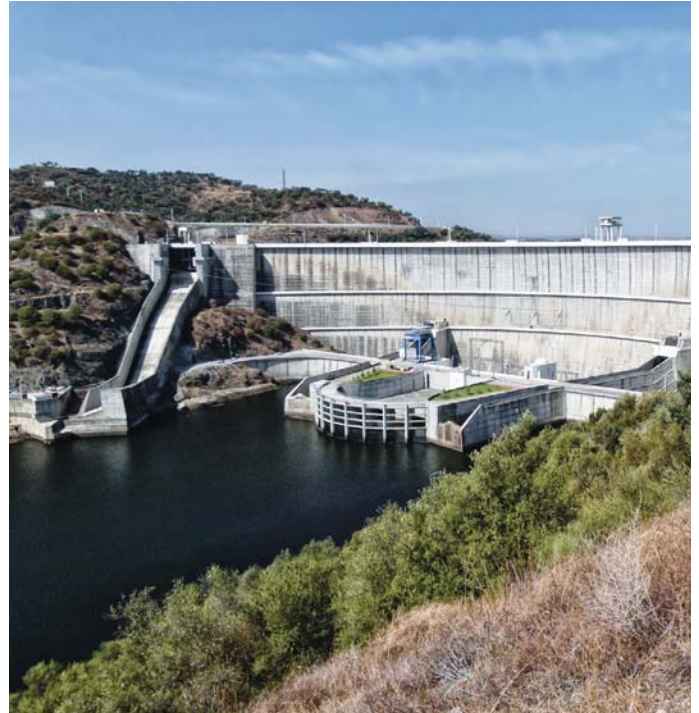
Each individual product can have a critical effect on an entire structure or its repair. Choosing the wrong solutions or applying them incorrectly can lead to component and structural damage and, in extreme cases, even endanger life.

Planners, engineers and applicators therefore have a significant responsibility to bear, of which we are only too aware.

It is not only your own good name that is at stake; businesses and people also have to be protected.

Hence – through reliable and sound technical advice and product solutions – we dedicate our fullest efforts, care and attention to ensuring that each project performed by our customers is executed to their enduring satisfaction and peace of mind. Because part of being MC really does mean accepting responsibility for lives and reputations.

We take building seriously.
BE SURE. BUILD SURE.



Injection systems



Admixtures for precast concrete



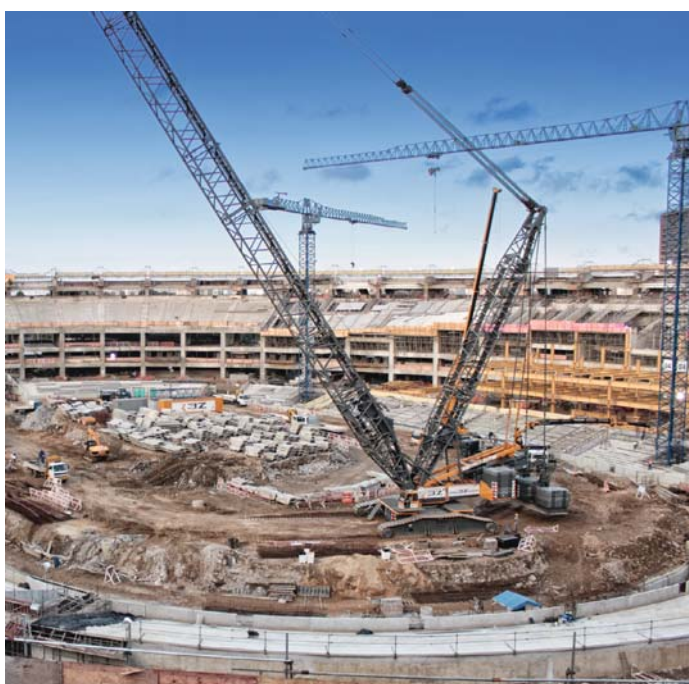
Admixtures
Concrete cosmetics
Grouting mortar



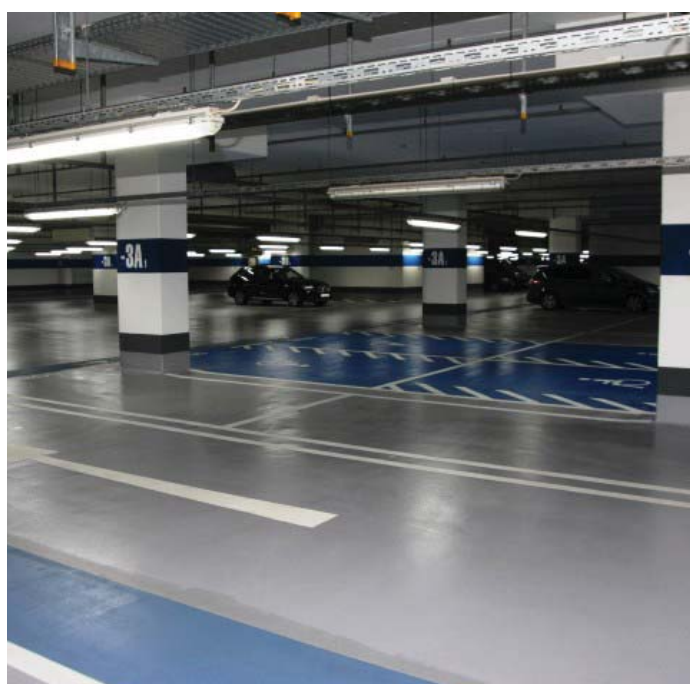
Admixtures
Concrete cosmetics



Floor coatings
Epoxy, Polyurethane



Injection systems
Concrete repair



Floor coatings
Waterproofing
Surface protection

MC solutions in demand throughout the world

MC solutions have been used in major construction and repair projects around the world for more than 50 years now. Developers, promoters, architects, planning engineers and applicators know they can rely both on the advice of our experienced consultants and on the high quality of our product systems.

MC – Building Chemicals d.o.o.

Kovinska 4a, 10090 Zagreb
Tel. +385 (1) 5587 797

www.mc-bauchemie.hr
infocro@mc-bauchemie.com



I WANT TO GET THE MOST OUT OF MY QUARRY

MasterSuna SBS: The solution for fine aggregates containing clay



35 %
Reduction
in sand costs*

25-ton
Reduction
in CO₂ emissions
per year*

Zero
Sand transportation*



QUANTIFIED SUSTAINABLE BENEFITS – REDUCE YOUR FOOTPRINT AND BOOST YOUR BOTTOM LINE

Clay containing fine aggregates were once regarded as unsuitable for the production of high-quality concrete. But this is no longer the case. With the new MasterSuna SBS sand blocker from BASF, it is even possible to convert difficult sands into a valuable resource. Thanks to MasterSuna SBS, the concrete producer BRONZO PERASSO in Marseille, France, no longer needs to transport sand from remote sites. That reduces sand and transportation costs, and saves up to 25 tons of CO₂ per year.

Discover more about this success story:

sustainability.master-builders-solutions.basf.com

BASF
We create chemistry

* Figures provided are based on an actual case from the concrete producer BRONZO PERASSO in Marseille, France

Cast off for non-metallic reinforcements

Textile concrete with AR glass or carbon reinforcements is economically and functionally far superior to standard steel concrete. The non-metallic reinforcements are alkali-resistant, non-corrosive and light. This is your introduction to modern concrete construction. Textile concrete is superbly suited to extreme conditions in a maritime environment where the wind and water are a permanent challenge.

Permanently and sustainably superior

- Six times stronger than steel
- Resistant to the effect of chloride
- Non-corrosive:
 - > Reduced concrete coverings
 - > Thin, streamlined and light components
- Lower transport costs for components
- Easy to handle during installation
- No renovation and maintenance costs



solidian[®]

Leading in construction with non-metallic reinforcement

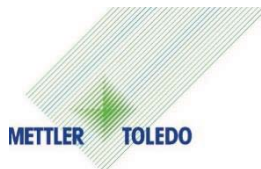
📍 Dr. Slavka Rozgaja 3
47000 Karlovac, Croatia

✉ info@solidian.hr
🌐 www.solidian.hr

☎ P +385 47 693 300
☎ F +385 47 434 203



CONFERENCE EXHIBITORS



GRAĐEVINAR

Journal of the Croatian Association of Civil Engineers

Scientific and Professional Papers
Professional news items

Indexed in:
Science Citation Index Expanded

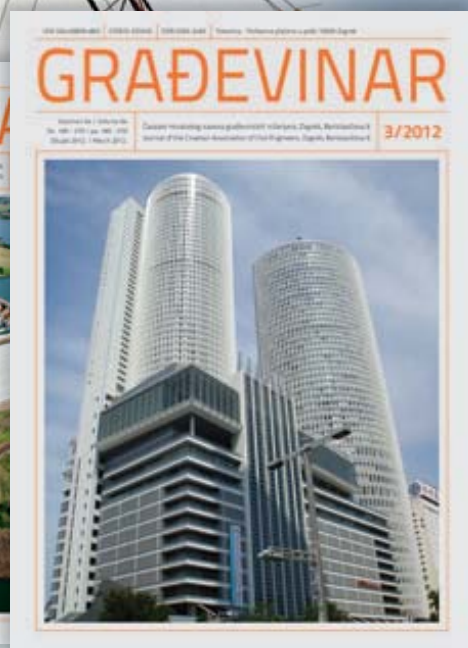
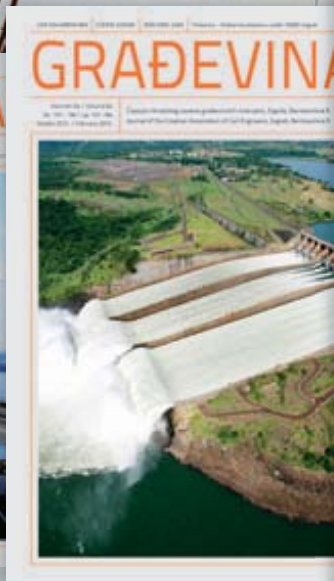
The journal is published regularly
12 times a year since 1949.

Papers are published in Croatian
language and, all papers in the
online edition are entirely in
Croatian and English

The biggest scientific & professional journal of civil engineering in Croatia

Journal published monthly
(12 issues/year)

Circulation: 3500 copies



GRADEVINAR

Journal of the Croatian Association of Civil Engineers

Editor-in-Chief

Prof. **Stjepan Lakusic**

University of Zagreb

Faculty of Civil Engineering

stjepan.lakusic@grad.hr

Journal GRADEVINAR (eng. CIVIL ENGINEER)
is a scientific/professional journal with a strong
focus on all aspects of Civil Engineering

12 issues/year
3500 copies/issue

The journal GRADEVINAR is a monthly publication that has been regularly appearing **12 times a year** without interruption for three decades now. As the journal is published each month, the publication process of reviewed and accepted papers is relatively fast. The Journal uses the **double blind review** process for evaluation of papers. All papers are printed in Croatian language, but the online edition of the journal features full versions of all papers in English language as well.

The journal GRADEVINAR encourages submission of good papers, not only to help disseminate technical information useful in the field of civil engineering, but also to provide authors with the opportunity to have their paper reviewed by peers and, when published, receive proper recognition for their efforts. The scientific/professional papers are grouped into four categories, depending on their contribution to the advancement of research or professional work.

According to its circulation (3,500 copies), GRADEVINAR is the biggest scientific/professional journal in the field of technical engineering in Croatia and wider region, and is **Indexed in Science Citation Index Expanded**.

On the homepage of Journal GRADEVINAR you can:

- Find all information about the journal
- Acquire information about the journal's most read papers
- Read all papers free of charge
- Find submission information

For more information and for submission guidelines, please visit us at
www.casopis-gradjevinar.hr

International Conference on Sustainable Materials, Systems and Structures (SMSS2019) – 20-22 March 2019 – Rovinj, Croatia
New Generation of Construction Materials

Edited by Marijana Serdar, Nina Štirmer, John Provis

RILEM Proceedings PRO 128
ISBN: 978-2-35158-217-6
VOL 1. ISBN: 978-2-35158-223-7
e-ISBN: 978-2-35158-218-3
2019 Edition

As part of the RILEM International Conference on Sustainable Materials, Systems and Structures (SMSS 2019) the segment New Generation of Construction Materials covers innovation, advances and improvement of construction materials, towards sustainable, intelligent and tailor-made solutions. This volume brings a selection of 100 peer-reviewed papers that were presented within the segment on construction materials. Topics include novel advances in raw materials for classical and alternative concretes, innovations in chemistry, application of nanotechnology in construction materials, and requirements for materials to suit the needs of construction automation.

The editors wish to thank the authors for their efforts at producing and delivering papers of a high standard. We are certain that this volume will be a valued reference of research topics in this important field and that it will, together with the other volumes from the SMSS conference, form a suitable base for discussion and suggestions for future development and research.

RILEM Publications S.a.r.l.
4 avenue du Recteur Poincaré
75016 Paris - FRANCE
Tel: + 33 1 42 24 64 46 Fax: + 33 9 70 29 51 20
E-mail : dg@rilem.net